December 2005

WASH123D: A Numerical Model of Flow, Thermal Transport, and Salinity, Sediment, and Water Quality Transport in WAterSHed Systems of 1-D Stream-River Network, 2-D Overland Regime, and 3-D Subsurface Media

by Gour-Tsyh (George) Yeh[1], Guobiao Huang[2], Fan Zhang[3], Hwai-Ping (Pearce) Cheng[4], and Hsin-Chi (Jerry) Lin[4]

[1]Department of Civil and Environmental Engineering, University of Central Florida
[2]Department of Civil and Environmental Engineering, The Pennsylvania State University
[3]Environemntal Sciences Division, Oak Ridge National Laboratory
[4]Engineer Research and Development Center, US Army Corps of Engineers

Approved for Public Release; Distribution is Unlimited

Prepared for the Office of Research and Development, US Environmental Protection Agency

Acknowledgements and Disclaimers

This research has been supported by a grant from the U.S. Environmental Protection Agency's Science to Achieve Results (STAR) program under Grant No. 827956 with University of Central Florida.

Although the research described in this report has been funded or in part by the U.S. Environmental Protection Agency's STAR program through grant 827956, it has not been subjected to any EPA review and therefore does not necessarily reflect the views of the Agency, and no official endorsement should be inferred.

EXECUTIVE SUMMARY

1 INTRODUCTION

This report presents the development of a numerical model simulating density-dependent water flow, thermal transport, and salinity transport and sediment and water quality transport in watershed systems of WAterSHed Systems of 1-D Stream-River Network, 2-D Overland Regime, and 3-D Subsurface Media (WASH123D). WASH123D is an integrated multimedia, multi-processes, physics-based computational model of various spatial-temporal scales:

- **Integrated Multimedia**
  - **Dentric Streams/Rivers/Canal/Open Channel,**
  - **Overland Regime (Land Surface),**
  - **Subsurface Media (Vadose and Saturated Zones), and**
  - **Ponds, Lakes/Reservoirs (Small/Shallow)**
- **Control Structures**
  - **Weirs, Gates, Culverts, Pumps, Levees, and Storage Ponds**
- **Management: Operational Rules for Pumps and Control Structures**
- **Integrated Multi-processes**
  - **Hydrological Cycles (Evaporation, Evapotranspiration, Infiltration, and Recharges);**
  - **Fluid Flow (Surface Runoff in Land Surface, Hydraulics and Hydrodynamics in River/Stream/Canal Networks, Interflow in Vadose Zones, and Groundwater Flow in Saturated Zones);**
  - **Salinity Transport and Thermal Transport (in Surface Waters and Groundwater);**
  - **Sediment Transport (in Surface Waters);**
  - **Water Quality Transport (Any Number of Reactive Constituents);**
  - **Biogeochemical Cycles (Nitrogen, Phosphorous, Carbon, Oxygen, etc.); and**
  - **Biota Kinetics (Algae, Phyotoplankton, Zooplakton, Caliform, Bacteria, Plants, etc.)**

2 THEORETICAL BASES

Theoretical bases of WASH123D are the conservation laws of fluids, energy, mass, and biogeochemical reaction principles with physics-based constitutional relationships. The governing equations and **particular features** of WASH123D are given as follows:

- **Fluid Flows**
  - **1D St Venant Equations for River Networks: kinematic, diffusive, and fully dynamic (MOC) waves**
  - **2D St Venant Equations for Overland Regime: kinematic, diffusive, and fully dynamic (MOC) waves, as well as Lumped Models such as SCS**

  - 3D Richard Equation for Subsurface Media (both Vadose and Saturated Zones): Saturated-unsaturated conditions

- Salinity, Thermal, and Sediment Transport
  - Modified Advection-Dispersion Equations with phenomenological approaches for erosion and deposition

- Water Quality Transport
  - Advection-Dispersion-Reaction Equations with reaction-based mechanistic approaches to water quality modeling - a general paradigm

3 TYPES OF BOUNDARY CONDITIONS

To enable the simulation of as wide a range of problems as possible, many types of boundary conditions including many particular features that can be anticipated in real-world problems are provided. These include global boundaries, internal boundaries and internal sources/sinks, and media interfaces:

- Global Boundaries
  - Flows
    - For subsurface flow - specify pressure head, fluxes, pressure gradients, radiation conditions or variable boundary conditions
    - For surface flow - specify water depth, flow rate, or rating curve.
  - Salinity, Sediment, and Reactive chemical Transport
    - Specify concentration, flux, concentration gradient or variable boundary conditions.
  - Thermal Transport
    - Specify temperature, heat flux, temperature gradient or variable boundary conditions, and heat and mass budgets at the air-media interface.

- Internal Sources/sinks and Internal Boundary Conditions
  - Pumps and Operational Rules
  - Junctions - explicitly enforced mass balance
  - Control Structures - weirs, gates, culverts, levees, and storage ponds.

- Media Interfaces
  - Continuity of Fluxes Across Media Interfaces
  - Continuity of State Variables Across Media Interfaces or
  - Linkage Terms for Special Cases.

4 OPTIONAL NUMERICAL METHODS AND STRATEGIES

To provide robust and efficient numerical solutions of the governing equations, many options and strategies are provided in WASH123D so a wide range of application-depending circumstances can be simulated. These options, strategies, and particular features are stated as follows:

- **Discretization**
  - **Flows**
    - **For subsurface flow: Use Galerkin Finite Element Methods (FEM)**
    - **For surface flow: Use Particle Tracking Methods for the kinematic wave approaches; Use Finite Element Methods or Particle Tracking Methods for the diffusive wave approaches; Use Lagrangian-Eluerian Finite Element Methods or FEM for the fully dynamic wave approaches.**
  - **Salinity, Thermal, Sediment, and Reaction-Based Water Quality Transport**
    - **Use Finite Element Methods or Particle Tracking Methods**

- **Solvers**
  - **Direct Band Matrix; Basic Point Iterations Methods; Basic Line Iterations; Preconditioned Preconditioned Conjugate Gradient Methods with Point Iterations, Incomplete Cholesky Decomposition, and Line Iterations as Preconditioners; Multigrid Methods**

- **Coupling Strategies between Transport and Reactive Chemistry**
  - **Fully Implicit Method**
  - **Mixed Prediction/Corrector (on kinetic reaction rates) and Operator-Splitting Method (on accumulation rates of immobile species)**
  - **Operator-Splitting Methods.**

In order not to introduce non-physics parameters, on the media interfaces, rigorous coupling of continuity of fluxes and continuity of state variables or formulations of fluxes when state variables are discontinuous are imposed:

- **Continuous of Fluxes**
- **Continuous of State Variables or Formulation of Fluxes**

To handle vast differences of flow and transport scales in system components of river/stream/canal networks, overland regime, and subsurface media, different time-step sizes are used.

5 DESIGN CAPABILITY OF WASH123D

The code consisted of eight modules to deal with multiple media:

(1) 1-D River/Stream Networks,
(2) 2-D Overland Regime,
(3) 3-D Subsurface Media (both Vadose and Saturated Zones);

(4) Coupled 1-D River/Stream Network and 2-D Overland Regime,
(5) Coupled 2-D Overland Regime and 3-D Subsurface,
(6) Coupled 3-D Subsurface and 1-D River Systems;

(7) Coupled 3-D Subsurface Media, 2-D Overland, and 1-D River Network; and

(8) Coupled 0-D Shallow Water Bodies and 1-D Canal Network.

For any of the above eight modules, flow only, transport only, or coupled flow and transport simulations can be carried out using WASH123D.

6 EXAMPLE PROBLEMS

A total of 17 flow problems and 15 water quality transport problems are presented in WASH123D. These example problems can serve as templates for users to apply WASH123D to research problems or practical field-scale problems. For the 17 flow examples, the following objectives are achieved:

- **Seven to demonstrate the design capability of WASH123D using seven different flow modules;**
- **Four to show the needs of various approaches to simulate various types of flow (critical, subcritical, and supercritical) in river networks and overland regime; and**
- **Five to illustrate some realistic problems using WASH123D**

For the 13 water quality transport problems: six examples for one-dimensional transport, four examples for two-dimensional transport, and three examples for three-dimensional transport. These examples are used to achieve the following objectives:

- **verify the correctness of computer implementation,**
- **demonstrate the need of various numerical options and coupling strategies between transport and biogeochemical processes for application-depending circumstances,**
- **illustrate how the generality of the water quality modeling paradigm embodies the widely used water quality models as specific examples; and**
- **validate the capability of the models to simulate laboratory experiments, and indicate its potential applications to field problems.**

TABLE OF CONTENTS

LIST OF FIGURES

LIST OF TABLES

1 INTRODUCTION

This report is to present a numerical model designed to simulate density-dependent water flow, thermal and salinity transport, and sediment and water quality transport in watershed systems of river/stream/canal networks, overland regime, and subsurface media. WASH123D is an integrated multimedia, multi-processes, physics-based computational model of various spatial-temporal scales. The model is developed to have design capability to simulate flow and transport processes in various component systems or combinations of component systems of a watershed. It can simulate problems of various spatial and temporal scales as long as the assumptions of continuum are valid.

1.1 Multimedia

WASH123D was developed to cover dentric river/stream/canal networks and overland regime (land surface) (top plate of Fig. 1.1-1) and subsurface media including vadose and saturated (groundwater) zones (bottom plate of Fig. 1.1-1). It incorporates natural junctions and control structures such as weirs, gates, culverts, levees, and pumps in river/stream/canal networks (Fig. 1.1-2). It also includes management structures such as storage ponds, pumping stations, culverts, and levees in the overland regime. In the subsurface media, management devices such as pumping/injecting wells, drainage pipes, and drainage channels are also included. Numerous management rules of these control structures and pumping operations have been implemented.

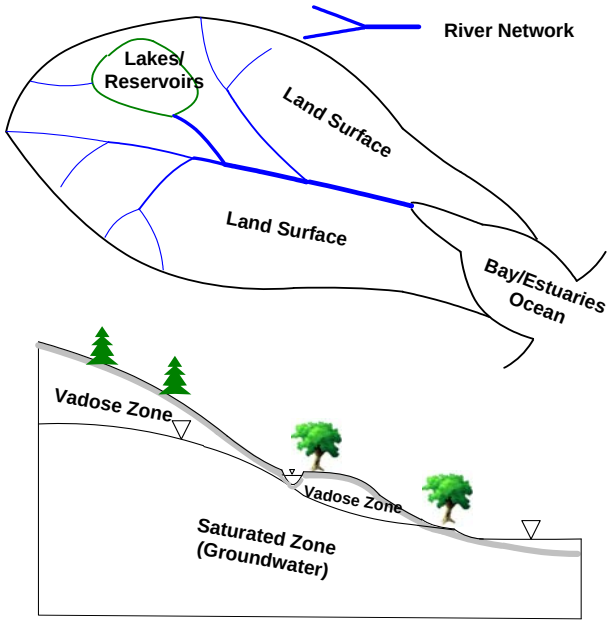

Fig. 1.1-1. Multimedia Included in WASH123D

Weirs

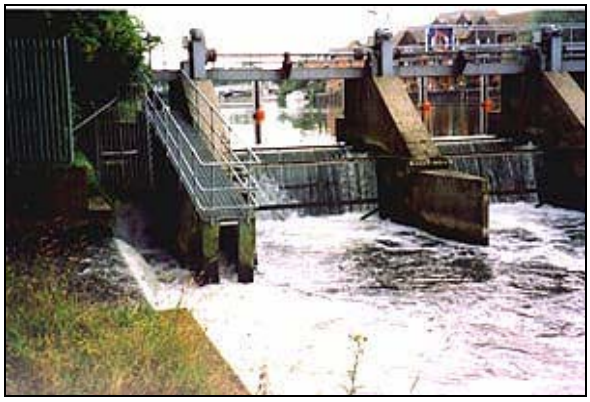

Gate

Culverts

Pumps

Levees

Storage Ponds

Fig. 1.1-2. Various Types of Control Structures Handled in WASH123D

1.2 Multi-Processes

WASH123D is designed to deal with physics-based multi-processes occurring in watersheds. These include density dependent flow and thermal and salinity transport over the entire hydrologic cycle (Fig. 1.2-1). The processes include (1) evaporation from surface waters (rivers, lakes, reservoirs, ponds, etc) in the terrestrial environment; (2) evportransipiration from plants, grass, and forest from the land surface; (3) infiltration to vadose zone through land surface and recharges (percolations) to groundwater through water tables; (4) overland flow and thermal and salinity transport in surface runoff; (5) hydraulics and hydrodynamics and thermal and salinity transport in densdric river networks; and (6) subsurface flow and thermal and salinity transport in both vadose and saturated zones.

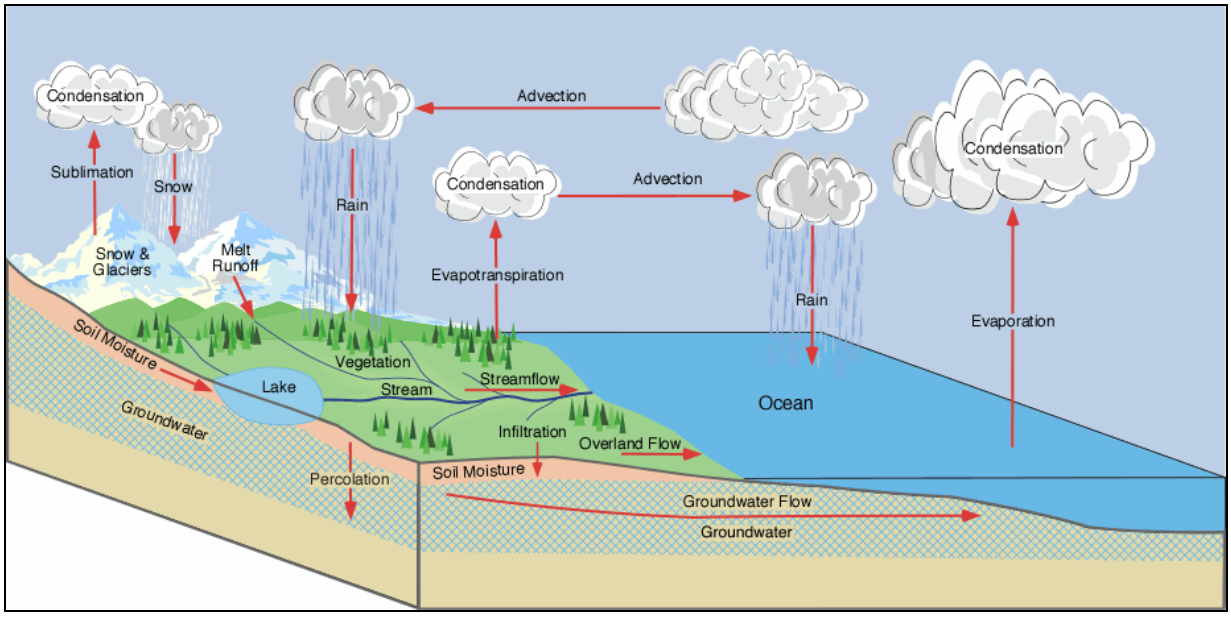

Fig. 1.2-1. Flow and Thermal and Salinity Transport Processes of Hydrologic Cycles in WASH123D

To enable the modeling of any number of water qualities including sediments, a general paradigm of reaction-based approaches is taken in WASH123D. As a result of this generic approach, WASH123D can easily be employed to model bigogeochemical cycles (including nitrogen, oxygen, phosphorous, and carbon cycles, etc. as shown in Fig. 1.2-2 and biota kinetics (including Algae, Phyotoplankton, Zooplakton, Caliform, Bacteria, Plants, etc.). In fact, once one's ability to transform biogeochemical processes into reaction networks and come up with rate equations for every reaction is achieved, one can employ WASH123D to model his/her system of reactive transport in surface runoff, surface water, and subsurface flows on watershed scales.

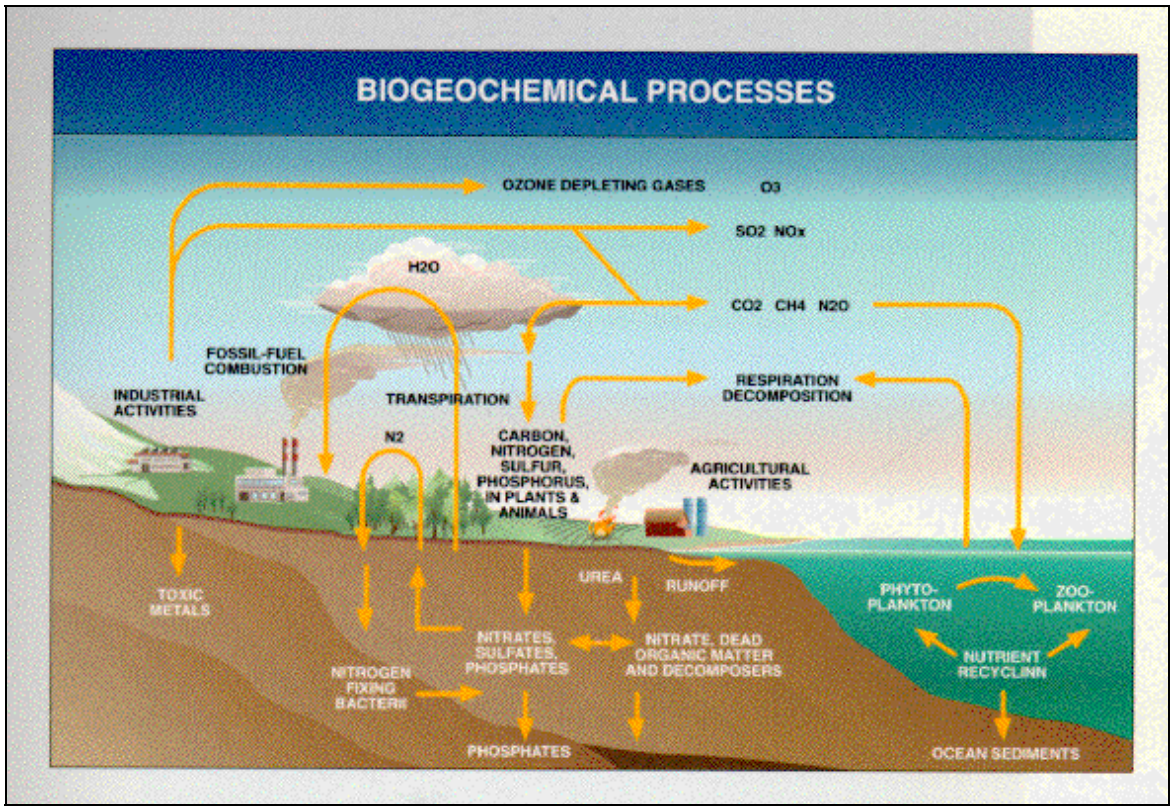

Fig. 1.2-2. Biogeochemical Cycles and Reactive Transport Included in WASH123D.

1.3 Theoretical Bases in WASH123D

The theoretical bases of fluid flows and transport processes built in WASH123D are based on the conservation laws of fluid, momentum, energy, and mass with associated constitution relationships between fluxes and state variables and appropriately formulated equations for source/sink terms. Various types of boundary conditions based on physics reasoning are essential to supplement the governing equations. Adequate initial conditions are either obtained from measurements or with simulations of steady-state versions of the governing equations.

1.3.1 Governing Equations

For fluid flows in river/stream/canal networks, one-dimensional St Venant Equations modified to include the effects of density due to temperature and salinity are employed, which are in fact the cross-section area averaged Navier-Stokes equations. For surface runoff over the land surfaces, two-dimensional St Venant Equations modified to take into account the effects of temperature- and salinity-dependent density. The two-dimensional St Venant Equations are in fact the vertically averaged Navier-Stokes equations.

The particular features in WASH123D are the inclusion of three approaches to model surface flow in a watershed system: the kinematic, diffusive, and dynamic wave models. The dynamic wave models completely describe water flow but they are very difficult to solve under some conditions (e.g., when the slope of ground surface is steep), regardless of what numerical approach is employed. On the other hand, the diffusion and/or kinematic models can handle a wide range of flow problems but are inaccurate when the inertial terms play significant roles. Thus, three options are provided in this report: the kinematic wave model, the diffusion wave model, and the dynamic wave model to accurately compute water flow over a wide range of conditions.

The subsurface flow is described with the modified Richards equation. The modification incorporates the effect of density due to temperature and salinity effects. The governing equation is derived based on continuity of fluid, continuity of solid mass, incompressibility of solids, and Darcy's law.

The principles of mass balance were employed to derive the modified advective-dispersive/diffusion transport equations governing the temporal-spatial distribution of salinity, water quality, suspended sediment, and bed sediment. For sediment transport, phenomenological equations for erosions and depositions are used. For biogeochemical transport, reaction rate equations can be provided based on mechanisms (pathways) or based on empirical formulations using experimental data for every slow reaction. Examples of mechanisms-based reaction rates includes forward-backward rate equations based on the collision theory, Monod-type rate equations based on the enzymatic kinetic theory (Segel, 1975), etc. Empirical rate equations include zero-order, first order, n-th order, Freundlich kinetics, etc. For every fast reaction, either the mass action equation based on the thermodynamic approach or user's defined algebraic equation can be used.

1.3.2 Boundary Conditions

To enable the simulation of as wide a range of problems as possible, many types of boundary conditions that can be anticipated in real-world problems are provided. These include global boundaries, internal boundaries and internal sources/sinks, and media interfaces. On global boundaries, five types of boundary conditions can be prescribed for subsurface flows: (1) specified pressure head, (2) specified flux, (3) specified pressure gradient, (4) variable conditions in which the model will iteratively determine head or flux conditions (this type of boundary conditions is normally specified at the atmospheric boundary), and (5) radiation conditions where the flux is proportional to the difference in head between the media and surface waters such as rivers or lakes/reservoirs/ponds. For surface water flows, three types of boundary conditions can be prescribed: (1) specified water depth, (2) specified flow rates, and (3) rating curves relating discharges to water depth. For scalor transport, four types of boundary conditions can be prescribed: (1) specified state variables (concentrations or temperature), (2) specified fluxes of state variables, (3) specified gradient fluxes of state variables, and (4) variable conditions in which fluxes are specified when the flow is coming into the region or the mass/energy is transported out of the region by advection when the flow is going out of the region. In addition, at the atmosphere-media interface, heat and mass budget balance must be satisfied for thermal transport.

On internal boundaries such as natural junctions and control structures of weirs, gates, culverts, levees, mass or energy balance is explicitly enforced by solving a set of flux continuity and state variable continuity (or flux) equations. For the internal sources/sinks, pumping and operation rules are simulated to ensure mass conservation.

On the media interfaces, continuity of fluxes and continuity of state variables or formulations of fluxes when state variables are discontinuous are imposed.

1.3.3 Numerical Methods

To provide robust and efficient numerical solutions of the governing equations, many options and strategies are provided in WASH123D so a wide range of application-depending circumstances can be simulated. For surface flow problems, the semi-Lagrangian method (backward particle tracking) was used to solve kinematic wave equations. The diffusion wave models were numerically approximated with the Galerkin finite element method or the semi-Lagrangian method. The dynamic model was first mathematically transformed into characteristic wave equations. Then it was numerically solved with the Lagrangian-Eulerian method. The subsurface flow-governing equations were discretized with the Galerkin finite element method. The dynamic wave model for surface water flows in conservative forms will be discretized with finite element methods in future update of WASH123D.

For scalor transport equations including thermal, salinity, sediment, and reactive chemical transport, either finite element methods or hybrid Lagrangian-Eulerian methods were used to approximate the governing equations. Three strategies were employed to handle the coupling between transport and biogeochemical reactions: (1) fully implicit scheme, (2) mixed predictor-corrector and operator-splitting methods, and (3) operator-splitting schemes. For the fully implicit scheme, one iteratively solves the transport equations and reaction equations. For the mixed predictor-corrector and operator-splitting method, the advection-dispersion transport equation is solved with the source/sink term evaluated at the previous time in the predictor step. The implicit finite difference was used to solve the system of ordinary equations governing the chemical kinetic and equilibrium reactions in the corrector step. The nonlinearity in flow and sediment transport equations is handled with the Picard method, while the nonlinear chemical system is solved using the Newton-Raphson method.

Several matrix solvers are provided to efficiently solve the system of linear algebraic equations resulting from the discretization of the governing equations and the incorporation of boundary conditions. These include direct band matrix solvers; basic point iteration solvers such as Gauss-Seidel iteration or successive over relaxation; basic line iteration solvers; preconditioned conjugate gradient methods with point iterations, incomplete Cholesky decomposition, and line iterations as preconditioners; and multigrid methods.

1.4 Design Capability of WASH123D

WASH123D includes seven modules: (1) one-dimensional river/stream network module, (2) two-dimensional overland module, (3) three-dimensional subsurface module, (4) coupled 1D and 2D module, (5) coupled 2D and 3D module, (6) coupled 3D and 1D module, and (7) coupled 1D, 2D, and 3D module. Each module can be used to simulate flows alone, sediment transport alone, water quality transport alone, or flow and sediment and water quality transport simultaneously. When both flow and transport are simulated, the flow fields are computed first. Then the transport is calculated using the computed flow fields at respective times. Temperature- and salinity-dependent flow is considered. A slightly different version of WASH123D also included 0-dimensional water, energy, and mass budget to simulate the change of stages, temperature, and concentrations of sediment and any biogeochemical species for well mixed surface water bodies such as small lakes, reservoirs, storage ponds, etc. This 0D module has been coupled to one-dimensional canal networks and it could be coupled with two-dimensional overland regime or three-dimensional subsurface media.

1.5 Organization of this Report

Chapter 2 provides a heuristic derivation of the governing equations and statements of boundary and initial conditions for flow in river/stream network (Section 2.1), surface runoff in the overland regime (Section 2.2), flow in the subsurface (Section 2.3) rigorous coupling of flows among various media (Section 2.4), sediment and water quality transport in river/stream network (Section 2.5), sediment and water quality transport in the overland regime (Section 2.6), water quality transport in the subsurface (Section 2.7), and coupling of transport among various media (Section 2.8).

Chapter 3 includes numerical approaches to solve governing equations for flows in the river/stream network (Section 3.1), overland (Section 3.2), and subsurface systems (Section 3.3). Numerical approximations of dynamic, diffusive, and kinematic wave models are thoroughly explored for solving flow problems in surface water. Numerical implementations of rigorously coupling fluid flow between media interfaces are addressed in Section 3.4. This chapter also describes the numerical approximation to solve both sediment and chemical transport in river/stream network (Section 3.5) and overland regimes (Section 3.6), and chemical transport in the subsurface (Section 3.7). Section 3.8 deals with detail coupling strategies in handling water quality (both sediments and biogeochemical constituents) transport problems across media interfaces. Section 3.9 presents detail computational structures of using different time-step sizes to deal with vastly different time scales of flow and transport problems in river/stream/canal networks, surface runoffs, and subsurface media.

Chapter 4 gives a total of 17 flow examples which could serve as templates for users in applying WASH123D to either research problems or real-world field applications. These examples are presented to demonstrate the design capability of WASH123D, to show the needs of various approaches to simulate flow in river networks and overland flow problems, and to illustrate some realistic problems using WASH123D.

Chapter 5 contains a total of 13 water quality transport problems: six examples for one-dimensional

problems, four examples for two-dimensional problems, and three examples for three-dimensional problems. These examples are used to (1) verify the correctness of computer implementation, (2) demonstrate the need of various numerical options and coupling between transport and biogeochemical processes depending on application circumstances, (3) show the generality of the water quality modeling paradigm that embodies the widely used water quality models as specific examples, (4) validate the capability of the models to simulate laboratory experiments, and indicate its potential applications to field problems.

Summary conclusions and recommendations for further research in the development of computational models for watersheds are addressed in Chapter 6.

2 MATHEMATICAL BASIS

In this section, we are to give governing equations, initial conditions, and boundary conditions for simulating water flow and chemical and sediment transport in watershed systems.

2.1 Water Flow in One-Dimensional River/Stream/Canal Network

The governing equations of water flow in one-dimensional river/stream/canal can be derived based on the conservation law of water mass and linear momentum (Singh, 1996), and can be written as follows.

The continuity equation:

$$\frac{\partial A}{\partial t}+\frac{\partial Q}{\partial x}=S_S+S_R-S_E+S_I+S_1+S_2 \qquad \textbf{(2.1.1)}$$

where t is time [t]; x is the axis along the river/stream/canal direction [L]; A is cross-sectional area of the river/stream [L^2]; Q is flow rate of the river/stream/canal [L^3/t]; S_S is the man-induced source [L^3/t/L]; S_R is the source due to rainfall [L^3/t/L]; S_E is the sink due to evapotranspiration [L^3/t/L]; S_I is the source due to exfiltration from the subsurface media [L^3//t/L]; S_1 and S_2 are the source terms contributed from overland flow [L^3/t/L].

The momentum equation:

$$\frac{\partial Q}{\partial t}+\frac{\partial VQ}{\partial x}=-gA\frac{\partial\left(Z_O+h\right)}{\partial x}-\frac{gAh}{c\rho}\frac{\partial\Delta\rho}{\partial x}-\frac{\partial F_x}{\partial x}+\left(M_S+M_R-M_E+M_I+M_1+M_2\right)+\frac{B\tau^S-P\tau^b}{\rho} \qquad \textbf{(2.1.2)}$$

where h is water depth [L]; V is river/stream/canal velocity [L/t]; g is gravity [L/t^2]; Z_o is bottom elevation [L]; $\Delta\rho=\rho-\rho_o$ is the density deviation [M/L^3] from the reference density (ρ_o), which is a function of temperature and salinity as well as other chemical concentrations; c is the shape factor of the cross-sectional area; F_x is the momentum flux due to eddy viscosity [L^4/t^2]; M_S is the external momentum-impulse from artificial sources/sinks [L^3/t^2]; M_R is the momentum-impulse gained from rainfall [L^3/t^2]; M_E is the momentum-impulse lost to evapotranspiration [L^3/t^2]; M_I is the momentum-impulse gained from the subsurface due to exfiltration [L^3/t^2]; M_1 and M_2 are the momentum-impulse gained from the overland flow [L^3/t^2]; ρ is the water density [M/L^3]; B is the top width of the cross-section [L]; τ^s is the surface shear stress [$M/t^2/L$]; P is the wet perimeter [L]; and τ^b is the bottom shear stress [$M/t^2/L$], which can be assumed proportional to the flow rate as $\tau^b/\rho=\boldsymbol{\kappa V}^2$ where $\kappa=gn^2/R^{1/3}$ and R is the hydraulic radius (L) and n is the Manning's roughness.

2.1.1 Fully Dynamic Wave Approaches

Equations (2.1.1) and (2.1.2) written in the conservative form are the governing equations for one-dimensional flow in river/stream/canals. Depending on the simplification of the momentum equation, one can have three approaches: fully dynamic wave, diffusive wave, and kinematic wave. For the fully dynamic wave approach, all terms in Eq. (2.1.2) are retained. Under such circumstances, the conservative form of the governing equations may be used or they may be cast in the advection form or in the characteristic form. In this report the characteristic form of the fully dynamic approach will be used as the main option because it is the most natural way and amenable to the advective numerical methods, e.g., the upstream approximation or the Lagrangian-Eulerian method.

For a non-prismatic river/stream/canal network, the cross-sectional area is a function not only of the water depth but also of the river distance, i.e.,

$$A(x,t) = A^{\#}\left(h(x,t),x\right) \tag{2.1.3}$$

where $A^{\#}$ is a function of the water depth $h(x,t)$ and the axis along the river/stream/canal direction x. Differentiating Eq. (2.1.3) with respect to x and t, respectively, we have

$$\frac{\partial A}{\partial t} = \frac{\partial A^{\#}}{\partial h}\frac{\partial h}{\partial t} + \frac{\partial A^{\#}}{\partial x}\frac{\partial x}{\partial t} = \frac{\partial A^{\#}}{\partial h}\frac{\partial h}{\partial t} = B\frac{\partial h}{\partial t} \tag{2.1.4}$$

and

$$\frac{\partial A}{\partial x} = \frac{\partial A^{\#}}{\partial h}\frac{\partial h}{\partial x} + \frac{\partial A^{\#}}{\partial x}\frac{\partial x}{\partial x} = \frac{\partial A^{\#}}{\partial h}\frac{\partial h}{\partial x} + \frac{\partial A^{\#}}{\partial x} = B\frac{\partial h}{\partial x} + \frac{\partial A^{\#}}{\partial x} \tag{2.1.5}$$

where $B(x,t) = B^{\#}(h,x) = \partial A^{\#}/\partial h$ is the top width of the cross-section, [L].

Substituting $Q = VA$ and Eqs. (2.1.4) and (2.1.5) into Eqs. (2.1.1) and (2.1.2), we obtain

$$\frac{\partial h}{\partial t} + V\frac{\partial h}{\partial x} + \frac{A}{B}\frac{\partial V}{\partial x} = \frac{1}{B}\left(S_S + S_R - S_E + S_I + S_1 + S_2\right) - \frac{V}{B}\frac{\partial A^{\#}}{\partial x} \tag{2.1.6}$$

$$\frac{\partial V}{\partial t} + V\frac{\partial V}{\partial x} + g\frac{\partial h}{\partial x} = -\frac{1}{A}\frac{\partial F_x}{\partial x} - g\frac{\partial Z_o}{\partial x} - \frac{gh}{c\rho}\frac{\partial \Delta\rho}{\partial x} + \frac{1}{A}\left[\begin{array}{l} -V\left(S_S + S_R - S_E + S_I + S_1 + S_2\right) + \\ \left(M_S + M_R - M_E + M_I + M_1 + M_2\right) + \dfrac{B\tau^S - P\tau^b}{\rho} \end{array}\right] \tag{2.1.7}$$

Equations (2.1.6) and (2.1.7) can be written in matrix form as

$$\frac{\partial \mathbf{E}}{\partial \mathrm{t}} + \mathbf{A}\frac{\partial \mathbf{E}}{\partial \mathrm{x}} = \mathbf{R} + \mathbf{D} \tag{2.1.8}$$

where

$$\mathbf{E} = \{h \quad V\}^T; \qquad \mathbf{A} = \begin{bmatrix} V & \frac{A}{B} \\ g & V \end{bmatrix}; \qquad \mathbf{R} = \{R_1 \quad R_2\}^T; \qquad \mathbf{D} = \{0 \quad D\}^T \tag{2.1.9}$$

in which

$$R_1 = \frac{1}{B}\left(S_S + S_R - S_E + S_I + S_1 + S_2\right) - \frac{V}{B}\frac{\partial A^{\#}}{\partial x} \tag{2.1.10}$$

$$R_2 = -g\frac{\partial Z_0}{\partial x} - \frac{gh}{c\rho}\frac{\partial(\Delta\rho)}{\partial x} + \frac{1}{A}\begin{bmatrix} -V\left(S_S + S_R - S_E + S_I + S_1 + S_2\right) + \\ \left(M_S + M_R - M_E + M_I + M_1 + M_2\right) + \dfrac{B\tau^s - P\tau^b}{\rho} \end{bmatrix} \tag{2.1.11}$$

$$D = -\frac{1}{A}\frac{\partial F_x}{\partial x} = \frac{1}{A}\frac{\partial}{\partial x}\left(A\varepsilon\frac{\partial V}{\partial x}\right) \qquad \textit{in which} \quad F_x = -A\varepsilon\frac{\partial V}{\partial x} \quad \textit{has been assumed} \tag{2.1.12}$$

where ε is the eddy viscosity.

The eigenvalues and eigenvectors of **A** are

$$\lambda_1 = V + \sqrt{\frac{gA}{B}} \qquad \mathbf{e_1} = \left\{\frac{1}{2}\sqrt{\frac{A}{gB}} \quad \frac{1}{2}\right\}^T \tag{2.1.13}$$

$$\lambda_2 = V - \sqrt{\frac{gA}{B}} \qquad \mathbf{e_2} = \left\{-\frac{1}{2}\sqrt{\frac{A}{gB}} \quad \frac{1}{2}\right\}^T \tag{2.1.14}$$

Denoting $c = \sqrt{\frac{gA}{B}}$, we define

$$\mathbf{L} = \begin{bmatrix} \frac{c}{2g} & -\frac{c}{2g} \\ \frac{1}{2} & \frac{1}{2} \end{bmatrix} \quad \textit{which gives} \quad \mathbf{L^{-1}} = \begin{bmatrix} \frac{g}{c} & 1 \\ -\frac{g}{c} & 1 \end{bmatrix} \tag{2.1.15}$$

where **L** and $\mathbf{L}^{-1}$, respectively, are the right and left eigenmatrices, respectively, of the matrix **A**. Set

$$\partial\mathbf{W} = \mathbf{L}^{-1}\partial\mathbf{E} = \begin{bmatrix} \frac{g}{c} & 1 \\ -\frac{g}{c} & 1 \end{bmatrix}\begin{Bmatrix} \partial h \\ \partial V \end{Bmatrix} \tag{2.1.16}$$

where **W** is a characteristic wave variable. Equation (2.1.16) transforms the primitive variable $\mathbf{E} = \{h, V\}^T$ to the characteristic variable $\mathbf{W} = \{W_1, W_2\}^T$.

Multiplying both side of Eq. (2.1.8) by $\mathbf{L^{-1}}$ yields

$$\mathbf{L^{-1}}\frac{\partial \mathbf{E}}{\partial \mathbf{t}} + \mathbf{L^{-1}A\,L\,L^{-1}}\frac{\partial \mathbf{E}}{\partial \mathrm{x}} = \mathbf{L^{-1}R} + \mathbf{L^{-1}D} \qquad \textbf{(2.1.17)}$$

Since by definition $\partial\mathbf{W} = \mathbf{L^{-1}}\partial\mathbf{E}$ and $\mathbf{L^{-1}AL}$ is a diagonal matrix whose entries are the eigenvalues of **A**, we have

$$\frac{\partial \mathbf{W}}{\partial \mathrm{t}} + \begin{bmatrix} V+c & 0 \\ 0 & V-c \end{bmatrix}\frac{\partial \mathbf{W}}{\partial \mathrm{x}} = \mathbf{L^{-1}R} + \mathbf{L^{-1}D} \qquad or \qquad \frac{D\mathbf{W}}{Dt} = \mathbf{L^{-1}R} + \mathbf{L^{-1}D} \qquad \textbf{(2.1.18)}$$

Substituting $\mathbf{L^{-1}}$ ($\mathbf{L^{-1}}$ is defined by Eq. (2.1.15)) into the right hand side of Eq. (2.1.18) and making an integral transformation so that $(g/c)\partial h = \partial\omega$, we obtain

$$\frac{D_{V+c}(V+\omega)}{D\tau} \equiv \frac{\partial(V+\omega)}{\partial t} + (V+c)\frac{\partial(V+\omega)}{\partial x} = \frac{g}{c}R_1 + R_2 + D \qquad \textbf{(2.1.19)}$$

$$\frac{D_{V-c}(V-\omega)}{D\tau} \equiv \frac{\partial(V-\omega)}{\partial t} + (V-c)\frac{\partial(V-\omega)}{\partial x} = -\frac{g}{c}R_1 + R_2 + D \qquad \textbf{(2.1.20)}$$

in which

$$c = \sqrt{\frac{gA}{B}}; \quad \omega = \int_0^h \frac{g}{c(s)}ds \qquad \textbf{(2.1.21)}$$

where c is the wave speed and ω is the transformed wave speed. Equation (2.1.19) simply states that the positive gravity wave ($V+\omega$) is advected by the speed ($V+c$) while Equation (2.1.20) states that the negative gravity wave ($V-\omega$) is advected by the speed ($V-c$).

For transient simulations, the water depth (or water stage) and the cross-sectionally averaged velocity must be given as the initial condition. In addition, appropriate boundary conditions need to be specified to match the corresponding physical system.

The system of Eqs. (2.1.19) and (2.1.20) are identical to the system of Eqs. (2.1.1) and (2.1.2) on the differential level. They offer advantages in their amenability to innovative advective numerical methods such as the upstream finite difference, upwind finite element, or semi-Lagrangian scheme. Furthermore, the implementation of boundary conditions is very straightforward. Only when the wave is coming into the region of interest, the boundary condition is required. For the wave that is going out of the region of interest, there is no need to specify a boundary condition.

Open upstream boundary condition:

The boundary condition at an upstream point depends on flow conditions. If the flow is supercritical, both waves are transported into the region and two boundary conditions are needed. The water depth and velocity at the boundary are determined entirely by the flow condition that prevails at the upstream. The governing equations for this case can be set up based on the continuity of mass as well as momentum between the boundary and the upstream as follows

$$VA = V_{up}A_{up} = Q_{up} \quad and \quad \rho VAV + \rho g h_c A = \rho V_{up}A_{up}V_{up} + \rho g h_{upc}A_{up} = M_{up} \quad \textbf{(2.1.22)}$$

where V_{up} is the cross-sectional averaged velocity from the incoming upstream fluid, A_{up} is the cross-sectional area in the upstream, Q_{up} is the flow rate of the incoming fluid from the upstream, h_c is the water depth to the centroid of the cross-sectional area of the boundary, h_{upc} is the water depth to the centroid of the upstream cross-sectional area, and M_{up} is the momentum-impulse of the incoming fluid from the upstream. It should be noted that both the water depth and velocity in the upstream must be measured to provide values of Q_{up} and M_{up}. If the flow is critical, the positive wave is transported into the region from upstream and the negative wave is immobile. The water depth and velocity at the boundary are determined by the flow conditions prevail at the upstream and by the condition of critical flow. The governing equations for this case may be set up based on the continuity of mass and the requirement of critical flow condition as

$$VA = Q_{up} \qquad and \qquad \frac{BQ^2}{gA^3} = 1 \qquad \textbf{(2.1.23)}$$

If the flow is subcritical, while the positive wave is transported into the region, the negative wave is transported out of the region. The water depth and velocity are determined by the flow condition prevail at upstream and by flow dynamics in the region. The governing equations are set up based on the continuity of mass between the boundary and the upstream, and on flow dynamics in the region

$$VA = Q_{up} \qquad and \qquad F_{-}(V,h) = 0 \qquad \textbf{(2.1.24)}$$

where $F_{-}(V, h)$, a function of velocity and water depth, is the negative wave boundary function.

In summary, the boundary condition at an open upstream boundary point is given by Eqs. (2.1.22), (2.1.23), and (2.1.24), respectively, for the case of supercritical, critical, and subcritical flows, respectively.

Open downstream boundary condition:

If the flow is supercritical on an open downstream boundary point, both waves are transported out of region. Under such circumstances, no boundary conditions are needed. The water depth and velocity on the boundary are determined by flow dynamics in the region. The governing equations for V and h are

$$F_{+}(V,h) = 0 \qquad and \qquad F_{-}(V,h) = 0 \qquad \textbf{(2.1.25)}$$

where $F_{+}(V, h)$, a function of V and h, is the positive wave boundary function. If the flow is critical, the water depth and velocity at the boundary are determined by flow dynamics in the region and by the condition of critical flow. Thus, the governing equations for critical flow are given by

$$F_{+}(V,h) = 0 \qquad and \qquad \frac{BQ^2}{gA^3} = 1 \qquad \textbf{(2.1.26)}$$

If the flow is subcritical, while the positive wave is transported out of the region, the negative wave is transported into the region. The water depth and velocity are determined by flow dynamics in the region and by what is the control on the boundary. The governing equations may be given by

$$F_+(V,h)=0 \quad and \quad VA=Q_{dn}(h) \qquad or \qquad F_+(V,h)=0 \quad and \quad h=h_{dn}(t) \qquad \textbf{(2.1.27)}$$

where $Q_{dn}(h)$, a function of h, is the rating curve function for the downstream boundary and $h_{dn}(t)$, a function of t, is the water depth at the downstream boundary. The adaptation of Eq. (2.1.27) depends on the physical configuration at the boundary.

In summary, the boundary condition at an open downstream boundary is given by Eqs. (2.1.25), (2.1.26), and (2.1.27), respectively, for the case of supercritical flow, critical flow, and subcritical flows, respectively.

Closed upstream boundary condition:

At the closed upstream boundary, physically all flow conditions can occur. When the supercritical flow happens, both positive and negative waves are transported into the region. Two boundary condition equations are needed. Because the boundary is closed, it is impermeable. The governing equations can be obtained by simply substituting $Q_{up} = 0$ and $M_{up} = 0$ into Eq. (2.1.22) to yield

$$VA=0 \qquad and \qquad \rho VAV+\rho g h_c A=0 \qquad \textbf{(2.1.28)}$$

The solutions for Eq. (2.1.28) are not unique. One possible solution is $V = 0$ and $h = 0$.

For the critical flow, the velocity is equal to the wave speed, $V = c$, the negative wave is immobile. On the other hand, the positive wave is transported into the region of interest, one boundary-condition equation is needed. Because the closed boundary is impermeable, the governing equations may be set up by imposing zero flow rate and the condition of critical flow as

$$VA=0 \qquad and \qquad \frac{BQ^2}{gA^3}=1 \qquad \textbf{(2.1.29)}$$

When the flow is subcritical, the positive wave is transported into the region of interest while the negative wave is transported out of the region of interest. Only the boundary condition for the positive wave is needed. Since no fluid from the outside world is transported into the region via the boundary, the boundary condition for the positive wave can be stated with $Q = VA = 0$. The governing equations for V and h are thus given by

$$VA=0 \qquad and \qquad F_-(V,h)=0 \qquad \textbf{(2.1.30)}$$

In summary, the boundary condition at a closed upstream point is given by Eqs. (2.1.28), (2.1.29), and (2.1.30), respectively, for the case of supercritical flow, critical flow, and subcritical flows, respectively.

Closed downstream boundary condition:

At the closed downstream boundary, physical condition dictates that the velocity at the boundary is zero. Since the velocity is zero, supercritical flow cannot occur at the closed boundary point because the water depth is greater or equal to zero. Therefore, the flow can only be either critical or subcritical. For critical flow, $c = V = 0$, which is very unlikely. Therefore, it is highly unlikely that critical flow will occur at the closed downstream boundary.

For the subcritical flow, the positive wave is transported out of the region and no boundary condition is needed for this wave. On the other hand, the negative wave is transported into the region of interest. The governing equations for V and h are

$$F_+(V,h) = 0 \qquad and \qquad V = 0 \tag{2.1.31}$$

which is based on the physics that $V = 0$ and the water depth is governed by internal flow dynamics.

In summary, supercritical flow cannot occur at a closed downstream point. The boundary condition at a closed downstream boundary point is either V = 0 and h = 0 for critical flow or is given by Eq. (2.1.31) for subcritical flow.

Natural internal boundary condition at junctions:

For the junction node J (Figure 2.1-1), we have one unknown: the water surface elevation or the stage, H_J. The governing equation for this junction is obtained as

$$\frac{d\forall_J}{dh_J}\frac{dh_J}{dt} = \sum_I^{N_J} Q_{IJ} = \sum_I^{N_J} V_{IJ} A_{IJ} \tag{2.1.32}$$

for the case when the storage effect of the junction is accounted for, or

$$\sum_I^{N_J} Q_{IJ} = \sum_I^{N_J} V_{IJ} A_{IJ} = 0 \tag{2.1.33}$$

for the case when the storage effect of the junction is not included.

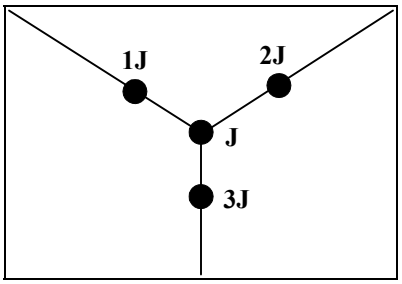

Fig. 2.1-1. Schematic of a Junction

In Eqs. (2.1.32) and (2.1.33), $\forall_J$ is the volume of the junction J; h_J is the water depth of the junction J; Q_{IJ} is the flow rate of the I^{th} reach to the J^{th} junction; I is the identification number of

river/stream/canal reach; N_J is the total number of river/stream/canal reaches that are connected to the junction J (it is 3 in the case shown); V_{IJ} and A_{IJ} are the velocity and cross sectional area, respectively, of the I^{th} reach at the location entering the J^{th} junction.

The node IJ located at the boundary between the I^{th} reach and the J^{th} junction is termed the natural internal boundary of reach I. The governing equations for the internal boundary node IJ depend on whether this node is a downstream or an upstream node in reference to the reach I. Let us say that node IJ is a downstream point if the flow is from the reach I toward the junction J. On the other hand, we say that the node IJ is an upstream point if the flow is from the junction J toward the reach I. With this definition, we can generate equations for any internal boundary node IJ, which will be stated in the following.

If IJ is a downstream internal boundary, we have three cases to consider: subcritical flow, critical flow, and supercritical flow. For the case of subcritical flow, the positive wave is going out of the reach and no boundary condition for this wave is needed. On the other hand, the negative wave is going into the region and its boundary condition is obtained by the assumption that no loss in energy between the junction and node IJ. The governing equations for node IJ are given as

$$F_+\left(V_{IJ}, h_{IJ}\right) = 0 \qquad and \qquad E_{IJ} = \frac{V_{IJ}^2}{2g} + h_{IJ} + Z_{oIJ} = H_J \tag{2.1.34}$$

where $F_+(V_{IJ},h_{IJ})$, a function of the velocity V_{IJ} (velocity at node IJ) and h_{IJ} (water depth at node IJ), is the positive wave boundary function; E_{IJ} is the energy line at node IJ, Z_{oIJ} is the bottom elevation at node IJ; and H_J is the water surface elevation of the junction J. The second equation of Eq. (2.1.34) is obtained from the assumption that the total energy is constant from the junction to the node IJ. In the case of critical flow, the positive wave is going out of the reach and there is no need of a boundary condition for this wave. The negative wave is immobile and its boundary condition is given by the condition of critical flow. The governing equations for node IJ under critical flow are given by

$$F_+\left(V_{IJ}, h_{IJ}\right) = 0 \qquad and \qquad \frac{Q_{IJ}^2 B_{IJ}}{g A_{IJ}^3} = 1 \tag{2.1.35}$$

where B_{IJ} is the top width of the cross-section of the I-th reach at node IJ and A_{IJ} is the cross-section area of the I-th reach at node IJ. In the case of supercritical flow, both positive and negative waves are going out of the reach, therefore no boundary conditions are needed and the governing equations for node IJ under supercritical flow are given by

$$F_+\left(V_{IJ}, h_{IJ}\right) = 0 \qquad and \qquad F_-\left(V_{IJ}, h_{IJ}\right) = 0 \tag{2.1.36}$$

where $F_-\left(V_{IJ}, h_{IJ}\right)$, a function of the velocity V_{IJ} and h_{IJ}, is the negative wave boundary function.

If IJ is an upstream point, we have also three cases to consider: subcritical, critical, and supercritical flows. For the case of subcritical flow, the positive wave is going into the reach and its boundary condition is obtained with the assumption that the specific energy is constant between the junction J and the node IJ. With this assumption, the governing equations for node IJ are given by

$$H_J = \frac{V_{IJ}^2}{2g} + h_{IJ} + Z_{oIJ} \qquad \text{and} \qquad F_{-}(V_{IJ}, h_{IJ}) = 0 \qquad \textbf{(2.1.37)}$$

In the case of critical flow, the positive wave is going into the reach from the junction and its boundary condition is obtained with the assumption of constant energy line between the junction and the node *IJ*, and the negative wave is immobile and its boundary condition is obtained from the condition of critical flow. The governing equations for node *IJ* under critical flow are given by

$$H_J = \frac{V_{IJ}^2}{2g} + h_{IJ} + Z_{oIJ} \qquad \text{and} \qquad \frac{Q_{IJ}^2 B_{IJ}}{g A_{IJ}^3} = 1 \qquad \textbf{(2.1.38)}$$

In the case of supercritical flow, both positive and negative waves are going into the region from the junction *J* to the reach *I*. Two boundary conditions are required for this case. One of the boundary conditions is obtained with the assumption of constant energy line between the junction *J* and the node *IJ*. The other boundary condition is obtained with the assumption that the supercritical flow at node *IJ* will become a critical flow in a very short distance (so short that it can be conceptually considered to locate at *IJ*). With these assumptions the governing equations for node *IJ* under supercritical flow is given by Eq. (2.1.38).

In summary, the governing equations at a natural internal boundary node of a reach connecting to junctions are given by one of Eq. (2.1.34) through (2.1.38) depending on whether the node IJ is a downstream or an upstream point and whether the flow is supercritical, critical, or subcritical.

Controlled internal boundary condition at control structures:

For any structure, *S* (which may be a weir, a gate, or a culvert), there are two river/stream/canal reaches connecting to the structure. The node *1S* located at the upstream of the structure is termed the controlled-internal boundary of the first reach while the Node *2S* located at the downstream of the structure is called the controlled-internal boundary of the second reach (Fig. 2.1-2). The specification of boundary conditions for the internal boundaries separated by a structure requires elaboration.

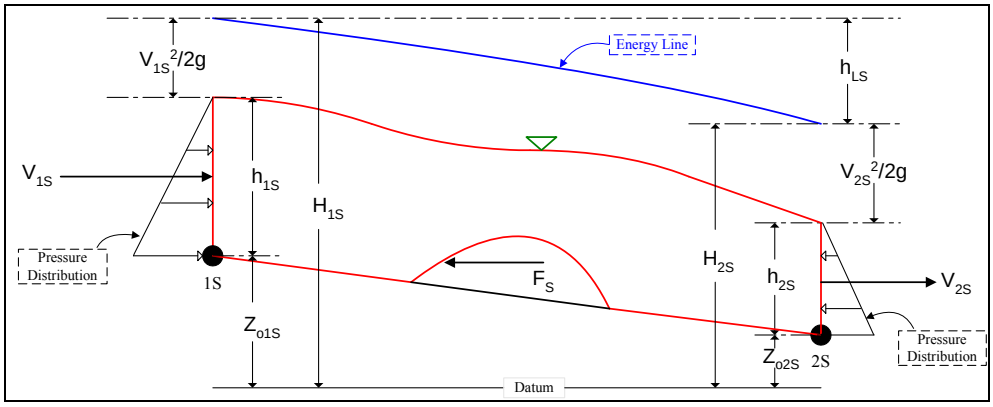

Fig. 2.1-2. The control volume (red outline) between Nodes 1S and 2S

The flow configuration around a structure and its surrounding reaches may be very dynamic under transient flows. Governing equations of flow at Nodes *1S* and *2S* depend on the changing dynamics of water stages around the structure. When both stages are below the height of the structure, the two reaches connecting the structure are decoupled. When at least one of the stages is above the structure, two reaches are either sequentially coupled or fully coupled via the structure. Here for sake of simplicity of discussions, we assume that the flow direction is from Reach *1* to Reach *2*. In other words, Reach *1* is an upstream reach and Reach *2* is a downstream reach. If the flow direction is reversed, we can have the boundary condition similarly prescribed.

There are five unknowns, V_{1S} (velocity of the upstream reach Node *1S*), h_{1S} (the water depth of the upstream Node *1S*), Q (the flow rate through the internal-boundary complex), V_{2S} (the velocity of the downstream reach Node *2S*), and h_{2S} (the water depth of the downstream Node *2S*); five equations must be set up for this internal-boundary complex consisting of a upstream reach node, a structure, and a downstream node. The governing equations for these five unknowns can be obtained depending on the flow conditions at the upstream and downstream reaches separated by the internal boundary structure. The flow condition can be supercritical, critical, or subcritical at Node *1S* and Node *2S*.

Node *1S* is a downstream point relative to the first reach or is the upstream point relative to the structure. The positive wave is transported out of *Reach 1* over the structure to *Reach 2*, and there is no need of a boundary condition for this wave. As for the negative wave, if the flow is supercritical, it is transported out of the reach, and there is no need to prescribe a boundary condition for this wave. Thus, the governing equations for Node *1S* under supercritical flow are given by

$$F_+(V_{1S}, h_{1S}) = 0, \qquad F_-(V_{1S}, h_{1S}) = 0, \qquad \textit{and} \quad Q = V_{1S} A_{1S} \tag{2.1.39}$$

where $F_+(V_{1S},h_{1S})$, a function of V_{1S} and h_{1S}, is the positive wave boundary function; and $F_-(V_{1S},h_{1S})$, a function of V_{1S} and h_{1S}, is the negative wave boundary function.

If the flow is critical, the negative wave is immobile and its governing equation must satisfy the condition of critical flow. Thus, the two governing equations for Node *1S* under critical flow are given by

$$F_+(V_{1S}, h_{1S}) = 0, \qquad \frac{Q^2 B_{1S}}{g A_{1S}^3} = 1, \qquad \textit{and} \quad Q = V_{1S} A_{1S} \tag{2.1.40}$$

where B_{1S} and A_{1S}, respectively, are the top width and the area, respectively, of the cross-section at Node *1S*.

If the flow is subcritical, the negative wave is transported into the reach from the downstream reach via the structure, and its boundary condition is obtained by equating the flow rates at Nodes *1S* and *2S*. Thus the governing equations for Node *1S* under subcritical flow are given by

$$F_+(V_{1S}, h_{1S}) = 0, \qquad V_{1S} A_{1S} = V_{2S} A_{2S}, \qquad \textit{and} \quad Q = V_{1S} A_{1S} \tag{2.1.41}$$

A comment is in order here. When the flow at Note *1S* is supercritical or critical, the flow in the

upstream reach is decouple from the flow in the downstream reach. Under such conditions, Eq. (2.1.39) or (2.1.40) is used to solve to the values of V_{1S} and h_{1S}, which then yield the flow rate Q, the energy level H_{1S} at Node *1S*, or the momentum-impulse M_{1S} at Node *1S*. These quantities (Q, H_{1S}, and M_{1S}) may serve as the boundary conditions for Node *2S*. As to which of these quantities is needed for the internal boundary Node *2S* depends on the flow condition at Node *2S*. This point will be taken up when the boundary conditions for Node *2S* are addressed. When the flow at Node *1S* is subcritical, then the flows in the upstream and downstream reaches are coupled via the second equation in Eq. (2.1.41).

On the other hand, Node *2S* is an upstream point relative to the second reach or a downstream point relative to the structure. If the flow is supercritical at Node *2S*, both the positive and the negative waves are coming into the reach from the upstream reach via the structure, and two boundary conditions are needed. These two boundary conditions can be obtained by the principle of mass continuity and the principle of momentum/impulse or the Bernoulli's equation between Nodes *1S* and *2S*. The structure between Nodes *1S* and *2S* will exert reaction force, F_S, on the fluid between two nodes or it induces energy loss, h_{LS}, between two nodes (Fig. 2.1-2). Thus, the governing equations for Node *2S* are

$$Q = V_{1S}A_{1S}, \qquad V_{2S}A_{2S} = V_{1S}A_{1S}, \qquad \textit{and} \qquad \begin{matrix} H_{2S} + h_{LS} = H_{1S} \\ \textit{or} \\ M_{2S} + F_S = M_{1S} \end{matrix} \tag{2.1.42}$$

where F_S is the force exerted by the structure on the fluid; h_{LS} is the energy loss between Nodes *1* and *2*; H_{2S} and H_{1S} (defined in Fig. 2.1-2), respectively, are the energy level at Nodes *2S* and *1S*, respectively; and M_{2S} ($=\rho V_{2S}A_{2S}V_{2S}+\rho g\, h_{2Sc}A_{2S}$) and M_{1S} ($=\rho V_{1S}A_{1S}V_{1S}+\rho g\, h_{1Sc}A_{1S}$), respectively, are the momentum-impulse at Nodes *2S* and *1S*, respectively (where ρ is the fluid density, g is the gravity constant, h_{2Sc} is the water depth to the centroid of the cross-sectional area at Node *2*, and h_{1Sc} is the water depth to the centroid of the cross-sectional area at Node *1*).

If the flow at Node *2S* is critical, one of the two boundary equations is obtained by the requirement of critical conditions while the other is obtained by the principle of mass continuity and the principle of momentum/impulse or the Bernoulli's equation between Nodes *1S* and *2S*. Thus, the governing conditions for Node *2S* are given as follows

$$\begin{matrix} \dfrac{Q^2 B_{2S}}{gA_{2S}^3} = 1, \qquad V_{2S}A_{2S} = V_{1S}A_{1S}, \qquad Q = V_{1S}A_{1S} \\ \textit{or} \\ \dfrac{Q^2 B_{2S}}{gA_{2S}^3} = 1, \qquad V_{2S}A_{2S} = V_{1S}A_{1S}, \qquad Q = V_{1S}A_{1S}, \quad \textit{and} \end{matrix} \qquad \begin{matrix} H_{2S} + h_{LS} = H_{1S} \\ \textit{or} \\ M_{2S} + F_{1S} = M_{1S} \end{matrix} \tag{2.1.43}$$

If the flow at Node *2S* is subcritical, the positive wave is transported into the reach from the upstream reach via the structure while the negative wave is transport out of the reach. The boundary condition for the positive wave is obtained by the principle of mass continuity and the principle of

momentum/impulse or the Bernoulli's equation between Nodes *1S* and *2S*. Thus the two governing equations for Node *2S* under subcritical flow are given as follows

$$F_{-}(V_{2S}, h_{2S}) = 0, \qquad V_{2S}A_{2S} = V_{1S}A_{1S}, \qquad Q = V_{1S}A_{1S}$$

or

$$F_{-}(V_{2S}, h_{2S}) = 0, \quad V_{2S}A_{2S} = V_{1S}A_{1S}, \quad Q = V_{1S}A_{1S}, \quad \textit{and} \quad \begin{matrix} H_{2S} + h_{LS} = H_{1S} \\ \textit{or} \\ M_{2S} + F_{1S} = M_{1S} \end{matrix} \qquad \textbf{(2.1.44)}$$

In summary, the governing equations for internal boundary nodes separated by a structure are given by any combination of Eq. (2.1.39), (2.1.40), or (2.1.41) and Eq. (2.1.42), (2.1.43), or (2.1.44). All combinations provide five governing equations for five unknowns (V_{1S}, h_{1S}, Q, V_{2S}, and h_{2S}), except for one combination.

The combination of Eq. (2.1.41) and Eq. (2.1.42) only generates four equations; one more equation is needed. This combination represents the situation that flow in the upstream reach is subcritical and in the downstream reach is supercritical. For this situation to occur, flow must under go a transitional state of critical flow over the structure, and the critical flow condition on the structure must be satisfied. Thus, the following additional governing equations can be set up by applying the principle of mass continuity and the principle of momentum-impulse or the Bernoulli equation to a control volume between Node 1S and the structure (Fig. 2.1-3) as

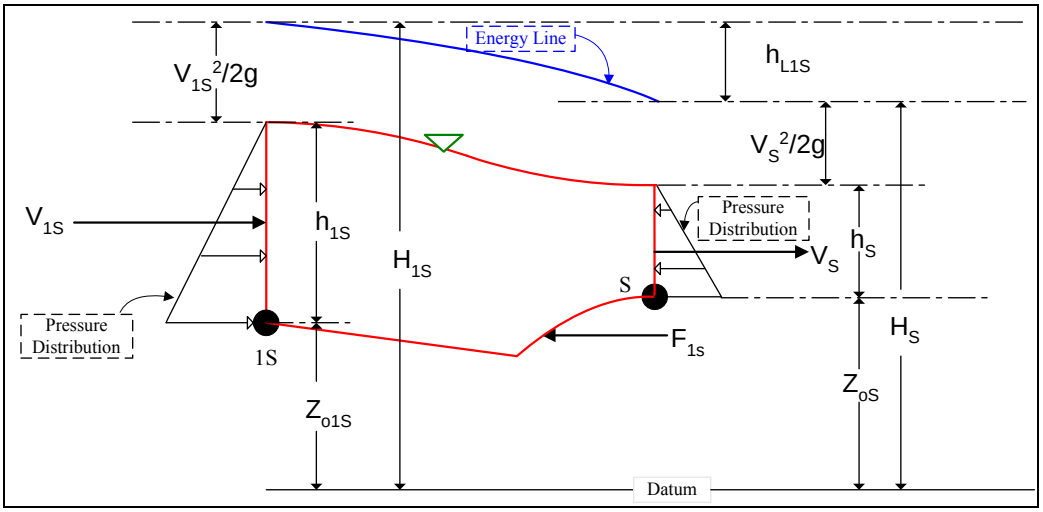

Fig. 2.1-3. The control volume (red outline) between Node 1S and structure.

$$\frac{Q^2 B_S}{gA_S^3} = 1, \qquad V_S A_S = V_{1S}A_{1S}, \qquad Q = V_{1S}A_{1S}, \quad \textit{and} \quad \begin{matrix} H_S + h_{L1S} = H_{1S} \\ \textit{or} \\ M_S + F_{1S} = M_{1S} \end{matrix} \qquad \textbf{(2.1.45)}$$

where A_S, B_S, and V_S, are the area, top width, and velocity of the cross-sectional area over the

structure; h_{L1S} is head loss between Node 1S and the structure; F_{1S} is the force the structure exerts on the fluid between Node 1S and the structure, H_S is the total head over the structure (Fig. 2.1-3); and M_S (= $\rho V_S A_S V_S$ + g $h_{Sc} A_S$) is the momentum-impulse at the structure (where h_{Sc} is the water depth to the centroid of the cross-sectional area at the structure). Now, Eq. (2.1.41), (2.1.42), and (2.1.45) give seven equations for seven unknowns (V_{1S}, h_{1S}, Q, V_{2S}, h_{2S}, V_S, and h_S).

The theoretical presentation about the governing equations for the internal-boundary complex is valid for any structure including weirs, gates, and culverts. The differences among various structures are characterized by the formulation of the head loss functions, $h_{LS}(Q, h_{1S}, h_{2S})$ and h_{L1S} (Q, h_{1S}, h_S), which depend on the flow rate Q and the water depth h_{1S}, and h_{2S}.

2.1.2 Diffusive Wave Approaches

In a diffusive approach, the inertia terms in the momentum equation is assumed negligible when compared with the other terms. By further assuming negligible eddy viscosity and $M_S = M_R = M_E = M_I = M_1 = M_2 = 0$, we approximate the river/stream/canal velocity with the following equation (Hergarten and Neugebauer, 1995).

$$V = \frac{-a}{n}\left[\frac{R}{1+\left(\frac{\partial Z_o}{\partial x}\right)^2}\right]^{2/3} \frac{1}{\sqrt{\left|-\frac{\partial H}{\partial x} - \frac{h}{c\rho}\frac{\partial \Delta\rho}{\partial x} + \frac{B\tau^S}{Ag\rho}\right|}}\left(\frac{\partial H}{\partial x} + \frac{h}{c\rho}\frac{\partial \Delta\rho}{\partial x} - \frac{B\tau^S}{Ag\rho}\right) \qquad \textbf{(2.1.46)}$$

where n is Manning's roughness [$tL^{-1/3}$], a is a unit-dependent factor ($a = 1$ for SI units and $a = 1.49$ for U.S. Customary units) to make the Manning's roughness unit-independent, R is the hydraulic radius [L], and $H = h + Z_o$ is the water stage.

Using the definition $Q = VA$ and substituting Eq. (2.1.46) into Eq. (2.1.1), we obtain

$$B\frac{\partial H}{\partial t} - \frac{\partial}{\partial x}\left(K\left[\frac{\partial H}{\partial x} + \frac{h}{c\rho}\frac{\partial \Delta\rho}{\partial x} - \frac{B\tau^S}{Ag\rho}\right]\right) = S_S + S_R - S_E + S_I + S_1 + S_2 \qquad \textbf{(2.1.47)}$$

in which

$$K = \frac{a\,A\,R^{2/3}}{n}\frac{1}{\left[1+\left(\frac{\partial Z_o}{\partial x}\right)^2\right]^{2/3}}\frac{1}{\sqrt{\left|-\frac{\partial H}{\partial x} - \frac{h}{c\rho}\frac{\partial \Delta\rho}{\partial x} + \frac{B\tau^S}{Ag\rho}\right|}} \qquad \textbf{(2.1.48)}$$

To achieve transient simulations, either water depth or stage must be given as the initial condition. In addition, appropriate boundary conditions need to be specified to match the corresponding physical system. In our model, four types of boundary conditions may be specified depending on physical configurations of the boundary. These boundary conditions are addressed below.

Dirichlet boundary condition: prescribed water depth or stage

On a Dirichlet boundary, either the water depth or stage can be prescribed as a function of time.

This boundary condition can be expressed as

$$h = h_d(t) \qquad or \qquad H = h + Z_o = H_d, \quad on \quad B_d \tag{2.1.49}$$

where $h_d(t)$ is a prescribed time-dependent water depth on the Dirichlet boundary [L], $H_d(t)$ is a prescribed time-dependent water stage [L], and B_d is the Dirichlet boundary point. A Dirichlet boundary point can locate at the upstream or down stream point, control structures, or even interior point.

Flux boundary condition: prescribed flow rate

On a flux boundary, a time-dependent flow rate is prescribed as a function of time as

$$-K\left(\frac{\partial H}{\partial x} + \frac{h}{c\rho}\frac{\partial \Delta\rho}{\partial x} - \frac{B\tau^S}{Ag\rho}\right) = Q_f(t) \quad on \quad B_f \tag{2.1.50}$$

where $Q_f(t)$ a prescribed time-dependent flow rate [L^3/t] and B_f is a flux boundary point. Mathematically, a flux boundary condition can be applied to an upstream or downstream point. However, in practice, it is often applied to an upstream boundary point.

Water depth-dependent boundary condition: prescribed rating curve

This condition is often used to describe the flow rate at a downstream river/stream boundary at which the flow rate is a function of water depth. It can be written as

$$-K\left(\frac{\partial H}{\partial x} + \frac{h}{c\rho}\frac{\partial \Delta\rho}{\partial x} - \frac{B\tau^S}{Ag\rho}\right) = Q_r(h(x_r, t)) \quad on \quad B_r \tag{2.1.51}$$

where $Q_r(h(x_r,t))$ is a water depth-dependent flow rate [L^3/t], x_r is the x-coordinate on the boundary B_r, and B_r is a boundary point on which the prescribed rating curve is applied.

Junction boundary condition:

This condition is applied to a boundary of a river/stream/canal reach that is connected to a junction (Fig. 2.1-1). For the junction complex consisting of N_J river/stream/canal reaches (e.g., in Fig. 2.1-1, $N_J = 3$) and one junction (say J), we have ($N_J + 1$) unknowns, which are flow rates, Q_{IJ} (Q_{IJ} is the flow rate from the I-th reach to junction J), and water stage at junction J, H_J. Therefore, we need to set up ($N_J + 1$) equations. The first equation is obtained by applying the continuity of mass at the junction to result in Eq. (2.1.35) for the case when the storage effect of the junction must be accounted for or Eq. (2.1.36) when this effect is negligible. The other N_J equations can be obtained by assuming the energy loss from any reach to the junction is negligible to result in

$$\frac{1}{2g}\left(\frac{Q_{IJ}}{A_{IJ}}\right)^2 + H_{IJ} = H_J, \quad I \in N_J \quad where \quad Q_{IJ} = -K\left(\frac{\partial H}{\partial x} + \frac{h}{c\rho}\frac{\partial \Delta\rho}{\partial x} - \frac{B\tau^S}{Ag\rho}\right)\Bigg|_{IJ} \tag{2.1.52}$$

where H_{IJ} is the water stage the internal boundary Node IJ of the I-th reach connecting to junction J.

Equations (2.1.32) or (2.1.33) along with Eq. (2.1.52) provide ($N_J + 1$) equations to solve for ($N_J + 1$) unknowns.

Weir boundary condition:

For any weir (*W*), there are two river/stream/canal reaches connecting to it. Node *1W* located just upstream of the weir is termed the controlled-internal boundary of the upstream reach while Node *2W* located just downstream of the weir is called the controlled-internal boundary of the downstream reach (Figure 2.1-4). The specification of boundary conditions for the internal boundaries for the diffusive wave approach is given as

$$-\mathbf{n}\cdot\mathrm{K}\left(\nabla H+\frac{h}{c\rho}\nabla(\Delta\rho)-\frac{B\tau^{S}}{Ag\rho}\right)\Big|_{1\mathrm{W}}=Q_{W}\left(h_{up},h_{dn}\right)\qquad \textit{and}$$
$$-\mathbf{n}\cdot\mathrm{K}\left(\nabla H+\frac{h}{c\rho}\nabla(\Delta\rho)-\frac{B\tau^{S}}{Ag\rho}\right)=Q_{W}\left(h_{up},h_{dn}\right) \qquad \textbf{(2.1.53)}$$

where Q_w is the weir discharge rate, which is a given function of the water depths h_{up} at Node *1W* and h_{dn} at Node *2W* (Fig. 2.1-5).

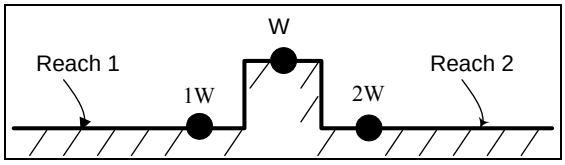

Fig. 2.1-4. Schematic of weir.

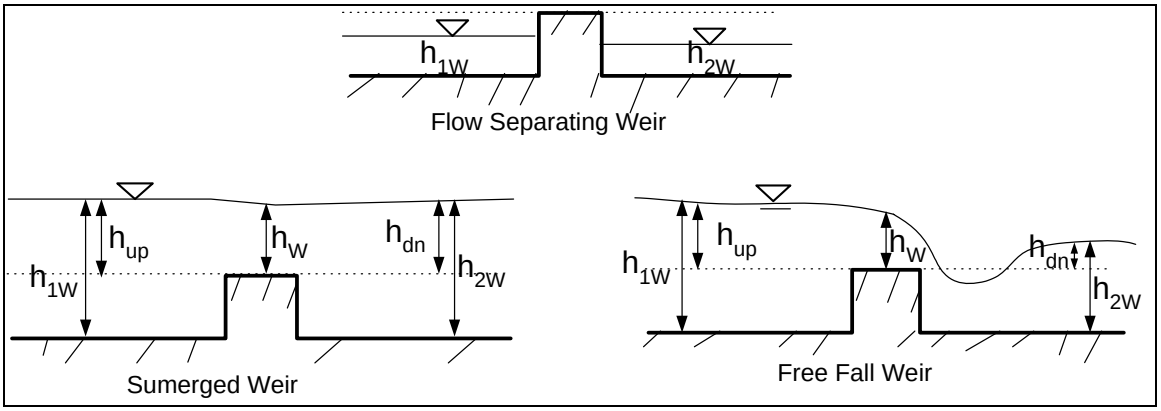

Fig. 2.1-5. Flow configurations around a weir.

The flow configuration around the weir and its surrounding reaches may be very dynamic under transient flows. Both of the water stages at Nodes *1W* and *2W* may be below the weir, both may be above the weir, or one below the weir while the other is above the weir (Fig. 2.1-5). When both stages are below the height of the weir, the two reaches connecting the weir are decoupled. When at least one of the stages is above the weir, two reaches are coupled via the weir. The weir discharge, Q_w, can be obtained by solving the continuity equation and the Bernoulli equation between Nodes *1W* and *2W*. The weir formulae under various stage conditions are given as

(1) For submerged flow

$$Q_W = C_W h_{dn} L_W \sqrt{2g\left(h_{up} - h_{dn}\right)} \quad if \quad h_{dn} \geq \frac{2}{3} h_{up} \quad and \quad h_{dn} < h_{up} \tag{2.1.54}$$

(2) For free fall flow

$$Q_W = \frac{2}{3\sqrt{3}} C_W h_{up} L \sqrt{2g h_{up}} \quad if \quad h_{dn} < \frac{2}{3} h_{up} \tag{2.1.55}$$

(3) For decoupled flow

$$Q_W = 0 \tag{2.1.56}$$

where C_w is the weir coefficient and L_w is the weir length. It should be noted that the above formulae are valid for broad weir. For other types of weirs, different weir discharge formulae may be used and they can easily be incorporated into the computer code.

Gate boundary condition:

For any gate (G), there are two river/stream/canal reaches connecting to it. Node *1G* located just upstream of the gate G is termed the controlled-internal boundary of the upstream reach while Node *2G* located just downstream of the gate G is called the controlled-internal boundary of the downstream reach (Fig. 2.1-6). The specification of boundary conditions for the internal boundaries separated by a gate can be made similar to that of a weir as follows.

$$\begin{aligned} -\mathbf{n}\cdot\mathbf{K}\left(\nabla H + \frac{h}{c\rho}\nabla(\Delta\rho) - \frac{B\tau^S}{Ag\rho}\right)\Big|_{1G} &= Q_g\left(h_{up}, h_{dn}\right) \quad and \\ -\mathbf{n}\cdot\mathbf{K}\left(\nabla H + \frac{h}{c\rho}\nabla(\Delta\rho) - \frac{B\tau^S}{Ag\rho}\right)\Big|_{2G} &= Q_g\left(h_{up}, h_{dn}\right) \end{aligned} \tag{2.1.57}$$

where Q_g is the gate discharge rate, which is a given function of the water depths h_{up} at *1G* and h_{dn} at *2G* (Fig. 2.1-7).

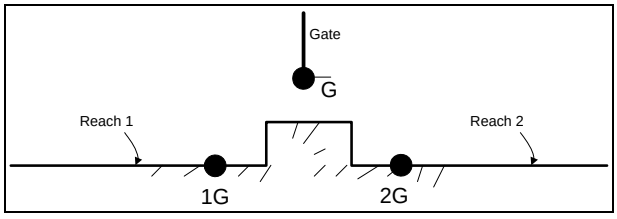

Fig. 2.1-6. Schematic of Gate.

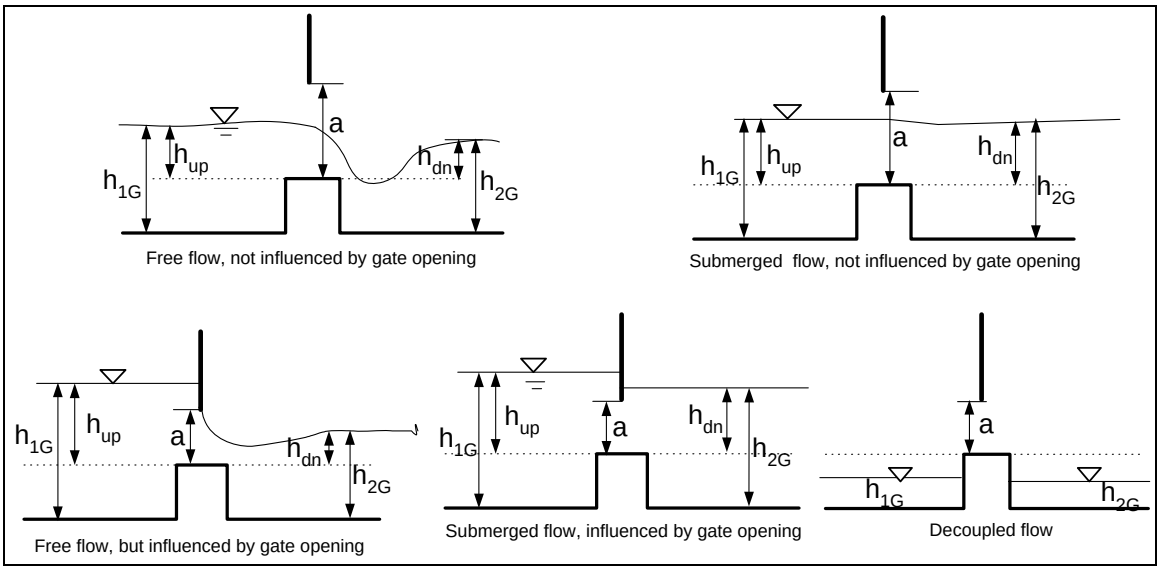

Fig. 2.1-7. Flow configurations around a gate.

The flow configuration around the gate and its surrounding reaches may be very dynamic under transient flows. Depending on the water stages at Nodes *1G* and *2G* (H_{1G} and H_{2G}), we have several configurations (Fig. 2.1-7). The gate discharge, Q_g, can be obtained by solving the continuity equation and the Bernoulli equation between Nodes *1G* and *2G*. The gate formulae under various stage conditions are given as

(1) For free fall flow and not influenced by the gate opening

$$Q_g = \frac{2}{3\sqrt{3}} C_g h_{up} L_g \sqrt{2gh_{up}} \quad if \quad h_{dn} < \frac{2}{3} h_{up} \quad and \quad a > \frac{2}{3} h_{up} \tag{2.1.58}$$

(2) For submerged flow and not influenced by the gate opening

$$Q_g = C_g h_{dn} L_g \sqrt{2g\left(h_{up} - h_{dn}\right)} \quad if \quad h_{dn} \geq \frac{2}{3} h_{up}, h_{dn} < h_{up}, \quad and \quad a > \frac{2}{3} h_{up} \tag{2.1.59}$$

(3) For free flow and influenced by the gate opening

$$Q_g = \frac{2}{3\sqrt{3}} C_g a L_g \sqrt{2gh_{up}} \quad if \quad h_{dn} < \frac{2}{3} h_{up} \quad and \quad a < \frac{2}{3} h_{up} \tag{2.1.60}$$

(4) For submerged flow and influenced by the gate opening

$$Q_g = C_g a L_g \sqrt{2g\left(h_{up} - h_{dn}\right)} \quad if \quad h_{dn} \geq \frac{2}{3} h_{up}, h_{dn} < h_{up}, \quad and \quad a < \frac{2}{3} h_{up} \tag{2.1.61}$$

(5) For decoupled flow

$$Q_g = 0 \tag{2.1.62}$$

where C_g is the gate coefficient, a is the gate opening, and L_g is the weir length.

Culvert boundary condition:

Similar to weirs and gates, the boundary conditions for the culvert can be stated as

$$\begin{aligned} -\mathbf{n}\cdot\mathbf{K}\left(\nabla H+\frac{h}{c\rho}\nabla(\Delta\rho)-\frac{B\tau^S}{Ag\rho}\right)\Big|_{1C}&=Q_C\left(h_{up},h_{dn}\right)\quad and\\ -\mathbf{n}\cdot\mathbf{K}\left(\nabla H+\frac{h}{c\rho}\nabla(\Delta\rho)-\frac{B\tau^S}{Ag\rho}\right)\Big|_{2C}&=Q_C\left(h_{up},h_{dn}\right)\end{aligned} \tag{2.1.63}$$

where Q_c is the discharge through the culvert or culverts, Node *1C* is the point upstream of the culvert and *2C* is the point downstream of the culvert, h_{up} is the water stage above the culvert at Node *1C*, and h_{dn} is the water stage above the culvert at Node *2C*. A wide range of culvert discharge formulae can be used and they can be easily incorporated in the computer code.

2.1.3 Kinematic Wave Approaches

In a kinematic approach, all the assumptions for the diffusive approach are hold. However, the velocity is given by modifying Eq. (2.1.46) with $\partial Z_o/\partial x$ replacing $\partial H/\partial x$ as follows

$$V=\frac{-a}{n}\left[\frac{R}{1+\left(\frac{\partial Z_0}{\partial x}\right)^2}\right]^{2/3}\frac{1}{\sqrt{\left|-\frac{\partial Z_o}{\partial x}-\frac{h}{c\rho}\frac{\partial\Delta\rho}{\partial x}+\frac{B\tau^S}{Ag\rho}\right|}}\left(\frac{\partial Z_o}{\partial x}+\frac{h}{c\rho}\frac{\partial\Delta\rho}{\partial x}-\frac{B\tau^S}{Ag\rho}\right) \tag{2.1.64}$$

Substituting Eq. (2.1.64) into Eq. (2.1.1) and using the definition $Q = VA$, we obtain

$$\frac{\partial A}{\partial t}+\frac{\partial VA}{\partial x}=S_S+S_R-S_E+S_I+S_1+S_2 \tag{2.1.65}$$

It is noted that Eq. (2.1.65) represents the advective transport of the cross-sectional area, A. It is an ideal equation amenable for numerically innovative advective transport algorithm.

To achieve transient simulations, either water depth or stage must be given as the initial condition. In addition, appropriate boundary conditions need to be specified to match the corresponding physical configuration. In a kinematic wave approach, boundary conditions are required only at upstream boundaries. An upstream boundary point can be an open boundary or a closed boundary. On an open upstream boundary, either the cross-sectional area (equivalent to water depth or water stage) or the flow rate can be specified as

$$A=A_{up}\quad or\quad \mathbf{n}\cdot\mathrm{VA}=\mathrm{Q_{up}}\quad on\quad B_{up} \tag{2.1.66}$$

where H_{up} is the water stage of the incoming upstream flow, Q_{up} is the flow rate of the incoming

upstream flow, and B_{up} is the open upstream boundary point. The flow rate through a closed upstream boundary point is by default equal to zero.

2.1.4 Thermal Transport

The thermal transport equation is derived based on the conservation principle of energy as:

$$\frac{\partial(\rho_W C_W AT)}{\partial t}+\frac{\partial(\rho_W C_W QT)}{\partial x}-\frac{\partial}{\partial x}\left(D^H A\frac{\partial T}{\partial x}\right) = S_h^a + S_h^r + S_h^n - S_h^b - S_h^e - S_h^s + S_h^i + S_h^{o1} + S_h^{o2} + S_h^c \quad \textbf{(2.1.67)}$$

where ρ_w is the water density [M/L^3]; C_w is the heat capacity of water [L^2/t^2/T]; T is the temperature [T]; D^H is the apparent thermal conductivity including the effect of dispersion, diffusion, and conduction [E/t/L/T = ML/t^3/T, where E is the unit of energy]; S_h^a is the heat source due to artificial injection/withdraw including rainfall [E/t/L = ML/t^3]; S_h^r is the heat source due to rainfall [E/t/L=ML/t^3]; S_h^n is the heat source due to net radiation [E/t/L = ML/t^3]; S_h^b is the heat sink due to back radiation from water surface to the atmosphere [E/t/L = ML/t^3]; S_h^e is the heat sink due to evaporation [E/t/L = ML/t^3]; S_h^s is the heat sink due to sensible heat flux [E/t/L = ML/t^3]; S_h^i is the heat source due to exfiltration from subsurface [E/t/L = ML/t^3]; S_h^{o1} is the heat source from overland flow via Bank *1* [E/t/L = ML/t^3]; S_h^{o2} is the heat source from overland flow via Bank *2* [E/t/L = ML/t^3]; and S_h^c is the heat source due to chemical reaction [E/t/L = ML/t^3]. In Eq. (2.1.67), S_h^r, S_h^i, S_h^{o1}, and S_h^{o2} are given by

$$S_h^r = C_W \rho_W S_R T^r; \qquad S_h^i = \begin{cases} C_W \rho_W S_I T^i & if \quad S_I \geq 0 \\ C_W \rho_W S_I T & if \quad S_I < 0 \end{cases} \quad \textbf{(2.1.68)}$$

and

$$S_h^{o1} = \begin{cases} C_W \rho_W S_1 T^{o1} & if \quad S_1 \geq 0 \\ C_W \rho_W S_1 T & if \quad S_1 < 0 \end{cases}; \qquad S_h^{o2} = \begin{cases} C_W \rho_W S_2 T^{o2} & if \quad S_2 \geq 0 \\ C_W \rho_W S_2 T & if \quad S_2 < 0 \end{cases} \quad \textbf{(2.1.69)}$$

where T^r is the temperature of the rainwater [T], T^i is the temperature of the exfiltration water from the subsurface flow [T], T^{o1} is the temperature of the water from overland flow via river Bank *1* [T], and T^{o2} is the temperature of the water from overland flow via river Bank *2* [T].

The heat source due to net radiation, S_h^n, heat sink due to back radiation, S_h^b, heat sink due to evaporation, S_h^e, and heat sink due to sensible heat, S_h^s, are given by their respective heat fluxes as follows

$$S_h^n = BH_n; \quad S_h^b = BH_b; \quad S_h^e = BH_e; \quad S_h^s = BH_s \quad \textbf{(2.1.70)}$$

where H_n, H_b, H_e, and H_s are the net radiation flux, back radiation flux, latent heat flux, and sensible heat flux, respectively. These fluxes depend on only meteorological condition and water temperature. They may be computed from follow equations (Yeh, 1969; Yeh et al., 1973; McCuen, 1989; Song and Li. 2000; and Jennifer et al., 2002).

Net radiation H_n

$$H_n = (1 - a_s)H_{so} + (1 - a_\ell)H_{\ell o} \qquad \textbf{(2.1.71)}$$

in which

$$H_{so} = H_o \cdot (0.61s + 0.35) \quad Btu / ft^2 / day \qquad \textbf{(2.1.72)}$$

and

$$H_{\ell o} = \varepsilon\sigma(T_a + 460)^4 \left[C + 0.031(e_a)^{1/2}\right] \qquad Btu / ft^2 / day \qquad \textbf{(2.1.73)}$$

where a_s and a_ℓ are the albedos of the water surface for short- and long-wave radiation respectively; H_{so} and $H_{\ell o}$ are the solar short- and long-wave radiation respectively; H_o is the solar constant, s is the percentage of possible sunshine; ε **= 0.97** is emissivity of water surface**;** $\sigma = 4.15 \times 10^{-8}$ Btu/ft^2/day/R^4 is the Stenfan-Boltzmann constant; T_a is air temperature in ^oF; C is the brunt coefficient; and e_a is the air vapor pressure in millimeter of mercury.

Back radiation H_b

$$H_b = \varepsilon\sigma(T_a + 460)^4 \quad Btu / ft^2 / day \qquad \textbf{(2.1.74)}$$

Sensible heat flux H_s

$$H_s = 0.26(73 + 7.3W)(T - T_a) \cdot (p / 760) \quad Btu / ft^2 / day \qquad \textbf{(2.1.75)}$$

where W is the wind speed in miles per hour and p is the atmospheric pressure in millimeter of mercury.

Latent heat flux of evaporation H_e

$$H_e = 0.26(73 + 7.3W)(e_w - e_a) \quad Btu / ft^2 / day \qquad \textbf{(2.1.76)}$$

where e_w is the saturated vapor pressure in millimeter of mercury at the water temperature T.

In addition to the initial boundary condition, boundary conditions must be specified for the temperature. Four types of global boundary conditions are provided in this report as follows.

Dirichlet boundary condition:

This condition is applied when the temperature is prescribed as a function of time on the boundaries:

$$T = T_{db}(x_b, t) \quad on \quad B_d \qquad \textbf{(2.1.77)}$$

where $T_{db}(x_b,t)$ is a time-dependent temperature on the Dirichlet boundary B_d [T].

Variable boundary condition:

This boundary condition is employed when the flow direction would change with time during simulations. Two cases are considered, regarding to the flow direction on the boundary.

< Case 1 > Flow is coming in from outside:

$$\rho_w C_w Q T - D^H A \frac{\partial T}{\partial x} = \rho_w C_w Q T_{vb}(x_b, t) \quad on \quad B_v \tag{2.1.78}$$

< Case 2 > Flow is going out from inside:

$$- D^H A \frac{\partial T}{\partial x} = 0 \quad on \quad B_v \tag{2.1.79}$$

where $T_{vb}(x_b,t)$ is a time-dependent temperature [T] through the variable boundary B_v, which is associated with the incoming flow.

Cauchy boundary condition:

This boundary condition is employed when the total heat-flow rate is given at the river/stream boundary. Usually, this boundary is an upstream boundary node. The conditions can be expressed as

$$\rho_w C_w Q T - D^H A \frac{\partial T}{\partial x} = \Phi_{cb}(x_b, t) \tag{2.1.80}$$

where $\Phi_{cb}(x_b,t)$ is total heat-flow rate (E/t = ML^2/t^3, where E denotes the unit of energy) through the Cauchy boundary, which takes a positive value if it is going out of the region and a negative value if it is coming into the region.

Neumann boundary condition:

This boundary condition is used when the conductive heat-flow rate is known at the river/stream boundary node. It can be written as

$$- D^H A \frac{\partial T}{\partial x} = \Phi_{nb}(x_b, t) \tag{2.1.81}$$

where $\Phi_{nb}(x_b,t)$ is the heat flux through the Neumann boundary.

In addition to the above four types of global boundary conditions, two types of internal boundary conditions are implemented: internal boundary nodes connecting to natural junctions and two internal boundary nodes for every control structures. These internal boundary conditions are mathematically stated similar to fluid flow of diffusive wave approaches.

Internal boundary condition at junctions:

If Node *IJ* is the internal node from Reach *I* connecting to Junction *J* (Fig. 2.1-1), the boundary conditions at Node *IJ* is given as

$$\left(\rho_w C_w QT - D^H A\frac{\partial T}{\partial x}\right)\Big|_{IJ} = \rho_w C_w \frac{1}{2} Q_{IJ}\left[(1+sign(Q_{IJ}))T_{IJ} + (1-sign(Q_{IJ}))T_J\right] \qquad \textbf{(2.1.82)}$$

where $sign(Q_{IJ})$ is equal 1.0 if the flow is from Reach I into Junction J, -1.0 if flow is from Junction J into Reach I; T_{IJ} is the temperature at Node IJ; and T_J is the temperature at Junction J which is given by

$$\sum_i \rho_w C_w \frac{1}{2} Q_{iJ}\left[(1+sign(Q_{iJ}))T_{iJ} + (1-sign(Q_{ij}))T_J\right] = 0 \qquad \textbf{(2.1.83)}$$

if the storage effect of Junction J is negligible or

$$\frac{d(\rho_w C_w V_J T_J)}{dt} = \sum_i \rho_w C_w \frac{1}{2} Q_{iJ}\left[(1+sign(Q_{iJ}))T_{iJ} + (1-sign(Q_{iJ}))T_J\right] \qquad \textbf{(2.1.84)}$$

if the storage effect of Junction J is significant.

Internal boundary condition at control structure:

If Nodes *1S* and *2S* are two internal boundary nodes connecting to Structure S (Fig. 2.1-2), the boundary conditions at Nodes *1S* and *2S* are given

$$\begin{aligned}\left(\rho_w C_w QT - D^H A\frac{\partial T}{\partial x}\right)\Big|_{1S} &= \left(\rho_w C_w QT - D^H A\frac{\partial T}{\partial x}\right)\Big|_{2S} \\ &= \rho_w C_w \frac{1}{2} Q_S\left[(1+sign(Q_S))T_{1S} + (1-sign(Q_S))T_{2S}\right]\end{aligned} \qquad \textbf{(2.1.85)}$$

where $sign(Q)$ is equal 1.0 if the flow is from Node *1S* to Node *2S*, -1.0 if flow is from Node *2S* to Node *1S*; T_{1S} is the temperature at Node *1S*; and T_{2S} is the temperature at Node *2S*.

2.1.5 Salinity Transport

$$\frac{\partial(AS)}{\partial t} + \frac{\partial(QS)}{\partial x} - \frac{\partial}{\partial x}\left(D^S A\frac{\partial S}{\partial x}\right) = M_s^{\,a} + M_s^{\,r} - M_s^{\,e} + M_s^{\,i} + M_s^{\,ol} + M_s^{\,o2} \qquad \textbf{(2.1.86)}$$

where S is the salinity [M/L^3]; D^S is the longitudinal dispersion coefficient for salinity [L^2/t]; $M_s^{\,a}$ is the artificial source of the salt [M/t/L]; $M_s^{\,r}$ is the salt source from rainfall [M/t/L]; $M_s^{\,e}$ is the salt sink from evaporation, which most likely would be zero [M/t/L]; $M_s^{\,i}$ is the salt source from subsurface [M/t/L]; $M_s^{\,o1}$ is the salt source from overland via River Bank *1* [M/t/L]; and $M_s^{\,o2}$ is the salt source from overland source viz River Bank *2* [M/L/t]. In Eq. (2.1.86), $M_s^{\,e}$ is likely to be zero and $M_s^{\,r}$, $M_s^{\,i}$, $M_s^{\,o1}$, and $M_s^{\,o2}$ are given by

$$M_s^{\,r} = S_R S^r; \qquad M_s^{\,i} = \begin{cases} S_I S^i & if \quad S_I \ge 0 \\ S_I S & if \quad S_I < 0 \end{cases} \qquad \textbf{(2.1.87)}$$

and

$$M_s^{ol} = \begin{cases} S_1 S^{ol} & if \quad S_1 \geq 0 \\ S_1 S & if \quad S_1 < 0 \end{cases}; \qquad M_s^{o2} = \begin{cases} S_2 S^{o2} & if \quad S_2 \geq 0 \\ S_2 S & if \quad S_2 < 0 \end{cases} \tag{2.1.88}$$

where S^r is the salinity of the rainwater [M/L^3], S^i is the salinity of the exfiltration water from the subsurface flow [M/L^3], S^{o1} is the salinity of the water from overland flow via River Bank *1* [M/L^3], and S^{o2} is the salinity of the water from overland flow via River Bank *2* [M/L^3].

As in thermal transport, four types of global boundary conditions for salinity transport are provided in this report as follows:

Dirichlet boundary condition:

This condition is applied when the salinity is prescribed as a function of time on the boundaries:

$$S = S_{db}\left(x_b, t\right) \tag{2.1.89}$$

where $S_{db}\left(x_b, t\right)$ is a time-dependent salinity on the Dirichlet boundary [M/L^3].

Variable boundary condition:

This boundary condition is employed when the flow direction would change with time during simulations. Two cases are considered, regarding to the flow direction on the boundary.

< Case 1 > Flow is coming in from outside:

$$QS - D^S A \frac{\partial S}{\partial x} = QS_{vb}\left(x_b, t\right) \tag{2.1.90}$$

< Case 2 > Flow is going out from inside:

$$-D^S A \frac{\partial S\left(x_b, t\right)}{\partial x} = 0 \tag{2.1.91}$$

where $S_{vb}\left(x_b, t\right)$ is a time-dependent salinity on the variable boundary [M/L^3], which is associated with the incoming flow.

Cauchy boundary condition:

This boundary condition is employed when the total salt-flow rate is given at the river/stream boundary. Usually, this boundary is an upstream boundary node. The conditions are expressed as

$$QS - D^S A \frac{\partial S}{\partial x} = \Phi_{cb}\left(x_b, t\right) \tag{2.1.92}$$

where $\Phi_{cb}\left(x_b, t\right)$ is total salt-flow rate on the Cauchy boundary [M/t], which takes a positive value if it is going out of the region and a negative value if it is coming into the region.

Neumann boundary condition:

This boundary condition is used when the dispersive salt-flow rate is known at the river/stream boundary node. It can be written as

$$-D^S A\frac{\partial S}{\partial x} = \Phi_{nb}\left(x_b, t\right) \tag{2.1.93}$$

where $\Phi_{nb}\left(x_b, t\right)$ is the salt rate due to salt concentration through the Neumann boundary [M/L].

The internal boundary conditions at junctions and control structures for salinity transport are stated similarly to those for thermal transport as follows.

Internal boundary condition at junctions:

If Node *IJ* is the internal node from Reach *I* connecting to Junction *J* (Fig. 2.1-1), the boundary condition at Node *IJ* is given as

$$\left(QS - D^S A\frac{\partial S}{\partial x}\right)\Big|_{IJ} = \frac{1}{2}Q_{IJ}\left[\left(1+sign\left(Q_{IJ}\right)\right)S_{IJ} + \left(1-sign\left(Q_{IJ}\right)\right)S_J\right] \tag{2.1.94}$$

where S_{IJ} is the salinity at Node *IJ* and S_J is the salinity at Junction *J*, which is governed by

$$\sum_i \frac{1}{2}Q_{IJ}\left[\left(1+sign\left(Q_{iJ}\right)\right)S_{iJ} + \left(1-sign\left(Q_{iJ}\right)\right)S_J\right] = 0 \tag{2.1.95}$$

if the storage effect of Junction *J* is negligible or

$$\frac{d\left(V_J S_J\right)}{dt} = \sum_i \frac{1}{2}Q_{iJ}\left[\left(1+sign\left(Q_{iJ}\right)\right)S_{iJ} + \left(1-sign\left(Q_{iJ}\right)\right)S_J\right] \tag{2.1.96}$$

if the storage effect of Junction *J* is significant.

Internal boundary condition at control structure:

If Nodes *1S* and *2S* are two internal boundary nodes connecting to Structure *S* (Fig. 2.1-2), the boundary conditions at nodes 1S and 2S are given

$$\left(QS - D^S A\frac{\partial S}{\partial x}\right)\Big|_{1S} = \left(QS - D^S A\frac{\partial S}{\partial x}\right)\Big|_{2S} = \frac{1}{2}Q_S\left[\left(1+sign\left(Q_S\right)\right)S_{1S} + \left(1-sign\left(Q_S\right)\right)S_{2S}\right] \tag{2.1.97}$$

where S_{1S} is the salinity at Node *1S* and S_{2S} is the salinity at Node *2S*.

2.2 Water Flow in Two-Dimensional Overland Regime

The governing equations for two-dimensional overland flow can be derived based on the conservation law of water mass and linear momentum [Wang and Connor, 1975]. The governing equations of a dynamic wave model in conservative form can be written as follows.

The continuity equation:

$$\frac{\partial h}{\partial t}+\frac{\partial (uh)}{\partial x}+\frac{\partial (vh)}{\partial y}=S+R-E+I \qquad \textbf{(2.2.1)}$$

where h is the water depth [L]; u is the velocity component in the x-direction [L/t]; v is the velocity component in the y-velocity [L/t]; S_S is the man-induced source [$L^3/t/L^2$]; S_R is the source due to rainfall [$L^3/t/L^2$]; S_E is the sink due to evapotranspiration [$L^3/t/L^2$]; and S_I is the source from subsurface media due to exfiltration [L/t]. It should be noted that $uh = q_x$ is the flux the x-direction [$L^3/t/L^2$] and $vh = q_y$ is the flux in the y-direction [$L^3/t/L^2$].

The x-momentum equation:

$$\frac{\partial (uh)}{\partial t}+\frac{\partial u(uh)}{\partial x}+\frac{\partial v(uh)}{\partial y}=-gh\frac{\partial (Z_o+h)}{\partial x}-\frac{gh^2}{2\rho}\frac{\partial \Delta\rho}{\partial x}-\frac{\partial F_{xx}}{\partial x}-\frac{\partial F_{yx}}{\partial y}+$$
$$\left(M_X{}^S+M_X{}^R-M_X{}^E+M_X{}^I\right)+\frac{\tau_x^s-\tau_x^b}{\rho} \qquad \textbf{(2.2.2)}$$

where Z_o is the bottom elevation of overland [L];]; $\Delta\rho = \rho - \rho_o$ is the density deviation [M/L^3] from the reference density (ρ_o), which is a function of temperature and salinity as well as other chemical concentrations; $M_X{}^S$ is the x-component of momentum-impulse from artificial sources/sinks [L^2/t^2]; $M_X{}^R$ is the x-component of momentum-impulse gained from rainfall [L^2/t^2]; $M_X{}^E$ is the x-component of momentum-impulse lost to evapotranspiration [L^2/t^2]; $M_X{}^I$ is the x-component of momentum-impulse gained from the subsurface media due to exfiltration [L^2/t^2]; F_{xx} and F_{yx} are the water fluxes due to eddy viscosity along the x-direction [L^3/t^2]; τ_x^s is the component of surface shear stress along the x-direction over unit horizontal overland area [$M/L/t^2$]; τ_x^b is the component of bottom shear stress along the x-direction over unit horizontal overland area [$M/L/t^2$], which can be assumed proportional to the x-component flow rate, i.e., $\tau_x^b/\rho = \kappa|\mathbf{V}|u$.

The y-momentum equation:

$$\frac{\partial (vh)}{\partial t}+\frac{\partial u(vh)}{\partial y}+\frac{\partial v(vh)}{\partial y}=-gh\frac{\partial (Z_o+h)}{\partial y}-gh\frac{gh^2}{2\rho}\frac{\partial \Delta\rho}{\partial y}-\frac{\partial F_{xy}}{\partial x}-\frac{\partial F_{yy}}{\partial y}+$$
$$\left(M_y{}^S+M_y{}^R-M_y^E+M_y{}^I\right)+\frac{\tau_y^s-\tau_y^b}{\rho} \qquad \textbf{(2.2.3)}$$

where M_y^S is the y-component of momentum-impulse from artificial sources/sinks [L^2/t^2]; M_y^R is the y-component of momentum-impulse gained from rainfall [L^2/t^2]; M_y^E is the y-component of momentum-impulse lost to evapotranspiration L^2/t^2]; M_y^I is the y-component of momentum-impulse gained from the subsurface media due to exfiltration [L^2/t^2]; F_{xy} and F_{yy} are the water fluxes due to eddy viscosity along the y-direction [L^3/t^2]; τ_y^s is the component of surface shear stress along the y-direction over unit horizontal overland area [M/L/t^2]; τ_y^b is the component of bottom shear stress along the y-direction over unit horizontal overland area [M/L/t^2], which can be assumed proportional to the y-component flow rate, i.e., $\tau_y^b/\rho = \kappa|\mathbf{V}|v$.

2.2.1 Fully Dynamic Wave Approaches

Eqs. (2.2.1) through (2.1.3) written in conservative form are the governing equations for two-dimensional flow in overland. Depending on the simplification of the momentum equation, one can have three approaches: fully dynamic wave, diffusive wave, and kinematic wave. For the fully dynamic wave approach, all terms in Eqs. (2.2.1) and (2.2.3) are retained. Under such circumstances, the conservative form of the governing equations may be used or they may be cast in the advection form or in the characteristic form. In this report, while the conservative form of fully dynamic wave equation is used as an option, the characteristic form of the fully dynamic approach will be used as a primary option. The characteristic form is the most natural way to deal with hyperbolic-dominant equations and amenable to the advective numerical methods, for example the upstream approximation or the Lagrangian-Eulerian method.

With an adequate mathematical manipulation, Eqs. (2.2.1) through (2.2.3) can be written in advective form as follows

$$\frac{\partial h}{\partial t} + u\frac{\partial h}{\partial x} + h\frac{\partial u}{\partial x} + v\frac{\partial h}{\partial y} + h\frac{\partial v}{\partial y} = \left(S + R - E + I\right) \tag{2.2.4}$$

$$\begin{aligned}\frac{\partial u}{\partial t} + g\frac{\partial h}{\partial x} + u\frac{\partial u}{\partial x} + v\frac{\partial u}{\partial y} &= -g\frac{\partial Z_o}{\partial x} - \frac{1}{h}\left[\frac{\partial F_{xx}}{\partial x} + \frac{\partial F_{yx}}{\partial y}\right] \\ &- \frac{u\left(S + R - E + I\right) - \left(M_X^S + M_X^R - M_x^E + M_X^I\right)}{h} + \frac{\tau_x^s - \tau_x^b}{\rho h}\end{aligned} \tag{2.2.5}$$

$$\begin{aligned}\frac{\partial v}{\partial t} + g\frac{\partial h}{\partial x} + u\frac{\partial v}{\partial x} + v\frac{\partial v}{\partial y} &= -g\frac{\partial Z_o}{\partial y} - \frac{gh^2}{2\rho}\frac{\partial \Delta\rho}{\partial y} - \frac{1}{h}\left[\frac{\partial F_{xy}}{\partial x} + \frac{\partial F_{yy}}{\partial y}\right] \\ &- \frac{v\left(S + R - E + I\right) - \left(M_y^S + M_y^R - M_y^E + M_y^I\right)}{h} + \frac{\tau_y^s - \tau_y^b}{\rho h}\end{aligned} \tag{2.2.6}$$

which can be written in matrix form as

$$\frac{\partial \mathbf{E}}{\partial t} + \mathbf{A}_x\frac{\partial \mathbf{E}}{\partial x} + \mathbf{A}_y\frac{\partial \mathbf{E}}{\partial y} = \mathbf{R} + \mathbf{D} \tag{2.2.7}$$

where

$$\mathbf{E} = \{\mathrm{h} \quad \mathrm{u} \quad \mathrm{v}\}^T; \quad \mathbf{A_x} = \begin{bmatrix} u & h & 0 \\ g & u & 0 \\ 0 & 0 & u \end{bmatrix}; \quad \mathbf{A_y} = \begin{bmatrix} v & 0 & h \\ 0 & v & 0 \\ g & 0 & v \end{bmatrix} \tag{2.2.8}$$

$$\mathbf{R} = \begin{Bmatrix} R_1 \\ R_2 \\ R_3 \end{Bmatrix} = \begin{Bmatrix} S + R - E + I \\ -g\dfrac{\partial Z_o}{\partial x} - \dfrac{gh^2}{2\rho}\dfrac{\partial \Delta\rho}{\partial x} - \dfrac{u\left(S_S + S_R - S_E + S_I\right) - \left(M_X{}^S + M_X{}^R - M_x{}^E + M_X{}^I\right)}{h} + \dfrac{\tau_x^s - \tau_x^b}{\rho h} \\ -g\dfrac{\partial Z_o}{\partial y} - \dfrac{gh^2}{2\rho}\dfrac{\partial \Delta\rho}{\partial y} - \dfrac{v\left(S_S + S_R - S_E + S_I\right) - \left(M_y{}^S + M_y{}^R - M_y{}^E + M_y{}^I\right)}{h} + \dfrac{\tau_y^s - \tau_y^b}{\rho h} \end{Bmatrix} \tag{2.2.9}$$

$$\mathbf{D} = \begin{Bmatrix} 0 \\ \mathrm{D_x} \\ D_y \end{Bmatrix} = \begin{Bmatrix} 0 \\ -\dfrac{1}{h}\left[\dfrac{\partial F_{xx}}{\partial x} + \dfrac{\partial F_{yx}}{\partial y}\right] \\ -\dfrac{1}{h}\left[\dfrac{\partial F_{xy}}{\partial x} + \dfrac{\partial F_{yy}}{\partial y}\right] \end{Bmatrix} = \begin{Bmatrix} 0 \\ \dfrac{1}{h}\left[\dfrac{\partial}{\partial x}\left(h\varepsilon_{xx}\dfrac{\partial u}{\partial x}\right) + \dfrac{\partial}{\partial y}\left(h\varepsilon_{xy}\dfrac{\partial u}{\partial y} + h\varepsilon_{yx}\dfrac{\partial v}{\partial x}\right)\right] \\ \dfrac{1}{h}\left[\dfrac{\partial}{\partial x}\left(h\varepsilon_{xy}\dfrac{\partial u}{\partial y} + h\varepsilon_{yx}\dfrac{\partial v}{\partial x}\right) + \dfrac{\partial v}{\partial y}\left(h\varepsilon_{yy}\dfrac{\partial v}{\partial y}\right)\right] \end{Bmatrix} \tag{2.2.10}$$

Let the matrix **B** be the linear combination of the matrices $\mathbf{A_x}$ and $\mathbf{A_y}$ as follows

$$\mathbf{B} = \mathbf{A} \cdot \mathbf{k} = \mathbf{A_x} k_x + \mathbf{A_y} k_y = \begin{bmatrix} uk_x + vk_y & hk_x & hk_y \\ gk_x & uk_x + vk_y & 0 \\ gk_y & 0 & uk_x + vk_y \end{bmatrix} \tag{2.2.11}$$

where **A** is a third rank vector with the matrices $\mathbf{A_x}$ and $\mathbf{A_y}$ as its components and **k** is a unit vector. The eigenvalues and eigenvectors of the defined matrix **B** are

$$\lambda_1 = uk_x + vk_y \qquad \mathbf{e_1} = \{0 \quad k_y \quad -k_x\}^T \tag{2.2.12}$$

$$\lambda_2 = uk_x + vk_y + \sqrt{gh} \qquad \mathbf{e_2} = \left\{\frac{\sqrt{gh}}{2} \quad \frac{gk_x}{2} \quad \frac{gk_y}{2}\right\}^T \tag{2.2.13}$$

$$\lambda_3 = uk_x + vk_y - \sqrt{gh} \qquad \mathbf{e_3} = \left\{-\frac{\sqrt{gh}}{2} \quad \frac{gk_x}{2} \quad \frac{gk_y}{2}\right\}^T \tag{2.2.14}$$

where k_x and k_y are the *x*- and *y*-component of the unit vector **k**.

Now we compose an eigenmatrix and its inverse from the eigenvectors of **B** as

$$\mathbf{L} = \begin{bmatrix} 0 & \frac{\sqrt{gh}}{2} & -\frac{\sqrt{gh}}{2} \\ k_y & \frac{gk_x}{2} & \frac{gk_x}{2} \\ -k_x & \frac{gk_y}{2} & \frac{gk_y}{2} \end{bmatrix} \quad and \quad \mathbf{L}^{-1} = \begin{bmatrix} 0 & k_y & -k_x \\ \frac{1}{\sqrt{gh}} & \frac{k_x}{g} & \frac{k_y}{g} \\ -\frac{1}{\sqrt{gh}} & \frac{k_x}{g} & \frac{k_y}{g} \end{bmatrix} \tag{2.2.15}$$

Let us define a characteristic vector **W** by

$$\partial\mathbf{W} = \mathbf{L}^{-1}\partial\mathbf{E} = \begin{bmatrix} 0 & k_y & -k_x \\ \frac{1}{\sqrt{gh}} & \frac{k_x}{g} & \frac{k_y}{g} \\ -\frac{1}{\sqrt{gh}} & \frac{k_x}{g} & \frac{k_y}{g} \end{bmatrix} \begin{Bmatrix} \partial h \\ \partial u \\ \partial v \end{Bmatrix} \quad in\ which \quad \mathbf{W} = \begin{Bmatrix} W_1 \\ W_2 \\ W_3 \end{Bmatrix}^T \tag{2.2.16}$$

where the first characteristic variable W_1 is a vorticity or shear wave. The second and third components, W_2 and W_3, are the amplitudes of the two gravity waves. The multiplication of Eq. (2.2.7) by $\mathbf{L}^{-1}$ yields

$$\mathbf{L}^{-1}\frac{\partial \mathbf{E}}{\partial \mathrm{t}} + \mathbf{L}^{-1}\mathbf{A}_\mathrm{x}\mathbf{L}\mathbf{L}^{-1}\frac{\partial \mathbf{E}}{\partial \mathrm{x}} + \mathbf{L}^{-1}\mathbf{A}_\mathrm{y}\mathbf{L}\mathbf{L}^{-1}\frac{\partial \mathbf{E}}{\partial \mathrm{y}} = \mathbf{L}^{-1}\mathbf{R} + \mathbf{L}^{-1}\mathbf{D} \tag{2.2.17}$$

or, with the transformation between **E** and **W** given by $\mathbf{L}^{-1}\partial\mathbf{E} = \partial\mathbf{W}$,

$$\frac{\partial \mathbf{W}}{\partial t} + \mathbf{L}^{-1}\mathbf{A}_\mathrm{x}\mathbf{L}\frac{\partial \mathbf{W}}{\partial x} + \mathbf{L}^{-1}\mathbf{A}_\mathrm{y}\mathbf{L}\frac{\partial \mathbf{W}}{\partial y} = \mathbf{L}^{-1}\mathbf{R} + \mathbf{L}^{-1}\mathbf{D} \tag{2.2.18}$$

Substituting $\mathbf{A}_\mathrm{x}$ and $\mathbf{A}_\mathrm{y}$ in Eq. (2.2.8) and $\mathbf{L}^{-1}$ and **L** in Eq. (2.2.15) into Eq. (2.2.18), and performing matrix multiplication, we obtain

$$\frac{\partial \mathbf{W}}{\partial t} + \begin{bmatrix} u & \frac{gck_y}{2} & -\frac{gck_y}{2} \\ \frac{hk_y}{c} & u+ck_x & 0 \\ \frac{hk_y}{c} & 0 & u-ck_x \end{bmatrix} \frac{\partial \mathbf{W}}{\partial x} + \begin{bmatrix} v & -\frac{gck_x}{2} & \frac{gck_x}{2} \\ -\frac{hk_x}{c} & v+ck_y & 0 \\ \frac{hk_x}{c} & 0 & v-ck_y \end{bmatrix} \frac{\partial \mathbf{W}}{\partial y} = \mathbf{L}^{-1}\mathbf{R} + \mathbf{L}^{-1}\mathbf{D} \tag{2.2.19}$$

where

$$\mathrm{c} = \sqrt{\mathrm{gh}} \tag{2.2.20}$$

It is noted that the coefficient matrices $\mathbf{L}^{-1}\mathbf{A}_x\mathbf{L}$ and $\mathbf{L}^{-1}\mathbf{A}_y\mathbf{L}$, respectively, of $(\partial\mathbf{W}/\partial x)$ and $(\partial\mathbf{W}/\partial y)$, respectively, are not diagonal matrices because $\mathbf{L}^{-1}$ is not an eigenmatrix of $\mathbf{A}_x$ nor of $\mathbf{A}_y$. Rearranging Eq. (2.2.19), we obtain

$$\frac{\partial \mathbf{W}}{\partial t}+\begin{bmatrix} u & 0 & 0 \\ 0 & u+ck_x & 0 \\ 0 & 0 & u-ck_x \end{bmatrix}\frac{\partial \mathbf{W}}{\partial x}+\begin{bmatrix} v & 0 & 0 \\ 0 & v+ck_y & 0 \\ 0 & 0 & v-ck_y \end{bmatrix}\frac{\partial \mathbf{W}}{\partial y}+\begin{Bmatrix} S_1 \\ S_2 \\ S_3 \end{Bmatrix}=\mathbf{L}^{-1}\left(\mathbf{R}+\mathbf{D}\right) \qquad \textbf{(2.2.21)}$$

where

$$\begin{Bmatrix} S_1 \\ S_2 \\ S_3 \end{Bmatrix}=\begin{Bmatrix} g\left(k_y\dfrac{\partial h}{\partial x}-k_x\dfrac{\partial h}{\partial y}\right) \\ \dfrac{h}{c}\left[k_yk_y\dfrac{\partial u}{\partial x}+k_xk_x\dfrac{\partial v}{\partial y}-k_xk_y\left(\dfrac{\partial u}{\partial y}+\dfrac{\partial v}{\partial x}\right)\right] \\ \dfrac{-h}{c}\left[k_yk_y\dfrac{\partial u}{\partial x}+k_xk_x^{(2)}\dfrac{\partial v}{\partial y}-k_xk_y\left(\dfrac{\partial u}{\partial y}+\dfrac{\partial v}{\partial x}\right)\right] \end{Bmatrix} \qquad \textbf{(2.2.22)}$$

For a general consideration, we define a new $\mathbf{L}^{*-1}$ (and its inverse $\mathbf{L}^*$) which plays the following transformation.

$$\partial\mathbf{W}=\mathbf{L}^{*-1}\,\partial\mathbf{E}=\begin{bmatrix} 0 & k_y^{(1)} & -k_x^{(1)} \\ \dfrac{1}{c} & \dfrac{k_x^{(2)}}{g} & \dfrac{k_y^{(2)}}{g} \\ -\dfrac{1}{c} & \dfrac{k_x^{(2)}}{g} & \dfrac{k_y^{(2)}}{g} \end{bmatrix}\begin{Bmatrix} \partial h \\ \partial u \\ \partial v \end{Bmatrix};\quad \mathbf{L}^*=\begin{bmatrix} 0 & \dfrac{c}{2} & -\dfrac{c}{2} \\ \dfrac{k_y^{(2)}}{k} & \dfrac{gk_x^{(2)}}{2k} & \dfrac{gk_x^{(2)}}{2k} \\ -\dfrac{k_x^{(2)}}{k} & \dfrac{gk_y^{(2)}}{2k} & \dfrac{gk_y^{(2)}}{2k} \end{bmatrix} \qquad \textbf{(2.2.23)}$$

where $k = \mathbf{k}^{(1)}\cdot\mathbf{k}^{(2)}$ is the inner product of $\mathbf{k}^{(1)}$ and $\mathbf{k}^{(2)}$. It should be noted that two unit wave directions $\mathbf{k}^{(1)}$ and $\mathbf{k}^{(2)}$ should not be orthogonal so that the transformation will not be singular. Multiplying both side of Eq. (2.2.7) by this new $\mathbf{L}^{*-1}$ and repeating mathematical manipulations involved in Eqs. (2.2.19) and (2.2.21), we have

$$\frac{\partial \mathbf{W}}{\partial t}+\begin{bmatrix} u & 0 & 0 \\ 0 & u+ck_x^{(2)} & 0 \\ 0 & 0 & u-ck_x^{(2)} \end{bmatrix}\frac{\partial \mathbf{W}}{\partial x}+\begin{bmatrix} v & 0 & 0 \\ 0 & v+ck_y^{(2)} & 0 \\ 0 & 0 & v-ck_y^{(2)} \end{bmatrix}\frac{\partial \mathbf{W}}{\partial y}+\begin{Bmatrix} S_1 \\ S_2 \\ S_3 \end{Bmatrix}=\mathbf{L}^{*-1}\left(\mathbf{R}+\mathbf{D}\right) \qquad \textbf{(2.2.24)}$$

where

$$\begin{Bmatrix} S_1 \\ S_2 \\ S_3 \end{Bmatrix} = \begin{Bmatrix} g\left(k_y^{(1)} \frac{\partial h}{\partial x} - k_x^{(1)} \frac{\partial h}{\partial y} \right) \\ \frac{h}{c}\left[k_y^{(2)} k_y^{(2)} \frac{\partial u}{\partial x} + k_x^{(2)} k_x^{(2)} \frac{\partial v}{\partial y} - k_x^{(2)} k_y^{(2)} \left(\frac{\partial u}{\partial y} + \frac{\partial v}{\partial x} \right) \right] \\ \frac{-h}{c}\left[k_y^{(2)} k_y^{(2)} \frac{\partial u}{\partial x} + k_x^{(2)} k_x^{(2)} \frac{\partial v}{\partial y} - k_x^{(2)} k_y^{(2)} \left(\frac{\partial u}{\partial y} + \frac{\partial v}{\partial x} \right) \right] \end{Bmatrix} \qquad \textbf{(2.2.25)}$$

Substituting $\mathbf{L}^{*-1}$ defined in Eq. (2.2.23) into the right hand side of Eq. (2.2.24), we obtain

$$\begin{Bmatrix} \frac{\partial W_1}{\partial t} + u\frac{\partial W_1}{\partial x} + v\frac{\partial W_1}{\partial y} \\ \frac{\partial W_2}{\partial t} + \left(u + ck_x^{(2)}\right)\frac{\partial W_2}{\partial x} + \left(v + ck_y^{(2)}\right)\frac{\partial W_2}{\partial y} \\ \frac{\partial W_3}{\partial t} + \left(u - ck_x^{(2)}\right)\frac{\partial W_3}{\partial x} + \left(v - ck_y^{(2)}\right)\frac{\partial W_3}{\partial y} \end{Bmatrix} + \begin{Bmatrix} S_1 \\ S_2 \\ S_3 \end{Bmatrix} = \begin{Bmatrix} A_1 \\ A_2 \\ A_3 \end{Bmatrix} + \begin{Bmatrix} B_1 \\ B_2 \\ B_3 \end{Bmatrix} \qquad \textbf{(2.2.26)}$$

where

$$\begin{Bmatrix} A_1 \\ A_2 \\ A_3 \end{Bmatrix} = \begin{Bmatrix} k_y^{(1)} R_2 - k_x^{(1)} R_3 \\ \frac{1}{c} R_1 + \frac{k_x^{(2)}}{g} R_2 + \frac{k_y^{(2)}}{g} R_3 \\ \frac{-1}{c} R_1 + \frac{k_x^{(2)}}{g} R_2 + \frac{k_y^{(2)}}{g} R_3 \end{Bmatrix} \quad \textit{and} \quad \begin{Bmatrix} B_1 \\ B_2 \\ B_3 \end{Bmatrix} = \begin{Bmatrix} k_y^{(1)} D_x - k_x^{(1)} D_y \\ \frac{k_x^{(2)}}{g} D_x + \frac{k_y^{(2)}}{g} D_y \\ \frac{k_x^{(2)}}{g} D_x + \frac{k_y^{(2)}}{g} D_y \end{Bmatrix} \qquad \textbf{(2.2.27)}$$

Writing out Eq. (2.2.26) in its three components, we have the following three equations for three unknowns W_1, W_2, and W_3

$$\frac{\partial W_1}{\partial t} + u\frac{\partial W_1}{\partial x} + v\frac{\partial W_1}{\partial y} + S_1 = A_1 + B_1 \qquad \textbf{(2.2.28)}$$

$$\frac{\partial W_2}{\partial t} + \left(u + ck_x^{(2)}\right)\frac{\partial W_2}{\partial x} + \left(v + ck_y^{(2)}\right)\frac{\partial W_2}{\partial y} + S_2 = A_2 + B_2 \qquad \textbf{(2.2.29)}$$

$$\frac{\partial W_3}{\partial t} + \left(u - ck_x^{(2)}\right)\frac{\partial W_3}{\partial x} + \left(v - ck_y^{(2)}\right)\frac{\partial W_3}{\partial y} + S_3 = A_3 + B_3 \qquad \textbf{(2.2.30)}$$

Equations (2.2.28), (2.29), and (2.230) indicate that the vorticity wave is advected by the velocity **V**, the positive gravity wave by $\mathbf{V} + c\mathbf{k}^{(2)}$, and the negative gravity wave by $\mathbf{V} - c\mathbf{k}^{(2)}$, where $\mathbf{k}^{(2)}$ is a unit vector.

We can write Eq. (2.2.26) in Lagrangian form as

$$\begin{Bmatrix} \frac{D_V W_1}{D\tau} \\ \frac{D_{V+ck^{(2)}} W_2}{D\tau} \\ \frac{D_{V-ck^{(2)}} W_3}{D\tau} \end{Bmatrix} + \begin{Bmatrix} S_1 \\ S_2 \\ S_3 \end{Bmatrix} = \begin{Bmatrix} A_1 \\ A_2 \\ A_3 \end{Bmatrix} + \begin{Bmatrix} B_1 \\ B_2 \\ B_3 \end{Bmatrix} \qquad \textbf{(2.2.31)}$$

where **V** is the transporting velocity of the vorticity wave W_1, (**V** + c**k**$^{(2)}$) is the transporting velocity of positive gravity wave W_2, and (**V** - c**k**$^{(2)}$) is the transporting velocity of negative gravity wave W_3. Substituting the definition of the characteristic variable **W** in Eq. (2.2.23) into Eq. (2.2.31), we have the following three equations for the three waves

$$k_y^{(1)} \frac{D_V u}{D\tau} - k_x^{(1)} \frac{D_V v}{D\tau} + S_1 = A_1 + B_1 \qquad \textbf{(2.2.32)}$$

$$\frac{2}{g} \frac{D_{V+ck^{(2)}} c}{D\tau} + \frac{k_x^{(2)}}{g} \frac{D_{V+ck^{(2)}} u}{D\tau} + \frac{k_y^{(2)}}{g} \frac{D_{V+ck(2)} v}{D\tau} + S_2 = A_2 + B_2 \qquad \textbf{(2.2.33)}$$

$$-\frac{2}{g} \frac{D_{V-ck^{(2)}} c}{D\tau} + \frac{k_x^{(2)}}{g} \frac{D_{V-ck^{(2)}} u}{D\tau} + \frac{k_y^{(2)}}{g} \frac{D_{V-ck^{(2)}} v}{D\tau} + S_3 = A_3 + B_3 \qquad \textbf{(2.2.34)}$$

It is noted that a diagonalization can be achieved with special selections of $k_x^{(1)}$, $k_y^{(1)}$, $k_x^{(2)}$, and $k_y^{(2)}$ to make S_1, S_2, and S_3 zeros.

In solving Eqs. (2.2.28) through (2.2.30) or Eqs. (2.2.32) through (2.2.34), the water depth h, and the velocity components, u and v, must be given initially or they can be obtained by simulating the steady-state version of Eqs. (2.2.28) through (2.2.30). In addition, appropriate boundary conditions need to be specified to match the corresponding physical system. The characteristics form of the governing equation offers great advantages over the primitive form in adapting appropriate numerical algorithms and in defining boundary conditions. Innovative hyperbolic numerical algorithms can be employed to approximate the system because each of the three equations is a decoupled advective transport equation of a wave. The specification of boundary conditions is made easy pending the wave direction. We demonstrate how boundary conditions are specified in the following. An overland boundary segment can be either open or closed. In the former case, the boundary condition for any wave is needed only when it is transported into the region of interest. When a wave is transported out of the region, there is no need to specify the boundary condition because internal flow dynamics due to this wave affects the boundary values of u, v, and h. In the later case, the flow rate on the boundary is zero.

Open upstream boundary condition:

At an open upstream boundary segment, the vorticity is always transported into the region from upstream. If the flow is supercritical, then both gravity waves also transported into the region from

upstream; thus three boundary conditions are needed. The water depth and velocity components at the boundary are determined entirely by the flow condition that prevails at the upstream. The governing equations for this case can be set up based on the continuity of mass as well as momentums between the upstream and boundary as

$$\mathbf{n}\cdot\mathbf{V}h = q_n^{(up)}(\mathbf{x}_b,t);\ \mathbf{n}\cdot\mathbf{V}uh + n_x\frac{gh^2}{2} = M_x^{up}(\mathbf{x}_b,t);\ and\ \mathbf{n}\cdot\mathbf{V}vh + n_y\frac{gh^2}{2} = M_y^{up}(\mathbf{x}_b,t) \quad \textbf{(2.2.35)}$$

where **n** is the outward unit vector of the boundary segment; $q_n^{up}(\mathbf{x}_b,t)$, a function of time *t*, is flow rate normal to the boundary from the upstream; $\mathbf{x}_b$ is the coordinate on the boundary; n_x is the *x*-component of **n**; $M_x^{up}(\mathbf{x}_b,t)$ is the *x*-momentum/impulse from the upstream; n_y is the *y*-component of **n**; and $M_y^{up}(\mathbf{x}_b,t)$ is the *y*-momentum/impulse from the upstream. It is noted that *u*, *v*, and *h* from the upstream must be given to provide q_n^{up}, M_x^{up} and M_y^{up}.

In the case of subcritical flow, one of the two gravity waves is transported into the region while the other is transported out of the region. The water depth and velocity are determined with the upstream flow condition and internal flow dynamics. The governing equations are set up based on the continuity of mass between the boundary and the upstream and on the flow dynamics in the region as

$$\begin{aligned}&\mathbf{n}\cdot\mathbf{V}h = q_n^{(up)}(\mathbf{x}_b,t)\ \ or\ \ h+Z_o = H_{up}(\mathbf{x}_b,t);\ \ell\cdot\mathbf{V}h = q_\ell^{(up)}(\mathbf{x}_b,t);\ and\ F_+(u,v,h)=0\\ &\qquad\qquad or\\ &\mathbf{n}\cdot\mathbf{V}h = q_n^{(up)}(\mathbf{x}_b,t)\ \ or\ h+Z_o = H_{up}(\mathbf{x}_b,t);\ \ell\cdot\mathbf{V}h = q_\ell^{(up)}(\mathbf{x}_b,t);\ and\ F_-(u,v,h)=0\end{aligned} \quad \textbf{(2.2.36)}$$

where ℓ is the unit vector parallel to the boundary segment; $H_{up}(\mathbf{x}_b,t)$, a function of time *t*, is the water stage in the incoming fluid from the upstream; $q_\ell^{up}(\mathbf{x}_b,t)$, a function of time *t*, is the flow rate parallel to the boundary.

Open downstream boundary condition:

At an open downstream boundary segment, the vorticity is always transported out of the region into downstream. If the flow is supercritical, then both gravity waves also transported out of the region into downstream; thus three is no need to specify the boundary conditions. The water depth and velocity components at the boundary are determined entirely by internal flow dynamics. The governing equations for this case are given by

$$F_\otimes(u,v,h)=0;\quad F_+(u,v,h)=0;\quad and\quad F_-(u,v,h)=0 \quad \textbf{(2.2.37)}$$

where $F_\otimes(u,v,h)$, a function of velocity and water depth, is the vorticity wave boundary function.

In the case of subcritical flow, one of the two gravity waves is transported into the region from downstream while the other is transported out of the region into downstream. The water depth and

velocity are determined by the internal flow dynamics and the control of the downstream boundary segment

$$\begin{aligned} &F_{\otimes}(u,v,h)=0;\quad F_{+}(u,v,h)=0;\ and\ h=h_{dn}(\mathbf{x}_b,t)\ or\ \mathbf{n}\cdot\mathbf{V}h=q_n^{dn}(h) \\ &\qquad\qquad or \\ &F_{\otimes}(u,v,h)=0;\quad F_{-}(u,v,h)=0;\ and\ \ h=h_{dn}(\mathbf{x}_b,t)\ or\ \mathbf{n}\cdot\mathbf{V}h=q_n^{dn}(h) \end{aligned} \qquad \textbf{(2.2.38)}$$

where $h^{dn}(t)$, a function of time t, is the water depth of the downstream boundary an $q_n^{dn}(h)$, a function of water depth h, is the rating curve of the downstream boundary.

Closed upstream boundary condition:

At the closed upstream boundary, physically all flow conditions can occur. The vorticity wave is always transported from the outside of the boundary into the region. When the supercritical flow happens, both gravity waves are also transported into the region. Thus, three boundary condition equations are needed. Because the boundary is closed, it is impermeable. The governing equations can be obtained by simply substituting $q_n^{up}=0$, $M_x^{up}=0$, and $M_y^{up}=0$ into Eq. (2.2.35) to yield

$$\mathbf{n}\cdot\mathbf{V}h=0;\quad \mathbf{n}\cdot\mathbf{V}uh+n_x\frac{gh^2}{2}=0;\quad and\quad \mathbf{n}\cdot\mathbf{V}vh+n_y\frac{gh^2}{2}=0 \qquad \textbf{(2.2.39)}$$

The solutions for Eq. (2.2.39) are not unique. One of the possible solution is $u=0$, $v=0$, and $h=0$.

When the flow is subcritical, one of the two gravity waves is transported from the outside of the boundary into the region while the other is transported from inside the boundary to the outside The boundary conditions are needed only for the incoming waves. Since no fluid from the outside world is transported into the region via the closed boundary, one of the two boundary condition equations can be stated with $\mathbf{n}\cdot\mathbf{V}=0$. The other boundary equation can be obtained by assuming no slip condition on the boundary. Thus, three governing equations are given as

$$\mathbf{n}\cdot\mathbf{V}h=0;\ \ell\cdot\mathbf{V}h=0;\ and\ F_{+}(u,v,h)=0\quad or\quad \mathbf{n}\cdot\mathbf{V}h=0;\ \ell\cdot\mathbf{V}h=0;\ and\ F_{-}(u,v,h)=0 \qquad \textbf{(2.2.40)}$$

depending on which wave is transported out of the region.

Closed downstream boundary condition:

At the closed downstream boundary, physical condition dictates that normal flow rate at the boundary is zero. The vorticity wave is always transported out of the region. If the flow is supercritical, both gravity waves are also transported out of the region. The velocity and water depth on the boundary is determined entirely by internal flow dynamics and no boundary condition is needed. The governing equations are given by the wave boundary functions subject to the constraint that fluid flux is zero as follows:

$$F_{\otimes}(u,v,h)=0;\ \ F_{+}(u,v,h)=0;\quad and\quad F_{-}(u,v,h)=0\quad subject\ to\quad \mathbf{n}\cdot\mathbf{V}=0 \qquad \textbf{(2.2.41)}$$

The only feasible solution of Eq. (2.1.31) is $u=0$, $v=0$, and $h=0$. Therefore, supercritical flow

cannot occur at a closed downstream segment.

In the case of subcritical flow, one of the two gravity waves is transported into the region while the other is transported out of the region. The water depth and velocity are determined with the internal flow dynamics and the condition of zero normal flux as

$$F_{\otimes}(u,v,h)=0;\ F_{+}(u,v,h)=0;\ and\ \mathbf{n}\cdot\mathbf{V}h=0\ \ or\ \ F_{\otimes}(u,v,h)=0;\ F_{-}(u,v,h)=0;\ and\ \mathbf{n}\cdot\mathbf{V}h=0 \qquad \textbf{(2.2.42)}$$

Overland-river interface boundary condition:

At the overland-river interface, the flux must be continuous as

$$(\mathbf{n}\bullet\mathbf{V})h\Big|_{Bank\,1}=S_1 \qquad and \qquad (\mathbf{n}\bullet\mathbf{V})h\Big|_{Bank\,2}=S_2 \qquad \textbf{(2.2.43)}$$

where S_1 and S_2 are sources of water which appear in Eq. (2.1.1)

2.2.2 Diffusive Wave Approaches

For diffusion wave models, the inertia terms in Eqs. (2.2.2) and (2.2.3) are assumed not important when compared to the others. With the further assumption that eddy viscosity is insignificant and $M_x^S=M_x^R=M_x^E=M_x^I=M_y^S=M_y^R=M_y^E=M_y^I=0$, we approximate the velocity $\mathbf{V}=(u,v)$ as follows

$$\mathbf{V}=\frac{-a}{n}\left[\frac{h}{1+(\nabla Z_o)^2}\right]^{2/3}\frac{1}{\sqrt{\left|-\nabla H-\frac{h}{2\rho}\nabla(\Delta\rho)+\frac{\tau^s}{\rho gh}\right|}}\left(\nabla H+\frac{h}{2\rho}\nabla(\Delta\rho)-\frac{\tau^s}{\rho gh}\right) \qquad \textbf{(2.2.44)}$$

Using the definition $\mathbf{q}=\mathbf{V}h$ and substituting Eq. (2.2.44) into Eq. (2.2.1), we obtain

$$\frac{\partial H}{\partial t}-\nabla\cdot\left[K\left(\nabla H+\frac{h}{2\rho}\nabla(\Delta\rho)-\frac{\boldsymbol{\tau}^s}{\rho gh}\right)\right]=S_S+S_R-S_E+S_I \qquad \textbf{(2.2.45)}$$

in which

$$K=\frac{a\,h^{5/3}}{n}\frac{1}{\left[1+(\nabla Z_o)^2\right]^{2/3}}\frac{1}{\sqrt{\left|-\nabla H-\frac{h}{2\rho}\nabla(\Delta\rho)+\frac{\tau^s}{\rho gh}\right|}} \qquad \textbf{(2.2.46)}$$

To achieve transient simulations, either water depth or stage must be given as the initial condition. In addition, appropriate boundary conditions need to be specified to match the corresponding physical system. In our model, four types of boundary conditions may be specified depending on physical configurations of the boundary. These boundary conditions are addressed below.

Dirichlet boundary condition: prescribed water depth or stage

On a Dirichlet boundary, either the water depth or stage can be prescribed as a function of time. This boundary condition can be expressed as

$$h = h_d\left(\mathbf{x}_b, t\right) \quad or \quad H = h + Z_0 = H_d(\mathbf{x}_b, t), \quad on \quad B_d \tag{2.2.47}$$

where $h_d\left(\mathbf{x}_b, t\right)$ is a prescribed time-dependent water depth on the Dirichlet boundary [L], $H_d(\mathbf{x}_b, t)$ is a prescribed time-dependent water stage [L], and B_d is the Dirichlet boundary segment. A Dirichlet boundary segment can locate at the up-streams or down-streams, control structures, or even interior points.

Flux boundary condition: prescribed flow rate

On a flux boundary, a time-dependent flow rate is prescribed as a function of time as

$$-\mathbf{n}\cdot K\left(\nabla H + \frac{h}{2\rho}\nabla\left(\Delta\rho\right) - \frac{\boldsymbol{\tau}^s}{\rho g h}\right) = q_f\left(\mathbf{x}_b, t\right) \quad on \quad B_f \tag{2.2.48}$$

where **n** is an outward unit vector at the flux boundary point, $q_f\left(\mathbf{x}_b, t\right)$ a prescribed time-dependent flow rate [L^3/t/L], and B_f is a flux boundary segment. Mathematically, a flux boundary condition can be applied to an upstream or downstream segment. However, in practice, it is often applied to an upstream boundary segment.

Water depth-dependent boundary condition: prescribed rating curve

This condition is often used to describe the flow rate at a downstream boundary at which the flow rate is a function of water depth. It can be written as

$$-\mathbf{n}\cdot K\left(\nabla H + \frac{h}{2\rho}\nabla\left(\Delta\rho\right) - \frac{\boldsymbol{\tau}^s}{\rho g h}\right) = q_r\left(h\left(x_r, t\right)\right) \quad on \quad B_r \tag{2.2.49}$$

where $q_r(h(x_r,t))$ is a water depth-dependent flow rate [L^3/t/L], $\mathbf{x}_r$ is the *x*-coordinate on the boundary B_r, and B_r is a boundary segment on which the prescribed rating curve is applied.

Overland-river interface boundary condition:

At the overland-river interface, the flux must be continuous as

$$\begin{aligned} -\mathbf{n}\cdot K\left(\nabla H + \frac{h}{2\rho}\nabla\left(\Delta\rho\right) - \frac{\boldsymbol{\tau}^s}{\rho g h}\right)\Big|_{Bank\,1} &= S_1 \quad and \\ -\mathbf{n}\cdot K\left(\nabla H + \frac{h}{2\rho}\nabla\left(\Delta\rho\right) - \frac{\boldsymbol{\tau}^s}{\rho g h}\right)\Big|_{Bank\,2} &= S_2 \end{aligned} \tag{2.2.50}$$

where S_1 and S_2 are sources of water which appear in Eq. (2.1.1)

2.2.3 Kinematic Wave Approaches

In a kinematic approach, all the assumptions for the diffusive approach are hold. However, the velocity is given by modifying Eq. (2.2.44) with ∇Z_0 replacing ∇H as follows

$$\mathbf{V} = \frac{-a}{n}\left[\frac{h}{1+\left(\nabla Z_o\right)^2}\right]^{2/3} \frac{1}{\sqrt{\left|-\nabla Z_o - \frac{h}{2\rho}\nabla\left(\Delta\rho\right)+\frac{\tau^s}{\rho g h}\right|}}\left(\nabla z_o + \frac{h}{2\rho}\nabla\left(\Delta\rho\right) - \frac{\tau^s}{\rho g h}\right) \qquad \textbf{(2.2.51)}$$

Substituting Eq. (2.2.51) into Eq. (2.2.1) and using the definition **q** = **V***h*, we obtain

$$\frac{\partial h}{\partial t} + \nabla\cdot\left(\mathbf{V}h\right) = S_S + S_R - S_E + S_I \qquad \textbf{(2.2.52)}$$

It is noted that Eq. (2.2.52) represents the advective transport of the water depth, *h*. It is an ideal equation amenable for numerically innovative advective transport algorithm.

To achieve transient simulations, either water depth or stage must be given as the initial condition. In addition, appropriate boundary conditions need to be specified to match the corresponding physical configuration. In a kinematic wave approach, boundary conditions are required only at upstream boundaries. An upstream boundary segment can be an open boundary or a closed boundary. On an open upstream boundary, either the water depth or the flow rate can be specified as

$$h = h_{up}\left(\mathbf{x}_{up}, t\right) \quad or \quad \mathbf{n}\cdot\mathbf{V}h = q_{up}\left(\mathbf{x}_{up}, t\right) \quad on \quad B_{up} \qquad \textbf{(2.2.53)}$$

where $h_{up}\left(\mathbf{x}_{up}, t\right)$ is the water depth of the incoming upstream flow, $q_{up}\left(\mathbf{x}_{up}, t\right)$ is the flow rate of the incoming upstream flow, $\mathbf{x}_{up}$ is the coordinate on the upstream boundary, and B_{up} is the open upstream boundary segment. The flow rate through a closed upstream boundary segment is by default equal to zero.

2.2.4 Thermal Transport

The thermal transport equation is derived based on the conservation principle of energy as:

$$\begin{aligned}\frac{\partial\left(\rho_w C_w h T\right)}{\partial t} + \nabla\cdot\left(\rho_w C_w \mathbf{q}\mathrm{T}\right) - \nabla\cdot\left(\mathbf{D}^{\mathrm{H}} h\cdot\nabla T\right) \\ = H_a + H_r + H_n - H_b - H_e - H_s + H_i + H_c\end{aligned} \qquad \textbf{(2.2.54)}$$

where ρ_w is the water density [M/L^3]; C_w is the heat capacity of water [L^2/t^2/T]; T is the temperature [T]; $\mathbf{D}^{\mathrm{H}}$ is the apparent thermal conductivity tensor including the effect of dispersion, diffusion, and

conduction [E/L/t/T = ML/t^3/T, where E is the unit of energy]; H_a is the heat source due to artificial injection/withdraw including rainfall [E/t/L^2 = M/t^3]; H_r is the heat source due to rainfall [E/t/L^2 = M/t^3]; H_n is the heat source due to net radiation [E/t/L^2 = M/t^3]; H_b is the heat sink due to back radiation from water surface to the atmosphere [E/t/L^2 = M/t^3]; H_e is the heat sink due to evaporation [E/t/L^2 = M/t^3]; H_s is the heat sink due to sensible heat flux [E/t/L^2 = M/t^3]; H_i is the heat source due to exfiltration from subsurface [E/t/L^2 = M/t^3]; and H_c is the heat source due to chemical reaction [E/t/L^2 = M/t^3]. In Eq. (2.2.54), H_r and H_i are given by

$$H_r = C_w \rho_w R T^r; \qquad H_i = \begin{cases} C_w \rho_w I T^i & if \quad I \geq 0 \\ C_w \rho_w I T & if \quad I < 0 \end{cases} \tag{2.2.55}$$

where R is the rainfall rate [L/t], T^r is the temperature of the rainwater [T], I is the exfiltration rate [L/t], and T^i is the temperature of the exfiltration water from the subsurface flow [T]. H_n, H_b, H_e, and H_s are the net radiation flux, back radiation flux, latent heat flux, and sensible heat flux, respectively. These fluxes depend on only meteorological condition and water temperature. The formulation of these heat/energy fluxes were presented in Section 2.1.

In addition to the initial boundary condition, boundary conditions must be specified for the temperature. Four types of global boundary conditions are provided in this report as follows.

Dirichlet boundary condition:

This condition is applied when the temperature is prescribed as a function of time on the boundaries:

$$T = T_{db}\left(\mathbf{x}_b, t\right) \qquad on \qquad B_d \tag{2.2.56}$$

where $T_{db}\left(\mathbf{x}_b, t\right)$ is a time-dependent temperature on the Dirichlet boundary B_d [T].

Variable boundary condition:

This boundary condition is employed when the flow direction would change with time during simulations. Two cases are considered, regarding to the flow direction on the boundary.

< Case 1 > Flow is coming in from outside:

$$\mathbf{n} \cdot \left(\rho_w C_w \mathbf{q} T - \mathbf{D}^{\mathbf{H}} h \cdot \nabla T \right) = \mathbf{n} \cdot \rho_w C_w \mathbf{q} T_{vb}\left(\mathbf{x}_b, t\right) \qquad on \qquad B_v \tag{2.2.57}$$

< Case 2 > Flow is going out from inside:

$$-\mathbf{n} \cdot \mathbf{D}^{\mathbf{H}} h \cdot \nabla T = 0 \qquad on \qquad B_v \tag{2.2.58}$$

where $T_{vb}\left(\mathbf{x}_b, t\right)$ is a time-dependent temperature on the variable boundary B_v [T], which is associated with the incoming flow.

Cauchy boundary condition:

This boundary condition is employed when the total heat-flow rate is given at the boundary. Usually, this boundary is a flow-in boundary. The conditions can be expressed as

$$\mathbf{n}\cdot\left(\rho_w C_w \mathbf{q}T - \mathbf{D}^{\mathbf{H}}h\cdot\nabla T\right) = \Phi_{cb}(t) \quad on \quad B_c \tag{2.2.59}$$

where $\Phi_{cb}(t)$ is total heat flux on the Cauchy boundary B_c [E/L/t = ML/t^3, where E denotes the unit of energy], which takes a positive value if it is going out of the region and a negative value if it is coming into the region.

Neumann boundary condition:

This boundary condition is used when the conductive heat-flow rate is known at the boundary. It can be written as

$$-\mathbf{n}\cdot\mathbf{D}^{\mathbf{H}}h\cdot\nabla T = \Phi_{nb}(\mathbf{x}_b, t) \quad on \quad B_n \tag{2.2.60}$$

where $\Phi_{nb}(\mathbf{x}_b, t)$ is the heat flux on the Neumann boundary B_n [E/L/t].

In addition to the four types of global boundary conditions, an internal boundary condition may be specified for the exchange of energy/heat flux between the overland and river/stream network. Mathematically, this boundary condition is described below.

Overland-river interface boundary condition:

$$\mathbf{n}\cdot\left(\rho_w C_w \mathbf{q}T - \mathbf{D}^{\mathbf{H}}h\cdot\nabla T\right)\Big|_{Bank\,1} = S_h^{o1} \quad and \quad \mathbf{n}\cdot\left(\rho_w C_w \mathbf{q}T - \mathbf{D}^{\mathbf{H}}h\cdot\nabla T\right)\Big|_{Bank\,2} = S_h^{o2} \tag{2.2.61}$$

where S_h^{o1} and S_h^{o2} are the heat sources, which appeared in Eq. (2.1.67). These heat sources can be calculated using Eq. (2.1.69) if the temperatures in the overland water and river water are discontinuous at the interfaces. If the temperatures are continuous, then these heat sources should be formulated by imposing the continuity of the temperatures in the overland water and river water at the interface.

2.2.5 Salinity Transport

$$\frac{\partial(hS)}{\partial ts} + \nabla\cdot(\mathbf{q}S) - \nabla\cdot\left(h\mathbf{D}^{\mathbf{S}}\cdot\nabla S\right) = M_s^{as} + M_s^{rs} - M_s^{es} + M_s^{is} \tag{2.2.62}$$

where S is the salinity [M/L^3]; $\mathbf{D}^{\mathbf{S}}$ is the longitudinal dispersion coefficient for salt [L^2/t]; M_s^{as} is the artificial source of the salt [M/t//L^2]; M_s^{rs} is the salt source from rainfall [M/t/L^2; M_s^{es} is the salt sink from evaporation [M/t/L^2]; M_s^{is} is the salt source from subsurface [M/t/L^2]. In Eq. (2.2.62), M_s^{es} is likely to be zero and M_s^{rs} and M_s^{is} are given by

$$M_s^{rs} = RS^r; \quad M_s^{is} = \begin{Bmatrix} IS^i & if\ I \ge 0 \\ IS & if\ I < 0 \end{Bmatrix} \tag{2.2.63}$$

where R is the rainfall rate [L/t], S^r is the salinity of the rainwater [M/L^3], I is the exfiltration rate [L/t], and S^i is the salinity of the exfiltration water from the subsurface flow [M/L^3].

As in thermal transport, four types of global boundary conditions for salinity transport are provided in this report as follows.

Dirichlet boundary condition:

This condition is applied when the salinity is prescribed as a function of time on the boundaries:

$$S = S_{db}\left(\mathbf{x}_b, t\right) \quad on \quad B_d \tag{2.2.64}$$

where $S_{db}\left(\mathbf{x}_b, t\right)$ is a time-dependent salinity on the Dirichlet boundary B_d [M/L^3].

Variable boundary condition:

This boundary condition is employed when the flow direction would change with time during simulations. Two cases are considered, regarding to the flow direction on the boundary.

< Case 1 > Flow is coming in from outside:

$$\mathbf{n}\cdot\left(\mathbf{q}S - h\mathbf{D}^{\mathbf{S}}\cdot\nabla S\right) = \mathbf{n}\cdot\mathbf{q}S_{vb}\left(\mathbf{x}_b, t\right) \quad on \quad B_v \tag{2.2.65}$$

< Case 2 > Flow is going out from inside:

$$-\mathbf{n}\cdot h\mathbf{D}^{\mathbf{S}}\cdot\nabla S = 0 \quad on \quad B_v \tag{2.2.66}$$

where $S_{vb}\left(\mathbf{x}_b, t\right)$ is a time-dependent salinity on the variable boundary B_v [M/L^3], which is associated with the incoming flow.

Cauchy boundary condition:

This boundary condition is employed when the total salt-flow rate is given at the boundary. Usually, this boundary is a flow-in boundary. The conditions are expressed as

$$\mathbf{n}\cdot\left(\mathbf{q}S - h\mathbf{D}^{\mathbf{S}}\cdot\nabla S\right) = S_{cb}\left(\mathbf{x}_b, t\right) \quad on \quad B_c \tag{2.2.67}$$

where $S_{cb}\left(\mathbf{x}_b, t\right)$ is total salt-flow rate on the Cauchy boundary B_c [M/L/t], which takes a positive value if it is going out of the region and a negative value if it is coming into the region.

Neumann boundary condition:

This boundary condition is used when the dispersive salt-flow rate is known at the boundary. t can be written as

$$-\mathbf{n}\cdot h\mathbf{D}^{\mathbf{S}}\cdot\nabla S = S_{nb}(t) \quad on \quad B_n \tag{2.2.68}$$

where $S_{nb}(t)$ is the salt flux on the Neumann boundary [M/L/t].

As in thermal transport, in addition to the four types of global boundary conditions, an internal boundary condition may be specified for the exchange of salt between the overland and river/stream network. Mathematically, this boundary condition is described below.

River-overland interface boundary condition:

$$\mathbf{n}\cdot\left(\mathbf{q}S-\mathbf{D}^{S}h\cdot\nabla S\right)\Big|_{Bank\,1} = M_s^{o1} \quad and \quad \mathbf{n}\cdot\left(\mathbf{q}S-\mathbf{D}^{S}h\cdot\nabla S\right)\Big|_{Bank\,2} = M_s^{o2} \tag{2.2.69}$$

where M_s^{o1} and M_s^{o2}, which appeared in Eq. (2.1.86), are the salt sources from overland into the rivers. These salt sources can be calculated using Eq. (2.1.88) if the salinity in the overland water and river water are discontinuous at the interfaces. If the salinity is continuous, then these salt sources should be formulated by imposing the continuity of salinity in the overland water and river water at the interface.

2.3 Water Flow in Three-Dimensional Subsurface Media

2.3.1 Water Flow

The governing equation of subsurface density dependent flow through saturated-unsaturated porous media can be derived based on the conservation law of water mass (Yeh, 1987; Yeh et al., 1994; Lin et al., 1997). It is written as follows.

$$\frac{\rho}{\rho_o}F\frac{\partial h}{\partial t} = \nabla\cdot\left[\mathbf{K}\cdot\left(\nabla h+\frac{\rho}{\rho_o}\nabla z\right)\right]+\frac{\rho^*}{\rho_o}q \tag{2.3.1}$$

where ρ is the density of water; ρ_o is the reference density of water; h is the referenced pressure head [L]; t is the time [t]; **K** is the hydraulic conductivity tensor [L/t]; z is the potential head [L]; ρ* is the density of source water; q is the source and/or sink [L^3/L^3/t]; and F is the water capacity [1/L] given by

$$F = a'\frac{\theta_e}{n_e}+\beta'\theta_e+n_e\frac{dS}{dh} \tag{2.3.2}$$

where a' is the modified compressibility of the medium [1/L], θ_e is the effective moisture content [L^3/L^3], n_e is the effectively porosity [L^3/L^3], β' is the compressibility of water [1/L], and S is the degree of saturation. The Darcy's velocity is given by

$$\mathbf{V} = -\mathbf{K} \cdot \left(\frac{\rho_o}{\rho} \nabla h + \nabla z \right) \tag{2.3.3}$$

To achieve transient simulation, the following initial condition needs to be given.

$$h = h_i(\mathbf{x}) \qquad in \quad R, \tag{2.3.4}$$

where R is the region of interest and h_i is the prescribed pressure head [L], which can be obtained by either field measurements or by solving the steady state version of Eq. (2.3.1).

Five types of boundary conditions are taken into account as follows.

Dirichlet boundary condition:

This boundary condition is used when pressure head can be prescribed on the boundary. It can be expressed as

$$h = h_d(\mathbf{x}, t) \qquad on \quad B_d(\mathbf{x}) = 0 \tag{2.3.5}$$

where $h_d(\mathbf{x},t)$ is the Dirichlet head on the boundary surface $B_d(\mathbf{x}) = 0$

Neumann boundary condition:

This boundary condition is employed when the flux results from pressure-head gradient is known as a function of time. It is written as

$$-\mathbf{n} \cdot \mathbf{K} \cdot \frac{\rho_o}{\rho} \nabla h = q_n(\mathbf{x}, t) \qquad on \quad B_n(\mathbf{x}) = 0 \tag{2.3.6}$$

where $q_n(\mathbf{x},t)$ is the Neumann flux and $B_n(\mathbf{x}) = 0$ is the Neumann boundary surface.

Cauchy boundary condition:

This boundary condition is employed when the flux results from total-head gradient is known as a function of time. It can be written as

$$-\mathbf{n} \cdot \left(\mathbf{K} \cdot \frac{\rho_o}{\rho} \nabla h + \mathbf{K} \cdot \nabla z \right) = q_c(\mathbf{x}, t) \qquad on \quad B_c(\mathbf{x}) = 0 \tag{2.3.7}$$

where $q_c(\mathbf{x},t)$ is the Cauchy flux and $B_c(\mathbf{x}) = 0$ is the Cauchy boundary surface.

River Boundary Condition:

This boundary condition is employed when there is a thin layer of medium separating the river and the subsurface media.

$$-\mathbf{n}\cdot\mathbf{K}\cdot\left(\frac{\rho_o}{\rho}\nabla h+\nabla z\right)=-\frac{K_R}{b_R}\left(h_R-h\right)\qquad on\quad B_r(\mathbf{x})=0 \tag{2.3.8}$$

where K_R is the hydraulic conductivity of the thin layer, b_R is the thickness of the thin layer, h_R is the water depth in the river, and $B_r(\mathbf{x}) = 0$ is the surface between the river and subsurface media.

Variable Boundary Condition:

This boundary condition is usually used for the ground surface boundary when the coupling of surface and subsurface systems is not taken into account.

(1) During precipitation periods:

$$h=h_p(\mathbf{x},t)\quad iff\quad -\mathbf{n}\cdot\mathbf{K}\cdot\left(\frac{\rho_o}{\rho}\nabla h+\nabla z\right)\geq q_p(\mathbf{x},t)\quad on\quad B_v(\mathbf{x})=0 \tag{2.3.9}$$

or

$$-\mathbf{n}\cdot\mathbf{K}\cdot\left(\frac{\rho_o}{\rho}\nabla h+\nabla z\right)=q_p(\mathbf{x},t)\quad iff\quad h\leq h_p\quad on\quad B_v(\mathbf{x})=0 \tag{2.3.10}$$

(2) During non-precipitation period:

$$h=h_p(\mathbf{x},t)\quad iff\quad -\mathbf{n}\cdot\mathbf{K}\cdot\left(\frac{\rho_o}{\rho}\nabla h+\nabla z\right)\geq 0\quad on\quad B_v(\mathbf{x})=0 \tag{2.3.11}$$

$$h=h_m(\mathbf{x},t)\quad iff\quad -\mathbf{n}\cdot\mathbf{K}\cdot\left(\frac{\rho_o}{\rho}\nabla h+\nabla z\right)\leq q_e\quad on\quad B_v(\mathbf{x})=0 \tag{2.3.12}$$

or

$$-\mathbf{n}\cdot\mathbf{K}\cdot\left(\frac{\rho_o}{\rho}\nabla h+\nabla z\right)=q_e(\mathbf{x},t)\quad iff\quad h\geq h_m\quad on\quad B_v(\mathbf{x})=0 \tag{2.3.13}$$

where $h_p(\mathbf{x},t)$ is ponding depth, $q_p(\mathbf{x},t)$ is the flux due to precipitation, $h_m(\mathbf{x},t)$ is the minimum pressure head, and $q_e(\mathbf{x},t)$ is the potential evaporation rate on the surfaces of the variable boundary condition $B_v(\mathbf{x}) = 0$. Only one of Eqs. (2.3.9) through (2.3.13) is used at any point on the variable boundary at any time.

2.3.2 Thermal Transport

The thermal transport equation is derived based on the conservation principle of energy as:

$$\frac{\partial\left[\left(\rho_w C_w\theta+\rho_b C_m\right)T\right]}{\partial t}+\nabla\cdot\left(\rho_w C_w\mathbf{V}T\right)-\nabla\cdot\left(\mathbf{D}^{\mathbf{H}}\cdot\nabla T\right)=H^a+H^c \tag{2.3.14}$$

where ρ_w is the water density [M/L^3]; C_w is the heat capacity of water [L^2/t^2/T]; θ is the moisture content [L^3/L^3]; ρ_b is the bulk density of the media [M/L^3]; C_m is the heat capacity of the matrix [L^2/t^2/T]; T is the temperature [T]; $\mathbf{D}^{\mathrm{H}}$ is the apparent thermal conductivity tensor including the effect of dispersion, diffusion, and conduction [E/t/L/T = ML/t^3/T, where E is the unit of energy]; H^a is the heat source due to artificial injection/withdraw [E/t/L^3 = M/L/t^3], and H^c is the heat source due to chemical reaction [E/t/L^3 = M/L/t^3].

In addition to the initial boundary condition, boundary conditions must be specified for the temperature. Five types of global boundary conditions are provided in this report as follows.

Dirichlet boundary condition:

This condition is applied when the temperature is prescribed as a function of time on the boundaries:

$$T(\mathbf{x},t) = T_{db}(\mathbf{x},t) \quad on \quad B_d(\mathbf{x}) = 0 \tag{2.3.15}$$

where $T_{db}(\mathbf{x},t)$ is a time-dependent temperature on the Dirichlet boundary $B_d(\mathbf{x}) = 0$ [T].

Variable boundary condition:

This boundary condition is employed when the flow direction would change with time during simulations. Two cases are considered, regarding to the flow direction on the boundary.

< Case 1 > Flow is coming in from outside:

$$\mathbf{n}\cdot\left(\rho_w C_w \mathbf{V}T - \mathbf{D}^{\mathbf{H}}\cdot\nabla T\right) = \mathbf{n}\cdot\rho_w C_w \mathbf{V}T_{vb}(\mathbf{x},t) \quad on \quad B_v(\mathbf{x}) = 0 \tag{2.3.16}$$

< Case 2 > Flow is going out from inside:

$$-\mathbf{n}\cdot\mathbf{D}^{\mathbf{H}}\cdot\nabla T = 0 \quad on \quad B_v(\mathbf{x}) = 0 \tag{2.3.17}$$

where $T_{vb}(\mathbf{x},t)$ is a time-dependent temperature on the variable boundary, $B_v(\mathbf{x}) = 0$, [T], which is associated with the incoming flow.

Cauchy boundary condition*:*

This boundary condition is employed when the total heat-flow rate is given at the river/stream boundary. Usually, this boundary is an upstream boundary node. The conditions can be expressed as

$$\mathbf{n}\cdot\left(\rho_w C_w \mathbf{V}T - \mathbf{D}^{\mathbf{H}}\cdot\nabla T\right) = H_{cb}(\mathbf{x},t) \quad on \quad B_c(\mathbf{x}) = 0 \tag{2.3.18}$$

where $H_{cb}(\mathbf{x},t)$ is total heat flux through the Cauchy boundary, $B_c(\mathbf{x}) = 0$, [E/L^2/t = M/t^3, where E denotes the unit of energy], which takes a positive value if it is going out of the region and a negative value if it is coming into the region.

Neumann boundary condition:

This boundary condition is used when the conductive heat-flow rate is known at the river/stream boundary node. It can be written as

$$-\mathbf{n}\cdot\mathbf{D}^{\mathbf{H}}\cdot\nabla T = H_{nb}(\mathbf{x},t) \quad on \quad B_n(\mathbf{x}) = 0 \tag{2.3.19}$$

where $H_{nb}(\mathbf{x},t)$ is the heat flux through the Neumann boundary, $B_n(\mathbf{x}) = 0$, [E/L^2/t].

Atmosphere-subsurface interface boundary condition:

At the interface of the atmosphere and subsurface media, a heat budget boundary condition is specified as

$$-\mathbf{n}\cdot\left(\rho_w C_w \mathbf{V}T - \mathbf{D}^{\mathbf{H}}\cdot\nabla T\right) = H_n - H_b - H_e - H_s \tag{2.3.20}$$

where H_n, H_b, H_e, and H_s are calculated using Eqs. (2.1.71) through (2.1.76).

In addition to the five types of global boundary conditions, two interface boundary conditions may be specified: one for the exchange of energy/heat flux between the subsurface media and river/stream network and the other for energy/heat exchange between the subsurface media and the overland. Mathematically, these boundary conditions are described below.

Subsurface-river interface boundary condition*:*

$$\int_P \mathbf{n}\cdot\left(\rho_w C_w \mathbf{V}T - \mathbf{D}^{\mathbf{H}}\cdot\nabla T\right)dP = S_h^i \tag{2.3.21}$$

where S_h^i is the heat sources in Eq. (2.1.67) and P is the wet perimeter of the river. The heat source can be calculated using Eq. (2.1.68) if the temperatures in the subsurface and river are discontinuous at the interfaces. If the temperatures are continues, then this heat source should be formulated by imposing the continuity of the temperatures in the subsurface and river water at the interfaces.

Subsurface-overland interface boundary condition:

$$\mathbf{n}\cdot\left(\rho_w C_w \mathbf{V}T - \mathbf{D}^{\mathbf{H}}\cdot\nabla T\right) = H_i \tag{2.3.22}$$

where H_i is the heat source in Eq. (2.2.54). This heat source can be calculated using Eq. (2.2.55) if the temperatures in the subsurface and overland are discontinuous at the interface. If the temperatures are continues, then this heat source should be formulated by imposing the continuity of the temperatures in the subsurface and overland at the interface.

2.3.3 Salinity Transport

$$\frac{\partial(\theta S)}{\partial t} + \nabla\cdot(\mathbf{V}S) - \nabla\cdot\left(\theta\mathbf{D}^{\mathbf{S}}\cdot\nabla S\right) = S^{as} \qquad \textbf{(2.3.23)}$$

where S is the salinity [M/L^3]; $\mathbf{D}^{\mathbf{S}}$ is the longitudinal dispersion coefficient [L^2/t]; and S^{as} is the artificial source of the salt [M/L^3/t].

As in thermal transport, four types of global boundary conditions for salinity transport are provided in this report as follows.

Dirichlet boundary condition:

This condition is applied when the salinity is prescribed as a function of time on the boundaries:

$$S(x,t) = S_{db}(\mathbf{x},t) \quad on \quad B_d(\mathbf{x}) = 0 \qquad \textbf{(2.3.24)}$$

where $S_{db}(\mathbf{x},t)$ is a time-dependent salinity on the Dirichlet boundary, $B_d(\mathbf{x}) = 0$, [M/L^3].

Variable boundary condition:

This boundary condition is employed when the flow direction would change with time during simulations. Two cases are considered, regarding to the flow direction on the boundary.

< Case 1 > Flow is coming in from outside:

$$\mathbf{n}\cdot\left(\mathbf{V}S - \theta\mathbf{D}^{\mathbf{S}}\cdot\nabla S\right) = \mathbf{n}\cdot VS_{vb}(\mathbf{x},t) \quad on \quad B_v(\mathbf{x}) = 0 \qquad \textbf{(2.3.25)}$$

< Case 2 > Flow is going out from inside:

$$-\mathbf{n}\cdot\theta\mathbf{D}^{\mathbf{S}}\cdot\nabla S = 0 \quad on \quad B_v(\mathbf{x}) = 0 \qquad \textbf{(2.3.26)}$$

where $S_{vb}(\mathbf{x},t)$ is a time-dependent salinity [M/L^3] on the variable boundary, $B_v(\mathbf{x}) = 0$, which is associated with the incoming flow.

Cauchy boundary condition:

This boundary condition is employed when the total salt-flow rate is given at pervious boundaries. Usually, this boundary is a flow-in boundary. The conditions are expressed as

$$\mathbf{n}\cdot\left(\mathbf{V}S - \theta\mathbf{D}^{\mathbf{S}}\cdot\nabla S\right) = Q_{scb}(\mathbf{x},t) \quad on \quad B_c(\mathbf{x}) = 0 \qquad \textbf{(2.3.27)}$$

where $Q_{scb}(\mathbf{x},t)$ is total salt-flow rate [M/L^2/t] through the Cauchy boundary, $B_c(\mathbf{x}) = 0$, which takes a positive value if it is going out of the region and a negative value if it is coming into the region.

Neumann boundary condition:

This boundary condition is used when the dispersive salt-flow rate is known at the boundary. It can be written as

$$-\mathbf{n}\cdot\theta\mathbf{D}^{\mathbf{S}}\cdot\nabla S = Q_{snb}\left(\mathbf{x},t\right) \tag{2.3.28}$$

where $Q_{snb}\left(\mathbf{x},t\right)$ is the salt flux through the Neumann boundary, $B_n(\mathbf{x}) = 0$, [M/L^2/t].

In addition to the four types of global boundary conditions, two interface boundary conditions may be specified: one for the exchange of salt flux between the subsurface media and river/stream network and the other for salt exchange between the subsurface media and the overland. Mathematically, these boundary conditions are described below.

Subsurface-river interface boundary condition:

$$\int_P \mathbf{n}\cdot\left(\mathbf{V}S - \theta\mathbf{D}^{\mathbf{S}}\cdot\nabla S\right)dP = M_s^i \tag{2.3.29}$$

where M_s^i is the salt source in Eq. (2.1.86) and P is the wet perimeter of the river. The salt source can be calculated using Eq. (2.1.87) if the salinity in the subsurface and river is discontinuous at the interfaces. If the salinity is continuous, then this salt source should be formulated by imposing the continuity of the salinity in the subsurface and river at the interface.

Subsurface-overland interface boundary condition:

$$\mathbf{n}\cdot\left(\mathbf{V}S - \theta\mathbf{D}^{\mathbf{S}}\cdot\nabla S\right) = M_s^{is} \tag{2.3.30}$$

where M_s^{is} is the salt source in Eq. (2.2.62). This salt source can be calculated using Eq. (2.2.63) if the salinity in the subsurface and overland is discontinuous at the interface. If the salinity is continuous, then this salt source should be formulated by imposing the continuity of the salinity in the subsurface and overland at the interface.

2.4 Coupling Fluid Flows Among Various Media

One of the critical issues in a first principle physics-based watershed model is its treatments of coupling among various media. There appear a number of watershed models that have dealt with each component medium on the bases of first principle in the past decade (MIKE11-MIKE SHE [Abbott et al., 1986a, 1986b], SHETRAN [Ewen et al., 2000], MODFLOW-HMS [HydroGeoLogic, Inc., 2001], InHM [VanderKwaak, 1999], GISWA [Wigmosta and Perkins, 1997], SFRSM-HSE [SFWMD, 2005], COSFLOW [Yeh et al., 1997], WASH123D Version 1.0 [Yeh et al., 1998]). However, rigorous considerations on coupling among media seemed lacking. For example, a linkage term is normally formulated between the river/stream/canal dynamics and subsurface fluid flow (e.g., MODNET [Walton et al., 1999]) or between overland and subsurface flows (e.g.,

MIKE11-MIKE SHE [http://www.dhisoftware.com/mikeshe/; http://www.dhisoftware.com/mikeshe/components]). The linkage term usually introduces non-physical parameters. As a result, such watershed models have degraded even though each media-component module has taken a first principle physics-based approach. A rigorous treatment of coupling media should be based the continuity of mass, momentum, and state variables. This is the approach taken in this report. Mathematical statements on coupling between pairs of media are address below.

2.4.1 Coupling between River/Stream/Canal and Overland Flows

The fluxes between overland regime and canals/streams/rivers network are dynamics and depend on the water surface elevations in the vicinity of the interface between canal/stream/river and overland regime (Fig. 2.4-1). The basic principle of coupling is to impose continuous of fluxes and the state variables (water surface elevations, temperature, and salinity in the overland and in the canal) if these state variables do not exhibit discontinuity. If the state variables exhibit discontinuity, then the linkage term is used to simulate the volumetric fluxes or simplified formulations of heat fluxes and salinity fluxes are imposed.

When a levee is present on the bank of the canal (left column in Fig. 2.4-1), there are several possibilities on the dynamic interactions between overland flow and river flow dynamics. If water surfaces in both the overland regime and river are below the top of the levee, the two flow systems are decoupled (Fig. 2.4-1a).

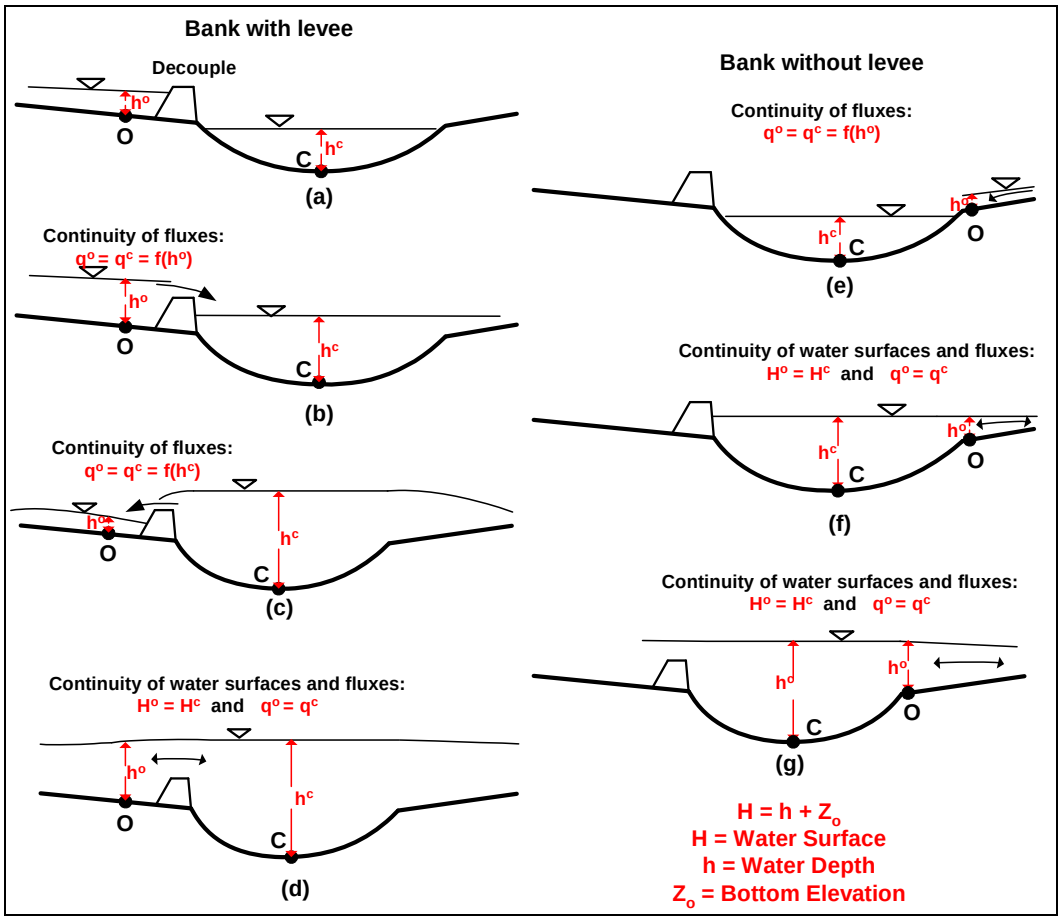

Fig. 2.4-1. Flow interactions between overland regime and canal: bank with levee (left column) and bank without levee (right column)

When the water surface in the overland regime is above the top of the levee and in the canal is below

the top of the levee (Fig. 2.4-1b), the flux is a function of the water depth in the overland regime given

$$q^{o} = q^{c} = f\left(h^{o}\right) \;\Rightarrow\; \mathbf{n}\cdot\mathbf{V}h\big|_{O} = S_1 = f\left(h^{o}; Z_{o|B}\right) \qquad \textbf{(2.4.1)}$$

where q^o is the outward normal flux of the overland flow, q^c is the lateral flow from the overland to the canal, h^o is the water depth in the overland regime, $f(h^o)$ is a prescribed function of h^o given by the shape and width of the levee, $\mathbf{n}$ is the outward unit vector (from the overland side) of the overland-canal interface, $\mathbf{V}$ is the velocity in the overland regime, S_1 is defined in Eq. (2.1.1), $Z_o|_B$ is the bottom elevation evaluated at the canal bank (in this case $Z_o|_B$ is the elevation of the top of the levee). The coupling of thermal and/or salinity transport between the overland regime and river networks for this case can be stated as

$$\begin{aligned} \mathbf{n}\cdot\left(\rho_w C_w \mathbf{q}T - \mathbf{D}^{\mathbf{H}} h\cdot\nabla T\right)\Big|_{Bank\,1} &= S_h^{o1} = \rho_w C_w S_1 T^o \qquad \textit{and} \\ \mathbf{n}\cdot\left(\mathbf{q}S - \mathbf{D}^{\mathbf{S}} h\cdot\nabla S\right)\Big|_{Bank\,1} &= M_s^{o1} = S_1 S^o \end{aligned} \qquad \textbf{(2.4.2)}$$

where T^o is the temperature of the overland water at the interface and S^o is the salinity of the overland water at the interface.

On the other hand, when the water surface in the overland regime is belowe the top of the levee and in the canal is above the top of the levee (Fig. 2.4-1c), the flux is a function of the water depth in the overland regime given by

$$q^{o} = q^{c} = f\left(h^{c}\right) \qquad \Rightarrow \qquad \mathbf{n}\cdot\mathbf{V}h\big|_{O} = S_1 = f\left(h^{c}; Z_o\big|_B\right) \qquad \textbf{(2.4.3)}$$

where h^c is the water depth in the canal and $f(h^c)$ is a prescribed function of h^c. The coupling of thermal and salinity transport between the overland regime and river networks for this case can be stated as

$$\begin{aligned} \mathbf{n}\cdot\left(\rho_w C_w \mathbf{q}T - \mathbf{D}^{\mathbf{H}} h\cdot\nabla T\right)\Big|_{Bank1} &= S_h^{o1} = \rho_w C_w S_1 T^c \qquad \textit{and} \\ \mathbf{n}\cdot\left(\mathbf{q}S - \mathbf{D}^{\mathbf{S}} h\cdot\nabla S\right)\Big|_{Bank1} &= M_s^{o1} = S_1 S^c \end{aligned} \qquad \textbf{(2.4.4)}$$

where T^c is the temperature of the canal water at the interface and S^c is the salinity of the canal water at the interface.

When the water surfaces in both the overland and canal are above the top of the levee (Fig. 2.4-1d), then the continuity of fluxes and state variables must be imposed as

$$q^o = q^c \;\Rightarrow \mathbf{n}\cdot\mathbf{V}h\big|_{O} = S_1 \quad \textit{and} \quad H^o = H^c \Rightarrow \left(h + Z_o\right)\big|_{O} = \left(h + Z_o\right)\big|_{C} \qquad \textbf{(2.4.5)}$$

where $(h + Z_o)|_O$ denotes that $(h + Z_o)$ is evaluated at point O (Fig. 2.4-1 d). Similarly, $(h + Z_o)|_C$ denotes that $(h + Z_o)$ is evaluated at point C. The coupling of thermal and/or salinity transport between the overland regime and river networks for this case can be obtained by formulating the fluxes

$$\mathbf{n}\cdot\left(\rho_w C_w \mathbf{q}T - \mathbf{D}^{\mathbf{H}} h\cdot\nabla T\right)\Big|_{Bank1} = S_h^{o1} = \rho_w C_w S_1 \frac{1}{2}\left(1+sign\left(S_1\right)T^o + \left(1-sign\left(S_1\right)\right)T^c\right)$$
$$and \quad \mathbf{n}\cdot\left(\mathbf{q}S - \mathbf{D}^{\mathbf{S}} h\cdot\nabla S\right)\Big|_{Bank1} = M_S^{o1} = S_1 \frac{1}{2}\left(\left(1+sign\left(S_1\right)\right)S^o + \left(1-sign\left(S_1\right)\right)S^c\right) \quad \textbf{(2.4.6)}$$

where *sign(S_1)* is 1.0 if the flow is from overland to canal, -1.0 if the flow is from canal to overland. For this case, the temperature and salinity in the canal may be the same as those in the overland water at the interface. If this is the case, we impose the continuity of temperature and/or salinity to yield the fluxes

$$\mathbf{n}\cdot\left(\rho_w C_w \mathbf{q}T - \mathbf{D}^{\mathbf{H}} h\cdot\nabla T\right)\Big|_{Bank1} = S_h^{o1} \quad and \quad T^o\Big|_{Bank1} = T^c$$
$$and \qquad \mathbf{n}\cdot\left(\mathbf{q}S - \mathbf{D}^{\mathbf{S}} h\cdot\nabla S\right)\Big|_{Bank1} = M_S^{o1} \quad and \quad S^o\Big|_{Bank1} = S^c \quad \textbf{(2.4.7)}$$

When a levee is not present on the bank of the canal (right column in Fig. 2.4-1), there are two possibilities on the dynamic interactions between overland flow and river flow dynamics. If water surface in the canal falls below the bank, the flux is either zero if the overland flow is not present or is nonzero and directed from the overland into the canal if overland flow is present (Fig. 2.4-1 e) as

$$q^o = q^c = f\left(h^o\right) \qquad \Rightarrow \qquad \mathbf{n}\cdot\mathbf{V}h\Big|_O = S_2 = f\left(h^o; Z_o\big|_B\right) \quad \textbf{(2.4.8)}$$

where S_2 is defined in Eq. (2.1.1) and $Z_o|_B$ is the bottom elevation evaluated at point *O* on the canal bank. The coupling of thermal and/or salinity transport between the overland regime and river networks for this case can be stated as

$$\mathbf{n}\cdot\left(\rho_w C_W \mathbf{q}T - \mathbf{D}^{\mathbf{H}} h\cdot\nabla T\right)\Big|_{Bank2} = S_h^{o2} = \rho_w C_w S_2 T^o \quad and$$
$$\mathbf{n}\cdot\left(\mathbf{q}S - \mathbf{D}^{\mathbf{S}} h\cdot\nabla S\right)\Big|_{Bank2} = M_s^{o2} = S_2 S^o \quad \textbf{(2.4.9)}$$

When the water surface in the canal is above the bank (Figs. 2.4-1f and 2.4-1.g), the flux direction can be either from the overland into the canal or from the canal into the overland depending on the flow dynamics in the overland and in the canal. The direction of the flux and its magnitude are obtained by imposing the continuity of flux and state variables

$$q^o = q^c \Rightarrow \mathbf{n}\cdot\mathbf{V}h\Big|_O = S_2 \quad and$$
$$H^o = H^c \Rightarrow \left(h+Z_o\right)\Big|_O = \left(h+Z_o\right)\Big|_C \quad \textbf{(2.4.10)}$$

The coupling of thermal and/or salinity transport between the overland regime and river networks for this case can be stated as

$$\mathbf{n}\cdot\left(\rho_w C_w \mathbf{q}T - \mathbf{D}^{\mathbf{H}} h\cdot\nabla T\right)\Big|_{Bank\,2} = S_h^{o2}$$
$$= \rho_w C_w S_2 \frac{1}{2}\left(\left(1+sign\left(S_2\right)\right)T^o + \left(1-sign\left(S_2\right)\right)T^c\right) \quad and \tag{2.4.11}$$
$$\mathbf{n}\cdot\left(\mathbf{q}S - \mathbf{D}^{\mathbf{S}} h\cdot\nabla S\right)\Big|_{Bank\,2} = M_S^{o2} = S_2\frac{1}{2}\left(\left(1+sign\left(S_2\right)\right)S^o + \left(1-sign\left(S_2\right)\right)S^c\right)$$

For these two cases (Fig. 2.4-1f and 2.4-1g), the temperature and salinity in the canal may be the same as those in the overland water at the interface. If this is the case, we impose the continuity of temperature and/or salinity to yield the fluxes

$$\mathbf{n}\cdot\left(\rho_w C_w \mathbf{q}T - \mathbf{D}^{\mathbf{H}} h\cdot\nabla T\right)\Big|_{Bank\,2} = S_h^{o1} \quad and \quad T^o\Big|_{Bank\,2} = T^c \quad and$$
$$\mathbf{n}\cdot\left(\mathbf{q}S - \mathbf{D}^{\mathbf{S}} h\cdot\nabla S\right)\Big|_{Bank\,2} = M_s^{o1} \quad and \quad S^o\Big|_{Bank\,2} = S^c \tag{2.4.12}$$

2.4.2 Coupling between Overland and Subsurface Flows

The fluxes between overland and subsurface media are obtained by imposing continuous of fluxes and state variables if these state variables do not exhibit discontinuity. If the state variables exhibit discontinuity, then a linkage term is used to simulate the fluxes. Consider the interaction between the overland subsurface and subsurface flows. There are two cases: in one case, there is no impermeable layers on the ground surface (Fig. 2.4-2a) and, in another case, there are thin layers of very impermeable layers such as pavements or sediment deposits on the ground surface (Fig. 2.4-2b).

For the case of no impermeable layers on the ground surface (Fig. 2.4-2a), it can easily be seen that the pressures in the overland flow (if it is present) and in the subsurface media will be continuous across the interface. Thus, the interaction must be simulated by imposing continuity of pressures and fluxes as

$$h^o = h^s \quad and \quad Q^o = Q^s \quad \Rightarrow \quad I = -\mathbf{n}\cdot\mathbf{K}\cdot\left(\frac{\rho_o}{\rho}\nabla h^s + \nabla z\right) \tag{2.4.13}$$

where h^o is the water depth in the overland if it is present, h^s is the pressure head in the subsurface, Q^o is the flux from the overland to the interface and Q^s is the flux from the interface to the subsurface media, I is defined in Eq. (2.2.1), **n** is an outward unit vector of the ground subsurface, **K** is the hydraulic conductivity tensor, and h^s is the pressure head in the subsurface media. The use of a linkage term such as $Q^o = Q^s = K(h^o - h^s)$, while may be convenient, is not appropriate because it introduces a non-physics parameter K. The calibration of K to match simulations with field data renders the coupled model ad hoc even though the overland and subsurface flows are each individually physics-based.

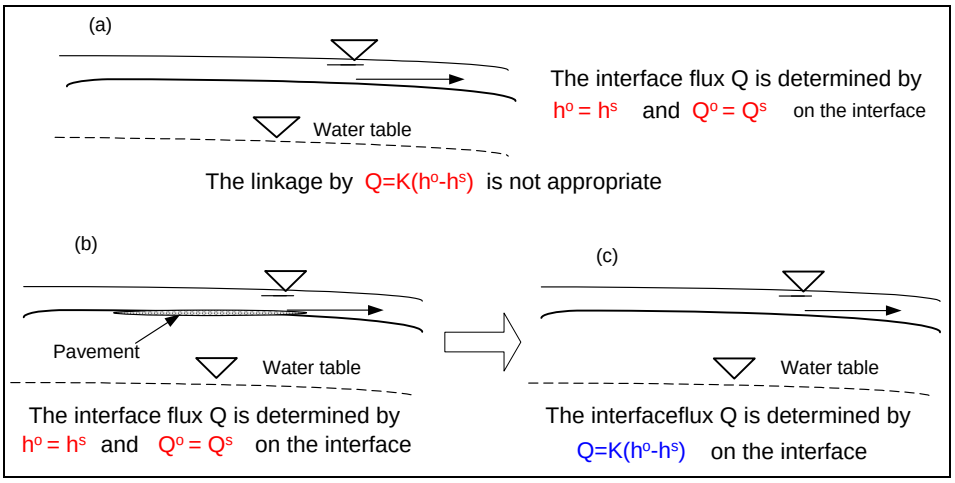

Fig. 2.4-2. Flow interactions between overland regime and subsurface media.

For the cases with thin impervious layers (Fig. 2.4-2b), one can include the impervious layers as part of the subsurface media or exclude these layers from the modeling. If one includes the thin layers, then it is obvious the pressures in the overland flow and in the layer are continuous across the interface, thus continuity of pressures and fluxes must imposed to simulate the interaction. On the other hand, if the thin layers are not included, it is obvious, the pressures in the overland flow and the subsurface are not continuous across the removed layers, then a linkage term is used to model the flux between across interface as

$$Q^o = Q^s \qquad \Rightarrow \qquad I = -n \cdot K \cdot \left(\frac{\rho_o}{\rho} \nabla h^s + \nabla z \right) = \frac{K_b}{b} \left(h^s - h^o \right) \tag{2.4.14}$$

where K_b and b are the hydraulic conductivity and thickness, respectively, of the removed bottom sediment layer. These parameters in the linkage term are the material properties and geometry of the removed layer. These parameters, in theory, can be obtained independent of model calibration.

The coupling of thermal and/or salinity transport between the overland regime and subsurface media can be stated as

$$\begin{aligned} &\mathbf{n} \cdot \left(\rho_w C_w V T - \mathbf{D^H} \cdot \nabla T \right) = H_i = \rho_w C_w I \frac{1}{2} \left(\left(1 + sign(I) \right) T^s + \left(1 - sign(I) \right) T^o \right) \\ &\textit{and} \quad \mathbf{n} \cdot \left(V S - \theta \mathbf{D^S} \cdot \nabla S \right) = M_s^{is} = I \frac{1}{2} \left(\left(1 + sign(I) \right) S^s + \left(1 - sign(I) \right) S^o \right) \end{aligned} \tag{2.4.15}$$

where *sign(I)* is 1.0 if I is positive and is -1.0 if negative; T^s is the temperature of subsurface water at the interface; T^o is the temperature of overland water at the interface; S^s is the salinity of subsurface water at the interface; and S^o is the salinity of overland water at the interface.

The temperature and salinity in the overland water may be the same as those in the subsurface water at the interface. If this is the case, we impose the continuity of temperature and/or salinity to yield the fluxes

$$\mathbf{n}\cdot\left(\rho_w C_w \mathbf{V}T - \mathbf{D}^{\mathbf{H}}\cdot\nabla T\right) = H_i \text{ and } T^s\Big|_{\text{on the surface}} = T^o \text{ and}$$
$$\mathbf{n}\cdot\left(\mathbf{V}S - \theta\mathbf{D}^{\mathbf{S}}\cdot\nabla S\right) = M_s^{is} \quad \text{and} \quad S^s\Big|_{\text{on the surface}} = S^o \tag{2.4.16}$$

2.4.3 Coupling between Subsurface and River/Stream/Canal Flows

The fluxes between canal and subsurface are obtained by imposing continuous of fluxes and state variables if these state variables do not exhibit discontinuity. If the state variables exhibit discontinuity, then a linkage term is used to simulate the fluxes. Consider the interaction between the canal and subsurface. There are two cases: in one case, there is not any thin layer of sediment materials (Fig. 2.4-3a) and, in another case, there are thin layers of sediment materials between the canal bottom and the top of surface media (Fig. 2.4-3b).

For the case of no thin layer of sediments (Fig. 2.4-3a), it can easily be seen that the pressures in the canal and in the subsurface media will be continuous across the interface of canal bottom and subsurface media. Thus, the interaction must be simulated by imposing continuity of pressure and flux as follows.

$$h^c = h^s \quad \text{and} \quad Q^c = Q^s \Rightarrow S_I = \int_P \left[-\mathbf{n}\cdot\mathbf{K}\cdot\left(\frac{\rho_O}{\rho}\nabla h^s + \nabla z\right)\right] dP \tag{2.4.17}$$

where h^c is the water depth in the canal, h^s is the pressure head in the subsurface, Q^c is the flux from the canal to the interface and Q^s is the flux from the interface to the subsurface media, S_I is defined in Eq. (2.1.1), **n** is an outward unit vector of the subsurface media interfacing the canal, **K** is the hydraulic conductivity tensor of the subsurface media, h^s is the pressure head in the subsurface media, and P is the wet perimeter of the canal. The use of a linkage term such as $Q^c = Q^s = K(h^c - h^s)$, while may be convenient, is not appropriate because it introduces a non-physics parameter K. The calibration of K to match simulations with field data renders the coupled model ad hoc even though the canal and subsurface flows are each individually physics-based.

For the cases with thin layers of sediments (Fig. 2.4-3b), one can include the sediment layers as part of the subsurface media or exclude these layers from the modeling. If one includes the thin layers, then it is obvious the pressures in the canal and in the sediment layer are continuous across the interface of canal bottom and the top of the thin layers, thus continuity of pressures must imposed to simulate the interaction. On the other hand, if the thin layers are excluded (Fig. 2.4-3c), the pressures in the canal and subsurface are not continuous across the bottom of canal and the top of subsurface media, then, a linkage term can be used to model the flux between the canal and surface media as

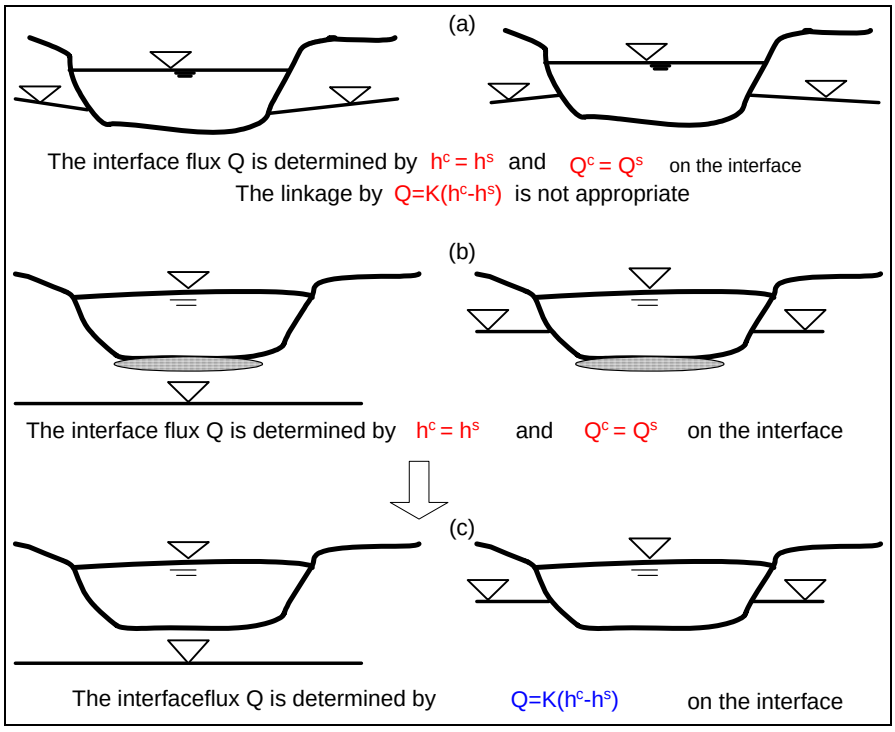

Fig. 2.4-3. Flow interactions between canal and subsurface media.

$$Q^c = Q^s \Rightarrow \int_P \left[-\mathbf{n}\cdot\mathbf{K}\cdot\left(\frac{\rho_o}{\rho}\nabla h^s + \nabla z\right)\right] dP = \int_P \frac{K_b}{b}\left(h^s - h^c\right) dP \qquad \textbf{(2.4.18)}$$

where K_b and b are the hydraulic conductivity and thickness, respectively, of the removed bottom sediment layer. These parameters in the linkage term are the material properties and geometry of the removed layer. These parameters, in theory, can be obtained independent of model calibration.

The coupling of thermal and/or salinity transport between the canal and subsurface media can be stated as

$$\int_P \mathbf{n}\cdot\left(\rho_w C_w \mathbf{V} T - \mathbf{D}^{\mathbf{H}}\cdot\nabla T\right) dP = S_h^i$$

$$= \rho_w C_w S_I \frac{1}{2}\left(\left(1+sign\left(S_I\right)\right)T^s + \left(1-sign\left(S_I\right)\right)T^c\right) \quad and \qquad \textbf{(2.4.19)}$$

$$\int_P \mathbf{n}\cdot\left(\mathbf{V}S - \theta\mathbf{D}^{\mathbf{S}}\cdot\nabla S\right) dP = M_s^i = S_I \frac{1}{2}\left(\left(1+sign\left(S_I\right)\right)S^s + \left(1-sign\left(S_I\right)\right)S^c\right)$$

where $sign(S_I)$ is 1.0 if S_I is positive and is -1.0 if negative; T^s is the temperature of subsurface water at the interface; T^c is the temperature of canal water at the interface; S^s is the salinity of subsurface water at the interface; and S^c is the salinity of canal water at the interface.

Similar to the interaction between the overland regime and subsurface media, the temperature and salinity in the canal water may be the same as those in the subsurface water at the interface. If this is

the case, we impose the continuity of temperature and/or salinity to yield the fluxes

$$\int_P \mathbf{n}\cdot\left(\rho_w C_w \mathbf{V}T - \mathbf{D}^{\mathbf{H}}\cdot\nabla T\right)dP = S_h^i \quad and \quad T^s\Big|_{on\ the\ surface} = T^c \quad and$$
$$\int_P \mathbf{n}\cdot\left(\mathbf{V}S - \theta\mathbf{D}^S\cdot\nabla S\right)dP = = M_s^i \quad and \quad S^s\Big|_{on\ the\ surface} = S^c \qquad \textbf{(2.4.20)}$$

2.5 Sediment and Water Quality Transport in 1D River/Stream/Canal Networks

In WASH123D, sediments are categorized based on their physical and chemical properties. For each category of sediment, we include mobile suspended sediment particles scattered in water column and immobile bed sediment particles accumulated in river/stream bed. The distribution of suspended sediment and bed sediment is controlled through hydrological transport as well as erosion and deposition processes.

In river/stream networks, there are six phases and three forms of biochemical species. As shown in Figure 2.5-1, the six phases are suspended sediment, bed sediment, mobile water, immobile water, suspension precipitate, and bed precipitate phases; and the three forms are dissolved biochemicals, particulate biochemicals sorbed onto sediments, and precipitates. Usually, biochemical species in the suspended sediment phase, the mobile water phase and the suspension precipitate phase are considered mobile. Biochemical species in the bed sediment phase, the immobile water phase and the bed precipitate phase are considered immobile.

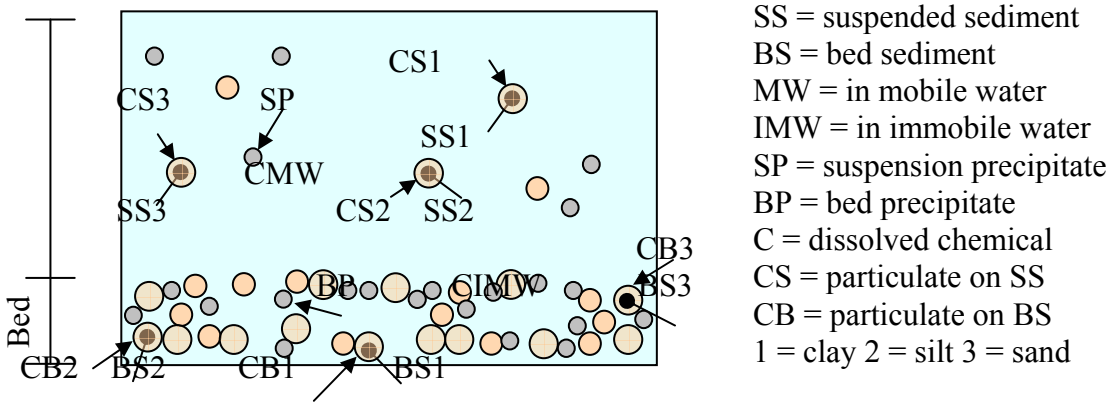

Fig. 2.5-1. Sediments and Chemicals in River/Stream Networks

A reactive system is completely defined by specifying biogeochemical reactions (Yeh, et al. 2001a). In the transport simulation, biogeochemical reactions can be divided into two classes (Rubin, 1983): (1) Fast/equilibrium reactions, and (2) Slow/kinetic reactions. The former are sufficiently fast compared to transport time scale and reversible, so that local equilibrium may be assumed. The latter are not sufficiently fast compared to transport time scale. They are either reversible or irreversible, where the local equilibrium formulation is inappropriate.

As shown in Figure 2.5-2, the biogeochemical reactions considered in the model can be categorized into ten types which take place between various phases: (1) aqueous complexation in column water, (2) adsorption/desorption or ion-exchange to suspended sediment, (3) precipitation/dissolution in water column, (4) adsorption/desorption or ion-exchange between column water and bed sediment, (5) aqueous complexation in pore water, (6) adsorption/desorption or ion-exchange to bed sediment, (7) precipitation/dissolution in bed, (8) volatilization reactions from water column to the atmopshere, (9) diffusion reactions between column and pore water, and (10) sedimentation reactions. Any individual reaction representing any of these chemical and physical processes may be simulated as kinetic or as equilibrium, which makes the code extremely flexible for application to a wide range of biogeochemical transport problems.

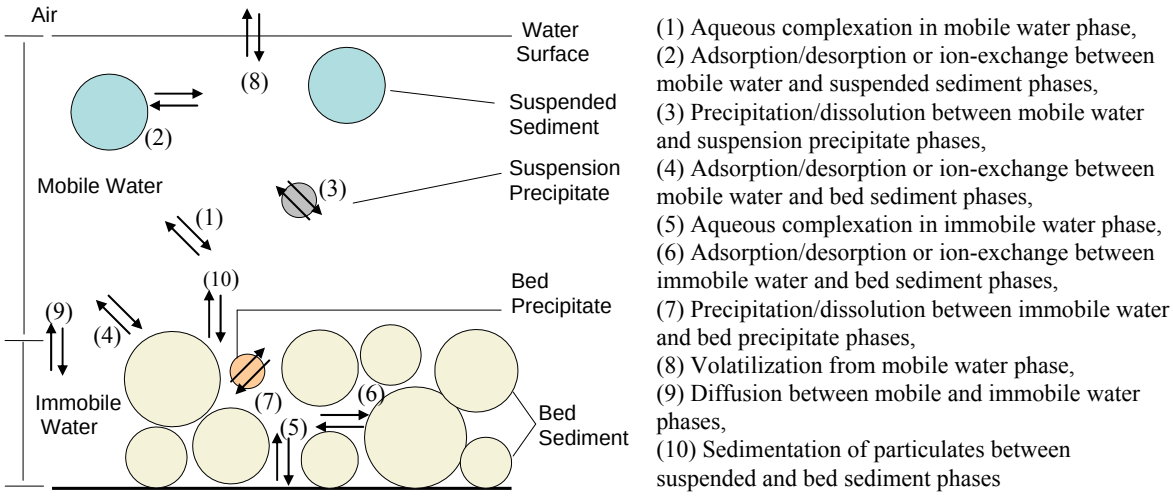

Fig. 2.5-2. Biogeochemical Reactions Considered in the Model

2.5.1 Bed Sediment

The balance equation for bed sediments is simply the statement that the rate of mass change is due to erosion/deposition as

$$\frac{\partial(PM_n)}{\partial t} = P(D_n - R_n) + M^{is}_{M_n}, \quad n \in [1, N_s] \qquad \textbf{(2.5.1)}$$

where P is the river/stream cross-sectional wetted perimeter [L], M_n is wetted perimeter-averaged concentration of the n-th bed sediment in mass per unit bed area [M/L^2], D_n is the deposition rate of the n-th sediment in mass per unit bed area per unit time [M/L^2/T], R_n is the erosion rate of the n-th sediment in mass per unit bed area per unit time [M/L^2/T], $M^{is}_{M_n}$ is the source of the n-th sediment from groundwater exfiltration in mass per unit river length [M/L/T], and N_S is the total number of sediment size fractions. Concentrations of all bed sediments must be given initially for transient simulations. No boundary condition is needed for bed sediments. In equation (2.5.1), we estimate the deposition and erosion rates using the different equations for cohesive and non-cohesive sediments.

For cohesive sediments, e.g., silt and clay, following equations are used (Yeh et al., 1998; Gerritsen

et al., 2000)

$$D_n = \min\left(V_{sn} S_n P_{Dn},\ S_n h/\Delta t\right) \qquad \text{where} \qquad P_{Dn} = \max\left(0,\ 1-\tau_b/\tau_{cDn}\right) \tag{2.5.2}$$

and

$$R_n = \min\left(E_{0n} P_{Rn},\ DMA_n/\Delta t\right) \qquad \text{where} \qquad P_{Rn} = \max\left(0,\ \tau_b/\tau_{cRn}-1\right) \tag{2.5.3}$$

where V_{sn} is the settling velocity of the n-th sediment [L/T], S_n is the cross-section-averaged suspended concentration of n-th sediment [M/L^3], h is the water depth [L], Δt is the time step size [T], τ_b is the bottom shear stress or the bottom friction stress [M/L/T^2], τ_{cDn} is the critical shear stress for the deposition of the n-th sediment [M/L/T^2], E_{0n} is the erodibility of the n-th sediment [M/L^2/T], DMA_n is the amount of locally available dry matter of n-th sediment, expressed as dry weight per unit area [M/L^2], τ_{cRn} is the critical shear stress for the erosion of the n-th sediment [M/L/T^2].

For Non-cohesive sediments, e.g., sand, we have two options.

Option 1 (Prandle et al., 2000)

$$D_n = \min\left(V_{sn} S_n N_{Dn},\ S_n h/\Delta t\right) \qquad \text{where} \qquad N_{Dn} = \max\left[0,\ 1-\left(V_{cDn}/V_{cRn}\right)^2\right] \tag{2.5.4}$$

and

$$R_n = \min\left(E_{0n} N_{Rn},\ DMA_n/\Delta t\right) \qquad \text{where} \qquad N_{Rn} = \max\left(0,\ V_{cDn}/V_{cRn}-1\right) \tag{2.5.5}$$

where V_{cDn} and V_{cRn} represent the critical friction velocities for the onset of deposition and erosion, respectively [L/T].

Option 2 (Yeh et al., 1998)

$$D_n = \max\left(\frac{G_{sAn}-G_{sn}}{\Delta L}, 0\right) \tag{2.5.6}$$

and

$$R_n = \max\left(\frac{G_{sn}-G_{sAn}}{\Delta L}, 0\right) \tag{2.5.7}$$

where G_{sAn} is the actual load rate of the n-th sediment per unit width at a upstream location [M/L/T], G_{sn} is the maximum load rate of the n-th size fraction sediment per unit width at a downstream location [M/L/T], ΔL is the distance between the upstream and the downstream locations.

$$G_{sAn} = S_n V R \tag{2.5.8}$$

and

$$G_{sn} = 10\frac{\rho^2 VRS(\tau_b-\tau_{crn})}{g d_n(\rho_{sn}-\rho)^2} \tag{2.5.9}$$

where V is the river/stream flow velocity [L/T], R is hydraulic radius [L], ρ is the density of water [M/L^3], S is the friction slope, τ_{crn} is the critical bottom shear stress of the n-th sediment at which sediment movement begins [M/L/T^2], g is gravity [L/T^2], d_n is the median diameter of the n-th sediment particle [L], and ρ_{sn} is the density of the n-th sediment [M/L^3].

It should be noted that equations (2.5.2) through (2.5.9) are the sample models programmed in the computer code to estimate sediment deposition and erosion rate. Any other phenomenological model equation can be easily incorporated in the code.

2.5.2 Suspended Sediments

The continuity equation of suspended sediment can be derived based on the conservation law of material mass as (Yeh et al., 2005):

$$\frac{\partial (AS_n)}{\partial t} + \frac{\partial (QS_n)}{\partial x} - \frac{\partial}{\partial x}\left(AK_x \frac{\partial S_n}{\partial x} \right) = M_{S_n}{}^{as} + M_{S_n}{}^{os1} + M_{S_n}{}^{os2} + M_{S_n}{}^{is} + (R_n - D_n)P, \quad n \in [1, N_s] \tag{2.5.10}$$

where S_n is the cross-sectional-averaged concentration of the *n*-th suspended sediment in the unit of mass per unit column volume [M/L^3], K_x is the dispersion coefficient [L^2/T], $M_{S_n}{}^{as}$ is the artificial source of the *n*-th suspended sediment [M/L/T], $M_{S_n}{}^{is}$ is the source of the n-th suspended sediment from groundwater exfiltration [M/L/T], and $M_{S_n}{}^{os1}$ and $M_{S_n}{}^{os2}$ are overland sources of the *n*-th suspended sediment from river bank *1* and *2*, respectively [M/L/T].

Concentrations of all suspended sediments must be given initially for transient simulations. Four types of boundary conditions are taken into account for suspended sediments, including Dirichlet, Variable, Cauchy, and Neumann boundary conditions (Yeh et al., 2005).

Dirichlet boundary condition: Dirichlet boundary conditions are prescribed on the boundary where the suspended sediment concentration is known,

$$S_n = S_{dn}(x_b, t) \qquad \text{on} \qquad B_d(x_b) \tag{2.5.11}$$

where x_b is the axis coordinate of the boundary node [L], $S_{dn}(x_b, t)$ is a time-dependent Dirichlet concentration of the *n*-th fraction size on the boundary $B_d(x_b)$ [M/L^3].

Variable boundary condition: Variable boundary conditions are normally specified on the boundary where the flow direction can change with time or on any open boundary. On the variable boundary, when the flow is directed into the region of the interest, the mass rate into the region is given by the product of the flow rate and concentration of the incoming fluid. When the flow is directed out of the region, the sediment mass is assumed carried out via advection. Mathematically, a variable boundary condition is given as

$$n\left(QS_n - AK_x \frac{\partial S_n}{\partial x} \right) = nQS_{vn}(x_b, t) \;\; if \;\; nQ \le 0 \;\; on \;\; B_v(x_b) \tag{2.5.12}$$

and

$$-nAK_x \frac{\partial S_n}{\partial x} = 0 \;\; if \;\; nQ \ge 0 \;\; on \;\; B_v(x_b) \tag{2.5.13}$$

where *n* is a unit outward direction, and $S_{vn}(x_b,t)$ is a time-dependent concentration at the boundary that is associated with the incoming flow on the variable boundary $B_v(x_b)$ [M/L^3].

Cauchy boundary condition: This boundary condition is employed when the total material flow rate is given. Usually, this boundary is an upstream flux boundary.

$$n\left(QS_n - AK_x\frac{\partial S_n}{\partial x}\right) = Q_{S_n c}(x_b,t) \;\; on \;\; B_c(x_b) \qquad \textbf{(2.5.14)}$$

where $Q_{S_n c}(x_b,t)$ is a time-dependent material flow rate at the Cauchy boundary boundary [M/t] $B_c(x_b)$.

Neumann boundary condition: This boundary condition is used when the diffusive material flow rate is known at the boundary node.

$$-nAK_x\frac{\partial S_n}{\partial x} = Q_{S_n n}(x_b,t) \;\; on \;\; B_n(x_b) \qquad \textbf{(2.5.15)}$$

where $Q_{S_n n}(x_b,t)$ is a time-dependent diffusive material flow rate at the boundary $B_n(x_b)$ [M/t].

2.5.3 Immobile Bed-Sediment Species

The balance equation for immobile species is simply the statement that the rate of mass change is due to biogeochemical reaction as:

$$\frac{\partial(Ph_b\rho_{bw}\theta_b C_{bw})}{\partial t} = Ph_b r_{Cbw}\big|_N' \qquad \textbf{(2.5.16)}$$

$$\frac{\partial(Ph_b\rho_{bw}\theta_b C_{bp})}{\partial t} = Ph_b r_{Cbp}\big|_N' \qquad \textbf{(2.5.17)}$$

$$\frac{\partial(PM_n C_{bsn})}{\partial t} = Ph_b r_{Cbsn}\big|_N' \qquad \textbf{(2.5.18)}$$

where h_b is the river/stream bed depth [L], ρ_{bw} is the density of bed pore-water [M/L^3], θ_b is the porosity of the bed sediment [L^3/L^3], C_{bw} is the concentration of dissolved chemical in the immobile pore-water phase in the unit of chemical mass per bed-water mass [M/M], $r_{Cbw}\big|_N$' is the production rate of C_{bw} due to all N reactions in the unit of chemical mass per bed volume per time [M/L^3/t], C_{bp} is the concentration of bed precipitate in the unit of chemical mass per bed-water mass [M/M], $r_{Cbp}\big|_N$' is the production rate of C_{bp} due to all N reactions in the unit of chemical mass per bed volume per time [M/L^3/t], C_{bsn} is the concentration of particulate sorbed on to bed sediment of the *n*-th fraction size in the unit of chemical mass per unit of bed-sediment mass [M/M], M_n is the concentration of the *n*-th bed sediment in the unit of sediment mass per bed area [M/L^2], $r_{Cbsn}\big|_N$' is the production rate of C_{bsn} due to all N reactions in the unit of chemical mass per bed volume per time [M/L^3/t].

Define

$$r_i\big|_N = Ph_b r_i\big|_N \,'/A \quad where \quad i = C_{bw},\ C_{bp},\ or\ C_{bsn} \tag{2.5.19}$$

Equation (2.5.16) through (2.5.18) can be modified as

$$\frac{\partial(Ph_b\rho_{bw}\theta_b C_{bw})}{\partial t} = Ar_{Cbw}\big|_N \tag{2.5.20}$$

$$\frac{\partial(Ph_b\rho_{bw}\theta_b C_{bp})}{\partial t} = Ar_{Cbp}\big|_N \tag{2.5.21}$$

$$\frac{\partial(PM_n C_{bsn})}{\partial t} = Ar_{Cbsn}\big|_N \tag{2.5.22}$$

Define

$$\rho_i = \begin{cases} Ph_b\rho_{bw}\theta_b / A, for\ C_{bw}\ and\ C_{bp} \\ PM_n / A, for\ C_{bsn} \end{cases} \tag{2.5.23}$$

Equation (2.5.20) through (2.5.22) can be summarized as

$$\frac{\partial(A\rho_i C_i)}{\partial t} = Ar_i\big|_N, \quad i \in M_{im} \tag{2.5.24}$$

where C_i is the concentration of species i, which is immobile, in the unit of chemical mass per unit phase mass [M/M], ρ_i is the density of the phase associated with species i [M/L^3], $r_i\big|_N$ is the production rate of species i due to all N reactions in the unit of chemical mass per column volume per time [M/L^3/t], and M_{im} is the number of immobile species. The concentrations of all immobile species must be given initially for transient simulations. No boundary conditions are needed for immobile species.

2.5.4 Mobile Column-Water Species

The continuity equation of mobile species can be derived based on the conservation law of material mass stating that the rate of mass change is due to both advective-dispersive transport and biogeochemical reactions as:

$$\frac{\partial(A\rho_w C_w)}{\partial t} + L(\rho_w C_w) = Ar_{Cw}\big|_N \tag{2.5.25}$$

$$\frac{\partial(A\rho_w C_p)}{\partial t} + L(\rho_w C_p) = Ar_{Cp}\big|_N \tag{2.5.26}$$

$$\frac{\partial(AS_n C_{sn})}{\partial t} + L(S_n C_{sn}) = Ar_{Csn}\big|_N \tag{2.5.27}$$

where ρ_w is the density of column water [M/L^3], C_w is the concentration of dissolved chemical in the mobile water phase in the unit of chemical mass per column-water mass [M/M], $r_{Cw}\big|_N$ is the production rate of C_w due to all N reactions in the unit of chemical mass per column volume per time [M/L^3/t], C_p is the concentration of suspension precipitate in the unit of chemical mass per column-water mass [M/M], $r_{Cp}\big|_N$ is the production rate of C_p due to all N reactions in the unit of chemical mass per column volume per time [M/L^3/t], C_{sn} is the concentration of particulate sorbed on to suspended sediment of the n-th fraction size in the unit of chemical mass per unit of sediment mass [M/M], S_n is the concentration of suspended sediment in the unit of sediment mass per column volume [M/L^3], $r_{Csn}\big|_N$ is the production rate of C_{sn} due to all N reactions in the unit of chemical mass per column volume per time [M/L^3/t], and L is an operator that will be defined in Eq. (2.5.30) later.

Define

$$\rho_i = \begin{cases} \rho_w \quad for \quad C_w \ and \ C_p \\ S_n \quad for \quad C_{sn} \end{cases} \tag{2.5.28}$$

Equation (2.5.25) through (2.5.27) can be summarized as

$$\frac{\partial(A\rho_i C_i)}{\partial t} + L(\rho_i C_i) = Ar_i\big|_N, \quad i \in M_m = M - M_{im} \tag{2.5.29}$$

where C_i is the concentration of species i, which is mobile, in the unit of chemical mass per unit phase mass [M/M], ρ_i is the density of the phase associated with species i [M/L^3], $r_i\big|_N$ is the production rate of species i due to all N reactions in the unit of chemical mass per column volume per time [M/L^3/t], M is the total number of chemical species, M_m is the number of mobile chemical species, and operator L is defined as

$$L(\rho_i C_i) = \frac{\partial(Q\rho_i C_i)}{\partial x} - \frac{\partial}{\partial x}\left[AK_x \frac{\partial(\rho_i C_i)}{\partial x}\right] - (M_{C_i}^{as} + M_{C_i}^{rs} - M_{C_i}^{es} + M_{C_i}^{os1} + M_{C_i}^{os2} + M_{C_i}^{is}) \tag{2.5.30}$$

where $M_{C_i}^{as}$ is the artificial source of species i [M/L/T], $M_{C_i}^{rs}$ is the rainfall source of species i [M/L/T], $M_{C_i}^{rs}$ is the sink of species i due to evaporation, $M_{C_i}^{os1}$ and $M_{C_i}^{os2}$ are the overland sources of species i from river bank *1* and *2*, respectively [M/L/T], and $M_{C_i}^{is}$ is the mass rate of the source of species i in river/stream from subsurface [M/L/T].

Concentrations of all mobile species must be given initially for transient simulations. Four types of boundary conditions are taken into account for mobile species, including Dirichlet, Variable, Cauchy, and Neumann boundary conditions (Yeh et al., 2005), which are similar to those for suspended sediment transport and are presented below:

Dirichlet boundary condition: On a Dirichlet boundary, the concentrations of all mobile species are prescribed

$$C_i = C_{idb}(x_b, t) \qquad i \in M_m \qquad on \qquad B_d(x) = 0 \tag{2.5.31}$$

where $C_{idb}(x_b,t)$ is the prescribed concentration of the *i*-th mobile species on the Dirichlet boundary $B_d(x)=0$ [M/M].

Variable boundary condition: On a variable boundary, the concentrations of all mobile species are known and they contribute to the increase of chemical masses in the region of interest when the flow is coming into the region. When the flow is going out of the region, the transport of all mobile species out of the region is assumed due to advection only, which implies that one must put an outgoing boundary far away from the source.

< Case 1 > Flow is coming in from outside (nQ < 0)

$$n\left(Q\rho_i C_i - AK_x\frac{\partial\rho_i C_i}{\partial x}\right)=(nQ)\rho_i C_{ivb}(x_b,t) \qquad i\in M_m \qquad on \qquad B_v(x)=0 \tag{2.5.32}$$

< Case 2 > Flow is going out from inside (nQ > 0).

$$-nAK_x\frac{\partial\rho_i C_i}{\partial x}=0 \qquad i\in M_m \qquad on \qquad B_v(x)=0 \tag{2.5.33}$$

where *n* is the unit outward direction and $C_{ivb}(x_b,t)$ is the concentration of the *i*-th species in the incoming fluid on the variable boundary $B_v(x)=0$ [M/M].

Cauchy boundary condition: On a Cauchy boundary chemical flux for any mobile species is prescribed

$$n\left(Q\rho_i C_i - AK_x\frac{\partial\rho_i C_i}{\partial x}\right)=Q_{C_i cb}(x_b,t) \qquad i\in M_m \qquad on \qquad B_c(x)=0 \tag{2.5.34}$$

where $Q_{C_i cb}(x_b,t)$ is the mass flux of C_i through the Cauchy boundary $B_c(x)=0$ [M/t].

Neumann boundary condition: On a Neumann boundary, chemical flux of any mobile species due to dispersion is prescribed

$$-nAK_x\frac{\partial\rho_i C_i}{\partial x}=Q_{C_i nb}(x_b,t) \qquad i\in M_m \qquad on \qquad B_n(x)=0 \tag{2.5.35}$$

where $Q_{C_i nb}(x_b,t)$ is the mass flux of C_i through the Neumann boundary $B_n(x)=0$ [M/t].

2.5.5 Diagonalization of Species Transport Equations

The temporal-spatial distribution of chemical species is described by a system of M_{im} mass balance equations [equation (2.5.24)], and M_m reactive transport equations [equation (2.5.29)]. These two equations can be recast in the following form

$$\frac{\partial(A\rho_i C_i)}{\partial t} + \alpha_i L(\rho_i C_i) = A r_i\big|_N, \quad i \in M \tag{2.5.36}$$

where M is the total number of chemical species, α_i is 0 for immobile species and 1 for mobile species.

The determination of $r_i\big|_N$ and associated parameters is a primary challenge in biogeochemical modeling. Instead of using an ad hoc method to formulate $r_i\big|_N$, we use reaction-based formulations (Steefel and Cappellen, 1998). In a reaction-based formulation, $r_i\big|_N$ is given by the summation of rates of all reactions that the i-th species participates in,

$$r_i\big|_N = \frac{d(\rho_i C_i)}{dt}\Big|_{reaction} = \sum_{k=1}^{N}\left[(\nu_{ik} - \mu_{ik})r_k\right], \quad i \in M \tag{2.5.37}$$

where ν_{ik} is the reaction stoichiometry of the i-th species in the k-th reaction associated with the products, μ_{ik} is the reaction stoichiometry of the i-th species in the k-th reaction associated with the reactants, and r_k is the rate of the k-th reaction.

Substituting equation (2.5.37) into equation (2.5.36) results in the transport equations of M chemical species described by

$$\frac{\partial(A\rho_i C_i)}{\partial t} + \alpha_i L(\rho_i C_i) = A\sum_{k=1}^{N}\left[(\nu_{ik} - \mu_{ik})r_k\right], \quad i \in M; \quad or \quad \mathbf{U}\frac{\partial \mathbf{C_A}}{\partial t} + \boldsymbol{\alpha} L(\mathbf{C}) = A\boldsymbol{\nu}\mathbf{r} \tag{2.5.38}$$

where $\mathbf{U}$ is a unit matrix, $\mathbf{C_A}$ is a vector with its components representing M species concentrations multiply the cross section area of the river [M/L], $\boldsymbol{\alpha}$ is a diagonal matrix with α_i as its diagonal component, $\mathbf{C}$ is a vector with its components representing M species concentrations [M/L^3], $\boldsymbol{\nu}$ is the reaction stoichiometry matrix, and $\mathbf{r}$ is the reaction rate vector with N reaction rates as its components. Equation (2.5.38) represents a mass balance for species i, which states that the rate of change of any species mass is due to advection-dispersion coupled with contributing reactions that describe the biogeochemical processes.

In a primitive approach, equation (2.5.38) is integrated to yield the distributions and evolutions of chemical species in a region of interest. However, when some fast equilibrium reactions take place in the system, this approach is not adequate (Fang et al., 2003). Here, we will take a diagonalization approach through decomposition. Equation (2.5.38) written in matrix form can be decomposed based on the type of biogeochemical reactions via Gauss-Jordan column reduction of reaction matrix $\boldsymbol{\nu}$. Among all the fast/equilibrium and slow/kinetic reactions, "redundant reactions" are defined as fast reactions that are linearly dependent on other fast reactions, and "irrelevant reactions" are kinetic reactions that are linearly dependent on only equilibrium reactions. In order to avoid singularity of the reaction matrix, redundant fast reactions are omitted from the system prior to decomposition. The removal of irrelevant slow reactions alleviates problems associated with rate formulation uncertainty and parameterization for these reactions.

Decomposition is performed by pivoting on the N_E equilibrium reactions and decoupling them from the N_K kinetic reactions. In other words, each fast reaction can be used to eliminate one chemical

species from simultaneous consideration. An incomplete Gauss-Jordan row decomposition of the reaction matrix $\boldsymbol{\nu}$ by pivoting on N_E equilibrium reactions will result in N_E equilibrium-variables and N_{KIV} kinetic-variables. To analyze the system behavior, it is advantageous to perform a complete decomposition, in which the reduction of the reaction matrix is done by pivoting on N_E equilibrium reactions and on N_{KI} linearly independent kinetic reactions to result in N_E equilibrium-variables, N_{KI} kinetic-variables, and N_C components. The complete decomposition is given as follows:

$$\begin{bmatrix} \mathbf{A}_{11} & \mathbf{0}_{12} & \mathbf{0}_{13} \\ \mathbf{A}_{21} & \mathbf{A}_{22} & \mathbf{0}_{23} \\ \mathbf{A}_{31} & \mathbf{A}_{32} & \mathbf{U}_{33} \end{bmatrix} \begin{Bmatrix} \dfrac{\partial \mathbf{C}_{A1}}{dt} \\ \dfrac{\partial \mathbf{C}_{A2}}{dt} \\ \dfrac{\partial \mathbf{C}_{A3}}{dt} \end{Bmatrix} + \begin{bmatrix} \mathbf{B}_{11} & \mathbf{0}_{12} & \mathbf{0}_{13} \\ \mathbf{B}_{21} & \mathbf{B}_{22} & \mathbf{0}_{23} \\ \mathbf{B}_{31} & \mathbf{B}_{32} & \boldsymbol{\alpha}_{33} \end{bmatrix} \mathrm{L}\left(\begin{Bmatrix} \mathbf{C}_1 \\ \mathbf{C}_2 \\ \mathbf{C}_3 \end{Bmatrix} \right) = \mathrm{A} \begin{bmatrix} \mathbf{D}_{11} & \mathbf{K}_{12} & \mathbf{K}_{13} \\ \mathbf{0}_{21} & \mathbf{D}_{22} & \mathbf{K}_{23} \\ \mathbf{0}_{31} & \mathbf{0}_{32} & \mathbf{0}_{33} \end{bmatrix} \begin{Bmatrix} \mathbf{r}_1 \\ \mathbf{r}_2 \\ \mathbf{r}_3 \end{Bmatrix} \quad \textbf{(2.5.39)}$$

where $\mathbf{A_{11}}$ is the submatrix of the reduced **U** matrix with size of $N_E \times N_E$, $\mathbf{A_{21}}$ is the submatrix of the reduced **U** matrix with size of $N_{KI} \times N_E$, and $\mathbf{A_{31}}$ is the submatrix of the reduced **U** matrix with size of $N_C \times N_E$; $\mathbf{0_{12}}$ is the zero submatrix of the reduced **U** matrix with size of $N_E \times N_{KI}$, $\mathbf{A_{22}}$ is the submatrix of the reduced **U** matrix with size of $N_{KI} \times N_{KI}$, and $\mathbf{A_{32}}$ is the submatrix of the reduced **U** matrix with size of $N_C \times N_{KI}$; $\mathbf{0_{13}}$ is the zero submatrix of the reduced **U** matrix with size of $N_E \times N_C$, $\mathbf{0_{23}}$ is the submatrix of the reduced **U** matrix with size of $N_{KI} \times N_C$, and $\mathbf{U_{33}}$ is the unit submatrix of the reduced **U** matrix with size of $N_C \times N_C$; $\mathbf{C_{A1}}$, $\mathbf{C_{A2}}$, and $\mathbf{C_{A3}}$ are the subvectors of the vector $\mathbf{C_A}$ with sizes of N_E, N_{KI}, and N_C, respectively; $\mathbf{B_{11}}$ is the submatrix of the reduced $\boldsymbol{\alpha}$ matrix with size of $N_E \times N_E$, $\mathbf{B_{21}}$ is the submatrix of the reduced $\boldsymbol{\alpha}$ matrix with size of $N_{KI} \times N_E$, and $\mathbf{B_{31}}$ is the submatrix of the reduced $\boldsymbol{\alpha}$ matrix with size of $N_C \times N_E$; $\mathbf{0_{12}}$ is the zero submatrix of the reduced $\boldsymbol{\alpha}$ matrix with size of $N_E \times N_{KI}$, $\mathbf{A_{22}}$ is the submatrix of the reduced $\boldsymbol{\alpha}$ matrix with size of $N_{KI} \times N_{KI}$, and $\mathbf{B_{32}}$ is the submatrix of the reduced $\boldsymbol{\alpha}$ matrix with size of $N_C \times N_{KI}$; $\mathbf{0_{13}}$ is the zero submatrix of the reduced $\boldsymbol{\alpha}$ matrix with size of $N_E \times N_C$, $\mathbf{0_{23}}$ is the submatrix of the reduced $\boldsymbol{\alpha}$ matrix with size of $N_{KI} \times N_C$, and $\boldsymbol{\alpha_{33}}$ is the diagonal submatrix of the reduced $\boldsymbol{\alpha}$ matrix with size of $N_C \times N_C$; $\mathbf{C_1}$, $\mathbf{C_2}$, and $\mathbf{C_3}$ are the subvectors of the vector **C** with sizes of N_E, N_{KI}, and N_C, respectively; $\mathbf{D_{11}}$ is the diagonal submatrix of the reduced $\boldsymbol{\nu}$ matrix with size of $N_E \times N_E$, $\mathbf{K_{12}}$ is the submatrix of the reduced $\boldsymbol{\nu}$ matrix with size of $N_E \times N_{KI}$, and $\mathbf{K_{13}}$ is the submatrix of the reduced $\boldsymbol{\nu}$ matrix with size of $N_E \times N_{KD(k)}$; $\mathbf{0_{21}}$ is the zero submatrix of the reduced $\boldsymbol{\nu}$ matrix with size of $N_{KI} \times N_E$, $\mathbf{D_{22}}$ is the diagonal submatrix of the reduced $\boldsymbol{\nu}$ matrix with size of $N_{KI} \times N_{KI}$, and $\mathbf{K_{23}}$ is the submatrix of the reduced $\boldsymbol{\nu}$ matrix with size of $N_{KI} \times N_{KD(k)}$; $\mathbf{0_{13}}$ is the zero submatrix of the reduced $\boldsymbol{\nu}$ matrix with size of $N_C \times N_E$, $\mathbf{0_{32}}$ is the zero submatrix of the reduced $\boldsymbol{\nu}$ matrix with size of $N_C \times N_{KI}$, and $\mathbf{0_{33}}$ is the zero submatrix of the reduced $\boldsymbol{\nu}$ matrix with size of $N_C \times N_{KD(k)}$; $\mathbf{r_1}$, $\mathbf{r_2}$, and $\mathbf{r_3}$ are the subvectors of the vector **r** with sizes of N_E, N_{KI}, and $N_{KD(k)}$, respectively.

For incomplete decomposition of the reaction matrix $\boldsymbol{\nu}$, Equation (2.5.39) can be connoted as

$$\begin{bmatrix} \mathbf{A}_{11} & \mathbf{0}_{12} \\ \mathbf{A}_{21} & \mathrm{U}_{22} \end{bmatrix} \begin{Bmatrix} \dfrac{\partial \mathbf{C}_{A1}}{dt} \\ \dfrac{\partial \mathbf{C}_{A2}}{dt} \end{Bmatrix} + \begin{bmatrix} \mathbf{B}_{11} & \mathbf{0}_{12} \\ \mathbf{B}_{21} & \boldsymbol{\alpha}_{22} \end{bmatrix} \mathrm{L}\left(\begin{Bmatrix} \mathbf{C}_1 \\ \mathbf{C}_2 \end{Bmatrix} \right) = \mathrm{A} \begin{bmatrix} \mathbf{D}_{11} & \mathbf{K}_{12} \\ \mathbf{0}_{21} & \mathbf{K}_{22} \end{bmatrix} \begin{Bmatrix} \mathbf{r}_1 \\ \mathbf{r}_2 \end{Bmatrix} \quad \textbf{(2.5.40)}$$

where $\mathbf{A_{11}}$ and $\mathbf{A_{21}}$ are the submatrices of the reduced **U** matrix with size of $N_E \times N_E$ and $N_{KIV} \times N_E$, respectively (note that $N_{KIV} = M - N_E = N_{KI} + N_C$); $\mathbf{0_{12}}$ and $\mathbf{U_{22}}$ are the zero- and unit-submatrices, respectively, of the reduced **U** matrix with size of $N_E \times N_{KIV}$ and $N_{KIV} \times N_{KIV}$, respectively; $\mathbf{C_{A1}}$ and $\mathbf{C_{A2}}$ are the subvectors of the vector $\mathbf{C_A}$ with sizes of N_E and N_{KIV}, respectively; $\mathbf{B_{11}}$ and $\mathbf{B_{21}}$ are the submatrices of the reduced $\boldsymbol{\alpha}$ matrix with sizes of $N_E \times N_E$ and $N_{KIV} \times N_E$, respectively; $\mathbf{0_{12}}$ and $\boldsymbol{\alpha}_{\mathbf{22}}$ are the zero- and unit- submatrices, respectively, of the reduced $\boldsymbol{\alpha}$ matrix with size of $N_E \times N_{KIV}$ and $N_{KIV} \times N_{KIV}$, respectively; $\mathbf{C_1}$ and $\mathbf{C_2}$ are the subvectors of the vector **C** with sizes of N_E and N_{KIV}, respectively; $\mathbf{D_{11}}$ is the diagonal submatrix of the reduced $\boldsymbol{\nu}$ matrix with size of $N_E \times N_E$ and $\mathbf{K_{12}}$ is the submatrix of the reduced $\boldsymbol{\nu}$ matrix with size of $N_E \times N_{KIV}$; $\mathbf{0_{21}}$ is the zero submatrix of the reduced $\boldsymbol{\nu}$ matrix with size of $N_{KIV} \times N_E$ and $\mathbf{K_{22}}$ is the submatrix of the reduced $\boldsymbol{\nu}$ matrix with size of $N_{KIV} \times N_E$; $\mathbf{r_1}$ and $\mathbf{r_2}$ are the subvectors of the vector **r** with sizes of N_E and N_{KIV}, respectively.

For reactions that are fast, equilibrium may be regarded as being reached instantaneously among the relevant species and the reaction rates may be regarded as infinite. An infinite rate is mathematically represented by a mass action equation or a user specified nonlinear algebraic equation. As a result, the decomposition of equation (2.5.38) to equation (2.5.40) effectively reduces a set of M species reactive transport equations into two subsets of equations. The first set contains N_E algebraic equations representing mass action laws for the equilibrium reactions, and the second set contains N_{KIV} kinetic-variable transport equations. These equation subsets are defined as

Algebraic Equations for Equilibrium Reactions

$$\frac{\partial(AE_i)}{\partial t} + L(E_i^m) = AD_{1ii}r_{1i} + A\sum_{j=1}^{N_K} K_{1ij}r_{2j},\ i \in N_E \quad \Rightarrow \quad r_{1i} = \infty \quad \Rightarrow \quad \frac{\partial(AE_i)}{\partial t} \approx \infty$$

which is replaced with a thermodynamically consistent equation: $K_i^e = \prod_{j\in M} A_j^{\nu_{ji}} \Big/ \prod_{j\in M} A_j^{\mu_{ji}}$ **(2.5.41)**

$$or\ \ F_i(C_1,..,C_M;p_1,p_2,..) = 0 \quad where\ E_i = \sum_{j=1}^{N_E} A_{1ij}C_{1j}\ \ and\ \ E_i^m = \sum_{j=1}^{N_E} B_{1ij}C_{1j}$$

where K_i^e is the equilibrium constant of the i-th fast reaction, A_j is the activity of the j-th species, $F_i(C_1,..,C_M; p_1,p_2,..)$ is an empirical function of all species and a number of parameters $p_1, p_2, \ldots$ for the i-th fast reaction. E_i was called an equilibrium-variable (Fang, et al., 2003) because $\frac{\partial(AE_i)}{\partial t} \approx \infty$ simply means that E_i can reach equilibrium instantaneously.

Transport Equations for Kinetic-Variables

$$\frac{\partial(AE_i)}{\partial t} + L(E_i^m) = A\sum_{j=1}^{N_K} K_{2nj}r_{2j},\ \ i \in N_{KIV} = M - N_E$$
$$where\ E_i = \sum_{j=1}^{N_E} A_{2ij}C_{1j} + C_{2i}\ and\ E_i^m = \sum_{j=1}^{N_E} B_{2ij}C_{1j} + \alpha_{1i}C_{2i} \qquad \textbf{(2.5.42)}$$

where E_i was called kinetic variable (Fang, et al., 2003) because as E_i is transported it is subject to only kinetic reactions. This is in contrast to Eq. (2.5.38) where as C_i is transported, it is subject to

both equilibrium and kinetic reactions.

Assign

$$R_i = \sum_{j=1}^{N_K} K_{2ij} r_{2j},\ \mathrm{i} \in N_{KIV} \qquad \textbf{(2.5.43)}$$

The reduction of Eq. (2.5.38) to Eq. (2.5.41) and (2.5.42) is equivalent to reducing M governing equations for immobile and mobile species to the mixed N_E algebraic equations for equilibrium variables and N_{KIV} transport equations for kinetic-variables specified as follows

$$\begin{aligned} &\frac{\partial (AE_i)}{\partial t} + \frac{\partial (QE_i^{\,m})}{\partial x} - \frac{\partial}{\partial x}\left(AK_x \frac{\partial E_i^{\,m}}{\partial x} \right) = M_{E_i}^{\ as} + M_{E_i}^{\ rs} - M_{E_i}^{\ es} \\ &+ M_{E_i}^{\ os1} + M_{E_i}^{\ os2} + M_{E_i}^{\ is} + AR_i,\ i \in N_{KIV} \end{aligned} \qquad \textbf{(2.5.44)}$$

where E_i is the concentration of the i-th kinetic-variable [M/L^3], E_i^m is the concentration of mobile part of the i-th kinetic-variable [M/L^3], $M_{E_i}^{\ as}$ is the artificial source of the i-th kinetic-variable [M/L/T], $M_{E_i}^{\ rs}$ is the rainfall source of the i-th kinetic-variable [M/L/T], $M_{E_i}^{\ es}$ is the evaporation sink of the i-th kinetic variable [M/L/T], $M_{E_i}^{\ os1}$ and $M_{E_i}^{\ os2}$ are overland sources of the i-th kinetic-variable from river banks *1* and *2*, respectively [M/L/T], $M_{E_i}^{\ is}$ is the mass rate of the source of the i-th kinetic-variable in river/stream from subsurface [M/L/T], R_i is the production rate of i-th kinetic-variable due to biogeochemical reactions [M/L^3/T], and N_{KIV} is the number of kinetic variable variables.

Boundary conditions for mobile species need to be transformed into corresponding boundary conditions for kinetic-variables, which are stated in the following.

Dirichlet boundary condition:

$$E_i^{\ m} = E_{i\ db}^{m}(x_b, t) \qquad i \in M_m \qquad on \qquad B_d(x) = 0 \qquad \textbf{(2.5.45)}$$

where $E_{i\ db}^{m}(x_b, t)$ is the specified concentration of the mobile portion of the i-th kinetic variable on the Dirichlet boundary $B_d(x) = 0$ [M/L3].

Variable boundary condition:

< Case 1 > Flow is coming in from outside (nQ < 0)

$$n\left(QE_i^m - AK_x \frac{\partial E_i^m}{\partial x} \right) = nQE_{i\ vb}^{m}(x_b, t) \qquad i \in M_m \qquad on \qquad B_v(x) = 0 \qquad \textbf{(2.5.46)}$$

< Case 2 > Flow is going out from inside (nQ > 0).

$$-nAK_x \frac{\partial E_i^m}{\partial x} = 0 \qquad i \in M_m \qquad on \qquad B_v(x) = 0 \tag{2.5.47}$$

where n is the unit outward direction and $E_{i\ vb}^{m}(x_b,t)$ is the concentration of the mobile portion of the i-th kinetic variable on the variable boundary $B_v(x) = 0$ [M/L^3].

Cauchy boundary condition:

$$n\left(QE_i^m - AK_x \frac{\partial E_i^m}{\partial x}\right) = Q_{E_i^m cb}(x_b,t) \qquad i \in M_m \qquad on \qquad B_c(x) = 0 \tag{2.5.48}$$

where $Q_{E_i^m cb}(x_b,t)$ is the mass flux of E_i^m through the Cauchy boundary $B_c(x) = 0$ [M/t].

Neumann boundary condition:

$$-nAK_x \frac{\partial E_i^m}{\partial x} = Q_{E_i^m{}_{nb}}(x_b,t) \qquad i \in M_m \qquad on \qquad B_n(x) = 0 \tag{2.5.49}$$

where $Q_{E_i^m nb}(x_b,t)$ is the mass flux of E_i^m through the Neumann boundary $B_n(x) = 0$ [M/t].

2.6 Sediment and Water Quality Transport in Two-Dimension Overland Regime

Researches on overland water quality modeling include studies of sediment (McDonald and Cheng, 1994; Harris and Wiberg, 2001; and Zeng and Beck, 2003) and water quality transport (Falconer and Lin, 1997; Tufford and McKellar, 1999; Shen et al., 2002; and Zheng et al., 2004) as well as thermal and salinity transport. Most of the existing overland water quality models simulate either specific systems (Cerco and Cole, 1995; Shen et al., 2002; and Zheng et al., 2004) or systems containing specific reactions (Brown and Barnwell, 1987; Ambrose et al, 1993; and Bonnet and Wessen, 2001). They may provide efficient monitoring and management tools because they are calibrated for specific environments, but the extension of a calibrated model to other environmental conditions needs to be carefully evaluated. With better understanding and mathematical formulation of complex biogeochemical interactions (Thomann, 1998; Somlyody et al., 1998; and Yeh et al., 2001a), models considering interactions among biogeochemicals based on reaction mechanism have a better potential for application to other systems (Steefel and Cappellen, 1998). Although a few reaction-based models can handle contaminant transport subject to kinetically controlled chemical reactions (Cheng et al., 2000; and Yeh et al., 2005), no existing overland water quality model, to our knowledge, has the design capability that permitts the use of a fully mechanistic approach to estimate both kinetically and equilibrium controlled reactive chemical transport in overland water systems.

This section presents a general two-dimensional depth-averaged numerical model simulating the water quality in overland shallow water systems using a general paradigm of diagonalized reaction-

based approaches. In our model, sediments are categorized based on their physical and chemical properties. For each category of sediment, we include mobile suspended sediment particles scattered in water column and immobile bed sediment particles accumulated in water bed. The distribution of suspended sediment and bed sediment is controlled through hydrological transport as well as erosion and deposition processes. There are six phases and three forms for biogeochemical species. As shown in Figure 2.6-1, the six phases are suspended sediment, bed sediment, mobile water, immobile water, suspension precipitate, and bed precipitate phases; and the three forms are dissolved chemicals, particulate chemicals sorbed onto sediments, and precipitates.

In the transport simulation, biogeochemical reactions can be divided into two classes (Rubin, 1983): (1) equilibrium-controlled "fast" reactions, and (2) kinetically-controlled "slow" reactions. The former are sufficiently fast compared to the transport time-scale and are reversible, so that local equilibrium may be assumed. The latter are not sufficiently fast compared to the transport time-scale. As shown in Figure 2.6-2, biogeochemical reactions taken into account in the model include aqueous complexation, adsorption/desorption, ion-exchange, precipitation/dissolution, volatilization, diffusion, and sedimentation, etc. Any individual reaction representing any of these chemical and physical processes may be simulated as kinetic or as equilibrium, which makes the code extremely flexible for application to a wide range of biogeochemical transport problems.

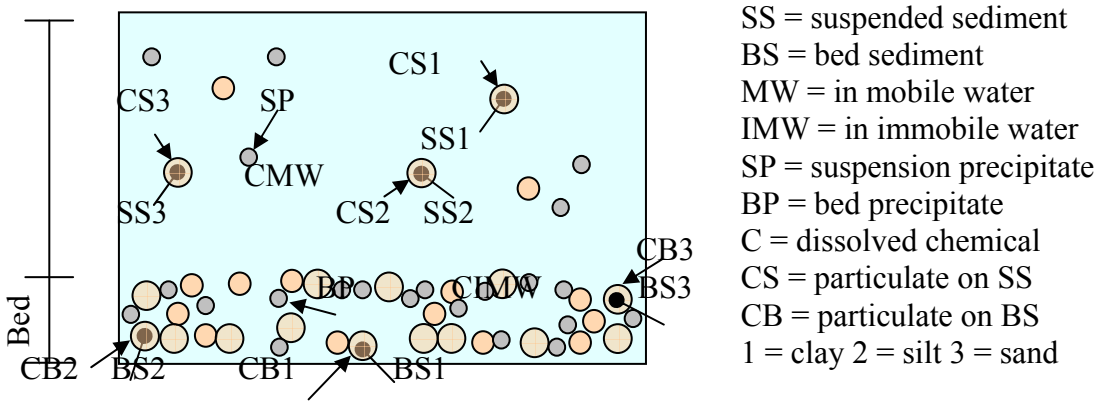

Fig. 2.6-1. Sediments and Chemicals in River/Stream Networks

2.6.1 Bed Sediment

The balance equation for bed sediments is simply the statement that the rate of mass change is due to erosion/deposition as (Yeh, et al., 2005)

$$\frac{\partial(M_n)}{\partial t} = (D_n - R_n) + M^{is}_{M_n}, \quad n \in [1, N_s] \qquad \textbf{(2.6.1)}$$

where M_n is the concentration of the n-th bed sediment in mass per unit bed area [M/L^2], D_n is the deposition rate of the n-th sediment in mass per unit bed area per unit time [M/L^2/T], R_n is the erosion rate of the n-th sediment in mass per unit bed area per unit time [M/L^2/T], $M^{is}_{M_n}$ is the source of the n-th sediment from groundwater exfiltration in mass per unit area [M/L^2/T], and N_S is the total number of sediment size fractions. Concentrations of all bed sediments must be given initially for

transient simulations. No boundary condition is needed for bed sediments. In equation (2.6.1), we estimate the deposition and erosion rates using the different equations for cohesive and non-cohesive sediments.

For cohesive sediments, e.g., silt and clay, following equations are used (Yeh et al., 1998; Gerritsen et al., 2000)

$$D_n = \min\left(V_{sn} S_n P_{Dn},\ S_n h/\Delta t\right) \qquad \text{where} \qquad P_{Dn} = \max\left(0,\ 1-\tau_b/\tau_{cDn}\right) \qquad \textbf{(2.6.2)}$$

and

$$R_n = \min\left(E_{0n} P_{Rn},\ DMA_n/\Delta t\right) \qquad \text{where} \qquad P_{Rn} = \max\left(0,\ \tau_b/\tau_{cRn}-1\right) \qquad \textbf{(2.6.3)}$$

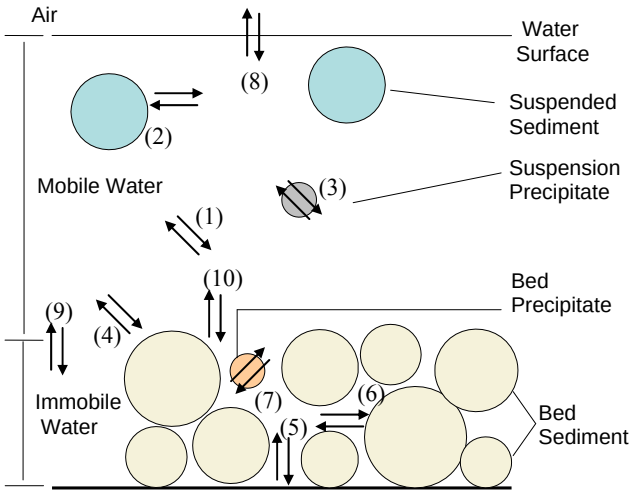

(1) Aqueous complexation in mobile water phase,
(2) Adsorption/desorption or ion-exchange between mobile water and suspended sediment phases,
(3) Precipitation/dissolution between mobile water and suspension precipitate phases,
(4) Adsorption/desorption or ion-exchange between mobile water and bed sediment phases,
(5) Aqueous complexation in immobile water phase,
(6) Adsorption/desorption or ion-exchange between immobile water and bed sediment phases,
(7) Precipitation/dissolution between immobile water and bed precipitate phases,
(8) Volatilization from mobile water phase,
(9) Diffusion between mobile and immobile water phases,
(10) Sedimentation of particulates between suspended and bed sediment phases

Fig. 2.6-2. Biogeochemical Reactions Considered in the Model

where V_{sn} is the settling velocity of the n-th sediment [L/T], S_n is the depth-averaged suspended concentration of n-th sediment [M/L^3], h is the water depth [L], Δt is the simulation time step size [T], τ_b is the bottom shear stress or the bottom friction stress [M/L/T^2], τ_{cDn} is the critical shear stress for the deposition of the n-th sediment [M/L/T^2], E_{0n} is the erodibility of the n-th sediment [M/L^2/T], DMA_n is the amount of locally available dry matter of n-th sediment, expressed as dry weight per unit area [M/L^2], τ_{cRn} is the critical shear stress for the erosion of the n-th sediment [M/L/T^2].

For Non-cohesive sediments, e.g., sand, we have two options.

Option 1 (Prandle et al., 2000)

$$D_n = \min\left(V_{sn} S_n N_{Dn},\ S_n h/\Delta t\right) \qquad \text{where} \qquad N_{Dn} = \max\left[0,\ 1-\left(V_{cDn}/V_{cRn}\right)^2\right] \qquad \textbf{(2.6.4)}$$

and

$$R_n = \min\left(E_{0n} N_{Rn},\ DMA_n/\Delta t\right) \qquad \text{where} \qquad N_{Rn} = \max\left(0,\ V_{cDn}/V_{cRn}-1\right) \qquad \textbf{(2.6.5)}$$

where V_{cDn} and V_{cRn} represent the critical friction velocities for the onset of deposition and erosion, respectively [L/T].

Option 2 (Yeh et al., 1998)

$$D_n = \max\left(\frac{G_{sAn} - G_{sn}}{\Delta L}, 0\right) \tag{2.6.6}$$

and

$$R_n = \max\left(\frac{G_{sn} - G_{sAn}}{\Delta L}, 0\right) \tag{2.6.7}$$

where G_{sAn} is the actual load rate of the n-th sediment per unit width at a upstream location [M/L/T], G_{sn} is the maximum load rate of the n-th size fraction sediment per unit width at a downstream location [M/L/T], ΔL is the distance between the upstream and the downstream locations.

$$G_{sAn} = S_n VR \tag{2.6.8}$$

and

$$G_{sn} = 10\frac{\rho^2 VRS(\tau_b - \tau_{crn})}{g d_n (\rho_{sn} - \rho)^2} \tag{2.6.9}$$

where V is the overland flow velocity [L/t], R is hydraulic radius [L], ρ is the density of water [M/L^3], S is the friction slope, τ_{crn} is the critical bottom shear stress of the n-th sediment at which sediment movement begins [M/L/t^2], g is gravity [L/t^2], d_n is the median diameter of the n-th sediment particle [L], and ρ_{sn} is the density of the n-th sediment [M/L^3].

It should be noted that equations (2.6.2) through (2.6.9) are the sample models programmed in the computer code to estimate sediment deposition and erosion rate. Any other phenomenological model equation can be easily incorporated in the code.

2.6.2 Suspended Sediments

The continuity equation of suspended sediment can be derived based on the conservation law of material mass as (Yeh et al., 2005):

$$\frac{\partial(hS_n)}{\partial t} + \nabla\bullet(\mathbf{q}S_n) - \nabla\bullet(h\mathbf{K}\nabla S_n) = M_{S_n^{as}} + M_{S_n^{rs}} + M_{S_n^{is}} + R_n - D_n, \quad n \in [1, N_s] \tag{2.6.10}$$

where S_n is the depth-averaged concentration of the n-th suspended sediment in the unit of mass per unit column volume [M/L^3], $\mathbf{K}$ is the dispersion coefficient tensor [L^2/t], and $M_{S_n^{as}}$, $M_{S_n^{rs}}$, and $M_{S_n^{is}}$ are the mass rate of artificial source, rainfall source, and groundwater source of the n-th suspended sediment [M/L^2/t].

Concentrations of all suspended sediments must be given initially for transient simulations. Five types of boundary conditions are taken into account for suspended sediments, including Dirichlet, Variable, Cauchy, Neumann, and river/stream-overland interface boundary conditions (Yeh et al., 2005).

Dirichlet boundary condition: Dirichlet boundary conditions are prescribed on the boundary where

the suspended sediment concentration is known,

$$S_n = S_{ndb}(x_b, y_b, t) \quad on \quad B_d(\mathbf{x}) = 0 \tag{2.6.11}$$

where x_b and y_b are the coordinates of the boundary node [L], and $S_{ndb}(x_b, y_b, t)$ is a time-dependent concentration of the *n*-th sediment size on the Dirichlet boundary $B_d(\mathbf{x}) = 0$ [M/L^3].

Variable boundary condition: Variable boundary conditions are normally specified on the boundary where the flow direction can change with time or on any open boundary. On the variable boundary, when the flow is directed into the region of the interest, the mass rate into the region is given by the product of the flow rate and concentration of the incoming fluid. When the flow is directed out of the region, the sediment mass is assumed carried out via advection. Mathematically, a variable boundary condition is given as

$$\mathbf{n}\bullet\left(\mathbf{q}S_n - h\mathbf{K}\bullet\nabla S_n\right) = \mathbf{n}\bullet\mathbf{q}S_{nvb}(x_b, y_b, t) \quad if \quad \mathbf{n}\bullet\mathbf{q} \le 0 \quad on \quad B_v(\mathbf{x}) = 0 \tag{2.6.12}$$

and

$$-\mathbf{n}\bullet\left(h\mathbf{K}\bullet\nabla S_n\right) = 0 \quad if \quad \mathbf{n}\bullet\mathbf{q} \ge 0 \quad on \quad B_v(\mathbf{x}) = 0 \tag{2.6.13}$$

where **n** is a unit outward direction and $S_{nvb}(x_b, y_b, t)$ is a time-dependent concentration of the *n*-th sediment in the incoming fluid at the boundary [M/L^3] $B_v(\mathbf{x}) = 0$.

Cauchy boundary condition: This boundary condition is employed when the total material flow rate is given. Usually, this boundary is an upstream flux boundary.

$$\mathbf{n}\bullet\left(\mathbf{q}S_n - h\mathbf{K}\bullet\nabla S_n\right) = Q_{S_n cb}(x_b, y_b, t) \quad on \quad B_c(\mathbf{x}) = 0 \tag{2.6.14}$$

where $Q_{S_n cb}(x_b, y_b, t)$ is a time-dependent material flow rate of the *n*-th sediment through the Cauchy boundary $B_c(\mathbf{x}) = 0$ [M/t/L].

Neumann boundary condition: This boundary condition is used when the diffusive material flow rate is known at the boundary node.

$$-\mathbf{n}\bullet h\mathbf{K}\bullet\nabla S_n = Q_{S_n nb}(x_b, y_b, t) \quad on \quad B_{nb}(\mathbf{x}) = 0 \tag{2.6.15}$$

where $Q_{S_n nb}(x_b, y_b, t)$ is a time-dependent diffusive material flow rate of the *n*-th sediment trough the Neumann boundary $B_{nb}(\mathbf{x}) = 0$ [M/t/L].

Overland-River/Stream interface boundary condition: The boundary condition is needed when one-dimensional sediment transport in river/stream networks is coupled with two-dimensional sediment transport in overland regime. We assume that the exchange of sediment mass between river/stream and overland flows is mainly due to advection. Under such circumstances, the interfacial boundary condition is stated as

$$\mathbf{n}\cdot\left(\mathbf{q}S_n - h\mathbf{K}\cdot\nabla S_n\right) = \left(\mathbf{n}\cdot\mathbf{q}\right)\frac{1}{2}\left\{\left[1 + sign\left(\mathbf{n}\cdot\mathbf{q}\right)\right]S_n + \left[1 - sign\left(\mathbf{n}\cdot\mathbf{q}\right)\right]S_{n1D}(x_b, y_b, t)\right\} \tag{2.6.16}$$

where $S_{n1D}(x_b, y_b, t)$ is the time-dependent concentration of the *n*-th sediment at the 1-D node corresponding to the boundary [M/L^3]. It is the contribution of 1D transport to the overland boundary.

2.6.3 Immobile Species

The balance equation for immobile species is simply the statement that the rate of mass change is due to biogeochemical reaction as:

$$\frac{\partial(h_b \rho_{bw} \theta_b C_{bw})}{\partial t} = h_b r_{Cbw}\big|_N' \qquad \textbf{(2.6.17)}$$

$$\frac{\partial(h_b \rho_{bw} \theta_b C_{bp})}{\partial t} = h_b r_{Cbp}\big|_N' \qquad \textbf{(2.6.18)}$$

$$\frac{\partial(M_n C_{bsn})}{\partial t} = h_b r_{Cbsn}\big|_N' \qquad \textbf{(2.6.19)}$$

where h_b is the bed depth [L], ρ_{bw} is the density of bed pore-water [M/L^3], θ_b is the porosity of the bed sediment [L^3/L^3], C_{bw} is the concentration of dissolved chemical in the immobile pore-water phase in the unit of chemical mass per bed-water mass [M/M], $r_{Cbw}\big|_N'$ is the production rate of C_{bw} due to all N reactions in the unit of chemical mass per bed volume per time [M/L^3/t], C_{bp} is the concentration of bed precipitate in the unit of chemical mass per bed-water mass [M/M], $r_{Cbp}\big|_N'$ is the production rate of C_{bp} due to all N reactions in the unit of chemical mass per bed volume per time [M/L^3/t], C_{bsn} is the concentration of particulate sorbed on to bed sediment of the *n*-th fraction size in the unit of chemical mass per unit of bed-sediment mass [M/M], M_n is the concentration of the *n*-th bed sediment in the unit of sediment mass per bed area [M/L^2], $r_{Cbsn}\big|_N'$ is the production rate of C_{bsn} due to all N reactions in the unit of chemical mass per bed volume per time [M/L^3/t].

Define

$$r_i\big|_N = h_b \cdot r_i\big|_N' / h \quad where \quad i = C_{bw},\ C_{bp},\ or\ C_{bsn} \qquad \textbf{(2.6.20)}$$

Equation (2.6.16) through (2.6.18) can be modified as

$$\frac{\partial(h_b \rho_{bw} \theta_b C_{bw})}{\partial t} = h r_{Cbw}\big|_N \qquad \textbf{(2.6.21)}$$

$$\frac{\partial(h_b \rho_{bw} \theta_b C_{bp})}{\partial t} = h \cdot r_{Cbp}\big|_N \qquad \textbf{(2.6.22)}$$

$$\frac{\partial(h_b M_n C_{bsn})}{\partial t} = h r_{Cbsn}\big|_N \qquad \textbf{(2.6.23)}$$

Define

$$\rho_i = \begin{cases} h_b \rho_{bw} \theta_b / h, \ for \ \ C_{bw} \ and \ C_{bp} \\ M_n / h, \ for \ \ C_{bsn} \end{cases} \quad \textbf{(2.6.24)}$$

Equation (2.6.21) through (2.6.23) can be summarized as

$$\frac{\partial (h \rho_i C_i)}{\partial t} = hr_i \big|_N, \ \ i \in M_{im} \quad \textbf{(2.6.25)}$$

where C_i is the concentration of species i, which is immobile, in the unit of chemical mass per unit phase mass [M/M], ρ_i is the density of the phase associated with species i [M/L^3], $r_i \big|_N$ is the production rate of species i due to all N reactions in the unit of chemical mass per column volume per time [M/L^3/t], and M_{im} is the number of immobile species. The concentrations of all immobile species must be given initially for transient simulations. No boundary conditions are needed for immobile species.

2.6.4 Mobile Species

The continuity equation of mobile species can be derived based on the conservation law of material mass stating that the rate of mass change is due to both advective-dispersive transport and biogeochemical reactions as:

$$\frac{\partial (h \rho_w C_w)}{\partial t} + L(\rho_w C_w) = hr_{Cw} \big|_N \quad \textbf{(2.6.26)}$$

$$\frac{\partial (h \rho_w C_p)}{\partial t} + L(\rho_w C_p) = hr_{Cp} \big|_N \quad \textbf{(2.6.27)}$$

$$\frac{\partial (h S_n C_{sn})}{\partial t} + L(S_n C_{sn}) = hr_{Csn} \big|_N \quad \textbf{(2.6.28)}$$

where ρ_w is the density of column water [M/L^3], C_w is the concentration of dissolved chemical in the mobile water phase in the unit of chemical mass per column-water mass [M/M], $r_{Cw} \big|_N$ is the production rate of C_w due to all N reactions in the unit of chemical mass per column volume per time [M/L^3/t], C_p is the concentration of suspension precipitate in the unit of chemical mass per column-water mass [M/M], $r_{Cp} \big|_N$ is the production rate of C_p due to all N reactions in the unit of chemical mass per column volume per time [M/L^3/t], C_{sn} is the concentration of particulate sorbed on to suspended sediment of the n-th fraction size in the unit of chemical mass per unit of sediment mass [M/M], S_n is the concentration of suspended sediment in the unit of sediment mass per column volume [M/L^3], $r_{Csn} \big|_N$ is the production rate of C_{sn} due to all N reactions in the unit of chemical mass per column volume per time [M/L^3/t], and the operator L is defined in Eq. (2.6.31) later.

Define

$$\rho_i = \begin{cases} \rho_w \ \ for \ \ C_w \ and \ C_p \\ S_n \ \ for \ \ C_{sn} \end{cases} \quad \textbf{(2.6.29)}$$

Equation (2.6.26) through (2.6.28) can be summarized as

$$\frac{\partial(h\rho_i C_i)}{\partial t} + L(\rho_i C_i) = hr_i\big|_N, \quad i \in M_m = M - M_{im} \tag{2.6.30}$$

where C_i is the concentration of species i, which is mobile, in the unit of chemical mass per unit phase mass [M/M], ρ_i is the density of the phase associated with species i [M/L^3], $r_i\big|_N$ is the production rate of species i due to all N reactions in the unit of chemical mass per column volume per time [M/L^3/t], M is the total number of chemical species, M_m is the number of mobile chemical species, and operator L is defined as

$$L(\rho_i C_i) = \nabla\cdot(\mathbf{q}\rho_i C_i) - \nabla\cdot\left[h\mathrm{K}\cdot\nabla(\rho_i C_i)\right] - (M_{C_i^{as}} + M_{C_i^{rs}} - M_{C_i^{es}} + M_{C_i^{rs}}) \tag{2.6.31}$$

where $M_{C_i^{as}}$ is the mass ratte of artificial source of species i [M/L^2/T], $M_{C_i^{rs}}$ is the mass rate of the rainfall source of species i [M/L^2/T], $M_{C_i^{es}}$ is the mass rate of the evaporation sink of species i [M/L^2/T], and $M_{C_c^{is}}$ is mass rate of the source of species i in the overland from subsurface [M/L^2/T].

Concentrations of all mobile species must be given initially for transient simulations. Similar to suspended sediment transport, five types of boundary conditions are taken into account for mobile species, including Dirichlet, Variable, Cauchy, Neumann, and river/stream-overland interface boundary conditions (Yeh et al., 2005).

Dirichlet boundary condition: Dirichlet boundary conditions are prescribed on the boundary where the suspended sediment concentration is known,

$$C_i = C_{idb}(x_b, y_b, t) \qquad i \in M_m \quad on \quad B_d(\mathbf{x}) = 0 \tag{2.6.32}$$

where x_b and y_b are the coordinates of the boundary node [L], and $C_{idb}(x_b, y_b, t)$ is a time-dependent concentration of the i-th mobile species on the Dirichlet boundary $B_d(\mathbf{x}) = 0$ [M/M].

Variable boundary condition: Variable boundary conditions are normally specified on the boundary where the flow direction can change with time or on any open boundary. On the variable boundary, when the flow is directed into the region of the interest, the mass rate into the region is given by the product of the flow rate and concentration of the incoming fluid. When the flow is directed out of the region, the sediment mass is assumed carried out via advection. Mathematically, a variable boundary condition is given as

$$\mathbf{n}\cdot\left(\mathbf{q}\rho_i C_i - h\mathbf{K}\cdot\nabla(\rho_i C_i)\right) = \mathbf{n}\cdot\mathbf{q}\rho_i C_{ivb}(x_b, y_b, t) \; if \; \mathbf{n}\cdot\mathbf{q} \le 0 \; on \; B_v(\mathbf{x}) = 0, \; i \in M_m \tag{2.6.33}$$

and

$$-\mathbf{n}\cdot\left(h\mathbf{K}\cdot\nabla(\rho_i C_i)\right) = 0 \qquad if \qquad \mathbf{n}\cdot\mathbf{q} \le 0 \qquad on \qquad B_v(\mathbf{x}) = 0, \qquad i \in M_m \tag{2.6.34}$$

where $\mathbf{n}$ is a unit outward direction and $C_{ivb}(x_b, y_b, t)$ is a time-dependent concentration of the i-th mobile species in the incoming fluid at the boundary [M/M] $B_v(\mathbf{x}) = 0$.

Cauchy boundary condition: This boundary condition is employed when the total material flow rate

is given. Usually, this boundary is an upstream flux boundary.

$$\mathbf{n}\cdot\left(\mathbf{q}\rho_i C_i - h\mathbf{K}\cdot\nabla(\rho_i C_i)\right) = Q_{C_i cb}(x_b, y_b, t) \qquad i \in M_m \qquad on \qquad B_c(\mathbf{x}) = 0 \tag{2.6.35}$$

where $Q_{C_i cb}(x_b, y_b, t)$ is a time-dependent material flow rate of the *i*-th mobile species through the Cauchy boundary $B_c(\mathbf{x}) = 0$ [M/t/L].

Neumann boundary condition: This boundary condition is used when the diffusive material flow rate is known at the boundary node.

$$-\mathbf{n}\cdot h\mathbf{K}\cdot\nabla(\rho_i C_i) = Q_{C_i nb}(x_b, y_b, t) \qquad i \in M_m \qquad on \quad B_{nb}(\mathbf{x}) = 0 \tag{2.6.36}$$

where $Q_{C_i nb}(x_b, y_b, t)$ is a time-dependent diffusive material flow rate of the *i*-th mobile species through the Neumann boundary $B_{nb}(\mathbf{x}) = 0$ [M/t/L].

Overland-river/stream interface boundary condition: The boundary condition is needed when one-dimensional sediment transport in river/stream networks is coupled with two-dimensional sediment transport in overland regime. We assume that the exchange of sediment mass between river/stream and overland flows is mainly due to advection. Under such circumstances, the interfacial boundary condition is stated as

$$\mathbf{n}\cdot\left(\mathbf{q}\rho_i C_i - h\mathbf{K}\cdot\nabla(\rho_i C_i)\right) = \left(\mathbf{n}\cdot\mathbf{q}\right)\frac{1}{2}\left\{\left[1 + sign\left(\mathbf{n}\cdot\mathbf{q}\right)\right]\rho_i C_i + \left[1 - sign\left(\mathbf{n}\cdot\mathbf{q}\right)\right]\rho_i C_{i1D}(x_b, y_b, t)\right\} \tag{2.6.37}$$

where $C_{i1D}(x_b, y_b, t)$ is the time-dependent concentration of the *i*-th species at the 1-D node corresponding to the overland-river/stream interfacial boundary point [M/M].

2.6.5 Diagonalization of Species Transport Equations

The temporal-spatial distribution of chemical species is described by a system of M_{im} mass balance equations [equation (2.6.25)], and M_m reactive transport equations [equation (2.6.30)]. These two equations can be recast in the following form

$$\frac{\partial(h\rho_i C_i)}{\partial t} + \alpha_i L(\rho_i C_i) = hr_i\big|_N, \quad i \in M \tag{2.6.38}$$

where *M* is the total number of chemical species, α_i is 0 for immobile species and 1 for mobile species.

The determination of $r_i\big|_N$ and associated parameters is a primary challenge in biogeochemical modeling. Instead of using an ad hoc method to formulate $r_i\big|_N$, we use reaction-based formulations (Steefel and Cappellen, 1998). In a reaction-based formulation, $r_i\big|_N$ is given by the summation of rates of all reactions that the *i*-th species participates in,

$$r_i\big|_N = \frac{d\left(\rho_i C_i\right)}{dt}\Big|_{reaction} = \sum_{k=1}^{N}\left[(\nu_{ik} - \mu_{ik})r_k\right], \quad i \in M \qquad \textbf{(2.6.39)}$$

where ν_{ik} is the reaction stoichiometry of the *i*-th species in the *k*-th reaction associated with the products, μ_{ik} is the reaction stoichiometry of the *i*-th species in the *k*-th reaction associated with the reactants, and r_k is the rate of the *k*-th reaction.

Substituting equation (2.6.39) into equation (2.6.38) results in the transport equations of *M* chemical species described by

$$\frac{\partial(h\rho_i C_i)}{\partial t} + \alpha_i L(\rho_i C_i) = h\sum_{k=1}^{N}\left[(\nu_{ik} - \mu_{ik})r_k\right], \quad i \in M; \quad or \quad \mathbf{U}\frac{\partial \mathbf{C}_h}{\partial t} + \boldsymbol{\alpha} L(\mathbf{C}) = h\boldsymbol{\nu}\mathbf{r} \qquad \textbf{(2.6.40)}$$

where **U** is a unit matrix, $\mathbf{C}_h$ is a vector with its components representing *M* species concentrations multiply the water depth [M/L^2], $\boldsymbol{\alpha}$ is a diagonal matrix with α_i as its diagonal component, **C** is a vector with its components representing M species concentrations [M/L^3], $\boldsymbol{\nu}$ is the reaction stoichiometry matrix, and **r** is the reaction rate vector with *N* reaction rates as its components. Equation (2.6.40) represents a mass balance for species *i*, which states that the rate of change of any species mass is due to advection-dispersion coupled with contributing reactions that describe the biogeochemical processes.

In a primitive approach, equation (2.6.40) is integrated to yield the distributions and evolutions of chemical species in a region of interest. However, when some fast equilibrium reactions take place in the system, this approach is not adequate (Fang et al., 2003). Here, we will take a diagonalization approach through decomposition. Equation (2.6.40) written in matrix form can be decomposed based on the type of biogeochemical reactions via Gauss-Jordan column reduction of reaction matrix $\boldsymbol{\nu}$. Among all the fast/equilibrium and slow/kinetic reactions, "redundant reactions" are defined as fast reactions that are linearly dependent on other fast reactions, and "irrelevant reactions" are kinetic reactions that are linearly dependent on only equilibrium reactions. In order to avoid singularity of the reaction matrix, redundant fast reactions are omitted from the system prior to decomposition. The removal of irrelevant slow reactions alleviates problems associated with rate formulation uncertainty and parameterization for these reactions.

Decomposition is performed by pivoting on the N_E equilibrium reactions and decoupling them from the N_K kinetic reactions. In other words, each fast reaction can be used to eliminate one chemical species from simultaneous consideration. An incomplete Gauss-Jordan row decomposition of the reaction matrix $\boldsymbol{\nu}$ by pivoting on N_E equilibrium reactions will result in N_E equilibrium-variables and N_{KIV} kinetic-variables. To analyze the system behavior, it is advantageous to perform a complete decomposition, in which the reduction of the reaction matrix is done by pivoting on N_E equilibrium reactions and on N_{KI} linearly independent kinetic reactions to result in N_E equilibrium-variables, N_{KI} kinetic-variables, and N_C components. The complete decomposition is given as follows:

$$\begin{bmatrix} \mathbf{A_{11}} & \mathbf{0_{12}} & \mathbf{0_{13}} \\ \mathbf{A_{21}} & \mathbf{A_{22}} & \mathbf{0_{23}} \\ \mathbf{A_{31}} & \mathbf{A_{32}} & \mathbf{U_{33}} \end{bmatrix} \begin{Bmatrix} \frac{\partial \mathbf{C}_{h1}}{dt} \\ \frac{\partial \mathbf{C}_{h2}}{dt} \\ \frac{\partial \mathbf{C}_{h3}}{dt} \end{Bmatrix} + \begin{bmatrix} \mathbf{B_{11}} & \mathbf{0_{12}} & \mathbf{0_{13}} \\ \mathbf{B_{21}} & \mathbf{B_{22}} & \mathbf{0_{23}} \\ \mathbf{B_{31}} & \mathbf{B_{32}} & \boldsymbol{\alpha}_{33} \end{bmatrix} \mathrm{L}\left(\begin{Bmatrix} \mathbf{C_1} \\ \mathbf{C_2} \\ \mathbf{C_3} \end{Bmatrix} \right) = \mathrm{h} \begin{bmatrix} \mathbf{D_{11}} & \mathbf{K_{12}} & \mathbf{K_{13}} \\ \mathbf{0_{21}} & \mathbf{D_{22}} & \mathbf{K_{23}} \\ \mathbf{0_{31}} & \mathbf{0_{32}} & \mathbf{0_{33}} \end{bmatrix} \begin{Bmatrix} \mathbf{r_1} \\ \mathbf{r_2} \\ \mathbf{r_3} \end{Bmatrix} \quad \textbf{(2.6.41)}$$

where $\mathbf{A_{11}}$ is the submatrix of the reduced **U** matrix with size of $N_E \times N_E$, $\mathbf{A_{21}}$ is the submatrix of the reduced **U** matrix with size of $N_{KI} \times N_E$, and $\mathbf{A_{31}}$ is the submatrix of the reduced **U** matrix with size of $N_C \times N_E$; $\mathbf{0_{12}}$ is the zero submatrix of the reduced **U** matrix with size of $N_E \times N_{KI}$, $\mathbf{A_{22}}$ is the submatrix of the reduced **U** matrix with size of $N_{KI} \times N_{KI}$, and $\mathbf{A_{32}}$ is the submatrix of the reduced **U** matrix with size of $N_C \times N_{KI}$; $\mathbf{0_{13}}$ is the zero submatrix of the reduced **U** matrix with size of $N_E \times N_C$, $\mathbf{0_{23}}$ is the submatrix of the reduced **U** matrix with size of $N_{KI} \times N_C$, and $\mathbf{U_{33}}$ is the unit submatrix of the reduced **U** matrix with size of $N_C \times N_C$; $\mathbf{C_{h1}}$, $\mathbf{C_{h2}}$, and $\mathbf{C_{h3}}$ are the subvectors of the vector $\mathbf{C_h}$ with sizes of N_E, N_{KI}, and N_C, respectively; $\mathbf{B_{11}}$ is the submatrix of the reduced $\boldsymbol{\alpha}$ matrix with size of $N_E \times N_E$, $\mathbf{B_{21}}$ is the submatrix of the reduced $\boldsymbol{\alpha}$ matrix with size of $N_{KI} \times N_E$, and $\mathbf{B_{31}}$ is the submatrix of the reduced $\boldsymbol{\alpha}$ matrix with size of $N_C \times N_E$; $\mathbf{0_{12}}$ is the zero submatrix of the reduced $\boldsymbol{\alpha}$ matrix with size of $N_E \times N_{KI}$, $\mathbf{A_{22}}$ is the submatrix of the reduced $\boldsymbol{\alpha}$ matrix with size of $N_{KI} \times N_{KI}$, and $\mathbf{B_{32}}$ is the submatrix of the reduced $\boldsymbol{\alpha}$ matrix with size of $N_C \times N_{KI}$; $\mathbf{0_{13}}$ is the zero submatrix of the reduced $\boldsymbol{\alpha}$ matrix with size of $N_E \times N_C$, $\mathbf{0_{23}}$ is the submatrix of the reduced $\boldsymbol{\alpha}$ matrix with size of $N_{KI} \times N_C$, and $\boldsymbol{\alpha}_{33}$ is the diagonal submatrix of the reduced $\boldsymbol{\alpha}$ matrix with size of $N_C \times N_C$; $\mathbf{C_1}$, $\mathbf{C_2}$, and $\mathbf{C_3}$ are the subvectors of the vector **C** with sizes of N_E, N_{KI}, and N_C, respectively; $\mathbf{D_{11}}$ is the diagonal submatrix of the reduced $\boldsymbol{\nu}$ matrix with size of $N_E \times N_E$, $\mathbf{K_{12}}$ is the submatrix of the reduced $\boldsymbol{\nu}$ matrix with size of $N_E \times N_{KI}$, and $\mathbf{K_{13}}$ is the submatrix of the reduced $\boldsymbol{\nu}$ matrix with size of $N_E \times N_{KD(k)}$; $\mathbf{0_{21}}$ is the zero submatrix of the reduced $\boldsymbol{\nu}$ matrix with size of $N_{KI} \times N_E$, $\mathbf{D_{22}}$ is the diagonal submatrix of the reduced $\boldsymbol{\nu}$ matrix with size of $N_{KI} \times N_{KI}$, and $\mathbf{K_{23}}$ is the submatrix of the reduced $\boldsymbol{\nu}$ matrix with size of $N_{KI} \times N_{KD(k)}$; $\mathbf{0_{13}}$ is the zero submatrix of the reduced $\boldsymbol{\nu}$ matrix with size of $N_C \times N_E$, $\mathbf{0_{32}}$ is the zero submatrix of the reduced $\boldsymbol{\nu}$ matrix with size of $N_C \times N_{KI}$, and $\mathbf{0_{33}}$ is the zero submatrix of the reduced $\boldsymbol{\nu}$ matrix with size of $N_C \times N_{KD(k)}$; $\mathbf{r_1}$, $\mathbf{r_2}$, and $\mathbf{r_3}$ are the subvectors of the vector **r** with sizes of N_E, N_{KI}, and $N_{KD(k)}$, respectively.

For incomplete decomposition of the reaction matrix $\boldsymbol{\nu}$, Equation (2.6.41) can be connoted as

$$\begin{bmatrix} \mathbf{A_{11}} & \mathbf{0_{12}} \\ \mathbf{A_{21}} & \mathrm{U}_{22} \end{bmatrix} \begin{Bmatrix} \frac{\partial \mathbf{C}_{h1}}{dt} \\ \frac{\partial \mathbf{C}_{h2}}{dt} \end{Bmatrix} + \begin{bmatrix} \mathbf{B_{11}} & \mathbf{0_{12}} \\ \mathbf{B_{21}} & \boldsymbol{\alpha}_{22} \end{bmatrix} \mathrm{L}\left(\begin{Bmatrix} \mathbf{C_1} \\ \mathbf{C_2} \end{Bmatrix} \right) = \mathrm{h} \begin{bmatrix} \mathbf{D_{11}} & \mathbf{K_{12}} \\ \mathbf{0_{21}} & \mathbf{K_{22}} \end{bmatrix} \begin{Bmatrix} \mathbf{r_1} \\ \mathbf{r_2} \end{Bmatrix} \quad \textbf{(2.6.42)}$$

where $\mathbf{A_{11}}$ and $\mathbf{A_{21}}$ are the submatrices of the reduced **U** matrix with size of $N_E \times N_E$ and $N_{KIV} \times N_E$, respectively (note that $N_{KIV} = M - N_E = N_{KI} + N_C$); $\mathbf{0_{12}}$ and $\mathbf{U_{22}}$ are the zero- and unit-submatrices, respectively, of the reduced **U** matrix with size of $N_E \times N_{KIV}$ and $N_{KIV} \times N_{KIV}$, respectively; $\mathbf{C_{h1}}$ and $\mathbf{C_{h2}}$ are the subvectors of the vector $\mathbf{C_h}$ with sizes of N_E and N_{KIV}, respectively; $\mathbf{B_{11}}$ and $\mathbf{B_{21}}$ are the submatrices of the reduced $\boldsymbol{\alpha}$ matrix with sizes of $N_E \times N_E$ and $N_{KIV} \times N_E$, respectively; $\mathbf{0_{12}}$ and $\boldsymbol{\alpha}_{22}$ are the zero- and unit- submatrices, respectively, of the reduced $\boldsymbol{\alpha}$ matrix with size of $N_E \times N_{KIV}$ and $N_{KIV} \times N_{KIV}$, respectively; $\mathbf{C_1}$ and $\mathbf{C_2}$ are the subvectors of the vector **C** with sizes of N_E and N_{KIV},

respectively; $\mathbf{D_{11}}$ is the diagonal submatrix of the reduced $\boldsymbol{\nu}$ matrix with size of $N_E \times N_E$ and $\mathbf{K_{12}}$ is the submatrix of the reduced $\boldsymbol{\nu}$ matrix with size of $N_E \times N_{KIV}$; $\mathbf{0_{21}}$ is the zero submatrix of the reduced $\boldsymbol{\nu}$ matrix with size of $N_{KIV} \times N_E$ and $\mathbf{K_{22}}$ is the submatrix of the reduced $\boldsymbol{\nu}$ matrix with size of $N_{KIV} \times N_E$; $\mathbf{r_1}$ and $\mathbf{r_2}$ are the subvectors of the vector $\mathbf{r}$ with sizes of N_E and N_{KIV}, respectively.

For reactions that are fast, equilibrium may be regarded as being reached instantaneously among the relevant species and the reaction rates may be regarded as infinite. An infinite rate is mathematically represented by a mass action equation or a user specified nonlinear algebraic equation. As a result, the decomposition of equation (2.6.40) to equation (2.6.42) effectively reduces a set of M species reactive transport equations into two subsets of equations. The first set contains N_E algebraic equations representing mass action laws for the equilibrium reactions, and the second set contains N_{KIV} kinetic-variable transport equations. These equation subsets are defined as

Algebraic Equations for Equilibrium Reactions

$$\frac{\partial(hE_i)}{\partial t} + L(E_i^m) = hD_{1ii}r_{1i} + h\sum_{j=1}^{N_K} K_{1ij}r_{2j},\ i \in N_E \quad \Rightarrow \quad r_{1i} = \infty \quad \Rightarrow \quad \frac{\partial(hE_i)}{\partial t} \approx \infty$$

which is replaced with a thermodynamically consistent equation: $K_i^e = \prod_{j\in M} A_j^{\nu_{ji}} \Big/ \prod_{j\in M} A_j^{\mu_{ji}}$ **(2.6.43)**

$$or\ \ F_i(C_1,..,C_M;p_1,p_2,..) = 0 \quad where\ E_i = \sum_{j=1}^{N_E} A_{1ij}C_{1j} \ \ and \ \ E_i^m = \sum_{j=1}^{N_E} B_{1ij}C_{1j}$$

where K_i^e is the equilibrium constant of the i-th fast reaction, A_j is the activity of the j-th species, $Fi(C_1,..,C_M; p_1,p_2,..)$ is an empirical function of all species and a number of parameters p, p2, … for the i-th fast reaction. E_i was called an equilibrium-variable (Fang, et al., 2003) because $\frac{\partial(hE_i)}{\partial t} \approx \infty$ simply means that E_i can reach equilibrium instantaneously.

Transport Equations for Kinetic-Variables

$$\frac{\partial(hE_i)}{\partial t} + L(E_i^m) = h\sum_{j=1}^{N_K} K_{2nj}r_{2j},\ \ i \in N_{KIV} = M - N_E$$
$$where\ E_i = \sum_{j=1}^{N_E} A_{2ij}C_{1j} + C_{2i}\ \ and\ \ E_i^m = \sum_{j=1}^{N_E} B_{2ij}C_{1j} + \alpha_{1i}C_{2i} \qquad \textbf{(2.6.44)}$$

where E_i was called a kinetic variable (Fang, et al., 2003) because as E_i is transported it is subject to only kinetic reactions. This is in contrast to Eq. (2.6.44) where as C_i is transported, it is subject to both equilibrium and kinetic reactions.

Assign

$$R_i = \sum_{j=1}^{N_K} K_{2ij}r_{2j},\ \mathrm{i} \in N_{KIV} \qquad \textbf{(2.6.45)}$$

The reduction of Eq. (2.6.40) to Eq. (2.6.43) and (2.6.44) is equivalent to reducing M governing

equations for immobile and mobile species to the mixed N_E algebraic equations for equilibrium variables and N_{KIV} transport equations for kinetic-variables specified as follows

$$\frac{\partial(hE_i)}{\partial t} + \nabla\bullet(\mathbf{q}E_i^m) - \nabla\bullet\left[(h\mathbf{K}\bullet\nabla E_i^m)\right] = M_{E_i^{as}} + M_{E_i^{rs}} + M_{E_i^{is}} + hR_i,\ i \in N_{KIV} \qquad \textbf{(2.6.46)}$$

where E_i is the concentration of the i-th kinetic-variable [M/L^3], E_i^m is the concentration of mobile part of the i-th kinetic-variable [M/L^3], $M_{E_i^{as}}$ is the artificial source of the i-th kinetic-variable [M/L^2/T], $M_{E_i^{rs}}$ is the rainfall source of the i-th kinetic-variable [M/L^2/T], $M_{E_i^{os1}}$ and $M_{E_i^{os2}}$ are overland sources of the i-th kinetic-variable from river banks *1* and *2*, respectively [M/L^2/T], $M_{E_i^{is}}$ is the mass rate of the source of the i-th kinetic-variable in the overland from subsurface [M/L^2/T], R_i is the production rate of i-th kinetic-variable due to biogeochemical reactions [M/L^3/T], and N_{KIV} is the number of kinetic variable variables.

Initial and boundary condition for chemical species need to be transformed into corresponding initial and boundary conditions for kinetic-variables, which are stated in the following.

Dirichlet boundary condition:

$$E_i^m = E_{i\ db}^m(x_b, y_b, t) \qquad i \in M_m \qquad on \qquad B_d(\mathbf{x}) = 0 \qquad \textbf{(2.6.47)}$$

where $E_{i\ db}^m(x_b, y_b, t)$ is the prescribed concentration of the mobile portion of the i-th kinetic variable on the Dirichlet boundary $B_d(\mathbf{x}) = 0$ [M/L^3].

Variable boundary condition:

< Case 1 > Flow is coming in from outside (nQ < 0)

$$\mathbf{n}\bullet\left(\mathbf{q}E_i^m - h\mathbf{K}\bullet\nabla E_i^m\right) = \mathbf{n}\bullet\mathbf{q}E_{i\ vb}^m(x_b, y_b, t) \qquad i \in M_i \qquad on \qquad B_v(\mathbf{x}) = 0 \qquad \textbf{(2.6.48)}$$

< Case 2 > Flow is going out from inside (nQ > 0).

$$-\mathbf{n}\bullet\left(h\mathbf{K}\bullet\nabla E_i^m\right) = 0 \qquad i \in M_m \qquad on \qquad B_v(\mathbf{x}) = 0 \qquad \textbf{(2.6.49)}$$

where $\mathbf{n}$ is the unit outward vector and $E_{i\ vb}^m(x_b, y_b, t)$ is the concentration of the mobile portion of the i-th kinetic variable on the variable boundary $B_v(\mathbf{x}) = 0$ [M/L^3].

Cauchy boundary condition:

$$\mathbf{n}\bullet\left(\mathbf{q}E_i^m - h\mathbf{K}\bullet\nabla E_i^m\right) = Q_{E_i^m cb}(x_b, y_b, t) \qquad i \in M_i \qquad on \qquad B_c(\mathbf{x}) = 0 \qquad \textbf{(2.6.50)}$$

where $Q_{E_i^m cb}(x_b, y_b, t)$ is the mass flux of E_i^m through the Cauchy boundary $B_c(\mathbf{x}) = 0$ [M/t/L].

Neumann boundary condition:

$$-\mathbf{n}\bullet\left(h\mathbf{K}\bullet\nabla E_i^m\right)=Q_{E_i^m nb}(x_b,y_b,t)\qquad i\in M_i\qquad on\qquad B_n(\mathbf{x})=0 \tag{2.6.51}$$

where $Q_{E_i^m nb}(x_b,y_b,t)$ is the mass flux of E_i^m through the Neumann boundary $B_n(\mathbf{x})=0$ [M/t/L].

Overland-river/stream interface boundary condition:

$$\mathbf{n}\cdot\left(\mathbf{q}E_i^m-h\mathbf{K}\cdot\nabla E_i^m\right)=\left(\mathbf{n}\cdot\mathbf{q}\right)\frac{1}{2}\left\{\left[1+sign\left(\mathbf{n}\cdot\mathbf{q}\right)\right]E_i^m+\left[1-sign\left(\mathbf{n}\cdot\mathbf{q}\right)\right]E_{i\ 1D}^m(x_b,y_b,t)\right\} \tag{2.6.52}$$

where $E_{i\ 1D}^m(x_b,y_b,t)$ is the time-dependent concentration of the mobile portion of the *i*-th kinetic variable at the 1-D node corresponding to the overland-river/stream interfacial boundary point [M/L^3].

2.7 Reactive Biogeochemical Transport in Three-Dimension Subsurface Media

Reactive chemical transport in the subsurface occurs over a broad range of geochemical environments at various space and time scales. Coupled models that simulate hydrological transport and complex biogeochemical reactions are important tools for quantitative predictions of the fate and transport of chemicals in groundwater. Biogeochemical reactions can be divided into two classes (Rubin, 1983): (1) equilibrium-controlled "fast" reactions, and (2) kinetically-controlled "slow" reactions. The former are sufficiently fast compared to the transport time-scale and are reversible, so that local equilibrium may be assumed. The latter are not sufficiently fast compared to the transport time-scale. They may be either reversible or irreversible. Local equilibrium conditions cannot be assumed.

Due to computational limitations, existing coupled models for subsurface reactive transport have various capabilities (Keum and Hahn, 2003). Some models couple transport with equilibrium chemistry (e.g., Cederberg et al., 1985; Liu and Narasimhan, 1989; Yeh and Tripathi, 1991; Parkhurst, 1995; and Parkhurst and Appelo, 1999), while some couple transport with kinetic chemistry (e.g., MacQuarrie et al., 1990; Tompson, 1993; Lensing et al., 1994; Wood et al., 1994; Adeel et al., 1995; Yeh et al., 1998; and Saiers et al., 2000). Models coupling transport with both equilibrium and kinetic reactions appeared in the mid-1990s (e.g., Steefel and Lasaga, 1994; Chilakapati, 1995; Chilakapati et al., 1998; Tebes-Stevens et al., 1998; Yeh et al., 2001b; Brun and Engesgaard, 2002). Most of these models either implicitly assumes that equilibrium reactions occur only among aqueous species or consider only limited reaction networks. These limitations affect the generality of the models. There appears to be few general-purpose transport models that can simulate generic reaction networks including mixed equilibrium/kinetic biochemical and geochemical reactions (Yeh et al., 2004).

This report presents a general mathematical framework and a three-dimensional numerical implementation to simulate reactive chemical transport in subsurface water subject to a defined flow field. Chemical species considered include dissolved species, suspension precipitates and surface species that encompass adsorbed species, ion-exchanged species and free sites. Biogeochemical

reactions taken into account in the model include aqueous complexation, adsorption/desorption, ion-exchange, precipitation/dissolution, reduction/oxidation, and volatilization. Any individual reaction representing any of these chemical and physical processes may be simulated as kinetic or as equilibrium, which makes the approach applicable to a wide range of biogeochemical transport problems. In the subsurface, all dissolved species are assumed mobile while all surface species and suspension precipitates are assumed immobile.

2.7.1 Immobile Species

The balance equation for immobile species is simply the statement that the rate of mass change is due to biogeochemical reaction as:

$$\frac{\partial(\theta\rho_w C_p)}{\partial t} = \theta r_{Cp}\big|_N \qquad \textbf{(2.7.1)}$$

and

$$\frac{\partial(\rho_b S_A C_s)}{\partial t} = \theta r_{Cs}\big|_N \qquad \textbf{(2.7.2)}$$

where ρ_w is the density of pore-water [M/L^3], θ is the porosity of the media [L^3/L^3], C_p is the concentration of precipitate in the unit of chemical mass per por-water mass [M/M], $r_{Cp}\big|_N$ is the production rate of C_p due to all N reactions in the unit of chemical mass per pore-water volume per time [M/L^3/t], ρ_b is the bulk density in dry media mass per unit media volume [M/L^3], S_A is the surface area per unit dry mass [L^2/M], C_s is the concentration of surface species in unit of chemical mass per surface area [M/L^2], and $r_{Cs}\big|_N$ is the production rate of C_s due to all N reactions in the unit of chemical mass per pore-water per time [M/L^3/t].

Equation (2.7.1) and (2.7.2) can be combined as

$$\frac{\partial(\theta\rho_i C_i)}{\partial t} = \theta r_i\big|_N, \quad i \in M_{im} \qquad \textbf{(2.7.3)}$$

where C_i is the concentration of the i-th immobile, $r_i\big|_N$ is the production rate of species i due to all N reactions in the unit of chemical mass per pore-water volume per time [M/L^3/t], M_{im} is the number of immobile species, and ρ_i is defined by

$$\rho_i = \begin{cases} \rho_w, & for\ C_p \\ \rho_b S_A / \theta, & for\ C_s \end{cases} \qquad \textbf{(2.7.4)}$$

The concentrations of all immobile species must be given initially for transient simulations. No boundary conditions are needed for immobile species.

2.7.2 Mobile Species

The continuity equation of mobile species, i.e. dissolved species in the water phase, can be derived

based on the mass conservation law stating that the rate of mass change is due to both advective-dispersive transport and biogeochemical reactions as

$$\frac{\partial(\theta\rho_i C_i)}{\partial t} + \nabla\cdot(\mathbf{V}\rho_i C_i) - \nabla\cdot[\theta\mathbf{D}\cdot\nabla(\rho_i C_i)] = M_{C_i}^{\ as} + \theta r_i\big|_N, \quad i \in M_m \qquad \textbf{(2.7.5)}$$

where C_i is the concentration of the i-th dissolved species in the unit of chemical mass per unit water mass [M/M], ρ_i is the density of water [i.e., $C_i = C_w$] [M/L^3], **V** is the Darcy velocity [L/t], **D** is the dispersion coefficient tensor [L^2/t], $r_i\big|_N$ is the production rate of species i due to all N reactions in the unit of chemical mass per volume of water per time [M/L^3/t], $M_{C_i}^{\ as}$ is the artificial source of C_i in unit of chemical mass per unit of medium volume [M/L^3/t], and M_m is the number of mobile chemical species.

Concentrations of all mobile species must be given initially for transient simulations. Similar to salinity transport, six types of boundary conditions are taken into account for mobile species, including Dirichlet, Variable, Cauchy, Neumann, river/stream-overland interface, and overland-subsurface interface boundary conditions (Yeh et al., 2005). These boundary conditions are stated below:

Dirichlet boundary condition: This condition is applied when the species concentration is prescribed as a function of time on the boundaries:

$$C_i(\mathbf{x},t) = C_{idb}(\mathbf{x},t) \quad on \quad B_d(\mathbf{x}) = 0 \qquad \textbf{(2.7.6)}$$

where $C_{idb}(\mathbf{x},t)$ is a time-dependent concentration of the i-th species on the Dirichlet boundary, $B_d(\mathbf{x}) = 0$, [M/M].

Variable boundary condition: This boundary condition is employed when the flow direction would change with time during simulations. Two cases are considered, regarding to the flow direction on the boundary.

< Case 1 > Flow is coming in from outside:

$$\mathbf{n}\cdot\left[\mathbf{V}\rho_i C_i - \theta\mathbf{D}\cdot\nabla(\rho_i C_i)\right] = (\mathbf{n}\cdot\mathbf{V})\rho_i C_{ivb}(\mathbf{x},t) \quad on \quad B_v(\mathbf{x}) = 0 \qquad \textbf{(2.7.7)}$$

< Case 2 > Flow is going out from inside:

$$-\mathbf{n}\cdot\left[\theta\mathbf{D}\cdot\nabla(\rho_i C_i)\right] = 0 \quad on \quad B_v(\mathbf{x}) = 0 \qquad \textbf{(2.7.8)}$$

where $C_{ivb}(\mathbf{x},t)$ is a time-dependent concentration of the i-th species [M/M] on the variable boundary, $B_v(\mathbf{x}) = 0$, which is associated with the incoming flow.

Cauchy boundary condition: This boundary condition is employed when the total salt-flow rate is given at pervious boundaries. Usually, this boundary is a flow-in boundary. The conditions are expressed as

$$\mathbf{n}\cdot\left[\mathbf{V}\rho_i C_i - \theta\mathbf{D}\cdot\nabla(\rho_i C_i)\right] = Q_{C_i cb}(\mathbf{x},t) \quad on \quad B_c(\mathbf{x}) = 0 \qquad \textbf{(2.7.9)}$$

where $Q_{C_i cb}(\mathbf{x},t)$ is total chemical flux of the *i*-th species [M/L^2/t] through the Cauchy boundary, $B_c(\mathbf{x}) = 0$, which takes a positive value if it is going out of the region and a negative value if it is coming into the region.

Neumann boundary condition: This boundary condition is used when the dispersive salt-flow rate is known at the boundary. It can be written as

$$-\mathbf{n}\cdot\left(\theta\mathbf{D}\cdot\nabla(\rho_i C_i)\right) = Q_{C_i nb}(\mathbf{x},t) \quad on \quad B_n(\mathbf{x}) = 0 \qquad \textbf{(2.7.10)}$$

where $Q_{C_i nb}(\mathbf{x},t)$ is the chemical flux of the *i*-th species through the Neumann boundary, $B_n(\mathbf{x}) = 0$, [M/L^2/t].

In addition to the four types of global boundary conditions, two interface boundary conditions may be specified: one for the exchange of chemicals between the subsurface media and river/stream network and the other for chemical exchange between the subsurface media and the overland. Mathematically, these boundary conditions are described below.

Subsurface-river interface boundary condition:

$$\mathbf{n}\cdot\left[\mathbf{V}\rho_i C_i - \theta\mathbf{D}\cdot\nabla(\rho_i C_i)\right] = (\mathbf{n}\cdot\mathbf{V})\frac{1}{2}\left\{\left[1+sign(\mathbf{n}\cdot\mathbf{V})\right]\rho_i C_i + \left[1-sign(\mathbf{n}\cdot\mathbf{V})\right]\rho_i C_{i1D}(x_b,y_b,z_b,t)\right\} \qquad \textbf{(2.7.11)}$$

where $C_{i1D}(x_b,y_b,z_b,t)$ is the time-dependent concentration of the *i*-th species at the 1-D node corresponding to the subsurface-river/stream interfacial boundary points [M/M].

Subsurface-overland interface boundary condition:

$$\mathbf{n}\cdot\left[\mathbf{V}\rho_i C_i - \theta\mathbf{D}\cdot\nabla(\rho_i C_i)\right] = (\mathbf{n}\cdot\mathbf{V})\frac{1}{2}\left\{\left[1+sign(\mathbf{n}\cdot\mathbf{V})\right]\rho_i C_i + \left[1-sign(\mathbf{n}\cdot\mathbf{V})\right]\rho_i C_{i2D}(x_b,y_b,z_b,t)\right\} \qquad \textbf{(2.7.12)}$$

where $C_{i2D}(x_b,y_b,z_b,t)$ is the time-dependent concentration of the *i*-th species at the 2-D node corresponding to the subsurface-overland interfacial boundary point [M/M].

2.7.3 Diagonalization of Species Transport Equations

The temporal-spatial distribution of chemical species is described by a system of M_{im} mass balance equations [equation (2.7.3)], and M_m reactive transport equations [equation (2.7.5)]. These two equations can be recast in the following form

$$\frac{\partial(\theta\rho_i C_i)}{\partial t} + \alpha_i L(\rho_i C_i) = \theta r_i\big|_N, \quad i \in M \qquad \textbf{(2.7.13)}$$

where L is an operator defined as

$$L(\rho_i C_i) = \nabla \cdot (\mathbf{V}\rho_i C_i) - \nabla \cdot [\theta \mathbf{D} \cdot \nabla(\rho_i C_i)] - M_{C_i}{}^{as} \qquad \textbf{(2.7.14)}$$

The determination of $r_i\,|_N$ and associated parameters is a primary challenge in biogeochemical modeling. Instead of using an ad hoc method to formulate $r_i\,|_N$, we use reaction-based formulations (Steefel and Cappellen, 1998). In a reaction-based formulation, $r_i\,|_N$ is given by the summation of rates of all reactions that the *i*-th species participates in,

$$r_i\,|_N = \frac{d(\rho_i C_i)}{dt}\Big|_{reaction} = \sum_{k=1}^{N}[(\nu_{ik} - \mu_{ik})r_k], \quad i \in M \qquad \textbf{(2.7.15)}$$

where ν_{ik} is the reaction stoichiometry of the *i*-th species in the *k*-th reaction associated with the products, μ_{ik} is the reaction stoichiometry of the *i*-th species in the *k*-th reaction associated with the reactants, and r_k is the rate of the *k*-th reaction.

Substituting equation (2.7.15) into equation (2.7.18) results in the transport equations of *M* chemical species described by

$$\frac{\partial(\theta\rho_i C_i)}{\partial t} + \alpha_i L(\rho_i C_i) = \theta\sum_{k=1}^{N}[(\nu_{ik} - \mu_{ik})r_k], \quad i \in M; \quad or \quad \mathbf{U}\frac{\partial \mathbf{C}_\theta}{\partial t} + \boldsymbol{\alpha} L(\mathbf{C}) = h\boldsymbol{\nu}\mathbf{r} \qquad \textbf{(2.7.16)}$$

where **U** is a unit matrix, $\mathbf{C}_{\boldsymbol{\theta}}$ is a vector with its components representing *M* species concentrations multiply the moisture content [M/L^3], $\boldsymbol{\alpha}$ is a diagonal matrix with α_i as its diagonal component, **C** is a vector with its components representing M species concentrations [M/L^3], $\boldsymbol{\nu}$ is the reaction stoichiometry matrix, and **r** is the reaction rate vector with *N* reaction rates as its components. Equation (2.7.16) represents a mass balance for species *i*, which states that the rate of change of any species mass is due to advection-dispersion coupled with contributing reactions that describe the biogeochemical processes.

In a primitive approach, equation (2.7.16) is integrated to yield the distributions and evolutions of chemical species in a region of interest. However, when some fast equilibrium reactions take place in the system, this approach is not adequate (Fang et al., 2003). Here, we will take a diagonalization approach through decomposition. Equation (2.7.16) written in matrix form can be decomposed based on the type of biogeochemical reactions via Gauss-Jordan column reduction of reaction matrix $\boldsymbol{\nu}$. Among all the fast/equilibrium and slow/kinetic reactions, "redundant reactions" are defined as fast reactions that are linearly dependent on other fast reactions, and "irrelevant reactions" are kinetic reactions that are linearly dependent on only equilibrium reactions. In order to avoid singularity of the reaction matrix, redundant fast reactions are omitted from the system prior to decomposition. The removal of irrelevant slow reactions alleviates problems associated with rate formulation uncertainty and parameterization for these reactions.

Decomposition is performed by pivoting on the N_E equilibrium reactions and decoupling them from the N_K kinetic reactions. In other words, each fast reaction can be used to eliminate one chemical species from simultaneous consideration. An incomplete Gauss-Jordan row decomposition of the reaction matrix $\boldsymbol{\nu}$ by pivoting on N_E equilibrium reactions will result in N_E equilibrium-variables and N_{KIV} kinetic-variables. To analyze the system behavior, it is advantageous to perform a

complete decomposition, in which the reduction of the reaction matrix is done by pivoting on N_E equilibrium reactions and on N_{KI} linearly independent kinetic reactions to result in N_E equilibrium-variables, N_{KI} kinetic-variables, and N_C components. The complete decomposition is given as follows:

$$\begin{bmatrix} \mathbf{A_{11}} & \mathbf{0_{12}} & \mathbf{0_{13}} \\ \mathbf{A_{21}} & \mathbf{A_{22}} & \mathbf{0_{23}} \\ \mathbf{A_{31}} & \mathbf{A_{32}} & \mathbf{U_{33}} \end{bmatrix} \begin{Bmatrix} \dfrac{\partial \mathbf{C}_{\theta 1}}{\mathrm{dt}} \\ \dfrac{\partial \mathbf{C}_{\theta 2}}{\mathrm{dt}} \\ \dfrac{\partial \mathbf{C}_{\theta 3}}{\mathrm{dt}} \end{Bmatrix} + \begin{bmatrix} \mathbf{B_{11}} & \mathbf{0_{12}} & \mathbf{0_{13}} \\ \mathbf{B_{21}} & \mathbf{B_{22}} & \mathbf{0_{23}} \\ \mathbf{B_{31}} & \mathbf{B_{32}} & \boldsymbol{\alpha}_{33} \end{bmatrix} \mathrm{L}\left(\begin{Bmatrix} \mathbf{C_1} \\ \mathbf{C_2} \\ \mathbf{C}_3 \end{Bmatrix} \right) = \theta \begin{bmatrix} \mathbf{D_{11}} & \mathbf{K_{12}} & \mathbf{K_{13}} \\ \mathbf{0_{21}} & \mathbf{D_{22}} & \mathbf{K_{23}} \\ \mathbf{0_{31}} & \mathbf{0_{32}} & \mathbf{0_{33}} \end{bmatrix} \begin{Bmatrix} \mathbf{r_1} \\ \mathbf{r_2} \\ \mathbf{r_3} \end{Bmatrix} \quad \textbf{(2.7.17)}$$

where $\mathbf{A_{11}}$ is the submatrix of the reduced **U** matrix with size of $N_E \times N_E$, $\mathbf{A_{21}}$ is the submatrix of the reduced **U** matrix with size of $N_{KI} \times N_E$, and $\mathbf{A_{31}}$ is the submatrix of the reduced **U** matrix with size of $N_C \times N_E$; $\mathbf{0_{12}}$ is the zero submatrix of the reduced **U** matrix with size of $N_E \times N_{KI}$, $\mathbf{A_{22}}$ is the submatrix of the reduced **U** matrix with size of $N_{KI} \times N_{KI}$, and $\mathbf{A_{32}}$ is the submatrix of the reduced **U** matrix with size of $N_C \times N_{KI}$; $\mathbf{0_{13}}$ is the zero submatrix of the reduced **U** matrix with size of $N_E \times N_C$, $\mathbf{0_{23}}$ is the submatrix of the reduced **U** matrix with size of $N_{KI} \times N_C$, and $\mathbf{U_{33}}$ is the unit submatrix of the reduced **U** matrix with size of $N_C \times N_C$; $\mathbf{C_{h1}}$, $\mathbf{C_{h2}}$, and $\mathbf{C_{h3}}$ are the subvectors of the vector $\mathbf{C_h}$ with sizes of N_E, N_{KI}, and N_C, respectively; $\mathbf{B_{11}}$ is the submatrix of the reduced $\boldsymbol{\alpha}$ matrix with size of $N_E \times N_E$, $\mathbf{B_{21}}$ is the submatrix of the reduced $\boldsymbol{\alpha}$ matrix with size of $N_{KI} \times N_E$, and $\mathbf{B_{31}}$ is the submatrix of the reduced $\boldsymbol{\alpha}$ matrix with size of $N_C \times N_E$; $\mathbf{0_{12}}$ is the zero submatrix of the reduced $\boldsymbol{\alpha}$ matrix with size of $N_E \times N_{KI}$, $\mathbf{A_{22}}$ is the submatrix of the reduced $\boldsymbol{\alpha}$ matrix with size of $N_{KI} \times N_{KI}$, and $\mathbf{B_{32}}$ is the submatrix of the reduced $\boldsymbol{\alpha}$ matrix with size of $N_C \times N_{KI}$; $\mathbf{0_{13}}$ is the zero submatrix of the reduced $\boldsymbol{\alpha}$ matrix with size of $N_E \times N_C$, $\mathbf{0_{23}}$ is the submatrix of the reduced $\boldsymbol{\alpha}$ matrix with size of $N_{KI} \times N_C$, and $\boldsymbol{\alpha}_{33}$ is the diagonal submatrix of the reduced $\boldsymbol{\alpha}$ matrix with size of $N_C \times N_C$; $\mathbf{C_1}$, $\mathbf{C_2}$, and $\mathbf{C_3}$ are the subvectors of the vector **C** with sizes of N_E, N_{KI}, and N_C, respectively; $\mathbf{D_{11}}$ is the diagonal submatrix of the reduced $\boldsymbol{\nu}$ matrix with size of $N_E \times N_E$, $\mathbf{K_{12}}$ is the submatrix of the reduced $\boldsymbol{\nu}$ matrix with size of $N_E \times N_{KI}$, and $\mathbf{K_{13}}$ is the submatrix of the reduced $\boldsymbol{\nu}$ matrix with size of $N_E \times N_{KD(k)}$; $\mathbf{0_{21}}$ is the zero submatrix of the reduced $\boldsymbol{\nu}$ matrix with size of $N_{KI} \times N_E$, $\mathbf{D_{22}}$ is the diagonal submatrix of the reduced $\boldsymbol{\nu}$ matrix with size of $N_{KI} \times N_{KI}$, and $\mathbf{K_{23}}$ is the submatrix of the reduced $\boldsymbol{\nu}$ matrix with size of $N_{KI} \times N_{KD(k)}$; $\mathbf{0_{13}}$ is the zero submatrix of the reduced $\boldsymbol{\nu}$ matrix with size of $N_C \times N_E$, $\mathbf{0_{32}}$ is the zero submatrix of the reduced $\boldsymbol{\nu}$ matrix with size of $N_C \times N_{KI}$, and $\mathbf{0_{33}}$ is the zero submatrix of the reduced $\boldsymbol{\nu}$ matrix with size of $N_C \times N_{KD(k)}$; $\mathbf{r_1}$, $\mathbf{r_2}$, and $\mathbf{r_3}$ are the subvectors of the vector **r** with sizes of N_E, N_{KI}, and $N_{KD(k)}$, respectively.

For incomplete decomposition of the reaction matrix $\boldsymbol{\nu}$, Equation (2.7.17) can be connoted as

$$\begin{bmatrix} \mathbf{A_{11}} & \mathbf{0_{12}} \\ \mathbf{A_{21}} & \mathrm{U}_{22} \end{bmatrix} \begin{Bmatrix} \dfrac{\partial \mathbf{C}_{\theta 1}}{\mathrm{dt}} \\ \dfrac{\partial \mathbf{C}_{\theta 2}}{\mathrm{dt}} \end{Bmatrix} + \begin{bmatrix} \mathbf{B_{11}} & \mathbf{0_{12}} \\ \mathbf{B_{21}} & \boldsymbol{\alpha}_{22} \end{bmatrix} \mathrm{L}\left(\begin{Bmatrix} \mathbf{C_1} \\ \mathbf{C}_2 \end{Bmatrix} \right) = \theta \begin{bmatrix} \mathbf{D_{11}} & \mathbf{K_{12}} \\ \mathbf{0_{21}} & \mathbf{K_{22}} \end{bmatrix} \begin{Bmatrix} \mathbf{r_1} \\ \mathbf{r_2} \end{Bmatrix} \quad \textbf{(2.7.18)}$$

where $\mathbf{A_{11}}$ and $\mathbf{A_{21}}$ are the submatrices of the reduced **U** matrix with size of $N_E \times N_E$ and $N_{KIV} \times N_E$, respectively (note that $N_{KIV} = M - N_E = N_{\mathrm{KI}} + N_C$); $\mathbf{0_{12}}$ and $\mathbf{U_{22}}$ are the zero- and unit-submatrices,

respectively, of the reduced **U** matrix with size of $N_E \times N_{KIV}$ and $N_{KIV} \times N_{KIV}$, respectively; $\mathbf{C_{\theta 1}}$ and $\mathbf{C_{\theta 2}}$ are the subvectors of the vector $\mathbf{C_\theta}$ with sizes of N_E and N_{KIV}, respectively; $\mathbf{B_{11}}$ and $\mathbf{B_{21}}$ are the submatrices of the reduced $\boldsymbol{\alpha}$ matrix with sizes of $N_E \times N_E$ and $N_{KIV} \times N_E$, respectively; $\mathbf{0_{12}}$ and $\boldsymbol{\alpha}_{22}$ are the zero- and unit- submatrices, respectively, of the reduced $\boldsymbol{\alpha}$ matrix with size of $N_E \times N_{KIV}$ and $N_{KIV} \times N_{KIV}$, respectively; $\mathbf{C_1}$ and $\mathbf{C_2}$ are the subvectors of the vector **C** with sizes of N_E and N_{KIV}, respectively; $\mathbf{D_{11}}$ is the diagonal submatrix of the reduced $\boldsymbol{\nu}$ matrix with size of $N_E \times N_E$ and $\mathbf{K_{12}}$ is the submatrix of the reduced $\boldsymbol{\nu}$ matrix with size of $N_E \times N_{KIV}$; $\mathbf{0_{21}}$ is the zero submatrix of the reduced $\boldsymbol{\nu}$ matrix with size of $N_{KIV} \times N_E$ and $\mathbf{K_{22}}$ is the submatrix of the reduced $\boldsymbol{\nu}$ matrix with size of $N_{KIV} \times N_E$; $\mathbf{r_1}$ and $\mathbf{r_2}$ are the subvectors of the vector **r** with sizes of N_E and N_{KIV}, respectively.

For reactions that are fast, equilibrium may be regarded as being reached instantaneously among the relevant species and the reaction rates may be regarded as infinite. An infinite rate is mathematically represented by a mass action equation or a user specified nonlinear algebraic equation. As a result, the decomposition of equation (2.7.16) to equation (2.7.18) effectively reduces a set of *M* species reactive transport equations into two subsets of equations. The first set contains N_E algebraic equations representing mass action laws for the equilibrium reactions, and the second set contains N_{KIV} kinetic-variable transport equations. These equation subsets are defined as

Algebraic Equations for Equilibrium Reactions

$$\frac{\partial(\theta E_i)}{\partial t} + L(E_i^m) = \theta D_{1ii} r_{1i} + \theta \sum_{j=1}^{N_K} K_{1ij} r_{2j},\ i \in N_E \quad \Rightarrow \quad r_{1i} = \infty \quad \Rightarrow \quad \frac{\partial(\theta E_i)}{\partial t} \approx \infty$$

which is replaced with a thermodynamically consistent equation: $K_i^e = \prod_{j \in M} A_j^{\nu_{ji}} \Big/ \prod_{j \in M} A_j^{\mu_{ji}}$ **(2.7.19)**

$$or\ \ F_i(C_1,..,C_M; p_1, p_2,..) = 0 \quad where\ E_i = \sum_{j=1}^{N_E} A_{1ij} C_{1j} \ \ and \ \ E_i^m = \sum_{j=1}^{N_E} B_{1ij} C_{1j}$$

where K_i^e is the equilibrium constant of the *i*-th fast reaction, A_j is the activity of the *j*-th species, $F_i(C_1,..,C_M; p_1,p_2,..)$ is an empirical function of all species and a number of parameters p, p2, … for the *i*-th fast reaction. E_i was called an equilibrium-variable (Fang, et al., 2003) because $\frac{\partial(\theta E_i)}{\partial t} \approx \infty$ simply means that E_i can reach equilibrium instantaneously.

Transport Equations for Kinetic-Variables

$$\frac{\partial(\theta E_i)}{\partial t} + L(E_i^m) = \theta \sum_{j=1}^{N_K} K_{2nj} r_{2j},\ \ i \in N_{KIV} = M - N_E$$
$$where\ E_i = \sum_{j=1}^{N_E} A_{2ij} C_{1j} + C_{2i} \ and \ E_i^m = \sum_{j=1}^{N_E} B_{2ij} C_{1j} + \alpha_{1i} C_{2i} \qquad \textbf{(2.7.20)}$$

where E_i was called a kinetic variable (Fang, et al., 2003) because as E_i is transported it is subject to only kinetic reactions. This is in contrast to Eq. (2.7.16) where as C_i is transported, it is subject to both equilibrium and kinetic reactions.

Assign

$$R_i = \sum_{j=1}^{N_K} K_{2ij} r_{2j},\ \mathrm{i} \in N_{KIV} \qquad \textbf{(2.7.21)}$$

The reduction of Eq. (2.7.15) to Eq. (2.7.18) and (2.7.19) is equivalent to reducing M governing equations for immobile and mobile species to N_E algebraic equations for equilibrium variables and N_{KIV} transport equations for kinetic-variables specified as follows

$$\frac{\partial(\theta E_i)}{\partial t} + \nabla\bullet(\mathbf{V}E_i^m) - \nabla\bullet\left[(\theta\mathbf{D}\bullet\nabla E_i^m)\right] = M_{E_i^{as}} + \theta R_i,\ i \in N_{KIV} \qquad \textbf{(2.7.22)}$$

where E_i is the concentration of the i-th kinetic-variable [M/L^3], E_i^m is the concentration of mobile part of the i-th kinetic-variable [M/L^3], $M_{E_i^{as}}$ is the artificial source of the i-th kinetic-variable [M/L^3/T], R_i is the production rate of i-th kinetic-variable due to biogeochemical reactions [M/L^3/T], and N_{KIV} is the number of kinetic variable variables.

Initial and boundary condition for chemical species need to be transformed into corresponding initial and boundary conditions for kinetic-variables, which are stated in the following.

Dirichlet boundary condition:

$$E_i^m = E_{id}^m(x_b, y_b, z_b, t) \qquad on \qquad B_d(\mathbf{x}) = 0 \qquad \textbf{(2.7.23)}$$

where $E_{id}^m(x_b, y_b, t)$ is the specified concentration of the mobile portion of the i-th kinetic variable on the Dirichlet boundary $B_d(\mathbf{x}) = 0$ [M/L^3].

Variable boundary condition:

< Case 1 > Flow is coming in from outside (nQ < 0)

$$\mathbf{n}\bullet\left(\mathbf{V}E_i^m - \theta\mathbf{D}\bullet\nabla E_i^m\right) = \mathbf{n}\bullet\mathbf{V}E_{iv}^m(x_b, y_b, z_b, t) \qquad on \qquad B_v(\mathbf{x}) = 0 \qquad \textbf{(2.7.24)}$$

< Case 2 > Flow is going out from inside (nQ > 0).

$$-\mathbf{n}\bullet\left(\theta\mathbf{D}\bullet\nabla E_i^m\right) = 0 \qquad on \qquad B_v(\mathbf{x}) = 0 \qquad \textbf{(2.7.25)}$$

where $\mathbf{n}$ is the unit outward vector and $E_{iv}^m(x_b, y_b, z_b, t)$ is the concentration of the mobile portion of the i-th kinetic variable on the variable boundary $B_v(\mathbf{x}) = 0$ [M/L^3].

Cauchy boundary condition:

$$\mathbf{n}\bullet\left(\mathbf{V}E_i^m - \theta\mathbf{D}\bullet\nabla E_i^m\right) = Q_{cE_i^m}(x_b, y_b, z_b, t) \qquad on \qquad B_c(\mathbf{x}) = 0 \qquad \textbf{(2.7.26)}$$

where $Q_{cE_i^m}(x_b, y_b z_b, t)$ is the mass flux of E_i^m through the Cauchy boundary $B_c(\mathbf{x}) = 0$ [M/t/L^2].

Neumann boundary condition:

$$-\mathbf{n}\bullet\left(\theta\mathbf{D}\bullet\nabla E_i^m\right)=Q_{nE_i^m}(x_b,y_b,z_b,t)\quad on\quad B_n(\mathbf{x})=0 \qquad \textbf{(2.7.27)}$$

where $Q_{nE_i^m}(x_b,y_b,z_b,t)$ is the mass flux of E_i^m through the Neumann boundary $B_n(\mathbf{x})=0$ [M/t/L^2].

Subsurface-river interface boundary condition:

$$\mathbf{n}\cdot\left[\mathbf{V}E_i^m-\theta\mathbf{D}\cdot\nabla(E_i^m)\right]=(\mathbf{n}\cdot\mathbf{V})\frac{1}{2}\left\{\left[1+sign(\mathbf{n}\cdot\mathbf{V})\right]E_i^m+\left[1-sign(\mathbf{n}\cdot\mathbf{V})\right]E_i^m(C_j^{1D}{}'s)\right\} \qquad \textbf{(2.7.28)}$$

Where $E_i^m(C_j^{1D}{}'s)$ is the mobile portion of the subsurface *i*-th kinetic variables with its argument being the linear combination of 1-D river/stream species concentrations $C_j^{1D}{}'s$ [M/L^3].

Subsurface-overland interface boundary condition:

$$\mathbf{n}\cdot\left[\mathbf{V}E_i^m-\theta\mathbf{D}\cdot\nabla(E_i^m)\right]=(\mathbf{n}\cdot\mathbf{V})\frac{1}{2}\left\{\left[1+sign(\mathbf{n}\cdot\mathbf{V})\right]E_i^m+\left[1-sign(\mathbf{n}\cdot\mathbf{V})\right]E_i^m(C_j^{2D}{}'s)\right\} \qquad \textbf{(2.7.29)}$$

where $E_i^m(C_j^{2D}{}'s)$ is the mobile portion of the subsurface *i*-th kinetic variables with its argument being the linear comination of 2-D overland species concentrations $C_j^{2D}{}'s$ [M/L^3].

2.8 Coupling Transport Among Various Media

As in coupling flows among various media, a rigorous treatment of coupling transport among media should be based the continuity of material fluxes and state variables. This rigorous treatment in coupling chemical transport among various media can be taken similar to the case of flows. We simply impose the continuity of material fluxes and species concentrations for all mobile (between river/stream networks and overland regime) dissolved aqueous species (between subsurface media and overland regime and between subsurface media and river/stream networks) .

However, because the state variables (dissolved chemical concentrations, suspend sediment concentrations, and mobile particulate chemical concentrations) in various media may not be continuous because these state variables are true three-dimensional distribution in subsurface media, but are vertically averaged quantities in overland regime and cross-sectional area averaged quantity in river/stream networks. Because of the averaging processes, mass fluxes between media can be considered due mainly to the advective transport. If this assumption is valid, the coupling of transport among various medial is much simpler than that for fluid flow.

2.8.1 Coupling between Overland Transport and River/StreamNetworks

The coupling of transport between overland and canal is similar to that of salinity transport. When a levee is present on the bank of the canal (left column in Fig. 2.4-1), there are several possibilities on the interactions between overland and river flow transport. If water surfaces in both the overland regime and river are below the top of the levee, the two flow systems are decoupled and transport in overland is decoupled from that in river networks (Fig. 2.4-1a).

When the water surface in the overland regime is above the top of the levee and in the canal is below the top of the levee (Fig. 2.4-1b), the flow is from the overland to river network and thus the transport is also one way from the overland to river network. The fluxes are given by

$$\mathbf{n}\cdot\left[\mathbf{q}\rho C-\mathbf{D}h\cdot\nabla(\rho C)\right]\Big|_{Bank\,1}=M_{C_i}^{\ osl}=S_1\rho C^{o} \qquad \textbf{(2.8.1)}$$

where C [denotes S_n with $\rho=1$ for supended sediment, C_w with $\rho=\rho_w$ for dissolved species, C_p with $\rho=\rho_w$ for precipitated species, C_{Sn} with $\rho=S_n$ for particulate species] is sediment concentration [M/L^3] or species concentrations [M/M] in the overland flow, $M_{C_i}^{\ osl}$ is the source rate of the i-th species in the canal from the overland via bank *1*, which appeared in Eq. (2.5.30) [M/t/L], C^o is the value of C in the overland water at the interface. When the water surface in the overland regime is below the top of the levee and in the canal is above the top of the levee (Fig. 2.4-1c), the flow is from the canal to overland and thus the transport is one way from the canal to overland. The fluxes are given by

$$\mathbf{n}\cdot\left[\mathbf{q}\rho C-\mathbf{D}h\cdot\nabla(\rho C)\right]\Big|_{Bank\,1}=M_{C_i}^{\ osl}=S_1\rho C^{c} \qquad \textbf{(2.8.2)}$$

where C^c is the value of C in the canal water. When the water surfaces in the overland and canal are above the top of the levee (Fig. 2.4-1d), flow direction can e either from the overland to the canl or from the canal to the overland depending on the flow dynamics in the overland and in the canal. If the state variable C is discontinues at the interface of the canal and overland, the fluxes are given by

$$\mathbf{n}\cdot\left[\mathbf{q}\rho C-\mathbf{D}h\cdot\nabla(\rho C)\right]\Big|_{Bank\,1}=M_{C_i}^{\ osl}=S_1\frac{1}{2}\left[\left(1+sign\left(S_1\right)\right)\rho C^{o}+\left(1-sign\left(S_1\right)\right)\rho C^{c}\right] \qquad \textbf{(2.8.3)}$$

If the state variable is continuous, the fluxes are modeled by imposing its continuity to yield the fluxes

$$\mathbf{n}\cdot\left[\mathbf{q}\rho C-\mathbf{D}h\cdot\nabla(\rho C)\right]\Big|_{Bank\,1}=M_{C_i}^{\ osl}\quad and\quad C^{o}\Big|_{Bank\,1}=C^{c} \qquad \textbf{(2.8.4)}$$

When a levee is not present on the bank of the canal (right column in Fig. 2.4-1), there are two possibilities on the interactions between overland and river transport. If water surface in the canal falls below the bank, the flux is either zero if the overland flow is not present or is nonzero and directed from the overland into the canal if overland flow is present (Fig. 2.4-1e). Under this circumstance, the fluxes are given by

$$\mathbf{n}\cdot\left[\mathbf{q}\rho C-\mathbf{D}h\cdot\nabla(\rho C)\right]\Big|_{Bank\,2}=M_{C_i}^{\ os2}=S_2\rho C^{o} \qquad \textbf{(2.8.5)}$$

where $M_{C_i}^{os2}$ is the source rate of the *i*-th species in the canal from the overland via bank *2*, which appeared in Eq. (2.5.30) [M/t/L],

When the water surface in the canal is above the bank (Figs. 2.4-1f and 2.4-1.g), the flow direction can be either from the overland into the canal or from the canal into the overland depending on the flow dynamics in the overland and in the canal. If the state variable is discontinuous, the fluxes are

$$\mathbf{n}\cdot\left[\mathbf{q}\rho C - \mathbf{D}h\cdot\nabla(\rho C)\right]\Big|_{Bank\,2} = M_{C_i}^{os2} = S_2\frac{1}{2}\left[\left(1+sign\left(S_2\right)\right)\rho C^{o} + \left(1-sign\left(S_2\right)\right)\rho C^{c}\right] \qquad \textbf{(2.8.6)}$$

If the state variable is continuous, we impose the continuity of the state variable to yield the fluxes

$$\mathbf{n}\cdot\left[\mathbf{q}\rho C - \mathbf{D}h\cdot\nabla(\rho C)\right]\Big|_{Bank\,2} = M_{C_i}^{os2} \quad and \quad C^{o}\Big|_{Bank\,2} = C^{c} \qquad \textbf{(2.8.7)}$$

Because kinetic variables *E* are chosen as the primary variables in the transport module, for reactive chemical transport, the interfacial boundary conditions in terms of species concentrations must be transformed into those in terms of kinetic variables. Since reaction networks in overland and river/stream/canal networks are identical, every corresponding kinetic variable in the overland and river/stream networks contains the same mobile portion. Thus, one simply replaces ρC with E_i^m in Eqs. (2.8.1) through (2.8.7). For completeness of this report, these equations are listed below.

For couling via bank 1:

When the water surface in the overland regime is above the top of the levee and in the canal is below the top of the levee (Fig. 2.4-1b), the flow is from the overland to river network and thus the transport is also one way from the overland to river network. The flux of the *i*-th kinetic variables are given by

$$\mathbf{n}\cdot\left[\mathbf{q}E_i^m - \mathbf{D}h\cdot\nabla E_i^m\right]\Big|_{Bank\,1} = M_{E_i}^{os1} = S_1\left(E_i^m\right)^{o} \qquad \textbf{(2.8.8)}$$

When the water surface in the overland regime is below the top of the levee and in the canal is above the top of the levee (Fig. 2.4-1c), the flow is from the canal to overland and thus the transport is one way from the canal to overland, the flux of the i-th kinetic variable is given as

$$\mathbf{n}\cdot\left[\mathbf{q}E_i^m - \mathbf{D}h\cdot\nabla E_i^m\right]\Big|_{Bank\,1} = M_{E_i}^{os1} = S_1\left(E_i^m\right)^{c} \qquad \textbf{(2.8.9)}$$

When the water surfaces in the overland and canal are above the top of the levee (Fig. 2.4-1d), flow direction can e either from the overland to the canl or from the canal to the overland depending on the flow dynamics in the overland and in the canal. If the state variable *E* is discontinues at the interface of the canal and overland, the fluxes are given by

$$\mathbf{n}\cdot\left[\mathbf{q}E_i^m - \mathbf{D}h\cdot\nabla E_i^m\right]\Big|_{Bank\,1} = M_{E_i}^{os1} = S_1\frac{1}{2}\left[\left(1+sign\left(S_1\right)\right)\left(E_i^m\right)^{o} + \left(1-sign\left(S_1\right)\right)\left(E_i^m\right)^{c}\right] \qquad \textbf{(2.8.10)}$$

If the state variable *E* is continuous, the fluxes are modeled by imposing its continuity to yield the

fluxes

$$\mathbf{n}\cdot\left[\mathbf{q}E_i^m - \mathbf{D}h\cdot\nabla E_i^m\right]\Big|_{Bank\,1} = M_{E_i}^{os1} \quad and \quad \left(E_i^m\right)^o\Big|_{Bank\,1} = \left(E_i^m\right)^c \tag{2.8.11}$$

In Equations (2.8.8) through (2.8.11), E_i^m is the concentration of the mobile portion of the *i*-th kinetic variable [M/L^3], $\left(E_i^m\right)^o$ is the value of E_i^m in the overland water at the interface [M/L^3], and $M_{E_i}^{os1}$ is the source of the kinetic variable E_i in the canal from the overland via bank *1* [M/t/L], which appeared in Eq. (2.5.44), and $\left(E_i^m\right)^c$ is the value of E_i^m in the canal water at the interface.

For couling via bank 2:

When a levee is not present on the bank of the canal (right column in Fig. 2.4-1), there are two possibilities on the interactions between overland and river transport. If water surface in the canal falls below the bank, the flux is either zero if the overland flow is not present or is nonzero and directed from the overland into the canal if overland flow is present (Fig. 2.4-1e). Under this circumstance, the fluxes are given by

$$\mathbf{n}\cdot\left[\mathbf{q}E_i^m - \mathbf{D}h\cdot\nabla E_i^m\right]\Big|_{Bank\,2} = M_{E_i}^{os2} = S_2\left(E_i^m\right)^o \tag{2.8.12}$$

When the water surface in the canal is above the bank (Figs. 2.4-1f and 2.4-1g), the flow direction can be either from the overland into the canal or from the canal into the overland depending on the flow dynamics in the overland and in the canal. If the state variable is discontinuous, the fluxes are

$$\mathbf{n}\cdot\left[\mathbf{q}E_i^m - \mathbf{D}h\cdot\nabla E_i^m\right]\Big|_{Bank\,2} = M_{E_i}^{os2} = S_2\frac{1}{2}\left[\left(1+sign\left(S_2\right)\right)\left(E_i^m\right)^o + \left(1-sign\left(S_2\right)\right)\left(E_i^m\right)^c\right] \tag{2.8.13}$$

If the state variable is continuous, we impose the continuity of the state variable to yield the fluxes

$$\mathbf{n}\cdot\left[\mathbf{q}E_i^m - \mathbf{D}h\cdot\nabla E_i^m\right]\Big|_{Bank\,2} = M_{E_i}^{os2} \quad and \quad \left(E_i^m\right)^o\Big|_{Bank\,2} = \left(E_i^m\right)^c \tag{2.8.14}$$

In Equstions (2.8.12) through (2.8.14), $M_{E_i}^{os2}$ is the source of the kinetic variable E_i in the canal from the overland via bank *2* [M/t/L], which appeared in Eq. (2.5.44).

2.8.2 Coupling between Subsurface and Overland Transport

The coupling of overland and subsurface transport is through the exchange of dissolved species only. Sediments, particulate species, and precipitated species in the overland flow will not exchange with adsorbed/ion exchanged and precipitated species in the subsurface flow. If the concentrations of dissolved chemicals in overland water and subsurface water at the ground surface are discontinuous, the chemical flux is given by

$$\mathbf{n}\cdot\left[\mathbf{V}\rho_w C_i^w - \theta\mathbf{D}\cdot\nabla(\rho_w C_i^w)\right] = M_{C_i^{is}} = \frac{S_I}{2}\left[\left(1+sign(S_I)\right)\rho_w\left(C_i^w\right)^s + \left(1-sign(S_I)\right)\rho_w\left(C_i^w\right)^o\right] \quad \textbf{(2.8.15)}$$

where $\left(C_i^w\right)^o$ is the concentration of the *i*-th dissolved species in the overland water and $\left(C_i^w\right)^s$ is the concentration of the *i*-th dissolved species of subsurface water at the interface and $M_{C_i^{is}}$ is mass rate of the source of the *i*-th dissolved species in overland from subsurface media [M/t/L^2], which appeared in Eq. (2.6.31). If the concentrations are continuous, we impose the continuity of dissolved concentration to yield the fluxes

$$\mathbf{n}\cdot\left[\mathbf{V}\rho_i C_i^w - \theta\mathbf{D}\cdot\nabla(\rho_i C_i^w)\right] = M_{C_i^{is}} \text{ and } \left(C_i^w\right)^s\Big|_{\text{on the interface}} = \left(C_i^w\right)^o \quad \textbf{(2.8.16)}$$

The transforemation of the interfacial boundary conditions, Eq. (2.8.15) and (2.8.16), to those in terms of kinetic variables is not straightforward because the reaction networks for the subsurface and overland may not be identical. If every kinetic-variable in the subsurface corresponding to that in the overland contains the same dissolved aqueous species, then the transformation is straightforwd as

$$\mathbf{n}\cdot\left[\mathbf{V}E_i^w - \theta\mathbf{D}\cdot\nabla(E_i^w)\right] = M_{E_i^{is}} = \frac{S_I}{2}\left[\left(1+sign(S_I)\right)\left(E_i^w\right)^s + \left(1-sign(S_I)\right)\left(E_i^w\right)^o\right] \quad \textbf{(2.8.17)}$$

for the case when the state variables are discontinuous, and

$$\mathbf{n}\cdot\left[\mathbf{V}E_i^w - \theta\mathbf{D}\cdot\nabla(E_i^w)\right] = M_{E_i^{is}} \text{ and } \left(E_i^w\right)^s\Big|_{\text{on the interface}} = \left(E_i^w\right)^o \quad \textbf{(2.8.18)}$$

for the case when the state variables are continuous. In Equstions (2.8.17) and (2.8.18), $\left(E_i^w\right)^o$ is the concentration of the dissolved portion of *i*-th kinetic variables in the overland water and $\left(E_i^w\right)^s$ is the concentration of the dissolved portion of the *i*-th kinetic variable in subsurface water at the interface and $M_{E_i^{is}}$ is the mass rate of the source of the *i*-th kinetic variable in overland from subsurface media [M/t/L^2], which appeared in Eq. (2.6.46).

It should be kept in mind that $\left(E_i^w\right)^o$ and $\left(E_i^w\right)^s$ (and as a matter of fact $\left(E_i^w\right)$) must have the same dissolved species content for Equations (2.8.17) and (2.8.18) to be valid. Otherwise, the coupling in terms of kinetic-variables requires further elaborations that will be addressed in Section 2.8.4.

2.8.3 Coupling between Subsurface and River/Stream/Canal Transport

Similar to the coupling between subsurface and overland, the transport between subsurface and canal is coupled and the fluxes between two media depend on if the dissolved concentration is continuous or not. For the case of discontinuous chemical concentration, the flux is given by

$$\mathbf{n}\cdot\left(\mathbf{V}\,\rho_w C_i^{\,w}-\theta\mathbf{D}\cdot\nabla\rho_w C_i^{\,w}\right)=\frac{\mathbf{n}\bullet\mathbf{V}}{2}\left(\left(1+sign\left(\mathbf{n}\bullet\mathbf{V}\right)\right)\rho_w\left(C_i^{\,w}\right)^s+\left(1-sign\left(\mathbf{n}\bullet\mathbf{V}\right)\right)\rho_w\left(C_i^{\,w}\right)^c\right)$$
$$M_{C_i}^{\,is}=\int_P\frac{\mathbf{n}\bullet\mathbf{V}}{2}\left(\left(1+sign\left(\mathbf{n}\bullet\mathbf{V}\right)\right)\rho_w\left(C_i^{\,w}\right)^s+\left(1-sign\left(\mathbf{n}\bullet\mathbf{V}\right)\right)\rho_w\left(C_i^{\,w}\right)^c\right)dP \qquad \textbf{(2.8.19)}$$

where $\left(C_i^{\,w}\right)^s$ and $\left(C_i^{\,w}\right)^c$ are the concentrations of the i-th dissolved species in the subsurface and canal waters. If the concentration is continuous, we impose its continuity to yield the flux

$$\int_P\mathbf{n}\cdot\left(\mathbf{V}\,\rho_w C_i^{\,w}-\theta\mathbf{D}\cdot\nabla(\rho_w C_i^{\,w})\right)dP=M_{C_i}^{\,is}\quad and\quad\left(C_i^{\,w}\right)^s\Big|_{\text{on the interface}}=\left(C_i^{\,w}\right)^c \qquad \textbf{(2.8.20)}$$

where $M_{C_i^{is}}$ is mass rate of the source of the *i*-th dissolved species in canal from subsurface media [M/t/L].

Similar to the coupling between subsurface and overland flows, the transforemation of the interfacial boundary conditions, Eq. (2.8.19) and (2.8.20), to those in terms of kinetic variables is not straightforward because the reaction networks for the subsurface and river/stream newtworks may not be identical. If every kinetic-variable in the subsurface corresponding to that in the river/stream contains the same dissolved aqueous species, then the transformation is straightforwd and is given in Eqs. (2.8.21) and (2.8.22), respectively, for the cases of discontinuity and conctinuity, respectively, in species concentrations,

$$\mathbf{n}\cdot\left(\mathbf{V}\,E_i^w-\theta\mathbf{D}\cdot\nabla E_i^w\right)=\frac{\mathbf{n}\bullet\mathbf{V}}{2}\left(\left(1+sign\left(\mathbf{n}\bullet\mathbf{V}\right)\right)\left(E_i^w\right)^s+\left(1-sign\left(\mathbf{n}\bullet\mathbf{V}\right)\right)\left(E_i^w\right)^c\right)$$
$$M_{E_i}^{\,is}=\int_P\frac{\mathbf{n}\bullet\mathbf{V}}{2}\left(\left(1+sign\left(\mathbf{n}\bullet\mathbf{V}\right)\right)\left(E_i^w\right)^s+\left(1-sign\left(\mathbf{n}\bullet\mathbf{V}\right)\right)\left(E_i^w\right)^c\right)dP \qquad \textbf{(2.8.21)}$$

and

$$\int_P\mathbf{n}\cdot\left(\mathbf{V}E_i^w-\theta\mathbf{D}\cdot\nabla(E_i^w)\right)dP=M_{E_i}^{\,is}\quad and\quad\left(E_i^w\right)^s\Big|_{\text{on the interface}}=\left(E_i^{\,w}\right)^c \qquad \textbf{(2.8.22)}$$

where $\left(E_i^{\,w}\right)^s$ and $\left(E_i^{\,w}\right)^c$ are the concentration of the dissolved portion of *i*-th kinetic variables in the subsurface and canal.

It should be kept in mind that $\left(E_i^{\,w}\right)^c$ and $\left(E_i^{\,w}\right)^s$ (and as a matter of fact $\left(E_i^{\,w}\right)$) must have the same content of dissolved species for Equations (2.8.21) and (2.8.22) to be valid. Otherwise, the coupling in terms of kinetic-variables requires further elaborations that will be addressed in Section 2.8.4.

2.8.4 Coupling of Reactive Transport between Groundwater and Surface Transport

Since reaction networks for groundwater and surface waters (in overland and river/stream flows) are likely to be different, the continuity of species fluxes and the continuity of species concentration or

the formulation of species fluxes must be transformed from those in terms of species concentration to those in terms of kinetic variables.

After decomposition of reaction networks, kinetic-variables and their corresponding dissolved portion are simply defined as linear combination of species

$$\{\mathbf{E}\}_g = [\mathbf{A}]_g \{\mathbf{C}\}_g, \quad \{\mathbf{E}^w\}_g = [\mathbf{B}]_g \{\mathbf{C}\}_g \qquad \textit{and} \qquad \{\mathbf{E}\}_s = [\mathbf{A}]_s \{\mathbf{C}\}_s, \quad \{\mathbf{E}^w\}_s = [\mathbf{B}]_s \{\mathbf{C}\}_s \tag{2.8.23}$$

where the subscript *g* denotes the groundwater system; the subscript *s* denote the surface water system; $\{\mathbf{E}\}$ and $\{\mathbf{E}^{\mathbf{w}}\}$ are the vectors of size *M*; and $[\mathbf{A}]$ and $[\mathbf{B}]$ are the decomposed unit matrices of size *M* x *M*. It is noted that the *i*-th reaction extent, E_i, is an equilibrium variable if its evolution is governed by an indepdendnt equilibrium raeaction and a set of linearly depending kinetic reactions; a kinetic variable if by an independent kinetic reaction and a set of linearly dependent kinetic reactions; a component if its concentration remains constant (Fang et al., 2003). Inverting Eq. (2.8.23), we have

$$\{\mathbf{C}\}_g = [\mathbf{A}]_g^{-1} \{\mathbf{E}\}_g \qquad \textit{and} \qquad \{\mathbf{C}\}_s = [\mathbf{A}]_s^{-1} \{\mathbf{E}\}_s \tag{2.8.24}$$

Continuity of flux of all aqueous requires

$$\begin{aligned} &\mathbf{n} \cdot \left(\mathbf{V} \{\mathbf{E}^w\}_g - \theta \mathbf{D} \cdot \nabla \{\mathbf{E}^w\}_g \right) = \mathbf{n} \cdot \left(\mathbf{V} [\mathbf{B}]_g \{\mathbf{C}^w\}_g - \theta \mathbf{D} \cdot \nabla [\mathbf{B}]_g \{\mathbf{C}^w\}_g \right), \\ &\textit{thus} \qquad \mathbf{n} \cdot \left(\mathbf{V} \{\mathbf{E}^w\}_g - \theta \mathbf{D} \cdot \nabla \{\mathbf{E}^w\}_g \right) = \mathbf{n} \cdot \left(\mathbf{V} [\mathbf{B}]_g \{\mathbf{C}^w\}_s - \theta \mathbf{D} \cdot \nabla [\mathbf{B}]_g \{\mathbf{C}^w\}_s \right) \\ &\qquad\qquad = \mathbf{n} \cdot \left(\mathbf{V} [\mathbf{B}]_g [\mathbf{A}]_s^{-1} \{\mathbf{E}\}_s - \theta \mathbf{D} \cdot \nabla [\mathbf{B}]_g [\mathbf{A}]_s^{-1} \{\mathbf{E}\}_s \right) \end{aligned} \tag{2.8.25}$$

Continuity of aqueous speces require

$$\{\mathbf{E}^w\}_g = [\mathbf{B}]_g \{\mathbf{C}^w\}_g = [\mathbf{B}]_g \{\mathbf{C}^w\}_s = [\mathbf{B}]_g [\mathbf{A}]_s^{-1} \{\mathbf{E}\}_s \tag{2.8.26}$$

2 MATHEMATICAL BASIS

In this section, we are to give governing equations, initial conditions, and boundary conditions for simulating water flow and chemical and sediment transport in watershed systems.

2.1 Water Flow in One-Dimensional River/Stream/Canal Network

The governing equations of water flow in one-dimensional river/stream/canal can be derived based on the conservation law of water mass and linear momentum (Singh, 1996), and can be written as follows.

The continuity equation:

$$\frac{\partial A}{\partial t}+\frac{\partial Q}{\partial x}=S_S+S_R-S_E+S_I+S_1+S_2 \qquad \textbf{(2.1.1)}$$

where t is time [t]; x is the axis along the river/stream/canal direction [L]; A is cross-sectional area of the river/stream [L^2]; Q is flow rate of the river/stream/canal [L^3/t]; S_S is the man-induced source [L^3/t/L]; S_R is the source due to rainfall [L^3/t/L]; S_E is the sink due to evapotranspiration [L^3/t/L]; S_I is the source due to exfiltration from the subsurface media [L^3//t/L]; S_1 and S_2 are the source terms contributed from overland flow [L^3/t/L].

The momentum equation:

$$\frac{\partial Q}{\partial t}+\frac{\partial VQ}{\partial x}=-gA\frac{\partial\left(Z_O+h\right)}{\partial x}-\frac{gAh}{c\rho}\frac{\partial\Delta\rho}{\partial x}-\frac{\partial F_x}{\partial x}+\left(M_S+M_R-M_E+M_I+M_1+M_2\right)+\frac{B\tau^S-P\tau^b}{\rho} \qquad \textbf{(2.1.2)}$$

where h is water depth [L]; V is river/stream/canal velocity [L/t]; g is gravity [L/t^2]; Z_o is bottom elevation [L]; $\Delta\rho=\rho-\rho_o$ is the density deviation [M/L^3] from the reference density (ρ_o), which is a function of temperature and salinity as well as other chemical concentrations; c is the shape factor of the cross-sectional area; F_x is the momentum flux due to eddy viscosity [L^4/t^2]; M_S is the external momentum-impulse from artificial sources/sinks [L^3/t^2]; M_R is the momentum-impulse gained from rainfall [L^3/t^2]; M_E is the momentum-impulse lost to evapotranspiration [L^3/t^2]; M_I is the momentum-impulse gained from the subsurface due to exfiltration [L^3/t^2]; M_1 and M_2 are the momentum-impulse gained from the overland flow [L^3/t^2]; ρ is the water density [M/L^3]; B is the top width of the cross-section [L]; τ^s is the surface shear stress [$M/t^2/L$]; P is the wet perimeter [L]; and τ^b is the bottom shear stress [$M/t^2/L$], which can be assumed proportional to the flow rate as $\tau^b/\rho=\boldsymbol{\kappa V}^2$ where $\kappa=gn^2/R^{1/3}$ and R is the hydraulic radius (L) and n is the Manning's roughness.

2.1.1 Fully Dynamic Wave Approaches

Equations (2.1.1) and (2.1.2) written in the conservative form are the governing equations for one-dimensional flow in river/stream/canals. Depending on the simplification of the momentum equation, one can have three approaches: fully dynamic wave, diffusive wave, and kinematic wave. For the fully dynamic wave approach, all terms in Eq. (2.1.2) are retained. Under such circumstances, the conservative form of the governing equations may be used or they may be cast in the advection form or in the characteristic form. In this report the characteristic form of the fully dynamic approach will be used as the main option because it is the most natural way and amenable to the advective numerical methods, e.g., the upstream approximation or the Lagrangian-Eulerian method.

For a non-prismatic river/stream/canal network, the cross-sectional area is a function not only of the water depth but also of the river distance, i.e.,

$$A(x,t) = A^{\#}\left(h(x,t),x\right) \tag{2.1.3}$$

where $A^{\#}$ is a function of the water depth $h(x,t)$ and the axis along the river/stream/canal direction x. Differentiating Eq. (2.1.3) with respect to x and t, respectively, we have

$$\frac{\partial A}{\partial t} = \frac{\partial A^{\#}}{\partial h}\frac{\partial h}{\partial t} + \frac{\partial A^{\#}}{\partial x}\frac{\partial x}{\partial t} = \frac{\partial A^{\#}}{\partial h}\frac{\partial h}{\partial t} = B\frac{\partial h}{\partial t} \tag{2.1.4}$$

and

$$\frac{\partial A}{\partial x} = \frac{\partial A^{\#}}{\partial h}\frac{\partial h}{\partial x} + \frac{\partial A^{\#}}{\partial x}\frac{\partial x}{\partial x} = \frac{\partial A^{\#}}{\partial h}\frac{\partial h}{\partial x} + \frac{\partial A^{\#}}{\partial x} = B\frac{\partial h}{\partial x} + \frac{\partial A^{\#}}{\partial x} \tag{2.1.5}$$

where $B(x,t) = B^{\#}(h,x) = \partial A^{\#}/\partial h$ is the top width of the cross-section, [L].

Substituting $Q = VA$ and Eqs. (2.1.4) and (2.1.5) into Eqs. (2.1.1) and (2.1.2), we obtain

$$\frac{\partial h}{\partial t} + V\frac{\partial h}{\partial x} + \frac{A}{B}\frac{\partial V}{\partial x} = \frac{1}{B}\left(S_S + S_R - S_E + S_I + S_1 + S_2\right) - \frac{V}{B}\frac{\partial A^{\#}}{\partial x} \tag{2.1.6}$$

$$\frac{\partial V}{\partial t} + V\frac{\partial V}{\partial x} + g\frac{\partial h}{\partial x} = -\frac{1}{A}\frac{\partial F_x}{\partial x} - g\frac{\partial Z_o}{\partial x} - \frac{gh}{c\rho}\frac{\partial \Delta\rho}{\partial x} + \frac{1}{A}\left[\begin{array}{l} -V\left(S_S + S_R - S_E + S_I + S_1 + S_2\right) + \\ \left(M_S + M_R - M_E + M_I + M_1 + M_2\right) + \dfrac{B\tau^S - P\tau^b}{\rho} \end{array}\right] \tag{2.1.7}$$

Equations (2.1.6) and (2.1.7) can be written in matrix form as

$$\frac{\partial \mathbf{E}}{\partial \mathrm{t}} + \mathbf{A}\frac{\partial \mathbf{E}}{\partial \mathrm{x}} = \mathbf{R} + \mathbf{D} \tag{2.1.8}$$

where

$$\mathbf{E} = \{h \quad V\}^T; \qquad \mathbf{A} = \begin{bmatrix} V & \frac{A}{B} \\ g & V \end{bmatrix}; \qquad \mathbf{R} = \{R_1 \quad R_2\}^T; \qquad \mathbf{D} = \{0 \quad D\}^T \tag{2.1.9}$$

in which

$$R_1 = \frac{1}{B}\left(S_S + S_R - S_E + S_I + S_1 + S_2\right) - \frac{V}{B}\frac{\partial A^{\#}}{\partial x} \tag{2.1.10}$$

$$R_2 = -g\frac{\partial Z_0}{\partial x} - \frac{gh}{c\rho}\frac{\partial(\Delta\rho)}{\partial x} + \frac{1}{A}\begin{bmatrix} -V\left(S_S + S_R - S_E + S_I + S_1 + S_2\right) + \\ \left(M_S + M_R - M_E + M_I + M_1 + M_2\right) + \dfrac{B\tau^s - P\tau^b}{\rho} \end{bmatrix} \tag{2.1.11}$$

$$D = -\frac{1}{A}\frac{\partial F_x}{\partial x} = \frac{1}{A}\frac{\partial}{\partial x}\left(A\varepsilon\frac{\partial V}{\partial x}\right) \qquad \textit{in which} \quad F_x = -A\varepsilon\frac{\partial V}{\partial x} \quad \textit{has been assumed} \tag{2.1.12}$$

where ε is the eddy viscosity.

The eigenvalues and eigenvectors of **A** are

$$\lambda_1 = V + \sqrt{\frac{gA}{B}} \qquad \mathbf{e_1} = \left\{\frac{1}{2}\sqrt{\frac{A}{gB}} \quad \frac{1}{2}\right\}^T \tag{2.1.13}$$

$$\lambda_2 = V - \sqrt{\frac{gA}{B}} \qquad \mathbf{e_2} = \left\{-\frac{1}{2}\sqrt{\frac{A}{gB}} \quad \frac{1}{2}\right\}^T \tag{2.1.14}$$

Denoting $c = \sqrt{\frac{gA}{B}}$, we define

$$\mathbf{L} = \begin{bmatrix} \frac{c}{2g} & -\frac{c}{2g} \\ \frac{1}{2} & \frac{1}{2} \end{bmatrix} \quad \textit{which gives} \quad \mathbf{L^{-1}} = \begin{bmatrix} \frac{g}{c} & 1 \\ -\frac{g}{c} & 1 \end{bmatrix} \tag{2.1.15}$$

where **L** and $\mathbf{L}^{-1}$, respectively, are the right and left eigenmatrices, respectively, of the matrix **A**. Set

$$\partial\mathbf{W} = \mathbf{L}^{-1}\partial\mathbf{E} = \begin{bmatrix} \frac{g}{c} & 1 \\ -\frac{g}{c} & 1 \end{bmatrix}\begin{Bmatrix} \partial h \\ \partial V \end{Bmatrix} \tag{2.1.16}$$

where **W** is a characteristic wave variable. Equation (2.1.16) transforms the primitive variable $\mathbf{E} = \{h, V\}^T$ to the characteristic variable $\mathbf{W} = \{W_1, W_2\}^T$.

Multiplying both side of Eq. (2.1.8) by $\mathbf{L^{-1}}$ yields

$$\mathbf{L^{-1}}\frac{\partial \mathbf{E}}{\partial \mathbf{t}} + \mathbf{L^{-1}A\,L\,L^{-1}}\frac{\partial \mathbf{E}}{\partial \mathrm{x}} = \mathbf{L^{-1}R} + \mathbf{L^{-1}D} \qquad \textbf{(2.1.17)}$$

Since by definition $\partial\mathbf{W} = \mathbf{L^{-1}}\partial\mathbf{E}$ and $\mathbf{L^{-1}AL}$ is a diagonal matrix whose entries are the eigenvalues of **A**, we have

$$\frac{\partial \mathbf{W}}{\partial \mathrm{t}} + \begin{bmatrix} V+c & 0 \\ 0 & V-c \end{bmatrix}\frac{\partial \mathbf{W}}{\partial \mathrm{x}} = \mathbf{L^{-1}R} + \mathbf{L^{-1}D} \qquad or \qquad \frac{D\mathbf{W}}{Dt} = \mathbf{L^{-1}R} + \mathbf{L^{-1}D} \qquad \textbf{(2.1.18)}$$

Substituting $\mathbf{L^{-1}}$ ($\mathbf{L^{-1}}$ is defined by Eq. (2.1.15)) into the right hand side of Eq. (2.1.18) and making an integral transformation so that $(g/c)\partial h = \partial\omega$, we obtain

$$\frac{D_{V+c}(V+\omega)}{D\tau} \equiv \frac{\partial(V+\omega)}{\partial t} + (V+c)\frac{\partial(V+\omega)}{\partial x} = \frac{g}{c}R_1 + R_2 + D \qquad \textbf{(2.1.19)}$$

$$\frac{D_{V-c}(V-\omega)}{D\tau} \equiv \frac{\partial(V-\omega)}{\partial t} + (V-c)\frac{\partial(V-\omega)}{\partial x} = -\frac{g}{c}R_1 + R_2 + D \qquad \textbf{(2.1.20)}$$

in which

$$c = \sqrt{\frac{gA}{B}}; \quad \omega = \int_0^h \frac{g}{c(s)}ds \qquad \textbf{(2.1.21)}$$

where c is the wave speed and ω is the transformed wave speed. Equation (2.1.19) simply states that the positive gravity wave ($V+\omega$) is advected by the speed ($V+c$) while Equation (2.1.20) states that the negative gravity wave ($V-\omega$) is advected by the speed ($V-c$).

For transient simulations, the water depth (or water stage) and the cross-sectionally averaged velocity must be given as the initial condition. In addition, appropriate boundary conditions need to be specified to match the corresponding physical system.

The system of Eqs. (2.1.19) and (2.1.20) are identical to the system of Eqs. (2.1.1) and (2.1.2) on the differential level. They offer advantages in their amenability to innovative advective numerical methods such as the upstream finite difference, upwind finite element, or semi-Lagrangian scheme. Furthermore, the implementation of boundary conditions is very straightforward. Only when the wave is coming into the region of interest, the boundary condition is required. For the wave that is going out of the region of interest, there is no need to specify a boundary condition.

Open upstream boundary condition:

The boundary condition at an upstream point depends on flow conditions. If the flow is supercritical, both waves are transported into the region and two boundary conditions are needed. The water depth and velocity at the boundary are determined entirely by the flow condition that prevails at the upstream. The governing equations for this case can be set up based on the continuity of mass as well as momentum between the boundary and the upstream as follows

$$VA = V_{up}A_{up} = Q_{up} \quad and \quad \rho VAV + \rho g h_c A = \rho V_{up}A_{up}V_{up} + \rho g h_{upc}A_{up} = M_{up} \quad \textbf{(2.1.22)}$$

where V_{up} is the cross-sectional averaged velocity from the incoming upstream fluid, A_{up} is the cross-sectional area in the upstream, Q_{up} is the flow rate of the incoming fluid from the upstream, h_c is the water depth to the centroid of the cross-sectional area of the boundary, h_{upc} is the water depth to the centroid of the upstream cross-sectional area, and M_{up} is the momentum-impulse of the incoming fluid from the upstream. It should be noted that both the water depth and velocity in the upstream must be measured to provide values of Q_{up} and M_{up}. If the flow is critical, the positive wave is transported into the region from upstream and the negative wave is immobile. The water depth and velocity at the boundary are determined by the flow conditions prevail at the upstream and by the condition of critical flow. The governing equations for this case may be set up based on the continuity of mass and the requirement of critical flow condition as

$$VA = Q_{up} \qquad and \qquad \frac{BQ^2}{gA^3} = 1 \qquad \textbf{(2.1.23)}$$

If the flow is subcritical, while the positive wave is transported into the region, the negative wave is transported out of the region. The water depth and velocity are determined by the flow condition prevail at upstream and by flow dynamics in the region. The governing equations are set up based on the continuity of mass between the boundary and the upstream, and on flow dynamics in the region

$$VA = Q_{up} \qquad and \qquad F_{-}(V,h) = 0 \qquad \textbf{(2.1.24)}$$

where $F_{-}(V, h)$, a function of velocity and water depth, is the negative wave boundary function.

In summary, the boundary condition at an open upstream boundary point is given by Eqs. (2.1.22), (2.1.23), and (2.1.24), respectively, for the case of supercritical, critical, and subcritical flows, respectively.

Open downstream boundary condition:

If the flow is supercritical on an open downstream boundary point, both waves are transported out of region. Under such circumstances, no boundary conditions are needed. The water depth and velocity on the boundary are determined by flow dynamics in the region. The governing equations for V and h are

$$F_{+}(V,h) = 0 \qquad and \qquad F_{-}(V,h) = 0 \qquad \textbf{(2.1.25)}$$

where $F_{+}(V, h)$, a function of V and h, is the positive wave boundary function. If the flow is critical, the water depth and velocity at the boundary are determined by flow dynamics in the region and by the condition of critical flow. Thus, the governing equations for critical flow are given by

$$F_{+}(V,h) = 0 \qquad and \qquad \frac{BQ^2}{gA^3} = 1 \qquad \textbf{(2.1.26)}$$

If the flow is subcritical, while the positive wave is transported out of the region, the negative wave is transported into the region. The water depth and velocity are determined by flow dynamics in the region and by what is the control on the boundary. The governing equations may be given by

$$F_+(V,h)=0 \quad and \quad VA=Q_{dn}(h) \qquad or \qquad F_+(V,h)=0 \quad and \quad h=h_{dn}(t) \qquad \textbf{(2.1.27)}$$

where $Q_{dn}(h)$, a function of h, is the rating curve function for the downstream boundary and $h_{dn}(t)$, a function of t, is the water depth at the downstream boundary. The adaptation of Eq. (2.1.27) depends on the physical configuration at the boundary.

In summary, the boundary condition at an open downstream boundary is given by Eqs. (2.1.25), (2.1.26), and (2.1.27), respectively, for the case of supercritical flow, critical flow, and subcritical flows, respectively.

Closed upstream boundary condition:

At the closed upstream boundary, physically all flow conditions can occur. When the supercritical flow happens, both positive and negative waves are transported into the region. Two boundary condition equations are needed. Because the boundary is closed, it is impermeable. The governing equations can be obtained by simply substituting $Q_{up} = 0$ and $M_{up} = 0$ into Eq. (2.1.22) to yield

$$VA=0 \qquad and \qquad \rho VAV+\rho g h_c A=0 \qquad \textbf{(2.1.28)}$$

The solutions for Eq. (2.1.28) are not unique. One possible solution is $V = 0$ and $h = 0$.

For the critical flow, the velocity is equal to the wave speed, $V = c$, the negative wave is immobile. On the other hand, the positive wave is transported into the region of interest, one boundary-condition equation is needed. Because the closed boundary is impermeable, the governing equations may be set up by imposing zero flow rate and the condition of critical flow as

$$VA=0 \qquad and \qquad \frac{BQ^2}{gA^3}=1 \qquad \textbf{(2.1.29)}$$

When the flow is subcritical, the positive wave is transported into the region of interest while the negative wave is transported out of the region of interest. Only the boundary condition for the positive wave is needed. Since no fluid from the outside world is transported into the region via the boundary, the boundary condition for the positive wave can be stated with $Q = VA = 0$. The governing equations for V and h are thus given by

$$VA=0 \qquad and \qquad F_-(V,h)=0 \qquad \textbf{(2.1.30)}$$

In summary, the boundary condition at a closed upstream point is given by Eqs. (2.1.28), (2.1.29), and (2.1.30), respectively, for the case of supercritical flow, critical flow, and subcritical flows, respectively.

Closed downstream boundary condition:

At the closed downstream boundary, physical condition dictates that the velocity at the boundary is zero. Since the velocity is zero, supercritical flow cannot occur at the closed boundary point because the water depth is greater or equal to zero. Therefore, the flow can only be either critical or subcritical. For critical flow, $c = V = 0$, which is very unlikely. Therefore, it is highly unlikely that critical flow will occur at the closed downstream boundary.

For the subcritical flow, the positive wave is transported out of the region and no boundary condition is needed for this wave. On the other hand, the negative wave is transported into the region of interest. The governing equations for V and h are

$$F_+(V,h) = 0 \qquad and \qquad V = 0 \tag{2.1.31}$$

which is based on the physics that $V = 0$ and the water depth is governed by internal flow dynamics.

In summary, supercritical flow cannot occur at a closed downstream point. The boundary condition at a closed downstream boundary point is either V = 0 and h = 0 for critical flow or is given by Eq. (2.1.31) for subcritical flow.

Natural internal boundary condition at junctions:

For the junction node J (Figure 2.1-1), we have one unknown: the water surface elevation or the stage, H_J. The governing equation for this junction is obtained as

$$\frac{d\forall_J}{dh_J}\frac{dh_J}{dt} = \sum_I^{N_J} Q_{IJ} = \sum_I^{N_J} V_{IJ} A_{IJ} \tag{2.1.32}$$

for the case when the storage effect of the junction is accounted for, or

$$\sum_I^{N_J} Q_{IJ} = \sum_I^{N_J} V_{IJ} A_{IJ} = 0 \tag{2.1.33}$$

for the case when the storage effect of the junction is not included.

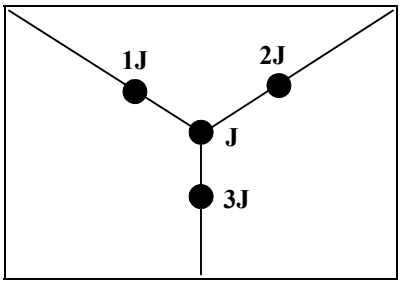

Fig. 2.1-1. Schematic of a Junction

In Eqs. (2.1.32) and (2.1.33), $\forall_J$ is the volume of the junction J; h_J is the water depth of the junction J; Q_{IJ} is the flow rate of the I^{th} reach to the J^{th} junction; I is the identification number of

river/stream/canal reach; N_J is the total number of river/stream/canal reaches that are connected to the junction J (it is 3 in the case shown); V_{IJ} and A_{IJ} are the velocity and cross sectional area, respectively, of the I^{th} reach at the location entering the J^{th} junction.

The node IJ located at the boundary between the I^{th} reach and the J^{th} junction is termed the natural internal boundary of reach I. The governing equations for the internal boundary node IJ depend on whether this node is a downstream or an upstream node in reference to the reach I. Let us say that node IJ is a downstream point if the flow is from the reach I toward the junction J. On the other hand, we say that the node IJ is an upstream point if the flow is from the junction J toward the reach I. With this definition, we can generate equations for any internal boundary node IJ, which will be stated in the following.

If IJ is a downstream internal boundary, we have three cases to consider: subcritical flow, critical flow, and supercritical flow. For the case of subcritical flow, the positive wave is going out of the reach and no boundary condition for this wave is needed. On the other hand, the negative wave is going into the region and its boundary condition is obtained by the assumption that no loss in energy between the junction and node IJ. The governing equations for node IJ are given as

$$F_+\left(V_{IJ}, h_{IJ}\right) = 0 \qquad and \qquad E_{IJ} = \frac{V_{IJ}^2}{2g} + h_{IJ} + Z_{oIJ} = H_J \tag{2.1.34}$$

where $F_+(V_{IJ},h_{IJ})$, a function of the velocity V_{IJ} (velocity at node IJ) and h_{IJ} (water depth at node IJ), is the positive wave boundary function; E_{IJ} is the energy line at node IJ, Z_{oIJ} is the bottom elevation at node IJ; and H_J is the water surface elevation of the junction J. The second equation of Eq. (2.1.34) is obtained from the assumption that the total energy is constant from the junction to the node IJ. In the case of critical flow, the positive wave is going out of the reach and there is no need of a boundary condition for this wave. The negative wave is immobile and its boundary condition is given by the condition of critical flow. The governing equations for node IJ under critical flow are given by

$$F_+\left(V_{IJ}, h_{IJ}\right) = 0 \qquad and \qquad \frac{Q_{IJ}^2 B_{IJ}}{g A_{IJ}^3} = 1 \tag{2.1.35}$$

where B_{IJ} is the top width of the cross-section of the I-th reach at node IJ and A_{IJ} is the cross-section area of the I-th reach at node IJ. In the case of supercritical flow, both positive and negative waves are going out of the reach, therefore no boundary conditions are needed and the governing equations for node IJ under supercritical flow are given by

$$F_+\left(V_{IJ}, h_{IJ}\right) = 0 \qquad and \qquad F_-\left(V_{IJ}, h_{IJ}\right) = 0 \tag{2.1.36}$$

where $F_-\left(V_{IJ}, h_{IJ}\right)$, a function of the velocity V_{IJ} and h_{IJ}, is the negative wave boundary function.

If IJ is an upstream point, we have also three cases to consider: subcritical, critical, and supercritical flows. For the case of subcritical flow, the positive wave is going into the reach and its boundary condition is obtained with the assumption that the specific energy is constant between the junction J and the node IJ. With this assumption, the governing equations for node IJ are given by

$$H_J = \frac{V_{IJ}^2}{2g} + h_{IJ} + Z_{oIJ} \qquad \text{and} \qquad F_{-}(V_{IJ}, h_{IJ}) = 0 \qquad \textbf{(2.1.37)}$$

In the case of critical flow, the positive wave is going into the reach from the junction and its boundary condition is obtained with the assumption of constant energy line between the junction and the node *IJ*, and the negative wave is immobile and its boundary condition is obtained from the condition of critical flow. The governing equations for node *IJ* under critical flow are given by

$$H_J = \frac{V_{IJ}^2}{2g} + h_{IJ} + Z_{oIJ} \qquad \text{and} \qquad \frac{Q_{IJ}^2 B_{IJ}}{g A_{IJ}^3} = 1 \qquad \textbf{(2.1.38)}$$

In the case of supercritical flow, both positive and negative waves are going into the region from the junction *J* to the reach *I*. Two boundary conditions are required for this case. One of the boundary conditions is obtained with the assumption of constant energy line between the junction *J* and the node *IJ*. The other boundary condition is obtained with the assumption that the supercritical flow at node *IJ* will become a critical flow in a very short distance (so short that it can be conceptually considered to locate at *IJ*). With these assumptions the governing equations for node *IJ* under supercritical flow is given by Eq. (2.1.38).

In summary, the governing equations at a natural internal boundary node of a reach connecting to junctions are given by one of Eq. (2.1.34) through (2.1.38) depending on whether the node IJ is a downstream or an upstream point and whether the flow is supercritical, critical, or subcritical.

Controlled internal boundary condition at control structures:

For any structure, *S* (which may be a weir, a gate, or a culvert), there are two river/stream/canal reaches connecting to the structure. The node *1S* located at the upstream of the structure is termed the controlled-internal boundary of the first reach while the Node *2S* located at the downstream of the structure is called the controlled-internal boundary of the second reach (Fig. 2.1-2). The specification of boundary conditions for the internal boundaries separated by a structure requires elaboration.

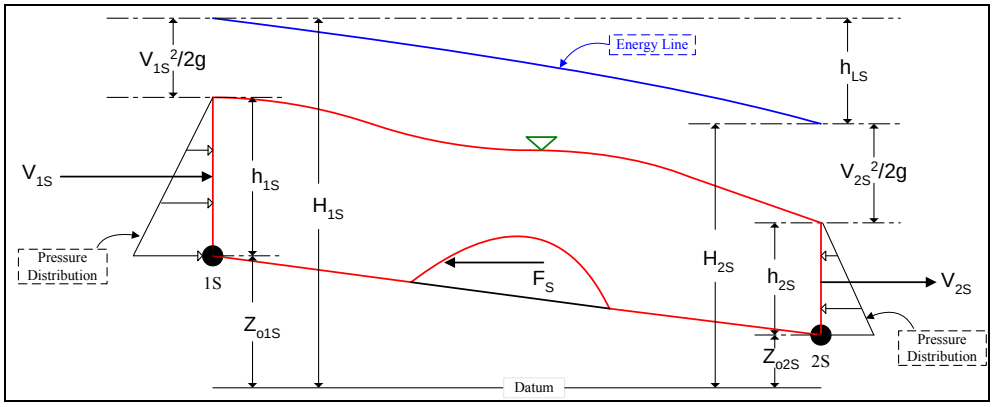

Fig. 2.1-2. The control volume (red outline) between Nodes 1S and 2S

The flow configuration around a structure and its surrounding reaches may be very dynamic under transient flows. Governing equations of flow at Nodes *1S* and *2S* depend on the changing dynamics of water stages around the structure. When both stages are below the height of the structure, the two reaches connecting the structure are decoupled. When at least one of the stages is above the structure, two reaches are either sequentially coupled or fully coupled via the structure. Here for sake of simplicity of discussions, we assume that the flow direction is from Reach *1* to Reach *2*. In other words, Reach *1* is an upstream reach and Reach *2* is a downstream reach. If the flow direction is reversed, we can have the boundary condition similarly prescribed.

There are five unknowns, V_{1S} (velocity of the upstream reach Node *1S*), h_{1S} (the water depth of the upstream Node *1S*), Q (the flow rate through the internal-boundary complex), V_{2S} (the velocity of the downstream reach Node *2S*), and h_{2S} (the water depth of the downstream Node *2S*); five equations must be set up for this internal-boundary complex consisting of a upstream reach node, a structure, and a downstream node. The governing equations for these five unknowns can be obtained depending on the flow conditions at the upstream and downstream reaches separated by the internal boundary structure. The flow condition can be supercritical, critical, or subcritical at Node *1S* and Node *2S*.

Node *1S* is a downstream point relative to the first reach or is the upstream point relative to the structure. The positive wave is transported out of *Reach 1* over the structure to *Reach 2*, and there is no need of a boundary condition for this wave. As for the negative wave, if the flow is supercritical, it is transported out of the reach, and there is no need to prescribe a boundary condition for this wave. Thus, the governing equations for Node *1S* under supercritical flow are given by

$$F_+(V_{1S}, h_{1S}) = 0, \qquad F_-(V_{1S}, h_{1S}) = 0, \qquad \textit{and} \quad Q = V_{1S} A_{1S} \tag{2.1.39}$$

where $F_+(V_{1S},h_{1S})$, a function of V_{1S} and h_{1S}, is the positive wave boundary function; and $F_-(V_{1S},h_{1S})$, a function of V_{1S} and h_{1S}, is the negative wave boundary function.

If the flow is critical, the negative wave is immobile and its governing equation must satisfy the condition of critical flow. Thus, the two governing equations for Node *1S* under critical flow are given by

$$F_+(V_{1S}, h_{1S}) = 0, \qquad \frac{Q^2 B_{1S}}{g A_{1S}^3} = 1, \qquad \textit{and} \quad Q = V_{1S} A_{1S} \tag{2.1.40}$$

where B_{1S} and A_{1S}, respectively, are the top width and the area, respectively, of the cross-section at Node *1S*.

If the flow is subcritical, the negative wave is transported into the reach from the downstream reach via the structure, and its boundary condition is obtained by equating the flow rates at Nodes *1S* and *2S*. Thus the governing equations for Node *1S* under subcritical flow are given by

$$F_+(V_{1S}, h_{1S}) = 0, \qquad V_{1S} A_{1S} = V_{2S} A_{2S}, \qquad \textit{and} \quad Q = V_{1S} A_{1S} \tag{2.1.41}$$

A comment is in order here. When the flow at Note *1S* is supercritical or critical, the flow in the

upstream reach is decouple from the flow in the downstream reach. Under such conditions, Eq. (2.1.39) or (2.1.40) is used to solve to the values of V_{1S} and h_{1S}, which then yield the flow rate Q, the energy level H_{1S} at Node *1S*, or the momentum-impulse M_{1S} at Node *1S*. These quantities (Q, H_{1S}, and M_{1S}) may serve as the boundary conditions for Node *2S*. As to which of these quantities is needed for the internal boundary Node *2S* depends on the flow condition at Node *2S*. This point will be taken up when the boundary conditions for Node *2S* are addressed. When the flow at Node *1S* is subcritical, then the flows in the upstream and downstream reaches are coupled via the second equation in Eq. (2.1.41).

On the other hand, Node *2S* is an upstream point relative to the second reach or a downstream point relative to the structure. If the flow is supercritical at Node *2S*, both the positive and the negative waves are coming into the reach from the upstream reach via the structure, and two boundary conditions are needed. These two boundary conditions can be obtained by the principle of mass continuity and the principle of momentum/impulse or the Bernoulli's equation between Nodes *1S* and *2S*. The structure between Nodes *1S* and *2S* will exert reaction force, F_S, on the fluid between two nodes or it induces energy loss, h_{LS}, between two nodes (Fig. 2.1-2). Thus, the governing equations for Node *2S* are

$$Q = V_{1S}A_{1S}, \qquad V_{2S}A_{2S} = V_{1S}A_{1S}, \qquad \textit{and} \qquad \begin{matrix} H_{2S} + h_{LS} = H_{1S} \\ \textit{or} \\ M_{2S} + F_S = M_{1S} \end{matrix} \tag{2.1.42}$$

where F_S is the force exerted by the structure on the fluid; h_{LS} is the energy loss between Nodes *1* and *2*; H_{2S} and H_{1S} (defined in Fig. 2.1-2), respectively, are the energy level at Nodes *2S* and *1S*, respectively; and M_{2S} ($=\rho V_{2S}A_{2S}V_{2S}+\rho g\, h_{2Sc}A_{2S}$) and M_{1S} ($=\rho V_{1S}A_{1S}V_{1S}+\rho g\, h_{1Sc}A_{1S}$), respectively, are the momentum-impulse at Nodes *2S* and *1S*, respectively (where ρ is the fluid density, g is the gravity constant, h_{2Sc} is the water depth to the centroid of the cross-sectional area at Node *2*, and h_{1Sc} is the water depth to the centroid of the cross-sectional area at Node *1*).

If the flow at Node *2S* is critical, one of the two boundary equations is obtained by the requirement of critical conditions while the other is obtained by the principle of mass continuity and the principle of momentum/impulse or the Bernoulli's equation between Nodes *1S* and *2S*. Thus, the governing conditions for Node *2S* are given as follows

$$\begin{matrix} \dfrac{Q^2 B_{2S}}{gA_{2S}^3} = 1, \qquad V_{2S}A_{2S} = V_{1S}A_{1S}, \qquad Q = V_{1S}A_{1S} \\ \textit{or} \\ \dfrac{Q^2 B_{2S}}{gA_{2S}^3} = 1, \qquad V_{2S}A_{2S} = V_{1S}A_{1S}, \qquad Q = V_{1S}A_{1S}, \quad \textit{and} \end{matrix} \qquad \begin{matrix} H_{2S} + h_{LS} = H_{1S} \\ \textit{or} \\ M_{2S} + F_{1S} = M_{1S} \end{matrix} \tag{2.1.43}$$

If the flow at Node *2S* is subcritical, the positive wave is transported into the reach from the upstream reach via the structure while the negative wave is transport out of the reach. The boundary condition for the positive wave is obtained by the principle of mass continuity and the principle of

momentum/impulse or the Bernoulli's equation between Nodes *1S* and *2S*. Thus the two governing equations for Node *2S* under subcritical flow are given as follows

$$F_{-}(V_{2S}, h_{2S}) = 0, \qquad V_{2S}A_{2S} = V_{1S}A_{1S}, \qquad Q = V_{1S}A_{1S}$$

or

$$F_{-}(V_{2S}, h_{2S}) = 0, \quad V_{2S}A_{2S} = V_{1S}A_{1S}, \quad Q = V_{1S}A_{1S}, \quad \textit{and} \quad \begin{matrix} H_{2S} + h_{LS} = H_{1S} \\ \textit{or} \\ M_{2S} + F_{1S} = M_{1S} \end{matrix} \qquad \textbf{(2.1.44)}$$

In summary, the governing equations for internal boundary nodes separated by a structure are given by any combination of Eq. (2.1.39), (2.1.40), or (2.1.41) and Eq. (2.1.42), (2.1.43), or (2.1.44). All combinations provide five governing equations for five unknowns (V_{1S}, h_{1S}, Q, V_{2S}, and h_{2S}), except for one combination.

The combination of Eq. (2.1.41) and Eq. (2.1.42) only generates four equations; one more equation is needed. This combination represents the situation that flow in the upstream reach is subcritical and in the downstream reach is supercritical. For this situation to occur, flow must under go a transitional state of critical flow over the structure, and the critical flow condition on the structure must be satisfied. Thus, the following additional governing equations can be set up by applying the principle of mass continuity and the principle of momentum-impulse or the Bernoulli equation to a control volume between Node 1S and the structure (Fig. 2.1-3) as

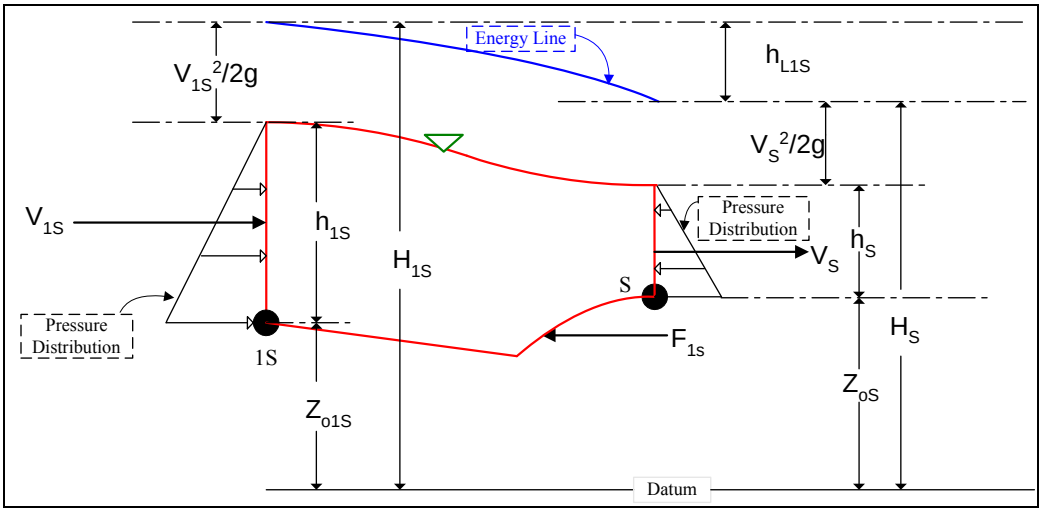

Fig. 2.1-3. The control volume (red outline) between Node 1S and structure.

$$\frac{Q^2 B_S}{gA_S^3} = 1, \qquad V_S A_S = V_{1S}A_{1S}, \qquad Q = V_{1S}A_{1S}, \quad \textit{and} \quad \begin{matrix} H_S + h_{L1S} = H_{1S} \\ \textit{or} \\ M_S + F_{1S} = M_{1S} \end{matrix} \qquad \textbf{(2.1.45)}$$

where A_S, B_S, and V_S, are the area, top width, and velocity of the cross-sectional area over the

structure; h_{L1S} is head loss between Node 1S and the structure; F_{1S} is the force the structure exerts on the fluid between Node 1S and the structure, H_S is the total head over the structure (Fig. 2.1-3); and M_S (= $\rho V_S A_S V_S$ + g $h_{Sc} A_S$) is the momentum-impulse at the structure (where h_{Sc} is the water depth to the centroid of the cross-sectional area at the structure). Now, Eq. (2.1.41), (2.1.42), and (2.1.45) give seven equations for seven unknowns (V_{1S}, h_{1S}, Q, V_{2S}, h_{2S}, V_S, and h_S).

The theoretical presentation about the governing equations for the internal-boundary complex is valid for any structure including weirs, gates, and culverts. The differences among various structures are characterized by the formulation of the head loss functions, $h_{LS}(Q, h_{1S}, h_{2S})$ and h_{L1S} (Q, h_{1S}, h_S), which depend on the flow rate Q and the water depth h_{1S}, and h_{2S}.

2.1.2 Diffusive Wave Approaches

In a diffusive approach, the inertia terms in the momentum equation is assumed negligible when compared with the other terms. By further assuming negligible eddy viscosity and $M_S = M_R = M_E = M_I = M_1 = M_2 = 0$, we approximate the river/stream/canal velocity with the following equation (Hergarten and Neugebauer, 1995).

$$V = \frac{-a}{n}\left[\frac{R}{1+\left(\frac{\partial Z_o}{\partial x}\right)^2}\right]^{2/3} \frac{1}{\sqrt{\left|-\frac{\partial H}{\partial x} - \frac{h}{c\rho}\frac{\partial \Delta\rho}{\partial x} + \frac{B\tau^S}{Ag\rho}\right|}}\left(\frac{\partial H}{\partial x} + \frac{h}{c\rho}\frac{\partial \Delta\rho}{\partial x} - \frac{B\tau^S}{Ag\rho}\right) \qquad \textbf{(2.1.46)}$$

where n is Manning's roughness [$tL^{-1/3}$], a is a unit-dependent factor ($a = 1$ for SI units and $a = 1.49$ for U.S. Customary units) to make the Manning's roughness unit-independent, R is the hydraulic radius [L], and $H = h + Z_o$ is the water stage.

Using the definition $Q = VA$ and substituting Eq. (2.1.46) into Eq. (2.1.1), we obtain

$$B\frac{\partial H}{\partial t} - \frac{\partial}{\partial x}\left(K\left[\frac{\partial H}{\partial x} + \frac{h}{c\rho}\frac{\partial \Delta\rho}{\partial x} - \frac{B\tau^S}{Ag\rho}\right]\right) = S_S + S_R - S_E + S_I + S_1 + S_2 \qquad \textbf{(2.1.47)}$$

in which

$$K = \frac{a\,A\,R^{2/3}}{n}\frac{1}{\left[1+\left(\frac{\partial Z_o}{\partial x}\right)^2\right]^{2/3}}\frac{1}{\sqrt{\left|-\frac{\partial H}{\partial x} - \frac{h}{c\rho}\frac{\partial \Delta\rho}{\partial x} + \frac{B\tau^S}{Ag\rho}\right|}} \qquad \textbf{(2.1.48)}$$

To achieve transient simulations, either water depth or stage must be given as the initial condition. In addition, appropriate boundary conditions need to be specified to match the corresponding physical system. In our model, four types of boundary conditions may be specified depending on physical configurations of the boundary. These boundary conditions are addressed below.

Dirichlet boundary condition: prescribed water depth or stage

On a Dirichlet boundary, either the water depth or stage can be prescribed as a function of time.

This boundary condition can be expressed as

$$h = h_d(t) \qquad or \qquad H = h + Z_o = H_d, \quad on \quad B_d \tag{2.1.49}$$

where $h_d(t)$ is a prescribed time-dependent water depth on the Dirichlet boundary [L], $H_d(t)$ is a prescribed time-dependent water stage [L], and B_d is the Dirichlet boundary point. A Dirichlet boundary point can locate at the upstream or down stream point, control structures, or even interior point.

Flux boundary condition: prescribed flow rate

On a flux boundary, a time-dependent flow rate is prescribed as a function of time as

$$-K\left(\frac{\partial H}{\partial x} + \frac{h}{c\rho}\frac{\partial \Delta\rho}{\partial x} - \frac{B\tau^S}{Ag\rho}\right) = Q_f(t) \quad on \quad B_f \tag{2.1.50}$$

where $Q_f(t)$ a prescribed time-dependent flow rate [L^3/t] and B_f is a flux boundary point. Mathematically, a flux boundary condition can be applied to an upstream or downstream point. However, in practice, it is often applied to an upstream boundary point.

Water depth-dependent boundary condition: prescribed rating curve

This condition is often used to describe the flow rate at a downstream river/stream boundary at which the flow rate is a function of water depth. It can be written as

$$-K\left(\frac{\partial H}{\partial x} + \frac{h}{c\rho}\frac{\partial \Delta\rho}{\partial x} - \frac{B\tau^S}{Ag\rho}\right) = Q_r(h(x_r, t)) \quad on \quad B_r \tag{2.1.51}$$

where $Q_r(h(x_r,t))$ is a water depth-dependent flow rate [L^3/t], x_r is the x-coordinate on the boundary B_r, and B_r is a boundary point on which the prescribed rating curve is applied.

Junction boundary condition:

This condition is applied to a boundary of a river/stream/canal reach that is connected to a junction (Fig. 2.1-1). For the junction complex consisting of N_J river/stream/canal reaches (e.g., in Fig. 2.1-1, $N_J = 3$) and one junction (say J), we have ($N_J + 1$) unknowns, which are flow rates, Q_{IJ} (Q_{IJ} is the flow rate from the I-th reach to junction J), and water stage at junction J, H_J. Therefore, we need to set up ($N_J + 1$) equations. The first equation is obtained by applying the continuity of mass at the junction to result in Eq. (2.1.35) for the case when the storage effect of the junction must be accounted for or Eq. (2.1.36) when this effect is negligible. The other N_J equations can be obtained by assuming the energy loss from any reach to the junction is negligible to result in

$$\frac{1}{2g}\left(\frac{Q_{IJ}}{A_{IJ}}\right)^2 + H_{IJ} = H_J, \quad I \in N_J \quad where \quad Q_{IJ} = -K\left(\frac{\partial H}{\partial x} + \frac{h}{c\rho}\frac{\partial \Delta\rho}{\partial x} - \frac{B\tau^S}{Ag\rho}\right)\Bigg|_{IJ} \tag{2.1.52}$$

where H_{IJ} is the water stage the internal boundary Node IJ of the I-th reach connecting to junction J.

Equations (2.1.32) or (2.1.33) along with Eq. (2.1.52) provide ($N_J + 1$) equations to solve for ($N_J + 1$) unknowns.

Weir boundary condition:

For any weir (*W*), there are two river/stream/canal reaches connecting to it. Node *1W* located just upstream of the weir is termed the controlled-internal boundary of the upstream reach while Node *2W* located just downstream of the weir is called the controlled-internal boundary of the downstream reach (Figure 2.1-4). The specification of boundary conditions for the internal boundaries for the diffusive wave approach is given as

$$-\mathbf{n}\cdot\mathrm{K}\left(\nabla H+\frac{h}{c\rho}\nabla(\Delta\rho)-\frac{B\tau^{S}}{Ag\rho}\right)\Big|_{1\mathrm{W}}=Q_{W}\left(h_{up},h_{dn}\right)\qquad \textit{and}$$
$$-\mathbf{n}\cdot\mathrm{K}\left(\nabla H+\frac{h}{c\rho}\nabla(\Delta\rho)-\frac{B\tau^{S}}{Ag\rho}\right)=Q_{W}\left(h_{up},h_{dn}\right) \qquad \textbf{(2.1.53)}$$

where Q_w is the weir discharge rate, which is a given function of the water depths h_{up} at Node *1W* and h_{dn} at Node *2W* (Fig. 2.1-5).

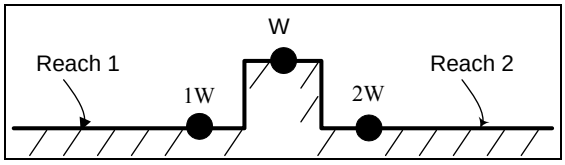

Fig. 2.1-4. Schematic of weir.

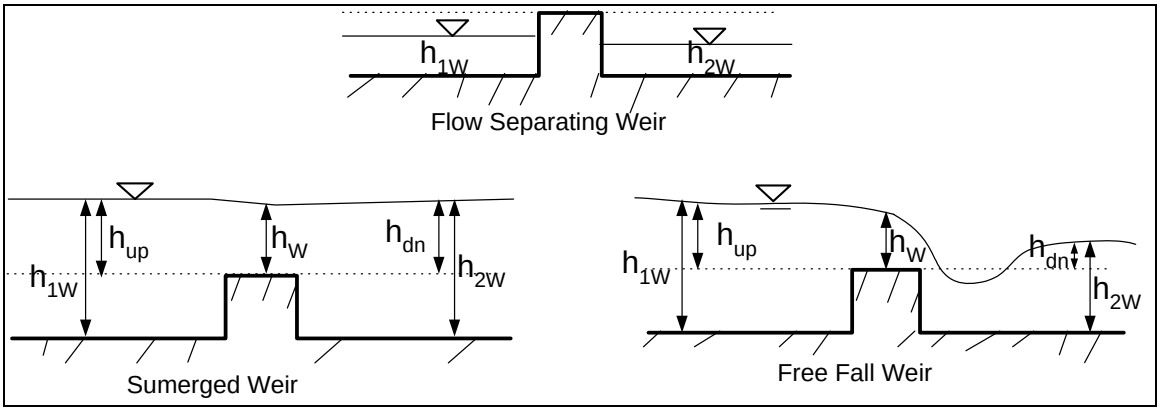

Fig. 2.1-5. Flow configurations around a weir.

The flow configuration around the weir and its surrounding reaches may be very dynamic under transient flows. Both of the water stages at Nodes *1W* and *2W* may be below the weir, both may be above the weir, or one below the weir while the other is above the weir (Fig. 2.1-5). When both stages are below the height of the weir, the two reaches connecting the weir are decoupled. When at least one of the stages is above the weir, two reaches are coupled via the weir. The weir discharge, Q_w, can be obtained by solving the continuity equation and the Bernoulli equation between Nodes *1W* and *2W*. The weir formulae under various stage conditions are given as

(1) For submerged flow

$$Q_W = C_W h_{dn} L_W \sqrt{2g\left(h_{up} - h_{dn}\right)} \quad if \quad h_{dn} \geq \frac{2}{3} h_{up} \quad and \quad h_{dn} < h_{up} \tag{2.1.54}$$

(2) For free fall flow

$$Q_W = \frac{2}{3\sqrt{3}} C_W h_{up} L \sqrt{2g h_{up}} \quad if \quad h_{dn} < \frac{2}{3} h_{up} \tag{2.1.55}$$

(3) For decoupled flow

$$Q_W = 0 \tag{2.1.56}$$

where C_w is the weir coefficient and L_w is the weir length. It should be noted that the above formulae are valid for broad weir. For other types of weirs, different weir discharge formulae may be used and they can easily be incorporated into the computer code.

Gate boundary condition:

For any gate (G), there are two river/stream/canal reaches connecting to it. Node *1G* located just upstream of the gate G is termed the controlled-internal boundary of the upstream reach while Node *2G* located just downstream of the gate G is called the controlled-internal boundary of the downstream reach (Fig. 2.1-6). The specification of boundary conditions for the internal boundaries separated by a gate can be made similar to that of a weir as follows.

$$\begin{aligned} -\mathbf{n}\cdot\mathbf{K}\left(\nabla H + \frac{h}{c\rho}\nabla(\Delta\rho) - \frac{B\tau^S}{Ag\rho}\right)\Big|_{1G} &= Q_g\left(h_{up}, h_{dn}\right) \quad and \\ -\mathbf{n}\cdot\mathbf{K}\left(\nabla H + \frac{h}{c\rho}\nabla(\Delta\rho) - \frac{B\tau^S}{Ag\rho}\right)\Big|_{2G} &= Q_g\left(h_{up}, h_{dn}\right) \end{aligned} \tag{2.1.57}$$

where Q_g is the gate discharge rate, which is a given function of the water depths h_{up} at *1G* and h_{dn} at *2G* (Fig. 2.1-7).

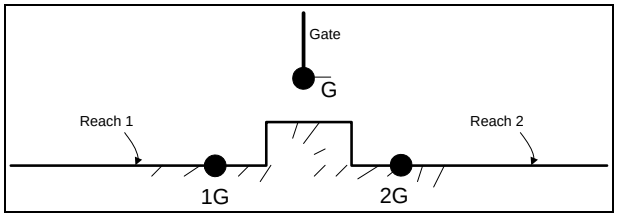

Fig. 2.1-6. Schematic of Gate.

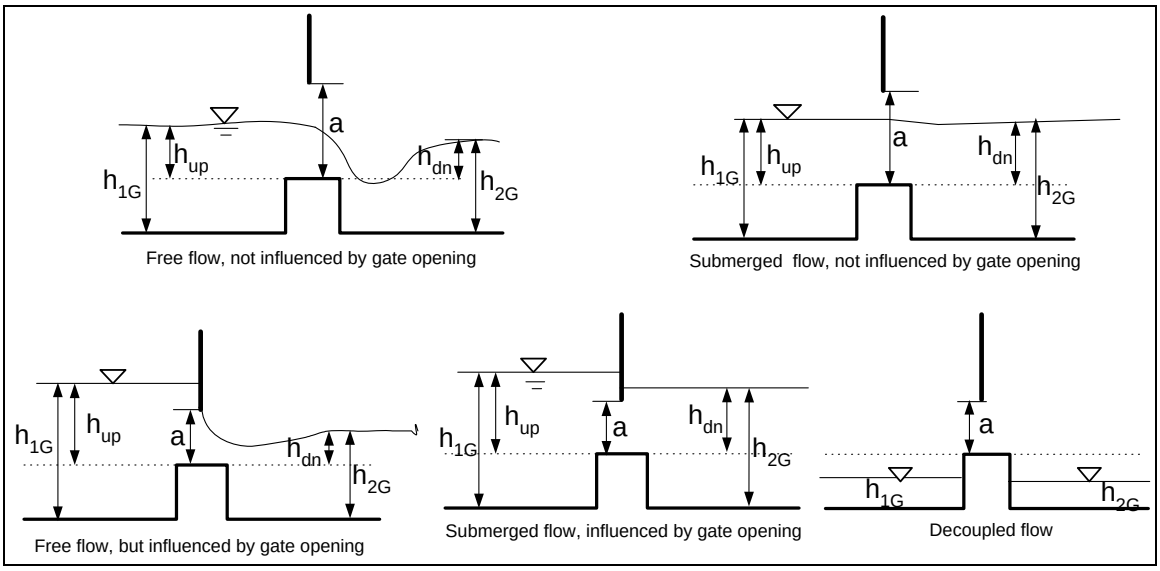

Fig. 2.1-7. Flow configurations around a gate.

The flow configuration around the gate and its surrounding reaches may be very dynamic under transient flows. Depending on the water stages at Nodes *1G* and *2G* (H_{1G} and H_{2G}), we have several configurations (Fig. 2.1-7). The gate discharge, Q_g, can be obtained by solving the continuity equation and the Bernoulli equation between Nodes *1G* and *2G*. The gate formulae under various stage conditions are given as

(1) For free fall flow and not influenced by the gate opening

$$Q_g = \frac{2}{3\sqrt{3}} C_g h_{up} L_g \sqrt{2gh_{up}} \quad if \quad h_{dn} < \frac{2}{3} h_{up} \quad and \quad a > \frac{2}{3} h_{up} \tag{2.1.58}$$

(2) For submerged flow and not influenced by the gate opening

$$Q_g = C_g h_{dn} L_g \sqrt{2g\left(h_{up} - h_{dn}\right)} \quad if \quad h_{dn} \geq \frac{2}{3} h_{up}, h_{dn} < h_{up}, \quad and \quad a > \frac{2}{3} h_{up} \tag{2.1.59}$$

(3) For free flow and influenced by the gate opening

$$Q_g = \frac{2}{3\sqrt{3}} C_g a L_g \sqrt{2gh_{up}} \quad if \quad h_{dn} < \frac{2}{3} h_{up} \quad and \quad a < \frac{2}{3} h_{up} \tag{2.1.60}$$

(4) For submerged flow and influenced by the gate opening

$$Q_g = C_g a L_g \sqrt{2g\left(h_{up} - h_{dn}\right)} \quad if \quad h_{dn} \geq \frac{2}{3} h_{up}, h_{dn} < h_{up}, \quad and \quad a < \frac{2}{3} h_{up} \tag{2.1.61}$$

(5) For decoupled flow

$$Q_g = 0 \tag{2.1.62}$$

where C_g is the gate coefficient, a is the gate opening, and L_g is the weir length.

Culvert boundary condition:

Similar to weirs and gates, the boundary conditions for the culvert can be stated as

$$\begin{aligned} -\mathbf{n}\cdot\mathbf{K}\left(\nabla H+\frac{h}{c\rho}\nabla(\Delta\rho)-\frac{B\tau^S}{Ag\rho}\right)\Big|_{1C}&=Q_C\left(h_{up},h_{dn}\right)\quad and\\ -\mathbf{n}\cdot\mathbf{K}\left(\nabla H+\frac{h}{c\rho}\nabla(\Delta\rho)-\frac{B\tau^S}{Ag\rho}\right)\Big|_{2C}&=Q_C\left(h_{up},h_{dn}\right)\end{aligned} \tag{2.1.63}$$

where Q_c is the discharge through the culvert or culverts, Node *1C* is the point upstream of the culvert and *2C* is the point downstream of the culvert, h_{up} is the water stage above the culvert at Node *1C*, and h_{dn} is the water stage above the culvert at Node *2C*. A wide range of culvert discharge formulae can be used and they can be easily incorporated in the computer code.

2.1.3 Kinematic Wave Approaches

In a kinematic approach, all the assumptions for the diffusive approach are hold. However, the velocity is given by modifying Eq. (2.1.46) with $\partial Z_o/\partial x$ replacing $\partial H/\partial x$ as follows

$$V=\frac{-a}{n}\left[\frac{R}{1+\left(\frac{\partial Z_0}{\partial x}\right)^2}\right]^{2/3}\frac{1}{\sqrt{\left|-\frac{\partial Z_o}{\partial x}-\frac{h}{c\rho}\frac{\partial\Delta\rho}{\partial x}+\frac{B\tau^S}{Ag\rho}\right|}}\left(\frac{\partial Z_o}{\partial x}+\frac{h}{c\rho}\frac{\partial\Delta\rho}{\partial x}-\frac{B\tau^S}{Ag\rho}\right) \tag{2.1.64}$$

Substituting Eq. (2.1.64) into Eq. (2.1.1) and using the definition $Q = VA$, we obtain

$$\frac{\partial A}{\partial t}+\frac{\partial VA}{\partial x}=S_S+S_R-S_E+S_I+S_1+S_2 \tag{2.1.65}$$

It is noted that Eq. (2.1.65) represents the advective transport of the cross-sectional area, A. It is an ideal equation amenable for numerically innovative advective transport algorithm.

To achieve transient simulations, either water depth or stage must be given as the initial condition. In addition, appropriate boundary conditions need to be specified to match the corresponding physical configuration. In a kinematic wave approach, boundary conditions are required only at upstream boundaries. An upstream boundary point can be an open boundary or a closed boundary. On an open upstream boundary, either the cross-sectional area (equivalent to water depth or water stage) or the flow rate can be specified as

$$A=A_{up}\quad or\quad \mathbf{n}\cdot\mathrm{VA}=\mathrm{Q_{up}}\quad on\quad B_{up} \tag{2.1.66}$$

where H_{up} is the water stage of the incoming upstream flow, Q_{up} is the flow rate of the incoming

upstream flow, and B_{up} is the open upstream boundary point. The flow rate through a closed upstream boundary point is by default equal to zero.

2.1.4 Thermal Transport

The thermal transport equation is derived based on the conservation principle of energy as:

$$\frac{\partial(\rho_W C_W AT)}{\partial t}+\frac{\partial(\rho_W C_W QT)}{\partial x}-\frac{\partial}{\partial x}\left(D^H A\frac{\partial T}{\partial x}\right) = S_h^a + S_h^r + S_h^n - S_h^b - S_h^e - S_h^s + S_h^i + S_h^{o1} + S_h^{o2} + S_h^c \quad \textbf{(2.1.67)}$$

where ρ_w is the water density [M/L^3]; C_w is the heat capacity of water [L^2/t^2/T]; T is the temperature [T]; D^H is the apparent thermal conductivity including the effect of dispersion, diffusion, and conduction [E/t/L/T = ML/t^3/T, where E is the unit of energy]; S_h^a is the heat source due to artificial injection/withdraw including rainfall [E/t/L = ML/t^3]; S_h^r is the heat source due to rainfall [E/t/L=ML/t^3]; S_h^n is the heat source due to net radiation [E/t/L = ML/t^3]; S_h^b is the heat sink due to back radiation from water surface to the atmosphere [E/t/L = ML/t^3]; S_h^e is the heat sink due to evaporation [E/t/L = ML/t^3]; S_h^s is the heat sink due to sensible heat flux [E/t/L = ML/t^3]; S_h^i is the heat source due to exfiltration from subsurface [E/t/L = ML/t^3]; S_h^{o1} is the heat source from overland flow via Bank *1* [E/t/L = ML/t^3]; S_h^{o2} is the heat source from overland flow via Bank *2* [E/t/L = ML/t^3]; and S_h^c is the heat source due to chemical reaction [E/t/L = ML/t^3]. In Eq. (2.1.67), S_h^r, S_h^i, S_h^{o1}, and S_h^{o2} are given by

$$S_h^r = C_W \rho_W S_R T^r; \qquad S_h^i = \begin{cases} C_W \rho_W S_I T^i & if \quad S_I \geq 0 \\ C_W \rho_W S_I T & if \quad S_I < 0 \end{cases} \quad \textbf{(2.1.68)}$$

and

$$S_h^{o1} = \begin{cases} C_W \rho_W S_1 T^{o1} & if \quad S_1 \geq 0 \\ C_W \rho_W S_1 T & if \quad S_1 < 0 \end{cases}; \qquad S_h^{o2} = \begin{cases} C_W \rho_W S_2 T^{o2} & if \quad S_2 \geq 0 \\ C_W \rho_W S_2 T & if \quad S_2 < 0 \end{cases} \quad \textbf{(2.1.69)}$$

where T^r is the temperature of the rainwater [T], T^i is the temperature of the exfiltration water from the subsurface flow [T], T^{o1} is the temperature of the water from overland flow via river Bank *1* [T], and T^{o2} is the temperature of the water from overland flow via river Bank *2* [T].

The heat source due to net radiation, S_h^n, heat sink due to back radiation, S_h^b, heat sink due to evaporation, S_h^e, and heat sink due to sensible heat, S_h^s, are given by their respective heat fluxes as follows

$$S_h^n = BH_n; \quad S_h^b = BH_b; \quad S_h^e = BH_e; \quad S_h^s = BH_s \quad \textbf{(2.1.70)}$$

where H_n, H_b, H_e, and H_s are the net radiation flux, back radiation flux, latent heat flux, and sensible heat flux, respectively. These fluxes depend on only meteorological condition and water temperature. They may be computed from follow equations (Yeh, 1969; Yeh et al., 1973; McCuen, 1989; Song and Li. 2000; and Jennifer et al., 2002).

Net radiation H_n

$$H_n = (1 - a_s)H_{so} + (1 - a_\ell)H_{\ell o} \qquad \textbf{(2.1.71)}$$

in which

$$H_{so} = H_o \cdot (0.61s + 0.35) \quad Btu / ft^2 / day \qquad \textbf{(2.1.72)}$$

and

$$H_{\ell o} = \varepsilon\sigma(T_a + 460)^4 \left[C + 0.031(e_a)^{1/2}\right] \qquad Btu / ft^2 / day \qquad \textbf{(2.1.73)}$$

where a_s and a_ℓ are the albedos of the water surface for short- and long-wave radiation respectively; H_{so} and $H_{\ell o}$ are the solar short- and long-wave radiation respectively; H_o is the solar constant, s is the percentage of possible sunshine; ε **= 0.97** is emissivity of water surface**;** $\sigma = 4.15 \times 10^{-8}$ Btu/ft^2/day/R^4 is the Stenfan-Boltzmann constant; T_a is air temperature in ^oF; C is the brunt coefficient; and e_a is the air vapor pressure in millimeter of mercury.

Back radiation H_b

$$H_b = \varepsilon\sigma(T_a + 460)^4 \quad Btu / ft^2 / day \qquad \textbf{(2.1.74)}$$

Sensible heat flux H_s

$$H_s = 0.26(73 + 7.3W)(T - T_a) \cdot (p / 760) \quad Btu / ft^2 / day \qquad \textbf{(2.1.75)}$$

where W is the wind speed in miles per hour and p is the atmospheric pressure in millimeter of mercury.

Latent heat flux of evaporation H_e

$$H_e = 0.26(73 + 7.3W)(e_w - e_a) \quad Btu / ft^2 / day \qquad \textbf{(2.1.76)}$$

where e_w is the saturated vapor pressure in millimeter of mercury at the water temperature T.

In addition to the initial boundary condition, boundary conditions must be specified for the temperature. Four types of global boundary conditions are provided in this report as follows.

Dirichlet boundary condition:

This condition is applied when the temperature is prescribed as a function of time on the boundaries:

$$T = T_{db}(x_b, t) \quad on \quad B_d \qquad \textbf{(2.1.77)}$$

where $T_{db}(x_b,t)$ is a time-dependent temperature on the Dirichlet boundary B_d [T].

Variable boundary condition:

This boundary condition is employed when the flow direction would change with time during simulations. Two cases are considered, regarding to the flow direction on the boundary.

< Case 1 > Flow is coming in from outside:

$$\rho_w C_w Q T - D^H A \frac{\partial T}{\partial x} = \rho_w C_w Q T_{vb}(x_b, t) \quad on \quad B_v \tag{2.1.78}$$

< Case 2 > Flow is going out from inside:

$$- D^H A \frac{\partial T}{\partial x} = 0 \quad on \quad B_v \tag{2.1.79}$$

where $T_{vb}(x_b,t)$ is a time-dependent temperature [T] through the variable boundary B_v, which is associated with the incoming flow.

Cauchy boundary condition:

This boundary condition is employed when the total heat-flow rate is given at the river/stream boundary. Usually, this boundary is an upstream boundary node. The conditions can be expressed as

$$\rho_w C_w Q T - D^H A \frac{\partial T}{\partial x} = \Phi_{cb}(x_b, t) \tag{2.1.80}$$

where $\Phi_{cb}(x_b,t)$ is total heat-flow rate (E/t = ML^2/t^3, where E denotes the unit of energy) through the Cauchy boundary, which takes a positive value if it is going out of the region and a negative value if it is coming into the region.

Neumann boundary condition:

This boundary condition is used when the conductive heat-flow rate is known at the river/stream boundary node. It can be written as

$$- D^H A \frac{\partial T}{\partial x} = \Phi_{nb}(x_b, t) \tag{2.1.81}$$

where $\Phi_{nb}(x_b,t)$ is the heat flux through the Neumann boundary.

In addition to the above four types of global boundary conditions, two types of internal boundary conditions are implemented: internal boundary nodes connecting to natural junctions and two internal boundary nodes for every control structures. These internal boundary conditions are mathematically stated similar to fluid flow of diffusive wave approaches.

Internal boundary condition at junctions:

If Node *IJ* is the internal node from Reach *I* connecting to Junction *J* (Fig. 2.1-1), the boundary conditions at Node *IJ* is given as

$$\left(\rho_w C_w QT - D^H A\frac{\partial T}{\partial x}\right)\Big|_{IJ} = \rho_w C_w \frac{1}{2} Q_{IJ}\left[(1+sign(Q_{IJ}))T_{IJ} + (1-sign(Q_{IJ}))T_J\right] \qquad \textbf{(2.1.82)}$$

where $sign(Q_{IJ})$ is equal 1.0 if the flow is from Reach I into Junction J, -1.0 if flow is from Junction J into Reach I; T_{IJ} is the temperature at Node IJ; and T_J is the temperature at Junction J which is given by

$$\sum_i \rho_w C_w \frac{1}{2} Q_{iJ}\left[(1+sign(Q_{iJ}))T_{iJ} + (1-sign(Q_{ij}))T_J\right] = 0 \qquad \textbf{(2.1.83)}$$

if the storage effect of Junction J is negligible or

$$\frac{d(\rho_w C_w V_J T_J)}{dt} = \sum_i \rho_w C_w \frac{1}{2} Q_{iJ}\left[(1+sign(Q_{iJ}))T_{iJ} + (1-sign(Q_{iJ}))T_J\right] \qquad \textbf{(2.1.84)}$$

if the storage effect of Junction J is significant.

Internal boundary condition at control structure:

If Nodes *1S* and *2S* are two internal boundary nodes connecting to Structure S (Fig. 2.1-2), the boundary conditions at Nodes *1S* and *2S* are given

$$\begin{aligned}\left(\rho_w C_w QT - D^H A\frac{\partial T}{\partial x}\right)\Big|_{1S} &= \left(\rho_w C_w QT - D^H A\frac{\partial T}{\partial x}\right)\Big|_{2S} \\ &= \rho_w C_w \frac{1}{2} Q_S\left[(1+sign(Q_S))T_{1S} + (1-sign(Q_S))T_{2S}\right]\end{aligned} \qquad \textbf{(2.1.85)}$$

where $sign(Q)$ is equal 1.0 if the flow is from Node *1S* to Node *2S*, -1.0 if flow is from Node *2S* to Node *1S*; T_{1S} is the temperature at Node *1S*; and T_{2S} is the temperature at Node *2S*.

2.1.5 Salinity Transport

$$\frac{\partial(AS)}{\partial t} + \frac{\partial(QS)}{\partial x} - \frac{\partial}{\partial x}\left(D^S A\frac{\partial S}{\partial x}\right) = M_s^{\,a} + M_s^{\,r} - M_s^{\,e} + M_s^{\,i} + M_s^{\,ol} + M_s^{\,o2} \qquad \textbf{(2.1.86)}$$

where S is the salinity [M/L^3]; D^S is the longitudinal dispersion coefficient for salinity [L^2/t]; $M_s^{\,a}$ is the artificial source of the salt [M/t/L]; $M_s^{\,r}$ is the salt source from rainfall [M/t/L]; $M_s^{\,e}$ is the salt sink from evaporation, which most likely would be zero [M/t/L]; $M_s^{\,i}$ is the salt source from subsurface [M/t/L]; $M_s^{\,o1}$ is the salt source from overland via River Bank *1* [M/t/L]; and $M_s^{\,o2}$ is the salt source from overland source viz River Bank *2* [M/L/t]. In Eq. (2.1.86), $M_s^{\,e}$ is likely to be zero and $M_s^{\,r}$, $M_s^{\,i}$, $M_s^{\,o1}$, and $M_s^{\,o2}$ are given by

$$M_s^{\,r} = S_R S^r; \qquad M_s^{\,i} = \begin{cases} S_I S^i & if \quad S_I \ge 0 \\ S_I S & if \quad S_I < 0 \end{cases} \qquad \textbf{(2.1.87)}$$

and

$$M_s^{ol} = \begin{cases} S_1 S^{ol} & if \quad S_1 \geq 0 \\ S_1 S & if \quad S_1 < 0 \end{cases}; \qquad M_s^{o2} = \begin{cases} S_2 S^{o2} & if \quad S_2 \geq 0 \\ S_2 S & if \quad S_2 < 0 \end{cases} \tag{2.1.88}$$

where S^r is the salinity of the rainwater [M/L^3], S^i is the salinity of the exfiltration water from the subsurface flow [M/L^3], S^{o1} is the salinity of the water from overland flow via River Bank *1* [M/L^3], and S^{o2} is the salinity of the water from overland flow via River Bank *2* [M/L^3].

As in thermal transport, four types of global boundary conditions for salinity transport are provided in this report as follows:

Dirichlet boundary condition:

This condition is applied when the salinity is prescribed as a function of time on the boundaries:

$$S = S_{db}\left(x_b, t\right) \tag{2.1.89}$$

where $S_{db}\left(x_b, t\right)$ is a time-dependent salinity on the Dirichlet boundary [M/L^3].

Variable boundary condition:

This boundary condition is employed when the flow direction would change with time during simulations. Two cases are considered, regarding to the flow direction on the boundary.

< Case 1 > Flow is coming in from outside:

$$QS - D^S A \frac{\partial S}{\partial x} = QS_{vb}\left(x_b, t\right) \tag{2.1.90}$$

< Case 2 > Flow is going out from inside:

$$-D^S A \frac{\partial S\left(x_b, t\right)}{\partial x} = 0 \tag{2.1.91}$$

where $S_{vb}\left(x_b, t\right)$ is a time-dependent salinity on the variable boundary [M/L^3], which is associated with the incoming flow.

Cauchy boundary condition:

This boundary condition is employed when the total salt-flow rate is given at the river/stream boundary. Usually, this boundary is an upstream boundary node. The conditions are expressed as

$$QS - D^S A \frac{\partial S}{\partial x} = \Phi_{cb}\left(x_b, t\right) \tag{2.1.92}$$

where $\Phi_{cb}\left(x_b, t\right)$ is total salt-flow rate on the Cauchy boundary [M/t], which takes a positive value if it is going out of the region and a negative value if it is coming into the region.

Neumann boundary condition:

This boundary condition is used when the dispersive salt-flow rate is known at the river/stream boundary node. It can be written as

$$-D^S A\frac{\partial S}{\partial x} = \Phi_{nb}\left(x_b, t\right) \tag{2.1.93}$$

where $\Phi_{nb}\left(x_b, t\right)$ is the salt rate due to salt concentration through the Neumann boundary [M/L].

The internal boundary conditions at junctions and control structures for salinity transport are stated similarly to those for thermal transport as follows.

Internal boundary condition at junctions:

If Node *IJ* is the internal node from Reach *I* connecting to Junction *J* (Fig. 2.1-1), the boundary condition at Node *IJ* is given as

$$\left(QS - D^S A\frac{\partial S}{\partial x}\right)\Big|_{IJ} = \frac{1}{2}Q_{IJ}\left[\left(1+sign\left(Q_{IJ}\right)\right)S_{IJ} + \left(1-sign\left(Q_{IJ}\right)\right)S_J\right] \tag{2.1.94}$$

where S_{IJ} is the salinity at Node *IJ* and S_J is the salinity at Junction *J*, which is governed by

$$\sum_i \frac{1}{2}Q_{IJ}\left[\left(1+sign\left(Q_{iJ}\right)\right)S_{iJ} + \left(1-sign\left(Q_{iJ}\right)\right)S_J\right] = 0 \tag{2.1.95}$$

if the storage effect of Junction *J* is negligible or

$$\frac{d\left(V_J S_J\right)}{dt} = \sum_i \frac{1}{2}Q_{iJ}\left[\left(1+sign\left(Q_{iJ}\right)\right)S_{iJ} + \left(1-sign\left(Q_{iJ}\right)\right)S_J\right] \tag{2.1.96}$$

if the storage effect of Junction *J* is significant.

Internal boundary condition at control structure:

If Nodes *1S* and *2S* are two internal boundary nodes connecting to Structure *S* (Fig. 2.1-2), the boundary conditions at nodes 1S and 2S are given

$$\left(QS - D^S A\frac{\partial S}{\partial x}\right)\Big|_{1S} = \left(QS - D^S A\frac{\partial S}{\partial x}\right)\Big|_{2S} = \frac{1}{2}Q_S\left[\left(1+sign\left(Q_S\right)\right)S_{1S} + \left(1-sign\left(Q_S\right)\right)S_{2S}\right] \tag{2.1.97}$$

where S_{1S} is the salinity at Node *1S* and S_{2S} is the salinity at Node *2S*.

2.2 Water Flow in Two-Dimensional Overland Regime

The governing equations for two-dimensional overland flow can be derived based on the conservation law of water mass and linear momentum [Wang and Connor, 1975]. The governing equations of a dynamic wave model in conservative form can be written as follows.

The continuity equation:

$$\frac{\partial h}{\partial t}+\frac{\partial (uh)}{\partial x}+\frac{\partial (vh)}{\partial y}=S+R-E+I \qquad \textbf{(2.2.1)}$$

where h is the water depth [L]; u is the velocity component in the x-direction [L/t]; v is the velocity component in the y-velocity [L/t]; S_S is the man-induced source [$L^3/t/L^2$]; S_R is the source due to rainfall [$L^3/t/L^2$]; S_E is the sink due to evapotranspiration [$L^3/t/L^2$]; and S_I is the source from subsurface media due to exfiltration [L/t]. It should be noted that $uh = q_x$ is the flux the x-direction [$L^3/t/L^2$] and $vh = q_y$ is the flux in the y-direction [$L^3/t/L^2$].

The x-momentum equation:

$$\frac{\partial (uh)}{\partial t}+\frac{\partial u(uh)}{\partial x}+\frac{\partial v(uh)}{\partial y}=-gh\frac{\partial (Z_o+h)}{\partial x}-\frac{gh^2}{2\rho}\frac{\partial \Delta\rho}{\partial x}-\frac{\partial F_{xx}}{\partial x}-\frac{\partial F_{yx}}{\partial y}+$$
$$\left(M_X{}^S+M_X{}^R-M_X{}^E+M_X{}^I\right)+\frac{\tau_x^s-\tau_x^b}{\rho} \qquad \textbf{(2.2.2)}$$

where Z_o is the bottom elevation of overland [L];]; $\Delta\rho = \rho - \rho_o$ is the density deviation [M/L^3] from the reference density (ρ_o), which is a function of temperature and salinity as well as other chemical concentrations; $M_X{}^S$ is the x-component of momentum-impulse from artificial sources/sinks [L^2/t^2]; $M_X{}^R$ is the x-component of momentum-impulse gained from rainfall [L^2/t^2]; $M_X{}^E$ is the x-component of momentum-impulse lost to evapotranspiration [L^2/t^2]; $M_X{}^I$ is the x-component of momentum-impulse gained from the subsurface media due to exfiltration [L^2/t^2]; F_{xx} and F_{yx} are the water fluxes due to eddy viscosity along the x-direction [L^3/t^2]; τ_x^s is the component of surface shear stress along the x-direction over unit horizontal overland area [$M/L/t^2$]; τ_x^b is the component of bottom shear stress along the x-direction over unit horizontal overland area [$M/L/t^2$], which can be assumed proportional to the x-component flow rate, i.e., $\tau_x^b/\rho = \kappa|\mathbf{V}|u$.

The y-momentum equation:

$$\frac{\partial (vh)}{\partial t}+\frac{\partial u(vh)}{\partial y}+\frac{\partial v(vh)}{\partial y}=-gh\frac{\partial (Z_o+h)}{\partial y}-gh\frac{gh^2}{2\rho}\frac{\partial \Delta\rho}{\partial y}-\frac{\partial F_{xy}}{\partial x}-\frac{\partial F_{yy}}{\partial y}+$$
$$\left(M_y{}^S+M_y{}^R-M_y^E+M_y{}^I\right)+\frac{\tau_y^s-\tau_y^b}{\rho} \qquad \textbf{(2.2.3)}$$

where M_y^S is the y-component of momentum-impulse from artificial sources/sinks [L^2/t^2]; M_y^R is the y-component of momentum-impulse gained from rainfall [L^2/t^2]; M_y^E is the y-component of momentum-impulse lost to evapotranspiration L^2/t^2]; M_y^I is the y-component of momentum-impulse gained from the subsurface media due to exfiltration [L^2/t^2]; F_{xy} and F_{yy} are the water fluxes due to eddy viscosity along the y-direction [L^3/t^2]; τ_y^s is the component of surface shear stress along the y-direction over unit horizontal overland area [M/L/t^2]; τ_y^b is the component of bottom shear stress along the y-direction over unit horizontal overland area [M/L/t^2], which can be assumed proportional to the y-component flow rate, i.e., $\tau_y^b/\rho = \kappa|\mathbf{V}|v$.

2.2.1 Fully Dynamic Wave Approaches

Eqs. (2.2.1) through (2.1.3) written in conservative form are the governing equations for two-dimensional flow in overland. Depending on the simplification of the momentum equation, one can have three approaches: fully dynamic wave, diffusive wave, and kinematic wave. For the fully dynamic wave approach, all terms in Eqs. (2.2.1) and (2.2.3) are retained. Under such circumstances, the conservative form of the governing equations may be used or they may be cast in the advection form or in the characteristic form. In this report, while the conservative form of fully dynamic wave equation is used as an option, the characteristic form of the fully dynamic approach will be used as a primary option. The characteristic form is the most natural way to deal with hyperbolic-dominant equations and amenable to the advective numerical methods, for example the upstream approximation or the Lagrangian-Eulerian method.

With an adequate mathematical manipulation, Eqs. (2.2.1) through (2.2.3) can be written in advective form as follows

$$\frac{\partial h}{\partial t} + u\frac{\partial h}{\partial x} + h\frac{\partial u}{\partial x} + v\frac{\partial h}{\partial y} + h\frac{\partial v}{\partial y} = \left(S + R - E + I\right) \tag{2.2.4}$$

$$\begin{aligned}\frac{\partial u}{\partial t} + g\frac{\partial h}{\partial x} + u\frac{\partial u}{\partial x} + v\frac{\partial u}{\partial y} &= -g\frac{\partial Z_o}{\partial x} - \frac{1}{h}\left[\frac{\partial F_{xx}}{\partial x} + \frac{\partial F_{yx}}{\partial y}\right] \\ &- \frac{u\left(S + R - E + I\right) - \left(M_X^S + M_X^R - M_x^E + M_X^I\right)}{h} + \frac{\tau_x^s - \tau_x^b}{\rho h}\end{aligned} \tag{2.2.5}$$

$$\begin{aligned}\frac{\partial v}{\partial t} + g\frac{\partial h}{\partial x} + u\frac{\partial v}{\partial x} + v\frac{\partial v}{\partial y} &= -g\frac{\partial Z_o}{\partial y} - \frac{gh^2}{2\rho}\frac{\partial \Delta\rho}{\partial y} - \frac{1}{h}\left[\frac{\partial F_{xy}}{\partial x} + \frac{\partial F_{yy}}{\partial y}\right] \\ &- \frac{v\left(S + R - E + I\right) - \left(M_y^S + M_y^R - M_y^E + M_y^I\right)}{h} + \frac{\tau_y^s - \tau_y^b}{\rho h}\end{aligned} \tag{2.2.6}$$

which can be written in matrix form as

$$\frac{\partial \mathbf{E}}{\partial t} + \mathbf{A}_x\frac{\partial \mathbf{E}}{\partial x} + \mathbf{A}_y\frac{\partial \mathbf{E}}{\partial y} = \mathbf{R} + \mathbf{D} \tag{2.2.7}$$

where

$$\mathbf{E} = \{\mathrm{h} \quad \mathrm{u} \quad \mathrm{v}\}^T; \quad \mathbf{A_x} = \begin{bmatrix} u & h & 0 \\ g & u & 0 \\ 0 & 0 & u \end{bmatrix}; \quad \mathbf{A_y} = \begin{bmatrix} v & 0 & h \\ 0 & v & 0 \\ g & 0 & v \end{bmatrix} \tag{2.2.8}$$

$$\mathbf{R} = \begin{Bmatrix} R_1 \\ R_2 \\ R_3 \end{Bmatrix} = \begin{Bmatrix} S + R - E + I \\ -g\dfrac{\partial Z_o}{\partial x} - \dfrac{gh^2}{2\rho}\dfrac{\partial \Delta\rho}{\partial x} - \dfrac{u\left(S_S + S_R - S_E + S_I\right) - \left(M_X{}^S + M_X{}^R - M_x{}^E + M_X{}^I\right)}{h} + \dfrac{\tau_x^s - \tau_x^b}{\rho h} \\ -g\dfrac{\partial Z_o}{\partial y} - \dfrac{gh^2}{2\rho}\dfrac{\partial \Delta\rho}{\partial y} - \dfrac{v\left(S_S + S_R - S_E + S_I\right) - \left(M_y{}^S + M_y{}^R - M_y{}^E + M_y{}^I\right)}{h} + \dfrac{\tau_y^s - \tau_y^b}{\rho h} \end{Bmatrix} \tag{2.2.9}$$

$$\mathbf{D} = \begin{Bmatrix} 0 \\ \mathrm{D_x} \\ D_y \end{Bmatrix} = \begin{Bmatrix} 0 \\ -\dfrac{1}{h}\left[\dfrac{\partial F_{xx}}{\partial x} + \dfrac{\partial F_{yx}}{\partial y}\right] \\ -\dfrac{1}{h}\left[\dfrac{\partial F_{xy}}{\partial x} + \dfrac{\partial F_{yy}}{\partial y}\right] \end{Bmatrix} = \begin{Bmatrix} 0 \\ \dfrac{1}{h}\left[\dfrac{\partial}{\partial x}\left(h\varepsilon_{xx}\dfrac{\partial u}{\partial x}\right) + \dfrac{\partial}{\partial y}\left(h\varepsilon_{xy}\dfrac{\partial u}{\partial y} + h\varepsilon_{yx}\dfrac{\partial v}{\partial x}\right)\right] \\ \dfrac{1}{h}\left[\dfrac{\partial}{\partial x}\left(h\varepsilon_{xy}\dfrac{\partial u}{\partial y} + h\varepsilon_{yx}\dfrac{\partial v}{\partial x}\right) + \dfrac{\partial v}{\partial y}\left(h\varepsilon_{yy}\dfrac{\partial v}{\partial y}\right)\right] \end{Bmatrix} \tag{2.2.10}$$

Let the matrix **B** be the linear combination of the matrices $\mathbf{A_x}$ and $\mathbf{A_y}$ as follows

$$\mathbf{B} = \mathbf{A} \cdot \mathbf{k} = \mathbf{A_x} k_x + \mathbf{A_y} k_y = \begin{bmatrix} uk_x + vk_y & hk_x & hk_y \\ gk_x & uk_x + vk_y & 0 \\ gk_y & 0 & uk_x + vk_y \end{bmatrix} \tag{2.2.11}$$

where **A** is a third rank vector with the matrices $\mathbf{A_x}$ and $\mathbf{A_y}$ as its components and **k** is a unit vector. The eigenvalues and eigenvectors of the defined matrix **B** are

$$\lambda_1 = uk_x + vk_y \qquad \mathbf{e_1} = \{0 \quad k_y \quad -k_x\}^T \tag{2.2.12}$$

$$\lambda_2 = uk_x + vk_y + \sqrt{gh} \qquad \mathbf{e_2} = \left\{\frac{\sqrt{gh}}{2} \quad \frac{gk_x}{2} \quad \frac{gk_y}{2}\right\}^T \tag{2.2.13}$$

$$\lambda_3 = uk_x + vk_y - \sqrt{gh} \qquad \mathbf{e_3} = \left\{-\frac{\sqrt{gh}}{2} \quad \frac{gk_x}{2} \quad \frac{gk_y}{2}\right\}^T \tag{2.2.14}$$

where k_x and k_y are the *x*- and *y*-component of the unit vector **k**.

Now we compose an eigenmatrix and its inverse from the eigenvectors of **B** as

$$\mathbf{L} = \begin{bmatrix} 0 & \frac{\sqrt{gh}}{2} & -\frac{\sqrt{gh}}{2} \\ k_y & \frac{gk_x}{2} & \frac{gk_x}{2} \\ -k_x & \frac{gk_y}{2} & \frac{gk_y}{2} \end{bmatrix} \quad and \quad \mathbf{L}^{-1} = \begin{bmatrix} 0 & k_y & -k_x \\ \frac{1}{\sqrt{gh}} & \frac{k_x}{g} & \frac{k_y}{g} \\ -\frac{1}{\sqrt{gh}} & \frac{k_x}{g} & \frac{k_y}{g} \end{bmatrix} \tag{2.2.15}$$

Let us define a characteristic vector **W** by

$$\partial\mathbf{W} = \mathbf{L}^{-1}\partial\mathbf{E} = \begin{bmatrix} 0 & k_y & -k_x \\ \frac{1}{\sqrt{gh}} & \frac{k_x}{g} & \frac{k_y}{g} \\ -\frac{1}{\sqrt{gh}} & \frac{k_x}{g} & \frac{k_y}{g} \end{bmatrix} \begin{Bmatrix} \partial h \\ \partial u \\ \partial v \end{Bmatrix} \quad in\ which \quad \mathbf{W} = \begin{Bmatrix} W_1 \\ W_2 \\ W_3 \end{Bmatrix}^T \tag{2.2.16}$$

where the first characteristic variable W_1 is a vorticity or shear wave. The second and third components, W_2 and W_3, are the amplitudes of the two gravity waves. The multiplication of Eq. (2.2.7) by $\mathbf{L}^{-1}$ yields

$$\mathbf{L}^{-1}\frac{\partial \mathbf{E}}{\partial \mathrm{t}} + \mathbf{L}^{-1}\mathbf{A}_\mathrm{x}\mathbf{L}\mathbf{L}^{-1}\frac{\partial \mathbf{E}}{\partial \mathrm{x}} + \mathbf{L}^{-1}\mathbf{A}_\mathrm{y}\mathbf{L}\mathbf{L}^{-1}\frac{\partial \mathbf{E}}{\partial \mathrm{y}} = \mathbf{L}^{-1}\mathbf{R} + \mathbf{L}^{-1}\mathbf{D} \tag{2.2.17}$$

or, with the transformation between **E** and **W** given by $\mathbf{L}^{-1}\partial\mathbf{E} = \partial\mathbf{W}$,

$$\frac{\partial \mathbf{W}}{\partial t} + \mathbf{L}^{-1}\mathbf{A}_\mathrm{x}\mathbf{L}\frac{\partial \mathbf{W}}{\partial x} + \mathbf{L}^{-1}\mathbf{A}_\mathrm{y}\mathbf{L}\frac{\partial \mathbf{W}}{\partial y} = \mathbf{L}^{-1}\mathbf{R} + \mathbf{L}^{-1}\mathbf{D} \tag{2.2.18}$$

Substituting $\mathbf{A}_\mathrm{x}$ and $\mathbf{A}_\mathrm{y}$ in Eq. (2.2.8) and $\mathbf{L}^{-1}$ and **L** in Eq. (2.2.15) into Eq. (2.2.18), and performing matrix multiplication, we obtain

$$\frac{\partial \mathbf{W}}{\partial t} + \begin{bmatrix} u & \frac{gck_y}{2} & -\frac{gck_y}{2} \\ \frac{hk_y}{c} & u+ck_x & 0 \\ \frac{hk_y}{c} & 0 & u-ck_x \end{bmatrix} \frac{\partial \mathbf{W}}{\partial x} + \begin{bmatrix} v & -\frac{gck_x}{2} & \frac{gck_x}{2} \\ -\frac{hk_x}{c} & v+ck_y & 0 \\ \frac{hk_x}{c} & 0 & v-ck_y \end{bmatrix} \frac{\partial \mathbf{W}}{\partial y} = \mathbf{L}^{-1}\mathbf{R} + \mathbf{L}^{-1}\mathbf{D} \tag{2.2.19}$$

where

$$\mathrm{c} = \sqrt{\mathrm{gh}} \tag{2.2.20}$$

It is noted that the coefficient matrices $\mathbf{L}^{-1}\mathbf{A}_x\mathbf{L}$ and $\mathbf{L}^{-1}\mathbf{A}_y\mathbf{L}$, respectively, of $(\partial\mathbf{W}/\partial x)$ and $(\partial\mathbf{W}/\partial y)$, respectively, are not diagonal matrices because $\mathbf{L}^{-1}$ is not an eigenmatrix of $\mathbf{A}_x$ nor of $\mathbf{A}_y$. Rearranging Eq. (2.2.19), we obtain

$$\frac{\partial \mathbf{W}}{\partial t}+\begin{bmatrix} u & 0 & 0 \\ 0 & u+ck_x & 0 \\ 0 & 0 & u-ck_x \end{bmatrix}\frac{\partial \mathbf{W}}{\partial x}+\begin{bmatrix} v & 0 & 0 \\ 0 & v+ck_y & 0 \\ 0 & 0 & v-ck_y \end{bmatrix}\frac{\partial \mathbf{W}}{\partial y}+\begin{Bmatrix} S_1 \\ S_2 \\ S_3 \end{Bmatrix}=\mathbf{L}^{-1}\left(\mathbf{R}+\mathbf{D}\right) \qquad \textbf{(2.2.21)}$$

where

$$\begin{Bmatrix} S_1 \\ S_2 \\ S_3 \end{Bmatrix}=\begin{Bmatrix} g\left(k_y\dfrac{\partial h}{\partial x}-k_x\dfrac{\partial h}{\partial y}\right) \\ \dfrac{h}{c}\left[k_yk_y\dfrac{\partial u}{\partial x}+k_xk_x\dfrac{\partial v}{\partial y}-k_xk_y\left(\dfrac{\partial u}{\partial y}+\dfrac{\partial v}{\partial x}\right)\right] \\ \dfrac{-h}{c}\left[k_yk_y\dfrac{\partial u}{\partial x}+k_xk_x^{(2)}\dfrac{\partial v}{\partial y}-k_xk_y\left(\dfrac{\partial u}{\partial y}+\dfrac{\partial v}{\partial x}\right)\right] \end{Bmatrix} \qquad \textbf{(2.2.22)}$$

For a general consideration, we define a new $\mathbf{L}^{*-1}$ (and its inverse $\mathbf{L}^*$) which plays the following transformation.

$$\partial\mathbf{W}=\mathbf{L}^{*-1}\,\partial\mathbf{E}=\begin{bmatrix} 0 & k_y^{(1)} & -k_x^{(1)} \\ \dfrac{1}{c} & \dfrac{k_x^{(2)}}{g} & \dfrac{k_y^{(2)}}{g} \\ -\dfrac{1}{c} & \dfrac{k_x^{(2)}}{g} & \dfrac{k_y^{(2)}}{g} \end{bmatrix}\begin{Bmatrix} \partial h \\ \partial u \\ \partial v \end{Bmatrix};\quad \mathbf{L}^*=\begin{bmatrix} 0 & \dfrac{c}{2} & -\dfrac{c}{2} \\ \dfrac{k_y^{(2)}}{k} & \dfrac{gk_x^{(2)}}{2k} & \dfrac{gk_x^{(2)}}{2k} \\ -\dfrac{k_x^{(2)}}{k} & \dfrac{gk_y^{(2)}}{2k} & \dfrac{gk_y^{(2)}}{2k} \end{bmatrix} \qquad \textbf{(2.2.23)}$$

where $k = \mathbf{k}^{(1)}\cdot\mathbf{k}^{(2)}$ is the inner product of $\mathbf{k}^{(1)}$ and $\mathbf{k}^{(2)}$. It should be noted that two unit wave directions $\mathbf{k}^{(1)}$ and $\mathbf{k}^{(2)}$ should not be orthogonal so that the transformation will not be singular. Multiplying both side of Eq. (2.2.7) by this new $\mathbf{L}^{*-1}$ and repeating mathematical manipulations involved in Eqs. (2.2.19) and (2.2.21), we have

$$\frac{\partial \mathbf{W}}{\partial t}+\begin{bmatrix} u & 0 & 0 \\ 0 & u+ck_x^{(2)} & 0 \\ 0 & 0 & u-ck_x^{(2)} \end{bmatrix}\frac{\partial \mathbf{W}}{\partial x}+\begin{bmatrix} v & 0 & 0 \\ 0 & v+ck_y^{(2)} & 0 \\ 0 & 0 & v-ck_y^{(2)} \end{bmatrix}\frac{\partial \mathbf{W}}{\partial y}+\begin{Bmatrix} S_1 \\ S_2 \\ S_3 \end{Bmatrix}=\mathbf{L}^{*-1}\left(\mathbf{R}+\mathbf{D}\right) \qquad \textbf{(2.2.24)}$$

where

$$\begin{Bmatrix} S_1 \\ S_2 \\ S_3 \end{Bmatrix} = \begin{Bmatrix} g\left(k_y^{(1)} \frac{\partial h}{\partial x} - k_x^{(1)} \frac{\partial h}{\partial y} \right) \\ \frac{h}{c}\left[k_y^{(2)} k_y^{(2)} \frac{\partial u}{\partial x} + k_x^{(2)} k_x^{(2)} \frac{\partial v}{\partial y} - k_x^{(2)} k_y^{(2)} \left(\frac{\partial u}{\partial y} + \frac{\partial v}{\partial x} \right) \right] \\ \frac{-h}{c}\left[k_y^{(2)} k_y^{(2)} \frac{\partial u}{\partial x} + k_x^{(2)} k_x^{(2)} \frac{\partial v}{\partial y} - k_x^{(2)} k_y^{(2)} \left(\frac{\partial u}{\partial y} + \frac{\partial v}{\partial x} \right) \right] \end{Bmatrix} \qquad \textbf{(2.2.25)}$$

Substituting $\mathbf{L}^{*-1}$ defined in Eq. (2.2.23) into the right hand side of Eq. (2.2.24), we obtain

$$\begin{Bmatrix} \frac{\partial W_1}{\partial t} + u\frac{\partial W_1}{\partial x} + v\frac{\partial W_1}{\partial y} \\ \frac{\partial W_2}{\partial t} + \left(u + ck_x^{(2)}\right)\frac{\partial W_2}{\partial x} + \left(v + ck_y^{(2)}\right)\frac{\partial W_2}{\partial y} \\ \frac{\partial W_3}{\partial t} + \left(u - ck_x^{(2)}\right)\frac{\partial W_3}{\partial x} + \left(v - ck_y^{(2)}\right)\frac{\partial W_3}{\partial y} \end{Bmatrix} + \begin{Bmatrix} S_1 \\ S_2 \\ S_3 \end{Bmatrix} = \begin{Bmatrix} A_1 \\ A_2 \\ A_3 \end{Bmatrix} + \begin{Bmatrix} B_1 \\ B_2 \\ B_3 \end{Bmatrix} \qquad \textbf{(2.2.26)}$$

where

$$\begin{Bmatrix} A_1 \\ A_2 \\ A_3 \end{Bmatrix} = \begin{Bmatrix} k_y^{(1)} R_2 - k_x^{(1)} R_3 \\ \frac{1}{c} R_1 + \frac{k_x^{(2)}}{g} R_2 + \frac{k_y^{(2)}}{g} R_3 \\ \frac{-1}{c} R_1 + \frac{k_x^{(2)}}{g} R_2 + \frac{k_y^{(2)}}{g} R_3 \end{Bmatrix} \quad \textit{and} \quad \begin{Bmatrix} B_1 \\ B_2 \\ B_3 \end{Bmatrix} = \begin{Bmatrix} k_y^{(1)} D_x - k_x^{(1)} D_y \\ \frac{k_x^{(2)}}{g} D_x + \frac{k_y^{(2)}}{g} D_y \\ \frac{k_x^{(2)}}{g} D_x + \frac{k_y^{(2)}}{g} D_y \end{Bmatrix} \qquad \textbf{(2.2.27)}$$

Writing out Eq. (2.2.26) in its three components, we have the following three equations for three unknowns W_1, W_2, and W_3

$$\frac{\partial W_1}{\partial t} + u\frac{\partial W_1}{\partial x} + v\frac{\partial W_1}{\partial y} + S_1 = A_1 + B_1 \qquad \textbf{(2.2.28)}$$

$$\frac{\partial W_2}{\partial t} + \left(u + ck_x^{(2)}\right)\frac{\partial W_2}{\partial x} + \left(v + ck_y^{(2)}\right)\frac{\partial W_2}{\partial y} + S_2 = A_2 + B_2 \qquad \textbf{(2.2.29)}$$

$$\frac{\partial W_3}{\partial t} + \left(u - ck_x^{(2)}\right)\frac{\partial W_3}{\partial x} + \left(v - ck_y^{(2)}\right)\frac{\partial W_3}{\partial y} + S_3 = A_3 + B_3 \qquad \textbf{(2.2.30)}$$

Equations (2.2.28), (2.29), and (2.230) indicate that the vorticity wave is advected by the velocity **V**, the positive gravity wave by $\mathbf{V} + c\mathbf{k}^{(2)}$, and the negative gravity wave by $\mathbf{V} - c\mathbf{k}^{(2)}$, where $\mathbf{k}^{(2)}$ is a unit vector.

We can write Eq. (2.2.26) in Lagrangian form as

$$\begin{Bmatrix} \frac{D_V W_1}{D\tau} \\ \frac{D_{V+ck^{(2)}} W_2}{D\tau} \\ \frac{D_{V-ck^{(2)}} W_3}{D\tau} \end{Bmatrix} + \begin{Bmatrix} S_1 \\ S_2 \\ S_3 \end{Bmatrix} = \begin{Bmatrix} A_1 \\ A_2 \\ A_3 \end{Bmatrix} + \begin{Bmatrix} B_1 \\ B_2 \\ B_3 \end{Bmatrix} \qquad \textbf{(2.2.31)}$$

where **V** is the transporting velocity of the vorticity wave W_1, (**V** + c**k**$^{(2)}$) is the transporting velocity of positive gravity wave W_2, and (**V** - c**k**$^{(2)}$) is the transporting velocity of negative gravity wave W_3. Substituting the definition of the characteristic variable **W** in Eq. (2.2.23) into Eq. (2.2.31), we have the following three equations for the three waves

$$k_y^{(1)} \frac{D_V u}{D\tau} - k_x^{(1)} \frac{D_V v}{D\tau} + S_1 = A_1 + B_1 \qquad \textbf{(2.2.32)}$$

$$\frac{2}{g} \frac{D_{V+ck^{(2)}} c}{D\tau} + \frac{k_x^{(2)}}{g} \frac{D_{V+ck^{(2)}} u}{D\tau} + \frac{k_y^{(2)}}{g} \frac{D_{V+ck(2)} v}{D\tau} + S_2 = A_2 + B_2 \qquad \textbf{(2.2.33)}$$

$$-\frac{2}{g} \frac{D_{V-ck^{(2)}} c}{D\tau} + \frac{k_x^{(2)}}{g} \frac{D_{V-ck^{(2)}} u}{D\tau} + \frac{k_y^{(2)}}{g} \frac{D_{V-ck^{(2)}} v}{D\tau} + S_3 = A_3 + B_3 \qquad \textbf{(2.2.34)}$$

It is noted that a diagonalization can be achieved with special selections of $k_x^{(1)}$, $k_y^{(1)}$, $k_x^{(2)}$, and $k_y^{(2)}$ to make S_1, S_2, and S_3 zeros.

In solving Eqs. (2.2.28) through (2.2.30) or Eqs. (2.2.32) through (2.2.34), the water depth h, and the velocity components, u and v, must be given initially or they can be obtained by simulating the steady-state version of Eqs. (2.2.28) through (2.2.30). In addition, appropriate boundary conditions need to be specified to match the corresponding physical system. The characteristics form of the governing equation offers great advantages over the primitive form in adapting appropriate numerical algorithms and in defining boundary conditions. Innovative hyperbolic numerical algorithms can be employed to approximate the system because each of the three equations is a decoupled advective transport equation of a wave. The specification of boundary conditions is made easy pending the wave direction. We demonstrate how boundary conditions are specified in the following. An overland boundary segment can be either open or closed. In the former case, the boundary condition for any wave is needed only when it is transported into the region of interest. When a wave is transported out of the region, there is no need to specify the boundary condition because internal flow dynamics due to this wave affects the boundary values of u, v, and h. In the later case, the flow rate on the boundary is zero.

Open upstream boundary condition:

At an open upstream boundary segment, the vorticity is always transported into the region from upstream. If the flow is supercritical, then both gravity waves also transported into the region from

upstream; thus three boundary conditions are needed. The water depth and velocity components at the boundary are determined entirely by the flow condition that prevails at the upstream. The governing equations for this case can be set up based on the continuity of mass as well as momentums between the upstream and boundary as

$$\mathbf{n}\cdot\mathbf{V}h = q_n^{(up)}(\mathbf{x}_b,t);\ \mathbf{n}\cdot\mathbf{V}uh + n_x\frac{gh^2}{2} = M_x^{up}(\mathbf{x}_b,t);\ and\ \mathbf{n}\cdot\mathbf{V}vh + n_y\frac{gh^2}{2} = M_y^{up}(\mathbf{x}_b,t) \quad \textbf{(2.2.35)}$$

where **n** is the outward unit vector of the boundary segment; $q_n^{up}(\mathbf{x}_b,t)$, a function of time *t*, is flow rate normal to the boundary from the upstream; $\mathbf{x}_b$ is the coordinate on the boundary; n_x is the *x*-component of **n**; $M_x^{up}(\mathbf{x}_b,t)$ is the *x*-momentum/impulse from the upstream; n_y is the *y*-component of **n**; and $M_y^{up}(\mathbf{x}_b,t)$ is the *y*-momentum/impulse from the upstream. It is noted that *u*, *v*, and *h* from the upstream must be given to provide q_n^{up}, M_x^{up} and M_y^{up}.

In the case of subcritical flow, one of the two gravity waves is transported into the region while the other is transported out of the region. The water depth and velocity are determined with the upstream flow condition and internal flow dynamics. The governing equations are set up based on the continuity of mass between the boundary and the upstream and on the flow dynamics in the region as

$$\begin{aligned}&\mathbf{n}\cdot\mathbf{V}h = q_n^{(up)}(\mathbf{x}_b,t)\ \ or\ \ h+Z_o = H_{up}(\mathbf{x}_b,t);\ \ell\cdot\mathbf{V}h = q_\ell^{(up)}(\mathbf{x}_b,t);\ and\ F_+(u,v,h)=0\\ &\qquad\qquad or\\ &\mathbf{n}\cdot\mathbf{V}h = q_n^{(up)}(\mathbf{x}_b,t)\ \ or\ h+Z_o = H_{up}(\mathbf{x}_b,t);\ \ell\cdot\mathbf{V}h = q_\ell^{(up)}(\mathbf{x}_b,t);\ and\ F_-(u,v,h)=0\end{aligned} \quad \textbf{(2.2.36)}$$

where ℓ is the unit vector parallel to the boundary segment; $H_{up}(\mathbf{x}_b,t)$, a function of time *t*, is the water stage in the incoming fluid from the upstream; $q_\ell^{up}(\mathbf{x}_b,t)$, a function of time *t*, is the flow rate parallel to the boundary.

Open downstream boundary condition:

At an open downstream boundary segment, the vorticity is always transported out of the region into downstream. If the flow is supercritical, then both gravity waves also transported out of the region into downstream; thus three is no need to specify the boundary conditions. The water depth and velocity components at the boundary are determined entirely by internal flow dynamics. The governing equations for this case are given by

$$F_\otimes(u,v,h)=0;\quad F_+(u,v,h)=0;\quad and\quad F_-(u,v,h)=0 \quad \textbf{(2.2.37)}$$

where $F_\otimes(u,v,h)$, a function of velocity and water depth, is the vorticity wave boundary function.

In the case of subcritical flow, one of the two gravity waves is transported into the region from downstream while the other is transported out of the region into downstream. The water depth and

velocity are determined by the internal flow dynamics and the control of the downstream boundary segment

$$\begin{aligned} &F_{\otimes}(u,v,h)=0;\quad F_{+}(u,v,h)=0;\ and\ h=h_{dn}(\mathbf{x}_b,t)\ or\ \mathbf{n}\cdot\mathbf{V}h=q_n^{dn}(h) \\ &\qquad\qquad or \\ &F_{\otimes}(u,v,h)=0;\quad F_{-}(u,v,h)=0;\ and\ \ h=h_{dn}(\mathbf{x}_b,t)\ or\ \mathbf{n}\cdot\mathbf{V}h=q_n^{dn}(h) \end{aligned} \qquad \textbf{(2.2.38)}$$

where $h^{dn}(t)$, a function of time t, is the water depth of the downstream boundary an $q_n^{dn}(h)$, a function of water depth h, is the rating curve of the downstream boundary.

Closed upstream boundary condition:

At the closed upstream boundary, physically all flow conditions can occur. The vorticity wave is always transported from the outside of the boundary into the region. When the supercritical flow happens, both gravity waves are also transported into the region. Thus, three boundary condition equations are needed. Because the boundary is closed, it is impermeable. The governing equations can be obtained by simply substituting $q_n^{up}=0$, $M_x^{up}=0$, and $M_y^{up}=0$ into Eq. (2.2.35) to yield

$$\mathbf{n}\cdot\mathbf{V}h=0;\quad \mathbf{n}\cdot\mathbf{V}uh+n_x\frac{gh^2}{2}=0;\quad and\quad \mathbf{n}\cdot\mathbf{V}vh+n_y\frac{gh^2}{2}=0 \qquad \textbf{(2.2.39)}$$

The solutions for Eq. (2.2.39) are not unique. One of the possible solution is $u=0$, $v=0$, and $h=0$.

When the flow is subcritical, one of the two gravity waves is transported from the outside of the boundary into the region while the other is transported from inside the boundary to the outside The boundary conditions are needed only for the incoming waves. Since no fluid from the outside world is transported into the region via the closed boundary, one of the two boundary condition equations can be stated with $\mathbf{n}\cdot\mathbf{V}=0$. The other boundary equation can be obtained by assuming no slip condition on the boundary. Thus, three governing equations are given as

$$\mathbf{n}\cdot\mathbf{V}h=0;\ \ell\cdot\mathbf{V}h=0;\ and\ F_{+}(u,v,h)=0\quad or\quad \mathbf{n}\cdot\mathbf{V}h=0;\ \ell\cdot\mathbf{V}h=0;\ and\ F_{-}(u,v,h)=0 \qquad \textbf{(2.2.40)}$$

depending on which wave is transported out of the region.

Closed downstream boundary condition:

At the closed downstream boundary, physical condition dictates that normal flow rate at the boundary is zero. The vorticity wave is always transported out of the region. If the flow is supercritical, both gravity waves are also transported out of the region. The velocity and water depth on the boundary is determined entirely by internal flow dynamics and no boundary condition is needed. The governing equations are given by the wave boundary functions subject to the constraint that fluid flux is zero as follows:

$$F_{\otimes}(u,v,h)=0;\ \ F_{+}(u,v,h)=0;\quad and\quad F_{-}(u,v,h)=0\quad subject\ to\quad \mathbf{n}\cdot\mathbf{V}=0 \qquad \textbf{(2.2.41)}$$

The only feasible solution of Eq. (2.1.31) is $u=0$, $v=0$, and $h=0$. Therefore, supercritical flow

cannot occur at a closed downstream segment.

In the case of subcritical flow, one of the two gravity waves is transported into the region while the other is transported out of the region. The water depth and velocity are determined with the internal flow dynamics and the condition of zero normal flux as

$$F_{\otimes}(u,v,h)=0;\ F_{+}(u,v,h)=0;\ and\ \mathbf{n}\cdot\mathbf{V}h=0\ \ or\ \ F_{\otimes}(u,v,h)=0;\ F_{-}(u,v,h)=0;\ and\ \mathbf{n}\cdot\mathbf{V}h=0 \qquad \textbf{(2.2.42)}$$

Overland-river interface boundary condition:

At the overland-river interface, the flux must be continuous as

$$(\mathbf{n}\bullet\mathbf{V})h\Big|_{Bank\,1}=S_1 \qquad and \qquad (\mathbf{n}\bullet\mathbf{V})h\Big|_{Bank\,2}=S_2 \qquad \textbf{(2.2.43)}$$

where S_1 and S_2 are sources of water which appear in Eq. (2.1.1)

2.2.2 Diffusive Wave Approaches

For diffusion wave models, the inertia terms in Eqs. (2.2.2) and (2.2.3) are assumed not important when compared to the others. With the further assumption that eddy viscosity is insignificant and $M_x^S=M_x^R=M_x^E=M_x^I=M_y^S=M_y^R=M_y^E=M_y^I=0$, we approximate the velocity $\mathbf{V}=(u,v)$ as follows

$$\mathbf{V}=\frac{-a}{n}\left[\frac{h}{1+(\nabla Z_o)^2}\right]^{2/3}\frac{1}{\sqrt{\left|-\nabla H-\frac{h}{2\rho}\nabla(\Delta\rho)+\frac{\tau^s}{\rho gh}\right|}}\left(\nabla H+\frac{h}{2\rho}\nabla(\Delta\rho)-\frac{\tau^s}{\rho gh}\right) \qquad \textbf{(2.2.44)}$$

Using the definition $\mathbf{q}=\mathbf{V}h$ and substituting Eq. (2.2.44) into Eq. (2.2.1), we obtain

$$\frac{\partial H}{\partial t}-\nabla\cdot\left[K\left(\nabla H+\frac{h}{2\rho}\nabla(\Delta\rho)-\frac{\boldsymbol{\tau}^s}{\rho gh}\right)\right]=S_S+S_R-S_E+S_I \qquad \textbf{(2.2.45)}$$

in which

$$K=\frac{a\,h^{5/3}}{n}\frac{1}{\left[1+(\nabla Z_o)^2\right]^{2/3}}\frac{1}{\sqrt{\left|-\nabla H-\frac{h}{2\rho}\nabla(\Delta\rho)+\frac{\tau^s}{\rho gh}\right|}} \qquad \textbf{(2.2.46)}$$

To achieve transient simulations, either water depth or stage must be given as the initial condition. In addition, appropriate boundary conditions need to be specified to match the corresponding physical system. In our model, four types of boundary conditions may be specified depending on physical configurations of the boundary. These boundary conditions are addressed below.

Dirichlet boundary condition: prescribed water depth or stage

On a Dirichlet boundary, either the water depth or stage can be prescribed as a function of time. This boundary condition can be expressed as

$$h = h_d\left(\mathbf{x}_b, t\right) \quad or \quad H = h + Z_0 = H_d(\mathbf{x}_b, t), \quad on \quad B_d \tag{2.2.47}$$

where $h_d\left(\mathbf{x}_b, t\right)$ is a prescribed time-dependent water depth on the Dirichlet boundary [L], $H_d(\mathbf{x}_b, t)$ is a prescribed time-dependent water stage [L], and B_d is the Dirichlet boundary segment. A Dirichlet boundary segment can locate at the up-streams or down-streams, control structures, or even interior points.

Flux boundary condition: prescribed flow rate

On a flux boundary, a time-dependent flow rate is prescribed as a function of time as

$$-\mathbf{n}\cdot K\left(\nabla H + \frac{h}{2\rho}\nabla\left(\Delta\rho\right) - \frac{\boldsymbol{\tau}^s}{\rho g h}\right) = q_f\left(\mathbf{x}_b, t\right) \quad on \quad B_f \tag{2.2.48}$$

where **n** is an outward unit vector at the flux boundary point, $q_f\left(\mathbf{x}_b, t\right)$ a prescribed time-dependent flow rate [L^3/t/L], and B_f is a flux boundary segment. Mathematically, a flux boundary condition can be applied to an upstream or downstream segment. However, in practice, it is often applied to an upstream boundary segment.

Water depth-dependent boundary condition: prescribed rating curve

This condition is often used to describe the flow rate at a downstream boundary at which the flow rate is a function of water depth. It can be written as

$$-\mathbf{n}\cdot K\left(\nabla H + \frac{h}{2\rho}\nabla\left(\Delta\rho\right) - \frac{\boldsymbol{\tau}^s}{\rho g h}\right) = q_r\left(h\left(x_r, t\right)\right) \quad on \quad B_r \tag{2.2.49}$$

where $q_r(h(x_r,t))$ is a water depth-dependent flow rate [L^3/t/L], $\mathbf{x}_r$ is the *x*-coordinate on the boundary B_r, and B_r is a boundary segment on which the prescribed rating curve is applied.

Overland-river interface boundary condition:

At the overland-river interface, the flux must be continuous as

$$\begin{aligned} -\mathbf{n}\cdot K\left(\nabla H + \frac{h}{2\rho}\nabla\left(\Delta\rho\right) - \frac{\boldsymbol{\tau}^s}{\rho g h}\right)\Big|_{Bank\,1} &= S_1 \quad and \\ -\mathbf{n}\cdot K\left(\nabla H + \frac{h}{2\rho}\nabla\left(\Delta\rho\right) - \frac{\boldsymbol{\tau}^s}{\rho g h}\right)\Big|_{Bank\,2} &= S_2 \end{aligned} \tag{2.2.50}$$

where S_1 and S_2 are sources of water which appear in Eq. (2.1.1)

2.2.3 Kinematic Wave Approaches

In a kinematic approach, all the assumptions for the diffusive approach are hold. However, the velocity is given by modifying Eq. (2.2.44) with ∇Z_0 replacing ∇H as follows

$$\mathbf{V} = \frac{-a}{n}\left[\frac{h}{1+\left(\nabla Z_o\right)^2}\right]^{2/3} \frac{1}{\sqrt{\left|-\nabla Z_o - \frac{h}{2\rho}\nabla\left(\Delta\rho\right)+\frac{\tau^s}{\rho g h}\right|}}\left(\nabla z_o + \frac{h}{2\rho}\nabla\left(\Delta\rho\right) - \frac{\tau^s}{\rho g h}\right) \qquad \textbf{(2.2.51)}$$

Substituting Eq. (2.2.51) into Eq. (2.2.1) and using the definition **q** = **V***h*, we obtain

$$\frac{\partial h}{\partial t} + \nabla\cdot\left(\mathbf{V}h\right) = S_S + S_R - S_E + S_I \qquad \textbf{(2.2.52)}$$

It is noted that Eq. (2.2.52) represents the advective transport of the water depth, *h*. It is an ideal equation amenable for numerically innovative advective transport algorithm.

To achieve transient simulations, either water depth or stage must be given as the initial condition. In addition, appropriate boundary conditions need to be specified to match the corresponding physical configuration. In a kinematic wave approach, boundary conditions are required only at upstream boundaries. An upstream boundary segment can be an open boundary or a closed boundary. On an open upstream boundary, either the water depth or the flow rate can be specified as

$$h = h_{up}\left(\mathbf{x}_{up}, t\right) \quad or \quad \mathbf{n}\cdot\mathbf{V}h = q_{up}\left(\mathbf{x}_{up}, t\right) \quad on \quad B_{up} \qquad \textbf{(2.2.53)}$$

where $h_{up}\left(\mathbf{x}_{up}, t\right)$ is the water depth of the incoming upstream flow, $q_{up}\left(\mathbf{x}_{up}, t\right)$ is the flow rate of the incoming upstream flow, $\mathbf{x}_{up}$ is the coordinate on the upstream boundary, and B_{up} is the open upstream boundary segment. The flow rate through a closed upstream boundary segment is by default equal to zero.

2.2.4 Thermal Transport

The thermal transport equation is derived based on the conservation principle of energy as:

$$\begin{aligned}\frac{\partial\left(\rho_w C_w h T\right)}{\partial t} + \nabla\cdot\left(\rho_w C_w \mathbf{q}\mathrm{T}\right) - \nabla\cdot\left(\mathbf{D}^{\mathrm{H}} h\cdot\nabla T\right) \\ = H_a + H_r + H_n - H_b - H_e - H_s + H_i + H_c\end{aligned} \qquad \textbf{(2.2.54)}$$

where ρ_w is the water density [M/L^3]; C_w is the heat capacity of water [L^2/t^2/T]; T is the temperature [T]; $\mathbf{D}^{\mathrm{H}}$ is the apparent thermal conductivity tensor including the effect of dispersion, diffusion, and

conduction [E/L/t/T = ML/t^3/T, where E is the unit of energy]; H_a is the heat source due to artificial injection/withdraw including rainfall [E/t/L^2 = M/t^3]; H_r is the heat source due to rainfall [E/t/L^2 = M/t^3]; H_n is the heat source due to net radiation [E/t/L^2 = M/t^3]; H_b is the heat sink due to back radiation from water surface to the atmosphere [E/t/L^2 = M/t^3]; H_e is the heat sink due to evaporation [E/t/L^2 = M/t^3]; H_s is the heat sink due to sensible heat flux [E/t/L^2 = M/t^3]; H_i is the heat source due to exfiltration from subsurface [E/t/L^2 = M/t^3]; and H_c is the heat source due to chemical reaction [E/t/L^2 = M/t^3]. In Eq. (2.2.54), H_r and H_i are given by

$$H_r = C_w \rho_w R T^r; \qquad H_i = \begin{cases} C_w \rho_w I T^i & if \quad I \geq 0 \\ C_w \rho_w I T & if \quad I < 0 \end{cases} \tag{2.2.55}$$

where R is the rainfall rate [L/t], T^r is the temperature of the rainwater [T], I is the exfiltration rate [L/t], and T^i is the temperature of the exfiltration water from the subsurface flow [T]. H_n, H_b, H_e, and H_s are the net radiation flux, back radiation flux, latent heat flux, and sensible heat flux, respectively. These fluxes depend on only meteorological condition and water temperature. The formulation of these heat/energy fluxes were presented in Section 2.1.

In addition to the initial boundary condition, boundary conditions must be specified for the temperature. Four types of global boundary conditions are provided in this report as follows.

Dirichlet boundary condition:

This condition is applied when the temperature is prescribed as a function of time on the boundaries:

$$T = T_{db}\left(\mathbf{x}_b, t\right) \qquad on \qquad B_d \tag{2.2.56}$$

where $T_{db}\left(\mathbf{x}_b, t\right)$ is a time-dependent temperature on the Dirichlet boundary B_d [T].

Variable boundary condition:

This boundary condition is employed when the flow direction would change with time during simulations. Two cases are considered, regarding to the flow direction on the boundary.

< Case 1 > Flow is coming in from outside:

$$\mathbf{n} \cdot \left(\rho_w C_w \mathbf{q} T - \mathbf{D}^{\mathbf{H}} h \cdot \nabla T \right) = \mathbf{n} \cdot \rho_w C_w \mathbf{q} T_{vb}\left(\mathbf{x}_b, t\right) \qquad on \qquad B_v \tag{2.2.57}$$

< Case 2 > Flow is going out from inside:

$$-\mathbf{n} \cdot \mathbf{D}^{\mathbf{H}} h \cdot \nabla T = 0 \qquad on \qquad B_v \tag{2.2.58}$$

where $T_{vb}\left(\mathbf{x}_b, t\right)$ is a time-dependent temperature on the variable boundary B_v [T], which is associated with the incoming flow.

Cauchy boundary condition:

This boundary condition is employed when the total heat-flow rate is given at the boundary. Usually, this boundary is a flow-in boundary. The conditions can be expressed as

$$\mathbf{n}\cdot\left(\rho_w C_w \mathbf{q}T - \mathbf{D}^{\mathbf{H}}h\cdot\nabla T\right) = \Phi_{cb}(t) \quad on \quad B_c \tag{2.2.59}$$

where $\Phi_{cb}(t)$ is total heat flux on the Cauchy boundary B_c [E/L/t = ML/t^3, where E denotes the unit of energy], which takes a positive value if it is going out of the region and a negative value if it is coming into the region.

Neumann boundary condition:

This boundary condition is used when the conductive heat-flow rate is known at the boundary. It can be written as

$$-\mathbf{n}\cdot\mathbf{D}^{\mathbf{H}}h\cdot\nabla T = \Phi_{nb}(\mathbf{x}_b, t) \quad on \quad B_n \tag{2.2.60}$$

where $\Phi_{nb}(\mathbf{x}_b, t)$ is the heat flux on the Neumann boundary B_n [E/L/t].

In addition to the four types of global boundary conditions, an internal boundary condition may be specified for the exchange of energy/heat flux between the overland and river/stream network. Mathematically, this boundary condition is described below.

Overland-river interface boundary condition:

$$\mathbf{n}\cdot\left(\rho_w C_w \mathbf{q}T - \mathbf{D}^{\mathbf{H}}h\cdot\nabla T\right)\Big|_{Bank\,1} = S_h^{o1} \quad and \quad \mathbf{n}\cdot\left(\rho_w C_w \mathbf{q}T - \mathbf{D}^{\mathbf{H}}h\cdot\nabla T\right)\Big|_{Bank\,2} = S_h^{o2} \tag{2.2.61}$$

where S_h^{o1} and S_h^{o2} are the heat sources, which appeared in Eq. (2.1.67). These heat sources can be calculated using Eq. (2.1.69) if the temperatures in the overland water and river water are discontinuous at the interfaces. If the temperatures are continuous, then these heat sources should be formulated by imposing the continuity of the temperatures in the overland water and river water at the interface.

2.2.5 Salinity Transport

$$\frac{\partial(hS)}{\partial ts} + \nabla\cdot(\mathbf{q}S) - \nabla\cdot\left(h\mathbf{D}^{\mathbf{S}}\cdot\nabla S\right) = M_s^{as} + M_s^{rs} - M_s^{es} + M_s^{is} \tag{2.2.62}$$

where S is the salinity [M/L^3]; $\mathbf{D}^{\mathbf{S}}$ is the longitudinal dispersion coefficient for salt [L^2/t]; M_s^{as} is the artificial source of the salt [M/t//L^2]; M_s^{rs} is the salt source from rainfall [M/t/L^2; M_s^{es} is the salt sink from evaporation [M/t/L^2]; M_s^{is} is the salt source from subsurface [M/t/L^2]. In Eq. (2.2.62), M_s^{es} is likely to be zero and M_s^{rs} and M_s^{is} are given by

$$M_s^{rs} = RS^r; \quad M_s^{is} = \begin{Bmatrix} IS^i & if\ I \ge 0 \\ IS & if\ I < 0 \end{Bmatrix} \tag{2.2.63}$$

where R is the rainfall rate [L/t], S^r is the salinity of the rainwater [M/L^3], I is the exfiltration rate [L/t], and S^i is the salinity of the exfiltration water from the subsurface flow [M/L^3].

As in thermal transport, four types of global boundary conditions for salinity transport are provided in this report as follows.

Dirichlet boundary condition:

This condition is applied when the salinity is prescribed as a function of time on the boundaries:

$$S = S_{db}\left(\mathbf{x}_b, t\right) \quad on \quad B_d \tag{2.2.64}$$

where $S_{db}\left(\mathbf{x}_b, t\right)$ is a time-dependent salinity on the Dirichlet boundary B_d [M/L^3].

Variable boundary condition:

This boundary condition is employed when the flow direction would change with time during simulations. Two cases are considered, regarding to the flow direction on the boundary.

< Case 1 > Flow is coming in from outside:

$$\mathbf{n}\cdot\left(\mathbf{q}S - h\mathbf{D}^{\mathbf{S}}\cdot\nabla S\right) = \mathbf{n}\cdot\mathbf{q}S_{vb}\left(\mathbf{x}_b, t\right) \quad on \quad B_v \tag{2.2.65}$$

< Case 2 > Flow is going out from inside:

$$-\mathbf{n}\cdot h\mathbf{D}^{\mathbf{S}}\cdot\nabla S = 0 \quad on \quad B_v \tag{2.2.66}$$

where $S_{vb}\left(\mathbf{x}_b, t\right)$ is a time-dependent salinity on the variable boundary B_v [M/L^3], which is associated with the incoming flow.

Cauchy boundary condition:

This boundary condition is employed when the total salt-flow rate is given at the boundary. Usually, this boundary is a flow-in boundary. The conditions are expressed as

$$\mathbf{n}\cdot\left(\mathbf{q}S - h\mathbf{D}^{\mathbf{S}}\cdot\nabla S\right) = S_{cb}\left(\mathbf{x}_b, t\right) \quad on \quad B_c \tag{2.2.67}$$

where $S_{cb}\left(\mathbf{x}_b, t\right)$ is total salt-flow rate on the Cauchy boundary B_c [M/L/t], which takes a positive value if it is going out of the region and a negative value if it is coming into the region.

Neumann boundary condition:

This boundary condition is used when the dispersive salt-flow rate is known at the boundary. t can be written as

$$-\mathbf{n}\cdot h\mathbf{D}^{\mathbf{S}}\cdot\nabla S = S_{nb}(t) \quad on \quad B_n \tag{2.2.68}$$

where $S_{nb}(t)$ is the salt flux on the Neumann boundary [M/L/t].

As in thermal transport, in addition to the four types of global boundary conditions, an internal boundary condition may be specified for the exchange of salt between the overland and river/stream network. Mathematically, this boundary condition is described below.

River-overland interface boundary condition:

$$\mathbf{n}\cdot\left(\mathbf{q}S-\mathbf{D}^{S}h\cdot\nabla S\right)\Big|_{Bank\,1} = M_s^{o1} \quad and \quad \mathbf{n}\cdot\left(\mathbf{q}S-\mathbf{D}^{S}h\cdot\nabla S\right)\Big|_{Bank\,2} = M_s^{o2} \tag{2.2.69}$$

where M_s^{o1} and M_s^{o2}, which appeared in Eq. (2.1.86), are the salt sources from overland into the rivers. These salt sources can be calculated using Eq. (2.1.88) if the salinity in the overland water and river water are discontinuous at the interfaces. If the salinity is continuous, then these salt sources should be formulated by imposing the continuity of salinity in the overland water and river water at the interface.

2.3 Water Flow in Three-Dimensional Subsurface Media

2.3.1 Water Flow

The governing equation of subsurface density dependent flow through saturated-unsaturated porous media can be derived based on the conservation law of water mass (Yeh, 1987; Yeh et al., 1994; Lin et al., 1997). It is written as follows.

$$\frac{\rho}{\rho_o}F\frac{\partial h}{\partial t} = \nabla\cdot\left[\mathbf{K}\cdot\left(\nabla h+\frac{\rho}{\rho_o}\nabla z\right)\right]+\frac{\rho^*}{\rho_o}q \tag{2.3.1}$$

where ρ is the density of water; ρ_o is the reference density of water; h is the referenced pressure head [L]; t is the time [t]; **K** is the hydraulic conductivity tensor [L/t]; z is the potential head [L]; ρ* is the density of source water; q is the source and/or sink [L^3/L^3/t]; and F is the water capacity [1/L] given by

$$F = a'\frac{\theta_e}{n_e}+\beta'\theta_e+n_e\frac{dS}{dh} \tag{2.3.2}$$

where a' is the modified compressibility of the medium [1/L], θ_e is the effective moisture content [L^3/L^3], n_e is the effectively porosity [L^3/L^3], β' is the compressibility of water [1/L], and S is the degree of saturation. The Darcy's velocity is given by

$$\mathbf{V} = -\mathbf{K} \cdot \left(\frac{\rho_o}{\rho} \nabla h + \nabla z \right) \tag{2.3.3}$$

To achieve transient simulation, the following initial condition needs to be given.

$$h = h_i(\mathbf{x}) \qquad in \quad R, \tag{2.3.4}$$

where R is the region of interest and h_i is the prescribed pressure head [L], which can be obtained by either field measurements or by solving the steady state version of Eq. (2.3.1).

Five types of boundary conditions are taken into account as follows.

Dirichlet boundary condition:

This boundary condition is used when pressure head can be prescribed on the boundary. It can be expressed as

$$h = h_d(\mathbf{x}, t) \qquad on \quad B_d(\mathbf{x}) = 0 \tag{2.3.5}$$

where $h_d(\mathbf{x},t)$ is the Dirichlet head on the boundary surface $B_d(\mathbf{x}) = 0$

Neumann boundary condition:

This boundary condition is employed when the flux results from pressure-head gradient is known as a function of time. It is written as

$$-\mathbf{n} \cdot \mathbf{K} \cdot \frac{\rho_o}{\rho} \nabla h = q_n(\mathbf{x}, t) \qquad on \quad B_n(\mathbf{x}) = 0 \tag{2.3.6}$$

where $q_n(\mathbf{x},t)$ is the Neumann flux and $B_n(\mathbf{x}) = 0$ is the Neumann boundary surface.

Cauchy boundary condition:

This boundary condition is employed when the flux results from total-head gradient is known as a function of time. It can be written as

$$-\mathbf{n} \cdot \left(\mathbf{K} \cdot \frac{\rho_o}{\rho} \nabla h + \mathbf{K} \cdot \nabla z \right) = q_c(\mathbf{x}, t) \qquad on \quad B_c(\mathbf{x}) = 0 \tag{2.3.7}$$

where $q_c(\mathbf{x},t)$ is the Cauchy flux and $B_c(\mathbf{x}) = 0$ is the Cauchy boundary surface.

River Boundary Condition:

This boundary condition is employed when there is a thin layer of medium separating the river and the subsurface media.

$$-\mathbf{n}\cdot\mathbf{K}\cdot\left(\frac{\rho_o}{\rho}\nabla h+\nabla z\right)=-\frac{K_R}{b_R}\left(h_R-h\right)\qquad on\quad B_r(\mathbf{x})=0 \tag{2.3.8}$$

where K_R is the hydraulic conductivity of the thin layer, b_R is the thickness of the thin layer, h_R is the water depth in the river, and $B_r(\mathbf{x}) = 0$ is the surface between the river and subsurface media.

Variable Boundary Condition:

This boundary condition is usually used for the ground surface boundary when the coupling of surface and subsurface systems is not taken into account.

(1) During precipitation periods:

$$h=h_p(\mathbf{x},t)\quad iff\quad -\mathbf{n}\cdot\mathbf{K}\cdot\left(\frac{\rho_o}{\rho}\nabla h+\nabla z\right)\geq q_p(\mathbf{x},t)\quad on\quad B_v(\mathbf{x})=0 \tag{2.3.9}$$

or

$$-\mathbf{n}\cdot\mathbf{K}\cdot\left(\frac{\rho_o}{\rho}\nabla h+\nabla z\right)=q_p(\mathbf{x},t)\quad iff\quad h\leq h_p\quad on\quad B_v(\mathbf{x})=0 \tag{2.3.10}$$

(2) During non-precipitation period:

$$h=h_p(\mathbf{x},t)\quad iff\quad -\mathbf{n}\cdot\mathbf{K}\cdot\left(\frac{\rho_o}{\rho}\nabla h+\nabla z\right)\geq 0\quad on\quad B_v(\mathbf{x})=0 \tag{2.3.11}$$

$$h=h_m(\mathbf{x},t)\quad iff\quad -\mathbf{n}\cdot\mathbf{K}\cdot\left(\frac{\rho_o}{\rho}\nabla h+\nabla z\right)\leq q_e\quad on\quad B_v(\mathbf{x})=0 \tag{2.3.12}$$

or

$$-\mathbf{n}\cdot\mathbf{K}\cdot\left(\frac{\rho_o}{\rho}\nabla h+\nabla z\right)=q_e(\mathbf{x},t)\quad iff\quad h\geq h_m\quad on\quad B_v(\mathbf{x})=0 \tag{2.3.13}$$

where $h_p(\mathbf{x},t)$ is ponding depth, $q_p(\mathbf{x},t)$ is the flux due to precipitation, $h_m(\mathbf{x},t)$ is the minimum pressure head, and $q_e(\mathbf{x},t)$ is the potential evaporation rate on the surfaces of the variable boundary condition $B_v(\mathbf{x}) = 0$. Only one of Eqs. (2.3.9) through (2.3.13) is used at any point on the variable boundary at any time.

2.3.2 Thermal Transport

The thermal transport equation is derived based on the conservation principle of energy as:

$$\frac{\partial\left[\left(\rho_w C_w\theta+\rho_b C_m\right)T\right]}{\partial t}+\nabla\cdot\left(\rho_w C_w\mathbf{V}T\right)-\nabla\cdot\left(\mathbf{D}^{\mathbf{H}}\cdot\nabla T\right)=H^a+H^c \tag{2.3.14}$$

where ρ_w is the water density [M/L^3]; C_w is the heat capacity of water [L^2/t^2/T]; θ is the moisture content [L^3/L^3]; ρ_b is the bulk density of the media [M/L^3]; C_m is the heat capacity of the matrix [L^2/t^2/T]; T is the temperature [T]; $\mathbf{D}^{\mathrm{H}}$ is the apparent thermal conductivity tensor including the effect of dispersion, diffusion, and conduction [E/t/L/T = ML/t^3/T, where E is the unit of energy]; H^a is the heat source due to artificial injection/withdraw [E/t/L^3 = M/L/t^3], and H^c is the heat source due to chemical reaction [E/t/L^3 = M/L/t^3].

In addition to the initial boundary condition, boundary conditions must be specified for the temperature. Five types of global boundary conditions are provided in this report as follows.

Dirichlet boundary condition:

This condition is applied when the temperature is prescribed as a function of time on the boundaries:

$$T(\mathbf{x},t) = T_{db}(\mathbf{x},t) \quad on \quad B_d(\mathbf{x}) = 0 \tag{2.3.15}$$

where $T_{db}(\mathbf{x},t)$ is a time-dependent temperature on the Dirichlet boundary $B_d(\mathbf{x}) = 0$ [T].

Variable boundary condition:

This boundary condition is employed when the flow direction would change with time during simulations. Two cases are considered, regarding to the flow direction on the boundary.

< Case 1 > Flow is coming in from outside:

$$\mathbf{n}\cdot\left(\rho_w C_w \mathbf{V}T - \mathbf{D}^{\mathbf{H}}\cdot\nabla T\right) = \mathbf{n}\cdot\rho_w C_w \mathbf{V}T_{vb}(\mathbf{x},t) \quad on \quad B_v(\mathbf{x}) = 0 \tag{2.3.16}$$

< Case 2 > Flow is going out from inside:

$$-\mathbf{n}\cdot\mathbf{D}^{\mathbf{H}}\cdot\nabla T = 0 \quad on \quad B_v(\mathbf{x}) = 0 \tag{2.3.17}$$

where $T_{vb}(\mathbf{x},t)$ is a time-dependent temperature on the variable boundary, $B_v(\mathbf{x}) = 0$, [T], which is associated with the incoming flow.

Cauchy boundary condition*:*

This boundary condition is employed when the total heat-flow rate is given at the river/stream boundary. Usually, this boundary is an upstream boundary node. The conditions can be expressed as

$$\mathbf{n}\cdot\left(\rho_w C_w \mathbf{V}T - \mathbf{D}^{\mathbf{H}}\cdot\nabla T\right) = H_{cb}(\mathbf{x},t) \quad on \quad B_c(\mathbf{x}) = 0 \tag{2.3.18}$$

where $H_{cb}(\mathbf{x},t)$ is total heat flux through the Cauchy boundary, $B_c(\mathbf{x}) = 0$, [E/L^2/t = M/t^3, where E denotes the unit of energy], which takes a positive value if it is going out of the region and a negative value if it is coming into the region.

Neumann boundary condition:

This boundary condition is used when the conductive heat-flow rate is known at the river/stream boundary node. It can be written as

$$-\mathbf{n}\cdot\mathbf{D}^{\mathbf{H}}\cdot\nabla T = H_{nb}(\mathbf{x},t) \quad on \quad B_n(\mathbf{x}) = 0 \tag{2.3.19}$$

where $H_{nb}(\mathbf{x},t)$ is the heat flux through the Neumann boundary, $B_n(\mathbf{x}) = 0$, [E/L^2/t].

Atmosphere-subsurface interface boundary condition:

At the interface of the atmosphere and subsurface media, a heat budget boundary condition is specified as

$$-\mathbf{n}\cdot\left(\rho_w C_w \mathbf{V}T - \mathbf{D}^{\mathbf{H}}\cdot\nabla T\right) = H_n - H_b - H_e - H_s \tag{2.3.20}$$

where H_n, H_b, H_e, and H_s are calculated using Eqs. (2.1.71) through (2.1.76).

In addition to the five types of global boundary conditions, two interface boundary conditions may be specified: one for the exchange of energy/heat flux between the subsurface media and river/stream network and the other for energy/heat exchange between the subsurface media and the overland. Mathematically, these boundary conditions are described below.

Subsurface-river interface boundary condition*:*

$$\int_P \mathbf{n}\cdot\left(\rho_w C_w \mathbf{V}T - \mathbf{D}^{\mathbf{H}}\cdot\nabla T\right)dP = S_h^i \tag{2.3.21}$$

where S_h^i is the heat sources in Eq. (2.1.67) and P is the wet perimeter of the river. The heat source can be calculated using Eq. (2.1.68) if the temperatures in the subsurface and river are discontinuous at the interfaces. If the temperatures are continues, then this heat source should be formulated by imposing the continuity of the temperatures in the subsurface and river water at the interfaces.

Subsurface-overland interface boundary condition:

$$\mathbf{n}\cdot\left(\rho_w C_w \mathbf{V}T - \mathbf{D}^{\mathbf{H}}\cdot\nabla T\right) = H_i \tag{2.3.22}$$

where H_i is the heat source in Eq. (2.2.54). This heat source can be calculated using Eq. (2.2.55) if the temperatures in the subsurface and overland are discontinuous at the interface. If the temperatures are continues, then this heat source should be formulated by imposing the continuity of the temperatures in the subsurface and overland at the interface.

2.3.3 Salinity Transport

$$\frac{\partial(\theta S)}{\partial t} + \nabla\cdot(\mathbf{V}S) - \nabla\cdot\left(\theta\mathbf{D}^{\mathbf{S}}\cdot\nabla S\right) = S^{as} \qquad \textbf{(2.3.23)}$$

where S is the salinity [M/L^3]; $\mathbf{D}^{\mathbf{S}}$ is the longitudinal dispersion coefficient [L^2/t]; and S^{as} is the artificial source of the salt [M/L^3/t].

As in thermal transport, four types of global boundary conditions for salinity transport are provided in this report as follows.

Dirichlet boundary condition:

This condition is applied when the salinity is prescribed as a function of time on the boundaries:

$$S(x,t) = S_{db}(\mathbf{x},t) \quad on \quad B_d(\mathbf{x}) = 0 \qquad \textbf{(2.3.24)}$$

where $S_{db}(\mathbf{x},t)$ is a time-dependent salinity on the Dirichlet boundary, $B_d(\mathbf{x}) = 0$, [M/L^3].

Variable boundary condition:

This boundary condition is employed when the flow direction would change with time during simulations. Two cases are considered, regarding to the flow direction on the boundary.

< Case 1 > Flow is coming in from outside:

$$\mathbf{n}\cdot\left(\mathbf{V}S - \theta\mathbf{D}^{\mathbf{S}}\cdot\nabla S\right) = \mathbf{n}\cdot VS_{vb}(\mathbf{x},t) \quad on \quad B_v(\mathbf{x}) = 0 \qquad \textbf{(2.3.25)}$$

< Case 2 > Flow is going out from inside:

$$-\mathbf{n}\cdot\theta\mathbf{D}^{\mathbf{S}}\cdot\nabla S = 0 \quad on \quad B_v(\mathbf{x}) = 0 \qquad \textbf{(2.3.26)}$$

where $S_{vb}(\mathbf{x},t)$ is a time-dependent salinity [M/L^3] on the variable boundary, $B_v(\mathbf{x}) = 0$, which is associated with the incoming flow.

Cauchy boundary condition:

This boundary condition is employed when the total salt-flow rate is given at pervious boundaries. Usually, this boundary is a flow-in boundary. The conditions are expressed as

$$\mathbf{n}\cdot\left(\mathbf{V}S - \theta\mathbf{D}^{\mathbf{S}}\cdot\nabla S\right) = Q_{scb}(\mathbf{x},t) \quad on \quad B_c(\mathbf{x}) = 0 \qquad \textbf{(2.3.27)}$$

where $Q_{scb}(\mathbf{x},t)$ is total salt-flow rate [M/L^2/t] through the Cauchy boundary, $B_c(\mathbf{x}) = 0$, which takes a positive value if it is going out of the region and a negative value if it is coming into the region.

Neumann boundary condition:

This boundary condition is used when the dispersive salt-flow rate is known at the boundary. It can be written as

$$-\mathbf{n}\cdot\theta\mathbf{D}^{\mathbf{S}}\cdot\nabla S = Q_{snb}\left(\mathbf{x},t\right) \tag{2.3.28}$$

where $Q_{snb}\left(\mathbf{x},t\right)$ is the salt flux through the Neumann boundary, $B_n(\mathbf{x}) = 0$, [M/L^2/t].

In addition to the four types of global boundary conditions, two interface boundary conditions may be specified: one for the exchange of salt flux between the subsurface media and river/stream network and the other for salt exchange between the subsurface media and the overland. Mathematically, these boundary conditions are described below.

Subsurface-river interface boundary condition:

$$\int_P \mathbf{n}\cdot\left(\mathbf{V}S - \theta\mathbf{D}^{\mathbf{S}}\cdot\nabla S\right)dP = M_s^i \tag{2.3.29}$$

where M_s^i is the salt source in Eq. (2.1.86) and P is the wet perimeter of the river. The salt source can be calculated using Eq. (2.1.87) if the salinity in the subsurface and river is discontinuous at the interfaces. If the salinity is continuous, then this salt source should be formulated by imposing the continuity of the salinity in the subsurface and river at the interface.

Subsurface-overland interface boundary condition:

$$\mathbf{n}\cdot\left(\mathbf{V}S - \theta\mathbf{D}^{\mathbf{S}}\cdot\nabla S\right) = M_s^{is} \tag{2.3.30}$$

where M_s^{is} is the salt source in Eq. (2.2.62). This salt source can be calculated using Eq. (2.2.63) if the salinity in the subsurface and overland is discontinuous at the interface. If the salinity is continuous, then this salt source should be formulated by imposing the continuity of the salinity in the subsurface and overland at the interface.

2.4 Coupling Fluid Flows Among Various Media

One of the critical issues in a first principle physics-based watershed model is its treatments of coupling among various media. There appear a number of watershed models that have dealt with each component medium on the bases of first principle in the past decade (MIKE11-MIKE SHE [Abbott et al., 1986a, 1986b], SHETRAN [Ewen et al., 2000], MODFLOW-HMS [HydroGeoLogic, Inc., 2001], InHM [VanderKwaak, 1999], GISWA [Wigmosta and Perkins, 1997], SFRSM-HSE [SFWMD, 2005], COSFLOW [Yeh et al., 1997], WASH123D Version 1.0 [Yeh et al., 1998]). However, rigorous considerations on coupling among media seemed lacking. For example, a linkage term is normally formulated between the river/stream/canal dynamics and subsurface fluid flow (e.g., MODNET [Walton et al., 1999]) or between overland and subsurface flows (e.g.,

MIKE11-MIKE SHE [http://www.dhisoftware.com/mikeshe/; http://www.dhisoftware.com/mikeshe/components]). The linkage term usually introduces non-physical parameters. As a result, such watershed models have degraded even though each media-component module has taken a first principle physics-based approach. A rigorous treatment of coupling media should be based the continuity of mass, momentum, and state variables. This is the approach taken in this report. Mathematical statements on coupling between pairs of media are address below.

2.4.1 Coupling between River/Stream/Canal and Overland Flows

The fluxes between overland regime and canals/streams/rivers network are dynamics and depend on the water surface elevations in the vicinity of the interface between canal/stream/river and overland regime (Fig. 2.4-1). The basic principle of coupling is to impose continuous of fluxes and the state variables (water surface elevations, temperature, and salinity in the overland and in the canal) if these state variables do not exhibit discontinuity. If the state variables exhibit discontinuity, then the linkage term is used to simulate the volumetric fluxes or simplified formulations of heat fluxes and salinity fluxes are imposed.

When a levee is present on the bank of the canal (left column in Fig. 2.4-1), there are several possibilities on the dynamic interactions between overland flow and river flow dynamics. If water surfaces in both the overland regime and river are below the top of the levee, the two flow systems are decoupled (Fig. 2.4-1a).

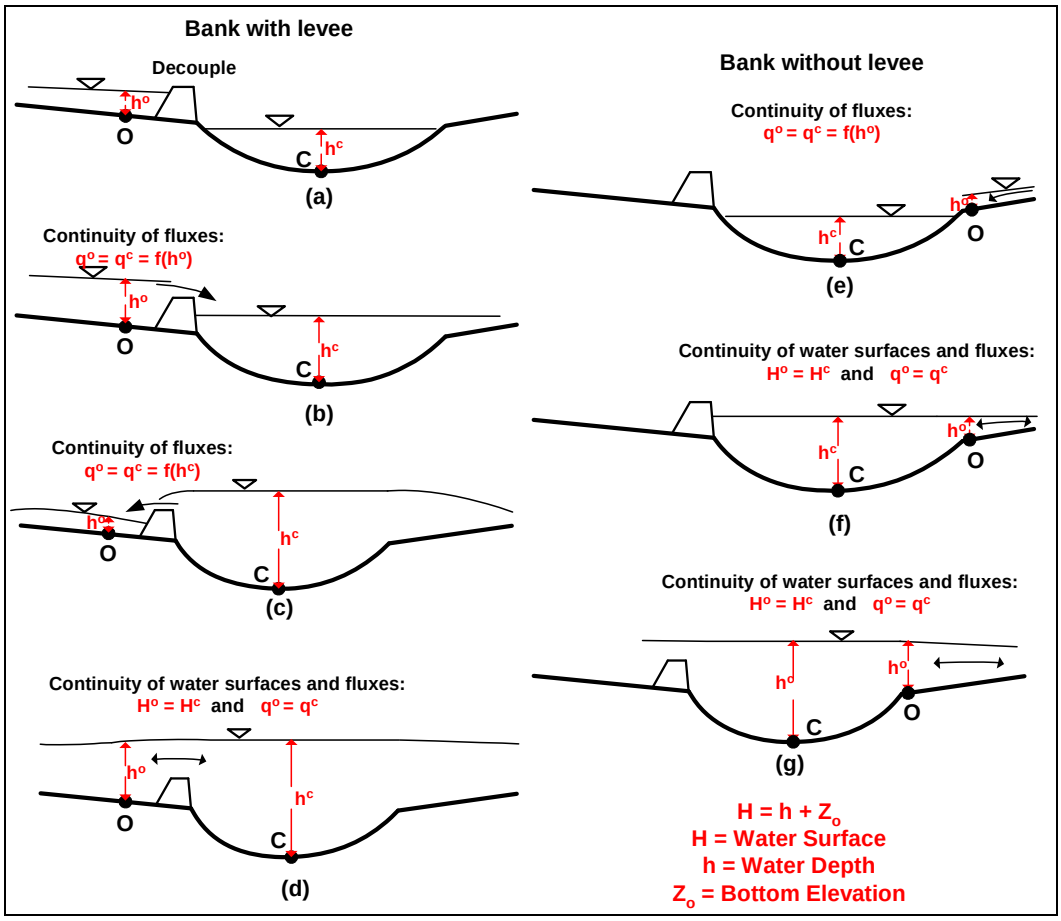

Fig. 2.4-1. Flow interactions between overland regime and canal: bank with levee (left column) and bank without levee (right column)

When the water surface in the overland regime is above the top of the levee and in the canal is below

the top of the levee (Fig. 2.4-1b), the flux is a function of the water depth in the overland regime given

$$q^{o} = q^{c} = f\left(h^{o}\right) \;\Rightarrow\; \mathbf{n}\cdot\mathbf{V}h\big|_{O} = S_1 = f\left(h^{o}; Z_{o|B}\right) \qquad \textbf{(2.4.1)}$$

where q^o is the outward normal flux of the overland flow, q^c is the lateral flow from the overland to the canal, h^o is the water depth in the overland regime, $f(h^o)$ is a prescribed function of h^o given by the shape and width of the levee, $\mathbf{n}$ is the outward unit vector (from the overland side) of the overland-canal interface, $\mathbf{V}$ is the velocity in the overland regime, S_1 is defined in Eq. (2.1.1), $Z_o|_B$ is the bottom elevation evaluated at the canal bank (in this case $Z_o|_B$ is the elevation of the top of the levee). The coupling of thermal and/or salinity transport between the overland regime and river networks for this case can be stated as

$$\begin{aligned} \mathbf{n}\cdot\left(\rho_w C_w \mathbf{q}T - \mathbf{D}^{\mathbf{H}} h\cdot\nabla T\right)\Big|_{Bank\,1} &= S_h^{o1} = \rho_w C_w S_1 T^o \qquad \textit{and} \\ \mathbf{n}\cdot\left(\mathbf{q}S - \mathbf{D}^{\mathbf{S}} h\cdot\nabla S\right)\Big|_{Bank\,1} &= M_s^{o1} = S_1 S^o \end{aligned} \qquad \textbf{(2.4.2)}$$

where T^o is the temperature of the overland water at the interface and S^o is the salinity of the overland water at the interface.

On the other hand, when the water surface in the overland regime is belowe the top of the levee and in the canal is above the top of the levee (Fig. 2.4-1c), the flux is a function of the water depth in the overland regime given by

$$q^{o} = q^{c} = f\left(h^{c}\right) \qquad \Rightarrow \qquad \mathbf{n}\cdot\mathbf{V}h\big|_{O} = S_1 = f\left(h^{c}; Z_o\big|_B\right) \qquad \textbf{(2.4.3)}$$

where h^c is the water depth in the canal and $f(h^c)$ is a prescribed function of h^c. The coupling of thermal and salinity transport between the overland regime and river networks for this case can be stated as

$$\begin{aligned} \mathbf{n}\cdot\left(\rho_w C_w \mathbf{q}T - \mathbf{D}^{\mathbf{H}} h\cdot\nabla T\right)\Big|_{Bank1} &= S_h^{o1} = \rho_w C_w S_1 T^c \qquad \textit{and} \\ \mathbf{n}\cdot\left(\mathbf{q}S - \mathbf{D}^{\mathbf{S}} h\cdot\nabla S\right)\Big|_{Bank1} &= M_s^{o1} = S_1 S^c \end{aligned} \qquad \textbf{(2.4.4)}$$

where T^c is the temperature of the canal water at the interface and S^c is the salinity of the canal water at the interface.

When the water surfaces in both the overland and canal are above the top of the levee (Fig. 2.4-1d), then the continuity of fluxes and state variables must be imposed as

$$q^o = q^c \;\Rightarrow \mathbf{n}\cdot\mathbf{V}h\big|_{O} = S_1 \quad \textit{and} \quad H^o = H^c \Rightarrow \left(h + Z_o\right)\big|_{O} = \left(h + Z_o\right)\big|_{C} \qquad \textbf{(2.4.5)}$$

where $(h + Z_o)|_O$ denotes that $(h + Z_o)$ is evaluated at point O (Fig. 2.4-1 d). Similarly, $(h + Z_o)|_C$ denotes that $(h + Z_o)$ is evaluated at point C. The coupling of thermal and/or salinity transport between the overland regime and river networks for this case can be obtained by formulating the fluxes

$$\mathbf{n}\cdot\left(\rho_w C_w \mathbf{q}T - \mathbf{D}^{\mathbf{H}} h\cdot\nabla T\right)\Big|_{Bank1} = S_h^{o1} = \rho_w C_w S_1 \frac{1}{2}\left(1+sign\left(S_1\right)T^o + \left(1-sign\left(S_1\right)\right)T^c\right)$$
$$and \quad \mathbf{n}\cdot\left(\mathbf{q}S - \mathbf{D}^{\mathbf{S}} h\cdot\nabla S\right)\Big|_{Bank1} = M_S^{o1} = S_1 \frac{1}{2}\left(\left(1+sign\left(S_1\right)\right)S^o + \left(1-sign\left(S_1\right)\right)S^c\right) \quad \textbf{(2.4.6)}$$

where *sign(S_1)* is 1.0 if the flow is from overland to canal, -1.0 if the flow is from canal to overland. For this case, the temperature and salinity in the canal may be the same as those in the overland water at the interface. If this is the case, we impose the continuity of temperature and/or salinity to yield the fluxes

$$\mathbf{n}\cdot\left(\rho_w C_w \mathbf{q}T - \mathbf{D}^{\mathbf{H}} h\cdot\nabla T\right)\Big|_{Bank1} = S_h^{o1} \quad and \quad T^o\Big|_{Bank1} = T^c$$
$$and \qquad \mathbf{n}\cdot\left(\mathbf{q}S - \mathbf{D}^{\mathbf{S}} h\cdot\nabla S\right)\Big|_{Bank1} = M_S^{o1} \quad and \quad S^o\Big|_{Bank1} = S^c \quad \textbf{(2.4.7)}$$

When a levee is not present on the bank of the canal (right column in Fig. 2.4-1), there are two possibilities on the dynamic interactions between overland flow and river flow dynamics. If water surface in the canal falls below the bank, the flux is either zero if the overland flow is not present or is nonzero and directed from the overland into the canal if overland flow is present (Fig. 2.4-1 e) as

$$q^o = q^c = f\left(h^o\right) \qquad \Rightarrow \qquad \mathbf{n}\cdot\mathbf{V}h\Big|_O = S_2 = f\left(h^o; Z_o\big|_B\right) \quad \textbf{(2.4.8)}$$

where S_2 is defined in Eq. (2.1.1) and $Z_o|_B$ is the bottom elevation evaluated at point *O* on the canal bank. The coupling of thermal and/or salinity transport between the overland regime and river networks for this case can be stated as

$$\mathbf{n}\cdot\left(\rho_w C_W \mathbf{q}T - \mathbf{D}^{\mathbf{H}} h\cdot\nabla T\right)\Big|_{Bank2} = S_h^{o2} = \rho_w C_w S_2 T^o \quad and$$
$$\mathbf{n}\cdot\left(\mathbf{q}S - \mathbf{D}^{\mathbf{S}} h\cdot\nabla S\right)\Big|_{Bank2} = M_s^{o2} = S_2 S^o \quad \textbf{(2.4.9)}$$

When the water surface in the canal is above the bank (Figs. 2.4-1f and 2.4-1.g), the flux direction can be either from the overland into the canal or from the canal into the overland depending on the flow dynamics in the overland and in the canal. The direction of the flux and its magnitude are obtained by imposing the continuity of flux and state variables

$$q^o = q^c \Rightarrow \mathbf{n}\cdot\mathbf{V}h\Big|_O = S_2 \quad and$$
$$H^o = H^c \Rightarrow \left(h+Z_o\right)\Big|_O = \left(h+Z_o\right)\Big|_C \quad \textbf{(2.4.10)}$$

The coupling of thermal and/or salinity transport between the overland regime and river networks for this case can be stated as

$$\mathbf{n}\cdot\left(\rho_w C_w \mathbf{q}T - \mathbf{D}^{\mathbf{H}} h\cdot\nabla T\right)\Big|_{Bank\,2} = S_h^{o2}$$
$$= \rho_w C_w S_2 \frac{1}{2}\left(\left(1+sign\left(S_2\right)\right)T^o + \left(1-sign\left(S_2\right)\right)T^c\right) \quad and \tag{2.4.11}$$
$$\mathbf{n}\cdot\left(\mathbf{q}S - \mathbf{D}^{\mathbf{S}} h\cdot\nabla S\right)\Big|_{Bank\,2} = M_S^{o2} = S_2\frac{1}{2}\left(\left(1+sign\left(S_2\right)\right)S^o + \left(1-sign\left(S_2\right)\right)S^c\right)$$

For these two cases (Fig. 2.4-1f and 2.4-1g), the temperature and salinity in the canal may be the same as those in the overland water at the interface. If this is the case, we impose the continuity of temperature and/or salinity to yield the fluxes

$$\mathbf{n}\cdot\left(\rho_w C_w \mathbf{q}T - \mathbf{D}^{\mathbf{H}} h\cdot\nabla T\right)\Big|_{Bank\,2} = S_h^{o1} \quad and \quad T^o\Big|_{Bank\,2} = T^c \quad and$$
$$\mathbf{n}\cdot\left(\mathbf{q}S - \mathbf{D}^{\mathbf{S}} h\cdot\nabla S\right)\Big|_{Bank\,2} = M_s^{o1} \quad and \quad S^o\Big|_{Bank\,2} = S^c \tag{2.4.12}$$

2.4.2 Coupling between Overland and Subsurface Flows

The fluxes between overland and subsurface media are obtained by imposing continuous of fluxes and state variables if these state variables do not exhibit discontinuity. If the state variables exhibit discontinuity, then a linkage term is used to simulate the fluxes. Consider the interaction between the overland subsurface and subsurface flows. There are two cases: in one case, there is no impermeable layers on the ground surface (Fig. 2.4-2a) and, in another case, there are thin layers of very impermeable layers such as pavements or sediment deposits on the ground surface (Fig. 2.4-2b).

For the case of no impermeable layers on the ground surface (Fig. 2.4-2a), it can easily be seen that the pressures in the overland flow (if it is present) and in the subsurface media will be continuous across the interface. Thus, the interaction must be simulated by imposing continuity of pressures and fluxes as

$$h^o = h^s \quad and \quad Q^o = Q^s \quad \Rightarrow \quad I = -\mathbf{n}\cdot\mathbf{K}\cdot\left(\frac{\rho_o}{\rho}\nabla h^s + \nabla z\right) \tag{2.4.13}$$

where h^o is the water depth in the overland if it is present, h^s is the pressure head in the subsurface, Q^o is the flux from the overland to the interface and Q^s is the flux from the interface to the subsurface media, I is defined in Eq. (2.2.1), **n** is an outward unit vector of the ground subsurface, **K** is the hydraulic conductivity tensor, and h^s is the pressure head in the subsurface media. The use of a linkage term such as $Q^o = Q^s = K(h^o - h^s)$, while may be convenient, is not appropriate because it introduces a non-physics parameter K. The calibration of K to match simulations with field data renders the coupled model ad hoc even though the overland and subsurface flows are each individually physics-based.

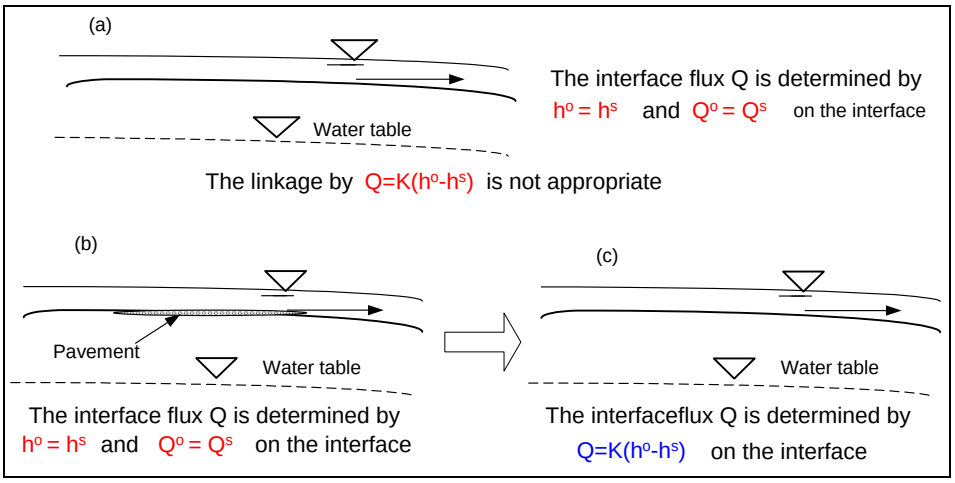

Fig. 2.4-2. Flow interactions between overland regime and subsurface media.

For the cases with thin impervious layers (Fig. 2.4-2b), one can include the impervious layers as part of the subsurface media or exclude these layers from the modeling. If one includes the thin layers, then it is obvious the pressures in the overland flow and in the layer are continuous across the interface, thus continuity of pressures and fluxes must imposed to simulate the interaction. On the other hand, if the thin layers are not included, it is obvious, the pressures in the overland flow and the subsurface are not continuous across the removed layers, then a linkage term is used to model the flux between across interface as

$$Q^o = Q^s \qquad \Rightarrow \qquad I = -n \cdot K \cdot \left(\frac{\rho_o}{\rho} \nabla h^s + \nabla z \right) = \frac{K_b}{b} \left(h^s - h^o \right) \tag{2.4.14}$$

where K_b and b are the hydraulic conductivity and thickness, respectively, of the removed bottom sediment layer. These parameters in the linkage term are the material properties and geometry of the removed layer. These parameters, in theory, can be obtained independent of model calibration.

The coupling of thermal and/or salinity transport between the overland regime and subsurface media can be stated as

$$\begin{aligned} &\mathbf{n} \cdot \left(\rho_w C_w V T - \mathbf{D^H} \cdot \nabla T \right) = H_i = \rho_w C_w I \frac{1}{2} \left(\left(1 + sign(I) \right) T^s + \left(1 - sign(I) \right) T^o \right) \\ &\textit{and} \quad \mathbf{n} \cdot \left(V S - \theta \mathbf{D^S} \cdot \nabla S \right) = M_s^{is} = I \frac{1}{2} \left(\left(1 + sign(I) \right) S^s + \left(1 - sign(I) \right) S^o \right) \end{aligned} \tag{2.4.15}$$

where *sign(I)* is 1.0 if I is positive and is -1.0 if negative; T^s is the temperature of subsurface water at the interface; T^o is the temperature of overland water at the interface; S^s is the salinity of subsurface water at the interface; and S^o is the salinity of overland water at the interface.

The temperature and salinity in the overland water may be the same as those in the subsurface water at the interface. If this is the case, we impose the continuity of temperature and/or salinity to yield the fluxes

$$\mathbf{n}\cdot\left(\rho_w C_w \mathbf{V}T - \mathbf{D}^{\mathbf{H}}\cdot\nabla T\right) = H_i \text{ and } T^s\Big|_{\text{on the surface}} = T^o \text{ and}$$
$$\mathbf{n}\cdot\left(\mathbf{V}S - \theta\mathbf{D}^{\mathbf{S}}\cdot\nabla S\right) = M_s^{is} \quad \text{and} \quad S^s\Big|_{\text{on the surface}} = S^o \tag{2.4.16}$$

2.4.3 Coupling between Subsurface and River/Stream/Canal Flows

The fluxes between canal and subsurface are obtained by imposing continuous of fluxes and state variables if these state variables do not exhibit discontinuity. If the state variables exhibit discontinuity, then a linkage term is used to simulate the fluxes. Consider the interaction between the canal and subsurface. There are two cases: in one case, there is not any thin layer of sediment materials (Fig. 2.4-3a) and, in another case, there are thin layers of sediment materials between the canal bottom and the top of surface media (Fig. 2.4-3b).

For the case of no thin layer of sediments (Fig. 2.4-3a), it can easily be seen that the pressures in the canal and in the subsurface media will be continuous across the interface of canal bottom and subsurface media. Thus, the interaction must be simulated by imposing continuity of pressure and flux as follows.

$$h^c = h^s \quad \text{and} \quad Q^c = Q^s \Rightarrow S_I = \int_P \left[-\mathbf{n}\cdot\mathbf{K}\cdot\left(\frac{\rho_O}{\rho}\nabla h^s + \nabla z\right)\right] dP \tag{2.4.17}$$

where h^c is the water depth in the canal, h^s is the pressure head in the subsurface, Q^c is the flux from the canal to the interface and Q^s is the flux from the interface to the subsurface media, S_I is defined in Eq. (2.1.1), **n** is an outward unit vector of the subsurface media interfacing the canal, **K** is the hydraulic conductivity tensor of the subsurface media, h^s is the pressure head in the subsurface media, and P is the wet perimeter of the canal. The use of a linkage term such as $Q^c = Q^s = K(h^c - h^s)$, while may be convenient, is not appropriate because it introduces a non-physics parameter K. The calibration of K to match simulations with field data renders the coupled model ad hoc even though the canal and subsurface flows are each individually physics-based.

For the cases with thin layers of sediments (Fig. 2.4-3b), one can include the sediment layers as part of the subsurface media or exclude these layers from the modeling. If one includes the thin layers, then it is obvious the pressures in the canal and in the sediment layer are continuous across the interface of canal bottom and the top of the thin layers, thus continuity of pressures must imposed to simulate the interaction. On the other hand, if the thin layers are excluded (Fig. 2.4-3c), the pressures in the canal and subsurface are not continuous across the bottom of canal and the top of subsurface media, then, a linkage term can be used to model the flux between the canal and surface media as

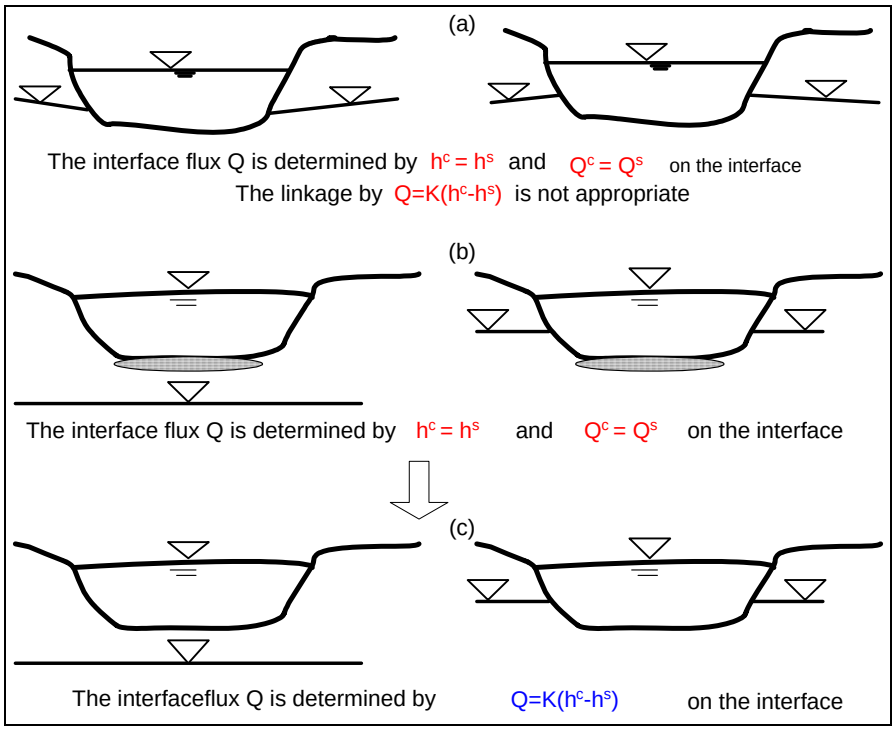

Fig. 2.4-3. Flow interactions between canal and subsurface media.

$$Q^c = Q^s \Rightarrow \int_P \left[-\mathbf{n}\cdot\mathbf{K}\cdot\left(\frac{\rho_o}{\rho}\nabla h^s + \nabla z\right)\right] dP = \int_P \frac{K_b}{b}\left(h^s - h^c\right) dP \qquad \textbf{(2.4.18)}$$

where K_b and b are the hydraulic conductivity and thickness, respectively, of the removed bottom sediment layer. These parameters in the linkage term are the material properties and geometry of the removed layer. These parameters, in theory, can be obtained independent of model calibration.

The coupling of thermal and/or salinity transport between the canal and subsurface media can be stated as

$$\int_P \mathbf{n}\cdot\left(\rho_w C_w \mathbf{V} T - \mathbf{D}^{\mathbf{H}}\cdot\nabla T\right) dP = S_h^i$$

$$= \rho_w C_w S_I \frac{1}{2}\left(\left(1+sign\left(S_I\right)\right)T^s + \left(1-sign\left(S_I\right)\right)T^c\right) \quad and \qquad \textbf{(2.4.19)}$$

$$\int_P \mathbf{n}\cdot\left(\mathbf{V}S - \theta\mathbf{D}^{\mathbf{S}}\cdot\nabla S\right) dP = M_s^i = S_I \frac{1}{2}\left(\left(1+sign\left(S_I\right)\right)S^s + \left(1-sign\left(S_I\right)\right)S^c\right)$$

where $sign(S_I)$ is 1.0 if S_I is positive and is -1.0 if negative; T^s is the temperature of subsurface water at the interface; T^c is the temperature of canal water at the interface; S^s is the salinity of subsurface water at the interface; and S^c is the salinity of canal water at the interface.

Similar to the interaction between the overland regime and subsurface media, the temperature and salinity in the canal water may be the same as those in the subsurface water at the interface. If this is

the case, we impose the continuity of temperature and/or salinity to yield the fluxes

$$\int_P \mathbf{n}\cdot\left(\rho_w C_w \mathbf{V}T - \mathbf{D}^{\mathbf{H}}\cdot\nabla T\right)dP = S_h^i \quad and \quad T^s\Big|_{on\ the\ surface} = T^c \quad and$$
$$\int_P \mathbf{n}\cdot\left(\mathbf{V}S - \theta\mathbf{D}^S\cdot\nabla S\right)dP = = M_s^i \quad and \quad S^s\Big|_{on\ the\ surface} = S^c \qquad \textbf{(2.4.20)}$$

2.5 Sediment and Water Quality Transport in 1D River/Stream/Canal Networks

In WASH123D, sediments are categorized based on their physical and chemical properties. For each category of sediment, we include mobile suspended sediment particles scattered in water column and immobile bed sediment particles accumulated in river/stream bed. The distribution of suspended sediment and bed sediment is controlled through hydrological transport as well as erosion and deposition processes.

In river/stream networks, there are six phases and three forms of biochemical species. As shown in Figure 2.5-1, the six phases are suspended sediment, bed sediment, mobile water, immobile water, suspension precipitate, and bed precipitate phases; and the three forms are dissolved biochemicals, particulate biochemicals sorbed onto sediments, and precipitates. Usually, biochemical species in the suspended sediment phase, the mobile water phase and the suspension precipitate phase are considered mobile. Biochemical species in the bed sediment phase, the immobile water phase and the bed precipitate phase are considered immobile.

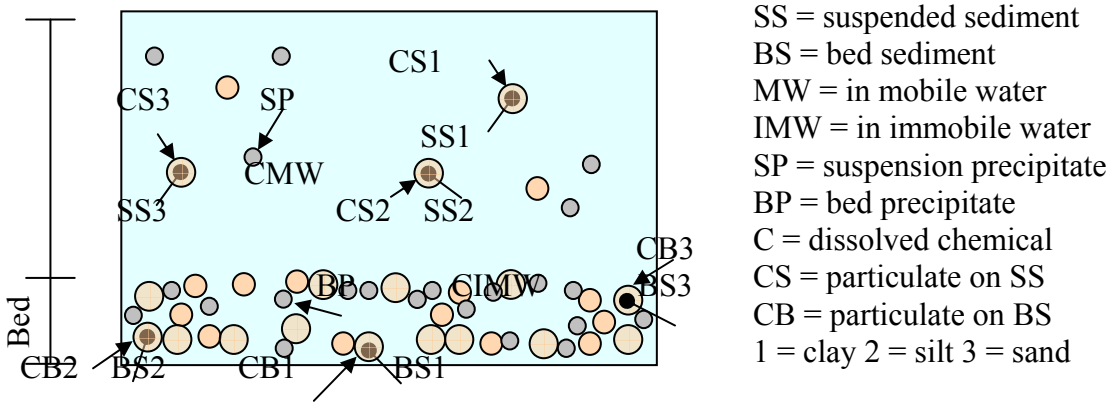

Fig. 2.5-1. Sediments and Chemicals in River/Stream Networks

A reactive system is completely defined by specifying biogeochemical reactions (Yeh, et al. 2001a). In the transport simulation, biogeochemical reactions can be divided into two classes (Rubin, 1983): (1) Fast/equilibrium reactions, and (2) Slow/kinetic reactions. The former are sufficiently fast compared to transport time scale and reversible, so that local equilibrium may be assumed. The latter are not sufficiently fast compared to transport time scale. They are either reversible or irreversible, where the local equilibrium formulation is inappropriate.

As shown in Figure 2.5-2, the biogeochemical reactions considered in the model can be categorized into ten types which take place between various phases: (1) aqueous complexation in column water, (2) adsorption/desorption or ion-exchange to suspended sediment, (3) precipitation/dissolution in water column, (4) adsorption/desorption or ion-exchange between column water and bed sediment, (5) aqueous complexation in pore water, (6) adsorption/desorption or ion-exchange to bed sediment, (7) precipitation/dissolution in bed, (8) volatilization reactions from water column to the atmopshere, (9) diffusion reactions between column and pore water, and (10) sedimentation reactions. Any individual reaction representing any of these chemical and physical processes may be simulated as kinetic or as equilibrium, which makes the code extremely flexible for application to a wide range of biogeochemical transport problems.

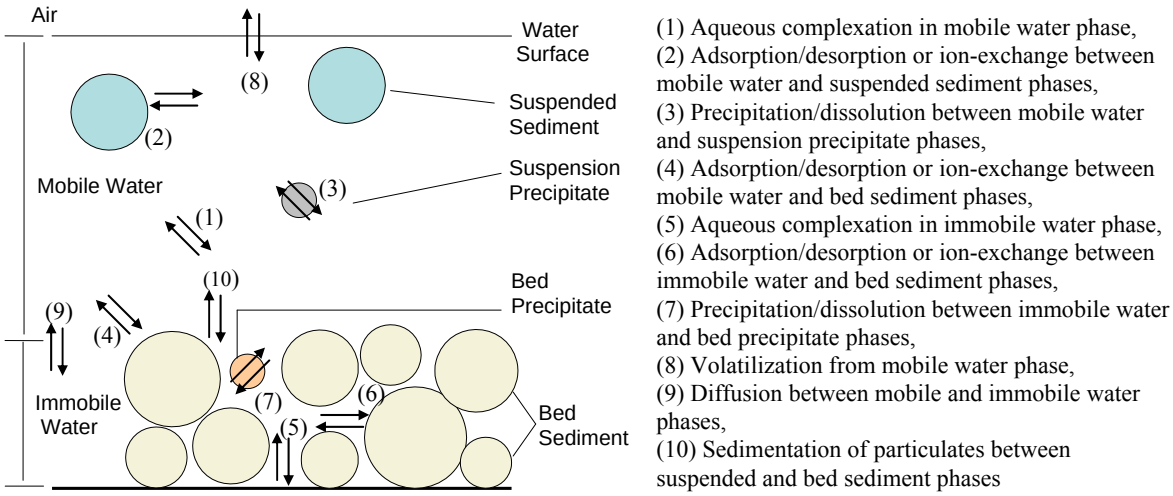

Fig. 2.5-2. Biogeochemical Reactions Considered in the Model

2.5.1 Bed Sediment

The balance equation for bed sediments is simply the statement that the rate of mass change is due to erosion/deposition as

$$\frac{\partial(PM_n)}{\partial t} = P(D_n - R_n) + M^{is}_{M_n}, \quad n \in [1, N_s] \qquad \textbf{(2.5.1)}$$

where P is the river/stream cross-sectional wetted perimeter [L], M_n is wetted perimeter-averaged concentration of the n-th bed sediment in mass per unit bed area [M/L^2], D_n is the deposition rate of the n-th sediment in mass per unit bed area per unit time [M/L^2/T], R_n is the erosion rate of the n-th sediment in mass per unit bed area per unit time [M/L^2/T], $M^{is}_{M_n}$ is the source of the n-th sediment from groundwater exfiltration in mass per unit river length [M/L/T], and N_S is the total number of sediment size fractions. Concentrations of all bed sediments must be given initially for transient simulations. No boundary condition is needed for bed sediments. In equation (2.5.1), we estimate the deposition and erosion rates using the different equations for cohesive and non-cohesive sediments.

For cohesive sediments, e.g., silt and clay, following equations are used (Yeh et al., 1998; Gerritsen

et al., 2000)

$$D_n = \min\left(V_{sn} S_n P_{Dn},\ S_n h/\Delta t\right) \qquad \text{where} \qquad P_{Dn} = \max\left(0,\ 1-\tau_b/\tau_{cDn}\right) \tag{2.5.2}$$

and

$$R_n = \min\left(E_{0n} P_{Rn},\ DMA_n/\Delta t\right) \qquad \text{where} \qquad P_{Rn} = \max\left(0,\ \tau_b/\tau_{cRn}-1\right) \tag{2.5.3}$$

where V_{sn} is the settling velocity of the n-th sediment [L/T], S_n is the cross-section-averaged suspended concentration of n-th sediment [M/L^3], h is the water depth [L], Δt is the time step size [T], τ_b is the bottom shear stress or the bottom friction stress [M/L/T^2], τ_{cDn} is the critical shear stress for the deposition of the n-th sediment [M/L/T^2], E_{0n} is the erodibility of the n-th sediment [M/L^2/T], DMA_n is the amount of locally available dry matter of n-th sediment, expressed as dry weight per unit area [M/L^2], τ_{cRn} is the critical shear stress for the erosion of the n-th sediment [M/L/T^2].

For Non-cohesive sediments, e.g., sand, we have two options.

Option 1 (Prandle et al., 2000)

$$D_n = \min\left(V_{sn} S_n N_{Dn},\ S_n h/\Delta t\right) \qquad \text{where} \qquad N_{Dn} = \max\left[0,\ 1-\left(V_{cDn}/V_{cRn}\right)^2\right] \tag{2.5.4}$$

and

$$R_n = \min\left(E_{0n} N_{Rn},\ DMA_n/\Delta t\right) \qquad \text{where} \qquad N_{Rn} = \max\left(0,\ V_{cDn}/V_{cRn}-1\right) \tag{2.5.5}$$

where V_{cDn} and V_{cRn} represent the critical friction velocities for the onset of deposition and erosion, respectively [L/T].

Option 2 (Yeh et al., 1998)

$$D_n = \max\left(\frac{G_{sAn}-G_{sn}}{\Delta L}, 0\right) \tag{2.5.6}$$

and

$$R_n = \max\left(\frac{G_{sn}-G_{sAn}}{\Delta L}, 0\right) \tag{2.5.7}$$

where G_{sAn} is the actual load rate of the n-th sediment per unit width at a upstream location [M/L/T], G_{sn} is the maximum load rate of the n-th size fraction sediment per unit width at a downstream location [M/L/T], ΔL is the distance between the upstream and the downstream locations.

$$G_{sAn} = S_n V R \tag{2.5.8}$$

and

$$G_{sn} = 10\frac{\rho^2 VRS(\tau_b-\tau_{crn})}{g d_n(\rho_{sn}-\rho)^2} \tag{2.5.9}$$

where V is the river/stream flow velocity [L/T], R is hydraulic radius [L], ρ is the density of water [M/L^3], S is the friction slope, τ_{crn} is the critical bottom shear stress of the n-th sediment at which sediment movement begins [M/L/T^2], g is gravity [L/T^2], d_n is the median diameter of the n-th sediment particle [L], and ρ_{sn} is the density of the n-th sediment [M/L^3].

It should be noted that equations (2.5.2) through (2.5.9) are the sample models programmed in the computer code to estimate sediment deposition and erosion rate. Any other phenomenological model equation can be easily incorporated in the code.

2.5.2 Suspended Sediments

The continuity equation of suspended sediment can be derived based on the conservation law of material mass as (Yeh et al., 2005):

$$\frac{\partial (AS_n)}{\partial t} + \frac{\partial (QS_n)}{\partial x} - \frac{\partial}{\partial x}\left(AK_x \frac{\partial S_n}{\partial x} \right) = M_{S_n}{}^{as} + M_{S_n}{}^{os1} + M_{S_n}{}^{os2} + M_{S_n}{}^{is} + (R_n - D_n)P, \quad n \in [1, N_s] \tag{2.5.10}$$

where S_n is the cross-sectional-averaged concentration of the *n*-th suspended sediment in the unit of mass per unit column volume [M/L^3], K_x is the dispersion coefficient [L^2/T], $M_{S_n}{}^{as}$ is the artificial source of the *n*-th suspended sediment [M/L/T], $M_{S_n}{}^{is}$ is the source of the n-th suspended sediment from groundwater exfiltration [M/L/T], and $M_{S_n}{}^{os1}$ and $M_{S_n}{}^{os2}$ are overland sources of the *n*-th suspended sediment from river bank *1* and *2*, respectively [M/L/T].

Concentrations of all suspended sediments must be given initially for transient simulations. Four types of boundary conditions are taken into account for suspended sediments, including Dirichlet, Variable, Cauchy, and Neumann boundary conditions (Yeh et al., 2005).

Dirichlet boundary condition: Dirichlet boundary conditions are prescribed on the boundary where the suspended sediment concentration is known,

$$S_n = S_{dn}(x_b, t) \qquad \text{on} \qquad B_d(x_b) \tag{2.5.11}$$

where x_b is the axis coordinate of the boundary node [L], $S_{dn}(x_b, t)$ is a time-dependent Dirichlet concentration of the *n*-th fraction size on the boundary $B_d(x_b)$ [M/L^3].

Variable boundary condition: Variable boundary conditions are normally specified on the boundary where the flow direction can change with time or on any open boundary. On the variable boundary, when the flow is directed into the region of the interest, the mass rate into the region is given by the product of the flow rate and concentration of the incoming fluid. When the flow is directed out of the region, the sediment mass is assumed carried out via advection. Mathematically, a variable boundary condition is given as

$$n\left(QS_n - AK_x \frac{\partial S_n}{\partial x} \right) = nQS_{vn}(x_b, t) \;\; if \;\; nQ \le 0 \;\; on \;\; B_v(x_b) \tag{2.5.12}$$

and

$$-nAK_x \frac{\partial S_n}{\partial x} = 0 \;\; if \;\; nQ \ge 0 \;\; on \;\; B_v(x_b) \tag{2.5.13}$$

where *n* is a unit outward direction, and $S_{vn}(x_b,t)$ is a time-dependent concentration at the boundary that is associated with the incoming flow on the variable boundary $B_v(x_b)$ [M/L^3].

Cauchy boundary condition: This boundary condition is employed when the total material flow rate is given. Usually, this boundary is an upstream flux boundary.

$$n\left(QS_n - AK_x\frac{\partial S_n}{\partial x}\right) = Q_{S_n c}(x_b,t) \;\; on \;\; B_c(x_b) \qquad \textbf{(2.5.14)}$$

where $Q_{S_n c}(x_b,t)$ is a time-dependent material flow rate at the Cauchy boundary boundary [M/t] $B_c(x_b)$.

Neumann boundary condition: This boundary condition is used when the diffusive material flow rate is known at the boundary node.

$$-nAK_x\frac{\partial S_n}{\partial x} = Q_{S_n n}(x_b,t) \;\; on \;\; B_n(x_b) \qquad \textbf{(2.5.15)}$$

where $Q_{S_n n}(x_b,t)$ is a time-dependent diffusive material flow rate at the boundary $B_n(x_b)$ [M/t].

2.5.3 Immobile Bed-Sediment Species

The balance equation for immobile species is simply the statement that the rate of mass change is due to biogeochemical reaction as:

$$\frac{\partial(Ph_b\rho_{bw}\theta_b C_{bw})}{\partial t} = Ph_b r_{Cbw}\big|_N' \qquad \textbf{(2.5.16)}$$

$$\frac{\partial(Ph_b\rho_{bw}\theta_b C_{bp})}{\partial t} = Ph_b r_{Cbp}\big|_N' \qquad \textbf{(2.5.17)}$$

$$\frac{\partial(PM_n C_{bsn})}{\partial t} = Ph_b r_{Cbsn}\big|_N' \qquad \textbf{(2.5.18)}$$

where h_b is the river/stream bed depth [L], ρ_{bw} is the density of bed pore-water [M/L^3], θ_b is the porosity of the bed sediment [L^3/L^3], C_{bw} is the concentration of dissolved chemical in the immobile pore-water phase in the unit of chemical mass per bed-water mass [M/M], $r_{Cbw}\big|_N$' is the production rate of C_{bw} due to all N reactions in the unit of chemical mass per bed volume per time [M/L^3/t], C_{bp} is the concentration of bed precipitate in the unit of chemical mass per bed-water mass [M/M], $r_{Cbp}\big|_N$' is the production rate of C_{bp} due to all N reactions in the unit of chemical mass per bed volume per time [M/L^3/t], C_{bsn} is the concentration of particulate sorbed on to bed sediment of the *n*-th fraction size in the unit of chemical mass per unit of bed-sediment mass [M/M], M_n is the concentration of the *n*-th bed sediment in the unit of sediment mass per bed area [M/L^2], $r_{Cbsn}\big|_N$' is the production rate of C_{bsn} due to all N reactions in the unit of chemical mass per bed volume per time [M/L^3/t].

Define

$$r_i\big|_N = Ph_b r_i\big|_N \,'/A \quad where \quad i = C_{bw},\ C_{bp},\ or\ C_{bsn} \tag{2.5.19}$$

Equation (2.5.16) through (2.5.18) can be modified as

$$\frac{\partial(Ph_b\rho_{bw}\theta_b C_{bw})}{\partial t} = Ar_{Cbw}\big|_N \tag{2.5.20}$$

$$\frac{\partial(Ph_b\rho_{bw}\theta_b C_{bp})}{\partial t} = Ar_{Cbp}\big|_N \tag{2.5.21}$$

$$\frac{\partial(PM_n C_{bsn})}{\partial t} = Ar_{Cbsn}\big|_N \tag{2.5.22}$$

Define

$$\rho_i = \begin{cases} Ph_b\rho_{bw}\theta_b / A, for\ C_{bw}\ and\ C_{bp} \\ PM_n / A, for\ C_{bsn} \end{cases} \tag{2.5.23}$$

Equation (2.5.20) through (2.5.22) can be summarized as

$$\frac{\partial(A\rho_i C_i)}{\partial t} = Ar_i\big|_N, \quad i \in M_{im} \tag{2.5.24}$$

where C_i is the concentration of species i, which is immobile, in the unit of chemical mass per unit phase mass [M/M], ρ_i is the density of the phase associated with species i [M/L^3], $r_i\big|_N$ is the production rate of species i due to all N reactions in the unit of chemical mass per column volume per time [M/L^3/t], and M_{im} is the number of immobile species. The concentrations of all immobile species must be given initially for transient simulations. No boundary conditions are needed for immobile species.

2.5.4 Mobile Column-Water Species

The continuity equation of mobile species can be derived based on the conservation law of material mass stating that the rate of mass change is due to both advective-dispersive transport and biogeochemical reactions as:

$$\frac{\partial(A\rho_w C_w)}{\partial t} + L(\rho_w C_w) = Ar_{Cw}\big|_N \tag{2.5.25}$$

$$\frac{\partial(A\rho_w C_p)}{\partial t} + L(\rho_w C_p) = Ar_{Cp}\big|_N \tag{2.5.26}$$

$$\frac{\partial(AS_n C_{sn})}{\partial t} + L(S_n C_{sn}) = Ar_{Csn}\big|_N \tag{2.5.27}$$

where ρ_w is the density of column water [M/L^3], C_w is the concentration of dissolved chemical in the mobile water phase in the unit of chemical mass per column-water mass [M/M], $r_{Cw}\big|_N$ is the production rate of C_w due to all N reactions in the unit of chemical mass per column volume per time [M/L^3/t], C_p is the concentration of suspension precipitate in the unit of chemical mass per column-water mass [M/M], $r_{Cp}\big|_N$ is the production rate of C_p due to all N reactions in the unit of chemical mass per column volume per time [M/L^3/t], C_{sn} is the concentration of particulate sorbed on to suspended sediment of the n-th fraction size in the unit of chemical mass per unit of sediment mass [M/M], S_n is the concentration of suspended sediment in the unit of sediment mass per column volume [M/L^3], $r_{Csn}\big|_N$ is the production rate of C_{sn} due to all N reactions in the unit of chemical mass per column volume per time [M/L^3/t], and L is an operator that will be defined in Eq. (2.5.30) later.

Define

$$\rho_i = \begin{cases} \rho_w \quad for \quad C_w \ and \ C_p \\ S_n \quad for \quad C_{sn} \end{cases} \tag{2.5.28}$$

Equation (2.5.25) through (2.5.27) can be summarized as

$$\frac{\partial(A\rho_i C_i)}{\partial t} + L(\rho_i C_i) = Ar_i\big|_N, \quad i \in M_m = M - M_{im} \tag{2.5.29}$$

where C_i is the concentration of species i, which is mobile, in the unit of chemical mass per unit phase mass [M/M], ρ_i is the density of the phase associated with species i [M/L^3], $r_i\big|_N$ is the production rate of species i due to all N reactions in the unit of chemical mass per column volume per time [M/L^3/t], M is the total number of chemical species, M_m is the number of mobile chemical species, and operator L is defined as

$$L(\rho_i C_i) = \frac{\partial(Q\rho_i C_i)}{\partial x} - \frac{\partial}{\partial x}\left[AK_x \frac{\partial(\rho_i C_i)}{\partial x}\right] - (M_{C_i}^{as} + M_{C_i}^{rs} - M_{C_i}^{es} + M_{C_i}^{os1} + M_{C_i}^{os2} + M_{C_i}^{is}) \tag{2.5.30}$$

where $M_{C_i}^{as}$ is the artificial source of species i [M/L/T], $M_{C_i}^{rs}$ is the rainfall source of species i [M/L/T], $M_{C_i}^{rs}$ is the sink of species i due to evaporation, $M_{C_i}^{os1}$ and $M_{C_i}^{os2}$ are the overland sources of species i from river bank *1* and *2*, respectively [M/L/T], and $M_{C_i}^{is}$ is the mass rate of the source of species i in river/stream from subsurface [M/L/T].

Concentrations of all mobile species must be given initially for transient simulations. Four types of boundary conditions are taken into account for mobile species, including Dirichlet, Variable, Cauchy, and Neumann boundary conditions (Yeh et al., 2005), which are similar to those for suspended sediment transport and are presented below:

Dirichlet boundary condition: On a Dirichlet boundary, the concentrations of all mobile species are prescribed

$$C_i = C_{idb}(x_b, t) \qquad i \in M_m \qquad on \qquad B_d(x) = 0 \tag{2.5.31}$$

where $C_{idb}(x_b,t)$ is the prescribed concentration of the *i*-th mobile species on the Dirichlet boundary $B_d(x)=0$ [M/M].

Variable boundary condition: On a variable boundary, the concentrations of all mobile species are known and they contribute to the increase of chemical masses in the region of interest when the flow is coming into the region. When the flow is going out of the region, the transport of all mobile species out of the region is assumed due to advection only, which implies that one must put an outgoing boundary far away from the source.

< Case 1 > Flow is coming in from outside (nQ < 0)

$$n\left(Q\rho_i C_i - AK_x\frac{\partial\rho_i C_i}{\partial x}\right)=(nQ)\rho_i C_{ivb}(x_b,t) \qquad i\in M_m \qquad on \qquad B_v(x)=0 \tag{2.5.32}$$

< Case 2 > Flow is going out from inside (nQ > 0).

$$-nAK_x\frac{\partial\rho_i C_i}{\partial x}=0 \qquad i\in M_m \qquad on \qquad B_v(x)=0 \tag{2.5.33}$$

where *n* is the unit outward direction and $C_{ivb}(x_b,t)$ is the concentration of the *i*-th species in the incoming fluid on the variable boundary $B_v(x)=0$ [M/M].

Cauchy boundary condition: On a Cauchy boundary chemical flux for any mobile species is prescribed

$$n\left(Q\rho_i C_i - AK_x\frac{\partial\rho_i C_i}{\partial x}\right)=Q_{C_i cb}(x_b,t) \qquad i\in M_m \qquad on \qquad B_c(x)=0 \tag{2.5.34}$$

where $Q_{C_i cb}(x_b,t)$ is the mass flux of C_i through the Cauchy boundary $B_c(x)=0$ [M/t].

Neumann boundary condition: On a Neumann boundary, chemical flux of any mobile species due to dispersion is prescribed

$$-nAK_x\frac{\partial\rho_i C_i}{\partial x}=Q_{C_i nb}(x_b,t) \qquad i\in M_m \qquad on \qquad B_n(x)=0 \tag{2.5.35}$$

where $Q_{C_i nb}(x_b,t)$ is the mass flux of C_i through the Neumann boundary $B_n(x)=0$ [M/t].

2.5.5 Diagonalization of Species Transport Equations

The temporal-spatial distribution of chemical species is described by a system of M_{im} mass balance equations [equation (2.5.24)], and M_m reactive transport equations [equation (2.5.29)]. These two equations can be recast in the following form

$$\frac{\partial(A\rho_i C_i)}{\partial t} + \alpha_i L(\rho_i C_i) = A r_i\big|_N, \quad i \in M \tag{2.5.36}$$

where M is the total number of chemical species, α_i is 0 for immobile species and 1 for mobile species.

The determination of $r_i\big|_N$ and associated parameters is a primary challenge in biogeochemical modeling. Instead of using an ad hoc method to formulate $r_i\big|_N$, we use reaction-based formulations (Steefel and Cappellen, 1998). In a reaction-based formulation, $r_i\big|_N$ is given by the summation of rates of all reactions that the i-th species participates in,

$$r_i\big|_N = \frac{d(\rho_i C_i)}{dt}\Big|_{reaction} = \sum_{k=1}^{N}\left[(\nu_{ik} - \mu_{ik})r_k\right], \quad i \in M \tag{2.5.37}$$

where ν_{ik} is the reaction stoichiometry of the i-th species in the k-th reaction associated with the products, μ_{ik} is the reaction stoichiometry of the i-th species in the k-th reaction associated with the reactants, and r_k is the rate of the k-th reaction.

Substituting equation (2.5.37) into equation (2.5.36) results in the transport equations of M chemical species described by

$$\frac{\partial(A\rho_i C_i)}{\partial t} + \alpha_i L(\rho_i C_i) = A\sum_{k=1}^{N}\left[(\nu_{ik} - \mu_{ik})r_k\right], \quad i \in M; \quad or \quad \mathbf{U}\frac{\partial \mathbf{C_A}}{\partial t} + \boldsymbol{\alpha} L(\mathbf{C}) = A\boldsymbol{\nu}\mathbf{r} \tag{2.5.38}$$

where $\mathbf{U}$ is a unit matrix, $\mathbf{C_A}$ is a vector with its components representing M species concentrations multiply the cross section area of the river [M/L], $\boldsymbol{\alpha}$ is a diagonal matrix with α_i as its diagonal component, $\mathbf{C}$ is a vector with its components representing M species concentrations [M/L^3], $\boldsymbol{\nu}$ is the reaction stoichiometry matrix, and $\mathbf{r}$ is the reaction rate vector with N reaction rates as its components. Equation (2.5.38) represents a mass balance for species i, which states that the rate of change of any species mass is due to advection-dispersion coupled with contributing reactions that describe the biogeochemical processes.

In a primitive approach, equation (2.5.38) is integrated to yield the distributions and evolutions of chemical species in a region of interest. However, when some fast equilibrium reactions take place in the system, this approach is not adequate (Fang et al., 2003). Here, we will take a diagonalization approach through decomposition. Equation (2.5.38) written in matrix form can be decomposed based on the type of biogeochemical reactions via Gauss-Jordan column reduction of reaction matrix $\boldsymbol{\nu}$. Among all the fast/equilibrium and slow/kinetic reactions, "redundant reactions" are defined as fast reactions that are linearly dependent on other fast reactions, and "irrelevant reactions" are kinetic reactions that are linearly dependent on only equilibrium reactions. In order to avoid singularity of the reaction matrix, redundant fast reactions are omitted from the system prior to decomposition. The removal of irrelevant slow reactions alleviates problems associated with rate formulation uncertainty and parameterization for these reactions.

Decomposition is performed by pivoting on the N_E equilibrium reactions and decoupling them from the N_K kinetic reactions. In other words, each fast reaction can be used to eliminate one chemical

species from simultaneous consideration. An incomplete Gauss-Jordan row decomposition of the reaction matrix $\boldsymbol{\nu}$ by pivoting on N_E equilibrium reactions will result in N_E equilibrium-variables and N_{KIV} kinetic-variables. To analyze the system behavior, it is advantageous to perform a complete decomposition, in which the reduction of the reaction matrix is done by pivoting on N_E equilibrium reactions and on N_{KI} linearly independent kinetic reactions to result in N_E equilibrium-variables, N_{KI} kinetic-variables, and N_C components. The complete decomposition is given as follows:

$$\begin{bmatrix} \mathbf{A}_{11} & \mathbf{0}_{12} & \mathbf{0}_{13} \\ \mathbf{A}_{21} & \mathbf{A}_{22} & \mathbf{0}_{23} \\ \mathbf{A}_{31} & \mathbf{A}_{32} & \mathbf{U}_{33} \end{bmatrix} \begin{Bmatrix} \dfrac{\partial \mathbf{C}_{A1}}{dt} \\ \dfrac{\partial \mathbf{C}_{A2}}{dt} \\ \dfrac{\partial \mathbf{C}_{A3}}{dt} \end{Bmatrix} + \begin{bmatrix} \mathbf{B}_{11} & \mathbf{0}_{12} & \mathbf{0}_{13} \\ \mathbf{B}_{21} & \mathbf{B}_{22} & \mathbf{0}_{23} \\ \mathbf{B}_{31} & \mathbf{B}_{32} & \boldsymbol{\alpha}_{33} \end{bmatrix} \mathrm{L}\left(\begin{Bmatrix} \mathbf{C}_1 \\ \mathbf{C}_2 \\ \mathbf{C}_3 \end{Bmatrix} \right) = \mathrm{A} \begin{bmatrix} \mathbf{D}_{11} & \mathbf{K}_{12} & \mathbf{K}_{13} \\ \mathbf{0}_{21} & \mathbf{D}_{22} & \mathbf{K}_{23} \\ \mathbf{0}_{31} & \mathbf{0}_{32} & \mathbf{0}_{33} \end{bmatrix} \begin{Bmatrix} \mathbf{r}_1 \\ \mathbf{r}_2 \\ \mathbf{r}_3 \end{Bmatrix} \quad \textbf{(2.5.39)}$$

where $\mathbf{A_{11}}$ is the submatrix of the reduced **U** matrix with size of $N_E \times N_E$, $\mathbf{A_{21}}$ is the submatrix of the reduced **U** matrix with size of $N_{KI} \times N_E$, and $\mathbf{A_{31}}$ is the submatrix of the reduced **U** matrix with size of $N_C \times N_E$; $\mathbf{0_{12}}$ is the zero submatrix of the reduced **U** matrix with size of $N_E \times N_{KI}$, $\mathbf{A_{22}}$ is the submatrix of the reduced **U** matrix with size of $N_{KI} \times N_{KI}$, and $\mathbf{A_{32}}$ is the submatrix of the reduced **U** matrix with size of $N_C \times N_{KI}$; $\mathbf{0_{13}}$ is the zero submatrix of the reduced **U** matrix with size of $N_E \times N_C$, $\mathbf{0_{23}}$ is the submatrix of the reduced **U** matrix with size of $N_{KI} \times N_C$, and $\mathbf{U_{33}}$ is the unit submatrix of the reduced **U** matrix with size of $N_C \times N_C$; $\mathbf{C_{A1}}$, $\mathbf{C_{A2}}$, and $\mathbf{C_{A3}}$ are the subvectors of the vector $\mathbf{C_A}$ with sizes of N_E, N_{KI}, and N_C, respectively; $\mathbf{B_{11}}$ is the submatrix of the reduced $\boldsymbol{\alpha}$ matrix with size of $N_E \times N_E$, $\mathbf{B_{21}}$ is the submatrix of the reduced $\boldsymbol{\alpha}$ matrix with size of $N_{KI} \times N_E$, and $\mathbf{B_{31}}$ is the submatrix of the reduced $\boldsymbol{\alpha}$ matrix with size of $N_C \times N_E$; $\mathbf{0_{12}}$ is the zero submatrix of the reduced $\boldsymbol{\alpha}$ matrix with size of $N_E \times N_{KI}$, $\mathbf{A_{22}}$ is the submatrix of the reduced $\boldsymbol{\alpha}$ matrix with size of $N_{KI} \times N_{KI}$, and $\mathbf{B_{32}}$ is the submatrix of the reduced $\boldsymbol{\alpha}$ matrix with size of $N_C \times N_{KI}$; $\mathbf{0_{13}}$ is the zero submatrix of the reduced $\boldsymbol{\alpha}$ matrix with size of $N_E \times N_C$, $\mathbf{0_{23}}$ is the submatrix of the reduced $\boldsymbol{\alpha}$ matrix with size of $N_{KI} \times N_C$, and $\boldsymbol{\alpha_{33}}$ is the diagonal submatrix of the reduced $\boldsymbol{\alpha}$ matrix with size of $N_C \times N_C$; $\mathbf{C_1}$, $\mathbf{C_2}$, and $\mathbf{C_3}$ are the subvectors of the vector **C** with sizes of N_E, N_{KI}, and N_C, respectively; $\mathbf{D_{11}}$ is the diagonal submatrix of the reduced $\boldsymbol{\nu}$ matrix with size of $N_E \times N_E$, $\mathbf{K_{12}}$ is the submatrix of the reduced $\boldsymbol{\nu}$ matrix with size of $N_E \times N_{KI}$, and $\mathbf{K_{13}}$ is the submatrix of the reduced $\boldsymbol{\nu}$ matrix with size of $N_E \times N_{KD(k)}$; $\mathbf{0_{21}}$ is the zero submatrix of the reduced $\boldsymbol{\nu}$ matrix with size of $N_{KI} \times N_E$, $\mathbf{D_{22}}$ is the diagonal submatrix of the reduced $\boldsymbol{\nu}$ matrix with size of $N_{KI} \times N_{KI}$, and $\mathbf{K_{23}}$ is the submatrix of the reduced $\boldsymbol{\nu}$ matrix with size of $N_{KI} \times N_{KD(k)}$; $\mathbf{0_{13}}$ is the zero submatrix of the reduced $\boldsymbol{\nu}$ matrix with size of $N_C \times N_E$, $\mathbf{0_{32}}$ is the zero submatrix of the reduced $\boldsymbol{\nu}$ matrix with size of $N_C \times N_{KI}$, and $\mathbf{0_{33}}$ is the zero submatrix of the reduced $\boldsymbol{\nu}$ matrix with size of $N_C \times N_{KD(k)}$; $\mathbf{r_1}$, $\mathbf{r_2}$, and $\mathbf{r_3}$ are the subvectors of the vector **r** with sizes of N_E, N_{KI}, and $N_{KD(k)}$, respectively.

For incomplete decomposition of the reaction matrix $\boldsymbol{\nu}$, Equation (2.5.39) can be connoted as

$$\begin{bmatrix} \mathbf{A}_{11} & \mathbf{0}_{12} \\ \mathbf{A}_{21} & \mathrm{U}_{22} \end{bmatrix} \begin{Bmatrix} \dfrac{\partial \mathbf{C}_{A1}}{dt} \\ \dfrac{\partial \mathbf{C}_{A2}}{dt} \end{Bmatrix} + \begin{bmatrix} \mathbf{B}_{11} & \mathbf{0}_{12} \\ \mathbf{B}_{21} & \boldsymbol{\alpha}_{22} \end{bmatrix} \mathrm{L}\left(\begin{Bmatrix} \mathbf{C}_1 \\ \mathbf{C}_2 \end{Bmatrix} \right) = \mathrm{A} \begin{bmatrix} \mathbf{D}_{11} & \mathbf{K}_{12} \\ \mathbf{0}_{21} & \mathbf{K}_{22} \end{bmatrix} \begin{Bmatrix} \mathbf{r}_1 \\ \mathbf{r}_2 \end{Bmatrix} \quad \textbf{(2.5.40)}$$

where $\mathbf{A_{11}}$ and $\mathbf{A_{21}}$ are the submatrices of the reduced **U** matrix with size of $N_E \times N_E$ and $N_{KIV} \times N_E$, respectively (note that $N_{KIV} = M - N_E = N_{KI} + N_C$); $\mathbf{0_{12}}$ and $\mathbf{U_{22}}$ are the zero- and unit-submatrices, respectively, of the reduced **U** matrix with size of $N_E \times N_{KIV}$ and $N_{KIV} \times N_{KIV}$, respectively; $\mathbf{C_{A1}}$ and $\mathbf{C_{A2}}$ are the subvectors of the vector $\mathbf{C_A}$ with sizes of N_E and N_{KIV}, respectively; $\mathbf{B_{11}}$ and $\mathbf{B_{21}}$ are the submatrices of the reduced $\boldsymbol{\alpha}$ matrix with sizes of $N_E \times N_E$ and $N_{KIV} \times N_E$, respectively; $\mathbf{0_{12}}$ and $\boldsymbol{\alpha}_{\mathbf{22}}$ are the zero- and unit- submatrices, respectively, of the reduced $\boldsymbol{\alpha}$ matrix with size of $N_E \times N_{KIV}$ and $N_{KIV} \times N_{KIV}$, respectively; $\mathbf{C_1}$ and $\mathbf{C_2}$ are the subvectors of the vector **C** with sizes of N_E and N_{KIV}, respectively; $\mathbf{D_{11}}$ is the diagonal submatrix of the reduced $\boldsymbol{\nu}$ matrix with size of $N_E \times N_E$ and $\mathbf{K_{12}}$ is the submatrix of the reduced $\boldsymbol{\nu}$ matrix with size of $N_E \times N_{KIV}$; $\mathbf{0_{21}}$ is the zero submatrix of the reduced $\boldsymbol{\nu}$ matrix with size of $N_{KIV} \times N_E$ and $\mathbf{K_{22}}$ is the submatrix of the reduced $\boldsymbol{\nu}$ matrix with size of $N_{KIV} \times N_E$; $\mathbf{r_1}$ and $\mathbf{r_2}$ are the subvectors of the vector **r** with sizes of N_E and N_{KIV}, respectively.

For reactions that are fast, equilibrium may be regarded as being reached instantaneously among the relevant species and the reaction rates may be regarded as infinite. An infinite rate is mathematically represented by a mass action equation or a user specified nonlinear algebraic equation. As a result, the decomposition of equation (2.5.38) to equation (2.5.40) effectively reduces a set of M species reactive transport equations into two subsets of equations. The first set contains N_E algebraic equations representing mass action laws for the equilibrium reactions, and the second set contains N_{KIV} kinetic-variable transport equations. These equation subsets are defined as

Algebraic Equations for Equilibrium Reactions

$$\frac{\partial(AE_i)}{\partial t} + L(E_i^m) = AD_{1ii}r_{1i} + A\sum_{j=1}^{N_K} K_{1ij}r_{2j},\ i \in N_E \quad \Rightarrow \quad r_{1i} = \infty \quad \Rightarrow \quad \frac{\partial(AE_i)}{\partial t} \approx \infty$$

which is replaced with a thermodynamically consistent equation: $K_i^e = \prod_{j\in M} A_j^{\nu_{ji}} \Big/ \prod_{j\in M} A_j^{\mu_{ji}}$ **(2.5.41)**

$$or\ \ F_i(C_1,..,C_M;p_1,p_2,..) = 0 \quad where\ E_i = \sum_{j=1}^{N_E} A_{1ij}C_{1j}\ \ and\ \ E_i^m = \sum_{j=1}^{N_E} B_{1ij}C_{1j}$$

where K_i^e is the equilibrium constant of the i-th fast reaction, A_j is the activity of the j-th species, $F_i(C_1,..,C_M; p_1,p_2,..)$ is an empirical function of all species and a number of parameters $p_1, p_2, \ldots$ for the i-th fast reaction. E_i was called an equilibrium-variable (Fang, et al., 2003) because $\frac{\partial(AE_i)}{\partial t} \approx \infty$ simply means that E_i can reach equilibrium instantaneously.

Transport Equations for Kinetic-Variables

$$\frac{\partial(AE_i)}{\partial t} + L(E_i^m) = A\sum_{j=1}^{N_K} K_{2nj}r_{2j},\ \ i \in N_{KIV} = M - N_E$$
$$where\ E_i = \sum_{j=1}^{N_E} A_{2ij}C_{1j} + C_{2i}\ and\ E_i^m = \sum_{j=1}^{N_E} B_{2ij}C_{1j} + \alpha_{1i}C_{2i} \qquad \textbf{(2.5.42)}$$

where E_i was called kinetic variable (Fang, et al., 2003) because as E_i is transported it is subject to only kinetic reactions. This is in contrast to Eq. (2.5.38) where as C_i is transported, it is subject to

both equilibrium and kinetic reactions.

Assign

$$R_i = \sum_{j=1}^{N_K} K_{2ij} r_{2j},\ \mathrm{i} \in N_{KIV} \qquad \textbf{(2.5.43)}$$

The reduction of Eq. (2.5.38) to Eq. (2.5.41) and (2.5.42) is equivalent to reducing M governing equations for immobile and mobile species to the mixed N_E algebraic equations for equilibrium variables and N_{KIV} transport equations for kinetic-variables specified as follows

$$\begin{aligned} &\frac{\partial (AE_i)}{\partial t} + \frac{\partial (QE_i^{\,m})}{\partial x} - \frac{\partial}{\partial x}\left(AK_x \frac{\partial E_i^{\,m}}{\partial x} \right) = M_{E_i}^{\ as} + M_{E_i}^{\ rs} - M_{E_i}^{\ es} \\ &+ M_{E_i}^{\ os1} + M_{E_i}^{\ os2} + M_{E_i}^{\ is} + AR_i,\ i \in N_{KIV} \end{aligned} \qquad \textbf{(2.5.44)}$$

where E_i is the concentration of the i-th kinetic-variable [M/L^3], E_i^m is the concentration of mobile part of the i-th kinetic-variable [M/L^3], $M_{E_i}^{\ as}$ is the artificial source of the i-th kinetic-variable [M/L/T], $M_{E_i}^{\ rs}$ is the rainfall source of the i-th kinetic-variable [M/L/T], $M_{E_i}^{\ es}$ is the evaporation sink of the i-th kinetic variable [M/L/T], $M_{E_i}^{\ os1}$ and $M_{E_i}^{\ os2}$ are overland sources of the i-th kinetic-variable from river banks *1* and *2*, respectively [M/L/T], $M_{E_i}^{\ is}$ is the mass rate of the source of the i-th kinetic-variable in river/stream from subsurface [M/L/T], R_i is the production rate of i-th kinetic-variable due to biogeochemical reactions [M/L^3/T], and N_{KIV} is the number of kinetic variable variables.

Boundary conditions for mobile species need to be transformed into corresponding boundary conditions for kinetic-variables, which are stated in the following.

Dirichlet boundary condition:

$$E_i^{\ m} = E_{i\ db}^{m}(x_b, t) \qquad i \in M_m \qquad on \qquad B_d(x) = 0 \qquad \textbf{(2.5.45)}$$

where $E_{i\ db}^{m}(x_b, t)$ is the specified concentration of the mobile portion of the i-th kinetic variable on the Dirichlet boundary $B_d(x) = 0$ [M/L3].

Variable boundary condition:

< Case 1 > Flow is coming in from outside (nQ < 0)

$$n\left(QE_i^m - AK_x \frac{\partial E_i^m}{\partial x} \right) = nQE_{i\ vb}^{m}(x_b, t) \qquad i \in M_m \qquad on \qquad B_v(x) = 0 \qquad \textbf{(2.5.46)}$$

< Case 2 > Flow is going out from inside (nQ > 0).

$$-nAK_x \frac{\partial E_i^m}{\partial x} = 0 \qquad i \in M_m \qquad on \qquad B_v(x) = 0 \tag{2.5.47}$$

where n is the unit outward direction and $E_{i\ vb}^{m}(x_b,t)$ is the concentration of the mobile portion of the i-th kinetic variable on the variable boundary $B_v(x) = 0$ [M/L^3].

Cauchy boundary condition:

$$n\left(QE_i^m - AK_x \frac{\partial E_i^m}{\partial x}\right) = Q_{E_i^m cb}(x_b,t) \qquad i \in M_m \qquad on \qquad B_c(x) = 0 \tag{2.5.48}$$

where $Q_{E_i^m cb}(x_b,t)$ is the mass flux of E_i^m through the Cauchy boundary $B_c(x) = 0$ [M/t].

Neumann boundary condition:

$$-nAK_x \frac{\partial E_i^m}{\partial x} = Q_{E_i^m{}_{nb}}(x_b,t) \qquad i \in M_m \qquad on \qquad B_n(x) = 0 \tag{2.5.49}$$

where $Q_{E_i^m nb}(x_b,t)$ is the mass flux of E_i^m through the Neumann boundary $B_n(x) = 0$ [M/t].

2.6 Sediment and Water Quality Transport in Two-Dimension Overland Regime

Researches on overland water quality modeling include studies of sediment (McDonald and Cheng, 1994; Harris and Wiberg, 2001; and Zeng and Beck, 2003) and water quality transport (Falconer and Lin, 1997; Tufford and McKellar, 1999; Shen et al., 2002; and Zheng et al., 2004) as well as thermal and salinity transport. Most of the existing overland water quality models simulate either specific systems (Cerco and Cole, 1995; Shen et al., 2002; and Zheng et al., 2004) or systems containing specific reactions (Brown and Barnwell, 1987; Ambrose et al, 1993; and Bonnet and Wessen, 2001). They may provide efficient monitoring and management tools because they are calibrated for specific environments, but the extension of a calibrated model to other environmental conditions needs to be carefully evaluated. With better understanding and mathematical formulation of complex biogeochemical interactions (Thomann, 1998; Somlyody et al., 1998; and Yeh et al., 2001a), models considering interactions among biogeochemicals based on reaction mechanism have a better potential for application to other systems (Steefel and Cappellen, 1998). Although a few reaction-based models can handle contaminant transport subject to kinetically controlled chemical reactions (Cheng et al., 2000; and Yeh et al., 2005), no existing overland water quality model, to our knowledge, has the design capability that permitts the use of a fully mechanistic approach to estimate both kinetically and equilibrium controlled reactive chemical transport in overland water systems.

This section presents a general two-dimensional depth-averaged numerical model simulating the water quality in overland shallow water systems using a general paradigm of diagonalized reaction-

based approaches. In our model, sediments are categorized based on their physical and chemical properties. For each category of sediment, we include mobile suspended sediment particles scattered in water column and immobile bed sediment particles accumulated in water bed. The distribution of suspended sediment and bed sediment is controlled through hydrological transport as well as erosion and deposition processes. There are six phases and three forms for biogeochemical species. As shown in Figure 2.6-1, the six phases are suspended sediment, bed sediment, mobile water, immobile water, suspension precipitate, and bed precipitate phases; and the three forms are dissolved chemicals, particulate chemicals sorbed onto sediments, and precipitates.

In the transport simulation, biogeochemical reactions can be divided into two classes (Rubin, 1983): (1) equilibrium-controlled "fast" reactions, and (2) kinetically-controlled "slow" reactions. The former are sufficiently fast compared to the transport time-scale and are reversible, so that local equilibrium may be assumed. The latter are not sufficiently fast compared to the transport time-scale. As shown in Figure 2.6-2, biogeochemical reactions taken into account in the model include aqueous complexation, adsorption/desorption, ion-exchange, precipitation/dissolution, volatilization, diffusion, and sedimentation, etc. Any individual reaction representing any of these chemical and physical processes may be simulated as kinetic or as equilibrium, which makes the code extremely flexible for application to a wide range of biogeochemical transport problems.

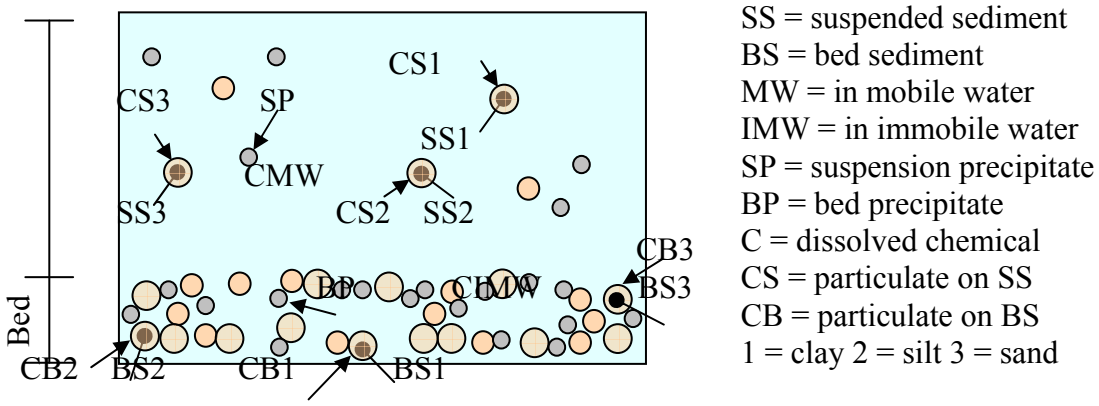

Fig. 2.6-1. Sediments and Chemicals in River/Stream Networks

2.6.1 Bed Sediment

The balance equation for bed sediments is simply the statement that the rate of mass change is due to erosion/deposition as (Yeh, et al., 2005)

$$\frac{\partial(M_n)}{\partial t} = (D_n - R_n) + M^{is}_{M_n}, \quad n \in [1, N_s] \qquad \textbf{(2.6.1)}$$

where M_n is the concentration of the n-th bed sediment in mass per unit bed area [M/L^2], D_n is the deposition rate of the n-th sediment in mass per unit bed area per unit time [M/L^2/T], R_n is the erosion rate of the n-th sediment in mass per unit bed area per unit time [M/L^2/T], $M^{is}_{M_n}$ is the source of the n-th sediment from groundwater exfiltration in mass per unit area [M/L^2/T], and N_S is the total number of sediment size fractions. Concentrations of all bed sediments must be given initially for

transient simulations. No boundary condition is needed for bed sediments. In equation (2.6.1), we estimate the deposition and erosion rates using the different equations for cohesive and non-cohesive sediments.

For cohesive sediments, e.g., silt and clay, following equations are used (Yeh et al., 1998; Gerritsen et al., 2000)

$$D_n = \min\left(V_{sn} S_n P_{Dn},\ S_n h/\Delta t\right) \qquad \text{where} \qquad P_{Dn} = \max\left(0,\ 1-\tau_b/\tau_{cDn}\right) \qquad \textbf{(2.6.2)}$$

and

$$R_n = \min\left(E_{0n} P_{Rn},\ DMA_n/\Delta t\right) \qquad \text{where} \qquad P_{Rn} = \max\left(0,\ \tau_b/\tau_{cRn}-1\right) \qquad \textbf{(2.6.3)}$$

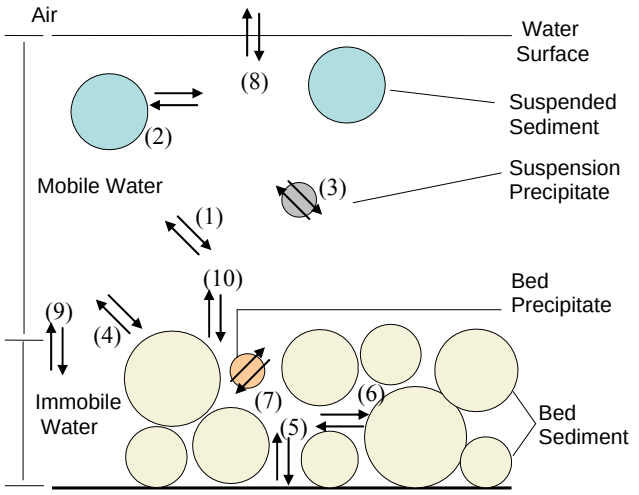

(1) Aqueous complexation in mobile water phase,
(2) Adsorption/desorption or ion-exchange between mobile water and suspended sediment phases,
(3) Precipitation/dissolution between mobile water and suspension precipitate phases,
(4) Adsorption/desorption or ion-exchange between mobile water and bed sediment phases,
(5) Aqueous complexation in immobile water phase,
(6) Adsorption/desorption or ion-exchange between immobile water and bed sediment phases,
(7) Precipitation/dissolution between immobile water and bed precipitate phases,
(8) Volatilization from mobile water phase,
(9) Diffusion between mobile and immobile water phases,
(10) Sedimentation of particulates between suspended and bed sediment phases

Fig. 2.6-2. Biogeochemical Reactions Considered in the Model

where V_{sn} is the settling velocity of the n-th sediment [L/T], S_n is the depth-averaged suspended concentration of n-th sediment [M/L^3], h is the water depth [L], Δt is the simulation time step size [T], τ_b is the bottom shear stress or the bottom friction stress [M/L/T^2], τ_{cDn} is the critical shear stress for the deposition of the n-th sediment [M/L/T^2], E_{0n} is the erodibility of the n-th sediment [M/L^2/T], DMA_n is the amount of locally available dry matter of n-th sediment, expressed as dry weight per unit area [M/L^2], τ_{cRn} is the critical shear stress for the erosion of the n-th sediment [M/L/T^2].

For Non-cohesive sediments, e.g., sand, we have two options.

Option 1 (Prandle et al., 2000)

$$D_n = \min\left(V_{sn} S_n N_{Dn},\ S_n h/\Delta t\right) \qquad \text{where} \qquad N_{Dn} = \max\left[0,\ 1-\left(V_{cDn}/V_{cRn}\right)^2\right] \qquad \textbf{(2.6.4)}$$

and

$$R_n = \min\left(E_{0n} N_{Rn},\ DMA_n/\Delta t\right) \qquad \text{where} \qquad N_{Rn} = \max\left(0,\ V_{cDn}/V_{cRn}-1\right) \qquad \textbf{(2.6.5)}$$

where V_{cDn} and V_{cRn} represent the critical friction velocities for the onset of deposition and erosion, respectively [L/T].

Option 2 (Yeh et al., 1998)

$$D_n = \max\left(\frac{G_{sAn} - G_{sn}}{\Delta L}, 0\right) \tag{2.6.6}$$

and

$$R_n = \max\left(\frac{G_{sn} - G_{sAn}}{\Delta L}, 0\right) \tag{2.6.7}$$

where G_{sAn} is the actual load rate of the n-th sediment per unit width at a upstream location [M/L/T], G_{sn} is the maximum load rate of the n-th size fraction sediment per unit width at a downstream location [M/L/T], ΔL is the distance between the upstream and the downstream locations.

$$G_{sAn} = S_n VR \tag{2.6.8}$$

and

$$G_{sn} = 10\frac{\rho^2 VRS(\tau_b - \tau_{crn})}{g d_n (\rho_{sn} - \rho)^2} \tag{2.6.9}$$

where V is the overland flow velocity [L/t], R is hydraulic radius [L], ρ is the density of water [M/L^3], S is the friction slope, τ_{crn} is the critical bottom shear stress of the n-th sediment at which sediment movement begins [M/L/t^2], g is gravity [L/t^2], d_n is the median diameter of the n-th sediment particle [L], and ρ_{sn} is the density of the n-th sediment [M/L^3].

It should be noted that equations (2.6.2) through (2.6.9) are the sample models programmed in the computer code to estimate sediment deposition and erosion rate. Any other phenomenological model equation can be easily incorporated in the code.

2.6.2 Suspended Sediments

The continuity equation of suspended sediment can be derived based on the conservation law of material mass as (Yeh et al., 2005):

$$\frac{\partial(hS_n)}{\partial t} + \nabla\bullet(\mathbf{q}S_n) - \nabla\bullet(h\mathbf{K}\nabla S_n) = M_{S_n^{as}} + M_{S_n^{rs}} + M_{S_n^{is}} + R_n - D_n, \quad n \in [1, N_s] \tag{2.6.10}$$

where S_n is the depth-averaged concentration of the n-th suspended sediment in the unit of mass per unit column volume [M/L^3], $\mathbf{K}$ is the dispersion coefficient tensor [L^2/t], and $M_{S_n^{as}}$, $M_{S_n^{rs}}$, and $M_{S_n^{is}}$ are the mass rate of artificial source, rainfall source, and groundwater source of the n-th suspended sediment [M/L^2/t].

Concentrations of all suspended sediments must be given initially for transient simulations. Five types of boundary conditions are taken into account for suspended sediments, including Dirichlet, Variable, Cauchy, Neumann, and river/stream-overland interface boundary conditions (Yeh et al., 2005).

Dirichlet boundary condition: Dirichlet boundary conditions are prescribed on the boundary where

the suspended sediment concentration is known,

$$S_n = S_{ndb}(x_b, y_b, t) \quad on \quad B_d(\mathbf{x}) = 0 \tag{2.6.11}$$

where x_b and y_b are the coordinates of the boundary node [L], and $S_{ndb}(x_b, y_b, t)$ is a time-dependent concentration of the *n*-th sediment size on the Dirichlet boundary $B_d(\mathbf{x}) = 0$ [M/L^3].

Variable boundary condition: Variable boundary conditions are normally specified on the boundary where the flow direction can change with time or on any open boundary. On the variable boundary, when the flow is directed into the region of the interest, the mass rate into the region is given by the product of the flow rate and concentration of the incoming fluid. When the flow is directed out of the region, the sediment mass is assumed carried out via advection. Mathematically, a variable boundary condition is given as

$$\mathbf{n}\bullet\left(\mathbf{q}S_n - h\mathbf{K}\bullet\nabla S_n\right) = \mathbf{n}\bullet\mathbf{q}S_{nvb}(x_b, y_b, t) \quad if \quad \mathbf{n}\bullet\mathbf{q} \le 0 \quad on \quad B_v(\mathbf{x}) = 0 \tag{2.6.12}$$

and

$$-\mathbf{n}\bullet\left(h\mathbf{K}\bullet\nabla S_n\right) = 0 \quad if \quad \mathbf{n}\bullet\mathbf{q} \ge 0 \quad on \quad B_v(\mathbf{x}) = 0 \tag{2.6.13}$$

where **n** is a unit outward direction and $S_{nvb}(x_b, y_b, t)$ is a time-dependent concentration of the *n*-th sediment in the incoming fluid at the boundary [M/L^3] $B_v(\mathbf{x}) = 0$.

Cauchy boundary condition: This boundary condition is employed when the total material flow rate is given. Usually, this boundary is an upstream flux boundary.

$$\mathbf{n}\bullet\left(\mathbf{q}S_n - h\mathbf{K}\bullet\nabla S_n\right) = Q_{S_n cb}(x_b, y_b, t) \quad on \quad B_c(\mathbf{x}) = 0 \tag{2.6.14}$$

where $Q_{S_n cb}(x_b, y_b, t)$ is a time-dependent material flow rate of the *n*-th sediment through the Cauchy boundary $B_c(\mathbf{x}) = 0$ [M/t/L].

Neumann boundary condition: This boundary condition is used when the diffusive material flow rate is known at the boundary node.

$$-\mathbf{n}\bullet h\mathbf{K}\bullet\nabla S_n = Q_{S_n nb}(x_b, y_b, t) \quad on \quad B_{nb}(\mathbf{x}) = 0 \tag{2.6.15}$$

where $Q_{S_n nb}(x_b, y_b, t)$ is a time-dependent diffusive material flow rate of the *n*-th sediment trough the Neumann boundary $B_{nb}(\mathbf{x}) = 0$ [M/t/L].

Overland-River/Stream interface boundary condition: The boundary condition is needed when one-dimensional sediment transport in river/stream networks is coupled with two-dimensional sediment transport in overland regime. We assume that the exchange of sediment mass between river/stream and overland flows is mainly due to advection. Under such circumstances, the interfacial boundary condition is stated as

$$\mathbf{n}\cdot\left(\mathbf{q}S_n - h\mathbf{K}\cdot\nabla S_n\right) = \left(\mathbf{n}\cdot\mathbf{q}\right)\frac{1}{2}\left\{\left[1 + sign\left(\mathbf{n}\cdot\mathbf{q}\right)\right]S_n + \left[1 - sign\left(\mathbf{n}\cdot\mathbf{q}\right)\right]S_{n1D}(x_b, y_b, t)\right\} \tag{2.6.16}$$

where $S_{n1D}(x_b, y_b, t)$ is the time-dependent concentration of the *n*-th sediment at the 1-D node corresponding to the boundary [M/L^3]. It is the contribution of 1D transport to the overland boundary.

2.6.3 Immobile Species

The balance equation for immobile species is simply the statement that the rate of mass change is due to biogeochemical reaction as:

$$\frac{\partial(h_b \rho_{bw} \theta_b C_{bw})}{\partial t} = h_b r_{Cbw}\big|_N' \qquad \textbf{(2.6.17)}$$

$$\frac{\partial(h_b \rho_{bw} \theta_b C_{bp})}{\partial t} = h_b r_{Cbp}\big|_N' \qquad \textbf{(2.6.18)}$$

$$\frac{\partial(M_n C_{bsn})}{\partial t} = h_b r_{Cbsn}\big|_N' \qquad \textbf{(2.6.19)}$$

where h_b is the bed depth [L], ρ_{bw} is the density of bed pore-water [M/L^3], θ_b is the porosity of the bed sediment [L^3/L^3], C_{bw} is the concentration of dissolved chemical in the immobile pore-water phase in the unit of chemical mass per bed-water mass [M/M], $r_{Cbw}\big|_N'$ is the production rate of C_{bw} due to all N reactions in the unit of chemical mass per bed volume per time [M/L^3/t], C_{bp} is the concentration of bed precipitate in the unit of chemical mass per bed-water mass [M/M], $r_{Cbp}\big|_N'$ is the production rate of C_{bp} due to all N reactions in the unit of chemical mass per bed volume per time [M/L^3/t], C_{bsn} is the concentration of particulate sorbed on to bed sediment of the *n*-th fraction size in the unit of chemical mass per unit of bed-sediment mass [M/M], M_n is the concentration of the *n*-th bed sediment in the unit of sediment mass per bed area [M/L^2], $r_{Cbsn}\big|_N'$ is the production rate of C_{bsn} due to all N reactions in the unit of chemical mass per bed volume per time [M/L^3/t].

Define

$$r_i\big|_N = h_b \cdot r_i\big|_N' / h \quad where \quad i = C_{bw},\ C_{bp},\ or\ C_{bsn} \qquad \textbf{(2.6.20)}$$

Equation (2.6.16) through (2.6.18) can be modified as

$$\frac{\partial(h_b \rho_{bw} \theta_b C_{bw})}{\partial t} = h r_{Cbw}\big|_N \qquad \textbf{(2.6.21)}$$

$$\frac{\partial(h_b \rho_{bw} \theta_b C_{bp})}{\partial t} = h \cdot r_{Cbp}\big|_N \qquad \textbf{(2.6.22)}$$

$$\frac{\partial(h_b M_n C_{bsn})}{\partial t} = h r_{Cbsn}\big|_N \qquad \textbf{(2.6.23)}$$

Define

$$\rho_i = \begin{cases} h_b \rho_{bw} \theta_b / h, \ for \ \ C_{bw} \ and \ C_{bp} \\ M_n / h, \ for \ \ C_{bsn} \end{cases} \quad \textbf{(2.6.24)}$$

Equation (2.6.21) through (2.6.23) can be summarized as

$$\frac{\partial (h \rho_i C_i)}{\partial t} = hr_i \big|_N, \ \ i \in M_{im} \quad \textbf{(2.6.25)}$$

where C_i is the concentration of species i, which is immobile, in the unit of chemical mass per unit phase mass [M/M], ρ_i is the density of the phase associated with species i [M/L^3], $r_i \big|_N$ is the production rate of species i due to all N reactions in the unit of chemical mass per column volume per time [M/L^3/t], and M_{im} is the number of immobile species. The concentrations of all immobile species must be given initially for transient simulations. No boundary conditions are needed for immobile species.

2.6.4 Mobile Species

The continuity equation of mobile species can be derived based on the conservation law of material mass stating that the rate of mass change is due to both advective-dispersive transport and biogeochemical reactions as:

$$\frac{\partial (h \rho_w C_w)}{\partial t} + L(\rho_w C_w) = hr_{Cw} \big|_N \quad \textbf{(2.6.26)}$$

$$\frac{\partial (h \rho_w C_p)}{\partial t} + L(\rho_w C_p) = hr_{Cp} \big|_N \quad \textbf{(2.6.27)}$$

$$\frac{\partial (h S_n C_{sn})}{\partial t} + L(S_n C_{sn}) = hr_{Csn} \big|_N \quad \textbf{(2.6.28)}$$

where ρ_w is the density of column water [M/L^3], C_w is the concentration of dissolved chemical in the mobile water phase in the unit of chemical mass per column-water mass [M/M], $r_{Cw} \big|_N$ is the production rate of C_w due to all N reactions in the unit of chemical mass per column volume per time [M/L^3/t], C_p is the concentration of suspension precipitate in the unit of chemical mass per column-water mass [M/M], $r_{Cp} \big|_N$ is the production rate of C_p due to all N reactions in the unit of chemical mass per column volume per time [M/L^3/t], C_{sn} is the concentration of particulate sorbed on to suspended sediment of the n-th fraction size in the unit of chemical mass per unit of sediment mass [M/M], S_n is the concentration of suspended sediment in the unit of sediment mass per column volume [M/L^3], $r_{Csn} \big|_N$ is the production rate of C_{sn} due to all N reactions in the unit of chemical mass per column volume per time [M/L^3/t], and the operator L is defined in Eq. (2.6.31) later.

Define

$$\rho_i = \begin{cases} \rho_w \ \ for \ \ C_w \ and \ C_p \\ S_n \ \ for \ \ C_{sn} \end{cases} \quad \textbf{(2.6.29)}$$

Equation (2.6.26) through (2.6.28) can be summarized as

$$\frac{\partial(h\rho_i C_i)}{\partial t} + L(\rho_i C_i) = hr_i\big|_N, \quad i \in M_m = M - M_{im} \tag{2.6.30}$$

where C_i is the concentration of species i, which is mobile, in the unit of chemical mass per unit phase mass [M/M], ρ_i is the density of the phase associated with species i [M/L^3], $r_i\big|_N$ is the production rate of species i due to all N reactions in the unit of chemical mass per column volume per time [M/L^3/t], M is the total number of chemical species, M_m is the number of mobile chemical species, and operator L is defined as

$$L(\rho_i C_i) = \nabla\cdot(\mathbf{q}\rho_i C_i) - \nabla\cdot\left[h\mathrm{K}\cdot\nabla(\rho_i C_i)\right] - (M_{C_i^{as}} + M_{C_i^{rs}} - M_{C_i^{es}} + M_{C_i^{rs}}) \tag{2.6.31}$$

where $M_{C_i^{as}}$ is the mass ratte of artificial source of species i [M/L^2/T], $M_{C_i^{rs}}$ is the mass rate of the rainfall source of species i [M/L^2/T], $M_{C_i^{es}}$ is the mass rate of the evaporation sink of species i [M/L^2/T], and $M_{C_c^{is}}$ is mass rate of the source of species i in the overland from subsurface [M/L^2/T].

Concentrations of all mobile species must be given initially for transient simulations. Similar to suspended sediment transport, five types of boundary conditions are taken into account for mobile species, including Dirichlet, Variable, Cauchy, Neumann, and river/stream-overland interface boundary conditions (Yeh et al., 2005).

Dirichlet boundary condition: Dirichlet boundary conditions are prescribed on the boundary where the suspended sediment concentration is known,

$$C_i = C_{idb}(x_b, y_b, t) \qquad i \in M_m \quad on \quad B_d(\mathbf{x}) = 0 \tag{2.6.32}$$

where x_b and y_b are the coordinates of the boundary node [L], and $C_{idb}(x_b, y_b, t)$ is a time-dependent concentration of the i-th mobile species on the Dirichlet boundary $B_d(\mathbf{x}) = 0$ [M/M].

Variable boundary condition: Variable boundary conditions are normally specified on the boundary where the flow direction can change with time or on any open boundary. On the variable boundary, when the flow is directed into the region of the interest, the mass rate into the region is given by the product of the flow rate and concentration of the incoming fluid. When the flow is directed out of the region, the sediment mass is assumed carried out via advection. Mathematically, a variable boundary condition is given as

$$\mathbf{n}\cdot\left(\mathbf{q}\rho_i C_i - h\mathbf{K}\cdot\nabla(\rho_i C_i)\right) = \mathbf{n}\cdot\mathbf{q}\rho_i C_{ivb}(x_b, y_b, t) \; if \; \mathbf{n}\cdot\mathbf{q} \le 0 \; on \; B_v(\mathbf{x}) = 0, \; i \in M_m \tag{2.6.33}$$

and

$$-\mathbf{n}\cdot\left(h\mathbf{K}\cdot\nabla(\rho_i C_i)\right) = 0 \qquad if \qquad \mathbf{n}\cdot\mathbf{q} \le 0 \qquad on \qquad B_v(\mathbf{x}) = 0, \qquad i \in M_m \tag{2.6.34}$$

where $\mathbf{n}$ is a unit outward direction and $C_{ivb}(x_b, y_b, t)$ is a time-dependent concentration of the i-th mobile species in the incoming fluid at the boundary [M/M] $B_v(\mathbf{x}) = 0$.

Cauchy boundary condition: This boundary condition is employed when the total material flow rate

is given. Usually, this boundary is an upstream flux boundary.

$$\mathbf{n}\cdot\left(\mathbf{q}\rho_i C_i - h\mathbf{K}\cdot\nabla(\rho_i C_i)\right) = Q_{C_i cb}(x_b, y_b, t) \qquad i \in M_m \qquad on \qquad B_c(\mathbf{x}) = 0 \tag{2.6.35}$$

where $Q_{C_i cb}(x_b, y_b, t)$ is a time-dependent material flow rate of the *i*-th mobile species through the Cauchy boundary $B_c(\mathbf{x}) = 0$ [M/t/L].

Neumann boundary condition: This boundary condition is used when the diffusive material flow rate is known at the boundary node.

$$-\mathbf{n}\cdot h\mathbf{K}\cdot\nabla(\rho_i C_i) = Q_{C_i nb}(x_b, y_b, t) \qquad i \in M_m \qquad on \quad B_{nb}(\mathbf{x}) = 0 \tag{2.6.36}$$

where $Q_{C_i nb}(x_b, y_b, t)$ is a time-dependent diffusive material flow rate of the *i*-th mobile species through the Neumann boundary $B_{nb}(\mathbf{x}) = 0$ [M/t/L].

Overland-river/stream interface boundary condition: The boundary condition is needed when one-dimensional sediment transport in river/stream networks is coupled with two-dimensional sediment transport in overland regime. We assume that the exchange of sediment mass between river/stream and overland flows is mainly due to advection. Under such circumstances, the interfacial boundary condition is stated as

$$\mathbf{n}\cdot\left(\mathbf{q}\rho_i C_i - h\mathbf{K}\cdot\nabla(\rho_i C_i)\right) = \left(\mathbf{n}\cdot\mathbf{q}\right)\frac{1}{2}\left\{\left[1 + sign\left(\mathbf{n}\cdot\mathbf{q}\right)\right]\rho_i C_i + \left[1 - sign\left(\mathbf{n}\cdot\mathbf{q}\right)\right]\rho_i C_{i1D}(x_b, y_b, t)\right\} \tag{2.6.37}$$

where $C_{i1D}(x_b, y_b, t)$ is the time-dependent concentration of the *i*-th species at the 1-D node corresponding to the overland-river/stream interfacial boundary point [M/M].

2.6.5 Diagonalization of Species Transport Equations

The temporal-spatial distribution of chemical species is described by a system of M_{im} mass balance equations [equation (2.6.25)], and M_m reactive transport equations [equation (2.6.30)]. These two equations can be recast in the following form

$$\frac{\partial(h\rho_i C_i)}{\partial t} + \alpha_i L(\rho_i C_i) = hr_i\big|_N, \quad i \in M \tag{2.6.38}$$

where *M* is the total number of chemical species, α_i is 0 for immobile species and 1 for mobile species.

The determination of $r_i\big|_N$ and associated parameters is a primary challenge in biogeochemical modeling. Instead of using an ad hoc method to formulate $r_i\big|_N$, we use reaction-based formulations (Steefel and Cappellen, 1998). In a reaction-based formulation, $r_i\big|_N$ is given by the summation of rates of all reactions that the *i*-th species participates in,

$$r_i\big|_N = \frac{d\left(\rho_i C_i\right)}{dt}\Big|_{reaction} = \sum_{k=1}^{N}\left[(\nu_{ik} - \mu_{ik})r_k\right], \quad i \in M \qquad \textbf{(2.6.39)}$$

where ν_{ik} is the reaction stoichiometry of the *i*-th species in the *k*-th reaction associated with the products, μ_{ik} is the reaction stoichiometry of the *i*-th species in the *k*-th reaction associated with the reactants, and r_k is the rate of the *k*-th reaction.

Substituting equation (2.6.39) into equation (2.6.38) results in the transport equations of *M* chemical species described by

$$\frac{\partial(h\rho_i C_i)}{\partial t} + \alpha_i L(\rho_i C_i) = h\sum_{k=1}^{N}\left[(\nu_{ik} - \mu_{ik})r_k\right], \quad i \in M; \quad or \quad \mathbf{U}\frac{\partial \mathbf{C}_h}{\partial t} + \boldsymbol{\alpha} L(\mathbf{C}) = h\boldsymbol{\nu}\mathbf{r} \qquad \textbf{(2.6.40)}$$

where **U** is a unit matrix, $\mathbf{C}_h$ is a vector with its components representing *M* species concentrations multiply the water depth [M/L^2], $\boldsymbol{\alpha}$ is a diagonal matrix with α_i as its diagonal component, **C** is a vector with its components representing M species concentrations [M/L^3], $\boldsymbol{\nu}$ is the reaction stoichiometry matrix, and **r** is the reaction rate vector with *N* reaction rates as its components. Equation (2.6.40) represents a mass balance for species *i*, which states that the rate of change of any species mass is due to advection-dispersion coupled with contributing reactions that describe the biogeochemical processes.

In a primitive approach, equation (2.6.40) is integrated to yield the distributions and evolutions of chemical species in a region of interest. However, when some fast equilibrium reactions take place in the system, this approach is not adequate (Fang et al., 2003). Here, we will take a diagonalization approach through decomposition. Equation (2.6.40) written in matrix form can be decomposed based on the type of biogeochemical reactions via Gauss-Jordan column reduction of reaction matrix $\boldsymbol{\nu}$. Among all the fast/equilibrium and slow/kinetic reactions, "redundant reactions" are defined as fast reactions that are linearly dependent on other fast reactions, and "irrelevant reactions" are kinetic reactions that are linearly dependent on only equilibrium reactions. In order to avoid singularity of the reaction matrix, redundant fast reactions are omitted from the system prior to decomposition. The removal of irrelevant slow reactions alleviates problems associated with rate formulation uncertainty and parameterization for these reactions.

Decomposition is performed by pivoting on the N_E equilibrium reactions and decoupling them from the N_K kinetic reactions. In other words, each fast reaction can be used to eliminate one chemical species from simultaneous consideration. An incomplete Gauss-Jordan row decomposition of the reaction matrix $\boldsymbol{\nu}$ by pivoting on N_E equilibrium reactions will result in N_E equilibrium-variables and N_{KIV} kinetic-variables. To analyze the system behavior, it is advantageous to perform a complete decomposition, in which the reduction of the reaction matrix is done by pivoting on N_E equilibrium reactions and on N_{KI} linearly independent kinetic reactions to result in N_E equilibrium-variables, N_{KI} kinetic-variables, and N_C components. The complete decomposition is given as follows:

$$\begin{bmatrix} \mathbf{A_{11}} & \mathbf{0_{12}} & \mathbf{0_{13}} \\ \mathbf{A_{21}} & \mathbf{A_{22}} & \mathbf{0_{23}} \\ \mathbf{A_{31}} & \mathbf{A_{32}} & \mathbf{U_{33}} \end{bmatrix} \begin{Bmatrix} \frac{\partial \mathbf{C}_{h1}}{dt} \\ \frac{\partial \mathbf{C}_{h2}}{dt} \\ \frac{\partial \mathbf{C}_{h3}}{dt} \end{Bmatrix} + \begin{bmatrix} \mathbf{B_{11}} & \mathbf{0_{12}} & \mathbf{0_{13}} \\ \mathbf{B_{21}} & \mathbf{B_{22}} & \mathbf{0_{23}} \\ \mathbf{B_{31}} & \mathbf{B_{32}} & \boldsymbol{\alpha}_{33} \end{bmatrix} \mathrm{L}\left(\begin{Bmatrix} \mathbf{C_1} \\ \mathbf{C_2} \\ \mathbf{C_3} \end{Bmatrix} \right) = \mathrm{h} \begin{bmatrix} \mathbf{D_{11}} & \mathbf{K_{12}} & \mathbf{K_{13}} \\ \mathbf{0_{21}} & \mathbf{D_{22}} & \mathbf{K_{23}} \\ \mathbf{0_{31}} & \mathbf{0_{32}} & \mathbf{0_{33}} \end{bmatrix} \begin{Bmatrix} \mathbf{r_1} \\ \mathbf{r_2} \\ \mathbf{r_3} \end{Bmatrix} \quad \textbf{(2.6.41)}$$

where $\mathbf{A_{11}}$ is the submatrix of the reduced **U** matrix with size of $N_E \times N_E$, $\mathbf{A_{21}}$ is the submatrix of the reduced **U** matrix with size of $N_{KI} \times N_E$, and $\mathbf{A_{31}}$ is the submatrix of the reduced **U** matrix with size of $N_C \times N_E$; $\mathbf{0_{12}}$ is the zero submatrix of the reduced **U** matrix with size of $N_E \times N_{KI}$, $\mathbf{A_{22}}$ is the submatrix of the reduced **U** matrix with size of $N_{KI} \times N_{KI}$, and $\mathbf{A_{32}}$ is the submatrix of the reduced **U** matrix with size of $N_C \times N_{KI}$; $\mathbf{0_{13}}$ is the zero submatrix of the reduced **U** matrix with size of $N_E \times N_C$, $\mathbf{0_{23}}$ is the submatrix of the reduced **U** matrix with size of $N_{KI} \times N_C$, and $\mathbf{U_{33}}$ is the unit submatrix of the reduced **U** matrix with size of $N_C \times N_C$; $\mathbf{C_{h1}}$, $\mathbf{C_{h2}}$, and $\mathbf{C_{h3}}$ are the subvectors of the vector $\mathbf{C_h}$ with sizes of N_E, N_{KI}, and N_C, respectively; $\mathbf{B_{11}}$ is the submatrix of the reduced $\boldsymbol{\alpha}$ matrix with size of $N_E \times N_E$, $\mathbf{B_{21}}$ is the submatrix of the reduced $\boldsymbol{\alpha}$ matrix with size of $N_{KI} \times N_E$, and $\mathbf{B_{31}}$ is the submatrix of the reduced $\boldsymbol{\alpha}$ matrix with size of $N_C \times N_E$; $\mathbf{0_{12}}$ is the zero submatrix of the reduced $\boldsymbol{\alpha}$ matrix with size of $N_E \times N_{KI}$, $\mathbf{A_{22}}$ is the submatrix of the reduced $\boldsymbol{\alpha}$ matrix with size of $N_{KI} \times N_{KI}$, and $\mathbf{B_{32}}$ is the submatrix of the reduced $\boldsymbol{\alpha}$ matrix with size of $N_C \times N_{KI}$; $\mathbf{0_{13}}$ is the zero submatrix of the reduced $\boldsymbol{\alpha}$ matrix with size of $N_E \times N_C$, $\mathbf{0_{23}}$ is the submatrix of the reduced $\boldsymbol{\alpha}$ matrix with size of $N_{KI} \times N_C$, and $\boldsymbol{\alpha}_{33}$ is the diagonal submatrix of the reduced $\boldsymbol{\alpha}$ matrix with size of $N_C \times N_C$; $\mathbf{C_1}$, $\mathbf{C_2}$, and $\mathbf{C_3}$ are the subvectors of the vector **C** with sizes of N_E, N_{KI}, and N_C, respectively; $\mathbf{D_{11}}$ is the diagonal submatrix of the reduced $\boldsymbol{\nu}$ matrix with size of $N_E \times N_E$, $\mathbf{K_{12}}$ is the submatrix of the reduced $\boldsymbol{\nu}$ matrix with size of $N_E \times N_{KI}$, and $\mathbf{K_{13}}$ is the submatrix of the reduced $\boldsymbol{\nu}$ matrix with size of $N_E \times N_{KD(k)}$; $\mathbf{0_{21}}$ is the zero submatrix of the reduced $\boldsymbol{\nu}$ matrix with size of $N_{KI} \times N_E$, $\mathbf{D_{22}}$ is the diagonal submatrix of the reduced $\boldsymbol{\nu}$ matrix with size of $N_{KI} \times N_{KI}$, and $\mathbf{K_{23}}$ is the submatrix of the reduced $\boldsymbol{\nu}$ matrix with size of $N_{KI} \times N_{KD(k)}$; $\mathbf{0_{13}}$ is the zero submatrix of the reduced $\boldsymbol{\nu}$ matrix with size of $N_C \times N_E$, $\mathbf{0_{32}}$ is the zero submatrix of the reduced $\boldsymbol{\nu}$ matrix with size of $N_C \times N_{KI}$, and $\mathbf{0_{33}}$ is the zero submatrix of the reduced $\boldsymbol{\nu}$ matrix with size of $N_C \times N_{KD(k)}$; $\mathbf{r_1}$, $\mathbf{r_2}$, and $\mathbf{r_3}$ are the subvectors of the vector **r** with sizes of N_E, N_{KI}, and $N_{KD(k)}$, respectively.

For incomplete decomposition of the reaction matrix $\boldsymbol{\nu}$, Equation (2.6.41) can be connoted as

$$\begin{bmatrix} \mathbf{A_{11}} & \mathbf{0_{12}} \\ \mathbf{A_{21}} & \mathrm{U}_{22} \end{bmatrix} \begin{Bmatrix} \frac{\partial \mathbf{C}_{h1}}{dt} \\ \frac{\partial \mathbf{C}_{h2}}{dt} \end{Bmatrix} + \begin{bmatrix} \mathbf{B_{11}} & \mathbf{0_{12}} \\ \mathbf{B_{21}} & \boldsymbol{\alpha}_{22} \end{bmatrix} \mathrm{L}\left(\begin{Bmatrix} \mathbf{C_1} \\ \mathbf{C_2} \end{Bmatrix} \right) = \mathrm{h} \begin{bmatrix} \mathbf{D_{11}} & \mathbf{K_{12}} \\ \mathbf{0_{21}} & \mathbf{K_{22}} \end{bmatrix} \begin{Bmatrix} \mathbf{r_1} \\ \mathbf{r_2} \end{Bmatrix} \quad \textbf{(2.6.42)}$$

where $\mathbf{A_{11}}$ and $\mathbf{A_{21}}$ are the submatrices of the reduced **U** matrix with size of $N_E \times N_E$ and $N_{KIV} \times N_E$, respectively (note that $N_{KIV} = M - N_E = N_{KI} + N_C$); $\mathbf{0_{12}}$ and $\mathbf{U_{22}}$ are the zero- and unit-submatrices, respectively, of the reduced **U** matrix with size of $N_E \times N_{KIV}$ and $N_{KIV} \times N_{KIV}$, respectively; $\mathbf{C_{h1}}$ and $\mathbf{C_{h2}}$ are the subvectors of the vector $\mathbf{C_h}$ with sizes of N_E and N_{KIV}, respectively; $\mathbf{B_{11}}$ and $\mathbf{B_{21}}$ are the submatrices of the reduced $\boldsymbol{\alpha}$ matrix with sizes of $N_E \times N_E$ and $N_{KIV} \times N_E$, respectively; $\mathbf{0_{12}}$ and $\boldsymbol{\alpha}_{22}$ are the zero- and unit- submatrices, respectively, of the reduced $\boldsymbol{\alpha}$ matrix with size of $N_E \times N_{KIV}$ and $N_{KIV} \times N_{KIV}$, respectively; $\mathbf{C_1}$ and $\mathbf{C_2}$ are the subvectors of the vector **C** with sizes of N_E and N_{KIV},

respectively; $\mathbf{D_{11}}$ is the diagonal submatrix of the reduced $\boldsymbol{\nu}$ matrix with size of $N_E \times N_E$ and $\mathbf{K_{12}}$ is the submatrix of the reduced $\boldsymbol{\nu}$ matrix with size of $N_E \times N_{KIV}$; $\mathbf{0_{21}}$ is the zero submatrix of the reduced $\boldsymbol{\nu}$ matrix with size of $N_{KIV} \times N_E$ and $\mathbf{K_{22}}$ is the submatrix of the reduced $\boldsymbol{\nu}$ matrix with size of $N_{KIV} \times N_E$; $\mathbf{r_1}$ and $\mathbf{r_2}$ are the subvectors of the vector $\mathbf{r}$ with sizes of N_E and N_{KIV}, respectively.

For reactions that are fast, equilibrium may be regarded as being reached instantaneously among the relevant species and the reaction rates may be regarded as infinite. An infinite rate is mathematically represented by a mass action equation or a user specified nonlinear algebraic equation. As a result, the decomposition of equation (2.6.40) to equation (2.6.42) effectively reduces a set of M species reactive transport equations into two subsets of equations. The first set contains N_E algebraic equations representing mass action laws for the equilibrium reactions, and the second set contains N_{KIV} kinetic-variable transport equations. These equation subsets are defined as

Algebraic Equations for Equilibrium Reactions

$$\frac{\partial(hE_i)}{\partial t} + L(E_i^m) = hD_{1ii}r_{1i} + h\sum_{j=1}^{N_K} K_{1ij}r_{2j},\ i \in N_E \quad \Rightarrow \quad r_{1i} = \infty \quad \Rightarrow \quad \frac{\partial(hE_i)}{\partial t} \approx \infty$$

which is replaced with a thermodynamically consistent equation: $K_i^e = \prod_{j\in M} A_j^{\nu_{ji}} \Big/ \prod_{j\in M} A_j^{\mu_{ji}}$ **(2.6.43)**

$$or\ \ F_i(C_1,..,C_M;p_1,p_2,..) = 0 \quad where\ E_i = \sum_{j=1}^{N_E} A_{1ij}C_{1j} \ \ and \ \ E_i^m = \sum_{j=1}^{N_E} B_{1ij}C_{1j}$$

where K_i^e is the equilibrium constant of the i-th fast reaction, A_j is the activity of the j-th species, $Fi(C_1,..,C_M; p_1,p_2,..)$ is an empirical function of all species and a number of parameters p, p2, … for the i-th fast reaction. E_i was called an equilibrium-variable (Fang, et al., 2003) because $\frac{\partial(hE_i)}{\partial t} \approx \infty$ simply means that E_i can reach equilibrium instantaneously.

Transport Equations for Kinetic-Variables

$$\frac{\partial(hE_i)}{\partial t} + L(E_i^m) = h\sum_{j=1}^{N_K} K_{2nj}r_{2j},\ \ i \in N_{KIV} = M - N_E$$
$$where\ E_i = \sum_{j=1}^{N_E} A_{2ij}C_{1j} + C_{2i}\ \ and\ \ E_i^m = \sum_{j=1}^{N_E} B_{2ij}C_{1j} + \alpha_{1i}C_{2i} \qquad \textbf{(2.6.44)}$$

where E_i was called a kinetic variable (Fang, et al., 2003) because as E_i is transported it is subject to only kinetic reactions. This is in contrast to Eq. (2.6.44) where as C_i is transported, it is subject to both equilibrium and kinetic reactions.

Assign

$$R_i = \sum_{j=1}^{N_K} K_{2ij}r_{2j},\ \mathrm{i} \in N_{KIV} \qquad \textbf{(2.6.45)}$$

The reduction of Eq. (2.6.40) to Eq. (2.6.43) and (2.6.44) is equivalent to reducing M governing

equations for immobile and mobile species to the mixed N_E algebraic equations for equilibrium variables and N_{KIV} transport equations for kinetic-variables specified as follows

$$\frac{\partial(hE_i)}{\partial t} + \nabla\bullet(\mathbf{q}E_i^m) - \nabla\bullet\left[(h\mathbf{K}\bullet\nabla E_i^m)\right] = M_{E_i^{as}} + M_{E_i^{rs}} + M_{E_i^{is}} + hR_i,\ i \in N_{KIV} \qquad \textbf{(2.6.46)}$$

where E_i is the concentration of the i-th kinetic-variable [M/L^3], E_i^m is the concentration of mobile part of the i-th kinetic-variable [M/L^3], $M_{E_i^{as}}$ is the artificial source of the i-th kinetic-variable [M/L^2/T], $M_{E_i^{rs}}$ is the rainfall source of the i-th kinetic-variable [M/L^2/T], $M_{E_i^{os1}}$ and $M_{E_i^{os2}}$ are overland sources of the i-th kinetic-variable from river banks *1* and *2*, respectively [M/L^2/T], $M_{E_i^{is}}$ is the mass rate of the source of the i-th kinetic-variable in the overland from subsurface [M/L^2/T], R_i is the production rate of i-th kinetic-variable due to biogeochemical reactions [M/L^3/T], and N_{KIV} is the number of kinetic variable variables.

Initial and boundary condition for chemical species need to be transformed into corresponding initial and boundary conditions for kinetic-variables, which are stated in the following.

Dirichlet boundary condition:

$$E_i^m = E_{i\ db}^m(x_b, y_b, t) \qquad i \in M_m \qquad on \qquad B_d(\mathbf{x}) = 0 \qquad \textbf{(2.6.47)}$$

where $E_{i\ db}^m(x_b, y_b, t)$ is the prescribed concentration of the mobile portion of the i-th kinetic variable on the Dirichlet boundary $B_d(\mathbf{x}) = 0$ [M/L^3].

Variable boundary condition:

< Case 1 > Flow is coming in from outside (nQ < 0)

$$\mathbf{n}\bullet\left(\mathbf{q}E_i^m - h\mathbf{K}\bullet\nabla E_i^m\right) = \mathbf{n}\bullet\mathbf{q}E_{i\ vb}^m(x_b, y_b, t) \qquad i \in M_i \qquad on \qquad B_v(\mathbf{x}) = 0 \qquad \textbf{(2.6.48)}$$

< Case 2 > Flow is going out from inside (nQ > 0).

$$-\mathbf{n}\bullet\left(h\mathbf{K}\bullet\nabla E_i^m\right) = 0 \qquad i \in M_m \qquad on \qquad B_v(\mathbf{x}) = 0 \qquad \textbf{(2.6.49)}$$

where $\mathbf{n}$ is the unit outward vector and $E_{i\ vb}^m(x_b, y_b, t)$ is the concentration of the mobile portion of the i-th kinetic variable on the variable boundary $B_v(\mathbf{x}) = 0$ [M/L^3].

Cauchy boundary condition:

$$\mathbf{n}\bullet\left(\mathbf{q}E_i^m - h\mathbf{K}\bullet\nabla E_i^m\right) = Q_{E_i^m cb}(x_b, y_b, t) \qquad i \in M_i \qquad on \qquad B_c(\mathbf{x}) = 0 \qquad \textbf{(2.6.50)}$$

where $Q_{E_i^m cb}(x_b, y_b, t)$ is the mass flux of E_i^m through the Cauchy boundary $B_c(\mathbf{x}) = 0$ [M/t/L].

Neumann boundary condition:

$$-\mathbf{n}\bullet\left(h\mathbf{K}\bullet\nabla E_i^m\right)=Q_{E_i^m nb}(x_b,y_b,t)\qquad i\in M_i\qquad on\qquad B_n(\mathbf{x})=0 \tag{2.6.51}$$

where $Q_{E_i^m nb}(x_b,y_b,t)$ is the mass flux of E_i^m through the Neumann boundary $B_n(\mathbf{x})=0$ [M/t/L].

Overland-river/stream interface boundary condition:

$$\mathbf{n}\cdot\left(\mathbf{q}E_i^m-h\mathbf{K}\cdot\nabla E_i^m\right)=\left(\mathbf{n}\cdot\mathbf{q}\right)\frac{1}{2}\left\{\left[1+sign\left(\mathbf{n}\cdot\mathbf{q}\right)\right]E_i^m+\left[1-sign\left(\mathbf{n}\cdot\mathbf{q}\right)\right]E_{i\ 1D}^m(x_b,y_b,t)\right\} \tag{2.6.52}$$

where $E_{i\ 1D}^m(x_b,y_b,t)$ is the time-dependent concentration of the mobile portion of the *i*-th kinetic variable at the 1-D node corresponding to the overland-river/stream interfacial boundary point [M/L^3].

2.7 Reactive Biogeochemical Transport in Three-Dimension Subsurface Media

Reactive chemical transport in the subsurface occurs over a broad range of geochemical environments at various space and time scales. Coupled models that simulate hydrological transport and complex biogeochemical reactions are important tools for quantitative predictions of the fate and transport of chemicals in groundwater. Biogeochemical reactions can be divided into two classes (Rubin, 1983): (1) equilibrium-controlled "fast" reactions, and (2) kinetically-controlled "slow" reactions. The former are sufficiently fast compared to the transport time-scale and are reversible, so that local equilibrium may be assumed. The latter are not sufficiently fast compared to the transport time-scale. They may be either reversible or irreversible. Local equilibrium conditions cannot be assumed.

Due to computational limitations, existing coupled models for subsurface reactive transport have various capabilities (Keum and Hahn, 2003). Some models couple transport with equilibrium chemistry (e.g., Cederberg et al., 1985; Liu and Narasimhan, 1989; Yeh and Tripathi, 1991; Parkhurst, 1995; and Parkhurst and Appelo, 1999), while some couple transport with kinetic chemistry (e.g., MacQuarrie et al., 1990; Tompson, 1993; Lensing et al., 1994; Wood et al., 1994; Adeel et al., 1995; Yeh et al., 1998; and Saiers et al., 2000). Models coupling transport with both equilibrium and kinetic reactions appeared in the mid-1990s (e.g., Steefel and Lasaga, 1994; Chilakapati, 1995; Chilakapati et al., 1998; Tebes-Stevens et al., 1998; Yeh et al., 2001b; Brun and Engesgaard, 2002). Most of these models either implicitly assumes that equilibrium reactions occur only among aqueous species or consider only limited reaction networks. These limitations affect the generality of the models. There appears to be few general-purpose transport models that can simulate generic reaction networks including mixed equilibrium/kinetic biochemical and geochemical reactions (Yeh et al., 2004).

This report presents a general mathematical framework and a three-dimensional numerical implementation to simulate reactive chemical transport in subsurface water subject to a defined flow field. Chemical species considered include dissolved species, suspension precipitates and surface species that encompass adsorbed species, ion-exchanged species and free sites. Biogeochemical

reactions taken into account in the model include aqueous complexation, adsorption/desorption, ion-exchange, precipitation/dissolution, reduction/oxidation, and volatilization. Any individual reaction representing any of these chemical and physical processes may be simulated as kinetic or as equilibrium, which makes the approach applicable to a wide range of biogeochemical transport problems. In the subsurface, all dissolved species are assumed mobile while all surface species and suspension precipitates are assumed immobile.

2.7.1 Immobile Species

The balance equation for immobile species is simply the statement that the rate of mass change is due to biogeochemical reaction as:

$$\frac{\partial(\theta\rho_w C_p)}{\partial t} = \theta r_{Cp}\big|_N \qquad \textbf{(2.7.1)}$$

and

$$\frac{\partial(\rho_b S_A C_s)}{\partial t} = \theta r_{Cs}\big|_N \qquad \textbf{(2.7.2)}$$

where ρ_w is the density of pore-water [M/L^3], θ is the porosity of the media [L^3/L^3], C_p is the concentration of precipitate in the unit of chemical mass per por-water mass [M/M], $r_{Cp}\big|_N$ is the production rate of C_p due to all N reactions in the unit of chemical mass per pore-water volume per time [M/L^3/t], ρ_b is the bulk density in dry media mass per unit media volume [M/L^3], S_A is the surface area per unit dry mass [L^2/M], C_s is the concentration of surface species in unit of chemical mass per surface area [M/L^2], and $r_{Cs}\big|_N$ is the production rate of C_s due to all N reactions in the unit of chemical mass per pore-water per time [M/L^3/t].

Equation (2.7.1) and (2.7.2) can be combined as

$$\frac{\partial(\theta\rho_i C_i)}{\partial t} = \theta r_i\big|_N, \quad i \in M_{im} \qquad \textbf{(2.7.3)}$$

where C_i is the concentration of the i-th immobile, $r_i\big|_N$ is the production rate of species i due to all N reactions in the unit of chemical mass per pore-water volume per time [M/L^3/t], M_{im} is the number of immobile species, and ρ_i is defined by

$$\rho_i = \begin{cases} \rho_w, & for\ C_p \\ \rho_b S_A / \theta, & for\ C_s \end{cases} \qquad \textbf{(2.7.4)}$$

The concentrations of all immobile species must be given initially for transient simulations. No boundary conditions are needed for immobile species.

2.7.2 Mobile Species

The continuity equation of mobile species, i.e. dissolved species in the water phase, can be derived

based on the mass conservation law stating that the rate of mass change is due to both advective-dispersive transport and biogeochemical reactions as

$$\frac{\partial(\theta\rho_i C_i)}{\partial t} + \nabla\cdot(\mathbf{V}\rho_i C_i) - \nabla\cdot[\theta\mathbf{D}\cdot\nabla(\rho_i C_i)] = M_{C_i}^{\ as} + \theta r_i\big|_N, \quad i \in M_m \qquad \textbf{(2.7.5)}$$

where C_i is the concentration of the i-th dissolved species in the unit of chemical mass per unit water mass [M/M], ρ_i is the density of water [i.e., $C_i = C_w$] [M/L^3], **V** is the Darcy velocity [L/t], **D** is the dispersion coefficient tensor [L^2/t], $r_i\big|_N$ is the production rate of species i due to all N reactions in the unit of chemical mass per volume of water per time [M/L^3/t], $M_{C_i}^{\ as}$ is the artificial source of C_i in unit of chemical mass per unit of medium volume [M/L^3/t], and M_m is the number of mobile chemical species.

Concentrations of all mobile species must be given initially for transient simulations. Similar to salinity transport, six types of boundary conditions are taken into account for mobile species, including Dirichlet, Variable, Cauchy, Neumann, river/stream-overland interface, and overland-subsurface interface boundary conditions (Yeh et al., 2005). These boundary conditions are stated below:

Dirichlet boundary condition: This condition is applied when the species concentration is prescribed as a function of time on the boundaries:

$$C_i(\mathbf{x},t) = C_{idb}(\mathbf{x},t) \quad on \quad B_d(\mathbf{x}) = 0 \qquad \textbf{(2.7.6)}$$

where $C_{idb}(\mathbf{x},t)$ is a time-dependent concentration of the i-th species on the Dirichlet boundary, $B_d(\mathbf{x}) = 0$, [M/M].

Variable boundary condition: This boundary condition is employed when the flow direction would change with time during simulations. Two cases are considered, regarding to the flow direction on the boundary.

< Case 1 > Flow is coming in from outside:

$$\mathbf{n}\cdot\left[\mathbf{V}\rho_i C_i - \theta\mathbf{D}\cdot\nabla(\rho_i C_i)\right] = (\mathbf{n}\cdot\mathbf{V})\rho_i C_{ivb}(\mathbf{x},t) \quad on \quad B_v(\mathbf{x}) = 0 \qquad \textbf{(2.7.7)}$$

< Case 2 > Flow is going out from inside:

$$-\mathbf{n}\cdot\left[\theta\mathbf{D}\cdot\nabla(\rho_i C_i)\right] = 0 \quad on \quad B_v(\mathbf{x}) = 0 \qquad \textbf{(2.7.8)}$$

where $C_{ivb}(\mathbf{x},t)$ is a time-dependent concentration of the i-th species [M/M] on the variable boundary, $B_v(\mathbf{x}) = 0$, which is associated with the incoming flow.

Cauchy boundary condition: This boundary condition is employed when the total salt-flow rate is given at pervious boundaries. Usually, this boundary is a flow-in boundary. The conditions are expressed as

$$\mathbf{n}\cdot\left[\mathbf{V}\rho_i C_i - \theta\mathbf{D}\cdot\nabla(\rho_i C_i)\right] = Q_{C_i cb}(\mathbf{x},t) \quad on \quad B_c(\mathbf{x}) = 0 \qquad \textbf{(2.7.9)}$$

where $Q_{C_i cb}(\mathbf{x},t)$ is total chemical flux of the *i*-th species [M/L^2/t] through the Cauchy boundary, $B_c(\mathbf{x}) = 0$, which takes a positive value if it is going out of the region and a negative value if it is coming into the region.

Neumann boundary condition: This boundary condition is used when the dispersive salt-flow rate is known at the boundary. It can be written as

$$-\mathbf{n}\cdot\left(\theta\mathbf{D}\cdot\nabla(\rho_i C_i)\right) = Q_{C_i nb}(\mathbf{x},t) \quad on \quad B_n(\mathbf{x}) = 0 \qquad \textbf{(2.7.10)}$$

where $Q_{C_i nb}(\mathbf{x},t)$ is the chemical flux of the *i*-th species through the Neumann boundary, $B_n(\mathbf{x}) = 0$, [M/L^2/t].

In addition to the four types of global boundary conditions, two interface boundary conditions may be specified: one for the exchange of chemicals between the subsurface media and river/stream network and the other for chemical exchange between the subsurface media and the overland. Mathematically, these boundary conditions are described below.

Subsurface-river interface boundary condition:

$$\mathbf{n}\cdot\left[\mathbf{V}\rho_i C_i - \theta\mathbf{D}\cdot\nabla(\rho_i C_i)\right] = (\mathbf{n}\cdot\mathbf{V})\frac{1}{2}\left\{\left[1+sign(\mathbf{n}\cdot\mathbf{V})\right]\rho_i C_i + \left[1-sign(\mathbf{n}\cdot\mathbf{V})\right]\rho_i C_{i1D}(x_b,y_b,z_b,t)\right\} \qquad \textbf{(2.7.11)}$$

where $C_{i1D}(x_b,y_b,z_b,t)$ is the time-dependent concentration of the *i*-th species at the 1-D node corresponding to the subsurface-river/stream interfacial boundary points [M/M].

Subsurface-overland interface boundary condition:

$$\mathbf{n}\cdot\left[\mathbf{V}\rho_i C_i - \theta\mathbf{D}\cdot\nabla(\rho_i C_i)\right] = (\mathbf{n}\cdot\mathbf{V})\frac{1}{2}\left\{\left[1+sign(\mathbf{n}\cdot\mathbf{V})\right]\rho_i C_i + \left[1-sign(\mathbf{n}\cdot\mathbf{V})\right]\rho_i C_{i2D}(x_b,y_b,z_b,t)\right\} \qquad \textbf{(2.7.12)}$$

where $C_{i2D}(x_b,y_b,z_b,t)$ is the time-dependent concentration of the *i*-th species at the 2-D node corresponding to the subsurface-overland interfacial boundary point [M/M].

2.7.3 Diagonalization of Species Transport Equations

The temporal-spatial distribution of chemical species is described by a system of M_{im} mass balance equations [equation (2.7.3)], and M_m reactive transport equations [equation (2.7.5)]. These two equations can be recast in the following form

$$\frac{\partial(\theta\rho_i C_i)}{\partial t} + \alpha_i L(\rho_i C_i) = \theta r_i\big|_N, \quad i \in M \qquad \textbf{(2.7.13)}$$

where L is an operator defined as

$$L(\rho_i C_i) = \nabla \cdot (\mathbf{V}\rho_i C_i) - \nabla \cdot [\theta \mathbf{D} \cdot \nabla(\rho_i C_i)] - M_{C_i}{}^{as} \qquad \textbf{(2.7.14)}$$

The determination of $r_i\,|_N$ and associated parameters is a primary challenge in biogeochemical modeling. Instead of using an ad hoc method to formulate $r_i\,|_N$, we use reaction-based formulations (Steefel and Cappellen, 1998). In a reaction-based formulation, $r_i\,|_N$ is given by the summation of rates of all reactions that the *i*-th species participates in,

$$r_i\,|_N = \frac{d(\rho_i C_i)}{dt}\Big|_{reaction} = \sum_{k=1}^{N}[(\nu_{ik} - \mu_{ik})r_k], \quad i \in M \qquad \textbf{(2.7.15)}$$

where ν_{ik} is the reaction stoichiometry of the *i*-th species in the *k*-th reaction associated with the products, μ_{ik} is the reaction stoichiometry of the *i*-th species in the *k*-th reaction associated with the reactants, and r_k is the rate of the *k*-th reaction.

Substituting equation (2.7.15) into equation (2.7.18) results in the transport equations of *M* chemical species described by

$$\frac{\partial(\theta\rho_i C_i)}{\partial t} + \alpha_i L(\rho_i C_i) = \theta\sum_{k=1}^{N}[(\nu_{ik} - \mu_{ik})r_k], \quad i \in M; \quad or \quad \mathbf{U}\frac{\partial \mathbf{C}_\theta}{\partial t} + \boldsymbol{\alpha} L(\mathbf{C}) = h\boldsymbol{\nu}\mathbf{r} \qquad \textbf{(2.7.16)}$$

where **U** is a unit matrix, $\mathbf{C}_{\boldsymbol{\theta}}$ is a vector with its components representing *M* species concentrations multiply the moisture content [M/L^3], $\boldsymbol{\alpha}$ is a diagonal matrix with α_i as its diagonal component, **C** is a vector with its components representing M species concentrations [M/L^3], $\boldsymbol{\nu}$ is the reaction stoichiometry matrix, and **r** is the reaction rate vector with *N* reaction rates as its components. Equation (2.7.16) represents a mass balance for species *i*, which states that the rate of change of any species mass is due to advection-dispersion coupled with contributing reactions that describe the biogeochemical processes.

In a primitive approach, equation (2.7.16) is integrated to yield the distributions and evolutions of chemical species in a region of interest. However, when some fast equilibrium reactions take place in the system, this approach is not adequate (Fang et al., 2003). Here, we will take a diagonalization approach through decomposition. Equation (2.7.16) written in matrix form can be decomposed based on the type of biogeochemical reactions via Gauss-Jordan column reduction of reaction matrix $\boldsymbol{\nu}$. Among all the fast/equilibrium and slow/kinetic reactions, "redundant reactions" are defined as fast reactions that are linearly dependent on other fast reactions, and "irrelevant reactions" are kinetic reactions that are linearly dependent on only equilibrium reactions. In order to avoid singularity of the reaction matrix, redundant fast reactions are omitted from the system prior to decomposition. The removal of irrelevant slow reactions alleviates problems associated with rate formulation uncertainty and parameterization for these reactions.

Decomposition is performed by pivoting on the N_E equilibrium reactions and decoupling them from the N_K kinetic reactions. In other words, each fast reaction can be used to eliminate one chemical species from simultaneous consideration. An incomplete Gauss-Jordan row decomposition of the reaction matrix $\boldsymbol{\nu}$ by pivoting on N_E equilibrium reactions will result in N_E equilibrium-variables and N_{KIV} kinetic-variables. To analyze the system behavior, it is advantageous to perform a

complete decomposition, in which the reduction of the reaction matrix is done by pivoting on N_E equilibrium reactions and on N_{KI} linearly independent kinetic reactions to result in N_E equilibrium-variables, N_{KI} kinetic-variables, and N_C components. The complete decomposition is given as follows:

$$\begin{bmatrix} \mathbf{A_{11}} & \mathbf{0_{12}} & \mathbf{0_{13}} \\ \mathbf{A_{21}} & \mathbf{A_{22}} & \mathbf{0_{23}} \\ \mathbf{A_{31}} & \mathbf{A_{32}} & \mathbf{U_{33}} \end{bmatrix} \begin{Bmatrix} \dfrac{\partial \mathbf{C}_{\theta 1}}{\mathrm{dt}} \\ \dfrac{\partial \mathbf{C}_{\theta 2}}{\mathrm{dt}} \\ \dfrac{\partial \mathbf{C}_{\theta 3}}{\mathrm{dt}} \end{Bmatrix} + \begin{bmatrix} \mathbf{B_{11}} & \mathbf{0_{12}} & \mathbf{0_{13}} \\ \mathbf{B_{21}} & \mathbf{B_{22}} & \mathbf{0_{23}} \\ \mathbf{B_{31}} & \mathbf{B_{32}} & \boldsymbol{\alpha}_{33} \end{bmatrix} \mathrm{L}\left(\begin{Bmatrix} \mathbf{C_1} \\ \mathbf{C_2} \\ \mathbf{C}_3 \end{Bmatrix} \right) = \theta \begin{bmatrix} \mathbf{D_{11}} & \mathbf{K_{12}} & \mathbf{K_{13}} \\ \mathbf{0_{21}} & \mathbf{D_{22}} & \mathbf{K_{23}} \\ \mathbf{0_{31}} & \mathbf{0_{32}} & \mathbf{0_{33}} \end{bmatrix} \begin{Bmatrix} \mathbf{r_1} \\ \mathbf{r_2} \\ \mathbf{r_3} \end{Bmatrix} \quad \textbf{(2.7.17)}$$

where $\mathbf{A_{11}}$ is the submatrix of the reduced **U** matrix with size of $N_E \times N_E$, $\mathbf{A_{21}}$ is the submatrix of the reduced **U** matrix with size of $N_{KI} \times N_E$, and $\mathbf{A_{31}}$ is the submatrix of the reduced **U** matrix with size of $N_C \times N_E$; $\mathbf{0_{12}}$ is the zero submatrix of the reduced **U** matrix with size of $N_E \times N_{KI}$, $\mathbf{A_{22}}$ is the submatrix of the reduced **U** matrix with size of $N_{KI} \times N_{KI}$, and $\mathbf{A_{32}}$ is the submatrix of the reduced **U** matrix with size of $N_C \times N_{KI}$; $\mathbf{0_{13}}$ is the zero submatrix of the reduced **U** matrix with size of $N_E \times N_C$, $\mathbf{0_{23}}$ is the submatrix of the reduced **U** matrix with size of $N_{KI} \times N_C$, and $\mathbf{U_{33}}$ is the unit submatrix of the reduced **U** matrix with size of $N_C \times N_C$; $\mathbf{C_{h1}}$, $\mathbf{C_{h2}}$, and $\mathbf{C_{h3}}$ are the subvectors of the vector $\mathbf{C_h}$ with sizes of N_E, N_{KI}, and N_C, respectively; $\mathbf{B_{11}}$ is the submatrix of the reduced $\boldsymbol{\alpha}$ matrix with size of $N_E \times N_E$, $\mathbf{B_{21}}$ is the submatrix of the reduced $\boldsymbol{\alpha}$ matrix with size of $N_{KI} \times N_E$, and $\mathbf{B_{31}}$ is the submatrix of the reduced $\boldsymbol{\alpha}$ matrix with size of $N_C \times N_E$; $\mathbf{0_{12}}$ is the zero submatrix of the reduced $\boldsymbol{\alpha}$ matrix with size of $N_E \times N_{KI}$, $\mathbf{A_{22}}$ is the submatrix of the reduced $\boldsymbol{\alpha}$ matrix with size of $N_{KI} \times N_{KI}$, and $\mathbf{B_{32}}$ is the submatrix of the reduced $\boldsymbol{\alpha}$ matrix with size of $N_C \times N_{KI}$; $\mathbf{0_{13}}$ is the zero submatrix of the reduced $\boldsymbol{\alpha}$ matrix with size of $N_E \times N_C$, $\mathbf{0_{23}}$ is the submatrix of the reduced $\boldsymbol{\alpha}$ matrix with size of $N_{KI} \times N_C$, and $\boldsymbol{\alpha}_{33}$ is the diagonal submatrix of the reduced $\boldsymbol{\alpha}$ matrix with size of $N_C \times N_C$; $\mathbf{C_1}$, $\mathbf{C_2}$, and $\mathbf{C_3}$ are the subvectors of the vector **C** with sizes of N_E, N_{KI}, and N_C, respectively; $\mathbf{D_{11}}$ is the diagonal submatrix of the reduced $\boldsymbol{\nu}$ matrix with size of $N_E \times N_E$, $\mathbf{K_{12}}$ is the submatrix of the reduced $\boldsymbol{\nu}$ matrix with size of $N_E \times N_{KI}$, and $\mathbf{K_{13}}$ is the submatrix of the reduced $\boldsymbol{\nu}$ matrix with size of $N_E \times N_{KD(k)}$; $\mathbf{0_{21}}$ is the zero submatrix of the reduced $\boldsymbol{\nu}$ matrix with size of $N_{KI} \times N_E$, $\mathbf{D_{22}}$ is the diagonal submatrix of the reduced $\boldsymbol{\nu}$ matrix with size of $N_{KI} \times N_{KI}$, and $\mathbf{K_{23}}$ is the submatrix of the reduced $\boldsymbol{\nu}$ matrix with size of $N_{KI} \times N_{KD(k)}$; $\mathbf{0_{13}}$ is the zero submatrix of the reduced $\boldsymbol{\nu}$ matrix with size of $N_C \times N_E$, $\mathbf{0_{32}}$ is the zero submatrix of the reduced $\boldsymbol{\nu}$ matrix with size of $N_C \times N_{KI}$, and $\mathbf{0_{33}}$ is the zero submatrix of the reduced $\boldsymbol{\nu}$ matrix with size of $N_C \times N_{KD(k)}$; $\mathbf{r_1}$, $\mathbf{r_2}$, and $\mathbf{r_3}$ are the subvectors of the vector **r** with sizes of N_E, N_{KI}, and $N_{KD(k)}$, respectively.

For incomplete decomposition of the reaction matrix $\boldsymbol{\nu}$, Equation (2.7.17) can be connoted as

$$\begin{bmatrix} \mathbf{A_{11}} & \mathbf{0_{12}} \\ \mathbf{A_{21}} & \mathrm{U}_{22} \end{bmatrix} \begin{Bmatrix} \dfrac{\partial \mathbf{C}_{\theta 1}}{\mathrm{dt}} \\ \dfrac{\partial \mathbf{C}_{\theta 2}}{\mathrm{dt}} \end{Bmatrix} + \begin{bmatrix} \mathbf{B_{11}} & \mathbf{0_{12}} \\ \mathbf{B_{21}} & \boldsymbol{\alpha}_{22} \end{bmatrix} \mathrm{L}\left(\begin{Bmatrix} \mathbf{C_1} \\ \mathbf{C}_2 \end{Bmatrix} \right) = \theta \begin{bmatrix} \mathbf{D_{11}} & \mathbf{K_{12}} \\ \mathbf{0_{21}} & \mathbf{K_{22}} \end{bmatrix} \begin{Bmatrix} \mathbf{r_1} \\ \mathbf{r_2} \end{Bmatrix} \quad \textbf{(2.7.18)}$$

where $\mathbf{A_{11}}$ and $\mathbf{A_{21}}$ are the submatrices of the reduced **U** matrix with size of $N_E \times N_E$ and $N_{KIV} \times N_E$, respectively (note that $N_{KIV} = M - N_E = N_{\mathrm{KI}} + N_C$); $\mathbf{0_{12}}$ and $\mathbf{U_{22}}$ are the zero- and unit-submatrices,

respectively, of the reduced **U** matrix with size of $N_E \times N_{KIV}$ and $N_{KIV} \times N_{KIV}$, respectively; $\mathbf{C_{\theta 1}}$ and $\mathbf{C_{\theta 2}}$ are the subvectors of the vector $\mathbf{C_\theta}$ with sizes of N_E and N_{KIV}, respectively; $\mathbf{B_{11}}$ and $\mathbf{B_{21}}$ are the submatrices of the reduced $\boldsymbol{\alpha}$ matrix with sizes of $N_E \times N_E$ and $N_{KIV} \times N_E$, respectively; $\mathbf{0_{12}}$ and $\boldsymbol{\alpha}_{22}$ are the zero- and unit- submatrices, respectively, of the reduced $\boldsymbol{\alpha}$ matrix with size of $N_E \times N_{KIV}$ and $N_{KIV} \times N_{KIV}$, respectively; $\mathbf{C_1}$ and $\mathbf{C_2}$ are the subvectors of the vector **C** with sizes of N_E and N_{KIV}, respectively; $\mathbf{D_{11}}$ is the diagonal submatrix of the reduced $\boldsymbol{\nu}$ matrix with size of $N_E \times N_E$ and $\mathbf{K_{12}}$ is the submatrix of the reduced $\boldsymbol{\nu}$ matrix with size of $N_E \times N_{KIV}$; $\mathbf{0_{21}}$ is the zero submatrix of the reduced $\boldsymbol{\nu}$ matrix with size of $N_{KIV} \times N_E$ and $\mathbf{K_{22}}$ is the submatrix of the reduced $\boldsymbol{\nu}$ matrix with size of $N_{KIV} \times N_E$; $\mathbf{r_1}$ and $\mathbf{r_2}$ are the subvectors of the vector **r** with sizes of N_E and N_{KIV}, respectively.

For reactions that are fast, equilibrium may be regarded as being reached instantaneously among the relevant species and the reaction rates may be regarded as infinite. An infinite rate is mathematically represented by a mass action equation or a user specified nonlinear algebraic equation. As a result, the decomposition of equation (2.7.16) to equation (2.7.18) effectively reduces a set of *M* species reactive transport equations into two subsets of equations. The first set contains N_E algebraic equations representing mass action laws for the equilibrium reactions, and the second set contains N_{KIV} kinetic-variable transport equations. These equation subsets are defined as

Algebraic Equations for Equilibrium Reactions

$$\frac{\partial(\theta E_i)}{\partial t} + L(E_i^m) = \theta D_{1ii} r_{1i} + \theta \sum_{j=1}^{N_K} K_{1ij} r_{2j},\ i \in N_E \quad \Rightarrow \quad r_{1i} = \infty \quad \Rightarrow \quad \frac{\partial(\theta E_i)}{\partial t} \approx \infty$$

which is replaced with a thermodynamically consistent equation: $K_i^e = \prod_{j \in M} A_j^{\nu_{ji}} \Big/ \prod_{j \in M} A_j^{\mu_{ji}}$ **(2.7.19)**

$$or\ \ F_i(C_1,..,C_M; p_1, p_2,..) = 0 \quad where\ E_i = \sum_{j=1}^{N_E} A_{1ij} C_{1j} \ \ and \ \ E_i^m = \sum_{j=1}^{N_E} B_{1ij} C_{1j}$$

where K_i^e is the equilibrium constant of the *i*-th fast reaction, A_j is the activity of the *j*-th species, $F_i(C_1,..,C_M; p_1,p_2,..)$ is an empirical function of all species and a number of parameters p, p2, … for the *i*-th fast reaction. E_i was called an equilibrium-variable (Fang, et al., 2003) because $\frac{\partial(\theta E_i)}{\partial t} \approx \infty$ simply means that E_i can reach equilibrium instantaneously.

Transport Equations for Kinetic-Variables

$$\frac{\partial(\theta E_i)}{\partial t} + L(E_i^m) = \theta \sum_{j=1}^{N_K} K_{2nj} r_{2j},\ \ i \in N_{KIV} = M - N_E$$
$$where\ E_i = \sum_{j=1}^{N_E} A_{2ij} C_{1j} + C_{2i} \ and \ E_i^m = \sum_{j=1}^{N_E} B_{2ij} C_{1j} + \alpha_{1i} C_{2i} \qquad \textbf{(2.7.20)}$$

where E_i was called a kinetic variable (Fang, et al., 2003) because as E_i is transported it is subject to only kinetic reactions. This is in contrast to Eq. (2.7.16) where as C_i is transported, it is subject to both equilibrium and kinetic reactions.

Assign

$$R_i = \sum_{j=1}^{N_K} K_{2ij} r_{2j},\ \mathrm{i} \in N_{KIV} \qquad \textbf{(2.7.21)}$$

The reduction of Eq. (2.7.15) to Eq. (2.7.18) and (2.7.19) is equivalent to reducing M governing equations for immobile and mobile species to N_E algebraic equations for equilibrium variables and N_{KIV} transport equations for kinetic-variables specified as follows

$$\frac{\partial(\theta E_i)}{\partial t} + \nabla\bullet(\mathbf{V}E_i^m) - \nabla\bullet\left[(\theta\mathbf{D}\bullet\nabla E_i^m)\right] = M_{E_i^{as}} + \theta R_i,\ i \in N_{KIV} \qquad \textbf{(2.7.22)}$$

where E_i is the concentration of the i-th kinetic-variable [M/L^3], E_i^m is the concentration of mobile part of the i-th kinetic-variable [M/L^3], $M_{E_i^{as}}$ is the artificial source of the i-th kinetic-variable [M/L^3/T], R_i is the production rate of i-th kinetic-variable due to biogeochemical reactions [M/L^3/T], and N_{KIV} is the number of kinetic variable variables.

Initial and boundary condition for chemical species need to be transformed into corresponding initial and boundary conditions for kinetic-variables, which are stated in the following.

Dirichlet boundary condition:

$$E_i^m = E_{id}^m(x_b, y_b, z_b, t) \qquad on \qquad B_d(\mathbf{x}) = 0 \qquad \textbf{(2.7.23)}$$

where $E_{id}^m(x_b, y_b, t)$ is the specified concentration of the mobile portion of the i-th kinetic variable on the Dirichlet boundary $B_d(\mathbf{x}) = 0$ [M/L^3].

Variable boundary condition:

< Case 1 > Flow is coming in from outside (nQ < 0)

$$\mathbf{n}\bullet\left(\mathbf{V}E_i^m - \theta\mathbf{D}\bullet\nabla E_i^m\right) = \mathbf{n}\bullet\mathbf{V}E_{iv}^m(x_b, y_b, z_b, t) \qquad on \qquad B_v(\mathbf{x}) = 0 \qquad \textbf{(2.7.24)}$$

< Case 2 > Flow is going out from inside (nQ > 0).

$$-\mathbf{n}\bullet\left(\theta\mathbf{D}\bullet\nabla E_i^m\right) = 0 \qquad on \qquad B_v(\mathbf{x}) = 0 \qquad \textbf{(2.7.25)}$$

where $\mathbf{n}$ is the unit outward vector and $E_{iv}^m(x_b, y_b, z_b, t)$ is the concentration of the mobile portion of the i-th kinetic variable on the variable boundary $B_v(\mathbf{x}) = 0$ [M/L^3].

Cauchy boundary condition:

$$\mathbf{n}\bullet\left(\mathbf{V}E_i^m - \theta\mathbf{D}\bullet\nabla E_i^m\right) = Q_{cE_i^m}(x_b, y_b, z_b, t) \qquad on \qquad B_c(\mathbf{x}) = 0 \qquad \textbf{(2.7.26)}$$

where $Q_{cE_i^m}(x_b, y_b z_b, t)$ is the mass flux of E_i^m through the Cauchy boundary $B_c(\mathbf{x}) = 0$ [M/t/L^2].

Neumann boundary condition:

$$-\mathbf{n}\bullet\left(\theta\mathbf{D}\bullet\nabla E_i^m\right)=Q_{nE_i^m}(x_b,y_b,z_b,t)\quad on\quad B_n(\mathbf{x})=0 \qquad \textbf{(2.7.27)}$$

where $Q_{nE_i^m}(x_b,y_b,z_b,t)$ is the mass flux of E_i^m through the Neumann boundary $B_n(\mathbf{x})=0$ [M/t/L^2].

Subsurface-river interface boundary condition:

$$\mathbf{n}\cdot\left[\mathbf{V}E_i^m-\theta\mathbf{D}\cdot\nabla(E_i^m)\right]=(\mathbf{n}\cdot\mathbf{V})\frac{1}{2}\left\{\left[1+sign(\mathbf{n}\cdot\mathbf{V})\right]E_i^m+\left[1-sign(\mathbf{n}\cdot\mathbf{V})\right]E_i^m(C_j^{1D}{}'s)\right\} \qquad \textbf{(2.7.28)}$$

Where $E_i^m(C_j^{1D}{}'s)$ is the mobile portion of the subsurface *i*-th kinetic variables with its argument being the linear combination of 1-D river/stream species concentrations $C_j^{1D}{}'s$ [M/L^3].

Subsurface-overland interface boundary condition:

$$\mathbf{n}\cdot\left[\mathbf{V}E_i^m-\theta\mathbf{D}\cdot\nabla(E_i^m)\right]=(\mathbf{n}\cdot\mathbf{V})\frac{1}{2}\left\{\left[1+sign(\mathbf{n}\cdot\mathbf{V})\right]E_i^m+\left[1-sign(\mathbf{n}\cdot\mathbf{V})\right]E_i^m(C_j^{2D}{}'s)\right\} \qquad \textbf{(2.7.29)}$$

where $E_i^m(C_j^{2D}{}'s)$ is the mobile portion of the subsurface *i*-th kinetic variables with its argument being the linear comination of 2-D overland species concentrations $C_j^{2D}{}'s$ [M/L^3].

2.8 Coupling Transport Among Various Media

As in coupling flows among various media, a rigorous treatment of coupling transport among media should be based the continuity of material fluxes and state variables. This rigorous treatment in coupling chemical transport among various media can be taken similar to the case of flows. We simply impose the continuity of material fluxes and species concentrations for all mobile (between river/stream networks and overland regime) dissolved aqueous species (between subsurface media and overland regime and between subsurface media and river/stream networks) .

However, because the state variables (dissolved chemical concentrations, suspend sediment concentrations, and mobile particulate chemical concentrations) in various media may not be continuous because these state variables are true three-dimensional distribution in subsurface media, but are vertically averaged quantities in overland regime and cross-sectional area averaged quantity in river/stream networks. Because of the averaging processes, mass fluxes between media can be considered due mainly to the advective transport. If this assumption is valid, the coupling of transport among various medial is much simpler than that for fluid flow.

2.8.1 Coupling between Overland Transport and River/StreamNetworks

The coupling of transport between overland and canal is similar to that of salinity transport. When a levee is present on the bank of the canal (left column in Fig. 2.4-1), there are several possibilities on the interactions between overland and river flow transport. If water surfaces in both the overland regime and river are below the top of the levee, the two flow systems are decoupled and transport in overland is decoupled from that in river networks (Fig. 2.4-1a).

When the water surface in the overland regime is above the top of the levee and in the canal is below the top of the levee (Fig. 2.4-1b), the flow is from the overland to river network and thus the transport is also one way from the overland to river network. The fluxes are given by

$$\mathbf{n}\cdot\left[\mathbf{q}\rho C-\mathbf{D}h\cdot\nabla(\rho C)\right]\Big|_{Bank\,1}=M_{C_i}^{\ osl}=S_1\rho C^{o} \qquad \textbf{(2.8.1)}$$

where C [denotes S_n with $\rho=1$ for supended sediment, C_w with $\rho=\rho_w$ for dissolved species, C_p with $\rho=\rho_w$ for precipitated species, C_{Sn} with $\rho=S_n$ for particulate species] is sediment concentration [M/L^3] or species concentrations [M/M] in the overland flow, $M_{C_i}^{\ osl}$ is the source rate of the i-th species in the canal from the overland via bank *1*, which appeared in Eq. (2.5.30) [M/t/L], C^o is the value of C in the overland water at the interface. When the water surface in the overland regime is below the top of the levee and in the canal is above the top of the levee (Fig. 2.4-1c), the flow is from the canal to overland and thus the transport is one way from the canal to overland. The fluxes are given by

$$\mathbf{n}\cdot\left[\mathbf{q}\rho C-\mathbf{D}h\cdot\nabla(\rho C)\right]\Big|_{Bank\,1}=M_{C_i}^{\ osl}=S_1\rho C^{c} \qquad \textbf{(2.8.2)}$$

where C^c is the value of C in the canal water. When the water surfaces in the overland and canal are above the top of the levee (Fig. 2.4-1d), flow direction can e either from the overland to the canl or from the canal to the overland depending on the flow dynamics in the overland and in the canal. If the state variable C is discontinues at the interface of the canal and overland, the fluxes are given by

$$\mathbf{n}\cdot\left[\mathbf{q}\rho C-\mathbf{D}h\cdot\nabla(\rho C)\right]\Big|_{Bank\,1}=M_{C_i}^{\ osl}=S_1\frac{1}{2}\left[\left(1+sign\left(S_1\right)\right)\rho C^{o}+\left(1-sign\left(S_1\right)\right)\rho C^{c}\right] \qquad \textbf{(2.8.3)}$$

If the state variable is continuous, the fluxes are modeled by imposing its continuity to yield the fluxes

$$\mathbf{n}\cdot\left[\mathbf{q}\rho C-\mathbf{D}h\cdot\nabla(\rho C)\right]\Big|_{Bank\,1}=M_{C_i}^{\ osl}\quad and\quad C^{o}\Big|_{Bank\,1}=C^{c} \qquad \textbf{(2.8.4)}$$

When a levee is not present on the bank of the canal (right column in Fig. 2.4-1), there are two possibilities on the interactions between overland and river transport. If water surface in the canal falls below the bank, the flux is either zero if the overland flow is not present or is nonzero and directed from the overland into the canal if overland flow is present (Fig. 2.4-1e). Under this circumstance, the fluxes are given by

$$\mathbf{n}\cdot\left[\mathbf{q}\rho C-\mathbf{D}h\cdot\nabla(\rho C)\right]\Big|_{Bank\,2}=M_{C_i}^{\ os2}=S_2\rho C^{o} \qquad \textbf{(2.8.5)}$$

where $M_{C_i}^{os2}$ is the source rate of the *i*-th species in the canal from the overland via bank *2*, which appeared in Eq. (2.5.30) [M/t/L],

When the water surface in the canal is above the bank (Figs. 2.4-1f and 2.4-1.g), the flow direction can be either from the overland into the canal or from the canal into the overland depending on the flow dynamics in the overland and in the canal. If the state variable is discontinuous, the fluxes are

$$\mathbf{n}\cdot\left[\mathbf{q}\rho C - \mathbf{D}h\cdot\nabla(\rho C)\right]\Big|_{Bank\,2} = M_{C_i}^{os2} = S_2\frac{1}{2}\left[\left(1+sign\left(S_2\right)\right)\rho C^{o} + \left(1-sign\left(S_2\right)\right)\rho C^{c}\right] \qquad \textbf{(2.8.6)}$$

If the state variable is continuous, we impose the continuity of the state variable to yield the fluxes

$$\mathbf{n}\cdot\left[\mathbf{q}\rho C - \mathbf{D}h\cdot\nabla(\rho C)\right]\Big|_{Bank\,2} = M_{C_i}^{os2} \quad and \quad C^{o}\Big|_{Bank\,2} = C^{c} \qquad \textbf{(2.8.7)}$$

Because kinetic variables *E* are chosen as the primary variables in the transport module, for reactive chemical transport, the interfacial boundary conditions in terms of species concentrations must be transformed into those in terms of kinetic variables. Since reaction networks in overland and river/stream/canal networks are identical, every corresponding kinetic variable in the overland and river/stream networks contains the same mobile portion. Thus, one simply replaces ρC with E_i^m in Eqs. (2.8.1) through (2.8.7). For completeness of this report, these equations are listed below.

For couling via bank 1:

When the water surface in the overland regime is above the top of the levee and in the canal is below the top of the levee (Fig. 2.4-1b), the flow is from the overland to river network and thus the transport is also one way from the overland to river network. The flux of the *i*-th kinetic variables are given by

$$\mathbf{n}\cdot\left[\mathbf{q}E_i^m - \mathbf{D}h\cdot\nabla E_i^m\right]\Big|_{Bank\,1} = M_{E_i}^{os1} = S_1\left(E_i^m\right)^{o} \qquad \textbf{(2.8.8)}$$

When the water surface in the overland regime is below the top of the levee and in the canal is above the top of the levee (Fig. 2.4-1c), the flow is from the canal to overland and thus the transport is one way from the canal to overland, the flux of the i-th kinetic variable is given as

$$\mathbf{n}\cdot\left[\mathbf{q}E_i^m - \mathbf{D}h\cdot\nabla E_i^m\right]\Big|_{Bank\,1} = M_{E_i}^{os1} = S_1\left(E_i^m\right)^{c} \qquad \textbf{(2.8.9)}$$

When the water surfaces in the overland and canal are above the top of the levee (Fig. 2.4-1d), flow direction can e either from the overland to the canl or from the canal to the overland depending on the flow dynamics in the overland and in the canal. If the state variable *E* is discontinues at the interface of the canal and overland, the fluxes are given by

$$\mathbf{n}\cdot\left[\mathbf{q}E_i^m - \mathbf{D}h\cdot\nabla E_i^m\right]\Big|_{Bank\,1} = M_{E_i}^{os1} = S_1\frac{1}{2}\left[\left(1+sign\left(S_1\right)\right)\left(E_i^m\right)^{o} + \left(1-sign\left(S_1\right)\right)\left(E_i^m\right)^{c}\right] \qquad \textbf{(2.8.10)}$$

If the state variable *E* is continuous, the fluxes are modeled by imposing its continuity to yield the

fluxes

$$\mathbf{n}\cdot\left[\mathbf{q}E_i^m - \mathbf{D}h\cdot\nabla E_i^m\right]\Big|_{Bank\,1} = M_{E_i}^{os1} \quad and \quad \left(E_i^m\right)^o\Big|_{Bank\,1} = \left(E_i^m\right)^c \tag{2.8.11}$$

In Equations (2.8.8) through (2.8.11), E_i^m is the concentration of the mobile portion of the *i*-th kinetic variable [M/L^3], $\left(E_i^m\right)^o$ is the value of E_i^m in the overland water at the interface [M/L^3], and $M_{E_i}^{os1}$ is the source of the kinetic variable E_i in the canal from the overland via bank *1* [M/t/L], which appeared in Eq. (2.5.44), and $\left(E_i^m\right)^c$ is the value of E_i^m in the canal water at the interface.

For couling via bank 2:

When a levee is not present on the bank of the canal (right column in Fig. 2.4-1), there are two possibilities on the interactions between overland and river transport. If water surface in the canal falls below the bank, the flux is either zero if the overland flow is not present or is nonzero and directed from the overland into the canal if overland flow is present (Fig. 2.4-1e). Under this circumstance, the fluxes are given by

$$\mathbf{n}\cdot\left[\mathbf{q}E_i^m - \mathbf{D}h\cdot\nabla E_i^m\right]\Big|_{Bank\,2} = M_{E_i}^{os2} = S_2\left(E_i^m\right)^o \tag{2.8.12}$$

When the water surface in the canal is above the bank (Figs. 2.4-1f and 2.4-1g), the flow direction can be either from the overland into the canal or from the canal into the overland depending on the flow dynamics in the overland and in the canal. If the state variable is discontinuous, the fluxes are

$$\mathbf{n}\cdot\left[\mathbf{q}E_i^m - \mathbf{D}h\cdot\nabla E_i^m\right]\Big|_{Bank\,2} = M_{E_i}^{os2} = S_2\frac{1}{2}\left[\left(1+sign\left(S_2\right)\right)\left(E_i^m\right)^o + \left(1-sign\left(S_2\right)\right)\left(E_i^m\right)^c\right] \tag{2.8.13}$$

If the state variable is continuous, we impose the continuity of the state variable to yield the fluxes

$$\mathbf{n}\cdot\left[\mathbf{q}E_i^m - \mathbf{D}h\cdot\nabla E_i^m\right]\Big|_{Bank\,2} = M_{E_i}^{os2} \quad and \quad \left(E_i^m\right)^o\Big|_{Bank\,2} = \left(E_i^m\right)^c \tag{2.8.14}$$

In Equstions (2.8.12) through (2.8.14), $M_{E_i}^{os2}$ is the source of the kinetic variable E_i in the canal from the overland via bank *2* [M/t/L], which appeared in Eq. (2.5.44).

2.8.2 Coupling between Subsurface and Overland Transport

The coupling of overland and subsurface transport is through the exchange of dissolved species only. Sediments, particulate species, and precipitated species in the overland flow will not exchange with adsorbed/ion exchanged and precipitated species in the subsurface flow. If the concentrations of dissolved chemicals in overland water and subsurface water at the ground surface are discontinuous, the chemical flux is given by

$$\mathbf{n}\cdot\left[\mathbf{V}\rho_w C_i^w - \theta\mathbf{D}\cdot\nabla(\rho_w C_i^w)\right] = M_{C_i^{is}} = \frac{S_I}{2}\left[\left(1+sign(S_I)\right)\rho_w\left(C_i^w\right)^s + \left(1-sign(S_I)\right)\rho_w\left(C_i^w\right)^o\right] \quad \textbf{(2.8.15)}$$

where $\left(C_i^w\right)^o$ is the concentration of the *i*-th dissolved species in the overland water and $\left(C_i^w\right)^s$ is the concentration of the *i*-th dissolved species of subsurface water at the interface and $M_{C_i^{is}}$ is mass rate of the source of the *i*-th dissolved species in overland from subsurface media [M/t/L^2], which appeared in Eq. (2.6.31). If the concentrations are continuous, we impose the continuity of dissolved concentration to yield the fluxes

$$\mathbf{n}\cdot\left[\mathbf{V}\rho_i C_i^w - \theta\mathbf{D}\cdot\nabla(\rho_i C_i^w)\right] = M_{C_i^{is}} \text{ and } \left(C_i^w\right)^s\Big|_{\text{on the interface}} = \left(C_i^w\right)^o \quad \textbf{(2.8.16)}$$

The transforemation of the interfacial boundary conditions, Eq. (2.8.15) and (2.8.16), to those in terms of kinetic variables is not straightforward because the reaction networks for the subsurface and overland may not be identical. If every kinetic-variable in the subsurface corresponding to that in the overland contains the same dissolved aqueous species, then the transformation is straightforwd as

$$\mathbf{n}\cdot\left[\mathbf{V}E_i^w - \theta\mathbf{D}\cdot\nabla(E_i^w)\right] = M_{E_i^{is}} = \frac{S_I}{2}\left[\left(1+sign(S_I)\right)\left(E_i^w\right)^s + \left(1-sign(S_I)\right)\left(E_i^w\right)^o\right] \quad \textbf{(2.8.17)}$$

for the case when the state variables are discontinuous, and

$$\mathbf{n}\cdot\left[\mathbf{V}E_i^w - \theta\mathbf{D}\cdot\nabla(E_i^w)\right] = M_{E_i^{is}} \text{ and } \left(E_i^w\right)^s\Big|_{\text{on the interface}} = \left(E_i^w\right)^o \quad \textbf{(2.8.18)}$$

for the case when the state variables are continuous. In Equstions (2.8.17) and (2.8.18), $\left(E_i^w\right)^o$ is the concentration of the dissolved portion of *i*-th kinetic variables in the overland water and $\left(E_i^w\right)^s$ is the concentration of the dissolved portion of the *i*-th kinetic variable in subsurface water at the interface and $M_{E_i^{is}}$ is the mass rate of the source of the *i*-th kinetic variable in overland from subsurface media [M/t/L^2], which appeared in Eq. (2.6.46).

It should be kept in mind that $\left(E_i^w\right)^o$ and $\left(E_i^w\right)^s$ (and as a matter of fact $\left(E_i^w\right)$) must have the same dissolved species content for Equations (2.8.17) and (2.8.18) to be valid. Otherwise, the coupling in terms of kinetic-variables requires further elaborations that will be addressed in Section 2.8.4.

2.8.3 Coupling between Subsurface and River/Stream/Canal Transport

Similar to the coupling between subsurface and overland, the transport between subsurface and canal is coupled and the fluxes between two media depend on if the dissolved concentration is continuous or not. For the case of discontinuous chemical concentration, the flux is given by

$$\mathbf{n}\cdot\left(\mathbf{V}\,\rho_w C_i^{\,w}-\theta\mathbf{D}\cdot\nabla\rho_w C_i^{\,w}\right)=\frac{\mathbf{n}\bullet\mathbf{V}}{2}\left(\left(1+sign\left(\mathbf{n}\bullet\mathbf{V}\right)\right)\rho_w\left(C_i^{\,w}\right)^s+\left(1-sign\left(\mathbf{n}\bullet\mathbf{V}\right)\right)\rho_w\left(C_i^{\,w}\right)^c\right)$$
$$M_{C_i}^{\,is}=\int_P\frac{\mathbf{n}\bullet\mathbf{V}}{2}\left(\left(1+sign\left(\mathbf{n}\bullet\mathbf{V}\right)\right)\rho_w\left(C_i^{\,w}\right)^s+\left(1-sign\left(\mathbf{n}\bullet\mathbf{V}\right)\right)\rho_w\left(C_i^{\,w}\right)^c\right)dP \qquad \textbf{(2.8.19)}$$

where $\left(C_i^{\,w}\right)^s$ and $\left(C_i^{\,w}\right)^c$ are the concentrations of the i-th dissolved species in the subsurface and canal waters. If the concentration is continuous, we impose its continuity to yield the flux

$$\int_P\mathbf{n}\cdot\left(\mathbf{V}\,\rho_w C_i^{\,w}-\theta\mathbf{D}\cdot\nabla(\rho_w C_i^{\,w})\right)dP=M_{C_i}^{\,is}\quad and\quad\left(C_i^{\,w}\right)^s\Big|_{\text{on the interface}}=\left(C_i^{\,w}\right)^c \qquad \textbf{(2.8.20)}$$

where $M_{C_i^{is}}$ is mass rate of the source of the *i*-th dissolved species in canal from subsurface media [M/t/L].

Similar to the coupling between subsurface and overland flows, the transforemation of the interfacial boundary conditions, Eq. (2.8.19) and (2.8.20), to those in terms of kinetic variables is not straightforward because the reaction networks for the subsurface and river/stream newtworks may not be identical. If every kinetic-variable in the subsurface corresponding to that in the river/stream contains the same dissolved aqueous species, then the transformation is straightforwd and is given in Eqs. (2.8.21) and (2.8.22), respectively, for the cases of discontinuity and conctinuity, respectively, in species concentrations,

$$\mathbf{n}\cdot\left(\mathbf{V}\,E_i^w-\theta\mathbf{D}\cdot\nabla E_i^w\right)=\frac{\mathbf{n}\bullet\mathbf{V}}{2}\left(\left(1+sign\left(\mathbf{n}\bullet\mathbf{V}\right)\right)\left(E_i^w\right)^s+\left(1-sign\left(\mathbf{n}\bullet\mathbf{V}\right)\right)\left(E_i^w\right)^c\right)$$
$$M_{E_i}^{\,is}=\int_P\frac{\mathbf{n}\bullet\mathbf{V}}{2}\left(\left(1+sign\left(\mathbf{n}\bullet\mathbf{V}\right)\right)\left(E_i^w\right)^s+\left(1-sign\left(\mathbf{n}\bullet\mathbf{V}\right)\right)\left(E_i^w\right)^c\right)dP \qquad \textbf{(2.8.21)}$$

and

$$\int_P\mathbf{n}\cdot\left(\mathbf{V}E_i^w-\theta\mathbf{D}\cdot\nabla(E_i^w)\right)dP=M_{E_i}^{\,is}\quad and\quad\left(E_i^w\right)^s\Big|_{\text{on the interface}}=\left(E_i^{\,w}\right)^c \qquad \textbf{(2.8.22)}$$

where $\left(E_i^{\,w}\right)^s$ and $\left(E_i^{\,w}\right)^c$ are the concentration of the dissolved portion of *i*-th kinetic variables in the subsurface and canal.

It should be kept in mind that $\left(E_i^{\,w}\right)^c$ and $\left(E_i^{\,w}\right)^s$ (and as a matter of fact $\left(E_i^{\,w}\right)$) must have the same content of dissolved species for Equations (2.8.21) and (2.8.22) to be valid. Otherwise, the coupling in terms of kinetic-variables requires further elaborations that will be addressed in Section 2.8.4.

2.8.4 Coupling of Reactive Transport between Groundwater and Surface Transport

Since reaction networks for groundwater and surface waters (in overland and river/stream flows) are likely to be different, the continuity of species fluxes and the continuity of species concentration or

the formulation of species fluxes must be transformed from those in terms of species concentration to those in terms of kinetic variables.

After decomposition of reaction networks, kinetic-variables and their corresponding dissolved portion are simply defined as linear combination of species

$$\{\mathbf{E}\}_g = [\mathbf{A}]_g \{\mathbf{C}\}_g, \quad \{\mathbf{E}^w\}_g = [\mathbf{B}]_g \{\mathbf{C}\}_g \qquad \textit{and} \qquad \{\mathbf{E}\}_s = [\mathbf{A}]_s \{\mathbf{C}\}_s, \quad \{\mathbf{E}^w\}_s = [\mathbf{B}]_s \{\mathbf{C}\}_s \tag{2.8.23}$$

where the subscript *g* denotes the groundwater system; the subscript *s* denote the surface water system; $\{\mathbf{E}\}$ and $\{\mathbf{E}^{\mathbf{w}}\}$ are the vectors of size *M*; and $[\mathbf{A}]$ and $[\mathbf{B}]$ are the decomposed unit matrices of size *M* x *M*. It is noted that the *i*-th reaction extent, E_i, is an equilibrium variable if its evolution is governed by an indepdendnt equilibrium raeaction and a set of linearly depending kinetic reactions; a kinetic variable if by an independent kinetic reaction and a set of linearly dependent kinetic reactions; a component if its concentration remains constant (Fang et al., 2003). Inverting Eq. (2.8.23), we have

$$\{\mathbf{C}\}_g = [\mathbf{A}]_g^{-1} \{\mathbf{E}\}_g \qquad \textit{and} \qquad \{\mathbf{C}\}_s = [\mathbf{A}]_s^{-1} \{\mathbf{E}\}_s \tag{2.8.24}$$

Continuity of flux of all aqueous requires

$$\begin{aligned} &\mathbf{n} \cdot \left(\mathbf{V} \{\mathbf{E}^w\}_g - \theta \mathbf{D} \cdot \nabla \{\mathbf{E}^w\}_g \right) = \mathbf{n} \cdot \left(\mathbf{V} [\mathbf{B}]_g \{\mathbf{C}^w\}_g - \theta \mathbf{D} \cdot \nabla [\mathbf{B}]_g \{\mathbf{C}^w\}_g \right), \\ &\textit{thus} \qquad \mathbf{n} \cdot \left(\mathbf{V} \{\mathbf{E}^w\}_g - \theta \mathbf{D} \cdot \nabla \{\mathbf{E}^w\}_g \right) = \mathbf{n} \cdot \left(\mathbf{V} [\mathbf{B}]_g \{\mathbf{C}^w\}_s - \theta \mathbf{D} \cdot \nabla [\mathbf{B}]_g \{\mathbf{C}^w\}_s \right) \\ &\qquad\qquad = \mathbf{n} \cdot \left(\mathbf{V} [\mathbf{B}]_g [\mathbf{A}]_s^{-1} \{\mathbf{E}\}_s - \theta \mathbf{D} \cdot \nabla [\mathbf{B}]_g [\mathbf{A}]_s^{-1} \{\mathbf{E}\}_s \right) \end{aligned} \tag{2.8.25}$$

Continuity of aqueous speces require

$$\{\mathbf{E}^w\}_g = [\mathbf{B}]_g \{\mathbf{C}^w\}_g = [\mathbf{B}]_g \{\mathbf{C}^w\}_s = [\mathbf{B}]_g [\mathbf{A}]_s^{-1} \{\mathbf{E}\}_s \tag{2.8.26}$$

3 NUMERICAL APPROACHES

In this chapter, we are to present the numerical approaches employed to solve the governing equations of flow and transport given in the previous section. In our model, transport is assumed not to influence flow. Three time scales are considered in the model. They are (1) for three-dimensional subsurface flow, (2) for three-dimensional subsurface transport and two-dimensional overland flow/transport, and (3) for one-dimensional river/stream/canal flow/transport. In general, a three-dimensional flow time step may include several two-dimensional flow time steps and a two-dimensional flow time step can cover many one-dimensional flow time steps. The time scale for three-dimensional subsurface transport is set to be the same as that for two-dimensional overland flow/transport because kinetic chemical reactions are taken into account. During each three-dimensional flow time step, we solve three-dimensional subsurface flow by employing the updated two-dimensional flow conditions to achieve the surface/subsurface interface boundary conditions and determine the infiltration/seepage for two-dimensional flow computation included in this three-dimensional flow time step. During each two-dimensional flow time step, we first solve three-dimensional reactive chemical transport with the updated two-dimensional transport result (i.e., at the previous time) used for implementing variable boundary conditions on the interface boundary and determine the dissolve chemical flux through the surface/subsurface interface. This flux is actually the source/sink to two-dimensional dissolve chemical transport through infiltration/seepage. Then we solve two-dimensional flow equations to determine the water stage/depth and velocity of overland flow. Finally, we solve two-dimensional reactive chemical transport equations for the distribution of dissolved chemicals, sediments, and particulate chemicals. Within a one-dimensional flow time step, the river/stream flow equations are solved first and the one-dimensional transport equations are solved by using the newly-computed flow results. The interaction between one-dimensional river/stream and two-dimenional overland flow/transport is taken into account by using the updated computational results. Depth or stage difference-dependent fluxes are employed to determine the flow through this one-dimensional/two-dimensional interface.

3.1 Solving One-Dimensional River/Stream/Canal Network Flow Equations

As mentioned earlier in this report, we desire to implement a hybrid model to accurately simulate surface water flow under a wide range of physical conditions though it is still under investigation and further study is required. In our investigation to date, we would apply the hybrid Lagrangian-Eulerian finite element method to solve dynamical wave models, the hybrid Lagrangian-Eulerian or conventional finite element method to solve diffusion wave models, and the semi-Lagrangian method for kinematic wave models. In this and the next subsections, we will present the numerical approaches used in the method of characteristics and the Lagrangian approach for solving the one-dimensional river/stream/canal flow and two-dimensional overland flow equations, respectively. In either approach, the Picard method is employed to deal with the nonlinearity.

3.1.1 The Lagrangian-Eulerian Finite Element Method for Dynamic Wave

Substituting Equations (2.1.10) through (2.1.12) into Equations (2.1.19) and (2.1.20) and rearranging

the resulting equations, we obtain

$$\frac{D_{V+c}(V+\omega)}{D\tau} = D - K_+ V + S_+ \tag{3.1.1}$$

$$\frac{D_{V-c}(V-\omega)}{D\tau} = D - K_- V + S_- \tag{3.1.2}$$

in which

$$D = \frac{1}{A}\frac{\partial}{\partial x}\left(\varepsilon A \frac{\partial V}{\partial x}\right); K_+ = \frac{g}{Bc}\frac{\partial A^{\#}}{\partial x} + \frac{(S_S + S_R - S_E + S_I + S_1 + S_2)}{A} + \frac{\kappa PV}{A} \tag{3.1.3}$$

$$\begin{aligned} S_+ = {} & \frac{g}{Bc}(S_S + S_R - S_E + S_I + S_1 + S_2) - g\frac{\partial Z_o}{\partial x} - \frac{gh}{c\rho}\frac{\partial \Delta\rho}{\partial x} \\ & + \frac{(M_S + M_R - M_E + M_I + M_1 + M_2)}{A} + \frac{B\tau^s}{\rho A} \end{aligned} \tag{3.1.4}$$

$$K_- = \frac{g}{Bc}\frac{\partial A^{\#}}{\partial x} + \frac{(S_S + S_R - S_E + S_I + S_1 + S_2)}{A} + \frac{\kappa PV}{A} \tag{3.1.5}$$

$$\begin{aligned} S_- = {} & -\frac{g}{Bc}(S_S + S_R - S_E + S_I + S_1 + S_2) - g\frac{\partial Z_o}{\partial x} - \frac{gh}{c\rho}\frac{\partial \Delta\rho}{\partial x} \\ & + \frac{M_S + M_R - M_E + M_I + M_1 + M_2}{A} + \frac{B\tau^s}{\rho A} \end{aligned} \tag{3.1.6}$$

where D is the diffusive transport of waves, K_+ is the decay coefficient of the positive gravity wave, S_+ is the source/sink of the positive wave, K_- is the decay coefficient of the negative gravity wave, and S_- is the source/sink of the negative wave.

Integrating Equations (3.1.1) and (3.1.2) along their respective characteristic lines from x_i at new time-level to x_{i1}^* and x_{i2}^* (Fig. 3.1-1), we obtain

$$\begin{aligned} \frac{(V_i + \omega_i) - (V_{il}^* + \omega_{il}^*)}{\Delta\tau_l} = {} & \frac{1}{2}(D_i + D_{il}^*) - \frac{1}{2}\left((K_+)_i V_i + (K_+)_{il}^* V_{il}^*\right) \\ & + \frac{1}{2}\left((S_+)_i + (S_+)_{il}^*\right), \quad I \in N \end{aligned} \tag{3.1.7}$$

$$\begin{aligned} \frac{(V_i - \omega_i) - (V_{i2}^* - \omega_{i2}^*)}{\Delta\tau_l} = {} & \frac{1}{2}(D_i + D_{i2}^*) - \frac{1}{2}\left((K_-)_i V_i + (K_-)_{i2}^* V_{i2}^*\right) \\ & + \frac{1}{2}\left((S_-)_i + (S_-)_{i2}^*\right), \quad I \in N \end{aligned} \tag{3.1.8}$$

where (referring to Figure 3.1-1) V_i, ω_i are the values of V and ω at x_i (x_i = coordinate of node i) at new time level; V_{i1}^* and ω_{i1}^* are the values of V and ω point x_{i1}^* (where x_{i1}^* is the location of a fictitious particle backward tracked from x_i along the first characteristics); $\Delta\tau_1$ is the time determined by backward tracking along the first characteristic; D_i is the value of D at node i at new time level; D_{i1}^* is the value of D at point x_{i1}^*; $(K_+)_i$ and $(S_+)_i$ are the values of K_+ and S_+, respectively at node i

at new time level; $(K_+)_{i1}^*$ and $(S_+)_{i1}^*$ are the values of K_+ and S_+, respectively at node x_{i1}^* ; N is the number of nodes; V_{i2}^* and ω_{i2}^* are the values of V and ω point x_{i2}^* (where x_{i2}^* is the location of a fictitious particle backward tracked from x_i along the second characteristics); $\Delta\tau_2$ is the time determined by backward tracking along the second characteristic; D_{i2}^* is the value of D at point x_{i2}^*; $(K_-)_i$ and $(S_-)_i$ are the values of K_- and S_-, respectively at node i at new time level; and $(K)_{i2}^*$ and $(S_-)_{i2}^*$ are the values of K_- and S_-, respectively at node x_{i2}^*.

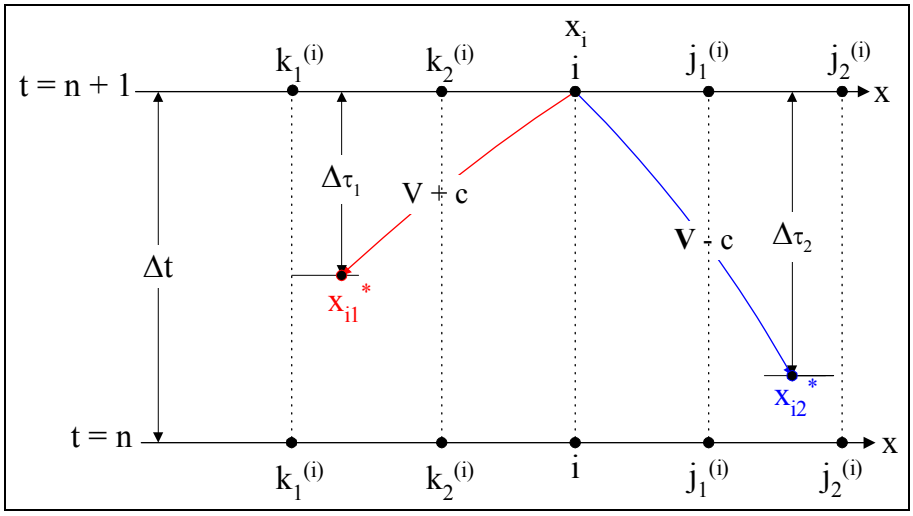

Fig. 3.1-1. Backward Tracking along Characteristics in One Dimension.

In Equations (3.1.7) and (3.1.8), the primitive variables at the backward tracked location are interpolated with those at the global nodes at both new time and old time as

$$V_{il}^* = a_{1(i)}V_{k_1^{(i)}}^{(n)} + a_{2(i)}V_{k_2^{(i)}}^{(n)} + a_{3(i)}V_{k_1^{(i)}} + a_{4(i)}V_{k_2^{(i)}} \qquad \textbf{(3.1.9)}$$

$$\omega_{il}^* = a_{1(i)}\omega_{k_1^{(i)}}^{(n)} + a_{2(i)}\omega_{k_2^{(i)}}^{(n)} + a_{3(i)}\omega_{k_1^{(i)}} + a_{4(i)}\omega_{k_2^{(i)}} \qquad \textbf{(3.1.10)}$$

$$V_{i2}^* = b_{1(i)}V_{j_1^{(i)}}^{(n)} + b_{2(i)}V_{j_2^{(i)}}^{(n)} + b_{3(i)}V_{j_1^{(i)}} + b_{4(i)}V_{j_2^{(i)}} \qquad \textbf{(3.1.11)}$$

$$\omega_{i2}^* = b_1\omega_{j_1^{(i)}}^{(n)} + b_2\omega_{j_2^{(i)}}^{(n)} + b_3\omega_{j_1^{(i)}} + b_4\omega_{j_2^{(i)}} \qquad \textbf{(3.1.12)}$$

in which the superscript (n) denotes time level (n); $k_1^{(i)}$ and $k_2^{(i)}$ are the two nodes of the element in which the backward tracking from node i, along the first characteristic, stops; $j_1^{(i)}$ and $j_2^{(i)}$ are the two nodes of the element in which the backward tracking from node i, along the second characteristic, stops; $a_{1(i)}$, $a_{2(i)}$, $a_{3(i)}$, $a_{4(i)}$, $b_{1(i)}$, $b_{2(i)}$, $b_{3(i)}$, and $b_{4(i)}$ are the interpolation parameters associated with the backtracking of the i-th node, all in the range of [0,1]. It should be noted that we may use two given parameters to determine where to stop in the backward tracking: one is for controlling tracking time and the other one is for controlling tracking distance. After the primitive variables at the backward tracked points are interpolated, all other parameters (such as the decay coefficients and source/sink terms) are functions of these variables and can be calculated.

To compute the eddy diffusion terms D_i, we rewrite the first equation in Equation (3.1.3) as

$$AD = \frac{\partial}{\partial x}\left(A\varepsilon \frac{\partial V}{\partial x} \right) \tag{3.1.13}$$

in which the momentum flux due to turbulence is modeled with the eddy diffusion hypothesis. Applying the Galerkin finite element method to Equation (3.1.13), we obtain the following matrix equation for D as

$$[a]\{D\} + [b]\{V\} = \{F\} \tag{3.1.14}$$

in which

$$\{D\} = \{D_1 \quad D_2 \quad D_3 \quad . \quad . \quad D_i \quad . \quad . \quad D_N\}^T \tag{3.1.15}$$

$$\{V\} = \{V_1 \quad V_2 \quad V_3 \quad . \quad . \quad V_i \quad . \quad . \quad V_N\}^T \tag{3.1.16}$$

$$\{F\} = \{F_1 \quad F_2 \quad F_3 \quad . \quad . \quad F_i \quad . \quad . \quad F_N\}^T \tag{3.1.17}$$

$$a_{ij} = \int_{x_l}^{X_N} N_i A N_j dx, \quad b_{ij} = \int_{x_l}^{X_N} \frac{dN_i}{dx} A\varepsilon \frac{dN_j}{dx} dx, \quad F_i = n\mathrm{N_i} A\varepsilon \frac{\partial V}{\partial x} \tag{3.1.18}$$

where N_i and N_j, functions of x, are the base functions of nodes at x_i and x_j, respectively.

Lumping the matrix [a], we can solve Eq. (3.1.14) for D_i as follows

$$D_i = \frac{1}{a_{ii}} F_i - \frac{1}{a_{ii}} \sum_j b_{ij} V_j \tag{3.1.19}$$

Following the identical procedure that leads Eq. (3.1.13) to Eq. (3.1.19), we have

$$D_i^{(n)} = \frac{1}{a_{ii}^{(n)}} F_i^{(n)} - \frac{1}{a_{ii}^{(n)}} \sum_j b_{ij}^{(n)} V_j^{(n)} \tag{3.1.20}$$

where $\{F^{(n)}\}$, $\{a^{(n)}\}$ and $\{b^{(n)}\}$, respectively, are defined similar to $\{F\}$, $\{a\}$ and $\{b\}$, respectively. Similar to Eqs. (3.1.9) and (3.1.10), $D_{i1}{}^*$ and $D_{i2}{}^*$ at the backward tracked location are interpolated with $\{D\}$ and $\{D^{(n)}\}$ as

$$D_{il}^* = a_{l(i)} D_{k_l^{(i)}}^{(n)} + a_{(i)} D_{k_2^{(i)}}^{(n)} + a_{3(i)} D_{k_{l(}^{(i)}} + a_{4(i)} D_{k_2^{(i)}} \tag{3.1.21}$$

and

$$D_{i2}^* = b_{l(i)} D_{k_l^{(i)}}^{(n)} + b_{(i)} D_{k_2^{(i)}}^{(n)} + b_{3(i)} D_{k_l^{(i)}} + b_{4(i)} D_{k_2^{(i)}} \tag{3.1.22}$$

Substituting Equations (3.1.9) through (3.1.12) and Equations (3.1.19) through (3.1.22) into Equations (3.1.7) and (3.1.8) and implementing boundary conditions given Section 2.1.1, we obtain a system of $2N$ simultaneous algebraic equations for the $2N$ unknowns (V_i for $i = 1, 2, .., N$ and ω_i for

$i = 1, 2, .., N$). If the eddy diffusion terms are not included and the backward tracking is performed to reach the time level n (Fig. 3.1-2), then Eqs. (3.1.7) and (3.1.8) are reduced to a set of N decoupled pairs of equations as

$$a_{ll}V_i + a_{12}\omega_i = b_1 \quad and \quad a_{21}V_i - a_{22}\omega_i = b_2, \quad i \in N \tag{3.1.23}$$

$$\begin{aligned} a_{11} &= 1 + \frac{\Delta\tau_1}{2}(K_+)_i, \quad a_{12} = 1, \quad b_1 = \left(1 - \frac{\Delta\tau_1}{2}(K_+)^*_{il}\right)V^*_{il} + \omega^*_{il} + \frac{\Delta\tau_1}{2}\left((S_+)_i + (S_+)^*_{il}\right), \\ a_{21} &= 1 + \frac{\Delta\tau 2}{2}(K_-)_i, \quad a_{22} = 1, \quad b_2 = \left(1 - \frac{\Delta\tau_2}{2}(K_-)^*_{i2}\right)V^*_{i2} + \omega^*_{i2} + \frac{\Delta\tau_2}{2}\left((S_-)_i + (S_-)^*_{i2}\right), \end{aligned} \tag{3.1.24}$$

Equation (3.1.23)) is applied to all interior nodes without having to make any modification. On a boundary point, there are several possibilities: (1) both equations in Eq. (3.1.23) are replaced with two boundary equations, (2) one of the two equations is replaced with a boundary condition equation while the other remains unchanged, and (3) both equations stay valid. These conditions are addressed below.

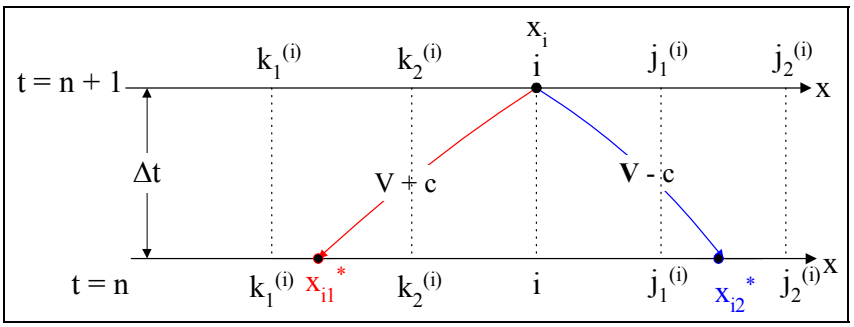

Fig. 3.1-2. Backward Tracking along Characteristics to the Toot in One Dimension.

Open upstream boundary condition:

If the flow is supercritical, Eq. (3.1.23) is replaced with

$$V_i A_i = Q_{up} \quad and \quad V_i^2 A_i + g(h_c)_i A_i = M_{up} \tag{3.1.25}$$

where V_i the cross-sectionally averaged velocity at node i, A_i is the cross-sectional area at node i, Q_{up} is the flow rate of the incoming fluid from the upstream, $(h_c)_i$ is the water depth to the centroid of the cross-sectional area at node i, and M_{up} is the momentum-impulse of the incoming fluid from the upstream. It should be noted that both the water depth and velocity in the upstream must be measured to provide values of Q_{up} and M_{up}. Equation (3.1.25) provides two equations for the solution of V_i and h_i. If the flow is critical, Eq. (3.1.23) for the boundary point i is replaced with

$$V_i A_i = Q_{up} \quad and \quad \frac{B_i Q_i^2}{g A_i^3} = 1 \tag{3.1.26}$$

where B_i is the top width of the cross-section at node i. Equation (3.1.26) provides two equations to

solve for V_i and h_i. If the flow is subcritical, Eq. (3.1.23) is replaced with

$$a_{11}V_i + a_{12}\omega_i = b_l \quad and \quad V_i A_i = Q_{up} \tag{3.1.27}$$

which is solved for V_i and h_i.

Open downstream boundary condition:

If the flow is supercritical, Eq. (3.1.23) is used to solve for V_i and h_i on node *i*. If the flow is critical, the following equation

$$a_{11}V_i + a_{12}\omega_i = b_1 \quad and \quad \frac{B_i Q_i^{\,2}}{g A_i^{\,3}} = 1 \tag{3.1.28}$$

is used to solve for V_i and h_i. If the flow is subcritical, the following equation is used to solve for V_i and h_i

$$a_{11}V_i + a_{12}\omega_i = b_1 \quad and \quad V_i A_i = Q_{dn}(h) \quad or \quad h_i = h_{dn}(t) \tag{3.1.29}$$

where $Q_{dn}(h)$, a function of h, is the rating curve function for the downstream boundary and $h_{dn}(t)$, a function of t, is the water depth at the downstream boundary. The adaption of Eq. (3.1.29) depends on the physical configuration at the boundary.

Closed upstream boundary condition:

If the flow is supercritical or critical, Eq. (3.1.23) is replaced with $V_i = 0$ and $h_i = 0$. If the flow is subcritical, $V_i = 0$ and the second equation in Eq. (3.1.23) is used to calculate h_i.

Closed downstream boundary conditions:

At the closed downstream boundary, physical condition dictates that the velocity at the boundary is zero. Therefore, supercritical flow cannot occur because c is greater or equal to zero. For critical flow, $V_i = 0$ and $h_i = 0$ at the closed boundary point x_i. For the subcritical flow, $V_i = 0$ and the first equation in Eq. (3.1.23) is used to calculate h_i.

Natural internal boundary condition at junctions:

For example, consider the junction node J joined by three reaches (Fig. 3.1-3), we have one unknown: the water surface elevation or the stage, H_J. The governing equation for this junction is

$$\frac{dV_J}{dh_J}\frac{dh_J}{dt} = \sum_{I=1}^{I=3} Q_{IJ} = \sum_{I=1}^{I=3} V_{IJ} A_{IJ} \tag{3.1.30}$$

for the case when the storage effect of the junction is accounted for, or

$$\sum_{I=1}^{I=3} Q_{IJ} = \sum_{I=1}^{I=3} V_{IJ} A_{IJ} = 0 \tag{3.1.31}$$

for the case when the storage effect of the junction is small.

For the node *IJ*, we need to set up two equations for V_{IJ} and h_{IJ}. Let us say that node *IJ* is a downstream point if the flow is from the node *IJ* toward the junction *J*. On the other hand, we say that the node *IJ* is an upstream point if the flow is from the junction *J* toward the node *IJ*. Now we can set up two equations for each node *IJ*. This is demonstrated as follows.

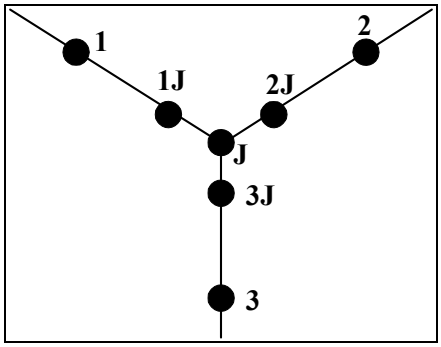

Fig. 3.1-3. A Three-Reach Junction

If *IJ* is a downstream point, we have three cases to consider:

(1). Subcritical flow –

$$a_{11}V_{IJ} + a_{12}\omega_{IJ} = b_1 \quad and \quad \frac{V_{IJ}^2}{2g} + h_{IJ} + Z_{oIJ} = H_J \qquad \textbf{(3.1.32)}$$

(2). Supercritical flow –

$$a_{11}V_{IJ} + a_{12}\omega_{IJ} = b_1 \quad and \quad a_{21}V_{IJ} - a_{22}\omega_{IJ} = b_2 \qquad \textbf{(3.1.33)}$$

(3). Critical flow –

$$a_{11}V_{IJ} + a_{12}\omega_{IJ} = b_1 \quad and \quad \frac{Q_{IJ}^2 B_{IJ}}{gA_{IJ}^3} = 1 \qquad \textbf{(3.1.34)}$$

If *IJ* is an upstream point, we have three cases to consider:

(1) Subcritical flow -

$$\frac{V_{IJ}^2}{2g} + h_{IJ} + Z_{oIJ} = H_J \quad and \quad a_{21}V_{IJ} - a_{22}\omega_{IJ} = b_2 \qquad \textbf{(3.1.35)}$$

(2). Supercritical flow –

$$\frac{V_{IJ}^2}{2g} + h_{IJ} + Z_{oIJ} = H_J \quad and \quad \frac{Q_{IJ}^2 B_{IJ}}{g A_{IJ}^3} = 1 \qquad \textbf{(3.1.36)}$$

(3). Critical flow –

$$\frac{V_{IJ}^2}{2g} + h_{IJ} + Z_{oIJ} = H_J \quad and \quad \frac{Q_{IJ}^2 B_{IJ}}{g A_{IJ}^3} = 1 \qquad \textbf{(3.1.37)}$$

Equation (3.1.30) or (3.1.31) and for I =1, 2, and 3, one of Eqs. (3.1.32) through (3.1.37) form 7 equations that can be solved for 7 unknowns V_{1J}, h_{1J}, V_{2J}, h_{2J}, V_{3J}, h_{3J}, and H_J. In theory, a substitution of the governing equations for the internal junction nodes into Eq. (3.1.30) or (3.1.31) eliminates all V_{IJ} and h_{IJ}, and the reduced Eq. (3.1.30) or (3.1.31) relates H_J to all unknowns at nodes other than that at node *IJ*. However, in practice, the 7 junction equations are solved simultaneously with all other discretized algebraic equations.

Controlled internal boundary condition at weirs:

For any weir (*W*), there are two river/stream/canal reaches connecting to it. The node *1W* located at the boundary between the 1^{th} reach and the W^{th} weir is termed the controlled internal boundary of the first reach while the node *2W* is called the controlled internal boundary of the second reach (Fig. 3.1-4). The specification of boundary conditions for the internal boundaries separated by a weir requires elaboration.

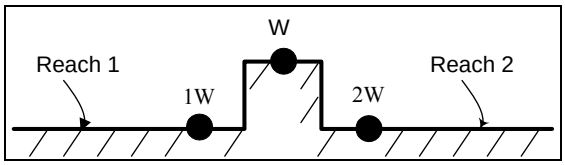

Fig. 3.1-4. A Flow-Control Weir

The flow configuration around the weir and its surrounding reaches may be very dynamic under transient flows. Both of the water stages at nodes *1W* and *2W* (H_{1W} and H_{2W}) may be below the weir, both may be above the weir, or one below the weir while the other is above the weir (Fig. 3.1-5). Governing equations of flow at internal boundary nodes *1W* and *2W* depend on the changing dynamics of water stages around the weir. When both stages H_{1W} and H_{2W} are below the height of the weir, the two reaches connecting the weir are decoupled. When at least one of the stages is above the weir, two reaches are either sequentially coupled or fully coupled via the weir. Here for sake of simplicity of discussions, we assume that the flow direction is from *Reach 1* to *Reach 2*. In other words, *Reach 1* is an upstream reach and *Reach 2* is a downstream reach. If the flow direction is reversed, we can have the boundary condition similarly prescribed.

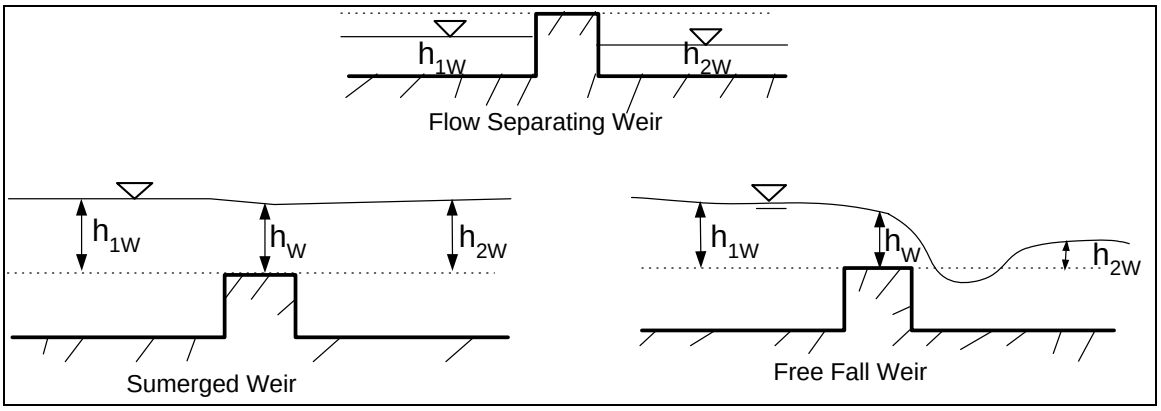

Fig. 3.1-5. Flow Configurations around a Weir.

There five unknowns, V_{1W} (velocity of the upstream reach node *1W*), h_{1W} (the water depth of the upstream node *1W*), Q_W (flow rate over the weir), V_{2W} (the velocity of the downstream reach node *2W*), and h_{2W} (the water depth of the downstream node *2W*); five equations must be set up for this weir complex consisting of a upstream reach node, a weir, and a downstream node. The governing equations for these five unknowns can be obtained depending on the flow conditions at the upstream and downstream reaches separated by a weir. The flow condition can be supercritical, critical, or subcritical at node *1W* and node *2W*. There are nine combinations. Five governing equations for each combination are given below.

Case 1: Supercritical flow at node 1W and supercritical flow at 2W (slowly varying flow)

$$a_{11}V_{1W} + a_{12}\omega_{1W} = b_1 \quad and \quad a_{21}V_{1W} - a_{22}\omega_{1W} = b_2 \tag{3.1.38}$$

$$\begin{aligned} &Q_W = V_{1W}A_{1W}; \quad H_{1W} = h_{1W} + Z_{o1W} + \frac{V_{1W}^2}{2g}; \\ &M_{1W} = \rho\left(V_{1W}A_{1W}V_{1W} + gh_{1Wc}A_{1W}\right) \end{aligned} \tag{3.1.39}$$

$$\begin{aligned} &u_{2W}A_{2W} = Q_W \quad and \quad h_{2W} + Z_{o2W} + \frac{V_{2W}^2}{2g} + h_{LW} = H_{1W} \quad or \\ &u_{2W}A_{2W} = Q_W \quad and \quad \rho\left(V_{2W}A_{2W}V_{2W} + gh_{2Wc}A_{2W}\right) + F_W = M_{1W} \end{aligned} \tag{3.1.40}$$

where h_{LW} is the head loss between nodes *1W* and *2W* and F_W is the force exerted by the weir between nodes *1W* and *2W*. For this case, the computation is straightforward. First Eq. (3.1.38), which constitutes two equations for two unknowns V_{1W} and h_{1W}, is used to solve for these two unknowns. Then the flow rate through the weir, Q_W, and the momentum-impulse and energy line at point *1W*, M_{1W} and H_{1W}, are simply calculated with Eq. (3.1.39). Finally, either the first two equations or the last two equations in Eq. (3.1.40) constitute two equations for two unknowns V_{2W} and h_{2W}. These two unknowns are obtained by solving either first two equations or the last two equations in Eq. (3.1.40).

Case 2: Supercritical flow at node 1W and critical flow at 2W

$$a_{11}V_{1W} + a_{12}\omega_{1W} = b_1 \quad and \quad a_{21}V_{1W} - a_{22}\omega_{1W} = b_2 \tag{3.1.41}$$

$$Q_W = V_{1W}A_{1W} \tag{3.1.42}$$

$$V_{2W}A_{2W} = Q_W \quad and \quad \frac{Q_W^2 B_{2W}}{gA_{2W}^3} = 1 \tag{3.1.43}$$

For this case, the computation is straightforward. First Eq. (3.1.41), which constitutes two equations for two unknowns V_{1W} and h_{1W}, is used to solve for these two unknowns. Then the flow rate through the weir Q_W is simply calculated with Eq. (3.1.42). Finally, Equation (3.1.43) constitutes two equations for two unknowns V_{2W} and h_{2W}. These two unknowns are obtained by solving the two equations in Eq. (3.1.43).

Case 3: Supercritical flow at node *1W* and subcritical flow at *2W* (Hydraulic Jump)

$$a_{11}V_{1W} + a_{12}\omega_{1W} = b_1 \quad and \quad a_{21}V_{1W} - a_{22}\omega_{1W} = b_2 \tag{3.1.44}$$

$$Q_W = V_{1W}A_{1W} \tag{3.1.45}$$

$$a_{21}V_{2W} - a_{22}\omega_{2W} = b_2 \quad and \quad u_{2W}A_{2W} = Q_W \tag{3.1.46}$$

For this case, the computation is straightforward. First Eq. (3.1.44), which constitutes two equations for two unknowns V_{1W} and h_{1W}, is used to solve for these two unknowns. Then the flow rate through the weir Q_W is simply calculated with Eq. (3.1.45). Finally, Equation (3.1.46) constitutes two equations for two unknowns V_{2W} and h_{2W}. These two unknowns are obtained by solving the two equations in Eq. (3.1.46).

Case 4: Critical flow at node 1W and supercritical flow at 2W

$$a_{11}V_{1W} + a_{12}\omega_{1W} = b_1 \quad and \quad \frac{Q_{1W}^2 B_{1W}}{gA_{1W}^3} = 1, \tag{3.1.47}$$

$$Q_W = V_{1W}A_{1W}; \;\; H_{1W} = h_{1W} + Z_{o1W} + \frac{V_{1W}^2}{2g}; \;\; M_{1W} = \rho\left(V_{1W}A_{1W}V_{1W} + gh_{1Wc}A_{1W}\right) \tag{3.1.48}$$

$$\begin{aligned} &u_{2W}A_{2W} = Q_W \quad and \quad h_{2W} + Z_{o2W} + \frac{V_{2W}^2}{2g} + h_{LW} = H_{1W} \quad or \\ &u_{2W}A_{2W} = Q_W \quad and \quad \rho\left(V_{2W}A_{2W}V_{2W} + gh_{2Wc}A_{2W}\right) + F_w = M_{1W} \end{aligned} \tag{3.1.49}$$

For this case, the computation is straightforward. First Eq. (3.1.47), which constitutes two equations for two unknowns V_{1W} and h_{1W}, is used to solve for these two unknowns. Then the flow rate through the weir Q_W and the momentum-impulse and energy line at point *1W*, M_{1W} and H_{1W}, are simply calculated with Eq. (3.1.48). Finally, either the first two equations or the last two equations in Eq. (3.1.49) constitute two equations for two unknowns V_{2W} and h_{2W}. These two unknowns are obtained

by solving either two equations or the last two equations in Eq. (3.1.49).

Case 5: Critical flow at node 1W and critical flow at 2W

$$a_{11}V_{1W} + a_{12}\omega_{1W} = b_1 \quad and \quad \frac{Q_{1W}^2 B_{1W}}{gA_{1W}^3} = 1, \tag{3.1.50}$$

$$Q_W = V_{1W} A_{1W} \tag{3.1.51}$$

$$V_{2W} A_{2W} = Q_W \quad and \quad \frac{Q_{2W}^2 B_{2W}}{gA_{2W}^3} = 1 \tag{3.1.52}$$

For this case, the computation is straightforward. First Eq. (3.1.50), which constitutes two equations for two unknowns V_{1W} and h_{1W}, is used to solve for these two unknowns. Then the flow rate through the weir Q_W is simply calculated with Eq. (3.1.51). Finally, Equation (3.1.52) constitutes two equations for two unknowns V_{2W} and h_{2W}. These two unknowns are obtained by solving the two equations in Eq. (3.1.52).

Case 6: Critical flow at node 1W and subcritical flow at 2W (Hydraulic Jump)

$$a_{11}V_{1W} + a_{12}\omega_{1W} = b_1 \quad and \quad \frac{Q_{1W}^2 B_{1W}}{gA_{1W}^3} = 1, \tag{3.1.53}$$

$$Q_W = V_{1W} A_{1W} \tag{3.1.54}$$

$$a_{21}V_{2W} - a_{22}\omega_{2W} = b_2 \quad and \quad V_{2W} A_{2W} = Q_W \tag{3.1.55}$$

For this case, the computation is straightforward. First Eq. (3.1.53), which constitutes two equations for two unknowns V_{1W} and h_{1W}, is used to solve for these two unknowns. Then the flow rate through the weir Q_W is simply calculated with Eq. (3.1.54). Finally, Equation (3.1.46) constitutes two equations for two unknowns V_{2W} and h_{2W}. These two unknowns are obtained by solving the two equations in Eq. (3.1.55).

Case 7: Subcritical flow at node 1W and Supercritical flow at 2W (Critical must occur at the weir)

$$a_{11}V_{1W} + a_{12}\omega_{1W} = b_1, \quad V_{1W}A_{1W} - Q_W = 0 \tag{3.1.56}$$

$$\frac{Q_W^2 B_W}{gA_W^3} = 1,\ V_W A_W = Q_W,\ and \qquad \begin{gathered} h_W + Z_{oW} + \frac{V_W^2}{2g} + h_{L1W} = h_{1W} + Z_{o1W} + \frac{V_{1W}^2}{2g} \\ or \\ \rho\left(V_W A_W V_W + g h_{Wc} A_W\right) + F_{1W} = \rho\left(V_{1W} A_{1W} V_{1W} + g h_{1Wc} A_{1W}\right) \end{gathered} \tag{3.1.57}$$

$$u_{2W}A_{2W} - Q_w = 0 \quad and \quad \begin{matrix} h_{2W} + Z_{o2W} + \dfrac{V_{2W}^2}{2g} + h_{L2W} = h_W + Z_{oW} + \dfrac{V_{W_p}}{2g} \\ or \\ \rho\left(V_{2W}A_{2W}V_{2W} + gh_{2Wc}A_{2W}\right) + F_{2W} = \rho\left(V_W A_W V_W + gh_{Wc}A_W\right) \end{matrix} \qquad \textbf{(3.1.58)}$$

where h_{L1W} is the head loss between the weir and node *1W*, F_{1W} is the force exerted by the weir between the weir and node *1W*, h_{L2W} is the head loss between the weir and node *2W*, and F_{2W} is the force exerted by the weir between the weir and node *2W*. For this case, in addition to the five unknowns, V_{1W}, h_{1W}, Q_W, V_{2W}, and h_{2W}, two more unknowns, h_W and V_W, appear in Eqs. (3.1.56) through (3.1.58). These seven unknowns are obtained by solving seven simultaneous equations contained in Eqs. (3.1.56) through (3.1.58).

Case 8: Subcritical flow at node 1W and critical flow at 2W

$$a_{11}V_{1W} + a_{12}\omega_{1W} = b_1, \quad V_{1W}A_{1W} - Q_W = 0 \qquad \textbf{(3.1.59)}$$

$$V_{2W}A_{2W} - Q_W = 0, \quad \frac{Q_W^2 B_{2W}}{gA_{2W}^3} = 1, \; and \quad \begin{matrix} h_{2W} + Z_{o2W} + \dfrac{V_{2W}^2}{2g} + h_{LW} = h_{1W} + Z_{o1W} + \dfrac{V_{1W}^2}{2g} \\ or \\ \rho\left(V_{2W}A_{2W}V_{2W} + gh_{2Wc}A_{2W}\right) + F_W = \rho\left(V_{1W}A_{1W}V_{1W} + gh_{1Wc}A_{1W}\right) \end{matrix} \qquad \textbf{(3.1.60}$$

For this case, five equations in Eqs. (3.1.59) and (3.1.60) are solved for the five unknowns, V_{1W}, h_{1W}, Q_W, V_{2W}, and h_{2W}.

Case 9: Subcritical flow at node 1W and Subcritical flow at 2W (slowly varying flow)

$$a_{11}V_{1W} + a_{12}\omega_{1W} = b_1, \quad V_{1W}A_{1W} - Q_W = 0 \qquad \textbf{(3.1.61)}$$

$$a_{21}V_{2W} - a_{22}\omega_{2W} = b_2, \quad V_{2W}A_{2W} - Q_W = 0$$

and

$$\begin{matrix} h_{2W} + Z_{o2W} + \dfrac{V_{2W}^2}{2g} + h_{LW} = h_{1W} + Z_{o1W} + \dfrac{V_{1W}^2}{2g} \\ or \\ \rho\left(V_{2W}A_{2W}V_{2W} + gh_{2Wc}A_{2W}\right) + F_W = \rho\left(V_{1W}A_{1W}V_{1W} + gh_{1Wc}A_{1W}\right) \end{matrix} \qquad \textbf{(3.1.62)}$$

For this case, five equations in Eqs. (3.1.59) and (3.1.60) are solved for the five unknowns, V_{1W}, h_{1W}, Q_W, V_{2W}, and h_{2W}

Controlled internal boundary condition at Gates:

For any gate (*G*), there are two river/stream/canal reaches connecting to it. The node *1G* located at the boundary between the 1^{th} reach and the G^{th} gate is termed the controlled internal boundary of the first reach while the node *2G* is called the controlled internal boundary of the second reach (Fig. 3.1-6). The specification of boundary conditions for the internal boundaries separated by a gate can be

made similar to that of a weir.

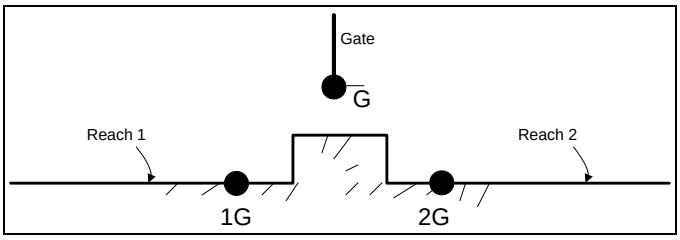

Fig. 3.1-6. A Flow-Control Gate.

The flow configuration around the gate and its surrounding reaches may be very dynamic under transient flows. Depending on the water stages at nodes *1G* and *2G* (H_{1G} and H_{2G}), we have several configurations (Fig. 3.1-7). Governing equations for flow at nodes *1G* and *2G* and through the gate depend on the changing dynamics of water stages around the gate. These equations can be obtained identical to those for a weir by changing the letter from *W* to *G*. Similar approaches can be used for culverts change the letter from *W* to *C* (for culverts). The only differences among various types of structures are the formulation of energy losses over the structures and/or the formulation of forces exerting on the fluids by the structures.

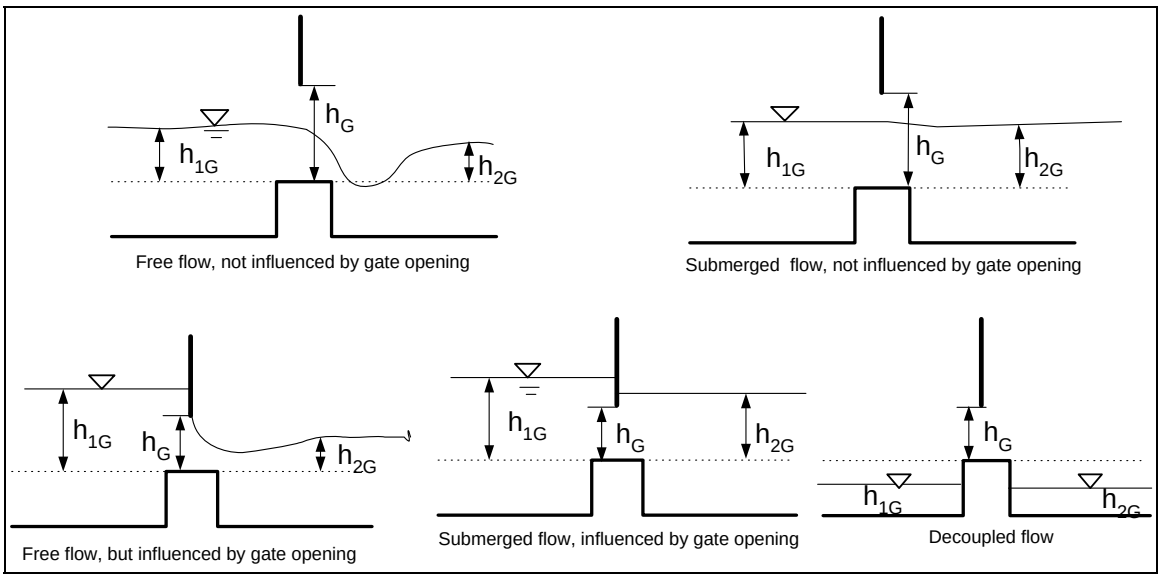

Fig. 3.1-7. Flow Configurations around a Gate.

3.1.2 Numerical Approximations of Diffusive Wave Approaches.

Two options are provided in this report to solve the diffusive wave flow equations. One is the finite element method and the other is the particle tracking method.

3.1.2.1 Galerkin Finite Element Method. Recall the diffusive wave is governed by Eq. (2.1.47) which is repeated here as

$$B\frac{\partial H}{\partial t}-\frac{\partial}{\partial x}\left(K\left[\frac{\partial H}{\partial x}+\frac{h}{c\rho}\frac{\partial \Delta\rho}{\partial x}-\frac{B\tau^s}{Ag\rho}\right]\right)=S_S+S_R-S_E+S_I+S_1+S_2 \qquad \textbf{(3.1.63)}$$

Applying the Galerkin finite element method to Eq. (3.1.63), we obtain the following matrix equation.

$$[M]\frac{d\{H\}}{dt}+[S]\{H\}=\{Q_{\rho w}\}+\{Q_B\}+\{Q_S\}+\{Q_R\}-\{Q_E\}+\{Q_I\}+\{Q_1\}+\{Q_2\} \qquad \textbf{(3.1.64)}$$

in which

$$M_{ij}=\int_{X_1}^{X_N}N_iBN_j dx,\quad S_{ij}=\int_{X_1}^{X_N}\frac{dN_i}{dx}K\frac{dN_j}{dx}dx,\quad Q_{\rho wi}=\int_{X_1}^{X_N}\frac{dN_i}{dx}K\left[\frac{h}{c\rho}\frac{\partial\Delta\rho}{\partial x}-\frac{B\tau^s}{Ag\rho}\right]$$
$$Q_i=nN_iK\left[\frac{\partial H}{\partial x}+\frac{h}{c\rho}\frac{\partial\Delta\rho}{\partial x}-\frac{B\tau^s}{Ag\rho}\right] \qquad \textbf{(3.1.65)}$$

$$Q_{Si}=\int_{X_1}^{X_N}N_iS_S dx,\quad Q_{Ri}=\int_{X_1}^{X_N}N_iS_R dx,\quad Q_{Ei}=\int_{X_1}^{X_N}N_iS_E dx,$$
$$Q_{Ii}=\int_{X_1}^{X_N}N_iS_I dx,\quad Q_{1i}=\int_{X_1}^{X_N}N_iS_1 dx,\quad Q_{2i}=\int_{X_1}^{X_N}N_iS_2 dx, \qquad \textbf{(3.1.66)}$$

where N_i and N_j are the base functions of nodes at x_i and x_j, respectively; n is the unit outward direction, $n = 1$ at a downstream point and $n = -1$ at an upstream point; $[M]$ is the mass matrix, $[S]$ is the stiff matrix, $\{H\}$ is the solution vector of H, $\{Q_{\rho w}\}$ is the load vector due to density and wind stress effects, $\{Q_B\}$ is the flow rate through the boundary nodes of a river/stream/canal reach, $\{Q_S\}$ is the flow rate from artificial source/sink, $\{Q_R\}$ is the flow rate from rainfall, $\{Q_E\}$ is the flow rate due evapotranspiration, $\{Q_I\}$ is the flow rate to infiltration, $\{Q_1\}$ is the flow rate from overland flow via river bank *1*, and $\{Q_2\}$ is the flow rate from overland flow via river bank *2*. It should be noted that $\{Q_I\}$ is the interaction between the river/stream/canal reach and subsurface flows and $\{Q_1\}$ and $\{Q_2\}$ between the river/stream/canal (via bank 1 and bank 2) and overland flows.

Approximating the time derivative term in Eq. (3.1.64) with a time-weighted finite difference, we reduce the diffusive equation and its boundary conditions to the following matrix equation

$$[C]\{H\}=\{L\}+\{Q_B\}+\{Q_I\}+\{Q_1\}+\{Q_2\} \qquad \textbf{(3.1.67)}$$

in which

$$[C]=\frac{[M]}{\Delta t}+\theta[S],\ \{L\}=\left(\frac{[M]}{\Delta t}-(1-\theta[S])\right)\{H^{(n)}\}+\{Q_{\rho w}\}+\{Q_S\}+\{Q_R\}-\{Q_E\} \qquad \textbf{(3.1.68)}$$

where $[C]$ is the coefficient matrix, $\{L\}$ is the load vector from initial condition, density and wind effects, artificial sink/sources, rainfall, and evapotranspiration; Δt is the time step size; θ is the time weighting factor; and $\{H^{(n)}\}$ is the value of $\{H\}$ at old time level n. The global and internal boundary (junctions, weirs, and gates) conditions must be used to provide $\{Q_B\}$ in Eq. (3.1.67). The interaction between the overland and river/stream/canal flows must be implemented to evaluate $\{Q_I\}$ and $\{Q_2\}$; and the interaction between the subsurface and river/stream/canal flows must be

implemented to calculate $\{Q_I\}$. The interactions will be addressed in Section 3.4.

For a global boundary node I, the corresponding algebraic equation from Eq. (3.1.67) is

$$C_{I,I-1}H_{I-1} + C_{I,I}H_I = L_1 + Q_{BI} + Q_{II} + Q_{1I} + Q_{2I} \qquad \textbf{(3.1.69)}$$

where $(I\text{-}1)$ is the corresponding interior node of the node I. In the above equation there are two unknowns H_I and Q_{BI}; either H_I or Q_{BI}, or the relationship between H_I and Q_{BI} must be specified. The numerical implementation of these boundary conditions are described as follows.

Dirichlet-boundary condition: prescribed water depth or state

If H_I is given on the boundary node I (Dirichlet boundary condition), all coefficients ($C_{I,I-1}$, $C_{I,I}$, $C_{I,I+1}$) and right-hand side (L_I, Q_{II}, Q_{1I}, Q_{2I}) obtained before the implementation of boundary conditions for this equation are stored in a temporary array, then an identity equation is created as

$$H_I = H_{Id}, \quad I \in N_D \qquad \textbf{(3.1.70)}$$

where H_{Id} is the prescribed total head on the Dirichlet node I and N_D is the number of Dirichlet boundary nodes. This process is repeated for every Dirichlet nodes. Note it is unnecessary to modify other equations that involving these unknowns, which was done in the previous version. By not modifying other equations, the symmetrical property of the matrix is preserved, which makes the iterative solvers more robust. The final set of equations will consist of N_D identity equations and (N - N_D) finite element equations for N unknowns H_i*'s*. After H_i*'s* are obtained, Eq. (3.1.69) is then used to back calculate N_D Q_{BI}*'s*.

If a direct solver is used to solve the matrix equation, the above procedure will solve N H_i*'s* accurately except for roundoff errors. However, if an iterative solver is used, a stopping criteria must be strict enough so that the converged solution of N H_i*'s* are accurate enough to the exact solution. With such accurate H_i*'s*, then one can be sure that the back-calculated N_D Q_{BI}*'s* are accurate.

Flux boundary condition: prescribed flow rate

If Q_{BI} is given (flux boundary condition), all coefficients ($C_{I,I-1}$, $C_{I,I}$, $C_{I,I+1}$) and right-hand side (L_I, Q_{II}, Q_{1I}, Q_{2I}) obtained before the implementation of boundary conditions for this equation are stored in a temporary array, then Eq. (3.1.69) is modified to incorporate the boundary conditions and used to solve for H_I. The modification of Eq. (3.1.69) is straightforward. Because Q_{BI} is a known quantity, it contributes to the load on the right hand side. This type of boundary conditions is very easy to implement. After H_i*'s* are obtained, the original Eq. (3.1.69), which is stored in a temporary array, is used to back calculate N_C Q_{BI}*'s* on flux boundaries (where N_C is the number of flux boundary nodes). These back-calculated Q_{BI}*'s* should be theoretically identical to the input Q_{BI}*'s*. However, because of round-off errors (in the case of direct solvers) or because of stopping criteria (in the case of iterative solvers), the back-calculated Q_{BI}*'s* will be slightly different from the input Q_{BI}*'s*. If the differences between the two are significant, it is an indication that the solvers have not yielded accurate solutions.

Water depth-dependent boundary condition: prescribed rating curve

If the relationship is given between Q_{BI} and H_I (rating curve boundary condition), all coefficients ($C_{I,I-1}$, $C_{I,I}$, $C_{I,I+1}$) and right-hand side (L_I, Q_{1I}, Q_{1I}, Q_{2I}) obtained before the implementation of boundary conditions for this equation are stored in a temporary array, then Eq. (3.1.69) is modified to incorporate the boundary conditions and used to solve for H_I. The rating-relationship is used to eliminate one of the unknowns, say Q_{BI}, and the modified Eq. (3.1.69) is used to solve for, say H_I. After H_I is solved, the original Eq. (3.1.69) (recall the original Eq. (3.1.69) must be and has been stored in a temporary array) is used to back-calculate Q_{BI}.

Junction boundary condition:

If the node *IJ* is an internal node that connects a junction *J*, then node *IJ* is treated as an internal boundary node. For example, consider three reaches with three internal nodes connecting to the junction *J* (Fig. 3.1-8). After applying the finite element method to Eq. (3.1.63), we have a total of (*1J* + *2J* + *3J*) algebraic equations. The algebraic equations for Nodes *1J*, *2J*, and *3J* can be written based on Eq. (3.1.69)

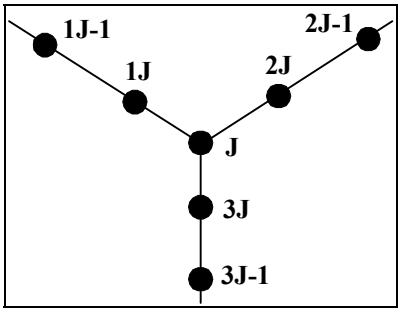

Fig. 3.1-8. A Three-Reach Junction

$$C^1_{1J,1J-1}H^1_{1J-1} + C^1_{1J,1J}H^1_{1J} = L^1_{1J} + Q^1_{1J} + Q^1_{I1J} + Q^1_{11J} + Q^1_{21J} \quad \textbf{(3.1.71)}$$

$$C^2_{2J,2J-1}H^2_{2J-1} + C^2_{2J,2J}H^2_{2J} = L^2_{2J} + Q^2_{2J} + Q^2_{I2J} + Q^2_{12J} + Q^2_{22J} \quad \textbf{(3.1.72)}$$

$$C^3_{3J,3J-1}H^3_{3J-1} + C^3_{3J,3J}H^3_{3J} = L^3_{3J} + Q^3_{3J} + Q^3_{I3J} + Q^3_{13J} + Q^3_{23J} \quad \textbf{(3.1.73)}$$

where the superscript denotes the reach number and subscript denotes local node number in a reach, for example, H_{1J}^{1} denotes the total head at the *1J*-th node in Reach *1*. For a convenient discussion, let us associate each of the unknowns, $H_1^1, \ldots, H_{1J-1}^1$ to each of the *1J-1* finite element equations in Reach *1*. Similarly, we associate each of the unknowns, $H_1^2, .., H_{2J-2}^2$ to each of the *2J-1* finite element equations in Reach *2* and each of the unknowns and $H_1^3, .., H_{3J-1}^3$ to each of the *3J-1* finite element equations in Reach *3*. The unknown, Q_{1J}^1, Q_{2J}^2, and Q_{3J}^3, are absent from these (*1J-1* + *2J-1* + *3J-1*) equations. In other words, we can say each equation governs one unknown. However, two unknowns, H_{1J}^1 and Q_{1J}^1, appear in Eq. (3.1.71). Similarly, Equation (3.1.72) has two unknowns, H_{2J}^2 and Q_{2J}^2, and Equation (3.1.73) has two unknowns, H_{3J}^3 and Q_{3J}^3. The number of unknowns, (1J + 2J + 3J) total heads and Q_{1J}^1, Q_{2J}^2, and Q_{3J}^3, is more than the number of equations, (*1J* + *2J* + *3J*) finite element equations. Three more governing equations must be set up, which can

be obtained based on the continuity of energy lines. This is described as follows.

Assume the entrance loss to the junction and exit loss from the junction are negligible, we have the following three equations

$$H_{1j}^{1} + \frac{1}{2g}\left(\frac{Q_{1J}^{1}}{A_{1J}^{1}}\right)^2 = h_J + Z_{oJ} \qquad \textbf{(3.1.74)}$$

$$H_{2j}^{2} + \frac{1}{2g}\left(\frac{Q_{2J}^{2}}{A_{2J}^{2}}\right)^2 = h_J + Z_{oJ} \qquad \textbf{(3.1.75)}$$

$$H_{3j}^{3} + \frac{1}{2g}\left(\frac{Q_{3J}^{3}}{A_{3J}^{3}}\right)^2 = h_J + Z_{oJ} \qquad \textbf{(3.1.76)}$$

where A_{1J}^{1}, A_{2J}^{2}, and A_{3J}^{3} are the cross-sectional area at *Nodes 1J* of *Reach 1*, *Node 2J* of *Reach 2*, and *Node 3J* of *Reach 3*, respectively; h_J is the water depth at the Junction J; and Z_{oJ} is the bottom elevation at the *Junction J*. It is noted that the second terms on the left hand side of Eqs. (3.1.74) through (3.1.76) are generally ignored in computation implementation to give more robust solutions.

The water depth at *Junction J* is not decoupled from river/stream/canal reaches. The water budget equation for the *Junction J* is

$$\frac{d\forall_J}{dh_J}\frac{dh_J}{dt} = \sum_{i=1}^{i=3} Q_{iJ}^{i} \qquad \textbf{(3.1.77)}$$

When $\frac{d\forall_J}{dh_J}$ is small, the water budget Eq. (3.1.77) is not employed. Instead, the following equation, resulting from the requirement that the summation of flow rates is equal to zero, is used

$$\sum_{i=1}^{i=3} Q_{iJ}^{i} = 0 \qquad \textbf{(3.1.78)}$$

Equations (3.1.71) through (3.1.76) and Eq. (3.1.77) or Eq. (3.1.78) constitute 7 equations for seven unknowns, A_{1J}^{1}, A_{2J}^{2}, A_{3J}^{3}, Q_{1J}^{1}, Q_{2J}^{2}, Q_{3J}^{3}, and h_J. If there are N_J junctions, there will be N_J blocks of seven equations. These N_J blocks of equations should be solved iteratively along with N_R block of finite element equations where N_R is the number of reaches. In other words, the whole system of algebraic equations can be solved with block iterations. Each block of equations can be solved directly. For example, each of N_R block of finite element equations can be solved with an efficient tri-diagonal matrix solver such as the Thomas algorithm. Each of the N_J block of seven equations can be solved with the Gaussian direct elimination with full pivoting.

Control Structure Boundary Condition:

The control structures may include weirs, gates, culverts, etc. For the two internal boundary nodes separated by a weir (Fig. 3.1-9), $Q_{1W} = Q_{2W} = Q_W$, where Q_W is given by

$$Q_W = C_W B_W h_{2W} \sqrt{h_{1W} - h_{2W}} \quad if \quad h_{1W} > h_{2W} > \frac{2}{3} h_{1W} \ (Submerged\ Weir) \qquad \textbf{(3.1.79)}$$

$$Q_W = \frac{2}{3\sqrt{3}} C_W B_W h_{1W} \sqrt{h_{1W}} \quad if \quad h_{2W} < \frac{2}{3} h_{1W} \ (Free\ Fall\ Weir) \qquad \textbf{(3.1.80)}$$

where C_W is the weir coefficient, B_W is the weir width [L]. The flow rate Q_W is equal to zero when both the upstream and downstream stages are below the weir elevation.

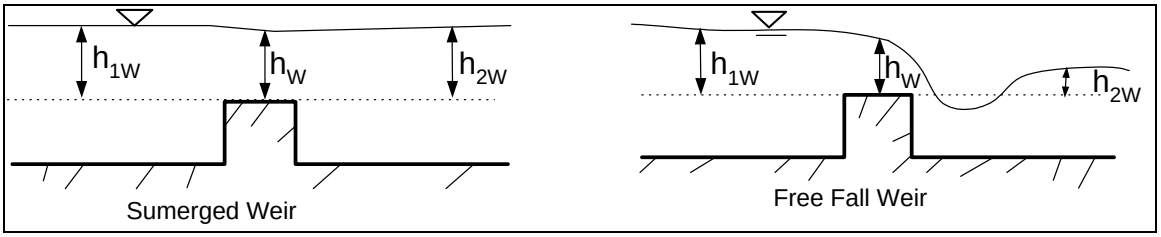

Fig. 3.1-9. Submerged versus Free Fall Weir.

Similarly, for two internal boundary nodes separated by a gate, $Q_{1G} = Q_{2G} = Q_G$. When the flow is not influenced by the gate opening (Fig. 3.1-10), the flow rate is given by

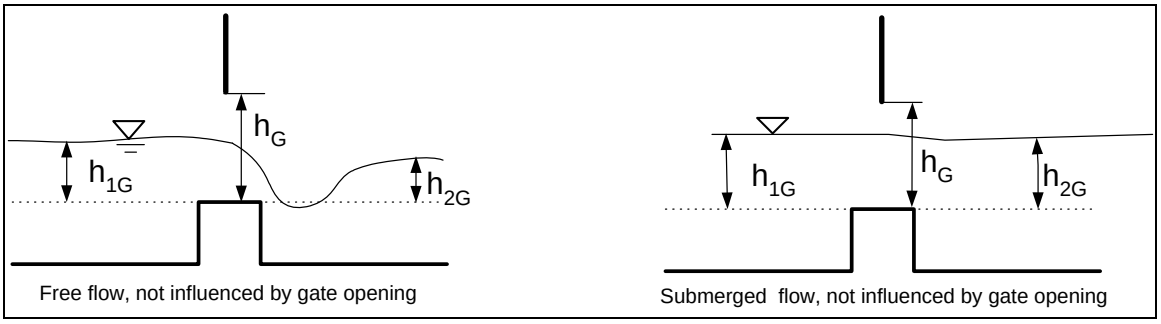

Fig. 3.1-10. Gate Opening Does Not Affect Flow.

$$Q_G = \frac{2}{3\sqrt{3}} C_G h_{1G} B_G \sqrt{h_{1G}} \quad if \quad h_{2G} < \frac{2}{3} h_{1G} \ and \ h_G > \frac{2}{3} h_{1G} \qquad \textbf{(3.1.81)}$$

$$Q_G = C_G B_G h_{2G} \sqrt{h_{1G} - h_{2G}} \quad if \quad h_{1G} > h_{2G} > \frac{2}{3} h_{1G} \ and \ h_G > \frac{2}{3} h_{1G} \qquad \textbf{(3.1.82)}$$

where C_G is the gate coefficient and B_G is the gate width [L]. When the gate opening affects the flow (Fig. 3.1-11), the flow rate is given by

$$Q_G = \frac{2}{3\sqrt{3}} C_G h_G B_G \sqrt{h_{1G}} \quad if \quad h_{2G} < \frac{2}{3} h_{1G} \ and \ h_G < \frac{2}{3} h_{1G} \qquad \textbf{(3.1.83)}$$

$$Q_G = C_G B_G h_G \sqrt{h_{1G} - h_{2G}} \quad if \quad h_{1G} > h_{2G} > \frac{2}{3} h_{1G} \; and \; h_G < \frac{2}{3} h_{1G} \qquad \textbf{(3.1.84)}$$

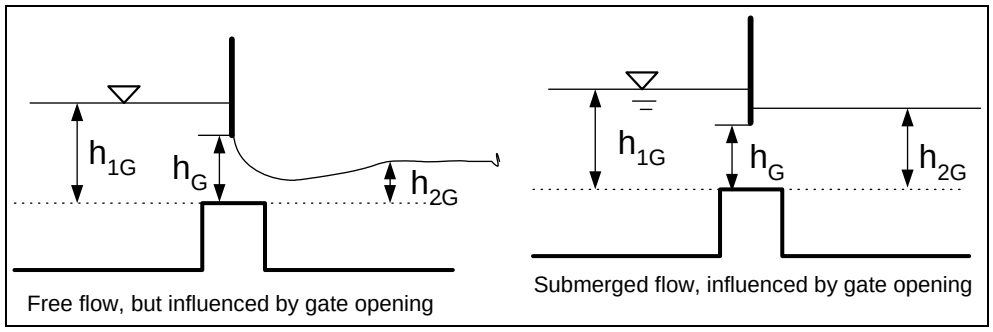

Fig. 3.1-11. Gate Opening Affects Flow.

For two internal boundary nodes separated by a culvert, $Q_{1C} = Q_{2C} = Q_C$. Various formulae for Q_C can be found in the literature.

3.1.2.2 The Hybrid Lagrangian-Eulerian Finite Element Method. When the hybrid Lagrangian-Eulerian finite element method is used to solve the diffusive wave equation, instead of Eq. (3.1.63), using the definition of Q = VA, we expand Eq. (2.1.1) to yield following diffusive wave equation in the Lagrangian form

$$\frac{D_V A}{D\tau} + KA = S_S + S_R - S_E + S_I + S_1 + S_2 \quad where \quad K = \frac{\partial V}{\partial x} \qquad \textbf{(3.1.85)}$$

To use the semi-Lagrangian method to solve the diffusive wave equation, we integrate Eq. (3.1.85) along its characteristic line from x_i at new time level to x_i^* at old time level or on the boundary (Fig. 3.1-12), we obtain

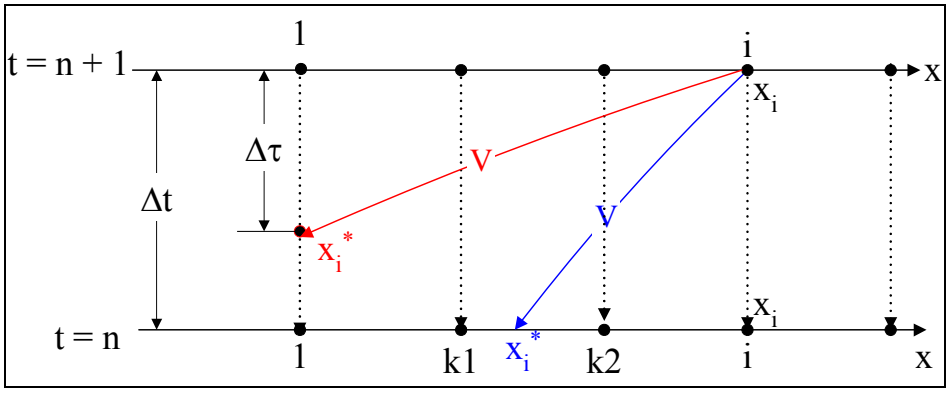

Fig. 3.1-12. Backward Particle Tracking in One Dimension.

$$\left(1+\frac{\Delta\tau}{2}K_i^{(n+1)}\right)A_i^{(n+1)}=\left(1-\frac{\Delta\tau}{2}K_i^{*}\right)A_i^{*}+\frac{\Delta\tau}{2}\left(S_{Si}^{(n+1)}+S_{Si}^{*}\right)+\frac{\Delta\tau}{2}\left(S_{Ri}^{(n+1)}+S_{Ri}^{*}\right)$$
$$-\frac{\Delta\tau}{2}\left(S_{Ei}^{(n+1)}+S_{Ei}^{*}\right)+\frac{\Delta\tau}{2}\left(S_{Ii}^{(n+1)}+S_{Ii}^{*}\right)+\frac{\Delta\tau}{2}\left(S_{1i}^{(n+1)}+S_{1i}^{*}\right)+\frac{\Delta\tau}{2}\left(S_{2i}^{(n+1)}+S_{2i}^{*}\right)$$

or analytically,

$$A_i^{(n+1)}=A_i^{*}e^{-\overline{K}\Delta\tau}+\frac{\overline{SS}}{\overline{K}}\left(1-e^{-\overline{K}\Delta\tau}\right)\quad or\quad A_i^{(n+1)}=\frac{\overline{SS}}{\overline{K}}+\left(A_i^{*}-\frac{\overline{SS}}{\overline{K}}\right)e^{-\overline{K}\Delta\tau} \tag{3.1.86}$$

If $A_i^{(n+1)}<0$ *set* $A_i^{(n+1}=0$, where $\overline{K}=\frac{1}{2}\left(K_i^{(n+1)}+K_i^{*}\right)$ *and*

$$\overline{SS}=\frac{1}{2}\left(\left(S_{Si}^{(n+1)}+S_{Ri}^{(n+1)}-S_{Ei}^{(n+1)}+S_{Ii}^{(n+1)}+S_{1i}^{(n+1)}+S_{2i}^{(n+1)}\right)+\left(S_{Si}^{*}+S_{Ri}^{*}-S_{Ei}^{*}+S_{Ii}^{*}+S_{1i}^{*}+S_{2i}^{*}\right)\right)$$

where $\Delta\tau$ is the tracking time, it is equal to Δt when the backward tracking is carried out all the way to the root of the characteristic and it is less than Δt when the backward tracking hits the boundary before Δt is consumed (Fig. 3.1-12); $K_i^{(n+1)}$, $A_i^{(n+1)}$, $S_{Si}^{(n+1)}$, $S_{Ri}^{(n+1)}$, $S_{Ei}^{(n+1)}$, $S_{Ii}^{(n+1)}$, $S_{1i}^{(n+1)}$, and $S_{2i}^{(n+1)}$ respectively, are the values of K, A, S_S, S_R, S_E, S_I, S_1, and S_2, respectively, at x_i at new time level $t = (n+1)\Delta t$; and K_i^{*}, A_i^{*}, S_{Si}^{*}, S_{Ri}^{*}, S_{Ei}^{*}, S_{Ii}^{*}, S_{1i}^{*}, and $\mathbf{S_{2i}}^{*}$, respectively, are the values of K, A, S_S, S_R, S_E, S_I, S_1, and S_2, respectively, at the location x_i^{*}. Since the velocity V and the decay coefficient K are functions of A, this is a nonlinear hyperbolic problem. Equation (3.1.86) is solved iteratively to yield the cross-sectional area A, and hence the water depth h. The iteration procedure is outlined as follows:

(i) Given the value of $A^{(k)}$ at the *k-th* iteration, compute h and H.
(ii) Apply finite element method to the following equation to obtain V

$$V=\frac{-a}{n}\left[\frac{R}{1+\left(\frac{\partial Z_0}{\partial x}\right)^2}\right]^{2/3}\frac{1}{\sqrt{\left|-\frac{\partial H}{\partial x}-\frac{h}{c\rho}\frac{\partial\Delta\rho}{\partial x}+\frac{B\tau^S}{Ag\rho}\right|}}\left(\frac{\partial H}{\partial x}+\frac{h}{c\rho}\frac{\partial\Delta\rho}{\partial x}-\frac{B\tau^S}{Ag\rho}\right) \tag{3.1.87}$$

(iii) Perform particle tracking to locate x^{*} and obtain all the *-superscripted quantities.
(iv) Apply the finite element method to the following equation to obtain K

$$K=\frac{\partial V}{\partial x} \tag{3.1.88}$$

(v) Solve Eq. (3.1.86) along with the boundary condition to obtain new $A^{(k+1)}$
(vi) Check if $A^{(k+1)}$ converges, if yes go to the next time step.
(vii) If $A^{(k+1)}$ does not converge, update A with $A^{(k)} \leftarrow \omega A^{(k+1)} + (1-\omega)A^{(k)}$ and repeat Steps (i) through (vi).

When the wave is transported out of the region at a boundary node (i.e., when $\mathbf{N}\cdot\mathbf{V} \geq 0$), a boundary condition is not needed. When the wave is transported into the region at a node (i.e., when $\mathbf{N}\cdot\mathbf{V} <$ 0), a boundary condition must be specified. As in the Galerkin finite element method, three types of

boundary conditions may be encountered.

Dirichlet boundary condition:

For the Dirichlet boundary, the water depth is prescribed, thus the cross sectional area, A, is computed from the relationship between the cross section area versus depth curve as

$$H_I = H_{Id}, \quad I \in N_D \Rightarrow A_I = A_{Id}, \quad I \in N_D \tag{3.1.89}$$

Flux boundary condition:

For the flux boundary, the flow rate is prescribed as function of time at the boundary node, from which the boundary value is computed as

$$A^{(n+1)} = \frac{Q_{up}(t)}{V^{(n+1,k)}} \tag{3.1.90}$$

where $Q_{up}(t)$, a function of time t, is the prescribed flow rate [L^3/t] and $V^{(n+1,k)}$ is the value of V at new time and previous iteration.

Water depth-dependent boundary condition: prescribed rating curve

For the boundary where a rating curve is used to describe the relationship between water depth, h, and the discharge, Q, the cross sectional area, A, on the boundary is computed with

$$V^{(n+1,k)} A^{(n+1)} = f(h) \tag{3.1.91}$$

where $f(h)$ is the rating curve which is a function of h. Equation (3.1.91) is solved iteratively to yield $A^{(n+1)}$.

Junction Boundary Condition:

If the node IJ is an internal boundary node that connects a junction J, then H_{IJ} is a function of water depth, h_{IJ-1}, of its immediately internal node and of water surface at the junction J, H_J. This functional relationship is obtained by applying the finite element method to Eq. (3.1.63) to yield the governing equation for *Node IJ* similar to Eqs. (3.1.71) through (3.73)

$$C^1_{1J,1J-1} H^1_{1J-1} + C^1_{1J,1J} H^1_{1J} = L^1_{1J} + Q^1_{1J} + Q^1_{I1J} + Q^1_{11J} + Q^1_{21J} \tag{3.1.92}$$

$$C^2_{2J,2J-1} H^2_{2J-1} + C^2_{2J,2J} H^2_{2J} = L^2_{2J} + Q^2_{2J} + Q^2_{I2J} + Q^2_{12J} + Q^2_{22J} \tag{3.1.93}$$

$$C^3_{3J,3J-1} H^3_{3J-1} + C^3_{3J,3J} H^3_{3J} = L^3_{3J} + Q^3_{3J} + Q^3_{I3J} + Q^3_{13J} + Q^3_{23J} \tag{3.1.94}$$

where the superscript denotes the reach number and subscript denotes node number in a reach, for example, H_{1J}^1 denotes the total head at the *1J-th* node in *Reach 1*. Equation (3.1.92) has two unknowns, H_{1J}^1 and Q_{1J}^1, the unknown $H_{1J\text{-}1}^1$ is obtained by inverting $A_{1J\text{-}1}^1$, which is obtained from

particle tracking in *Reach 1*. Similarly, Equation (3.1.93) has two unknowns, H_{2J}^{2} and Q_{2J}^{2}, and Equation (3.1.94) has two unknowns, H_{3J}^{3} and Q_{3J}^{3}. The number of unknowns (6) is more than the number of equations (3). Three more governing equations must be set up, which can be obtained based on the continuity of energy lines. This is described as follows.

Assume the entrance loss to the junction and exit loss from the junction are negligible, we have the following three equations

$$H_{1j}^{1} + \frac{1}{2g}\left(\frac{Q_{1J}^{1}}{A_{1J}^{1}}\right)^{2} = h_J + Z_{oJ} \qquad \textbf{(3.1.95)}$$

$$H_{2j}^{2} + \frac{1}{2g}\left(\frac{Q_{2J}^{2}}{A_{2J}^{2}}\right)^{2} = h_J + Z_{oJ} \qquad \textbf{(3.1.96)}$$

$$H_{3j}^{3} + \frac{1}{2g}\left(\frac{Q_{3J}^{3}}{A_{3J}^{3}}\right)^{2} = h_J + Z_{oJ} \qquad \textbf{(3.1.97)}$$

where A_{1J}^{1}, A_{2J}^{2}, and A_{3J}^{3} are the cross-sectional area at Nodes *1J* of Reach *1*, Node *2J* of Reach *2*, and Node *3J* of Reach *3*, respectively; h_J is the water depth at the Junction *J*; and Z_{oJ} is the bottom elevation at the Junction *J*. It is noted that the second terms on the left hand side of Eqs. (3.1.95) through (3.1.97) are generally ignored in computation implementation to give more robust solutions.

The water depth at Junction *J* is not decoupled from river/stream/canal reaches. The water budget equation for the Junction J is

$$\frac{d\forall_J}{dh_J}\frac{dh_J}{dt} = \sum_{i=1}^{i=3} Q_{iJ}^{i} \qquad \textbf{(3.1.98)}$$

When $\frac{d\forall_J}{dh_J}$ is small, the water budget Eq. (3.1.98) is not employed. Instead, the following equation, resulting from the requirement that the summation of flow rates is equal to zero, is used

$$\sum_{i=3}^{i=3} Q_{iJ}^{i} = 0 \qquad \textbf{(3.1.99)}$$

Equations (3.1.92) through (3.1.97) and Eq. (3.1.98) or Eq. (3.1.99) constitute 7 equations for seven unknowns, A_{1J}^{1}, A_{2J}^{2}, A_{3J}^{3}, Q_{1J}^{1}, Q_{2J}^{2}, Q_{3J}^{3}, and h_J. These equations should be solved iteratively along with particle tracking for all internal nodes of the three reaches connecting the junction node J. The seven linearized equations can be solved with the Gaussian direct elimination with full pivoting.

Control structure boundary condition:

To facilitate the implementation of internal boundary conditions of control structures, we discretize

the two internal boundary nodes of every structure with the finite element method. Then we can implement the boundary conditions similar to that in finite element modeling of diffusive wave approaches.

3.1.3 The Semi-Lagrangian Method for Kinematic Wave

To use the Lagrangian method to solve the kinematic wave equation, Eq. (2.1.65) is rewritten in the Lagrangian form as follows

$$\frac{D_V A}{D\tau} + KA = S_S + S_R - S_E + S_I + S_1 + S_2 \quad where \quad K = \frac{\partial V}{\partial x} \tag{3.1.100}$$

in which K is the decay coefficient of the wave and S is the source/sink of the wave. Integrating Eq. (3.1.100) along its characteristic line from x_i at new time level to x_i^* (Fig. 3.1-12), we obtain

$$\left(1+\frac{\Delta\tau}{2}K_i\right)A_i^{(n+1)} = \left(1-\frac{\Delta\tau}{2}K_i^*\right)A_i^* + \frac{\Delta\tau}{2}\left(S_{Si}^{(n+1)} + S_{Si}^*\right) + \frac{\Delta\tau}{2}\left(S_{Ri}^{(n+1)} + S_{Ri}^*\right)$$
$$-\frac{\Delta\tau}{2}\left(S_{Ei}^{(n+1)} + S_{Ei}^*\right) + \frac{\Delta\tau}{2}\left(S_{Ii}^{(n+1)} + S_{Ii}^*\right) + \frac{\Delta\tau}{2}\left(S_{Ii}^{(n+1)} + S_{Ii}^*\right) + \frac{\Delta\tau}{2}\left(S_{2i}^{(n+1)} + S_{2i}^*\right)$$

or analytically,

$$A_i^{(n+1)} = A_i^* e^{-\overline{K}\Delta\tau} + \frac{\overline{SS}}{\overline{K}}\left(1-e^{-\overline{K}\Delta\tau}\right) \quad or \quad A_i^{(n+1)} = \frac{\overline{SS}}{\overline{K}} + \left(A_i^* - \frac{\overline{SS}}{\overline{K}}\right)e^{-\overline{K}\Delta\tau} \tag{3.1.101}$$

If $A_i^{(n+1)} < 0$ *set* $A_i^{(n+1} = 0$, where $\overline{K} = \frac{1}{2}\left(K_i^{(n+1)} + K_i^*\right)$ *and*

$$\overline{SS} = \frac{1}{2}\left(\left(S_{Si}^{(n+1)} + S_{Ri}^{(n+1)} - S_{Ei}^{(n+1)} + S_{Ii}^{(n+1)} + S_{1i}^{(n+1)} + S_{2i}^{(n+1)}\right) + \left(S_{Si}^* + S_{Ri}^* - S_{Ei}^* + S_{Ii}^* + S_{1i}^* + S_{2i}^*\right)\right)$$

where $\Delta\tau$ is the tracking time, it is equal to Δt when the backward tracking is carried out all the way to the root of the characteristic and it is less than Δt when the backward tracking hits the boundary before Δt is consumed (Fig. 3.1-12); $K_i^{(n+1)}$, $A_i^{(n+1)}$, $S_{Si}^{(n+1)}$, $S_{Ri}^{(n+1)}$, $S_{Ei}^{(n+1)}$, $S_{Ii}^{(n+1)}$, $S_{1i}^{(n+1)}$, and $S_{2i}^{(n+1)}$ respectively, are the values of K, A, S_S, S_R, S_E, S_I, S_1, and S_2, respectively, at x_i at new time level $t = (n+1)\Delta t$; and K_i^*, A_i^*, S_{Si}^*, S_{Ri}^*, S_{Ei}^*, S_{Ii}^*, S_{1i}^*, and S_{2i}^*, respectively, are the values of K, A, S_S, S_R, S_E, S_I, S_1, and S_2, respectively, at the location x_i^*. Because of density and wind effects, the velocity V and the decay coefficient K are functions of A, this is nonlinear problem. However, because the nonlinearity due to density and wind effects are normally very weak, Equation (3.1.101) is considered a linear hyperbolic problem with the nonlinear effects evaluated using the values of A at previous time. This equation is used to compute the cross-sectional area A, and hence the water depth h, at all nodes except for the upstream boundary node.

Because the wave is transported into the region at an upstream node, a boundary condition must be specified. The flow rate is normally given as a function of time at an upstream node, from which the boundary value is computed as

$$A_i^{(n+1)} = \frac{Q_{up}(t)}{V_i^{(n+1)}} \tag{3.1.102}$$

where $Q_{up}(t)$, a function of time t, is the prescribed flow rate [L^3/t].

3.1.4 Numerical Approximations of Thermal Transport

Two options are provided in this report to solve the thermal transport equation. One is the finite element method and the other is the particle tracking method.

3.1.4.1 Finite Element Method. Recall the thermal transport equation is governed by Eq. (2.1.67) which is rewritten in a slightly different form as

$$\begin{aligned} &\rho_W C_W A\frac{\partial T}{\partial t} + \frac{\partial(\rho_W C_W A)}{\partial t}T + \frac{\partial(\rho_W C_W QT)}{\partial x} - \frac{\partial}{\partial x}\left(D^H A\frac{\partial T}{\partial x}\right) \\ &\quad = S_h^a + S_h^r + S_h^n - S_h^b - S_h^e - S_h^s + S_h^i + S_h^{o1} + S_h^{o2} + S_h^c \end{aligned} \tag{3.1.103}$$

Applying the finite element method to Eq. (3.1.103), we obtain the following matrix equation

$$\begin{aligned} &[M]\frac{d\{T\}}{dt} + [V]\{T\} + [D]\{T\} + [K]\{T\} = -\{\Phi_B\} + \{\Phi^a\} \\ &\quad + \{\Phi^r\} + \{\Phi^n\} - \{\Phi^b\} - \{\Phi^e\} - \{\Phi^s\} + \{\Phi^i\} + \{\Phi^{o1}\} + \{\Phi^{o2}\} + \{\Phi^c\} \end{aligned} \tag{3.1.104}$$

in which

$$\begin{aligned} &M_{ij} = \int_{X_1}^{X_N} N_i \rho_W C_W A N_j dx, \quad V_{ij} = \int_{X_1}^{X_N} \frac{dW_i}{dx}\rho_W C_W Q N_j dx, \quad D_{ij} = \int_{X_1}^{X_N} \frac{dN_i}{dx} D^H A \frac{dN_j}{dx} dx, \\ &K_{ij} = \int_{X_1}^{X_N} N_i \frac{\partial \rho_W C_W A}{\partial t} N_j dx, \quad \Phi_{Bi} = \left(W_i \rho_W C_W QT - N_i D^H A \frac{\partial T}{\partial x}\right)\Big|_{x+X_1}^{x=X_N} \end{aligned} \tag{3.1.105}$$

$$\Phi_i^a = \int_{X_1}^{X_N} N_i S_h^a dx, \quad \Phi_i^r = \int_{X_1}^{X_N} N_i S_h^r dx, \quad \Phi_i^n = \int_{X_1}^{X_N} N_i S_h^n dx \tag{3.1.106}$$

$$\Phi_i^b = \int_{X_1}^{X_N} N_i S_h^b dx, \quad \Phi_i^e = \int_{X_1}^{X_N} N_i S_h^e dx, \quad \Phi_i^s = \int_{X_1}^{X_N} N_i S_h^s dx, \quad \Phi_i^c = \int_{X_1}^{X_N} N_i S_h^c dx, \tag{3.1.107}$$

$$\Phi_i^i = \int_{X_1}^{X_N} N_i S_h^i dx, \quad \Phi_i^{o1} = \int_{X_1}^{X_N} N_i S_h^{o1} dx, \quad \Phi_i^{o2} = \int_{X_1}^{X_N} N_i S_h^{o2} dx \tag{3.1.108}$$

where $W_i(x)$ is the weighting function of node at x_i; $N_i(x)$ and $N_j(x)$, functions of x, are the base functions of nodes at x_i and x_j, respectively; [M] is the mass matrix, [V] is the stiff matrix due to advective transport; [D] is the stiff matrix due to dispersion/diffusion/conduction; {T} is the solution vector of temperature; $\{\Phi_B\}$ is the vector due to boundary conditions, which can contribute to load

vector and/or coefficient matrix; $\{\Phi^a\}$ is the load vector due to artificial energy source; $\{\Phi^r\}$ is the load vector due to energy in rainfall; $\{\Phi^n\}$ is the load vector due to net radiation; $\{\Phi^b\}$ is the vector due to backward radiation, which is a nonlinear function of temperature and contributes to both the load vector and coefficient matrix; $\{\Phi^e\}$ is the vector due to energy consumed for evaporation, which is a nonlinear function of temperature and contributes to both the load vector and coefficient matrix; $\{\Phi^s\}$ is the vector due to sensible heat, which is a linear function of temperature and contributes to both the load vector and coefficient matrix; $\{\Phi^c\}$ is the vector due to chemical reaction, which is not considered in this version, but can be added easily; $\{\Phi^i\}$ is the vector due to interaction with subsurface exfiltraing water; $\{\Phi^{o1}\}$ is the vector due to interaction with overland water via river bank 1; and $\{\Phi^{o2}\}$ is the vector due to interaction with overland water via river bank 2.

Approximating the time derivative term in Eq. (3.1.104) with a time-weighted finite difference, we reduce the advective-diffusive equation and its boundary conditions to the following matrix equation

$$[C]\{T\} = \{L\} - \{\Phi_B\} - \{\Phi^b\} - \{\Phi^e\} - \{\Phi^s\} + \{\Phi^i\} + \{\Phi^{o1}\} + \{\Phi^{o2}\} \qquad \textbf{(3.1.109)}$$

in which

$$[C] = \frac{[M]}{\Delta t} + \theta([D] + [K]) + \theta_V [V],$$
$$\{L\} = \left(\frac{[M]}{\Delta t} - (1-\theta)([DS] + [K]) - (1-\theta_V)[V] \right) \{T^{(n)}\} + \{\Phi^a\} + \{\Phi^r\} + \{\Phi^n\} \qquad \textbf{(3.1.110)}$$

where [C] is the coefficient matrix, {L} is the load vector from initial condition, artificial sink/sources, rainfall, and net radiation; Δt is the time step size; θ is the time weighting factor for the dispersion and linear terms; θ_v is the time weighting factor for the velocity term; and $\{T^{(n)}\}$ is the value of {T} at old time level n. The global and internal boundary (junctions, weirs, and gates) conditions must be used to provide $\{\Phi_B\}$ in Eq. (3.1.109). The interaction between the overland and river/stream/canal flows must be implemented to evaluate $\{\Phi^{o1}\}$ and $\{\Phi^{o2}\}$; and the interaction between the subsurface and river/stream/canal flows must be implemented to calculate $\{\Phi^i\}$. The interactions will be addressed in Section 3.4.

For a global boundary node I, the corresponding algebraic equation from Eq. (3.1.109) is

$$C_{I,I-1}T_{I-1} + C_{I,I}T_I + C_{I,I+1}T_{I+1} = L_I - \left(\Phi_I^b + \Phi_I^e + \Phi_I^s\right) + \left(\Phi_I^i + \Phi_I^{o1} + \Phi_I^{o2}\right) - \Phi_{BI} \qquad \textbf{(3.1.111)}$$

In the above equations there are two unknowns T_I and Φ_{BI}; either T_I or Φ_{BI}, or the relationship between T_I and Φ_{BI} must be specified. The numerical implementation of these boundary conditions is described as follows.

Direchlet boundary condition: prescribed temperature

If T_I is given on the boundary node I (Dirichlet boundary condition), all coefficients ($C_{I,I-1}$, $C_{I,I}$, $C_{I,I+1}$) and right-hand side (L_I, Φ_I^b, Φ_I^e, Φ_I^s, Φ_I^i, Φ_I^{o1}, Φ_I^{o2}) obtained before the implementation of boundary conditions for this equation are stored in a temporary array, then an identity equation is created as

$$T_I = T_{Id}, \quad I \in N_D \tag{3.1.112}$$

where T_{Id} is the prescribed temperature on the Dirichlet node I and N_D is the number of Dirichlet boundary nodes. This process is repeated for every Dirichlet nodes. Note it is unnecessary to modify other equations that involving these unknowns, which was done in the previous version. By not modifying other equations, the symmetrical property of the matrix is preserved, which makes the iterative solvers more robust. The final set of equations will consist of N_D identity equations and (N - N_D) finite element equations for N unknowns T_i's. After T_i's for all nodes are solved from the matrix equation, Eq. (3.1.111) is then used to back calculate N_D Φ_{BI}'s.

If a direct solver is used to solve the matrix equation, the above procedure will solve N T_i's accurately except for roundoff errors. However, if an iterative solver is used, stopping criteria must be strict enough so that the converged solutions of N T_i's are accurate enough to the exact solution. With such accurate T_i's, then can be sure that the back-calculated ND Φ_{BI}'s are accurate.

Cauchy boundary condition: prescribed heat flux

If Φ_{BI} is given (Cauchy flux boundary condition), all coefficients ($C_{I,I-1}$, $C_{I,I}$, $C_{I,I+1}$) and right-hand side (L_I, Φ_I^a, Φ_I^r, Φ_I^n, Φ_I^i, Φ_I^{o1}, Φ_I^{o2}) obtained before the implementation of boundary conditions for this equation are stored in a temporary array, then Eq. (3.1.111) is modified to incorporate the boundary conditions and used to solve for T_I. The modification of Eq. (3.1.111) is straightforward. Because Φ_{BI} is a known quantity, it contributes to the load on the right hand side. This type of boundary conditions is very easy to implement. After T_i's are obtained, the original Eq. (3.1.111), which is stored in a temporary array, is used to back calculate N_C Φ_{BI}'s on flux boundaries (where N_C is the number of flux boundary nodes). These back-calculated Φ_{BI}'s should be theoretically identical to the input Φ_{BI}'s. However, because of round-off errors (in the case of direct solvers) or because of stopping criteria (in the case of iterative solvers), the back-calculated Φ_{BI}'s will be slightly different from the input Φ_{BI}'s. If the differences between the two are significant, it is an indication that the solvers have not yielded accurate solutions.

Neumann boundary condition: prescribed gradient of temperature

At Neumann boundaries, the temperature gradient is prescribed, thus, the flux due to temperature gradient is given. For this case, all coefficients ($C_{I,I-1}$, $C_{I,I}$, $C_{I,I+1}$) and right-hand side (L_I, Φ_I^a, Φ_I^r, Φ_I^n, Φ_I^i, Φ_I^{o1}, Φ_I^{o2}) obtained before the implementation of boundary conditions for this equation are stored in a temporary array, then Eq. (3.1.111) is modified to incorporate the boundary conditions and used to solve for T_I. For the Neumann boundary condition, Φ_{BI} contributes to both the matrix coefficient and load vector, thus both the coefficient matrix [C] and the load vector {L} must be modified. Recall

$$\Phi_{Bi} = \left(W_i \rho_W C_W Q T - N_i D^H A \frac{\partial T}{\partial x} \right) \Big|_{\substack{x=X_N \\ x=X_1}} \tag{3.1.113}$$

Apply this equation to Node I, we have

$$\Phi_{BI} \equiv n_I \rho_W C_W Q T_I - n_I D^H A \frac{\partial T}{\partial x}\Big|_{x=X_I} = n_I \rho_W C_W Q T_I - \Phi_{nbI} \qquad \textbf{(3.1.114)}$$

where n_I is the unit outward normal vector at the boundary node I, Φ_{nbI} is the Neumann boundary flux at node I. Substitution of Eq. (3.1.114) into Eq. (3.1.111), we have the modified coefficient matrix and load vector; thus the modified Eq. (3.1.111). This modified equation is used to solve T_I. After T_I is solved, the original Eq. (3.1.111) (recall the original Eq. (3.1.111) must be and has been stored in a temporary array) is used to back-calculate Φ_{BI}.

Variable Boundary Condition:

At the variable boundary condition Node I, the implementation of boundary conditions can be made identical to that for a Cauchy boundary condition node if the flow is directed into the river/stream/canal reach. If the flow is going out of the reach, the boundary condition is implemented similar to the implementation of Neuman boundary condition with $\Phi_{nbI} = 0$. The assumption of zero Neumann flux implies that a Neuman node must be far away from the source/sink.

Junction boundary condition:

If the node IJ is an internal node that connects a junction J, then node IJ is treated as an internal boundary node. For example, consider three reaches with three internal nodes connecting to the junction J (Fig. 3.1-8). After applying the finite element method to Eq. (3.1.103), we have a total of (1J + 2J + 3J) algebraic equations. The algebraic equations for Nodes 1J, 2J, and 3J can be written based on Eq. (3.1.111)

$$C^1_{1J,1J-1}T^1_{1J-1} + C^1_{1J,1J}T^1_{1J} = L^1_{1J} - \left(\Phi^{b1}_{1J} + \Phi^{e1}_{1J} + \Phi^{s1}_{1J}\right) + \left(\Phi^{i1}_{1J} + \Phi^{o11}_{1J} + \Phi^{o21}_{1J}\right) - \Phi^1_{1J} \qquad \textbf{(3.1.115}$$

$$C^2_{2J,2J-1}T^2_{2J-1} + C^2_{2J,2J}T^2_{2J} = L^2_{2J} - \left(\Phi^{b2}_{2J} + \Phi^{e2}_{2J} + \Phi^{s2}_{2J}\right) + \left(\Phi^{i2}_{2J} + \Phi^{o12}_{2J} + \Phi^{o22}_{2J}\right) - \Phi^2_{2J} \qquad \textbf{(3.1.116}$$

$$C^3_{3J,3J-1}T^3_{3J-1} + C^3_{3J,3J}T^3_{3J} = L^3_{3J} - \left(\Phi^{a3}_{3J} + \Phi^{r3}_{3J} + \Phi^{n3}_{3J}\right) + \left(\Phi^{i3}_{3J} + \Phi^{o13}_{3J} + \Phi^{o23}_{3J}\right) - \Phi^3_{3J} \qquad \textbf{(3.1.117}$$

where the superscript denotes the reach number and subscript denotes local node number in a reach, for example, $T_{1J}{}^1$ denotes the temperature at the 1J-th node in Reach 1. For a convenient discussion, let us associate each of the unknowns, $T_1{}^1$, - - $T_{1J-1}{}^1$ to each of the 1J-1 finite element equations in Reach 1. Similarly, we associate each of the unknowns, $T_1{}^2$, - - $T_{2J-2}{}^2$ to each of the 2J-1 finite element equations in Reach 2 and each of the unknowns and $T_1{}^3$, - - $T_{3J-1}{}^3$ to each of the 3J-1 finite element equations in Reach 3. The unknown, $\Phi_{1J}{}^1$, $\Phi_{2J}{}^2$, and $\Phi_{3J}{}^3$, are absent from these (1J-1 + 2J-1 + 3J-1) equations. In other words, we can say each equation governs one unknown. However, two unknowns, $T_{1J}{}^1$ and $\Phi_{1J}{}^1$, appear in Eq. (3.1.115). Similarly, Equation (3.1.116) has two unknowns, $T_{2J}{}^2$ and $\Phi_{2J}{}^2$, and Equation (3.1.117) has two unknowns, $T_{3J}{}^3$ and $\Phi_{3J}{}^3$. The number of unknowns, (1J + 2J + 3J) temperatures and $\Phi_{1J}{}^1$, $\Phi_{2J}{}^2$, and $\Phi_{3J}{}^3$, is more than the number of equations, (1J + 2J + 3J) finite element equations. Three more governing equations must be set up, which can be obtained with the assumption that the energy flux is due mainly to advection as

$$\Phi_{1J}^{1} \equiv \left(\rho_W C_W QT - D^H A \frac{\partial T}{\partial x} \right)\Big|_{1J}$$
$$= \rho_W C_W \frac{1}{2} Q_{1J}^{1} \left[\left(1 + sign\left(Q_{1J}^{1}\right)\right) T_{1J}^{1} + \left(1 - sign\left(Q_{1J}^{1}\right)\right) T_J \right] \quad \textbf{(3.1.118)}$$

$$\Phi_{2J}^{2} \equiv \left(\rho_W C_W QT - D^H A \frac{\partial T}{\partial x} \right)\Big|_{2J}$$
$$= \rho_W C_W \frac{1}{2} Q_{2J}^{2} \left[\left(1 + sign\left(Q_{2J}^{2}\right)\right) T_{2J}^{2} + \left(1 - sign\left(Q_{2J}^{2}\right)\right) T_J \right] \quad \textbf{(3.1.119)}$$

$$\Phi_{3J}^{3} \equiv \left(\rho_W C_W QT - D^H A \frac{\partial T}{\partial x} \right)\Big|_{3J}$$
$$= \rho_W C_W \frac{1}{2} Q_{3J}^{3} \left[\left(1 + sign\left(Q_{3J}^{3}\right)\right) T_{3J}^{3} + \left(1 - sign\left(Q_{3J}^{3}\right)\right) T_J \right] \quad \textbf{(3.1.120}$$

where $Q_{1J}{}^1$, $Q_{2J}{}^2$, and $Q_{3J}{}^3$, respectively, are the volumetric flow rates from/to Nodes 1J, 2J, and 3J, respectively, to/from the junction J [cf. Eqs. (3.1.71), (3.1.72), and (3.1.73), respectively].

Equations (3.1.118) through (3.1.120) introduce one additional unknown, T_J. One additional equation must be set up which can be done based on the energy budget at the junction J. The rate of change of energy at the junction J must be equal to the net energy rate from all reaches that join at J. This energy budget can be written as

$$\frac{d\left(\rho_W C_W V_J T_J\right)}{dt} = \sum_i \Phi_{iJ}^{i} \quad \textbf{(3.1.121)}$$

When the storage effect of the junction is small, the energy budget Eq. (3.1.121) is not employed. Instead, the following equation, resulting from the requirement that the summation of heat flux is equal to zero, is used

$$\sum_{i=1}^{i=3} \Phi_{iJ}^{i} = 0 \quad \textbf{(3.1.122)}$$

Equations (3.1.115) through (3.1.120) and Eq. (3.1.121) or Eq. (3.1.122) constitute 7 equations for seven unknowns, $T_{1J}{}^1$, $T_{2J}{}^2$, $T_{3J}{}^3$, $\Phi_{1J}{}^1$, $\Phi_{2J}{}^2$, $\Phi_{3J}{}^3$, and T_J. If there are N_J junctions, there will be N_J blocks of seven equations. These N_J blocks of equations should be solved iteratively along with N_R block of finite element equations where N_R is the number of reaches. In other words, the whole system of algebraic equations can be solved with block iterations. Each block of equations can be solved directly. For example, each of N_R blocks of finite element equations can be solved with an efficient tri-diagonal matrix solver such as the Thomas algorithm. Each of the N_J blocks of seven equations can be solved with the Gaussian direct elimination with full pivoting.

Control structure boundary condition:

The control structures may include weirs, gates, culverts, etc. For the two internal boundary nodes 1S and 2S separated by a structure, the boundary conditions at these two nodes are given by

$$\Phi_{1S} \equiv \left(\rho_W C_W QT - D^H A \frac{\partial T}{\partial x} \right)\Big|_{1S} = \rho_W C_W \frac{1}{2} Q[(1 + sign(Q))T_{1S} + (1 - sign(Q))T_{2S}] \quad \textbf{(3.1.123)}$$

$$\Phi_{2S} \equiv \left(\rho_W C_W QT - D^H A \frac{\partial T}{\partial x} \right)\Big|_{2S} = \rho_W C_W \frac{1}{2} Q[(1 + sign(Q))T_{1S} + (1 - sign(Q))T_{2S}] \quad \textbf{(3.1.124)}$$

where Φ_{1S} is the energy flux through node 1S; Φ_{2s} is the energy flux through node 2S; and Q is the flow rate through the structure S; sign(Q) is equal 1.0 if the flow is from node 1S to node 2S, -1.0 if flow is from node 2S to node 1S; T_{1S} is the temperature at node 1S; and T_{2S} is the temperature at node 2S.

3.1.4.2 The Hybrid Lagrangian-Eulerian Finite Element Method. When the hybrid Lagrangian-Eulerian finite element method is used to solve the thermal transport equation, we expand Eq. (3.1.103) to yield following advection-dispersion equation in the Lagrangian form

$$\frac{D_V T}{Dt} + KT = D + \Phi^S + \Phi^I + \Phi^{O1} + \Phi^{O2} \quad where \quad V = \frac{Q}{A} \qquad \textbf{(3.1.125)}$$

in which

$$K = \frac{1}{\rho_W C_W A}\frac{\partial \rho_W C_W A}{\partial t} + \frac{1}{\rho_W C_W A}\frac{\partial \rho_W C_W Q}{\partial x}, \quad D = \frac{1}{\rho_W C_W A}\frac{\partial}{\partial x}\left(D^H A \frac{\partial T}{\partial x} \right)$$

$$\Phi^S = \frac{S_h^a + S_h^r + S_h^n - S_h^b - S_h^e - S_h^s}{\rho_W C_W A}, \qquad \textbf{(3.1.126)}$$

$$and \quad \Phi^I = \frac{S_h^i}{\rho_W C_W A}, \quad \Phi^{O1} = \frac{S_h^{o1}}{\rho_W C_W A}, \quad \Phi^{O2} = \frac{S_h^{o2}}{\rho_W C_W A}$$

To use the semi-Lagrangian method to solve the thermal transport equation, we integrate Eq. (3.1.125) along its characteristic line from x_i at new time level to x_i^* (Fig. 3.1-12), we obtain

$$\left(1 + \frac{\Delta\tau}{2} K_i^{(n+1)}\right) T_i^{(n+1)} = \left(1 - \frac{\Delta\tau}{2} K_i^*\right) T_i^* + \frac{\Delta\tau}{2}\left(D_i^{(n+1)} + D_i^*\right) + \frac{\Delta\tau}{2}\left(\Phi_i^{S^{(n+1)}} + \Phi_i^{S^*}\right)$$
$$+ \frac{\Delta\tau}{2}\left(\Phi_i^{I^{(n+1)}} + \Phi_i^{I^*}\right) + \frac{\Delta\tau}{2}\left(\Phi_i^{O1^{(n+1)}} + \Phi_i^{O1^*}\right) + \frac{\Delta\tau}{2}\left(\Phi_i^{O2^{(n+1)}} + \Phi_i^{O2^*}\right), \quad i \in N \qquad \textbf{(3.1.127)}$$

where $\Delta\tau$ is the tracking time, it is equal to Δt when the backward tracking is carried out all the way to the root of the characteristic and it is less than Δt when the backward tracking hits the boundary before Δt is consumed; $K_i^{(n+1)}$, $T_i^{(n+1)}$, $D_i^{(n+1)}$, $\Phi_i^{S(n+1)}$, $\Phi_i^{I(n+1)}$, $\Phi_i^{O1(n+1)}$, and $\Phi_i^{O2(n+1)}$ respectively, are the values of K, T, D, Φ^S, Φ^I, Φ^{O1}, and Φ^{O2}, respectively, at x_i at new time level $t = (n+1)\Delta t$; and K_i^*, T_i^*, D_i^*, Φ_i^{S*}, Φ_i^{I*}, Φ_i^{O1*}, and Φ_i^{O2*}, respectively, are the values of K, T, D, Φ^S, Φ^I, Φ^{O1}, and Φ^{O2}, respectively, at the location x_i^*.

To compute the dispersion/diffusion terms $D_i^{(n+1)}$ and D_i^*, we rewrite the second equation in Eq.

(3.1.126) as

$$\rho_W C_W AD = \frac{\partial}{\partial x}\left(D^H A \frac{\partial T}{\partial x} \right) \qquad \textbf{(3.1.128)}$$

Applying the Galerkin finite element method to Eq. (3.1.128) at new time level (n+1), we obtain the following matrix equation for $\{D^{(n+1)}\}$ as

$$\left[a^{(n+1)}\right]\left\{D^{(n+1)}\right\} + \left[b^{(n+1)}\right]\left\{T^{(n+1)}\right\} = \left\{B^{(n+1)}\right\} \qquad \textbf{(3.1.129)}$$

in which

$$\left\{D^{(n+1)}\right\} = \left\{D_1^{(n+1)} \quad D_2^{(n+1)} \quad . \quad . \quad D_i^{(n+1)} \quad . \quad . \quad D_N^{(n+1)}\right\}^{Transpose} \qquad \textbf{(3.1.130)}$$

$$\left\{T^{(n+1)}\right\} = \left\{T_1^{(n+1)} \quad T_2^{(n+1)} \quad . \quad . \quad T_i^{(n+1)} \quad . \quad . \quad T_N^{(n+1)}\right\}^{Transpose} \qquad \textbf{(3.1.131)}$$

$$\left\{B^{(n+1)}\right\} = \left\{B_1^{(n+1)} \quad B_2^{(n+1)} \quad . \quad . \quad B_i^{(n+1)} \quad . \quad . \quad B_N^{(n+1)}\right\}^{Transpose} \qquad \textbf{(3.1.132)}$$

$$a_{ij}^{(n+1)} = \int_{X_1}^{X_N} N_i \left(\rho_W C_W A\right)\Big|_{(n+1)} N_j dx, \quad b_{ij}^{(n+1)} = \int_{X_1}^{X_N} \frac{dN_i}{dx}\left(D^H A\right)\Big|_{(n+1)} \frac{dN_j}{dx} dx,$$
$$B_i^{(n+1)} = N_i \left(D^H A\right)\Big|_{(n+1)} \frac{\partial T^{(n+1)}}{\partial x}\Big|_{X=X_1}^{X=X_N} \qquad \textbf{(3.1.133)}$$

where the superscript (n+1) denotes the time level; N_i and N_j are the base functions of nodes at x_i and x_j, respectively.

Lumping the matrix $[a^{(n+1)}]$, we can solve Eq. (3.1.129) for $D_I^{(n+1)}$ as follows

$$\begin{aligned} D_I^{(n+1)} &= -\frac{1}{a_{II}^{(n+1)}} \sum_j b_{Ij}^{(n+1)} T_j^{(n+1)} \quad if \quad I \in \{2,3,..,N-1\} \\ D_I^{(n+1)} &= \frac{1}{a_{II}^{(n+1)}} B_1^{(n+1)} - \frac{1}{a_{II}^{(n+1)}} \sum_j b_{Ij}^{(n+1)} T_j^{(n+1)} \quad if \quad I \in \{1,N\} \end{aligned} \qquad \textbf{(3.1.134)}$$

where $a_{II}^{(n+1)}$ is the lumped $a_{ii}^{(n+1)}$. Following the identical procedure that leads Eq. (3.1.128) to Eq. (3.1.134), we have

$$\begin{aligned} D_I^{(n)} &= -\frac{1}{a_{II}^{(n)}} \sum_j b_{Ij}^{(n)} T_j^{(n)} \quad if \quad I \in \{2,3,..,N-1\} \\ D_I^{(n)} &= \frac{1}{a_{II}^{(n)}} B_1^{(n)} - \frac{1}{a_{II}^{(n)}} \sum_j b_{Ij}^{(n)} T_j^{(n)} \quad if \quad I \in \{1,N\} \end{aligned} \qquad \textbf{(3.1.135)}$$

where $\{B^{(n)}\}$, $\{a^{(n)}\}$ and $\{b^{(n)}\}$, respectively, are defined similar to $\{B^{(n+1)}\}$, $\{a^{(n+1)}\}$ and $\{b^{(n+1)}\}$, respectively.

With $\{D^{(n)}\}$ calculated with Eq. (3.1.135), $\{D^*\}$ can be interpolated. Substituting Eq. (3.1.134) into

Eq. (3.1.127) and implementing boundary conditions given in Section 2.1.4, we obtain a system of N simultaneous algebraic equations N unknowns ($T_i^{(n+1)}$ for i = 1, 2, .., N.) If the dispersion/diffusion term is not included, then Eq. (3.1.127) is reduced to a set of N decoupled equations as

$$a_{ii}T_i^{(n+1)} = b_i, i \in N \tag{3.1.136}$$

where

$$a_{ii} = \left(1 + \frac{\Delta\tau}{2}K_i^{(n+1)}\right) \tag{3.1.137}$$

$$\begin{aligned} b_i = &\left(1 - \frac{\Delta\tau}{2}K_i^*\right)T_i^* + \frac{\Delta\tau}{2}\left(\Phi_i^{S^{(n+1)}} + \Phi_i^{S*}\right) \\ &+ \frac{\Delta\tau}{2}\left(\Phi_i^{I^{(n+1)}} + \Phi_i^{I*}\right) + \frac{\Delta\tau}{2}\left(\Phi_i^{O1^{(n+1)}} + \Phi_i^{O1*}\right) + \frac{\Delta\tau}{2}\left(\Phi_i^{O2^{(n+1)}} + \Phi_i^{O2*}\right), \quad i \in N \end{aligned} \tag{3.1.138}$$

Equations (3.1.136) is applied to all interior nodes without having to make any modification. On a boundary point, there two possibilities: Eq. (3.1.136) is replaced with a boundary equations when the flow is directed into the reach or Eq. (3.1.136) is still valid when the flow is direct out of the reach. In other words, when the thermal energy is transported out of the region at a boundary node (i.e., when $\mathbf{n}\bullet\mathbf{V} \geq 0$), a boundary condition is not needed and Equation (3.1.136) is used to compute the $T_i^{(n+1)}$. When the thermal energy is transported into the region at a node (i.e., when $\mathbf{n}\bullet\mathbf{V} < 0$), a boundary condition must be specified.

Alternatively, to facilitate the implementation of boundary condition at incoming flow node, the algebraic equation for the boundary node is obtained by applying the finite element method to the boundary node. For this alternative approach, the implementation of boundary conditions at global boundary nodes, internal junction nodes, and internal nodes connecting to control structures is identical to that in the finite element approximation of solving the thermal transport equation.

3.1.5 Numerical Approximations of Salinity Transport

Two options are provided in this report to solve the salinity transport equation. One is the finite element method and the other is the particle tracking method.

3.1.5.1 Finite Element Method. Recall the salinity transport equation is governed by Eq. (2.1.86) which is rewritten in a slightly different form as

$$A\frac{\partial S}{\partial t} + \frac{\partial A}{\partial t}S + \frac{\partial (QS)}{\partial x} - \frac{\partial}{\partial x}\left(D^S A\frac{\partial S}{\partial x}\right) = M_S^a + M_S^r + M_S^i + M_S^{o1} + M_S^{o2} \tag{3.1.139}$$

Applying the finite element method to Eq. (3.1.139), we obtain the following matrix equation

$$\begin{aligned} &[M]\frac{d\{S\}}{dt} + [V]\{S\} + [D]\{S\} + [K]\{S\} \\ &\qquad = -\{\Psi^B\} + \{\Psi^a\} + \{\Psi^T\} + \{\Psi^i\} + \{\Psi^{o1}\} + \{\Psi^{o2}\} \end{aligned} \tag{3.1.140}$$

in which

$$M_{ij} = \int_{X_1}^{X_N} N_i A N_j dx, \quad V_{ij} = \int_{X_1}^{X_N} \frac{dW_i}{dx} Q N_j dx, \quad D_{ij} = \int_{X_1}^{X_N} \frac{dN_i}{dx} D^S A \frac{dN_j}{dx} dx,$$
$$K_{ij} = \int_{X_1}^{X_N} N_i \frac{\partial A}{\partial t} N_j dx, \quad \Psi_i^B = \left(W_i Q S - N_i D^S A \frac{\partial T}{\partial x} \right) \Big|_{x=X_1}^{x=X_N} \tag{3.1.141}$$

$$\Psi_i^a = \int_{X_1}^{X_N} N_i M_s^a dx, \quad \Psi_i^r = \int_{X_1}^{X_N} N_i M_s^r dx \tag{3.1.142}$$

$$\Psi_i^i = \int_{X_1}^{X_N} N_i M_s^i dx, \quad \Psi_i^{o1} = \int_{X_1}^{X_N} N_i M_s^{o1} dx, \quad \Psi_i^{o2} = \int_{X_1}^{X_N} N_i M_s^{o2} dx \tag{3.1.143}$$

where W_i is the weighting function of node at x_i; N_i and N_j are the base functions of nodes at x_i and x_j, respectively; [M] is the mass matrix, [V] is the stiff matrix due to advective transport; [D] is the stiff matrix due to dispersion/diffusion/conduction; [K] is the stiff matrix due to the linear term; {S} is the solution vector of salinity; $\{\Psi^B\}$ is the vector due to boundary conditions, which can contribute to load vector and/or coefficient matrix; $\{\Psi^a\}$ is the load vector due to artificial salt source; $\{\Psi^r\}$ is the load vector due to salt in rainfall; $\{\Psi^i\}$ is the vector due to interaction with subsurface exfiltraing water; $\{\Psi^{o1}\}$ is the vector due to interaction with overland water via river bank 1; and $\{\Psi^{o2}\}$ is the vector due to interaction with overland water via river bank 2.

Approximating the time derivative term in Eq. (3.1.140) with a time-weighted finite difference, we reduce the advective-diffusive equation and its boundary conditions to the following matrix equation.

$$[C]\{S\} = \{L\} - \{\Psi^B\} - \{\Psi^i\} + \{\Psi^{o1}\} + \{\Psi^{o2}\} \tag{3.1.144}$$

in which

$$[C] = \frac{[M]}{\Delta t} + \theta([D] + [K]) + \theta_V [V],$$
$$\{L\} = \left(\frac{[M]}{\Delta t} - (1-\theta)([D] + [K]) - (1-\theta_V)[V] \right) \{S^{(n)}\} + \{\Psi^a\} + \{\Psi^r\} \tag{3.1.145}$$

where [C] is the coefficient matrix, {L} is the load vector from initial condition, artificial sink/sources and rainfall; Δt is the time step size; θ is the time weighting factor for the dispersion and linear terms; θ_v is the time weighting factor for the velocity term; and $\{S^{(n)}\}$ is the value of {S} at old time level n. The global and internal boundary (junctions, weirs, and gates) conditions must be used to provide $\{\Phi_B\}$ in Eq. (3.1.144). The interaction between the overland and river/stream/canal flows must be implemented to evaluate $\{\Psi^{o1}\}$ and $\{\Psi^{o2}\}$; and the interaction between the subsurface and river/stream/canal flows must be implemented to calculate $\{\Psi^i\}$. The interactions will be addressed in Section 3.4.

For a global boundary node I, the corresponding algebraic equation from Eq. (3.1.144) is

$$C_{I,I-1}S_{I-1} + C_{I,I}S_I + C_{I,I+1}S_{I+1} = L_I + \left(\Psi_I^i + \Psi_I^{o1} + \Psi_I^{o2}\right) - \Psi_I^B \qquad \textbf{(3.1.146)}$$

In the above equations there are two unknowns T_I and Φ_{BI}; either T_I or Φ_{BI}, or the relationship between T_I and Ψ_I^B must be specified. The numerical implementation of these boundary conditions is described as follows.

Direchlet boundary condition: prescribed salinity

If S_I is given on the boundary node I (Dirichlet boundary condition), all coefficients ($C_{I,I-1}$, $C_{I,I}$, $C_{I,I+1}$) and right-hand side (L_I, Ψ_I^i, Ψ_I^{o1}, Ψ_I^{o2}) obtained before the implementation of boundary conditions for this equation are stored in a temporary array, then an identity equation is created as

$$S_I = S_{Id}, \quad I \in N_D \qquad \textbf{(3.1.147)}$$

where S_{Id} is the prescribed salinity on the Dirichlet node I and N_D is the number of Dirichlet boundary nodes. This process is repeated for every Dirichlet nodes. Note it is unnecessary to modify other equations that involving these unknowns, which was done in the previous version. By not modifying other equations, the symmetrical property of the matrix is preserved, which makes the iterative solvers more robust. The final set of equations will consist of N_D identity equations and (N - N_D) finite element equations for N unknowns S_i's. After S_i's for all nodes are solved from the matrix equation, Eq. (3.1.146) is then used to back calculate N_D Ψ_I^B's.

If a direct solver is used to solve the matrix equation, the above procedure will solve N S_i's accurately except for roundoff errors. However, if an iterative solver is used, stopping criteria must be strict enough so that the converged solution of N S_i's are accurate enough to the exact solution. With such accurate S_is, then can be sure that the back-calculated ND Ψ_I^B's are accurate.

Cauchy boundary condition: prescribed salt flux

If Ψ_I^B is given (Cauchy flux boundary condition), all coefficients ($C_{I,I-1}$, $C_{I,I}$, $C_{I,I+1}$) and right-hand side (L_I, Ψ_I^i, Ψ_I^{o1}, Ψ_I^{o2}) obtained before the implementation of boundary conditions for this equation are stored in a temporary array, then Eq. (3.1.146) is modified to incorporate the boundary conditions and used to solve for S_I. The modification of Eq. (3.1.146) is straightforward. Because Ψ_I^B is a known quantity, it contributes to the load on the right hand side. This type of boundary conditions is very easy to implement. After S_is are obtained, the original Eq. (3.1.146), which is stored in a temporary array, isused to back calculate N_C Ψ_I^B's on flux boundaries (where N_C is the number of flux boundary nodes). These back-calculated Ψ_I^B's should be theoretically identical to the input Ψ_I^B's. However, because of round-off errors (in the case of direct solvers) or because of stopping criteria (in the case of iterative solvers), the back-calculated will be slightly different from the input Ψ_I^B's. If the differences between the two are significant, it is an indication that the solvers have not yielded accurate solutions.

Neumann boundary condition: prescribed gradient of salinity

At Neumann boundaries, the temperature gradient is prescribed, thus, the flux due to temperature gradient is given. For this case, all coefficients ($C_{I,I-1}$, $C_{I,I}$, $C_{I,I+1}$) and right-hand side (L_I, Ψ_I^i, Ψ_I^{o1}, Ψ_I^{o2}) obtained before the implementation of boundary conditions for this equation are stored in a temporary array, then Eq. (3.1.146) is modified to incorporate the boundary conditions and used to solve for S_I. For the Neumann boundary condition, Ψ_I^B contributes to both the matrix coefficient and load vector, thus both the coefficient matrix [C] and the load vector {L} must be modified. Recall

$$\Psi_i^B = \left(W_i QS - N_i D^S A \frac{\partial S}{\partial x} \right) \Big|_{\substack{x=X_N \\ x=X_1}} \tag{3.1.148}$$

Apply this equation to Node I, we have

$$\Psi_I^B \equiv n_I QS_I - n_I D^S A \frac{\partial S}{\partial x} \Big|_{x=X_I} = n_I QS_I - \Psi_I^{nb} \tag{3.1.149}$$

where n_I is the unit outward normal vector at the boundary node I, Ψ_I^{nb} is the Neumann boundary flux at node I. Substitution of Eq. (3.1.149) into Eq. (3.1.146), we have the modified coefficient matrix and load vector; thus the modified Eq. (3.1.146). This modified equation is used to solve S_I. After S_I is solved, the original Eq. (3.1.146) (recall the original Eq. (3.1.146) must be and has been stored in a temporary array) is used to back-calculate Ψ_I^B.

Variable boundary condition:

At the variable boundary condition Node I, the implementation of boundary conditions can be made identical to that for a Cauchy boundary condition node if the flow is directed into the river/stream/canal reach. If the flow is going out of the reach, the boundary condition is implemented similar to the implementation of Neuman boundary condition with $\Psi_I^{nb} = 0$. The assumption of zero Neumann flux implies that a Neuman node must be far away from the source/sink.

Junction boundary condition:

If the node IJ is an internal node that connects a junction J, then node IJ is treated as an internal boundary node. For example, consider three reaches with three internal nodes connecting to the junction J (Fig. 3.1-8). After applying the finite element method to Eq. (3.1.139), we have a total of (1J + 2J + 3J) algebraic equations. The algebraic equations for Nodes 1J, 2J, and 3J can be written based on Eq. (3.1.146)

$$C^1_{1J,1J-1} S^1_{1J-1} + C^1_{1J,1J} S^1_{1J} = L^1_{1J} + \left(\Psi^{i1}_{1J} + \Psi^{o11}_{1J} + \Psi^{o21}_{1J} \right) - \Psi^1_{1J} \tag{3.1.150}$$

$$C^2_{2J,2J-1} S^2_{2J-1} + C^2_{2J,2J} S^2_{2J} = L^2_{2J} + \left(\Psi^{i2}_{2J} + \Psi^{o12}_{2J} + \Psi^{o22}_{2J} \right) - \Psi^2_{2J} \tag{3.1.151}$$

$$C^3_{3J,3J-1} S^3_{3J-1} + C^3_{3J,3J} S^3_{3J} = L^3_{3J} + \left(\Psi^{i3}_{3J} + \Psi^{o13}_{3J} + \Psi^{o23}_{3J} \right) - \Psi^3_{1J} \tag{3.1.152}$$

where the superscript denotes the reach number and subscript denotes local node number in a reach, for example, S_{1J}^{1} denotes the salinity at the 1J-th node in Reach 1. For a convenient discussion, let us associate each of the unknowns, S_1^1, …, S_{1J-1}^1 to each of the 1J-1 finite element equations in Reach 1. Similarly, we associate each of the unknowns, S_1^2, …, S_{2J-2}^2 to each of the 2J-1 finite element equations in Reach 2 and each of the unknowns and S_1^3, …, S_{3J-1}^3 to each of the 3J-1 finite element equations in Reach 3. The unknowns, Ψ_{1J}^1, Ψ_{2J}^2, and Ψ_{3J}^3, are absent from these (1J-1 + 2J-1 + 3J-1) equations. In other words, we can say each equation governs one unknown. However, two unknowns, S_{1J}^1 and Ψ_{1J}^1, appear in Equation (3.1.150). Similarly, Equation (3.1.151) has two unknowns, S_{2J}^2 and Ψ_{2J}^2, and Equation (3.1.152) has two unknowns, S_{3J}^3 and Ψ_{3J}^3. The number of unknowns, (1J + 2J + 3J) salinities and Ψ_{1J}^1, Ψ_{2J}^2, and Ψ_{3J}^3, is more than the number of equations, (1J + 2J + 3J) finite element equations. Three more governing equations must be set up, which can be obtained with the assumption that the salt flux is due mainly to advection as

$$\Psi_{1J}^1 \equiv \left(QS - D^S A \frac{\partial S}{\partial x} \right)\Big|_{1J} = \frac{1}{2} Q_{1J}^1 \left[\left(1 + sign\left(Q_{1J}^1\right)\right) S_{1J}^1 + \left(1 - sign\left(Q_{1J}^1\right)\right) S_J \right] \qquad \textbf{(3.1.153)}$$

$$\Psi_{2J}^2 \equiv \left(QS - D^S A \frac{\partial S}{\partial x} \right)\Big|_{2J} = \frac{1}{2} Q_{2J}^2 \left[\left(1 + sign\left(Q_{2J}^2\right)\right) S_{2J}^2 + \left(1 - sign\left(Q_{2J}^2\right)\right) S_J \right] \qquad \textbf{(3.1.154)}$$

$$\Psi_{3J}^3 \equiv \left(QS - D^S A \frac{\partial S}{\partial x} \right)\Big|_{3J} = \frac{1}{2} Q_{3J}^3 \left[\left(1 + sign\left(Q_{3J}^3\right)\right) S_{3J}^3 + \left(1 - sign\left(Q_{3J}^3\right)\right) S_J \right] \qquad \textbf{(3.1.155)}$$

where Q_{1J}^1, Q_{2J}^2, and Q_{3J}^3, respectively, are the volumetric flow rates from/to Nodes 1J, 2J, and 3J, respectively, to/from the junction J [cf. Eqs. (3.1.71), (3.1.72), and (3.1.73), respectively].

Equations (3.1.153) through (3.1.155) introduce one additional unknown, S_J. One additional equation must be set up which can be done based on the energy budget at the junction J. The rate of change of energy at the junction J must be equal to the net energy rate from all reaches that join at J. This energy budget can be written as

$$\frac{d\left(V_J S_J\right)}{dt} = \sum_i \Psi_{iJ}^i \qquad \textbf{(3.1.156)}$$

When the storage effect of the junction is small, the salt budget Eq. (3.1.156) is not employed. Instead, the following equation, resulting from the requirement that the summation of salt flux is equal to zero, is used

$$\sum_{i=1}^{i=3} \Psi_{iJ}^i = 0 \qquad \textbf{(3.1.157)}$$

Equations (3.1.150) through (3.1.155) and Eq. (3.1.156) or Eq. (3.1.157) constitute 7 equations for seven unknowns, S_{1J}^1, S_{2J}^2, S_{3J}^3, Ψ_{1J}^1, Ψ_{2J}^2, Ψ_{3J}^3, and S_J. If there are N_J junctions, there will be N_J blocks of seven equations. These N_J blocks of equations should be solved iteratively along with N_R block of finite element equations where N_R is the number of reaches. In other words, the whole system of algebraic equations can be solved with block iterations. Each block of equations can be solved directly. For example, each of N_R blocks of finite element equations can be solved with an

efficient tri-diagonal matrix solver such as the Thomas algorithm. Each of the N_J blocks of seven equations can be solved with the Gaussian direct elimination with full pivoting.

Control structure boundary condition:

The control structures may include weirs, gates, culverts, etc. For the two internal boundary nodes 1S and 2S separated by a structure, the boundary conditions at these two nodes are given by

$$\Psi_{1S} = \left(QS - D^S A \frac{\partial S}{\partial x} \right)\Big|_{1S} = \frac{1}{2} Q\left[(1 + sign(Q)) S_{1S} + (1 - sign(Q)) S_{2S} \right] \qquad \textbf{(3.1.158)}$$

$$\Psi_{2S} = \left(QS - D^S A \frac{\partial S}{\partial x} \right)\Big|_{2S} = \frac{1}{2} Q\left[(1 + sign(Q)) S_{2S} + (1 - sign(Q)) S_{2S} \right] \qquad \textbf{(3.1.159)}$$

where Ψ_{1S} is the salt flux through node 1S; Φ_{2s} is the salt flux through node 2S; and Q is the flow rate through the structure S; sign(Q) is equal 1.0 if the flow is from node 1S to node 2S, -1.0 if flow is from node 2S to node 1S; S_{1S} is the temperature at node 1S; and S_{2S} is the temperature at node 2S.

3.1.5.2 The Hybrid Lagrangian-Eulerian Finite Element Method. When the hybrid Lagrangian-Eulerian finite element method is used to solve the salt transport equation, we expand Eq. (3.1.139) to yield following advection-dispersion equation in the Lagrangian form

$$\frac{D_V S}{Dt} + KS = D + \Psi^S + \Psi^I + \Psi^{O1} + \Psi^{O2} \quad where \quad V = \frac{Q}{A} \qquad \textbf{(3.1.160)}$$

in which

$$K = \frac{1}{A}\frac{\partial A}{\partial t} + \frac{1}{A}\frac{\partial Q}{\partial x}, \quad D = \frac{1}{A}\frac{\partial}{\partial x}\left(D^S A \frac{\partial S}{\partial x} \right)$$
$$\Psi^S = \frac{M_s^a + M_s^r}{A}, \quad and \quad \Psi^I = \frac{M_s^i}{A}, \Psi^{O1} = \frac{M_s^{o1}}{A}, \Psi^{O2} = \frac{M_s^{O2}}{A} \qquad \textbf{(3.1.161)}$$

To use the semi-Lagrangian method to solve the thermal transport equation, we integrate Eq. (3.1.160) along its characteristic line from x_i at new time level to x_i^* (Fig. 3.1-12), we obtain

$$\left(1 + \frac{\Delta\tau}{2} K_i^{(n+1)}\right) S_i^{(n+1)} = \left(1 - \frac{\Delta\tau}{2} K_i^*\right) S_i^* + \frac{\Delta\tau}{2}\left(D_i^{(n+1)} + D_i^*\right) + \frac{\Delta\tau}{2}\left(\Psi_i^{S^{(n+1)}} + \Psi_i^{S^*}\right)$$
$$+ \frac{\Delta\tau}{2}\left(\Psi_i^{I^{(n+1)}} + \Psi_i^{I^*}\right) + \frac{\Delta\tau}{2}\left(\Psi_i^{O1^{(n+1)}} + \Psi_i^{O1^*}\right) + \frac{\Delta\tau}{2}\left(\Psi_i^{O2^{(n+1)}} + \Psi_i^{O2^*}\right), \quad i \in N \qquad \textbf{(3.1.162)}$$

where $\Delta\tau$ is the tracking time, it is equal to Δt when the backward tracking is carried out all the way to the root of the characteristic and it is less than Δt when the backward tracking hits the boundary before Δt is consumed; $K_i^{(n+1)}$, $S_i^{(n+1)}$, $D_i^{(n+1)}$, $\Psi_i^{S(n+1)}$, $\Psi_i^{I(n+1)}$, $\Psi_i^{O1(n+1)}$, and $\Psi_i^{O2(n+1)}$ respectively, are the values of K, S, D, Ψ^S, Ψ^I, Ψ^{O1}, and Ψ^{O2}, respectively, at x_i at new time level $t = (n+1)\Delta t$; and K_i^*, S_i^*, D_i^*, Ψ_i^{S*}, Ψ_i^{I*}, Ψ_i^{O1*}, and Ψ_i^{O2*}, respectively, are the values of K, S, D, Ψ^S, Ψ^I, Ψ^{O1}, and Ψ^{O2}, respectively, at the location x_i^*.

To compute the dispersion/diffusion terms $D_i^{(n+1)}$ and D_i^*, we rewrite the second equation in Eq. (3.1.161) as

$$AD = \frac{\partial}{\partial x}\left(D^S A \frac{\partial S}{\partial x} \right) \tag{3.1.163}$$

Applying the finite element method to Eq. (3.1.163) at new time level (n+1), we obtain the following matrix equation for $\{D^{(n+1)}\}$ as

$$\left[a^{(n+1)}\right]\left\{D^{(n+1)}\right\} + \left[b^{(n+1)}\right]\left\{S^{(n+1)}\right\} = \left\{B^{(n+1)}\right\} \tag{3.1.164}$$

in which

$$\left\{D^{(n+1)}\right\} = \left\{D_1^{(n+1)} \quad D_2^{(n+1)} \quad . \quad . \quad D_i^{(n+1)} \quad . \quad . \quad D_N^{(n+1)}\right\}^{Transpose} \tag{3.1.165}$$

$$\left\{S^{(n+1)}\right\} = \left\{S_1^{(n+1)} \quad S_2^{(n+1)} \quad . \quad . \quad S_i^{(n+1)} \quad . \quad . \quad S_N^{(n+1)}\right\}^{Transpose} \tag{3.1.166}$$

$$\left\{B^{(n+1)}\right\} = \left\{B_1^{(n+1)} \quad B_2^{(n+1)} \quad . \quad . \quad B_i^{(n+1)} \quad . \quad . \quad B_N^{(n+1)}\right\}^{Transpose} \tag{3.1.167}$$

$$\begin{gathered} a_{ij}^{(n+1)} = \int_{X_1}^{X_N} N_i A\Big|_{(n+1)} N_j dx, \quad b_{ij}^{(n+1)} = \int_{X_1}^{X_N} \frac{dN_i}{dx}\left(D^S A\right)\Big|_{(n+1)} \frac{dN_j}{dx} dx, \\ B_i^{(n+1)} = nN_i\left(D^S A\right)\Big|_{(n+1)} \frac{\partial S^{(n+1)}}{\partial x}\Big|_{x=x_1}^{x=x_N} \end{gathered} \tag{3.1.168}$$

where the superscript (n+1) denotes the time level; N_i and N_j are the base functions of nodes at x_i and x_j, respectively.

Lumping the matrix $[a^{(n+1)}]$, we can solve Eq. (3.1.164) for $D_I^{(n+1)}$ as follows

$$\begin{aligned} D_I^{(n+1)} &= -\frac{1}{a_{II}^{(n+1)}} \sum_j b_{Ij}^{(n+1)} S_j^{(n+1)} \quad \text{if} \quad I \in \{2,3,..,N-1\} \\ D_I^{(n+1)} &= \frac{1}{a_{II}^{(n+1)}} B_I^{(n+1)} - \frac{1}{a_{II}^{(n+1)}} \sum_j b_{Ij}^{(n+1)} S_j^{(n+1)} \quad \text{if} \quad I \in \{1,N\} \end{aligned} \tag{3.1.169}$$

where $a_{II}^{(n+1)}$ is the lumped $a_{ii}^{(n+1)}$. Following the identical procedure that leads Eq. (3.1.163) to Eq. (3.1.169), we have

$$\begin{aligned} D_I^{(n)} &= -\frac{1}{a_{II}^{(n)}} \sum_j b_{Ij}^{(n)} S_j^{(n)} \quad \text{if} \quad I \in \{2,3,..,N-1\} \\ D_I^{(n)} &= \frac{1}{a_{II}^{(n)}} B_I^{(n)} - \frac{1}{a_{II}^{(n)}} \sum_j b_{Ij}^{(n)} S_j^{(n)} \quad \text{if} \quad I \in \{1,N\} \end{aligned} \tag{3.1.170}$$

where $\{B^{(n)}\}$, $\{a^{(n)}\}$ and $\{b^{(n)}\}$, respectively, are defined similar to $\{B^{(n+1)}\}$, $\{a^{(n+1)}\}$ and $\{b^{(n+1)}\}$, respectively.

With $\{D^{(n)}\}$ calculated with Eq. (3.1.170), $\{D^{*}\}$ can be interpolated. Substituting Eq. (3.1.169) into Eq. (3.1.162) and implementing boundary conditions given in Section 2.1.4, we obtain a system of N simultaneous algebraic equations N unknowns ($S_i^{(n+1)}$ for i = 1, 2, .., N.) If the dispersion/diffusion term is not included, then Eq. (3.1.162) is reduced to a set of N decoupled equations as

$$a_{ii} S_i^{(n+1)} = b_i, \quad i \in N \tag{3.1.171}$$

where

$$a_{ii} = \left(1 + \frac{\Delta\tau}{2} K_i^{(n+1)}\right) \tag{3.1.172}$$

$$\begin{aligned} b_i = \left(1 - \frac{\Delta\tau}{2} K_i^{*}\right) S_i^{*} + \frac{\Delta\tau}{2}\left(\Psi_i^{S^{(n+1)}} + \Psi_i^{S*}\right) + \frac{\Delta\tau}{2}\left(\Psi_i^{I^{(n+1)}} + \Psi_i^{1*}\right) \\ + \frac{\Delta\tau}{2}\left(\Psi_i^{O1^{(n+1)}} + \Psi_i^{O1*}\right) + \frac{\Delta\tau}{2}\left(\Psi_i^{O2^{(n+1)}} + \Psi_i^{O2*}\right), \quad i \in N \end{aligned} \tag{3.1.173}$$

Equation (3.1.171) is applied to all interior nodes without having to make any modification. On a boundary point, there are two possibilities: Eq. (3.1.171) is replaced with a boundary equation when the flow is directed into the reach or Eq. (3.1.171) is still valid when the flow is direct out of the reach. In other words, when the salt is transported out of the region at a boundary node (i.e., when $\mathbf{N}\bullet\mathbf{V} \geq 0$), a boundary condition is not needed and Equation (3.1.171) is used to compute the $S_i^{(n+1)}$. When the salt is transported into the region at a node (i.e., when $\mathbf{N}\bullet\mathbf{V} < 0$), a boundary condition must be specified.

Alternatively, to facilitate the implementation of boundary condition at incoming flow node, the algebraic equation for the boundary node is obtained by applying the finite element method to the boundary node rather than the use of particle tracking. For this alternative approach, the implementation of boundary conditions at global boundary nodes, internal junction nodes, and internal nodes connecting to control structures is identical to that in the finite element approximation of solving the salt transport equation.

3.2 Solving the Two-Dimensional Overland Flow Equations

As in solving the one-dimensional flow equations for river/stream/canal networks, we employ a variety of numerical approaches to solve two-dimensional overland flow equations. For fully dynamic wave models, we cast the governing equations in characteristic forms and solve the governing equations with the hybrid Lagrangian-Eulerian finite element method. For diffusive wave models, we use either the conventional finite element methods or hybrid Lagrangian-Eulerian finite element methods. For kinematic wave models, we use semi-Lagrangian methods.

3.2.1 The Lagrangian-Eulerian Finite Element Method for Dynamic Waves

To facilitate the application of hybrid Lagrangian-Eulerian finite element method to fully dynamic wave models, substituting A_1, A_2, A_3, B_1, B_2, and B_3 in Eq. (2.2.27); R_1, R_2, and R_3 in Eq. (2.2.9); and

D_x and D_y in (2.2.10) into Eqs. (2.2.28) through and (2.2.30), and rearranging the resulting equations, we obtain

$$k_y^{(1)}\frac{D_V u}{D\tau} - k_x^{(1)}\frac{D_V v}{D\tau} + S_1 = D_\otimes - k_y^{(1)}Ku + k_x^{(1)}Kv + S_\otimes \qquad \textbf{(3.2.1)}$$

$$2\frac{D_{V+ck^{(2)}}c}{D\tau} + k_x^{(2)}\frac{D_{V+ck^{(2)}}u}{D\tau} + k_y^{(2)}\frac{D_{V+ck^{(2)}}v}{D\tau} + S_2 = D_\pm - k_x^{(2)}Ku - k_y^{(2)}Kv + S_+ \qquad \textbf{(3.2.2)}$$

$$-2\frac{D_{V-ck^{(2)}}c}{D\tau} + k_x^{(2)}\frac{D_{v-ck^{(2)}}u}{D\tau} + k_y^{(2)}\frac{D_{V-ck^{(2)}}v}{D\tau} + S_3 = D_\pm - k_X^{(2)}Ku - k_y^{(2)}Kv + S_- \qquad \textbf{(3.2.3)}$$

in which

$$D_\otimes = k_y^{(1)}D_x - k_x^{(1)}D_y,\quad D_\pm = k_x^{(2)}D_x + k_y^{(2)}D_y,\quad \textit{and}\quad K = \frac{S_S + S_R - S_E + S_I}{h} + \frac{\kappa|V|}{h} \qquad \textbf{(3.2.4)}$$

$$D_x = \frac{1}{h}\left[\frac{\partial}{\partial x}\left(h\varepsilon_{xx}\frac{\partial u}{\partial x}\right) + \frac{\partial}{\partial y}\left(h\varepsilon_{xy}\frac{\partial u}{\partial y} + h\varepsilon_{yx}\frac{\partial v}{\partial x}\right)\right] \qquad \textbf{(3.2.5)}$$

$$D_y = \frac{1}{h}\left[\frac{\partial}{\partial x}\left(h\varepsilon_{xy}\frac{\partial u}{\partial y} + h\varepsilon_{yx}\frac{\partial v}{\partial x}\right) + \frac{\partial}{\partial y}\left(h\varepsilon_{yy}\frac{\partial v}{\partial y}\right)\right] \qquad \textbf{(3.2.6)}$$

$$\begin{aligned} S_\otimes = {} & k_y^{(1)}\left(-g\frac{\partial Z_o}{\partial x} + \frac{\left(M_x^{\,S} + M_x^{\,R} - M_x^{E} + M_x^{\,I}\right)}{h} + \frac{\tau_x^s}{\rho h}\right) \\ & - k_x^{(1)}\left(-g\frac{\partial Z_o}{\partial y} + \frac{\left(M_y^{\,S} + M_y^{\,R} - M_y^{E} + M_y^{\,I}\right)}{h} + \frac{\tau_y^s}{\rho h}\right) \end{aligned} \qquad \textbf{(3.2.7)}$$

$$\begin{aligned} S_+ = {} & \frac{g}{c}\left(S_S + S_R - S_E + S_I\right) + k_x^{(2)}\left(-g\frac{\partial Z_o}{\partial x} + \frac{\left(M_x^{\,S} + M_x^{\,R} - M_x^{E} + M_x^{\,I}\right)}{h} + \frac{\tau^S}{\rho h}\right) \\ & + k_y^{(2)}\left(-g\frac{\partial Z_o}{\partial y} + \frac{\left(M_y^{\,S} + M_y^{\,R} - M_y^{E} + M_y^{\,I}\right)}{h} + \frac{\tau_y^s}{\rho h}\right) \end{aligned} \qquad \textbf{(3.2.8)}$$

$$\begin{aligned} S_- = {} & -\frac{g}{c}\left(S_S + S_R - S_E + S_I\right) + k_x^{(2)}\left(-g\frac{\partial Z_o}{\partial x} + \frac{M_x^{\,S} + M_x^{\,R} - M_x^{E} + M_x^{\,I}}{h} + \frac{\tau_X^s}{\rho h}\right) \\ & + k_y^{(2)}\left(-g\frac{\partial Z_o}{\partial y} + \frac{\left(M_y^{\,S} + M_y^{\,R} - M_y^{E} + M_y^{\,I}\right)}{h} + \frac{\tau_y^s}{\rho h}\right) \end{aligned} \qquad \textbf{(3.2.9)}$$

where $D_\otimes$ is the diffusive transport of the vorticity wave; $D_\pm$ is the diffusive transport of the positive and negative gravity waves; K is the decay coefficient for all three waves; and $S_\otimes$, S_+, and S_- are the sources/sinks of the vorticity, positive, and negative waves, respectively.

Integrating Eqs. (3.2.1) through (3.2.3) along their respective characteristic lines from x to x_1*, x_2*,

and x_3* (Fig. 3.2-1), we obtain

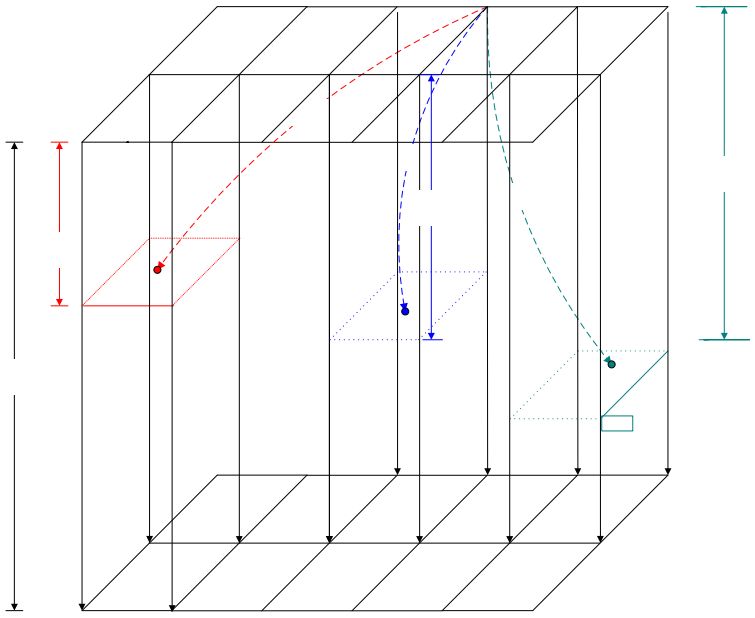

Fig. 3.2-1. Backward Particle Tracking along Characteristic Lines in Two Dimensions.

$$\overline{k_y^{(1)}}\frac{u-u_1^*}{\Delta\tau_1}-\overline{k_x^{(1)}}\frac{v-v_1^*}{\Delta\tau_1}+\frac{1}{2}\left(S_1+(S_1)_1^*\right)$$
$$=\frac{1}{2}\left(D_\otimes+(D_\otimes)_1^*\right)-\frac{1}{2}\left(k_y^{(1)}Ku-k_x^{(1)}Kv+\left(k_y^{(1)}Ku\right)_1^*-\left(k_x^{(1)}Kv\right)_1^*\right)+\frac{1}{2}\left(S_\otimes+(S_\otimes)_1^*\right) \quad \textbf{(3.2.10)}$$

$$\frac{2c-2c_2^*}{\Delta\tau_2}+\overline{k_x^{(2)}}\frac{u-u_2^*}{\Delta\tau_2}+\overline{k_y^{(2)}}\frac{v-v_2^*}{\Delta\tau_2}+\frac{1}{2}\left(S_2+(S_2)_2^*\right)$$
$$=\frac{1}{2}\left(D_\pm+(D_\pm)_2^*\right)-\frac{1}{2}\left(k_x^{(2)}Ku+k_y^{(2)}Kv+\left(k_x^{(2)}Ku\right)_2^*+\left(k_y^{(2)}Kv\right)_2^*\right)+\frac{1}{2}\left(S_+ +(S_+)_2^*\right) \quad \textbf{(3.2.11)}$$

$$-\frac{2c-2c_3^*}{\Delta\tau_3}+\overline{k_x^{(2)}}\frac{u-u_3^*}{\Delta\tau_3}+\overline{k_y^{(2)}}\frac{v-v_3^*}{\Delta\tau_3}+\frac{1}{2}\left(S_3+(S_3)_3^*\right)$$
$$=\frac{1}{2}\left(D_\pm+(D_\pm)_3^*\right)-\frac{1}{2}\left(k_x^{(2)}Ku+k_y^{(2)}Kv+\left(k_x^{(2)}Ku\right)_3^*+\left(k_y^{(2)}Kv\right)_3^*\right)+\frac{1}{2}\left(S_- +(S_-)_3^*\right) \quad \textbf{(3.2.12)}$$

where u_1^*, v_1^*, and $\Delta\tau_1$ are determined by backward tracking along the first characteristic; c_2^*, u_2^*, v_2^*, and $\Delta\tau_2$ are determined by backward tracking along the second characteristic; c_3^*, u_3^*, v_3^*, and $\Delta\tau_3$ are determined by backward tracking along the third characteristic; and all other variables with a superscript * are determined similarly at the roots of particle tracking.

In Eqs. (3.2.11) through (3.2.13), the primitive variables at the backward tracked locations are interpolated with those at the global nodes and at both new and old time levels as

$$c_1^* = a_1\, c_{k1}^n + a_2\, c_{k2}^n + a_3\, c_{k3}^n + a_4\, c_{k4}^n + a_5\, c_{k1} + a_6\, c_{k2} + a_7\, c_{k3} + a_8\, c_{k4} \qquad \textbf{(3.2.13)}$$

$$u_1^* = a_1\, u_{k1}^n + a_2\, u_{k2}^n + a_3\, u_{k3}^n + a_4\, u_{k4}^n + a_5\, u_{k1} + a_6\, u_{k2} + a_7\, u_{k3} + a_8\, u_{k4} \qquad \textbf{(3.2.14)}$$

$$v_1^* = a_1\, v_{k1}^n + a_2\, u_{k2}^n + a_3\, v_{k3}^n + a_4\, v_{k4}^n + a_5\, v_{k1} + a_6\, v_{k2} + a_7\, v_{k3} + a_8\, v_{k4} \qquad \textbf{(3.2.15)}$$

$$c_2^* = b_1\, c_{j1}^n + b_2\, c_{j2}^n + b_3\, c_{j3}^n + b_4\, c_{j4}^n + b_5\, c_{j1} + b_6\, cj + b_7\, c_{j3} + b_8\, c_{j4} \qquad \textbf{(3.2.16)}$$

$$u_2^* = b_1\, u_{j1}^n + b_2\, u_{j2}^n + b_3\, u_{j3}^n + b_4\, u_{j4}^n + b_5\, c_{j1} + b_6\, u_{j2} + b_7\, u_{j3} + b_8\, u_{j4} \qquad \textbf{(3.2.17)}$$

$$v_2^* = b_1\, v_{j1}^n + b_2\, v_{j2}^n + b_3\, v_{j3}^n + b_4\, v_{j4}^n + b_5\, v_{j1} + b_6\, v_{j2} + b_7\, v_{j3} + b_8\, v_{j4} \qquad \textbf{(3.2.18)}$$

$$c_3^* = d_1\, c_{m1}^n + d_2\, c_{m2}^n + d_3\, c_{m3}^n + d_4\, c_{m4}^n + d_5\, c_{m1} + d_6\, c_{m2} + d_7\, c_{m3} + d_8\, c_{m4} \qquad \textbf{(3.2.19)}$$

$$u_3^* = d_1\, u_{m1}^n + d_2\, u_{m2}^n + d_3\, u_{m3}^n + d_4\, {}^n_{m4} + d_5\, u_{m1} + d_6\, {}_{m2} + d_7\, u_{m3} + d_8\, u_{m4} \qquad \textbf{(3.2.20)}$$

$$v_3^* = d_1\, v_{m1}^n + d_2\, v_{m2}^n + d_3\, v_{m3}^n + d_4\, v_{m4}^n + d_5\, v_{mk1} + d_6\, v_{m2} + d_7\, v_{m3} + d_8\, v_{m4} \qquad \textbf{(3.2.21)}$$

where a_1 through a_8, b_1 through b_8, and d_1 through d_8 are interpolation parameters, all in the ranges of [0,1]; $k1$, $k2$, $k3$, and $k4$ are nodes of the element that the backward tracking, along the first characteristic, stops at; $j1$, $j2$, $j3$, and $j4$ are nodes of the element that the backward tracking, along the second characteristic, stops at; $m1$, $m2$, $m3$, and $m4$ are nodes of the element that the backward tracking, along the third characteristic, stops at (Fig. 3.2-1). It should be noted that we may use two given parameters to determine where to stop in the backward tracking: one is for controlling tracking time and the other one is for controlling tracking distance. After the primitive variables at the backward tracked points are interpolated, all other parameters (such as the decay coefficients and source/sink terms) are functions of these variables and can be calculated.

To calculate D_x and D_y, we multiple Eqs. (3.2.5) and (3.2.6) by h to yield

$$hD_x = \frac{\partial}{\partial x}\left(h\varepsilon_{xx}\frac{\partial u}{\partial x}\right) + \frac{\partial}{\partial y}\left(h\varepsilon_{xy}\frac{\partial u}{\partial y} + h\varepsilon_{yx}\frac{\partial v}{\partial x}\right) \qquad \textbf{(3.2.22)}$$

$$hD_y = \frac{\partial}{\partial x}\left(h\varepsilon_{xy}\frac{\partial u}{\partial y} + h\varepsilon_{yx}\frac{\partial v}{\partial x}\right) + \frac{\partial}{\partial y}\left(h\varepsilon_{yy}\frac{\partial v}{\partial y}\right) \qquad \textbf{(3.2.23)}$$

Applying the Galerkin finite element method to Eqs. (3.2.22) and (3.2.23), we obtain the following matrix equations for D_x and D_y

$$[QA]\{D_x\} + [QB]\{u\} + [QC]\{v\} = \{F_x\} \qquad \textbf{(3.2.24)}$$

$$[QA]\{D_y\}+[QD]\{u\}+[QE]\{v\}=\{F_y\} \tag{3.2.25}$$

where

$$QA_{ij}=\int_R N_i h N_j dR \tag{3.2.26}$$

$$QB_{ij}=\int_R \nabla N_i^* \begin{bmatrix} h\varepsilon_{xx} & 0 \\ 0 & h\varepsilon_{xy} \end{bmatrix}\cdot\nabla N_j dR;\quad QC_{ij}=\int_R \nabla N_i^* \begin{bmatrix} 0 & 0 \\ h\varepsilon_{xy} & 0 \end{bmatrix}\cdot\nabla N_j dR \tag{3.2.27}$$

$$QD_{ij}=\int_R \nabla N_i^* \begin{bmatrix} 0 & h\varepsilon_{xy} \\ 0 & 0 \end{bmatrix}\cdot\nabla N_j dR;\quad QE_{ij}=\int_R \nabla N_i^* \begin{bmatrix} h\varepsilon_{xy} & 0 \\ 0 & h\varepsilon_{yy} \end{bmatrix}\cdot\nabla N_j dR \tag{3.2.28}$$

$$F_{xi}=\sum_{e\in M_e}\int_{B_e}\left\{N_a^e\mathbf{n}\cdot\begin{bmatrix} h\varepsilon_{xx} & 0 \\ 0 & h\varepsilon_{xy} \end{bmatrix}\cdot\nabla u+N_a^e\mathbf{n}\cdot\begin{bmatrix} 0 & 0 \\ h\varepsilon_{xy} & 0 \end{bmatrix}\cdot\nabla v\right\}dB \tag{3.2.29}$$

$$F_{yi}=\sum_{e\in M_e}\int_{B_e}\left\{N_a^e\mathbf{n}\cdot\begin{bmatrix} 0 & h\varepsilon_{xy} \\ 0 & 0 \end{bmatrix}\cdot\nabla u+N_a^e\mathbf{n}\cdot\begin{bmatrix} h\varepsilon_{xy} & 0 \\ 0 & h\varepsilon_{yy} \end{bmatrix}\cdot\nabla v\right\}dB \tag{3.2.30}$$

Lumping the matrix [QA], we can explicitly compute $\{D_x\}$ and $\{D_y\}$ in terms of {u} and {v}.

$$D_{xi}=\frac{1}{QA_{ii}}F_{xi}-\frac{1}{QA_{ii}}\sum_j QB_{ij}u_j-\frac{1}{QA_{ii}}\sum_j QC_{ij}v_j \tag{3.2.31}$$

and

$$D_{yi}=\frac{1}{QA_{ii}}F_{yi}-\frac{1}{QA_{ii}}\sum_j QD_{ij}u_j-\frac{1}{QA_{ii}}\sum_j QE_{ij}v_j \tag{3.2.32}$$

Following the identical procedure that leads Eqs. (3.2.22) and (3.2.23) to Eqs. (3.2.31) and (2.3.32), we have

$$D_{xi}^{(n)}=\frac{1}{QA_{ii}^{(n)}}F_{xi}^{(n)}-\frac{1}{QA_{ii}^{(n)}}\sum_j QB_{ij}^{(n)}u_j^{(n)}-\frac{1}{QA_{ii}^{(n)}}\sum_j QC_{ij}^{(n)}v_j^{(n)} \tag{3.2.33}$$

and

$$D_{yi}^{(n)}=\frac{1}{QA_{ii}^{(n)}}F_{yi}^{(n)}-\frac{1}{QA_{ii}^{(n)}}\sum_j QD_{ij}^{(n)}u_j^{(n)}-\frac{1}{QA_{ii}^{(n)}}\sum_j QE_{ij}^{(n)}v_j^{(n)} \tag{3.2.34}$$

where the superscript (n) denotes that the variables are to be evaluated at the old time level n.

Similar to Eqs. (3.2.13) through (3.2.21), $(D_{xi}^*)_1$, $(D_{xi}^*)_2$, and $(D_{xi}^*)_3$ and $(D_{yi}^*)_1$, $(D_{yi}^*)_2$, and $(D_{yi}^*)_3$ at the backward tracked location are interpolated with {D} and $\{D^{(n)}\}$ as

$$\left(D_{xi}^*\right)_1=a_1D_{xk1}^n+a_2D_{xk2}^n+a_3D_{xk3}^n+a_4D_{xk4}^n+a_5D_{xk1}+a_6D_{xk2}+a_7D_{xk3}+a_8D_{xk4} \tag{3.2.35}$$

$$\left(D_{xi}^{*}\right)_2 = b_1 D_{xj1}^{n} + b_2 D_{xj2}^{n} + b_3 D_{xj3}^{n} + b_4 D_{xj4}^{n} + b_5 D_{xj1} + b_6 D_{xj2} + b_7 D_{xj3} + b_8 D_{xj4} \quad \textbf{(3.2.36)}$$

$$\left(D_{xi}^{*}\right)_3 = d_1 D_{xm1}^{n} + d_2 D_{xm2}^{n} + d_3 D_{xm3}^{n} + d_4 D_{xm4}^{n} + d_5 D_{xm1} + d_6 D_{xm2} + d_7 D_{xm3} + d_8 D_{xm4} \quad \textbf{(3.2.37)}$$

$$\left(D_{yi}^{*}\right)_1 = a_1 D_{yk1}^{n} + a_2 D_{yk2}^{n} + a_3 D_{yk3}^{n} + a_4 D_{yk4}^{n} + a_5 D_{yk1} + a_6 D_{yk2} + a_7 D_{yk3} + a_8 D_{yk4} \quad \textbf{(3.2.38)}$$

$$\left(D_{yi}^{*}\right)_2 = b_1 D_{yj1}^{n} + b_2 D_{yj2}^{n} + b_3 D_{yj3}^{n} + b_4 D_{yj4}^{n} + b_5 D_{yj1} + b_6 D_{yj2} + b_7 D_{yj3} + b_8 D_{yj4} \quad \textbf{(3.2.39)}$$

$$\left(D_{yi}^{*}\right)_3 = d_1 D_{ym1}^{n} + d_2 D_{ym2}^{n} + d_3 D_{ym3}^{n} + d_4 D_{ym4}^{n} + d_5 D_{ym1} + d_6 D_{ym2} + d_7 D_{ym3} + d_8 D_{ym4} \quad \textbf{(3.2.40)}$$

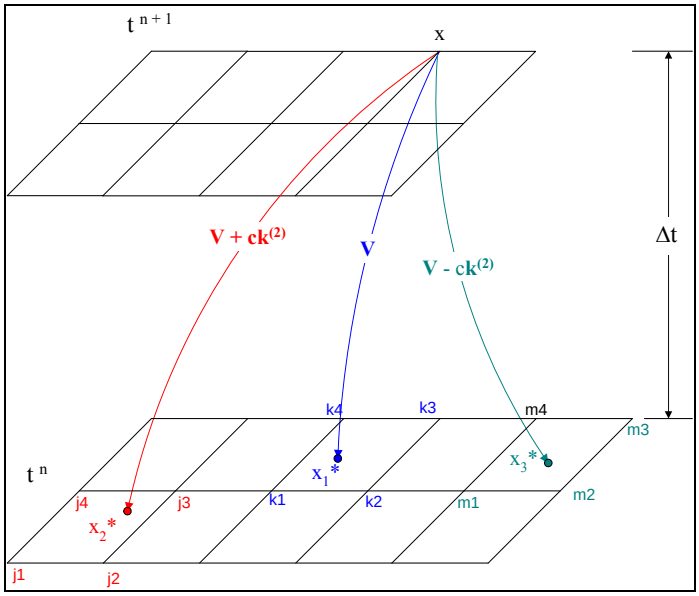

Fig. 3.2-2. Backward Tracking Along Characteristic Line to the Root in Two Dimensions

Substituting Eqs. (3.2.13) through (3.2.21) and Eqs. (3.2.35) through (3.2.40) into Eqs. (3.2.10) through (3.2.12) and implementing boundary conditions given Section 2.2.1, we obtain a system of $3N$ simultaneous algebraic equations for the $3N$ unknowns (u_i for $i = 1, 2, .., N$, v_i for $i = 1, 2, .., N$, and and c_i for $i = 1,2, .., N$). If the eddy diffusion terms are not included and the backward tracking is performed to reach the time level n (Fig. 3.2-2), then Eqs. (3.2.8) through (3.2.10) are reduced to a set of N decoupled triplets of equations as

$$\begin{aligned} a_{11}u + a_{12}v + a_{13}c &= B_1, \\ a_{21}u + a_{22}v + a_{23}c &= B_2, \\ a_{31}u + a_{32}v + a_{33}c &= B_3, \quad \text{for all interior nodes} \end{aligned} \quad \textbf{(3.2.41)}$$

where

$$a_{11} = \overline{k_y^{(1)}} + \frac{\Delta\tau_1}{2}\left(\overline{k_y^{(1)}} K_+\right), \qquad a_{12} = \overline{-k_x^{(1)}} - \frac{\Delta\tau_1}{2}\left(\overline{k_x^{(1)}} K_+\right), \qquad a_{13} = 0,$$

$$B_1 = \left(\overline{k_y^{(1)}} - \frac{\Delta\tau_1}{2}\left(k_y^{(1)} K\right)_1^*\right) u_i^* - \left(\overline{k_x^{(1)}} - \frac{\Delta\tau_1}{2}\left(k_x^{(1)} K\right)_1^*\right) v_1^* \qquad \textbf{(3.2.42)}$$

$$- \frac{\tau_1}{2}\left(S_1 + (S_1)_1^*\right) + \frac{\tau_1}{2}\left(S_\oplus + (S_\oplus)_1^*\right)$$

$$a_{21} = \overline{k_x^{(2)}} + \frac{\Delta\tau_2}{2}\left(k_x^{(2)} K\right), \qquad a_{22} = \overline{k_y^{(2)}} + \frac{\Delta\tau_2}{2}\left(k_x^{(2)} K\right), \qquad a_{23} = 2,$$

$$B_2 = \left(\overline{k_x^{(2)}} - \frac{\Delta\tau_2}{2}\left(k_x^{(2)} K\right)_2^*\right) u_2^* + \left(\overline{k_y^{(2)}} - \frac{\Delta\tau_2}{2}\left(k_y^{(2)} K\right)_2^*\right) v_2^* + 2c_2^* \qquad \textbf{(3.2.43)}$$

$$- \frac{\tau_2}{2}\left(S_2 + (S_2)_2^*\right) + \frac{\tau_2}{2}\left(S_+ + (S_+)_2^*\right)$$

$$a_{31} = \overline{k_x^{(2)}} + \frac{\Delta\tau_2}{2}\left(k_x^{(2)} K\right), \qquad a_{32} = \overline{k_y^{(2)}} + \frac{\Delta\tau_2}{2}\left(k_x^{(2)} K\right), \qquad a_{33} = -2,$$

$$B_3 = \left(\overline{k_x^{(2)}} - \frac{\Delta\tau_3}{2}\left(k_x^{(2)} K\right)_3^*\right) u_3^* + \left(\overline{k_y^{(2)}} - \frac{\Delta\tau_3}{2}\left(k_y^{(2)} K\right)_3^*\right) v_3^* + 2c_3^* \qquad \textbf{(3.2.44)}$$

$$- \frac{\tau_3}{2}\left(S_3 + (S_3)_3^*\right) + \frac{\tau_3}{2}\left(S_+ + (S_+)_3^*\right)$$

Equations (3.2.41) is applied to all interior nodes without having to make any modification. On a boundary point, any one of the three equations in Eq. (3.2.41) must be replaced by a boundary condition equation if its corresponding wave is directed into the region from the outside world. On the other hand, if the corresponding wave is going out of the region, then the equation is valid. These conditions are addressed below for four types of physical boundaries: open upstream, open downstream, closed upstream, and closed downstream boundary nodes.

Open upstream boundary condition:

If the flow is supercritical, all three waves are directed into the region from the outside world, thus Eq. (3.2.41) is replaced with

$$\mathbf{n} \cdot \mathbf{V}h = q_n^{(up)}(t); \qquad \mathbf{n} \cdot \mathbf{V}uh + n_x \frac{gh^2}{2} = M_x^{up}; \qquad \mathbf{n} \cdot \mathbf{V}vh + n_y \frac{gh^2}{2} = M_y^{up} \qquad \textbf{(3.2.45)}$$

where $\mathbf{V} = (u, v)$ is the vertically averaged velocity with u as the x-component and v the y-component; $\mathbf{n}$ is the outward unit vector normal to the boundary; q_n^{up}(t) is the flow rate of the incoming fluid from the upstream; and M_x^{up} and M_y^{up}, respectively, are the x- and y-components, respectively, of the momentum-impulse from the upstream.

If the flow is subcritical, one of the gravitational wave is going out of the region, thus Eq. (3.2.41) for the boundary point i is replaced with

$$\mathbf{n}\cdot\mathbf{V}h = q_n^{(up)}(t); \qquad \mathbf{l}\cdot\mathbf{V}h = q_\ell^{(up)}(t); \qquad a_{21}u + a_{22}v + a_{23}c = B_2$$

or **(3.2.46)**

$$\mathbf{n}\cdot\mathbf{V}h = q_n^{(up)}(t); \qquad \mathbf{l}\cdot\mathbf{V}h = q_\ell^{(up)}(t); \qquad a_{31}u + a_{32}v + a_{33}c = B_3$$

where **l** is the unit vector parallel to the boundary segment and $q_\ell^{(up)}$, a function of time t, is the flow rate parallel to the boundary.

Open downstream boundary condition:

If the flow is supercritical, all three waves are transported out of the region and Eq. (3.2.41) remains valid for the boundary point; thus

$$\begin{aligned} &a_{11}u + a_{12}v + a_{13}c = B_1, \\ &a_{21}u + a_{22}v + a_{23}c = B_2, \\ &a_{31}u + a_{32}v + a_{33}c = B_3, \quad \textit{for all interior nodes} \end{aligned} \qquad \textbf{(3.2.47)}$$

If the flow is subcritical, the vorticity wave and one the gravity waves are transported out of the region while the other gravity wave is transported into the region. Under such circumstance, Equation (3.2.41) may be replaced with

$$a_{11}u + a_{12}v + a_{13}c = B_1; \qquad a_{21}u + a_{22}v + a_{23}c_3 = B_2; \qquad h = h^{dn}(t) \;\; or \;\; \mathbf{n}\cdot\mathbf{V}h = q_n^{dn}(h)$$

or **(3.2.48)**

$$a_{11}u + a_{12}v + a_{13}c = B_1; \qquad a_{31}u + a_{32}v + a_{33}c = B_3; \qquad h = h^{dn}(t) \;\; or \;\; \mathbf{n}\cdot\mathbf{V}h = q_n^{dn}(h)$$

where $q_n^{dn}(h)$, a function of h, is the rating curve function for the downstream boundary and $h^{dn}(t)$, a function of t, is the water depth at the downstream boundary. As to which three equations in of Eq. (3.2.48) must be used depends on the physical configuration at the boundary.

Closed upstream boundary condition:

If the flow is supercritical, all three waves are transported from the boundary into the region of interest. Since neither flow nor momentum-impulse is transported from the outside world onto the boundary, the following boundary condition can be used

$$\mathbf{n}\cdot\mathbf{V}h = 0; \qquad \mathbf{n}\cdot\mathbf{V}uh + n_x\frac{gh^2}{2} = 0; \qquad \mathbf{n}\cdot\mathbf{V}vh + n_y\frac{gh^2}{2} = 0 \qquad \textbf{(3.2.49)}$$

The solution of Eq. (3.2.49) is not unique. One of the possible solution is h = 0, u = 0, and v = 0. If the flow is subcritical, one of the two gravity waves is transported out of the region, thus Equation (3.2.41) can be replaced with

$$\mathbf{n}\cdot\mathbf{V}h=0;\qquad \mathbf{l}\cdot\mathbf{V}h=0;\qquad a_{21}u=a_{22}v+a_{23}c_3=B_2$$

or **(3.2.50)**

$$\mathbf{n}\cdot\mathbf{V}h=0;\qquad \mathbf{l}\cdot\mathbf{V}h=0;\qquad a_{31}u=a_{32}v+a_{33}c=B_3$$

Closed downstream boundary condition:

At the closed downstream boundary, physical condition dictates that the normal flux should be zero. In the meantime, one of the gravity wave is transported out of the region. Thus, the water depth and velocity on the boundary are determined by the internal flow dynamics and the condition of zero normal flux. The boundary condition can be stated as

$$a_{11}u+a_{12}v+a_{13}c=B_1;\qquad a_{21}u+a_{22}v+a_{23}c_3=B_2;\qquad \mathbf{n}\cdot\mathbf{V}h=0$$

or **(3.2.51)**

$$a_{11}u+a_{12}v+a_{13}c=B_1;\qquad a_{31}u+a_{32}v+a_{33}c=B_3;\qquad \mathbf{n}\cdot\mathbf{V}h=0$$

3.2.2 Numerical Approximation of Diffusive Wave Equations

Two options are provided in this report to solve the diffusive wave flow equations. One is the finite element method and the other is the particle tracking method.

3.2.2.1 Galerkin Finite Element Method. Recall the diffusive wave is governed by Eq. (2.2.44) which is repeated here as

$$\frac{\partial H}{\partial t}-\nabla\cdot\left[K\left(\nabla H+\frac{h}{2\rho}\nabla(\Delta\rho)-\frac{\tau^s}{\rho g h}\right)\right]=S_S+S_R-S_E+S_I \qquad \textbf{(3.2.52)}$$

Applying the Galerkin finite element method to Eq. (3.2.52), we obtain the following matrix equation

$$[M]\frac{d\{H\}}{dt}+[S]\{H\}=\{Q_{\rho w}\}+\{Q_B\}+\{Q_S\}+\{Q_R\}-\{Q_E\}+\{Q_I\} \qquad \textbf{(3.2.53)}$$

in which

$$M_{ij}=\int_{\Re}N_iN_jd\Re,\qquad S_{ij}=\int_{\Re}\nabla N_i\cdot\mathbf{K}\cdot\nabla N_jd\Re,$$

$$Q_{\rho wi}=\int_{\Re}\nabla N_i\cdot\mathbf{K}\cdot\left[\frac{h}{2\rho}\nabla(\Delta\rho)-\frac{\boldsymbol{\tau}^s}{hg\rho}\right]d\Re,\quad Q_{Bi}=\int_B N_i\mathbf{n}\cdot\mathbf{K}\cdot\left[\nabla H+\frac{h}{2\rho}\nabla(\Delta\rho)-\frac{\boldsymbol{\tau}^s}{hg\rho}\right]dB \qquad \textbf{(3.2.54)}$$

$$Q_{Si}=\int_{\Re}N_iS_Sd\Re,\quad Q_{Ri}=\int_{\Re}N_iS_Rd\Re,\quad Q_{Ei}=\int_{\Re}N_iS_Ed\Re,\quad Q_{Ii}=\int_{\Re}N_iS_Id\Re \qquad \textbf{(3.2.55)}$$

where N_i and N_j are the base functions of nodes at x_i and x_j, respectively; **n** is the outward-normal unit vector; [M] is the mass matrix, [S] is the stiff matrix, {H} is the solution vector of H, $\{Q_{\rho w}\}$ is the load vector due to density and wind stress effects, $\{Q_B\}$ is the flow rate through the boundary nodes, $\{Q_S\}$ is the flow rate from artificial source/sink, $\{Q_R\}$ is the flow rate from rainfall, $\{Q_E\}$ is the flow rate due to evapotranspiration, and $\{Q_I\}$ is the flow rate to infiltration. It should be noted

that $\{Q_I\}$ is the interaction between the overland and subsurface flows.

Approximating the time derivative term in Eq. (3.2.53) with a time-weighted finite difference, we reduce the diffusive equation and its boundary conditions to the following matrix equation

$$[C]\{H\} = \{L\} + \{Q_B\} + \{Q_I\} \tag{3.2.56}$$

in which

$$[C] = \frac{[M]}{\Delta t} + \theta[S], \quad \{L\} = \left(\frac{[M]}{\Delta t} - (1-\theta)[S]\right)\{H^{(n)}\} + \{Q_{\rho w}\} + \{Q_S\} + \{Q_R\} - \{Q_E\} \tag{3.2.57}$$

where [C] is the coefficient matrix, {L} is the load vector from initial condition, density and wind effects, artificial sink/sources, rainfall, and evapotranspiration; Δt is the time step size; θ is the time weighting factor; and $\{H^{(n)}\}$ is the value of {H} at old time level n. The global boundary conditions must be used to provide $\{Q_B\}$ in Eq. (3.2.56). The interaction between the overland and subsurface flows must be implemented to calculate $\{Q_I\}$. The interactions will be addressed in Section 3.4.

For a global boundary node I, the corresponding algebraic equation from Eq. (3.2.56) is

$$C_{I,1}H_1 + \ldots + C_{I,I}H_I + \ldots + C_{I,N}H_N = L_I + Q_{II} + Q_{BI} \tag{3.2.58}$$

In the above equation there are two unknowns H_I and Q_{BI}; either H_I or Q_{BI}, or the relationship between H_I and Q_{BI} must be specified. The numerical implementation of these boundary conditions is described as follows.

Dirichlet boundary condition: prescribed water depth or stage

If H_I is given on the boundary node I (Dirichlet boundary condition), all coefficients ($C_{I,1}$, ..., $C_{I,I}$, ..., $C_{I,N}$) and right-hand side (L_I and Q_{II}) obtained before the implementation of boundary conditions for this equation are stored in a temporary array, then an identity equation is created as

$$H_I = H_{Id}, \quad I \in N_D \tag{3.2.59}$$

where H_{Id} is the prescribed total head on the Dirichlet node I and N_D is the number of Dirichlet boundary nodes. This process is repeated for every Dirichlet nodes. Note it is unnecessary to modify other equations that involving this unknown, which was done in the previous version. By not modifying other equations, the symmetrical property of the matrix is preserved, which makes the iterative solvers more robust. The final set of equations will consist of N_D identity equations and (N - N_D) finite element equations for N unknowns H_i's. After H_i's are obtained, Eq. (3.2.58) is then used to back calculate N_D Q_{BI}'s.

If a direct solver is used to solve the matrix equation, the above procedure will solve N H_i's accurately except for roundoff errors. However, if an iterative solver is used, a stopping criterion must be strict enough so that the converged solution of N H_i's is accurate enough to the exact solution. With such accurate H_i's, then one can be sure that the back-calculated N_D Q_{BI}'s are accurate.

Flux boundary condition: prescribed flow rate

If Q_{BI} is given (flux boundary condition), all coefficients ($C_{I,1}$, ..., $C_{I,I}$, ..., $C_{I,N}$) and the right-hand side (L_I and Q_{II}) obtained before the implementation of boundary conditions for this equation are stored in a temporary array, then Eq. (3.2.58) is modified to incorporate the boundary conditions and used to solve for H_I. The modification of Eq. (3.2.58) is straightforward. Because Q_{BI} is a known quantity, it contributes to the load on the right hand side. This type of boundary conditions is easy to implement. After H_i's are obtained, the original Eq. (3.2.58), which is stored in a temporary array, is used to back calculate N_C Q_{BI}'s on flux boundaries (where N_C is the number of flux boundary nodes). These back-calculated Q_{BI}'s should be theoretically identical to the input Q_{BI}'s. However, because of round-off errors (in the case of direct solvers) or because of stopping criteria (in the case of iterative solvers), the back-calculated Q_{BI}'s will be slightly different from the input Q_{BI}'s. If the differences between the two are significant, it is an indication that the solvers have not yielded accurate solutions.

Water depth-dependent boundary condition: prescribed rating curve

If the relationship is given between Q_{BI} and H_I (rating curve boundary condition), all coefficients ($C_{I,1}$, ..., $C_{I,I}$, ..., $C_{I,N}$) and the right-hand side (L_I and Q_{II}) obtained before the implementation of boundary conditions for this equation are stored in a temporary array, then Eq. (3.2.58) is modified to incorporate the boundary conditions and used to solve for H_I. The rating-relationship is used to eliminate one of the unknowns, say Q_{BI}, and the modified Eq. (3.2.58) is used to solve for, say H_I. After H_I is solved, the original Eq. (3.2.58) (recall the original Eq. (3.2.58) must be and has been stored in a temporary array) is used to back-calculate Q_{BI}.

3.2.2.2 The Hybrid Lagrangian-Eulerian Finite Element Method. When the hybrid Lagrangian-Eulerian finite element method is used to solve the diffusive wave equation, instead of Eq. (3.2.52), we expand Eq. (2.2.1) to yield following diffusive wave equation in the Lagrangian form

$$\frac{D_V h}{D\tau} + Kh = S_S + S_R - S_E + S_I \quad where \quad K = \nabla \cdot \mathbf{V} \tag{3.2.60}$$

To use the semi-Lagrangian method to solve the diffusive wave equation, we integrate Eq. (3.2.60) along its characteristic line from x_i at new time level to x_i^* at old time level or on the boundary (Fig. 3.2-3), we obtain

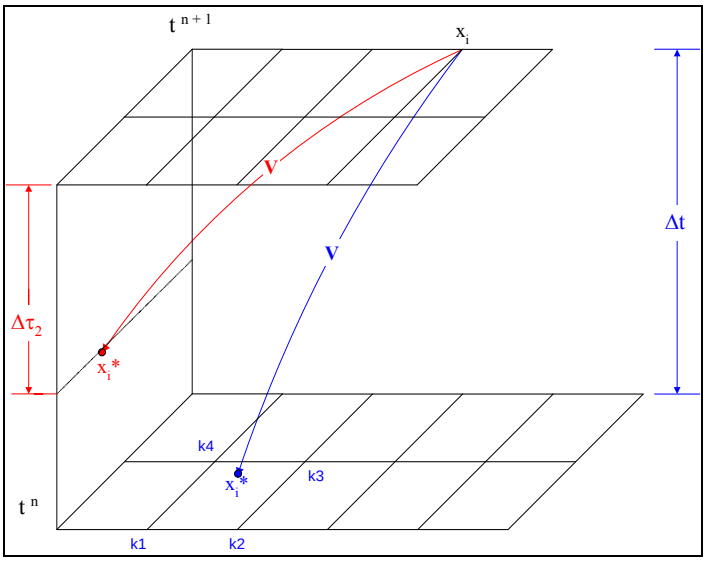

Fig. 3.2-3. Backward Particle Tracking in Two Dimension.

$$\left(1+\frac{\Delta\tau}{2}K_i^{(n+1)}\right)h_i^{(n+1)}=\left(1-\frac{\Delta\tau}{2}K_i^{*}\right)h_i^{*}+\frac{\Delta\tau}{2}\left(S_{Si}^{(n+1)}+S_{Si}^{*}\right)+\frac{\Delta\tau}{2}\left(S_{Ri}^{(n+1)}+S_{Ri}^{*}\right)$$
$$-\frac{\Delta\tau}{2}\left(S_{Ei}^{(n+1)}+S_{Ei}^{*}\right)+\frac{\Delta\tau}{2}\left(S_{Ii}^{(n+1)}+S_{Ii}^{*}\right) \qquad \textbf{(3.2.61)}$$

where $\Delta\tau$ is the tracking time, it is equal to Δt when the backward tracking is carried out all the way to the root of the characteristic and it is less than Δt when the backward tracking hits the boundary before Δt is consumed (Fig. 3.2-3); $K_i^{(n+1)}$), $h_i^{(n+1)}$, $S_{Si}^{(n+1)}$, $S_{Ri}^{(n+1)}$, $S_{Ei}^{(n+1)}$, and $S_{Ii}^{(n+1)}$, respectively, are the values of K, h, S_S, S_R, S_E, and S_I, respectively, at x_i at new time level $t = (n+1)\Delta t$; and K_i^{*}, h_i^{*}, S_{Si}^{*}, S_{Ri}^{*}, S_{Ei}^{*}, and S_{Ii}^{*}, respectively, are the values of K, h, S_S, S_R, S_E, and S_I, respectively, at the location x_i^{*}. Since the velocity **V** and the decay coefficient K are functions of h, this is a nonlinear hyperbolic problem.

Equation (3.2.61) is solved iteratively to yield the water depth h, and hence the water stage H. The iteration procedure is outlined as follows:

(i) Guess the value of $h^{(k)}$ at the k-th iteration, compute H.
(ii) Apply finite element method to the following equation to obtain V

$$V=\frac{-a}{n}\left[\frac{h}{1+\left(\nabla Z_O\right)^2}\right]^{2/3}\frac{1}{\sqrt{\left|-\nabla H-\frac{h}{2\rho}\nabla(\Delta\rho)+\frac{\tau^s}{\rho g h}\right|}}\left(\nabla H+\frac{h}{2\rho}\nabla(\Delta\rho)-\frac{\tau^s}{\rho g h}\right) \qquad \textbf{(3.2.62)}$$

(iii) Perform particle tracking to locate x^* and obtain all the *-superscripted quantities.
(iv) Apply the finite element method to the following equation to obtain K

$$K=\nabla\cdot\mathbf{V} \qquad \textbf{(3.2.63)}$$

(v) Solve Eq. (3.2.61) along with the boundary condition to obtain new $h^{(k+1)}$
(vi) Check if $h^{(k+1)}$ converges, if yes go to the next time step.
(vii) If $h^{(k+1)}$ does not converge, update h with $h^{(k)} \leftarrow \omega h^{(k+1)} + (1-\omega)h^{(k)}$ and repeat Steps (i) through (vi).

When the wave is transported out of the region at a boundary node (i.e., when $\mathbf{N}\bullet\mathbf{V} \geq 0$), a boundary condition is not needed. When the wave is transported into the region at a node (i.e., when $\mathbf{N}\bullet\mathbf{V} < 0$), a boundary condition must be specified. As in the finite element method, three types of boundary conditions may be encountered.

Dirichlet boundary condition:

For the Dirichlet boundary, the water depth is prescribed as

$$h_I = h_{Id}, \quad I \in N_D \tag{3.2.64}$$

Flux boundary condition:

For the flux boundary, the flow rate is prescribed as function of time at the boundary node, from which the boundary value is computed as

$$h^{(n+1)} = \frac{q_{up}(t)}{V^{(n+1,k)}} \tag{3.2.65}$$

where $q_{up}(t)$, a function of time t, is the prescribed flow rate [$L^3/t/L$] and $V^{(n+1,k)}$ is the value of V at new time and previous iteration.

Water depth-dependent boundary condition: prescribed rating curve

For the boundary where a rating curve is used to describe the relationship between water depth, h, and volumetric flow rate, q; thus, the water depth, h, on the boundary is computed with

$$V^{(n+1,k)} h^{(n+1)} = f(h) \tag{3.2.66}$$

where f(h) is the rating curve which is a function of h. Equation (3.1.91) is solved iteratively to yield $h^{(n+1)}$.

3.2.3 The Semi-Lagrangian Method for Kinematic Wave

To use the semi-Lagrangian method to solve the kinematic wave equation, Eq. (2.2.50) is rewritten in the Lagrangian form as follows

$$\frac{D_V h}{D\tau} + Kh = S_S + S_R - S_E + S_I \quad where \quad K = \nabla \cdot \mathbf{V} \tag{3.2.67}$$

in which K is the decay coefficient of the wave. Integrating Eq. (3.1.100) along its characteristic line from x_i at new time level to x_i^* at old time level or on the boundary (Fig. 3.2-3), we obtain

$$\left(1+\frac{\Delta\tau}{2}K_i\right)h_i^{(n+1)}=\left(1-\frac{\Delta\tau}{2}K_i^{*}\right)h_i^{*}+\frac{\Delta\tau}{2}\left(S_{Si}^{(n+1)}+S_{Si}^{*}\right)+\frac{\Delta\tau}{2}\left(S_{Ri}^{(n+1)}+S_{Ri}^{*}\right)$$
$$-\frac{\Delta\tau}{2}\left(S_{Ei}^{(n+1)}+S_{Ei}^{*}\right)+\frac{\Delta\tau}{2}\left(S_{Ii}^{(n+1)}+S_{Ii}^{*}\right) \qquad \textbf{(3.2.68)}$$

where $\Delta\tau$ is the tracking time, it is equal to Δt when the backward tracking is carried out all the way to the root of the characteristic and it is less than Δt when the backward tracking hits the boundary before Δt is consumed; $K_i^{(n+1)}$, $h_i^{(n+1)}$, $S_{Si}^{(n+1)}$, $S_{Ri}^{(n+1)}$, $S_{Ei}^{(n+1)}$, and $S_{Ii}^{(n+1)}$, respectively, are the values of K, h, S_S, S_R, S_E, and S_I, respectively, at x_i at new time level $t = (n+1)\Delta t$; and K_i^{*}, h_i^{*}, S_{Si}^{*}, S_{Ri}^{*}, S_{Ei}^{*}, and S_{Ii}^{*}, respectively, are the values of K, h, S_S, S_R, S_E, and S_I, respectively, at the location x_i^{*}. Because of density and wind effects, the velocity **V** and the decay coefficient K are functions of h, this is a nonlinear problem. However, because the nonlinearity due to density and wind effects are normally very weak, Equation (3.2.68) is considered a linear hyperbolic problem with the nonlinear effects evaluated using the values of h at previous time. This equation is used to compute the water depth, h, at all nodes except for the upstream boundary node.

Because the wave is transported into the region at an upstream node, a boundary condition must be specified. The flow rate is normally given as a function of time at an upstream node, from which the boundary value is computed as

$$h_1^{(n+1)}=\frac{q_{up}(t)}{V_i^{(n+1)}} \qquad \textbf{(3.2.69)}$$

where $q_{up}(t)$, a function of time t, is the prescribed flow rate [$L^3/t/L$].

3.2.2 Numerical Approximations of Thermal Transport

Two options are provided in this report to solve the thermal transport equation. One is the finite element method and the other is the particle tracking method.

3.2.4.1 Finite Element Method. Recall the thermal transport equation is governed by Eq. (2.2.52) which is rewritten in a slightly different form as

$$\rho_W C_W h\frac{\partial T}{\partial t}+\frac{\partial(\rho_W C_W h)}{\partial t}T+\nabla\cdot(\rho_W C_W\mathbf{q}T)-\nabla\cdot(\mathbf{D}^H h\cdot\nabla T)$$
$$=H_a+H_r+H_n-H_b-H_e-H_s+H_i+H_c \qquad \textbf{(3.2.70)}$$

Applying the finite element method to Eq. (3.2.70), we obtain the following matrix equation

$$[M]\frac{d\{T\}}{dt}+[V]\{T\}+[D]\{T\}+[K]\{T\}$$
$$=-\{\Phi^B\}+\{\Phi^a\}+\{\Phi^r\}+\{\Phi^n\}-\{\Phi^b\}-\{\Phi^e\}-\{\Phi^s\}+\{\Phi^i\}+\{\Phi^c\} \qquad \textbf{(3.2.71)}$$

in which

$$M_{ij} = \int_R N_i \rho_W C_W h N_j dR, \qquad V_{ij} = \int_R \nabla W_i \rho_W C_W \mathbf{q} N_j dR, \qquad D_{ij} = \int_R \nabla N_i \mathbf{D}^{\mathbf{H}} h \nabla N_j dR,$$
$$K_{ij} = \int_R N_i \frac{\partial \rho_W C_W h}{\partial t} N_j dR, \qquad \Phi_i^B = \int_B \mathbf{n} \cdot \left(W_i \rho_W C_W \mathbf{q} T - N_i \mathbf{D}^{\mathbf{H}} h \nabla T \right) dB \tag{3.2.72}$$

$$\Phi_i^a = \int_R N_i H_a R, \qquad \Phi_i^r = \int_R N_i H_r dR, \qquad \Phi_i^n = \int_R N_i H_n dR \tag{3.2.73}$$

$$\Phi_i^b = \int_R N_i H_b dR, \qquad \Phi_i^e = \int_R N_i H_e dR, \qquad \Phi_i^s = \int_R N_i H_s dR, \qquad \Phi_i^c = \int_R N_i H_c dR, \tag{3.2.74}$$

$$\Phi_i^i = \int_R N_i H_i dx \tag{3.2.75}$$

where W_i is the weighting function of node at x_i; N_i and N_j are the base functions of nodes at x_i and x_j, respectively; [M] is the mass matrix, [V] is the stiff matrix due to advective transport; [D] is the stiff matrix due to dispersion/diffusion/conduction; {T} is the solution vector of temperature; $\{\Phi^B\}$ is the vector due to boundary conditions, which can contribute to load vector and/or coefficient matrix; $\{\Phi^a\}$ is the load vector due to artificial energy source; $\{\Phi^r\}$ is the load vector due to energy contained in rainfall; $\{\Phi^n\}$ is the load vector due to net radiation; $\{\Phi^b\}$ is the vector due to backward radiation, which is a nonlinear function of temperature and contributes to both the load vector and coefficient matrix; $\{\Phi^e\}$ is the vector due to energy consumed for evaporation, which is a nonlinear function of temperature and contributes to both the load vector and coefficient matrix; $\{\Phi^s\}$ is the vector due to sensible heat, which is a linear function of temperature and contributes to both the load vector and coefficient matrix; $\{\Phi^c\}$ is the vector due to chemical reaction, which is not considered in this version, but can be added easily; and $\{\Phi^i\}$ is the vector due to interaction with subsurface exfiltraing water.

Approximating the time derivative term in Eq. (3.2.71) with a time-weighted finite difference, we reduce the advective-diffusive equation and its boundary conditions to the following matrix equation

$$[C]\{T\} = \{L\} - \{\Phi^B\} - \{\Phi^b\} - \{\Phi^e\} - \{\Phi^s\} + \{\Phi^i\} \tag{3.2.76}$$

in which

$$[C] = \frac{[M]}{\Delta t} + \theta([D] + [K]) + \theta_V [V],$$
$$\{L\} = \left(\frac{[M]}{\Delta t} - (1-\theta)([DS] + [K]) - (1-\theta_V)[V] \right) \{T^{(n)}\} + \{\Phi^a\} + \{\Phi^r\} + \{\Phi^n\} \tag{3.2.77}$$

where [C] is the coefficient matrix, {L} is the load vector from initial condition, artificial sink/sources, rainfall, and net radiation; Δt is the time step size; θ is the time weighting factor for the dispersion and linear terms; θ_v is the time weighting factor for the velocity term; and $\{T^{(n)}\}$ is the value of {T} at old time level n. The global boundary conditions must be used to provide $\{\Phi^B\}$ in Eq. (3.2.76). The interaction between the overland and subsurface flows must be implemented to calculate $\{\Phi^i\}$. The interactions will be addressed in Section 3.4.

For a global boundary node I, the corresponding algebraic equation from Eq. (3.2.76) is

$$C_{I1}T1 + .. + C_{I,1}TI + .. + C_{I,N}T_N = L_I - \left(\Phi_I^b + \Phi_i^e + \Phi_I^S\right) + \Phi_I^i - \Phi_I^B \qquad \textbf{(3.2.78)}$$

In the above equations there are two unknowns T_I and Φ_I^B; either T_I or Φ_I^B, or the relationship between T_I and Φ_I^B must be specified. The numerical implementation of these boundary conditions is described as follows.

Direchlet boundary condition: prescribed temperature

If T_I is given on the boundary node I (Dirichlet boundary condition), all coefficients ($C_{I,1}$, .., $C_{I,I}$, .., $C_{I,N}$) and the right-hand side terms (L_I, Φ_I^b, Φ_I^e, Φ_I^s, Φ_I^i) obtained before the implementation of boundary conditions for this equation are stored in a temporary array, then an identity equation is created as

$$T_I = T_{Id}, \quad I \in N_D \qquad \textbf{(3.2.79)}$$

where T_{Id} is the prescribed temperature on the Dirichlet node I and N_D is the number of Dirichlet boundary nodes. This process is repeated for every Dirichlet nodes. Note it is unnecessary to modify other equations that involving this unknown, which was done in the previous version. By not modifying other equations, the symmetrical property of the matrix is preserved, which makes the iterative solvers more robust. The final set of equations will consist of N_D identity equations and (N - N_D) finite element equations for N unknowns T_i's. After T_i's for all nodes are solved from the matrix equation, Eq. (3.2.78) is then used to back calculate N_D Φ_I^B's.

If a direct solver is used to solve the matrix equation, the above procedure will solve N T_i's accurately except for roundoff errors. However, if an iterative solver is used, a stopping criterion must be strict enough so that the converged solution of N T_i's are accurate enough to the exact solution. With such accurate T_i's, then can be sure that the back-calculated ND Φ_I^B's are accurate.

Cauchy boundary condition: prescribed heat flux

If Φ_{BI} is given (Cauchy flux boundary condition), all coefficients ($C_{I,1}$, .., $C_{I,I}$, .., $C_{I,N}$) and right-hand side terms (L_I, Φ_I^a, Φ_I^r, Φ_I^n, Φ_I^i) obtained before the implementation of boundary conditions for this equation are stored in a temporary array, then Eq. (3.2.78) is modified to incorporate the boundary conditions and used to solve for T_I. The modification of Eq. (3.2.78) is straightforward. Because Φ_I^B is a known quantity, it contributes to the load on the right hand side. This type of boundary conditions is very easy to implement. After T_i's are obtained, the original Eq. (3.2.78), which is stored in a temporary array, is used to back calculate N_C Φ_I^B's on flux boundaries (where N_C is the number of flux boundary nodes). These back-calculated Φ_I^B's should be theoretically identical to the input Φ_I^B's. However, because of round-off errors (in the case of direct solvers) or because of stopping criteria (in the case of iterative solvers), the back-calculated Φ_I^B's will be slightly different from the input Φ_I^B's. If the differences between the two are significant, it is an indication that the solvers have not yielded accurate solutions.

Neumann boundary condition: prescribed gradient of temperature

At Neumann boundaries, the temperature gradient is prescribed, thus, the flux due to temperature gradient is given. For this case, all coefficients ($C_{I,1}$, .., $C_{I,I}$, .., $C_{I,N}$) and right-hand side terms (L_I, Φ_I^a, Φ_I^r, Φ_I^n, Φ_I^i) obtained before the implementation of boundary conditions for this equation are stored in a temporary array, then Eq. (3.2.78) is modified to incorporate the boundary conditions and used to solve for T_I. For the Neumann boundary condition, Φ_I^B contributes to both the matrix coefficient and load vector, thus both the coefficient matrix [C] and the load vector {L} must be modified. Recall

$$\Phi_i^B = \int_B \mathbf{n} \cdot \left(W_i \rho_W C_W \mathbf{q} T - N_i \mathbf{D}^{\mathbf{H}} h \nabla T \right) dB \tag{3.2.80}$$

Substituting Eq. (2.2.58) into Eq. (3.2.80), we have

$$\begin{aligned} &\left\{ \Phi^B \right\} \equiv \left[CB \right] \left\{ T \right\} + \left\{ LB \right\} \\ &\textit{in which} \qquad CB_{i,j} = \int_B n \cdot W_i \rho_W C_W q N_j dB \qquad \textit{and} \qquad LB_i = \int_B N_i \varphi_{nb}(t) dB \end{aligned} \tag{3.2.81}$$

where [CB] and {LB} are the coefficient matrix and load vector due to Neumann boundary. Adding the I-th equation in Eq. (3.2.81) to Eq. (3.2.78), we obtained a modified equation, which can be solved for solve T_I. After T_I is solved, the original Eq. (3.2.78) (recall the original Eq. (3.2.78) must be and has been stored in a temporary array) is used to back-calculate Φ_I^B.

Variable boundary condition:

At the variable boundary condition Node I, the implementation of boundary conditions can be made identical to that for a Cauchy boundary condition node if the flow is directed into the region. If the flow is going out of the region, the boundary condition is implemented similar to the implementation of Neuman boundary condition with $LB_I = 0$. The assumption of zero Neumann flux implies that a Neuman node must be far away from the source/sink.

3.2.4.2 The Hybrid Lagrangian-Eulerian Finite Element Method. When the hybrid Lagrangian-Eulerian finite element method is used to solve the thermal transport equation, we expand Eq. (3.2.70) to yield following advection-dispersion equation in the Lagrangian form

$$\frac{D_V T}{Dt} + KT = D + \Phi^S + \Phi^I \quad \textit{where} \quad \mathbf{V} = \frac{\mathbf{q}}{h} \tag{3.2.82}$$

in which

$$\begin{aligned} &K = \frac{1}{\rho_W C_W h} \frac{\partial \rho_W C_W h}{\partial t} + \frac{1}{\rho_W C_W h} \nabla \cdot \left(\rho_W C_W \mathbf{q} \right), \qquad D = \frac{1}{\rho_W C_W h} \nabla \cdot \left(h \mathbf{D}^H \cdot \nabla T \right) \\ &\Phi^S = \frac{H_a + H_r + H_n - H_b - H_c - H_s}{\rho_W C_W h}, \qquad \Phi^I = \frac{H_i}{\rho_W C_W h} \end{aligned} \tag{3.2.83}$$

To use the semi-Lagrangian method to solve the thermal transport equation, we integrate Eq. (3.2.82) along its characteristic line from x_i at new time level to x_i^* at old time level or on the

boundary (Fig. 3.2-3), we obtain

$$\left(1+\frac{\Delta\tau}{2}K_i^{(n+1)}\right)T_1^{(n+1)}=\left(1-\frac{\Delta\tau}{2}K_i^{*}\right)T_i^{*}+ \\ \frac{\Delta\tau}{2}\left(D_i^{(n+1)}+D_i^{*}\right)+\frac{\Delta\tau}{2}\left(\Phi_i^{S^{(n+1)}}+\Phi_i^{S^{*}}\right)+\frac{\Delta\tau}{2}\left(\Phi_i^{I^{(n+1)}}+\Phi_i^{I^{*}}\right),\quad i\in N \tag{3.2.84}$$

where $\Delta\tau$ is the tracking time, it is equal to Δt when the backward tracking is carried out all the way to the root of the characteristic and it is less than Δt when the backward tracking hits the boundary before Δt is consumed; $K_i^{(n+1)}$, $T_i^{(n+1)}$, $D_i^{(n+1)}$, $\Phi_i^{S(n+1)}$, and $\Phi_i^{I(n+1)}$ respectively, are the values of K, T, D, Φ^S, and Φ^I, respectively, at x_i at new time level $t = (n+1)\Delta t$; and K_i^{*}, T_i^{*}, D_i^{*}, Φ_i^{S*}, and Φ_i^{I*}, respectively, are the values of K, T, D, Φ^S, and Φ^I, respectively, at the location x_i^{*}.

To compute the dispersion/diffusion terms $D_i^{(n+1)}$ and D_i^{*}, we rewrite the second equation in Eq. (3.2.83) as

$$\rho_W C_W hD=\nabla\cdot\left(\mathbf{D}^{\mathbf{H}}h\cdot\nabla T\right) \tag{3.2.85}$$

Applying the Galerkin finite element method to Eq. (3.2.85) at new time level (n+1), we obtain the following matrix equation for $\{D^{(n+1)}\}$ as

$$\left[a^{(n+1)}\right]\left\{D^{(n+1)}\right\}+\left[b^{(n+1)}\right]\left\{T^{(n+1)}\right\}=\left\{B^{(N+1)}\right\} \tag{3.2.86}$$

in which

$$\left\{D^{(n+1)}\right\}=\left\{D_1^{(n+1)}\quad D_2^{(n+1)}\quad \cdot\ \cdot\quad D_i^{(n+1)}\quad \cdot\ \cdot\quad D_N^{(n+1)}\right\}^{Transpose} \tag{3.2.87}$$

$$\left\{T^{(n+1)}\right\}=\left\{T_1^{(n+1)}\quad T_2^{(n+1)}\quad \cdot\ \cdot\quad T_i^{(n+1)}\quad \cdot\ \cdot\quad T_N^{(n+1)}\right\}^{Transpose} \tag{3.2.88}$$

$$\left\{\mathbf{B}^{(n+1)}\right\}=\left\{B_1^{(n+1)}\quad B_2^{(n+1)}\quad \cdot\ \cdot\quad B_i^{(n+1)}\quad \cdot\ \cdot\quad B_N^{(n+1)}\right\}^{Transpose} \tag{3.2.89}$$

$$a_{ij}^{(n+1)}=\int_R N_i\left(\rho_W C_W h\right)\Big|_{(n+1)}N_j dR,\qquad b_{ij}^{(n+1)}=\int_R \nabla N_i\cdot\left(\mathbf{D}^{\mathbf{H}}h\right)\Big|_{(n+1)}\cdot\nabla N_j dR, \\ B_i^{(n+1)}=\int_B \mathbf{n}\cdot N_i\left(\mathbf{D}^{\mathbf{H}}h\right)\Big|_{(n+1)}\cdot\nabla T^{(n+1)}dB \tag{3.2.90}$$

where the superscript (n+1) denotes the time level; N and N are the base functions of nodes at x_i and x_j, respectively.

Lumping the matrix $[a^{(n+1)}]$, we can solve Eq. (3.2.86) for $D_I^{(n+1)}$ as follows

$$D_I^{(n+1)}=-\frac{1}{a_{II}^{(n+1)}}\sum_j b_{Ij}^{(n+1)}T_j^{(n+1)}\quad if\quad I\quad is\ an\ \text{interior point} \\ D_I^{(n+1)}=\frac{1}{a_{II}^{(n+1)}}B_I^{(n+1)}-\frac{1}{a_{II}^{(n+1)}}\sum_j b_{Ij}^{(n+1)}T_j^{(n+1)}\quad if\quad I\quad is\ a\ boundary\ \text{point} \tag{3.2.91}$$

where $a_{II}^{(n+1)}$ is the lumped $a_{ii}^{(n+1)}$. Following the identical procedure that leads Eq. (3.2.85) to Eq. (3.2.91), we have

$$D_I^{(n)} = -\frac{1}{a_{II}^{(n)}} \sum_j b_{Ij}^{(n)} T_j^{(n)} \quad if\ I\ is\ an\ \text{interior point}$$
$$D_I^{(n)} = \frac{1}{a_{II}^{(n)}} B_I^{(n)} - \frac{1}{a_{II}^{(n)}} \sum_j b_{Ij}^{(n)} T_j^{(n)} \quad if\ I\ is\ a\ boundary\ \text{point} \qquad \textbf{(3.2.92)}$$

where $\{B^{(n)}\}$, $\{a^{(n)}\}$ and $\{b^{(n)}\}$, respectively, are defined similar to $\{B^{(n+1)}\}$, $\{a^{(n+1)}\}$ and $\{b^{(n+1)}\}$, respectively.

With $\{D^{(n)}\}$ calculated with Eq. (3.2.92), $\{D^*\}$ can be interpolated. Substituting Eq. (3.2.91) into Eq. (3.2.84) and implementing boundary conditions given in Section 2.2.4, we obtain a system of N simultaneous algebraic equations N unknowns ($T_i^{(n+1)}$ for i = 1, 2, .., N.) If the dispersion/diffusion term is not included, then Eq. (3.2.84) is reduced to a set of N decoupled equations as

$$a_{ii} T_i^{(n+1)} = b_i, \quad i \in N \qquad \textbf{(3.2.93)}$$

where

$$a_{ii} = \left(1 + \frac{\Delta\tau}{2} K_i^{(n+1)}\right) \qquad \textbf{(3.2.94)}$$

$$b_i = \left(1 - \frac{\Delta\tau}{2} K_i^*\right) T_i^* + \frac{\Delta\tau}{2}\left(\Phi_i^{S^{(n+1)}} + \Phi i_i^{S*}\right) + \frac{\Delta\tau}{2}\left(\Phi_i^{I^{(n+1)}} + \Phi_i^{I*}\right), \quad i \in N \qquad \textbf{(3.2.95)}$$

Equation (3.2.93) is applied to all interior nodes without having to make any modification. On a boundary point, there two possibilities: Eq. (3.2.93) is replaced with a boundary equation when the flow is directed into the region or Eq. (3.2.93) is still valid when the flow is direct out of the region. In other words, when the thermal energy is transported out of the region at a boundary node (i.e., when $\mathbf{N}\bullet\mathbf{V} \geq 0$), a boundary condition is not needed and Equation (3.2.93) is used to compute the $T_i^{(n+1)}$. When the thermal energy is transported into the region at a node (i.e., when $\mathbf{N}\bullet\mathbf{V} < 0$), a boundary condition must be specified.

Alternatively, to facilitate the implementation of boundary condition at incoming flow node, the algebraic equation for the boundary node is obtained by applying the finite element method to the boundary node. For this alternative approach, the implementation of boundary conditions at global boundary nodes is identical to that in the finite element approximation of solving the thermal transport equation.

3.2.4 Numerical Approximations of Salinity Transport

Two options are provided in this report to solve the salinity transport equation. One is the finite element method and the other is the particle tracking method.

3.2.5.1 Finite Element Method. Recall the salinity transport equation is governed by Eq. (2.2.60) which is rewritten in a slightly different form as

$$h\frac{\partial S}{\partial t}+\frac{\partial h}{\partial t}S+\nabla\cdot(\mathbf{q}S)-\nabla\cdot\left(\mathbf{D}^{s}h\cdot\nabla h\right)=M_s^{as}+M_x^{rs}-M_s^{es}+M_s^{is} \qquad \textbf{(3.2.96)}$$

Applying the finite element method to Eq. (3.2.96), we obtain the following matrix equation

$$[M]\frac{d\{S\}}{dt}+[V]\{S\}+[D]\{S\}+[K]\{S\}=-\{\Psi^B\}+\{\Psi^a\}+\{\Psi^r\}-\{\Psi^e\}+\{\Psi^i\} \qquad \textbf{(3.2.97)}$$

in which

$$\begin{aligned}&M_{ij}=\int_R N_i h N_j dx, \qquad V_{ij}=\int_R \nabla W_i\cdot\mathbf{q}N_j dR, \qquad D_{ij}=\int_R \nabla N_i\cdot\mathbf{D}^{s}h\cdot\nabla N_j dR,\\ &K_{ij}=\int_r N_i\frac{\partial h}{\partial t}N_j dR, \qquad \Psi_i^B=\int_B \mathbf{n}\cdot\left(W_i\mathbf{q}S-N_i\mathbf{D}^{s}h\cdot\nabla S\right)dB\end{aligned} \qquad \textbf{(3.2.98)}$$

$$\Psi_i^a=\int_R N_i M_S^{as}dR,\ \ \Psi_i^r=\int_R N_i M_s^{rs}dR,\ \ \Psi_i^e=\int_R N_i M_s^{es}dR,\ \ \Psi_i^i=\int_R N_i M_s^{is}dR \qquad \textbf{(3.2.99)}$$

where W_i is the weighting function of node at x_i; N_i and N_j are the base functions of nodes at x_i and x_j, respectively; [M] is the mass matrix, [V] is the stiff matrix due to advective transport; [D] is the stiff matrix due to dispersion/diffusion/conduction; [K] is the stiff matrix due to the linear term; {S} is the solution vector of salinity; $\{\Psi^B\}$ is the vector due to boundary conditions, which can contribute to load vector and/or coefficient matrix; $\{\Psi^a\}$ is the load vector due to artificial salt source; $\{\Psi^r\}$ is the load vector due to salt in rainfall; $\{\Psi^e\}$ is the vector due to evapotranspiration, which is most likely to be zero; and $\{\Psi^i\}$ is the vector due to interaction with subsurface exfiltraing water.

Approximating the time derivative term in Eq. (3.2.97) with a time-weighted finite difference, we reduce the advective-diffusive equation and its boundary conditions to the following matrix equation.

$$[C]\{S\}=\{L\}-\{\Psi^B\}+\{\Psi^i\} \qquad \textbf{(3.2.100)}$$

in which

$$\begin{aligned}&[C]=\frac{[M]}{\Delta t}+\theta([D]+[K])+\theta_V[V],\\ &\{L\}=\left(\frac{[M]}{\Delta t}-(1-\theta)([D]+[K])-(1-\theta_V)[V]\right)\{S^{(n)}\}+\{\Psi^a\}+\{\Psi^r\}\end{aligned} \qquad \textbf{(3.2.101)}$$

where [C] is the coefficient matrix, {L} is the load vector from initial condition, artificial sink/sources and rainfall; Δt is the time step size; θ is the time weighting factor for the dispersion and linear terms; θ_v is the time weighting factor for the velocity term; and $\{S^{(n)}\}$ is the value of {S} at old time level n. The global boundary conditions must be used to provide $\{\Psi^B\}$ in Eq. (3.2.100). The interaction between the overland and subsurface flows must be implemented to calculate $\{\Psi^i\}$. The interactions will be addressed in Section 3.4.

For a global boundary node I, the corresponding algebraic equation from Eq. (3.2.100) is

$$C_{I,1}S_1 + .. + C_{I,I}S_I + .. + C_{I,N}S_N = L_I + \Psi_I^i - \Psi_I^B \qquad \textbf{(3.2.102)}$$

In the above equations there are two unknowns T_I and Ψ_I^B; either T_I or Ψ_I^B, or the relationship between T_I and Ψ_I^B must be specified. The numerical implementations of these boundary conditions are described as follows.

Dirichlet boundary condition: prescribed salinity

If S_I is given on the boundary node I (Dirichlet boundary condition), all coefficients ($C_{I,1}$, .., $C_{I,I}$, .., $C_{I,N}$) and the right-hand side terms (L_I and Ψ_I^i) obtained before the implementation of boundary conditions for this equation are stored in a temporary array, then an identity equation is created as

$$S_I = S_{Id}, \quad I \in N_D \qquad \textbf{(3.2.103)}$$

where S_{Id} is the prescribed salinity on the Dirichlet node I and N_D is the number of Dirichlet boundary nodes. This process is repeated for every Dirichlet nodes. Note it is unnecessary to modify other equations that involving this unknown, which was done in the previous version. By not modifying other equations, the symmetrical property of the matrix is preserved, which makes the iterative solvers more robust. The final set of equations will consist of N_D identity equations and (N - N_D) finite element equations for N unknowns S_i's. After S_i's for all nodes are solved from the matrix equation, Eq. (3.2.100) is then used to back calculate N_D Ψ_I^B's.

If a direct solver is used to solve the matrix equation, the above procedure will solve N S_i's accurately except for roundoff errors. However, if an iterative solver is used, a stopping criterion must be strict enough so that the converged solution of N S_i's are accurate enough to the exact solution. With such accurate S_i's, then can be sure that the back-calculated ND Ψ_{BI}'s are accurate.

Cauchy boundary condition: prescribed salt flux

If Ψ_I^B is given (Cauchy flux boundary condition), all coefficients ($C_{I,1}$, .., $C_{I,I}$, .., $C_{I,N}$) and the right-hand side terms (L_I and Ψ_I^i) obtained before the implementation of boundary conditions for this equation are stored in a temporary array, then Eq. (3.2.102) is modified to incorporate the boundary conditions and used to solve for S_I. The modification of Eq. (3.2.102) is straightforward. Because Ψ_I^B is a known quantity, it contributes to the load on the right hand side. This type of boundary conditions is very easy to implement. After S_i's are obtained, the original Eq. (3.2.102), which is stored in a temporary array, is used to back calculate N_C Ψ_I^B's on flux boundaries (where N_C is the number of flux boundary nodes). These back-calculated Ψ_I^B's should be theoretically identical to the input Ψ_I^B's. However, because of round-off errors (in the case of direct solvers) or because of stopping criteria (in the case of iterative solvers), the back-calculated Ψ_I^B's will be slightly different from the input Ψ_I^B's. If the differences between the two are significant, it is an indication that the solvers have not yielded accurate solutions.

Neumann boundary condition: prescribed gradient of salinity

At Neumann boundaries, the temperature gradient is prescribed, thus, the flux due to temperature

gradient is given. For this case, all coefficients ($C_{I,}$ .., $C_{I,I}$, .., $C_{I,N}$) and the right-hand side terms (L_I and Ψ_I^i) obtained before the implementation of boundary conditions for this equation are stored in a temporary array, then Eq. (3.2.102) is modified to incorporate the boundary conditions and used to solve for S_I. For the Neumann boundary condition, Ψ_I^B contributes to both the matrix coefficient and load vector, thus both the coefficient matrix [C] and the load vector {L} must be modified. Recall

$$\Psi_i^B = \int_B \mathbf{n} \cdot \left(W_i \mathbf{q} S - N_i D^S h \nabla S \right) dB \qquad \textbf{(3.2.104)}$$

Substituting Eq. (2.2.66) into Eq. (3.2.104), we have

$$\begin{aligned} &\left\{ \Psi^B \right\} \equiv \left[CB \right] \left\{ S \right\} + \left\{ LB \right\} \\ &\textit{in which} \qquad CB_{i,j} = \int_B \mathbf{n} \cdot W_i \mathbf{q} N_j dB \quad \textit{and} \quad LB_i = \int_B N_i \Psi_{nb}(t) dB \end{aligned} \qquad \textbf{(3.2.105)}$$

where [CB] and {LB} are the coefficient matrix and load vector due to Neumann boundary. Adding the I-th equation in Eq. (3.2.105) to Eq. (3.2.102), we obtained a modified equation, which can be solved for solve S_I. After S_I is solved, the original Eq. (3.2.102) (recall the original Eq. (3.2.102) must be and has been stored in a temporary array) is used to back-calculate Ψ_I^B.

Variable boundary condition:

At the variable boundary condition Node I, the implementation of boundary conditions can be made identical to that for a Cauchy boundary condition node if the flow is directed into the river/stream/canal reach. If the flow is going out of the reach, the boundary condition is implemented similar to the implementation of Neuman boundary condition with $\Psi_I^{nb} = 0$. The assumption of zero Neumann flux implies that a Neuman node must be far away from the source/sink.

3.2.5.2 The Hybrid Lagrangian-Eulerian Finite Element Method. When the hybrid Lagrangian-Eulerian finite element method is used to solve the salt transport equation, we expand Eq. (3.2.96) to yield following advection-dispersion equation in the Lagrangian form

$$\frac{D_V S}{Dt} + KS = D + \Psi^S + \Psi^I \quad \textit{where} \quad \mathbf{V} = \frac{\mathbf{q}}{h} \qquad \textbf{(3.2.106)}$$

in which

$$K = \frac{1}{h}\frac{\partial h}{\partial t} + \frac{1}{h}\nabla \cdot (\mathbf{q}), \qquad D = \frac{1}{h}\nabla \cdot \left(h \mathbf{D}^S \cdot \nabla S \right), \qquad \Psi^S = \frac{M_s^{as} + M_s^{rs} - M_s^{es}}{h}, \qquad \Psi^I = \frac{M_s^{is}}{h} \qquad \textbf{(3.2.107)}$$

To use the semi-Lagrangian method to solve the thermal transport equation, we integrate Eq. (3.2.106) along its characteristic line from x_i at new time level to x_i^* at old time level or on the boundary (Fig. 3.2-3), we obtain

$$\left(1+\frac{\Delta\tau}{2}K_i^{(n+1)}\right)S_i^{(n+1)}=\left(1-\frac{\Delta\tau}{2}K_i^{*}\right)S_i^{*}+\frac{\Delta\tau}{2}\left(D_i^{(n+1)}+D_i^{*}\right)$$
$$+\frac{\Delta\tau}{2}\left(\Psi_i^{S^{(n+1)}}+\Psi_i^{S^{*}}\right)+\frac{\Delta\tau}{2}\left(\Psi_i^{I^{(n+1)}}+\Psi_i^{I^{*}}\right),\quad i\in N \tag{3.2.108}$$

where $\Delta\tau$ is the tracking time, it is equal to Δt when the backward tracking is carried out all the way to the root of the characteristic and it is less than Δt when the backward tracking hits the boundary before Δt is consumed; $K_i^{(n+1)}$, $T_i^{(n+1)}$, $D_i^{(n+1)}$, $\Psi_i^{S(n+1)}$, and $\Psi_i^{I(n+1)}$ respectively, are the values of K, T, D, Ψ^S, and Ψ^I, respectively, at x_i at new time level $t = (n+1)\Delta t$; and K_i^{*}, T_i^{*}, D_i^{*}, Ψ_i^{S*}, and Ψ_i^{I*}, respectively, are the values of K, T, D, Ψ^S, and Ψ^I, respectively, at the location x_i^{*}.

To compute the dispersion/diffusion terms $D_i^{(n+1)}$ and D_i^{*}, we rewrite the second equation in Eq. (3.2.107) as

$$hD=\nabla\cdot\left(h\mathbf{D}^S\cdot\nabla S\right) \tag{3.2.109}$$

Applying the Galerkin finite element method to Eq. (3.2.109) at new time level (n+1), we obtain the following matrix equation for $\{D^{(n+1)}\}$ as

$$\left[a^{(n+1)}\right]\left\{D^{(n+1)}\right\}+\left[b^{(n+1)}\right]\left\{S^{(n+1)}\right\}=\left\{B^{(n+1)}\right\} \tag{3.2.110}$$

in which

$$\left\{D^{(n+1)}\right\}=\left\{D_1^{(n+1)}\quad D_2^{(n+1)}\quad\ldots\quad D_i^{(n+1)}\quad\ldots\quad D_N^{(n+1)}\right\}^{Transpose} \tag{3.2.111}$$

$$\left\{S^{(n+1)}\right\}=\left\{S_1^{(n+1)}\quad S_2^{(n+1)}\quad\ldots\quad S_i^{(n+1)}\quad\ldots\quad S_N^{(n+1)}\right\}^{Transpose} \tag{3.2.112}$$

$$\left\{B^{(n+1)}\right\}=\left\{B_1^{(n+1)}\quad B_2^{(n+1)}\quad\ldots\quad B_i^{(n+1)}\quad\ldots\quad B_N^{(n+1)}\right\}^{Transpose} \tag{3.2.113}$$

$$a_{ij}^{(n+1)}=\int_R N_i(h)\Big|_{(n+1)}N_j\,dR,\qquad b_{ij}^{(n+1)}=\int_R\nabla N_i\cdot\left(h\mathbf{D}^S\right)\Big|_{(n+1)}\cdot\nabla N_j\,dR,$$
$$B_i^{(n+1)}=\int_B\mathbf{n}\cdot N_i\left(h\mathbf{D}^S\right)\Big|_{(n+1)}\cdot\nabla S^{(n+1)}\,dB \tag{3.2.114}$$

where the superscript (n+1) denotes the time level; N and N are the base functions of nodes at x_i and x_j, respectively.

Lumping the matrix $[a^{(n+1)}]$, we can solve Eq. (3.2.110) for $D_I^{(n+1)}$ as follows

$$D_I^{(n+1)}=-\frac{1}{a_{II}^{(n+1)}}\sum_j b_{Ij}^{(n+1)}S_j^{(n+1)}\quad if\quad I\ is\ an\ interior\ point$$
$$D_I^{(n+1)}=\frac{1}{a_{II}^{(n+1)}}B_I^{(n+1)}-\frac{1}{a_{II}^{(n+1)}}\sum_j b_{Ij}^{(n+1)}S_j^{(n+1)}\quad if\quad I\ is\ a\ boundary\ point \tag{3.2.115}$$

where $a_{II}^{(n+1)}$ is the lumped $a_{ii}^{(n+1)}$. Following the identical procedure that leads Eq. (3.2.109) to Eq.

(3.2.115), we have

$$D_I^{(n)} = -\frac{1}{a_{II}^{(n)}}\sum_j b_{Ij}^{(n)} S_j^{(n)} \quad if \quad I \text{ is an interior point}$$
$$D_I^{(n)} = \frac{1}{a_{II}^{(n)}} B_I^{(n)} - \frac{1}{a_{II}^{(n)}}\sum_j b_{Ij}^{(n)} S_j^{(n)} \quad if \quad I \text{ is a boundary point} \qquad \textbf{(3.2.116)}$$

where $\{B^{(n)}\}$, $\{a^{(n)}\}$ and $\{b^{(n)}\}$, respectively, are defined similar to $\{B^{(n+1)}\}$, $\{a^{(n+1)}\}$ and $\{b^{(n+1)}\}$, respectively.

With $\{D^{(n)}\}$ calculated with Eq. (3.2.116), $\{D^*\}$ can be interpolated. Substituting Eq. (3.2.115) into Eq. (3.2.108) and implementing boundary conditions given in Section 2.2.5, we obtain a system of N simultaneous algebraic equations N unknowns ($S_i^{(n+1)}$ for i = 1, 2, .., N.) If the dispersion/diffusion term is not included, then Eq. (3.2.108) is reduced to a set of N decoupled equations as

$$a_{ii} S_i^{(n+1)} = b_i, \quad i \in N \qquad \textbf{(3.2.117)}$$

where

$$a_{ii} = \left(1 + \frac{\Delta\tau}{2} K_i^{(n+1)}\right) \qquad \textbf{(3.2.118)}$$

$$b_i = \left(1 - \frac{\Delta\tau}{2} K_i^*\right) S_i^* + \frac{\Delta\tau}{2}\left(\Psi_i^{S^{(n+1)}} + \Psi_i^{S^*}\right) + \frac{\Delta\tau}{2}\left(\Psi_i^{I^{(n+1)}} + \Psi_i^{I^*}\right), \quad i \in N \qquad \textbf{(3.2.119)}$$

Equation (3.2.117) is applied to all interior nodes without having to make any modification. On a boundary point, there two possibilities: Eq. (3.2.117) is replaced with a boundary equation when the flow is directed into the region or Eq. (3.2.117) is still valid when the flow is direct out of the region. In other words, when the salt is transported out of the region at a boundary node (i.e., when $\mathbf{N}\bullet\mathbf{V} \geq 0$), a boundary condition is not needed and Equation (3.2.117) is used to compute the $S_i^{(n+1)}$. When the salt is transported into the region at a node (i.e., when $\mathbf{N}\bullet\mathbf{V} < 0$), a boundary condition must be specified.

Alternatively, to facilitate the implementation of boundary condition at incoming flow node, the algebraic equation for the boundary node is obtained by applying the finite element method to the boundary node. For this alternative approach, the implementation of boundary conditions at global boundary nodes is identical to that in the finite element approximation of solving the salt transport equation.

3.3 Solving the Three-Dimensional Subsurface Flow Equations

The Richards equation is discretized with the Galerkin finite element method in space and with the finite difference method in time. In our model, the steady-state version of subsurface flow equations can be solved for determining the initial subsurface flow condition when boundary conditions are complicated and/or unsaturated zones are taken into account. The details of solving the Richards

equation and the salt transport has been described in detail elsewhere (Yeh et al, 1994; Lin et al., 1997). The numerical solution of thermal transport equations follows similar to that for two-dimensional thermal equation in overland flow. These numerical solutions are summarized below for the completeness of this report.

3.3.1 Finite Element Approximations of the Flow Equations

Finite element disretization in space. When using the finite element method, the referenced pressure head in Eq. (2.3.1) is approximated by:

$$h \approx \hat{h} = \sum_{j=1}^{N} h_j(t) N_j(x, y, z) \tag{3.3.1}$$

where h_j and N_j are the amplitude of h and the base function, respectively, at nodal point j and N is the total number of nodes. After defining a residual and forcing the weighted residual to zero, the flow equation, Eq.(2.3.1), is approximated as:

$$\begin{aligned} &\left[\int_R N_i \frac{\rho}{\rho_o} F N_j dR\right]\frac{dh_j}{dt} + \left[\int_R (\nabla N_i)\cdot \mathbf{K} \cdot (\nabla N_j) dR\right] h_j \\ &\quad = \int_R N_i \frac{\rho^*}{\rho_o} q\, dR - \int_R (\nabla N_i)\cdot \mathbf{K} \cdot \frac{\rho}{\rho_o}\nabla z dR + \int_B \mathbf{n}\cdot \mathbf{K} \cdot \left(\nabla h + \frac{\rho}{\rho_o}\nabla z\right) N_i dB \end{aligned} \tag{3.3.2}$$

In matrix form, Eq.(3.3.2) is written as:

$$[M]\left\{\frac{dh}{dt}\right\} + [S]\{h\} = \{Q\} + \{G\} + \{B\} \tag{3.3.3}$$

where {dh/dt} and {h} are the column vectors containing the values of dh/dt and h, respectively, at all nodes; [M] is the mass matrix resulting from the storage term; [S] is the stiff matrix resulting from the action of conductivity; {Q}, {G}, and {B} are the load vectors from the internal source/sink, gravity force, and boundary conditions, respectively. The mass matrix, [M], and stiff matrix, [S], are defined as:

$$M_{ij} = \sum_{e\in M_e} \int_{R_e} N_\alpha^e \frac{\rho}{\rho_o} F N_\beta^e dR \quad \text{and} \quad S_{ij} = \sum_{e\in M_e} \int_{R_e} (\nabla N_\alpha^e)\cdot \mathbf{K} \cdot (\nabla N_\beta^e) dR \tag{3.3.4}$$

where R_e is the region of element e, M_e is the set of elements that have a local side α-β coinciding with the global side i-j, and N_α^e is the α-th local base function of element e. The three load vectors, {Q}, {G}, and {B}, are defined as:

$$Q_i = \sum_{e\in M_e} \int_{R_e} N_\alpha^e \frac{\rho}{\rho_o} q dR, \qquad G_i = -\sum_{e\in M_e} \int_{R_e} (\nabla N_\alpha^e)\cdot \mathbf{K} \cdot \frac{\rho}{\rho_o}\nabla z\, dR \tag{3.3.5}$$

$$B_i = -\sum_{e \in N_{se}} \int_{B_e} N_\alpha^e n \cdot \left[-K \cdot \left\{ \nabla h + \frac{\rho}{\rho_o} \nabla z \right\} \right] dB \qquad \textbf{(3.3.6)}$$

where N_{se} is the set of boundary segments that have a local node α coinciding with the global node i, and B_e is the length of boundary segment e.

Finite element evaluation of Darcy velocity. In most numerical models, Darcy velocity components are calculated numerically by taking the derivatives of the simulated h as

$$\mathbf{V} = -\mathbf{K} \cdot \left(\frac{\rho}{\rho_o} (\nabla N_j) h_j + \nabla z \right) \qquad \textbf{(3.3.7)}$$

The above formulation results in velocity field which is not continuous at element boundaries and nodal points if the variation of h is other than linear or constants. The alternative approach would be to apply the Galerkin finite element method to Eq. (2.3.3), thus one obtains

$$[U]\{V_x\} = \{D_x\}; \quad [U]\{V_y\} = \{D_y\}; \quad [U]\{V_z\} = \{D_z\} \qquad \textbf{(3.3.8)}$$

where the matrix [U] and the load vectors $\{D_x\}$, $\{D_y\}$, and $\{D_z\}$ are given by

$$U_{ij} = \sum_{e \in M_e} \int_{R_e} N_\alpha^e N_\beta^e dR, \qquad D_{xi} = \sum_{e \in M_e} \int_{R_e} N_\alpha^e \mathbf{i} \cdot \mathbf{K} \cdot \left\{ \frac{\rho_o}{\rho} \nabla h + \nabla z \right\} dR, \qquad \textbf{(3.3.9)}$$

$$D_{yi} = -\sum_{e \in M_e} \int_{R_e} N_\alpha^e \mathbf{j} \cdot \mathbf{K} \cdot \left\{ \frac{\rho_o}{\rho} \nabla h + \nabla z \right\} dR, \qquad D_{zi} = \sum_{e \in M_e} \int_{R_e} N_\alpha^e \mathbf{k} \cdot \mathbf{K} \cdot \left\{ \frac{\rho_o}{\rho} \nabla h + \nabla z \right\} dR \qquad \textbf{(3.3.10)}$$

where V_x, V_y, and V_z are the Darcy velocity components along the x-, y-, and z-directions, respectively and **i**, **j**, and **k** are the unit vector along the x-, y-, and z-coordinates, respectively.

Finite difference discretization in time. We derive a matrix equation by integrating Eq. (3.3.3). An important advantage in finite element approximation over the finite difference approximation is the inherent ability to handle complex boundaries and obtain the normal derivatives therein. In the time dimension, such advantages are not evident. Thus, finite difference methods are typically used in the approximation of the time derivative. Two time-marching methods are adopted in the present model.

The first one is the time weighted method written as:

$$\frac{[M]}{\Delta t}\left(\{h\}_{t+\Delta t} - \{h\}_t\right) + \omega[S]\{h\}_{t+\Delta t} + (1-\omega)[S]\{h_t\} = \{Q\} + \{G\} + \{B\} \qquad \textbf{(3.3.11)}$$

where [M], [S], {Q}, {G}, and {B} are evaluated at $(t + \omega\Delta t)$. In the Crank-Nicolson centered-in-time approach $\omega = 0.5$, in the backward-difference (implicit difference) $\omega = 1.0$, and in the forward-difference (explicit scheme) $\omega = 0.0$. The central-Nicolson algorithm has a truncation error of $O(\Delta t^2)$, but its propagation-of-error characteristics frequently lead to oscillatory nonlinear instability.

Both the backward-difference and forward-difference have a truncation error of O(Δt). The backward-difference is quite resistant to oscillatory nonlinear instability. On the other hand, the forward difference is only conditionally stable even for linear problems, not to mention nonlinear problems.

In the second method, the values of unknown variables are assumed to vary linearly with time during the time interval, Δt. In this mid-difference method, the recurrence formula is written as:

$$\left(\frac{2}{\Delta t}[M]+[S]\right)\{h\}_{t+\Delta t/2}-\frac{2}{\Delta t}[M]\{h\}_t=\{Q\}+\{G\}+\{B\} \qquad \textbf{(3.3.12)}$$

and

$$\{h\}_{t+\Delta t}=2\{h\}_{t+\Delta t/2}-\{h\}_t, \qquad \textbf{(3.3.13)}$$

where [M], [S], {Q}, and {B} are evaluated at (t+Δt/2).

Equations (3.3.11) and (3.3.12) can be written as a matrix equation

$$[A]\{h\}=\{L\}+\{B\}, \qquad \textbf{(3.3.14)}$$

where [A] is the assembled coefficient matrix, {h} is the unknown vector to be found and represents the values of discretized pressure field at new time, {L} is the load vector due to initial conditions and all types of sources/sinks, and {B} is the load vector due to boundary conditions including the global boundary and media-interface boundaries. Take for example, Eq. (3.3.11) with ω = 1.0, [C] and {L} represent the following:

$$[A]=\frac{[M]}{\Delta t}+[S] \quad and \quad \{L\}=\frac{[M]}{\Delta t}\{h\}_t+\{Q\}+\{G\} \qquad \textbf{(3.3.15)}$$

where $\{h\}_t$ is the vector of the discretized pressure field at previous time.

Mass lumping. Referring to the mass matrix, [M], one may recall that this is a unit matrix if the finite difference formulation is used in spatial discretization. Hence, by proper scaling, the mass matrix can be reduced to the finite-difference equivalent by lumping (Clough 1971). In many cases, the lumped mass matrix would result in better solution, in particular, if it is used in conjunction with the central or backward-difference time marching (Yeh and Ward 1980). Under such circumstances, it is preferred to the consistent mass matrix (mass matrix without lumping). Therefore, options are provided for the lumping of the matrix [M]. More explicitly, [M] will be lumped according to:

$$M_{ij}=\sum_{e\varepsilon Me}\left(\sum_{\beta=1}^{N_e}\int_{R_e}N_\alpha^e\frac{\rho}{\rho_o}FN_\beta^e dR\right) \quad if \quad j=i \quad and \quad M_{ij}=0 \quad if \quad j\neq i \qquad \textbf{(3.3.16)}$$

Implementation of global Boundary Conditions. For any interior node I, its algebraic equation is obtained by the I-th row of Eq. (3.3.14) as

$$A_{I,1}h_1+\ldots+A_{I,I}h_I+\ldots+A_{I,N}h_N=L_I \qquad \textbf{(3.3.17)}$$

Note that B_I is absent from Eq. (3.3.17) for all interior nodes. For the purpose of discussion, one may consider Eq. (3.3.17) to correspond the unknown h_I (one equation, one unknown). For any boundary node I, the corresponding algebraic equation from Eq. (3.3.14) is

$$A_{I,1}h_1 + \ldots + A_{I,I}h_I + \ldots + A_{I,N}h_N = L_I + B_I \qquad \textbf{(3.3.18)}$$

In the above equation there are two unknowns h_I and B_I; either h_I or B_I, or the relationship between h_I and B_I must be specified. Before the implementation of global boundary and media-interface boundary conditions, the coefficient matrix ($A_{I,1}$, .., $A_{I,I}$, .., $A_{I,N}$) and the right hand load term (L_I) must be stored in a temporary array. Then Eq. (3.3.18) is modified with the implementation of boundary conditions. After the implementation, the modified equations are solved for the primary unknown h_I's. The final step is to back calculate B_I's using unmodified Eq. (3.3.18).

The global and interface (river-subsurface media interface or overland-subsurface media interface) conditions must be used to provide {B} for all boundary nodes in Eq. (3.3.18). The interface boundary condition will be addressed in Sub-sections 3.4.2 through 3.4.4. The global boundary conditions are addressed below.

Dirichlet boundary condition: prescribed pressure head

For a Dirichlet node I, we simply rewrite Eq. (3.3.18) as

$$h_I = h_d \qquad \textbf{(3.3.19)}$$

which is obtained by modifying both the corresponding coefficient matrix and load vector as

$$A_{I,1} = 0, .., A_{I,I-1} = 0, A_{I,I+1} = 1, A_{I,I+1} = 0, .., A_{I,N} = 0 \quad and \quad L_I + B_I = h_d \qquad \textbf{(3.3.20)}$$

Thus, it is seen that for a Dirichlet node, both the matrix coefficient and the load vector are modified.

Cauchy boundary condition: prescribed total flux

For the Cauchy boundary condition given by Eq.(2.3.7), we simply substitute Eq.(2.3.7) into Eq.(3.3.6) to yield the value of B_I for the Cauchy node I:

$$B_I = -\int_{B_c} N_I \frac{\rho}{\rho_o} q_c dB\,, \qquad \textbf{(3.3.21)}$$

Thus, the modification of Eq. (3.3.18) is to simply add B_I to L_I.

Neumann boundary condition: prescribed gradient flux

For the Neumann boundary condition given by Eq.(2.3.6), we substitute Eq.(2.3.6) into Eq.(3.3.6) to yield the value of B_I for the Neumann node I:

$$B_I = \int N_I \left(\mathbf{n} \cdot \mathbf{K} \cdot \frac{\rho}{\rho_o} \nabla z - q_n \right) dB \qquad \textbf{(3.3.22)}$$

If the hydraulic conductivity is evaluated using the value of pressure head from previous iteration, then this boundary condition only contribute to the modification of the load vector in Eq. (3.3.18). Therefore, the modification of Eq. (3.3.18) is to simply add B_I to L_I.

Variable boundary condition: Dirichlet or Cauchy boundary condition

The implementation of variable-type boundary condition is more involved. During the iteration of boundary conditions on the variable boundary, one of Eqs.(2.3.9) through (2.3.12) is used at a node. If either Eq.(2.3.10) or (2.3.13) is used, we substitute it into Eq.(3.3.6) to yield the value of B_I for the variable node I:

$$B_I = -\int_{B_V} N_I \frac{\rho}{\rho_o} q_p dB, \quad or \quad B_I = -\int_{B_V} N_I \frac{\rho}{\rho_o} q_e dB \qquad \textbf{(3.3.23)}$$

which is independent of the pressure head h. Thus, if Eq. (2.3.10) or (2.3.13) is chosen during the iterative process, the implementation of the boundary condition is to simply add B_I to L_I in Eq. (3.3.8) which is the corresponding algebraic equation for boundary node I. On the other hand, if Eq. (2.3.9), (2.3.11), or (2.3.12) is chosen, we override Eq. (3.3.8) with an identity equation as in the implementation of Dirichlet boundary conditions:

$$\begin{aligned} &A_{I,1} = 0, .., A_{I,I-1} = 0, A_{I,I} = 1, A_{I,I+1} = 0, .., A_{I,N} = 0 \quad and \\ &\qquad L_I + B_I = h_p \quad if \quad Eq. \ (2.3.9) \ is \ used \quad or \\ &\qquad L_I + B_I = h_p \quad if \quad Eq. \ (2.3.11) \ is \ used \quad or \\ &\qquad L_I + B_I = h_m \quad if \quad Eq. \ (2.3.12) \ is \ used \end{aligned} \qquad \textbf{(3.3.24)}$$

River boundary condition:

For the the river boundary condition given by Eq.(2.3.8), we simply substitute Eq.(2.3.8) into Eq.(3.3.6) to yield the following integrals:

$$B_I = \int_{B_r} N_I \frac{\rho}{\rho_o} \frac{K_R}{b_R} h_R dB \quad and \quad B_{I,J} = \int_{B_r} N_I \frac{\rho}{\rho_o} \frac{K_R}{b_R} J_J dB \qquad \textbf{(3.3.25)}$$

The integrals B_I and $B_{I,J}$, respectively, are added to L_I and subtracted from $A_{I,J}$, respectively, in Eq. (3.3.18) to complete the modification of this algebraic equation for the node I.

After the incorporation of boundary conditions, we obtain the following matrix equation

$$[C]\{h\} = \{R\} \quad where \quad [C] = [A] + [B] \quad and \quad \{R\} = \{L\} + [\{B\}] \qquad \textbf{(3.3.26)}$$

where [C] is the final coefficient matrix; {R} is the final right-hand side vector; and [B] and {B} the

coefficient matrix and load vector contributed from boundary conditions. For saturated-unsaturated flow simulations, [C] and {R} are highly nonlinear functions of the pressure head {h}.

Solution of the matrix equation. Equation (3.3.26) is in general a banded sparse matrix equation. It may be solved numerically by either direct method or iteration methods. In direct methods, a sequence of operation is performed only once. This would result in an exact solution except for round-off error. In this method, one is concerned with the efficiency and magnitude of round-off error associated with the sequence of operations. On the other hand, in an iterative method, one attempts to the solution by a process of successive approximations. This involves in making an initial guess, then improving the guess by some iterative process until an error criterion is obtained. Therefore, in this technique, one must be concerned with convergence, and the rate of convergence. The round-off errors tend to be self-corrected.

For practical purposes, the most advantages of direct method are: (1) the efficient computation when the bandwidth of the matrix [C] is small, and (2) the fact that no problem of convergency is encountered when the matrix equation is linear or less severity in convergence than iterative methods even when the matrix equation is nonlinear. The most disadvantages of direct methods are the excessive requirements on CPU storage and CPU time when a large number of nodes is needed for discretization. On the other hand, the most advantages of iterative methods are the efficiencies in terms of CPU storage and CPU time when large problems are encountered. Their most disadvantages are the requirements that the matrix [C] must be well conditioned to guarantee a convergent solution. For three dimensional problems, the bandwidth of the matrix is usually large, thus the direction solution method is not practical. Only the iterative methods are implemented in the three-dimensional flow module of WASH123D. Four iteration methods are used in solving the linearized matrix equation: (1) block iteration, (2) successive point iteration, (3) incomplete Cholesky preconditioned conjugate gradient method, and (4) algebraic multigrid method.

The matrix equation, Eq. (3.326), is nonlinear because both the hydraulic conductivity and the water capacity are functions of the pressure head h. To solve the nonlinear matrix equation, two approaches can be taken: (1) the Picard method and (2) the Newton-Ralphson method. The Newton-Ralphson method has a second order of convergent rate and is very robust. However, the Newton-Ralphson method would destroy the symmetrical property of the coefficient matrix resulting from the finite element approximation. As a result the solution of the linearized matrix equation requires extra care. Many of the iterative methods will not warrant a convergent solution for the non-symmetric linearized matrix equation. Thus, the Picard method is used in this report to solve the nonlinear problems.

In the Picard method, an initial estimate is made of the unknown {h}. Using this estimate, we then compute the coefficient matrix [C] and solve the linearized matrix equation by the method of linear algebra. The new estimate is now obtained by the weighted average of the new solution and the previous estimate:

$$\left\{h^{(k+1}\right\} = \omega\{h\} + (1-\omega)\left\{h^{\,k}\right\} \qquad \textbf{(3.3.27)}$$

where $\{h^{(k+1)}\}$ is the new estimate, $\{h^k\}$ is the previous estimate, {h} is the new solution, and ω is the iteration parameter. The procedure is repeated until the new solution {h} is within a tolerance error.

If ω is greater than or equal to 0 but is less than 1, the iteration is under-relaxation. If ω = 1, the method is the exact relaxation. If ω is greater than 1 but less than or equal to 2, the iteration is termed over-relaxation. The under-relaxation should be used to overcome cases when nonconvergency or the slow convergent rate is due to fluctuation rather than due to "blowup" computations. Over-relaxation should be used to speed up convergent rate when it decreases monotonically.

In summary, there are 16 optional numerical schemes here to deal with as wide a range of problems as possible. These are the combinations of: (1) two ways of treating the mass matrix (lumping and no-lumping); (2) two ways of approximating the time derivatives (time-weighting and mid-difference), and (3) four ways of solving the linearized matrix equation.

3.3.2 Numerical Approximations of Thermal Transport Equations

Two options are provided in this report to solve the thermal transport equation. One is the finite element method and the other is the particle tracking method.

3.3.2.1 Finite Element Method. Recall the thermal transport equation is governed by Eq. (2.3.14) that is rewritten in a slightly different form as

$$\begin{aligned}&\left(\rho_W C_W\theta+\rho_b C_m\right)\frac{\partial T}{\partial t}+\frac{\partial\left(\rho_W C_W\theta+\rho_b C_m\right)}{\partial t}T\\&\quad+\nabla\cdot\left(\rho_W C_W\mathbf{V}T\right)-\nabla\cdot\left(\mathbf{D}^{\mathbf{H}}h\cdot\nabla T\right)=H^{a}+H^{C}\end{aligned}\qquad\textbf{(3.3.28)}$$

Applying the finite element method to Eq. (3.3.28), we obtain the following matrix equation

$$[M]\frac{d\{T\}}{dt}+[V]\{T\}+[D]\{T\}+[K]\{T\}=-\{\Phi^{B}\}+\{\Phi^{a}\}+\{\Phi^{C}\}\qquad\textbf{(3.3.29)}$$

in which

$$\begin{aligned}&M_{ij}=\int_R N_i\left(\rho_W C_W\theta+\rho_b C_m\right)N_j dR,\qquad V_{ij}=\int_R\nabla W_i\rho_W C_W\mathbf{V}N_j dR,\\&D_{ij}=\int_R\nabla N_i\cdot\mathbf{D}^{\mathbf{H}}\nabla N_j dR,\qquad K_{ij}=\int_R N_i\frac{\partial\left(\rho_W C_W\theta\right)+\rho_b C_m}{\partial t}N_j dR,\\&\Phi_i^{B}=\int_B\mathbf{n}\cdot\left(W_i\rho_W C_W\mathbf{V}T-N_i\mathbf{D}^{\mathbf{H}}\nabla T\right)dB\end{aligned}\qquad\textbf{(3.3.30)}$$

$$\Phi_i^{a}=\int_R N_i H_a R,\qquad\Phi_i^{r}=\int_R N_i H_r dR,\qquad\Phi_i^{C}=\int_R N_i H_C dR\qquad\textbf{(3.3.31)}$$

where W_i is the weighting function of node x_i; N_i and N_j are the base functions of nodes x_i and x_j, respectively; [M] is the mass matrix, [V] is the stiff matrix due to advective transport; [D] is the stiff matrix due to dispersion/diffusion/conduction; {T} is the solution vector of temperature; $\{\Phi^B\}$ is the vector due to boundary conditions, which can contribute to load vector and/or coefficient matrix; $\{\Phi^a\}$ is the load vector due to artificial energy source; $\{\Phi^r\}$ is the load vector due to energy contained in rainfall; and $\{\Phi^c\}$ is the vector due to chemical reaction, which is not considered in this

version, but can be added easily.

Approximating the time derivative term in Eq. (3.3.29) with a time-weighted finite difference, we reduce the advective-diffusive equation and its boundary conditions to the following matrix equation

$$[C]\{T\} = \{L\} - \{\Phi^B\} \tag{3.3.32}$$

in which

$$\begin{aligned} [C] &= \frac{[M]}{\Delta t} + \theta([D] + [K]) + \theta_V [V], \\ \{L\} &= \left(\frac{[M]}{\Delta t} - (1-\theta)([DS] + [K]) - (1-\theta_V)[V] \right) \{T^{(n)}\} + \{\Phi^a\} + \{\Phi^r\} \end{aligned} \tag{3.3.33}$$

where [C] is the coefficient matrix, {L} is the load vector from initial condition, artificial sink/sources, rainfall, and net radiation; Δt is the time step size; θ is the time weighting factor for the dispersion and linear terms; θ_v is the time weighting factor for the velocity term; and $\{T^{(n)}\}$ is the value of {T} at old time level n. The global boundary conditions must be used to provide $\{\Phi^B\}$ in Eq. (3.3.32).

For a global boundary node I, the corresponding algebraic equation from Eq. (3.3.32) is

$$C_{I1}T_1 + .. + C_{I,I}T_I + .. + C_{I,N}T_N = L_I - \Phi_I^B \tag{3.3.34}$$

In the above equations there are two unknowns T_I and Φ_I^B; either T_I or Φ_I^B, or the relationship between T_I and Φ_I^B must be specified. The numerical implementation of these boundary conditions is described as follows.

Direchlet boundary condition: prescribed temperature

If T_I is given on the boundary node I (Dirichlet boundary condition), all coefficients ($C_{I,1}$, .., $C_{I,I}$, .., $C_{I,N}$) and the right-hand side term (L_I) obtained before the implementation of boundary conditions for this equation are stored in a temporary array, then an identity equation is created as

$$T_I = T_{Idb}, \quad I \in N_D \tag{3.3.35}$$

where T_{Idb} is the prescribed temperature on the Dirichlet node I and N_D is the number of Dirichlet boundary nodes. This process is repeated for every Dirichlet nodes. Note it is unnecessary to modify other equations that involving these unknowns, which was done in the previous version. By not modifying other equations, the symmetrical property of the matrix is preserved, which makes the iterative solvers more robust. The final set of equations will consist of N_D identity equations and (N - N_D) finite element equations for N unknowns T_i's. After T_i's for all nodes are solved from the matrix equation, Eq. (3.3.34) is then used to back calculate N_D Φ_I^B's.

If a direct solver is used to solve the matrix equation, the above procedure will solve N T_i's accurately except for roundoff errors. However, if an iterative solver is used, a stopping criterion must be strict enough so that the converged solution of N T_i's are accurate enough to the exact solution. With such accurate T_i's, then can be sure that the back-calculated ND Φ_I^B's are accurate.

Cauchy boundary condition: prescribed heat flux

If Φ_{BI} is given (Cauchy flux boundary condition), all coefficients ($C_{I,1}$, .., $C_{I,I}$, .., $C_{I,N}$) and right-hand side term (L_I) obtained before the implementation of boundary conditions for this equation are stored in a temporary array, then Eq. (3.3.34) is modified to incorporate the boundary conditions and used to solve for T_I. The modification of Eq. (3.3.34) is straightforward. Because Φ_I^B is a known quantity, it contributes to the load on the right hand side. This type of boundary conditions is very easy to implement. After T_is are obtained, the original Eq. (3.3.34), which is stored in a temporary array, is used to back calculate N_C Φ_I^B's on flux boundaries (where N_C is the number of flux boundary nodes). These back-calculated Φ_I^B's should be theoretically identical to the input Φ_I^B's. However, because of round-off errors (in the case of direct solvers) or because of stopping criteria (in the case of iterative solvers), the back-calculated Φ_I^B's will be slightly different from the input Φ_I^B's. If the differences between the two are significant, it is an indication that the solvers have not yielded accurate solutions.

Neumann boundary condition: prescribed gradient of temperature

At Neumann boundaries, the temperature gradient is prescribed, thus, the flux due to temperature gradient is given. For this case, all coefficients ($C_{I,1}$, .., $C_{I,I}$, .., $C_{I,N}$) and right-hand side term (L_I) obtained before the implementation of boundary conditions for this equation are stored in a temporary array, then Eq. (3.3.34) is modified to incorporate the boundary conditions and used to solve for T_I. For the Neumann boundary condition, Φ_I^B contributes to both the matrix coefficient and load vector, thus both the coefficient matrix [C] and the load vector {L} must be modified. Recall

$$\Phi_i^B = \int_B \mathbf{n} \cdot \left(W_i \rho_W C_W \mathbf{V} T - N \mathbf{D}^{\mathbf{H}} \nabla T \right) dB \qquad \textbf{(3.3.36)}$$

Substituting Eq. (2.3.19) into Eq. (3.3.36), we have

$$\left\{ \Phi^B \right\} \equiv \left[CB \right] \left\{ T \right\} + \left\{ LB \right\}$$
$$\textit{in which} \qquad CB_{ij} = -\int_B \mathbf{n} \cdot W_i \rho_W C_W \mathbf{V} N_j dB \quad \textit{and} \quad LB_i = -\int_B N_i \varphi_{nb}(t) dB \qquad \textbf{(3.3.37)}$$

where [CB] and {LB} are the coefficient matrix and load vector due to Neumann boundary. Adding the I-th equation in Eq. (3.3.37) to Eq. (3.3.34), we obtained a modified equation, which can be solved for solve T_I. After T_I is solved, the original Eq. (3.3.34) (recall the original Eq. (3.3.34) must be and has been stored in a temporary array) is used to back-calculate Φ_I^B.

Variable boundary condition:

At the variable boundary condition Node I, the implementation of boundary conditions can be made identical to that for a Cauchy boundary condition node if the flow is directed into the region. If the flow is going out of the region, the boundary condition is implemented similar to the implementation of Neuman boundary condition with $LB_I = 0$. The assumption of zero Neumann flux implies that a

Neuman node must be far away from the source/sink.

Atmosphere-subsurface media interface boundary condition:

At the atmosphere-media interface, the heat flux is a nonlinear function of the temperature since the back radiation and the heat flux due to evaporation and sensible heat are both function of temperature. To implement this boundary condition, we first expand Eq. (2.3.20) in Taylor series as follows:

$$-\mathbf{n}\cdot\left(\rho_W C_W \mathbf{V}T - \mathbf{D}^{\mathbf{H}}\cdot\nabla T\right) = F\left(T^{(k)}\right) + \left.\frac{dF}{dT}\right|_{T=T^{(k)}}\left(T - T^{(k)}\right) \qquad \textbf{(3.3.38)}$$
$$where\ F = H_n - H_b - H_e - H_s$$

where T(k) is the value of T at previous iteration. Substituting Eq. (3.3.38) into Eq. (3.3.36), we have

$$\left\{\Phi^B\right\} \equiv \left[CB\right]\left\{T\right\} + \left\{LB\right\} \quad in\ which$$
$$CB_{ij} = \int_B N_i \left.\frac{dF}{dT}\right|_{T=T^{(k)}} N_j dB \quad and \quad LB_i = \int_B N_i \left(F\left(T^{(k)}\right) - \left.\frac{dF}{dT}\right|_{T=T^{(k)}} T^{(k)} \right) dB \qquad \textbf{(3.3.39)}$$

where [CB] and {LB} are the coefficient matrix and load vector due to the atmosphere-media boundary condition. Adding the I-th equation in Eq. (3.3.39) to Eq. (3.3.34), we obtained a modified equation, which can be solved for solve T_I. After T_I is solved, the original Eq. (3.3.34) is used to back-calculate Φ_I^B.

Subsurface-river interface boundary condition:

This type of boundary condition will be addressed in Sub-Sections 3.4.3 and 3.4.4.

Subsurface-overland interface boundary condition:

This type of boundary condition will be addressed in Sub-Section 3.4.2.

3.3.2.2 The Hybrid Lagrangian-Eulerian Finite Element Method. When the hybrid Lagrangian-Eulerian finite element method is used to solve the thermal transport equation, we expand Eq. (3.2.70) to yield following advection-dispersion equation in the Lagrangian form

$$\frac{D_{\mathbf{U}}T}{Dt} + KT = D + \Phi^S \quad where \quad \mathbf{U} = \frac{\rho_W C_r \mathbf{V}}{\left(\rho_W C_W \theta + \rho_b C_m\right)} \qquad \textbf{(3.3.40)}$$

in which

$$K = \frac{1}{\left(\rho_W C_W \theta + \rho_b C_m\right)} \frac{\partial\left(\rho_W C_W \theta + \rho_b C_m\right)}{\partial t} + \frac{1}{\left(\rho_W C_W \theta + \rho_b C_m\right)} \nabla\cdot\left(\rho_W C_W \mathbf{V}\right),$$
$$D = \frac{1}{\left(\rho_W C_W \theta\right) + \rho_b C_m} \nabla\cdot\left(\mathbf{D}^{\mathbf{H}}\cdot\nabla T\right) \quad and \quad \Phi^S = \frac{H^a + H^r}{\left(\rho_W C_W \theta + \rho_b C_m\right)} \qquad \textbf{(3.3.41)}$$

To use the semi-Lagrangian method to solve the thermal transport equation, we integrate Eq. (3.3.40) along its characteristic line from x_i at new time level to x_i^* at old time level or on the boundary, we obtain

$$\left(1+\frac{\Delta\tau}{2}K_i^{(n+1)}\right)T_i^{(n+1)} = \left(1-\frac{\Delta\tau}{2}K_i^{*}\right)T_i^{*}+\frac{\Delta\tau}{2}\left(D_i^{(n+1)}+D_i^{*}\right)+\frac{\Delta\tau}{2}\left(\Phi_i^{S^{(n+1)}}+\Phi_i^{S^{*}}\right), \quad i\in N \tag{3.3.42}$$

where $\Delta\tau$ is the tracking time, it is equal to Δt when the backward tracking is carried out all the way to the root of the characteristic and it is less than Δt when the backward tracking hits the boundary before Δt is consumed; $K_i^{(n+1)}$, $T_i^{(n+1)}$, $D_i^{(n+1)}$, and $\Phi_i^{S(n+1)}$, respectively, are the values of K, T, D, and Φ^S, respectively, at x_i at new time level $t = (n+1)\Delta t$; and K_i^*, T_i^*, D_i^*, and Φ_i^{S*}, respectively, are the values of K, T, D, and Φ^S, respectively, at the location x_i^*.

To compute the dispersion/diffusion terms $D_i^{(n+1)}$ and D_i^*, we rewrite the second equation in Eq. (3.3.41) as

$$\left(\rho_W C_W\theta+\rho_b C_m\right)D=\nabla\cdot\left(\mathbf{D}^{\mathbf{H}}\cdot\nabla T\right) \tag{3.3.43}$$

Applying the Galerkin finite element method to Eq. (3.3.43) at new time level (n+1), we obtain the following matrix equation for $\{D^{(n+1)}\}$ as

$$\left[a^{(n+1)}\right]\left\{D^{(n+1)}\right\}+\left[b^{(n+1)}\right]\left\{T^{(n+1)}\right\}=\left\{B^{(n+1)}\right\} \tag{3.3.44}$$

in which

$$\left\{D^{(n+1)}\right\}=\left\{D_1^{(n+1)} \quad D_2^{(n+1)} \quad . \quad . \quad D_i^{(n+1)} \quad . \quad . \quad D_N^{(n+1)}\right\}^{Transpose} \tag{3.3.45}$$

$$\left\{T^{(n+1)}\right\}=\left\{T_1^{(n+1)} \quad T_2^{(n+1)} \quad . \quad . \quad T_i^{(n+1)} \quad . \quad . \quad T_N^{(n+1)}\right\}^{Transpose} \tag{3.3.46}$$

$$\left\{B^{(n+1)}\right\}=\left\{B_1^{(n+1)} \quad B_2^{(n+1)} \quad . \quad . \quad B_i^{(n+1)} \quad . \quad . \quad B_N^{(n+1)}\right\}^{Transpose} \tag{3.3.47}$$

$$a_{ij}^{(n+1)}=\int_R N_i\left(\rho_W C_W\theta+\rho_b C_m\right)\Big|_{(n+1)}N_j dR, \quad b_{ij}^{(n+1)}=\int_R \nabla N_i\cdot\left(\mathbf{D}^{\mathbf{H}}\right)\Big|_{(n+1)}\cdot\nabla N_j dR,$$
$$B_i^{(n+1)}=\int_B n\cdot N_i\left(D^H\right)\Big|_{(n+1)}\cdot\nabla T^{(n+1)}dB \tag{3.3.48}$$

where the superscript (n+1) denotes the time level; N and N are the base functions of nodes at x_i and x_j, respectively.

Lumping the matrix $[a^{(n+1)}]$, we can solve Eq. (3.3.44) for $D_I^{(n+1)}$ as follows

$$D_I^{(n+1)} = -\frac{1}{a_{II}^{(n+1)}}\sum_j b_{Ij}^{(n+1)} T_j^{(n+1)} \quad if \quad I\ is\ an\ \text{interior point}$$
$$D_I^{(n+1)} = \frac{1}{a_{II}^{(n+1)}} B_I^{(n+1)} - \frac{1}{a_{II}^{(n+1)}}\sum_j b_{Ij}^{(n+1)} T_j^{(n+1)} \quad if \quad I\ is\ a\ boundary\ \text{point} \qquad \textbf{(3.3.49)}$$

where $a_{II}^{(n+1)}$ is the lumped $a_{ii}^{(n+1)}$. Following the identical procedure that leads Eq. (3.3.43) to Eq. (3.3.49), we have

$$D_I^{(n)} = -\frac{1}{a_{II}^{(n)}}\sum_j b_{Ij}^{(n)} T_j^{(n)} \quad if \quad I\ is\ an\ \text{interior point}$$
$$D_I^{(n)} = \frac{1}{a_{II}^{(n)}} B_I^{(n)} - \frac{1}{a_{II}^{(n)}}\sum_j b_{Ij}^{(n)} T_j^{(n)} \quad if \quad I\ is\ a\ boundary\ \text{point} \qquad \textbf{(3.3.50)}$$

where $\{B^{(n)}\}$, $\{a^{(n)}\}$ and $\{b^{(n)}\}$, respectively, are defined similar to $\{B^{(n+1)}\}$, $\{a^{(n+1)}\}$ and $\{b^{(n+1)}\}$, respectively.

With $\{D^{(n)}\}$ calculated with Eq. (3.3.50), $\{D^*\}$ can be interpolated. Substituting Eq. (3.3.49) into Eq. (3.3.42) and implementing boundary conditions given in Section 2.3.2, we obtain a system of N simultaneous algebraic equations N unknowns ($T_i^{(n+1)}$ for i = 1, 2, .., N.) If the dispersion/diffusion term is not included, then Eq. (3.3.42) is reduced to a set of N decoupled equations as

$$a_{ii} T_i^{(n+1)} = b_i, \quad i \in N \qquad \textbf{(3.3.51)}$$

where

$$a_{ii} = \left(1 + \frac{\Delta\tau}{2} K_i^{(n+1)}\right)$$
$$b_i = \left(1 - \frac{\Delta\tau}{2} K_i^*\right) T_i^* + \frac{\Delta\tau}{2}\left(\Phi_i^{S^{(n+1)}} + \Phi_i^{S*}\right), \quad i \in N \qquad \textbf{(3.3.52)}$$

Equations (3.3.51) is applied to all interior nodes without having to make any modification. On a boundary point, there are two possibilities: Eq. (3.3.51) is replaced with a boundary equation when the flow is directed into the region or Eq. (3.3.51) is still valid when the flow is direct out of the region. In other words, when the thermal energy is transported out of the region at a boundary node (i.e., when $\mathbf{N}\bullet\mathbf{V} \geq 0$), a boundary condition is not needed and Equation (3.3.51) is used to compute the $T_i^{(n+1)}$. When the thermal energy is transported into the region at a node (i.e., when $\mathbf{N}\bullet\mathbf{V} < 0$), a boundary condition must be specified.

Alternatively, to facilitate the implementation of boundary condition at incoming flow node, the algebraic equation for the boundary node is obtained by applying the finite element method to the boundary node. For this alternative approach, the implementation of boundary conditions at global boundary nodes is identical to that in the finite element approximation of solving the thermal transport equation.

3.3.3 Numerical Approximations of Salinity Transport

Two options are provided in this report to solve the salinity transport equation. One is the finite element method and the other is the particle tracking method.

3.3.3.1 Finite Element Method. Recall the salinity transport equation is governed by Eq. (2.3.23) which is rewritten in a slightly different form as

$$\theta\frac{\partial S}{\partial t}+\frac{\partial \theta}{\partial t}S+\nabla\cdot(\mathbf{V}S)-\nabla\cdot(\theta\mathbf{D}\cdot\nabla h)=S^{as} \tag{3.3.53}$$

Applying the finite element method to Eq. (3.3.53), we obtain the following matrix equation

$$[M]\frac{d\{S\}}{dt}+[V]\{S\}+[D]\{S\}+[K]\{S\}=-\{\Psi^{B}\}+\{\Psi^{a}\} \tag{3.3.54}$$

in which

$$\begin{aligned}
&M_{ij}=\int_R N_i\theta N_j dx, \qquad V_{ij}=\int_R W_i\cdot\mathbf{V}N_j dR, \qquad D_{ij}=\int_R \nabla N_i\cdot\theta\mathbf{D}\cdot\nabla N_j dR,\\
&K_{ij}=\int_R N_i\frac{\partial\theta}{\partial t}N_j dR, \qquad \Psi_i^{B}=\int_B \mathbf{n}\cdot(W_i\mathbf{V}S-N_i\theta\mathbf{D}\cdot\nabla S)dB, \qquad \Psi_i^{a}=\int_R N_i S^{as}dR
\end{aligned} \tag{3.3.55}$$

$$\Psi_i^{a}=\int_R N_i M_s^{as}dR, \qquad \Psi_i^{r}=\int_R N_i M_s^{rs}dR, \qquad \Psi_i^{e}=\int_R N_i M_s^{es}dR, \qquad \Psi_i^{i}=\int_R N_i M_s^{is}dR \tag{3.3.56}$$

where W_i is the weighting function of node x_i; N_i and N_j are the base functions of nodes x_i and x_j, respectively; [M] is the mass matrix, [V] is the stiff matrix due to advective transport; [D] is the stiff matrix due to dispersion/diffusion/conduction; [K] is the stiff matrix due to the linear term; {S} is the solution vector of salinity; $\{\Psi^B\}$ is the vector due to boundary conditions, which can contribute to load vector and/or coefficient matrix; and $\{\Psi^a\}$ is the load vector due to artificial salt source.

Approximating the time derivative term in Eq. (3.3.54) with a time-weighted finite difference, we reduce the advective-diffusive equation and its boundary conditions to the following matrix equation.

$$[C]\{S\}=\{L\}-\{\Psi^{B}\} \tag{3.3.57}$$

in which

$$\begin{aligned}
&[C]=\frac{[M]}{\Delta t}+\theta([D]+[K])+\theta_V[V],\\
&\{L\}=\left(\frac{[M]}{\Delta t}-(1-\theta)([D]+[K])-(1-\theta_V)[V]\right)\{S^{(n)}\}+\{\Psi^{a}\}
\end{aligned} \tag{3.3.58}$$

where [C] is the coefficient matrix, {L} is the load vector from initial condition, artificial sink/sources and rainfall; Δt is the time step size; θ is the time weighting factor for the dispersion and linear terms; θ_v is the time weighting factor for the velocity term; and $\{S^{(n)}\}$ is the value of {S} at old time level n. The global boundary conditions must be used to provide $\{\Psi^B\}$ in Eq. (3.3.57).

For a global boundary node I, the corresponding algebraic equation from Eq. (3.3.57) is

$$C_{I,1}S_1 + .. + C_{I,I}S_I + .. + C_{I,N}S_N = L_I - \Psi_I^B \qquad \textbf{(3.3.59)}$$

In the above equations there are two unknowns T_I and Ψ_I^B; either T_I or Ψ_I^B, or the relationship between T_I and Ψ_I^B must be specified. The numerical implementation of these boundary conditions are described as follows.

Dirichlet boundary condition: prescribed salinity

If S_I is given on the boundary node I (Dirichlet boundary condition), all coefficients ($C_{I,1}$, .., $C_{I,I}$, .., $C_{I,N}$) and the right-hand side term (L_I) obtained before the implementation of boundary conditions for this equation are stored in a temporary array, then an identity equation is created as

$$S_I = S_{Id}, \quad I \in N_D \qquad \textbf{(3.3.60)}$$

where S_{Id} is the prescribed salinity on the Dirichlet node I and N_D is the number of Dirichlet boundary nodes. This process is repeated for every Dirichlet nodes. Note it is unnecessary to modify other equations that involving this unknowns, which was done in the previous version. By not modifying other equations, the symmetrical property of the matrix is preserved, which makes the iterative solvers more robust. The final set of equations will consist of N_D identity equations and (N - N_D) finite element equations for N unknowns S_i's. After S_i's for all nodes are solved from the matrix equation, Eq. (3.3.59) is then used to back calculate N_D Ψ_I^B's.

If a direct solver is used to solve the matrix equation, the above procedure will solve N S_i's accurately except for roundoff errors. However, if an iterative solver is used, a stopping criterion must be strict enough so that the converged solution of N S_i's are accurate enough to the exact solution. With such accurate S_i's, then can we be sure that the back-calculated ND Ψ_{BI}'s are accurate.

Cauchy boundary condition: prescribed salt flux

If Ψ_I^B is given (Cauchy flux boundary condition), all coefficients ($C_{I,1}$, .., $C_{I,I}$, .., $C_{I,N}$) and the right-hand side term (L_I) obtained before the implementation of boundary conditions for this equation are stored in a temporary array, then Eq. (3.3.59) is modified to incorporate the boundary conditions and used to solve for S_I. The modification of Eq. (3.3.59) is straightforward. Because Ψ_I^B is a known quantity, it contributes to the load on the right hand side. This type of boundary conditions is very easy to implement. After S_i's are obtained, the original Eq. (3.3.59), which is stored in a temporary array, is used to back calculate N_C Ψ_I^B's on flux boundaries (where N_C is the number of flux boundary nodes). These back-calculated Ψ_I^B's should be theoretically identical to the input Ψ_I^B's. However, because of round-off errors (in the case of direct solvers) or because of stopping criteria (in the case of iterative solvers), the back-calculated Ψ_I^B's will be slightly different from the input Ψ_I^B's. If the differences between the two are significant, it is an indication that the solvers have not yielded accurate solutions.

Neumann boundary condition: prescribed gradient of salinity

At Neumann boundaries, the temperature gradient is prescribed, thus, the flux due to temperature

gradient is given. For this case, all coefficients ($C_{I,}$, .., $C_{I,I}$, .., $C_{I,N}$) and the right-hand side term (L_I) obtained before the implementation of boundary conditions for this equation are stored in a temporary array, then Eq. (3.3.59) is modified to incorporate the boundary conditions and used to solve for S_I. For the Neumann boundary condition, Ψ_I^B contributes to both the matrix coefficient and load vector, thus both the coefficient matrix [C] and the load vector {L} must be modified. Recall

$$\Psi_i^B = \int_B \mathbf{n} \cdot \left(W_i \mathbf{V} S - N_i \theta \mathbf{D} \nabla S \right) dB \tag{3.3.61}$$

Substituting Eq. (2.3.28) into Eq. (3.3.61), we have

$$\begin{aligned} &\left\{ \Psi^B \right\} \equiv \left[CB \right] \left\{ S \right\} + \left\{ LB \right\} \\ &\textit{in which} \qquad CB_{i,j} = \int_B \mathbf{n} \cdot W_i \mathbf{V} N_j dB \quad \textit{and} \quad LB_i = \int_B N_i Q_{Snb}(t) dB \end{aligned} \tag{3.3.62}$$

where [CB] and {LB} are the coefficient matrix and load vector due to Neumann boundary. Adding the I-th equation in Eq. (3.3.62) to Eq. (3.3.59), we obtained a modified equation, which can be solved for solve S_I. After S_I is solved, the original Eq. (3.3.59) is used to back-calculate Ψ_I^B.

Variable boundary condition:

At the variable boundary condition Node I, the implementation of boundary conditions can be made identical to that for a Cauchy boundary condition node if the flow is directed into the river/stream/canal reach. If the flow is going out of the reach, the boundary condition is implemented similar to the implementation of Neuman boundary condition with $\Psi_I^{nb} = 0$. The assumption of zero Neumann flux implies that a Neuman node must be far away from the source/sink.

Subsurface-river interface boundary condition:

This type of boundary condition will be addressed in Sub-Sections 3.4.3 and 3.4.4.

Subsurface-overland interface boundary condition:

This type of boundary condition will be addressed in Sub-Section 3.4.2.

3.3.3.2 The Hybrid Lagrangian-Eulerian Finite Element Method. When the hybrid Lagrangian-Eulerian finite element method is used to solve the salt transport equation, we expand Eq. (3.3.53) to yield following advection-dispersion equation in the Lagrangian form

$$\frac{D_U S}{Dt} + KS = D + \Psi^S \quad \textit{where} \quad \mathbf{U} = \frac{\mathbf{V}}{\theta} \tag{3.3.63}$$

in which

$$K = \frac{1}{\theta}\frac{\partial \theta}{\partial t} + \frac{1}{\theta} \nabla \cdot (\mathbf{V}), \quad D = \frac{1}{\theta} \nabla \cdot \left(\theta \mathbf{D} \cdot \nabla S \right) \quad \textit{and} \quad \Psi^S = \frac{S^{as}}{\theta} \tag{3.3.64}$$

To use the semi-Lagrangian method to solve the thermal transport equation, we integrate Eq. (3.3.63) along its characteristic line from x_i at new time level to x_i^* at old time level or on the boundary, we obtain

$$\left(1+\frac{\Delta\tau}{2}K_i^{(n+1)}\right)S_i^{(n+1)} = \left(1-\frac{\Delta\tau}{2}K_i^{*}\right)S_i^{*}+\frac{\Delta\tau}{2}\left(D_i^{(n+1)}+D_i^{*}\right)+\frac{\Delta\tau}{2}\left(\Psi_i^{S^{(n+1)}}+\Psi_i^{S*}\right),\quad i\in N \tag{3.3.65}$$

where $\Delta\tau$ is the tracking time, it is equal to Δt when the backward tracking is carried out all the way to the root of the characteristic and it is less than Δt when the backward tracking hits the boundary before Δt is consumed; $K_i^{(n+1)}$, $T_i^{(n+1)}$, $D_i^{(n+1)}$, and $\Psi_i^{S(n+1)}$, respectively, are the values of K, T, D, and Ψ^S, respectively, at x_i at new time level $t = (n+1)\Delta t$; and K_i^*, T_i^*, D_i^*, and Ψ_i^{S*}, respectively, are the values of K, T, D, and Ψ^S, respectively, at the location x_i^*.

To compute the dispersion/diffusion terms $D_i^{(n+1)}$ and D_i^*, we rewrite the second equation in Eq. (3.3.64) as

$$\theta D = \nabla\cdot\left(\theta\mathbf{D}\cdot\nabla S\right) \tag{3.3.66}$$

Applying the Galerkin finite element method to Eq. (3.3.66) at new time level (n+1), we obtain the following matrix equation for $\{D^{(n+1)}\}$ as

$$\left[a^{(n+1)}\right]\left\{D^{(n+1)}\right\}+\left[b^{(n+1)}\right]\left\{S^{(n+1)}\right\}=\left\{B^{(n+1)}\right\} \tag{3.3.67}$$

in which

$$\left\{D^{(n+1)}\right\}=\left\{D_1^{(n+1)}\quad D_2^{(n+1)}\quad .\ .\quad D_i^{(n+1)}\quad .\ .\quad D_N^{(n+1)}\right\}^{Transpose} \tag{3.3.68}$$

$$\left\{S^{(n+1)}\right\}=\left\{S_1^{(n+1)}\quad S_2^{(n+1)}\quad .\ .\quad S_i^{(n+1)}\quad .\ .\quad S_N^{(n+1)}\right\}^{Transpose} \tag{3.3.69}$$

$$\left\{B^{(n+1)}\right\}=\left\{B_1^{(n+1)}\quad B_2^{(n+1)}\quad .\ .\quad B_i^{(n+1)}\quad .\ .\quad B_N^{(n+1)}\right\}^{Transpose} \tag{3.3.70}$$

$$a_{ij}^{(n+1)}=\int_R N_i(\theta)\Big|_{(n+1)}N_j dR,\quad b_{ij}^{(n+1)}=\int_R \nabla N_i\cdot\left(\theta\mathbf{D}\right)\Big|_{(n+1)}\cdot\nabla N_j dR,$$
$$B_i^{(n+1)}=\int_B n\cdot N_i\left(\theta\mathbf{D}\right)\Big|_{(n+1)}\cdot\nabla S^{(n+1)}dB \tag{3.3.71}$$

where the superscript (n+1) denotes the time level; N and N are the base functions of nodes at x_i and x_j, respectively.

Lumping the matrix $[a^{(n+1)}]$, we can solve Eq. (3.2.110) for $D_I^{(n+1)}$ as follows

$$D_I^{(n+1)} = -\frac{1}{a_{II}^{(n+1)}}\sum_j b_{Ij}^{(n+1)} S_j^{(n+1)} \quad if \quad I\ is\ an\ \text{interior point}$$
$$D_I^{(n+1)} = \frac{1}{a_{II}^{(n+1)}} B_I^{(n+1)} - \frac{1}{a_{II}^{(n+1)}}\sum_j b_{Ij}^{(n+1)} S_j^{(n+1)} \quad if \quad I\ is\ a\ boundary\ \text{point} \qquad \textbf{(3.3.72)}$$

where $a_{II}^{(n+1)}$ is the lumped $a_{ii}^{(n+1)}$. Following the identical procedure that leads Eq. (3.3.66) to Eq. (3.3.72), we have

$$D_I^{(n)} = -\frac{1}{a_{II}^{(n)}}\sum_j b_{Ij}^{(n)} S_j^{(n)} \quad if \quad I\ is\ an\ \text{interior point}$$
$$D_I^{(n)} = \frac{1}{a_{II}^{(n)}} B_I^{(n)} - \frac{1}{a_{II}^{(n)}}\sum_j b_{Ij}^{(n)} S_j^{(n)} \quad if \quad I\ is\ a\ boundary\ \text{point} \qquad \textbf{(3.3.73)}$$

where $\{B^{(n)}\}$, $\{a^{(n)}\}$ and $\{b^{(n)}\}$, respectively, are defined similar to $\{B^{(n+1)}\}$, $\{a^{(n+1)}\}$ and $\{b^{(n+1)}\}$, respectively.

With $\{D^{(n)}\}$ calculated with Eq. (3.3.73), $\{D^*\}$ can be interpolated. Substituting Eq. (3.3.72) into Eq. (3.3.65) and implementing boundary conditions given in Section 2.3.3, we obtain a system of N simultaneous algebraic equations N unknowns ($S_i^{(n+1)}$ for i = 1, 2, .., N.) If the dispersion/diffusion term is not included, then Eq. (3.3.65) is reduced to a set of N decoupled equations as

$$a_{ii} S_i^{(n+1)} = b_i, \quad i \in N \qquad \textbf{(3.3.74)}$$

where

$$a_{ii} = \left(a + \frac{\Delta\tau}{2} K_i^{(n+1)}\right), \quad b_i = \left(1 - \frac{\Delta\tau}{2} K_i^*\right) S_i^* + \frac{\Delta\tau}{2}\left(\Psi_i^{S^{(n+1)}} + \Psi_i^{S^*}\right), \quad i \in N \qquad \textbf{(3.3.75)}$$

Equations (3.3.75) is applied to all interior nodes without having to make any modification. On a boundary point, there two possibilities: Eq. (3.3.75) is replaced with a boundary equation when the flow is directed into the region or Eq. (3.3.75) is still valid when the flow is direct out of the region. In other words, when the salt is transported out of the region at a boundary node (i.e., when $\mathbf{N}\bullet\mathbf{V} \geq 0$), a boundary condition is not needed and Equation (3.3.75) is used to compute the $S_i^{(n+1)}$. When the salt is transported into the region at a node (i.e., when $\mathbf{N}\bullet\mathbf{V} < 0$), a boundary condition must be specified.

Alternatively, to facilitate the implementation of boundary condition at incoming flow node, the algebraic equation for the boundary node is obtained by applying the finite element method to the boundary node. For this alternative approach, the implementation of boundary conditions at global boundary nodes is identical to that in the finite element approximation of solving the salt transport equation.

3.4 Numerical Implementation of Flow Coupling among Various Media

This section addresses numerical implement of coupling flow simulations among various media including (1) between 1D river and 2D overland flows, (2) between 2D overland and 3D subsurface flows, (3) between 3D subsurface and 1D overland flows, and (4) among 1D river, 2D overland, and 3D subsurface flows. Without loss of generality, numerical implementations of coupling for water flow equations are heuristically given for finite element approximations of diffusive wave models. For Largrangian-Eulerian approximations of diffusive wave models, semi-Largrangian approximations of kinematic wave models, or particle tracking approximations of fully dynamic wave models in surface waters, the implementations of numerical coupling among various media remain valid.

3.4.1 Coupling between 1-D River Networks and 2-D Overland Flows

The interaction between one-dimensional river and two-dimensional overland flows involves two cases: one is between overland and river nodes (left frame in Fig. 3.4-1) and the other is between overland and junction nodes (right frame in Fig. 3.4-1). For every river node (Node *I* in the left frame of Fig. 3.4-1), there will be associated with two overland nodes (Nodes *J* and *K* in the left frame of Fig. 3.4-1). For every junction node (Node *L* in the right frame of Fig. 3.4-1), there will be associated with a number of overland nodes such as Nodes *J*, *K*, *O*, etc (right frame of Fig. 3.4-1). It should be noted that nodes, such as Nodes *J* and *K* in the right frame of Figure 3.4-1, contribute flow to both the river as source/sink of Node *I* and the Junction as source/sink of Node *L*.

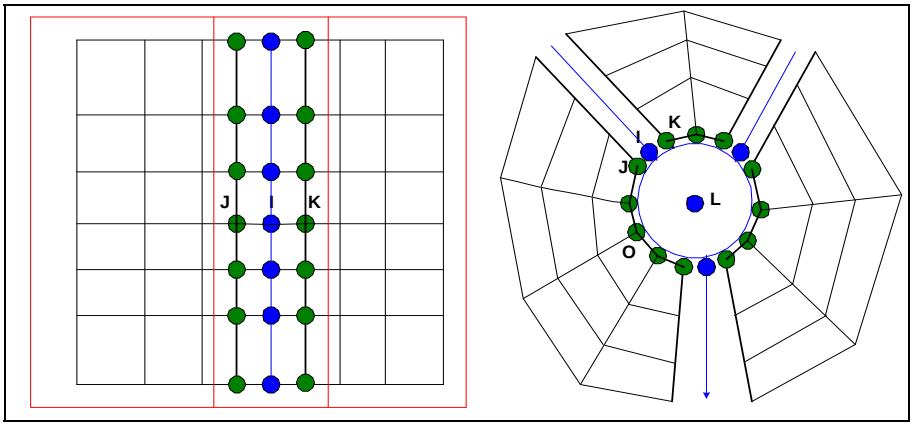

Fig. 3.4-1. Depiction of Interacting River Nodes and Overland Nodes (left) and Junction Nodes and Overland Nodes (Right)

3.4.1.1 Couple Flow Rates between the River Network and the Overland Regime.

Numerical approximations of the diffusive water flow equation for one-dimensional river with finite element methods yield the following matrix

$$\begin{bmatrix} -- & -- & -- & -- & -- & -- & -- \\ -- & -- & -- & -- & -- & -- & -- \\ -- & -- & -- & -- & -- & -- & -- \\ A^c_{I1} & A^c_{I2} & -- & A^c_{I1} & -- & -- & A^c_{IN} \\ -- & -- & -- & -- & -- & -- & -- \\ -- & -- & -- & -- & -- & -- & -- \\ -- & -- & -- & -- & -- & -- & -- \end{bmatrix} \begin{Bmatrix} H_1^c \\ H_2^c \\ -- \\ H_I^c \\ -- \\ -- \\ H_N^c \end{Bmatrix} = \begin{Bmatrix} R_1^c \\ R_2^c \\ -- \\ R_I^c \\ -- \\ -- \\ R_N^c \end{Bmatrix} + \begin{Bmatrix} Q_1^{o1} \\ Q_2^{o1} \\ -- \\ Q_I^{o1} \\ -- \\ -- \\ Q_N^{o1} \end{Bmatrix} + \begin{Bmatrix} Q_1^{o2} \\ Q_2^{o2} \\ -- \\ Q_I^{o2} \\ -- \\ -- \\ Q_N^{o2} \end{Bmatrix} \qquad \textbf{(3.4.1)}$$

where the superscript *c* denotes the canal (channel, river, or stream); A_{IJ} is the I-th row, J-th column of the coefficient matrix [*A*]; H_I denotes the water surface at Node *I*; R_I is *I*-th entry of the load vector {*R*}; *N* is the number of nodes in the canal; Q_I is the rates of water source/sink from/to the overland flow to/from canal node *I*; and the superscripts, *o1* and o2, respectively, denote canal bank 1 and 2, respectively. Every canal node *I* involves 3 unknowns, H_I^c, Q_I^{o1}, and Q_I^{o2}. However, Eq. (3.4.1) gives just one algebraic equation for every canal node *I*. Clearly, two additional algebraic equations are need for every canal node *I*.

Applications of finite element methods to two-dimensional diffusive wave flow equations yield the following matrix

$$\begin{bmatrix} A^o_{11} & A^o_{12} & -- & -- & -- & -- & A^o_{1M} \\ A^o_{21} & -- & -- & -- & -- & -- & A^o_{2M} \\ -- & -- & -- & -- & -- & -- & -- \\ A^o_{J1} & A^o_{J2} & -- & A^o_{JJ} & -- & -- & A^o_{1M} \\ -- & -- & -- & -- & -- & -- & -- \\ A^o_{K1} & A^o_{K2} & -- & -- & A^o_{KK} & -- & A^o_{KM} \\ -- & -- & -- & -- & -- & -- & -- \\ A^o_{M1} & A^o_{M2} & -- & -- & -- & -- & A^o_{MM} \end{bmatrix} \begin{Bmatrix} H_1^o \\ H_2^o \\ -- \\ H_J^o \\ -- \\ H_K^o \\ -- \\ H_M^o \end{Bmatrix} = \begin{Bmatrix} R_1^o \\ R_2^o \\ -- \\ R_J^o \\ -- \\ R_K^o \\ -- \\ R_M^o \end{Bmatrix} - \begin{Bmatrix} -- \\ -- \\ -- \\ Q_J^o \\ -- \\ Q_K^o \\ -- \\ -- \end{Bmatrix} \qquad \textbf{(3.4.2)}$$

where the superscript *o* denotes the overland; A_{IJ} is the *I*-th row, *J*-th column of the coefficient matrix [*A*]; H_I denotes the water surface at Node *I*; R_I is *I*-th entry of the load vector {*R*}; *M* is the number of nodes in the overland ; and Q_J and Q_K are the rates of water sink/source from/to the overland to/from the canal via nodes *J* and *K*, respectively. Equation (3.4.2) indicates that there is one unknown corresponding to one algebraic equation for every interior node. However, for every algebraic equation corresponding an overland-canal interface node, there are two unknowns, the water surface and the flow rate. Therefore, for every overland-river interface node, one additional equation is needed. Since for every canal node, there are associated two overland-interface nodes, four additional equations are needed for every canal node *I* for the four additional unknowns Q_I^o, Q_K^o, Q_I^{o1}, and Q_I^{o2}.

The additional equations are obtained by two interface boundary conditions. The first one is the continuity of flux. The second one is the imposition of continuity of water surfaces between canal

and overland nodes or the formulation of flow rates. Two of the additional equations are obtained from the interface condition between the canal node *I* and the overland node *J* as

$$Q_J^o = Q_I^{o1}; \qquad H_J^o = H_I^c \quad or \quad Q_I^{o1} = f_1\left(h_J^o, h_I^c\right) \tag{3.4.3}$$

where f_1 is a prescribed function of water depths h_J^o and h_I^c at the overland node *J* and the canal node *I*. The other two additional equations are obtained from the interface condition between the canal node *I* and the overland node *K*

$$Q_K^o = Q_I^{o2}; \qquad H_K^o = H_I^c \quad or \quad Q_I^{o2} = f_2\left(h_K^o, h_I^c\right) \tag{3.4.4}$$

where f_2 is a prescribed function of water depths h_K^o and h_I^c at the overland node *K* and the canal node *I*.

When the direct contribution of flow from the overland regime to a junction node *L* (Fig. 3.4-1) is significant, Equations (3.1.77) or (3.1.78) must be modified

$$\frac{d\forall_L}{dh_L}\frac{dh_L}{dt} = \sum_{i=1}^{i=3} Q_{iL}^i + \sum_{O\in N_O} Q_O^o \tag{3.4.5}$$

or

$$\sum_{i=1}^{i=3} Q_{iL}^i + \sum_{O\in N_O} Q_O^o = \sum_{i=1}^{i=3} V_{iL}^i A_{iL}^i + \sum_{O\in N_O} Q_O^o = 0 \tag{3.4.6}$$

where h_L and $\forall_L$ are the water depth and volume at the junction node *L*, Q_{iL}^i is the flux contributed from the node *iL* of the reach *i*, Q_O^o is the flux contributed from the overland node *O* to the junction and N_O is the number of overland nodes interfacing with the junction *L*. Additional N_O unknowns have been introduced in Equation (3.4.5) or (3.4.6). For each overland-junction interface node, say *O* (the right frame in Fig. 3.4-1), the finite element equation written out of Eq. (3.4.2) is

$$A_{O1}^o H_1^o + A_{O2}^o H_2^o + .. + A_{OO}^o H_O^o + .. + A_{OM}^o H_M^o = R_O^o - Q_O^o \tag{3.4.7}$$

It is seen that Equation (3.4.7) involves two unknowns, H_O^o and Q_O^o. One equation must be supplemented to the finite element equation to close the system. This equation is obtained by either imposing the continuity of water surfaces between nodes *O* and *L* or formulating flux as

$$H_O^o = H_L \quad or \quad Q_O^o = f_o\left(h_O^o, h_L\right) \tag{3.4.8}$$

where f_o is a prescribed function of water depths at nodes *O* and *L*.

Finally, for each reach-junction interface node, say node *I* (the right frame in Fig. 3.4-1) which we shall say Node *1L* of the first reach connecting to Junction *L*, the formulation of Q_{1L}^1 (or Q_I^1) is similar to that of Equation (3.4.9) as

$$H_I^1 = H_L \quad or \quad Q_I^1 = f_1\left(h_I^1, h_L\right) \tag{3.4.9}$$

where the superscript *1* denotes reach number and the subscript *I* denote node number.

3.4.1.1 Couple thermal or Salt Rate between the River Network and the Overland Regime.

Numerical approximations of thermal or salt transport equation for one-dimensional river with finite element methods yield the following matrix

$$\begin{bmatrix} -- & -- & -- & -- & -- & -- & -- \\ -- & -- & -- & -- & -- & -- & -- \\ -- & -- & -- & -- & -- & -- & -- \\ C_{I1}^c & C_{I2}^c & -- & C_{I1}^c & -- & -- & C_{IN}^c \\ -- & -- & -- & -- & -- & -- & -- \\ -- & -- & -- & -- & -- & -- & -- \\ -- & -- & -- & -- & -- & -- & -- \end{bmatrix} \begin{Bmatrix} E_1^c \\ E_2^c \\ -- \\ E_I^c \\ -- \\ -- \\ E_N^c \end{Bmatrix} = \begin{Bmatrix} R_1^c \\ R_2^c \\ -- \\ R_I^c \\ -- \\ -- \\ R_N^c \end{Bmatrix} + \begin{Bmatrix} M_1^{o1} \\ M_2^{o1} \\ -- \\ M_I^{o1} \\ -- \\ -- \\ M_N^{01} \end{Bmatrix} + \begin{Bmatrix} M_1^{o2} \\ M_2^{o2} \\ -- \\ M_I^{o2} \\ -- \\ -- \\ M_N^{o2} \end{Bmatrix} \qquad \textbf{(3.4.10)}$$

where the superscript *c* denotes the canal (channel, river, or stream); C_{IJ} is the I-th row, J-th column of the coefficient matrix [*C*]; E_I denotes the temperature or salinity at Node *I*; R_I is *I*-th entry of the load vector {*R*}; *N* is the number of nodes in the canal; M_I is the rate of energy or salt source/sink from/to the overland flow to/from canal node *I*; and the superscripts, *o1* and o2, respectively, denote canal bank 1 and 2, respectively. Every canal node *I* involves 3 unknowns, E_I^c, M_I^{o1}, and M_I^{o2}. However, Eq. (3.4.10) gives just one algebraic equation for every canal node *I*. Clearly, two additional algebraic equations are need for every canal node *I*.

Applications of finite element methods to two-dimensional thermal or salt transport equation yield the following matrix

$$\begin{bmatrix} C_{11}^o & C_{12}^o & -- & -- & -- & -- & C_{1M}^o \\ C_{21}^o & -- & -- & -- & -- & -- & C_{2M}^o \\ -- & -- & -- & -- & -- & -- & -- \\ C_{J1}^o & C_{J2}^o & -- & C_{jj}^o & -- & -- & C_{IM}^o \\ -- & -- & -- & -- & -- & -- & -- \\ C_{K1}^o & C_{K2}^o & -- & -- & C_{KK}^o & -- & C_{KM}^o \\ -- & -- & -- & -- & -- & -- & -- \\ C_{M1}^o & C_{M2}^o & -- & -- & -- & -- & C_{MM}^o \end{bmatrix} \begin{Bmatrix} E_1^o \\ E_2^o \\ -- \\ E_J^o \\ -- \\ E_K^o \\ -- \\ E_M^o \end{Bmatrix} = \begin{Bmatrix} R_1^o \\ R_2^o \\ -- \\ R_J^o \\ -- \\ R_K^o \\ -- \\ R_M^o \end{Bmatrix} - \begin{Bmatrix} -- \\ -- \\ -- \\ M_J^o \\ -- \\ M_K^o \\ -- \\ -- \end{Bmatrix} \qquad \textbf{(3.4.11)}$$

where the superscript *o* denotes the overland; C_{IJ} is the *I*-th row, *J*-th column of the coefficient matrix [*C*]; E_I denotes the temperature or salinity at Node *I*; R_I is *I*-th entry of the load vector {*R*}; *M* is the number of nodes in the overland; and M_J and M_K are the rates of thermal or salt sink/source from/to the overland to/from the canal via nodes *J* and *K*, respectively. Equation (3.4.11) indicates that there is one unknown corresponding to one algebraic equation for every interior node. However, for every algebraic equation corresponding to an overland-canal interface node, there are

two unknowns, the temperature or salinity and the thermal or salt flux. Therefore, for every overland-river interface node, one additional equation is needed. Since for every canal node, there are associated two overland-interface nodes, four additional equations are needed for every canal node I for the four additional unknowns M_I^o, M_K^o, M_I^{o1}, and M_I^{o2}.

The additional equations are obtained by two interface boundary conditions. The first one is the continuity of flux. The second one is the assumption that the thermal or salinity rates through the interface node are due mainly to water flow (i.e., advection). Two of the additional equations are obtained from the interface condition between the canal node I and the overland node J as

$$M_I^{o1} = \rho_W C_W Q_I^{o1} \frac{1}{2}\left(\left(1+sign\left(Q_I^{o1}\right)\right)E_J^o + \left(1-sign\left(Q_I^{o1}\right)\right)E_I^c\right) \quad and$$
$$M_J^o = \rho_W C_W Q_J^o \frac{1}{2}\left(\left(1+sign\left(Q_J^o\right)\right)E_J^o + \left(1-sign\left(Q_J^o\right)\right)E_I^c\right) \qquad \textbf{(3.4.12)}$$

for thermal transport or

$$M_I^{o1} = Q_I^{o1} \frac{1}{2}\left(\left(1+sign\left(Q_I^{o1}\right)\right)E_J^o + \left(1-sign\left(Q_I^{o1}\right)\right)E_I^c\right) \quad and$$
$$M_J^o = Q_J^o \frac{1}{2}\left(\left(1+sign\left(Q_J^o\right)\right)E_J^o + \left(1-sign\left(Q_J^o\right)\right)E_I^c\right) \qquad \textbf{(3.4.13)}$$

for salt transport. It should be noted that in Equations (3.4.12) and (3.4.13) $Q_I^{o1} = Q_J^o$, thus the continuity $M_I^{o1} = M_J^o$ is preserved.

The other two additional equations are obtained from the interface condition between the canal node I and the overland node K as follows.

$$M_I^{o2} = \rho_W C_W Q_I^{o2} \frac{1}{2}\left(\left(1+sign\left(Q_I^{o2}\right)\right)E_K^o + \left(1-sign\left(Q_I^{o2}\right)\right)E_I^c\right) \quad and$$
$$M_K^o = \rho_W C_W Q_K^o \frac{1}{2}\left(\left(1+sign\left(Q_K^o\right)\right)E_K^o + \left(1-sign\left(Q_K^o\right)\right)E_I^c\right) \qquad \textbf{(3.4.14)}$$

for thermal transport or

$$M_I^{o2} = Q_I^{o2} \frac{1}{2}\left(\left(1+sign\left(Q_I^{o2}\right)\right)E_K^o + \left(1-sign\left(Q_I^{o2}\right)\right)E_I^c\right) \qquad and$$
$$M_K^o = Q_K^o \frac{1}{2}\left(\left(1+sign\left(Q_K^o\right)\right)E_K^o + \left(1-sign\left(Q_K^o\right)\right)E_I^c\right) \qquad \textbf{(3.4.15)}$$

for salt transport. It should be noted that in Equations (3.4.12) and (3.4.13) $Q_I^{o2} = Q_K^o$, thus the continuity $M_I^{o2} = M_I^o$ is preserved.

When the direct contribution of energy or salt from the overland regime to a junction node L (Fig. 3.4-1) is significant, Equations (3.1.121) and (3.1.122) or Equations (3.1.156) and (3.1.157) must be modified

$$\frac{d\rho_W C_W \forall_L E_L}{dt} = \sum_i \Phi_{iL}^i + \sum_{O \in N_O} M_O^o \quad or \quad \sum_i \Phi_{iL}^i + \sum_{O \in N_O} M_O^o = 0 \tag{3.4.16}$$

with E_L denoting T_L (where T_L is the temperature at the junction *L*) for thermal transport or

$$\frac{d\forall_L S_L}{dt} = \sum_i \Psi_{iL}^i + \sum_{O \in N_O} M_O^o \quad or \quad \sum_i \Psi_{iL}^i + \sum_{O \in N_O} M_O^o = 0 \tag{3.4.17}$$

with E_L denoting S_L (where S_L is the salinity at the junction *L*) for salt transport. Additional N_O unknowns have been introduced in Equation (3.4.16) or (3.4.17). For each overland-junction interface node, say *O* (the right frame in Fig. 3.4-1), the finite element equation written out of Eq. (3.4.11) is

$$C_{O1}^o E_1^o + C_{O2}^o E_2^o + .. + C_{OO}^o E_O^o + .. + C_{OM}^o E_M^o = R_O^o - M_O^o \tag{3.4.18}$$

It is seen that Equation (3.4.18) involves two unknowns, E_O^o and M_O^o. One equation must be supplemented to the finite element equation to close the system. This equation is obtained by formulating energy or salt rates

$$M_O^o = \rho_W C_W Q_O^o \frac{1}{2}\left(\left(1 + sign\left(Q_O^o\right)\right)E_O^o + \left(1 - sign\left(Q_O^o\right)\right)E_L\right) \tag{3.4.19}$$

for thermal transport or

$$M_O^o = Q_O^o \frac{1}{2}\left(\left(1 + sign\left(Q_O^o\right)\right)E_O^o + \left(1 - sign\left(Q_O^o\right)\right)E_L\right) \tag{3.4.20}$$

for salt transport. Finally, the formulation of Φ_{iL}^i or Ψ_{iL}^i is identical to that of M_O^o in Equation (3.4.19) or (3.4.20).

3.4.2 Coupling between 2-D Overland and 3-D Subsurface Flows

The interaction between two-dimensional overland and three-dimensional subsurface flows is rather simple. For every subsurface node (Node *J* in Fig. 3.4-2), there will be associated an overland nodes (Node *I* in Fig. 3.4-2).

3.4.2.1 Couple Flow Rates between the Overland Regime and Subsurface Media.

Numerical approximations of the diffusive water flow equation for two-dimensional overland with finite element methods yield the following matrix

$$\begin{bmatrix} -- & -- & -- & -- & -- & -- & -- \\ -- & -- & -- & -- & -- & -- & -- \\ -- & -- & -- & -- & -- & -- & -- \\ A_{I1}^{o} & A_{I2}^{o} & -- & A_{II}^{o} & -- & -- & A_{IN}^{o} \\ -- & -- & -- & -- & -- & -- & -- \\ -- & -- & -- & -- & -- & -- & -- \\ -- & -- & -- & -- & -- & -- & -- \end{bmatrix} \begin{Bmatrix} H_1^{o} \\ H_2^{o} \\ -- \\ H_I^{o} \\ -- \\ -- \\ H_N^{o} \end{Bmatrix} = \begin{Bmatrix} R_1^{o} \\ R_2^{o} \\ -- \\ R_I^{o} \\ -- \\ -- \\ R_N^{o} \end{Bmatrix} + \begin{Bmatrix} Q_1^{io} \\ Q_2^{io} \\ -- \\ Q_I^{io} \\ -- \\ -- \\ Q_N^{io} \end{Bmatrix} \qquad \textbf{(3.4.21)}$$

where the superscript o denotes the overland; A_{IJ} is the I-th row, J-th column of the coefficient matrix $[A]$; H_I denotes the water surface at Node I; R_I is I-th entry of the load vector $\{R\}$; N is the number of nodes in the overland; and Q_I is the rates of water sink/source from/to the overland node I to/from the corresponding subsurface node (e.g., Node J in Fig. 3.4-2) due to infiltration (the superscripts, *io*, denotes the infiltration from overland). Every overland node I involves two unknowns, H_I^{o} and and Q_I^{io}. However, Eq. (3.4.21) gives just one algebraic equation for every canal node I. Clearly, one additional algebraic equation is needed every overland node I.

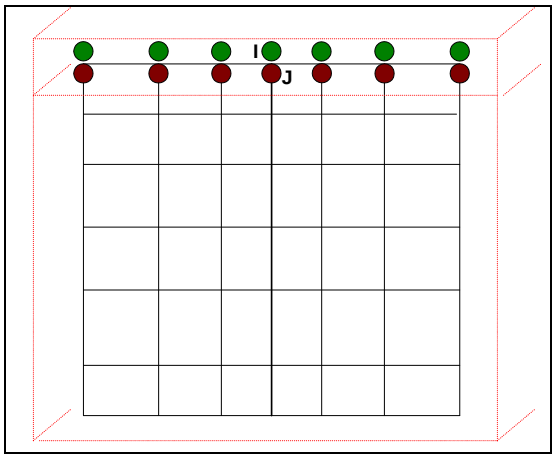

Fig. 3.4-2. Depiction of Interacting Subsurface Nodes and Overland Nodes

Applications of finite element methods to the three-dimensional subsurface flow equation yield the following matrix

$$\begin{bmatrix} A_{11}^{s} & A_{12}^{s} & -- & -- & -- & -- & A_{1M}^{s} \\ A_{21}^{s} & -- & -- & -- & -- & -- & A_{2M}^{s} \\ -- & -- & -- & -- & -- & -- & -- \\ A_{J1}^{s} & A_{J2}^{s} & -- & A_{JJ}^{s} & -- & -- & A_{IM}^{s} \\ -- & -- & -- & -- & -- & -- & -- \\ -- & -- & -- & -- & -- & -- & -- \\ A_{M1}^{o} & A_{M2}^{o} & -- & -- & -- & -- & A_{MM}^{o} \end{bmatrix} \begin{Bmatrix} H_1^{s} \\ H_2^{s} \\ -- \\ H_J^{s} \\ -- \\ -- \\ H_M^{s} \end{Bmatrix} = \begin{Bmatrix} R_1^{s} \\ R_2^{s} \\ -- \\ R_J^{s} \\ -- \\ -- \\ R_M^{s} \end{Bmatrix} - \begin{Bmatrix} -- \\ -- \\ -- \\ Q_J^{s} \\ -- \\ -- \\ -- \end{Bmatrix} \qquad \textbf{(3.4.22)}$$

where the superscript so denotes the subsurface media; A_{IJ} is the I-th row, J-th column of the coefficient matrix $[A]$; H_J denotes the total head at Node J; R_J is J-th entry of the load vector $\{R\}$; M

is the number of nodes in the subsurface media; and Q_J is the rates of water source/sink from/to the overland to/from the subsurface media at node J. Equation (3.4.22) indicates that there is one unknown corresponding to one algebraic equation for every interior node. However, for every algebraic equation corresponding to a subsurface-overland interface node, there are two unknowns, the total head and the flow rate. Therefore, for every subsurface media node interfacing with an overland node, one additional equation is needed. Since for every overland node, there is associated one subsurface-interface node, two additional equations are needed for every overland node I for the two additional unknowns Q_I^{io} and Q_J^s.

The additional equations are obtained by the interface boundary condition between the overland node I and the subsurface media node J as

$$Q_J^s = Q_I^{io}; \qquad H_J^s = H_I^o \quad or \quad Q_I^{io} = K\left(H_J^s - H_I^o\right) \tag{3.4.23}$$

where K is the exchange coefficient representing the property of the medium separating the overland and subsurface media, but not being included as part of the media.

3.4.2.2 Couple thermal or Salt Rate between the Overland Regime and Subsurface Media.

Numerical approximations of thermal or salt transport equation for two-dimensional overland regime with finite element methods yield the following matrix

$$\begin{bmatrix} -- & -- & -- & -- & -- & -- & -- \\ -- & -- & -- & -- & -- & -- & -- \\ -- & -- & -- & -- & -- & -- & -- \\ C_{I1}^o & C_{I2}^o & -- & C_{II}^o & -- & -- & C_{IN}^o \\ -- & -- & -- & -- & -- & -- & -- \\ -- & -- & -- & -- & -- & -- & -- \\ -- & -- & -- & -- & -- & -- & -- \end{bmatrix} \begin{Bmatrix} E_1^o \\ E_2^o \\ -- \\ E_I^o \\ -- \\ -- \\ E_N^o \end{Bmatrix} = \begin{Bmatrix} R_1^o \\ R_2^o \\ -- \\ R_I^o \\ -- \\ -- \\ R_N^o \end{Bmatrix} + \begin{Bmatrix} M_1^{io} \\ M_2^{io} \\ -- \\ M_I^{io} \\ -- \\ -- \\ M_N^{io} \end{Bmatrix} \tag{3.4.24}$$

where the superscript o denotes the overland; C_{IJ} is the I-th row, J-th column of the coefficient matrix $[C]$; E_I denotes the temperature or salinity at Node I; R_I is I-th entry of the load vector $\{R\}$; N is the number of nodes in the overland; and M_I is the rate of energy or salt source/sink from/to the subsurface to/from the overland node I (the superscript, io, denotes the infiltration from overland). Every overland node I involves two unknowns, E_I^o, and M_I^{io}. However, Eq. (3.4.24) gives just one algebraic equation for every canal node I. Clearly, one additional algebraic equation is need for every overland node I.

Applications of finite element methods to three-dimensional thermal or salt transport equations for subsurface media yield the following matrix

$$\begin{bmatrix} C^s_{11} & C^s_{12} & -- & -- & -- & -- & C^s_{1M} \\ C^s_{21} & -- & -- & -- & -- & -- & C^s_{2M} \\ -- & -- & -- & -- & -- & -- & -- \\ C^s_{J1} & C^s_{J2} & -- & C^s_{JJ} & -- & -- & C^s_{IM} \\ -- & -- & -- & -- & -- & -- & -- \\ -- & -- & -- & -- & -- & -- & -- \\ C^s_{M1} & C^s_{M2} & -- & -- & -- & -- & C^s_{MM} \end{bmatrix} \begin{Bmatrix} E^s_1 \\ E^s_2 \\ -- \\ E^s_J \\ -- \\ -- \\ E^s_M \end{Bmatrix} = \begin{Bmatrix} R^s_1 \\ R^s_2 \\ -- \\ R^s_J \\ -- \\ -- \\ R^s_M \end{Bmatrix} - \begin{Bmatrix} -- \\ -- \\ -- \\ M^s_J \\ -- \\ -- \\ -- \end{Bmatrix} \qquad \textbf{(3.4.25)}$$

where the superscript *s* denotes the subsurface media; C_{IJ} is the *I*-th row, *J*-th column of the coefficient matrix [*C*]; E_J denotes the temperature or salinity at Node *J*; R_J is *J*-th entry of the load vector {*R*}; *M* is the number of nodes in the overland ; and M_J is the rate of thermal or salt sink/source from/to the subsurface node *J* to/from the corresponding overland node *I*. Equation (3.4.25) indicates that there is one unknown corresponding to one algebraic equation for every interior node. However, for every algebraic equation corresponding an subsurface-overland interface node, there are two unknowns, the temperature or salinity and the thermal or salt flux. Therefore, for every subsurface-overland interface node, one additional equation is needed. Since for every overland node, there is associated one subsurface-interface nodes, two additional equations are needed for every overland node *I* and its corresponding subsurface node *J* for the two additional unknowns M_I^{io} and M_J^s.

The additional equations are obtained from the interface condition between the overland *I* and the subsurface *J* as

$$\begin{aligned} M_I^{io} &= \rho_W C_W Q_I^{io} \frac{1}{2}\left(\left(1+sign\left(Q_I^{io}\right)\right)E_J^s + \left(1-sign\left(Q_I^{io}\right)\right)E_I^o\right) \quad and \\ M_J^s &= \rho_W C_W Q_J^s \frac{1}{2}\left(\left(1+sign\left(Q_J^s\right)\right)E_J^s + \left(1-sign\left(Q_J^s\right)\right)E_I^o\right) \end{aligned} \qquad \textbf{(3.4.26)}$$

for thermal transport or

$$\begin{aligned} M_I^{io} &= Q_I^{io} \frac{1}{2}\left(\left(1+sign\left(Q_I^{io}\right)\right)E_J^s + \left(1-sign\left(Q_I^{io}\right)\right)E_I^o\right) \quad and \\ M_J^s &= Q_J^s \frac{1}{2}\left(\left(1+sign\left(Q_J^s\right)\right)E_J^s + \left(1-sign\left(Q_J^s\right)\right)E_I^o\right) \end{aligned} \qquad \textbf{(3.4.27)}$$

for salt transport. It should be noted that in Equations (3.4.26) or (3.4.27) $Q_I^{io} = Q_J^s$, thus the continuity $M_I^{io} = M_J^s$ is preserved.

3.4.3 Coupling between 3-D Subsurface and 1-D Surface Flows

The interaction between three-dimensional subsurface and one-dimensional river flows involves three options: (1) river is discretized as finite-width and finite-depth on the three-dimensional subsurface media (Fig. 3.4-3), (2) river is discretized as finite-width and zero-depth on the three-dimensional subsurface media (Fig. 3.4-4), and (3) river is discretized as zero-width and zero-depth on the three-dimensional subsurface media (Fig. 3.4-5). Option 1 is the most realistic one.

However, because of the computational demands, it is normally used in small scale studies involving the investigations of infiltration and discharge between river and subsurface media on a local scale. Option 2 is normally used in medium scale studies while Option 3 is normally employed in large scale investigations. In Option 1, for every river node there are associated with a number of subsurface interfacing nodes such as *K*, .., *J*, .., and *L*(Fig. 3.4-3). In Option 2, for every river node there are associated with three subsurface interfacing nodes *K*, *J*, and *L* (Fig. 3.4-4). In Option 3, for every river node there is associated with one subsurface interfacing node *J* (Fig. 3.4-5).

3.4.3.1 Couple Flow Rates between the River Network and the Subsurface Media.

Numerical approximations of the diffusive water flow equation for one-dimensional river with finite element methods yield the following matrix

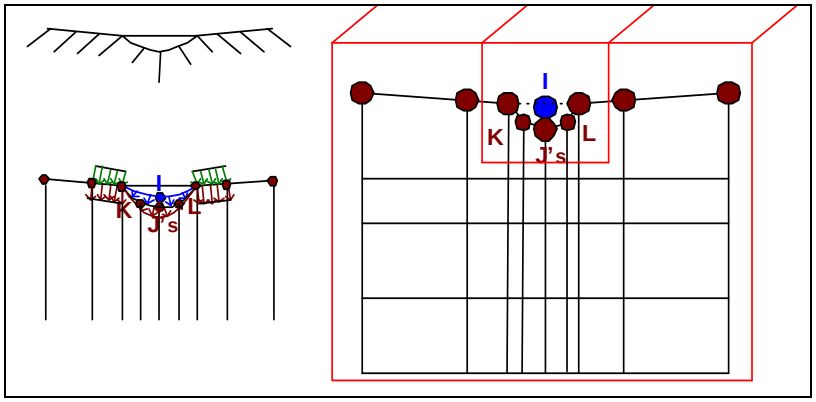

Fig. 3.4-3. Rivers Are Discretized as Finite-Width and Finite-Depth on the Subsurface Media

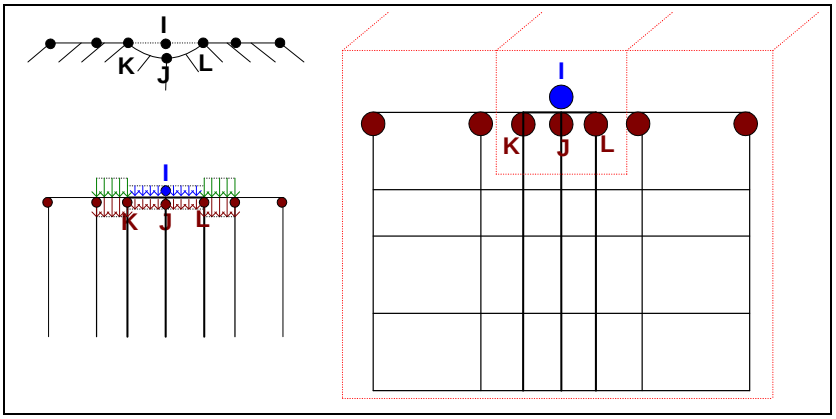

Fig. 3.4-4. Rivers Are Discretized as Finite-Width and Zero-Depth on the Subsurface Media

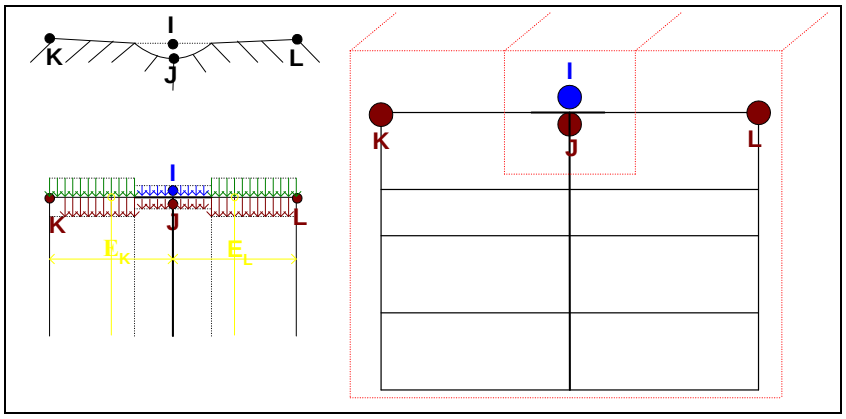

Fig. 3.4-5. Rivers Are Discretized as Zero-Width and Zero-Depth on the Subsurface Media

$$\begin{bmatrix} -- & -- & -- & -- & -- & -- & -- \\ -- & -- & -- & -- & -- & -- & -- \\ -- & -- & -- & -- & -- & -- & -- \\ A_{I1}^c & A_{I2}^c & -- & A_{II}^c & -- & -- & A_{IN}^c \\ -- & -- & -- & -- & -- & -- & -- \\ -- & -- & -- & -- & -- & -- & -- \\ -- & -- & -- & -- & -- & -- & -- \end{bmatrix} \begin{Bmatrix} H_1^c \\ H_2^c \\ -- \\ H_I^c \\ -- \\ -- \\ H_N^c \end{Bmatrix} = \begin{Bmatrix} R_1^c \\ R_2^c \\ -- \\ R_I^c \\ -- \\ -- \\ R_N^c \end{Bmatrix} + \begin{Bmatrix} Q_1^{ic} \\ Q_2^{ic} \\ -- \\ Q_I^{ic} \\ -- \\ -- \\ Q_N^{ic} \end{Bmatrix} \tag{3.4.28}$$

where the superscript c denotes the canal (channel, river, or stream); A_{IJ} is the I-th row, J-th column of the coefficient matrix $[A]$; H_I denotes the water surface at Node I; R_I is I-th entry of the load vector $\{R\}$; N is the number of nodes in the canal; Q_I is the rates of water sink/source from/to the river node I to/from the subsurface media. Every canal node I involves two unknowns, H_I^c and Q_I^{ic}. However, Eq. (3.4.28) gives just one algebraic equation for every canal node I. Clearly, one additional algebraic equation is need for every canal node I.

For example, taking Option 2 where there are three nodes associated with one canal node, the applications of finite element methods to three-dimensional subsurface flow equations yield

$$\begin{bmatrix} A_{11}^s & A_{12}^s & -- & -- & -- & -- & A_{1M}^s \\ A_{21}^s & -- & -- & -- & -- & -- & A_{2M}^s \\ -- & -- & -- & -- & -- & -- & -- \\ A_{K1}^s & A_{K2}^s & A_{KK}^s & -- & -- & -- & A_{KM}^s \\ A_{J1}^s & A_{J2}^s & -- & A_{JJ}^s & -- & -- & A_{IM}^s \\ A_{L1}^s & A_{L2}^s & A_{>>}^s & -- & -- & -- & A_{LM}^s \\ -- & -- & -- & -- & -- & -- & -- \\ A_{M1}^s & A_{M2}^s & -- & -- & -- & -- & A_{MM}^s \end{bmatrix} \begin{Bmatrix} H_1^s \\ H_2^s \\ -- \\ H_K^s \\ H_J^s \\ H_L^s \\ -- \\ H_M^s \end{Bmatrix} = \begin{Bmatrix} R_1^s \\ R_2^s \\ -- \\ R_K^s \\ R_J^s \\ R_L^s \\ -- \\ R_M^s \end{Bmatrix} - \begin{Bmatrix} -- \\ -- \\ -- \\ Q_K^s \\ Q_J^s \\ Q_L^s \\ -- \\ -- \end{Bmatrix} \tag{3.4.29}$$

where the superscript *s* denotes the subsurface meida; A_{IJ} is the *I*-th row, *J*-th column of the coefficient matrix [*A*]; H_J denotes the total head at Node *J*; R_J is *J*-th entry of the load vector {*R*}; *M* is the number of nodes in the subsurface media; and Q_J is the rate of water source/sink from/to the canal to/from the subsurface via node *J*. Equation (3.4.29) indicates that there is one unknown corresponding to one algebraic equation for every interior node. However, for every algebraic equation corresponding to a subsurface-canal interface node, there are two unknowns, the total head and the flow rate. Therefore, for every subsurface-river interface node, one additional equation is needed. Since for every canal node, there are associated three subsurface-interface nodes, four additional equations are needed for every canal node *I* for the four additional unknowns Q_I^{ic}, Q_K^s, Q_J^s, and Q_L^s.

The additional equations are obtained the interface condition between the canal node *I* and the subsurface nodes *K*, *J*, and *L* as

$$\begin{aligned} &Q_I^{ic} + Q_K^{rain} + Q_L^{rain} = Q_K^s + Q_J^s + Q_L^s; \qquad H_J^s = H_I^c \quad or \quad Q_J^s = K_e\left(H_J^s - H_I^c\right); \\ &H_K^s = H_K^{ponding} \quad or \quad Q_K^s = Q_K^{rain} + \frac{1}{4}Q_I^{ic}; \qquad H_L^s = H_L^{ponding} \quad or \quad Q_L^s = Q_L^{rain} + \frac{1}{4}Q_I^{ic} \end{aligned} \tag{3.4.30}$$

where Q_K^{rain} and Q_L^{rain} are the rainfall fluxes through nodes K and L, respectively; $H_K^{ponding}$ and $H_L^{ponding}$ are the allowable ponding depth at nodes K and L, respectively; and K_e is the exchange coefficient representing the material property of a layer separating the river and subsurface media but the layer is not included in the geometrical discretization.

In Option 1, for every canal node *I*, there are associated a number of subsurface-interface nodes, say N_S, (N_S + 1) additional equations are needed for every canal node *I* for the additional unknowns Q_I^{ic}, Q_K^s, .., Q_J^s, .., and Q_L^s. These equations are listed below:

$$\begin{aligned} &Q_I^{ic} + Q_K^{rain} + Q_L^{rain} = Q_K^s + \sum_J^{N_S} Q_J^s + Q_L^s; \\ &H_J^s = H_I^c \quad or \quad Q_J^s = K_e\left(H_J^s - H_I^c\right) \ for\ J \in \ on\ River\ Bottom; \\ &H_K^s = H_K^{ponding} \quad or \quad Q_K^s = Q_K^{rain} + \frac{1}{4}Q_I^{ic}; \qquad H_L^s = H_L^{ponding} \quad or \quad Q_L^s = Q_L^{rain} + \frac{1}{4}Q_I^{ic} \end{aligned} \tag{3.4.31}$$

In Option 3, for every canal node *I*, there are associated three subsurface-interface nodes *K*, *J*, and *L* as in Option 2. However, while in Option 2, nodes *K* and *J* are located at the interactions of river banks and subsurface media, in Option 3, nodes *K* and *L* can be located far way from the river banks and node *J* interacts directly with the canal node *I*. The four interaction equations are modified according to the continuity of fluxes as

$$\begin{aligned} &Q_J^s = Q_I^{ic} + Q_K^{rain}\left(1 - \frac{P}{E_K}\right) + Q_L^{rain}\left(1 - \frac{P}{E_L}\right); \qquad H_I^c = H_J^s \quad or \quad Q_I^{ic} = K\left(H_J^s - H_I^c\right); \\ &H_K^s = H_K^{ponding} \quad or \quad Q_K^s = Q_K^{rain}; \qquad H_L^s = H_L^{ponding} \quad or \quad Q_L^s = Q_L^{rain} \end{aligned} \tag{3.4.32}$$

where P is the wet perimeter of the canal and E_K and E_L are the element length of KJ and JL,

respectively.

3.4.3.2 Couple thermal or Salt Rate between the River Network and the Subsurface.

Numerical approximations of thermal or salt transport equation for one-dimensional river with finite element methods yield the following matrix

$$\begin{bmatrix} -- & -- & -- & -- & -- & -- & -- \\ -- & -- & -- & -- & -- & -- & -- \\ -- & -- & -- & -- & -- & -- & -- \\ C_{I1}^c & C_{I2}^c & -- & C_{II}^c & -- & -- & C_{IN}^c \\ -- & -- & -- & -- & -- & -- & -- \\ -- & -- & -- & -- & -- & -- & -- \\ -- & -- & -- & -- & -- & -- & -- \end{bmatrix} \begin{Bmatrix} E_1^c \\ E_2^c \\ -- \\ E_I^c \\ -- \\ -- \\ E_N^c \end{Bmatrix} = \begin{Bmatrix} R_1^c \\ R_2^c \\ -- \\ R_I^c \\ -- \\ -- \\ R_N^c \end{Bmatrix} + \begin{Bmatrix} M_1^{ic} \\ M_2^{ic} \\ -- \\ M_I^{ic} \\ -- \\ -- \\ M_N^{ic} \end{Bmatrix} \qquad \textbf{(3.4.33)}$$

where the superscript *c* denotes the canal (channel, river, or stream); C_{IJ} is the I-th row, J-th column of the coefficient matrix [*C*]; E_I denotes the temperature or salinity at Node *I*; R_I is *I*-th entry of the load vector {*R*}; *N* is the number of nodes in the canal; and M_I^{ic} is the rate of energy or salt source/sink from/to the subsurface to/from canal node *I* due to infiltration/exfiltration. Every canal node *I* involves two unknowns, E_I^c and M_I^{ic}. However, Eq. (3.4.33) gives just one algebraic equation for every canal node *I*. Clearly, one additional algebraic equation is need for every canal node *I*.

For example, taking Option 2 where there are three nodes associated with one canal node, the applications of finite element methods to three-dimensional thermal or salt transport equation in the subsurface media yields

$$\begin{bmatrix} C_{11}^s & C_{12}^s & -- & -- & -- & -- & C_{1M}^s \\ C_{21}^s & -- & -- & -- & -- & -- & C_{2M}^s \\ -- & -- & -- & -- & -- & -- & -- \\ C_{K1}^s & C_{K2}^s & C_{KK}^s & -- & -- & -- & C_{KM}^s \\ C_{J1}^s & C_{J2}^s & -- & C_{JJ}^s & -- & -- & C_{1M}^s \\ C_{L1}^s & C_{L2}^s & C_{<<}^s & -- & -- & -- & C_{LM}^s \\ -- & -- & -- & -- & -- & -- & -- \\ C_{M1}^s & C_{M2}^s & -- & -- & -- & -- & C_{MM}^s \end{bmatrix} \begin{Bmatrix} E_1^s \\ E_2^s \\ -- \\ E_K^s \\ E_J^s \\ E_L^s \\ -- \\ E_M^s \end{Bmatrix} = \begin{Bmatrix} R_1^s \\ R_2^s \\ -- \\ R_K^s \\ R_J^s \\ R_L^s \\ -- \\ R_M^s \end{Bmatrix} - \begin{Bmatrix} -- \\ -- \\ -- \\ M_K^s \\ M_J^s \\ M_L^s \\ -- \\ -- \end{Bmatrix} \qquad \textbf{(3.4.34)}$$

where the superscript *s* denotes the subsurface media; C_{IJ} is the *I*-th row, *J*-th column of the coefficient matrix [*C*]; E_J denotes the temperature or salinity at Node *J*; R_J is *J*-th entry of the load vector {*R*}; *M* is the number of nodes in the overland ; and M_K, M_J and M_L are the rates of thermal or salt sink/source from/to the subsurface water to/from the canal via nodes *K*, *J* and *L*, respectively. Equation (3.4.34) indicates that there is one unknown corresponding to one algebraic equation for

every interior node. However, for every algebraic equation corresponding an subsurface-canal interface node, there are two unknowns, the temperature or salinity and the thermal or salt flux. Therefore, for every subsurface-river interface node, one additional equation is needed. Since for every canal node, there are associated three subsurface-interface nodes, four additional equations are needed for every canal node I for the four additional unknowns M_I^{ic}, M_K^s, M_J^s, and M_L^s.

These four additional equations are obtained by the interface condition between the canal node I and the subsurface nodes K, J, and L as

$$M_I^{ic} = Q_I^{ic}\frac{\rho_W C_W}{2}\left(1-sign(Q_I^{ic})\right)E_I^c + \frac{\rho_W C_W}{2}\left(1+sign(Q_I^{ic})\right)\times \left(Q_K^s E_K^s + Q_J^s E_J^s + Q_L^s E_L^s - Q_K^{rains} E_K^{rain} - Q_L^{rains} E_L^{rain}\right) \tag{3.4.35}$$

and

$$\begin{aligned} M_K^s &= \rho_W C_W Q_K^s \frac{1}{2}\left(\left(1+sign\left(Q_K^s\right)\right)E_K^s + \left(1-sign\left(Q_K^s\right)\right)E_I^c\right), \\ M_J^s &= \rho_W C_W Q_J^s \frac{1}{2}\left(\left(1+sign\left(Q_J^s\right)\right)E_J^s + \left(1-sign\left(Q_J^s\right)\right)E_I^c\right), \\ M_L^s &= \rho_W C_W Q_L^s \frac{1}{2}\left(\left(1+sign\left(Q_L^s\right)\right)E_L^s + \left(1-sign\left(Q_L^s\right)\right)E_I^c\right) \end{aligned} \tag{3.4.36}$$

for thermal transport or

$$M_I^{ic} = Q_I^{ic}\frac{1}{2}\left(1-sign(Q_I^{ic})\right)E_I^c + \frac{1}{2}\left(1+sign(Q_I^{ic})\right)\times \left(Q_K^s E_K^s + Q_J^s E_J^s + Q_L^s E_L^s - Q_K^{rains} E_K^{rain} - Q_L^{rains} E_L^{rain}\right) \tag{3.4.37}$$

and

$$\begin{aligned} M_K^s &= Q_K^s \frac{1}{2}\left(\left(1+sign\left(Q_K^s\right)\right)E_K^s + \left(1-sign\left(Q_K^s\right)\right)E_I^c\right), \\ M_J^s &= Q_J^s \frac{1}{2}\left(\left(1+sign\left(Q_J^s\right)\right)E_J^s + \left(1-sign\left(Q_J^s\right)\right)E_I^c\right), \\ M_L^s &= Q_L^s \frac{1}{2}\left(\left(1+sign\left(Q_L^s\right)\right)E_L^s + \left(1-sign\left(Q_L^s\right)\right)E_I^c\right) \end{aligned} \tag{3.4.38}$$

for salt transport. For Option 1 and Option 3, the coupling can be done similarly.

3.4.4 Coupling Among River, Overland, and Subsurface Flows

The interaction among one-dimensional river, two-dimensional overland, and three-dimensional subsurface flows involves three options: (1) river is discretized as finite-width and finite-depth on the three-dimensional subsurface media (Fig. 3.4-6), (2) river is discretized as finite-width and zero-depth on the three-dimensional subsurface media (Fig. 3.4-7), and (3) river is discretized as zero-width and zero-depth on the three-dimensional subsurface media (Fig. 3.4-8). Option 1 is the most realistic one. However, because of the computational demands, it is normally used in small scale studies involving the investigations of infiltration and discharge between river and subsurface media on a local scale. Option 2 is normally used in medium scale studies while Option 3 is normally

employed in large scale investigations. In Option 1, for every river node there are associated with two overland nodes *M* and *N* and a number of subsurface interfacing nodes such as *K*. , *J*, .., and *L* (Fig. 3.4-6). In Option 2, for every river node *I*, there are associated with two overland nodes *M* and *N* and three subsurface interfacing nodes *K*, *J*, and *L* (Fig. 3.4-7). In Option 3, for every river node *I*, there is associated with two overland nodes *M* and *N* one subsurface node *J* (Fig. 3.4-8).

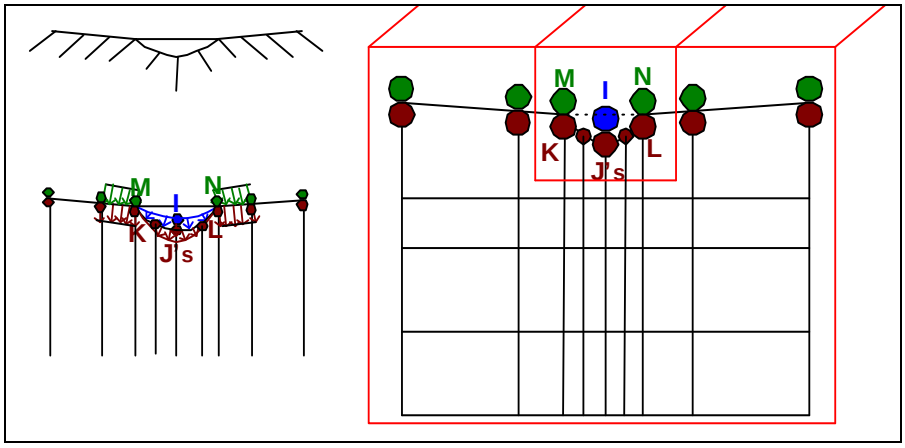

Fig. 3.4-6. Interfacing Nodes for Every River Node when Rivers Are Discretized as Finite-Width and Finite-Depth

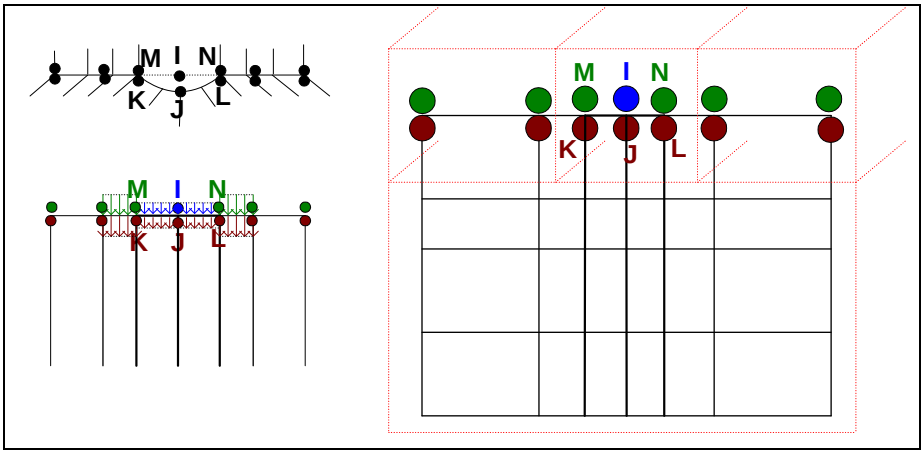

Fig. 3.4-7. Interfacing Nodes for Every River Node when Rivers Are Discretized as Finite-Width and Zero-Depth

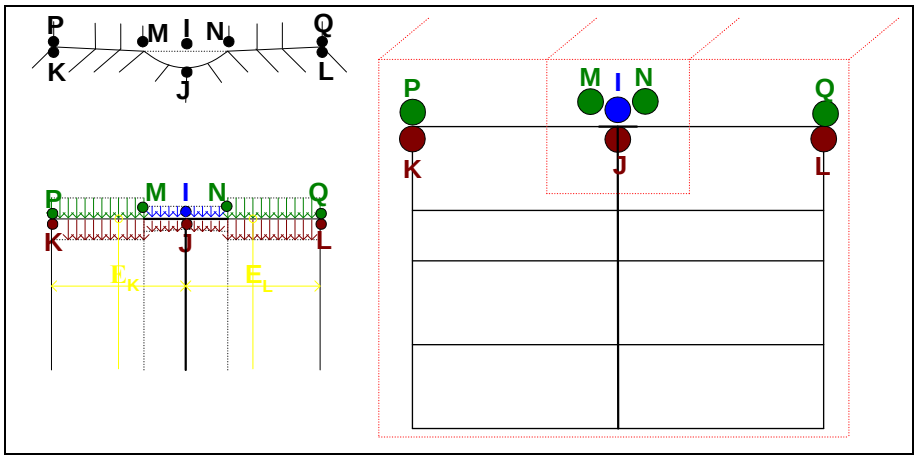

Fig. 3.4-8. Interfacing Nodes for Every River Node when Rivers Are Discretized as Zero-Width and Zero-Depth

3.4.4.1 Couple Flow Rates among River, Overland, and Subsurface Media.

Numerical approximations of flow equations in river, overland, and subsurface would result in a system of algebraic equations. For every river node *I* (Fig. 3.4-7), one or two algebraic equations (for diffusive wave or fully dynamic wave approaches) are obtained governing the water surface (diffusive wave approach) or the water surface and discharge (dynamic wave approach) for the node. The algebraic equation(s) also includes three additional unknowns: two are flow rates from overland to the river via two river banks (Q_I^{o1} and Q_I^{o2})and the other is the flow rate from the subsurface media to river via infiltration/exfiltration ($Q_I^{ic.}$) In the meantime, for the overland node *M* that interfaces with the river node *I* and other subsurface nodes (Fig. 3.4-7), there are two additional unknowns besides the state variables: one is the boundary flux from the overland to the river (Q_M^{o}) and the other is the infiltration and/or exfiltration flux from overland to the subsurface (Q_M^{io}). Similarly for the overland node *N* that interfaces with the river node *I* and other subsurface nodes (Fig. 3.4-7), there are two additional unknowns besides the state variables: one is the boundary flux from the overland to the river (Q_N^{o}) and the other is the infiltration and/or exfiltration flux from overland to the subsurface (Q_N^{io}). For the subsurface node *K* that interfaces with the river node *I* and overland node *M* (Fig. 3.4-7), there is one additional unknown (Q_K^{s}) beside the state variable. Similarly, for the subsurface nodes *L* that interfaces with the river node *I* and overland node *N*, there is one additional unknown (Q_L^{s}). Finally for the subsurface node J that interfaces with the river node I, there is one additional unknown (Q_J^{s}) beside the state variable (the pressure head or total head at node *J*). Thus, in Option 2, one needs to set up 10 equations that describe the interactions among flows in river, overland, and subsurface. These ten equations can be derived based on the continuity of fluxes and state variables and formulation of each flux at each individual node as follows.

Interaction between Overland Node *M* and Canal Node *I*. Two equations are obtained based on the continuity of flux and state variable or formulation of flux as

$$Q_M^o = Q_I^{o1}; \qquad H_M^o = H_I^c \quad or \quad Q_I^{o1} = f_1\left(H_M^o, H_I^c\right) \tag{3.4.39}$$

Interaction between Overland Node *N* and Canal Node *I*. Two equations are obtained based on

the continuity of flux and state variable or formulation of flux as

$$Q_N^o = Q_I^{o2}; \qquad H_N^o = H_I^c \quad or \quad Q_I^{o2} = f_2\left(H_N^o, H_I^c\right) \tag{3.4.40}$$

Interaction between Overland Node *M*, Subsurface Node *K*, and Canal Node *I*. Two equations are obtained based on the continuity of flux and state variable or formulation of flux as

$$Q_K^s = Q_M^{io} + \frac{1}{4}Q_I^{ic}; \qquad H_K^s = H_M^o \quad or \quad Q_M^{io} = K_e\left(H_K^s - H_M^o\right) \tag{3.4.41}$$

Interaction between River Bank Node *N*, Subsurface Node *L*, and Canal Node *I*. Two equations are obtained based on the continuity of flux and state variable or formulation of flux as

$$Q_L^s = Q_N^{io} + \frac{1}{4}Q_I^{ic}; \qquad H_L^s = H_N^o \quad or \quad Q_N^{io} = K_e\left(H_L^s - H_N^o\right) \tag{3.4.42}$$

Interaction between Subsurface Node *J* and Canal Node *I*. Two equations are obtained based on the continuity of flux and state variable or formulation of flux as

$$Q_J^s = \frac{1}{2}Q_I^{ic}; \qquad H_J^s = H_I^c \quad or \quad Q_J^s = K_e\left(H_J^s - H_I^c\right) \tag{3.4.43}$$

3.4.4.2 Couple thermal or Salt Rate among River, Overland, and Subsurface Media.

Similar to the coupling of flows among river, overland, and subsurface media, the coupling of thermal or salinity transport are achieved by imposing the continuity of energy/salt fluxes and formulation of individual node fluxes.

Interaction between Overland Node *M* and Canal Node *I*. Two equations are obtained based on the continuity of fluxes and the formulation of fluxes as

$$\begin{aligned} M_I^{o1} &= \rho_W C_W Q_I^{o1} \frac{1}{2}\left(\left(1 + sign\left(Q_I^{o1}\right)\right)E_M^o + \left(1 - sign\left((Q_I^{o1}\right)\right)E_I^c\right) \quad and \\ M_M^o &= \rho_W C_W Q_M^o \frac{1}{2}\left(\left(1 + sign\left(Q_M^o\right)\right)E_M^o + \left(1 - sign\left((Q_M^o\right)\right)E_I^c\right) \end{aligned} \tag{3.4.44}$$

for thermal transport or

$$\begin{aligned} M_I^{o1} &= Q_I^{o1} \frac{1}{2}\left(\left(1 + sign\left(Q_I^{o1}\right)\right)E_M^o + \left(1 - sign\left((Q_I^{o1}\right)\right)E_I^c\right) \quad and \\ M_M^o &= Q_M^o \frac{1}{2}\left(\left(1 + sign\left(Q_M^o\right)\right)E_M^o + \left(1 - sign\left((Q_M^o\right)\right)E_I^c\right) \end{aligned} \tag{3.4.45}$$

for salt transport.

Interaction between Overland Node *N* and Canal Node *I*. Two equations are obtained based on the continuity of fluxes and the formulation of fluxes as

$$M_I^{o2} = \rho_W C_W Q_I^{o2} \frac{1}{2}\left(\left(1+sign\left(Q_I^{o2}\right)\right)E_N^o + \left(1-sign\left((Q_I^{o2}\right)\right)E_I^c\right) \quad and$$
$$M_N^o = \rho_W C_W Q_N^o \frac{1}{2}\left(\left(1+sign\left(Q_N^o\right)\right)E_N^o + \left(1-sign\left((Q_N^o\right)\right)E_I^c\right) \qquad (3.4.46)$$

for thermal transport or

$$M_I^{o2} = Q_I^{o2} \frac{1}{2}\left(\left(1+sign\left(Q_I^{o2}\right)\right)E_N^o + \left(1-sign\left(Q_I^{o2}\right)\right)E_I^c\right) \quad and$$
$$M_N^o = Q_N^o \frac{1}{2}\left(\left(1+sign\left(Q_N^o\right)\right)E_N^o + \left(1-sign\left(Q_N^o\right)\right)E_I^c\right) \qquad (3.4.47)$$

Interaction between Overland Node *M*, Subsurface Node *K*, and Canal Node *I*. Two equations are obtained based on the continuity of fluxes and the formulation of fluxes as

$$M_M^{io} = \rho_W C_W \left\{\frac{1}{2}\left(1-sign\left(Q_M^{io}\right)\right)Q_M^{io}E_M^o + \frac{1}{2}\left(1+sign\left(Q_M^{io}\right)\right)\left(Q_K^s E_K^s - \frac{1}{4}Q_I^{ic}E_I^c\right)\right\} \quad and$$
$$M_K^s = \rho_W C_W \left\{\frac{1}{2}\left(1+sign\left(Q_K^s\right)\right)Q_K^s E_K^s + \frac{1}{2}\left(1-sign\left(Q_K^s\right)\right)\left(Q_M^{io}E_M^o + \frac{1}{4}Q_I^{ic}E_I^c\right)\right\} \qquad (3.4.48)$$

for thermal transport and

$$M_M^{io} = \left\{\frac{1}{2}\left(1-sign\left(Q_M^{io}\right)\right)Q_M^{io}E_M^o + \frac{1}{2}\left(1+sign\left(Q_M^{io}\right)\right)\left(Q_K^s E_K^s - \frac{1}{4}Q_I^{ic}E_I^c\right)\right\} \quad and$$
$$M_K^s = \left\{\frac{1}{2}\left(1+sign\left(Q_K^s\right)\right)Q_K^s E_K^s + \frac{1}{2}\left(1-sign\left(Q_K^s\right)\right)\left(Q_M^{io}E_M^o + \frac{1}{4}Q_I^{ic}E_I^c\right)\right\} \qquad (3.4.49)$$

for salt transport.

Interaction between River Bank Node *N*, Subsurface Node *L*, and Canal Node *I*. Two equations are obtained based on the continuity of fluxes and the formulation of flux as

$$M_N^{io} = \rho_W C_W \left\{\frac{1}{2}\left(1-sign\left(Q_N^{io}\right)\right)Q_N^{io}E_N^o + \frac{1}{2}\left(1+sign\left(Q_N^{io}\right)\right)\left(Q_L^s E_L^s - \frac{1}{4}Q_I^{ic}E_I^c\right)\right\} \quad and$$
$$M_L^s = \rho_W C_W \left\{\frac{1}{2}\left(1+sign\left(Q_L^s\right)\right)Q_L^s E_L^s + \frac{1}{2}\left(1-sign\left(Q_L^s\right)\right)\left(Q_N^{io}E_N^o + \frac{1}{4}Q_I^{ic}E_I^c\right)\right\} \qquad (3.4.50)$$

for thermal transport and

$$M_N^{io} = \left\{\frac{1}{2}\left(1-sign\left(Q_N^{io}\right)\right)Q_N^{io}E_N^o + \frac{1}{2}\left(1+sign\left(Q_N^{io}\right)\right)\left(Q_L^s E_L^s - \frac{1}{4}Q_I^{ic}E_I^c\right)\right\} \quad and$$
$$M_L^s = \left\{\frac{1}{2}\left(1+sign\left(Q_L^s\right)\right)Q_L^s E_L^s + \frac{1}{2}\left(1-sign\left(Q_L^s\right)\right)\left(Q_N^{io}E_N^o + \frac{1}{4}Q_I^{ic}E_I^c\right)\right\} \qquad (3.4.51)$$

for salt transport.

Interaction between Subsurface Node *J* and Canal Node *I*. Two equations are obtained based on the continuity of fluxes and the formulation of fluxes as

$$M_I^{ic} = \rho_W C_W \left(\frac{1}{2}\left(1 + sign\left(Q_I^{ic}\right)\right) 2Q_J^s E_J^s + \frac{1}{2}\left(1 - sign\left(Q_I^{ic}\right)\right) Q_I^{ic} E_I^c \right) \quad and$$
$$M_J^s = \rho_W C_W \left(\frac{1}{2}\left(1 + sign\left(Q_J^s\right)\right) Q_J^s E_J^s + \frac{1}{2}\left(1 - sign\left(Q_J^s\right)\right) \frac{1}{2} Q_I^{ic} E_I^c \right) \qquad \textbf{(3.4.52)}$$

for thermal transport and

$$M_I^{ic} = \left(\frac{1}{2}\left(1 + sign\left(Q_I^{ic}\right)\right) 2Q_J^s E_J^s + \frac{1}{2}\left(1 - sign\left(Q_I^{ic}\right)\right) Q_I^{ic} E_I^c \right) \quad and$$
$$M_J^s = \left(\frac{1}{2}\left(1 + sign\left(Q_J^s\right)\right) Q_J^s E_J^s + \frac{1}{2}\left(1 - sign\left(Q_J^s\right)\right) \frac{1}{2} Q_I^{ic} E_I^c \right) \qquad \textbf{(3.4.53)}$$

for salt transport.

3.5 Solving One-Dimensional River/Stream/Canal Network Water Quality Transport Equations

In this section, we present the numerical approaches employed to solve the governing equations of reactive chemical transport in 1-D river/stream/canal networks. Ideally, one would like to use a numerical approach that is accurate, efficient, and robust. Depending on the specific problem at hand, different numerical approaches may be more suitable. For research applications, accuracy is a primary requirement, because one does not want to distort physics due to numerical errors. On the other hand, for large field-scale problems, efficiency and robustness are primary concerns as long as accuracy remains within the bounds of uncertainty associated with model parameters. Thus, to provide accuracy for research applications and efficiency and robustness for practical applications, three coupling strategies were investigated to deal with reactive chemistry. They are: (1) a fully-implicit scheme, (2) a mixed predictor-corrector/operator-splitting method, and (3) an operator-splitting method. For each time-step, we first solve the advective-dispersive transport equation with or without reaction terms, kinetic-variable by kinetic-variable. We then solve the reactive chemical system node-by-node to yield concentrations of all species.

Five numerical options are provided to solve the advective-dispersive transport equations: Option 1- application of the Finite Element Method (FEM) to the conservative form of the transport equations, Option 2 - application of the FEM to the advective form of the transport equations, Option 3 - application of the modified Lagrangian-Eulerian (LE) approach to the Largrangian form of the transport equations, Option 4 - LE approach for all interior nodes and downstream boundary nodes with the FEM applied to the conservative form of the transport equations for the upstream flux boundaries, and Option 5 - LE approach for all interior and downstream boundary nodes with the FEM applied to the advective form of the transport equations for upstream flux boundaries.

3.5.1 One-Dimensional Bed Sediment Balance Equation

At n+1-th time step, the continuity equation for 1-D bed sediment transport, equation (2.5.1), is approximated as follows.

$$\frac{P^{n+1}M_n^{\,n+1} - P^nM_n^{\,n}}{\Delta t} = W_1P^{n+1}\left(D_n^{\,n+1} - R_n^{\,n+1}\right) + W_2P^n\left(D_n^{\,n} - R_n^{\,n}\right) \qquad \textbf{(3.5.1.1)}$$

where W_1 and W_2 are time weighting factors satisfying

$$W_1 + W_2 = 1,\ \ 0 < W_1 < 1,\ \ and\ \ \ 0 < W_2 < 1 \qquad \textbf{(3.5.1.2)}$$

So that

$$M_n^{\,n+1} = \left\{P^nM_n^{\,n} + \left[W_1P^{n+1}\left(D_n^{\,n+1} - R_n^{\,n+1}\right) + W_2P^n\left(D_n^{\,n} - R_n^{\,n}\right)\right]\Delta t\right\} \Big/ P^{n+1} \qquad \textbf{(3.5.1.3)}$$

If the calculated $M_n^{\,n+1} < 0$, assign $M_n^{\,n+1} = 0$, so that solve equation (3.5.1.3) and get

$$R_n^{\,n+1} = \left\{P^nM_n^{\,n} + \left[W_1P^{n+1}D_n^{\,n+1} + W_2P^n\left(D_n^{\,n} - R_n^{\,n}\right)\right]\Delta t\right\} \Big/ W_1P^{n+1}\Delta t \qquad \textbf{(3.5.1.4)}$$

3.5.2 Application of the Finite Element Method to the Conservative Form of the Sediment Transport Equations to Solve 1-D Suspended Sediment Transport

Recall governing equation for 1-D suspended sediment transport, equation (2.5.10), as following.

$$\frac{\partial(AS_n)}{\partial t} + \frac{\partial(QS_n)}{\partial x} - \frac{\partial}{\partial x}\left(K_xA\frac{\partial S_n}{\partial x}\right) = M_{S_n}^{\,as} + M_{S_n}^{\,os1} + M_{S_n}^{\,os2} + (R_n - D_n)P, \quad \text{n} \in [1,\text{N}_\text{s}] \qquad \textbf{(3.5.2.1)}$$

Assign

$$R_{HS} = (R_n - D_n)P \quad and \quad L_{HS} = 0 \qquad \textbf{(3.5.2.2)}$$

where the right hand side term R_{HS} and left hand side term L_{HS} should be continuously calculated as follows.

$$\begin{aligned} &If\ S_s \le 0,\ \ M_{S_n}^{\,as} = S_s * S_n,\ \ and\ \ \ L_{HS} = L_{HS} - S_s; \\ &Else\ S_s > 0,\ \ M_{S_n}^{\,as} = M_{S_n}^{\,as},\ \ R_{HS} = R_{HS} + M_{S_n}^{\,as} \end{aligned} \qquad \textbf{(3.5.2.3)}$$

$$\begin{aligned} &If\ S_1 \le 0,\ M_{S_n}^{\,os1} = S_1 * S_n,\ \ and\ \ L_{HS} = L_{HS} - S_1; \\ &Else\ S_1 > 0,\ M_{S_n}^{\,os1} = M_{S_n}^{\,os1},\ \ R_{HS} = R_{HS} + M_{S_n}^{\,os1} \end{aligned} \qquad \textbf{(3.5.2.4)}$$

$$\begin{aligned} &If\ S_2 \le 0,\ M_{S_n}^{\,os2} = S_2 * S_n,\ \ and\ \ \ L_{HS} = L_{HS} - S_2 \\ &Else\ S_2 > 0,\ M_{S_n}^{\,os2} = M_{S_n}^{\,os2},\ \ R_{HS} = R_{HS} + M_{S_n}^{\,os2} \end{aligned} \qquad \textbf{(3.5.2.5)}$$

Then equation (3.5.2.1) is simplified as

$$\frac{\partial(AS_n)}{\partial t}+\frac{\partial(QS_n)}{\partial x}-\frac{\partial}{\partial x}\left(K_x A\frac{\partial S_n}{\partial x}\right)+L_{HS}*S_n=R_{HS} \qquad \textbf{(3.5.2.6)}$$

Use Galerkin or Petrov-Galerkin FEM for the spatial discretization of transport equations. For Galerkin method, choose weighting function identical to base functions. For Petrov-Galerkin method, apply weighting function one-order higher than the base function to advection term. Integrate Equation (3.5.2.6) in the spatial dimensions over the entire region as follows.

$$\int_{x_1}^{x_N} N_i\left[\frac{\partial(AS_n)}{\partial t}-\frac{\partial}{\partial x}\left(K_x A\frac{\partial S_n}{\partial x}\right)+L_{HS}*S_n\right]dx+\int_{x_1}^{x_N} W_i\frac{\partial(QS_n)}{\partial x}dx=\int_{x_1}^{x_N} N_i R_{HS}dx \qquad \textbf{(3.5.2.7)}$$

Integrating by parts, we obtain

$$\begin{aligned}&\int_{x_1}^{x_N} N_i\frac{\partial(AS_n)}{\partial t}dx-\int_{x_1}^{x_N}\frac{dW_i}{dx}QS_n dx+\int_{x_1}^{x_N}\frac{dN_i}{dx}K_x A\frac{\partial S_n}{\partial x}dx+\int_{x_1}^{x_N} N_i L_{HS}*S_n dx\\&\quad=\int_{x_1}^{x_N} N_i R_{HS}dx-W_i QS_n\Big|_{X_1}^{X_N}+N_i K_x A\frac{\partial S_n}{\partial x}\Big|_{X_1}^{X_N}\end{aligned} \qquad \textbf{(3.5.2.8)}$$

Approximate solution S_n by a linear combination of the base functions as shown by Equation (3.5.2.9).

$$S_n\approx\widehat{S}_n=\sum_{j=1}^{N}S_{nj}(t)N_j(x) \qquad \textbf{(3.5.2.9)}$$

Substituting Equation (3.5.2.9) into Equation (3.5.2.8), we obtain

$$\begin{aligned}&\sum_{j=1}^{N}\left[\left(\int_{x_1}^{x_N} N_i\left(\frac{\partial A}{\partial t}+L_{HS}\right)N_j dx-\int_{x_1}^{x_N}\frac{dW_i}{dx}QN_j dx+\int_{x_1}^{x_N}\frac{dN_i}{dx}K_x A\frac{dN_j}{dx}dx\right)S_{nj}(t)\right]\\&+\sum_{j=1}^{N}\left[\left(\int_{x_1}^{x_N} N_i AN_j dx\right)\frac{\partial S_{nj}(t)}{\partial t}\right]=\int_{x_1}^{x_N} N_i R_{HS}dx-\sum n\left(W_i QS_n-N_i K_x A\frac{\partial S_n}{\partial x}\right)_b\end{aligned} \qquad \textbf{(3.5.2.10)}$$

Equation (3.5.2.10) can be written in matrix form as

$$([L1]+[L2]+[L3])\{S_n\}+[M]\left\{\frac{\partial S_n}{\partial t}\right\}=\{SS\}+\{B\} \qquad \textbf{(3.5.2.11)}$$

The matrices [L1], [L2], [L3], [M] and load vectors {SS}, {B} are given by

$$M_{ij}=\int_{x_1}^{x_N} N_i AN_j dx \qquad \textbf{(3.5.2.12)}$$

$$L1_{ij}=\int_{x_1}^{x_N} N_i\left(\frac{\partial A}{\partial t}+L_{HS}\right)N_j dx \qquad \textbf{(3.5.2.13)}$$

$$L2_{ij}=-\int_{x_1}^{x_N}\frac{dW_i}{dx}QN_j dx \qquad \textbf{(3.5.2.14)}$$

$$L3_{ij} = \int_{x_1}^{x_N} \frac{dN_i}{dx} K_x A \frac{dN_j}{dx} dx \qquad \textbf{(3.5.2.15)}$$

$$SS_i = \int_{x_1}^{x_N} N_i R_{HS} dx \qquad \textbf{(3.5.2.16)}$$

$$B_i = -n\left(W_i Q S_n - N_i K_x A \frac{\partial S_n}{\partial x} \right)_b \qquad \textbf{(3.5.2.17)}$$

where all the terms listed above are calculated with the corresponding time weighting value.

At n+1-th time step, equation (3.5.2.11) is transformed as

$$[L]\left\{W_1 S_n + W_2 S_n^{\,p}\right\} + [M]\left\{\frac{S_n - S_n^{\,p}}{\Delta t}\right\} = \{SS\} + \{B\} \ \textit{where}\ [L] = [L1] + [L2] + [L3] \qquad \textbf{(3.5.2.18)}$$

So that

$$[CMATRX]\left\{S_n^{\,n+1}\right\} = \{RLD\} \qquad \textbf{(3.5.2.19)}$$

where

$$[CMATRX] = \frac{[M]}{\Delta t} + W_1[L] \qquad \textbf{(3.5.2.20)}$$

$$\{RLD\} = \left(\frac{[M]}{\Delta t} - W_2[L]\right)\left\{S_n^{\,n}\right\} + \{SS\} + \{B\} \qquad \textbf{(3.5.2.21)}$$

The above equations are used to solve the suspended sediment concentration at interior nodes where boundary term {B} is zero.

The equation employed to determine the suspended sediment at junctions can be derived based on the conservation law of material mass and written as follows.

$$\frac{d\forall_j (S_n)_j}{dt} = (M_n^{\,s})_j + (M_n^{\,os})_j + [(R_n)_j - (D_n)_j] A_{JTj} + \sum_{k=1}^{NJRTH_j} Flux_k \qquad \textbf{(3.5.2.22)}$$

where $\forall_j$ is the junction volume, $(S_n)_j$ is the suspended sediment concentration at the junction, $(M_n^{\,s})_j$ is artificial source at the junction, $(M_n^{\,os})_j$ is overland source at the junction, $(R_n)_j$ is erosion rate at the junction, $(D_n)_j$ is deposition rate at the junction, A_{JTj} is the bed area of the junction j, $NJTRH_j$ is the number of river/stream reaches connected to the junction, and $Flux_k$ is the material flux contributed from k-th reach to the junction.

$$Flux_k = n_k\left(Q^k S_n^{\,k} - K_x A \frac{\partial S_n^{\,k}}{\partial x} \right) \qquad \textbf{(3.5.2.23)}$$

To solve equation (3.5.2.22) at n+1-th time step, assign

$$L_{HSj} = \frac{V_j^{n+1}}{\Delta t} \tag{3.5.2.24}$$

$$R_{HSj} = \frac{V_j^{n}(S_n)_j^{n}}{\Delta t} + W_2 R_{HSj}^{n} + W_1[(R_n)_j^{n+1} - (D_n)_j^{n+1}]A_{JTj}^{n+1} \tag{3.5.2.25}$$

where

$$R_{HSj}^{n} = (M_n^{s})_j^{n} + (M_n^{os})_j^{n} + [(R_n)_j^{n} - (D_n)_j^{n}]A_{JTj}^{n} \tag{3.5.2.26}$$

Continue the calculation as follows

$$(M_n^{s})_j = \begin{cases} (M_n^{s})_j, & if\ (S_s)_j > 0 \quad \Rightarrow \quad R_{HSj} = R_{HSj} + W_1(M_n^{s})_j \\ (S_s)_j * (S_n)_j, & if\ (S_s)_j \le 0 \quad \Rightarrow \quad L_{HSj} = L_{HSj} - W_1(S_s)_j \end{cases} \tag{3.5.2.27}$$

$$(M_n^{os})_j = \begin{cases} (M_n^{os})_j, & if\ (S_{os})_j > 0 \quad \Rightarrow \quad R_{HSj} = R_{HSj} + W_1(M_n^{os})_j \\ (S_{os})_j * (S_n)_j, & if\ (S_{os})_j \le 0 \quad \Rightarrow \quad L_{HSj} = L_{HSj} - W_1(S_{os})_j \end{cases} \tag{3.5.2.28}$$

Finally, the ordinary differential equation, Eq. (3.5.2.22), is reduced the algebraic equation as follows

$$L_{HSj}(S_n)_j - \sum_{k=1}^{NJRTH_j} Flux_k = R_{HSj} \tag{3.5.2.29}$$

So that at junction *j*

$$L_{HSj}(S_n)_j - W_1 \sum_{k=1}^{NJRTH_j} Flux_k^{n+1} = R_{HSj} + W_2 \sum_{k=1}^{NJRTH_j} Flux_k^{n} \tag{3.5.2.30}$$

For a reach node neighboring the junctions, assign

$$\{RLDW\} = \left(\frac{[M]}{\Delta t} - W_2[L]\right)\{S_n^{p}\} + \{SS\} \tag{3.5.2.31}$$

Equation (3.5.2.19) is written as

$$[CMATRX]\{S_n\} + \{Flux\} = \{RLDW\} \tag{3.5.2.32}$$

If $nQ > 0$, flow is going from reach to the junction

$$Flux_k = nQ^k S_n^{k} \tag{3.5.2.33}$$

If $nQ < 0$, flow is going from junction to the reach,

$$Flux_k = nQ^k (S_n)_j \tag{3.5.2.34}$$

So that equations (3.5.2.30) and (3.5.2.32) become a set of equation of $(S_n)_j$ and $(S_n)^k$.

For boundary node $i = b$, the boundary term {B} should be calculated as follows.

$$B_i = -n\left(W_i Q S_n - N_i K_x A \frac{\partial S_n}{\partial x}\right)_b = -n\left(Q S_n - K_x A \frac{\partial S_n}{\partial x}\right)_b \quad \textbf{(3.5.2.35)}$$

Dirichlet boundary condition

$$S_n = S_n(x_b, t) \quad \textbf{(3.5.2.36)}$$

Variable boundary condition

When flow is coming in from outside ($nQ < 0$)

$$n\left(Q S_n - A K_x \frac{\partial S_n}{\partial x}\right) = nQ S_n(x_b, t) \quad \Rightarrow \quad B_i = -nQ S_n(x_b, t) \quad \textbf{(3.5.2.37)}$$

When Flow is going out from inside ($nQ > 0$)

$$-nA K_x \frac{\partial S_n}{\partial x} = 0 \quad \Rightarrow \quad B_i = -nQ S_n \quad \textbf{(3.5.2.38)}$$

which must be assembled into the matrix for the boundary point.

Cauchy boundary condition

$$n\left(Q S_n - A K_x \frac{\partial S_n}{\partial x}\right) = Q_{Sn}(x_b, t) \quad \Rightarrow \quad B_i = -Q_{S_n}(x_b, t) \quad \textbf{(3.5.2.39)}$$

Neumann boundary condition

$$-nA K_x \frac{\partial S_n}{\partial x} = Q_{Sn}(x_b, t) \quad \Rightarrow \quad B_i = -nQ S_n - Q_{S_n}(x_b, t) \quad \textbf{(3.5.2.40)}$$

3.5.3 Application of the Finite Element Method to the Advective Form of the Transport Equations to Solve 1-D Suspended Sediment Transport

Recall governing equation for 1-D suspended sediment transport, equation (2.5.10), as following.

$$\frac{\partial (A S_n)}{\partial t} + \frac{\partial (Q S_n)}{\partial x} - \frac{\partial}{\partial x}\left(K_x A \frac{\partial S_n}{\partial x}\right) = M_{S_n}{}^{as} + M_{S_n}{}^{os1} + M_{S_n}{}^{os2} + (R_n - D_n)P, \quad n \in [1, N_s] \quad \textbf{(3.5.3.1)}$$

Conversion to advection form of equation (3.5.3.1) is expressed as

$$A \frac{\partial S_n}{\partial t} + Q \frac{\partial S_n}{\partial x} - \frac{\partial}{\partial x}\left(K_x A \frac{\partial S_n}{\partial x}\right) + \left(\frac{\partial A}{\partial t} + \frac{\partial Q}{\partial x}\right) S_n = M_{S_n}{}^{as} + M_{S_n}{}^{os1} + M_{S_n}{}^{os2} + (R_n - D_n)P \quad \textbf{(3.5.3.2)}$$

According to governing equation for 1-D flow, equation (2.1.1), assign

$$R_{HS} = (R_n - D_n)P \quad and \quad L_{HS} = S_S + S_R - S_E + S_I + S_1 + S_2 \tag{3.5.3.3}$$

where the right hand side term *RHS* and left hand side term *LHS* should be continuously calculated in the same way as that in section 3.5.2. Then equation (3.5.3.2) is simplified as

$$\mathrm{A}\frac{\partial \mathrm{S_n}}{\partial \mathrm{t}} + \mathrm{Q}\frac{\partial \mathrm{S_n}}{\partial \mathrm{x}} - \frac{\partial}{\partial \mathrm{x}}\left(\mathrm{K_x A}\frac{\partial \mathrm{S_n}}{\partial \mathrm{x}}\right) + \mathrm{L_{HS}} * \mathrm{S_n} = \mathrm{R_{HS}} \tag{3.5.3.4}$$

Use Galerkin or Petrov-Galerkin FEM for the spatial discretization of transport equations. Integrate Equation (3.5.3.4) in the spatial dimensions over the entire region as follows.

$$\int_{x_1}^{x_N} N_i \left[A\frac{\partial S_n}{\partial t} - \frac{\partial}{\partial x}\left(K_x A\frac{\partial S_n}{\partial x}\right) + L_{HS} * S_n \right] dx + \int_{x_1}^{x_N} W_i Q\frac{\partial S_n}{\partial x} dx = \int_{x_1}^{x_N} N_i R_{HS} dx \tag{3.5.3.5}$$

Integrating by parts for the dispersion/diffusion term, we obtain

$$\begin{aligned} &\int_{x_1}^{x_N} N_i A\frac{\partial S_n}{\partial t} dx + \int_{x_1}^{x_N} W_i Q\frac{\partial S_n}{\partial x} dx + \int_{x_1}^{x_N} \frac{dN_i}{dx} K_x A\frac{\partial S_n}{\partial x} dx + \int_{x_1}^{x_N} N_i L_{HS} * S_n dx \\ &\qquad = \int_{x_1}^{x_N} N_i R_{HS} dx + N_i K_x A\frac{\partial S_n}{\partial x}\Big|_{x_1}^{x_N} \end{aligned} \tag{3.5.3.6}$$

Approximate solution S_n by a linear combination of the base functions as shown by Equation (3.5.3.7).

$$S_n \approx \widehat{S}_n = \sum_{j=1}^{N} S_{nj}(t) N_j(x) \tag{3.5.3.7}$$

Substituting Equation (3.5.3.7) into Equation (3.5.3.6), we obtain

$$\begin{aligned} &\sum_{j=1}^{N}\left[\left(\int_{x_1}^{x_N} N_i L_{HS}\ N_j dx + \int_{x_1}^{x_N} W_i Q\frac{dN_j}{dx} dx + \int_{x_1}^{x_N} \frac{dN_i}{dx} K_x A\frac{dN_j}{dx} dx\right) S_{nj}(t)\right] \\ &+ \sum_{j=1}^{N}\left[\left(\int_{x_1}^{x_N} N_i A N_j dx\right)\frac{\partial S_{nj}(t)}{\partial t}\right] = \int_{x_1}^{x_N} N_i R_{HS} dx + \sum n\left(N_i K_x A\frac{\partial S_n}{\partial x}\right)_b \end{aligned} \tag{3.5.3.8}$$

Equation (3.5.3.8) can be written in matrix form as

$$([L1] + [L2] + [L3])\{S_n\} + [M]\left\{\frac{\partial S_n}{\partial t}\right\} = \{SS\} + \{B\} \tag{3.5.3.9}$$

The matrices [*L*1], [*L*2], [*L*3], [*M*] and load vectors {*SS*}, {*B*} are given by

$$M_{ij} = \int_{x_1}^{x_N} N_i A N_j dx \tag{3.5.3.10}$$

$$L1_{ij} = \int_{x_1}^{x_N} N_i L_{HS} N_j dx \tag{3.5.3.11}$$

$$L2_{ij} = \int_{x_1}^{x_N} W_i Q \frac{dN_j}{dx} dx \qquad \textbf{(3.5.3.12)}$$

$$L3_{ij} = \int_{x_1}^{x_N} \frac{dN_i}{dx} K_x A \frac{dN_j}{dx} dx \qquad \textbf{(3.5.3.13)}$$

$$SS_i = \int_{x_1}^{x_N} N_i R_{HS} dx \qquad \textbf{(3.5.3.14)}$$

$$B_i = -n\left(-N_i K_x A \frac{\partial S_n}{\partial x} \right)_b \qquad \textbf{(3.5.3.15)}$$

where all the terms listed above are calculated with the corresponding time weighting value.

At n+1-th time step, equation (3.5.3.9) is approximated as

$$[L]\left\{W_1 S_n^{n+1} + W_2 S_n^{n}\right\} + [M]\left\{\frac{S_n^{n+1} - S_n^{n}}{\Delta t}\right\} = \{SS\} + \{B\} \ \textit{where}\ [L] = [L1] + [L2] + [L3] \qquad \textbf{(3.5.3.16)}$$

So that

$$[CMATRX]\left\{S_n^{n+1}\right\} = \{RLD\} \qquad \textbf{(3.5.3.17)}$$

where

$$[CMATRX] = \frac{[M]}{\Delta t} + W_1[L] \qquad \textbf{(3.5.3.18)}$$

$$\{RLD\} = \left(\frac{[M]}{\Delta t} - W_2[L]\right)\left\{S_n^{n}\right\} + \{SS\} + \{B\} \qquad \textbf{(3.5.3.19)}$$

The above equations are used to solve the suspended sediment concentration at interior nodes where boundary term $\{B\}$ is zero.

At internal boundary points neighboring the junctions, assign

$$\{RLDW\} = \left(\frac{[M]}{\Delta t} - W_2[L]\right)\left\{S_n^{p}\right\} + \{SS\} + \{nQS_n\} \qquad \textbf{(3.5.3.20)}$$

Equation (3.5.3.17) is modified as

$$[CMATRX]\{S_n\} + \{Flux\} = \{RLDW\} \qquad \textbf{(3.5.3.21)}$$

So that junction concentration can be solved by equations (3.5.2.30) and (3.5.3.21).

For a global boundary node $i = b$, the boundary term $\{B\}$ should be calculated as follows.

$$B_i = n\left(N_i K_x A \frac{\partial S_n}{\partial x} \right)_b = n\left(K_x A \frac{\partial S_n}{\partial x} \right)_b \qquad \textbf{(3.5.3.22)}$$

Dirichlet boundary condition

$$S_n = S_n(x_b, t) \qquad \textbf{(3.5.3.23)}$$

Variable boundary condition

When flow is coming in from outside ($nQ < 0$)

$$n\left(QS_n - AK_x \frac{\partial S_n}{\partial x}\right) = nQS_n(x_b, t) \quad \Rightarrow \quad B_i = nQS_n - nQS_n(x_b, t) \qquad \textbf{(3.5.3.24)}$$

When Flow is going out from inside ($nQ > 0$)

$$-nAK_x \frac{\partial S_n}{\partial x} = 0 \quad \Rightarrow \quad B_i = 0 \qquad \textbf{(3.5.3.25)}$$

Cauchy boundary condition

$$\mathrm{n}\left(\mathrm{QS_n} - \mathrm{AK_x}\frac{\partial \mathrm{S_n}}{\partial \mathrm{x}}\right) = \mathrm{Q_{Sn}}(\mathrm{x_b}, \mathrm{t}) \Rightarrow \mathrm{B_i} = \mathrm{nQS_n} - \mathrm{Q_{S_n}}(\mathrm{x_b}, \mathrm{t}) \qquad \textbf{(3.5.3.26)}$$

Neumann boundary condition

$$-nAK_x \frac{\partial S_n}{\partial x} = Q_{Sn}(t) \quad \Rightarrow \quad B_i = -Q_{S_n}(t) \qquad \textbf{(3.5.3.27)}$$

3.5.4 Application of the Modified Lagrangian-Eulerian Approach to the Largrangian Form of the Transport Equations to Solve 1-D Suspended Sediment Transport

Recall governing equation for 1-D suspended sediment transport in advection form, equation (3.5.3.2), as follows

$$A\frac{\partial S_n}{\partial t} + Q\frac{\partial S_n}{\partial x} - \frac{\partial}{\partial x}\left(K_x A\frac{\partial S_n}{\partial x}\right) + \left(\frac{\partial A}{\partial t} + \frac{\partial Q}{\partial x}\right)S_n = M_{s_n}{}^{as} + M_{s_n}{}^{os1} + M_{s_n}{}^{os2} + (R_n - D_n)P \qquad \textbf{(3.5.4.1)}$$

Assign and calculate R_{HS} and L_{HS} the same as that in section (3.5.3). Then equation (3.5.4.1) is simplified as

$$A\frac{\partial S_n}{\partial t} + Q\frac{\partial S_n}{\partial x} - \frac{\partial}{\partial x}\left(K_x A\frac{\partial S_n}{\partial x}\right) + L_{HS} * S_n = R_{HS} \qquad \textbf{(3.5.4.2)}$$

Equation (3.5.4.2) in the Lagrangian and Eulerian form is written as follows. In the Lagrangian step

$$A\frac{dS_n}{d\tau} = A\frac{\partial S_n}{\partial t} + Q\frac{\partial S_n}{\partial x} = 0 \quad \Rightarrow \quad \frac{\partial S_n}{\partial t} + V\frac{\partial S_n}{\partial x} = 0 \qquad \textbf{(3.5.4.3)}$$

where τ is the tracking time, and particle-tracking velocity V is the flow velocity. In the Eulerian step

$$A\frac{dS_n}{d\tau} - \frac{\partial}{\partial x}\left(K_x A\frac{\partial S_n}{\partial x}\right) + L_{HS} * S_n = R_{HS} \qquad \textbf{(3.5.4.4)}$$

Equation (3.5.4.4) written in a slightly different form is shown as follows.

$$\frac{dS_n}{d\tau} - D + K * S_n = R_L \qquad \textbf{(3.5.4.5)}$$

where

$$AD = \frac{\partial}{\partial x}\left(K_x A \frac{\partial S_n}{\partial x} \right) \qquad \textbf{(3.5.4.6)}$$

$$K = \frac{L_{HS}}{A} \qquad \textbf{(3.5.4.7)}$$

$$R_L = \frac{R_{HS}}{A} \qquad \textbf{(3.5.4.8)}$$

Integrating Eq. (3.5.4.5) along a characteristic line to yield the following matrix equation as

$$\begin{aligned} &\frac{[\mathbf{U}]}{\Delta\tau}\left\{S_n{}^{n+1}\right\} - W_1\left\{D^{n+1}\right\} + W_1\left[\mathbf{K}^{n+1}\right]\left\{S_n{}^{n+1}\right\} = \\ &\frac{[\mathbf{U}]}{\Delta\tau}\left\{S_n{}^{*}\right\} + W_2\left\{D^{*}\right\} - W_2\left\{\left(KS_n\right)^{*}\right\} + W_1\left\{R_L{}^{n+1}\right\} + W_2\left\{R_L{}^{*}\right\} \end{aligned} \qquad \textbf{(3.5.4.9)}$$

where * corresponds to the previous time step value at the location where node i is backwardly tracked in the Lagrangian step, [**U**] is the unit matrix, and [$\mathbf{K}^{n+1}$] is a diagonal matrix with K calculated at the (n+1)-th time step as its diagonal components..

The diffusion term D expressed in term of S_n is solved by the following procedure. Approximate D by a linear combination of the base functions as follows.

$$D \approx \hat{D} = \sum_{j=1}^{N} D_j(t) N_j(x) \qquad \textbf{(3.5.4.10)}$$

Applying the Galerkin finite element method to Eq. (3.5.4.6), we obtain

$$\int_{x_1}^{x_N} N_i AD dx = \int_{x_1}^{x_N} N_i A \sum_{j=1}^{N} D_j(t) N_j(x) dx = \int_{x_1}^{x_N} N_i \frac{\partial}{\partial x}\left(K_x A \frac{\partial S_n}{\partial x} \right) dx \qquad \textbf{(3.5.4.11)}$$

Integrating by parts, we obtain

$$\sum_{j=1}^{N}\left[\left(\int_{x_1}^{x_N} N_i A N_j dx \right) * D_j \right] = -\int_{x_1}^{x_N} \frac{dN_i}{dx} K_x A \frac{\partial S_n}{\partial x} dx + N_i K_x A \frac{\partial S_n}{\partial x}\Bigg|_{X_1}^{X_N} \qquad \textbf{(3.5.4.12)}$$

Approximate S_n by a linear combination of the base functions as follows.

$$S_n \approx \hat{S}_n = \sum_{j=1}^{N} S_{nj}(t) N_j(x) \qquad \textbf{(3.5.4.13)}$$

Substituting Eq. (3.5.4.13) into Eq. (3.5.4.12), we have

$$\sum_{j=1}^{N}\left[\left(\int_{x_1}^{x_N} N_i A N_j dx\right) * D_j\right] = -\sum_{j=1}^{N}\left[\left(\int_{x_1}^{x_N} \frac{dN_i}{dx} K_x A \frac{dN_j}{\partial x} dx\right) * (S_n)_j\right] + N_i K_x A \frac{\partial S_n}{\partial x}\Bigg|_{X_1}^{X_N} \quad \textbf{(3.5.4.14)}$$

Assign matrices [QA], [QD] and load vector {B} as following.

$$QA_{ij} = \int_{x_1}^{x_N} N_i A N_j dx \quad \textbf{(3.5.4.15)}$$

$$QD_{ij} = \int_{x_1}^{x_N} \frac{dN_i}{dx} K_x A \frac{dN_j}{dx} dx \quad \textbf{(3.5.4.16)}$$

$$B_i = \left(nN_i K_x A \frac{\partial S_n}{\partial x}\right)_b \quad \textbf{(3.5.4.17)}$$

Equation (3.5.4.14) is expressed as

$$[QA]\{D\} = -[QD]\{S_n\} + \{QB\} \quad \textbf{(3.5.4.18)}$$

Lump matrix [QA] into diagonal matrix and update

$$QD_{ij} = QD_{ij} / QA_{ii} \quad \textbf{(3.5.4.19)}$$

$$B_i = QB_i / QA_{ii} \quad \textbf{(3.5.4.20)}$$

Then

$$\{D\} = -[QD]\{S_n\} + \{B\} \quad \textbf{(3.5.4.21)}$$

where {B} is calculated as follows

Dirichlet boundary condition

$$S_n = S_n(x_b, t) \;\Rightarrow\; B_i = nN_i K_x A \frac{(S_n)_j - S_n(x_b, t)}{\Delta x} \Big/ QA_{ii} \quad \textbf{(3.5.4.22)}$$

where *j* is the interior node connected to the boundary node.

Variable boundary condition

When flow is coming in from outside (nQ < 0)

$$n\left(QS_n - AK_x \frac{\partial S_n}{\partial x}\right) = nQS_n(x_b, t) \;\Rightarrow\; B_i = \left[nQS_n - nQS_n(x_b, t)\right] / QA_{ii} \quad \textbf{(3.5.4.23)}$$

When Flow is going out from inside ($nQ > 0$)

$$-nAK_x \frac{\partial S_n}{\partial x} = 0 \;\Rightarrow\; B_i = 0 \quad \textbf{(3.5.4.24)}$$

Cauchy boundary condition

$$n\left(QS_n - AK_x\frac{\partial S_n}{\partial x}\right) = Q_{Sn}(x_b,t) \;\Rightarrow\; B_i = \left[nQS_n - Q_{Sn}(x_b,t)\right]/QA_{ii} \qquad \textbf{(3.5.4.25)}$$

Neumann boundary condition

$$-nAK_x\frac{\partial S_n}{\partial x} = Q_{Sn}(x_b,t) \;\Rightarrow\; B_i = -Q_{Sn}(x_b,t)/QA_{ii} \qquad \textbf{(3.5.4.26)}$$

According to equation (3.5.4.21), Equation (3.5.4.9) can be modified as follows

$$[CMATRX]\left\{S_n^{\,n+1}\right\} = \{RLD\} \qquad \textbf{(3.5.4.27)}$$

where

$$[CMATRX] = \frac{[U]}{\Delta\tau} + W_1[QD^{n+1}] + W_1\left[K^{n+1}\right] \qquad \textbf{(3.5.4.28)}$$

$$\{RLD\} = \frac{[U]}{\Delta\tau}\left\{S_n^{\,*}\right\} + W_2\left\{D^*\right\} - W_2\left\{\left(KS_n\right)^*\right\} + W_1\left\{R_L^{\,n+1}\right\} + W_2\left\{R_L^{\,*}\right\} + W_1\{B^{n+1}\} \qquad \textbf{(3.5.4.29)}$$

The above equations are used to solve the suspended sediment concentration at interior nodes where boundary term $\{B^{n+1}\}$ is zero.

At the junctions, if $nQ > 0$, flow is going from the reach to the junction, assign

$$\{RLDW\} = \{RLD\} + \{nQS_n\}/QA_{ii}^{\,n+1} - W_1\left\{B^{n+1}\right\} - W_2[QB^n]\{S_n^{\,n}\}/QA_{ii} \qquad \textbf{(3.5.4.30)}$$

Equation (3.5.4.30) is written as

$$[CMATRX]\left\{S_n^{\,n+1}\right\} + \left\{Flux/QA_{ii}^{\,n+1}\right\} = \{RLDW\} \qquad \textbf{(3.5.4.31)}$$

If $nQ < 0$, flow in going from junction to the reach, apply equation (3.5.2.23)

$$Flux_i = n\left[Q(S_n)_i - K_xA\frac{(S_n)_j - (S_n)_i}{\Delta x}\right] \qquad \textbf{(3.5.4.32)}$$

where j is the interior node connected to the junction node i.

Junction concentration can be solved with equations (3.5.2.30), (3.5.4.31) and (3.5.4.32).

For boundary node $i = b$, the boundary term $\{B^{n+1}\}$ in equation (3.5.4.29) should be calculated as follows.

Dirichlet boundary condition

$$S_n = S_n(x_b,t) \qquad \textbf{(3.5.4.33)}$$

The above equation is used for Dirichlet boundary node rather than equation (3.5.4.29).

Variable boundary condition

When flow is coming in from outside ($nQ < 0$), equation (3.5.4.29) cannot be applied because $\Delta\tau$ equations zero. Applying boundary condition, we have

$$n\left[Q(S_n)_i - AK_x\frac{(S_n)_j - (S_n)_i}{\Delta x}\right] = nQS_n(x_b,t) \qquad \textbf{(3.5.4.34)}$$

where j is the interior node connected to the boundary node i.

When Flow is going out from inside ($nQ > 0$), the boundary term $\{B^{n+1}\}$ in equation (3.5.4.29) should be calculated as follows.

$$-nAK_x\frac{\partial S_n}{\partial x} = 0 \;\Rightarrow\; B_i = 0 \qquad \textbf{(3.5.4.35)}$$

Cauchy boundary condition

Equation (3.5.4.29) cannot be applied because $\Delta\tau$ equations zero. Applying boundary condition, we have

$$n\left[Q(S_n)_i - AK_x\frac{(S_n)_j - (S_n)_i}{\Delta x}\right] = Q_{Sn}(x_b,t) \qquad \textbf{(3.5.4.36)}$$

Neumann boundary condition

The boundary term $\{B^{n+1}\}$ in equation (3.5.4.29) should be calculated as follows.

$$-n\mathrm{AK_x}\frac{\partial \mathrm{S_n}}{\partial \mathrm{x}} = \mathrm{Q_{Sn}(x_b,t)} \;\Rightarrow\; B_i = -Q_{Sn}(x_b,t)/QA_{ii} \qquad \textbf{(3.5.4.37)}$$

3.5.5 Aplication of the Lagrangian-Eulerian Approach for All Interior Nodes and Downstream Boundary Nodes with the Finite Element Method Applied to the Conservative Form of the Transport Equations for the Upstream Flux Boundaries to Solve 1-D Suspended Sediment Transport

For this option, the matrix equation for interior and downstream boundary nodes is obtained through the same procedure as that in section 3.5.4, and the matrix equation for junction and upstream boundary nodes is obtained through the same procedure as that in section 3.5.2.

3.5.6 Application of the Lagrangian-Eulerian Approach for All Interior Nodes and Downstream Boundary Nodes with the Finite Element Method Applied to the Advective Form of the Transport Equations for the Upstream Flux Boundaries to Solve

1-D Suspended Sediment Transport

For this option, the matrix equation for interior and downstream boundary nodes is obtained through the same procedure as that in section 3.5.4, and the matrix equation for junction and upstream boundary nodes is obtained through the same procedure as that in section 3.5.3.

3.5.7 Finite Application of the Finite Element Method to the Conservative Form of the Transport Equations to Solve 1-D Kinetic Variable Transport

3.5.7.1 Fully implicit scheme

Recall the continuity equation for kinetic-variables, equation (2.5.44), can be written in slightly different form by expanding the time derivative term as

$$A\frac{\partial E_n}{\partial t}+\frac{\partial A}{\partial t}E_n+\frac{\partial (QE_n{}^m)}{\partial x}-\frac{\partial}{\partial x}\left(K_x A\frac{\partial E_n{}^m}{\partial x}\right)=M_{E_n}{}^{as}+M_{E_n}{}^{rs}+M_{E_n}{}^{is}+M_{E_n}{}^{os1}+M_{E_n}{}^{os2}+AR_{E_n} \qquad \textbf{(3.5.7.1.1)}$$

where E_n is the concentration of the *n*-th kinetic variable, $E_n{}^m$ is the mobile concentration of the *n*-th kinetic variable, $M_{E_n}{}^{as}$ is the rate of artificial source of the *n*-th kinetic variable E_n, $M_{E_n}{}^{rs}$ is the rate of rainfall source/evaporation sink of the *n*-th kinetic variable E_n, , $M_{E_n}{}^{os1}$ is the rate of overland source from Bank *1* of the *n*-th kinetic variable E_n, $M_{E_n}{}^{os2}$ is the rate of overland source from Bank *2* of the *n*-th kinetic variable E_n, $M_{E_n}{}^{is}$ is the rate of exfiltration source of the *n*-th kinetic variable E_n, and R_{E_n} and is the rate of reaction of the *n*-th kinetic variable E_n.

At (*n*+*1*)-th time step, equation (3.5.7.1.1) is approximated by

$$A\frac{(E_n)^{n+1}-(E_n)^n}{\Delta t}+\frac{\partial A}{\partial t}E_n+\frac{\partial (QE_n{}^m)}{\partial x}-\frac{\partial}{\partial x}\left(K_x A\frac{\partial E_n{}^m}{\partial x}\right)=M_{E_n}{}^{as}+M_{E_n}{}^{rs}+M_{E_n}{}^{is}+M_{E_n}{}^{os1}+M_{E_n}{}^{os2}+AR_{E_n} \qquad \textbf{(3.5.7.1.2)}$$

where the superscripts ^{n} and $^{n+1}$ represent the time step number. Terms without superscript should be the corresponding average values calculated with time weighting factors W_1 and W_2.

According to the fully-implicit scheme, equation (3.5.7.1.2) can be separated into two equations as follows

$$A\frac{(E_n)^{n+1/2}-(E_n)^n}{\Delta t}+\frac{\partial A}{\partial t}E_n+\frac{\partial (QE_n{}^m)}{\partial x}-\frac{\partial}{\partial x}\left(K_x A\frac{\partial E_n{}^m}{\partial x}\right)=M_{E_n}{}^{as}+M_{E_n}{}^{rs}+M_{E_n}{}^{is}+M_{E_n}{}^{os1}+M_{E_n}{}^{os2}+AR_{E_n} \qquad \textbf{(3.5.7.1.3)}$$

$$\frac{(E_n)^{n+1}-(E_n)^{n+1/2}}{\Delta t}=0 \qquad \textbf{(3.5.7.1.4)}$$

First, we express $E_n{}^m$ in terms of $(E_n{}^m/E_n)\cdot E_n$ to make E_n's as primary dependent variables, so that $E_n{}^{n+1/2}$ can be solved from Eq. (3.5.7.1.3). Second, we solve equation (3.5.7.1.4) together with algebraic equations for equilibrium reactions using BIOGEOCHEM to obtain all individual species

concentrations. Iteration between these two steps is needed because the new reaction terms R_n^{n+1} and the equation coefficients in equation (3.5.7.1.3) need to be updated with the calculation results of (3.5.7.1.4). To improve the standard SIA method, the nonlinear reaction terms are approximated by the Newton-Raphson linearization.

To solve equation (3.5.7.1.3), assign

$$R_{HSn} = 0 \quad and \quad L_{HSn} = 0 \tag{3.5.7.1.5}$$

Then the right hand side R_{HSn} and left hand side L_{HSn} should be continuously calculated as following

$$M_{E_n}^{rs} = \begin{cases} S_R * E_{n^{rs}}, \ if \ S_R > 0 \ \Rightarrow \ R_{HSn} = R_{HSn} + M_{E_n}^{rs} \\ S_R * E_n^{\ m}, \ if \ S_R \le 0 \ \Rightarrow \ L_{HSn} = L_{HSn} - S_R \end{cases} \tag{3.5.7.1.6}$$

$$M_{E_n}^{as} = \begin{cases} S_S * E_{n^{as}}, \ if \ S_S > 0 \ \Rightarrow \ R_{HSn} = R_{HSn} + M_{E_n}^{as}, \\ S_S * E_n^{\ m}, \ if \ S_S \le 0 \ \Rightarrow \ L_{HSn} = L_{HSn} - S_S \end{cases} \tag{3.5.7.1.7}$$

$$M_{E_n}^{os1} = \begin{cases} S_1 * E_n^{\ m}{}_{os1}, \ if \ S_1 > 0 \ \Rightarrow \ R_{HSn} = R_{HSn} + M_{E_n}^{os1} \\ S_1 * E_n^{\ m}, \ if \ S_1 \le 0 \ \Rightarrow \ L_{HSn} = L_{HSn} - S_1 \end{cases} \tag{3.5.7.1.8}$$

$$M_{E_n}^{os2} = \begin{cases} S_2 * E_n^{\ m}{}_{os2}, \ if \ S_2 > 0 \ \Rightarrow \ R_{HSn} = R_{HSn} + M_{E_n}^{os2} \\ S_2 * E_n^{\ m}, \ if \ S_2 \le 0 \ \Rightarrow \ L_{HSn} = L_{HSn} - S_2 \end{cases} \tag{3.5.7.1.9}$$

$$M_{E_n}^{is} = \begin{cases} S_I * E_n^{\ m}{}_{is}, \ if \ S_I > 0 \ \Rightarrow \ R_{HSn} = R_{HSn} + M_{E_n}^{is} \\ S_I * E_n^{\ m}, \ if \ S_I \le 0 \ \Rightarrow \ L_{HSn} = L_{HSn} - S_I \end{cases} \tag{3.5.7.1.10}$$

where $E_{n^{rs}}$ is the concentration of E_n in the rainfall source, $E_{n^{es}}$ is the concentration of E_n in the evaporation source, $E_{n^{as}}$ is the concentration of E_n in the artificial source, $E_{n^{os1}}$ is the concentration of E_n in the overland source from bank 1, $E_{n^{os2}}$ is the concentration of E_n in the overland source from bank 2, and $E_{n^{is}}$ is the concentration of E_n in the exfiltration source from subsurface media.

Equation (3.5.7.1.3) is then simplified as

$$A\frac{(E_n)^{n+1/2} - (E_n)^n}{\Delta t} + \frac{\partial A}{\partial t}E_n + \frac{\partial (QE_n^{\ m})}{\partial x} - \frac{\partial}{\partial x}\left(K_x A \frac{\partial E_n^{\ m}}{\partial x}\right) + L_{HSn} * E_n^{\ m} = R_{HSn} + AR_{E_n} \tag{3.5.7.1.11}$$

Express $E_n^{\ m}$ in terms of $(E_n^{\ m}/E_n)E_n$ to make E_n's as primary dependent variables,

$$A\frac{\partial E_n}{\partial t} + \frac{\partial A}{\partial t}E_n + \frac{\partial}{\partial x}\left(Q\frac{E_n^{\ m}}{E_n}E_n\right) - \frac{\partial}{\partial x}\left(K_x A \frac{E_n^{\ m}}{E_n}\frac{\partial E_n}{\partial x}\right) - \frac{\partial}{\partial x}\left(K_x A \frac{\partial (E_n^{\ m}/E_n)}{\partial x}E_n\right) + L_{HSn}\frac{E_n^{\ m}}{E_n} = R_{HSn} + AR_{E_n} \tag{3.5.7.1.12}$$

Use Galerkin or Petrov-Galerkin FEM for the spatial discretization of transport equations. Integrate Equation (3.5.7.1.12) in the spatial dimensions over the entire region as follows.

$$\int_{x_1}^{x_N} N_i \left[A\frac{\partial E_n}{\partial t} - \frac{\partial}{\partial x}\left(K_x A \frac{E_n{}^m}{E_n}\frac{\partial E_n}{\partial x}\right)\right]dx + \int_{x_1}^{x_N} W_i \left[\frac{\partial}{\partial x}\left(Q\frac{E_n{}^m}{E_n}E_n\right) - \frac{\partial}{\partial x}\left(K_x A \frac{\partial (E_n{}^m/E_n)}{\partial x}E_n\right)\right]dx$$
$$+\int_{x_1}^{x_N} N_i \left(L_{HSn}\frac{E_n{}^m}{E_n} + \frac{\partial A}{\partial t}\right)E_n dx = \int_{x_1}^{x_N} N_i (R_{HSn} + AR_{E_n})dx \qquad \textbf{(3.5.7.1.13)}$$

Integrating by parts, we obtain

$$\int_{x_1}^{x_N} N_i A\frac{\partial E_n}{\partial t}dx + \int_{x_1}^{x_N}\frac{dN_i}{dx}\left(K_x A\frac{E_n{}^m}{E_n}\right)\frac{\partial E_n}{\partial x}dx - \int_{x_1}^{x_N}\frac{dW_i}{dx}\left(Q\frac{E_n{}^m}{E_n}\right)E_n dx + \int_{x_1}^{x_N}\frac{dW_i}{dx}\left(K_x A\frac{\partial (E_n{}^m/E_n)}{\partial x}\right)E_n dx$$
$$+\int_{x_1}^{x_N} N_i\left(L_{HSn}\frac{E_n{}^m}{E_n} + \frac{\partial A}{\partial t}\right)E_n dx = \int_{x_1}^{x_N} N_i\left(R_{HSn} + AR_{E_n}\right)dx + N_i K_x A\frac{E_n{}^m}{E_n}\frac{\partial E_n}{\partial x}\Bigg|_{B1}^{B2} - W_i Q E_n{}^m\Big|_{B1}^{B2} + W_i K_x A\frac{\partial (E_n{}^m/E_n)}{\partial x}E_n\Bigg|_{B1}^{B2} \qquad \textbf{(3.5.7.1.14)}$$

Approximate solution E_n by a linear combination of the base functions as follows

$$E_n \approx \hat{E}_n = \sum_{j=1}^{N} E_{nj}(t)N_j(x) \qquad \textbf{(3.5.7.1.15)}$$

Substituting Equation (3.5.7.1.15) into Equation (3.5.7.1.14), we obtain

$$\sum_{j=1}^{N}\left\{\left[\begin{array}{l} -\int_{x_1}^{x_N}\frac{dW_i}{dx}\left(Q\frac{E_n{}^m}{E_n}\right)N_j dx + \int_{x_1}^{x_N}\frac{dW_i}{dx}\left(K_x A\frac{\partial (E_n{}^m/E_n)}{\partial x}\right)N_j dx \\ +\int_{x_1}^{x_N}\frac{dN_i}{dx}\left(K_x A\frac{E_n{}^m}{E_n}\right)\frac{dN_j}{dx}dx + \int_{x_1}^{x_N} N_i\left(L_{HSn}\frac{E_n{}^m}{E_n} + \frac{\partial A}{\partial t}\right)N_j dx \end{array}\right]E_{nj}(t)\right\} + \sum_{j=1}^{N}\left[\left(\int_{x_1}^{x_N} N_i A N_j dx\right)\frac{\partial E_{nj}(t)}{\partial t}\right] =$$
$$\int_{x_1}^{x_N} N_i\left(R_{HS} + AR_{E_n}\right)dx - \sum n\left[-N_i\left(K_x A\frac{E_n{}^m}{E_n}\right)\frac{\partial E_n}{\partial x} + W_i Q E_n{}^m - W_i\left(K_x A\frac{\partial (E_n{}^m/E_n)}{\partial x}\right)E_n\right]_b \qquad \textbf{(3.5.7.1.16)}$$

Equation (3.5.7.1.16) can be written in matrix form as

$$([L1]+[L2]+[L3]+[L4])\{E_n\} + [M]\left\{\frac{\partial E_n}{\partial t}\right\} = \{S\} + \{B\} \qquad \textbf{(3.5.7.1.17)}$$

The matrices [$L1$], [$L2$], [$L3$], [$L4$], [M] and load vectors $\{S\}$, $\{B\}$ are given by

$$L1_{ij} = -\int_{x_1}^{x_N}\frac{dW_i}{dx}\left(Q\frac{E_n{}^m}{E_n}\right)N_j dx \qquad \textbf{(3.5.7.1.18)}$$

$$L2_{ij} = \int_{x_1}^{x_N}\frac{dW_i}{dx}\left(K_x A\frac{\partial (E_n{}^m/E_n)}{\partial x}\right)N_j dx \qquad \textbf{(3.5.7.1.19)}$$

$$L3_{ij} = \int_{x_1}^{x_N}\frac{dN_i}{dx}\left(K_x A\frac{E_n{}^m}{E_n}\right)\frac{dN_j}{dx}dx \qquad \textbf{(3.5.7.1.20)}$$

$$L4_{ij} = \int_{x_1}^{x_N} N_i\left(L_{HSn}\frac{E_n{}^m}{E_n} + \frac{\partial A}{\partial t}\right)N_j dx \qquad \textbf{(3.5.7.1.21)}$$

$$M_{ij} = \int_{x_1}^{x_N} N_i A N_j dx \qquad \textbf{(3.5.7.1.22)}$$

$$S_i = \int_{x_1}^{x_N} N_i \left(R_{HSn} + AR_{E_n} \right) dx \qquad \textbf{(3.5.7.1.23)}$$

$$B_i = -n \left[W_i Q E_n{}^m - W_i \left(K_x A \frac{\partial (E_n{}^m / E_n)}{\partial x} \right) E_n - N_i \left(K_x A \frac{E_n{}^m}{E_n} \right) \frac{\partial E_n}{\partial x} \right]_b \qquad \textbf{(3.5.7.1.24)}$$

To calculate [$L2$] through equation (3.5.7.1.19), assign

$$PPX = \frac{\partial (E_n{}^m / E_n)}{\partial x} \qquad \textbf{(3.5.7.1.25)}$$

Then

$$\int_{x_1}^{x_N} N_i PPX dx = \int_{x_1}^{x_N} N_i \frac{\partial (E_n{}^m / E_n)}{\partial x} dx \qquad \textbf{(3.5.7.1.26)}$$

$$\sum_{j=1}^{N} \left[\left(\int_{x_1}^{x_N} N_i N_j dx \right) PPX_j \right] = \sum_{j=1}^{N} \left[\left(\int_{x_1}^{x_N} N_i \frac{dN_j}{dx} dx \right) \left(\frac{E_n{}^m}{E_n} \right)_j \right] \qquad \textbf{(3.5.7.1.27)}$$

So that

$$[QP1]\{PPX\} = [QP2]\left\{ \frac{E_n{}^m}{E_n} \right\} \qquad \textbf{(3.5.7.1.28)}$$

Lump [$QP1$] into diagonal matrix and assign

$$QP_{ij} = QP2_{ij} / QP1_{ii} \qquad \textbf{(3.5.7.1.29)}$$

Then

$$\{PPX\} = [QP]\left\{ \frac{E_n{}^m}{E_n} \right\} \qquad \textbf{(3.5.7.1.30)}$$

Equation (3.5.7.1.17) can be simplified as

$$[L]\{E_n\} + [M]\left\{ \frac{\partial E_n}{\partial t} \right\} = \{S\} + \{B\}, \quad where [L] = [L1] + [L2] + [L3] + [L4] \qquad \textbf{(3.5.7.1.31)}$$

Further,

$$[L]\left\{ W_1 E_n{}^{n+1/2} + W_2 E_n{}^n \right\} + \frac{[M]}{\Delta t}\left\{ E_n{}^{n+1/2} - E_n{}^n \right\} = \{S\} + \{B\} \qquad \textbf{(3.5.7.1.32)}$$

So that

$$[CMATRX]\left\{ E_n{}^{n+1/2} \right\} = \{RLD\} \qquad \textbf{(3.5.7.1.33)}$$

where

$$[CMATRX] = \frac{[M]}{\Delta t} + W_1 * [L] \qquad \textbf{(3.5.7.1.34)}$$

$$\{RLD\} = \left(\frac{[M]}{\Delta t} - W_2[L] \right) \{E_n{}^n\} + \{S\} + \{B\} \qquad \textbf{(3.5.7.1.35)}$$

The above equations are used to solve for the kinetic variable concentration at interior nodes, where the boundary term $\{B\}$ is zero.

The equation employed to determine the kinetic variable at junctions can be derived based on the conservation law of material mass and written as follows.

$$\forall_j \frac{d(E_n)_j}{dt} + \frac{d\forall_j}{dt}(E_n)_j = (M_{E_n}{}^{as})_j + (M_{E_n}{}^{rs})_j + (M_{E_n}{}^{os})_j + (M_{E_n}{}^{is})_j + \forall_j (R_{E_n})_j + \sum_{k=1}^{NJRTH_j} Flux_k \qquad \textbf{(3.5.7.1.36)}$$

where $\forall_j$ is the junction volume, $(E_n)_j$ is the concentration of the n-th kinetic variable at Junction j, $(M_{E_n}{}^{as})_j$ is the rate of artificial source of E_n at Junction j, $(M_{E_n}{}^{rs})_j$ is the rate of rainfall source at Junction j, $(M_{E_n}{}^{os})_j$ is the rate of overland source at Junction j, $(M_{E_n}{}^{is})_j$ is exfiltration source at the junction, $(R_{E_n})_j$ is the rate kinetic variable concentration change due to reactions at the junction, $NJTRH_j$ is the number of river/stream reaches connected to the junction, and $Flux_k$ is the material flux of the kinetic variable contributed from the k-th reach to the junction.

$$Flux_k = n\left[Q^k (E_n{}^m)^k - K_x A \frac{\partial (E_n{}^m)^k}{\partial x} \right] \qquad \textbf{(3.5.7.1.37)}$$

At n+1-th time step, equation (3.5.7.1.36) is approximated by

$$\forall_j \frac{(E_n)_j{}^{n+1} - (E_n)_j{}^n}{\Delta t} + \frac{d\forall_j}{dt}(E_n)_j = (M_{E_n}{}^{as})_j + (M_{E_n}{}^{rs})_j + (M_{E_n}{}^{os})_j + (M_{E_n}{}^{is})_j + \forall_j (R_{E_n})_j + \sum_{k=1}^{NJRTH_j} Flux_k \qquad \textbf{(3.5.7.1.38)}$$

which can be separated into two equations, according to Fully-implicit scheme, as follows

$$\forall_j \frac{(E_n)_j{}^{n+1/2} - (E_n)_j{}^n}{\Delta t} + \frac{d\forall_j}{dt}(E_n)_j = (M_{E_n}{}^{as})_j + (M_{E_n}{}^{rs})_j + (M_{E_n}{}^{os})_j + (M_{E_n}{}^{is})_j + \forall_j (R_{E_n})_j + \sum_{k=1}^{NJRTH_j} Flux_k \qquad \textbf{(3.5.7.1.39)}$$

$$\frac{(E_n)_j{}^{n+1} - (E_n)_j{}^{n+1/2}}{\Delta t} = 0 \qquad \textbf{(3.5.7.1.40)}$$

First, solve equation (3.5.7.1.39) and get $(E_n)_j{}^{n+1/2}$. Second, solve equation (3.5.7.1.40) together with algebraic equations for equilibrium reactions using BIOGEOCHEM scheme to get the individual species concentration.

To solve equation (3.5.7.1.39), assign

$$(L_{HSn})_j = \frac{\forall_j}{\Delta t} + \frac{\partial \forall}{\partial t} \qquad \textbf{(3.5.7.1.41)}$$

$$(R_{HSn})_j = \frac{\forall_j{}^n (E_n)_j{}^n}{\Delta t} + W_2 (R_{HSn})_j{}^n + \forall_j (R_{E_n})_j \qquad \textbf{(3.5.7.1.42)}$$

$$Flux_k = W_1 \cdot Flux_k{}^{n+1} + W_2 \cdot Flux_k{}^n \qquad \textbf{(3.5.7.1.43)}$$

Continue the calculation as follows

$$(M_{E_n}{}^{as})_j = \begin{cases} (S_S)_j * (E_{n^{as}})_j, & if\ (S_S)_j > 0 \ \Rightarrow\ (R_{HSn})_j = (R_{HSn})_j + W_1 (S_S)_j * (E_{n^{as}})_j \\ (S_S)_j * (E_n{}^m)_j, & if\ (S_S)_j \le 0 \ \Rightarrow\ (L_{HS_n})_j = (L_{HSn})_j - W_1 (S_S)_j * E_n{}^m / E_n \end{cases} \quad \textbf{(3.5.7.1.44)}$$

$$(M_{E_n}{}^{os})_j = \begin{cases} (S_{os})_j * (E_{n^{os}})_j, & if\ (S_{os})_j > 0 \ \Rightarrow\ (R_{HSn})_j = (R_{HSn})_j + W_1 (S_{os})_j * (E_{n^{os}})_j \\ (S_{os})_j * (E_n{}^m)_j, & if\ (S_{os})_j \le 0 \ \Rightarrow\ (L_{HSn})_j = (L_{HSn})_j - W_1 (S_{os})_j * E_n{}^m / E_n \end{cases} \quad \textbf{(3.5.7.1.45)}$$

where $(S_{os})_j$ is the flow rate of overland source to Junction *j* and $(E_{n^{os}})_j$ is the concentration of E_n in the overland source into Junction *j*.

$$(M_{E_n}{}^{rs})_j = \begin{cases} (S_R)_j * (E_{n^{rs}})_j, & if\ (S_R)_j > 0 \ \Rightarrow\ (R_{HSn})_j = (R_{HSn})_j + W_1 (S_R)_j * (R_n)_j \\ (S_R)_j * (E_n{}^m)_j, & if\ (S_R)_j \le 0 \ \Rightarrow\ (L_{HSn})_j = (L_{HSn})_j - W_1 (S_R)_j * E_n{}^m / E_n \end{cases} \quad \textbf{(3.5.7.1.46)}$$

$$(M_{E_n}{}^{is})_j = \begin{cases} (S_I)_j * (E_{n^{is}})_j, & if\ (S_I)_j > 0 \ \Rightarrow\ (R_{HSn})_j = (R_{HSn})_j + W_1 (S_I)_j * (E_{n^{is}})_j \\ (S_I)_j * (E_n{}^m)_j, & if\ (S_I)_j \le 0 \ \Rightarrow\ (L_{HSn})_j = (L_{HSn})_j - W_1 (S_I)_j * E_n{}^m / E_n \end{cases} \quad \textbf{(3.5.7.1.47)}$$

Then equation (3.5.7.1.39) is approximated by

$$(L_{HSn})_j (E_n)_j - \sum_{k=1}^{NJRTH_j} Flux_k = (R_{HSn})_j \quad \textbf{(3.5.7.1.48)}$$

Assign

$$\{RLDW\} = \left(\frac{[M]}{\Delta t} - W_2 * [L] \right) \{E_n{}^n\} + \{S\} \quad \textbf{(3.5.7.1.49)}$$

Equation (3.5.7.1.33) is modified as

$$[CMATRX] \{E_n{}^{n+1/2}\} + \{Flux\} = \{RLDW\} \quad \textbf{(3.5.7.1.50)}$$

The flux term in both equations (3.5.7.1.48) and (3.5.7.1.50) is specified as follows.

If $nQ > 0$, flow is going from reach to the junction

$$Flux_k = Q^k (E_n{}^m)^k = W_1 (Q^k)^{n+1} \frac{[(E_n{}^m)^k]^{n+1/2}}{[(E_n)^k]^{n+1/2}} [(E_n)^k]^{n+1/2} + W_2 (Q^k)^n [(E_n{}^m)^k]^n \quad \textbf{(3.5.7.1.51)}$$

where the superscript n denotes the old time step, the superscript $n+1/2$ denotes the intermediate time step, $Flux_k$ is the flux of the *n*-th kinetic variable from the *k*-th reach to Junction *j*, Q^k is the flow rate from the *k*-th reach to Junction *j*, $(E_n)^k$ is the concentration of the *n*-th kinetic variable of the *k*-th reach, and $(E_n^m)^k$ is the mobile concentration of the *n*-th kinetic variable of the *k*-th reach.

If $nQ < 0$, flow is going from junction to the reach,

$$Flux_k = -Q^k (E_n{}^m)_j = -W_1 (Q^k)^{n+1} \frac{[(E_n{}^m)_j]^{n+1/2}}{[(E_n)_j]^{n+1/2}} [(E_n)_j]^{n+1/2} - W_2 (Q^k)^n [(E_n{}^m)_j]^n \quad \textbf{(3.5.7.1.52)}$$

So that equations (3.5.7.1.48) and (3.5.7.1.50) become a set of equation of $(E_n)_j$ and $(E_n)^k$.

For boundary node $i = b$ (use B as the input boundary value), the boundary term $\{B\}$ should be continuously calculated as follows.

$$\begin{aligned} B_i &= -n\left[W_i Q E_n{}^m - N_i K_x A \frac{E_n{}^m}{E_n} \frac{\partial E_n}{\partial x} - W_i K_x A \frac{\partial (E_n{}^m / E_n)}{\partial x} E_n \right]_b \\ &= -n\left[Q E_n{}^m - K_x A \frac{E_n{}^m}{E_n} \frac{\partial E_n}{\partial x} - K_x A \frac{\partial (E_n{}^m / E_n)}{\partial x} E_n \right]_b = -n\left(Q E_n{}^m - K_x A \frac{\partial E_n{}^m}{\partial x} \right)_b \end{aligned} \quad \textbf{(3.5.7.1.53)}$$

Dirichlet boundary condition

$$E_n{}^m = E_n{}^m (x_b, t) \quad \textbf{(3.5.7.1.54)}$$

Variable boundary condition

When flow is coming in from outside ($nQ < 0$)

$$n\left(Q E_n{}^m - A K_x \frac{\partial E_n{}^m}{\partial x} \right) = n Q E_n{}^m (x_b, t) \;\Rightarrow\; B_i = -n Q E_n{}^m (x_b, t) \quad \textbf{(3.5.7.1.55)}$$

When Flow is going out from inside ($nQ > 0$)

$$-nAK_x \frac{\partial E_n{}^m}{\partial x} = 0 \;\Rightarrow\; B_i = -n Q E_n{}^m \quad \textbf{(3.5.7.1.56)}$$

Cauchy boundary condition

$$n\left(Q E_n{}^m - A K_x \frac{\partial E_n{}^m}{\partial x} \right) = Q_{En} (x_b, t) \;\Rightarrow\; B_i = -Q_{En} (x_b, t) \quad \textbf{(3.5.7.1.57)}$$

Neumann boundary condition

$$-nAK_x \frac{\partial E_n{}^m}{\partial x} = Q_{En} (x_b, t) \;\Rightarrow\; B_i = -n Q E_n{}^m - Q_{En} (x_b, t) \quad \textbf{(3.5.7.1.58)}$$

3.5.7.2 Mixed Predictor-corrector/Operator-Splitting Scheme

Recall the continuity equation for kinetic-variables, equation (3.5.7.1.1), as follows.

$$A \frac{\partial E_n}{\partial t} + \frac{\partial A}{\partial t} E_n + \frac{\partial (Q E_n{}^m)}{\partial x} - \frac{\partial}{\partial x}\left(K_x A \frac{\partial E_n{}^m}{\partial x} \right) = M_{E_n}{}^{as} + M_{E_n}{}^{rs} + M_{E_n}{}^{is} + M_{E_n}{}^{os1} + M_{E_n}{}^{os2} + A R_{E_n} \quad \textbf{(3.5.7.2.1)}$$

At (n+1)-th time step, equation (3.5.7.2.1) is approximated by

$$A\frac{(E_n)^{n+1}-(E_n)^n}{\Delta t}+\frac{\partial A}{\partial t}E_n+\frac{\partial(QE_n{}^m)}{\partial x}-\frac{\partial}{\partial x}\left(K_xA\frac{\partial E_n{}^m}{\partial x}\right)=M_{E_n}{}^{as}+M_{E_n}{}^{rs}+M_{E_n}{}^{is}+M_{E_n}{}^{os1}+M_{E_n}{}^{os2}+AR_{E_n} \quad \textbf{(3.5.7.2.2)}$$

According to Mixed Predictor-corrector/Operator-Splitting Scheme, equation (3.5.7.2.2) can be separated into two equations as follows

$$A\frac{(E_n{}^m)^{n+1/2}-(E_n{}^m)^n}{\Delta t}+\frac{\partial A}{\partial t}E_n^m+\frac{\partial(QE_n{}^m)}{\partial x}-\frac{\partial}{\partial x}\left(K_xA\frac{\partial E_n{}^m}{\partial x}\right)=M_{E_n}{}^{as}+M_{E_n}{}^{rs}+M_{E_n}{}^{os1}+M_{E_n}{}^{os2}+M_{E_n}{}^{is}$$
$$+AR_{E_n}{}^n-A\frac{\partial(\ell nA)}{\partial t}(E_n^{im})^n \quad \textbf{(3.5.7.2.3)}$$

$$\frac{E_n{}^{n+1}-[(E_n{}^m)^{n+1/2}+(E_n{}^{im})^n]}{\Delta t}=R_{E_n}{}^{n+1}-R_{E_n}{}^n-\frac{\partial(\ell nA)}{\partial t}(E_n^{im})^{n+1}+\frac{\partial(\ell nA)}{\partial t}(E_n^{im})^n \quad \textbf{(3.5.7.2.4)}$$

First, solve equation (3.5.7.2.3) and obtain $(E_n{}^m)^{n+1/2}$. Second, solve equation (3.5.7.2.4) together with algebraic equations for equilibrium reactions using BIOGEOCHEM scheme to obtain $(E_n)^{n+1}$ and the individual species concentration.

To solve equation (3.5.7.2.3), assign and calculate R_{HSn} and L_{HSn} same as that in section (3.5.7.1). Then equation (3.5.7.2.3) is simplified as

$$A\frac{(E_n{}^m)^{n+1/2}-(E_n{}^m)^n}{\Delta t}+\frac{\partial A}{\partial t}E_n^m+\frac{\partial(QE_n{}^m)}{\partial x}-\frac{\partial}{\partial x}\left(K_xA\frac{\partial E_n{}^m}{\partial x}\right)+L_{HSn}E_n{}^m=R_{HSn}+AR_{E_n}{}^n-\frac{\partial A}{\partial t}(E_n^{im})^n \quad \textbf{(3.5.7.2.5)}$$

Use Galerkin or Petrov-Galerkin FEM for the spatial discretization of transport equations. Integrate Equation (3.5.7.2.5) in the spatial dimensions over the entire region as follows.

$$\int_{x_1}^{x_N}N_i\left[A\frac{\partial E_n{}^m}{\partial t}-\frac{\partial}{\partial x}\left(K_xA\frac{\partial E_n{}^m}{\partial x}\right)\right]dx+\int_{x_1}^{x_N}W_i\frac{\partial\left(QE_n{}^m\right)}{\partial x}dx+\int_{x_1}^{x_N}N_i\left(L_{HSn}+\frac{\partial A}{\partial t}\right)E_n{}^m dx=$$
$$\int_{x_1}^{x_N}N_i\left(R_{HSn}+AR_{E_n}{}^n-\frac{\partial A}{\partial t}(E_n^{im})^n\right)dx \quad \textbf{(3.5.7.2.6)}$$

Integrating by parts, we obtain

$$\int_{x_1}^{x_N}N_iA\frac{\partial E_n{}^m}{\partial t}dx+\int_{x_1}^{x_N}\frac{dN_i}{dx}K_xA\frac{\partial E_n{}^m}{\partial x}dx-\int_{x_1}^{x_N}\frac{dW_i}{dx}QE_n{}^m dx+\int_{x_1}^{x_N}N_i\left(L_{HSn}+\frac{\partial A}{\partial t}\right)E_n{}^m dx$$
$$=\int_{x_1}^{x_N}N_i\left(R_{HSn}+AR_{E_n}{}^n-\frac{\partial A}{\partial t}(E_n^{im})^n\right)dx-W_iQE_n{}^m\Big|_{B1}^{B2}+N_iK_xA\frac{\partial E_n{}^m}{\partial x}\Big|_{B1}^{B2} \quad \textbf{(3.5.7.2.7)}$$

Approximate solution $E_n{}^m$ by a linear combination of the base functions as follows

$$E_n{}^m\approx\hat{E}_n{}^m=\sum_{j=1}^{N}E_{nj}{}^m(t)N_j(x) \quad \textbf{(3.5.7.2.8)}$$

Substituting Equation (3.5.7.2.8) into Equation (3.5.7.2.7), we obtain

$$\sum_{j=1}^{N}\left[\left(-\int_{x_1}^{x_N}\frac{dW_i}{dx}QN_j dx+\int_{x_1}^{x_N}\frac{dN_i}{dx}K_x A\frac{dN_j}{dx}dx+\int_{x_1}^{x_N}N_i\left(L_{HSn}+\frac{\partial A}{\partial t}\right)N_j dx\right)E_{nj}{}^m(t)\right]$$
$$+\sum_{j=1}^{N}\left[\left(\int_{x_1}^{x_N}N_i AN_j dx\right)\frac{\partial E_{nj}{}^m(t)}{\partial t}\right]=\int_{x_1}^{x_N}N_i\left(R_{HSn}+AR_{E_n}{}^n-\frac{\partial A}{\partial t}(E_n^{im})^n\right)dx-\sum n\left[W_i QE_n{}^m-N_i K_x A\frac{\partial E_n{}^m}{\partial x}\right]_b \quad \textbf{(3.5.7.2.9)}$$

Equation (3.5.7.2.9) can be written in matrix form as

$$([L1]+[L2]+[L3])\{E_n{}^m\}+[M]\left\{\frac{\partial E_n{}^m}{\partial t}\right\}=\{S\}+\{B\} \quad \textbf{(3.5.7.2.10)}$$

The matrices $[L1]$, $[L2]$, $[L3]$, $[M]$ and load vectors $\{S\}$, $\{B\}$ are given by

$$L1_{ij}=-\int_{x_1}^{x_N}\frac{dW_i}{dx}QN_j dx \quad \textbf{(3.5.7.2.11)}$$

$$L2_{ij}=\int_{x_1}^{x_N}\frac{dN_i}{dx}K_x A\frac{dN_j}{dx}dx \quad \textbf{(3.5.7.2.12)}$$

$$L3_{ij}=\int_{x_1}^{x_N}N_i\left(L_{HSn}+\frac{\partial A}{\partial t}\right)N_j dx \quad \textbf{(3.5.7.2.13)}$$

$$M_{ij}=\int_{x_1}^{x_N}N_i AN_j dx \quad \textbf{(3.5.7.2.14)}$$

$$S_i=\int_{x_1}^{x_N}N_i\left(R_{HSn}+AR_{E_n}{}^n-\frac{\partial A}{\partial t}(E_n^{im})^n\right)dx \quad \textbf{(3.5.7.2.15)}$$

$$B_i=-n\left(W_i QE_n{}^m-N_i K_x A\frac{\partial E_n{}^m}{\partial x}\right)_b \quad \textbf{(3.5.7.2.16)}$$

where all the terms listed above are calculated with the corresponding time weighting values. Equation (3.5.7.2.10) is then simplified as

$$[L]\{E_n{}^m\}+[M]\left\{\frac{\partial E_n{}^m}{\partial t}\right\}=\{S\}+\{B\},\ \ where[L]=[L1]+[L2]+[L3] \quad \textbf{(3.5.7.2.17)}$$

Further,

$$[L]\{W_1*(E_n{}^m)^{n+1/2}+W_2*(E_n{}^m)^n\}+[M]\left\{\frac{(E_n{}^m)^{n+1/2}-(E_n{}^m)^n}{\Delta t}\right\}=\{S\}+\{B\} \quad \textbf{(3.5.7.2.18)}$$

So that

$$[CMATRX]\{(E_n{}^m)^{n+1/2}\}=\{RLD\} \quad \textbf{(3.5.7.2.19)}$$

where

$$[CMATRX]=\frac{[M]}{\Delta t}+W_1*[L] \quad \textbf{(3.5.7.2.20)}$$

$$\{RLD\} = \left(\frac{[M]}{\Delta t} - W_2 * [L] \right) \left\{ (E_n{}^m)^n \right\} + \{S\} + \{B\} \qquad \textbf{(3.5.7.2.21)}$$

The above equations are used to solve for the kinetic variable concentration at interior nodes, where the boundary term {B} is zero.

For junction nodes, recall equation (3.5.7.1.38) as follows.

$$\forall_j \frac{(E_n)_j{}^{n+1} - (E_n)_j{}^n}{\Delta t} + \frac{d\forall_j}{dt}(E_n)_j = (M_{E_n}{}^{as})_j + (M_{E_n}{}^{rs})_j + (M_{E_n}{}^{os})_j + (M_{E_n}{}^{is})_j + \forall_j (R_{E_n})_j + \sum_{k=1}^{NJRTH_j} Flux_k \qquad \textbf{(3.5.7.2.22)}$$

which can be separated into two equations, according to mixed Predictor-corrector/operator-splitting scheme, as follows

$$\begin{aligned} &\forall_j \frac{(E_n^m)_j{}^{n+1/2} - (E_n^m)_j{}^n}{\Delta t} + \frac{d\forall_j}{dt}(E_n^m)_j = (M_{E_n}{}^{as})_j + (M_{E_n}{}^{rs})_j + (M_{E_n}{}^{os})_j + (M_{E_n}{}^{is})_j + \\ &\forall_j (R_{E_n})_j{}^n - \frac{d\forall_j}{dt}(E_n^{im})_j{}^n + \sum_{k=1}^{NJRTH_j} Flux_k \end{aligned} \qquad \textbf{(3.5.7.2.23)}$$

$$\frac{(E_n)_j{}^{n+1} - [(E_n{}^m)_j{}^{n+1/2} + (E_n{}^{im})_j{}^n]}{\Delta t} = \forall_j (R_{E_n})_j{}^{n+1} - \forall_j (R_{E_n})_j{}^n - \frac{\partial(\ell n \forall_j)}{\partial t}(E_n^{im})_j{}^{n+1} + \frac{\partial(\ell n \forall_j)}{\partial t}(E_n^{im})_j{}^n \qquad \textbf{(3.5.7.2.24)}$$

First, solve equation (3.5.7.2.23) and get $(E_n{}^m)_j{}^{n+1/2}$. Second, solve equation (3.5.7.2.24) together with algebraic equations for equilibrium reactions using BIOGEOCHEM scheme to obtain the individual species concentration.

To solve equation (3.5.7.2.23), assign

$$(L_{HSn})_j = \frac{\forall_j^n}{\Delta t} + \frac{d\forall_j}{dt} \qquad \textbf{(3.5.7.2.25)}$$

$$(R_{HSn})_j = \frac{\forall_j^n (E_n{}^m)_j{}^n}{\Delta t} + W_2 (R_{HSn})_j{}^n + \forall_j (R_{E_n})_j{}^n - \frac{d\forall_j}{dt}(E_n^{im})_j{}^n \qquad \textbf{(3.5.7.2.26)}$$

$$Flux_k = W_1 \cdot Flux_k{}^{n+1} + W_2 \cdot Flux_k{}^n \qquad \textbf{(3.5.7.2.27)}$$

Continue the calculation as follows

$$(M_{E_n}{}^{as})_j = \begin{cases} (S_S)_j * (E_{n^{as}})_j, & if\ (S_S)_j > 0 \ \Rightarrow\ (R_{HSn})_j = (R_{HSn})_j + W_1 (S_S)_j * (E_{n^{as}})_j \\ (S_S)_j * (E_n{}^m)_j, & if\ (S_S)_j \le 0 \ \Rightarrow\ (L_{HSn})_j = (L_{HSn})_j - W_1 (S_S)_j \end{cases} \qquad \textbf{(3.5.7.2.28)}$$

$$(M_{E_n}{}^{os})_j = \begin{cases} (S_{os})_j * (E_{n^{os}})_j, & if\ (S_{os})_j > 0 \ \Rightarrow\ (R_{HSn})_j = (R_{HSn})_j + W_1 (S_{os})_j * (E_{n^{os}})_j \\ (S_{os})_j * (E_n{}^m)_j, & if\ (S_{os})_j \le 0 \ \Rightarrow\ (L_{HSn})_j = (L_{HSn})_j - W_1 (S)_j \end{cases} \qquad \textbf{(3.5.7.2.29)}$$

$$(M_{E_n}{}^{rs})_j = \begin{cases} (S_R)_j * (E_{n^{rs}})_j, & if\ (S_R)_j > 0 \ \Rightarrow\ (R_{HSn})_j = (R_{HSn})_j + W_1 (S_R)_j * (E_{n^{rs}})_j \\ (S_R)_j * (E_n{}^m)_j, & if\ (S_R)_j \le 0 \ \Rightarrow\ (L_{HSn})_j = (L_{HSn})_j - W_1 (S_R)_j \end{cases} \qquad \textbf{(3.5.7.2.30)}$$

$$(M_{E_n}{}^{is})_j = \begin{cases} (S_I)_j * (E_{n^{is}})_j, & if\ (S_I)_j > 0 \ \Rightarrow\ (R_{HSn})_j = (R_{HSn})_j + W_1(S_I)_j * (E_{n^{is}})_j \\ (S_I)_j * (E_n{}^m)_j, & if\ (S_I)_j \le 0 \ \Rightarrow\ (L_{HSn})_j = (L_{HSn})_j - W_1(S_I)_j \end{cases} \quad \textbf{(3.5.7.2.31)}$$

Then equation (3.5.7.2.23) is approximated by

$$(L_{HSn})_j (E_n{}^m)_j - \sum_{k=1}^{NJRTH_j} Flux_k = (R_{HSn})_j \quad \textbf{(3.5.7.2.32)}$$

Assign

$$\{RLDW\} = \left(\frac{[M]}{\Delta t} - W_2 * [L] \right) \left\{ (E_n{}^m)^n \right\} + \{S\} \quad \textbf{(3.5.7.2.33)}$$

Equation (3.5.7.2.19) is modified as

$$[CMATRX] \left\{ (E_n{}^m)^{n+1/2} \right\} + \{Flux\} = \{RLDW\} \quad \textbf{(3.5.7.2.34)}$$

The flux term in both equations (3.5.7.2.32) and (3.5.7.2.34) is specified as follows.

If nQ >0, flow is going from reach to the junction

$$Flux_k = Q^k (E_n{}^m)^k = W_1 (Q^k)^{n+1} [(E_n{}^m)^k]^{n+1/2} + W_2 (Q^k)^n [(E_n{}^m)^k]^n \quad \textbf{(3.5.7.2.35)}$$

If nQ < 0, flow is going from junction to the reach,

$$Flux_k = -Q^k (E_n{}^m)_j = -W_1 (Q^k)^{n+1} [(E_n{}^m)_j]^{n+1/2} - W_2 (Q^k)^n [(E_n{}^m)_j]^n \quad \textbf{(3.5.7.2.36)}$$

So that equations (3.5.7.2.32) and (3.5.7.2.34) become a set of equations of $(E_n{}^m)_j$ and $(E_n{}^m)^k$.

For boundary node $i = b$, the boundary term $\{B\}$ should be continuously calculated same as that using Fully-implicit scheme in section 3.5.5.1.

3.5.7.3 Operator-splitting

Recall the continuity equation for kinetic-variables, equation (3.5.7.1.1), as follows.

$$A \frac{\partial E_n}{\partial t} + \frac{\partial A}{\partial t} E_n + \frac{\partial (Q E_n{}^m)}{\partial x} - \frac{\partial}{\partial x} \left(K_x A \frac{\partial E_n{}^m}{\partial x} \right) = M_{E_n}{}^{as} + M_{E_n}{}^{rs} + M_{E_n}{}^{is} + M_{E_n}{}^{os1} + M_{E_n}{}^{os2} + AR_{E_n} \quad \textbf{(3.5.7.3.1)}$$

At (n+1)-th time step, equation (3.5.7.3.1) is approximated by

$$A \frac{(E_n)^{n+1} - (E_n)^n}{\Delta t} + \frac{\partial A}{\partial t} E_n + \frac{\partial (Q E_n{}^m)}{\partial x} - \frac{\partial}{\partial x} \left(K_x A \frac{\partial E_n{}^m}{\partial x} \right) = M_{E_n}{}^{as} + M_{E_n}{}^{rs} + M_{E_n}{}^{is} + M_{E_n}{}^{os1} + M_{E_n}{}^{os2} + AR_{E_n} \quad \textbf{(3.5.7.3.2)}$$

According to Operator-splitting scheme, equation (3.5.7.3.2) can be separated into two equations as follows

$$A\frac{({E_n}^m)^{n+1/2}-({E_n}^m)^n}{\Delta t}+\frac{\partial A}{\partial t}{E_n}^m+\frac{\partial(Q{E_n}^m)}{\partial x}-\frac{\partial}{\partial x}\left(K_xA\frac{\partial {E_n}^m}{\partial x}\right)={M_{E_n}}^{as}+{M_{E_n}}^{rs}+{M_{E_n}}^{os1}+{M_{E_n}}^{os2}+{M_{E_n}}^{is} \quad \textbf{(3.5.7.3.3)}$$

$$\frac{{E_n}^{n+1}-[({E_n}^m)^{n+1/2}+({E_n}^{im})^n]}{\Delta t}={R_{E_n}}^{n+1}-\frac{\partial(\ell nA)}{\partial t}(E_n^{im})^{n+1} \quad \textbf{(3.5.7.3.4)}$$

First, solve equation (3.5.7.3.3) and get $({E_n}^m)^{n+1/2}$. Second, solve equation (3.5.7.3.4) together with algebraic equations for equilibrium reactions using BIOGEOCHEM scheme to obtain $(E_n)^{n+1}$ and the individual species concentration.

To solve equation (3.5.7.3.3), assign and calculate R_{HSn} and L_{HSn} same as that in section (3.5.7.1). Then equation (3.5.7.3.3) is simplified as

$$A\frac{({E_n}^m)^{n+1/2}-({E_n}^m)^n}{\Delta t}+\frac{\partial A}{\partial t}{E_n}^m+\frac{\partial(Q{E_n}^m)}{\partial x}-\frac{\partial}{\partial x}\left(K_xA\frac{\partial {E_n}^m}{\partial x}\right)+\left(L_{HSn}+\frac{\partial A}{\partial t}\right){E_n}^m=R_{HSn} \quad \textbf{(3.5.7.3.5)}$$

Use Galerkin or Petrov-Galerkin FEM for the spatial discretization of transport equations. Integrate Equation (3.5.7.3.5) in the spatial dimensions over the entire region as follows.

$$\int_{x_1}^{x_N}N_i\left[A\frac{\partial {E_n}^m}{\partial t}-\frac{\partial}{\partial x}\left(K_xA\frac{\partial {E_n}^m}{\partial x}\right)\right]dx+\int_{x_1}^{x_N}W_i\frac{\partial\left(Q{E_n}^m\right)}{\partial x}dx+\int_{x_1}^{x_N}N_i\left(L_{HSn}+\frac{\partial A}{\partial t}\right){E_n}^m dx=\int_{x_1}^{x_N}N_iR_{HSn}dx \quad \textbf{(3.5.7.3.6)}$$

Integrating by parts, we obtain

$$\begin{aligned}&\int_{x_1}^{x_N}N_iA\frac{\partial {E_n}^m}{\partial t}dx+\int_{x_1}^{x_N}\frac{dN_i}{dx}K_xA\frac{\partial {E_n}^m}{\partial x}dx-\int_{x_1}^{x_N}\frac{dW_i}{dx}Q{E_n}^m dx+\int_{x_1}^{x_N}N_i\left(L_{HSn}+\frac{\partial A}{\partial t}\right){E_n}^m dx\\&=\int_{x_1}^{x_N}N_iR_{HSn}dx-W_iQ{E_n}^m\Big|_{B1}^{B2}+N_iK_xA\frac{\partial {E_n}^m}{\partial x}\Big|_{B1}^{B2}\end{aligned} \quad \textbf{(3.5.7.3.7)}$$

Approximate solution ${E_n}^m$ by a linear combination of the base functions as follows

$${E_n}^m\approx\hat{E}_n^m=\sum_{j=1}^{N}{E_{nj}}^m(t)N_j(x) \quad \textbf{(3.5.7.3.8)}$$

Substituting Equation (3.5.7.3.8) into Equation (3.5.7.3.7), we obtain

$$\begin{aligned}&\sum_{j=1}^{N}\left[\left(-\int_{x_1}^{x_N}\frac{dW_i}{dx}QN_jdx+\int_{x_1}^{x_N}\frac{dN_i}{dx}K_xA\frac{dN_j}{dx}dx+\int_{x_1}^{x_N}N_i\left(L_{HSn}+\frac{\partial A}{\partial t}\right)N_jdx\right){E_{nj}}^m(t)\right]\\&+\sum_{j=1}^{N}\left[\left(\int_{x_1}^{x_N}N_iAN_jdx\right)\frac{d{E_{nj}}^m(t)}{dt}\right]=\int_{x_1}^{x_N}N_iR_{HSn}dx-\sum n\left[W_iQ{E_n}^m-N_iK_xA\frac{\partial {E_n}^m}{\partial x}\right]_b\end{aligned} \quad \textbf{(3.5.7.3.9)}$$

Equation (3.5.8.2.19) can be written in matrix form as

$$([L1]+[L2]+[L3])\left\{{E_n}^m\right\}+[M]\left\{\frac{d{E_n}^m}{dt}\right\}=\{S\}+\{B\} \quad \textbf{(3.5.7.3.10)}$$

The matrices [$L1$], [$L2$], [$L3$], [M] and load vectors $\{S\}$, $\{B\}$ are given by

$$L1_{ij} = -\int_{x_1}^{x_N} \frac{dW_i}{dx} QN_j dx \qquad \textbf{(3.5.7.3.11)}$$

$$L2_{ij} = \int_{x_1}^{x_N} \frac{dN_i}{dx} K_x A \frac{dN_j}{dx} dx \qquad \textbf{(3.5.7.3.12)}$$

$$L3_{ij} = \int_{x_1}^{x_N} N_i \left(L_{HSn} + \frac{\partial A}{\partial t} \right) N_j dx \qquad \textbf{(3.5.7.3.13)}$$

$$M_{ij} = \int_{x_1}^{x_N} N_i A N_j dx \qquad \textbf{(3.5.7.3.14)}$$

$$S_i = \int_{x_1}^{x_N} N_i R_{HSn} dx \qquad \textbf{(3.5.7.3.15)}$$

$$B_i = -n \left(W_i Q E_n{}^m - N_i K_x A \frac{\partial E_n{}^m}{\partial x} \right)_b \qquad \textbf{(3.5.7.3.16)}$$

where all the terms listed above are calculated with the corresponding time weighting values.

Equation (3.5.7.2.10) is simplified as

$$[L]\left\{E_n{}^m\right\} + [M]\left\{\frac{dE_n{}^m}{dt}\right\} = \{S\} + \{B\}, \quad where [L] = [L1] + [L2] + [L3] \qquad \textbf{(3.5.7.3.17)}$$

Further,

$$[L]\left\{W_1 * (E_n{}^m)^{n+1/2} + W_2 * (E_n{}^m)^n\right\} + [M]\left\{\frac{(E_n{}^m)^{n+1/2} - (E_n{}^m)^n}{\Delta t}\right\} = \{S\} + \{B\} \qquad \textbf{(3.5.7.3.18)}$$

So that

$$[CMATRX]\left\{(E_n{}^m)^{n+1/2}\right\} = \{RLD\} \qquad \textbf{(3.5.7.3.19)}$$

$$[CMATRX] = \frac{[M]}{\Delta t} + W_1 * [L] \qquad \textbf{(3.5.7.3.20)}$$

$$\{RLD\} = \left(\frac{[M]}{\Delta t} - W_2 * [L]\right)\left\{(E_n{}^m)^n\right\} + \{S\} + \{B\} \qquad \textbf{(3.5.7.3.21)}$$

The above equations are used to solve for the kinetic variable concentration at interior nodes, where the boundary term $\{B\}$ is zero.

For junction nodes, recall equation (3.5.7.2.22) as follows.

$$\forall_j \frac{(E_n)_j{}^{n+1} - (E_n)_j{}^n}{\Delta t} + \frac{d\forall_j}{dt}(E_n)_j = (M_{E_n}{}^{as})_j + (M_{E_n}{}^{rs})_j + (M_{E_n}{}^{os})_j + (M_{E_n}{}^{is})_j + \forall_j (R_{E_n})_j + \sum_{k=1}^{NJRTH_j} Flux_k \qquad \textbf{(3.5.7.3.22)}$$

which can be separated into two equations, according to Operator-splitting scheme, as follows

$$\cancel{V_j}\frac{(E_n^m)_j^{n+1/2}-(E_n^m)_j^{n}}{\Delta t}+\frac{d\cancel{V_j}}{dt}(E_n^m)_j=(M_{E_n}{}^{as})_j+(M_{E_n}{}^{rs})_j+(M_{E_n}{}^{os})_j+(M_{E_n}{}^{is})_j+\sum_{k=1}^{NJRTH_j}Flux_k \qquad \textbf{(3.5.7.3.23)}$$

$$\frac{(E_n)_j^{n+1}-[(E_n{}^m)_j^{n+1/2}+(E_n{}^{im})_j^{n}]}{\Delta t}=\cancel{V_j}(R_{E_n})_j^{n+1}-\frac{\partial(\ell n\cancel{V_j})}{\partial t}(E_n^{im})_j^{n+1} \qquad \textbf{(3.5.7.3.24)}$$

First, solve equation (3.5.7.3.23) and get $(E_n{}^m)_j^{n+1/2}$. Second, solve equation (3.5.7.3.24) together with algebraic equations for equilibrium reactions using BIOGEOCHEM scheme to obtain the individual species concentration and $(E_n)_j^{n+1}$.

To solve equation (3.5.7.3.23), assign

$$(L_{HSn})_j=\frac{\cancel{V_j^n}}{\Delta t}+\frac{d\cancel{V_j}}{dt} \qquad \textbf{(3.5.7.3.25)}$$

$$(R_{HSn})_j=\frac{\cancel{V_j^n}(E_n{}^m)_j^n}{\Delta t}+W_2(R_{HSn})_j^n \qquad \textbf{(3.5.7.3.26)}$$

$$\mathrm{Flux_k}=\mathrm{W_1}\cdot\mathrm{Flux_k}^{\mathrm{n+1}}+\mathrm{W_2}\cdot\mathrm{Flux_k}^{\mathrm{n}} \qquad \textbf{(3.5.7.3.27)}$$

Continue the calculation as follows

$$(M_{E_n}{}^{as})_j=\begin{cases}(S_S)_j*(E_{n^{as}})_j, & if\ (S_S)_j>0 \ \Rightarrow\ (R_{HSn})_j=(R_{HSn})_j+W_1(S_S)_j*(E_{n^{as}})_j\\ (S_S)_j*(E_n{}^m)_j, & if\ (S_S)_j\le 0 \ \Rightarrow\ (L_{HSn})_j=(L_{HSn})_j-W_1(S_S)_j\end{cases} \qquad \textbf{(3.5.7.3.28)}$$

$$(M_{E_n}{}^{os})_j=\begin{cases}(S_{os})_j*(E_{n^{os}})_j, & if\ (S_{os})_j>0 \ \Rightarrow\ (R_{HSn})_j=(R_{HSn})_j+W_1(S_{os})_j*(E_{n^{os}})_j\\ (S_{os})_j*(E_n{}^m)_j, & if\ (S_{os})_j\le 0 \ \Rightarrow\ (L_{HSn})_j=(L_{HSn})_j-W_1(S)_j\end{cases} \qquad \textbf{(3.5.7.3.29)}$$

$$(M_{E_n}{}^{rs})_j=\begin{cases}(S_R)_j*(E_{n^{rs}})_j, & if\ (S_R)_j>0 \ \Rightarrow\ (R_{HSn})_j=(R_{HSn})_j+W_1(S_R)_j*(E_{n^{rs}})_j\\ (S_R)_j*(E_n{}^m)_j, & if\ (S_R)_j\le 0 \ \Rightarrow\ (L_{HSn})_j=(L_{HSn})_j-W_1(S_R)_j\end{cases} \qquad \textbf{(3.5.7.3.30)}$$

$$(M_{E_n}{}^{is})_j=\begin{cases}(S_I)_j*(E_{n^{is}})_j, & if\ (S_I)_j>0 \ \Rightarrow\ (R_{HSn})_j=(R_{HSn})_j+W_1(S_I)_j*(E_{n^{is}})_j\\ (S_I)_j*(E_n{}^m)_j, & if\ (S_I)_j\le 0 \ \Rightarrow\ (L_{HSn})_j=(L_{HSn})_j-W_1(S_I)_j\end{cases} \qquad \textbf{(3.5.7.3.31)}$$

Then equation (3.5.7.3.23) is approximated by

$$(L_{HSn})_j(E_n{}^m)_j-\sum_{k=1}^{NJRTH_j}Flux_k=(R_{HSn})_j \qquad \textbf{(3.5.7.3.32)}$$

Assign

$$\{RLDW\}=\left(\frac{[M]}{\Delta t}-W_2*[L]\right)\{(E_n{}^m)^n\}+\{S\} \qquad \textbf{(3.5.7.3.33)}$$

Equation (3.5.7.3.19) is modified as

$$[CMATRX]\{(E_n{}^m)^{n+1/2}\}+\{Flux\}=\{RLDW\} \qquad \textbf{(3.5.7.3.34)}$$

The flux term in both equation (3.5.7.3.32) and (3.5.7.3.34) is specified as follows.

If $nQ > 0$, flow is going from reach to the junction

$$Flux_k = Q^k (E_n{}^m)^k = W_1 (Q^k)^{n+1} [(E_n{}^m)^k]^{n+1/2} + W_2 (Q^k)^n [(E_n{}^m)^k]^n \quad \textbf{(3.5.7.3.35)}$$

If $nQ < 0$, flow is going from junction to the reach,

$$Flux_k = -Q^k (E_n{}^m)_j = -W_1 (Q^k)^{n+1} [(E_n{}^m)_j]^{n+1/2} - W_2 (Q^k)^n [(E_n{}^m)_j]^n \quad \textbf{(3.5.7.3.36)}$$

Equations (3.5.7.3.32) and (3.5.7.3.34) become a set of equation of $(E_n{}^m)_j$ and $(E_n{}^m)^k$.

For boundary node $i = b$, the boundary term {B} should be continuously calculated same as that using Fully-implicit scheme in section 3.5.5.1.

3.5.8 Finite Application of the Finite Element Method to the Advective Form of the Transport Equations to Solve 1-D Kinetic Variable

3.5.8.1 Fully-implicit scheme

Recall the continuity equation for kinetic-variables, equation (2.5.44), as follows.

$$A\frac{\partial E_n}{\partial t} + \frac{\partial A}{\partial t}E_n + \frac{\partial (QE_n{}^m)}{\partial x} - \frac{\partial}{\partial x}\left(K_x A \frac{\partial E_n{}^m}{\partial x}\right) = M_{E_n}{}^{as} + M_{E_n}{}^{rs} + M_{E_n}{}^{is} + M_{E_n}{}^{os1} + M_{E_n}{}^{os2} + AR_{E_n} \quad \textbf{(3.5.8.1.1)}$$

According to the governing equation of water flow in 1-D river/stream

$$\frac{\partial A}{\partial t} + \frac{\partial Q}{\partial x} = S_S + S_R + S_I + S_1 + S_2 \quad \textbf{(3.5.8.1.2)}$$

Equation (3.5.8.1.1) can be modified as follows.

$$\begin{aligned} &A\frac{\partial E_n}{\partial t} + \frac{\partial A}{\partial t}E_n + Q\frac{\partial E_n{}^m}{\partial x} - \frac{\partial}{\partial x}\left(K_x A \frac{\partial E_n{}^m}{\partial x}\right) - \left[\frac{\partial A}{\partial t} - (S_S + S_R + S_I + S_1 + S_2)\right]E_n{}^m \\ &\quad = M_{E_n}{}^{as} + M_{E_n}{}^{rs} + M_{E_n}{}^{is} + M_{E_n}{}^{os1} + M_{E_n}{}^{os2} + AR_{E_n} \end{aligned} \quad \textbf{(3.5.8.1.3)}$$

At n+1-th time step, equation (3.5.8.1.3) is approximated by

$$\begin{aligned} &A\frac{(E_n)^{n+1} - (E_n)^n}{\Delta t} + \frac{\partial A}{\partial t}E_n + Q\frac{\partial E_n{}^m}{\partial x} - \frac{\partial}{\partial x}\left(K_x A \frac{\partial E_n{}^m}{\partial x}\right) - \left[\frac{\partial A}{\partial t} - (S_R + S_R + S_1 + S_2 + S_I)\right]E_n{}^m \\ &\quad = M_{E_n}{}^{as} + M_{E_n}{}^{rs} + M_{E_n}{}^{is} + M_{E_n}{}^{os1} + M_{E_n}{}^{os2} + AR_n \end{aligned} \quad \textbf{(3.5.8.1.4)}$$

According to Fully-implicit scheme, equation (3.5.8.1.4) can be separated into two equations as follows

$$\begin{aligned} &A\frac{(E_n)^{n+1/2} - (E_n)^n}{\Delta t} + \frac{\partial A}{\partial t}E_n + Q\frac{\partial E_n{}^m}{\partial x} - \frac{\partial}{\partial x}\left(K_x A \frac{\partial E_n{}^m}{\partial x}\right) - \left[\frac{\partial A}{\partial t} - (S_S + S_R + S_I + S_1 + S_2)\right]E_n{}^m = \\ &\quad M_{E_n}{}^{as} + M_{E_n}{}^{rs} + M_{E_n}{}^{is} + M_{E_n}{}^{os1} + M_{E_n}{}^{os2} + AR_{E_n} \end{aligned} \quad \textbf{(3.5.8.1.5)}$$

$$\frac{(E_n)^{n+1}-(E_n)^{n+1/2}}{\Delta t}=0 \qquad \textbf{(3.5.8.1.6)}$$

First, solve equation (3.5.8.1.5) and get $(E_n)^{n+1/2}$. Second, solve equation (3.5.8.1.6) together with algebraic equations for equilibrium reactions using BIOGEOCHEM scheme to obtain the individual species concentration. Iteration between these two steps is needed because reaction term in equation (3.5.8.1.5) needs to be updated by the results of (3.5.8.1.6).

To solve equation (3.5.8.1.5), assign

$$R_{HSn}=0 \quad and \quad L_{HSn}=(S_S+S_R+S_I+S_1+S_2)-\frac{\partial A}{\partial t} \qquad \textbf{(3.5.8.1.7)}$$

Then the right hand side RHS_n and left hand side LHS_n should be continuously calculated same as that in section (3.5.7.1). Equation (3.5.8.1.5) is then simplified as

$$A\frac{(E_n)^{n+1/2}-(E_n)^n}{\Delta t}+\frac{\partial A}{\partial t}E_n+Q\frac{\partial E_n{}^m}{\partial x}-\frac{\partial}{\partial x}\left(K_xA\frac{\partial E_n{}^m}{\partial x}\right)+L_{HSn}E_n{}^m=R_{HSn}+AR_{E_n} \qquad \textbf{(3.5.8.1.8)}$$

Express $E_n{}^m$ in terms of $(E_n{}^m/E_n)\,E_n{}^m$ to make E_n's as primary dependent variables,

$$A\frac{\partial E_n}{\partial t}+\frac{\partial A}{\partial t}E_n+Q\frac{\partial}{\partial x}\left(\frac{E_n{}^m}{E_n}E_n\right)-\frac{\partial}{\partial x}\left(K_xA\frac{E_n{}^m}{E_n}\frac{\partial E_n}{\partial x}\right)-\frac{\partial}{\partial x}\left(K_xA\frac{\partial(E_n{}^m/E_n)}{\partial x}E_n\right)+L_{HSn}\frac{E_n{}^m}{E_n}E_n=R_{HSn}+AR_{E_n} \qquad \textbf{(3.5.8.1.9)}$$

Use Galerkin or Petrov-Galerkin FEM for the spatial discretization of transport equations. Integrate Equation (3.5.8.1.9) in the spatial dimensions over the entire region as follows.

$$\begin{aligned}&\int_{x_1}^{x_N}N_i\left[A\frac{\partial E_n}{\partial t}-\frac{\partial}{\partial x}\left(K_xA\frac{E_n{}^m}{E_n}\frac{\partial E_n}{\partial x}\right)\right]dx+\int_{x_1}^{x_N}W_i\left[Q\frac{\partial}{\partial x}\left(\frac{E_n{}^m}{E_n}E_n\right)-\frac{\partial}{\partial x}\left(K_xA\frac{\partial(E_n{}^m/E_n)}{\partial x}E_n\right)\right]dx\\&+\int_{x_1}^{x_N}N_i\left(L_{HSn}\frac{E_n{}^m}{E_n}+\frac{\partial A}{\partial t}\right)E_n dx=\int_{x_1}^{x_N}N_i\left(R_{HSn}+AR_n\right)dx\end{aligned} \qquad \textbf{(3.5.8.1.10)}$$

Integrating by parts, we obtain

$$\begin{aligned}&\int_{x_1}^{x_N}N_iA\frac{\partial E_n}{\partial t}dx+\int_{x_1}^{x_N}W_iQ\frac{E_n{}^m}{E_n}\frac{\partial E_n}{\partial x}dx+\int_{x_1}^{x_N}W_iQ\frac{\partial(E_n{}^m/E_n)}{\partial x}E_n dx+\int_{x_1}^{x_N}\frac{dN_i}{dx}K_xA\frac{E_n{}^m}{E_n}\frac{\partial E_n}{\partial x}dx\\&\qquad+\int_{x_1}^{x_N}\frac{dW_i}{dx}K_xA\frac{\partial(E_n{}^m/E_n)}{\partial x}E_n dx+\int_{x_1}^{x_N}N_i\left(L_{HSn}\frac{E_n{}^m}{E_n}+\frac{\partial A}{\partial t}\right)E_n dx\\&=\int_{x_1}^{x_N}N_i\left(R_{HSn}+AR_{E_n}\right)dx+N_iK_xA\frac{E_n{}^m}{E_n}\frac{\partial E_n}{\partial x}\Bigg|_{B1}^{B2}+W_iK_xA\frac{\partial(E_n{}^m/E_n)}{\partial x}E_n\Bigg|_{B1}^{B2}\end{aligned} \qquad \textbf{(3.5.8.1.11)}$$

Approximate solution E_n by a linear combination of the base functions as follows

$$E_n\approx\hat{E}_n=\sum_{j=1}^{N}E_{nj}(t)N_j(x) \qquad \textbf{(3.5.8.1.12)}$$

Substituting Equation (3.5.8.1.12) into Equation (3.5.8.1.11), we obtain

$$\sum_{j=1}^{N}\left\{\left[\begin{array}{l}\int_{x_1}^{x_N} W_i Q\frac{E_n^{\,m}}{E_n}\frac{dN_j}{dx}dx+\int_{x_1}^{x_N} W_i Q\frac{\partial(E_n^{\,m}/E_n)}{\partial x}N_j dx+\int_{x_1}^{x_N}\frac{dW_i}{dx}K_x A\frac{\partial(E_n^{\,m}/E_n)}{\partial x}N_j dx \\ \quad+\int_{x_1}^{x_N}\frac{dN_i}{dx}K_x A\frac{E_n^{\,m}}{E_n}\frac{dN_j}{dx}dx+\int_{x_1}^{x_N} N_i\left(L_{HSn}\frac{E_n^{\,m}}{E_n}+\frac{\partial A}{\partial t}\right)N_j dx\end{array}\right]E_{nj}(t)\right\}$$
$$+\sum_{j=1}^{N}\left[\left(\int_{x_1}^{x_N} N_i A N_j dx\right)\frac{\partial E_{nj}(t)}{\partial t}\right]=\int_{x_1}^{x_N} N_i\left(R_{HSn}+AR_{E_n}\right)dx+\sum n\left[N_i K_x A\frac{E_n^{\,m}}{E_n}\frac{\partial E_n}{\partial x}+W_i K_x A\frac{\partial(E_n^{\,m}/E_n)}{\partial x}E_n\right]_b \quad \textbf{(3.5.8.1.13)}$$

Equation (3.5.8.1.13) can be written in matrix form as

$$([L1]+[L2]+[L3]+[L4]+[L5])\{E_n\}+[M]\left\{\frac{\partial E_n}{\partial t}\right\}=\{S\}+\{B\} \quad \textbf{(3.5.8.1.14)}$$

The matrices $[L1]$, $[L2]$, $[L3]$, $[L4]$, $[L5]$, $[M]$ and load vectors $\{S\}$, $\{B\}$ are given by

$$L1_{ij}=\int_{x_1}^{x_N} W_i Q\frac{E_n^{\,m}}{E_n}\frac{dN_j}{dx}dx \quad \textbf{(3.5.8.1.15)}$$

$$L2_{ij}=\int_{x_1}^{x_N} W_i Q\frac{\partial(E_n^{\,m}/E_n)}{\partial x}N_j dx \quad \textbf{(3.5.8.1.16)}$$

$$L3_{ij}=\int_{x_1}^{x_N}\frac{dW_i}{dx}K_x A\frac{\partial(E_n^{\,m}/E_n)}{\partial x}N_j dx \quad \textbf{(3.5.8.1.17)}$$

$$L4_{ij}=\int_{x_1}^{x_N}\frac{dN_i}{dx}K_x A\frac{E_n^{\,m}}{E_n}\frac{dN_j}{dx}dx \quad \textbf{(3.5.8.1.18)}$$

$$L5_{ij}=\int_{x_1}^{x_N} N_i\left(L_{HSn}\frac{E_n^{\,m}}{E_n}+\frac{\partial A}{\partial t}\right)N_j dx \quad \textbf{(3.5.8.1.19)}$$

$$M_{ij}=\int_{x_1}^{x_N} N_i A N_j dx \quad \textbf{(3.5.8.1.20)}$$

$$S_i=\int_{x_1}^{x_N} N_i\left(R_{HSn}+AR_{E_n}\right)dx \quad \textbf{(3.5.8.1.21)}$$

$$B_i=n\left[N_i K_x A\frac{E_n^{\,m}}{E_n}\frac{\partial E_n}{\partial x}+W_i K_x A\frac{\partial(E_n^{\,m}/E_n)}{\partial x}E_n\right]_b \quad \textbf{(3.5.8.1.22)}$$

Equation (3.5.8.1.14) is then simplified as

$$[L]\{E_n\}+[M]\left\{\frac{\partial E_n}{\partial t}\right\}=\{S\}+\{B\},\ \ where[L]=[L1]+[L2]+[L3]+[L4]+[L5] \quad \textbf{(3.5.8.1.23)}$$

Further,

$$[L]\left\{W_1 * E_n^{\,n+1/2}+W_2 * E_n^{\,n}\right\}+\frac{[M]}{\Delta t}\left\{E_n^{\,n+1/2}-E_n^{\,n}\right\}=\{S\}+\{B\} \quad \textbf{(3.5.8.1.24)}$$

So that

$$[CMATRX]\left\{E_n^{\,n+1/2}\right\} = \{RLD\} \quad \textbf{(3.5.8.1.25)}$$

where

$$[CMATRX] = \frac{[M]}{\Delta t} + W_1 * [L] \quad \textbf{(3.5.8.1.26)}$$

$$\{RLD\} = \left(\frac{[M]}{\Delta t} - W_2 * [L]\right)\left\{E_n^{\,n}\right\} + \{S\} + \{B\} \quad \textbf{(3.5.8.1.27)}$$

The above equations are used to solve for the kinetic variable concentration at interior nodes, where the boundary term {B} is zero.

At the junction nodes, assign

$$\{RLDW\} = \frac{[M]}{\Delta t} - W_2 * [L]\left\{E_n^{\,n}\right\} + \{S\} + \{nQE_n^{\,m}\} \quad \textbf{(3.5.8.1.28)}$$

Equation (3.5.8.1.25) is modified as

$$[CMATRX]\left\{E_n^{\,n+1/2}\right\} + Flux = \{RLDW\} \quad \textbf{(3.5.8.1.29)}$$

Junction concentration can be solved by the matrix equation assembled with equation (3.5.7.1.48), and (3.5.8.1.29).

For boundary node $i = b$, the boundary term $\{B\}$ should be continuously calculated as follows.

$$B_i = \left[N_i K_x A \frac{E_n^{\,m}}{E_n} \frac{\partial E_n}{\partial x} + W_i K_x A \frac{\partial (E_n^{\,m}/E_n)}{\partial x} E_n \right]_b = n\left[K_x A \frac{E_n^{\,m}}{E_n} \frac{\partial E_n}{\partial x} + K_x A \frac{\partial (E_n^{\,m}/E_n)}{\partial x} E_n \right]_b = n\left(K_x A \frac{\partial E_n^{\,m}}{\partial x} \right)_b \quad \textbf{(3.5.8.1.30)}$$

Dirichlet boundary condition

$$E_n^{\,m} = E_n^{\,m}(x_b, t) \quad \textbf{(3.5.8.1.31)}$$

Variable boundary condition

When flow is coming in from outside ($nQ < 0$)

$$n\left(QE_n^{\,m} - AK_x \frac{\partial E_n^{\,m}}{\partial x} \right) = nQE_n^{\,m}(x_b, t) \;\Rightarrow\; B_i = nQE_n^{\,m} - nQE_n^{\,m}(x_b, t) \quad \textbf{(3.5.8.1.32)}$$

When Flow is going out from inside (nQ > 0)

$$-\mathrm{nAK_x} \frac{\partial \mathrm{E_n^{\,m}}}{\partial \mathrm{x}} = 0 \Rightarrow \mathrm{B_i} = 0 \quad \textbf{(3.5.8.1.33)}$$

Cauchy boundary condition

$$n\left(QE_n^{\,m} - AK_x \frac{\partial E_n^{\,m}}{\partial x} \right) = Q_{En}(x_b, t) \;\Rightarrow\; B_i = nQE_n^{\,m} - Q_{En}(x_b, t) \quad \textbf{(3.5.8.1.34)}$$

Neumann boundary condition

$$-nAK_x \frac{\partial E_n^{\ m}}{\partial x} = Q_{En}(x_b,t) \quad \Rightarrow \quad B_i = -Q_{En}(x_b,t) \tag{3.5.8.1.35}$$

3.5.8.2 Mixed Predictor-corrector/Operator-Splitting Scheme

Recall the continuity equation for kinetic-variables, equation (3.5.8.1.3), as follows.

$$\begin{aligned} &A\frac{\partial E_n}{\partial t} + \frac{\partial A}{\partial t}E_n + Q\frac{\partial E_n^{\ m}}{\partial x} - \frac{\partial}{\partial x}\left(K_x A\frac{\partial E_n^{\ m}}{\partial x}\right) - \left[\frac{\partial A}{\partial t} - (S_S + S_R + S_I + S_1 + S_2)\right]E_n^{\ m} = \\ &M_{E_n}^{\ as} + M_{E_n}^{\ rs} + M_{E_n}^{\ is} + M_{E_n}^{\ os1} + M_{E_n}^{\ os2} + AR_{E_n} \end{aligned} \tag{3.5.8.2.1}$$

At $n+1$-th time step, equation (3.5.8.2.1) is approximated by

$$\begin{aligned} &A\frac{(E_n)^{n+1} - (E_n)^n}{\Delta t} + \frac{\partial A}{\partial t}E_n + Q\frac{\partial E_n^{\ m}}{\partial x} - \frac{\partial}{\partial x}\left(K_x A\frac{\partial E_n^{\ m}}{\partial x}\right) - \left[\frac{\partial A}{\partial t} - (S_S + S_R + S_1 + S_2 + S_I)\right]E_n^{\ m} \\ &= M_{E_n}^{\ as} + M_{E_n}^{\ rs} + M_{E_n}^{\ os1} + M_{E_n}^{\ os2} + M_{E_n}^{\ is} + AR_{E_n} \end{aligned} \tag{3.5.8.2.2}$$

According to mixed predictor corrector/operator-splitting scheme, equation (3.5.8.2.2) can be separated into two equations as follows

$$\begin{aligned} &A\frac{(E_n^m)^{n+1} - (E_n^m)^n}{\Delta t} + \frac{\partial A}{\partial t}E_n^m + Q\frac{\partial E_n^{\ m}}{\partial x} - \frac{\partial}{\partial x}\left(K_x A\frac{\partial E_n^{\ m}}{\partial x}\right) - \left[\frac{\partial A}{\partial t} - (S_S + S_R + S_1 + S_2 + S_I)\right]E_n^{\ m} \\ &= M_{E_n}^{\ as} + M_{E_n}^{\ rs} + M_{E_n}^{\ os1} + M_{E_n}^{\ os2} + M_{E_n}^{\ is} + AR_{E_n}^{\ n} - \frac{\partial A}{\partial t}(E_n^{im})^n \end{aligned} \tag{3.5.8.2.3}$$

$$\frac{E_n^{\ n+1} - [(E_n^{\ m})^{n+1/2} + (E_n^{\ im})^n]}{\Delta t} = R_{E_n}^{\ n+1} - R_{E_n}^{\ n} - \frac{\partial(\ell nA)}{\partial t}(E_n^{im})^{n+1} + \frac{\partial(\ell nA)}{\partial t}(E_n^{im})^n \tag{3.5.8.2.4}$$

First, solve equation (3.5.8.2.3) and get $(E_n^m)^{n+1/2}$. Second, solve equation (3.5.8.2.4) together with algebraic equations for equilibrium reactions using BIOGEOCHEM scheme to obtain $E_n^{\ n+1}$ and the individual species concentration.

To solve equation (3.5.8.2.3), assign and calculate R_{HSn} and L_{HSn} in the same way as that in Section (3.5.7.2). Equation (3.5.8.2.3) is then simplified as

$$A\frac{(E_n^{\ m})^{n+1/2} - (E_n^{\ m})^n}{\Delta t} + \frac{\partial A}{\partial t}E_n^m + Q\frac{\partial E_n^{\ m}}{\partial x} - \frac{\partial}{\partial x}\left(K_x A\frac{\partial E_n^{\ m}}{\partial x}\right) + L_{HS_n}E_n^{\ m} = R_{HS_n} + AR_{E_n}^{\ n} - \frac{\partial A}{\partial t}(E_n^{im})^n \tag{3.5.8.2.5}$$

Use Galerkin or Petrov-Galerkin FEM for the spatial discretization of transport equations. For Galerkin method, choose weighting function identical to base functions. Integrate Equation (3.5.8.2.5) in the spatial dimensions over the entire region as follows.

$$\int_{x_1}^{x_N} N_i \left[A\frac{\partial E_n^{\,m}}{\partial t} - \frac{\partial}{\partial x}\left(K_x A \frac{\partial E_n^{\,m}}{\partial x} \right) \right] dx + \int_{x_1}^{x_N} W_i Q \frac{\partial E_n^{\,m}}{\partial x} dx + \int_{x_1}^{x_N} N_i \left(L_{HS_n} + \frac{\partial A}{\partial t} \right) E_n^{\,m} dx = \int_{x_1}^{x_N} N_i \left[R_{HS_n} + A(R_{E_n})^n - \frac{\partial A}{\partial t}(E_n^{im})^n \right] dx \quad \textbf{(3.5.8.2.6)}$$

Integrating by parts, we obtain

$$\int_{x_1}^{x_N} N_i A \frac{\partial E_n^{\,m}}{\partial t} dx + \int_{x_1}^{x_N} \frac{dN_i}{dx} K_x A \frac{\partial E_n^{\,m}}{\partial x} dx + \int_{x_1}^{x_N} W_i Q \frac{\partial E_n^{\,m}}{\partial x} dx + \int_{x_1}^{x_N} N_i \left(L_{HS_n} + \frac{\partial A}{\partial t} \right) E_n^{\,m} dx = \int_{x_1}^{x_N} N_i \left[R_{HS_n} + A(R_{E_n})^n - \frac{\partial A}{\partial t}(E_n^{im})^n \right] dx + N_i K_x A \frac{\partial E_n^{\,m}}{\partial x}\Big|_{B1}^{B2} \quad \textbf{(3.5.8.2.7)}$$

Approximate solution $E_n^{\,m}$ by a linear combination of the base functions as follows

$$E_n^{\,m} \approx \hat{E}_n^{\,m} = \sum_{j=1}^{N} E_{nj}^{\,m}(t) N_j(x) \quad \textbf{(3.5.8.2.8)}$$

Substituting Equation (3.5.8.2.8) into Equation (3.5.8.2.7), we obtain

$$\sum_{j=1}^{N} \left[\left(\int_{x_1}^{x_N} W_i Q \frac{dN_j}{dx} dx + \int_{x_1}^{x_N} \frac{dN_i}{dx} K_x A \frac{dN_j}{dx} dx + \int_{x_1}^{x_N} N_i \left(L_{HS_n} + \frac{\partial A}{\partial t} \right) N_j dx \right) E_{nj}^{\,m}(t) \right] + \sum_{j=1}^{N} \left[\left(\int_{x_1}^{x_N} N_i A N_j dx \right) \frac{\partial E_{nj}^{\,m}(t)}{\partial t} \right] = \int_{x_1}^{x_N} N_i \left[R_{HS_n} + A(R_{E_n})^n - \frac{\partial A}{\partial t}(E_n^{im})^n \right] dx + \sum n \left(N_i K_x A \frac{\partial E_n^{\,m}}{\partial x} \right)_b \quad \textbf{(3.5.8.2.9)}$$

Equation (3.5.8.2.9) can be written in matrix form as

$$([L1]+[L2]+[L3])\{E_n^{\,m}\} + [M]\left\{ \frac{\partial E_n^{\,m}}{\partial t} \right\} = \{S\} + \{B\} \quad \textbf{(3.5.8.2.10)}$$

The matrices $[L1]$, $[L2]$, $[L3]$, $[M]$ and load vectors $\{S\}$, $\{B\}$ are given by

$$L1_{ij} = \int_{x_1}^{x_N} W_i Q \frac{dN_j}{dx} dx \quad \textbf{(3.5.8.2.11)}$$

$$L2_{ij} = \int_{x_1}^{x_N} \frac{dN_i}{dx} K_x A \frac{dN_j}{dx} dx \quad \textbf{(3.5.8.2.12)}$$

$$L3_{ij} = \int_{x_1}^{x_N} N_i \left(L_{HS_n} + \frac{\partial A}{\partial t} \right) N_j dx \quad \textbf{(3.5.8.2.13)}$$

$$M_{ij} = \int_{x_1}^{x_N} N_i A N_j dx \quad \textbf{(3.5.8.2.14)}$$

$$S_i = \int_{x_1}^{x_N} N_i \left[R_{HS_n} + A(R_{E_n})^n - \frac{\partial A}{\partial t}(E_n^{im})^n \right] dx \quad \textbf{(3.5.8.2.15)}$$

$$B_i = n\left(N_i K_x A \frac{\partial E_n^{\ m}}{\partial x} \right)_b \qquad \textbf{(3.5.8.2.16)}$$

where all the terms listed above are calculated with the corresponding time weighting values. Equation (3.5.8.2.10) is then simplified as

$$[L]\left\{E_n^{\ m}\right\} + [M]\left\{\frac{\partial E_n^{\ m}}{\partial t}\right\} = \{S\} + \{B\}, \quad where [L] = [L1] + [L2] + [L3] \qquad \textbf{(3.5.8.2.17)}$$

Further,

$$[L]\left\{W_1 * (E_n^{\ m})^{n+1/2} + W_2 * (E_n^{\ m})^n\right\} + [M]\left\{\frac{(E_n^{\ m})^{n+1/2} - (E_n^{\ m})^n}{\Delta t}\right\} = \{S\} + \{B\} \qquad \textbf{(3.5.8.2.18)}$$

So that

$$[CMATRX]\left\{(E_n^{\ m})^{n+1/2}\right\} = \{RLD\} \qquad \textbf{(3.5.8.2.19)}$$

where

$$[CMATRX] = \frac{[M]}{\Delta t} + W_1[L] \qquad \textbf{(3.5.8.2.20)}$$

$$\{RLD\} = \left(\frac{[M]}{\Delta t} - W_2[L]\right)\left\{(E_n^{\ m})^n\right\} + \{S\} + \{B\} \qquad \textbf{(3.5.8.2.21)}$$

The above equations are used to solve for the kinetic variable concentration at interior nodes where boundary term {B} is zero.

For junction nodes, assign

$$\{RLDW\} = \frac{[M]}{\Delta t} - W_2[L]\left\{(E_n^{\ m})^n\right\} + \{S\} + \{nQE_n^{\ m}\} \qquad \textbf{(3.5.8.2.22)}$$

Equation (3.5.8.2.18) is modified as

$$[CMATRX]\left\{(E_n^{\ m})^{n+1/2}\right\} + Flux = \{RLDW\} \qquad \textbf{(3.5.8.2.23)}$$

Junction concentration can be solved by the matrix equation assembled with equation (3.5.7.2.32) and (3.5.8.2.23).

For boundary node $i = b$, the boundary term $\{B\}$ should be continuously calculated same as that using Fully-implicit scheme in section (3.5.8.1).

3.5.8.3 Operator-splitting

Recall the continuity equation for kinetic-variables, equation (3.5.8.1.3), as follows.

$$A\frac{\partial E_n}{\partial t} + \frac{\partial A}{\partial t}E_n + Q\frac{\partial E_n^{\ m}}{\partial x} - \frac{\partial}{\partial x}\left(K_x A \frac{\partial E_n^{\ m}}{\partial x}\right) - \left[\frac{\partial A}{\partial t} - (S_S + S_R + S_I + S_1 + S_2)\right]E_n^{\ m} = M_{E_n}^{\ as} + M_{E_n}^{\ rs} + M_{E_n}^{\ is} + M_{E_n}^{\ os1} + M_{E_n}^{\ os2} + AR_{E_n} \qquad \textbf{(3.5.8.3.1)}$$

At $n+1$-th time step, equation (3.5.8.3.1) is approximated by

$$A\frac{(E_n)^{n+1}-(E_n)^n}{\Delta t}+\frac{\partial A}{\partial t}E_n+Q\frac{\partial {E_n}^m}{\partial x}-\frac{\partial}{\partial x}\left(K_xA\frac{\partial {E_n}^m}{\partial x}\right)-\left[\frac{\partial A}{\partial t}-(S_S+S_R+S_1+S_2+S_I)\right]{E_n}^m$$
$$={M_{E_n}}^{as}+{M_{E_n}}^{rs}+{M_{E_n}}^{os1}+{M_{E_n}}^{os2}+{M_{E_n}}^{is}+AR_{E_n} \quad \textbf{(3.5.8.3.2)}$$

According to Operator-splitting scheme, equation (3.5.8.3.2) can be separated into two equations as follows

$$A\frac{(E_n^m)^{n+1}-(E_n^m)^n}{\Delta t}+\frac{\partial A}{\partial t}E_n^m+Q\frac{\partial {E_n}^m}{\partial x}-\frac{\partial}{\partial x}\left(K_xA\frac{\partial {E_n}^m}{\partial x}\right)-\left[\frac{\partial A}{\partial t}-(S_S+S_R+S_1+S_2+S_I)\right]{E_n}^m$$
$$={M_{E_n}}^{as}+{M_{E_n}}^{rs}+{M_{E_n}}^{os1}+{M_{E_n}}^{os2}+{M_{E_n}}^{is} \quad \textbf{(3.5.8.3.3)}$$

$$\frac{{E_n}^{n+1}-[({E_n}^m)^{n+1/2}+({E_n}^{im})^n]}{\Delta t}={R_{E_n}}^{n+1}-\frac{\partial(\ell nA)}{\partial t}(E_n^{im})^{n+1} \quad \textbf{(3.5.8.3.4)}$$

First, solve equation (3.5.8.3.3) and get $(E_n^m)^{n+1/2}$. Second, solve equation (3.5.8.3.4) together with algebraic equations for equilibrium reactions using BIOGEOCHEM scheme to obtain $(E_n)^{n+1}$ and the individual species concentration.

To solve equation (3.5.8.3.3), assign and calculate R_{HSn} and L_{HSn} same as that in section (3.5.8.1). Equation (3.5.8.3.3) is then simplified as

$$A\frac{({E_n}^m)^{n+1/2}-({E_n}^m)^n}{\Delta t}+\frac{\partial A}{\partial t}E_n^m+Q\frac{\partial {E_n}^m}{\partial x}-\frac{\partial}{\partial x}\left(K_xA\frac{\partial {E_n}^m}{\partial x}\right)+L_{HS_n}{E_n}^m=R_{HS_n} \quad \textbf{(3.5.8.3.5)}$$

Use Galerkin or Petrov-Galerkin FEM for the spatial discretization of transport equations. For Galerkin method, choose weighting function identical to base functions. Integrate Equation (3.5.8.3.5) in the spatial dimensions over the entire region as follows.

$$\int_{x_1}^{x_N}N_i\left[A\frac{\partial {E_n}^m}{\partial t}-\frac{\partial}{\partial x}\left(K_xA\frac{\partial {E_n}^m}{\partial x}\right)\right]dx+\int_{x_1}^{x_N}W_iQ\frac{\partial {E_n}^m}{\partial x}dx+\int_{x_1}^{x_N}N_i\left(L_{HS_n}+\frac{\partial A}{\partial t}\right){E_n}^m dx=\int_{x_1}^{x_N}N_iR_{HS_n}dx \quad \textbf{(3.5.8.3.6)}$$

Integrating by parts, we obtain

$$\int_{x_1}^{x_N}N_iA\frac{\partial {E_n}^m}{\partial t}dx+\int_{x_1}^{x_N}\frac{dN_i}{dx}K_xA\frac{\partial {E_n}^m}{\partial x}dx+\int_{x_1}^{x_N}W_iQ\frac{\partial {E_n}^m}{\partial x}dx+\int_{x_1}^{x_N}N_i\left(L_{HS_n}+\frac{\partial A}{\partial t}\right){E_n}^m dx$$
$$=\int_{x_1}^{x_N}N_iR_{HS_n}dx+N_iK_xA\frac{\partial {E_n}^m}{\partial x}\Bigg|_{B1}^{B2} \quad \textbf{(3.5.8.3.7)}$$

Approximate solution ${E_n}^m$ by a linear combination of the base functions as follows

$${E_n}^m\approx{\hat{E}_n}^m=\sum_{j=1}^{N}{E_{nj}}^m(t)N_j(x) \quad \textbf{(3.5.8.3.8)}$$

Substituting Equation (3.5.8.3.8) into Equation (3.5.8.3.7), we obtain

$$\sum_{j=1}^{N}\left[\left(\int_{x_1}^{x_N} W_i Q\frac{dN_j}{dx}dx+\int_{x_1}^{x_N}\frac{dN_i}{dx}K_x A\frac{dN_j}{dx}dx+\int_{x_1}^{x_N} N_i\left(L_{HS_n}+\frac{\partial A}{\partial t}\right)N_j dx\right)E_{nj}{}^m(t)\right]$$
$$+\sum_{j=1}^{N}\left[\left(\int_{x_1}^{x_N} N_i A N_j dx\right)\frac{\partial E_{nj}{}^m(t)}{\partial t}\right]=\int_{x_1}^{x_N} N_i R_{HS_n}dx+\sum n\left(N_i K_x A\frac{\partial E_n{}^m}{\partial x}\right)_b \quad \textbf{(3.5.8.3.9)}$$

Equation (3.5.8.3.9) can be written in matrix form as

$$([L1]+[L2]+[L3])\{E_n{}^m\}+[M]\left\{\frac{\partial E_n{}^m}{\partial t}\right\}=\{S\}+\{B\} \quad \textbf{(3.5.8.3.10)}$$

The matrices $[L1]$, $[L2]$, $[L3]$, $[M]$ and load vectors $\{S\}$, $\{B\}$ are given by

$$L1_{ij}=\int_{x_1}^{x_N} W_i Q\frac{dN_j}{dx}dx \quad \textbf{(3.5.8.3.11)}$$

$$L2_{ij}=\int_{x_1}^{x_N}\frac{dN_i}{dx}K_x A\frac{dN_j}{dx}dx \quad \textbf{(3.5.8.3.12)}$$

$$L3_{ij}=\int_{x_1}^{x_N} N_i\left(L_{HS_n}+\frac{\partial A}{\partial t}\right)N_j dx \quad \textbf{(3.5.8.3.13)}$$

$$M_{ij}=\int_{x_1}^{x_N} N_i A N_j dx \quad \textbf{(3.5.8.3.14)}$$

$$S_i=\int_{x_1}^{x_N} N_i R_{HS_n}dx \quad \textbf{(3.5.8.3.15)}$$

$$B_i=n\left(N_i K_x A\frac{\partial E_n{}^m}{\partial x}\right)_b \quad \textbf{(3.5.8.3.16)}$$

where all the terms listed above are calculated with the corresponding time weighting values. Equation (3.5.8.3.10) is then simplified as

$$[L]\{E_n{}^m\}+[M]\left\{\frac{\partial E_n{}^m}{\partial t}\right\}=\{S\}+\{B\},\ \ where[L]=[L1]+[L2]+[L3] \quad \textbf{(3.5.8.3.17)}$$

Further,

$$[L]\left\{W_1*(E_n{}^m)^{n+1/2}+W_2*(E_n{}^m)^n\right\}+[M]\left\{\frac{(E_n{}^m)^{n+1/2}-(E_n{}^m)^n}{\Delta t}\right\}=\{S\}+\{B\} \quad \textbf{(3.5.8.3.18)}$$

So that

$$[CMATRX]\left\{(\mathrm{E_n}{}^m)^{n+1/2}\right\}=\{RLD\} \quad \textbf{(3.5.8.3.19)}$$

where

$$[CMATRX]=\frac{[M]}{\Delta t}+W_1[L] \quad \textbf{(3.5.8.3.20)}$$

$$\{RLD\}=\left(\frac{[M]}{\Delta t}-W_2[L]\right)\left\{(E_n{}^m)^n\right\}+\{S\}+\{B\} \quad \textbf{(3.5.8.3.21)}$$

The above equations are used to solve for the kinetic variable concentration at interior nodes where boundary term $\{B\}$ is zero.

For junction nodes, assign

$$\{RLDW\} = \frac{[M]}{\Delta t} - W_2[L]\left\{(E_n{}^m)^n\right\} + \{S\} + \{nQE_n{}^m\} \qquad \textbf{(3.5.8.3.22)}$$

Equation (3.5.8.3.18) is modified as

$$[CMATRX]\left\{(E_n{}^m)^{n+1/2}\right\} + Flux = \{RLDW\} \qquad \textbf{(3.5.8.3.23)}$$

Junction concentration can be solved by the matrix equation assembled with equation (3.5.7.3.33) and (3.5.8.3.23).

For boundary node i = b, the boundary term {B} should be continuously calculated same as that using Fully-implicit scheme in section (3.5.8.1).

3.5.9 Application of the Modified Lagrangian-Eulerian Approach to the Largrangian Form of the Transport Equations

3.5.9.1 Fully-implicit scheme

The continuity equation for kinetic-variables in advective form at *(n+1)*-th time step, is shown as follows.

$$A\frac{(E_n)^{n+1} - (E_n)^n}{\Delta t} + \frac{\partial A}{\partial t}E_n + Q\frac{\partial E_n{}^m}{\partial x} - \frac{\partial}{\partial x}\left(K_x A\frac{\partial E_n{}^m}{\partial x}\right) + \left[(S_S + S_R + S_1 + S_2 + S_I) - \frac{\partial A}{\partial t}\right]E_n{}^m = M_{E_n}{}^{as} + M_{E_n}{}^{rs} + M_{E_n}{}^{os1} + M_{E_n}{}^{os2} + M_{E_n}{}^{is} + AR_{E_n} \qquad \textbf{(3.5.9.1.1)}$$

[Option 1]

Express $E_n{}^m$ in terms of $E_n{}^m / E_n * E_n$ to make E_n's as primary dependent variables, equation (3.5.9.1.1) is modified as

$$A\frac{(E_n)^{n+1} - (E_n)^n}{\Delta t} + \frac{\partial A}{\partial t}E_n + Q\frac{\partial \frac{E_n{}^m}{E_n}E_n}{\partial x} - \frac{\partial}{\partial x}\left(K_x A\frac{\partial \frac{E_n{}^m}{E_n}E_n}{\partial x}\right) + \left[(S_S + S_R + S_1 + S_2 + S_I) - \frac{\partial A}{\partial t}\right]\frac{E_n{}^m}{E_n}E_n = M_{E_n}{}^{as} + M_{E_n}{}^{rs} + M_{E_n}{}^{os1} + M_{E_n}{}^{os2} + M_{E_n}{}^{is} + AR_{E_n} \qquad \textbf{(3.5.9.1.2)}$$

According to Fully-implicit scheme, equation (3.5.9.1.2) can be separated into two equations as follows

$$A\frac{(E_n)^{n+1/2}-(E_n)^n}{\Delta t}+\frac{\partial A}{\partial t}E_n+Q\frac{\partial\frac{E_n^{\ m}}{E_n}E_n}{\partial x}-\frac{\partial}{\partial x}\left(K_xA\frac{\partial\frac{E_n^{\ m}}{E_n}E_n}{\partial x}\right)+$$

$$\left[(S_S+S_R+S_1+S_2+S_I)-\frac{\partial A}{\partial t}\right]\frac{E_n^{\ m}}{E_n}E_n=M_{E_n}^{\ as}+M_{E_n}^{\ rs}+M_{E_n}^{\ os1}+M_{E_n}^{\ os2}+M_{E_n}^{\ is}+AR_{E_n} \quad \textbf{(3.5.9.1.3)}$$

$$\frac{(E_n)^{n+1}-(E_n)^{n+1/2}}{\Delta t}=0 \quad \textbf{(3.5.9.1.4)}$$

First, solve equation (3.5.9.1.3) and get $(E_n)^{n+1/2}$. Second, solve equation (3.5.9.1.4) together with algebraic equations for equilibrium reactions using BIOGEOCHEM scheme to obtain the individual species concentration. Iteration between these two steps is needed because reaction term in equation (3.5.9.1.3) needs to be updated by the results of (3.5.9.1.4).

To solve equation (3.5.9.1.3), assign

$$R_{HS_n}=0 \quad and \quad L_{HS_n}=\left[(S_S+S_R+S_1+S_2+S_I)-\frac{\partial A}{\partial t}\right]\frac{E_n^{\ m}}{E_n} \quad \textbf{(3.5.9.1.5)}$$

Then the right hand side R_{HSn} and left hand side L_{HSn} should be continuously calculated as following.

$$M_{E_n}^{\ rs}=\begin{cases}S_R*E_{n^{rs}}, & if\ S_R>0 \ \Rightarrow\ R_{HSn}=R_{HSn}+M_{E_n}^{\ rs}\\ S_R*E_n^{\ m}, & if\ S_R\le 0 \ \Rightarrow\ L_{HSn}=L_{HSn}-S_R\end{cases} \quad \textbf{(3.5.9.1.6)}$$

$$M_{E_n}^{\ as}=\begin{cases}S_S*E_{n^{as}}, & if\ S_S>0 \ \Rightarrow\ R_{HSn}=R_{HSn}+M_{E_n}^{\ as},\\ S_S*E_n^{\ m}, & if\ S_S\le 0 \ \Rightarrow\ L_{HSn}=L_{HSn}-S_S\end{cases} \quad \textbf{(3.5.9.1.7)}$$

$$M_{E_n}^{\ os1}=\begin{cases}S_1*E_n^{\ m_{os1}}, & if\ S_1>0 \ \Rightarrow\ R_{HSn}=R_{HSn}+M_{E_n}^{\ os1}\\ S_1*E_n^{\ m}, & if\ S_1\le 0 \ \Rightarrow\ L_{HSn}=L_{HSn}-S_1\end{cases} \quad \textbf{(3.5.9.1.8)}$$

$$M_{E_n}^{\ os2}=\begin{cases}S_2*E_n^{\ m_{os2}}, & if\ S_2>0 \ \Rightarrow\ R_{HSn}=R_{HSn}+M_{E_n}^{\ os2}\\ S_2*E_n^{\ m}, & if\ S_2\le 0 \ \Rightarrow\ L_{HSn}=L_{HSn}-S_2\end{cases} \quad \textbf{(3.5.9.1.9)}$$

$$M_{E_n}^{\ is}=\begin{cases}S_I*E_n^{\ m_{is}}, & if\ S_I>0 \ \Rightarrow\ R_{HSn}=R_{HSn}+M_{E_n}^{\ is}\\ S_I*E_n^{\ m}, & if\ S_I\le 0 \ \Rightarrow\ L_{HSn}=L_{HSn}-S_I\end{cases} \quad \textbf{(3.5.9.1.10)}$$

Equation (3.5.9.1.3) is then simplified as

$$A\frac{(E_n)^{n+1/2}-(E_n)^n}{\Delta t}+\frac{\partial A}{\partial t}E_n+\left(Q\frac{E_n^{\ m}}{E_n}-K_xA\frac{\partial\frac{E_n^{\ m}}{E_n}}{\partial x}\right)\frac{\partial E_n}{\partial x}-\frac{\partial}{\partial x}\left(K_xA\frac{E_n^{\ m}}{E_n}\frac{\partial E_n}{\partial x}\right)+$$

$$\left[Q\frac{\partial\frac{E_n^{\ m}}{E_n}}{\partial x}-\frac{\partial}{\partial x}\left(K_xA\frac{\partial\frac{E_n^{\ m}}{E_n}}{\partial x}\right)+L_{HS_n}\right]E_n=R_{HS_n}+AR_{E_n} \quad \textbf{(3.5.9.1.11)}$$

Assign the true transport velocity V_{true} as follows.

$$AV_{true} = Q\frac{E_n{}^m}{E_n} - K_x A\frac{\partial}{\partial x}\left(\frac{E_n{}^m}{E_n}\right) \quad \textbf{(3.5.9.1.12)}$$

$$K_{true} = K_x\frac{E_n{}^m}{E_n} \quad \textbf{(3.5.9.1.13)}$$

$$L = Q\frac{\partial}{\partial x}\left(\frac{E_n{}^m}{E_n}\right) - \frac{\partial}{\partial x}\left[K_x A\frac{\partial}{\partial x}\left(\frac{E_n{}^m}{E_n}\right)\right] + L_{HS_n} \quad \textbf{(3.5.9.1.14)}$$

Then equation (3.5.9.1.11) is simplified as

$$A\frac{(E_n)^{n+1/2} - (E_n)^n}{\Delta t} + AV_{true}\frac{\partial E_n}{\partial x} - \frac{\partial}{\partial x}\left(K_{true}A\frac{\partial E_n}{\partial x}\right) + \left(\frac{\partial A}{\partial t} + L\right)E_n = R_{HS_n} + AR_{E_n} \quad \textbf{(3.5.9.1.15)}$$

Equation (13.5.7.1.15) in the Lagrangian and Eulerian form is as follows.

$$\frac{dE_n}{d\tau} = \frac{(E_n)^{n+1/2} - (E_n)^n}{\Delta t} + V_{true}\frac{\partial E_n}{\partial x} = 0 \quad \textbf{(3.5.9.1.16)}$$

$$A\frac{dE_n}{d\tau} - \frac{\partial}{\partial x}\left(K_{true}A\frac{\partial E_n}{\partial x}\right) + \left(\frac{\partial A}{\partial t} + L\right)E_n = R_{HS_n} + AR_{E_n} \quad \textbf{(3.5.9.1.17)}$$

First, solve equation (3.5.9.1.16) to obtain the Lagrangian values by particle tracking. Then, deal with Eulerian equation (3.5.9.1.17) by finite element method.

Equation (3.5.9.1.17) written in a slightly different form is shown as follows.

$$\frac{dE_n}{d\tau} - D + KE_n = R_L \quad \textbf{(3.5.9.1.18)}$$

where

$$D = \frac{1}{A}\frac{\partial}{\partial x}\left(K_{true}A\frac{\partial E_n}{\partial x}\right) \quad \textbf{(3.5.9.1.19)}$$

$$K = \frac{\left(\frac{\partial A}{\partial t} + L\right)}{A} \quad \textbf{(3.5.9.1.20)}$$

$$R_L = \frac{R_{HS_n} + AR_{E_n}}{A} \quad \textbf{(3.5.9.1.21)}$$

Equation (3.5.9.1.18) written in matrix form is then expressed as

$$\frac{[U]}{\Delta\tau}\left\{E_n{}^{n+1/2}\right\} - W_1\left\{D^{n+1}\right\} + W_1\left[K^{n+1}\right]\left\{E_n{}^{n+1/2}\right\} = \frac{[U]}{\Delta\tau}\left\{E_n{}^*\right\} + W_2\left\{D^*\right\} - W_2\left\{\left(KE_n\right)^*\right\} + W_1\left\{R_L{}^{n+1}\right\} + W_2\left\{R_L{}^*\right\} \quad \textbf{(3.5.9.1.22)}$$

where $[K^{n+1}]$ is the diagonal matrix with K calculated at the $(n+1)$-th time step as its components, the diffusion term D expressed in term of E_n is solved by the following procedure.

Approximate D by a linear combination of the base functions as follows.

$$D \approx \hat{D} = \sum_{j=1}^{N} D_j(t) N_j(x) \tag{3.5.9.1.23}$$

According to equation (3.5.9.1.19), the integration of equation (3.5.9.1.22) can be written as

$$\int_{x_1}^{x_N} N_i AD dx = \int_{x_1}^{x_N} N_i A \sum_{j=1}^{N} D_j(t) N_j(x) dx = \int_{x_1}^{x_N} N_i \frac{\partial}{\partial x}\left(K_{true} A \frac{\partial E_n}{\partial x} \right) dx \tag{3.5.9.1.24}$$

Integrating by parts, we obtain

$$\sum_{j=1}^{N} \left[\left(\int_{x_1}^{x_N} N_i A N_j dx \right) D_j \right] = -\int_{x_1}^{x_N} \frac{dN_i}{dx} (K_{true} A) \frac{\partial E_n}{\partial x} dx + N_i K_{true} A \frac{\partial E_n}{\partial x} \Big|_{B1}^{B2} \tag{3.5.9.1.25}$$

Approximate E_n by a linear combination of the base functions as follows.

$$E_n \approx \hat{E}_n = \sum_{j=1}^{N} E_{nj}(t) N_j(x) \tag{3.5.9.1.26}$$

Equation (3.5.9.1.25) is further expressed as

$$\sum_{j=1}^{N} \left[\left(\int_{x_1}^{x_N} N_i A N_j dx \right) D_j \right] = -\sum_{j=1}^{N} \left[\left(\int_{x_1}^{x_N} \frac{dN_i}{dx} (K_{true} A) \frac{dN_j}{\partial x} dx \right) (E_n)_j \right] + N_i K_{true} A \frac{\partial E_n}{\partial x} \Big|_{B1}^{B2} \tag{3.5.9.1.27}$$

Assign matrices $[A1]$ and $[A2]$ and load vector $\{B1\}$ as following

$$A1_{ij} = \int_{x_1}^{x_N} N_i A N_j dx \tag{3.5.9.1.28}$$

$$A2_{ij} = \int_{x_1}^{x_N} \frac{dN_i}{dx} (K_{true} A) \frac{dN_j}{dx} dx \tag{3.5.9.1.29}$$

$$B1_i = \left(nN_i K_{true} A \frac{\partial E_n}{\partial x} \right)_b \tag{3.5.9.1.30}$$

Equation (3.5.9.1.27) is expressed as

$$[A1]\{D\} = -[A2]\{E_n\} + \{B1\} \tag{3.5.9.1.31}$$

Lump matrix $[A1]$ into diagonal matrix and assign

$$QE_{ij} = A2_{ij} / A1_{ii} \tag{3.5.9.1.32}$$

$$B_i = B1_i / A1_{ii} \tag{3.5.9.1.33}$$

Then

$$\{D\} = -[QE]\{E_n\} + \{B\} \tag{3.5.9.1.34}$$

where boundary term $\{B\}$ is calculated as follows

$$B_i = \left(nN_i K_x A \frac{\partial E_n^{\,m}}{\partial x} \right)_b \Big/ A1_{ii} - \left[nN_i K_x A \frac{\partial}{\partial x}\left(\frac{E_n^{\,m}}{E_n} \right) E_n \right]_b \Big/ A1_{ii} \qquad \textbf{(3.5.9.1.35)}$$

Dirichlet boundary condition

$$\begin{aligned} & E_n^{\,m} = E_n^{\,m}(x_b, t) \;\Rightarrow \\ & B_i = nN_i K_x A \frac{(E_n^{\,m})_j - E_n^{\,m}(x_b, t)}{\Delta x} \Big/ A1_{ii} - nN_i K_x A \frac{(E_n^{\,m}/E_n)_j - (E_n^{\,m}/E_n)_i}{\Delta x} (E_n)_i \Big/ A1_{ii} \end{aligned} \qquad \textbf{(3.5.9.1.36)}$$

where j is the interior node connected to the boundary node.

Variable boundary condition

When flow is coming in from outside (nQ < 0)

$$\begin{aligned} & n\left(QE_n^{\,m} - AK_x \frac{\partial E_n^{\,m}}{\partial x} \right) = nQE_n^{\,m}(x_b, t) \;\Rightarrow \\ & B_i = \left[nQE_n^{\,m} - nQE_n^{\,m}(x_b, t) \right] \Big/ A1_{ii} - nN_i K_x A \frac{(E_n^{\,m}/E_n)_j - (E_n^{\,m}/E_n)_i}{\Delta x} (E_n)_i \Big/ A1_{ii} \end{aligned} \qquad \textbf{(3.5.9.1.37)}$$

where j is the interior node connected to the boundary node.

When Flow is going out from inside (nQ > 0)

$$-nAK_x \frac{\partial E_n^{\,m}}{\partial x} = 0 \;\Rightarrow\; B_i = -nN_i K_x A \frac{(E_n^{\,m}/E_n)_j - (E_n^{\,m}/E_n)_i}{\Delta x} (E_n)_i \Big/ A1_{ii} \qquad \textbf{(3.5.9.1.38)}$$

where j is the interior node connected to the boundary node.

Cauchy boundary condition

$$\begin{aligned} & n\left(QE_n^{\,m} - AK_x \frac{\partial E_n^{\,m}}{\partial x} \right) = Q_{En}(x_b, t) \;\Rightarrow \\ & B_i = \left[nQE_n^{\,m} - Q_{En}(x_b, t) \right] \Big/ A1_{ii} - nN_i K_x A \frac{(E_n^{\,m}/E_n)_j - (E_n^{\,m}/E_n)_i}{\Delta x} (E_n)_i \Big/ A1_{ii} \end{aligned} \qquad \textbf{(3.5.9.1.39)}$$

where j is the interior node connected to the boundary node.

Neumann boundary condition

$$-nAK_x \frac{\partial E_n^{\,m}}{\partial x} = Q_{En}(x_b, t) \;\Rightarrow\; B_i = -Q_{En}(x_b, t) - nN_i K_x A \frac{(E_n^{\,m}/E_n)_j - (E_n^{\,m}/E_n)_i}{\Delta x} (E_n)_i \Big/ A1_{ii} \qquad \textbf{(3.5.9.1.40)}$$

where j is the interior node connected to the boundary node.

Equation (3.5.9.1.22) can be written as matrix equation as following

$$\frac{[U]}{\Delta\tau}\left\{E_n^{\,n+1/2}\right\}+W_1[QE^{n+1}]\left\{E_n^{\,n+1/2}\right\}+W_1\left[K^{n+1}\right]\left\{E_n^{\,n+1/2}\right\}$$
$$=\frac{[U]}{\Delta\tau}\left\{E_n^{\,*}\right\}-W_2\left\{\left(KE_n\right)^{*}\right\}+W_2\left\{D^{*}\right\}+W_1\left\{R_L^{\,n+1}\right\}+W_2\left\{R_L^{\,*}\right\}+W_1\left\{B^{n+1}\right\} \qquad \textbf{(3.5.9.1.41)}$$

[Option 2]

Express $E_n^{\,m}$ in terms of E_n-$E_n^{\,m}$ and $E_n^{\,m}/E_n$*E_n to make E_n's as primary dependent variables, equation (3.5.9.1.1) is modified as

$$A\frac{(E_n)^{n+1}-(E_n)^n}{\Delta t}+\frac{\partial A}{\partial t}E_n+Q\frac{\partial E_n}{\partial x}-\frac{\partial}{\partial x}\left(K_xA\frac{\partial E_n}{\partial x}\right)+\left[(S_S+S_R+S_1+S_2+S_I)-\frac{\partial A}{\partial t}\right]\frac{E_n^{\,m}}{E_n}E_n$$
$$=\left[Q\frac{\partial E_n^{\,im}}{\partial x}-\frac{\partial}{\partial x}\left(K_xA\frac{\partial E_n^{\,im}}{\partial x}\right)\right]+M_{E_n}^{\,as}+M_{E_n}^{\,rs}+M_{E_n}^{\,os1}+M_{E_n}^{\,os2}+M_{E_n}^{\,is}+AR_{E_n} \qquad \textbf{(3.5.9.1.42)}$$

According to Fully-implicit scheme, equation (3.5.9.1.42) can be separated into two equations as follows

$$A\frac{(E_n)^{n+1/2}-(E_n)^n}{\Delta t}+\frac{\partial A}{\partial t}E_n+Q\frac{\partial E_n}{\partial x}-\frac{\partial}{\partial x}\left(K_xA\frac{\partial E_n}{\partial x}\right)+\left[(S_S+S_R+S_1+S_2+S_I)-\frac{\partial A}{\partial t}\right]\frac{E_n^{\,m}}{E_n}E_n$$
$$=\left[Q\frac{\partial E_n^{\,im}}{\partial x}-\frac{\partial}{\partial x}\left(K_xA\frac{\partial E_n^{\,im}}{\partial x}\right)\right]+M_{E_n}^{\,as}+M_{E_n}^{\,rs}+M_{E_n}^{\,os1}+M_{E_n}^{\,os2}+M_{E_n}^{\,is}+AR_{E_n} \qquad \textbf{(3.5.9.1.43)}$$

$$\frac{(E_n)^{n+1}-(E_n)^{n+1/2}}{\Delta t}=0 \qquad \textbf{(3.5.9.1.44)}$$

First, solve equation (3.5.9.1.43) and get $E_n^{\,n+1/2}$. Second, solve equation (3.5.9.1.44) together with algebraic equations for equilibrium reactions using BIOGEOCHEM scheme to obtain the individual species concentration and $(E_n)^{n+1}$. Iteration between these two steps is needed because reaction term in equation (3.5.9.1.43) needs to be updated by the results of (3.5.9.1.44).

To solve equation (3.5.9.1.43), assign

$$R_{HS_n}=0 \quad and \quad L_{HS_n}=\left[(S_S+S_R+S_1+S_2+S_I)-\frac{\partial A}{\partial t}\right]\frac{E_n^{\,m}}{E_n} \qquad \textbf{(3.5.9.1.45)}$$

Then the right hand side R_{HSn} and left hand side L_{HSn} should be continuously calculated as following.

$$M_{E_n}^{\,rs}=\begin{cases}S_R*E_{n^{rs}}, & if\ S_R>0 \ \Rightarrow\ R_{HS_n}=R_{HS_n}+M_{E_n}^{\,rs}\\ S_R*E_n^{\,m}, & if\ S_R\le 0 \ \Rightarrow\ L_{HS_n}=L_{HS_n}-S_R*E_n^{\,m}/E_n\end{cases} \qquad \textbf{(3.5.9.1.46)}$$

$$M_{E_n}^{\,as}=\begin{cases}S_S*E_{n^{as}}, & if\ S_S>0 \ \Rightarrow\ R_{HS_n}=R_{HS_n}+M_{E_n}^{\,as},\\ S_S*E_n^{\,m}, & if\ S_S\le 0 \ \Rightarrow\ LHS_n=L_{HS_n}-S_S*E_n^{\,m}/E_n\end{cases} \qquad \textbf{(3.5.9.1.47)}$$

$$M_{E_n}^{\,os1}=\begin{cases}S_1*E_{n\ os1}^{m}, & if\ S_1>0 \ \Rightarrow\ R_{HS_n}=R_{HS_n}+M_{E_n}^{\,os1}\\ S_1*E_n^{\,m}, & if\ S_1\le 0 \ \Rightarrow\ L_{HS_n}=L_{HS_n}-S_1*E_n^{\,m}/E_n\end{cases} \qquad \textbf{(3.5.9.1.48)}$$

$$M_{E_n}^{os2} = \begin{cases} S_2 * E_n^{m}{}_{os2}, & if\ S_2 > 0 \ \Rightarrow\ R_{HS_n} = R_{HS_n} + M_{E_n}^{os2} \\ S_2 * E_n^{m}, & if\ S_2 \le 0 \ \Rightarrow\ L_{HS_n} = L_{HS_n} - S_2 * E_n^{m} / E_n \end{cases} \quad \textbf{(3.5.9.1.49)}$$

$$M_{E_n}^{is} = \begin{cases} S_I * E_n^{m}{}_{is}, & if\ S_I > 0 \ \Rightarrow\ R_{HS_n} = R_{HS_n} + M_{E_n}^{is} \\ S_I * E_n^{m}, & if\ S_I \le 0 \ \Rightarrow\ L_{HS_n} = L_{HS_n} - S_I * E_n^{m} / E_n \end{cases} \quad \textbf{(3.5.9.1.50)}$$

Equation (3.5.9.1.43) is then simplified as

$$A\frac{(E_n)^{n+1/2} - (E_n)^n}{\Delta t} + \frac{\partial A}{\partial t}E_n + Q\frac{\partial E_n}{\partial x} - \frac{\partial}{\partial x}\left(K_x A\frac{\partial E_n}{\partial x}\right) + L_{HS_n}E_n = \left[Q\frac{\partial E_n^{im}}{\partial x} - \frac{\partial}{\partial x}\left(K_x A\frac{\partial E_n^{im}}{\partial x}\right)\right] + R_{HS_n} + AR_{E_n} \quad \textbf{(3.5.9.1.51)}$$

Assign the true transport velocity V_{true} as follows.

$$AV_{true} = Q \quad \textbf{(3.5.9.1.52)}$$

Then equation (3.5.9.1.51) is simplified as

$$A\frac{(E_n)^{n+1/2} - (E_n)^n}{\Delta t} + A^n V_{true}\frac{\partial E_n}{\partial x} - \frac{\partial}{\partial x}\left(K_x A\frac{\partial E_n}{\partial x}\right) + \left(L_{HS_n} + \frac{\partial A}{\partial t}\right)E_n = \left[Q\frac{\partial E_n^{im}}{\partial x} - \frac{\partial}{\partial x}\left(K_x A\frac{\partial E_n^{im}}{\partial x}\right)\right] + R_{HS_n} + AR_{E_n} \quad \textbf{(3.5.9.1.53)}$$

Equation (13.5.9.1.53) in the Lagrangian and Eulerian form is as follows.

$$\frac{dE_n}{d\tau} = \frac{(E_n)^{n+1/2} - (E_n)^n}{\Delta t} + V_{true}\frac{\partial E_n}{\partial x} = 0 \quad \textbf{(3.5.9.1.54)}$$

$$A\frac{dE_n}{d\tau} - \frac{\partial}{\partial x}\left(K_x A\frac{\partial E_n}{\partial x}\right) + \left(L_{HS_n} + \frac{\partial A}{\partial t}\right)E_n = \left[Q\frac{\partial E_n^{im}}{\partial x} - \frac{\partial}{\partial x}\left(K_x A\frac{\partial E_n^{im}}{\partial x}\right)\right] + R_{HSn} + AR_{E_n} \quad \textbf{(3.5.9.1.55)}$$

First, solve equation (3.5.9.1.54) to obtain the Lagrangian values by particle tracking. Then, deal with Eulerian equation (3.5.9.1.55) by finite element method.

Equation (3.5.9.1.55) written in a slightly different form is shown as follows.

$$\frac{dE_n}{d\tau} - D + K * E_n = T + R_L \quad \textbf{(3.5.9.1.56)}$$

where

$$D = \frac{1}{A}\frac{\partial}{\partial x}\left(K_x A\frac{\partial E_n}{\partial x}\right) \quad \textbf{(3.5.9.1.57)}$$

$$K = \frac{\left(L_{HS_n} + \frac{\partial A}{\partial t}\right)}{A} \quad \textbf{(3.5.9.1.58)}$$

$$R_L = \frac{R_{HS_n} + AR_{E_n}}{A} \quad \textbf{(3.5.9.1.59)}$$

$$T = \frac{1}{A}\left[Q\frac{\partial E_n^{im}}{\partial x} - \frac{\partial}{\partial x}\left(K_x A\frac{\partial E_n^{im}}{\partial x}\right)\right] \quad \textbf{(3.5.9.1.60)}$$

Equation (3.5.9.1.56) written in matrix form is then expressed as

$$\begin{aligned}&\frac{[U]}{\Delta\tau}\left\{E_n^{\,n+1/2}\right\}-W_1\left\{D^{n+1}\right\}+W_1\left[K^{n+1}\right]\left\{E_n^{\,n+1/2}\right\}=\\&\frac{[U]}{\Delta\tau}\left\{E_n^{\,*}\right\}+W_2\left\{D^{*}\right\}-W_2\left\{\left(KE_n\right)^{*}\right\}+W_1\left\{T^{n+1}\right\}+W_2\left\{T^{*}\right\}+W_1\left\{R_L^{\,n+1}\right\}+W_2\left\{R_L^{\,*}\right\}\end{aligned} \qquad \textbf{(3.5.9.1.61)}$$

where $[K^{n+1}]$ is the diagonal matrix with K calculated at $(n+1)$-th time step as its components, the diffusion term D expressed in term of E_n and term T expressed in term of $E_n^{\,im}$ is solved by the following procedure.

Approximate D by a linear combination of the base functions as follows.

$$D \approx \hat{D} = \sum_{j=1}^{N} D_j(t) N_j(x) \qquad \textbf{(3.5.9.1.62)}$$

According to equation (3.5.9.1.57), the integration of equation (3.5.9.1.62) can be written as

$$\int_{x_1}^{x_N} N_i A D dx = \int_{x_1}^{x_N} N_i A \sum_{j=1}^{N} D_j(t) N_j(x) dx = \int_{x_1}^{x_N} N_i \frac{\partial}{\partial x}\left(K_x A \frac{\partial E_n}{\partial x}\right) dx \qquad \textbf{(3.5.9.1.63)}$$

Integrating by parts, we obtain

$$\sum_{j=1}^{N}\left[\left(\int_{x_1}^{x_N} N_i A N_j dx\right) D_j\right] = -\int_{x_1}^{x_N} \frac{dN_i}{dx}(K_x A)\frac{\partial E_n}{\partial x} dx + N_i K_x A \frac{\partial E_n}{\partial x}\bigg|_{B1}^{B2} \qquad \textbf{(3.5.9.1.64)}$$

Approximate E_n by a linear combination of the base functions as follows.

$$E_n \approx \hat{E}_n = \sum_{j=1}^{N} E_{nj}(t) N_j(x) \qquad \textbf{(3.5.9.1.65)}$$

Equation (3.5.9.1.64) is further expressed as

$$\sum_{j=1}^{N}\left[\left(\int_{x_1}^{x_N} N_i A N_j dx\right) D_j\right] = -\sum_{j=1}^{N}\left[\left(\int_{x_1}^{x_N} \frac{dN_i}{dx}(K_x A)\frac{dN_j}{\partial x} dx\right)(E_n)_j\right] + N_i K_x A \frac{\partial E_n}{\partial x}\bigg|_{B1}^{B2} \qquad \textbf{(3.5.9.1.66)}$$

Assign matrices [$A1$] and [$A2$] and load vector { $B1$ } as following

$$A1_{ij} = \int_{x_1}^{x_N} N_i A N_j dx \qquad \textbf{(3.5.9.1.67)}$$

$$A2_{ij} = \int_{x_1}^{x_N} \frac{dN_i}{dx}(K_x A)\frac{dN_j}{dx} dx \qquad \textbf{(3.5.9.1.68)}$$

$$B1_i = \left(nN_i K_x A \frac{\partial E_n}{\partial x}\right)_b \qquad \textbf{(3.5.9.1.69)}$$

Equation (3.5.9.1.66) is expressed as

$$[A1]\{D\} = -[A2]\{E_n\} + \{B1\} \qquad \textbf{(3.5.9.1.70)}$$

Lump matrix [$A1$] into diagonal matrix and assign

$$QE_{ij} = A2_{ij} / A1_{ii} \tag{3.5.9.1.71}$$

$$QB1_i = B1_i / A1_{ii} \tag{3.5.9.1.72}$$

Then

$$\{D\} = -[QE]\{E_n\} + \{QB1\} \tag{3.5.9.1.73}$$

Approximate T by a linear combination of the base functions as follows.

$$T \approx \hat{T} = \sum_{j=1}^{N} T_j(t) N_j(x) \tag{3.5.9.1.74}$$

According to equation (3.5.9.1.60), the integration of equation (3.5.9.1.74) can be written as

$$\int_{x_1}^{x_N} N_i A T dx = \int_{x_1}^{x_N} N_i A \sum_{j=1}^{N} T_j(t) N_j(x) dx = \int_{x_1}^{x_N} N_i \left[Q \frac{\partial E_n^{\ im}}{\partial x} - \frac{\partial}{\partial x}\left(K_x A \frac{\partial E_n^{\ im}}{\partial x} \right) \right] dx \tag{3.5.9.1.75}$$

Integrating by parts, we obtain

$$\sum_{j=1}^{N} \left[\left(\int_{x_1}^{x_N} N_i A N_j dx \right) T_j \right] = \int_{x_1}^{x_N} N_i Q \frac{\partial E_n^{\ im}}{\partial x} dx + \int_{x_1}^{x_N} \frac{dN_i}{dx} K_x A \frac{\partial E_n^{\ im}}{\partial x} dx + N_i K_x A \frac{\partial E_n^{\ im}}{\partial x} \Bigg|_{B1}^{B2} \tag{3.5.9.1.76}$$

Approximate $E_n^{\ im}$ by a linear combination of the base functions as follows.

$$E_n^{\ im} \approx \hat{E}_n^{\ im} = \sum_{j=1}^{N} E_{nj}^{\ im}(t) N_j(x) \tag{3.5.9.1.77}$$

Equation (3.5.9.1.76) is further expressed as

$$\begin{aligned} \sum_{j=1}^{N} \left[\left(\int_{x_1}^{x_N} N_i A N_j dx \right) T_j \right] &= \sum_{j=1}^{N} \left[\left(\int_{x_1}^{x_N} N_i Q \frac{dN_j}{dx} dx \right) (E_n^{\ im})_j \right] \\ + \sum_{j=1}^{N} \left[\left(\int_{x_1}^{x_N} \frac{dN_i}{dx} K_x A \frac{dN_j}{dx} dx \right) (E_n^{\ im})_j \right] &+ N_i K_x A \frac{\partial E_n^{\ im}}{\partial x} \Bigg|_{B1}^{B2} \end{aligned} \tag{3.5.9.1.78}$$

Assign matrices [$A3$], and load vector {$B2$} as following

$$A3_{ij} = \int_{x_1}^{x_N} N_i Q \frac{dN_j}{dx} dx \tag{3.5.9.1.79}$$

$$B2_i = \left(-nN_i K_x A \frac{\partial E_n^{\ im}}{\partial x} \right)_b \tag{3.5.9.1.80}$$

Assign

$$QT_{ij} = (A2_{ij} + A3_{ij}) / A1_{ii} \tag{3.5.9.1.81}$$

$$QB2_i = B2_i / A1_{ii} \tag{3.5.9.1.82}$$

Equation (3.5.9.1.78) is expressed as

$$\{T\} = [QT]\left\{E_n^{\,im}\right\} + \{QB2\} \qquad \textbf{(3.5.9.1.83)}$$

So that

$$\{D\} + \{T\} = -[QE]\{E_n\} + [QT]\left\{E_n^{\,im}\right\} + \{B\} \qquad \textbf{(3.5.9.1.84)}$$

where boundary term $\{B\}$ is calculated as follows

$$B_i = QB1_i + QB2_i = \left(nK_x A \frac{\partial E_n^{\,m}}{\partial x} \right)_b \Big/ A1_{ii} \qquad \textbf{(3.5.9.1.85)}$$

Dirichlet boundary condition

$$E_n^{\,m} = E_n^{\,m}(x_b, t) \;\Rightarrow\; B_i = nN_i K_x A \frac{(E_n^{\,m})_j - E_n^{\,m}(x_b, t)}{\Delta x} \Big/ A1_{ii} \qquad \textbf{(3.5.9.1.86)}$$

where j is the interior node connected to the boundary node.

Variable boundary condition

When flow is coming in from outside ($nQ < 0$)

$$n\left(QE_n^{\,m} - AK_x \frac{\partial E_n^{\,m}}{\partial x} \right) = nQE_n^{\,m}(x_b, t) \;\Rightarrow\; B_i = \left[nQE_n^{\,m} - nQE_n^{\,m}(x_b, t) \right] \Big/ A1_{ii} \qquad \textbf{(3.5.9.1.87)}$$

When Flow is going out from inside (nQ > 0)

$$-nAK_x \frac{\partial E_n^{\,m}}{\partial x} = 0 \;\Rightarrow\; B_i = 0 \qquad \textbf{(3.5.9.1.88)}$$

Cauchy boundary condition

$$n\left(QE_n^{\,m} - AK_x \frac{\partial E_n^{\,m}}{\partial x} \right) = Q_{En}(x_b, t) \;\Rightarrow\; B_i = \left[nQE_n^{\,m} - Q_{En}(x_b, t) \right] \Big/ A1_{ii} \qquad \textbf{(3.5.9.1.89)}$$

Neumann boundary condition

$$-nAK_x \frac{\partial E_n^{\,m}}{\partial x} = Q_{En}(x_b, t) \;\Rightarrow\; B_i = -Q_{En}(x_b, t) \qquad \textbf{(3.5.9.1.90)}$$

Equation (3.5.9.1.61) can be written as matrix equation as following

$$\begin{aligned} &\frac{[U]}{\Delta\tau}\left\{E_n^{\,n+1/2}\right\} + W_1[QE^{n+1}]\left\{E_n^{\,n+1/2}\right\} + W_1\left[K^{n+1}\right]\left\{E_n^{\,n+1/2}\right\} - W_1[QT^{n+1}]\left\{\left(E_n^{\,im}\right)^{n+1/2}\right\} \\ &= \frac{[U]}{\Delta\tau}\left\{E_n^{\,*}\right\} - W_2\left\{\left(KE_n\right)^*\right\} + W_2\left(\left\{D^*\right\} + \left\{T^*\right\}\right) + W_1\left\{R_L^{\,n+1}\right\} + W_2\left\{R_L^{\,*}\right\} + W_1\left\{B^{n+1}\right\} \end{aligned} \qquad \textbf{(3.5.9.1.91)}$$

So that

$$[CMATRX]\left\{E_n^{\,n+1/2}\right\} = \{RLD\} \qquad \textbf{(3.5.9.1.92)}$$

where

$$[CMATRX]=\frac{[U]}{\Delta\tau}+W_1[QE^{n+1}]+W_1\left[K^{n+1}\right]-W_1[QT^{n+1}\frac{E_n^{im}}{E_n}] \quad \textbf{(3.5.9.1.93)}$$

$$\{RLD\}=\frac{[U]}{\Delta\tau}\left\{E_n^*\right\}-W_2\left\{\left(KE_n\right)^*\right\}+W_2\left(\left\{D^*\right\}+\left\{T^*\right\}\right)+W_1\left\{R_L^{n+1}\right\}+W_2\left\{R_L^*\right\}+W_1\left\{B^{n+1}\right\} \quad \textbf{(3.5.9.1.94)}$$

At junctions, if nQ > 0, flow is going from reach to the junction. Assign

$$\left\{RLDW\right\}=\left\{RLD\right\}+\left\{nQE_n^m/A1_{ii}^{n+1}\right\}-W_1\left\{B^{n+1}\right\}-W_2\left\{\left(nK_xA\frac{\partial E_n^m}{\partial x}\right)^n\Big/A1_{ii}^{n+1}\right\} \quad \textbf{(3.5.9.1.95)}$$

Equation (3.5.9.1.89) is modified as

$$[CMATRX]\left\{\mathrm{E_n}^{n+1/2}\right\}+Flux/A1_{ii}=\{RLDW\} \quad \textbf{(3.5.9.1.96)}$$

If nQ < 0, flow is going from junction to the reach, apply equation (3.5.7.1.57),

$$Flux_i=n\left[Q(E_n^m)_i-K_xA\frac{(E_n^m)_J-(E_n^m)_i}{\Delta x}\right] \quad \textbf{(3.5.9.1.97)}$$

So that junction concentration and flux can be solved by the matrix equation assembled with equation (3.5.7.1.48), (3.5.9.1.96) and (3.5.9.1.97).

3.5.9.2 Mixed Predictor-corrector/Operator-Splitting Scheme

The continuity equation for kinetic-variables in advective form is shown as follows.

$$\begin{aligned}A\frac{\partial E_n}{\partial t}+\frac{\partial A}{\partial t}E_n+Q\frac{\partial E_n^m}{\partial x}-\frac{\partial}{\partial x}\left(K_xA\frac{\partial E_n^m}{\partial x}\right)+\left[(S_S+S_R+S_1+S_2+S_I)-\frac{\partial A}{\partial t}\right]E_n^m\\=M_{E_n}^{as}+M_{E_n}^{rs}+M_{E_n}^{os1}+M_{E_n}^{os2}+M_{E_n}^{is}+AR_{E_n}\end{aligned} \quad \textbf{(3.5.9.2.1)}$$

At ($n+1$)-th time step, equation (3.5.9.2.1) is approximated by

$$\begin{aligned}A\frac{(E_n)^{n+1}-(E_n)^n}{\Delta t}+\frac{\partial A}{\partial t}E_n+Q\frac{\partial E_n^m}{\partial x}-\frac{\partial}{\partial x}\left(K_xA\frac{\partial E_n^m}{\partial x}\right)+\left[(S_S+S_R+S_1+S_2+S_I)-\frac{\partial A}{\partial t}\right]E_n^m\\=M_{E_n}^{as}+M_{E_n}^{rs}+M_{E_n}^{os1}+M_{E_n}^{os2}+M_{E_n}^{is}+AR_{E_n}\end{aligned} \quad \textbf{(3.5.9.2.2)}$$

According to Mixed Predictor-corrector/Operator-Splitting Scheme, equation (3.5.9.2.2) can be separated into two equations as follows

$$\begin{aligned}A\frac{(E_n^m)^{n+1/2}-(E_n^m)^n}{\Delta t}+\frac{\partial A}{\partial t}E_n^m+Q\frac{\partial E_n^m}{\partial x}-\frac{\partial}{\partial x}\left(K_xA\frac{\partial E_n^m}{\partial x}\right)+\left[(S_S+S_R+S_1+S_2+S_I)-\frac{\partial A}{\partial t}\right]E_n^m\\=M_{E_n}^{as}+M_{E_n}^{rs}+M_{E_n}^{os1}+M_{E_n}^{os2}+M_{E_n}^{is}+AR_{E_n}^{\ n}-\frac{\partial A}{\partial t}(E_n^{im})^n\end{aligned} \quad \textbf{(3.5.9.2.3)}$$

$$\frac{E_n^{n+1}-[(E_n^m)^{n+1/2}+(E_n^{im})^n]}{\Delta t}=R_{E_n}^{\ n+1}-R_{E_n}^{\ n}-\frac{\partial(\ell nA)}{\partial t}(E_n^{im})^{n+1}+\frac{\partial(\ell nA)}{\partial t}(E_n^{im})^n \quad \textbf{(3.5.9.2.4)}$$

First, solve equation (3.5.9.2.3) and get $(E_n{}^m)^{n+1/2}$. Second, solve equation (3.5.9.2.4) together with algebraic equations for equilibrium reactions using BIOGEOCHEM scheme to obtain the individual species concentration.

To solve equation (3.5.9.2.3), assign and calculate R_{HSn} and L_{HSn} the same as that in section (3.5.7.2). Equation (3.5.9.2.3) is then simplified as

$$A\frac{(E_n{}^m)^{n+1/2}-(E_n{}^m)^n}{\Delta t}+\frac{\partial A}{\partial t}E_n^m+Q\frac{\partial E_n{}^m}{\partial x}-\frac{\partial}{\partial x}\left(K_xA\frac{\partial E_n{}^m}{\partial x}\right)+L_{HS_n}E_n{}^m=R_{HS_n}+AR_n{}^n-\frac{\partial A}{\partial t}(E_n^{im})^n \qquad \textbf{(3.5.9.2.5)}$$

Assign the true transport velocity V_{true} as follows.

$$AV_{true}=Q \qquad \textbf{(3.5.9.2.6)}$$

Then equation (3.5.9.2.5) is simplified as

$$A\frac{(E_n{}^m)^{n+1/2}-(E_n{}^m)^n}{\Delta t}+AV_{true}\frac{\partial E_n{}^m}{\partial x}-\frac{\partial}{\partial x}\left(K_xA\frac{\partial E_n{}^m}{\partial x}\right)+\left(L_{HS_n}+\frac{\partial A}{\partial t}\right)E_n{}^m=R_{HS_n}+AR_{E_n}{}^n-\frac{\partial A}{\partial t}(E_n^{im})^n \qquad \textbf{(3.5.9.2.7)}$$

Equation (3.5.9.2.7) in the Lagrangian and Eulerian form is as follows.

$$\frac{dE_n{}^m}{d\tau}=\frac{(E_n{}^m)^{n+1/2}-(E_n{}^m)^n}{\Delta t}+V_{true}\frac{\partial E_n{}^m}{\partial x}=0 \qquad \textbf{(3.5.9.2.8)}$$

$$A\frac{dE_n{}^m}{d\tau}-\frac{\partial}{\partial x}\left(K_xA\frac{\partial E_n{}^m}{\partial x}\right)+\left(L_{HS_n}+\frac{\partial A}{\partial t}\right)E_n{}^m=R_{HS_n}+AR_{E_n}{}^n-\frac{\partial A}{\partial t}(E_n^{im})^n \qquad \textbf{(3.5.9.2.9)}$$

First, solve equation (3.5.9.2.8) to obtain the Lagrangian values by particle tracking. Then, deal with Eulerian equation (3.5.9.2.9) by finite element method.

Equation (3.5.9.2.9) written in a slightly different form is shown as follows.

$$\frac{dE_n{}^m}{d\tau}-D+K*E_n{}^m=R_L \qquad \textbf{(3.5.9.2.10)}$$

where

$$D=\frac{1}{A}\frac{\partial}{\partial x}\left(K_xA\frac{\partial E_n{}^m}{\partial x}\right) \qquad \textbf{(3.5.9.2.11)}$$

$$K=\frac{\left(L_{HS_n}+\frac{\partial A}{\partial t}\right)}{A} \qquad \textbf{(3.5.9.2.12)}$$

$$R_L=\frac{R_{HS_n}+AR_{E_n}{}^n-\frac{\partial A}{\partial t}(E_n^{im})^n}{A} \qquad \textbf{(3.5.9.2.13)}$$

Equation (3.5.9.2.10) written in matrix form is then expressed as

$$\frac{[U]}{\Delta\tau}\left\{\left(E_n^{\,m}\right)^{n+1/2}\right\}-W_1\left\{D^{n+1}\right\}+W_1\left[K^{n+1}\right]\left\{\left(E_n^{\,m}\right)^{n+1/2}\right\}=$$
$$\frac{[U]}{\Delta\tau}\left\{\left(E_n^{\,m}\right)^{*}\right\}+W_2\left\{D^{*}\right\}-W_2\left\{\left(KE_n^{\,m}\right)^{*}\right\}+W_1\left\{R_L^{\,n+1}\right\}+W_2\left\{R_L^{\,*}\right\} \quad \textbf{(3.5.9.2.14)}$$

According to section 3.5.9.1,

$$\{D\}=-[QE]\left\{E_n^{\,m}\right\}+\{B\} \quad \textbf{(3.5.9.2.15)}$$

where *[QE*] and {*B*} are the same as those in section 3.5.9.1.

Equation (3.5.9.2.14) can be written as matrix equation as following

$$\frac{[U]}{\Delta\tau}\left\{\left(E_n^{\,m}\right)^{n+1/2}\right\}+W_1[QE^{n+1}]\left\{\left(E_n^{\,m}\right)^{n+1/2}\right\}+W_1\left[K^{n+1}\right]\left\{\left(E_n^{\,m}\right)^{n+1/2}\right\}$$
$$=\frac{[U]}{\Delta\tau}\left\{\left(E_n^{\,m}\right)^{*}\right\}-W_2\left\{\left(KE_n^{\,m}\right)^{*}\right\}+W_2\left\{D^{*}\right\}+W_1\left\{R_L^{\,n+1}\right\}+W_2\left\{R_L^{\,*}\right\}+W_1\left\{B^{n+1}\right\} \quad \textbf{(3.5.9.2.16)}$$

So that

$$[CMATRX]\left\{\left(E_n^{\,m}\right)^{n+1/2}\right\}=\{RLD\} \quad \textbf{(3.5.9.2.17)}$$

where

$$[CMATRX]=\frac{[U]}{\Delta\tau}+W_1[QE^{n+1}]+W_1\left[K^{n+1}\right] \quad \textbf{(3.5.9.2.18)}$$

$$\{RLD\}=\frac{[U]}{\Delta\tau}\left\{\left(E_n^{\,m}\right)^{*}\right\}-W_2\left\{\left(KE_n^{\,m}\right)^{*}\right\}+W_2\left\{D^{*}\right\}+W_1\left\{R_L^{\,n+1}\right\}+W_2\left\{R_L^{\,*}\right\}+W_1\left\{B^{n+1}\right\} \quad \textbf{(3.5.9.2.19)}$$

At junctions, if $nQ > 0$, flow is going from reach to the junction. Assign

$$\left\{RLDW\right\}=\left\{RLD\right\}+\left\{nQE_n^{\,m}/A1_{ii}^{\,n+1}\right\}-W_1\left\{B^{n+1}\right\}-W_2\left\{\left(nK_xA\frac{\partial E_n^{\,m}}{\partial x}\right)^{n}\Big/A1_{ii}^{\,n+1}\right\} \quad \textbf{(3.5.9.2.20)}$$

Equation (3.5.9.1.17) is modified as

$$[CMATRX]\left\{(E_n^{\,m})^{n+1/2}\right\}+Flux/A1_{ii}=\{RLDW\} \quad \textbf{(3.5.9.2.21)}$$

If nQ < 0, flow is going from junction to the reach, apply equation (3.5.7.1.37),

$$Flux_i=n\left[Q(E_n^{\,m})_i-K_xA\frac{(E_n^{\,m})_j-(E_n^{\,m})_i}{\Delta x}\right] \quad \textbf{(3.5.9.2.22)}$$

Junction concentration can be solved by the matrix equation assembled with equation (3.5.7.2.32), (3.5.9.2.21) and (3.5.9.2.22).

3.5.9.3 Operator-Splitting

The continuity equation for kinetic-variables in advective form is shown as follows.

$$A\frac{\partial E_n}{\partial t}+\frac{\partial A}{\partial t}E_n+Q\frac{\partial E_n{}^m}{\partial x}-\frac{\partial}{\partial x}\left(K_xA\frac{\partial E_n{}^m}{\partial x}\right)+\left[(S_S+S_R+S_1+S_2+S_I)-\frac{\partial A}{\partial t}\right]E_n{}^m$$
$$=M_{E_n}{}^{as}+M_{E_n}{}^{rs}+M_{E_n}{}^{os1}+M_{E_n}{}^{os2}+M_{E_n}{}^{is}+AR_{E_n} \qquad \textbf{(3.5.9.3.1)}$$

At n+1-th time step, equation (3.5.9.3.1) is approximated by

$$A\frac{(E_n)^{n+1}-(E_n)^n}{\Delta t}+\frac{\partial A}{\partial t}E_n+Q\frac{\partial E_n{}^m}{\partial x}-\frac{\partial}{\partial x}\left(K_xA\frac{\partial E_n{}^m}{\partial x}\right)+\left[(S_S+S_R+S_1+S_2+S_I)-\frac{\partial A}{\partial t}\right]E_n{}^m$$
$$=M_{E_n}{}^{as}+M_{E_n}{}^{rs}+M_{E_n}{}^{os1}+M_{E_n}{}^{os2}+M_{E_n}{}^{is}+AR_{E_n} \qquad \textbf{(3.5.9.3.2)}$$

According to Operator-splitting scheme, equation (3.5.9.3.2) can be separated into two equations as follows

$$A\frac{(E_n{}^m)^{n+1/2}-(E_n{}^m)^n}{\Delta t}+\frac{\partial A}{\partial t}E_n^m+Q\frac{\partial E_n{}^m}{\partial x}-\frac{\partial}{\partial x}\left(K_xA\frac{\partial E_n{}^m}{\partial x}\right)+\left[(S_S+S_R+S_1+S_2+S_I)-\frac{\partial A}{\partial t}\right]E_n{}^m$$
$$=M_{E_n}{}^{as}+M_{E_n}{}^{rs}+M_{E_n}{}^{os1}+M_{E_n}{}^{os2}+M_{E_n}{}^{is} \qquad \textbf{(3.5.9.3.3)}$$

$$\frac{(E_n)^{n+1}-[(E_n{}^m)^{n+1/2}+(E_n{}^{im})^n]}{\Delta t}=AR_{E_n}{}^{n+1}-\frac{\partial(\ell nA)}{\partial t}(E_n^{im})^{n+1} \qquad \textbf{(3.5.9.3.4)}$$

First, solve equation (3.5.9.3.3) and get $(E_n{}^m)^{n+1/2}$. Second, solve equation (3.5.9.3.4) together with algebraic equations for equilibrium reactions using BIOGEOCHEM scheme to obtain the individual species concentration.

To solve equation (3.5.9.3.3), assign and calculate R_{HSn} and L_{HSn} the same as that in section (3.5.8.1). Equation (3.5.9.3.3) is then simplified as

$$A\frac{(E_n{}^m)^{n+1/2}-(E_n{}^m)^n}{\Delta t}+\frac{\partial A}{\partial t}E_n^m+Q\frac{\partial E_n{}^m}{\partial x}-\frac{\partial}{\partial x}\left(K_xA\frac{\partial E_n{}^m}{\partial x}\right)+L_{HS_n}E_n{}^m=R_{HS_n} \qquad \textbf{(3.5.9.3.5)}$$

Assign the true transport velocity V_{true} as follows.

$$AV_{true}=Q \qquad \textbf{(3.5.9.3.6)}$$

Then equation (3.5.9.3.5) is simplified as

$$A\frac{(E_n{}^m)^{n+1/2}-(E_n{}^m)^n}{\Delta t}+AV_{true}\frac{\partial E_n{}^m}{\partial x}-\frac{\partial}{\partial x}\left(K_xA\frac{\partial E_n{}^m}{\partial x}\right)+\left(L_{HS_n}+\frac{\partial A}{\partial t}\right)E_n{}^m=R_{HS_n} \qquad \textbf{(3.5.9.3.7)}$$

Equation (3.5.9.3.7) in the Lagrangian and Eulerian form is as follows.

$$\frac{dE_n{}^m}{d\tau}=\frac{(E_n{}^m)^{n+1/2}-(E_n{}^m)^n}{\Delta t}+V_{true}\frac{\partial E_n{}^m}{\partial x}=0 \qquad \textbf{(3.5.9.3.8)}$$

$$A\frac{dE_n{}^m}{d\tau}-\frac{\partial}{\partial x}\left(K_xA\frac{\partial E_n{}^m}{\partial x}\right)+\left(L_{HS_n}+\frac{\partial A}{\partial t}\right)E_n{}^m=R_{HS_n} \qquad \textbf{(3.5.9.3.9)}$$

First, solve equation (3.5.9.3.8) to obtain the lagrangian values by particle tracking. Then, deal with Eulerian equation (3.5.9.3.9) by finite element method.

Equation (3.5.9.3.9) written in a slightly different form is shown as follows.

$$\frac{dE_n^{\ m}}{d\tau} - D + K * E_n^{\ m} = R_L \qquad \textbf{(3.5.9.3.10)}$$

where

$$D = \frac{1}{A}\frac{\partial}{\partial x}\left(K_x A \frac{\partial E_n^{\ m}}{\partial x} \right) \qquad \textbf{(3.5.9.3.11)}$$

$$K = \frac{\left(L_{HS_n} + \frac{\partial A}{\partial t} \right)}{A} \qquad \textbf{(3.5.9.3.12)}$$

$$R_L = \frac{R_{HS_n}}{A} \qquad \textbf{(3.5.9.3.13)}$$

Equation (3.5.9.3.10) written in matrix form is then expressed as

$$\begin{aligned} &\frac{[U]}{\Delta\tau}\left\{\left(E_n^{\ m}\right)^{n+1/2}\right\} - W_1\left\{D^{n+1}\right\} + W_1\left[K^{n+1}\right]\left\{\left(E_n^{\ m}\right)^{n+1/2}\right\} = \\ &\frac{[U]}{\Delta\tau}\left\{\left(E_n^{\ m}\right)^{*}\right\} + W_2\left\{D^{*}\right\} - W_2\left\{\left(KE_n^{\ m}\right)^{*}\right\} + W_1\left\{R_L^{\ n+1}\right\} + W_2\left\{R_L^{\ *}\right\} \end{aligned} \qquad \textbf{(3.5.9.3.14)}$$

According to section 3.5.9.1,

$$\{D\} = -[QE]\left\{E_n^{\ m}\right\} + \{B\} \qquad \textbf{(3.5.9.3.15)}$$

where $[QE]$ and $\{B\}$ are the same as those in section 3.5.9.1.

Equation (3.5.9.3.14) can be written as matrix equation as following

$$\begin{aligned} &\frac{[U]}{\Delta\tau}\left\{\left(E_n^{\ m}\right)^{n+1/2}\right\} + W_1[QE^{n+1}]\left\{\left(E_n^{\ m}\right)^{n+1/2}\right\} + W_1\left[K^{n+1}\right]\left\{\left(E_n^{\ m}\right)^{n+1/2}\right\} \\ &= \frac{[U]}{\Delta\tau}\left\{\left(E_n^{\ m}\right)^{*}\right\} - W_2\left\{\left(KE_n^{\ m}\right)^{*}\right\} + W_2\left\{D^{*}\right\} + W_1\left\{R_L^{\ n+1}\right\} + W_2\left\{R_L^{\ *}\right\} + W_1\left\{B^{n+1}\right\} \end{aligned} \qquad \textbf{(3.5.9.3.16)}$$

So that

$$[CMATRX]\left\{\left(E_n^{\ m}\right)^{n+1/2}\right\} = \{RLD\} \qquad \textbf{(3.5.9.3.17)}$$

where

$$[CMATRX] = \frac{[U]}{\Delta\tau} + W_1[\mathrm{QE}^{\mathrm{n+1}}] + W_1\left[K^{n+1}\right] \qquad \textbf{(3.5.9.3.18)}$$

$$\{RLD\} = \frac{[U]}{\Delta\tau}\left\{\left(E_n^{\ m}\right)^{*}\right\} - W_2\left\{\left(KE_n^{\ m}\right)^{*}\right\} + W_2\left\{D^{*}\right\} + W_1\left\{R_L^{\ n+1}\right\} + W_2\left\{R_L^{\ *}\right\} + W_1\left\{\mathrm{B}^{\mathrm{n+1}}\right\} \qquad \textbf{(3.5.9.3.19)}$$

At junctions, if $nQ > 0$, flow is going from reach to the junction. Assign

$$\{RLDW\} = \{RLD\} + \left\{nQE_n^{\ m} / A1_{ii}^{\ n+1}\right\} - W_1\left\{B^{n+1}\right\} - W_2\left\{\left(nK_x A \frac{\partial E_n^{\ m}}{\partial x} \right)^n \Big/ A1_{ii}^{\ n+1}\right\} \qquad \textbf{(3.5.9.3.20)}$$

Equation (3.5.9.1.19) is modified as

$$[CMATRX]\left\{(E_n^{\,m})^{n+1/2}\right\} + Flux/A1_{ii} = \{RLDW\} \qquad \textbf{(3.5.9.3.21)}$$

If $nQ < 0$, flow is going from junction to the reach, apply equation (3.5.7.1.37),

$$Flux_i = n\left[Q(E_n^{\,m})_i - K_x A\frac{(E_n^{\,m})_j - (E_n^{\,m})_i}{\Delta x}\right] \qquad \textbf{(3.5.9.3.22)}$$

Junction concentration can be solved by the matrix equation assembled with equation (3.5.7.3.32), (3.5.9.3.21) and (3.5.9.3.22).

3.5.10 Application of the Lagrangian-Eulerian Approach for All Interior Nodes and Downstream Boundary Nodes with the Finite Element Method Applied to the Conservative Form of the Transport Equations for the Upstream Flux Boundaries to Solve 1-D Kinetic Variable Transport

3.5.10.1 Fully-Implicit Scheme

For this option, the matrix equation for interior and downstream boundary nodes is obtained through the same procedure as that in section 3.5.9.1, and the matrix equation for junction and upstream boundary nodes is obtained through the same procedure as that in section 3.5.7.1.

3.5.10.2 Mixed Predictor-Corrector and Operator-Splitting Method

For this option, the matrix equation for interior and downstream boundary nodes is obtained through the same procedure as that in section 3.5.9.2, and the matrix equation for junction and upstream boundary nodes is obtained through the same procedure as that in section 3.5.7.2.

3.5.10.3 Operator-Splitting Approach

For this option, the matrix equation for interior and downstream boundary nodes is obtained through the same procedure as that in section 3.5.9.3, and the matrix equation for junction and upstream boundary nodes is obtained through the same procedure as that in section 3.5.7.3.

3.5.11 Application of the Lagrangian-Eulerian Approach for All Interior Nodes and Downstream Boundary Nodes with the Finite Element Method Applied to the Advective Form of the Transport Equations for the Upstream Flux Boundaries to Solve 1-D Kinetic Variable Transport

3.5.11.1 Fully-Implicit Scheme

For this option, the matrix equation for interior and downstream boundary nodes is obtained through the same procedure as that in section 3.5.9.1, and the matrix equation for junction and upstream boundary nodes is obtained through the same procedure as that in section 3.5.8.1.

3.5.11.2 Mixed Predictor-Corrector and Operator-Splitting Method

For this option, the matrix equation for interior and downstream boundary nodes is obtained through the same procedure as that in section 3.5.9.2, and the matrix equation for junction and upstream boundary nodes is obtained through the same procedure as that in section 3.5.8.2.

3.5.11.3 Operator-Splitting Approach

For this option, the matrix equation for interior and downstream boundary nodes is obtained through the same procedure as that in section 3.5.9.3, and the matrix equation for junction and upstream boundary nodes is obtained through the same procedure as that in section 3.5.8.3

3.6 Solving Two-Dimensional Overland Water Quality Transport Equations

In this section, we present the numerical approaches employed to solve the governing equations of reactive chemical transport. Ideally, one would like to use a numerical approach that is accurate, efficient, and robust. Depending on the specific problem at hand, different numerical approaches may be more suitable. For research applications, accuracy is a primary requirement, because one does not want to distort physics due to numerical errors. On the other hand, for large field-scale problems, efficiency and robustness are primary concerns as long as accuracy remains within the bounds of uncertainty associated with model parameters. Thus, to provide accuracy for research applications and efficiency and robustness for practical applications, three coupling strategies were investigated to deal with reactive chemistry. They are: (1) a fully-implicit scheme, (2) a mixed predictor-corrector/operator-splitting method, and (3) an operator-splitting method. For each time-tep, we first solve the advective-dispersive transport equation with or without reaction terms, kinetic-variable by kinetic-variable. We then solve the reactive chemical system node-by-node to yield concentrations of all species.

Five numerical options are provided to solve the advective-dispersive transport equations: Option 1- application of the Finite Element Method (FEM) to the conservative form of the transport equations, Option 2 - application of the FEM to the advective form of the transport equations, Option 3 - application of the modified Lagrangian-Eulerian (LE) approach to the Largrangian form of the transport equations, Option 4 - LE approach for all interior nodes and downstream boundary nodes with the FEM applied to the conservative form of the transport equations for the upstream flux boundaries, and Option 5 - LE approach for all interior and downstream boundary nodes with the FEM applied to the advective form of the transport equations for upstream flux boundaries.

3.6.1 Two-Dimensional Bed Sediment Balance Equation

At n+1-th time step, the continuity equation for 2-D bed sediment transport, equation (3.2.1), is approximated as

$$\frac{M_n^{n+1} - M_n^{n}}{\Delta t} \approx W_1(D_n^{n+1} - R_n^{n+1}) + W_2(D_n^{n} - R_n^{n}) \tag{3.6.1.1}$$

So that

$$M_n^{n+1} = M_n^{n} + W_1\left(D_n^{n+1} - R_n^{n+1}\right)\Delta t + W_2\left(D_n^{n} - R_n^{n}\right)\Delta t \tag{3.6.1.2}$$

If the calculated $M_n^{n+1} < 0$, assign $M_n^{n+1} = 0$, so that

$$R_n^{n+1} \approx \left(M_n^{n} - M_n^{n+1}\right)/\left(W_1\Delta t\right) + W_2\left(D_n^{n} - R_n^{n}\right)/W_1 + D_n^{n+1} \tag{3.6.1.3}$$

3.6.2 Application of the Finite Element Method to the Conservative Form of the Transport Equations to Solve 2-D Suspended Sediment Transport

Recall the governing equation for 2-D suspended sediment transport, equation (2.6.10), as follows

$$\frac{\partial(hS_n)}{\partial t} + \nabla\cdot(\mathbf{q}S_n) - \nabla\cdot(h\mathbf{K}\cdot\nabla S_n) = M_{S_n^{as}} + M_{S_n^{rs}} + R_n - D_n,\ n\in[1,N_s] \tag{3.6.2.1}$$

Assign and calculate the right hand side term R_{HS} and left hand side term L_{HS} as follows.

$$\begin{aligned} &Assign\ \ L_{HS} = 0\ \ and\ \ R_{HS} = R_n - D_n \qquad then\ continuously\ calculate \\ &(1):\ \ If\ \ S_S \le 0,\ \ L_{HS} = L_{HS} - S_S,\ \ ELSE\ \ \ R_{HS} = R_{HS} + S_S * S_n^{as} \\ &(2):\ \ If\ \ S_R \le 0,\ \ L_{HS} = L_{HS} - S_R,\ \ ELSE\ \ \ R_{HS} = R_{HS} + S_R * S_n^{rs} \end{aligned} \tag{3.6.2.2}$$

where S_n^{as} is the concentration of the *n*-th fraction suspended sediment in the artificial source and S_n^{rs} is the concentration of the *n*-th fraction suspended sediment in the rainfall source. Then equation (3.6.2.1) is modified as

$$\frac{\partial(hS_n)}{\partial t} + \nabla\cdot(\mathbf{q}S_n) - \nabla\cdot(h\mathbf{K}\cdot\nabla S_n) + L_{HS} * S_n = R_{HS} \tag{3.6.2.3}$$

Use Galerkin or Petrov-Galerkin finite-element method for the spatial descretization of transport equation: choose weighting function identical to base function. For Petriov-Galerkin method, apply weighting function one-order higher than the base function to advection term. Integrate equation (3.6.2.3) in the spatial dimensions over the entire region as follows.

$$\int_R N_i\left[\frac{\partial(hS_n)}{\partial t} - \nabla\cdot(h\mathbf{K}\cdot\nabla S_n) + L_{HS} * S_n\right] dR + \int_R W_i\nabla\cdot(\mathbf{q}S_n)\ dR = \int_R N_i R_{HS}\ dR \tag{3.6.2.4}$$

Further, we obtain

$$\begin{aligned} &\int_R N_i \frac{\partial(hS_n)}{\partial t}\ dR - \int_R \nabla W_i\cdot\mathbf{q}S_n\ dR + \int_R \nabla N_i\cdot(h\mathbf{K}\cdot\nabla S_n)\ dR + \int_R N_i\ L_{HS} * S_n dR \\ &\qquad = \int_R N_i\ R_{HS} dR - \int_B \mathbf{n}\cdot W_i\mathbf{q}S_n\ dB + \int_B \mathbf{n}\cdot N_i(h\mathbf{K}\cdot\nabla S_n)\ dB \end{aligned} \tag{3.6.2.5}$$

Approximate solution S_n by a linear combination of the base functions as shown by equation (3.6.2.6).

$$S_n \approx \hat{S}_n = \sum_{j=1}^{N} S_{nj}(t) N_j(R) \tag{3.6.2.6}$$

Substituting equation (3.6.2.6) into equation (3.6.2.5), we obtain

$$\begin{aligned} &\sum_{j=1}^{N}\left\{\left[\int_R N_i\left(\frac{\partial h}{\partial t}+L_{HS}\right)N_j\ dR-\int_R \nabla W_i\cdot\mathbf{q}N_j\ dR+\int_R \nabla N_i\cdot h\mathbf{K}\cdot\nabla N_j\ dR\right]S_{nj}(t)\right\} \\ &+\sum_{j=1}^{N}\left[\left(\int_R N_i h N_j\ dR\right)\frac{dS_{nj}(t)}{dt}\right]=\int_R N_i R_{HS}\ dR-\int_B \mathbf{n}\cdot(W_i\mathbf{q}S_n-N_i h\mathbf{K}\cdot\nabla S_n)dB \end{aligned} \tag{3.6.2.7}$$

Equation (3.6.2.7) can be written in matrix form as

$$[CMATRX1]\left\{\frac{dS_n}{dt}\right\}+([Q1]+[Q2]+[Q3])\{S_n\}=\{SS\}+\{B\} \tag{3.6.2.8}$$

where the matrices [CMATRX1], [Q1], [Q2], [Q3] and load vectors {RLD}, and {B} are given by

$$CMATRX1_{ij}=\int_R N_i h N_j dR \tag{3.6.2.9}$$

$$Q1_{ij}=\int_R N_i\left(\frac{\partial h}{\partial t}+L_{HS}\right)N_j dR \tag{3.6.2.10}$$

$$Q2_{ij}=-\int_R \nabla W_i\cdot\mathbf{q}N_j dR \tag{3.6.2.11}$$

$$Q3_{ij}=-\int_R \nabla N_i\cdot h\mathbf{K}\cdot\nabla N_j dR \tag{3.6.2.12}$$

$$SS_{ij}=\int_R N_i R_{HS} dR \tag{3.6.2.13}$$

$$B_i=-\int_B n\cdot(W_i\mathbf{q}S_n-N_i h\mathbf{K}\cdot\nabla S_n)dB \tag{3.6.2.14}$$

where all the integrations are evaluated with the corresponding time weighting values.

At n+1-th time step, equation (3.6.2.8) is approximated as

$$[CMATRX1]\left\{\frac{S_n{}^{n+1}-S_n{}^{n}}{\Delta t}\right\}+[CMATRX2]\{W_1 S_n{}^{n+1}+W_2 S_n{}^{n}\}=\{SS\}+\{B\} \tag{3.6.2.15}$$

where

$$[CMATRX2]=[Q1]+[Q2]+[Q3] \tag{3.6.2.16}$$

So that

$$[CMATRX]\{S_n{}^{n+1}\}=\{RLD\}+\{QB\} \tag{3.6.2.17}$$

where

$$[CMATRX]=\frac{[CMATRX1]}{\Delta t}+W_1[CMATRX2] \tag{3.6.2.18}$$

$$\{RLD\} = \left(\frac{[CMATRX1]}{\Delta t} - W_2[CMATRX2] \right) \{S_n{}^n\} + \{SS\} \qquad \textbf{(3.6.2.19)}$$

For interior nodes i, B_i is zero, for boundary nodes i = b, B_i is calculated according to the specified boundary condition and shown as follows.

Dirichlet boundary condition

$$S_n = S_n(x_b, y_b, t) \qquad \textbf{(3.6.2.20)}$$

Variable boundary condition

< Case 1 > Flow is going in from outside ($\mathbf{n} \cdot \mathbf{q} < 0$).

$$\mathbf{n} \cdot \left(\mathbf{q} S_n - h\mathbf{K} \cdot \nabla S_n \right) = \mathbf{n} \cdot \mathbf{q} S_n(x_b, y_b, t) \;\; \Rightarrow \;\; B_i = -\int_B \mathbf{n} \cdot W_i \mathbf{q} S_n(x_b, y_b, t) dB \qquad \textbf{(3.6.2.21)}$$

< Case 2 > Flow is going out from inside ($\mathbf{n} \cdot \mathbf{q} > 0$).

$$-\mathbf{n} \cdot \left(h\mathbf{K} \cdot \nabla S_n \right) = 0 \;\; \Rightarrow \;\; B_i = -\int_B \mathbf{n} \cdot W_i \mathbf{q} S_n dB \qquad \textbf{(3.6.2.22)}$$

Cauchy boundary condition

$$\mathbf{n} \cdot \left(\mathbf{q} S_n - h\mathbf{K} \cdot \nabla S_n \right) = Q_{Sn}(x_b, y_b, t) \;\; \Rightarrow \;\; B_i = -\int_B W_i Q_{Sn}(x_b, y_b, t) dB \qquad \textbf{(3.6.2.23)}$$

Neumann boundary condition

$$-\mathbf{n} \cdot \left(h\mathbf{K} \cdot \nabla S_n \right) = Q_{Sn}(x_b, y_b, t) \;\; \Rightarrow \;\; B_i = -\int_B \mathbf{n} \cdot W_i \mathbf{q} S_n dB + \int_B N_i Q_{Sn}(x_b, y_b, t) dB \qquad \textbf{(3.6.2.24)}$$

River/stream-overland interface boundary condition

$$\begin{aligned} &\mathbf{n} \cdot \left(\mathbf{q} S_n - h\mathbf{K} \cdot \nabla S_n \right) = (\mathbf{n} \cdot \mathbf{q}) \frac{1}{2} \left\{ \left[1 + sign(\mathbf{n} \cdot \mathbf{q}) \right] S_n + \left[1 - sign(\mathbf{n} \cdot \mathbf{q}) \right] S_n^{1D}(x_b, y_b, t) \right\} \\ &\Rightarrow \;\; B_i = -\int_B W_i (\mathbf{n} \cdot \mathbf{q}) \frac{1}{2} \left\{ \left[1 + sign(\mathbf{n} \cdot \mathbf{q}) \right] S_n + \left[1 - sign(\mathbf{n} \cdot \mathbf{q}) \right] S_n^{1D}(x_b, y_b, t) \right\} dB \end{aligned} \qquad \textbf{(3.6.2.25)}$$

3.6.3 Application of the Finite Element Method to the Advective Form of the Transport Equations to Solve 2-D Suspended Sediment Transport

Conversion of the governing equation for 2-D suspended sediment transport, equation (2.6.10), to advection form is expressed as

$$h \frac{\partial S_n}{\partial t} + \mathbf{q} \cdot \nabla S_n - \nabla \cdot (h\mathbf{K} \cdot \nabla S_n) + \left(\frac{\partial h}{\partial t} + \nabla \cdot \mathbf{q} \right) S_n = M_{S_n^{as}} + M_{S_n^{rs}} + R_n - D_n \qquad \textbf{(3.6.3.1)}$$

According to governing equation for 2-D water flow, equation (2.2.1), assign and calculate the right-

hand side term R_{HS} and left hand side term L_{HS} as follows.

$$\begin{aligned}&\text{Assign } L_{HS} = S_S + S_R - S_E + S_I \text{ and } R_{HS} = R_n - D_n \quad \text{then continuously calculate}\\&(1):\ If\ S_S \le 0,\ L_{HS} = L_{HS} - S_S,\ ELSE\ \ R_{HS} = R_{HS} + S_S * S_n^{as}\\&(2):\ If\ S_R \le 0,\ L_{HS} = L_{HS} - S_R,\ ELSE\ \ R_{HS} = R_{HS} + S_R * S_n^{rs}\end{aligned} \tag{3.6.3.2}$$

Then equation (3.6.3.1) is modified as

$$h\frac{\partial S_n}{\partial t} + \mathbf{q}\cdot\nabla S_n - \nabla\cdot(h\mathbf{K}\cdot\nabla S_n) + L_{HS} * S_n = R_{HS} \tag{3.6.3.3}$$

Use Galerkin or Petrov-Galerkin finite-element method for the spatial descretization of transport equation. Integrate equation (3.6.3.3) in the spatial dimensions over the entire region as follows.

$$\int_R N_i\left[h\frac{\partial S_n}{\partial t} - \nabla\cdot(h\mathbf{K}\cdot\nabla S_n) + L_{HS} * S_n\right]dR + \int_R W_i\mathbf{q}\cdot\nabla S_n dR = \int_R N_i R_{HS} dR \tag{3.6.3.4}$$

Further, we obtain

$$\begin{aligned}&\int_R N_i h\frac{\partial S_n}{\partial t}dR + \int_R W_i\mathbf{q}\cdot\nabla S_n dR + \int_R \nabla N_i\cdot(h\mathbf{K}\cdot\nabla S_n)\,dR + \int_R N_i\ L_{HS} * S_n dR\\&\qquad = \int_R N_i R_{HS} dR + \int_B \mathbf{n}\cdot N_i(h\mathbf{K}\cdot\nabla S_n)\,dB\end{aligned} \tag{3.6.3.5}$$

Approximate solution S_n by a linear combination of the base functions as shown by equation (3.6.3.6).

$$S_n \approx \hat{S}_n = \sum_{j=1}^{N} S_{nj}(t)N_j(R) \tag{3.6.3.6}$$

Substituting equation (3.6.3.6) into equation (3.6.3.5), we obtain

$$\begin{aligned}&\sum_{j=1}^{N}\left\{\left[\int_R N_i L_{HS} N_j dR + \int_R W_i\mathbf{q}\cdot\nabla N_j dR + \int_R \nabla N_i\cdot\left(h\mathbf{K}\cdot\nabla N_j\right)dR\right]S_{nj}(t)\right\}\\&+\sum_{j=1}^{N}\left[\left(\int_R N_i h N_j dR\right)\frac{dS_{nj}(t)}{dt}\right] = \int_R N_i R_{HS} dR + \int_B \mathbf{n}\cdot(N_i h\mathbf{K}\cdot\nabla S_n)dB\end{aligned} \tag{3.6.3.7}$$

Equation (3.6.3.7) can be written in matrix form as

$$[CMATRX1]\left\{\frac{dS_n}{dt}\right\} + ([Q1] + [Q2] + [Q3])\{S_n\} = \{SS\} + \{B\} \tag{3.6.3.8}$$

where the matrices [CMATRX1], [Q1], [Q2], [Q3] and load vectors {RLD}, and {B} are given by

$$CMATRX1_{ij} = \int_R N_i h N_j dR \tag{3.6.3.9}$$

$$Q1_{ij} = \int_R N_i L_{HS} N_j dR \tag{3.6.3.10}$$

$$Q2_{ij} = \int_R W_i\mathbf{q}\cdot\nabla N_j dR \tag{3.6.3.11}$$

$$Q3_{ij} = -\int_R \nabla N_i \cdot h\mathbf{K} \cdot \nabla N_j dR \tag{3.6.3.12}$$

$$SS_{ij} = \int_R N_i R_{HS} dR \tag{3.6.3.13}$$

$$B_i = \int_B \mathbf{n} \cdot (N_i h\mathbf{K} \cdot \nabla S_n) dB \tag{3.6.3.14}$$

where all the integrations are evaluated with the corresponding time weighting values.

At n+1-th time step, equation (3.6.3.8) is approximated as

$$[CMATRX1]\left\{\frac{S_n^{n+1} - S_n^n}{\Delta t}\right\} + [CMATRX2]\{W_1 S_n^{n+1} + W_2 S_n^n\} = \{SS\} + \{B\} \tag{3.6.3.15}$$

where

$$[CMATRX2] = [Q1] + [Q2] + [Q3] \tag{3.6.3.16}$$

So that

$$[CMATRX]\{S_n^{n+1}\} = \{RLD\} + \{QB\} \tag{3.6.3.17}$$

where

$$[CMATRX] = \frac{[CMATRX1]}{\Delta t} + W_1[CMATRX2] \tag{3.6.3.18}$$

$$\{RLD\} = \left(\frac{[CMATRX1]}{\Delta t} - W_2[CMATRX2]\right)\{S_n^n\} + \{SS\} \tag{3.6.3.19}$$

For interior nodes i, B_i is zero, for boundary nodes i = b, B_i is calculated according to the specified boundary condition and shown as follows.

Dirichlet boundary condition

$$S_n = S_n(x_b, y_b, t) \tag{3.6.3.20}$$

Variable boundary condition

< Case 1 > when flow is going in from outside ($\mathbf{n}\cdot\mathbf{q} < 0$)

$$\mathbf{n}\cdot\left(\mathbf{q}S_n - h\mathbf{K}\cdot\nabla S_n\right) = \mathbf{n}\cdot\mathbf{q}S_n(x_b, y_b, t) \;\Rightarrow\; B_i = \int_B \mathbf{n}\cdot N_i\mathbf{q}S_n dB - \int_B \mathbf{n}\cdot N_i\mathbf{q}S_n(x_b, y_b, t)dB \tag{3.6.3.21}$$

< Case 2 > Flow is going out from inside ($\mathbf{n}\cdot\mathbf{q} > 0$):

$$-\mathbf{n}\cdot\left(h\mathbf{K}\cdot\nabla S_n\right) = 0 \;\Rightarrow\; B_i = 0 \tag{3.6.3.22}$$

Cauchy boundary condition

$$\mathbf{n}\cdot\left(qS_n - h\mathbf{K}\cdot\nabla S_n\right) = Q_{Sn}(x_b, y_b, t) \;\Rightarrow\; B_i = \int_B N_i\mathbf{n}\cdot\mathbf{q}S_n dB - \int_B N_i Q_{Sn}(x_b, y_b, t)dB \tag{3.6.3.23}$$

Neumann boundary condition

$$-\mathbf{n}\cdot\left(h\mathbf{K}\cdot\nabla S_n\right) = Q_{Sn}(x_b, y_b, t) \;\Rightarrow\; B_i = -\int_B N_i Q_{Sn}(x_b, y_b, t)dB \tag{3.6.3.24}$$

River/stream-overland interface boundary condition

$$\begin{aligned}&\mathbf{n}\cdot\left(\mathbf{q}S_n - h\mathbf{K}\cdot\nabla S_n\right) = \left(\mathbf{n}\cdot\mathbf{q}\right)\frac{1}{2}\left\{\left[1 + sign\left(\mathbf{n}\cdot\mathbf{q}\right)\right]S_n + \left[1 - sign\left(\mathbf{n}\cdot\mathbf{q}\right)\right]S_n^{1D}(x_b, y_b, t)\right\}\\ \Rightarrow\; &B_i = \int_B N_i\mathbf{n}\cdot\mathbf{q}S_n dB - \int_B N_i\left(\mathbf{n}\cdot\mathbf{q}\right)\frac{1}{2}\left\{\left[1 + sign\left(\mathbf{n}\cdot\mathbf{q}\right)\right]S_n + \left[1 - sign\left(\mathbf{n}\cdot\mathbf{q}\right)\right]S_n^{1D}(x_b, y_b, t)\right\}dB\end{aligned} \tag{3.6.3.25}$$

3.6.4 Application of the Modified Lagrangian-Eulerian Approach to the Largrangian Form of the Transport Equations to Solve 2-D Suspended Sediment Transport

Recall governing equation for 2-D suspended sediment transport in advection form, equation (3.6.3.1), as follows

$$h\frac{\partial S_n}{\partial t} + \mathbf{q}\cdot\nabla \mathrm{S_n} - \nabla\cdot(\mathrm{h}\mathbf{K}\cdot\nabla \mathrm{S_n}) + \left(\frac{\partial h}{\partial t} + \nabla\cdot\mathbf{q}\right)\mathrm{S_n} = M_n^{\ as} + R_n - D_n \tag{3.6.4.1}$$

Assign and calculate R_{HS} and L_{HS} in the same way as that in section 3.6.3. Then equation (3.6.4.1) is simplified as

$$h\frac{\partial S_n}{\partial t} + \mathbf{q}\cdot\nabla \mathrm{S_n} - \nabla\cdot(\mathrm{h}\mathbf{K}\cdot\nabla \mathrm{S_n}) + L_{HS} * \mathrm{S_n} = R_{HS} \tag{3.6.4.2}$$

Equation (3.6.4.2) in the Lagrangian and Eulerian form is written as follows.

In lagrangian step,

$$h\frac{dS_n}{d\tau} = h\frac{\partial S_n}{\partial t} + \mathbf{q}\cdot\nabla S_n = 0 \quad \Rightarrow \quad \frac{\partial S_n}{\partial t} + \mathbf{v}\cdot\nabla S_n = 0 \tag{3.6.4.3}$$

where particle-tracking velocity **v** is the flow velocity.

In Eulerian step,

$$h\frac{dS_n}{d\tau} - \nabla\cdot(\mathrm{h}\mathbf{K}\cdot\nabla \mathrm{S_n}) + L_{HS} * \mathrm{S_n} = R_{HS} \tag{3.6.4.4}$$

where $\Delta\tau$ is the tracking time, * corresponds to the previous time step value at the location where node i is tracked through particle tracking in Lagrangian step.

Equation (3.6.4.4) written in a slightly different form is shown as

$$\frac{dS_n}{d\tau} - D + K * \mathrm{S_n} = RL \tag{3.6.4.5}$$

where

$$D = \frac{1}{h}\nabla\cdot(h\mathbf{K}\cdot\nabla S_n) \tag{3.6.4.6}$$

$$K = \frac{L_{HS}}{h} \tag{3.6.4.7}$$

$$RL = \frac{R_{HS}}{h} \tag{3.6.4.8}$$

Equation (3.6.4.5) written in matrix form is then expressed as

$$\begin{aligned} &\frac{[U]}{\Delta\tau}\left\{S_n{}^{n+1}\right\} - W_1\left\{D^{n+1}\right\} + W_1\left[K^{n+1}\right]\left\{S_n{}^{n+1}\right\} = \\ &\frac{[U]}{\Delta\tau}\left\{S_n{}^{*}\right\} + W_2\left\{D^{*}\right\} - W_2\left\{\left(KS_n\right)^{*}\right\} + W_1\left\{RL^{n+1}\right\} + W_2\left\{RL^{*}\right\} \end{aligned} \tag{3.6.4.9}$$

where $[K^{n+1}]$ is a diagonal matrix with K calculated at n+1-th time step as its diagonal components..

The diffusion term D expressed in term of S_n is solved by the following procedure.

Approximate D by a linear combination of the base functions as follows.

$$D \approx \hat{D} = \sum_{j=1}^{N} D_j(t) N_j(R) \tag{3.6.4.10}$$

where N is the number of nodes. According to equation (3.6.4.6), the integration of equation (3.6.4.10) can be written as

$$\int_R N_i h D dR = \int_R N_i h \sum_{j=1}^{N} D_j(t) N_j(R) dR = \int_R N_i \nabla\cdot(h\mathbf{K}\cdot\nabla S_n) dR \tag{3.6.4.11}$$

Further, we obtain

$$\sum_{j=1}^{N}\left[\left(\int_R N_i h N_j dR\right) * D_j\right] = -\int_R \nabla N_i \cdot (h\mathbf{K}\cdot\nabla S_n) dR + \int_B \mathbf{n}\cdot N_i (h\mathbf{K}\cdot\nabla S_n) dB \quad \textbf{(3.6.4.12)}$$

Approximate S_n by a linear combination of the base functions as follows.

$$S_n \approx \widehat{S}_n = \sum_{j=1}^{N} S_{nj}(t) N_j(R) \quad \textbf{(3.6.4.13)}$$

Equation (3.6.4.12) is further expressed as

$$\sum_{j=1}^{N}\left[\left(\int_R N_i h N_j dR\right) * D_j\right] = -\sum_{j=1}^{N}\left[\left(\int_R \nabla N_i \cdot (h\mathbf{K}\cdot\nabla N_j) dR\right) * (S_n)_j\right] + \int_B \mathbf{n}\cdot N_i (h\mathbf{K}\cdot\nabla S_n) dB \quad \textbf{(3.6.4.14)}$$

Assign matrices [QA] and [QD] and load vector {QB} as following.

$$QA_{ij} = \int_R N_i h N_j dR \quad \textbf{(3.6.4.15)}$$

$$QD_{ij} = \int_R \nabla N_i \cdot (h\mathbf{K}\cdot\nabla N_j) dR \quad \textbf{(3.6.4.16)}$$

$$QB_i = \int_B \mathbf{n}\cdot N_i (h\mathbf{K}\cdot\nabla S_n) dB \quad \textbf{(3.6.4.17)}$$

Equation (3.6.4.14) is expressed as

$$[QA]\{D\} = -[QD]\{S_n\} + \{QB\} \quad \textbf{(3.6.4.18)}$$

Lump matrix [QA] into diagonal matrix and update

$$QD_{ij} = QD_{ij} / QA_{ii} \quad \textbf{(3.6.4.19)}$$

$$B_i = QB_i / QA_{ii} \quad \textbf{(3.6.4.20)}$$

Then

$$\{D\} = -[QD]\{S_n\} + \{B\} \quad \textbf{(3.6.4.21)}$$

According to equation (3.6.4.21), Equation (3.6.4.9) can be modified as following

$$[CMATRX]\{S_n^{n+1}\} = \{RLD\} \quad \textbf{(3.6.4.22)}$$

where

$$[CMATRX] = \frac{[U]}{\Delta\tau} + W_1[QD^{n+1}] + W_1\left[K^{n+1}\right] \quad \textbf{(3.6.4.23)}$$

$$\{RLD\} = \frac{[U]}{\Delta\tau}\{S_n^*\} + W_2\{D^*\} - W_2\{(KS_n)^*\} + W_1\{RL^{n+1}\} + W_2\{RL^*\} + W_1\{B^{n+1}\} \quad \textbf{(3.6.4.24)}$$

For interior nodes, the boundary term {B} is zero. For boundary node i = b, {B} should be

calculated as follows.

Dirichlet boundary condition

$$S_n = S_n(x_b, y_b, t) \;\Rightarrow\; B_i = \int_B \mathbf{n} \cdot N_i (h\mathbf{K} \cdot \nabla S_n) dB \Big/ QA_{ii} \tag{3.6.4.25}$$

Variable boundary condition

< Case 1 > when flow is going in from outside ($\mathbf{n} \cdot \mathbf{q} < 0$)

$$\begin{aligned} &\mathbf{n} \cdot (\mathbf{q} S_n - h\mathbf{K} \cdot \nabla S_n) = \mathbf{n} \cdot \mathbf{q} S_n(x_b, y_b, t) \\ \Rightarrow\; &B_i = \int_B \mathbf{n} \cdot N_i \mathbf{q} S_n dB \Big/ QA_{ii} - \int_B \mathbf{n} \cdot N_i \mathbf{q} S_n(x_b, y_b, t) dB \Big/ QA_{ii} \end{aligned} \tag{3.6.4.26}$$

< Case 2 > Flow is going out from inside ($\mathbf{n} \cdot \mathbf{q} > 0$):

$$-\mathbf{n} \cdot (h\mathbf{K} \cdot \nabla S_n) = 0 \;\Rightarrow\; B_i = 0 \tag{3.6.4.27}$$

Cauchy boundary condition

$$\begin{aligned} &\mathbf{n} \cdot (\mathbf{q} S_n - h\mathbf{K} \cdot \nabla S_n) = Q_{Sn}(x_b, y_b, t) \\ \Rightarrow\; &B_i = \int_B N_i \mathbf{n} \cdot \mathbf{q} S_n dB \Big/ QA_{ii} - \int_B N_i Q_{Sn}(x_b, y_b, t) dB \Big/ QA_{ii} \end{aligned} \tag{3.6.4.28}$$

Neumann boundary condition

$$-\mathbf{n} \cdot (h\mathbf{K} \cdot \nabla S_n) = Q_{Sn}(x_b, y_b, t) \;\Rightarrow\; B_i = -\int_B N_i Q_{Sn}(x_b, y_b, t) dB \Big/ QA_{ii} \tag{3.6.4.29}$$

River/stream-overland interface boundary condition

$$\begin{aligned} &\mathbf{n} \cdot (\mathbf{q} S_n - h\mathbf{K} \cdot \nabla S_n) = (\mathbf{n} \cdot \mathbf{q}) \frac{1}{2} \left\{ \left[1 + sign(\mathbf{n} \cdot \mathbf{q}) \right] S_n + \left[1 - sign(\mathbf{n} \cdot \mathbf{q}) \right] S_n^{1D}(x_b, y_b, t) \right\} \\ \Rightarrow\; &B_i = \int_B N_i \mathbf{n} \cdot \mathbf{q} S_n dB \Big/ QA_{ii} - \int_B N_i (\mathbf{n} \cdot \mathbf{q}) \frac{1}{2} \left\{ \left[1 + sign(\mathbf{n} \cdot \mathbf{q}) \right] S_n + \left[1 - sign(\mathbf{n} \cdot \mathbf{q}) \right] S_n^{1D}(x_b, y_b, t) \right\} dB \Big/ QA_{ii} \end{aligned} \tag{3.6.4.30}$$

At upstream flux boundary nodes, equation (3.6.4.9) cannot be applied because $\Delta\tau$ equals zero. Thus, we propose a modified LE approach in which the matrix equation for upstream boundary nodes is obtained by explicitly applying the finite element method to the boundary conditions. Applying FEM at the upstream variable boundary side, we get

$$\int_B N_i \mathbf{n} \cdot (\mathbf{q} S_n - h\mathbf{K} \cdot \nabla S_n) dB = \int_B N_i \mathbf{n} \cdot \mathbf{q} S_n(x_b, y_b, t) dB \tag{3.6.4.31}$$

So that the following matrix equation can be assembled at the upstream variable boundary node

$$[QF]\{S_n\} = [QB]\{B\} \tag{3.6.4.32}$$

in which

$$QF_{ij} = \int_B (N_i \mathbf{n} \cdot \mathbf{q} N_j - N_i \mathbf{n} \cdot h\mathbf{K} \cdot \nabla N_j) dB \quad \textbf{(3.6.4.33)}$$

$$QB_{ij} = \int_B N_i \mathbf{n} \cdot \mathbf{q} N_j dB \quad \textbf{(3.6.4.34)}$$

$$B_i = S_n(x_b, y_b, t) \quad \textbf{(3.6.4.35)}$$

Similarly, equation (3.6.2.32) can be applied to Cauchy boundary with [QB] and {B} defined differently as

$$QB_{ij} = \int_B N_i N_j dB \quad \textbf{(3.6.4.36)}$$

$$B_i = Q_{S_n}(x_b, y_b, t) \quad \textbf{(3.6.4.37)}$$

At upstream river/stream-overland interface boundary, [QB] is calculated by equation (3.6.2.34), and {B} is defined as

$$B_i = S_n^{1D}(x_b, y_b, t) \quad \textbf{(3.6.4.38)}$$

3.6.5 Application of the Lagrangian-Eulerian Approach for All Interior Nodes and Downstream Boundary Nodes with the Finite Element Method Applied to the Conservative Form of the Transport Equations for the Upstream Flux Boundaries to Solve 2-D Suspended Sediment Transport

For this option, the matrix equation for interior and downstream boundary nodes is obtained through the same procedure as that in section 3.6.4, and the matrix equation for upstream boundary nodes is obtained through the same procedure as that in section 3.6.2.

3.6.6 Application of the Lagrangian-Eulerian Approach for All Interior Nodes and Downstream Boundary Nodes with the Finite Element Method Applied to the Advective Form of the Transport Equations for the Upstream Flux Boundaries to Solve 2-D Suspended Sediment Transport

For this option, the matrix equation for interior and downstream boundary nodes is obtained through the same procedure as that in section 3.6.4, and the matrix equation for upstream boundary nodes is obtained through the same procedure as that in section 3.6.3.

3.6.7 Application of the Finite Element Method to the Conservative Form of the Transport Equations to Solve 2-D Kinetic Variable Transport

3.6.7.1 Fully-implicit scheme

Recall the governing equation for 2-D kinetic variable transport, equation (2.6.46), as follows

$$h\frac{\partial E_n}{\partial t}+\frac{\partial h}{\partial t}E_n+\nabla\cdot(\mathbf{q}E_n^{\,m})-\nabla\cdot(h\mathbf{K}\cdot\nabla E_n^{\,m})=M_{E_n^{as}}+M_{E_n^{rs}}+M_{E_n^{is}}+hR_{E_n},\ n\in[1,\ M-N_E] \qquad \textbf{(3.6.7.1.1)}$$

At n+1-th time step, equation (3.6.7.1.1) is approximated by

$$h\frac{(E_n)^{n+1}-(E_n)^n}{\Delta t}+\frac{\partial h}{\partial t}E_n+\nabla\cdot(qE_n^{\,m})-\nabla\cdot(hK\cdot\nabla E_n^{\,m})=M_{E_n^{as}}+M_{E_n^{rs}}+M_{E_n^{is}}+hR_{E_n} \qquad \textbf{(3.6.7.1.2)}$$

where the superscripts n and n+1 represent the time step number. Terms without superscript should be the corresponding average values calculated with time weighting factors W_1 and W_2.

According to Fully-implicit scheme, equation (3.6.7.1.2) can be separated into two equations as follows

$$h\frac{(E_n)^{n+1/2}-(E_n)^n}{\Delta t}+\frac{\partial h}{\partial t}E_n+\nabla\cdot(\mathbf{q}E_n^{\,m})-\nabla\cdot(h\mathbf{K}\cdot\nabla E_n^{\,m})=M_{E_n^{as}}+M_{E_n^{rs}}+M_{E_n^{is}}+hR_{E_n} \qquad \textbf{(3.6.7.1.3)}$$

$$\frac{(E_n)^{n+1}-(E_n)^{n+1/2}}{\Delta t}=0 \qquad \textbf{(3.6.7.1.4)}$$

First, we express $E_n^{\,m}$ in terms of $(E_n^{\,m}/E_n)\cdot E_n$ to make E_n's as primary dependent variables, so that $E_n^{\,n+1/2}$ can be solved through equation (3.6.7.1.3). Second, we solve equation (3.6.7.1.4) together with algebraic equations for equilibrium reactions using BIOGEOCHEM to obtain all individual species concentrations. Iteration between these two steps is needed because the new reaction terms $RA_n^{\,n+1}$ and the equation coefficients in equation (3.6.7.1.3) need to be updated by the calculation results of (3.6.7.1.4). To improve the standard SIA method, the nonlinear reaction terms are approximated by the Newton-Raphson linearization.

To solve equation (3.6.7.1.3), assign

$$R_{HS}=0 \quad and \quad L_{HS}=0 \qquad \textbf{(3.6.7.1.5)}$$

Then the right hand side R_{HS} and left hand side L_{HS} should be continuously calculated as following.

$$M_{E_n}^{\,rs}=\begin{cases}S_R*E_{n^{rs}},\ if\ S_R>0 \ \Rightarrow\ R_{HSn}=R_{HSn}+M_{E_n}^{\,rs}\\ S_R*E_n^{\,m},\ if\ S_R\le 0 \ \Rightarrow\ L_{HSn}=L_{HSn}-S_R\end{cases} \qquad \textbf{(3.6.7.1.6)}$$

$$M_{E_n}^{\,as}=\begin{cases}S_S*E_{n^{as}},\ if\ S_S>0 \ \Rightarrow\ R_{HSn}=R_{HSn}+M_{E_n}^{\,as},\\ S_S*E_n^{\,m},\ if\ S_S\le 0 \ \Rightarrow\ L_{HSn}=L_{HSn}-S_S\end{cases} \qquad \textbf{(3.6.7.1.7)}$$

$$M_{E_n}^{\,is}=\begin{cases}S_I*E_n^{\,m_{\,is}},\ if\ S_I>0 \ \Rightarrow\ R_{HSn}=R_{HSn}+M_{E_n}^{\,is}\\ S_I*E_n^{\,m},\ if\ S_I\le 0 \ \Rightarrow\ L_{HSn}=L_{HSn}-S_I\end{cases} \qquad \textbf{(3.6.7.1.8)}$$

Equation (3.6.7.1.3) is then simplified as:

$$h\frac{(E_n)^{n+1/2}-(E_n)^n}{\Delta t}+\frac{\partial h}{\partial t}E_n+\nabla\cdot(\mathbf{q}E_n{}^m)-\nabla\cdot(h\mathbf{K}\cdot\nabla E_n{}^m)+L_{HS}E_n{}^m=R_{HS}+hR_{E_n} \quad \textbf{(3.6.7.1.9)}$$

Express $E_n{}^m$ in terms of $(E_n{}^m/E_n)\,E_n{}^m$ to make E_n's as primary dependent variables,

$$\begin{aligned}&h\frac{(E_n)^{n+1/2}-(E_n)^n}{\Delta t}+\nabla\cdot\left(\mathbf{q}\frac{E_n{}^m}{E_n}E_n\right)-\nabla\cdot\left(h\mathbf{K}\cdot\frac{E_n{}^m}{E_n}\nabla E_n\right)\\&-\nabla\cdot\left[h\mathbf{K}\cdot\left(\nabla\frac{E_n{}^m}{E_n}\right)E_n\right]+\left(L_{HS}\frac{E_n{}^m}{E_n}+\frac{\partial h}{\partial t}\right)E_n=R_{HS}+hR_{E_n}\end{aligned} \quad \textbf{(3.6.7.1.10)}$$

Use Galerkin or Petrov-Galerkin finite-element method for the spatial descretization of transport equation. Integrate equation (3.6.7.1.10) in the spatial dimensions over the entire region as follows.

$$\begin{aligned}&\int_R N_i\left[h\frac{\partial E_n}{\partial t}-\nabla\cdot\left(h\mathbf{K}\cdot\frac{E_n{}^m}{E_n}\nabla E_n\right)\right]dR+\int_R W_i\left\{\nabla\cdot\left(\mathbf{q}\frac{E_n{}^m}{E_n}E_n\right)-\nabla\cdot\left[h\mathbf{K}\cdot\left(\nabla\frac{E_n{}^m}{E_n}\right)E_n\right]\right\}dR\\&+\int_R N_i\left(L_{HS}\frac{E_n{}^m}{E_n}+\frac{\partial h}{\partial t}\right)E_n dR=\int_R N_i(R_{HS}+hR_{E_n})dR\end{aligned} \quad \textbf{(3.6.7.1.11)}$$

Further, we obtain

$$\begin{aligned}&\int_R N_i h\frac{\partial E_n}{\partial t}dR-\int_R\nabla W_i\cdot\mathbf{q}\frac{E_n{}^m}{E_n}E_n dR+\int_R\nabla N_i\cdot\left(h\mathbf{K}\cdot\frac{E_n{}^m}{E_n}\nabla E_n\right)dR+\int_R\nabla W_i\cdot\left[h\mathbf{K}\cdot\left(\nabla\frac{E_n{}^m}{E_n}\right)E_n\right]dR\\&+\int_R N_i\left(L_{HS}\frac{E_n{}^m}{E_n}+\frac{\partial h}{\partial t}\right)E_n dR=\int_R N_i(R_{HS}+hR_{E_n})dR\\&-\int_B\mathbf{n}\cdot W_i\mathbf{q}\frac{E_n{}^m}{E_n}E_n dB+\int_B\mathbf{n}\cdot\left(N_i h\mathbf{K}\cdot\frac{E_n{}^m}{E_n}\nabla E_n\right)dB+\int_B\mathbf{n}\cdot\left[W_i h\mathbf{K}\cdot\left(\nabla\frac{E_n{}^m}{E_n}\right)E_n\right]dB\end{aligned} \quad \textbf{(3.6.7.1.12)}$$

Approximate solution E_n by a linear combination of the base functions as follows

$$E_n\approx\hat{E}_n=\sum_{j=1}^{N}E_{nj}(t)N_j(R) \quad \textbf{(3.6.7.1.13)}$$

Substituting Equation (3.6.7.1.13) into Equation (3.6.7.1.12), we obtain

$$\begin{aligned}&\sum_{j=1}^{N}\left\{\begin{bmatrix}-\int_R\nabla W_i\cdot\mathbf{q}\frac{E_n{}^m}{E_n}N_j dR+\int_R\nabla W_i\cdot\left[h\mathbf{K}\cdot\left(\nabla\frac{E_n{}^m}{E_n}\right)N_j\right]dR\\+\int_R\nabla N_i\cdot\left(h\mathbf{K}\cdot\frac{E_n{}^m}{E_n}\nabla N_j\right)dR+\int_R N_i\left(L_{HS}\frac{E_n{}^m}{E_n}+\frac{\partial h}{\partial t}\right)N_j dR\end{bmatrix}E_{nj}(t)\right\}\\&+\sum_{j=1}^{N}\left[\left(\int_R N_i h N_j dR\right)\frac{\partial E_{nj}(t)}{\partial t}\right]=\int_R N_i\left(R_{HS}+hR_{E_n}\right)dR\\&-\int_B\mathbf{n}\cdot W_i\mathbf{q}\frac{E_n{}^m}{E_n}E_n dB+\int_B\mathbf{n}\cdot\left(N_i h\mathbf{K}\cdot\frac{E_n{}^m}{E_n}\nabla E_n\right)dB+\int_B\mathbf{n}\cdot\left[W_i h\mathbf{K}\cdot\left(\nabla\frac{E_n{}^m}{E_n}\right)E_n\right]dB\end{aligned} \quad \textbf{(3.6.7.1.14)}$$

Equation (3.6.7.1.14) can be written in matrix form as

$$[CMATRX1]\left\{\frac{\partial E_n}{\partial t}\right\}+([Q1]+[Q2]+[Q3]+[Q4])\{E_n\}=\{SS\}+\{B\} \quad \textbf{(3.6.7.1.15)}$$

The matrices [CMATRX1], [Q1], [Q2], [Q3], [Q4], and load vectors {SS}, {B} are given by

$$CMATRX1_{ij} = \int_R N_i h N_j dR \qquad \textbf{(3.6.7.1.16)}$$

$$Q1_{ij} = -\int_R \nabla W_i \cdot \mathbf{q} \frac{E_n^{\,m}}{E_n} N_j dR \qquad \textbf{(3.6.7.1.17)}$$

$$Q2_{ij} = \int_R \nabla W_i \cdot \left[h\mathbf{K} \cdot \left(\nabla \frac{E_n^{\,m}}{E_n} \right) N_j \right] dR \qquad \textbf{(3.6.7.1.18)}$$

$$Q3_{ij} = \int_R \nabla N_i \cdot \left(h\mathbf{K} \cdot \frac{E_n^{\,m}}{E_n} \nabla N_j \right) dR \qquad \textbf{(3.6.7.1.19)}$$

$$Q4_{ij} = \int_R N_i \left(L_{HS} \frac{E_n^{\,m}}{E_n} + \frac{\partial h}{\partial t} \right) N_j dR \qquad \textbf{(3.6.7.1.20)}$$

$$SS_i = \int_R N_i \left(R_{HS} + hR_{E_n} \right) dR \qquad \textbf{(3.6.7.1.21)}$$

$$B_i = -\int_B \mathbf{n} \cdot W_i \mathbf{q} \frac{E_n^{\,m}}{E_n} E_n dB + \int_B \mathbf{n} \cdot \left(N_i h\mathbf{K} \cdot \frac{E_n^{\,m}}{E_n} \nabla E_n \right) dB + \int_B \mathbf{n} \cdot \left[W_i h\mathbf{K} \cdot \left(\nabla \frac{E_n^{\,m}}{E_n} \right) E_n \right] dB \qquad \textbf{(3.6.7.1.22)}$$

Equation (3.6.7.1.15) is then simplified as

$$[CMATRX1]\left\{ \frac{\partial E_n}{\partial t} \right\} + [CMATRX2]\{E_n\} = \{SS\} + \{B\} \qquad \textbf{(3.6.7.1.23)}$$

where

$$[CMATRX2] = [Q1] + [Q2] + [Q3] + [Q4] \qquad \textbf{(3.6.7.1.24)}$$

Further,

$$[CMATRX1]\frac{\left(\{E_n^{\,n+1/2}\} - \{E_n^{\,n}\}\right)}{\Delta t} + [CMATRX2]\left(W_1\{E_n^{\,n+1/2}\} + W_2\{E_n^{\,n}\}\right) = \{SS\} + \{B\} \qquad \textbf{(3.6.7.1.25)}$$

So that

$$[CMATRX]\left\{E_n^{\,n+1/2}\right\} = \{RLD\} \qquad \textbf{(3.6.7.1.26)}$$

where

$$[CMATRX] = \frac{[CMATRX1]}{\Delta t} + W_1 * [CMATRX2] \qquad \textbf{(3.6.7.1.27)}$$

$$\{RLD\} = \left(\frac{[CMATRX1]}{\Delta t} - W_2 * [CMATRX2] \right)\left\{E_n^{\,n}\right\} + \{SS\} + \{B\} \qquad \textbf{(3.6.7.1.28)}$$

For interior nodes i, B_i is zero, for boundary nodes i = b, B_i is calculated according to the specified boundary condition and shown as follows.

$$B_i = -\int_B \mathbf{n} \cdot W_i \mathbf{q} E_n^{\,m} dB + \int_B \mathbf{n} \cdot \left(N_i h\mathbf{K} \cdot \nabla E_n^{\,m} \right) dB \qquad \textbf{(3.6.7.1.29)}$$

Dirichlet boundary condition

$$E_n^{\ m} = E_n^{\ m}(x_b, y_b, t) \qquad \textbf{(3.6.7.1.30)}$$

Variable boundary condition

< Case 1 > when flow is going in from outside (**n**·**q** <0)

$$\mathbf{n}\cdot\left(\mathbf{q}E_n^{\ m} - h\mathbf{K}\cdot\nabla E_n^{\ m}\right) = \mathbf{n}\cdot\mathbf{q}E_n^{\ m}(x_b, y_b, t) \quad \Rightarrow \quad B_i = -\int_B \mathbf{n}\cdot W_i\mathbf{q}E_n^{\ m}(x_b, y_b, t)dB \qquad \textbf{(3.6.7.1.31)}$$

< Case 2 > Flow is going out from inside (**n**·**q** > 0):

$$-\mathbf{n}\cdot\left(h\mathbf{K}\cdot\nabla E_n^{\ m}\right) = 0 \quad \Rightarrow \quad B_i = -\int_B \mathbf{n}\cdot W_i\mathbf{q}E_n^{\ m}dB \qquad \textbf{(3.6.7.1.32)}$$

Cauchy boundary condition

$$\mathrm{n}\cdot\left(\mathbf{q}E_n^{\ m} - h\mathbf{K}\cdot\nabla E_n^{\ m}\right) = Q_{En}^{\ m}(x_b, y_b, t) \quad \Rightarrow \quad B_i = -\int_B W_i Q_{En}^{\ m}(x_b, y_b, t)dB \qquad \textbf{(3.6.7.1.33)}$$

Neumann boundary condition

$$-\mathbf{n}\cdot\left(h\mathbf{K}\cdot\nabla E_n^{\ m}\right) = Q_{En}^{\ m}(x_b, y_b, t) \Rightarrow \quad B_i \quad = -\int_B \mathbf{n}\cdot W_i\mathbf{q}E_n dB - \int_B N_i Q_{En}^{\ m}(x_b, y_b, t)dB \qquad \textbf{(3.6.7.1.34)}$$

River/stream-overland interface boundary condition

$$\begin{aligned}\mathbf{n}\cdot\left(\mathbf{q}E_n^{\ m} - h\mathbf{K}\cdot\nabla E_n^{\ m}\right) &= (\mathbf{n}\cdot\mathbf{q})\frac{1}{2}\left\{\left[1+sign(\mathbf{n}\cdot\mathbf{q})\right]E_n^{\ m} + \left[1-sign(\mathbf{n}\cdot\mathbf{q})\right]\left(E_n^{1D}\right)^m(x_b, y_b, t)\right\} \\ \Rightarrow \quad B_i &= -\int_B W_i(\mathbf{n}\cdot\mathbf{q})\frac{1}{2}\left\{\left[1+sign(\mathbf{n}\cdot\mathbf{q})\right]E_n^{\ m} + \left[1-sign(\mathbf{n}\cdot\mathbf{q})\right]\left(E_n^{1D}\right)^m(x_b, y_b, t)\right\}dB\end{aligned} \qquad \textbf{(3.6.7.1.35)}$$

Note: In the equation (3.6.7.1.18), assign

3.6.7.2 Mixed Predictor-corrector/Operator-splitting scheme

Recall the governing equation for 2-D kinetic variable transport at n+1-th time step, equation (3.6.7.1.2), as follows

$$h\frac{(E_n)^{n+1} - (E_n)^n}{\Delta t} + \frac{\partial h}{\partial t}E_n + \nabla\cdot(\mathbf{q}E_n^{\ m}) - \nabla\cdot(h\mathbf{K}\cdot\nabla E_n^{\ m}) = M_{E_n^{\ as}} + M_{E_n^{\ rs}} + M_{E_n^{\ is}} + hR_{E_n} \qquad \textbf{(3.6.7.2.1)}$$

According to mixed Predictor-corrector/Operator-splitting scheme, equation (3.6.7.2.1) can be separated into two equations as follows

$$\begin{aligned}&h\frac{(E_n^{\ m})^{n+1/2} - (E_n^{\ m})^n}{\Delta t} + \frac{\partial h}{\partial t}E_n^m + \nabla\cdot(\mathbf{q}E_n^{\ m}) - \nabla\cdot(h\mathbf{K}\cdot\nabla E_n^{\ m}) = \\ &M_{E_n^{\ as}} + M_{E_n^{\ rs}} + M_{E_n^{\ is}} + h\left(R_{E_n}\right)^n - \frac{\partial h}{\partial t}(E_n^{im})^n\end{aligned} \qquad \textbf{(3.6.7.2.2)}$$

$$\frac{E_n^{n+1}-[(E_n^m)^{n+1/2}+(E_n^{im})^n]}{\Delta t}=hR_{E_n}^{n+1}-h(R_{E_n})^n-\frac{\partial \ell n(h)}{\partial t}(E_n^{im})^{n+1}+\frac{\partial \ell n(h)}{\partial t}(E_n^{im})^n \qquad \textbf{(3.6.7.2.3)}$$

First, solve equation (3.6.7.2.2) and get $(E_n^m)^{n+1/2}$. Second, solve equation (3.6.7.2.3) together with algebraic equations for equilibrium reactions using BIOGEOCHEM scheme to obtain the individual species concentration.

Assign and calculate the right hand side R_{HS} and left hand side L_{HS} the same as that in section 3.6.7.1, equation (3.6.7.2.2) is then simplified as:

$$h\frac{(E_n^m)^{n+1/2}-(E_n^m)^n}{\Delta t}+\nabla\cdot(\mathbf{q}E_n^m)-\nabla\cdot(h\mathbf{K}\cdot\nabla E_n^m)+\left(L_{HS}+\frac{\partial h}{\partial t}\right)E_n^m=R_{HS}+h\left(R_{E_n}\right)^n-\frac{\partial h}{\partial t}(E_n^{im})^n \qquad \textbf{(3.6.7.2.4)}$$

Use Galerkin or Petrov-Galerkin finite-element method for the spatial descretization of transport equation. Integrate equation (3.6.7.2.4) in the spatial dimensions over the entire region as follows

$$\begin{aligned}&\int_R N_i\left[h^n\frac{\partial E_n^m}{\partial t}-\nabla\cdot\left(h\mathbf{K}\cdot\nabla E_n^m\right)\right]dR+\int_R W_i\nabla\cdot\left(\mathbf{q}E_n^m\right)dR\\&\quad+\int_R N_i\left(L_{HS}+\frac{\partial h}{\partial t}\right)E_n^m dR=\int_R N_i\left(R_{HS}+hR_{E_n}^n-\frac{\partial h}{\partial t}(E_n^{im})^n\right)dR\end{aligned} \qquad \textbf{(3.6.7.2.5)}$$

Further, we obtain

$$\begin{aligned}&\int_R N_i h\frac{\partial E_n^m}{\partial t}dR-\int_R\nabla W_i\cdot\mathbf{q}E_n^m dR+\int_R\nabla N_i\cdot\left(h\mathbf{K}\cdot\nabla E_n^m\right)dR+\int_R N_i\left(L_{HS}+\frac{\partial h}{\partial t}\right)E_n^m dR\\&=\int_R N_i\left(R_{HS}+hR_{E_n}^n-\frac{\partial h}{\partial t}(E_n^{im})^n\right)dR-\int_B\mathbf{n}\cdot W_i\mathbf{q}E_n^m dB+\int_B\mathbf{n}\cdot\left(N_i h\mathbf{K}\cdot\nabla E_n^m\right)dB\end{aligned} \qquad \textbf{(3.6.7.2.6)}$$

Approximate solution E_n^m by a linear combination of the base functions as follows

$$E_n^m\approx\hat{E}_n^m=\sum_{j=1}^N E_{nj}^m(t)N_j(R) \qquad \textbf{(3.6.7.2.7)}$$

Substituting Equation (3.6.7.2.7) into Equation (3.6.7.2.6), we obtain

$$\begin{aligned}&\sum_{j=1}^N\left\{\left[-\int_R\nabla W_i\cdot\mathbf{q}N_j dR+\int_R\nabla N_i\cdot\left(h\mathbf{K}\cdot\nabla N_j\right)dR+\int_R N_i\left(L_{HS}+\frac{\partial h}{\partial t}\right)N_j dR\right]E_{nj}^m(t)\right\}\\&\quad+\sum_{j=1}^N\left[\left(\int_R N_i h^n N_j dR\right)\frac{\partial E_{nj}^m(t)}{\partial t}\right]=\int_R N_i\left(R_{HS}+hR_{E_n}^n-\frac{\partial h}{\partial t}(E_n^{im})^n\right)dR\\&\quad-\int_B\mathbf{n}\cdot W_i\mathbf{q}E_n^m dB+\int_B\mathbf{n}\cdot\left(N_i h\mathbf{K}\cdot\nabla E_n^m\right)dB\end{aligned} \qquad \textbf{(3.6.7.2.8)}$$

Equation (3.6.7.2.8) can be written in matrix form as

$$[CMATRX1]\left\{\frac{\partial E_n^m}{\partial t}\right\}+([Q1]+[Q3]+[Q4])\left\{E_n^m\right\}=\{SS\}+\{B\} \qquad \textbf{(3.6.7.2.9)}$$

The matrices [CMATRX1], [Q1], [Q3], [Q4], and load vectors {SS}, {B} are given by

$$CMATRX1_{ij} = \int_R N_i h N_j dR \tag{3.6.7.2.10}$$

$$Q1_{ij} = -\int_R \nabla W_i \cdot \mathbf{q} N_j dR \tag{3.6.7.2.11}$$

$$Q3_{ij} = \int_R \nabla N_i \cdot \left(h\mathbf{K} \cdot \nabla N_j\right) dR \tag{3.6.7.2.12}$$

$$Q4_{ij} = \int_R N_i \left(L_{HS} + \frac{\partial h}{\partial t}\right) N_j dR \tag{3.6.7.2.13}$$

$$SS_i = \int_R N_i \left(R_{HS} + hR_{E_n}{}^n - \frac{\partial h}{\partial t}(E_n^{im})^n\right) dR \tag{3.6.7.2.14}$$

$$B_i = -\int_B \mathbf{n} \cdot W_i \mathbf{q} E_n{}^m dB + \int_B \mathbf{n} \cdot \left(N_i h\mathbf{K} \cdot \nabla E_n{}^m\right) dB \tag{3.6.7.2.15}$$

Equation (3.6.7.2.9) is then simplified as

$$[CMATRX1]\left\{\frac{\partial E_n}{\partial t}\right\} + [CMATRX2]\{E_n\} = \{SS\} + \{B\} \tag{3.6.7.2.16}$$

where

$$[CMATRX2] = [Q1] + [Q3] + [Q4] \tag{3.6.7.2.17}$$

Further,

$$\begin{aligned} &[CMATRX1]\frac{\left[\{(E_n{}^m)^{n+1/2}\} - \{(E_n{}^m)^n\}\right]}{\Delta t} \\ &+[CMATRX2]\left[W_1\{(E_n{}^m)^{n+1/2}\} + W_2\{(E_n{}^m)^n\}\right] = \{SS\} + \{B\} \end{aligned} \tag{3.6.7.2.18}$$

So that

$$[CMATRX]\left\{(E_n{}^m)^{n+1/2}\right\} = \{RLD\} \tag{3.6.7.2.19}$$

where

$$[CMATRX] = \frac{[CMATRX1]}{\Delta t} + W_1 * [CMATRX2] \tag{3.6.7.2.20}$$

$$\{RLD\} = \left(\frac{[CMATRX1]}{\Delta t} - W_2 * [CMATRX2]\right)\left\{(E_n{}^m)^n\right\} + \{SS\} + \{B\} \tag{3.6.7.2.21}$$

For interior nodes i, B_i is zero, for boundary nodes i = b, B_i is the same as that in section 3.6.7.1.

3.6.7.3 Operator-splitting scheme

Recall the governing equation for 2-D kinetic variable transport at n+1-th time step, equation (3.6.7.1.2), as follows

$$h\frac{(E_n)^{n+1} - (E_n)^n}{\Delta t} + \frac{\partial h}{\partial t}E_n + \nabla \cdot (\mathbf{q}E_n{}^m) - \nabla \cdot (h\mathbf{K} \cdot \nabla E_n{}^m) = M_{E_n{}^{as}} + M_{E_n{}^{rs}} + M_{E_n{}^{is}} + hR_{E_n} \tag{3.6.7.3.1}$$

According to Operator-splitting scheme, equation (3.6.7.3.1) can be separated into two equations as follows

$$h\frac{(E_n{}^m)^{n+1/2}-(E_n{}^m)^n}{\Delta t}+\frac{\partial h}{\partial t}E_n^m+\nabla\cdot(\mathbf{q}E_n{}^m)-\nabla\cdot(h\mathbf{K}\cdot\nabla E_n{}^m)=M_{E_n{}^{as}}+M_{E_n{}^{rs}}+M_{E_n{}^{is}} \quad \textbf{(3.6.7.3.2)}$$

$$\frac{(E_n)^{n+1}-[(E_n{}^m)^{n+1/2}+(E_n{}^{im})^n]}{\Delta t}=hR_{E_n}{}^{n+1}-\frac{\partial \ell nh}{\partial t}(E_n^{im})^{n+1} \quad \textbf{(3.6.7.3.3)}$$

First, solve equation (3.6.7.3.2) and get $(E_n{}^m)^{n+1/2}$. Second, solve equation (3.6.7.3.3) together with algebraic equations for equilibrium reactions using BIOGEOCHEM scheme to obtain the individual species concentration.

Equation (3.6.7.3.2) can be solved through the same procedure as that in section 3.6.7.2, except for the load vectors {SS}, which is calculated by the following equation.

$$SS_i=\sum_{e=1}^{M_e}\int_{R_e}N_i{}^eR_{HS}dR \quad \textbf{(3.6.7.3.4)}$$

3.6.8 Application of the Finite Element Method to the Advective Form of the Transport Equations to Solve 2-D Kinetic Variable Transport

3.6.8.1 Fully-implicit scheme

Conversion of the equation for 2-D kinetic variable transport Fully-implicit scheme transport step, equation (3.6.7.1.3), to advection form is expressed as

$$\begin{aligned}&h\frac{(E_n)^{n+1/2}-(E_n)^n}{\Delta t}+\frac{\partial h}{\partial t}E_n+\mathbf{q}\cdot\nabla E_n{}^m-\nabla\cdot(h\mathbf{K}\cdot\nabla E_n{}^m)+(\nabla\cdot\mathbf{q})E_n{}^m=\\&M_{E_n{}^{as}}+M_{E_n{}^{rs}}+M_{E_n{}^{is}}+hR_{E_n}\end{aligned} \quad \textbf{(3.6.8.1.1)}$$

where $\partial h/\partial t+\nabla\cdot\mathbf{q}=S_S+S_R+S_I$ according to governing equation for 2-D flow.

To solve equation (3.6.8.1.1), assign

$$R_{HS}=0 \quad and \quad L_{HS}=S_S+S_R+S_I-\partial h/\partial t \quad \textbf{(3.6.8.1.2)}$$

Then the right hand side R_{HS} and left hand side L_{HS} should be continuously calculated the same as that in section 3.6.7.1. Equation (3.6.8.1.1) is then simplified as:

$$h\frac{\partial E_n}{\partial t}+\frac{\partial h}{\partial t}E_n+\mathbf{q}\cdot\nabla E_n{}^m-\nabla\cdot(h\mathbf{K}\cdot\nabla E_n{}^m)+L_{HS}E_n{}^m=R_{HS}+hR_{E_n} \quad \textbf{(3.6.8.1.3)}$$

Express $E_n{}^m$ in terms of $(E_n{}^m/E_n)\,E_n{}^m$ to make E_n's as primary dependent variables,

$$\begin{aligned}&h\frac{\partial E_n}{\partial t}+\mathbf{q}\cdot\nabla\left(\frac{E_n{}^m}{E_n}E_n\right)-\nabla\cdot\left(h\mathbf{K}\cdot\frac{E_n{}^m}{E_n}\nabla E_n\right)\\&-\nabla\cdot\left[h\mathbf{K}\cdot\left(\nabla\frac{E_n{}^m}{E_n}\right)E_n\right]+\left(L_{HS}\frac{E_n{}^m}{E_n}+\frac{\partial h}{\partial t}\right)E_n=R_HS+hR_{E_n}\end{aligned} \quad \textbf{(3.6.8.1.4)}$$

Use Galerkin or Petrov-Galerkin finite-element method for the spatial descretization of transport equation. Integrate equation (3.6.8.1.4) in the spatial dimensions over the entire region as follows.

$$\int_R N_i\left[h\frac{\partial E_n}{\partial t}-\nabla\cdot\left(h\mathbf{K}\cdot\frac{{E_n}^m}{E_n}\nabla E_n\right)\right]dR+\int_R W_i\left\{\mathbf{q}\cdot\nabla\left(\frac{{E_n}^m}{E_n}E_n\right)-\nabla\cdot\left[h\mathbf{K}\cdot\left(\nabla\frac{{E_n}^m}{E_n}\right)E_n\right]\right\}dR$$
$$+\int_R N_i\left(L_{HS}\frac{{E_n}^m}{E_n}+\frac{\partial h}{\partial t}\right)E_n dR=\int_R N_i(R_{HS}+hR_{E_n})dR \qquad \textbf{(3.6.8.1.5)}$$

Further, we obtain

$$\int_R N_i h\frac{\partial E_n}{\partial t}dR-\int_R W_i\mathbf{q}\cdot\nabla\frac{{E_n}^m}{E_n}E_n dR+\int_R\nabla N_i\cdot\left(h\mathbf{K}\cdot\frac{{E_n}^m}{E_n}\nabla E_n\right)dR$$
$$+\int_R\nabla W_i\cdot\left[h\mathbf{K}\cdot\left(\nabla\frac{{E_n}^m}{E_n}\right)E_n\right]dR+\int_R N_i\left(L_{HS}\frac{{E_n}^m}{E_n}+\frac{\partial h}{\partial t}\right)E_n dR \qquad \textbf{(3.6.8.1.6)}$$
$$=\int_R N_i(R_{HS}+hR_{E_n})dR+\int_B n\cdot\left(N_i hK\cdot\frac{{E_n}^m}{E_n}\nabla E_n\right)dB+\int_B n\cdot\left[W_i hK\cdot\left(\nabla\frac{{E_n}^m}{E_n}\right)E_n\right]dB$$

Approximate solution E_n by a linear combination of the base functions as follows

$$E_n\approx\hat{E}_n=\sum_{j=1}^{N}E_{nj}(t)N_j(R) \qquad \textbf{(3.6.8.1.7)}$$

Substituting Equation (3.6.8.1.7) into Equation (3.6.8.1.6), we obtain

$$\sum_{j=1}^{N}\left\{\left[\int_R W_i\mathbf{q}\cdot\frac{{E_n}^m}{E_n}\nabla N_j dR+\int_R W_i\mathbf{q}\cdot\left(\nabla\frac{{E_n}^m}{E_n}\right)N_j dR+\int_R\nabla W_i\cdot\left[h\mathbf{K}\cdot\left(\nabla\frac{{E_n}^m}{E_n}\right)N_j\right]dR\right.\right.$$
$$\left.\left.+\int_R\nabla N_i\cdot\left(h\mathbf{K}\cdot\frac{{E_n}^m}{E_n}\nabla N_j\right)dR+\int_R N_i\left(L_{HS}\frac{{E_n}^m}{E_n}+\frac{\partial h}{\partial t}\right)N_j dR\right]E_{nj}(t)\right\}$$
$$+\sum_{j=1}^{N}\left[\left(\int_R N_i hN_j dR\right)\frac{\partial E_{nj}(t)}{\partial t}\right]=\int_R N_i\left(R_{HS}+hR_{E_n}\right)dR \qquad \textbf{(3.6.8.1.8)}$$
$$+\int_B n\cdot\left(N_i h\mathbf{K}\cdot\frac{{E_n}^m}{E_n}\nabla E_n\right)dB+\int_B n\cdot\left[W_i h\mathbf{K}\cdot\left(\nabla\frac{{E_n}^m}{E_n}\right)E_n\right]dB$$

Equation (3.6.8.1.8) can be written in matrix form as

$$[CMATRX1]\left\{\frac{\partial E_n}{\partial t}\right\}+([Q1]+[Q2]+[Q3]+[Q4]+[Q5])\{E_n\}=\{SS\}+\{B\} \qquad \textbf{(3.6.8.1.9)}$$

The matrices [CMATRX1], [Q1], [Q2], [Q3], [Q4], [Q5], and load vectors {SS}, {B} are given by

$$CMATRX1_{ij}=\int_R N_i hN_j dR \qquad \textbf{(3.6.8.1.10)}$$

$$Q1_{ij}=\int_R W_i\mathbf{q}\cdot\frac{{E_n}^m}{E_n}\nabla N_j dR \qquad \textbf{(3.6.8.1.11)}$$

$$Q2_{ij} = \int_R W_i \mathbf{q} \cdot \left(\nabla \frac{E_n^{\,m}}{E_n} \right) N_j \, dR \qquad \textbf{(3.6.8.1.12)}$$

$$Q3_{ij} = \int_R \nabla W_i \cdot \left[h\mathbf{K} \cdot \left(\nabla \frac{E_n^{\,m}}{E_n} \right) N_j \right] dR \qquad \textbf{(3.6.8.1.13)}$$

$$Q4_{ij} = \int_R \nabla N_i \cdot \left(h\mathbf{K} \cdot \frac{E_n^{\,m}}{E_n} \nabla N_j \right) dR \qquad \textbf{(3.6.8.1.14)}$$

$$Q5_{ij} = \int_R N_i \left(L_{HS} \frac{E_n^{\,m}}{E_n} + \frac{\partial h}{\partial t} \right) N_j dR \qquad \textbf{(3.6.8.1.15)}$$

$$SS_i = \int_R N_i \left(R_{HS} + hR_{E_n} \right) dR \qquad \textbf{(3.6.8.1.16)}$$

$$B_i = \int_B \mathbf{n} \cdot \left(N_i h\mathbf{K} \cdot \frac{E_n^{\,m}}{E_n} \nabla E_n \right) dB + \int_B \mathbf{n} \cdot \left[W_i h\mathbf{K} \cdot \left(\nabla \frac{E_n^{\,m}}{E_n} \right) E_n \right] dB \qquad \textbf{(3.6.8.1.17)}$$

Equation (3.6.8.1.9) is then simplified as

$$[CMATRX1]\left\{ \frac{\partial E_n}{\partial t} \right\} + [CMATRX2]\{E_n\} = \{SS\} + \{B\} \qquad \textbf{(3.6.8.1.18)}$$

where

$$[CMATRX2] = [Q1] + [Q2] + [Q3] + [Q4] + [Q5] \qquad \textbf{(3.6.8.1.19)}$$

Further,

$$[CMATRX1]\frac{\left(\{E_n^{\,n+1/2}\} - \{E_n^{\,n}\} \right)}{\Delta t} + [CMATRX2]\left(W_1 \{E_n^{\,n+1/2}\} + W_2 \{E_n^{\,n}\} \right) = \{SS\} + \{B\} \qquad \textbf{(3.6.8.1.20)}$$

So that

$$[CMATRX]\left\{ E_n^{\,n+1/2} \right\} = \{RLD\} \qquad \textbf{(3.6.8.1.21)}$$

where

$$[CMATRX] = \frac{[CMATRX1]}{\Delta t} + W_1 * [CMATRX2] \qquad \textbf{(3.6.8.1.22)}$$

$$\{\mathrm{RLD}\} = \left(\frac{[\mathrm{CMATRX1}]}{\Delta \mathrm{t}} - \mathrm{W}_2 * [\mathrm{CMATRX2}] \right) \left\{ \mathrm{E_n}^{\,\mathrm{n}} \right\} + \{\mathrm{SS}\} + \{\mathrm{B}\} \qquad \textbf{(3.6.8.1.23)}$$

For interior nodes i, B_i is zero, for boundary nodes i = b, B_i is calculated according to the specified boundary condition and shown as follows.

$$B_i = \int_B \mathbf{n} \cdot \left(N_i h\mathbf{K} \cdot \nabla E_n^{\,m} \right) dB \qquad \textbf{(3.6.8.1.24)}$$

Dirichlet boundary condition

$$E_n^{\,m} = E_n^{\,m}(x_b, y_b, t) \qquad \textbf{(3.6.8.1.25)}$$

Variable boundary condition

< Case 1 > when flow is going in from outside ($\mathbf{n}\cdot\mathbf{q} < 0$)

$$\mathbf{n}\cdot\left(\mathbf{q}E_n^{\ m} - h\mathbf{K}\cdot\nabla E_n^{\ m}\right) = \mathbf{n}\cdot\mathbf{q}E_n^{\ m}(x_b,y_b,t) \;\Rightarrow\; B_i = \int_B \mathbf{n}\cdot N_i\mathbf{q}E_n^{\ m}dB - \int_B \mathbf{n}\cdot N_i\mathbf{q}E_n^{\ m}(x_b,y_b,t)dB \qquad \textbf{(3.6.8.1.26)}$$

< Case 2 > Flow is going out from inside ($\mathbf{n}\cdot\mathbf{q} > 0$):

$$-\mathbf{n}\cdot\left(h\mathbf{K}\cdot\nabla E_n^{\ m}\right) = 0 \;\Rightarrow\; B_i = 0 \qquad \textbf{(3.6.8.1.27)}$$

Cauchy boundary condition

$$\mathbf{n}\cdot\left(\mathbf{q}E_n^{\ m} - h\mathbf{K}\cdot\nabla E_n^{\ m}\right) = Q_{En}^{\ m}(x_b,y_b,t) \;\Rightarrow\; B_i = \int_B N_i\mathbf{n}\cdot\mathbf{q}E_n^{\ m}dB - \int_B N_iQ_{En}^{\ m}(x_b,y_b,t)dB \qquad \textbf{(3.6.8.1.28)}$$

Neumann boundary condition

$$-\mathbf{n}\cdot\left(h\mathbf{K}\cdot\nabla E_n^{\ m}\right) = Q_{En}^{\ m}(x_b,y_b,t) \;\Rightarrow\; B_i = -\int_B N_iQ_{En}^{\ m}(x_b,y_b,t)dB \qquad \textbf{(3.6.8.1.29)}$$

River/stream-overland interface boundary condition

$$\mathbf{n}\cdot\left(\mathbf{q}E_n^{\ m} - h\mathbf{K}\cdot\nabla E_n^{\ m}\right) = (\mathbf{n}\cdot\mathbf{q})\frac{1}{2}\left\{\left[1+sign(\mathbf{n}\cdot\mathbf{q})\right]E_n^{\ m} + \left[1-sign(\mathbf{n}\cdot\mathbf{q})\right]\left(E_n^{1D}\right)^m(x_b,y_b,t)\right\} \;\Rightarrow$$
$$B_i = \int_B N_i\mathbf{n}\cdot\mathbf{q}E_n^{\ m}dB - \int_B N_i(\mathbf{n}\cdot\mathbf{q})\frac{1}{2}\left\{\left[1+sign(\mathbf{n}\cdot\mathbf{q})\right]E_n^{\ m} + \left[1-sign(\mathbf{n}\cdot\mathbf{q})\right]\left(E_n^{1D}\right)^m(x_b,y_b,t)\right\}dB \qquad \textbf{(3.6.8.1.30)}$$

3.6.8.2 Mixed Predictor-corrector/Operator-splitting scheme

Conversion of the equation for 2-D kinetic variable transport mixed Predictor-corrector/Operator-splitting scheme transport step, equation (3.6.7.2.3), to advection form is expressed as

$$h\frac{(E_n^{\ m})^{n+1/2} - (E_n^{\ m})^n}{\Delta t} + \frac{\partial h}{\partial t}E_n^m + \mathbf{q}\cdot\nabla E_n^{\ m} - \nabla\cdot(h\mathbf{K}\cdot\nabla E_n^{\ m}) + (\nabla\cdot\mathbf{q})E_n^{\ m} =$$
$$M_{E_n^{as}} + M_{E_n^{rs}} + M_{E_n^{is}} + hR_{E_n}^{\ n} - \frac{\partial h}{\partial t}(E_n^{im})^n \qquad \textbf{(3.6.8.2.1)}$$

where $\partial h/\partial t + \nabla\cdot\mathbf{q} = S_S + S_R + S_I$ according to governing equation for 2-D flow.

To solve equation (3.6.8.2.1), assign the right hand side R_{HS} and left hand side L_{HS} the same as that in section 3.6.8.1. Equation (3.6.8.2.1) is then simplified as:

$$h\frac{\partial E_n^{\ m}}{\partial t} + \frac{\partial h}{\partial t}E_n^m + \mathbf{q}\cdot\nabla E_n^{\ m} - \nabla\cdot(h\mathbf{K}\cdot\nabla E_n^{\ m}) + L_{HS}E_n^{\ m} = R_{HS} + hR_{E_n}^{\ n} - \frac{\partial h}{\partial t}(E_n^{im})^n \qquad \textbf{(3.6.8.2.2)}$$

Use Galerkin or Petrov-Galerkin finite-element method for the spatial descretization of transport equation. Integrate equation (3.6.8.2.4) in the spatial dimensions over the entire region as follows.

$$\int_R N_i \left[h\frac{\partial E_n{}^m}{\partial t} - \nabla \cdot \left(h\mathbf{K} \cdot \nabla E_n{}^m \right) \right] dR + \int_R W_i \mathbf{q} \cdot \nabla E_n{}^m dR + \int_R N_i \left(L_{HS} + \frac{\partial h}{\partial t} \right) E_n{}^m dR = \int_R N_i \left(R_{HS} + hR_{E_n}{}^n - \frac{\partial h}{\partial t} (E_n^{im})^n \right) dR \quad \textbf{(3.6.8.2.3)}$$

Further, we obtain

$$\int_R N_i h \frac{\partial E_n{}^m}{\partial t} dR - \int_R W_i \mathbf{q} \cdot \nabla E_n{}^m dR + \int_R \nabla N_i \cdot \left(h\mathbf{K} \cdot \nabla E_n{}^m \right) dR + \int_R N_i \left(L_{HS} + \frac{\partial h}{\partial t} \right) E_n{}^m dR = \int_R N_i \left(R_{HS} + hR_{E_n}{}^n - \frac{\partial h}{\partial t} (E_n^{im})^n \right) dR + \int_B n \cdot \left(N_i hK \cdot \nabla E_n{}^m \right) dB \quad \textbf{(3.6.8.2.4)}$$

Approximate solution $E_n{}^m$ by a linear combination of the base functions as follows

$$E_n{}^m \approx \hat{E}_n{}^m = \sum_{j=1}^{N} E_{nj}{}^m(t) N_j(R) \quad \textbf{(3.6.8.2.5)}$$

Substituting Equation (3.6.8.2.5) into Equation (3.6.8.2.4), we obtain

$$\sum_{j=1}^{N} \left\{ \left[\int_R W_i \mathbf{q} \cdot \nabla N_j dR + \int_R \nabla N_i \cdot \left(h\mathbf{K} \cdot \nabla N_j \right) dR + \int_R N_i \left(L_{HS} + \frac{\partial h}{\partial t} \right) N_j dR \right] E_{nj}{}^m(t) \right\} + \sum_{j=1}^{N} \left[\left(\int_R N_i h N_j dR \right) \frac{\partial E_{nj}{}^m(t)}{\partial t} \right] = \int_R N_i \left(R_{HS} + hR_{E_n}{}^n - \frac{\partial h}{\partial t} (E_n^{im})^n \right) dR + \int_B \mathbf{n} \cdot \left(N_i h\mathbf{K} \cdot \nabla E_n{}^m \right) dB \quad \textbf{(3.6.8.2.6)}$$

Equation (3.6.8.2.6) can be written in matrix form as

$$[CMATRX1] \left\{ \frac{\partial E_n}{\partial t} \right\} + ([Q1] + [Q4] + [Q5]) \{E_n\} = \{SS\} + \{B\} \quad \textbf{(3.6.8.2.7)}$$

The matrices [CMATRX1], [Q1], [Q4], [Q5], and load vectors {SS}, {B} are given by

$$CMATRX1_{ij} = \int_R N_i h N_j dR \quad \textbf{(3.6.8.2.8)}$$

$$Q1_{ij} = \int_R W_i \mathbf{q} \cdot \nabla N_j dR \quad \textbf{(3.6.8.2.9)}$$

$$Q4_{ij} = \int_R \nabla N_i \cdot \left(h\mathbf{K} \cdot \nabla N_j \right) dR \quad \textbf{(3.6.8.2.10)}$$

$$Q5_{ij} = \int_R N_i \left(L_{HS} + \frac{\partial h}{\partial t} \right) N_j dR \quad \textbf{(3.6.8.2.11)}$$

$$SS_i = \int_R N_i \left(R_{HS} + hR_{E_n}{}^n - \frac{\partial h}{\partial t} (E_n^{im})^n \right) dR \quad \textbf{(3.6.8.2.12)}$$

$$B_i = \int_B \mathbf{n} \cdot \left(N_i h\mathbf{K} \cdot \nabla E_n \right) dB \quad \textbf{(3.6.8.2.13)}$$

Equation (3.6.8.2.7) is then simplified as

$$[CMATRX1]\left\{\frac{\partial E_n}{\partial t}\right\}+[CMATRX2]\{E_n\}=\{SS\}+\{B\} \quad \textbf{(3.6.8.2.14)}$$

where

$$[CMATRX2]=[Q1]+[Q4]+[Q5] \quad \textbf{(3.6.8.2.15)}$$

Further,

$$[CMATRX1]\frac{\left(\{E_n{}^{n+1/2}\}-\{E_n{}^{n}\}\right)}{\Delta t}+[CMATRX2]\left(W_1\{E_n{}^{n+1/2}\}+W_2\{E_n{}^{n}\}\right)=\{SS\}+\{B\} \quad \textbf{(3.6.8.2.16)}$$

So that

$$[CMATRX]\left\{E_n{}^{n+1/2}\right\}=\{RLD\} \quad \textbf{(3.6.8.2.17)}$$

where

$$[CMATRX]=\frac{[CMATRX1]}{\Delta t}+W_1*[CMATRX2] \quad \textbf{(3.6.8.2.18)}$$

$$\{RLD\}=\left(\frac{[CMATRX1]}{\Delta t}-W_2*[CMATRX2]\right)\left\{E_n{}^{n}\right\}+\{SS\}+\{B\} \quad \textbf{(3.6.8.2.19)}$$

For interior nodes i, B_i is zero, for boundary nodes i = b, B_i is calculated according to the specified boundary condition calculated the same as that in section 3.6.8.1.

3.6.8.3 Operator-splitting scheme

Conversion of the equation for 2-D kinetic variable transport operator spitting scheme transport step, equation (3.6.7.3.3), to advection form is expressed as

$$h\frac{(E_n{}^{m})^{n+1/2}-(E_n{}^{m})^{n}}{\Delta t}+\frac{\partial h}{\partial t}E_n^m+\mathbf{q}\cdot\nabla E_n{}^{m}-\nabla\cdot(h\mathbf{K}\cdot\nabla E_n{}^{m})+\left(\nabla\cdot\mathbf{q}\right)E_n{}^{m}=M_{E_n{}^{as}}+M_{E_n{}^{rs}}+M_{E_n{}^{is}} \quad \textbf{(3.6.8.3.1)}$$

where $\partial h/\partial t+\nabla\cdot q=S_S+S_R+S_I$ according to governing equation for 2-D flow.

Equation (3.6.8.3.1) can be solved through the same procedure as that in section 3.6.8.2, except for the load vectors {SS}, which is calculated by the following equation.

$$SS_i=\sum_{e=1}^{M_e}\int_{R_e}N_i{}^{e}R_{HS}dR \quad \textbf{(3.6.8.3.2)}$$

3.6.9 Application of the Modified Lagrangian-Eulerian Approach to the Largrangian Form of the Transport Equations to Solve 2-D Kinetic Variable Transport

3.6.9.1 Fully-implicit scheme

Recall the equation for 2-D kinetic variable transport Fully-implicit scheme transport step in advection form, equation (3.6.8.1.1), as follows

$$h\frac{(E_n)^{n+1/2}-(E_n)^{n}}{\Delta t}+\frac{\partial h}{\partial t}E_n+\mathbf{q}\cdot\nabla E_n{}^{m}-\nabla\cdot(h\mathbf{K}\cdot\nabla E_n{}^{m})+\left(\nabla\cdot\mathbf{q}\right)E_n{}^{m}=M_{E_n{}^{as}}+M_{E_n{}^{rs}}+M_{E_n{}^{is}}+hR_{E_n} \quad \textbf{(3.6.9.1.1)}$$

Express E_n^m in terms of $(E_n^m/E_n)E_n$ or E_n-E_n^{im} to make E_n's as primary dependent variables, equation (3.6.9.1.1) is modified as

$$\begin{aligned} & h\frac{\partial E_n}{\partial t}+\frac{\partial h}{\partial t}E_n+\mathbf{q}\cdot\nabla E_n-\nabla\cdot\left(h\mathbf{K}\cdot\nabla E_n\right)+\left(\nabla\cdot\mathbf{q}\right)\frac{E_n^{\ m}}{E_n}E_n \\ &=\mathbf{q}\cdot\nabla E_n^{\ im}-\nabla\cdot\left(h\mathbf{K}\cdot\nabla E_n^{\ im}\right)M_{E_n^{\ as}}+M_{E_n^{\ rs}}+M_{E_n^{\ is}}+hR_{E_n} \end{aligned} \qquad \textbf{(3.6.9.1.2)}$$

To solve equation (3.6.9.1.2), assign

$$R_{HS}=0 \quad and \quad L_{HS}=\left(S_S+S_R+S_I-\partial h/\partial t\right)E_n^{\ m}/E_n \qquad \textbf{(3.6.9.1.3)}$$

Then the right hand side R_{HS} and left hand side L_{HS} should be continuously calculated as following.

$$M_{E_n^{\ rs}}=\begin{cases} S_R*E_{n^{rs}}, & if\ S_R>0 \ \Rightarrow\ R_{HSn}=R_{HSn}+M_{E_n^{\ rs}} \\ S_R*E_n^{\ m}, & if\ S_R\le 0 \ \Rightarrow\ L_{HSn}=L_{HSn}-S_R \end{cases} \qquad \textbf{(3.6.9.1.4)}$$

$$M_{E_n^{\ as}}=\begin{cases} S_S*E_{n^{as}}, & if\ S_S>0 \ \Rightarrow\ R_{HSn}=R_{HSn}+M_{E_n^{\ as}}, \\ S_S*E_n^{\ m}, & if\ S_S\le 0 \ \Rightarrow\ L_{HSn}=L_{HSn}-S_S \end{cases} \qquad \textbf{(3.6.9.1.5)}$$

$$M_{E_n^{\ is}}=\begin{cases} S_I*E_n^{\ m_{\ is}}, & if\ S_I>0 \ \Rightarrow\ R_{HSn}=R_{HSn}+M_{E_n^{\ is}} \\ S_I*E_n^{\ m}, & if\ S_I\le 0 \ \Rightarrow\ L_{HSn}=L_{HSn}-S_I \end{cases} \qquad \textbf{(3.6.9.1.6)}$$

Equation (3.6.8.1.1) is then simplified as:

$$h\frac{\partial E_n}{\partial t}+\frac{\partial h}{\partial t}E_n+\mathbf{q}\cdot\nabla E_n-\nabla\cdot(h\mathbf{K}\cdot\nabla E_n)+L_{HS}E_n=\mathbf{q}\cdot\nabla E_n^{\ im}-\nabla\cdot\left(h\mathbf{K}\cdot\nabla E_n^{\ im}\right)+R_{HS}+hR_{E_n} \qquad \textbf{(3.6.9.1.7)}$$

Assign the true transport velocity $\mathbf{v}_{\text{true}}$ as follows

$$h\mathbf{v}_{true}=\mathbf{q} \qquad \textbf{(3.6.9.1.8)}$$

Equation (3.6.9.1.7) in the Lagrangian and Eulerian form is written as follows. In Lagrangian step,

$$h\frac{dE_n}{d\tau}=h\frac{\partial E_n}{\partial t}+\mathbf{q}\cdot\nabla E_n=0 \ \Rightarrow\ \frac{dE_n}{d\tau}=\frac{\partial E_n}{\partial t}+\mathbf{v}_{\text{true}}\cdot\nabla E_n=0 \qquad \textbf{(3.6.9.1.9)}$$

In Eulerian step,

$$h\frac{dE_n}{d\tau}-\nabla\cdot(h\mathbf{K}\cdot\nabla E_n)+\left(L_{HS}+\frac{\partial h}{\partial t}\right)E_n=\mathbf{q}\cdot\nabla E_n^{\ im}-\nabla\cdot\left(h\mathbf{K}\cdot\nabla E_n^{\ im}\right)+R_{HS}+hR_{E_n} \qquad \textbf{(3.6.9.1.10)}$$

Equation (3.6.9.1.10) written in a slightly different form is shown as

$$\frac{dE_n}{d\tau}-D+KE_n=T+R_L \qquad \textbf{(3.6.9.1.11)}$$

where

$$D=\frac{1}{h}\nabla\cdot(h\mathbf{K}\cdot\nabla E_n) \qquad \textbf{(3.6.9.1.12)}$$

$$K = \frac{\left(L_{HS} + \frac{\partial h}{\partial t}\right)}{h} \quad \textbf{(3.6.9.1.13)}$$

$$R_L = \frac{R_{HS} + hR_{E_n}}{h} \quad \textbf{(3.6.9.1.14)}$$

$$T = \frac{1}{h}\left[\mathbf{q} \cdot \nabla E_n^{\,im} - \nabla \cdot \left(h\mathbf{K} \cdot \nabla E_n^{\,im}\right)\right] \quad \textbf{(3.6.9.1.15)}$$

According to section 3.6.4,

$$[A1]\{D\} = -[A2]\{E_n\} + \{B1\} \quad \textbf{(3.6.9.1.16)}$$

where

$$A1_{ij} = \int_R N_i h N_j dR \quad \textbf{(3.6.9.1.17)}$$

$$A2_{ij} = \int_R \nabla N_i \cdot (h\mathbf{K} \cdot \nabla N_j) dR \quad \textbf{(3.6.9.1.18)}$$

$$B1_i = \int_B \mathbf{n} N_i \cdot (h\mathbf{K} \cdot \nabla E_n) dB \quad \textbf{(3.6.9.1.19)}$$

Lump matrix [A1] into diagonal matrix and assign

$$QE_{ij} = A2_{ij} / A1_{ii} \quad \textbf{(3.6.9.1.20)}$$

$$QB1_i = B1_i / A1_{ii} \quad \textbf{(3.6.9.1.21)}$$

Then

$$\{D\} = \{D1\} + \{QB1\} \quad \textbf{(3.6.9.1.22)}$$

where

$$\{D1\} = -[QE]\{E_n\} \quad \textbf{(3.6.9.1.23)}$$

Approximate T by a linear combination of the base functions as follows:

$$T \approx \hat{T} = \sum_{j=1}^{N} T_j(t) N_j(R) \quad \textbf{(3.6.9.1.24)}$$

According to equation (3.6.9.1.24), the integration of equation (3.6.9.1.15) can be written as

$$\int_R N_i h T dR = \int_R N_i h \sum_{j=1}^{N} T_j(t) N_j(R) dR = \int_R N_i \left[\mathbf{q} \cdot \nabla E_n^{\,im} - \nabla \cdot \left(h\mathbf{K} \cdot \nabla E_n^{\,im}\right)\right] dR \quad \textbf{(3.6.9.1.25)}$$

Further, we obtain

$$\sum_{j=1}^{N}\left[\left(\int_R N_i h N_j dR\right) T_j\right] = \int_R N_i \mathbf{q} \cdot \nabla E_n^{\,im} dR + \int_R \nabla N_i \cdot \left(h\mathbf{K} \cdot \nabla E_n^{\,im}\right) dR - \int_B \mathbf{n} \cdot N_i \left(h\mathbf{K} \cdot \nabla E_n^{\,im}\right) dB \quad \textbf{(3.6.9.1.26)}$$

Approximate $E_n^{\,im}$ by a linear combination of the base functions as follows:

$$E_n^{\,im} \approx \hat{E}_n^{\,im} = \sum_{j=1}^{N} E_{nj}^{\,im}(t) N_j(R) \qquad \textbf{(3.6.9.1.27)}$$

Equation (3.6.9.1.26) is further expressed as

$$\begin{aligned} \sum_{j=1}^{N}\left[\left(\int_R N_i h N_j dR\right) T_j\right] &= \sum_{j=1}^{N}\left[\left(\int_R N_i \mathbf{q}\cdot\nabla N_j dR\right)(E_n^{\,im})_j\right] \\ +\sum_{j=1}^{N}\left[\left(\int_R \nabla N_i\cdot\left(h\mathbf{K}\cdot\nabla N_j\right)dR\right)(E_n^{\,im})_j\right] &- \int_B \mathbf{n}\cdot N_i\left(h\mathbf{K}\cdot\nabla E_n^{\,im}\right)dB \end{aligned} \qquad \textbf{(3.6.9.1.28)}$$

Assign matrices [A3], and load vector {B2} as following

$$A3_{ij} = \int_R N_i \mathbf{q}\cdot\nabla N_j dR \qquad \textbf{(3.6.9.1.29)}$$

$$B2_i = -\int_B \mathbf{n}\cdot N_i\left(h\mathbf{K}\cdot\nabla E_n^{\,im}\right)dB \qquad \textbf{(3.6.9.1.30)}$$

Assign

$$QT_{ij} = (A2_{ij} + A3_{ij}) / A1_{ii} \qquad \textbf{(3.6.9.1.31)}$$

$$QB2_i = B2_i / A1_{ii} \qquad \textbf{(3.6.9.1.32)}$$

Equation (3.6.9.1.28) is expressed as

$$\{T\} = \{T1\} + \{QB2\} \qquad \textbf{(3.6.9.1.33)}$$

where

$$\{T1\} = [QT]\left\{E_n^{\,im}\right\} \qquad \textbf{(3.6.9.1.34)}$$

So that equation (3.6.9.1.11) is then expressed as

$$\frac{dE_n}{d\tau} - D1 + KE_n = T1 + R_L + B \qquad \textbf{(3.6.9.1.35)}$$

where B=B1+B2. For boundary node i = b, the boundary term {B} should be calculated as follows.

For Dirichlet boundary condition

$$E_n^{\,m} = E_n^{\,m}(x_b, y_b, t) \;\Rightarrow\; B_i = \int_B \mathbf{n}\cdot N_i\left(h\mathbf{K}\cdot\nabla E_n^{\,m}\right)dB \Big/ A1_{ii} \qquad \textbf{(3.6.9.1.36)}$$

Variable boundary condition

< Case 1 > when flow is going in from outside ($\mathbf{n}\cdot\mathbf{q} < 0$)

$$\begin{aligned} \mathbf{n}\cdot\left(\mathbf{q}E_n^{\,m} - h\mathbf{K}\cdot\nabla E_n^{\,m}\right) &= \mathbf{n}\cdot\mathbf{q}E_n^{\,m}(x_b, y_b, t) \;\Rightarrow \\ B_i = \int_B \mathbf{n}N_i\cdot\mathbf{q}E_n^{\,m}dB \Big/ A1_{ii} &- \int_B \mathbf{n}N_i\cdot\mathbf{q}E_n^{\,m}(x_b, y_b, t)dB \Big/ A1_{ii} \end{aligned} \qquad \textbf{(3.6.9.1.37)}$$

< Case 2 > Flow is going out from inside ($\mathbf{n}\cdot\mathbf{q} > 0$):

$$-\mathbf{n}\cdot\left[h\mathbf{K}\cdot\nabla E_n^{\ m}(x_b,y_b,t)\right]=0 \;\Rightarrow\; B_i=0 \qquad \textbf{(3.6.9.1.38)}$$

Cauchy boundary condition

$$\begin{aligned}&\mathbf{n}\cdot\left[\mathbf{q}E_n^{\ m}(x_b,y_b,t)-h\mathbf{K}\cdot\nabla E_n^{\ m}(x_b,y_b,t)\right]=q_b(t)\\ &\Rightarrow\; B_i=\int_B N_i\left[\mathbf{n}\cdot\mathbf{q}E_n^{\ m}(x_b,y_b,t)-q_b(t)\right]dB\Big/QA_{ii}\\ &=\sum_{j=1}^{N}\left[\left(\int_B N_i\mathbf{n}\cdot\mathbf{q}N_j dB\right)E_{nj}^{\ m}(t)\right]\Big/QA_{ii}-\left(\int_B N_i dB\right)B\Big/QA_{ii}\end{aligned} \qquad \textbf{(3.6.9.1.39)}$$

Neumann boundary condition

$$-\mathbf{n}\cdot\left[h\mathbf{K}\cdot\nabla E_n^{\ m}(x_b,y_b,t)\right]=q_b(t) \;\Rightarrow\; B_i=-\int_B N_i q_b(t)dB\Big/QA_{ii}=-\left(\int_B N_i dB\right)B\Big/QA_{ii} \qquad \textbf{(3.6.9.1.40)}$$

River/stream-overland interface boundary condition

$$\begin{aligned}&\mathbf{n}\cdot\left[\mathbf{q}E_n^{\ m}(x_b,y_b,t)-h\mathbf{K}\cdot\nabla E_n^{\ m}(x_b,y_b,t)\right]=q_b(h_b(t)) \;\Rightarrow\\ &B_i=\int_B N_i\left[\mathbf{n}\cdot\mathbf{q}E_n^{\ m}(x_b,y_b,t)-q_b(h_b(t))\right]dB\Big/QA_{ii}\\ &=\sum_{j=1}^{N}\left[\left(\int_B N_i\mathbf{n}\cdot\mathbf{q}N_j dB\right)E_{nj}^{\ m}(t)\right]\Big/QA_{ii}-\left(\int_B N_i dB\right)B\Big/QA_{ii}\end{aligned} \qquad \textbf{(3.6.9.1.41)}$$

Equation (3.6.9.1.35) written in matrix form is then expressed as

$$\begin{aligned}&\frac{[U]}{\Delta\tau}\left(\{E_n\}-\{E_n^{\ *}\}\right)-W_1\{D1\}-W_2\{D1^*\}+W_1\{K\}^T[U]\{E_n\}+W_2\{K^*\}^T[U]\{E_n^{\ *}\}\\ &=W_1\{T1\}+W_2\{T1^*\}+W_1\{RL\}+W_2\{RL^*\}+W_1\{B\}+W_2\{B^*\}\end{aligned} \qquad \textbf{(3.6.9.1.42)}$$

At upstream flux boundary nodes, equation (3.6.9.1.42) cannot be applied because $\Delta\tau$ equals zero. Thus, we propose a modified LE approach in which the matrix equation for upstream boundary nodes is obtained by explicitly applying the finite element method to the boundary conditions. For example, at the upstream variable boundary

$$\int_B N_i n\cdot(qE_n^{\ m}-hK\cdot\nabla E_n^{\ m})dB=\int_B N_i n\cdot qE_n^{\ m}(x_b,y_b,t)dB \qquad \textbf{(3.6.9.1.43)}$$

So that the following matrix equation can be assembled at the boundary nodes

$$[QF]\{E_n^{\ m}\}=[QB]\{B\} \qquad \textbf{(3.6.9.1.44)}$$

in which

$$QF_{ij}=\int_B(N_i\mathbf{n}\cdot\mathbf{q}N_j-N_i\mathbf{n}\cdot h\mathbf{K}\cdot\nabla N_j)dB \qquad \textbf{(3.6.9.1.45)}$$

$$QB_{ij} = \int_B N_i \mathbf{n} \cdot \mathbf{q} N_j dB \qquad \textbf{(3.6.9.1.46)}$$

$$B_i = E_n^{\ m}(x_b, y_b, t) \qquad \textbf{(3.6.9.1.47)}$$

3.6.9.2 Mixed Predictor-corrector/Operator-splitting scheme

Recall the simplified equation for 2-D kinetic variable transport mixed Predictor-corrector/Operator-splitting scheme transport step in advection form, equation (3.6.8.2.2), as follows

$$h\frac{\partial E_n^{\ m}}{\partial t} + \mathbf{q}\cdot\nabla E_n^{\ m} - \nabla\cdot(h\mathbf{K}\cdot\nabla E_n^{\ m}) + \left(L_{HS} + \frac{\partial h}{\partial t}\right)E_n^{\ m} = R_{HS} + hR_{E_n}^{\ n} - \frac{\partial h}{\partial t}(E_n^{im})^n \qquad \textbf{(3.6.9.2.1)}$$

Assign the true transport velocity $\mathbf{v}_{\text{true}}$ as follows

$$h\mathbf{v}_{true} = \mathbf{q} = W_1\mathbf{q}^{n+1} + W_2\mathbf{q}^n \qquad \textbf{(3.6.9.2.2)}$$

Equation (3.6.9.2.1) in the Lagrangian and Eulerian form is written as follows. In lagrangian step,

$$h\frac{dE_n^{\ m}}{d\tau} = h\frac{\partial E_n^{\ m}}{\partial t} + \mathbf{q}\cdot\nabla E_n^{\ m} = 0 \quad \Rightarrow \quad \frac{\partial E_n^{\ m}}{\partial t} + \mathbf{v}_{true}\cdot\nabla E_n^{\ m} = 0 \qquad \textbf{(3.6.9.2.3)}$$

In Eulerian step,

$$h\frac{dE_n^{\ m}}{d\tau} - \nabla\cdot(h\mathbf{K}\cdot\nabla E_n^{\ m}) + \left(L_{HS} + \frac{\partial h}{\partial t}\right)E_n^{\ m} = R_{HS} + hR_{E_n}^{\ n} - \frac{\partial h}{\partial t}(E_n^{im})^n \qquad \textbf{(3.6.9.2.4)}$$

Equation (3.6.9.3.4) written in a slightly different form is shown as

$$\frac{dE_n^{\ m}}{d\tau} - D + K * E_n^{\ m} = R_L \qquad \textbf{(3.6.9.2.5)}$$

where

$$D = \frac{1}{h}\nabla\cdot(h\mathbf{K}\cdot\nabla E_n^{\ m}) \qquad \textbf{(3.6.9.2.6)}$$

$$K = \frac{\left(L_{HS} + \frac{\partial h}{\partial t}\right)}{h} \qquad \textbf{(3.6.9.2.7)}$$

$$R_L = \frac{R_{HS} + hR_{E_n}^{\ n} - \frac{\partial h}{\partial t}(E_n^{im})^n}{h} \qquad \textbf{(3.6.9.2.8)}$$

Equation (3.6.9.2.5) written in matrix form is then expressed as

$$\begin{aligned}\frac{[\mathrm{U}]}{\Delta\tau}\left(\{\mathrm{E_n}^{\mathrm{m}}\} - \{\mathrm{E_n}^{\mathrm{m^*}}\}\right) - \mathrm{W_1}\{\mathrm{D}\} - \mathrm{W_2}\{\mathrm{D^*}\} + \mathrm{W_1}\{\mathrm{K}\}^{\mathrm{T}}[\mathrm{U}]\{\mathrm{E_n}^{\mathrm{m}}\} + \mathrm{W_2}\left\{\mathrm{K^*}\right\}^{\mathrm{T}}[\mathrm{U}]\{\mathrm{E_n}^{\mathrm{m^*}}\} \\ = \mathrm{W_1}\{\mathrm{R_L}\} + \mathrm{W_2}\left\{\left(\mathrm{R_L}\right)^*\right\}\end{aligned} \qquad \textbf{(3.6.9.2.9)}$$

Same as that in section 3.6.9.1,

$$\{D\} = -[QD]\{E_n^m\} + \{QB\} \quad \textbf{(3.6.9.2.10)}$$

At upstream flux boundary nodes, equation (3.6.9.2.9) cannot be applied because $\Delta\tau$ equals zero. Thus, we propose a modified LE approach in which the matrix equation for upstream boundary nodes is obtained by explicitly applying the finite element method to the boundary conditions.

3.6.9.3 Operator-splitting scheme

Equation (3.6.8.3.2) can be solved through the same procedure as that in section 3.6.9.2, except that

$$R_L = \frac{R_{HS}}{h} \quad \textbf{(3.6.9.3.1)}$$

3.6.10 Application of the Lagrangian-Eulerian Approach for All Interior Nodes and Downstream Boundary Nodes with the Finite Element Method Applied to the Conservative Form of the Transport Equations for the Upstream Flux Boundaries to Solve 2-D Kinetic Variable Transport

3.6.10.1 Fully-Implicit Scheme

For this option, the matrix equation for interior and downstream boundary nodes is obtained through the same procedure as that in section 3.6.9.1, and the matrix equation for upstream boundary nodes is obtained through the same procedure as that in section 3.6.7.1.

3.6.10.2 Mixed Predictor-Corrector and Operator-Splitting Method

For this option, the matrix equation for interior and downstream boundary nodes is obtained through the same procedure as that in section 3.6.9.2, and the matrix equation for upstream boundary nodes is obtained through the same procedure as that in section 3.6.7.2.

3.6.10.3 Operator-Splitting Approach

For this option, the matrix equation for interior and downstream boundary nodes is obtained through the same procedure as that in section 3.6.9.3, and the matrix equation for upstream boundary nodes is obtained through the same procedure as that in section 3.6.7.3.

3.6.11 Application of the Lagrangian-Eulerian Approach for All Interior Nodes and Downstream Boundary Nodes with the Finite Element Method Applied to the Advective Form of the Transport Equations for the Upstream Flux Boundaries to Solve 2-D Kinetic Variable Transport

3.6.11.1 Fully-Implicit Scheme

For this option, the matrix equation for interior and downstream boundary nodes is obtained through

the same procedure as that in section 3.6.9.1, and the matrix equation for upstream boundary nodes is obtained through the same procedure as that in section 3.6.8.1.

3.6.11.2 Mixed Predictor-Corrector and Operator-Splitting Method

For this option, the matrix equation for interior and downstream boundary nodes is obtained through the same procedure as that in section 3.6.9.2, and the matrix equation for upstream boundary nodes is obtained through the same procedure as that in section 3.6.8.2.

3.6.11.3 Operator-Splitting Approach

For this option, the matrix equation for interior and downstream boundary nodes is obtained through the same procedure as that in section 3.6.9.3, and the matrix equation for upstream boundary nodes is obtained through the same procedure as that in section 3.6.8.3.

3.7 Solving Three-Dimensional Subsurface Water Quality Transport Equations

In this section, we present the numerical approaches employed to solve the governing equations of reactive chemical transport. Ideally, one would like to use a numerical approach that is accurate, efficient, and robust. Depending on the specific problem at hand, different numerical approaches may be more suitable. For research applications, accuracy is a primary requirement, because one does not want to distort physics due to numerical errors. On the other hand, for large field-scale problems, efficiency and robustness are primary concerns as long as accuracy remains within the bounds of uncertainty associated with model parameters. Thus, to provide accuracy for research applications and efficiency and robustness for practical applications, three coupling strategies were investigated to deal with reactive chemistry. They are: (1) a fully-implicit scheme, (2) a mixed predictor-corrector/operator-splitting method, and (3) an operator-splitting method. For each time-step, we first solve the advective-dispersive transport equation with or without reaction terms, kinetic-variable by kinetic-variable. We then solve the reactive chemical system node-by-node to yield concentrations of all species.

Five numerical options are provided to solve the advective-dispersive transport equations: Option 1- application of the Finite Element Method (FEM) to the conservative form of the transport equations, Option 2 - application of the FEM to the advective form of the transport equations, Option 3 - application of the modified Lagrangian-Eulerian (LE) approach to the Largrangian form of the transport equations, Option 4 - LE approach for all interior nodes and downstream boundary nodes with the FEM applied to the conservative form of the transport equations for the upstream flux boundaries, and Option 5 - LE approach for all interior and downstream boundary nodes with the FEM applied to the advective form of the transport equations for upstream flux boundaries.

3.7.1 Application of the Finite Element Method to the Conservative Form of the Reactive Chemical Transport Equations

3.7.1.1 Fully-Implicit Scheme

Assign the right-hand side term R_{HS} and left hand side term L_{HS} as follows.

$$\begin{aligned} &If\ q \le 0, \quad M_{E_n}{}^{as} = qE_n{}^{m}, \quad L_{HS} = -q, \quad R_{HS} = 0 \\ &Else\ q > 0, \quad M_{E_n}{}^{as} = qE_{n^{as}}, \quad L_{HS} = 0, \quad R_{HS} = M_{E_n}{}^{as} \end{aligned} \tag{3.7.1.1.1}$$

Then equation (2.7.22) is modified as

$$\theta \frac{\partial E_n}{\partial t} + \frac{\partial \theta}{\partial t} E_n + \nabla \cdot (\mathbf{V} E_n{}^{m}) - \nabla \cdot (\theta \mathbf{D} \cdot \nabla E_n{}^{m}) + L_{HS} E_n{}^{m} = R_{HS} + \theta R_{E_n} \tag{3.7.1.1.2}$$

According to the fully-implicit scheme, equation (3.7.1.1.2) can be separated into two equations as follows.

$$\theta \frac{E_n{}^{n+1/2} - E_n{}^{n}}{\Delta t} + \frac{\partial \theta}{\partial t} E_n + \nabla \cdot (\mathbf{V} E_n{}^{m}) - \nabla \cdot (\theta \mathbf{D} \cdot \nabla E_n{}^{m}) + L_{HS} E_n{}^{m} = R_{HS} + \theta R_{E_n} \tag{3.7.1.1.3}$$

$$\frac{E_n{}^{n+1} - E_n{}^{n+1/2}}{\Delta t} = 0 \tag{3.7.1.1.4}$$

First, we express $E_n{}^{m}$ in terms of $(E_n{}^{m}/E_n)\cdot E_n$ or $(E_n – E_n{}^{im})$ to make E_n's as primary dependent variables, so that $E_n{}^{n+1/2}$ can be solved through equation (3.7.1.1.3). It is noted that the approach of expressing $E_n{}^{m}$ in terms of $(E_n{}^{m}/E_n)\cdot E_n$ improves model accuracy but is less robust than the approach of expressing $E_n{}^{m}$ in terms of $(E_n – E_n{}^{im})$ taken in Yeh et al. [2004]. Second, we solve equation (3.7.1.1.4) together with algebraic equations for equilibrium reactions using BIOGEOCHEM [Fang et al., 2003] to obtain all individual species concentrations. Iteration between these two steps is needed because the new reaction terms $RA_n{}^{n+1}$ and the equation coefficients in equation (3.7.1.1.3) need to be updated by the calculation results of (3.7.1.1.4). To improve the standard SIA method, the nonlinear reaction terms are approximated by the Newton-Raphson linearization.

Option 1: Express $E_n{}^{m}$ in terms of $(E_n{}^{m}/E_n)\ E_n{}^{m}$

$$\begin{aligned} &\theta \frac{\partial E_n}{\partial t} + \nabla \cdot \left(\mathbf{V} \frac{E_n{}^{m}}{E_n} E_n \right) - \nabla \cdot \left(\theta \mathbf{D} \cdot \frac{E_n{}^{m}}{E_n} \nabla E_n \right) \\ &- \nabla \cdot \left[\theta \mathbf{D} \cdot \left(\nabla \frac{E_n{}^{m}}{E_n} \right) E_n \right] + \left(L_{HS} \frac{E_n{}^{m}}{E_n} + \frac{\partial \theta}{\partial t} \right) E_n = R_{HS} + \theta R_{E_n} \end{aligned} \tag{3.7.1.1.5}$$

Use Galerkin or Petrov-Galerkin Finite-Element Method for the spatial descretization of transport equation: choose weighting function identical to base function. For Petriov-Galerkin method, apply weighting function one-order higher than the base function to advection term. Integrate equation (3.7.1.1.5) in the spatial dimensions over the entire region as follows.

$$\int_R N_i \left[\theta \frac{\partial E_n}{\partial t} - \nabla \cdot \left(\theta \mathbf{D} \cdot \frac{{E_n}^m}{E_n} \nabla E_n \right) + \left(L_{HS} \frac{{E_n}^m}{E_n} + \frac{\partial \theta}{\partial t} \right) E_n \right] dR$$
$$+ \int_R W_i \left\{ \nabla \cdot \left(\mathbf{V} \frac{{E_n}^m}{E_n} E_n \right) - \nabla \cdot \left[\theta \mathbf{D} \cdot \left(\nabla \frac{{E_n}^m}{E_n} \right) E_n \right] \right\} dR = \int_R N_i (R_{HS} + \theta R_{E_n}) dR \quad \textbf{(3.7.1.1.6)}$$

Further, we obtain

$$\int_R N_i \theta \frac{\partial E_n}{\partial t} dR - \int_R \nabla W_i \cdot \mathbf{V} \frac{{E_n}^m}{E_n} E_n dR + \int_R \nabla N_i \cdot \left(\theta \mathbf{D} \cdot \frac{{E_n}^m}{E_n} \nabla E_n \right) dR$$
$$+ \int_R \nabla W_i \cdot \left[\theta \mathbf{D} \cdot \left(\nabla \frac{{E_n}^m}{E_n} \right) E_n \right] dR + \int_R N_i \left(L_{HS} \frac{{E_n}^m}{E_n} + \frac{\partial \theta}{\partial t} \right) E_n dR = \int_R N_i (R_{HS} + \theta R_{E_n}) dR \quad \textbf{(3.7.1.1.7)}$$
$$- \int_B \mathbf{n} \cdot W_i \mathbf{V} \frac{{E_n}^m}{E_n} E_n dB + \int_B \mathbf{n} \cdot \left(N_i \theta \mathbf{D} \cdot \frac{{E_n}^m}{E_n} \nabla E_n \right) dB + \int_B \mathbf{n} \cdot \left[W_i \theta \mathbf{D} \cdot \left(\nabla \frac{{E_n}^m}{E_n} \right) E_n \right] dB$$

Approximate solution E_n by a linear combination of the base functions as follows.

$$E_n \approx \hat{E}_n = \sum_{j=1}^{N} E_{nj}(t) N_j(R) \quad \textbf{(3.7.1.1.8)}$$

Substituting equation (3.7.1.1.8) into equation (3.7.1.1.7), we obtain

$$\sum_{j=1}^{N} \left[\left(\int_R N_i \theta N_j dR \right) \frac{\partial E_{nj}(t)}{\partial t} \right]$$
$$+ \sum_{j=1}^{N} \left\{ \left\{ - \int_R \nabla W_i \cdot \mathbf{V} \frac{{E_n}^m}{E_n} N_j dR + \int_R \nabla W_i \cdot \left[\theta \mathbf{D} \cdot \left(\nabla \frac{{E_n}^m}{E_n} \right) N_j \right] dR \right\} E_{nj}(t) \right\}$$
$$+ \sum_{j=1}^{N} \left\{ \left[\int_R \nabla N_i \cdot \left(\theta \mathbf{D} \cdot \frac{{E_n}^m}{E_n} \nabla N_j \right) dR + \int_R N_i \left(L_{HS} \frac{{E_n}^m}{E_n} + \frac{\partial \theta}{\partial t} \right) N_j dR \right] E_{nj}(t) \right\} \quad \textbf{(3.7.1.1.9)}$$
$$= \int_R N_i (R_{HS} + \theta R_{E_n}) dR - \int_B \mathbf{n} \cdot W_i \mathbf{V} {E_n}^m dB + \int_B \mathbf{n} \cdot \left(N_i \theta \mathbf{D} \cdot \nabla {E_n}^m \right) dB$$

Equation (3.7.1.1.9) can be written in matrix form as

$$[Q1] \left\{ \frac{\partial E_n}{\partial t} \right\} + [Q2] \{E_n\} + [Q3] \{E_n\} = \{RLS\} + \{B\} \quad \textbf{(3.7.1.1.10)}$$

where the matrices [Q1], [Q2], [Q3] and load vectors {RLS}, and {B} are given by

$$Q1_{ij} = \int_R N_i \theta N_j dR \quad \textbf{(3.7.1.1.11)}$$

$$Q2_{ij} = -\int_R \nabla W_i \cdot \mathbf{V} \frac{E_n^{\,m}}{E_n} N_j dR + \int_R \nabla W_i \cdot \left[\theta \mathbf{D} \cdot \left(\nabla \frac{E_n^{\,m}}{E_n} \right) N_j \right] dR \qquad \textbf{(3.7.1.1.12)}$$

$$Q3_{ij} = \int_R \nabla N_i \cdot \left(\theta \mathbf{D} \cdot \frac{E_n^{\,m}}{E_n} \nabla N_j \right) dR + \int_R N_i \left(L_{HS} \frac{E_n^{\,m}}{E_n} + \frac{\partial \theta}{\partial t} \right) N_j dR \qquad \textbf{(3.7.1.1.13)}$$

$$RLS_i = \int_R N_i (R_{HS} + \theta R_{E_n}) dR \qquad \textbf{(3.7.1.1.14)}$$

$$B_i = -\int_B \mathbf{n} \cdot W_i \mathbf{V} E_n^{\,m} dB + \int_B \mathbf{n} \cdot \left(N_i \theta \mathbf{D} \cdot \nabla E_n^{\,m} \right) dB \qquad \textbf{(3.7.1.1.15)}$$

At n+1-th time step, equation (3.7.1.1.10) is approximated as

$$\begin{aligned} [Q1] \frac{\left\{ E_n^{\,n+1/2} \right\} - \left\{ E_n^{\,n} \right\}}{\Delta t} &+ W_{V1}[Q2^{n+1}] \left\{ E_n^{\,n+1/2} \right\} + W_{V2}[Q2^n] \left\{ E_n^{\,n} \right\} \\ &+ W_1[Q3^{n+1}] \left\{ E_n^{\,n+1/2} \right\} + W_2[Q3^n] \left\{ E_n^{\,n} \right\} \\ &= W_1\{RLS^{n+1}\} + W_2\{RLS^n\} + W_1\{B^{n+1}\} + W_2\{B^n\} \end{aligned} \qquad \textbf{(3.7.1.1.16)}$$

where W_{V1}, W_{V2}, W_1 and W_2 are time weighting factors, matrices and vectors with superscripts $^{n+1}$ and ^{n} are evaluated over the region at the new time step n+1 and at the old time step n, respectively.

So that

$$\begin{aligned} &\left(\frac{[Q1]}{\Delta t} + W_{V1}[Q2^{n+1}] + W_1[Q3^{n+1}] \right) \left\{ E_n^{\,n+1/2} \right\} \\ &= \left(\frac{[Q1]}{\Delta t} - W_{V2}[Q2^n] - W_2[Q3^n] \right) \left\{ E_n^{\,n} \right\} + W_1\{SS^{n+1}\} + W_2\{SS^n\} + W_1\{B^{n+1}\} + W_2\{B^n\} \end{aligned} \qquad \textbf{(3.7.1.1.17)}$$

Option 2: Express $E_n^{\,m}$ in terms of E_n-$E_n^{\,im}$

Use Galerkin or Petrov-Galerkin Finite-Element Method for the spatial descretization of transport equation. Integrate equation (3.7.1.1.3) in the spatial dimensions over the entire region as follows.

$$\begin{aligned} \int_R N_i \left[\theta \frac{\partial E_n}{\partial t} + \frac{\partial \theta}{\partial t} E_n - \nabla \cdot \left(\theta \mathbf{D} \cdot E_n^{\,m} \right) + L_{HS} E_n^{\,m} \right] dR + \int_R W_i \left[\nabla \cdot \left(\mathbf{V} E_n^{\,m} \right) \right] dR \\ = \int_R N_i (R_{HS} + \theta R_{E_n}) dR \end{aligned} \qquad \textbf{(3.7.1.1.18)}$$

Further, we obtain

$$\int_R N_i\left(\theta\frac{\partial E_n}{\partial t}+\frac{\partial\theta}{\partial t}E_n\right)dR-\int_R\nabla W_i\cdot\mathbf{V}E_n{}^m dR+\int_R\nabla N_i\cdot\left(\theta\mathbf{D}\cdot\nabla E_n{}^m\right)dR+\int_R N_i L_{HS}E_n{}^m dR$$
$$=\int_R N_i(R_{HS}+\theta R_{E_n})dR-\int_B\mathbf{n}\cdot W_i\mathbf{V}E_n{}^m dB+\int_B\mathbf{n}\cdot\left(N_i\theta\mathbf{D}\cdot\nabla E_n{}^m\right)dB \quad \textbf{(3.7.1.1.19)}$$

Approximate solution E_n by a linear combination of the base functions as equation (3.7.1.1.8). Substituting equation (3.7.1.1.8) into equation (3.7.1.1.19), we obtain

$$\sum_{j=1}^N\left[\left(\int_R N_i\theta^n N_j dR\right)\frac{\partial E_{nj}(t)}{\partial t}\right]+\sum_{j=1}^N\left[\left(-\int_R\nabla W_i\cdot\mathbf{V}N_j dR\right)E_{nj}{}^m(t)\right]+$$
$$\sum_{j=1}^N\left[\left(\int_R N_i\frac{\partial\theta}{\partial t}N_j dR\right)E_{nj}(t)\right]+\sum_{j=1}^N\left\{\left[\int_R\nabla N_i\cdot\left(\theta\mathbf{D}\cdot\nabla N_j\right)dR+\int_R N_i L_{HS}N_j dR\right]E_{nj}{}^m(t)\right\} \quad \textbf{(3.7.1.1.20)}$$
$$=\int_R N_i(R_{HS}+\theta R_{E_n})dR-\int_B\mathbf{n}\cdot W_i\mathbf{V}E_n{}^m dB+\int_B\mathbf{n}\cdot\left(N_i\theta\mathbf{D}\cdot\nabla E_n{}^m\right)dB$$

Equation (3.7.1.1.20) can be written in matrix form as

$$[Q1]\left\{\frac{\partial E_n}{\partial t}\right\}+[Q4]\{E_n\}+[Q2]\{E_n{}^m\}+[Q3]\{E_n{}^m\}=\{RLS\}+\{B\} \quad \textbf{(3.7.1.1.21)}$$

where the matrices [Q1], [Q4], [Q2], [Q3] and load vectors {RLS}, and {B} are given by

$$Q1_{ij}=\int_R N_i\theta N_j dR,\qquad Q4_{ij}=\int_R N_i\frac{\partial\theta}{\partial t}N_j dR \quad \textbf{(3.7.1.1.22)}$$

$$Q2_{ij}=-\int_R\nabla W_i\cdot\mathbf{V}N_j dR \quad \textbf{(3.7.1.1.23)}$$

$$Q3_{ij}=\int_R\nabla N_i\cdot\left(\theta\mathbf{D}\cdot\nabla N_j\right)dR+\int_R N_i L_{HS}N_j dR \quad \textbf{(3.7.1.1.24)}$$

$$RLS_i=\int_R N_i(R_{HS}+\theta R_{E_n})dR \quad \textbf{(3.7.1.1.25)}$$

$$B_i=-\int_B\mathbf{n}\cdot W_i\mathbf{V}E_n{}^m dB+\int_B\mathbf{n}\cdot\left(N_i\theta\mathbf{D}\cdot\nabla E_n{}^m\right)dB \quad \textbf{(3.7.1.1.26)}$$

Express $E_n{}^m$ in terms of E_n-$E_n{}^{im}$, equation (3.7.1.1.21) is modified as

$$[Q1]\left\{\frac{\partial E_n}{\partial t}\right\}+[Q4]\{E_n\}+[Q2]\{E_n\}+[Q3]\{E_n\}=[Q2]\{E_n{}^{im}\}+[Q3]\{E_n{}^{im}\}$$
$$+\{RLS\}+\{B\} \quad \textbf{(3.7.1.1.27)}$$

At n+1-th time step, equation (3.7.1.1.27) is approximated as

$$[Q1]\frac{\left\{E_n^{\,n+1/2}\right\}-\left\{E_n^{\,n}\right\}}{\Delta t}+[Q4]\left\{E_n^{\,n+1/2}\right\}+W_{V1}[Q2^{n+1}]\left\{E_n^{\,n+1/2}\right\}+W_{V2}[Q2^{n}]\left\{E_n^{\,n}\right\}$$
$$+W_1[Q3^{n+1}]\left\{E_n^{\,n+1/2}\right\}+W_2[Q3^{n}]\left\{E_n^{\,n}\right\}=W_{V1}[Q2^{n+1}]\left\{\left(E_n^{\,im}\right)^{n+1/2}\right\} \quad \textbf{(3.7.1.1.28)}$$
$$+W_{V2}[Q2^{n}]\left\{\left(E_n^{\,im}\right)^{n}\right\}+W_1[Q3^{n+1}]\left\{\left(E_n^{\,im}\right)^{n+1/2}\right\}+W_2[Q3^{n}]\left\{\left(E_n^{\,im}\right)^{n}\right\}$$
$$+W_1\{RLS^{n+1}\}+W_2\{RLS^{n}\}+W_1\{B^{n+1}\}+W_2\{B^{n}\}$$

So that

$$\left(\frac{[Q1]}{\Delta t}+[Q4]+W_{V1}[Q2^{n+1}]+W_1[Q3^{n+1}]\right)\left\{E_n^{\,n+1/2}\right\}=\frac{[Q1]}{\Delta t}\left\{E_n^{\,n}\right\}-$$
$$\left(W_{V2}[Q2^{n}]+W_2[Q3^{n}]\right)*\left\{\left(E_n^{\,m}\right)^{n}\right\}+\left(W_{V1}[Q2^{n+1}]+W_1[Q3^{n+1}]\right)\left\{\left(E_n^{\,im}\right)^{n+1/2}\right\}+ \quad \textbf{(3.7.1.1.29)}$$
$$W_1\{SS^{n+1}\}+W_2\{SS^{n}\}+W_1\{B^{n+1}\}+W_2\{B^{n}\}$$

For interior nodes i, B_i is zero, for boundary nodes i = b, B_i is calculated according to the specified boundary condition and shown as follows.

Dirichlet boundary condition

$$E_n^{\,m}=E_n^{\,m}(x_b,y_b,z_b,t) \quad \textbf{(3.7.1.1.30)}$$

Variable boundary condition

< Case 1 > when flow is going in from outside ($\mathbf{n}\cdot\mathbf{V}<0$)

$$\mathbf{n}\cdot(\mathbf{V}E_n^{\,m}-\theta\mathbf{D}\cdot\nabla E_n^{\,m})=\mathbf{n}\cdot\mathbf{V}E_n^{\,m}(x_b,y_b,z_b,t)\ \Rightarrow\ B_i=-\int_{\mathbf{B}}\mathbf{n}\cdot N_i\mathbf{V}E_n^{\,m}(x_b,y_b,z_b,t)dB \quad \textbf{(3.7.1.1.31)}$$

< Case 2 > Flow is going out from inside ($\mathbf{n}\cdot\mathbf{V}>0$):

$$-\mathbf{n}\cdot(\theta\mathbf{D}\cdot\nabla E_n^{\,m})=0\ \Rightarrow\ B_i=-\int_{B}\mathbf{n}\cdot N_i\mathbf{V}E_n^{\,m}dB \quad \textbf{(3.7.1.1.32)}$$

Cauchy boundary condition

$$\mathbf{n}\cdot(\mathbf{V}E_n^{\,m}-\theta\mathbf{D}\cdot\nabla E_n^{\,m})=Q_{E_n^{\,m}}(x_b,y_b,z_b,t)\ \Rightarrow\ B_i=-\int_{B}N_iQ_{E_n^{\,m}}(x_b,y_b,z_b,t)dB \quad \textbf{(3.7.1.1.33)}$$

Neumann boundary condition

$$-\mathbf{n}\cdot(\theta\mathbf{D}\cdot\nabla {E_n}^m) = Q_{{E_n}^m}(x_b, y_b, z_b, t)$$

$$\Rightarrow \quad B_i = -\int_B \mathbf{n}\cdot N_i \mathbf{V} {E_n}^m dB - \int_B N_i Q_{{E_n}^m}(x_b, y_b, z_b, t) dB \qquad \textbf{(3.7.1.1.34)}$$

River/stream-subsurface interface boundary condition

$$\mathbf{n}\cdot(\mathbf{V}{E_n}^m - \theta\mathbf{D}\cdot\nabla {E_n}^m)$$

$$= \frac{\mathbf{n}\cdot\mathbf{V}}{2}\left\{ [1+sign(\mathbf{n}\cdot\mathbf{V})]{E_n}^m + [1-sign(\mathbf{n}\cdot\mathbf{V})]\left({E_n}^m\right)^{1D}\right\} \quad \Rightarrow \qquad \textbf{(3.7.1.1.35)}$$

$$B_i = -\int_B N_i \frac{\mathbf{n}\cdot\mathbf{V}}{2}\left\{ [1+sign(\mathbf{n}\cdot\mathbf{V})]{E_n}^m + [1-sign(\mathbf{n}\cdot\mathbf{V})]\left({E_n}^m\right)^{1D}\right\} dB$$

Overland-subsurface interface boundary condition

$$\mathbf{n}\cdot(\mathbf{V}{E_n}^m - \theta\mathbf{D}\cdot\nabla {E_n}^m)$$

$$= \frac{\mathbf{n}\cdot\mathbf{V}}{2}\left\{ [1+sign(\mathbf{n}\cdot\mathbf{V})]{E_n}^m + [1-sign(\mathbf{n}\cdot\mathbf{V})]\left({E_n}^m\right)^{2D}\right\} \quad \Rightarrow \qquad \textbf{(3.7.1.1.36)}$$

$$B_i = -\int_B N_i \frac{\mathbf{n}\cdot\mathbf{V}}{2}\left\{ [1+sign(\mathbf{n}\cdot\mathbf{V})]{E_n}^m + [1-sign(\mathbf{n}\cdot\mathbf{V})]\left({E_n}^m\right)^{2D}\right\} dB$$

3.7.1.2 Mixed Predictor-Corrector and Operator-Splitting Method

According to the mixed predictor-corrector (on reaction rates) and operator-splitting (on immobile part of the kinetic variable) method, equation (3.7.1.1.2) can be separated into two equations as follows.

$$\theta\frac{\left({E_n}^m\right)^{n+1/2} - \left({E_n}^m\right)^n}{\Delta t} + \frac{\partial\theta}{\partial t}E_n^m + \nabla\cdot(\mathbf{V}{E_n}^m) - \nabla\cdot(\theta\mathbf{D}\cdot\nabla {E_n}^m)$$

$$+ L_{HS}{E_n}^m = R_{HS} + \theta {R_{E_n}}^n - \frac{\partial\theta}{\partial t}(E_n^{im})^n \qquad \textbf{(3.7.1.2.1)}$$

$$\frac{{E_n}^{n+1} - [(E_n^m)^{n+1/2} + (E_n^{im})^{n+1/2}]}{\Delta t} = \theta {R_{E_n}}^{n+1} - \theta {R_{E_n}}^n - \frac{\partial \ell n\theta}{\partial t}(E_n^{im})^{n+1} + \frac{\partial \ell n\theta}{\partial t}(E_n^{im})^n \qquad \textbf{(3.7.1.2.2)}$$

First, solve equation (3.7.1.2.1) and get $(E_n^m)^{n+1/2}$. Second, solve equation (3.7.1.2.2) together with algebraic equations representing equilibrium reactions using BIOGEOCHM scheme to obtain the individual species concentration.

Use Galerkin or Petrov-Galerkin Finite-Element Method for the spatial descretization of transport equation. Integrate equation (3.7.1.2.1) in the spatial dimensions over the entire region as follows.

$$\int_R N_i \left[\theta \frac{\partial E_n^{\ m}}{\partial t} - \nabla \cdot (\theta \mathbf{D} \cdot \nabla E_n^{\ m}) + \left(L_{HS} + \frac{\partial \theta}{\partial t} \right) E_n^{\ m} \right] dR + \int_R W_i \nabla \cdot \mathbf{V} E_n^{\ m} dR = \int_R N_i \left(R_{HS} + \theta R_{E_n}^{\ n} - \frac{\partial \theta}{\partial t} (E_n^{im})^n \right) dR \quad \textbf{(3.7.1.2.3)}$$

Further, we obtain

$$\int_R N_i \theta \frac{\partial E_n^{\ m}}{\partial t} dR - \int_R \nabla W_i \cdot \mathbf{V} E_n^{\ m} dR + \int_R \nabla N_i \cdot (\theta \mathbf{D} \cdot \nabla E_n^{\ m}) dR + \int_R N_i \left(L_{HS} + \frac{\partial \theta}{\partial t} \right) E_n^{\ m} dR = \int_R N_i \left(R_{HS} + \theta R_{E_n}^{\ n} - \frac{\partial \theta}{\partial t} (E_n^{im})^n \right) dR - \int_B \mathbf{n} \cdot W_i \mathbf{V} E_n^{\ m} dB + \int_B \mathbf{n} \cdot N_i (\theta \mathbf{D} \cdot \nabla E_n^{\ m}) dB \quad \textbf{(3.7.1.2.4)}$$

Approximate solution $E_n^{\ m}$ by a linear combination of the base functions as follows.

$$E_n^{\ m} \approx \hat{E}_n^{\ m} = \sum_{j=1}^{N} E_{nj}^{\ m}(t) N_j(R) \quad \textbf{(3.7.1.2.5)}$$

Substituting equation (3.7.1.2.5) into equation (3.7.1.2.4), we obtain

$$\sum_{j=1}^{N} \left[\left(\int_R N_i \theta N_j dR \right) \frac{\partial E_{nj}^{\ m}(t)}{\partial t} \right] - \sum_{j=1}^{N} \left[\left(\int_R \nabla W_i \cdot \mathbf{V} N_j dR \right) E_{nj}^{\ m}(t) \right] + \sum_{j=1}^{N} \left\{ \left[\int_R \nabla N_i \cdot (\theta \mathbf{D} \cdot \nabla N_j) dR + \int_R N_i \left(L_{HS} + \frac{\partial \theta}{\partial t} \right) N_j dR \right] E_{nj}^{\ m}(t) \right\} = \int_R N_i \left(R_{HS} + \theta R_{E_n}^{\ n} - \frac{\partial \theta}{\partial t} (E_n^{im})^n \right) dR - \int_B \mathbf{n} \cdot W_i \mathbf{V} E_n^{\ m} dB + \int_B \mathbf{n} \cdot N_i (\theta \mathbf{D} \cdot \nabla E_n^{\ m}) dB \quad \textbf{(3.7.1.2.6)}$$

Equation (3.7.1.2.6) can be written in matrix form as

$$[Q1] \left\{ \frac{dE_n^{\ m}}{dt} \right\} + [Q2] \left\{ E_n^{\ m} \right\} + [Q3] \left\{ E_n^{\ m} \right\} = \{RLS\} + \{B\} \quad \textbf{(3.7.1.2.7)}$$

where the matrices [Q1], [Q2], and [Q3], and load vectors {RLS} and {B} are given by

$$Q1_{ij} = \int_R N_i \theta N_j dR \quad \textbf{(3.7.1.2.8)}$$

$$Q2_{ij} = -\int_R \nabla W_i \cdot \mathbf{V} N_j dR \quad \textbf{(3.7.1.2.9)}$$

$$Q3_{ij} = \int_R \nabla N_i \cdot \left(\theta \mathbf{D} \cdot \nabla N_j \right) dR + \int_R N_i \left(L_{HS} + \frac{\partial \theta}{\partial t} \right) N_j dR \quad \textbf{(3.7.1.2.10)}$$

$$RLS_i = \int_R N_i \left(R_{HS} + \theta R_{E_n}{}^n - \frac{\partial \theta}{\partial t}(E_n^{im})^n \right) dR \qquad \textbf{(3.7.1.2.11)}$$

$$B_i = -\int_{\mathbf{B}} \mathbf{n} \cdot W_i \mathbf{V} E_n{}^m dB + \int_B \mathbf{n} \cdot (N_i \theta \mathbf{D} \cdot \nabla E_n{}^m) dB \qquad \textbf{(3.7.1.2.12)}$$

At n+1-th time step, equation (3.7.1.2.7) is approximated as

$$[Q1]\frac{\left\{ \left(E_n{}^m\right)^{n+1/2} \right\} - \left\{ \left(E_n{}^m\right)^n \right\}}{\Delta t} + W_{V1}[Q2^{n+1}] \left\{ \left(E_n{}^m\right)^{n+1/2} \right\} + W_{V2}[Q2^n] \left\{ \left(E_n{}^m\right)^n \right\}$$
$$+W_1[Q3^{n+1}] \left\{ \left(E_n{}^m\right)^{n+1/2} \right\} + W_2[Q3^n] \left\{ \left(E_n{}^m\right)^n \right\} = W_1\{RLS^{n+1}\} + W_2\{RLS^n\} + W_1\{B^{n+1}\} + W_2\{B^n\} \qquad \textbf{(3.7.1.2.13)}$$

So that

$$\left(\frac{[Q1]}{\Delta t} + W_{V1}[Q2^{n+1}] + W_1[Q3^{n+1}] \right) \left\{ \left(E_n{}^m\right)^{n+1/2} \right\} = \left(\frac{[Q1]}{\Delta t} - W_{V2}[Q2^n] - W_2[Q3^n] \right) *$$
$$\left\{ \left(E_n{}^m\right)^n \right\} + W_1\{RLS^{n+1}\} + W_2\{RLS^n\} + W_1\{B^{n+1}\} + W_2\{B^n\} \qquad \textbf{(3.7.1.2.14)}$$

The boundary term {B} is calculated according to the specified boundary conditions the same as that in section 3.7.1.1.

3.7.1.3 Operator-Splitting Approach

According to the operator-splitting approach, equation (3.7.1.1.2) can be separated into two equations as follows.

$$\theta \frac{\left(E_n{}^m\right)^{n+1/2} - \left(E_n{}^m\right)^n}{\Delta t} + \nabla \cdot (\mathbf{V} E_n{}^m) - \nabla \cdot (\theta \mathbf{D} \cdot \nabla E_n{}^m) + \left(L_{HS} + \frac{\partial \theta}{\partial t} \right) E_n{}^m = R_{HS} \qquad \textbf{(3.7.1.3.1)}$$

$$\frac{E_n{}^{n+1} - [(E_n{}^m)^{n+1/2} + (E_n{}^{im})^n]}{\Delta t} = \theta R_{E_n}{}^{n+1} - \frac{\partial \ell n \theta}{\partial t}(E_n^{im})^{n+1} \qquad \textbf{(3.7.1.3.2)}$$

First, solve equation (3.7.1.3.1) and get $(E_n{}^m)^{n+1/2}$. Second, solve equation (3.7.1.3.2) together with algebraic equations representing equilibrium reactions using BIOGEOCHM scheme to obtain the individual species concentration.

Equation (3.7.1.3.1) can be solved through the same procedure as that in section 4.1.2, except for the load vectors {RLS}, which is calculated by the following equation.

$$RLS_i = \int_R N_i R_{HS} dR \qquad \textbf{(3.7.1.3.3)}$$

3.7.2 Application of the Finite Element Method to the Advective Form of the Reactive

3.7.2.1 Fully-Implicit Scheme

Conversion of equation (2.7.22) to advection form is expressed as

$$\theta\frac{\partial E_n}{\partial t}+\frac{\partial \theta}{\partial t}E_n+\mathbf{V}\cdot\nabla {E_n}^m-\nabla\cdot(\theta\mathbf{D}\cdot\nabla {E_n}^m)+(\nabla\cdot\mathbf{V}){E_n}^m=M_{{E_n}^{as}}+\theta R_{E_n},\quad n\in[1,M\text{ - }N_E] \qquad \textbf{(3.7.2.1.1)}$$

According to equation (2.3.1), the right-hand side term R_{HS} and left hand side term L_{HS} can be assigned as follows.

$$\begin{aligned} &If\ q\le 0,\ M_{{E_n}^{as}}=q{E_n}^m,\quad L_{HS}=\left(-\mathbf{V}\bullet\ell n\left(\frac{\rho}{\rho_o}\right)-F\frac{\partial h}{\partial t}\right),\quad RHS=0\\ &Else\ q>0,\ M_{{E_n}^{as}}=M_{{E_n}^{as}},\ L_{HS}=\left(q-\mathbf{V}\bullet\ell n\left(\frac{\rho}{\rho_o}\right)-F\frac{\partial h}{\partial t}\right),\quad R_{HS}=M_{{E_n}^{as}}\end{aligned} \qquad \textbf{(3.7.2.1.2)}$$

Then equation (3.7.2.1.1) is modified as

$$\theta\frac{\partial E_n}{\partial t}+\frac{\partial \theta}{\partial t}E_n+\mathbf{V}\cdot\nabla {E_n}^m-\nabla\cdot(\theta\mathbf{D}\cdot\nabla {E_n}^m)+L_{HS}{E_n}^m=R_{HS}+\theta R_{E_n} \qquad \textbf{(3.7.2.1.3)}$$

According to the fully-implicit scheme, equation (3.7.2.1.3) can be separated into two equations as follows.

$$\theta\frac{{E_n}^{n+1/2}-{E_n}^n}{\Delta t}+\frac{\partial \theta}{\partial t}E_n+\mathbf{V}\cdot\nabla {E_n}^m-\nabla\cdot(\theta\mathbf{D}\cdot\nabla {E_n}^m)+L_{HS}*{E_n}^m=R_{HS}+\theta R_{E_n} \qquad \textbf{(3.7.2.1.4)}$$

$$\frac{{E_n}^{n+1}-{E_n}^{n+1/2}}{\Delta t}=0 \qquad \textbf{(3.7.2.1.5)}$$

First, solve equation (3.7.2.1.4) and get $(E_n)^{n+1/2}$. Second, solve equation (3.7.2.1.5) together with algebraic equations representing equilibrium reactions using BIOGEOCHEM scheme to obtain the individual species concentration. Iteration is needed because reaction term in equation (3.7.2.1.4) needs to be updated by the results of (3.7.2.1.5).

Option 1: Express E_n^m in terms of (E_n^m/E_n) E_n

$$\begin{aligned}&\theta\frac{\partial E_n}{\partial t}+\mathbf{V}\cdot\nabla\left(\frac{{E_n}^m}{E_n}E_n\right)-\nabla\cdot\left(\theta\mathbf{D}\cdot\frac{{E_n}^m}{E_n}\nabla E_n\right)\\ &-\nabla\cdot\left[\theta\mathbf{D}\cdot\left(\nabla\frac{{E_n}^m}{E_n}\right)E_n\right]+\left(L_{HS}\frac{{E_n}^m}{E_n}+\frac{\partial\theta}{\partial t}\right)E_n=R_{HS}+\theta R_{E_n}\end{aligned} \qquad \textbf{(3.7.2.1.6)}$$

Use Galerkin or Petrov-Galerkin Finite-Element Method for the spatial descretization of transport equation. Integrate equation (3.7.2.1.6) in the spatial dimensions over the entire region as follows.

$$\int_R N_i\left[\theta\frac{\partial E_n}{\partial t}-\nabla\cdot\left(\theta\mathbf{D}\cdot\frac{{E_n}^m}{E_n}\nabla E_n\right)+\left(L_{HS}\frac{{E_n}^m}{E_n}+\frac{\partial\theta}{\partial t}\right)E_n\right]dR$$
$$+\int_R W_i\left\{\mathbf{V}\cdot\nabla\left(\frac{{E_n}^m}{E_n}E_n\right)-\nabla\cdot\left[\theta\mathbf{D}\cdot\left(\nabla\frac{{E_n}^m}{E_n}\right)E_n\right]\right\}dR=\int_R N_i(R_{HS}+\theta R_{E_n})dR \quad \textbf{(3.7.2.1.7)}$$

Further, we obtain

$$\int_R N_i\theta\frac{\partial E_n}{\partial t}dR+\int_R W_{\mathbf{i}}\mathbf{V}\cdot\nabla\left(\frac{{E_n}^m}{E_n}E_n\right)dR+\int_R\nabla N_i\cdot\left(\theta\mathbf{D}\cdot\frac{{E_n}^m}{E_n}\nabla E_n\right)dR$$
$$+\int_R\nabla W_i\cdot\left[\theta\mathbf{D}\cdot\left(\nabla\frac{{E_n}^m}{E_n}\right)E_n\right]dR+\int_R N_i\left(L_{HS}\frac{{E_n}^m}{E_n}+\frac{\partial\theta}{\partial t}\right)E_n dR=\int_R N_i(R_{HS}+\theta R_{E_n})dR \quad \textbf{(3.7.2.1.8)}$$
$$+\int_B\mathbf{n}\cdot\left(N_i\theta\mathbf{D}\cdot\frac{{E_n}^m}{E_n}\nabla E_n\right)dB+\int_B\mathbf{n}\cdot\left[W_i\theta\mathbf{D}\cdot\left(\nabla\frac{{E_n}^m}{E_n}\right)E_n\right]dB$$

Approximate solution E_n by a linear combination of the base functions as follows.

$$E_n\approx\hat{E}_n=\sum_{j=1}^{N}E_{nj}(t)N_j(R) \quad \textbf{(3.7.2.1.9)}$$

Substituting equation (3.7.2.1.9) into equation (3.7.2.1.8), we obtain

$$\sum_{j=1}^{N}\left[\left(\int_R N_i\theta N_j\right)\frac{\partial E_{nj}(t)}{\partial t}dR\right]+\sum_{j=1}^{N}\left\{\left[\int_R W_i\mathbf{V}\cdot\left(\nabla\frac{{E_n}^m}{E_n}\right)N_j dR\right]E_{nj}(t)\right\}$$
$$+\sum_{j=1}^{N}\left[\left(\int_R W_i\mathbf{V}\cdot\frac{{E_n}^m}{E_n}\nabla N_j dR\right)E_{nj}(t)\right]+\sum_{j=1}^{N}\left\{\left\{\int_R\nabla W_i\cdot\left[\theta\mathbf{D}\cdot\left(\nabla\frac{{E_n}^m}{E_n}\right)N_j\right]dR\right\}E_{nj}(t)\right\} \quad \textbf{(3.7.2.1.10)}$$
$$+\sum_{j=1}^{N}\left\{\left[\int_R\nabla N_i\cdot\left(\theta\mathbf{D}\cdot\frac{{E_n}^m}{E_n}\nabla N_j\right)dR+\int_R N_i\left(L_{HS}\frac{{E_n}^m}{E_n}+\frac{\partial\theta}{\partial t}\right)N_j dR\right]E_{nj}(t)\right\}$$
$$=\int_R N_i(R_{HS}+\theta R_{E_n})dR+\int_B\mathbf{n}\cdot\left(N_i\theta\mathbf{D}\cdot\nabla{E_n}^m\right)dB$$

Equation (3.7.2.1.10) can be written in matrix form as

$$[Q1]\left\{\frac{\partial E_n}{\partial t}\right\}+[Q2]\{E_n\}+[Q3]\{E_n\}=\{RLS\}+\{B\} \quad \textbf{(3.7.2.1.11)}$$

where the matrices [Q1], [Q2], [Q3] and load vectors {SS}, and {B} are given by

$$Q1_{ij}=\int_R N_i\theta^n N_j dR \quad \textbf{(3.7.2.1.12)}$$

$$Q2_{ij} = \int_R W_i \mathbf{V} \cdot \left(\nabla \frac{E_n^{\ m}}{E_n} \right) N_j dR$$
$$+ \int_R W_i \mathbf{V} \cdot \frac{E_n^{\ m}}{E_n} \nabla N_j dR + \int_R \nabla W_i \cdot \left[\theta \mathbf{D} \cdot \left(\nabla \frac{E_n^{\ m}}{E_n} \right) N_j \right] dR \quad \textbf{(3.7.2.1.13)}$$

$$Q3_{ij} = \int_R \nabla N_i \cdot \left(\theta \mathbf{D} \cdot \frac{E_n^{\ m}}{E_n} \nabla N_j \right) dR + \int_R N_i \left(L_{HS} \frac{E_n^{\ m}}{E_n} + \frac{\partial \theta}{\partial t} \right) N_j dR \quad \textbf{(3.7.2.1.14)}$$

$$RLS_i = \int_R N_i (R_{HS} + \theta R_{E_n}) dR \quad \textbf{(3.7.2.1.15)}$$

$$B_i = \int_B \mathbf{n} \cdot \left(N_i \theta \mathbf{D} \cdot \nabla E_n^{\ m} \right) dB \quad \textbf{(3.7.2.1.16)}$$

At n+1-th time step, equation (3.7.2.1.11) is approximated as

$$[Q1] \frac{\left\{ E_n^{\ n+1/2} \right\} - \left\{ E_n^{\ n} \right\}}{\Delta t} + W_{V1}[Q2^{n+1}] \left\{ E_n^{\ n+1/2} \right\} + W_{V2}[Q2^n] \left\{ E_n^{\ n} \right\} + W_1[Q3^{n+1}] \left\{ E_n^{\ n+1/2} \right\}$$
$$+ W_2[Q3^n] \left\{ E_n^{\ n} \right\} = W_1\{RLS^{n+1}\} + W_2\{RLS^n\} + W_1\{B^{n+1}\} + W_2\{B^n\} \quad \textbf{(3.7.2.1.17)}$$

So that

$$\left(\frac{[Q1]}{\Delta t} + W_{V1}[Q2^{n+1}] + W_1[Q3^{n+1}] \right) \left\{ E_n^{\ n+1/2} \right\} = \left(\frac{[Q1]}{\Delta t} - W_{V2}[Q2^n] - W_2[Q3^n] \right) \left\{ E_n^{\ n} \right\}$$
$$+ W_1\{RLS^{n+1}\} + W_2\{RLS^n\} + W_1\{B^{n+1}\} + W_2\{B^n\} \quad \textbf{(3.7.2.1.18)}$$

Option 2: Express $E_n^{\ m}$ in terms of E_n-$E_n^{\ im}$

Use Galerkin or Petrov-Galerkin Finite-Element Method for the spatial descretization of transport equation. Integrate equation (3.7.2.1.6) in the spatial dimensions over the entire region as follows.

$$\int_R N_i \left[\theta \frac{\partial E_n}{\partial t} + \frac{\partial \theta}{\partial t} E_n - \nabla \cdot \left(\theta \mathbf{D} \cdot \nabla E_n^{\ m} \right) + L_{HS} \cdot E_n^{\ m} \right] dR + \int_R W_i \mathbf{V} \cdot \nabla E_n^{\ m} dR =$$
$$\int_R N_i (R_{HS} + \theta R_{E_n}) dR \quad \textbf{(3.7.2.1.19)}$$

Further, we obtain

$$\int_R N_i \theta \frac{\partial E_n}{\partial t} dR + \int_R N_i \frac{\partial \theta}{\partial t} E_n dR + \int_R W_i \mathbf{V} \cdot \nabla E_n^{\ m} dR + \int_R \nabla N_i \cdot \left(\theta \mathbf{D} \cdot \nabla E_n^{\ m} \right) dR +$$
$$\int_R N_i L_{HS} \cdot E_n^{\ m} dR = \int_R N_i (R_{HS} + \theta R_{E_n}) dR + \int_B \mathbf{n} \cdot \left(N_i \theta \mathbf{D} \cdot \nabla E_n^{\ m} \right) dB \quad \textbf{(3.7.2.1.20)}$$

Approximate solution E_n by a linear combination of the base functions as equation (3.7.2.1.9). Substituting equation (3.7.2.1.9) into equation (3.7.2.1.20), we obtain

$$\sum_{j=1}^{N}\left[\left(\int_R N_i\theta N_j\right)\frac{\partial E_{nj}(t)}{\partial t}dR\right]+\sum_{j=1}^{N}\left[\left(\int_R N_i\frac{\partial\theta}{\partial t}N_j\right)E_{nj}(t)dR\right]+$$
$$\sum_{j=1}^{N}\left\{\left[\int_R W_i\mathbf{V}\cdot\nabla N_j dR\right]E_{nj}{}^m(t)\right\}+\sum_{j=1}^{N}\left\{\left[\int_R\nabla N_i\cdot\left(\theta\mathbf{D}\cdot\nabla N_j\right)dR+\int_R N_i L_{HS}N_j dR\right]E_{nj}{}^m(t)\right\} \quad \textbf{(3.7.2.1.21)}$$
$$=\int_R N_i(R_{HS}+\theta R_{E_n})dR\ +\int_B\mathbf{n}\cdot\left(N_i\theta\mathbf{D}\cdot\nabla E_n{}^m\right)dB$$

Equation (3.7.2.1.21) can be written in matrix form as

$$[Q1]\left\{\frac{\partial E_n}{\partial t}\right\}+[Q4]\{E_n\}+[Q2]\{E_n{}^m\}+[Q3]\{E_n{}^m\}=\{RLS\}+\{B\} \quad \textbf{(3.7.2.1.22)}$$

where the matrices [Q1], [Q2], [Q3] and load vectors {SS}, and {B} are given by

$$Q1_{ij}=\int_R N_i\theta N_j dR,\qquad Q4_{ij}=\int_R N_i\frac{\partial\theta}{\partial t}N_j dR \quad \textbf{(3.7.2.1.23)}$$

$$Q2_{ij}=\int_R W_i\mathbf{V}\cdot\nabla N_j dR \quad \textbf{(3.7.2.1.24)}$$

$$Q3_{ij}=\int_R\nabla N_i\cdot\left(\theta\mathbf{D}\cdot\nabla N_j\right)dR+\int_R N_i L_{HS}N_j dR \quad \textbf{(3.7.2.1.25)}$$

$$RLS_i=\int_R N_i(R_{HS}+\theta R_{E_n})dR \quad \textbf{(3.7.2.1.26)}$$

$$B_i=\int_B\mathbf{n}\cdot\left(N_i\theta\mathbf{D}\cdot\nabla E_n{}^m\right)dB \quad \textbf{(3.7.2.1.27)}$$

Express $E_n{}^m$ in terms of E_n-$E_n{}^{im}$, equation (3.7.2.1.22) is modified as

$$[Q1]\left\{\frac{\partial E_n}{\partial t}\right\}+[Q4]\{E_n\}+[Q2]\{E_n\}+[Q3]\{E_n\}=$$
$$[Q2]\{E_n{}^{im}\}+[Q3]\{E_n{}^{im}\}+\{RLS\}+\{B\} \quad \textbf{(3.7.2.1.28)}$$

At n+1-th time step, equation (3.7.2.1.28) is approximated as

$$[Q1]\frac{\left\{ E_n^{\,n+1/2} \right\}-\left\{ E_n^{\,n} \right\}}{\Delta t}+[Q4]\left\{ E_n^{\,n+1/2} \right\}+W_{V1}[Q2^{n+1}]\left\{ E_n^{\,n+1/2} \right\}+W_{V2}[Q2^{n}]\left\{ E_n^{\,n} \right\}$$
$$+W_1[Q3^{n+1}]\left\{ E_n^{\,n+1/2} \right\}+W_2[Q3^{n}]\left\{ E_n^{\,n} \right\}=W_{V1}[Q2^{n+1}]\left\{ \left(E_n^{\,im} \right)^{n+1/2} \right\} \qquad \textbf{(3.7.2.1.29)}$$
$$+W_{V2}[Q2^{n}]\left\{ \left(E_n^{\,im} \right)^{n} \right\}+W_1[Q3^{n+1}]\left\{ \left(E_n^{\,im} \right)^{n+1/2} \right\}+W_2[Q3^{n}]\left\{ \left(E_n^{\,im} \right)^{n} \right\}$$
$$+W_1\{RLS^{n+1}\}+W_2\{RLS^{n}\}+W_1\{B^{n+1}\}+W_2\{B^{n}\}$$

So that

$$\left(\frac{[Q1]}{\Delta t}+[Q4]+W_{V1}[Q2^{n+1}]+W_1[Q3^{n+1}] \right)\left\{ E_n^{\,n+1/2} \right\}=\frac{[Q1]}{\Delta t}\left\{ E_n^{\,n} \right\}$$
$$-\left(W_{V2}[Q2^{n}]+W_2[Q3^{n}] \right)\left\{ \left(E_n^{\,m} \right)^{n} \right\}+\left(W_{V1}[Q2^{n}]+W_1[Q3^{n}] \right)\left\{ \left(E_n^{\,im} \right)^{n+1/2} \right\}+ \qquad \textbf{(3.7.2.1.30)}$$
$$W_1\{RLS^{n+1}\}+W_2\{RLS^{n}\}+W_1\{B^{n+1}\}+W_2\{B^{n}\}$$

For interior nodes i, B_i is zero, for boundary nodes i = b, B_i is calculated according to the specified boundary condition and shown as follows.

Dirichlet boundary condition

$$E_n^{\,m}=E_n^{\,m}(x_b,y_b,z_b,t) \qquad \textbf{(3.7.2.1.31)}$$

Variable boundary condition

< Case 1 > when flow is going in from outside ($\mathbf{n}\cdot\mathbf{V} < 0$)

$$\mathbf{n}\cdot(\mathbf{V}E_n^{\,m}-\theta\mathbf{D}\cdot\nabla E_n^{\,m})=\mathbf{n}\cdot\mathbf{V}E_n^{\,m}(x_b,y_b,z_b,t)$$
$$\Rightarrow\quad B_i=\int_{\mathbf{B}}\mathbf{n}\cdot N_i\mathbf{V}E_n^{\,m}dB-\int_{\mathbf{B}}\mathbf{n}\cdot N_i\mathbf{V}E_n^{\,m}(x_b,y_b,z_b,t)dB \qquad \textbf{(3.7.2.1.32)}$$

< Case 2 > Flow is going out from inside ($\mathbf{n}\cdot\mathbf{V} > 0$):

$$-\mathbf{n}\cdot(\theta\mathbf{D}\cdot\nabla E_n^{\,m})=0\quad\Rightarrow\quad B_i=0 \qquad \textbf{(3.7.2.1.33)}$$

Cauchy boundary condition

$$n\cdot(\mathbf{V}E_n^{\,m}-\theta\mathbf{D}\cdot\nabla E_n^{\,m})=Q_{E_n^{\,m}}(x_b,y_b,z_b,t)$$
$$\Rightarrow\quad B_i=\int_{\mathbf{B}}\mathbf{n}\cdot N_i\mathbf{V}E_n^{\,m}dB-\int_{B}N_iQ_{E_n^{\,m}}(x_b,y_b,z_b,t)dB \qquad \textbf{(3.7.2.1.34)}$$

Neumann boundary condition

$$-\mathbf{n}\cdot(\theta\mathbf{D}\cdot\nabla E_n^{\,m})=Q_{E_n^{\,m}}(x_b,y_b,z_b,t)\quad\Rightarrow\quad B_i=-\int_{B}N_iQ_{E_n^{\,m}}(x_b,y_b,z_b,t)dB \qquad \textbf{(3.7.2.1.35)}$$

River/stream-subsurface interface boundary condition

$$\mathbf{n}\cdot(\mathbf{V}E_n^{\,m}-\theta\mathbf{D}\cdot\nabla E_n^{\,m})=\frac{\mathbf{n}\cdot\mathbf{V}}{2}\left\{\,[1+sign(\mathbf{n}\cdot\mathbf{V})]E_n^{\,m}+[1-sign(\mathbf{n}\cdot\mathbf{V})]\left(E_n^{\,m}\right)^{1D}\right\}\;\Rightarrow$$
$$B_i=\int_B\mathbf{n}\cdot N_i\mathbf{V}E_n^{\,m}dB-\int_B N_i\frac{\mathbf{n}\cdot\mathbf{V}}{2}\left\{\,[1+sign(\mathbf{n}\cdot\mathbf{V})]E_n^{\,m}+[1-sign(\mathbf{n}\cdot\mathbf{V})]\left(E_n^{\,m}\right)^{1D}\right\}dB \qquad \textbf{(3.7.2.1.36)}$$

Overland-subsurface interface boundary condition

$$\mathbf{n}\cdot(\mathbf{V}E_n^{\,m}-\theta\mathbf{D}\cdot\nabla E_n^{\,m})=\frac{\mathbf{n}\cdot\mathbf{V}}{2}\left\{\,[1+sign(\mathbf{n}\cdot\mathbf{V})]E_n^{\,m}+[1-sign(\mathbf{n}\times\mathbf{V})]\left(E_n^{\,m}\right)^{2D}\right\}\;\Rightarrow$$
$$B_i=\int_{\mathbf{B}}\mathbf{n}\cdot N_i\mathbf{V}E_n^{\,m}dB-\int_B N_i\frac{\mathbf{n}\cdot\mathbf{V}}{2}\left\{\,[1+sign(\mathbf{n}\cdot\mathbf{V})]E_n^{\,m}+[1-sign(\mathbf{n}\cdot\mathbf{V})]\left(E_n^{\,m}\right)^{2D}\right\}dB \qquad \textbf{(3.7.2.1.37)}$$

3.7.2.2 Mixed Predictor-Corrector and Operator-Splitting Method

According to the mixed predictor-corrector (on reaction rates) and operator-splitting (on immobile part of the kinetic variable) method, equation (3.7.2.1.3) can be separated into two equations as follows.

$$\theta\frac{\left(E_n^{\,m}\right)^{n+1/2}-\left(E_n^{\,m}\right)^n}{\Delta t}+\frac{\partial\theta}{\partial t}E_n^m+\mathbf{V}\cdot\nabla E_n^{\,m}-\nabla\cdot(\theta\mathbf{D}\cdot\nabla E_n^{\,m})+L_{HS}E_n^{\,m}=$$
$$R_{HS}+\theta R_{E_n}^{\;n}-\frac{\partial\theta}{\partial t}(E_n^{im})^n \qquad \textbf{(3.7.2.2.1)}$$

$$\frac{E_n^{\,n+1}-[(E_n^{\,m})^{n+1/2}+(E_n^{\,im})^n]}{\Delta t}=R_{E_n}^{\;n+1}-R_{E_n}^{\;n}-\frac{\partial\ell n\theta}{\partial t}(E_n^{im})^{n+1}+\frac{\partial\ell n\theta}{\partial t}(E_n^{im})^n \qquad \textbf{(3.7.2.2.2)}$$

First, solve equation (3.7.2.2.1) and get $(E_n^{\,m})^{n+1/2}$. Second, solve equation (3.7.2.2.2) together with algebraic equations representing equilibrium reactions using BIOGEOCHM scheme to obtain the individual species concentration.

Use Galerkin or Petrov-Galerkin Finite-Element Method for the spatial descretization of transport equation. Integrate equation (3.7.2.2.1) in the spatial dimensions over the entire region as follows.

$$\int_R N_i\left[\theta\frac{\partial E_n^{\,m}}{\partial t}-\nabla\cdot(\theta\mathbf{D}\cdot\nabla E_n^{\,m})+\left(L_{HS}+\frac{\partial\theta}{\partial t}\right)E_n^{\,m}\right]dR+\int_R W_i\mathbf{V}\cdot\nabla E_n^{\,m}dR=$$
$$\int_R N_i\left(R_{HS}+\theta R_{E_n}^{\;n}-\frac{\partial\theta}{\partial t}(E_n^{im})^n\right)dR \qquad \textbf{(3.7.2.2.3)}$$

Further, we obtain

$$\int_R N_i \theta \frac{\partial E_n{}^m}{\partial t} dR + \int_R W_i \mathbf{V} \cdot \nabla E_n{}^m dR + \int_R \nabla N_i \cdot (\theta \mathbf{D} \cdot \nabla E_n{}^m) dR + \int_R N_i \left(L_{HS} + \frac{\partial \theta}{\partial t} \right) E_n{}^m dR$$
$$= \int_R N_i \left(R_{HS} + \theta R_{E_n}{}^n - \frac{\partial \theta}{\partial t} (E_n^{im})^n \right) dR + \int_B \mathbf{n} \cdot N_i (\theta \mathbf{D} \cdot \nabla E_n{}^m) dB \quad \textbf{(3.7.2.2.4)}$$

Approximate solution $E_n{}^m$ by a linear combination of the base functions as follows.

$$E_n{}^m \approx \hat{E}_n{}^m = \sum_{j=1}^{N} E_{nj}{}^m(t) N_j(R) \quad \textbf{(3.7.2.2.5)}$$

Substituting equation (3.7.2.2.5) into equation (3.7.2.2.4), we obtain

$$\sum_{j=1}^{N} \left[\left(\int_R N_i \theta^n N_j dR \right) \frac{\partial E_{nj}{}^m(t)}{\partial t} \right] + \sum_{j=1}^{N} \left[\left(\int_R W_i \mathbf{V} \cdot \nabla N_j dR \right) E_{nj}{}^m(t) \right]$$
$$+ \sum_{j=1}^{N} \left\{ \left[\int_R \nabla N_i \cdot (\theta \mathbf{D} \cdot \nabla N_j) dR + \int_R N_i \left(L_{HS} + \frac{\partial \theta}{\partial t} \right) N_j dR \right] E_{nj}{}^m(t) \right\} \quad \textbf{(3.7.2.2.6)}$$
$$= \int_R N_i \left(R_{HS} + \theta R_{E_n}{}^n - \frac{\partial \theta}{\partial t} (E_n^{im})^n \right) dR + \int_B \mathbf{n} \cdot N_i (\theta \mathbf{D} \cdot \nabla E_n{}^m) dB$$

Equation (3.7.2.2.6) can be written in matrix form as

$$[Q1] \left\{ \frac{dE_n{}^m}{dt} \right\} + [Q2] \left\{ E_n{}^m \right\} + [Q3] \left\{ E_n{}^m \right\} = \{RLS\} + \{B\} \quad \textbf{(3.7.2.2.7)}$$

where the matrices [Q1], [Q2], and [Q3], and load vectors {RLS} and {B} are given by

$$Q1_{ij} = \int_R N_i \theta N_j dR \quad \textbf{(3.7.2.2.8)}$$

$$Q2_{ij} = \int_R W_i \mathbf{V} \cdot \nabla N_j dR \quad \textbf{(3.7.2.2.9)}$$

$$Q3_{ij} = \int_R \nabla N_i \cdot \left(\theta \mathbf{D} \cdot \nabla N_j \right) dR + \int_R N_i \left(L_{HS} + \frac{\partial \theta}{\partial t} \right) N_j dR \quad \textbf{(3.7.2.2.10)}$$

$$RLS_i = \int_R N_i \left(R_{HS} + \theta R_{E_n}{}^n - \frac{\partial \theta}{\partial t} (E_n^{im})^n \right) dR \quad \textbf{(3.7.2.2.11)}$$

$$B_i = \int_B \mathbf{n} \cdot (N_i \theta \mathbf{D} \cdot \nabla E_n{}^m) dB \quad \textbf{(3.7.2.2.12)}$$

At n+1-th time step, equation (3.7.2.2.7) is approximated as

$$[Q1]\frac{\left\{\left(E_n^{\,m}\right)^{n+1/2}\right\}-\left\{\left(E_n^{\,m}\right)^{n}\right\}}{\Delta t}+W_{V1}[Q2^{n+1}]\left\{\left(E_n^{\,m}\right)^{n+1/2}\right\}$$
$$+W_{V2}[Q2^{n}]\left\{\left(E_n^{\,m}\right)^{n}\right\}+W_1[Q3^{n+1}]\left\{\left(E_n^{\,m}\right)^{n+1/2}\right\}+W_2[Q3^{n}]\left\{\left(E_n^{\,m}\right)^{n}\right\} \qquad \textbf{(3.7.2.2.13)}$$
$$=W_1\{RLS^{n+1}\}+W_2\{RLS^{n}\}+W_1\{B^{n+1}\}+W_2\{B^{n}\}$$

So that

$$\left(\frac{[Q1^{n}]}{\Delta t}+W_{V1}[Q2^{n+1}]+W_1[Q3^{n+1}]\right)\left\{\left(E_n^{\,m}\right)^{n+1/2}\right\}=\left(\frac{[Q1^{n}]}{\Delta t}-W_{V2}[Q2^{n}]-W_2[Q3^{n}]\right)* \qquad \textbf{(3.7.2.2.14)}$$
$$\left\{\left(E_n^{\,m}\right)^{n}\right\}+W_1\{RLS^{n+1}\}+W_2\{RLS^{n}\}+W_1\{B^{n+1}\}+W_2\{B^{n}\}$$

The boundary term {B} is calculated according the same as that in section 3.7.2.1.

3.7.3 Operator-Splitting Approach

According to the operator-splitting approach, equation (3.7.2.1.2) can be separated into two equations as follows.

$$\theta\frac{\left(E_n^{\,m}\right)^{n+1/2}-\left(E_n^{\,m}\right)^{n}}{\Delta t}+\mathbf{V}\cdot\nabla E_n^{\,m}-\nabla\cdot(\theta\mathbf{D}\cdot\nabla E_n^{\,m})+\left(L_{HS}+\frac{\partial\theta}{\partial t}\right)E_n^{\,m}=R_{HS} \qquad \textbf{(3.7.2.3.1)}$$

$$\frac{E_n^{\,n+1}-[(E_n^{\,m})^{n+1/2}+(E_n^{\,im})^{n}]}{\Delta t}=R_{E_n}^{\,n+1}-\frac{\partial\ell n\theta}{\partial t}(E_n^{im})^{n+1} \qquad \textbf{(3.7.2.3.2)}$$

First, solve equation (3.7.2.3.1) and get $(E_n^{\,m})^{n+1/2}$. Second, solve equation (3.7.2.3.2) together with algebraic equations representing equilibrium reactions using BIOGEOCHM scheme to obtain the individual species concentration.

Equation (3.7.2.3.1) can be solved through the same procedure as that in section 4.1.2, except for the load vectors {RLS}, which is calculated by the following equation.

$$RLS_i=\int_R N_i R_{HS}\,dR \qquad \textbf{(3.7.2.3.3)}$$

3.7.4 Application of the Modified Lagrangian-Eulerian Approach to the Largrangian Form of the Reactive Transport Equations

3.7.4.1 Fully-Implicit Scheme

Option 1: Express $E_n^{\,m}$ in terms of $(E_n^{\,m}/E_n)\,E_n$

Express $E_n^{\,m}$ in terms of $(E_n^{\,m}/E_n)\,E_n$ to make E_n's as primary dependent variables, equation

(3.7.2.1.4) is modified as

$$\theta\frac{\partial E_n}{\partial t}+\frac{\partial \theta}{\partial t}E_n+\left[\mathbf{V}\frac{E_n^{\,m}}{E_n}-\theta\mathbf{D}\cdot\left(\nabla\frac{E_n^{\,m}}{E_n}\right)\right]\cdot\nabla\left(E_n\right)-\nabla\cdot\left(\theta\mathbf{D}\cdot\frac{E_n^{\,m}}{E_n}\nabla E_n\right)$$
$$\left\{\mathbf{V}\cdot\nabla\left(\frac{E_n^{\,m}}{E_n}\right)-\nabla\cdot\left[\theta\mathbf{D}\cdot\left(\nabla\frac{E_n^{\,m}}{E_n}\right)\right]+L_{HS}\frac{E_n^{\,m}}{E_n}\right\}E_n=R_{HS}+\theta R_{E_n} \qquad \textbf{(3.7.3.1.1)}$$

Assign the particle tracking velocity $\mathbf{V}_{\text{track}}$ as follows

$$\mathbf{V}_{track}=\frac{1}{\theta}\left[\mathbf{V}\frac{E_n^{\,m}}{E_n}-\theta\mathbf{D}\cdot\left(\nabla\frac{E_n^{\,m}}{E_n}\right)\right] \qquad \textbf{(3.7.3.1.2)}$$

Equation (3.7.3.1.1) in Lagrangian-Eulerian form is written as

In Lagrangian step,

$$\frac{DE_n}{D\tau}=\frac{\partial E_n}{\partial t}+\mathbf{V}_{track}\cdot\nabla E_n=0 \qquad \textbf{(3.7.3.1.3)}$$

In Eulerian step,

$$\frac{DE_n}{D\tau}-D+KE_n=R_L \qquad \textbf{(3.7.3.1.4)}$$

where

$$\theta D=\nabla\cdot\left(\theta\mathbf{D}\frac{E_n^{\,m}}{E_n}\cdot\nabla E_n\right) \qquad \textbf{(3.7.3.1.5)}$$

$$K=\frac{1}{\theta}\left\{\mathbf{V}\cdot\nabla\left(\frac{E_n^{\,m}}{E_n}\right)-\nabla\cdot\left[\theta\mathbf{D}\cdot\left(\nabla\frac{E_n^{\,m}}{E_n}\right)\right]+\left(\frac{\partial\theta}{\partial t}+L_{HS}\frac{E_n^{\,m}}{E_n}\right)\right\} \qquad \textbf{(3.7.3.1.6)}$$

$$R_L=\frac{1}{\theta}\left(R_{HS}+\theta R_{E_n}\right) \qquad \textbf{(3.7.3.1.7)}$$

The integration of equation (3.7.3.1.5) can be written as

$$\int_R N_i\theta D\,dR=-\int_R\nabla N_i\cdot(\theta\mathbf{D}\frac{E_n^{\,m}}{E_n}\cdot\nabla E_n)dR+\int_B\mathbf{n}\cdot N_i(\theta\mathbf{D}\frac{E_n^{\,m}}{E_n}\cdot\nabla E_n)dB \qquad \textbf{(3.7.3.1.8)}$$

Approximate D and E_n by linear combination of the base functions as follows.

$$D\approx\hat{D}=\sum_{j=1}^{N}D_j(t)N_j(R) \qquad \textbf{(3.7.3.1.9)}$$

$$E_n \approx \hat{E}_n = \sum_{j=1}^{N} E_{nj}(t) N_j(R) \qquad \textbf{(3.7.3.1.10)}$$

Put Equations (3.7.3.1.9) and (3.7.3.1.10) into Equation (3.7.3.1.8), we obtain

$$\begin{aligned} &\sum_{j=1}^{N}\left[\left(\int_R N_i \theta N_j dR\right) * D_j\right] \\ &= -\sum_{j=1}^{N}\left[\left(\int_R \nabla N_i \cdot (\theta \mathbf{D} \frac{E_n^{\ m}}{E_n} \cdot \nabla N_j) dR\right) E_{nj}\right] + \int_B \mathbf{n} \cdot N_i (\theta \mathbf{D} \frac{E_n^{\ m}}{E_n} \cdot \nabla E_n) dB \end{aligned} \qquad \textbf{(3.7.3.1.11)}$$

Assign matrices [QA] and [QD] and load vector {B} as following.

$$QA_{ij} = \int_R N_i \theta N_j dR \qquad \textbf{(3.7.3.1.12)}$$

$$QD_{ij} = \int_R \nabla N_i \cdot (\theta \mathbf{D} \frac{E_n^{\ m}}{E_n} \cdot \nabla N_j) dR \qquad \textbf{(3.7.3.1.13)}$$

$$B_i = \int_B \mathbf{n} \cdot N_i (\theta \mathbf{D} \frac{E_n^{\ m}}{E_n} \cdot \nabla E_n) dB \qquad \textbf{(3.7.3.1.14)}$$

Equation (3.7.3.1.11) is expressed as

$$[QA]\{D\} = -[QD]\{E_n\} + \{B\} \qquad \textbf{(3.7.3.1.15)}$$

Lump matrix [QA] into diagonal matrix and update

$$QD_{ij} = QD_{ij} / QA_{ii} \qquad \textbf{(3.7.3.1.16)}$$

$$B_i = \int_B \mathbf{n} \cdot N_i (\theta \mathbf{D} \cdot \nabla E_n^{\ m}) dB \Big/ QA_{ii} - \int_B \mathbf{n} \cdot N_i (\theta \mathbf{D} \cdot \nabla \frac{E_n^{\ m}}{E_n} E_n) dB \Big/ QA_{ii} \qquad \textbf{(3.7.3.1.17)}$$

Then

$$\{D\} = -[QD]\{E_n\} + \{B\} \qquad \textbf{(3.7.3.1.18)}$$

Equation (3.7.3.1.4) written in matrix form is then expressed as

$$\begin{aligned} &\left(\frac{[U]}{\Delta\tau} + W_1[QD^{n+1}] + W_1\left[K^{n+1}\right]\right)\left\{E_n^{\ n+1/2}\right\} = \\ &\frac{[U]}{\Delta\tau}\left\{E_n^{\ *}\right\} - W_2\left([K]\left\{E_n^{\ m}\right\}\right)^* + W_2\{D\}^* + W_1\left\{R_L^{\ n+1}\right\} + W_2\left\{R_L^{\ *}\right\} + W_1\left\{B^{n+1}\right\} \end{aligned} \qquad \textbf{(3.7.3.1.19)}$$

where [U] is the unit matrix, $\Delta\tau$ is the tracking time, W_1 and W_2 are time weighting factors, matrices

and vectors with $^{n+1}$ and $^{n+1/2}$ are evaluated over the region at the new time step n+1. Matrices and vectors with superscript * corresponds to the n-th time step values interpolated at the location where a node is tracked through particle tracking in Lagrangian step.

For interior nodes i, B_i is zero, for boundary nodes i = b, B_i is calculated according to the specified boundary condition and shown as follows.

Dirichlet boundary condition

$$E_n^{\,m} = E_n^{\,m}(x_b, y_b, z_b, t) \;\Rightarrow$$
$$B_i = \int_B \mathbf{n} \cdot N_i(\theta \mathbf{D} \cdot \nabla E_n^{\,m}) dB \Big/ QA_{ii} - \int_B \mathbf{n} \cdot N_i(\theta \mathbf{D} \cdot \nabla \frac{E_n^{\,m}}{E_n} E_n) dB \Big/ QA_{ii} \qquad \textbf{(3.7.3.1.20)}$$

Variable boundary condition

< Case 1 > when flow is going in from outside ($\mathbf{n}\cdot\mathbf{V} < 0$)

$$\mathbf{n} \cdot (\mathbf{V} E_n^{\,m} - \theta \mathbf{D} \cdot \nabla E_n^{\,m}) = \mathbf{n} \cdot V E_n^{\,m}(x_b, y_b, z_b, t) \quad \Rightarrow \quad B_i = \int_{\mathbf{B}} \mathbf{n} \cdot N_i \mathbf{V} E_n^{\,m} dB \Big/ QA_{ii}$$
$$- \int_B \mathbf{n} \cdot N_i \mathbf{V} E_n^{\,m}(x_b, y_b, z_b, t) dB \Big/ QA_{ii} - \int_B \mathbf{n} \cdot N_i(\theta \mathbf{D} \cdot \nabla \frac{E_n^{\,m}}{E_n} E_n) dB \Big/ QA_{ii} \qquad \textbf{(3.7.3.1.21)}$$

< Case 2 > Flow is going out from inside ($\mathbf{n}\cdot\mathbf{V} > 0$):

$$-\mathbf{n} \cdot (\theta \mathbf{D} \cdot \nabla E_n^{\,m}) = 0 \quad \Rightarrow \quad B_i = -\int_B \mathbf{n} \cdot N_i(\theta \mathbf{D} \cdot \nabla \frac{E_n^{\,m}}{E_n} E_n) dB \Big/ QA_{ii} \qquad \textbf{(3.7.3.1.22)}$$

Cauchy boundary condition

$$n \cdot (V E_n^{\,m} - \theta D \cdot \nabla E_n^{\,m}) = Q_{E_n^{\,m}}(x_b, y_b, z_b, t) \quad \Rightarrow \quad B_i = \int_B \mathbf{n} \cdot N_i \mathbf{V} E_n^{\,m} dB \Big/ QA_{ii}$$
$$- \int_B N_i Q_{E_n^{\,m}}(x_b, y_b, z_b, t) dB \Big/ QA_{ii} - \int_B \mathbf{n} \cdot N_i(\theta \mathbf{D} \cdot \nabla \frac{E_n^{\,m}}{E_n} E_n) dB \Big/ QA_{ii} \qquad \textbf{(3.7.3.1.23)}$$

Neumann boundary condition

$$-\mathbf{n} \cdot (\theta \mathbf{D} \cdot \nabla E_n^{\,m}) = Q_{E_n^{\,m}}(x_b, y_b, z_b, t) \quad \Rightarrow \quad B_i = -\int_B N_i Q_{E_n^{\,m}}(x_b, y_b, z_b, t) dB \Big/ QA_{ii}$$
$$- \int_B \mathbf{n} \cdot N_i(\theta \mathbf{D} \cdot \nabla \frac{E_n^{\,m}}{E_n} E_n) dB \Big/ QA_{ii} \qquad \textbf{(3.7.3.1.24)}$$

River/stream-subsurface interface boundary condition

$$\mathbf{n}\cdot(\mathbf{V}E_n^{\ m}-\theta\mathbf{D}\cdot\nabla E_n^{\ m})=\frac{\mathbf{n}\cdot\mathbf{V}}{2}\Big\{\ [1+sign(\mathbf{n}\cdot\mathbf{V})]E_n^{\ m}+[1-sign(\mathbf{n}\cdot\mathbf{V})]\Big(E_n^{\ m}\Big)^{1D}\Big\}$$

$$\Rightarrow\quad B_i=\int_B\mathbf{n}\cdot N_i\mathbf{V}E_n^{\ m}dB\Big/QA_{ii}-\int_B\mathbf{n}\cdot N_i(\theta\mathbf{D}\cdot\nabla\frac{E_n^{\ m}}{E_n}E_n)dB\Big/QA_{ii} \qquad \textbf{(3.7.3.1.25)}$$

$$-\int_B N_i\frac{\mathbf{n}\cdot\mathbf{V}}{2}\Big\{\ [1+sign(\mathbf{n}\cdot\mathbf{V})]E_n^{\ m}+[1-sign(\mathbf{n}\cdot\mathbf{V})]\Big(E_n^{\ m}\Big)^{1D}\Big\}dB\Big/QA_{ii}$$

Overland-subsurface interface boundary condition

$$\mathbf{n}\cdot(\mathbf{V}E_n^{\ m}-\theta\mathbf{D}\cdot\nabla E_n^{\ m})=\frac{\mathbf{n}\cdot\mathbf{V}}{2}\Big\{\ [1+sign(\mathbf{n}\cdot\mathbf{V})]E_n^{\ m}+[1-sign(\mathbf{n}\cdot\mathbf{V})]\Big(E_n^{\ m}\Big)^{2D}\Big\}$$

$$\Rightarrow\quad B_i=\int_B\mathbf{n}\cdot N_i\mathbf{V}E_n^{\ m}dB\Big/QA_{ii}-\int_B\mathbf{n}\cdot N_i(\theta\mathbf{D}\cdot\nabla\frac{E_n^{\ m}}{E_n}E_n)dB\Big/QA_{ii} \qquad \textbf{(3.7.3.1.26)}$$

$$-\int_B N_i\frac{\mathbf{n}\cdot\mathbf{V}}{2}\Big\{\ [1+sign(\mathbf{n}\cdot\mathbf{V})]E_n^{\ m}+[1-sign(\mathbf{n}\cdot\mathbf{V})]\Big(E_n^{\ m}\Big)^{2D}\Big\}dB\Big/QA_{ii}$$

Option 2: Express $E_n^{\ m}$ in terms of E_n-$E_n^{\ m}$

Express $E_n^{\ m}$ in terms of E_n-$E_n^{\ m}$ to make E_n's as primary dependent variables, equation (3.7.2.1.4) is modified as

$$\begin{aligned}&\theta\frac{\partial E_n}{\partial t}+\frac{\partial\theta}{\partial t}E_n+\mathbf{V}\cdot\nabla E_n-\nabla\cdot\Big(\theta\mathbf{D}\cdot\nabla E_n\Big)\ +L_{HS}E_n\\&=\mathbf{V}\cdot\nabla E_n^{\ im}-\nabla\cdot\Big(\theta\mathbf{D}\cdot\nabla E_n^{\ im}\Big)+L_{HS}E_n^{\ im}+R_{HS}+\theta R_{E_n}\end{aligned} \qquad \textbf{(3.7.3.1.27)}$$

Assign the particle tracking velocity $\mathbf{V}_{track}$ as follows

$$\mathbf{V}_{track}=\frac{1}{\theta}\mathbf{V} \qquad \textbf{(3.7.3.1.28)}$$

Equation (3.7.3.1.27) in Lagrangian-Eulerian form is written as

In Lagrangian step,

$$\frac{DE_n}{D\tau}=\frac{\partial E_n}{\partial t}+\mathbf{V}_{track}\cdot\nabla E_n=0 \qquad \textbf{(3.7.3.1.29)}$$

In Eulerian step,

$$\frac{DE_n}{D\tau}-D+KE_n=T+R_L \qquad \textbf{(3.7.3.1.30)}$$

where

$$\theta D = \nabla \cdot (\theta \mathbf{D} \cdot \nabla E_n) \tag{3.7.3.1.31}$$

$$K = \frac{L_{HS} + \frac{\partial \theta}{\partial t}}{\theta} \tag{3.7.3.1.32}$$

$$\theta T = \mathbf{V} \cdot \nabla E_n^{\ im} - \nabla \cdot \left(\theta \mathbf{D} \cdot \nabla E_n^{\ im} \right) \tag{3.7.3.1.33}$$

$$R_L = \frac{1}{\theta^n} \left(L_{HS} E_n^{\ im} + R_{HS} + \theta R_{E_n} \right) \tag{3.7.3.1.34}$$

The integration of equation (3.7.3.1.31) can be written as

$$\int_R N_i \theta D dR = -\int_R \nabla N_i \cdot (\theta \mathbf{D} \cdot \nabla E_n) dR + \int_B \mathbf{n} \cdot N_i (\theta \mathbf{D} \cdot \nabla E_n) dB \tag{3.7.3.1.35}$$

Approximate D and E_n by linear combination of the base functions as follows.

$$D \approx \hat{D} = \sum_{j=1}^{N} D_j(t) N_j(R) \tag{3.7.3.1.36}$$

$$E_n \approx \hat{E}_n = \sum_{j=1}^{N} E_{nj}(t) N_j(R) \tag{3.7.3.1.37}$$

Put Equations (3.7.3.1.36) and (3.7.3.1.37) into Equation (3.7.3.1.35), we obtain

$$\begin{aligned} &\sum_{j=1}^{N} \left[\left(\int_R N_i \theta N_j dR \right) D_j \right] \\ &= -\sum_{j=1}^{N} \left[\left(\int_R \nabla N_i \cdot (\theta \mathbf{D} \cdot \nabla N_j) dR \right) E_{nj} \right] + \int_B \mathbf{n} \cdot N_i (\theta \mathbf{D} \cdot \nabla E_n) dB \end{aligned} \tag{3.7.3.1.38}$$

Assign matrices [QA] and [QD] and load vector {B} as following.

$$QA_{ij} = \int_R N_i \theta N_j dR \tag{3.7.3.1.39}$$

$$QD_{ij} = \int_R \nabla N_i \cdot (\theta \mathbf{D} \cdot \nabla N_j) dR \tag{3.7.3.1.40}$$

$$B1_i = \int_B \mathbf{n} \cdot N_i (\theta \mathbf{D} \cdot \nabla E_n) dB \tag{3.7.3.1.41}$$

Equation (3.7.3.1.31) is expressed as

$$[QA]\{D\} = -[QD]\{E_n\} + \{B1\} \quad \textbf{(3.7.3.1.42)}$$

Similarly,

$$[QA]\{T\} = [QT]\{E_n^{\,im}\} + \{B2\} \quad \textbf{(3.7.3.1.43)}$$

where

$$QT_{ij} = \int_R N_i \mathbf{V} \cdot \nabla N_j dR - \int_R \nabla N_i \cdot (\theta \mathbf{D} \cdot \nabla N_j) dR \quad \textbf{(3.7.3.1.44)}$$

$$B2_i = -\int_B \mathbf{n} \cdot N_i (\theta \mathbf{D} \cdot \nabla E_n^{\,im}) dB \quad \textbf{(3.7.3.1.45)}$$

Lump matrix [QA] into diagonal matrix and update

$$QD_{ij} = QD_{ij} / QA_{ii} \quad \textbf{(3.7.3.1.46)}$$

$$B1_i = B1_i / QA_{ii} \quad \textbf{(3.7.3.1.47)}$$

$$QT_{ij} = QT_{ij} / QA_{ii} \quad \textbf{(3.7.3.1.48)}$$

$$B2_i = B2_i / QA_{ii} \quad \textbf{(3.7.3.1.49)}$$

Then

$$\{D\} = -[QD]\{E_n\} + \{B1\} \quad \textbf{(3.7.3.1.50)}$$

$$\{T\} = [QT]\{E_n^{\,im}\} + \{B2\} \quad \textbf{(3.7.3.1.51)}$$

Assign

$$B_i = B1_i + B2_i = \int_B \mathbf{n} \cdot N_i (\theta \mathbf{D} \cdot \nabla E_n^{\,m}) dB \Big/ QA_{ii} \quad \textbf{(3.7.3.1.52)}$$

So that

$$\{D\} + \{T\} = -[QD]\{E_n\} + [QT]\{E_n^{\,im}\} + \{B\} \quad \textbf{(3.7.3.1.53)}$$

Equation (3.7.3.1.30) written in matrix form is then expressed as

$$\begin{aligned} &\left(\frac{[U]}{\Delta\tau} + W_1[QD^{n+1}] + W_1\left[K^{n+1}\right]\right)\left\{E_n^{\,n+1/2}\right\} = \frac{[U]}{\Delta\tau}\left\{E_n^{\,*}\right\} - W_2\left([K]\{E_n\}\right)^* \\ &+W_1[QT^{n+1}]\left\{\left(E_n^{\,im}\right)^{n+1}\right\} + W_2(\{D\} + \{T\})^* + W_1\left\{R_L^{\,n+1}\right\} + W_2\left\{R_L^{\,*}\right\} + W_1\left\{B^{n+1}\right\} \end{aligned} \quad \textbf{(3.7.3.1.54)}$$

For interior nodes i, B_i is zero, for boundary nodes i = b, B_i is calculated according to the specified boundary condition and shown as follows.

Dirichlet boundary condition

$$E_n^{\,m} = E_n^{\,m}(x_b, y_b, z_b, t) \;\Rightarrow\; B_i = \int_B \mathbf{n} \cdot N_i(\theta \mathbf{D} \cdot \nabla E_n^{\,m}) dB \Big/ QA_{ii} \tag{3.7.3.1.55}$$

Variable boundary condition

< Case 1 > when flow is going in from outside ($\mathbf{n} \cdot \mathbf{V} < 0$)

$$\begin{aligned} &\mathbf{n} \cdot (\mathbf{V} E_n^{\,m} - \theta \mathbf{D} \cdot \nabla E_n^{\,m}) = \mathbf{n} \cdot \mathbf{V} E_n^{\,m}(x_b, y_b, z_b, t) \\ \Rightarrow\; &B_i = \int_B \mathbf{n} \cdot N_i \mathbf{V} E_n^{\,m} dB \Big/ QA_{ii} - \int_{\mathbf{B}} \mathbf{n} \cdot N_i \mathbf{V} E_n^{\,m}(x_b, y_b, z_b, t) dB \Big/ QA_{ii} \end{aligned} \tag{3.7.3.1.56}$$

< Case 2 > Flow is going out from inside ($\mathbf{n} \cdot \mathbf{V} > 0$):

$$-n \cdot (\theta \mathbf{D} \cdot \nabla E_n^{\,m}) = 0 \quad \Rightarrow \quad B_i = 0 \tag{3.7.3.1.57}$$

Cauchy boundary condition

$$\begin{aligned} &\mathbf{n} \cdot (\mathbf{V} E_n^{\,m} - \theta \mathbf{D} \cdot \nabla E_n^{\,m}) = Q_{E_n^{\,m}}(x_b, y_b, z_b, t) \\ \Rightarrow\quad &B_i = \int_B \mathbf{n} \cdot N_i \mathbf{V} E_n^{\,m} dB \Big/ QA_{ii} - \int_B N_i Q_{E_n^{\,m}}(x_b, y_b, z_b, t) dB \Big/ QA_{ii} \end{aligned} \tag{3.7.3.1.58}$$

Neumann boundary condition

$$-\mathbf{n} \cdot (\theta \mathbf{D} \cdot \nabla E_n^{\,m}) = Q_{E_n^{\,m}}(x_b, y_b, z_b, t) \;\Rightarrow\; B_i = -\int_B N_i Q_{E_n^{\,m}}(x_b, y_b, z_b, t) dB \Big/ QA_{ii} \tag{3.7.3.1.59}$$

River/stream-subsurface interface boundary condition

$$\begin{aligned} \mathbf{n} \cdot (\mathbf{V} E_n^{\,m} - \theta \mathbf{D} \cdot \nabla E_n^{\,m}) &= \frac{\mathbf{n} \cdot \mathbf{V}}{2} \left\{ [1 + sign(\mathbf{n} \cdot \mathbf{V})] E_n^{\,m} + [1 - sign(\mathbf{n} \cdot \mathbf{V})] \left(E_n^{\,m} \right)^{1D} \right\} \\ \Rightarrow\quad B_i &= \int_B \mathbf{n} \cdot N_i \mathbf{V} E_n^{\,m} dB \Big/ QA_{ii} \\ - \int_B N_i \frac{\mathbf{n} \cdot \mathbf{V}}{2} &\left\{ [1 + sign(\mathbf{n} \cdot \mathbf{V})] E_n^{\,m} + [1 - sign(\mathbf{n} \cdot \mathbf{V})] \left(E_n^{\,m} \right)^{1D} \right\} dB \Big/ QA_{ii} \end{aligned} \tag{3.7.3.1.60}$$

Overland-subsurface interface boundary condition

$$\mathbf{n}\cdot(\mathbf{V}E_n^{\,m}-\theta\mathbf{D}\cdot\nabla E_n^{\,m})=\frac{\mathbf{n}\cdot\mathbf{V}}{2}\left\{\,[1+sign(\mathbf{n}\cdot\mathbf{V})]E_n^{\,m}+[1-sign(\mathbf{n}\cdot\mathbf{V})]\left(E_n^{\,m}\right)^{2D}\right\}$$

$$\Rightarrow\quad B_i=\int_B\mathbf{n}\cdot N_i\mathbf{V}E_n^{\,m}dB\Big/QA_{ii} \qquad \textbf{(3.7.3.1.61)}$$

$$-\int_B N_i\frac{\mathbf{n}\cdot\mathbf{V}}{2}\left\{\,[1+sign(\mathbf{n}\cdot\mathbf{V})]E_n^{\,m}+[1-sign(\mathbf{n}\cdot\mathbf{V})]\left(E_n^{\,m}\right)^{2D}\right\}dB\Big/QA_{ii}$$

At upstream flux boundary nodes, equation (3.7.3.1.19) and (3.7.3.1.54) cannot be applied because $\Delta\tau$ equals zero. Thus, we propose a modified LE approach in which the matrix equation for upstream boundary nodes is obtained by explicitly applying the finite element method to the boundary conditions. For example, at the upstream variable boundary

$$\int_B N_i\mathbf{n}\cdot(\mathbf{V}E_n^{\,m}-\theta\mathbf{D}\cdot\nabla E_n^{\,m})dB=\int_B N_i\mathbf{n}\cdot\mathbf{V}E_n^{\,m}(x_b,y_b,z_b,t)dB \qquad \textbf{(3.7.3.1.62)}$$

So that the following matrix equation can be assembled at the boundary nodes

$$[QF]\{E_n^{\,m}\}=[QB]\{B\} \qquad \textbf{(3.7.3.1.63)}$$

in which

$$QF_{ij}=\int_B(N_i\mathbf{n}\cdot\mathbf{V}N_j-N_i\mathbf{n}\cdot\theta\mathbf{D}\cdot\nabla N_j)dB \qquad \textbf{(3.7.3.1.64)}$$

$$QB_{ij}=\int_B N_i\mathbf{n}\cdot\mathbf{V}N_j dB \qquad \textbf{(3.7.3.1.65)}$$

$$B_j=E_n^{\,m}{}_j(x_b,y_b,z_b,t) \qquad \textbf{(3.7.3.1.66)}$$

where $E_n^{\,m}{}_j(x_b,y_b,z_b,t)$ is the value of $E_n^{\,m}(x_b,y_b,z_b,t)$ evaluated at point *j*.

3.7.4.2 Mixed Predictor-Corrector and Operator-Splitting Method

Equation (3.7.2.2.1) in Lagrangian-Eulerian form is written as follows.

In Lagrangian step,

$$\frac{DE_n^{\,m}}{D\tau}=\frac{\partial E_n^{\,m}}{\partial t}+\mathbf{V}_{track}\cdot\nabla E_n^{\,m}=0 \qquad \textbf{(3.7.3.2.1)}$$

where particle tracking velocity is $\mathbf{V}_{\text{track}}$ is defined in Equation (3.7.3.1.28) .

In Eulerian step,

$$\frac{DE_n^{\ m}}{D\tau} - D + KE_n^{\ m} = R_L \qquad \textbf{(3.7.3.2.2)}$$

where

$$\theta D = \nabla \cdot (\theta \mathbf{D} \cdot \nabla E_n^{\ m}) \qquad \textbf{(3.7.3.2.3)}$$

$$K = \frac{L_{HS} + \frac{\partial \theta}{\partial t}}{\theta} \qquad \textbf{(3.7.3.2.4)}$$

$$R_L = \frac{1}{\theta}\left(R_{HS} + \theta R_{E_n}^{\ n} - \frac{\partial \theta}{\partial t}(E_n^{im})^n \right) \qquad \textbf{(3.7.3.2.5)}$$

According to equation (3.7.3.1.50)

$$[QA]\{D\} = -[QD]\{E_n^{\ m}\} + \{B\} \qquad \textbf{(3.7.3.2.6)}$$

$$QA_{ij} = \int_R N_i \theta^n N_j dR \qquad \textbf{(3.7.3.2.7)}$$

$$QD_{ij} = \int_R \nabla N_i \cdot (\theta \mathbf{D} \cdot \nabla N_j) dR \qquad \textbf{(3.7.3.2.8)}$$

$$B_i = \int_B n \cdot N_i (\theta \mathbf{D} \cdot \nabla E_n^{\ m}) dB \qquad \textbf{(3.7.3.2.9)}$$

Lump matrix [QA] into diagonal matrix and update

$$QD_{ij} = QD_{ij} / QA_{ii} \qquad \textbf{(3.7.3.2.10)}$$

$$B_i = B_i / QA_{ii} \qquad \textbf{(3.7.3.2.11)}$$

Then

$$\{D\} = -[QD]\{E_n^{\ m}\} + \{B\} \qquad \textbf{(3.7.3.2.12)}$$

Equation (3.7.3.2.2) written in matrix form is then expressed as

$$\begin{aligned} &\left(\frac{[U]}{\Delta\tau} + W_1[QD^{n+1}] + W_1[K^{n+1}] \right)\left\{ \left(E_n^{\ m}\right)^{n+1/2} \right\} = \frac{[U]}{\Delta\tau}\left\{ \left(E_n^{\ m}\right)^* \right\} \\ &+ W_2\left\{ D^* \right\} - W_2\left([K]\left\{ E_n^{\ m} \right\} \right)^* + W_1\left\{ RL^{n+1} \right\} + W_2\left\{ RL^* \right\} + W_1\left\{ B^{n+1} \right\} \end{aligned} \qquad \textbf{(3.7.3.2.13)}$$

At upstream flux boundary nodes, equation (3.7.3.2.13) cannot be applied because $\Delta\tau$ equals zero.

Thus, we propose a modified LE approach in which the matrix equation for upstream boundary nodes is obtained by explicitly applying the finite element method to the boundary conditions as in Section 3.7.3.1.

3.7.4.3 Operator-Splitting Approach

Equation (3.7.2.3.1) can be solved through the same procedure as that in section 4.5.2, except that

$$RL = \frac{R_{HS}}{\theta^n} \qquad \textbf{(3.7.3.3.1)}$$

3.7.5 Application of the Lagrangian-Eulerian Approach for All Interior Nodes and Downstream Boundary Nodes with the Finite Element Method Applied to the Conservative Form of the Reactive Transport Equations for the Upstream Flux Boundaries

3.7.5.1 Fully-Implicit Scheme

For this option, the matrix equation for interior and downstream boundary nodes is obtained through the same procedure as that in section 3.7.3.1, and the matrix equation for upstream boundary nodes is obtained through the same procedure as that in section 3.7.1.1.

3.7.5.2 Mixed Predictor-Corrector and Operator-Splitting Method

For this option, the matrix equation for interior and downstream boundary nodes is obtained through the same procedure as that in section 3.7.3.2, and the matrix equation for upstream boundary nodes is obtained through the same procedure as that in section 3.7.1.2.

3.7.5.3 Operator-Splitting Approach

For this option, the matrix equation for interior and downstream boundary nodes is obtained through the same procedure as that in section 3.7.3.3, and the matrix equation for upstream boundary nodes is obtained through the same procedure as that in section 3.7.1.3.

3.7.6 Application of the Lagrangian-Eulerian Approach for All Interior Nodes and Downstream Boundary Nodes with the Finite Element Method Applied to the Advective Form of the Reactive Transport Equations for the Upstream Flux Boundaries

3.7.6.1 Fully-Implicit Scheme

For this option, the matrix equation for interior and downstream boundary nodes is obtained through the same procedure as that in section 3.7.3.1, and the matrix equation for upstream boundary nodes is obtained through the same procedure as that in section 3.7.2.1.

3.7.6.2 Mixed Predictor-Corrector and Operator-Splitting Method

For this option, the matrix equation for interior and downstream boundary nodes is obtained through the same procedure as that in section 3.7.3.2, and the matrix equation for upstream boundary nodes is obtained through the same procedure as that in section 3.7.2.2.

3.7.6.3 Operator-Splitting Approach

For this option, the matrix equation for interior and downstream boundary nodes is obtained through the same procedure as that in section 3.7.3.3, and the matrix equation for upstream boundary nodes is obtained through the same procedure as that in section 3.7.2.3.

3.8 Numerical Implementation of Reactive Transport Coupling among Various Media

This section addresses numerical implement of coupling reactive chemical transport simulations among various media including (1) between 1D river and 2D surface runoff, (2) between 2D surface runoff and 3D subsurface media, (3) between 3D subsurface media and 1D river networks, and (4) among 1D river networks, 2D surface runoff, and 3D subsurface media. For sediment transport simulations, only the coupling between 1D river network and 2D surface runoff is needed, which is similar to the coupling of reactive chemical transport between the two media. Without loss of generality, numerical implementations of coupling for scalar transport (including sediment and kinetic-variable transport) are heuristically given for finite element approximations of the conservative form of transport equations. For Largrangian-Eulerian approximations or finite element approximation of the advective form of transport equations, the implementations of numerical coupling among various media remain valid except care must be taken that the fluxes denote the total fluxes of advective and dispersive/diffusive fluxes.

3.8.1 Coupling between 1D-River and 2D-Overland Water Quality Transport

The interaction between one-dimensional river and two-dimensional surface runoff involves two cases: one is between surface runoff and river nodes (left frame in Fig. 3.8-1) and the other is between surface runoff and junction nodes (right frame in Fig. 3.8-1). For every river node (Node *I* in the left frame of Fig. 3.8-1), there will be associated with two overland nodes (Nodes *J* and *K* in the left frame of Fig. 3.8-1). For every junction node (Node *L* in the right frame of Fig. 3.8-1), there will be associated with a number of overland nodes such as Nodes *J*, *K*, *O*, etc (right frame of Fig. 3.8-1). It should be noted that nodes, such as Nodes *J* and *K* in the right frame of Figure 3.8-1, contribute fluxes to both the river as source/sink of Node *I* and the Junction as source/sink of Node *L*.

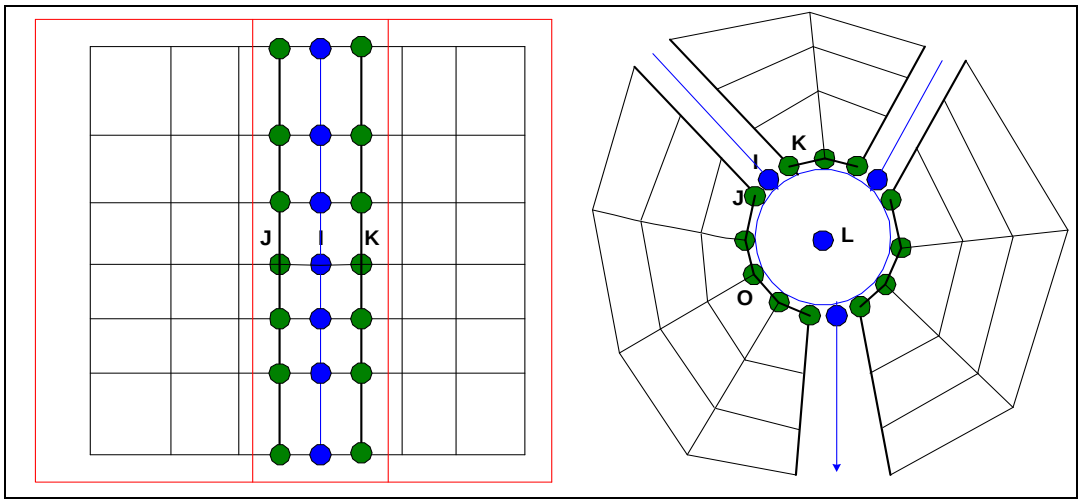

Fig. 3.8-1. Depiction of Interacting River Nodes and Overland Nodes (left) and Junction Node and Overland Nodes (Right)

Numerical approximations of suspended-sediment or kinetic-variable transport equations for one-dimensional river with finite element methods yield the following matrix

$$\begin{bmatrix} -- & -- & -- & -- & -- & -- & -- \\ -- & -- & -- & -- & -- & -- & -- \\ -- & -- & -- & -- & -- & -- & -- \\ C_{I1}^{c} & C_{I2}^{c} & -- & C_{I1}^{c} & -- & -- & C_{IN}^{c} \\ -- & -- & -- & -- & -- & -- & -- \\ -- & -- & -- & -- & -- & -- & -- \\ -- & -- & -- & -- & -- & -- & -- \end{bmatrix} \begin{Bmatrix} E_1^c \\ E_2^c \\ -- \\ E_I^c \\ -- \\ -- \\ E_N^c \end{Bmatrix} = \begin{Bmatrix} R_1^c \\ R_2^c \\ -- \\ R_I^c \\ -- \\ -- \\ R_N^c \end{Bmatrix} + \begin{Bmatrix} M_1^{o1} \\ M_2^{o1} \\ -- \\ M_I^{o1} \\ -- \\ -- \\ M_N^{01} \end{Bmatrix} + \begin{Bmatrix} M_1^{o2} \\ M_2^{o2} \\ -- \\ M_I^{o2} \\ -- \\ -- \\ M_N^{o2} \end{Bmatrix} \qquad \textbf{(3.8.1)}$$

where the superscript *c* denotes the canal (channel, river, or stream); C_{IJ} is the I-th row, J-th column of the coefficient matrix [*C*]; E_I denotes the concentration of a suspended sediment or a kinetic variable at Node *I*; R_I is *I*-th entry of the load vector {*R*}; *N* is the number of nodes in the canal; M_I is the rate of suspended-sediment or kinetic-variable source/sink from (to) the overland flow to (from)canal node *I*; and the superscripts, *o1* and o2, respectively, denote canal bank 1 and 2, respectively. Every canal node *I* involves 3 unknowns, E_I^c, M_I^{o1}, and M_I^{o2}. However, Eq. (3.8.1) gives just one algebraic equation for every canal node *I*. Clearly, two additional algebraic equations are need for every canal node *I*. It should be noted that M_I^{o1} and M_I^{o2}denote the following integrations in transforming Eq. (2.5.10) and its initial and boundary conditions or Eq. (2.5.44) and its initial and boundary conditions to Eq. (3.8.1)

$$M_I^{o1} = \int_{X_1}^{X_N} N_I M_{S_n}^{os1} dx \quad and \quad M_I^{o2} = \int_{X_1}^{X_N} N_I M_{S_n}^{os2} dx \qquad \textbf{(3.8.2)}$$

for the transport of the *n*-th suspended-sediment fraction

$$M_I^{o1} = \int_{X_1}^{X_N} N_I M_{E_i}^{os1} dx \quad and \quad M_I^{o2} = \int_{X_1}^{X_N} N_I M_{E_i}^{os2} dx \tag{3.8.3}$$

for the transport of the *i*-th kinetic variable.

Applications of finite element methods to two-dimensional suspended-sediment or kinetic-variable transport equation yield the following matrix

$$\begin{bmatrix} C_{11}^o & C_{12}^o & -- & -- & -- & -- & C_{1M}^o \\ C_{21}^o & -- & -- & -- & -- & -- & C_{2M}^o \\ -- & -- & -- & -- & -- & -- & -- \\ C_{J1}^o & C_{J2}^o & -- & C_{jj}^o & -- & -- & C_{IM}^o \\ -- & -- & -- & -- & -- & -- & -- \\ C_{K1}^o & C_{K2}^o & -- & -- & C_{KK}^o & -- & C_{KM}^o \\ -- & -- & -- & -- & -- & -- & -- \\ C_{M1}^o & C_{M2}^o & -- & -- & -- & -- & C_{MM}^o \end{bmatrix} \begin{Bmatrix} E_1^o \\ E_2^o \\ -- \\ E_J^o \\ -- \\ E_K^o \\ -- \\ E_M^o \end{Bmatrix} = \begin{Bmatrix} R_1^o \\ R_2^o \\ -- \\ R_J^o \\ -- \\ R_K^o \\ -- \\ R_M^o \end{Bmatrix} - \begin{Bmatrix} -- \\ -- \\ -- \\ M_J^o \\ -- \\ M_K^o \\ -- \\ -- \end{Bmatrix} \tag{3.8.4}$$

where the superscript *o* denotes the overland; C_{IJ} is the *I*-th row, *J*-th column of the coefficient matrix [*C*]; E_I denotes the concentration of suspended sediment or kinetic variable at Node *I*; R_I is *I*-th entry of the load vector {*R*}; *M* is the number of nodes in the overland ; and M_J and M_K are the fluxes [M/t] of suspended sediment or kinetic variable from (to) the overland to (from) the canal via nodes *J* and *K*, respectively. Equation (3.8.4) indicates that there is one unknown corresponding to one algebraic equation for every interior node. However, for every algebraic equation corresponding to an overland-canal interface node, there are two unknowns, the concentration of suspended sediment or kinetic variable and the sediment or chemical fluxes. Therefore, for every overland-river interface node, one additional equation is needed. Since for every canal node, there are associated two overland-interface nodes, four additional equations are needed for every canal node *I* for the four additional unknowns M_J^o, M_K^o, M_I^{o1}, and M_I^{o2}.

Before we proceed further, let us refresh ourselves that M_J^o and M_K^o denote the following integration in transforming Eq. (2.6.10) and its initial and boundary conditions or Eq. (2.6.46) and its initial and boundary conditions to Eq. (3.8.4)

$$M_J^o = \int_B \mathbf{n}\bullet\left(W_J \mathbf{q} S_n - N_J h \mathbf{K}\bullet\nabla S_n\right) dB \quad and \quad M_K^o = \int_B \mathbf{n}\bullet\left(W_K \mathbf{q} S_n - N_K h \mathbf{K}\bullet\nabla S_n\right) dB \tag{3.8.5}$$

for the transport of the *n*-th suspended-sediment fraction

$$M_J^o = \int_B \mathbf{n}\bullet\left(W_J \mathbf{q} E_i^m - N_J h \mathbf{K}\bullet\nabla E_i^m\right) dB \quad and \quad M_K^o = \int_B \mathbf{n}\bullet\left(W_K \mathbf{q} E_i^m - N_K h \mathbf{K}\bullet\nabla E_i^m\right) dB \tag{3.8.6}$$

for the transport of the *i*-th kinetic variable.

The additional equations are obtained from two interface boundary conditions: one is the continuity

of flux and the other is the assumption that the flux of suspended sediments or kinetic variables through the interface node is due mainly to water flow (i.e., advection). Two of the four additional equations are obtained from the interface condition between the canal node *I* and the overland node *J* as

$$M_J^o = M_I^{o1} \quad and \quad M_J^o = Q_J^o \frac{1}{2}\left(\left(1 + sign\left(Q_J^o\right)\right)E_J^o + \left(1 - sign\left(Q_J^o\right)\right)E_I^c\right) \tag{3.8.7}$$

For suspended sediment transport, E_J^o and E_I^c denote

$$E_J^o = S_{nJ}{}^o \quad and \quad E_I^c = S_{nI}{}^c \tag{3.8.8}$$

where $S_{nJ}{}^o$ is the concentration of the suspended sediment of the *n*-th fraction at Node *J* in the overland domain and $S_{nI}{}^c$ is the concentration of the suspended sediment of the *n*-th fraction at Node *I* in the canal domain. For the transport of kinetic variables, E_J^o and E_I^c denote

$$E_J^o = E_i^m{}_J{}^o \quad and \quad E_I^c = E_i^m{}_I{}^c \tag{3.8.9}$$

where $E_i^m{}_J{}^o$ is the concentration of the mobile portion of the *i*-th kinetic variable at Node *J* in the overland domain and $E_i^m{}_I{}^c$ is the concentration of the mobile portion of the *i*-th kinetic variable at Node *I* in the canal domain.

The other two additional equations are obtained from the interface condition between the canal Node *I* and the overland Node *K* as follows

$$M_K^o = M_I^{o1} \quad and \quad M_K^o = Q_K^o \frac{1}{2}\left(\left(1 + sign\left(Q_K^o\right)\right)E_K^o + \left(1 - sign\left(Q_K^o\right)\right)E_I^c\right) \tag{3.8.10}$$

The definition of E_K^o is similar to that of E_J^o.

When the direct contribution of suspended sediment or chemicals from the overland regime to a junction node *L* (Fig. 3.8-1) is significant, the mass balance equation can be written as

$$\frac{d\forall_L E_L}{dt} = \sum_i \Psi_{iL}^i + \sum_{O \in N_O} M_O^o \quad or \quad \sum_i \Psi_{iL}^i + \sum_{O \in N_O} M_O^o = 0 \tag{3.8.11}$$

where $\forall_L$ is the volume of the *L*-th junction, Ψ_{iL}^i is the mass flux from the *iL*-th node of *i*-th reach to the *L*-th junction, and M_O^o is the mass flux from the *O*-th node of the overland regime (superscript *o* t represent overland regime). Additional N_O unknowns have been introduced in Equation (3.8.11). For each overland-junction interface node, say *O* (the right frame in Fig. 3.8.1), the finite element equation written out of Eq. (3.8.4) is

$$C_{O1}^o E_1^o + C_{O2}^o E_2^o + .. + C_{OO}^o E_O^o + .. + C_{OM}^o E_M^o = R_O^o - M_O^o \tag{3.8.12}$$

It is seen that Equation (3.4.17) involves two unknowns, E_O^o and M_O^o. One equation must be supplemented to the finite element equation to close the system. This equation is obtained by formulating fluxes as

$$M_O^o = Q_O^o \frac{1}{2}\left(\left(1 + sign\left(Q_O^o\right)\right)E_O^o + \left(1 - sign\left(Q_O^o\right)\right)E_L\right) \qquad \textbf{(3.8.13)}$$

Equations (3.8.11), (3.8.12), and (3.8.13) for a system of equations for the set of unknowns E_L, E_O^o and M_O^o.

3.8.2 Coupling between 2D-Overalnd and 3D-Subsurface Water Quality Transport

The interaction between two-dimensional overland and three-dimensional subsurface water quality transport is not as straightforward as that between 1D-river and 2D-overland regime because the *i*-th kinetic variable in the 2D-voerland is not necessary to have the same set of species as the *i*-th kinetic variable in the 3D-subsurface media. We will assume that there is no exchange of suspended sediment between 2D-overland and 3D-subsurface media. Only exchanges of aqueous-phase species take place. For every subsurface node (Node *J* in Fig. 3.8-2), there will be associated an overland nodes (Node *I* in Fig. 3.8-2).

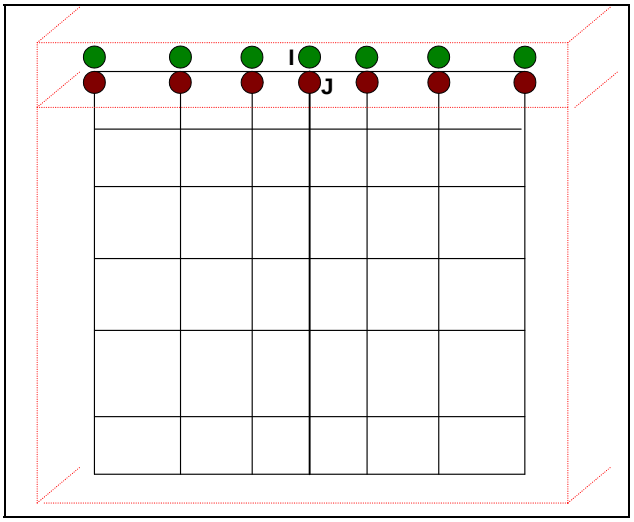

Fig. 3.8-2. Depiction of Interacting Subsurface Nodes and Overland Nodes

Numerical approximations of kinetic-variable transport equation for two-dimensional overland regime with finite element methods yield the following matrix

$$\begin{bmatrix} -- & -- & -- & -- & -- & -- & -- \\ -- & -- & -- & -- & -- & -- & -- \\ -- & -- & -- & -- & -- & -- & -- \\ C_{I1}^{o} & C_{I2}^{o} & -- & C_{II}^{o} & -- & -- & C_{IN}^{o} \\ -- & -- & -- & -- & -- & -- & -- \\ -- & -- & -- & -- & -- & -- & -- \\ -- & -- & -- & -- & -- & -- & -- \end{bmatrix} \begin{Bmatrix} E_1^{o} \\ E_2^{o} \\ -- \\ E_I^{o} \\ -- \\ -- \\ E_N^{o} \end{Bmatrix} = \begin{Bmatrix} R_1^{o} \\ R_2^{o} \\ -- \\ R_I^{o} \\ -- \\ -- \\ R_N^{o} \end{Bmatrix} + \begin{Bmatrix} M_1^{io} \\ M_2^{io} \\ -- \\ M_I^{io} \\ -- \\ -- \\ M_N^{io} \end{Bmatrix} \qquad \textbf{(3.8.14)}$$

where the superscript *o* denotes the overland; C_{IJ} is the I-th row, J-th column of the coefficient matrix [*C*]; E_I denotes the concentration of a kinetic variable at Node *I*; R_I is *I*-th entry of the load vector {*R*}; *N* is the number of nodes in the overland; and M_I is the rate of the kinetic-variable source/sink from (to) the subsurface to (from) the overland node *I* (the superscript, *io*, denotes the exfiltration from subsurface media to overland). Every overland node *I* involves two unknowns, E_I^o, and M_I^{io}. However, Eq. (3.8.14) gives just one algebraic equation for every canal node *I*. Clearly, one additional algebraic equation is need for every overland node *I*. To formulate this equation, it is noted that, for the *i*-th overland kinetic variable, M_I^{io} is the source/sink rate of the *i*-th kinetic variable at the I-th node due to infiltration (negative value) or exfitration (positive value). This equation is obtained as follows

$$M_I^{io} = (Q_I^{io})\frac{1}{2}\left(\left(1 + sign\left(Q_I^{io}\right)\right) \sum_{j \in M_a} a_{ij}^o C_{jJ}^s + \left(1 - sign\left(Q_I^{io}\right)\right) \sum_{j \in M_a} a_{ij}^o C_{jI}^o \right) \qquad \textbf{(3.8.15)}$$

where M_a is the set of aqueous species, a_{ij}^o is the *ij*-th entry of the decomposed unit matrix via diagonalization of the reaction network in the overland domain, C_{jJ}^s is the concentration of the *j*-th subsurface species at the *J*-th node of the subsurface domain, and C_{jI}^o is the concentration of the *j*-th overland species at the *I*-th node of the overland domain.

Applications of finite element methods to three-dimensional kinetic-variable transport equations for subsurface media yield the following matrix

$$\begin{bmatrix} C_{11}^s & C_{12}^s & -- & -- & -- & -- & C_{1M}^s \\ C_{21}^s & -- & -- & -- & -- & -- & C_{2M}^s \\ -- & -- & -- & -- & -- & -- & -- \\ C_{J1}^s & C_{J2}^s & -- & C_{JJ}^s & -- & -- & C_{IM}^s \\ -- & -- & -- & -- & -- & -- & -- \\ -- & -- & -- & -- & -- & -- & -- \\ C_{M1}^s & C_{M2}^s & -- & -- & -- & -- & C_{MM}^s \end{bmatrix} \begin{Bmatrix} E_1^s \\ E_2^s \\ -- \\ E_J^s \\ -- \\ -- \\ E_M^s \end{Bmatrix} = \begin{Bmatrix} R_1^s \\ R_2^s \\ -- \\ R_J^s \\ -- \\ -- \\ R_M^s \end{Bmatrix} - \begin{Bmatrix} -- \\ -- \\ -- \\ M_J^s \\ -- \\ -- \\ -- \end{Bmatrix} \qquad \textbf{(3.8.16)}$$

where the superscript *s* denotes the subsurface media; C_{IJ} is the *I*-th row, *J*-th column of the

coefficient matrix [C]; E_J denotes the temperature or salinity at Node J; R_J is J-th entry of the load vector $\{R\}$; M is the number of nodes in the subsurface; and M_J is the rate of thermal or salt sink/source from/to the subsurface node J to/from the corresponding overland node I. Equation (3.8.15) indicates that there is one unknown corresponding to one algebraic equation for every interior node. However, for every algebraic equation corresponding to a subsurface-overland interface node, there are two unknowns, the concentration of the i-th subsurface kinetic variable at node J, E_J^s, and its flux, M_J^s. Therefore, one additional equation is needed. This equation is obtained from

$$M_J^s = (Q_J^s)\frac{1}{2}\left(\left(1+sign\left(Q_J^s\right)\right)\sum_{j\in M_a} a_{ij}^s C_{jJ}^s + \left(1-sign\left(Q_J^s\right)\right)\sum_{j\in M_a} a_{ij}^s C_{jI}^o\right) \qquad \textbf{(3.8.17)}$$

where a_{ij}^s is the ij-th entry of the decomposed unit matrix via diagonalization of the reaction network in the subsurface media.

3.8.3 Coupling between 3-D Subsurface and 1-D Surface Flows

The interaction between three-dimensional subsurface and one-dimensional river water quality transport involves three options: (1) river is discretized as finite-width and finite-depth on the three-dimensional subsurface media (Fig. 3.8-3), (2) river is discretized as finite-width and zero-depth on the three-dimensional subsurface media (Fig. 3.4-4), and (3) river is discretized as zero-width and zero-depth on the three-dimensional subsurface media (Fig. 3.4-5). Option 1 is the most realistic one. However, because of the computational demands, it is normally used in small scale studies involving the investigations of infiltration and discharge between river and subsurface media on a local scale. Option 2 is normally used in medium scale studies while Option 3 is normally employed in large scale investigations. In Option 1, for every river node there are associated with a number of subsurface interfacing nodes such as K, .., J, .., and L(Fig. 3.8-3). In Option 2, for every river node there are associated with three subsurface interfacing nodes K, J, and L (Fig. 3.8-4). In Option 3, for every river node there is associated with one subsurface interfacing node J (Fig. 3.8-5).

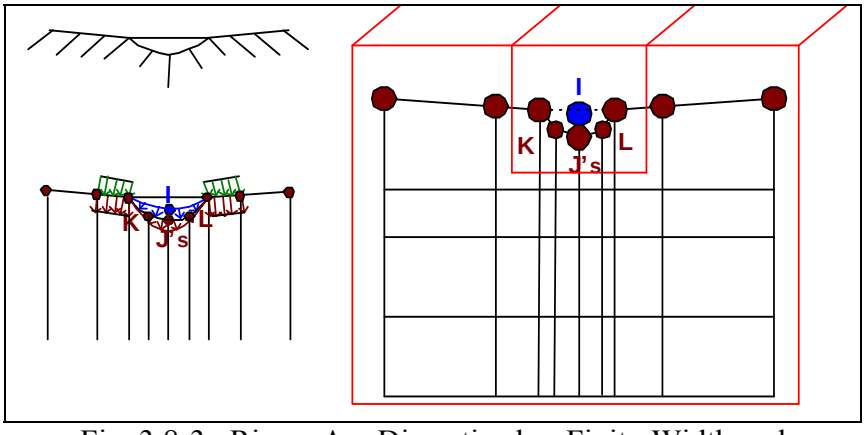

Fig. 3.8-3. Rivers Are Discretized as Finite-Width and Finite-Depth on the Subsurface Media

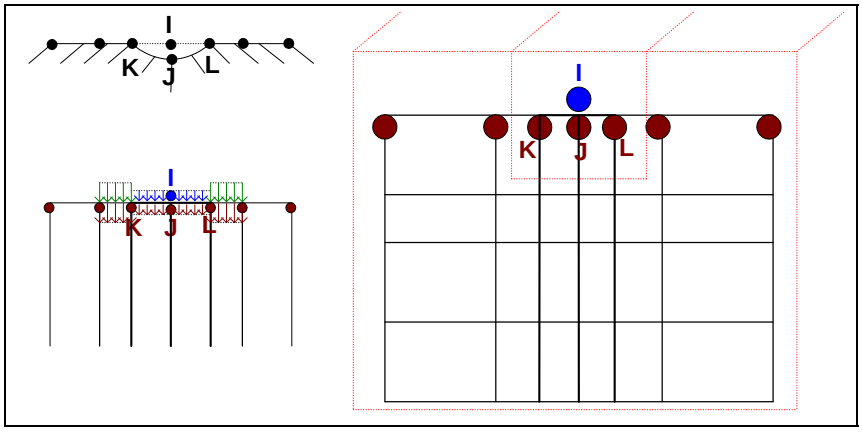

Fig. 3.8-4. Rivers Are Discretized as Finite-Width and Zero-Depth on the Subsurface Media

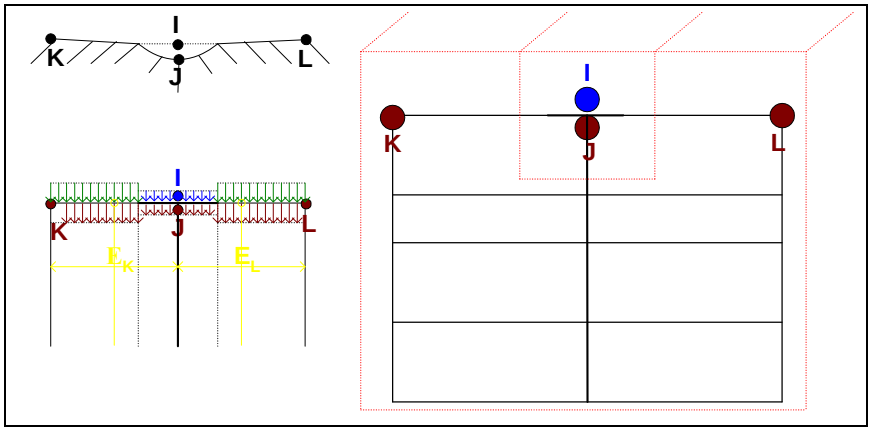

Fig. 3.8-5. Rivers Are Discretized as Zero-Width and Zero-Depth on the Subsurface Media

Numerical approximations of i-th kinetic-variable transport equation for one-dimensional river with finite element methods yield the following matrix

$$\begin{bmatrix} -- & -- & -- & -- & -- & -- & -- \\ -- & -- & -- & -- & -- & -- & -- \\ -- & -- & -- & -- & -- & -- & -- \\ C^c_{I1} & C^c_{I2} & -- & C^c_{II} & -- & -- & C^c_{IN} \\ -- & -- & -- & -- & -- & -- & -- \\ -- & -- & -- & -- & -- & -- & -- \\ -- & -- & -- & -- & -- & -- & -- \end{bmatrix} \begin{Bmatrix} E^c_1 \\ E^c_2 \\ -- \\ E^c_I \\ -- \\ -- \\ E^c_N \end{Bmatrix} = \begin{Bmatrix} R^c_1 \\ R^c_2 \\ -- \\ R^c_I \\ -- \\ -- \\ R^c_N \end{Bmatrix} + \begin{Bmatrix} M^{ic}_1 \\ M^{ic}_2 \\ -- \\ M^{ic}_I \\ -- \\ -- \\ M^{ic}_N \end{Bmatrix} \qquad \textbf{(3.8.18)}$$

where the superscript *c* denotes the canal (channel, river, or stream); C_{IJ} is the I-th row, J-th column

of the coefficient matrix [C]; E_I denotes the temperature or salinity at Node I; R_I is I-th entry of the load vector {R}; N is the number of nodes in the canal; and M_I^{ic} is the mass rate of the kinetic-variable source/sink from (to) the subsurface to (from) canal node I due to infiltration/exfiltration. Every canal node I involves two unknowns, E_I^c and M_I^{ic}. However, Eq. (3.8.18) gives just one algebraic equation for every canal node I. Clearly, one additional algebraic equation is need for every canal node I.

For example, taking Option 2 where there are three nodes associated with one canal node, the applications of finite element methods to three-dimensional kinetic-variable transport equation in the subsurface media yields

$$\begin{bmatrix} C_{11}^s & C_{12}^s & -- & -- & -- & -- & C_{1M}^s \\ C_{21}^s & -- & -- & -- & -- & -- & C_{2M}^s \\ -- & -- & -- & -- & -- & -- & -- \\ C_{K1}^s & C_{K2}^s & C_{KK}^s & -- & -- & -- & C_{KM}^s \\ C_{J1}^s & C_{J2}^s & -- & C_{JJ}^s & -- & -- & C_{1M}^s \\ C_{L1}^s & C_{L2}^s & C_{<<}^s & -- & -- & -- & C_{LM}^s \\ -- & -- & -- & -- & -- & -- & -- \\ C_{M1}^s & C_{M2}^s & -- & -- & -- & -- & C_{MM}^s \end{bmatrix} \begin{Bmatrix} E_1^s \\ E_2^s \\ -- \\ E_K^s \\ E_J^s \\ E_L^s \\ -- \\ E_M^s \end{Bmatrix} = \begin{Bmatrix} R_1^s \\ R_2^s \\ -- \\ R_K^s \\ R_J^s \\ R_L^s \\ -- \\ R_M^s \end{Bmatrix} - \begin{Bmatrix} -- \\ -- \\ -- \\ M_K^s \\ M_J^s \\ M_L^s \\ -- \\ -- \end{Bmatrix} \qquad \textbf{(3.8.19)}$$

where the superscript s denotes the subsurface media; C_{IJ} is the I-th row, J-th column of the coefficient matrix [C]; E_J denotes the temperature or salinity at Node J; R_J is J-th entry of the load vector {R}; M is the number of nodes in the overland ; and M_K, M_J and M_L are the rates of thermal or salt sink/source from/to the subsurface water to/from the canal via nodes K, J and L, respectively. Equation (3.8.19) indicates that there is one unknown corresponding to one algebraic equation for every interior node. However, for every algebraic equation corresponding a subsurface-canal interface node, there are two unknowns, concentration of the kinetic variable and its flux. Therefore, for every subsurface-river interface node, one additional equation is needed. Since for every canal node, there are associated three subsurface-interface nodes, four additional equations are needed for every canal node I for the four additional unknowns M_I^{ic}, M_K^s, M_J^s, and M_L^s.

These four additional equations are obtained with the assumptions that only aqueous species are involved in the exchange between the canal node I and the subsurface nodes K, J, and L and the exchange is mainly due to advection. These assumptions result in the following four equations:

$$M_I^{ic} = \frac{1}{2}(Q_I^{ic})\left(\left(1-sign\left(Q_I^{ic}\right)\right)\sum_{j\in M_a} a_{ij}^c C_{jI}^c\right)+\frac{1}{2}\left(1+sign(Q_I^{ic})\right)\times$$
$$\left(Q_K^s\sum_{j\in M_a} a_{ij}^c C_{jK}^s + Q_J^s\sum_{j\in M_a} a_{ij}^c C_{jJ}^s + Q_L^s\sum_{j\in M_a} a_{ij}^c C_{jL}^s - Q_K^{rains}\sum_{j\in M_a} a_{ij}^c C_{jK}^{rain} - Q_L^{rains}\sum_{j\in M_a} a_{ij}^c C_{jL}^{rain}\right) \qquad \textbf{(3.8.20)}$$

$$M_J^s = \frac{1}{2}(Q_J^s)\left(\left(1 - sign\left(Q_J^s\right)\right)\sum_{j\in M_a} a_{ij}^s C_{jI}^c\right) + \frac{1}{2}(Q_J^s)\left(\left(1 + sign\left(Q_J^s\right)\right)\sum_{j\in M_a} a_{ij}^s C_{jJ}^s\right) \quad \textbf{(3.8.21)}$$

$$M_K^s = \frac{1}{2}(Q_K^s)\left(\left(1 - sign\left(Q_K^s\right)\right)\sum_{j\in M_a} a_{ij}^s C_{jI}^c\right) + \frac{1}{2}(Q_K^s)\left(\left(1 + sign\left(Q_K^s\right)\right)\sum_{j\in M_a} a_{ij}^s C_{jK}^s\right) \quad \textbf{(3.8.22}$$

$$M_L^s = \frac{1}{2}(Q_L^s)\left(\left(1 - sign\left(Q_L^s\right)\right)\sum_{j\in M_a} a_{ij}^s C_{jI}^c\right) + \frac{1}{2}(Q_L^s)\left(\left(1 + sign\left(Q_L^s\right)\right)\sum_{j\in M_a} a_{ij}^s C_{jL}^s\right) \quad \textbf{(3.8.23)}$$

where M_a is the set of aqueous species, a_{ij}^c is the *ij*-th entry of the decomposed unit matrix via diagonalization of the reaction network in the canal domain, C_{jI}^c is the concentration of the *j*-th canal species at the I-th node of the canal domain, C_{jJ}^s is the concentration of the *j*-th subsurface species at the *J*-th node of the subsurface domain, C_{jK}^s is the concentration of the *j*-th subsurface species at the *K*-th node of the subsurface domain, C_{jL}^s is the concentration of the *j*-th subsurface species at the *L*-th node of the subsurface domain, C_{jK}^{rain} is the concentration of the *j*-th species of the rainfall that falls on the *K*-th node of the subsurface domain, C_{jL}^{rain} is the concentration of the *j*-th species of the rainfall that falls on the *L*-th node of the subsurface domain, and a_{ij}^s is the *ij*-th entry of the decomposed unit matrix via diagonalization of the reaction network in the subsurface domain.

3.8.4 Coupling Among River, Overland, and Subsurface Flows

The interaction among one-dimensional river, two-dimensional overland, and three-dimensional subsurface flows involves three options: (1) river is discretized as finite-width and finite-depth on the three-dimensional subsurface media (Fig. 3.8-6), (2) river is discretized as finite-width and zero-depth on the three-dimensional subsurface media (Fig. 3.8-7), and (3) river is discretized as zero-width and zero-depth on the three-dimensional subsurface media (Fig. 3.4-8). Option 1 is the most realistic one. However, because of the computational demands, it is normally used in small scale studies involving the investigations of infiltration and discharge between river and subsurface media on a local scale. Option 2 is normally used in medium scale studies while Option 3 is normally employed in large scale investigations. In Option 1, for every river node there are associated with two overland nodes *M* and *N* and a number of subsurface interfacing nodes such as *K*. , *J*, .., and *L* (Fig. 3.8-6). In Option 2, for every river node *I*, there are associated with two overland nodes *M* and *N* and three subsurface interfacing nodes *K*, *J*, and *L* (Fig. 3.4-7). In Option 3, for every river node *I*, there is associated with two overland nodes *M* and *N* one subsurface node *J* (Fig. 3.8-8).

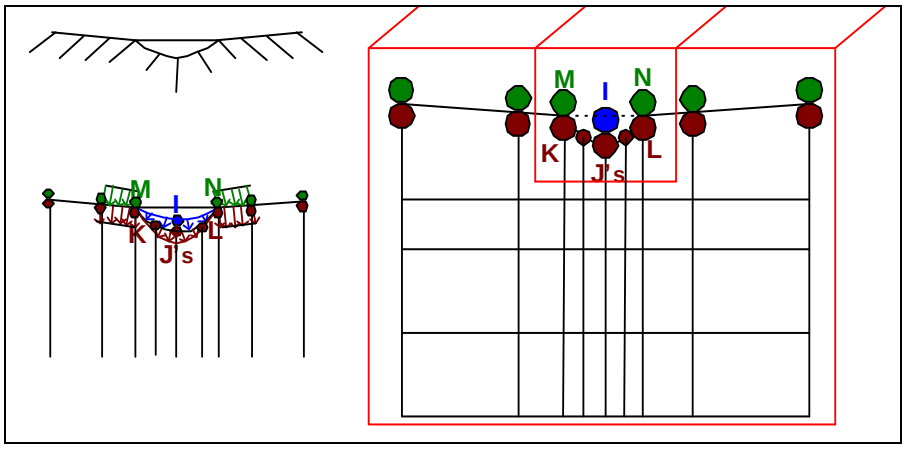

Fig. 3.8-6. Interfacing Nodes for Every River Node when Rivers Are Discretized as Finite-Width and Finite-Depth

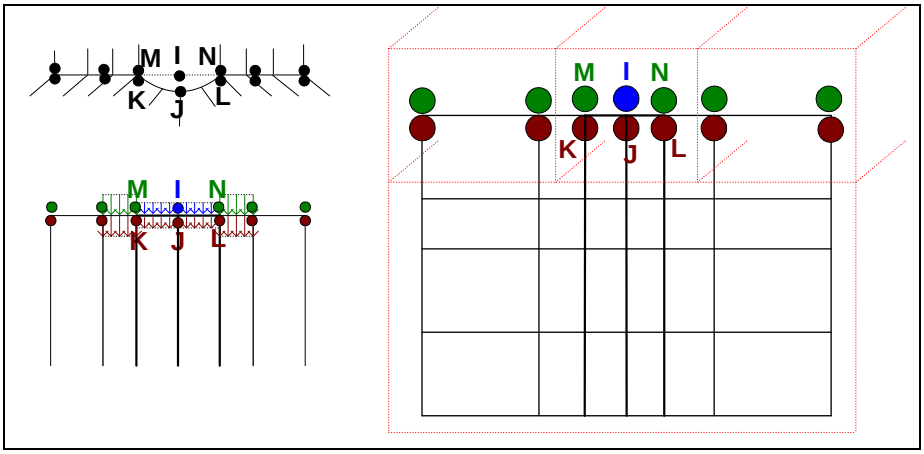

Fig. 3.8-7. Interfacing Nodes for Every River Node when Rivers Are Discretized as Finite-Width and Zero-Depth

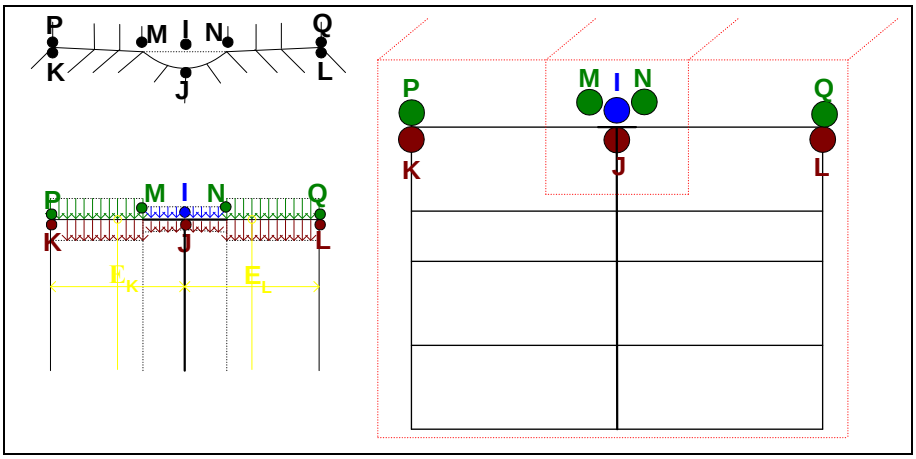

Fig. 3.8-8. Interfacing Nodes for Every River Node when Rivers Are Discretized as Zero-Width and Zero-Depth

Similar to the coupling of salt transport among river, overland, and subsurface media, the coupling of water quality transport is achieved by imposing the continuity of water quality fluxes and formulation of individual node fluxes.

Interaction between Overland Node *M* and Canal Node *I*. Two equations are obtained based on the continuity of fluxes and the formulation of fluxes as

$$\begin{aligned} M_I^{o1} &= Q_I^{o1}\frac{1}{2}\left(\left(1+sign\left(Q_I^{o1}\right)\right)E_M^o+\left(1-sign\left((Q_I^{o1}\right)\right)E_I^c\right) \quad and \\ M_M^o &= Q_M^o\frac{1}{2}\left(\left(1+sign\left(Q_M^o\right)\right)E_M^o+\left(1-sign\left((Q_M^o\right)\right)E_I^c\right) \end{aligned} \tag{3.8.24}$$

Interaction between Overland Node *N* and Canal Node *I*. Two equations are obtained based on the continuity of fluxes and the formulation of fluxes as

$$\begin{aligned} M_I^{o2} &= Q_I^{o2}\frac{1}{2}\left(\left(1+sign\left(Q_I^{o2}\right)\right)E_N^o+\left(1-sign\left((Q_I^{o2}\right)\right)E_I^c\right) \quad and \\ M_N^o &= Q_N^o\frac{1}{2}\left(\left(1+sign\left(Q_N^o\right)\right)E_N^o+\left(1-sign\left((Q_N^o\right)\right)E_I^c\right) \end{aligned} \tag{3.8.25}$$

Interaction between Overland Node *M*, Subsurface Node *K*, and Canal Node *I*. Two equations are obtained based on the continuity of fluxes and the formulation of fluxes as

$$M_M^{io}=\left\{\frac{1}{2}\left(1-sign\left(Q_M^{io}\right)\right)Q_M^{io}\sum_{j\in M_a}a_{ij}^oC_{jM}^o+\frac{1}{2}\left(1+sign\left(Q_M^{io}\right)\right)\left(Q_K^s\sum_{j\in M_a}a_{ij}^oC_{jK}^s-\frac{1}{4}Q_I^{ic}\sum_{j\in M_a}a_{ij}^oC_{jI}^cE_I^c\right)\right\}$$

$$and \tag{3.8.26}$$

$$M_K^s=\left\{\frac{1}{2}\left(1+sign\left(Q_K^s\right)\right)Q_K^s\sum_{j\in M_a}a_{ij}^sC_{jK}^s+\frac{1}{2}\left(1-sign\left(Q_K^s\right)\right)\left(Q_M^{io}\sum_{j\in M_a}a_{ij}^sC_{jM}^o+\frac{1}{4}Q_I^{ic}\sum_{j\in M_a}a_{ij}^sC_{jI}^c\right)\right\}$$

where M_a is the set of aqueous species, a_{ij}^o is the *ij*-th entry of the decomposed unit matrix via diagonalization of the reaction network in the overland domain.

Interaction between River Bank Node *N*, Subsurface Node *L*, and Canal Node *I*. Two equations are obtained based on the continuity of fluxes and the formulation of fluxes

$$M_N^{io}=\left\{\frac{1}{2}\left(1-sign\left(Q_N^{io}\right)\right)Q_N^{io}\sum_{j\in M_a}a_{ij}^oC_{jN}^o+\frac{1}{2}\left(1+sign\left(Q_N^{io}\right)\right)\left(Q_L^s\sum_{j\in M_a}a_{ij}^oC_{jL}^s-\frac{1}{4}Q_I^{ic}\sum_{j\in M_a}a_{ij}^oC_{jI}^c\right)\right\}$$

$$and \tag{3.8.27}$$

$$M_L^s=\left\{\frac{1}{2}\left(1+sign\left(Q_L^s\right)\right)Q_L^s\sum_{j\in M_a}a_{ij}^sC_{jL}^s+\frac{1}{2}\left(1-sign\left(Q_L^s\right)\right)\left(Q_N^{io}\sum_{j\in M_a}a_{ij}^sC_{jN}^o+\frac{1}{4}Q_I^{ic}\sum_{j\in M_a}a_{ij}^sC_{jI}^c\right)\right\}$$

Interaction between Subsurface Node *J* and Canal Node *I*. Two equations are obtained based on the continuity of fluxes and the formulation of fluxes as

$$M_I^{ic} = \left(\frac{1}{2}\left(1 + sign\left(Q_I^{ic}\right)\right) 2Q_J^s \sum_{j \in M_a} a_{ij}^c C_{jJ}^s + \frac{1}{2}\left(1 - sign\left(Q_I^{ic}\right)\right) Q_I^{ic} \sum_{j \in M_a} a_{ij}^c C_{jI}^c \right) \quad and$$

$$M_J^s = \left(\frac{1}{2}\left(1 + sign\left(Q_J^s\right)\right) Q_J^s \sum_{j \in M_a} a_{ij}^s C_{jJ}^s + \frac{1}{2}\left(1 - sign\left(Q_J^s\right)\right) \frac{1}{2} Q_I^{ic} \sum_{j \in M_a} a_{ij}^s C_{jI}^c \right) \qquad \textbf{(3.8.28)}$$

3.9 Vastly Different Time Scales among Various Media

The time scales for hydrology and hydraulics and water quality transport in river/stream/canal networks, overland regime and subsurface media are vastly different. The time scale for flow and transport may be in the order of seconds and minutes in 1D-river/stream/canal networks, minutes in 2D-overland regime, and hours, days or even weeks in 3D-subsurface media. To handle this kind of very different time-scale problems, the approach of using variable time-step sizes among different domains is taken. Figure 3.9-1 shows the model structure of over-all coupling between various interfacial media. In Figure 3.9-1, Δt = GT is the global time-step size (it is noted that total simulation time may consist of several Δt's); GTS is the number of time steps in each GT and Δt_{GT} is the time-step size; 3DF is the number of time steps for 3D flow simulations in each GT and Δt_{3DF} is time step size; 2DF is the number of time steps for 2D flow simulations and Δt_{2DF} is the time step size; 1DF is the number of time steps for 1D flow simulations and Δt_{1DF} is the time step size.

Figures 3.9-2 shows the detail structure on 1D only river/stream/canal networks simulations. For flow computation in one time step, we first linearize all coefficients in and boundary conditions (by linearize boundary conditions, we mean, for example, to fix variable-type boundary conditions if they are prescribed) for the governing equations using previous iterates and solve the linearized equations within the nonlinear loop. Within the nonlinear loop, first solve flow equations to obtain HQW1, where HQW1 is the water depth and discharge for the 1D case; then for every several flow time steps, solve salinity and thermal transport equation to yield C1 and T1, where C1 and T1 are the salt concentration and temperature, respectively. When fluid flow and salt and thermal transport are solved to convergences, repeat one more nonlinear loop to provide flow fields (i.e., HQW1) for the simulation of reactive chemical transport. The solution of reactive chemical transport would render CR1, where CR1 is the concentration of reactive biogeochemical species for 1D. After density-dependent flow fields, salinity, temperature, and reactive chemical transport are solved, proceed to the next time step. Figures 3.9-3 and 3.9-4 show detail computational structures for simulations in 2D overland and 3D subsurface media, respectively.

Figures 3.9-5, 3.9-6, and 3.9-7 show detail structures for simulating in coupled 1D and 2D, coupled 2D and 3D, and coupled 3D and 1D flow and transport, respectively. In all eight figures, the naming convention of the state-variables is systematic combination of H, Q, C, T, CR, R, W, P, 0, 1, 2, and 3. H denotes water depth or head, Q denotes discharge, C denote salt concentration, T denote temperature, CR denote concentration of reactive entities, R denotes source/sinks, W denotes working iterative values, P denotes previous time, 0 denote initial values, 1 denote 1D, 2 denotes 2D,

and 3 denotes 3D. For example, HQW1 (at convergence, HQW1 would be HQ1) is the water depth and discharge of the iterative working values for 1D case; CR2 is the concentrations of reactive entities for 2D cases; TP1 is the temperature at the previous time step for 1D cases. DIV denotes the divergence of the velocity, i.e. DIV = $\nabla \cdot \mathbf{V}$.

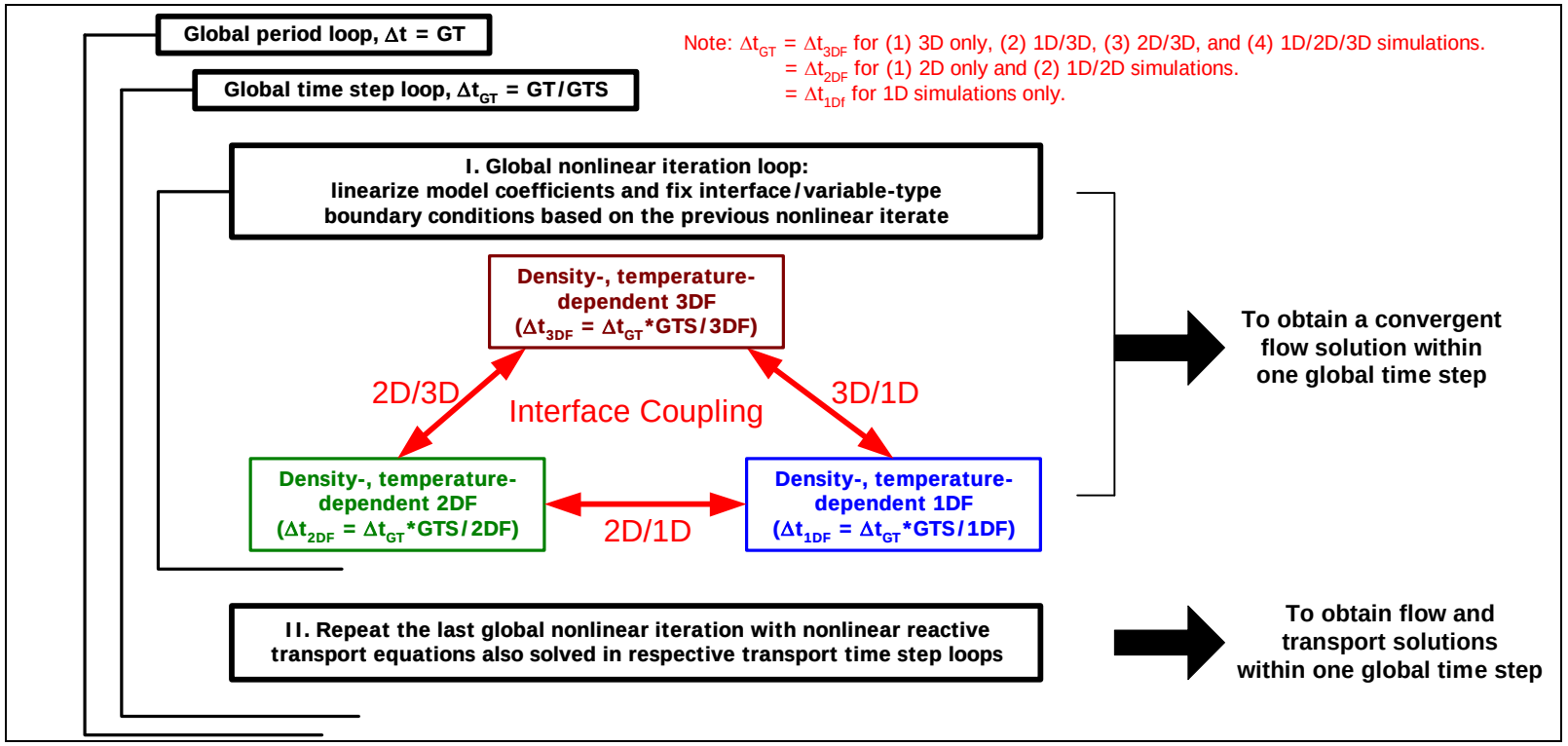

Fig. 3.9-1. Overall Coupled Structure of WASH123D

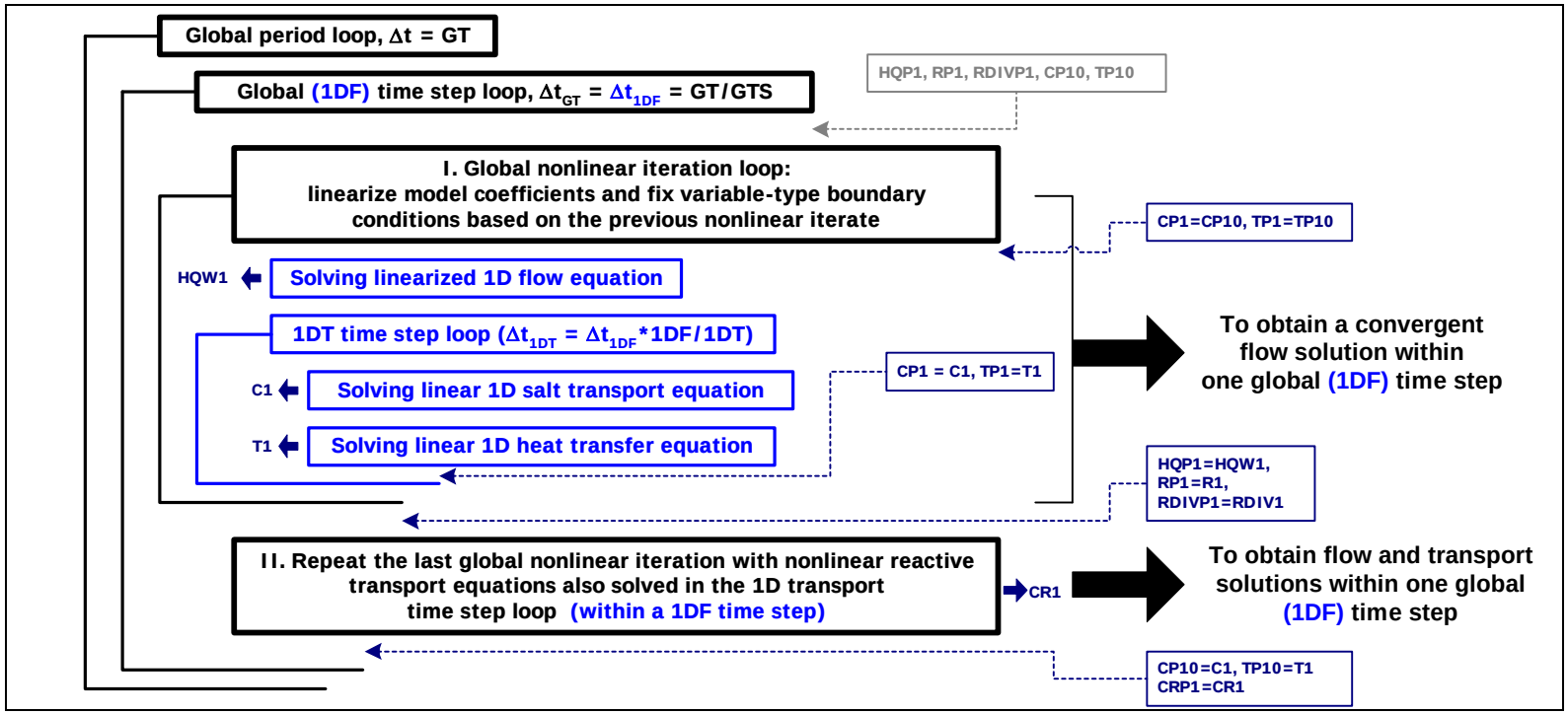

Fig. 3.9-2. Computation Structure of WASH123D for 1D only Simulations

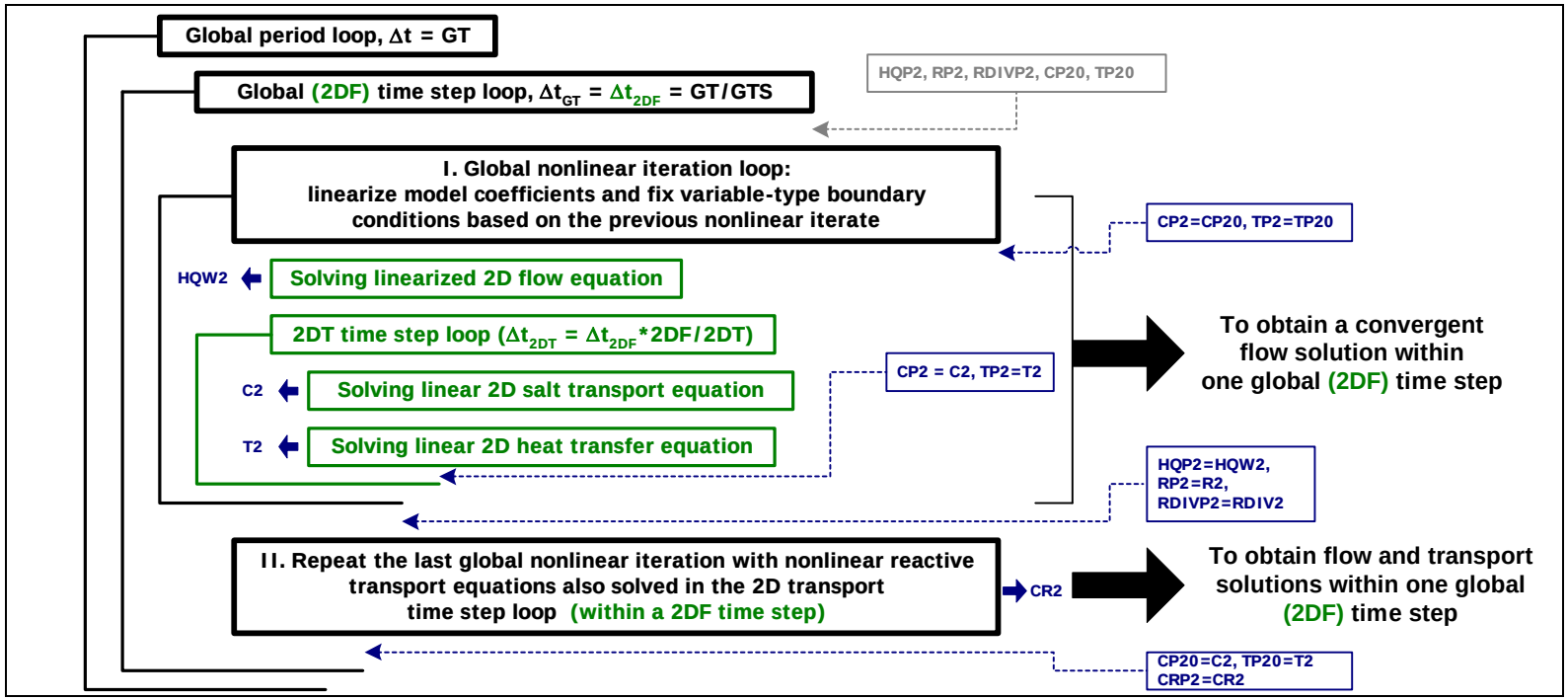

Fig. 3.9-3. Computation Structure of WASH123D for 2D only Simulations

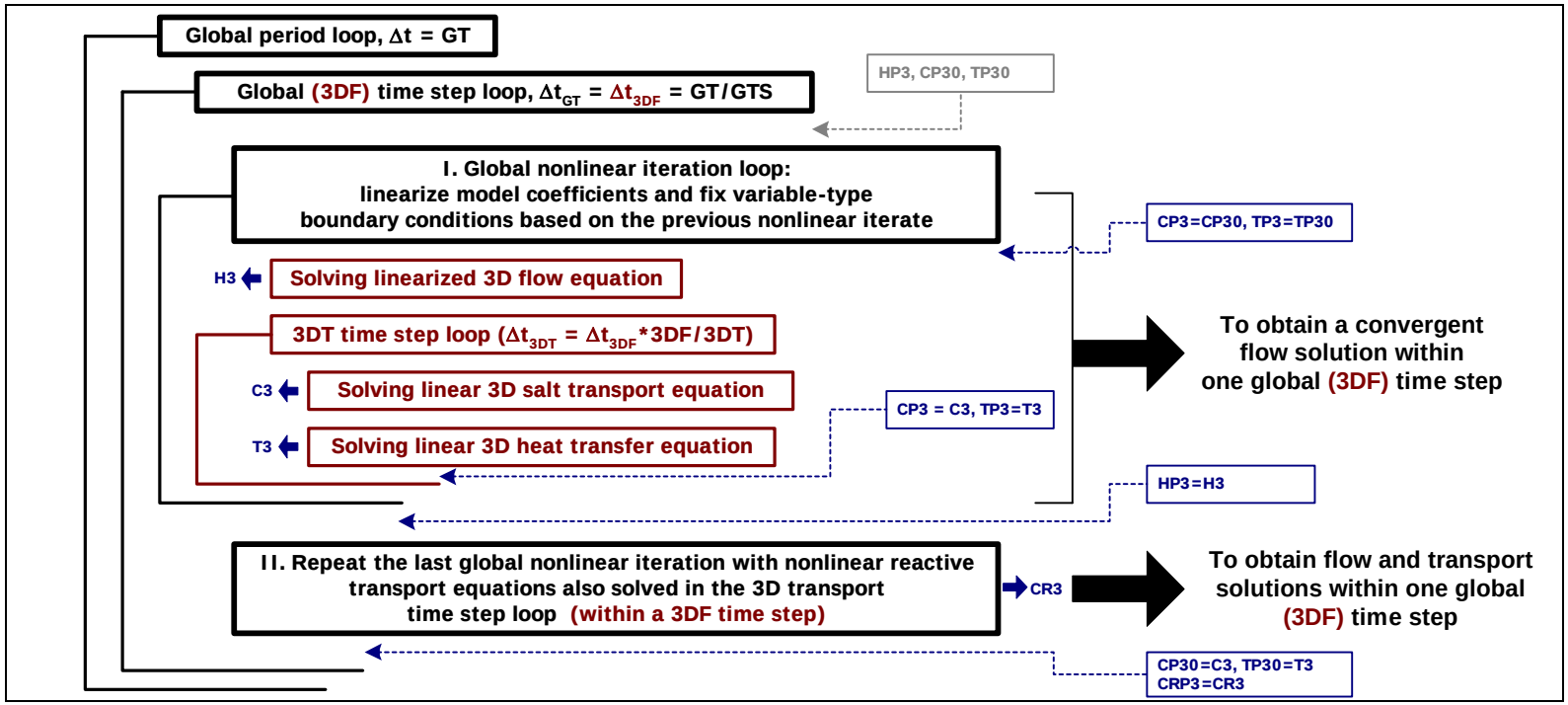

Fig. 3.9-4. Computation Structure of WASH123D for 3D only Simulations

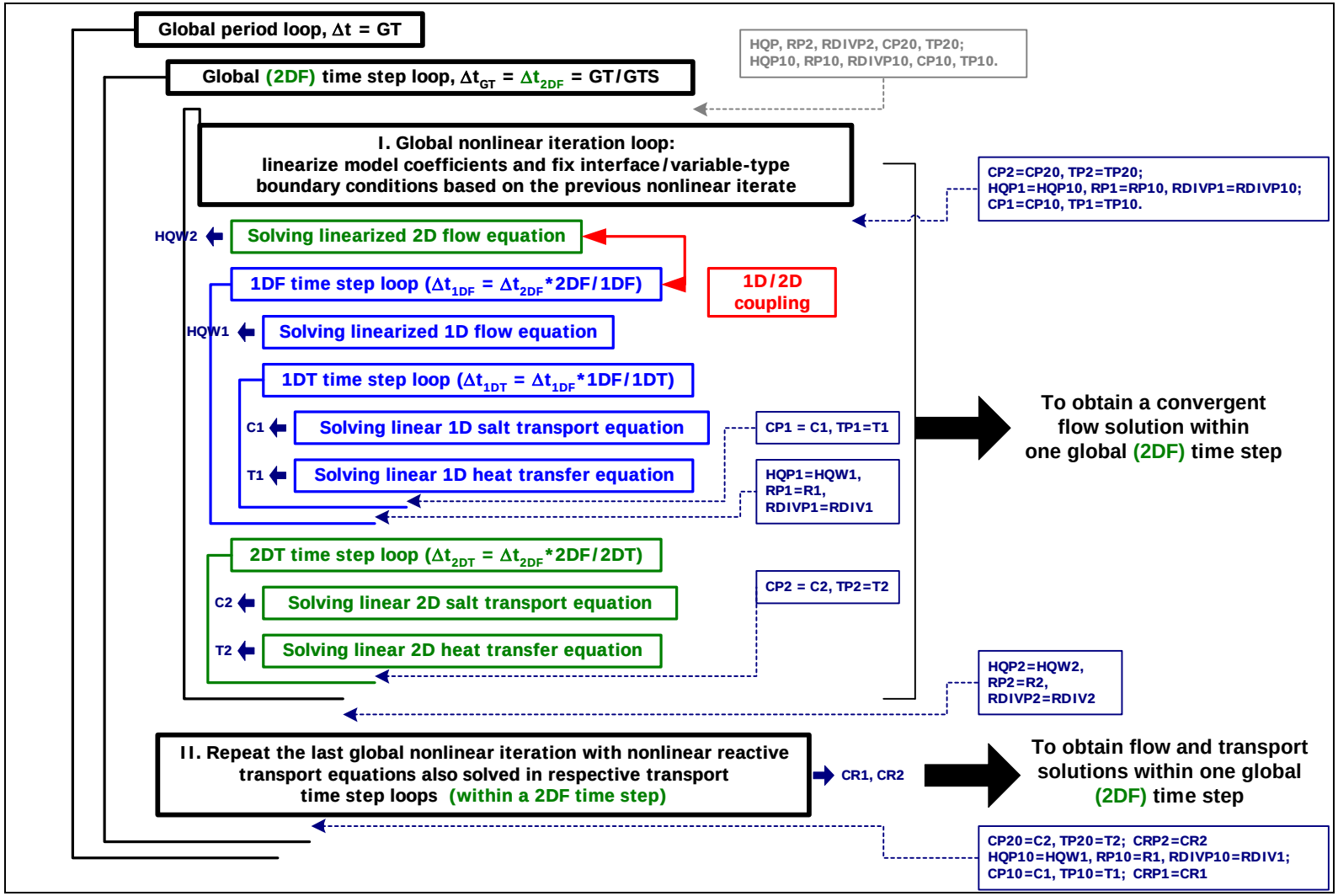

Fig. 3.9-5. Computation Structure of WASH123D for Coupled 1D/2D Simulations

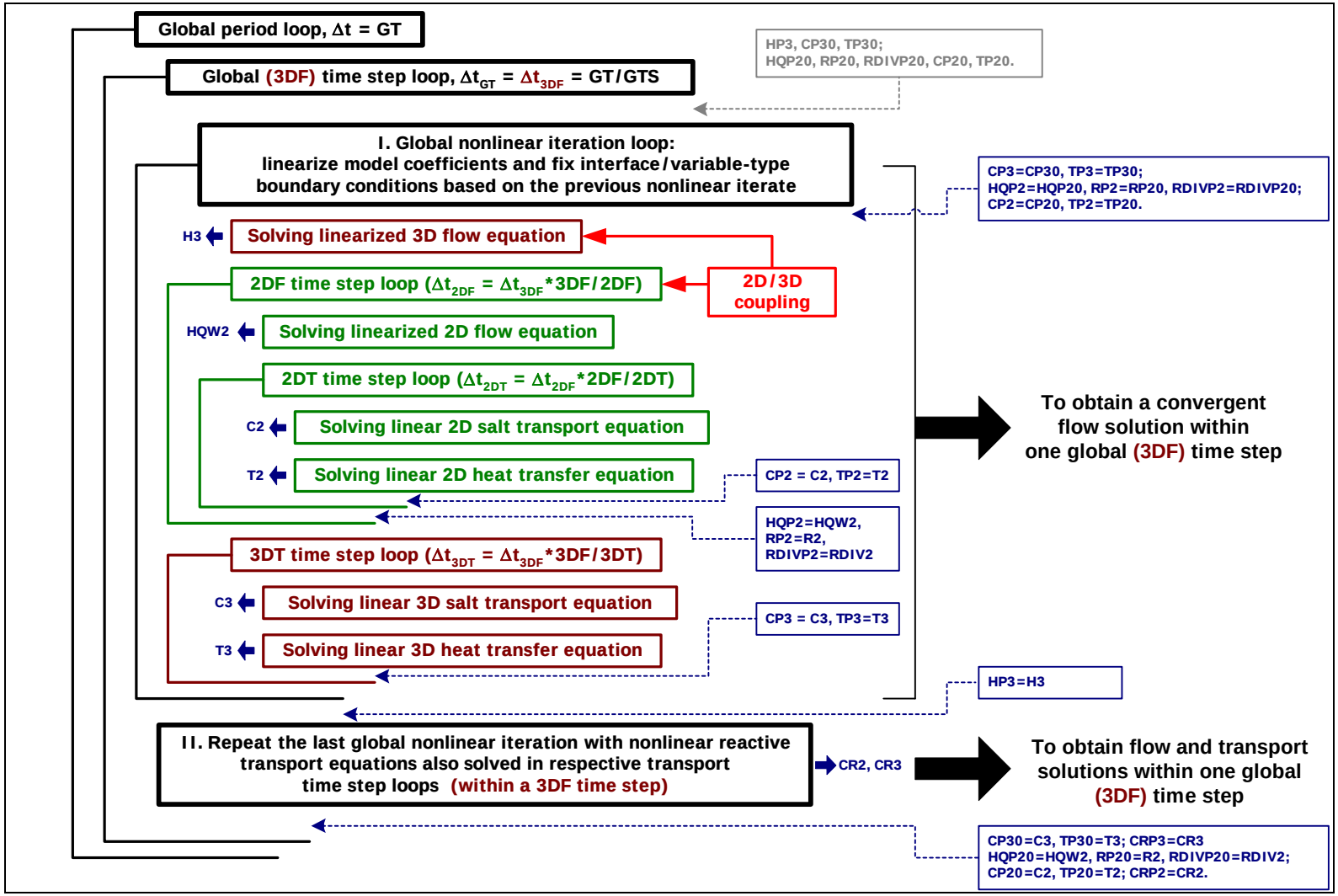

Fig. 3.9-6. Computation Structure of WASH123D for Coupled 2D/3D Simulations

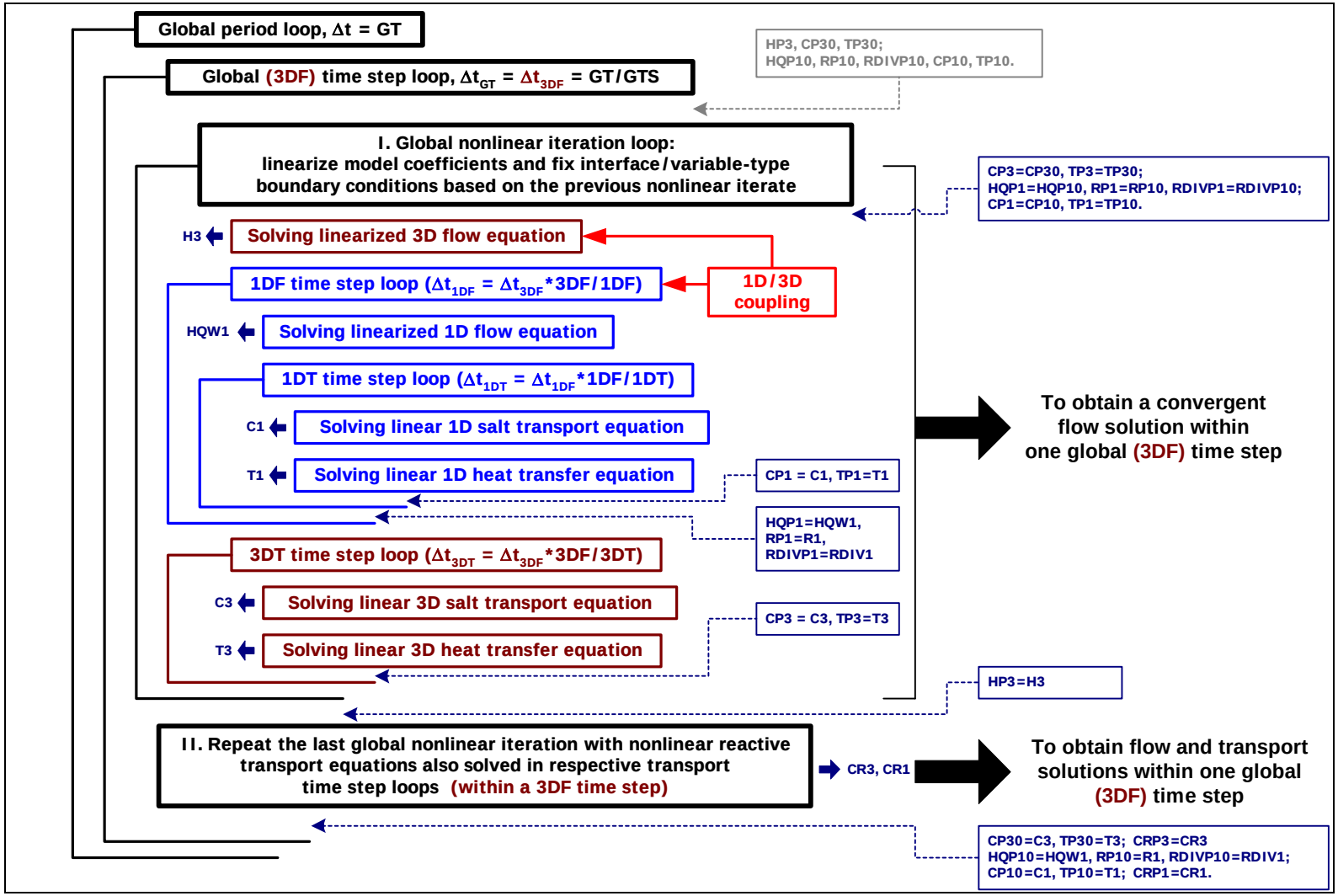

Fig. 3.9-7. Computation Structure of WASH123D for Coupled 3D/1D Simulations

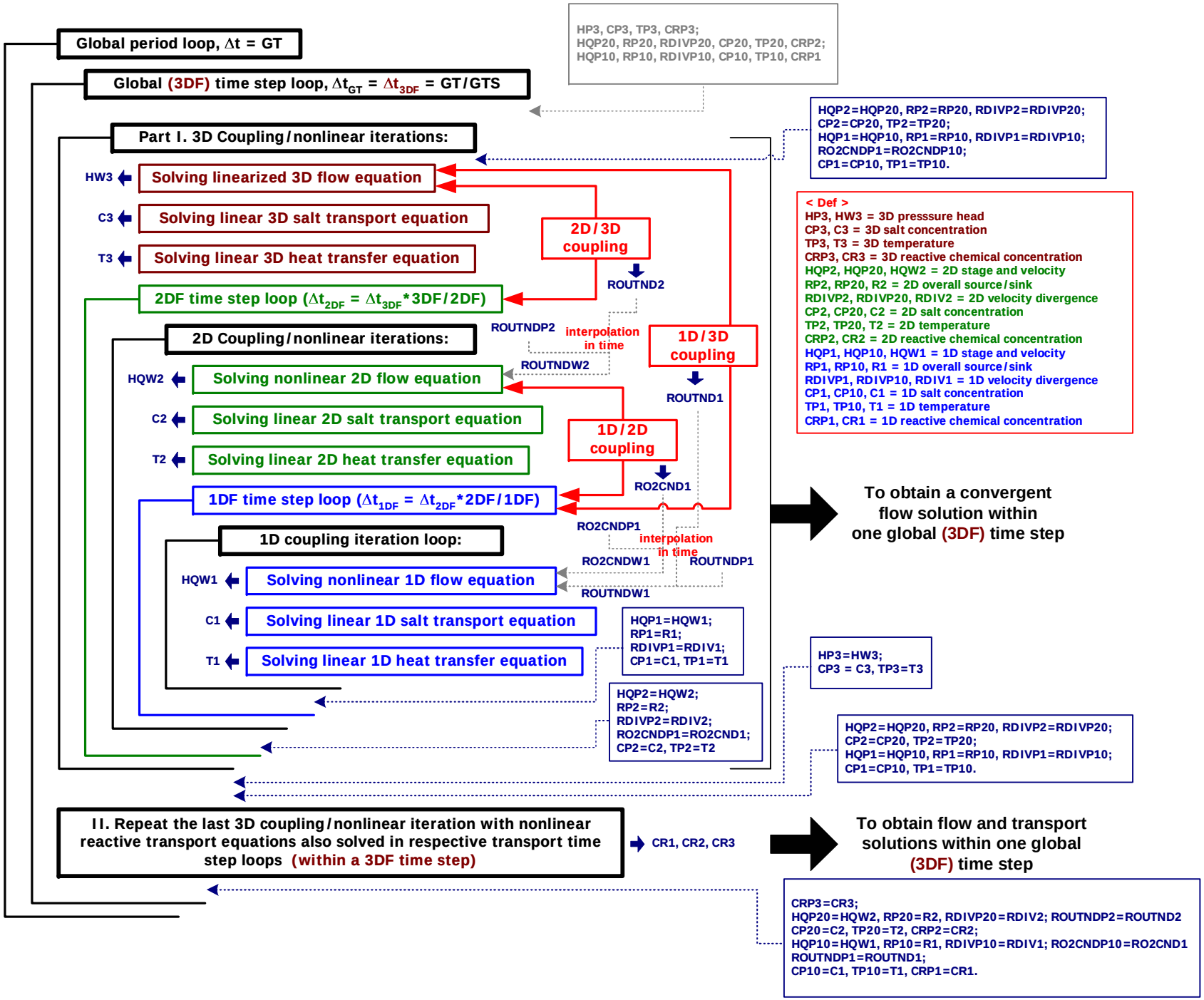

Fig. 3.9-8. Computation Structure of WASH123D for Coupled 1D/2D/3D Simulations

4 HYDRLOGY AND HYHRAULICS FLOW EXAMPLES

In this chapter, we are to present a total of 17 problems to demonstrate the design capability of WASH123D, to show the needs of various approaches to simulate flow river network and overland flow problems, and to illustrate some realistic problems using WASH123D. Section 4.1 present 7 examples to demonstrate the design capability and flexibility of seven flow modules in WASH123D. Section 4.2 includes four simple example problems to show possible differences in simulations using the kinematics-wave, diffusive-wave, and fully dynamic-wave approaches. Section 4.3 include six realistic-real world examples to illustrate the types of flow problems WASH123D can deal with.

4.1 Design Capability of WASH123D

Seven examples are used in this section to demonstrate the design flexibility to simulate hydrology and hydraulics in WASH123D. Example 1 is to simulate hydraulics in one-dimensional flows in river/stream/canal networks. Example 2 is to simulate two-dimensional overland flows in a complex topography. Example 3 is to model three-dimensional variably saturated flows in subsurface media. Example 4 is to simulate coupled one-dimensional river flow and two-dimensional overland flow. Example 5 is to model coupled two-dimensional overland and three-dimensional subsurface flow. Example 6 is to simulate coupled three-dimensional subsurface and one-dimensional river flows. Example 7 is to simulate one-dimensional river, two-dimensional overland, and three-dimensional subsurface flow problems.

4.1.1 One-Dimensional Flows in River/Stream/Canal Networks

This example simulates water flow in a channel network system in order to investigate how the change of upstream headwater would affect the downstream flow at various locations. The system was composed of five channel reaches that were connected via two junctions (Fig. 4.1.1-1). Reaches 1, 2, and 4 were 100 m long, and each was discretized with 11 nodes and 10 elements: Nodes 1 through 11 for Reach 1, 12 through 22 for Reach 2, and 44 through 54 for Reach 4. Reaches 3 and 5 were 200 m long, and each was discretized with 21 nodes and 20 elements: Nodes 23 through 43 for Reach 3, and 55 through 75 for Reach 5. In this case, Nodes 11, 12, and 23 were associated with with Junction 1, while Nodes 43, 54, and 55 with Junction 2, where zero capacity was assumed for both junctions.

Reaches 1 and 3 had a uniform channel width of 10 m, a uniform bottom elevation slope of -0.001 along the downstream direction, and a constant Manning's roughness of 0.03. Reaches 2, 4, and 5 had a narrower channel width of 5 m, same bottom elevation slope at -0.001, and a higher Manning's roughness of 0.035. Initially, the network was dry everywhere. As the simulation starts, a uniform rainfall of 10-4 m/s was applied on all Reaches. At Nodes 1 and 44, both served as upstream boundary nodes, water stage was controlled. Figures 4.1.1-2 and 4.1.1-3 depicted the time-dependent water depth controlled at Nodes 1 (single hump) and 44 (double humps), respectively. A depth-dependent outgoing normal flux, as shown in Figure 4.1.1-4, was applied at the two

downstream boundary nodes (i.e., Nodes 22 and 75). No infiltration was considered. A two-hour simulation was performed with a fixed time step size of 0.002 and 0.001 second used for time periods of 0 through 10 min and 10 min through 2 hrs, respectively. The semi-Lagrangian approach was used to solve the 1-D diffusion flow equation.

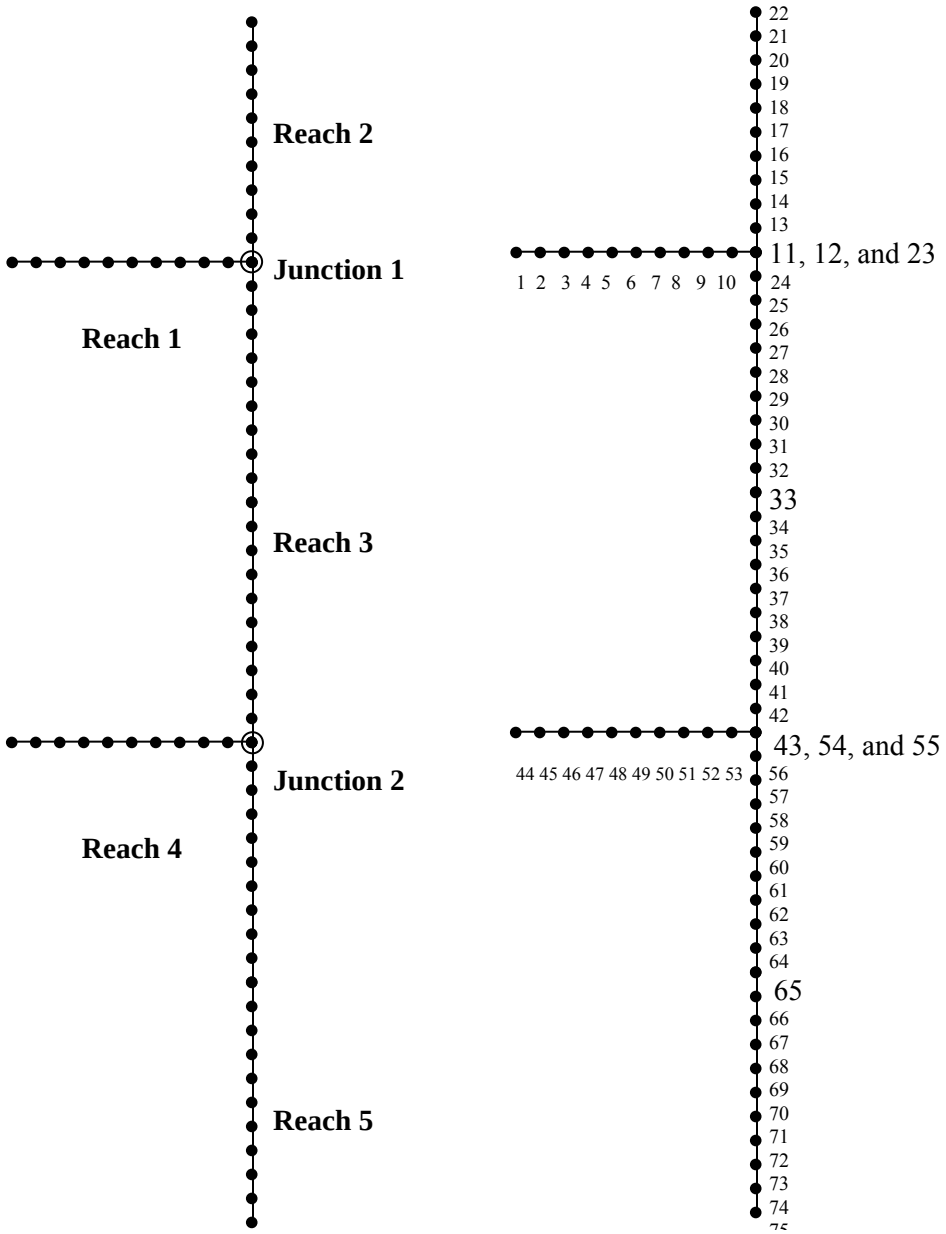

Fig. 4.1.1-1. Channel Network Configuration of Example 4.1.1

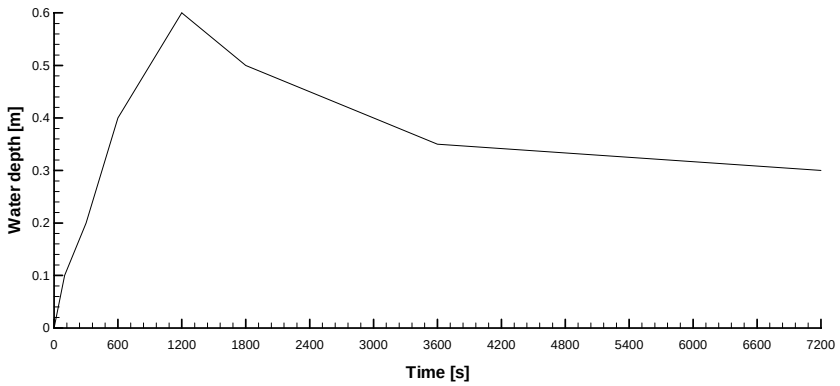

Fig. 4.1.1-2. Water Depth at Node 1 for Example 4.1.1

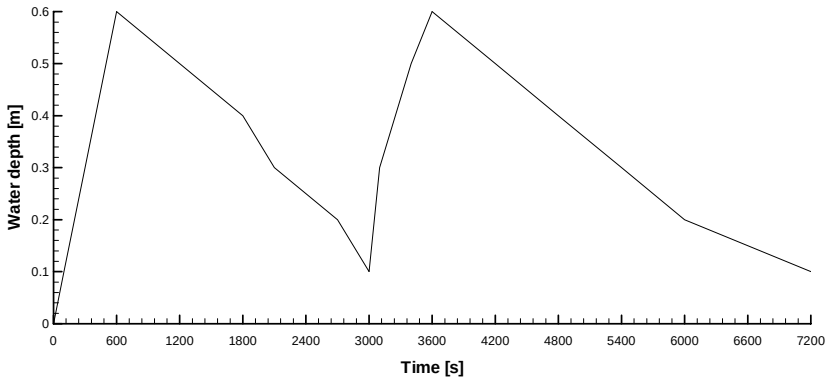

Fig. 4.1.1-3. Water Depth at Node 44 for Example 4.1.1

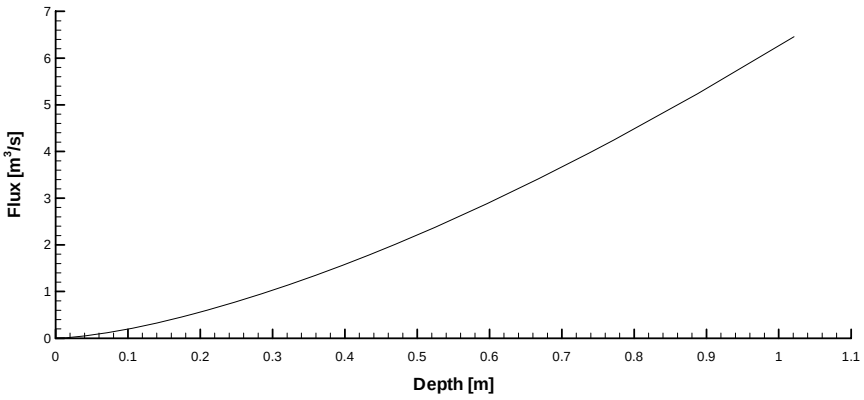

Fig. 4.1.1-4. Water Depth Dependent Outgoing Normal Flux for Example 4.1.1

Figure 4.1.1-5 plots the water stage change at nodes 5, 17, 26, 40, 48, and 70 during the simulation period. It is observed that the change of headwater at Node 44 at time = 3,000 s (i.e., the second hump) not only affected nearby downstream locations (Nodes 48, 40, and 70) but also had influence on those far-away location (Nodes 26, 17, and 5), even some of them were upstream nodes (e.g., Node 5). This result demonstrates how headwater control may impact the flow in the whole channel network system when the bottom elevation slope of the system is small (0.001 in this case). It also indicates that WASH123D can be used to deal with water management issues on a design level. Table 4.1.1-1 presents partial numerical results of water depth at Time = 7,200 s.

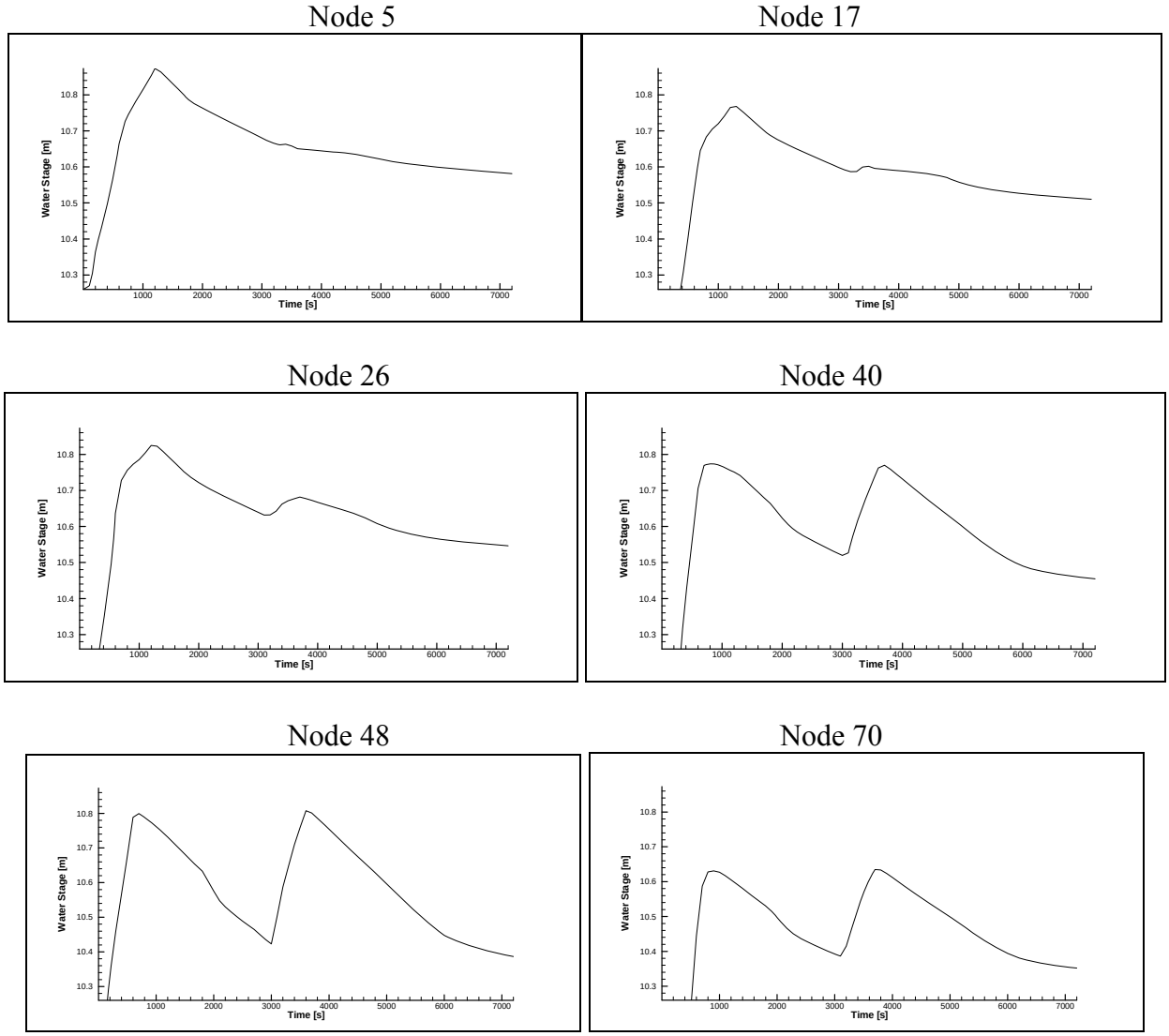

Fig. 4.1.1-5. Water Stages at Various Locations for Example 4.1.1

Table 4.1.1-1 Partial numerical results of water depth distribution at Time = 7,200 s

Node ID	Water Depth [m]
1	0.30000000E+000
2	0.30500313E+000
3	0.31027116E+000
4	0.31560379E+000
5	0.32115150E+000
6	0.32679867E+000
7	0.33262904E+000
8	0.33857747E+000
9	0.34468589E+000
10	0.35092209E+000
11	0.35729881E+000
12	0.35729881E+000
13	0.35044212E+000
14	0.34308253E+000
15	0.33470995E+000
16	0.32577832E+000
17	0.31517319E+000
18	0.30385018E+000
19	0.28953972E+000
20	0.27406891E+000
.	.
.	.
41	0.26021083E+000
42	0.24632798E+000
43	0.22884521E+000
44	0.10000000E+000
45	0.13593196E+000
46	0.14919869E+000
47	0.16705594E+000
48	0.17672218E+000
49	0.18889280E+000
50	0.19708776E+000
.	.
.	.
70	0.18695757E+000
71	0.17995510E+000
72	0.16943911E+000
73	0.15877223E+000
74	0.13962945E+000
75	0.11806921E+000

4.1.2 Two-Dimensional Overland Flows Complex Topography.

TIn this example, 2-D overland flow on a region of non-uniform slope was computed by solving the

2-D depth-average diffusion wave equation with the semi-Lagrangian approach. The computational domain embraces a rectangular area of 800 m wide (in the y direction) and 1,500 m long (in the x direction), which was discretized with 24,022 triangular elements and 12,242 nodes (Fig. 4.1.2-1).

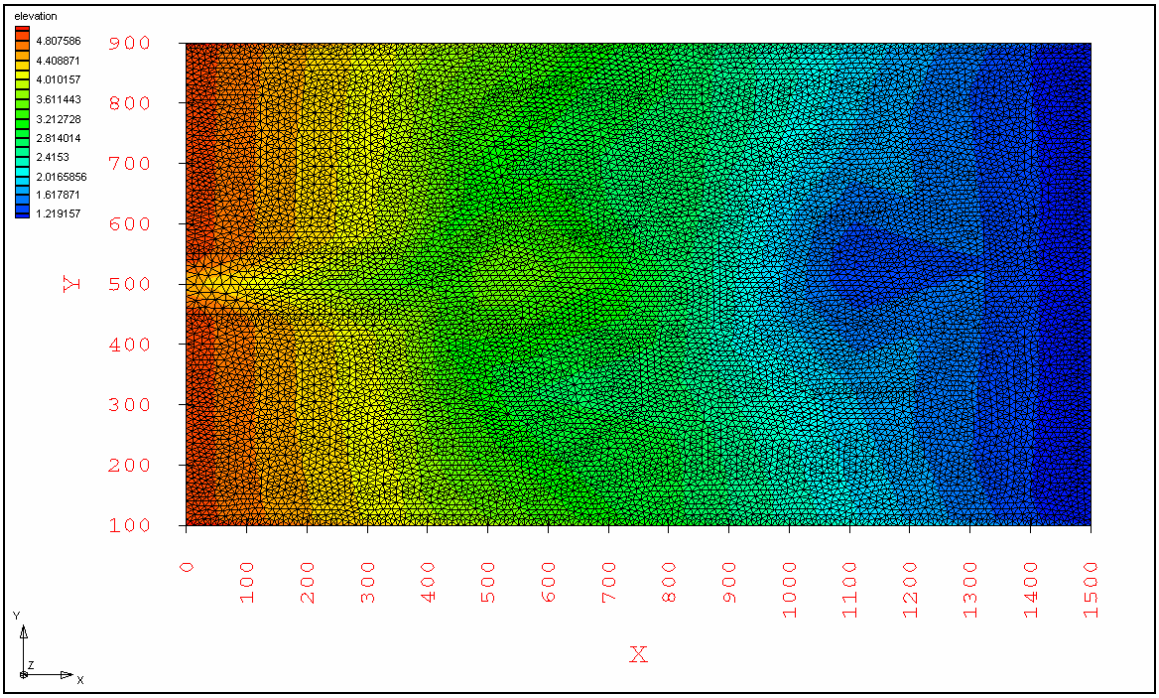

Fig. 4.1.2-1. Domain Discretization of Example 4.1.2

The Manning's roughness was set to 0.025 throughout the entire domain. A time-dependent rainfall rate was applied to the whole region and is given in Figure 4.1.2-2. For a computation, a time-dependent water stage boundary condition (Fig. 4.1.2-3) was applied to the boundary nodes on the left side (i.e., x = 0 m), a water depth-dependent outgoing normal flux boundary condition (Fig. 4.1.2-4) was applied to the downstream boundary element sides (i.e., x = 1,500 m), and a zero water depth boundary condition was applied to the other two sides (i.e., y = 100 m and 900 m).

Water depth was set to 0.001m initially throughout the region. Variable time step sizes of 0.1 s, 0.2 second, and 0.1 second were used from time periods of 0 through 600 seconds, 600 through 2,400 seconds, and 2,400 through 3,600 seconds, respectively. Simulation results of water depth and flow velocity were shown in Figures 4.1.2-5 and 4.1.2-6, respectively. The reasonable result shown in this example demonstrates the capability of WASH123D in computing overland flow with complex terrain. Table 4.1.2-1 also lists partial numerical results of water depth at Time = 1,800 seconds and 3,600 seconds, respectively.

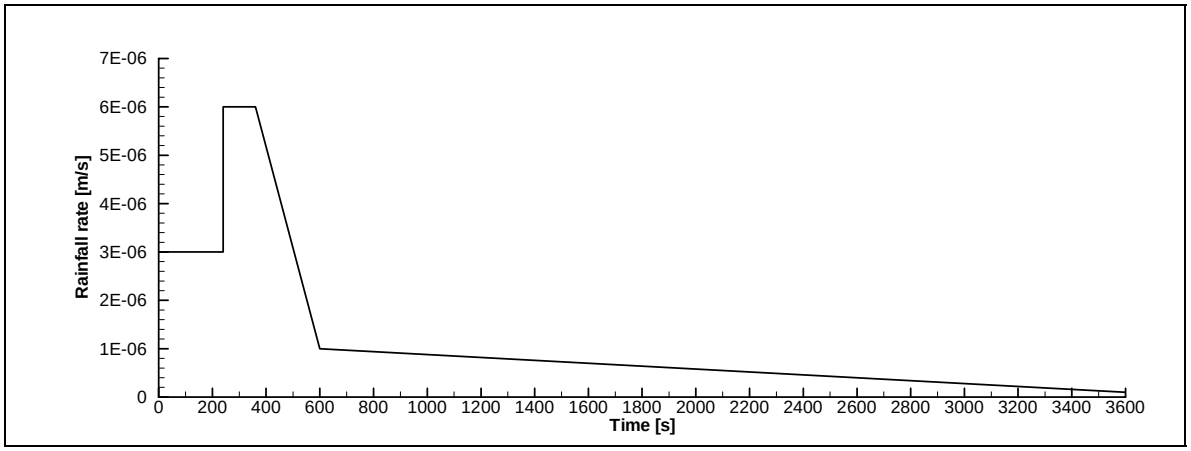

Fig. 4.1.2-2. Time-dependent Rainfall for Example 4.1.2

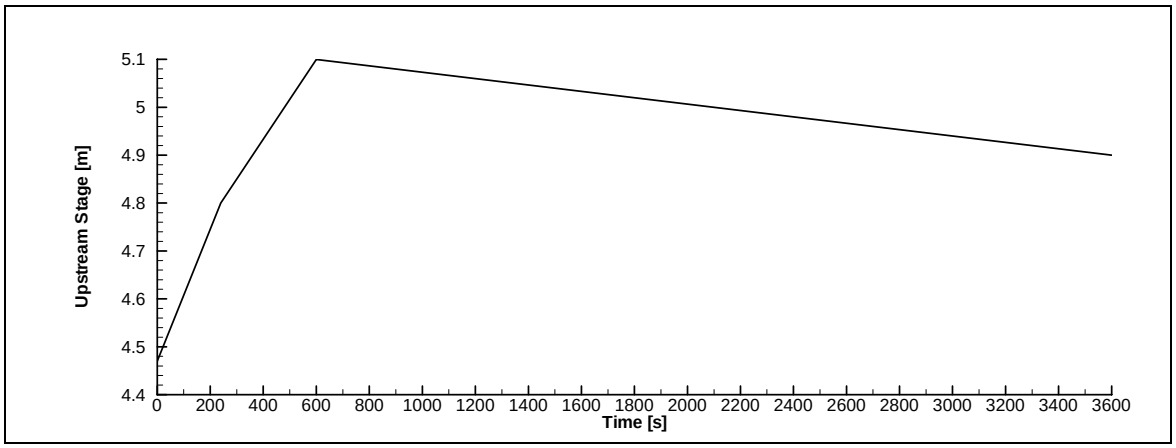

Fig. 4.1.2-3. Time-dependent Upstream Water Stage for Example 4.1.2

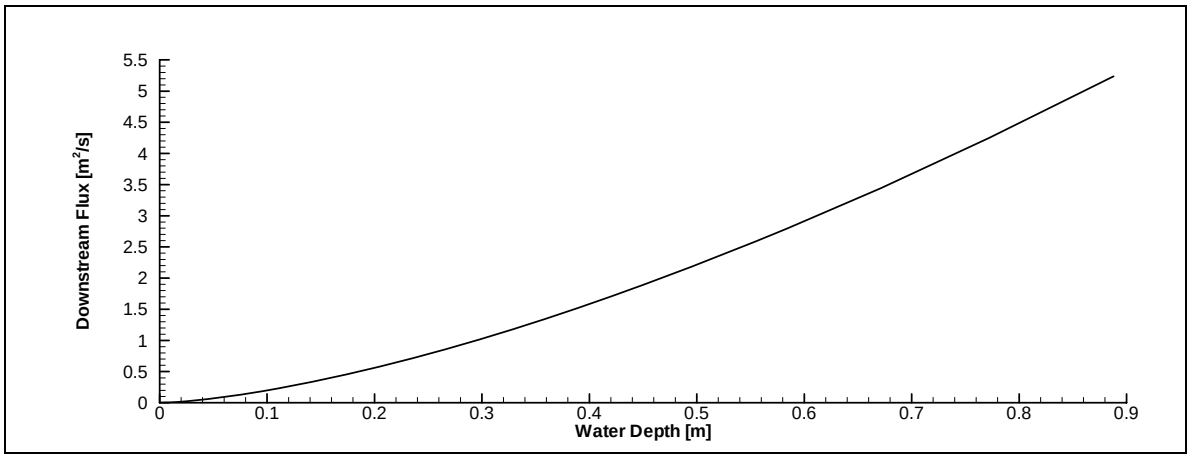

Fig. 4.1.2-4. Water Depth-Dependent Downstream Flux Rate for Example 4.1.2

Time = 600 s

Time = 1,200 s

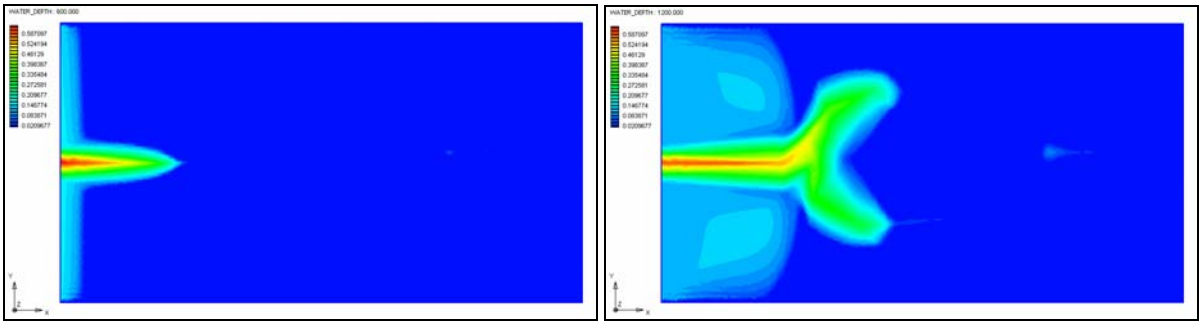

Time = 1,800 s

Time = 2,400 s

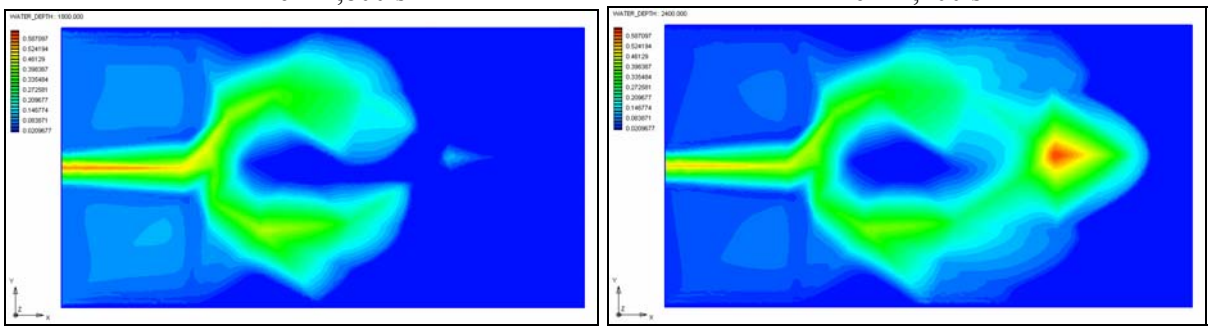

Time = 3,000 s

Time = 3,600 s

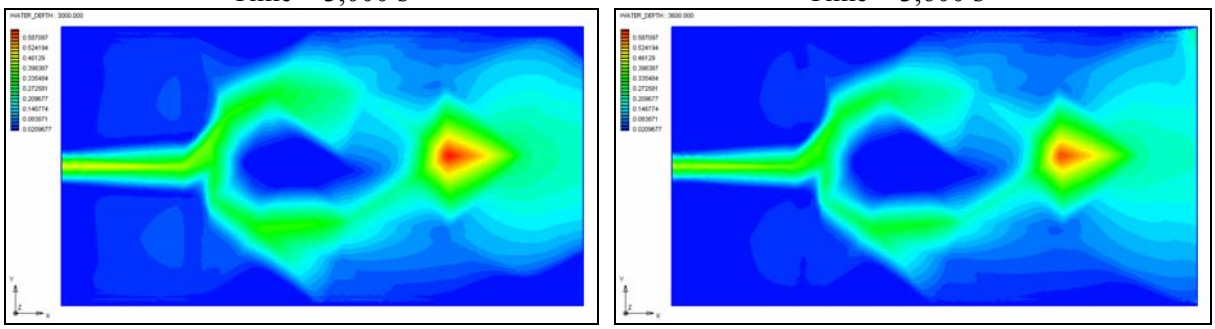

Fig. 4.1.2-5. Water Depth Distribution at Various Times for Example 4.1.2

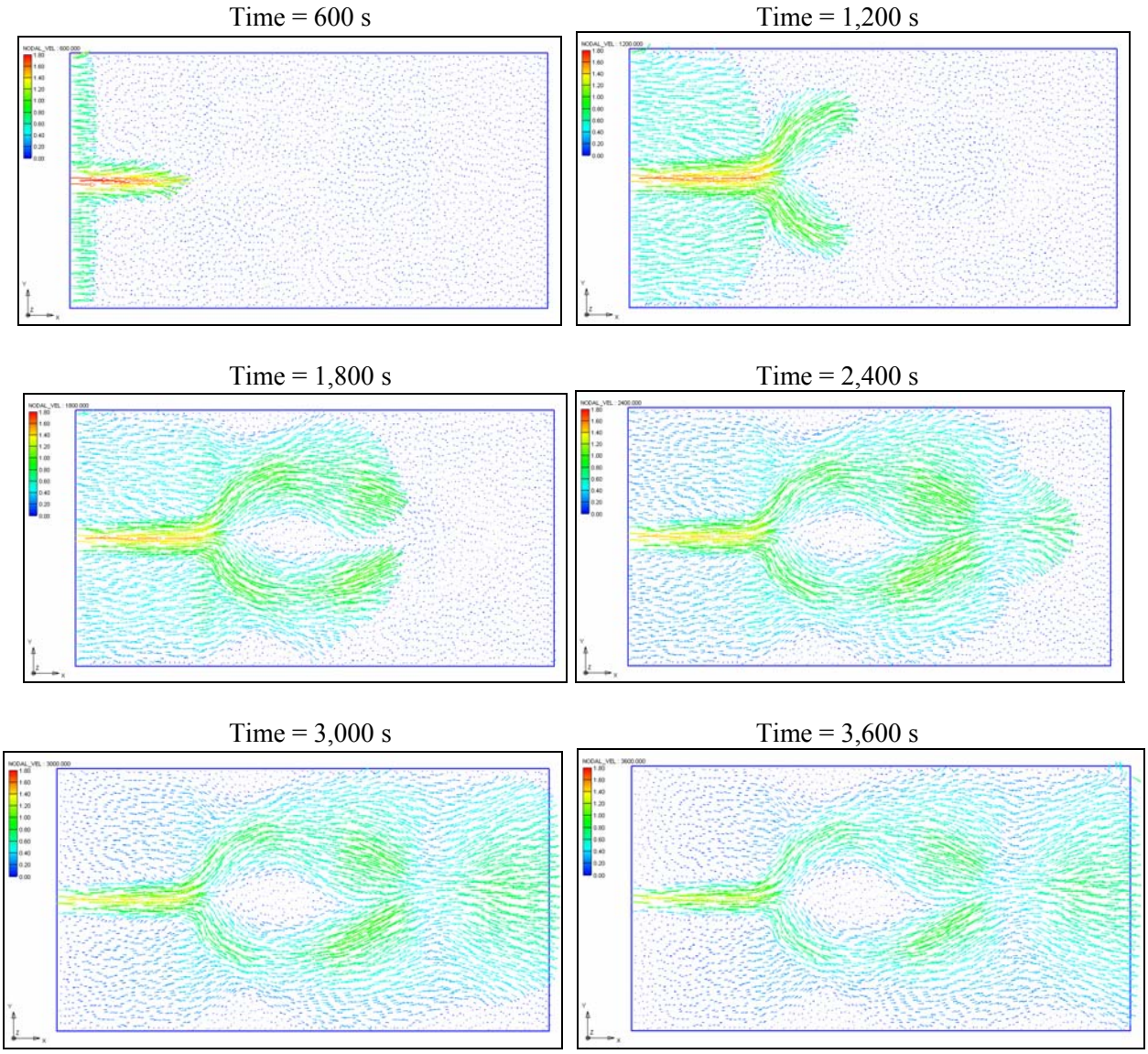

Fig. 4.1.2-6. Flow Velocity Distribution at Various Times for Example 4.1.2

Table 4.1.2-1 Partial numerical results of water depth at Time = 1,800 s and 3,600 s

Time [s]		1,800	3,600
Water Depth [m]	Node 1	0.00000000E+000	0.00000000E+000
	Node 2	0.26090607E-002	0.10483699E-002
	Node 3	0.96222901E-002	0.10416206E-002
	Node 4	0.49737288E-002	0.10289529E-002
	Node 5	0.51648537E-002	0.10290203E-002
	Node 6	0.49025188E-002	0.10295436E-002
	Node 7	0.44320597E-002	0.10298545E-002
	Node 8	0.41718356E-002	0.10299471E-002
	Node 9	0.40598833E-002	0.10300189E-002
	Node 10	0.39577560E-002	0.10299620E-002
	Node 11	0.39489289E-002	0.10299892E-002
	Node 12	0.39715800E-002	0.10299585E-002
	Node 13	0.39699679E-002	0.10299746E-002
	Node 14	0.39984312E-002	0.10301055E-002
	Node 15	0.40032635E-002	0.10300571E-002
	Node 16	0.39609258E-002	0.10298948E-002
	Node 17	0.40035252E-002	0.10300201E-002
	Node 18	0.40222042E-002	0.10300089E-002
	Node 19	0.40323242E-002	0.10299806E-002
	Node 20	0.40586892E-002	0.10299574E-002
	Node 21	0.40794709E-002	0.10300354E-002
	Node 22	0.40799779E-002	0.10300547E-002
	Node 23	0.41178206E-002	0.10300545E-002
	Node 24	0.40928576E-002	0.10299279E-002
	Node 25	0.41204993E-002	0.10299628E-002
	Node 26	0.41837656E-002	0.10300589E-002
	Node 27	0.41255215E-002	0.10298985E-002
	Node 28	0.41787453E-002	0.10300411E-002
	Node 29	0.41646828E-002	0.10299727E-002
	Node 30	0.41751149E-002	0.10299484E-002

4.1.3 Three-Dimensional Variably Saturated Flows in Subsurface Media.

This example was designed to demonstrate a 3-D flow simulation with the 3DFEMWATER model (Yeh, 1987). Since the computational results from our watershed model matches that from 3DFEMWATER perfectly, the 3-D subsurface flow module of WASH123D is verified with this example.

The dimension and discretization of the domain of interest are depicted in Figures 4.1.3-1 and 4.1.3-2, respectively. It was bounded on the left (x = 0 m) and right (x = 1,000 m) by hydraulically connected rivers; on the front (y = -400 m), back (y = 400 m), and bottom (z = 0 m) by impervious aquifuges; and on the top (z = 72 m) by an air-soil interface. A pumping well was placed at (x,y) = (540,0), and the screen of the well was from z = 0 through 30 m. Water table was assumed to be horizontal and was 60 m above the bottom of the aquifer before pumping. The saturated hydraulic conductivity has components K_{xx} = 5 m/d (= 0.208 m/hr), K_{yy} = 0.5 m/d (= 0.0208 m/hr), and K_{zz} = 2 m/d (= 0.083 m/hr). The porosity of the medium was 0.25 and the field capacity was 0.0125. The following three equations were employed to describe the unsaturated hydraulic properties. They were translated into x-y series that can be used in the WASH123D input file to represent pressure head-dependent moisture content, relative conductivity, and water capacity, respectively (i.e., θ vs. h, K_r vs. h, and dθ/dh vs. h).

$$\theta = \theta_r + (\theta_s - \theta_r)\frac{1}{1+\left(\alpha\left|h_a - h\right|\right)^{\beta}} = 0.0125 + \frac{0.2375}{1+0.25h^2} \qquad \textbf{(4.1.3.1)}$$

$$K_r = \left[\frac{\theta - \theta_r}{\theta_s - \theta_r}\right]^2 = \frac{(\theta - 0.0125)^2}{0.2375^2} \qquad \textbf{(4.1.3.2)}$$

$$\frac{d\theta}{dh} = -(\theta_s - \theta_r)\frac{\beta\left(\alpha\left|h_a - h\right|\right)^{\beta-1}\cdot\alpha}{\left[1+\left(\alpha\left|h_a - h\right|\right)^{\beta}\right]^2} = -0.2375\frac{0.5h}{(1+0.25h^2)^2} \qquad \textbf{(4.1.3.3)}$$

where θ_s (= 0.25) is the porosity; θ_r (= 0.0125) is the minimum moisture content that is associated with the minimum pressure head h_a (= 0.0); α (= 0.5) and β (= 2.0) are the parameters used to compute the moisture content and relative hydraulic conductivity.

Because the example problem was symmetric about the pumping well in the y direction, the computational domain was taken as x ∈ [0 m, 1000 m], y ∈ [0 m, 400 m], z ∈ [0 m, 72 m]. The boundary conditions were given as shown in Figure 4.1.3-3: pressure head maintained at 30 m at the pumping well during pumping; pressure head assumed hydrostatic on two vertical planes at (1) x = 0 m and z ∈ [0 m, 60 m] and (2) x = 1000 m and z ∈ [0 m, 60 m]; no flux imposed on all other boundary faces.

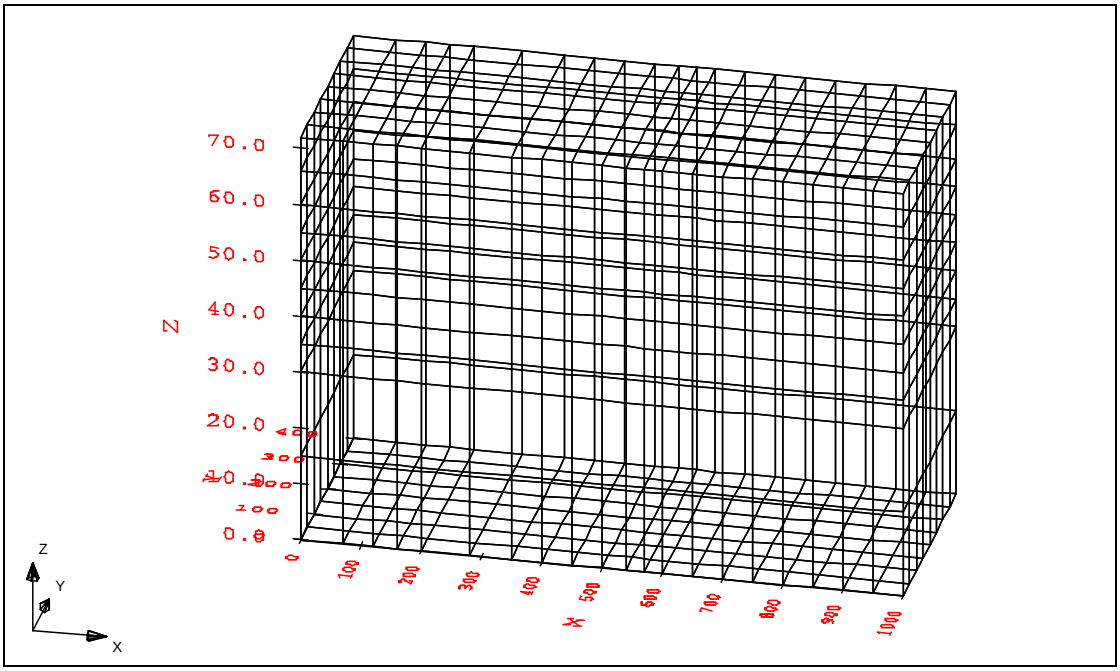

Fig. 4.1.3-1. Domain and Descretization of Example 4.1.3

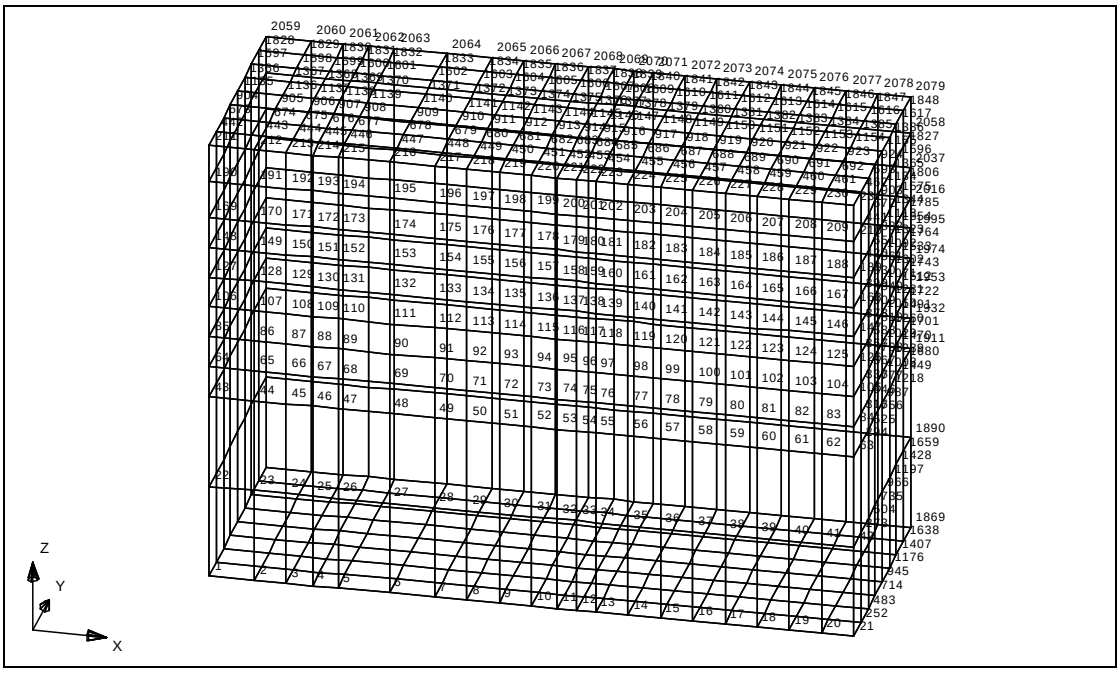

Fig. 4.1.3-2. Node Numbering for Example 4.1.3

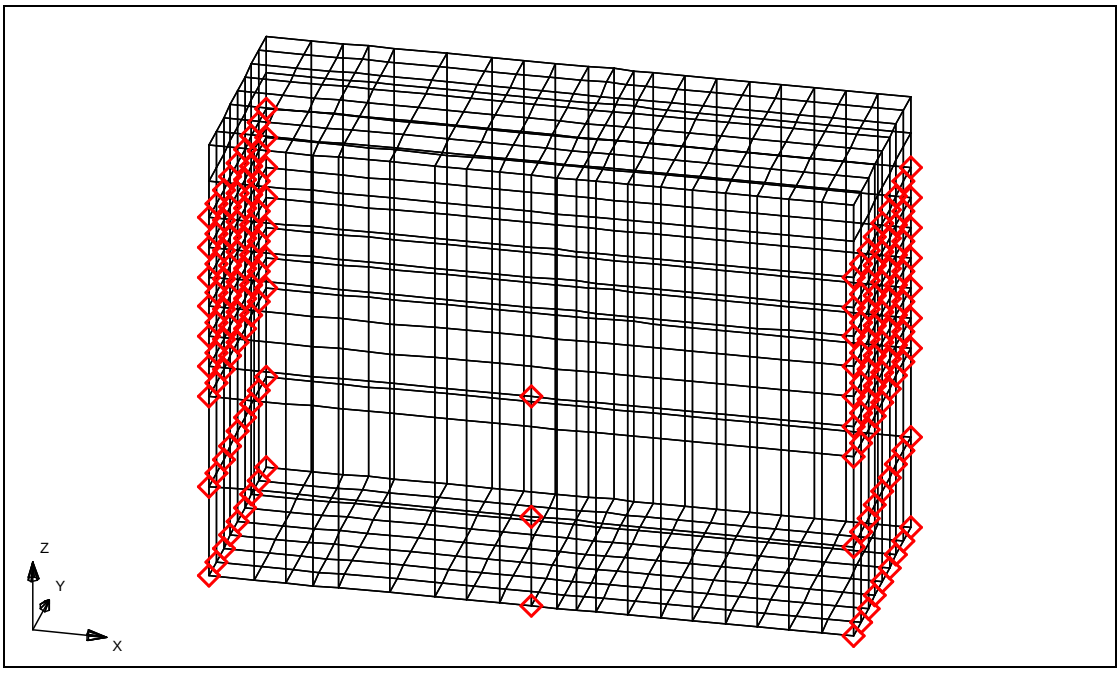

Fig. 4.1.3-3. Dirichlet Boundary Conditions for Example 4.1.3

The steady-state solution was determined with the absolute error tolerance of pressure head of 0.01 m and 0.00001 m for nonlinear iterations and linear matrix solvers, respectively. Simulation results of total head and flow velocity were shown in Figure 4.1.3-4 and Figure 4.1.3-5, respectively. Table 4.1.3-1 shows partial numerical results of pressure head that are corresponding to Figure 4.1.3-4.

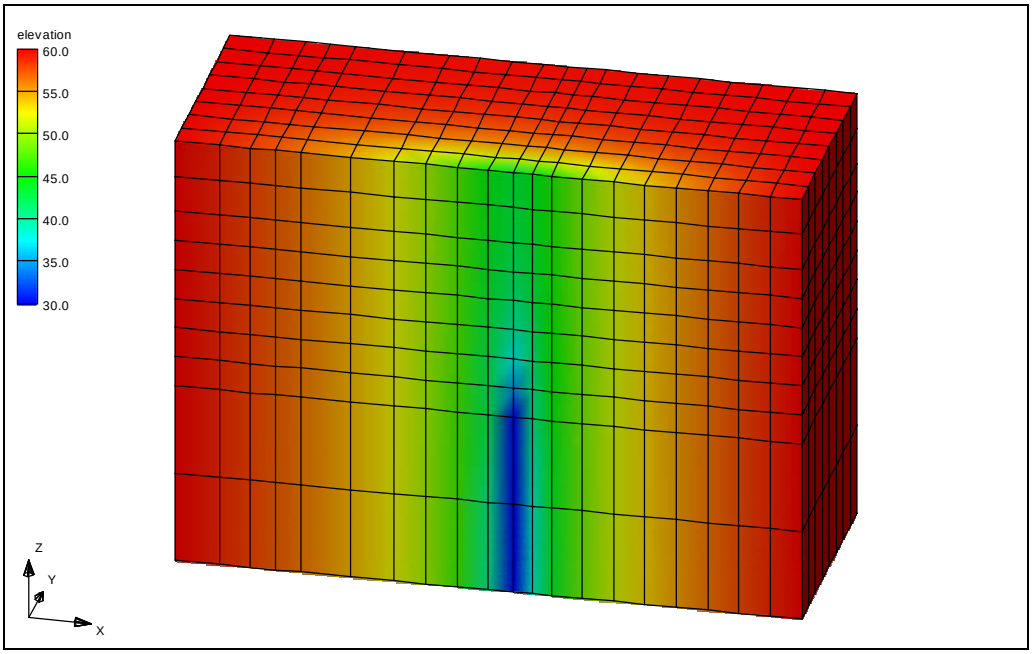

Fig. 4.1.3-4. Total Head Distribution for Example 4.1.3

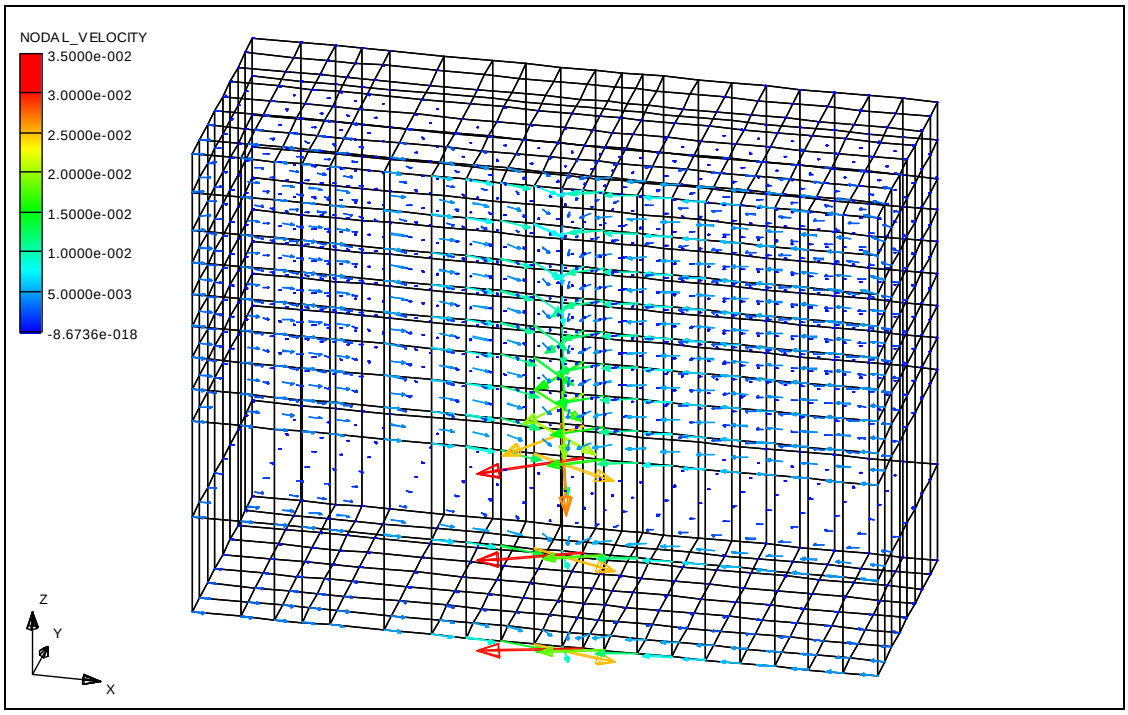

Fig. 4.1.3-5. Flow Velocity Distribution for Example 4.1.3

Table 4.1.3-1 Partial Numerical Results of Pressure Head

Node ID	Pressure Head [m]	Node ID	Pressure Head [m]
1	0.60000000E+002	211	-0.12140085E+002
2	0.58755458E+002	212	-0.13229426E+002
3	0.57839757E+002	213	-0.14165134E+002
4	0.57072146E+002	214	-0.14927611E+002
5	0.56255441E+002	215	-0.15744612E+002
6	0.54376744E+002	216	-0.17622228E+002
7	0.52233408E+002	217	-0.19744420E+002
8	0.50117077E+002	218	-0.21763400E+002
9	0.46862747E+002	219	-0.24469933E+002
10	0.40317625E+002	220	-0.27569262E+002
11	0.30000000E+002	221	-0.28751296E+002
12	0.38291482E+002	222	-0.27948658E+002
13	0.43660431E+002	223	-0.26172644E+002
14	0.48621638E+002	224	-0.23011554E+002
15	0.51443050E+002	225	-0.20489174E+002
16	0.53448674E+002	226	-0.18539230E+002

4.1.4 Coupled One-Dimensional and Two-Dimensional Flows.

This example demonstrates the capability of WASH123D in handling coupled 1-D channel and 2-D overland flow problems. Here we considered a spreader canal that was expected to distribute water to its downstream overland regime. The 2-D overland domain was discretized with 151 elements and 171 nodes, and the 1-D spreader canal was composed of 11 elements and 12 nodes (Fig.4.1.4-1). In WASH123D, all 2-D elements that are connected to 1-D nodes are defined as channel-related elements, and they are not included in 2-D overland computation. Therefore, the 2-D computational domain contained 127 (= 151 - 24) 2-D elements and 159 (= 171 - 12) 2-D nodes. The canal was 2 m wide and its cross-sectional area was proportional to its depth. The canal was as deep as 0.1 m at the entrance (i.e. the first 1-D node, marked in red in Fig. 4.1.4-1) and as shallow as 0.025 m at the turning point near Node 123 (i.e., the 6-th 1-D node).

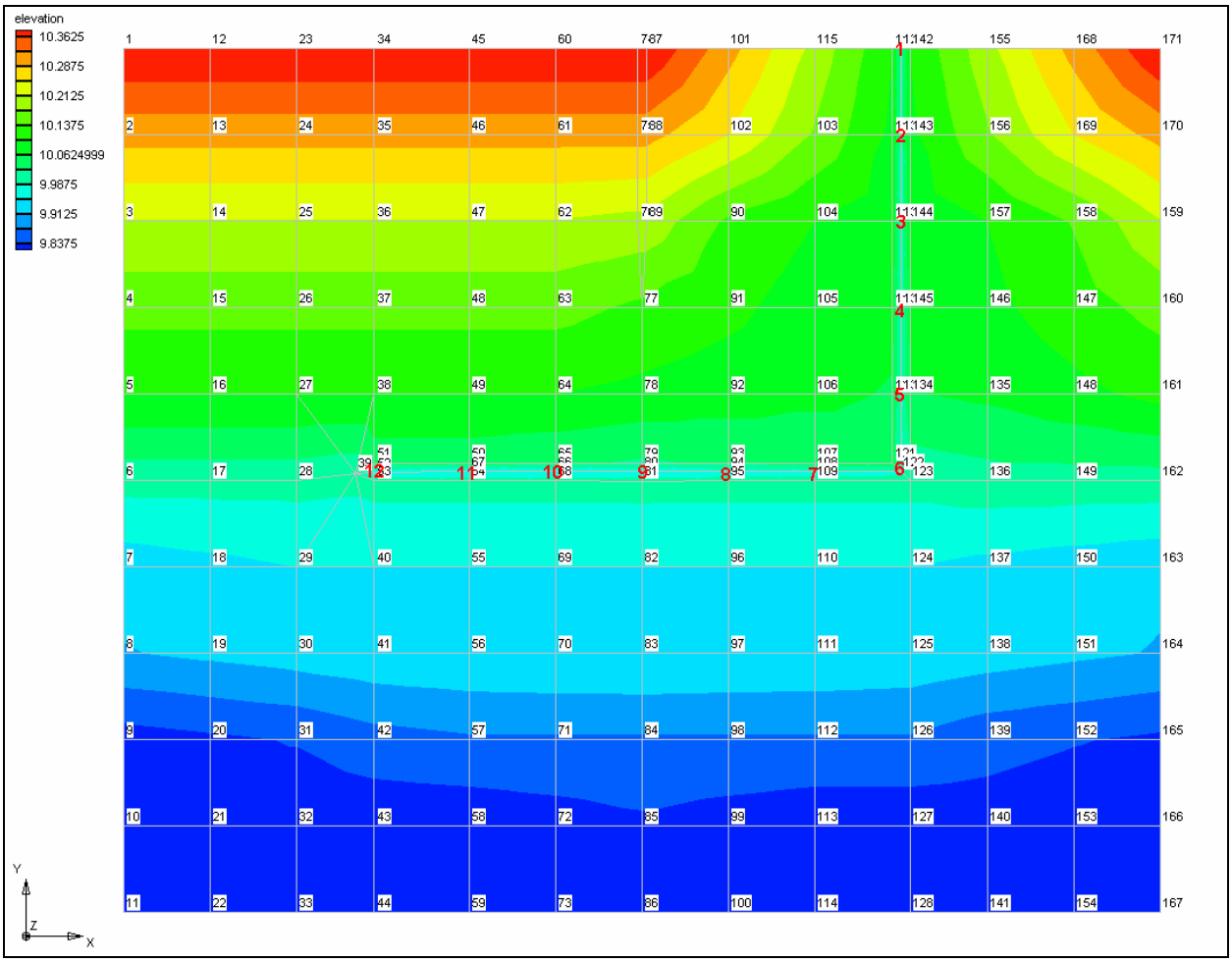

Fig. 4.1.4-1. Discretization and Surface Elevation of Example 4.1.4

The Manning's roughness was set to 0.01 for both 2-D overland and 1-D canal flow. In computing 2-D overland flow, a Dirichlet boundary condition of zero depth was specified for Nodes 1, 12, 23, 34, 45, 60, 74, 87, and 171; a depth-dependent flux boundary condition was given on the bottom

boundary (i.e., the boundary that emprises Nodes 11, 22, 33, …, 167); and a channel-overland interaction boundary condition was specified for the channel-related overland boundary sides, which included a depth-dependent flux when flow was from overland to canal and a canal stage condition when flooding occurred. A time-dependent water depth was controlled at the upstream 1-D node (i.e., the entrance, Fig. 4.1.4-2), and a zero-velocity condition was applied at the downstream dead-end node.

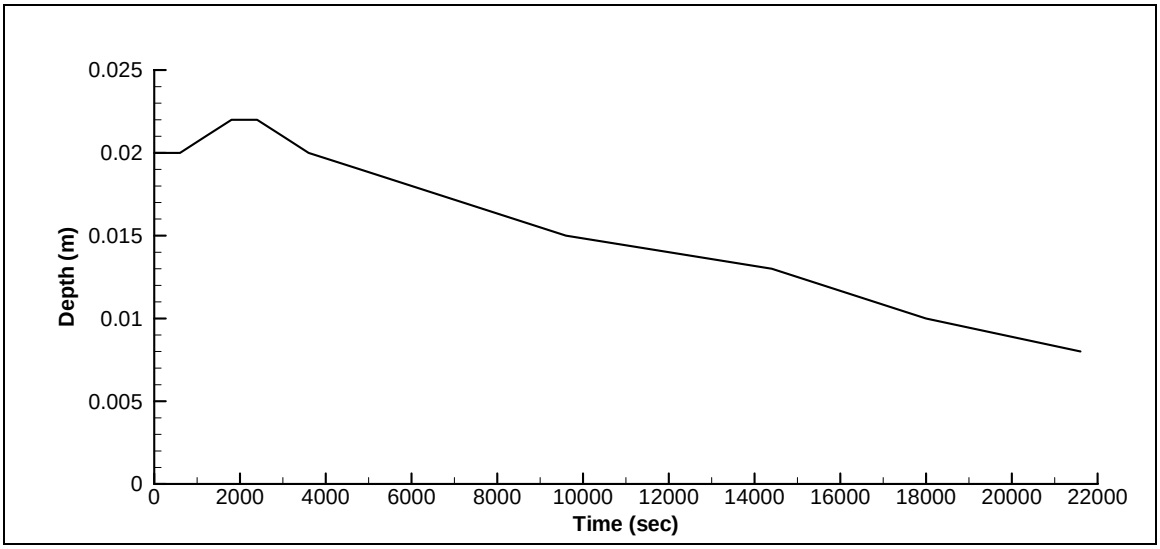

Fig. 4.1.4-2. Time-dependent Water Depth at the Upstream Canal Node for Example 4.1.4

Initially, the overland domain was completely dry, while a constant depth of 0.02 m was given for the 1-D spreader canal so that water flow from the spreader canal to its downstream overland regime can be expected within a short period of time, which allowed us to verify the algorithm of coupling 1-D channel and 2-D overland flow effectively. A constant rainfall rate of 10^{-8} m/s was then applied throughout the entire simulation period of 21,600 seconds (6 hours). The time-step size for computing 2-D overland flow was 4 seconds, and each 2-D time step contained four 1-D time steps.

Figure 4.1.4-3 plots the variation of water depth with time at four 1-D canal nodes: 3, 6, 9, and 12. Also, a dash line that represents the bank height over which canal water will overflow to the downstream overland regime is given as reference for each node (marked with respective colors), except for Node 3 where the associated bank height is 0.09 m (see the first plot in Figure 4.1.4-5 also). Figure 4.1.4-4 provides a zoom-in plot of Figure 4.1.4-3 for the period of time from 0 through 750 s, where the three plus symbols indicate the moments that water started to flow from canal to overland at Nodes 6, 9, and 12. It is consistent with what is plotted in Figure 4.1.4-5, where the computed water depth and flow direction distribution of overland flow is given. The first plot in Figure 4.1.4-44 also provides the information of bank height of each channel-related overland boundary nodes.

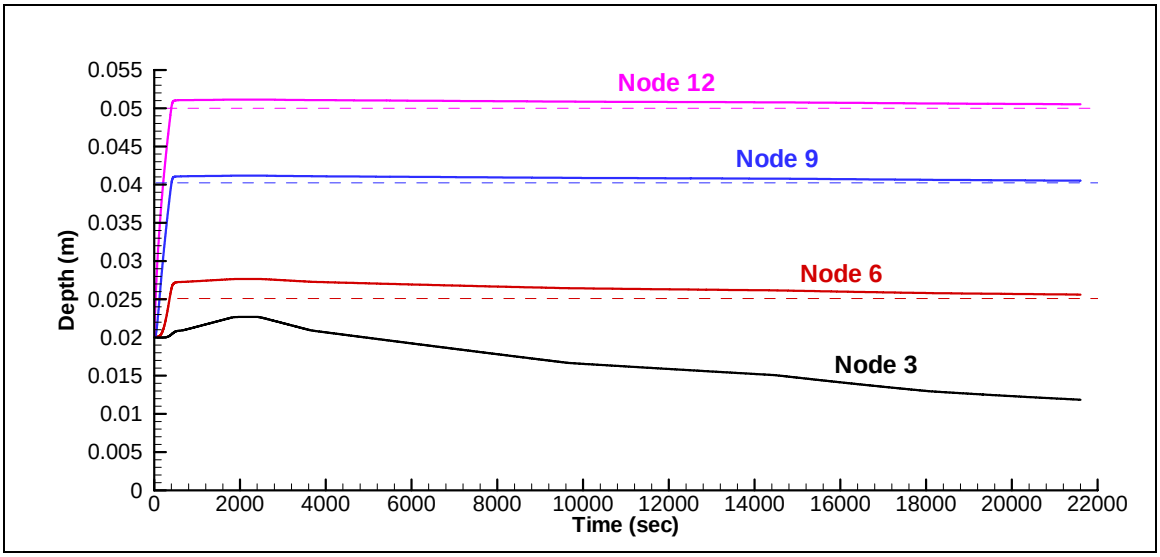

Fig. 4.1.4-3. Computed Water Depth at Various 1-D Canal Locations for Example 4.1.4 (Time = 0 through 21,600 s)

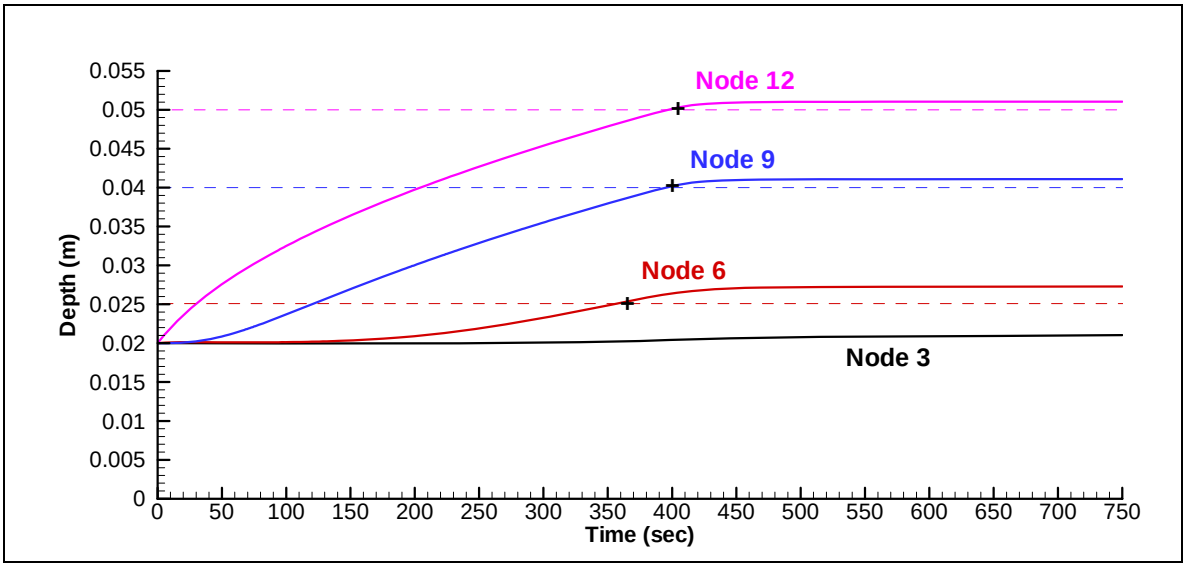

Fig. 4.1.4-4. Computed Water Depth at Various 1-D Canal Locations for Example 4.1.4 (Time = 0 through 750 s).

Time = 400 s

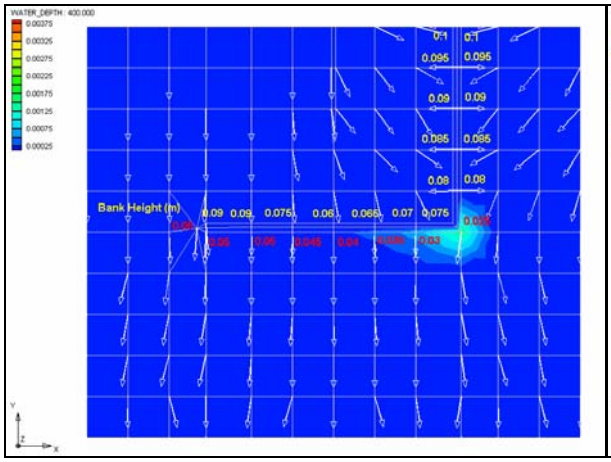

Time = 600 s

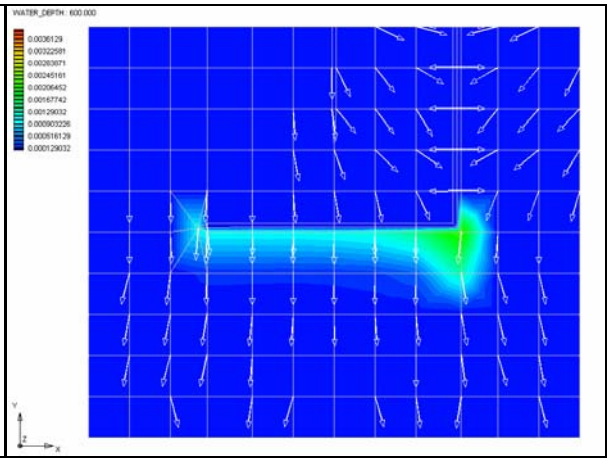

Time = 1,200 s

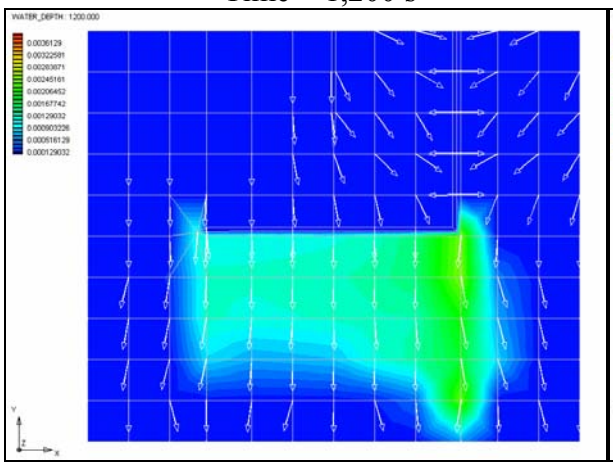

Time = 2,400 s

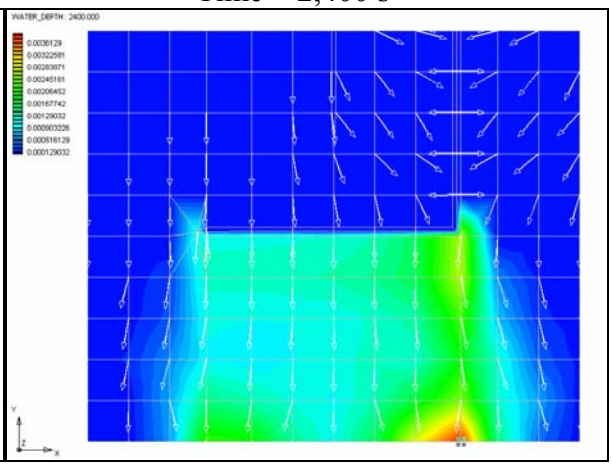

Time = 3,600 s

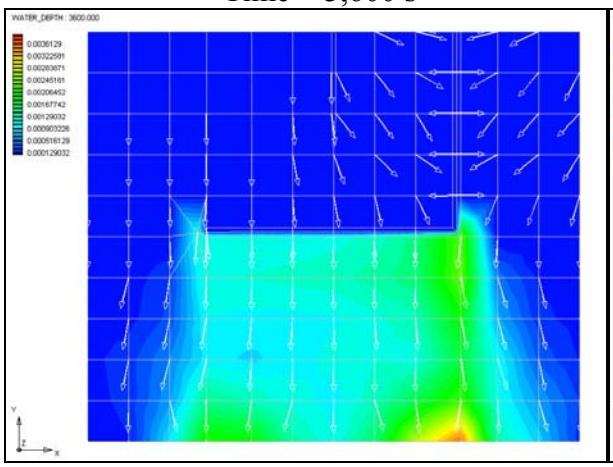

Time = 7,200 s

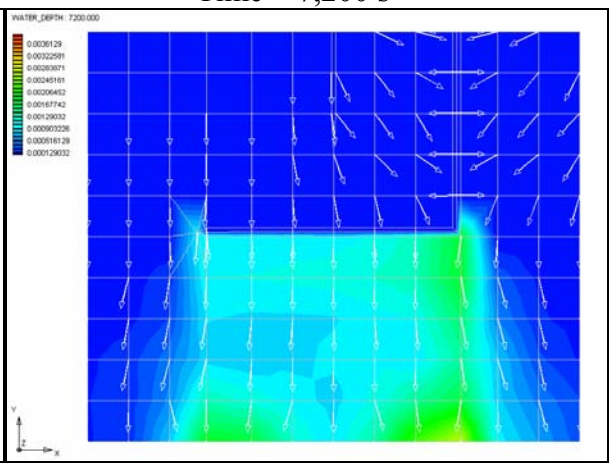

Time = 10,800 s

Time = 16,200 s

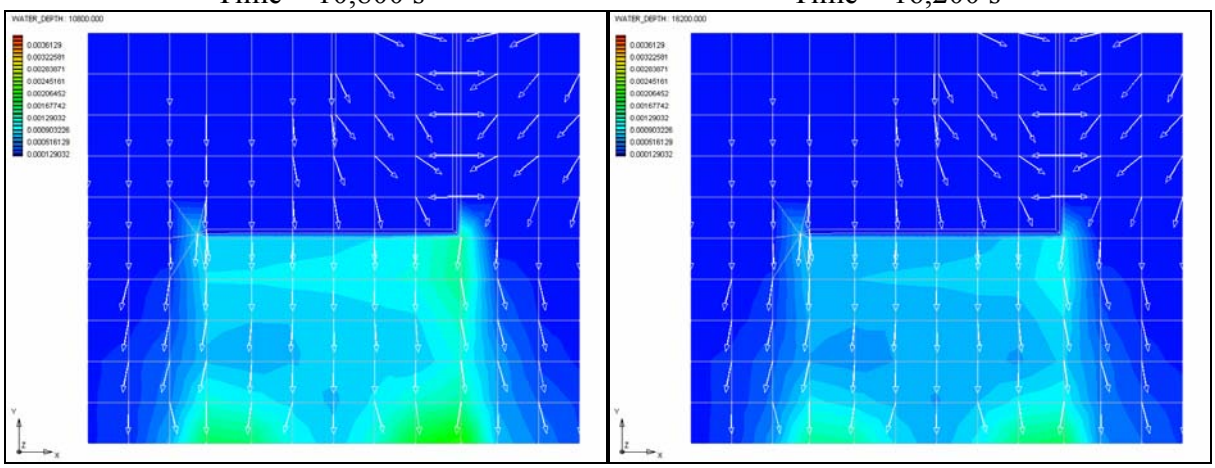

Time = 21,600 s

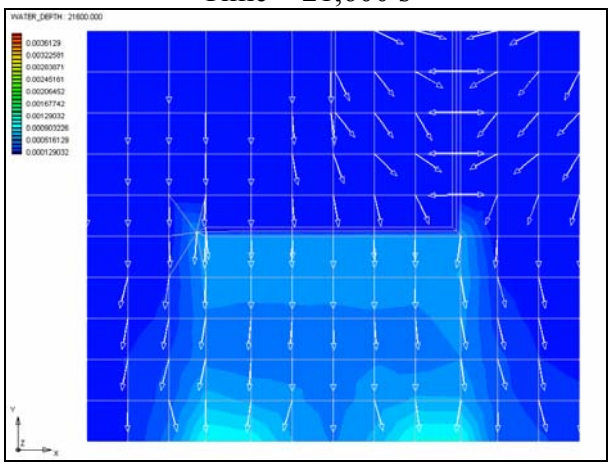

Fig. 4.1.4-5. Distribution of Water Depth and Flow Direction in the Land Surface at Various Times for Example 4.1.4

4.1.5 Coupled Two-Dimensional and Three-Dimensional Flows.

This example is designed to test coupled overland/subsurface flow within a hypothetic domain, where ground surface has a gradually changing slope in the x-direction (Fig. 4.1.5-1). Figure 4.5-1 depicts the simulation domain, dimension, and discretization of the example, where the dimension in the z direction is magnified five times for better visualization.

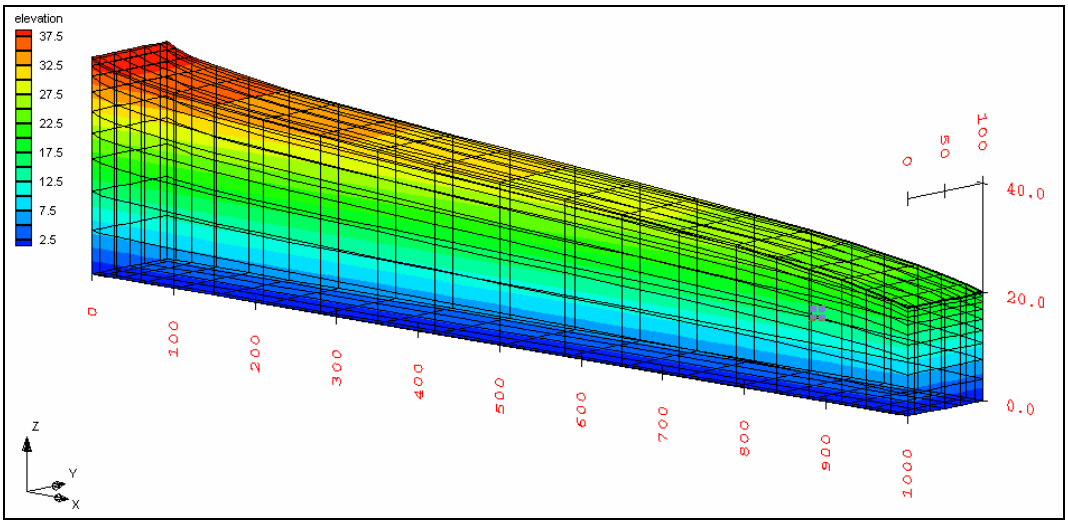

Fig. 4.1.5-1. Domain, Dimension, and Discretization of Example 4.1.5-1

The subsurface porous medium is uniformly distributed throughout the entire domain and the corresponding saturated hydraulic conductivity has components $K_{xx} = 2\text{x}10^{-4}$ m/s, $K_{yy} = 10^{-5}$ m/s, and $K_{zz} = 10^{-5}$ m/s. The following soil characteristic equations are used to describe the hydraulic properties in unsaturated zones.

$$\begin{aligned} &\theta = 0.3 && if\ \ 0 < h \\ &\theta = 0.15 + 0.0015(h+100) && if\ \ -100 < h < 0 \\ &\theta = 0.15 && if\ \ h < -100 \end{aligned} \qquad \textbf{(4.1.5.1)}$$

$$\begin{aligned} &K_r = 1 && if\ \ 0 < h \\ &K_r = \frac{h+100}{100} && if\ \ -100 < h < 0 \\ &K_r = 0 && if\ \ h < -100 \end{aligned} \qquad \textbf{(4.1.5.2)}$$

$$\frac{d\theta}{dh} = 0.0 \quad if\ \ 0 < h \quad \text{or} \quad if\ \ h < -100; \quad \frac{d\theta}{dh} = 0.0015 \quad if\ \ -100 < h < 0 \qquad \textbf{(4.1.5.3)}$$

In this example, the initial flow condition was computed by solving the steady-state flow governing equation based on the given boundary conditions: an impermeable boundary condition applied to the front (y = 0 m), back (y = 100 m), and bottom (z = 0 m) boundaries; a total head of 26 m specified

on the lower part of the left boundary (x = 0 m and z ≤ 26 m); a total head of 13 m specified on the lower part of the right boundary (x = 1000 m and z ≤ 13 m); a variable boundary condition of a zero ponding depth and a zero rainfall rate used for the top boundary (i.e., the ground surface, Figure 4.1.5-2).

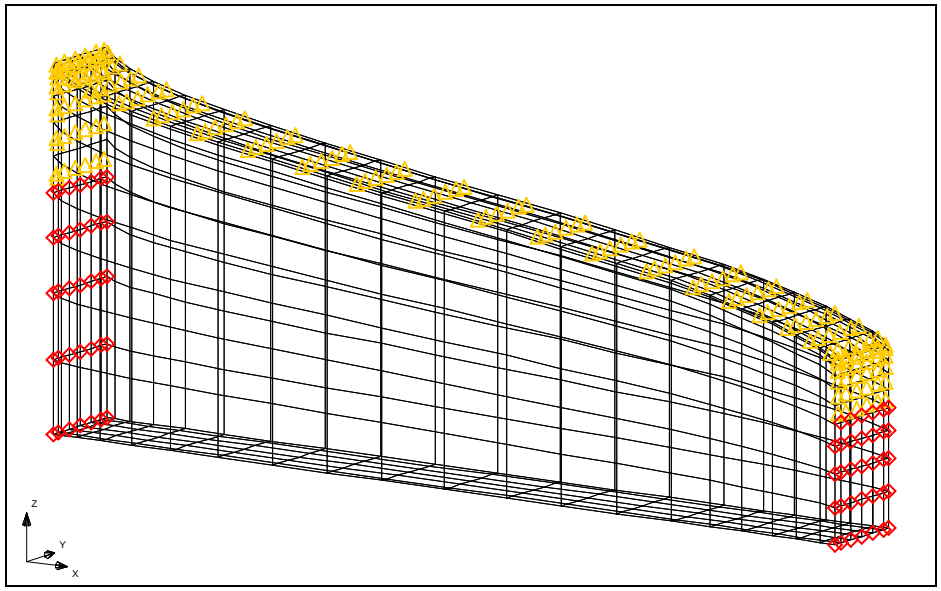

Fig. 4.1.5-2. The Setup of Boundary Conditions for Example 4.1.5
(Dirichlet boundary nodes are marked in red and variable-boundary sides are marked in yellow)

As the six-hour transient simulation began, we had a rainfall of 2×10^{-5} m/s during the first twenty minutes, followed by a no-rain period of one hour, a rain of 10^{-5} m/s for 1 hour, and 1.5×10^{-5} m/s afterwards till the end of the simulation (time = 6 hours). The overland water depth was set to zero on the highest location (i.e., at x = 0 m) to mimic a water divide, while a depth-dependent flux was given as the boundary condition to characterize water flow at the lowest location (i.e., at x = 1,000 m). The rest of the overland boundary (i.e., at y = 0 m and y = 100 m) was assumed streamline boundary and no-through flux boundary condition was applied. During the transient simulation, the computed overland water depth was used as the ponding depth for implementing the variable boundary condition on the top boundary in computing 3-D subsurface flow. The remaining boundary conditions for computed 3-D subsurface flow were set identical to those mentioned above for the initial steady-state simulation. The Manning's roughness was 0.02. The diffusion wave model was used to compute overland flow. An absolute error of 10^{-4} m was used to determine convergence for 2-D overland flow, and absolute errors of 10^{-3} m and 10^{-6} m were employed to settle nonlinear convergent solutions and linearized convergent solutions, respectively, in computing 3-D subsurface flow. The time step sizes for 3-D and 2-D computation were 10 seconds and 2 seconds, respectively.

Simulation results of subsurface pressure head/flow velocity and overland water depth are plotted in Figures 4.1.5-3 and 4.1.5-4, respectively. In Figure 4.1.5-3, the unsaturated zone is highlighted with white color. Although there was no water observed on ground surface from Time = 0 through 7,200 seconds due to infiltration, the time-dependent rainfall has changed the elevation of water table during this period of time. The constant rainfall rate after Time = 4,800 seconds not only raised

water table but also generated surface runoff after the soil could no longer take all the rainfall, and we observed water depth on ground surface at both Time = 10,800 seconds and 21,600 second. Figures 4.1.5-3 and 4.1.5-4 show consistent results for this coupled 2-D/3-D example. Table 1 gives the numerical results of water depth along the x direction that are corresponding to Figure 4.1.5-4.

Time = 0 s

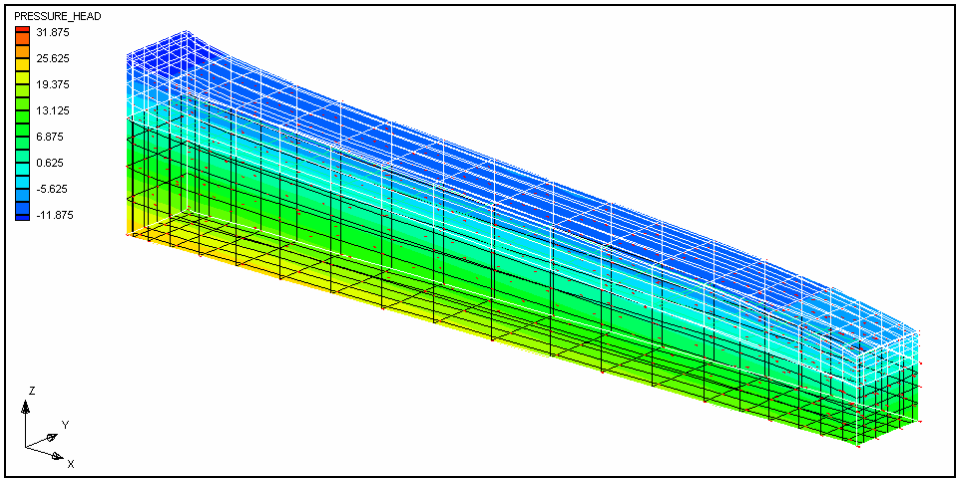

Time = 1,200 s

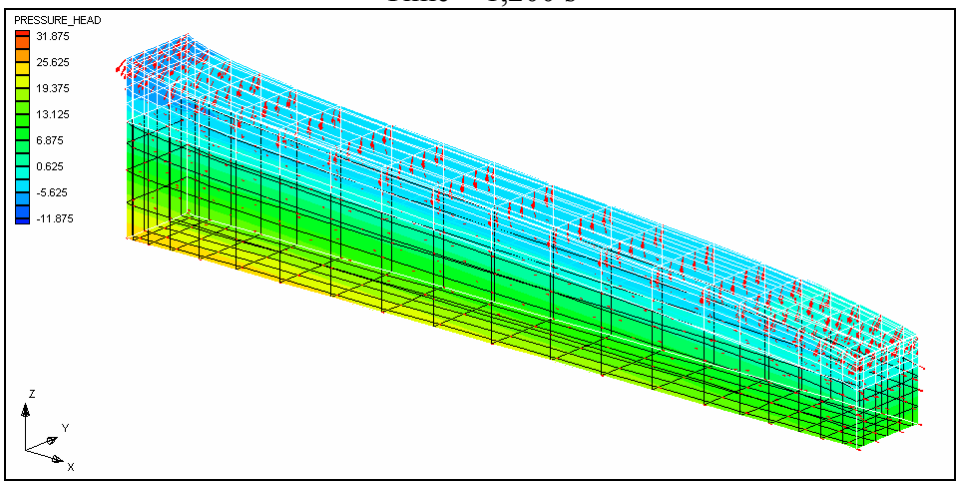

Time = 4,800 s

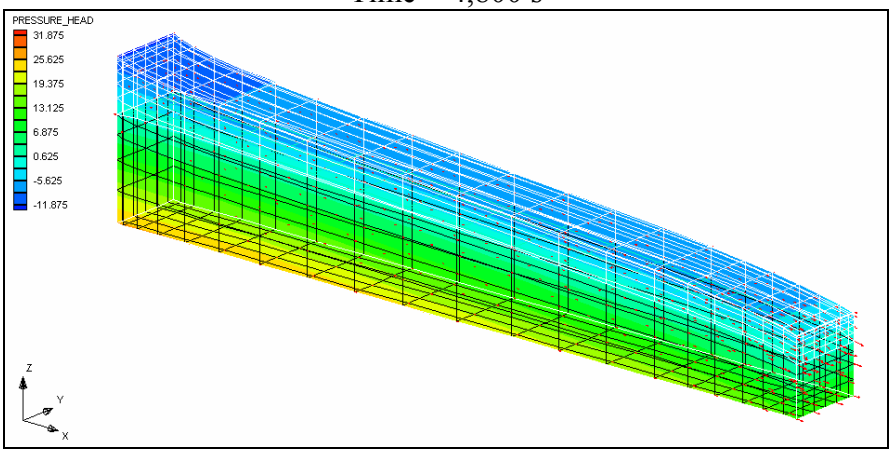

Time = 7,200 s

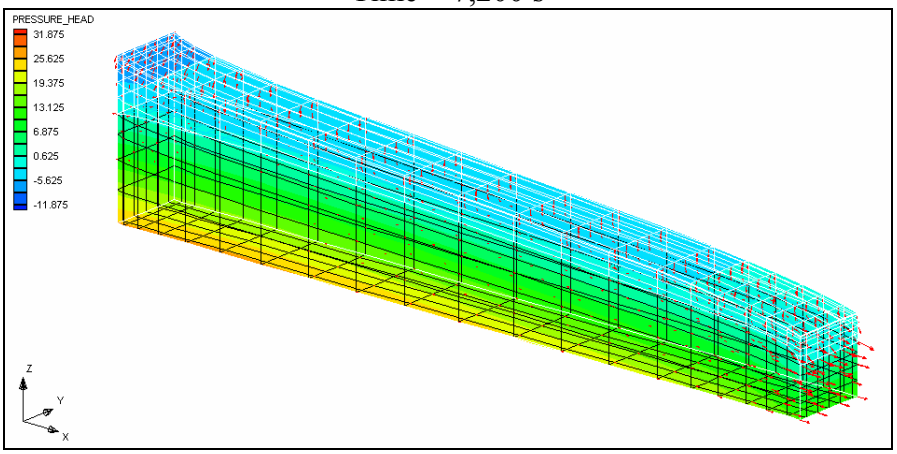

Time = 10,800 s

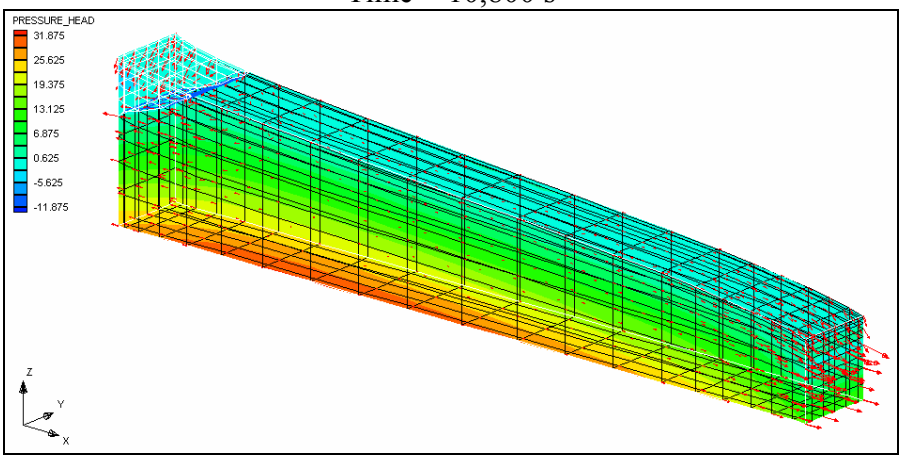

Time = 21,600 s

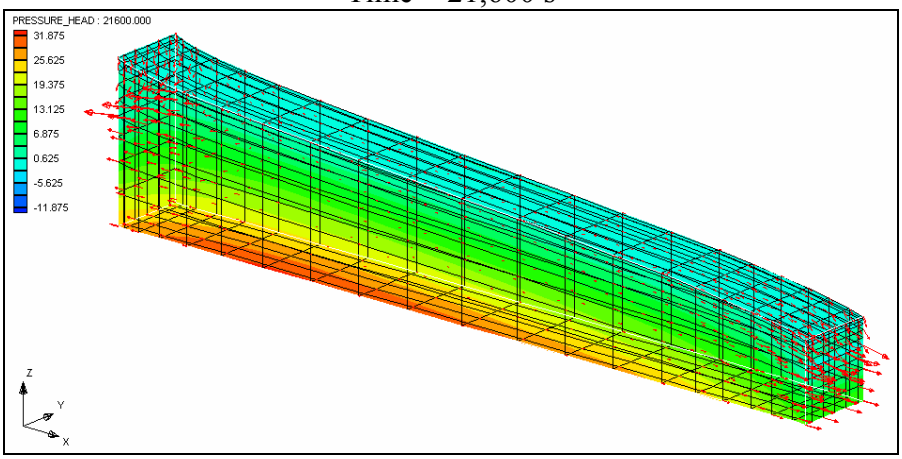

Fig. 4.1.5-3. Pressure Head Distribution at Various Times for Example 4.1.5

Time = 1,200 s

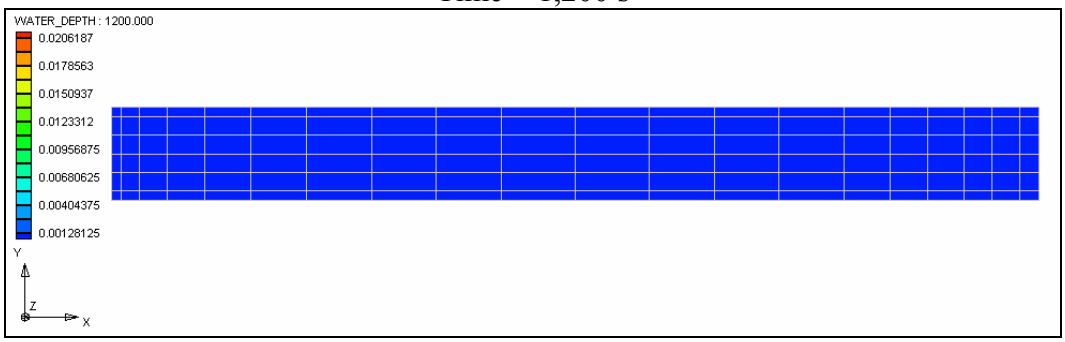

Time = 4,800 s

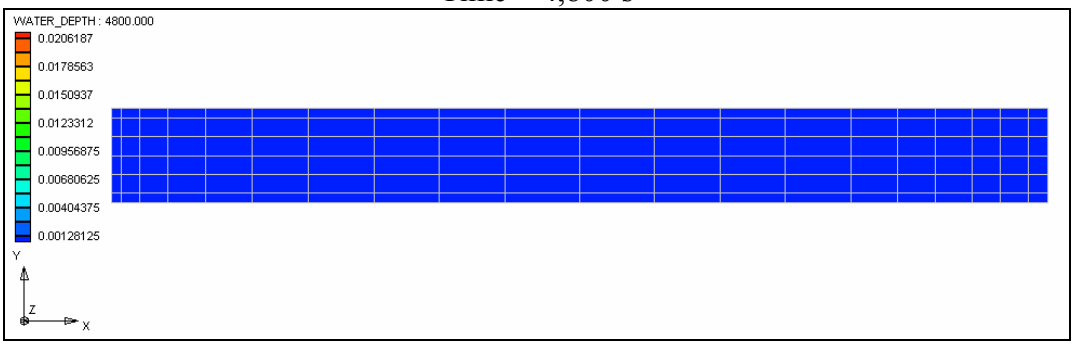

Time = 7,200 s

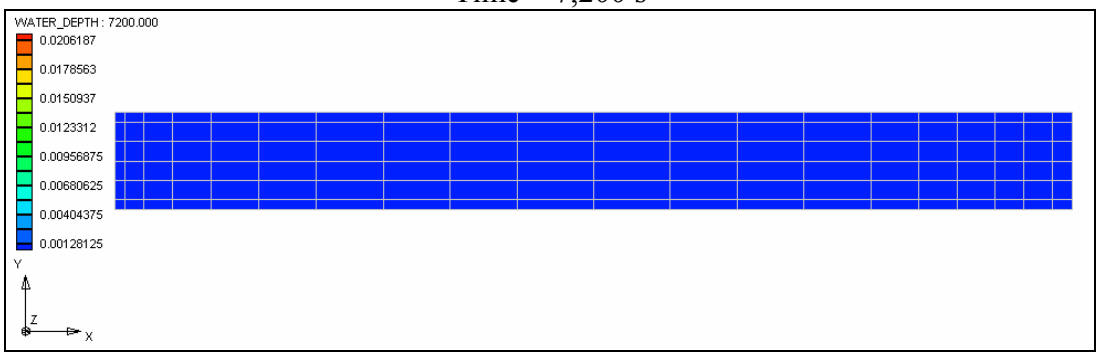

Time = 10,800 s

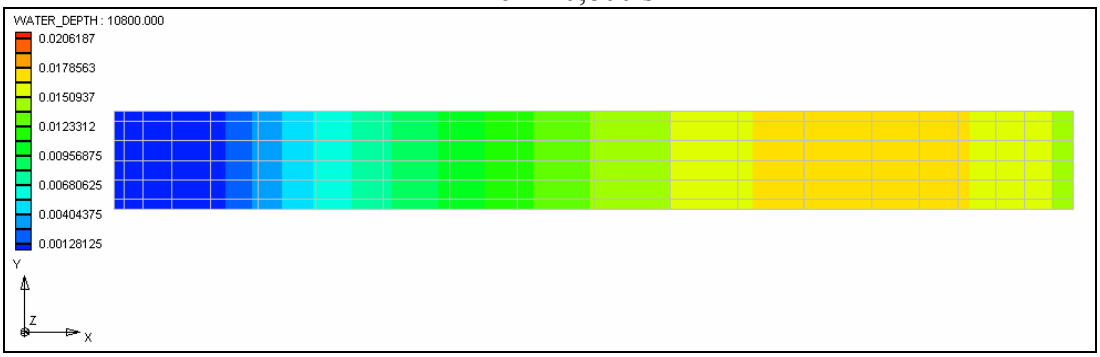

Time = 21,600 s

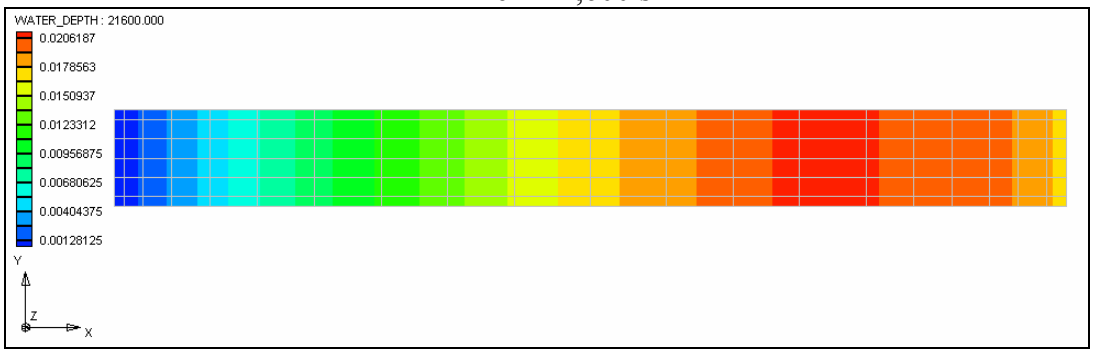

Fig. 4.1.5-4. Overland Water Depth Distribution at Various Times for Example 4.1.5

Table 4.1.5-1 Partial Results of Water Depth along the x-Direction for Example 4.1.5

Time [s]		1,200	4,800	7,200	10,800	21,600
Water Depth [m]	X = 0	0.000000E+00	0.000000E+00	0.000000E+00	0.000000E+000	0.000000E+000
	X = 10	0.000000E+00	0.000000E+00	0.000000E+00	0.000000E+000	0.566370E-003
	X = 30	0.000000E+00	0.000000E+00	0.000000E+00	0.000000E+000	0.150968E-002
	X = 60	0.000000E+00	0.000000E+00	0.000000E+00	0.000000E+000	0.285450E-002
	X = 100	0.000000E+00	0.000000E+00	0.000000E+00	0.494521E-003	0.458664E-002
	X = 150	0.000000E+00	0.000000E+00	0.000000E+00	0.295229E-002	0.665658E-002
	X = 210	0.000000E+00	0.000000E+00	0.000000E+00	0.552909E-002	0.894692E-002
	X = 280	0.000000E+00	0.000000E+00	0.000000E+00	0.790493E-002	0.111607E-001
	X = 350	0.000000E+00	0.000000E+00	0.000000E+00	0.991641E-002	0.131597E-001
	X = 420	0.000000E+00	0.000000E+00	0.000000E+00	0.119154E-001	0.152891E-001
	X = 500	0.000000E+00	0.000000E+00	0.000000E+00	0.137984E-001	0.173210E-001
	X = 580	0.000000E+00	0.000000E+00	0.000000E+00	0.150824E-001	0.186713E-001
	X = 650	0.000000E+00	0.000000E+00	0.000000E+00	0.162323E-001	0.199247E-001
	X = 720	0.000000E+00	0.000000E+00	0.000000E+00	0.172655E-001	0.210734E-001
	X = 790	0.000000E+00	0.000000E+00	0.000000E+00	0.170996E-001	0.207789E-001
	X = 840	0.000000E+00	0.000000E+00	0.000000E+00	0.166321E-001	0.201513E-001
	X = 880	0.000000E+00	0.000000E+00	0.000000E+00	0.165685E-001	0.200295E-001
	X = 920	0.000000E+00	0.000000E+00	0.000000E+00	0.162621E-001	0.196289E-001
	X = 950	0.000000E+00	0.000000E+00	0.000000E+00	0.158421E-001	0.191035E-001
	X = 980	0.000000E+00	0.000000E+00	0.000000E+00	0.150275E-001	0.181227E-001
	X = 1000	0.000000E+00	0.000000E+00	0.000000E+00	0.142089E-001	0.171431E-001

4.1.6 Coupled Three-Dimensional and One-Dimensional Flows.

This example is designed to simulate a losing stream passing through an underlying unconfined aquifer. The 3-D subsurface domain is represented by a 900 m x 800 m x 50 m area with a sloped land surface and the porous media extends to 50 m below land surface. A stream is located at the center of the domain (Fig.4.1.6-1). The saturated hydraulic conductivity of the soil is $K_{xx}=1.0^{-4}$ m/s, $K_{yy}=1.0^{-5}$ m/s and $K_{zz}=5.0^{-6}$ m/s. The effective porosity is 0.3. The unsaturated characteristic functions are linear.

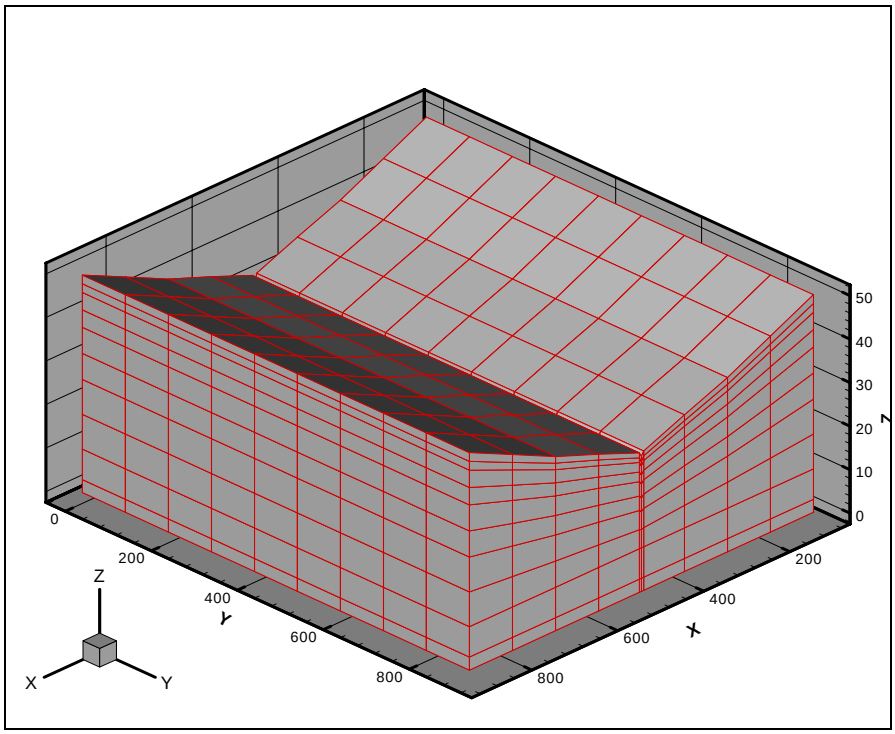

Fig. 4.1.6-1. 3-D Finite Element Mesh of Example 4.1.6

At the beginning of the simulation, a constant total head of 35 m is applied to the aquifer. A total head of 35 m was also applied as specified head boundary conditions to the lower part of the subsurface boundaries at the location of both stream ends. Other subsurface boundary surfaces were either variable boundary (top surface) or impermeable (other sides).

The stream is initially dry. An unsaturated zone hydraulically separates the stream and the aquifer. The length of the stream is 900 m. It was divided into 9 elements and 10 nodes. The bottom slope is 5/1,000. The cross-section is rectangular. The Manning's n is 0.03.

A discharge hydrograph is applied at the upstream end of the stream (Fig.4.1.6-2). The inflow hydrograph has a peak discharge of 40 m^3/s and duration of 7,200 seconds (2 hours). A rating curve was applied at the stream outlet. The total simulation time is 14,200 seconds (4 hours). A time step of 600 sec and 10 sec were used for 3-D subsurface and channel flows, respectively.

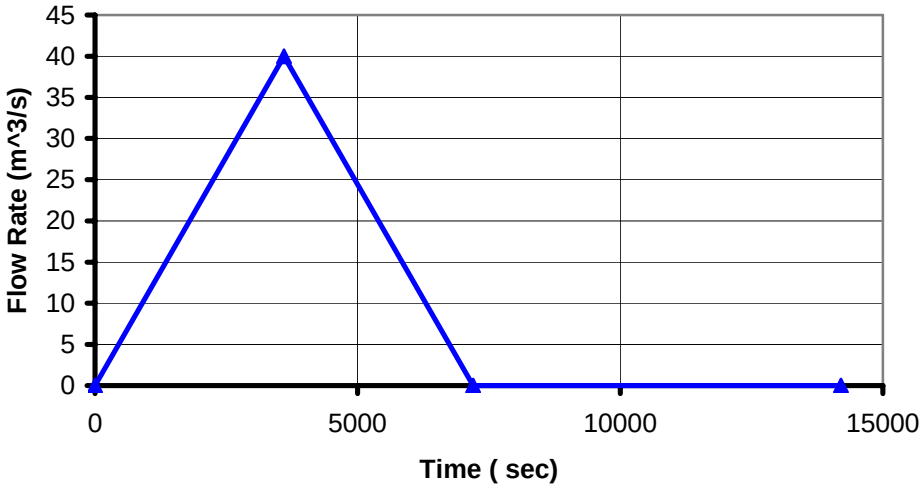

Fig. 4.1.6-2. Inflow Hydrograph for Example 4.1.6

The simulation results show that the saturated area in the subsurface domain expanded along the stream due to seepage from the channel (Fig. 4.1.6-4 and 4.1.6-5). The outflow hydrograph was modified by the infiltration into the subsurface. The peak discharge at x=600.0 m was less than the peak value without infiltration. And the time to peak was also delayed (Fig. 4.1.6-3).

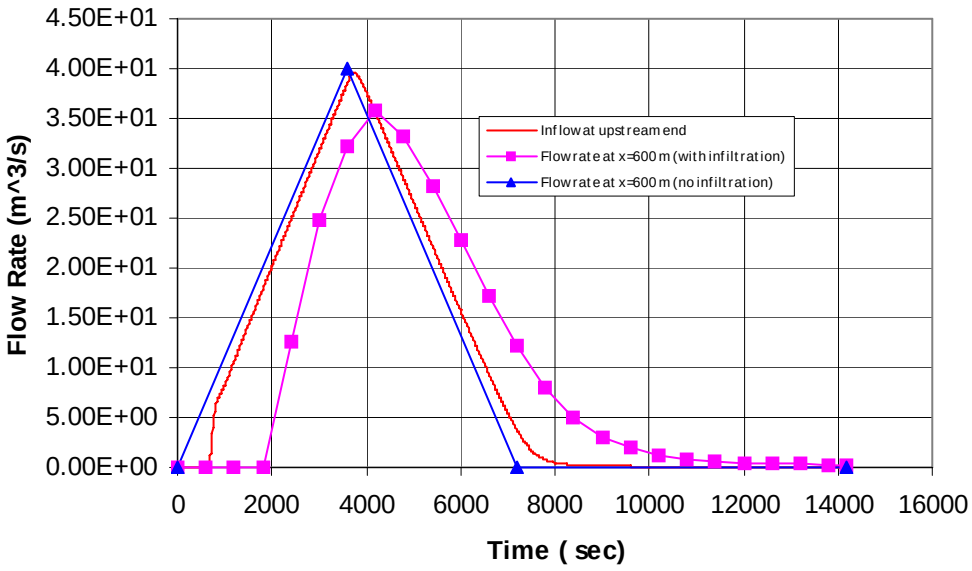

Fig. 4.1.6-3. Discharge Hydrograph (x = 0 and x = 600 m) for Example 4.1.6

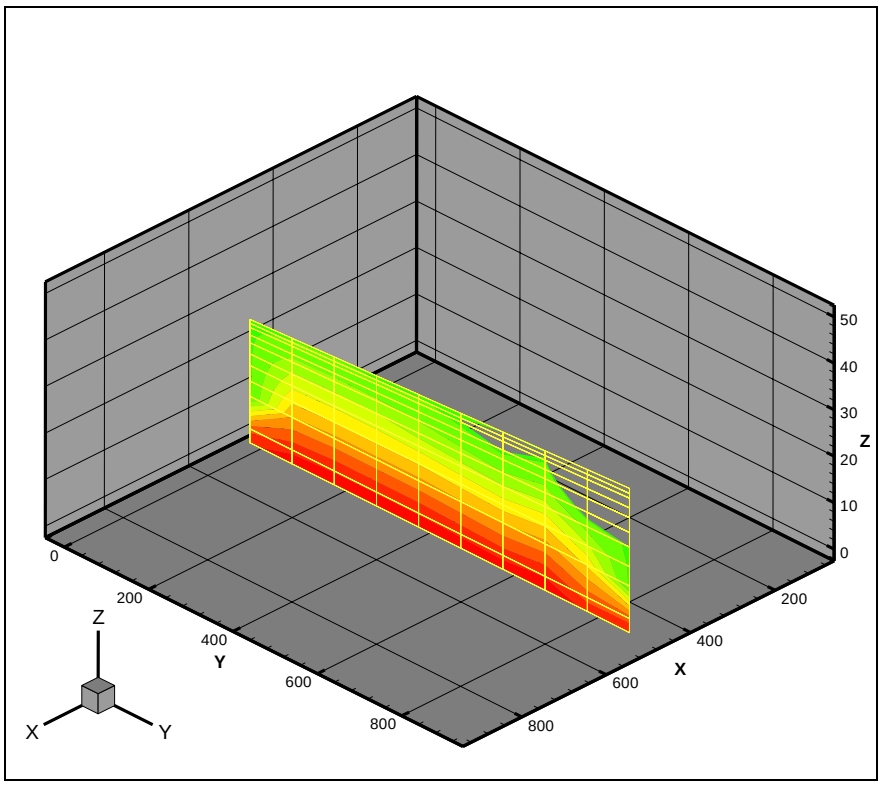

Fig. 4.1.6-4. Pressure Head Distribution at X = 500 m (Time=14,200 seconds)

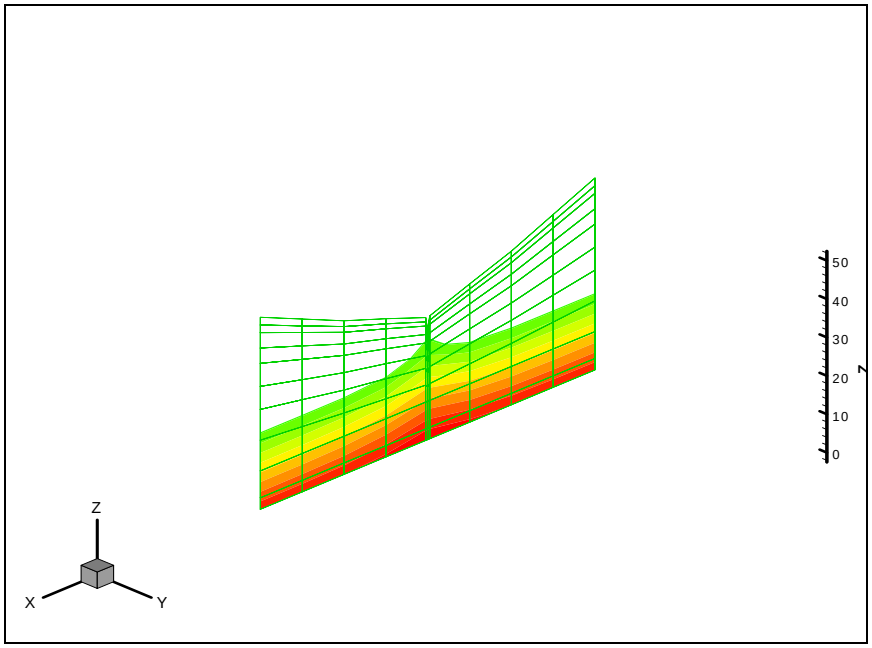

Fig. 4.1.6-5. Pressure Head Distribution at Y=430 m (time=14,200 seconds)

4.1.7 Coupled One-Dimensional, Two-Dimensional, and Three-Dimensional Flows.

This example demonstrates the capability of WASH123D in handling coupled 1-D channel, 2-D overland, and 3-D variably saturated subsurface flow problems. A spreader canal that was consisted of an upstream boundary node, a downstream boundary node, a junction, and a dead end was assumed in a hypothetic watershed. The 2-D overland domain was discretized with 154 elements and 175 nodes, and the 1-D spreader canal was composed of 14 elements and 17 nodes, where 1-D Nodes 1 through 6 were included in the first reach, 7 through 13 in the second reach, 14 through 17 in the third reach, and 1-D Nodes 6, 7, and 14 connected at the junction (Fig. 4.1.7-1). By excluding those 2-D nodes that coincided with 1-D nodes, the 2-D computational domain contained 124 (= 154 - 30) 2-D elements and 160 (= 175 - 15) 2-D nodes. The canal was 4 m wide for the first reach, 2 m wide for the second and third reaches, and its cross-sectional area was proportional to its depth. The canal was as deep as 0.1 m at the entrance (i.e. the first 1-D node, written in red in Fig. 4.1.7-1) and as shallow as 0.025 m at the junction. Figure 4.1.7-1 also provides the figures of bank height for all channel-related overland nodes (written in dark blue). The 3-D domain contained 1,050 nodes and 770 elements (Fig. 4.1.7-2), where the overland/canal domain coincided with its top boundary (i.e., ground surface).

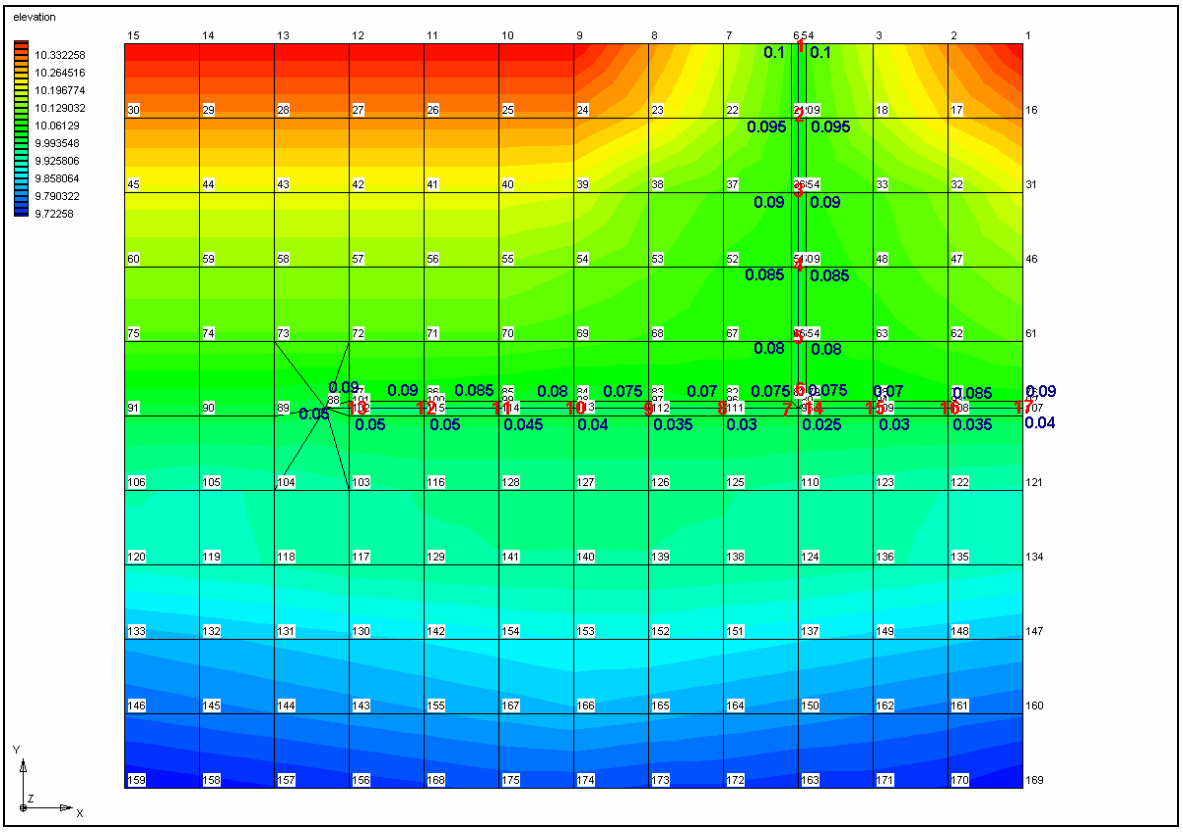

Fig. 4.1.7-1. 1-D/2-D Discretization and Surface Elevation of Example 4.1.7

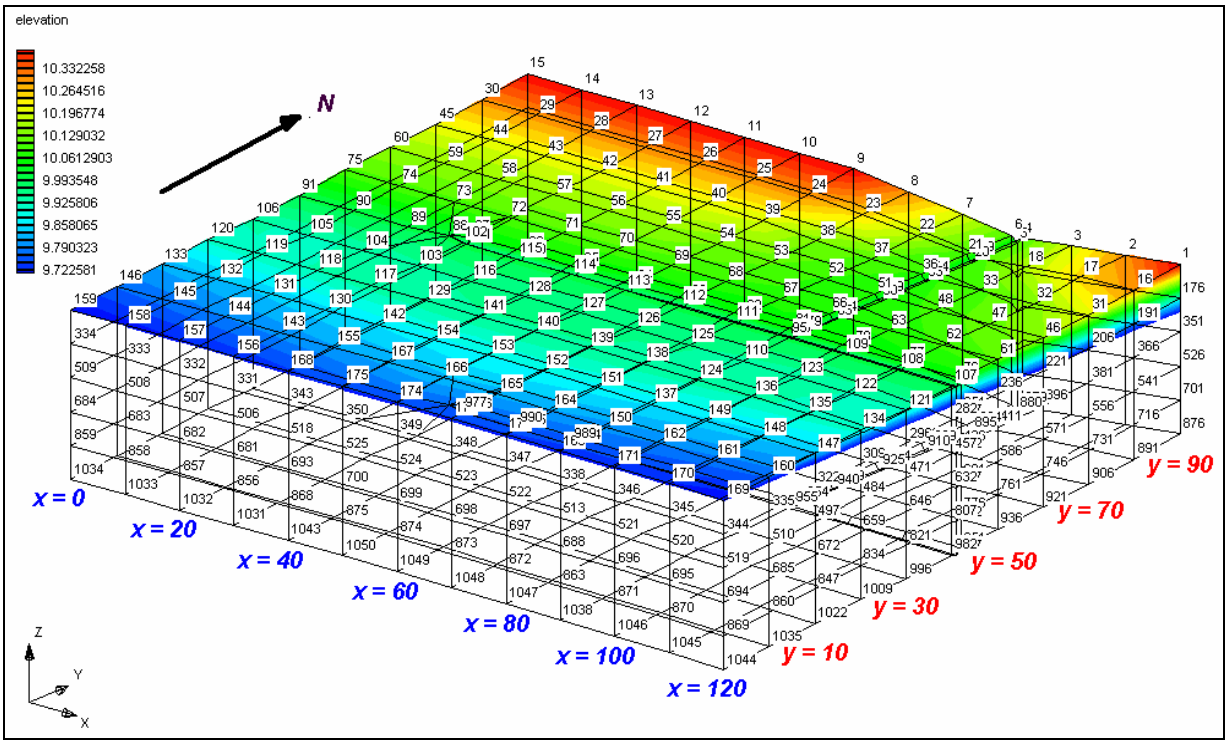

Fig. 4.1.7-2. 3-D Discretization of Example 4.1.7

To compute 3-D subsurface flow, a total head of 10.01 m was specified on the northern boundary and 9.5 m on the southern boundary. The east, west, and bottom boundaries were assumed impermeable. The Manning's roughness was set to 0.01 for both 2-D overland and 1-D canal flow. In computing 2-D overland flow, a Dirichlet boundary condition of zero depth was specified for Nodes 1, 9, 10, 11, 12, 13, 14, and 15, which represented high grounds; a depth-dependent flux boundary condition was given on the low ground (or south) boundary (i.e., the boundary that emprises Nodes 159, 158, 157, …, 169); and a channel-overland interaction boundary condition was specified for the channel-related overland boundary sides, which included a depth-dependent flux when flow was from overland to canal and a canal stage condition when flooding occurred. A time-dependent water depth was controlled at both the upstream and downstream 1-D nodes (i.e., Nodes 1 and 17 in red in Fig. 4.1.7-1), which started at 0.01 m at time = 0 second, then increased linearly to 0.04 m at time = 1,800 seconds, and stayed at 0.04 m for the rest of the simulation (i.e., to time = 14,400 s). A zero-velocity condition was applied at the dead-end node.

The initial subsurface head distribution (Fig. 4.1.7-3) was computed by solving for a steady-state subsurface flow solution, where Dirichlet boundary conditions were applied to the north and the south boundaries as mentioned above, a rainfall rate of 10^{-8} m/s was assumed as the variable boundary flux on the top boundary, and a ponding depth of 0.01m was enforced and applied to those subsurface boundary nodes that were corresponding to 1-D canal nodes. At the beginning of the simulation, the overland domain was completely dry, while a constant depth of 0.01 m was assumed at every node in the 1-D spreader canal. A constant rainfall rate of 10^{-7} m/s was applied throughout the entire simulation period of 14,400 seconds. The time-step size was set to 50 seconds for computing 3-D subsurface flow, 10 seconds for 2-D overland flow, and 2 seconds for 1-D channel

flow. It is noted that after the transient simulation began, the top boundary of 3-D subsurface served as the interface between surface and subsurface domains, and the boundary condition that was applied on it depended on both rainfall and water depth on ground surface.

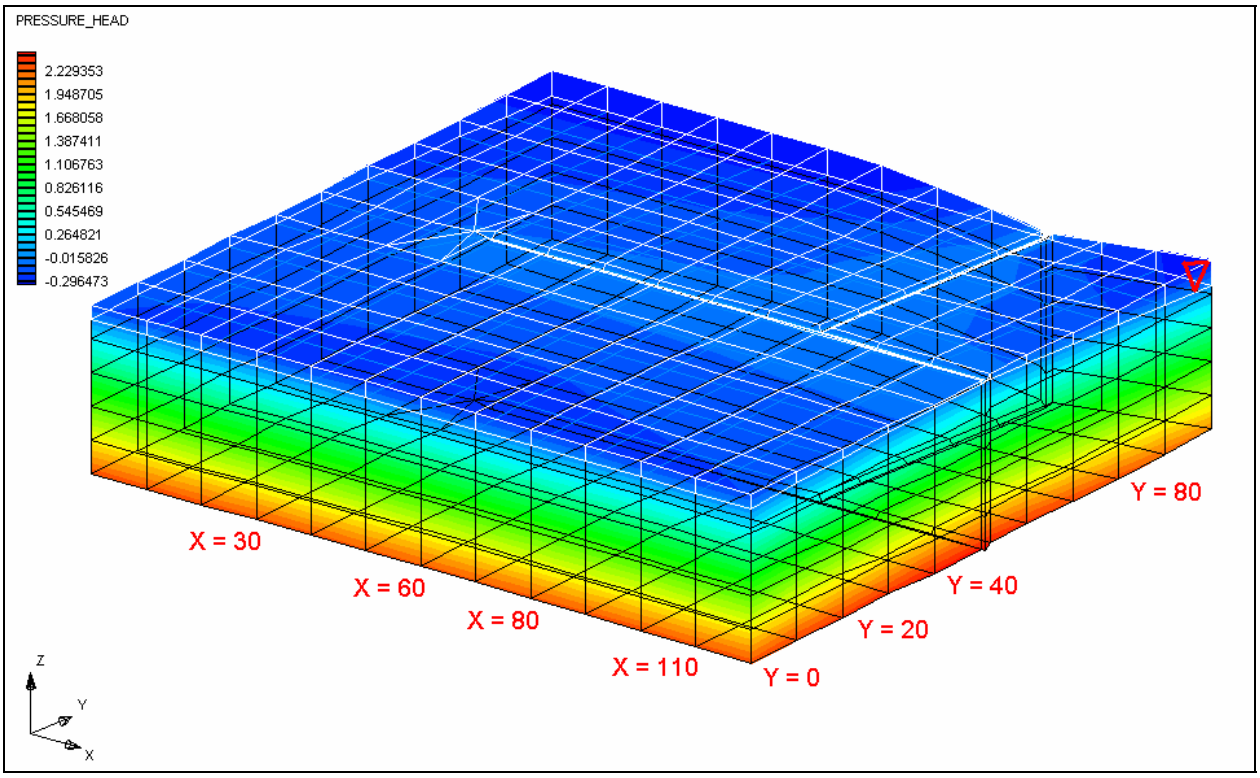

Fig. 4.1.7-3. The Computed Initial Steady-State Pressure Head Distribution of Example 4.1.7

Figure 4.1.7-4 plots the variation of water depth with time at five 1-D canal nodes: 3, 6, 9, 12, and 15. Also, a dash line that represents the bank height over which canal water will overflow to the downstream overland regime is given as reference for Nodes 6, 9, 12, and 15 (marked with respective colors). The bank height was 0.09 m for Node 3, which is out of scale in Figure 4.1.7-4. Figure 4.1.7-5 provides a zoom-in plot of Figure 4.1.7-4 for the period of Time = 0 through 2,000 s, where the four "X" symbols indicate the moments that water started to flow from canal to overland at Nodes 6, 9, 12, and 15.

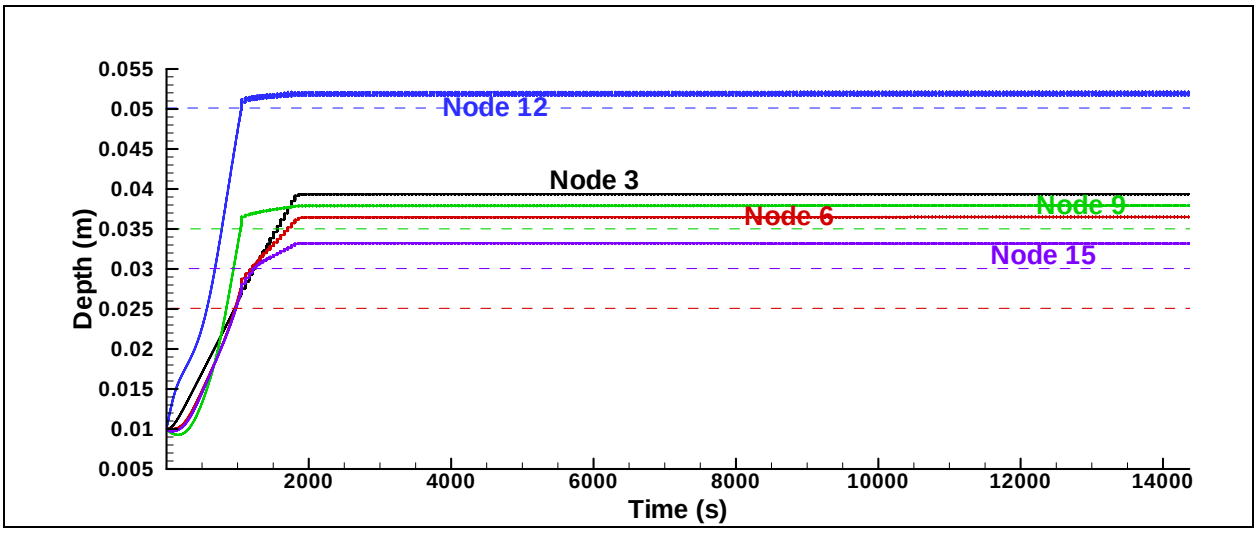

Fig. 4.1.7-4. Computed Water Depth at Various 1-D Canal Locations for Example 4.1.7 (Time = 0 through 14,400 s).

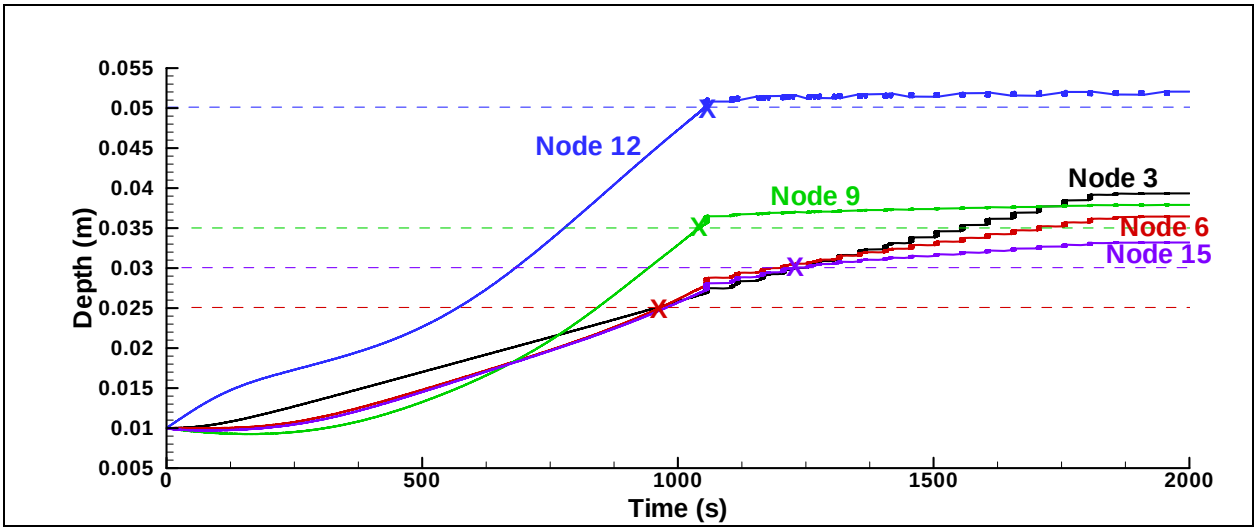

Fig. 4.1.7-5. Computed Water Depth at Various 1-D Canal Locations for Example 4.1.7 (Time = 0 through 750 s)

Figure 4.1.7-6 plots the distribution of water depth in the overland domain at various times. Figures 4.1.7-7 and 4.1.7-8 plot the distribution of subsurface pressure head on several x and y, respectively, cross sections at various times, where the unsaturated zone is highlighted in white and water table is marked in red.

Time = 1,200 s

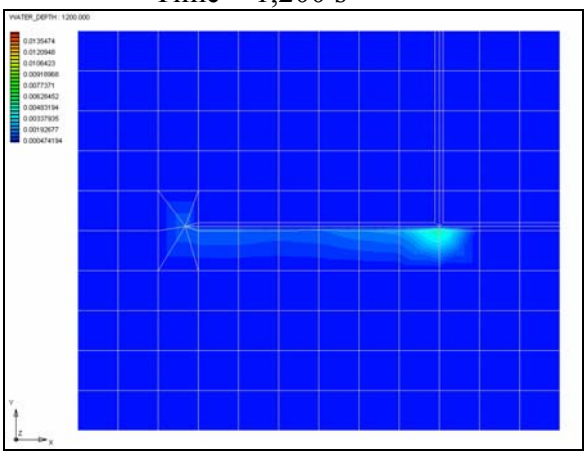

Time = 2,400 s

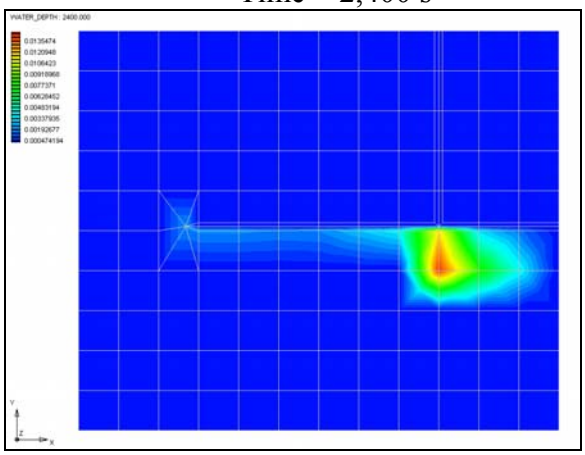

Time = 3,600 s

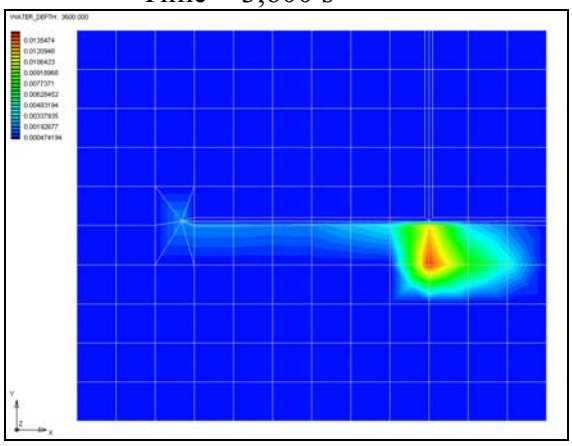

Time = 4,800 s

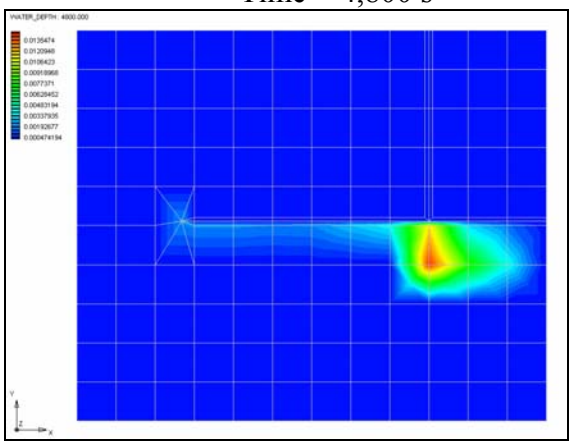

Time = 6,000 s

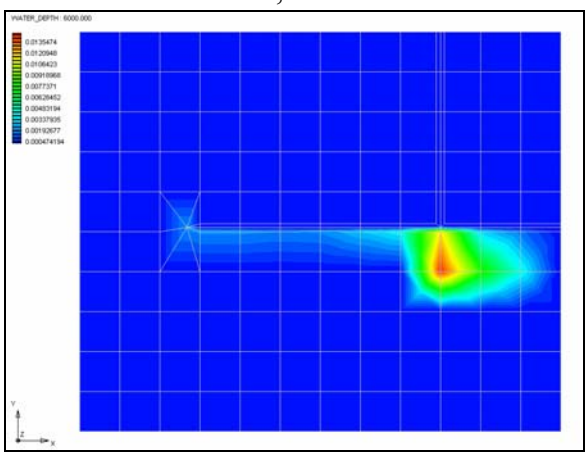

Time = 7,200 s

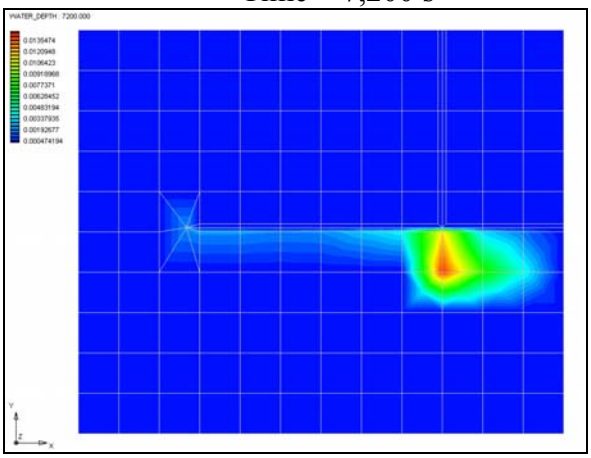

Fig. 4.1.7-6. Computed Distribution of Water Depth of Overland at Various Times (Example 4.1.7, Part 1)

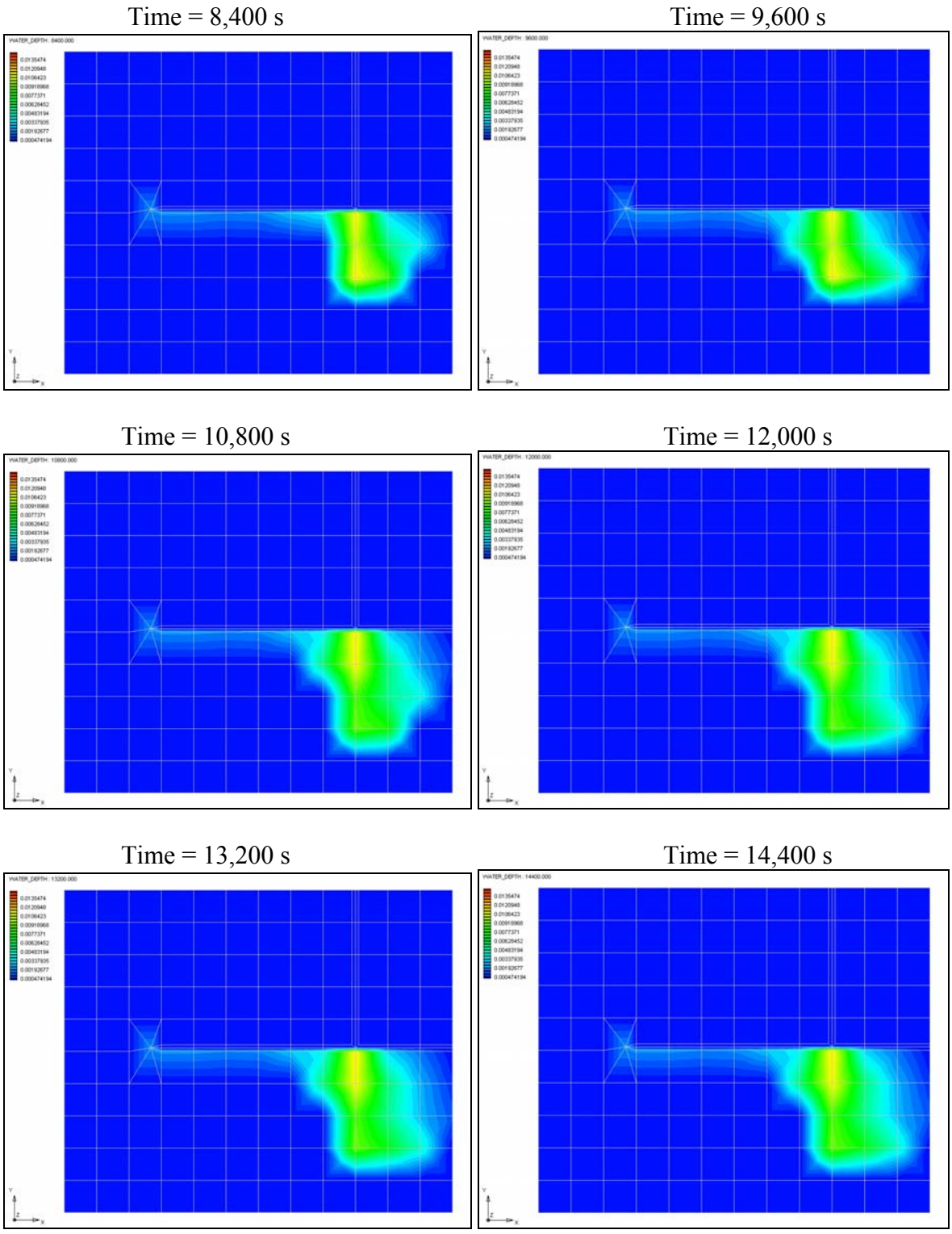

Fig. 4.1.7-6. Computed Distribution of Water Depth of Overland at Various Times (Example 4.1.7, Part 2)

Time = 1,200 s

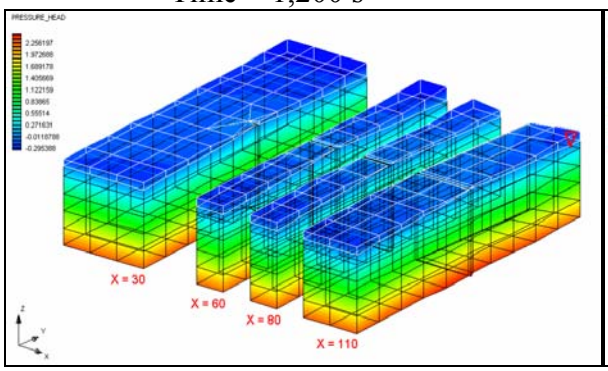

Time = 2,400 s

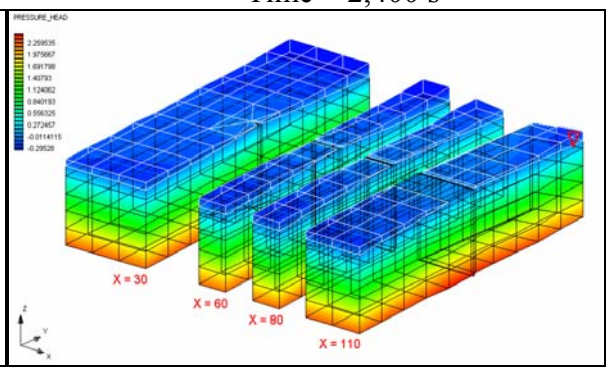

Time = 3,600 s

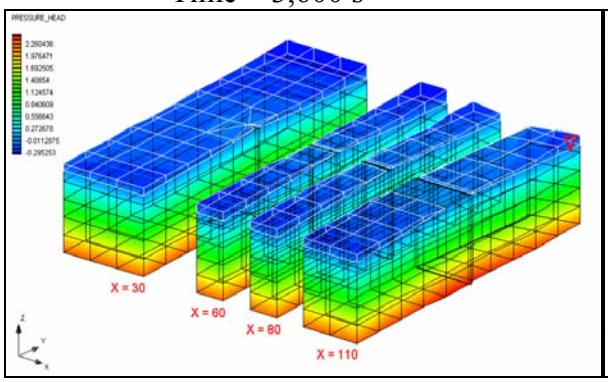

Time = 4,800 s

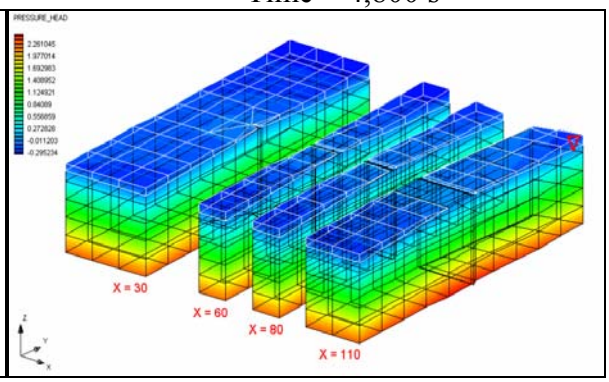

Time = 6,000 s

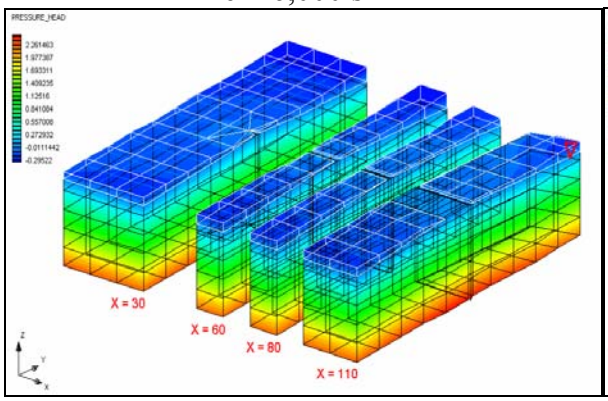

Time = 7,200 s

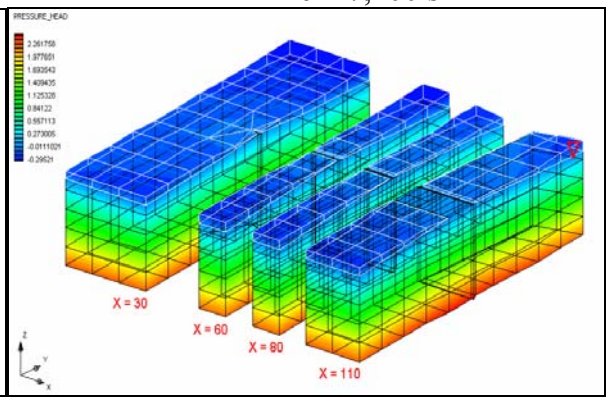

Fig. 4.1.7-7. Computed Pressure Head Distribution on Several X Cross Sections at Various Times (Example 4.1.7, Part 1)

Time = 8,400 s

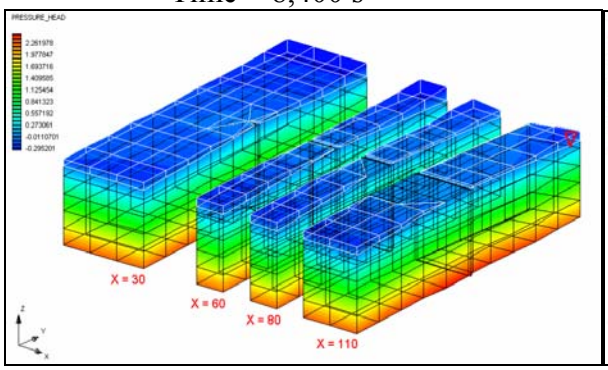

Time = 9,600 s

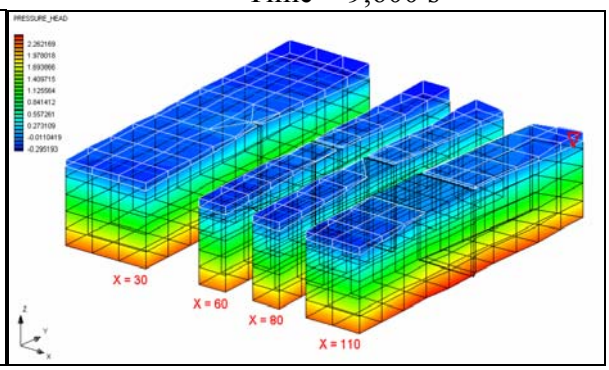

Time = 10,800 s

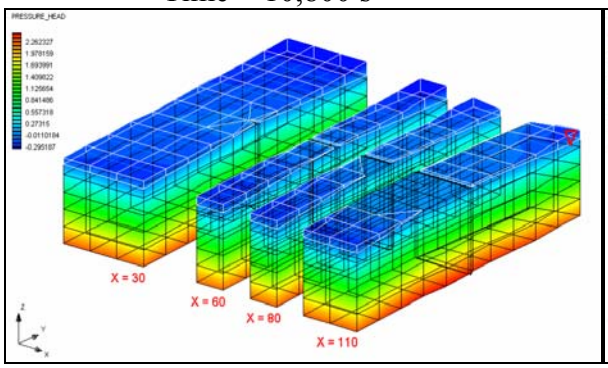

Time = 12,000 s

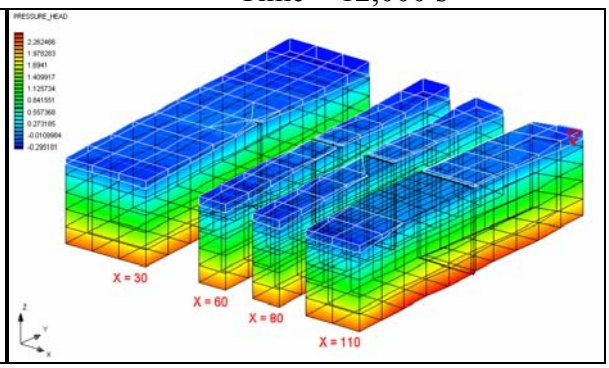

Time = 13,200 s

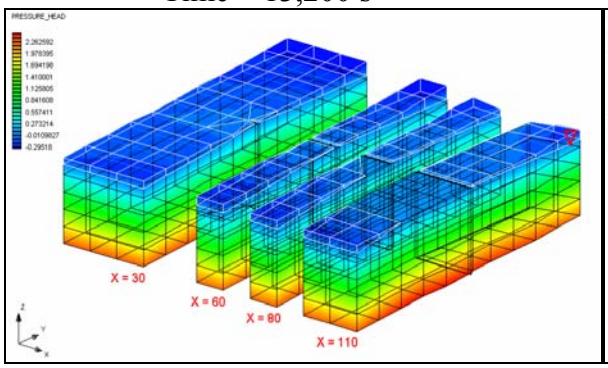

Time = 14,400 s

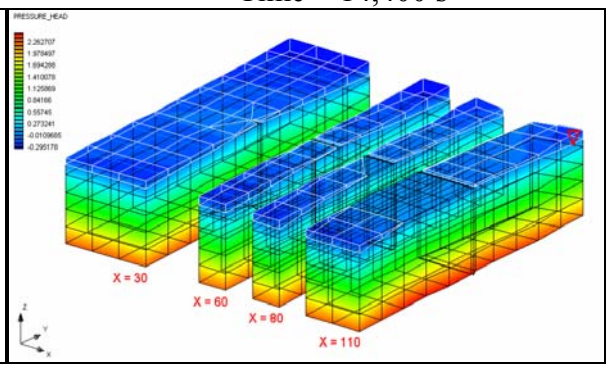

Fig. 4.1.7-7. Computed Pressure Head Distribution on Several X Cross Sections at Various Times (Example 4.1.7, Part 2)

Time = 1,200 s

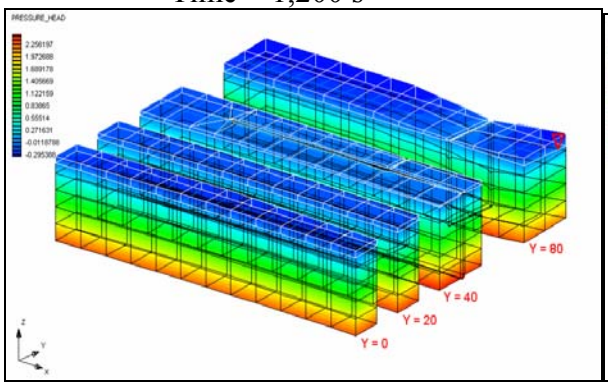

Time = 2,400 s

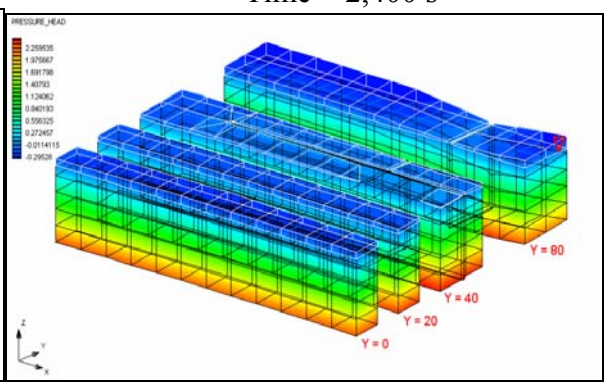

Time = 3,600 s

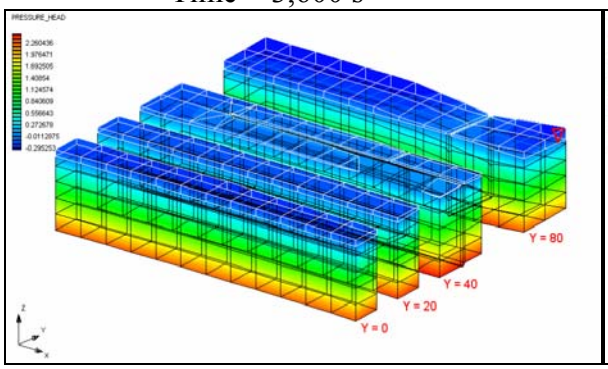

Time = 4,800 s

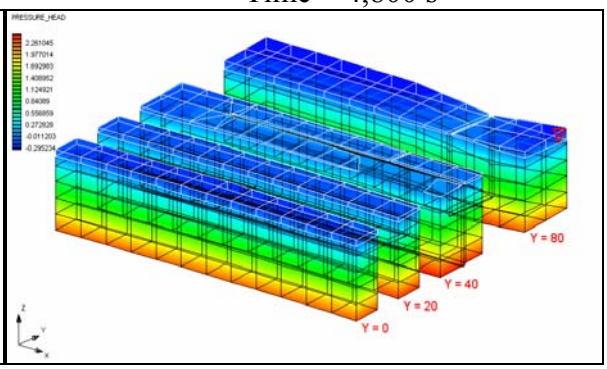

Time = 6,000 s

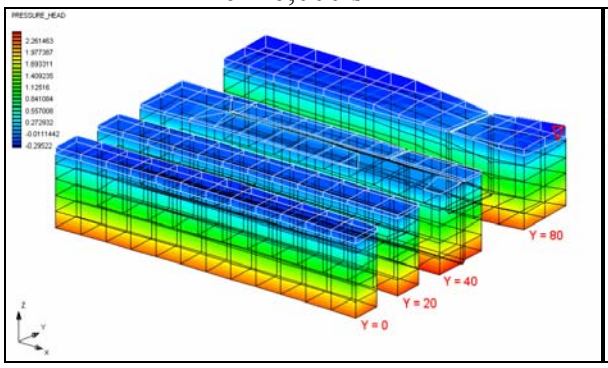

Time = 7,200 s

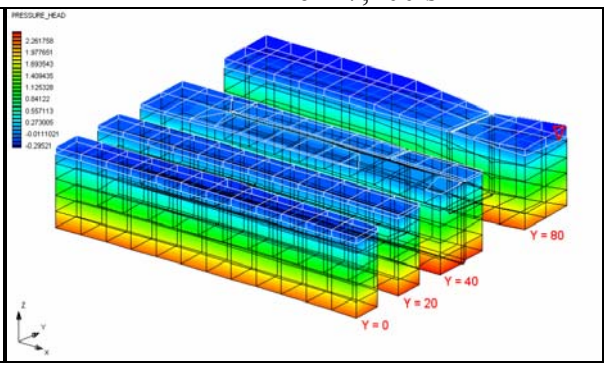

Fig. 4.1.7-8. Computed Pressure Head Distribution on Several Y Cross Sections at Various Times (Example 4.1.7, Part 1)

Time = 8,400 s

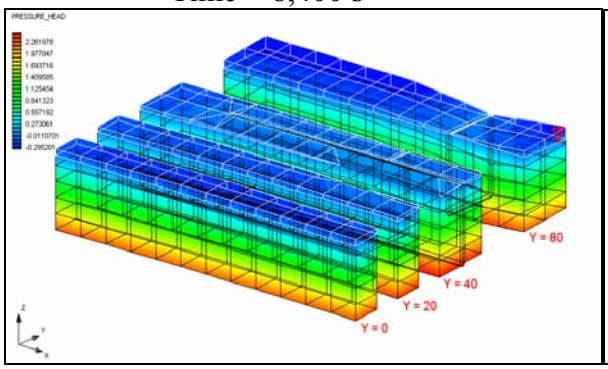

Time = 9,600 s

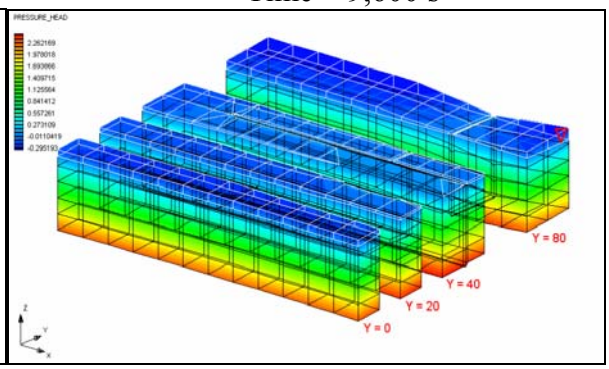

Time = 10,800 s

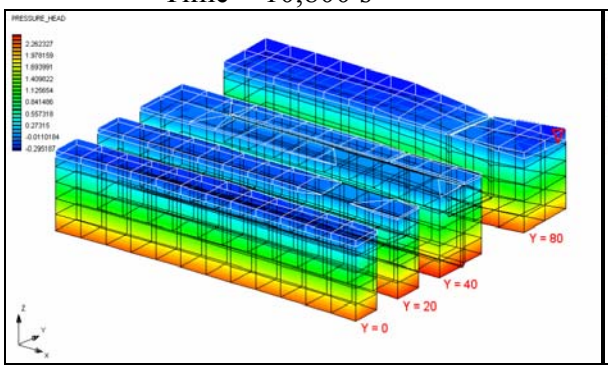

Time = 12,000 s

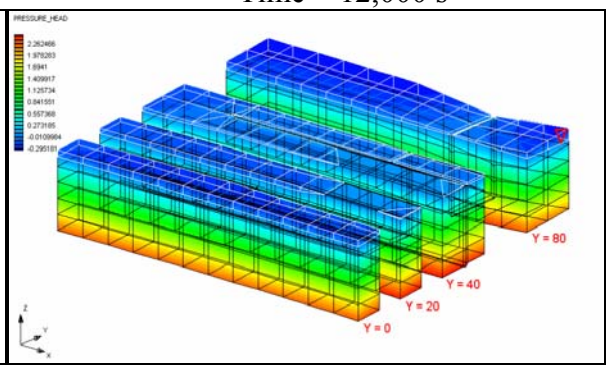

Time = 13,200 s

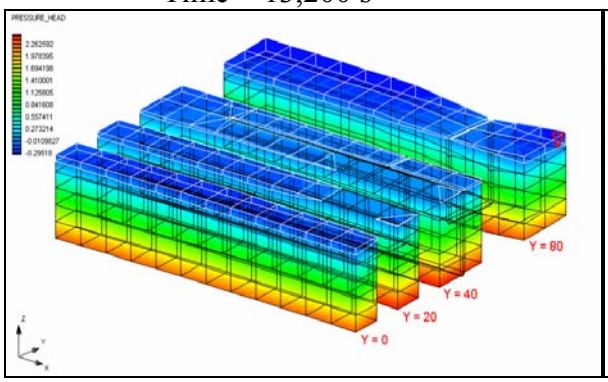

Time = 14,400 s

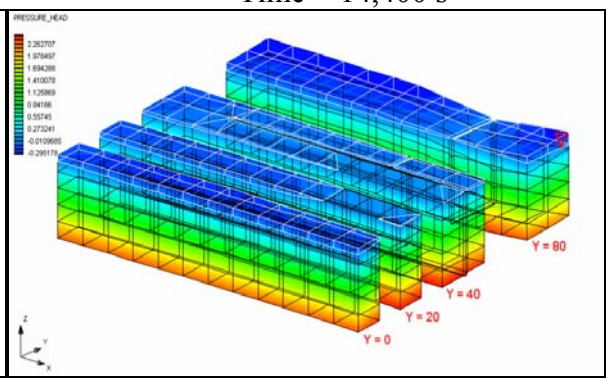

Fig. 4.1.7-8. Computed Pressure Head Distribution on Several Y Cross Sections at Various Times (Example 4.1.7, Part 2)

It is observed from Figure4.1.7-4 that the 1-D canal flow may be considered to be reaching a steady state after time = 3,000 seconds. However, the change of water depth and pressure head with time in Figures 4.1.7-6 and in Figures 4.1.7-7 and 4.1.7-8, respectively, shows that 2-D overland flow and 3-D subsurface flow have not reached a steady state even at the end of the simulation.

From Figure 4.1.7-6, it is observed that the overland water seems to be confined within a certain region during Time = 2,400 s through Time = 7,200 s and during Time = 12,000 s through Time = 14,400 s. After a close examination on the numerical results, we determine that this confinement was caused by infiltration at the respective downstream locations, which was greatly influenced by the Dirichlet boundary condition (total head = 9.5 m) that was specified on the southern boundary. As time passes, infiltration from overland to subsurface raised water table, and the overland water front moved further downstream when water table arose to near ground surface and water coming in from the upstream could overcome infiltration.

Figures 4.1.7-6 through 4.1.7-8 show consistent results between overland water depth and subsurface pressure head. This has verified that we have successfully implemented the coupling of surface and subsurface flow in WASH123D.

4.2 Three Optional Approaches to Modeling Flow in WASH123D

Three approaches are taken to model flow problems in WASH123D: kinematics-wave, diffusive-wave, and fully dynamic-wave models. In this section, four example problems are presented to show possible differences in simulations using these three different approaches and to illustrate that only fully dynamic-wave approaches can be taken to model very rapidly varying transient flow problems.

4.2.1 One-Dimensional River Flows

Three cases are presented for the one-dimensional problems in the river/stream/canal system. Case 1 is a steady-state subcritical flow problem, which shows there are some errors in the diffusive wave approximation even for this simple problem. Case 2 is a steady-state mixed subcritical and supercritical problem, which is designed to demonstrate the magnitude of errors introduced with the diffusive wave approximation. Case 3 is a steady-state, mixed subcritical and supercritical problem with a hydraulic jump. This problem demonstrates that the diffusive wave approximation is not adequate for this complicated problem. In all three cases, steady-state simulations were achieved via transient simulations with constant boundary and source conditions.

1. Subcritical Flow. This is the test problem published by MacDonald et al. (1997), where an analytical solution for the problem is available. The channel is rectangular with a width of 10 m. The total length is 1,000 m. A constant flow of 20 m^3/s passes through. The flow is subcritical over the entire channel. A water depth of 0.748409 m is specified at the downstream outlet. The Manning's n value is 0.03. The bed slope is given by an analytical function of the water depth. Simulated steady-state profiles of water depth with diffusive wave (DIW) and fully dynamic wave

(FDW) approaches are given in Figure 4.2.1-1. It is seen that the FDW approach yields excellently accurate results while the DIW approach produces some errors.

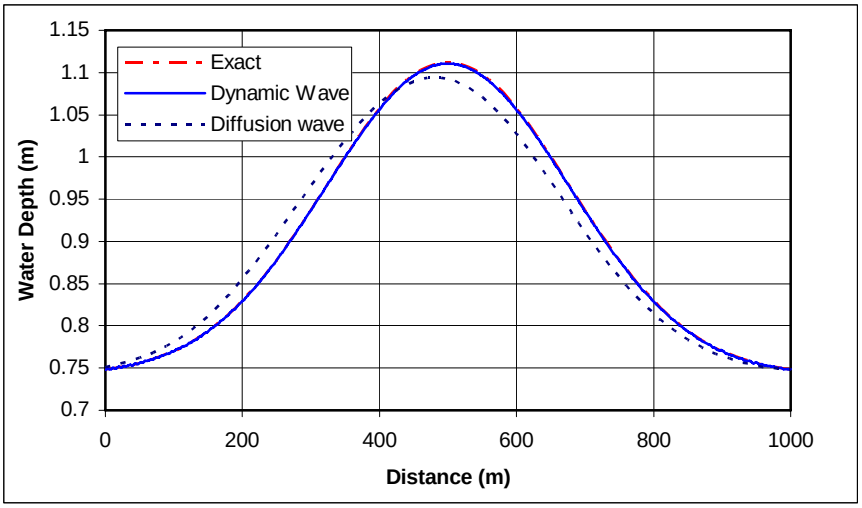

Fig. 4.2.1-1. Comparison of Simulated Water Depth Profile with Exact Solutions

2. Mixed Subcritical and Supercrical Flow. This test case was described in MacDonald et al. (1997). A 1,000 m of rectangular channel with a width of 10 m is given a constant flow rate of 20 m^3/s. The bottom slope is variable such that the flow condition at the inflow is subcritical and is supercritical at the outlet. The Manning's n value is 0.02. For the dynamic wave approach, one inflow boundary condition is specified at the upstream and no boundary condition is needed at the downstream since supercritical flows occur therein. For diffusive wave model, two boundary conditions must be given: one is the upstream boundary condition where the inflow rate is prescribed as in the case of FDW approach and the other is the downstream boundary condition. In this case, the known water depth at outlet is specified as the Dirichlet boundary conditions.

The dynamic wave model is able to solve this mixed flow problem with good accuracy (Fig. 4.2.1-2). No numerical instabilities have been encountered. The diffusive wave model also provides satisfactory results (4% error in water depth). The Froude number profile plot shown in Figure 4.2.1-3 confirms the mixed flow condition. It is interesting to note that the DIW model requires more input data than the FDW model, yet yields poorer simulations.

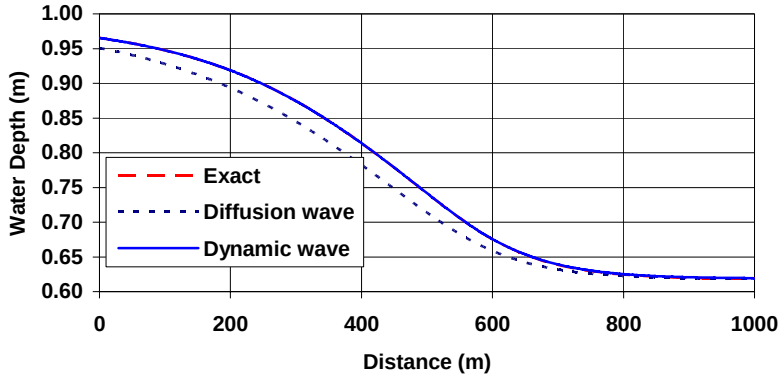

Fig. 4.2.1-2. Comparison of Simulated Water Depth Profile with Exact Solutions

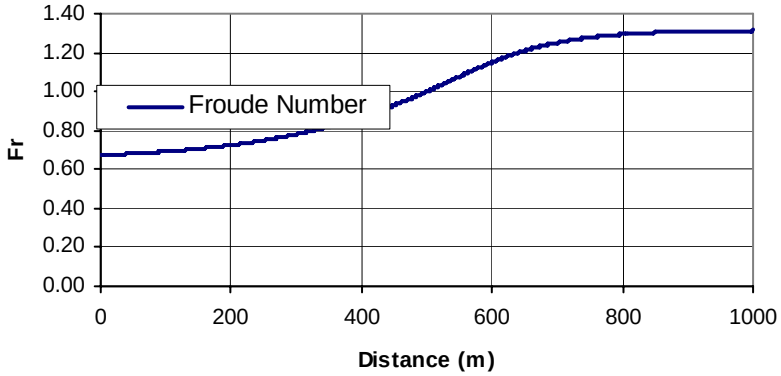

Fig. 4.2.1-3. Froude Number Profile

3. Mixed Subcritical and Supercrical Flow with Hydraulic Jump. This test case was described in MacDonald et al. (1997). The channel is trapezoidal with a total length of 1,000 m. The upstream inflow is a constant discharge 20 m^3/s. At the downstream outlet, a specified water depth of 1.349963 m is applied. The side slope of the trapezoidal cross-section is 1:1. The Manning's n value is 0.02. There is an abrupt change in the bed slope at x = 500 m, causing a hydraulic jump. The bottom elevation and bed slope were given in MacDonald et al. (1997). Both inflow and outflow boundaries are subcritical. The analytical solution of the steady state water depth is provided in MacDonald et al. (1997)

$$h(x)=\begin{cases} 0.723449\left[1-\tanh\left(\dfrac{x}{1,000}-\dfrac{3}{10}\right)\right] & 0\le x\le 300 \\ 0.723449\left\{1-\frac{1}{6}\tanh\left[6\left(\dfrac{x}{1,000}-\dfrac{3}{10}\right)\right]\right\} & 300\le x\le 600 \\ \dfrac{3}{4}+\sum_{k=1}^{3}a_k\exp\left[-20k\left(\dfrac{x}{1,000}-\dfrac{3}{10}\right)\right]+\dfrac{3}{5}\exp\left(\dfrac{x}{1,000}-\dfrac{3}{10}\right) & 600\le x\le 1,000 \end{cases} \quad \textbf{(4.1.3.4)}$$

This is a non-trivial problem with source terms (roughness and bed slope) and is more realistic in testing the performance of the FEM based method of characteristics. As expected, the accuracy of the diffusive wave approximation for this mixed flow case is not satisfactory. The error induced by diffusive wave approximation is high at the supercritical zone (Fig. 4.2.1-4).

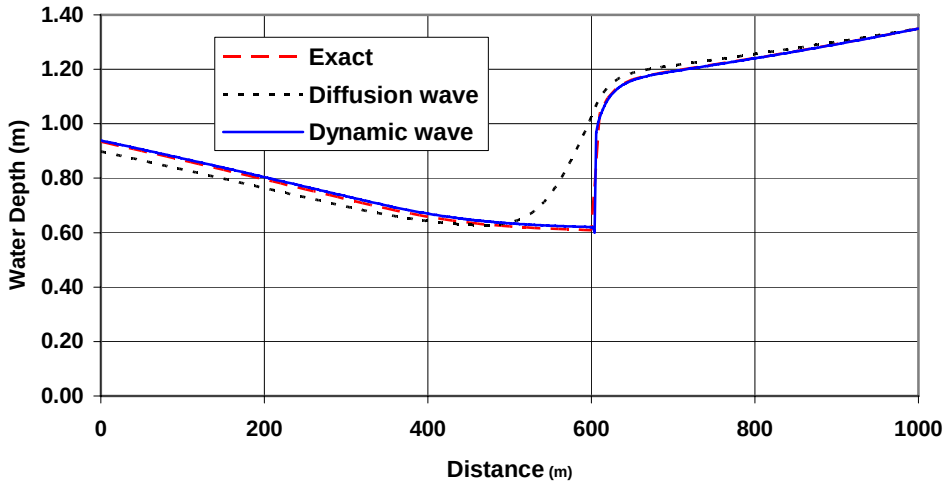

Fig. 4.2.1-4. Comparison of Simulated Water Depth Profile with Exact Solution

4.2.2 Two-Dimensional Overland Flows.

A rainfall-runoff process on an impervious curved surface is simulated (Fig. 4.2.2-1). The domain is 150 m x 40 m. The bottom elevation ranges from 0.11 m to 0.31 m over a horizontal length of 150 m. The overland domain is divided into 80 elements and 105 nodes. A specified water depth of 0.1 m is applied to the downstream end boundary. All other sides are assumed to be no-flow boundaries. A Manning's n value of 0.02 is used. The rainfall intensity is 3.0-5 m/s for 1,800 seconds (30 minutes). The purpose of this numerical experiment is to compare the simulation results obtained with different computational methods for 2-D overland flow and validate the numerical implementation for dynamic, diffusive and kinematic wave models. The average bottom slope is 0.00133.

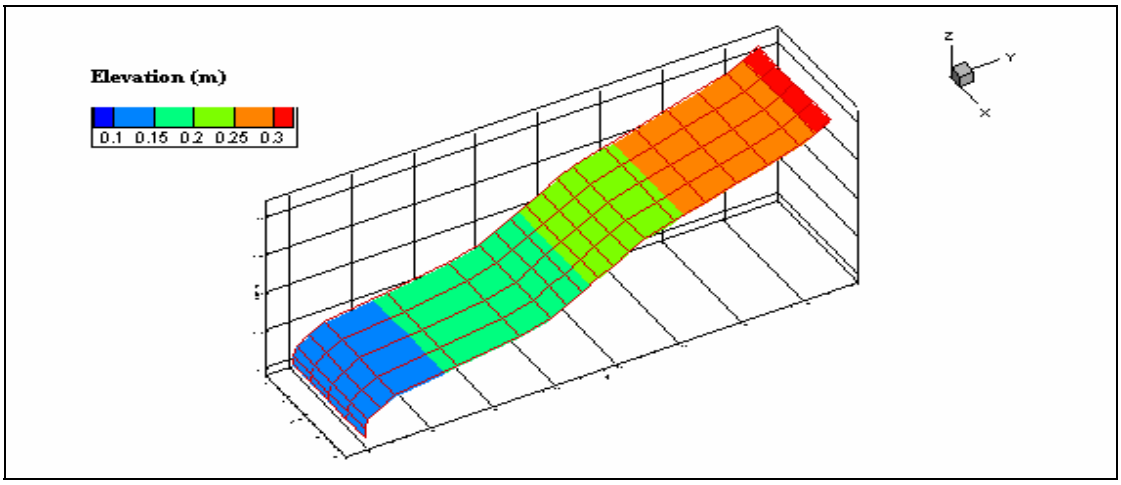

Fig. 4.2.2-1. Topography of the Land Surface

The fully dynamic wave equations and diffusive wave and kinematic wave approximations were applied to this problem. The simulation results were compared. The computed water levels at Node 28 (x = 20 m, y = 30 m, Z_o = 0.152 m) were compared (Fig. 4.4.2-2). This location is close to the downstream end. The maximum value of water level, found to be 0.173 m, 0.180 m and 0.181 m, was obtained with fully dynamic wave (MOC), diffusive wave (SL), and kinematic wave (SL) approaches. The difference between the dynamic wave and diffusive wave models is about 6%. This may indicate the diffusive wave approximation is not accurate for this problem. Similar conclusions can be made for the kinematic wave model. Water levels at Node 88 (x = 20 m, y = 130 m and Z_o = 0.278 m), which represent the flow at upper part of the surface, were compared (Fig. 4.2.2-3). The maximum water depth at this site is 0.01124 m, 0.0094 m and 0.00776 m for FDW (MOC), DIW (SL), and KIW (SL), respectively. The differences between the fully dynamic wave and diffusive/kinematic wave models at the upstream nodes are smaller than those at the downstream nodes as expected.

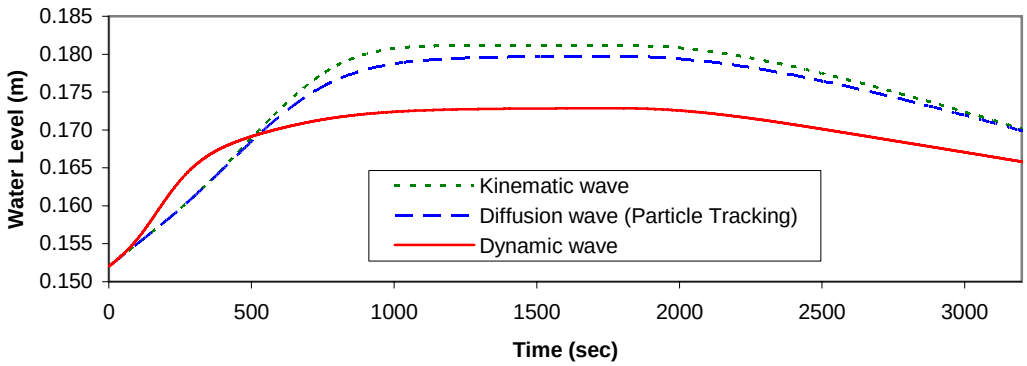

Fig. 4.2.2-2. Comparison of Simulated Water Levels at a Node Closed to Downstream

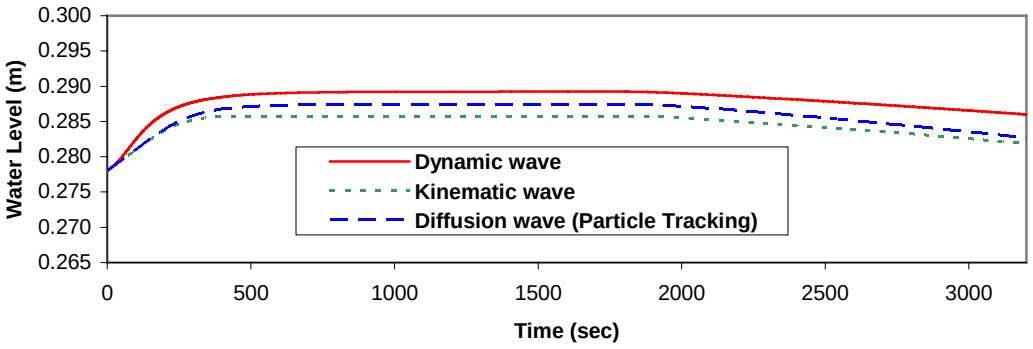

Fig. 4.2.2-3. Comparison of Simulated Water Levels at a Node Closed to Upstream

4.2.3 Circular Dam Break Problems.

This is a typically idealized dam break problem designed to test the performance of the two-dimensional method of characteristics (2-D MOC) in solving two-dimensional fully dynamic wave problems. This example has been extensively applied in the hydraulic literature to test performance of new numerical schemes for two-dimensional shallow water equations.

An idealized circular dam is located on a frictionless horizontal bottom (40 m x 40 m). A nominal circular thin wall is located at the circle from the center with a radius of 2.5 m. At the beginning of the simulation, the circular wall has collapsed instantly. At time t = 0, the water depth in the dam is 2.5 m, and a water depth of 0.5 m is presented elsewhere (Fig. 4.2.3-1).

This is a symmetrical wave propagation problem. The radial direction is the wave direction. Isotropic nature of the solution may be destroyed in some grid orientation dependent numerical schemes such as a finite volume method.

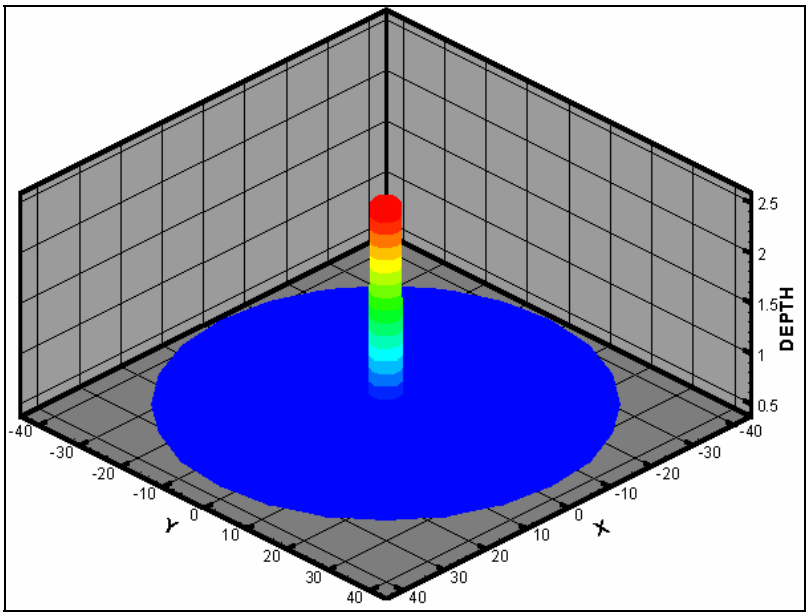

Fig. 4.2.3-1. Three-Dimensional Plot of Initial Water Depth

The most important and difficult aspect of the 2-D MOC method is the selection of the characteristic directions for the three characteristics. In this case, the wave directions are known *a priori* from the physical nature of the flow. It was found that if the characteristic directions were chosen along the radial direction at each node, the computation was very stable. When the selection of the characteristic directions is updated through the solution process, the convergence rate and the isotropic nature of the solution were very sensitive to time step and mesh size.

The computational mesh comprises 2,854 linear triangular elements and 1,440 nodes. Starting from the center of the circular dam, nodes are located evenly on circles with increasing radius. This is designed to follow the physical nature by taking advantage of finite element method (Fig. 4.2.3-2).

The time step size is 0.01 second and the total simulation time is 3.0 seconds. The following plots of water surface elevations (Fig. 4.2.3-3, 4.2.3-4 and 4.2.3-5) demonstrate the development of water wave movement. It can be seen that water depth has dropped below the initial water depth of 0.5 m outside of the dam. These numerical results are consistent with those presented in the hydraulic literatures.

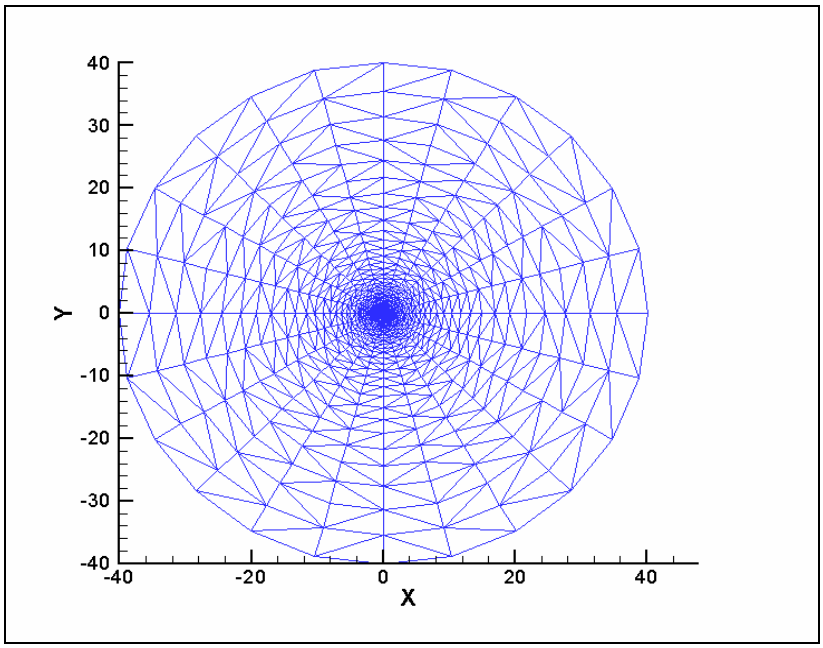

Fig. 4.2.3-2. Two-Dimensional Finite Element Mesh of Example 4.2.3

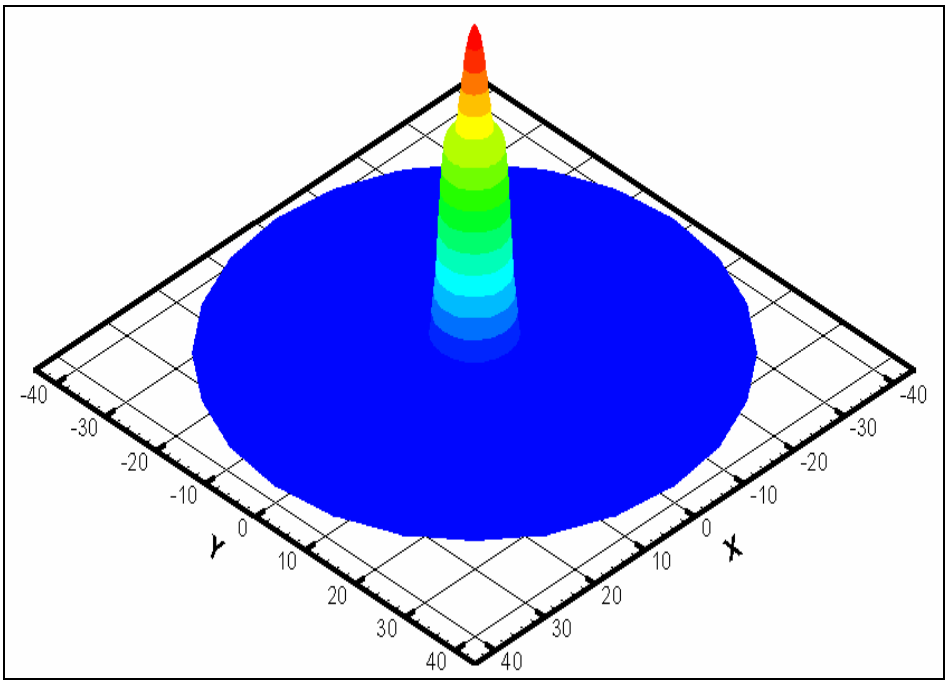

Fig. 4.2.3-3. Water Surface Elevation at Time = 0.7 s for Example 4.2.3

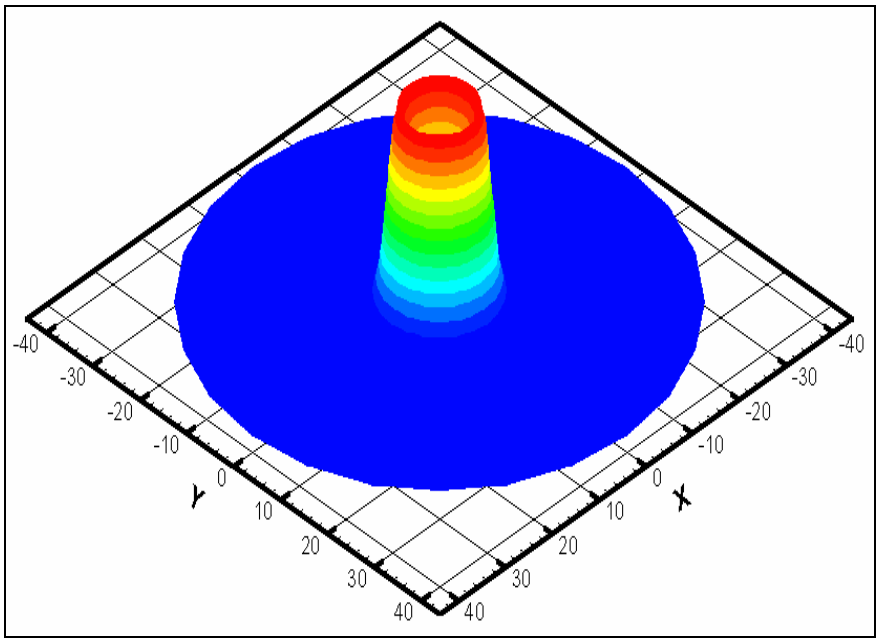

Fig. 4.2.3-4. Water Surface Elevation at Time = 1.4 s for Example 4.2.3

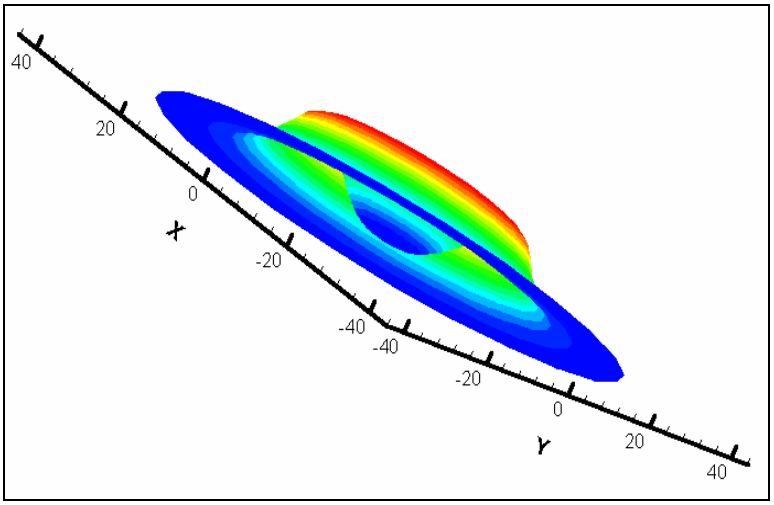

Fig. 4.2.3-5. Bottom View of Water Surface Elevation at Time = 2.8 s for Example 4.2.3

The symmetrical nature of the solution was preserved quite well. This is demonstrated in the stage hydrograph at nodes at the center of the circular domain (Fig. 4.2.3-6).

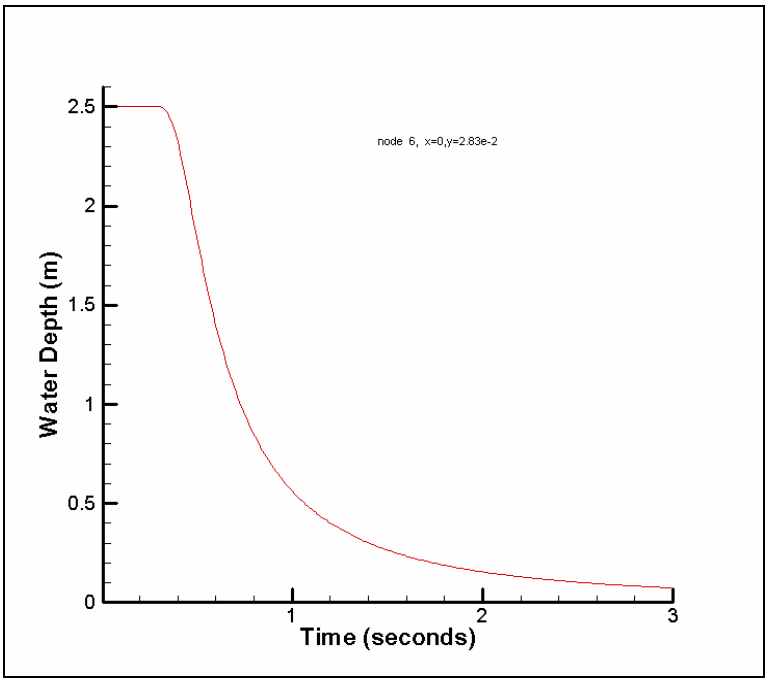

Fig. 4.2.3-6. Water Depth Hydrograph for a Location near the Center of the Circular Dam

The depth hydrograph in Figure 4.2.3-6 confirms that there is a depression in water surface after the dam break. The water depth decreases from 2.5 m to below 0.5 m.

An animation showing the circular dam break over the entire simulation period is attached in Appendix A (File Name: dambkcir(4-2-3).avi).

4.2.4 Two-Dimensional Dam Break Problems.

This a two-dimensional frictionless partial dam break problem that has been extensively used in hydraulic literature for testing numerical performance. The water depth behind the dam is assumed to 10 m. The downstream water depth was set to 0.05 m, so it is a nearly dry-bed simulation. This problem is very difficult to solve numerically with conventional finite difference or finite element methods.

The rectangular channel is horizontal with a dimension of 200 x 200 m in length and width, respectively. The initial water depth is 10 m in the reservoir and 0.05 m in the downstream. The breach or opening of sluice gates is 75 m, between x = 95-170 m. The domain was divided into 40 x 40 rectangular elements and the elements at the location of the dam are excluded (Fig. 4.2.4-1).

The two-dimensional fully dynamic wave model was applied to this problem and solved with the Method of Characteristics (MOC). A time step of 0.15 second was used. Figures 4.2.4-2 through 4.2.4-4 depict the water stages at various time = 2.0 s, 5.0 s, 7.0 s, respectively. This demonstrates that the 2-D MOC can solve this kind of sharp front problem without having to use higher order numerical schemes, all of which produce wiggles and peak clipping. Diffusive or kinematic wave approaches cannot adequately simulate this type of problems.

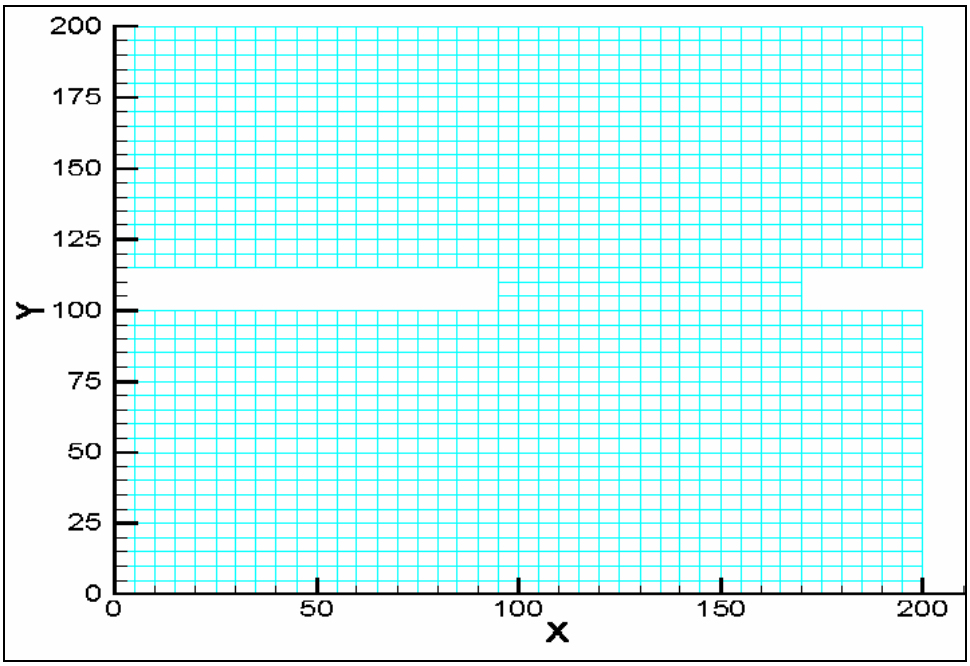

Fig. 4.2.4-1. Problem Description and Finite Element Discretization for Problem 4.2.4

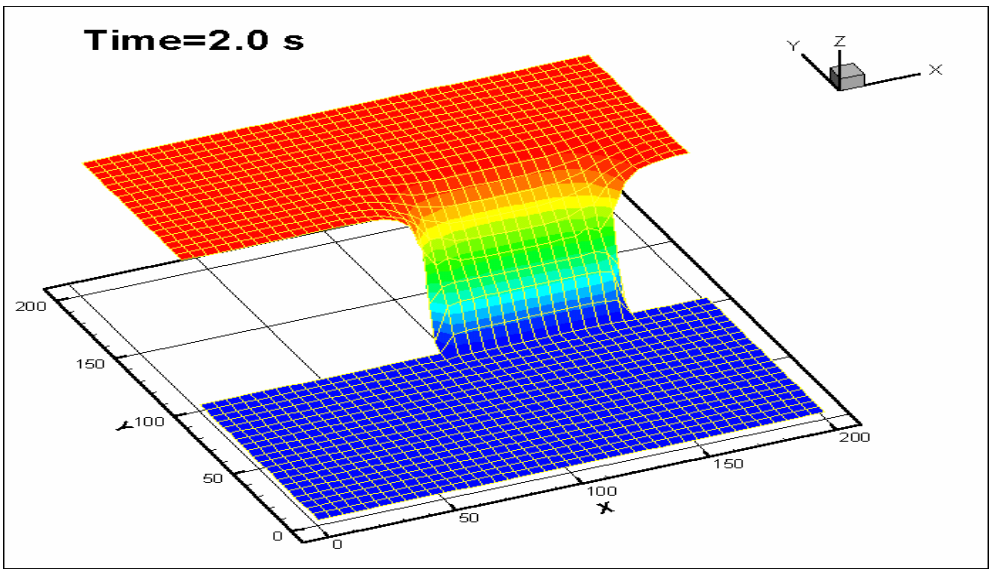

Fig. 4.2.4-2. 3-Dimensonal Perspective View of Water Surface at time = 2 s for Problem 4.2.4

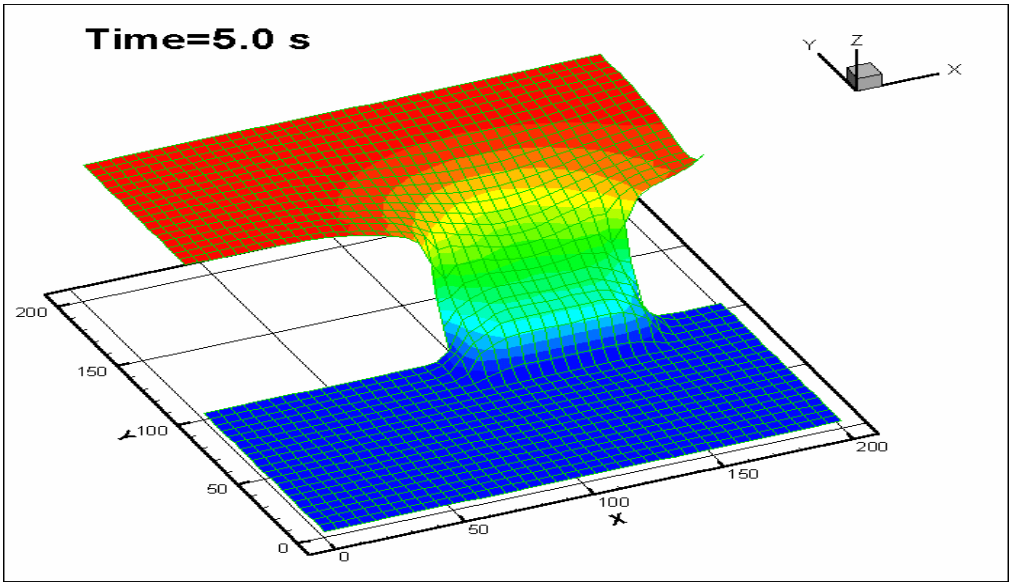

Fig. 4.2.4-3. 3-Dimensonal Perspective View of Water Surface at time = 5 s for Problem 4.2.4

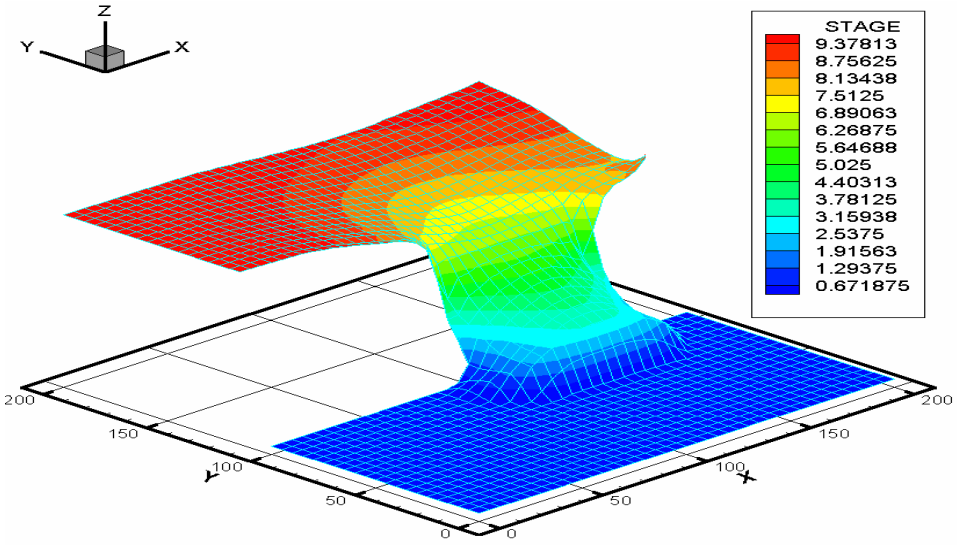

Fig. 4.2.4-4. 3-Dimensonal Perspective View of Water Surface at time = 7 s for Problem 4.2.4

An animation showing the two-dimensional dam break over the entire simulation period is attached in Appendix A (File Name: dambk2d_dry(4-2-4).avi).

4.3 Preliminary Field Applications Using WASH123D

WASH123D is developed to be a primary, first-principle, physics-based tool to simulate realistic, real-world, field problems. In this section, six example problems are presented to illustrate the types of problems that WASH123D can be used for field applications. No attempt is made to conduct thorough calibration and verification studies because this is not the purposes of this report. Preliminary calibrations have been made for some of the examples though. The first example involves the modeling of aquifer storage recovers. The second example is to design a spreader canal. The third example is the application of WASH123D to Biscayne Bay Coastal Wetland (BBCW) watershed to investigate the redistribution of overland flows and the overland fluxes to Biscayne Bay. The fourth example involves the modeling of stormwater treatment area (STA). The fifth example is the employment of WASH123D to model reservoirs and canal networks in Northern Beach County in Florida. The sixth example is the employment of WASH123D to model interactions among canal networks, overland flow, and subsurface flow in Dade County in South Florida.

4.3.1 Aquifer Storage Recover (ASR)

Aquifer Storage and Recovery (ASR) is means to store fresh water deep underground in brackish water aquifers. This stored water can be recovered at a later date during emergencies or times of water shortage. ASR is expected to provide a cost-effective solution to many of the world's water management needs. However, the quality of the stored water may degrade over time due to mixing and buoyancy stratification. Water quality may further be reduced during extraction due to upcoming of saline water underlying the ASR well. This water quality degradation may reduce the volume of the available fresh water during recovery to the point that the ASR well is no longer cost effective.

A simple case of a single ASR well is simulated. Some data is referred to the 1989 ASR pilot project at Lake Okeechobee, Florida (CH_2M Hill, 1989). But overall it is for demonstration purpose only. Three-dimensional density driven flow and transport is simulated. The injected freshwater is stored and mixed with the brackish water in the aquifer. The diameter of the ASR well is 24 inches. The screened area is located at 1,300 ft to 1,600 ft below land surface. So the storage zone is in the artesian aquifers with a confining layer of 400 ft overlying it. The saturated hydraulic conductivity is 177.6 ft/day. The effective porosity is 0.25. Only the storage zone will be simulated. The thickness of the aquifer is 300 ft. A rectangular area, with a scale of 1,600 x 1,600 ft is chosen for the modeling domain. The boundary is set far away from the ASR well, so that injected water is stored within the domain.

Specified head boundary conditions are assigned in the direction of natural groundwater flow to represent the background groundwater flow. Variable boundary conditions are specified at the perimeter of the ASR well. The boundary condition at the screen of the ASR well can be specified head or flux depending on the injection pumping pressure. During the recover period, the head condition is specified on the boundary.

The three-dimensional finite element mesh contains three layers. The total number of subsurface nodes is 3,280 and the total number of elements is 4,674. The size of the elements is designed to be finest within the vicinity of the well (Fig. 4.3.1-1).

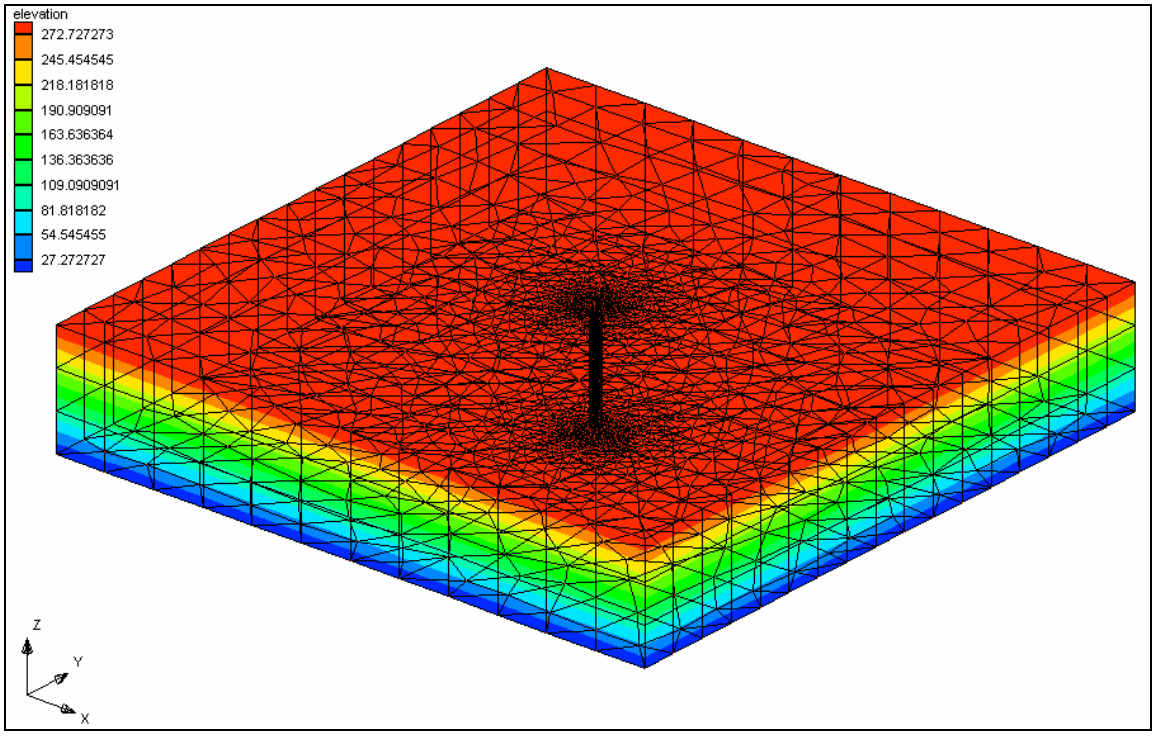

Fig. 4.3.1-1. Three-Dimensional Finite Element Mesh for ASR

The injection/recovery processes were simulated for 720 hours. The injection stopped at time = 360 hours and then recovery started till the end of the simulation. The total head distributions and saline concentrations at different times were plotted in Figures 4.3.1-2 to 4.3.1-5 and Figures 4.3.1-6 to 4.3.1.9, respectively, in the following. The spatial distributions of the total head and concentration presented these figures demonstrated the impact of the background flow and density effect.

From the animations (Files totalhead_inject(4-3-1).avi and totalhead_recov(4-3-1).avi in Appendix A), it is seen that the steady-state simulations were achieved in one–time step. This is so because the compressibility of the water and media were assumed zero which makes the aquifer specific storativity zero. On the other hand, from the animation (File concentration(4-3-1).avi in Appendix A), one can see that the concentration distribution is highly transient. This is so because the storage coefficient for salt transport is the porosity of the aquifer.

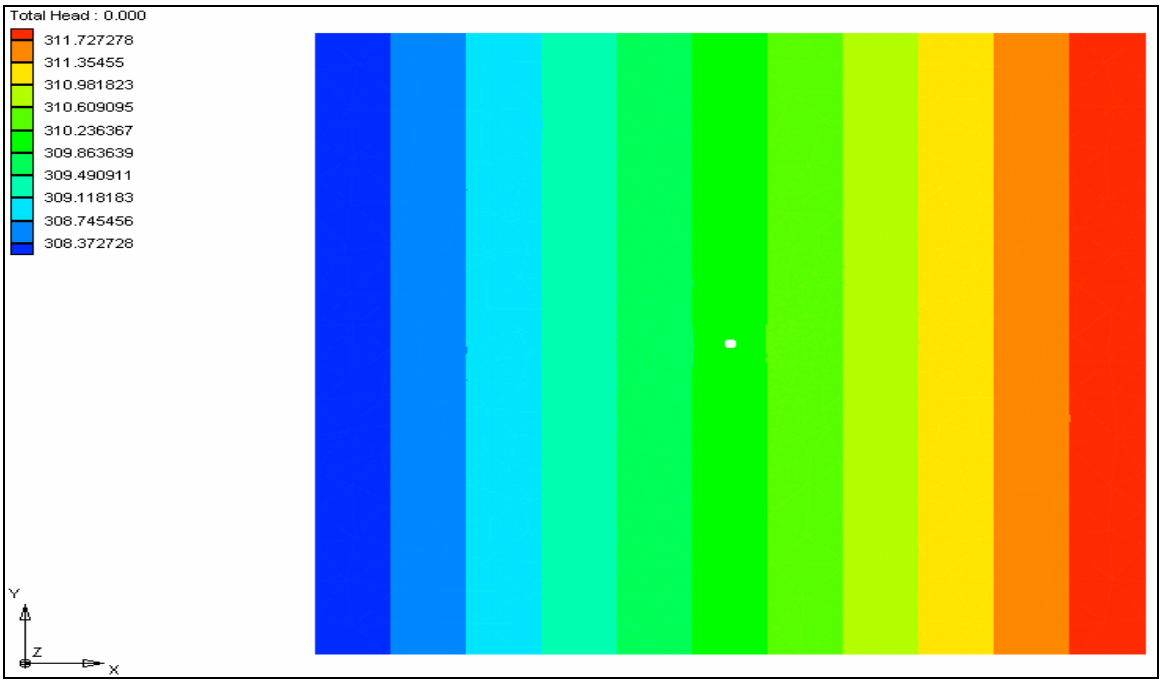

Fig. 4.3.1-2. Total Head Distribution (Time = 0 hour)

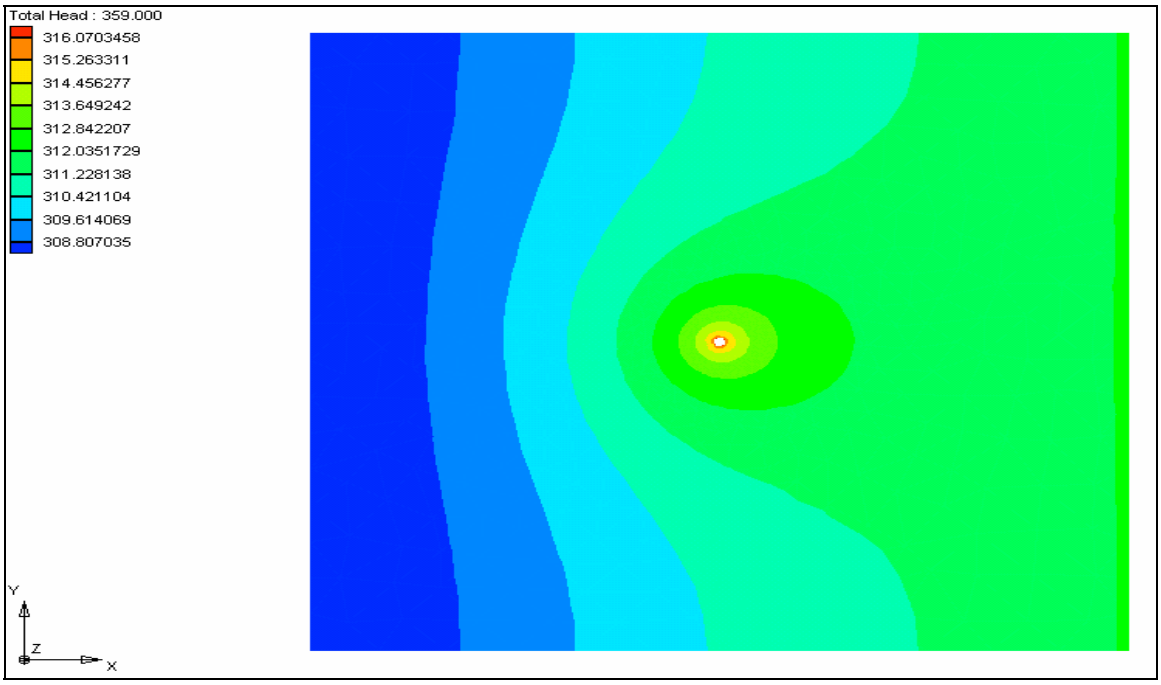

Fig. 4.3.1-3. Total Head Distribution (Time = 359 hours)

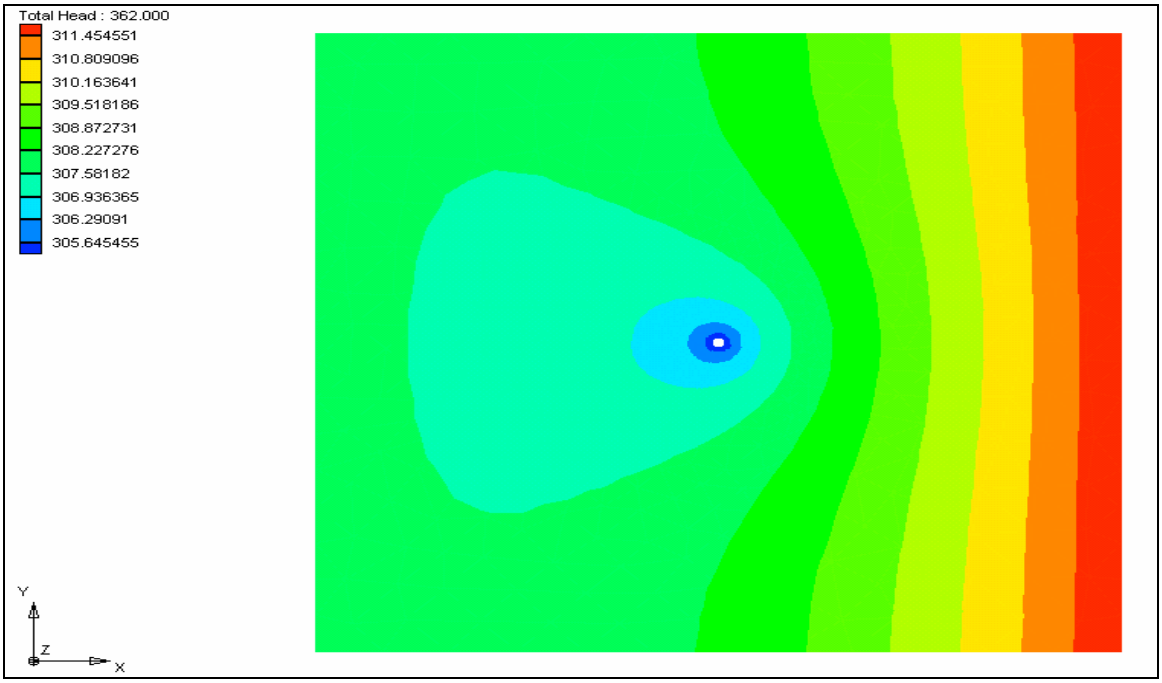

Fig. 4.3.1-4. Total Head Distribution (Time = 362 hours)

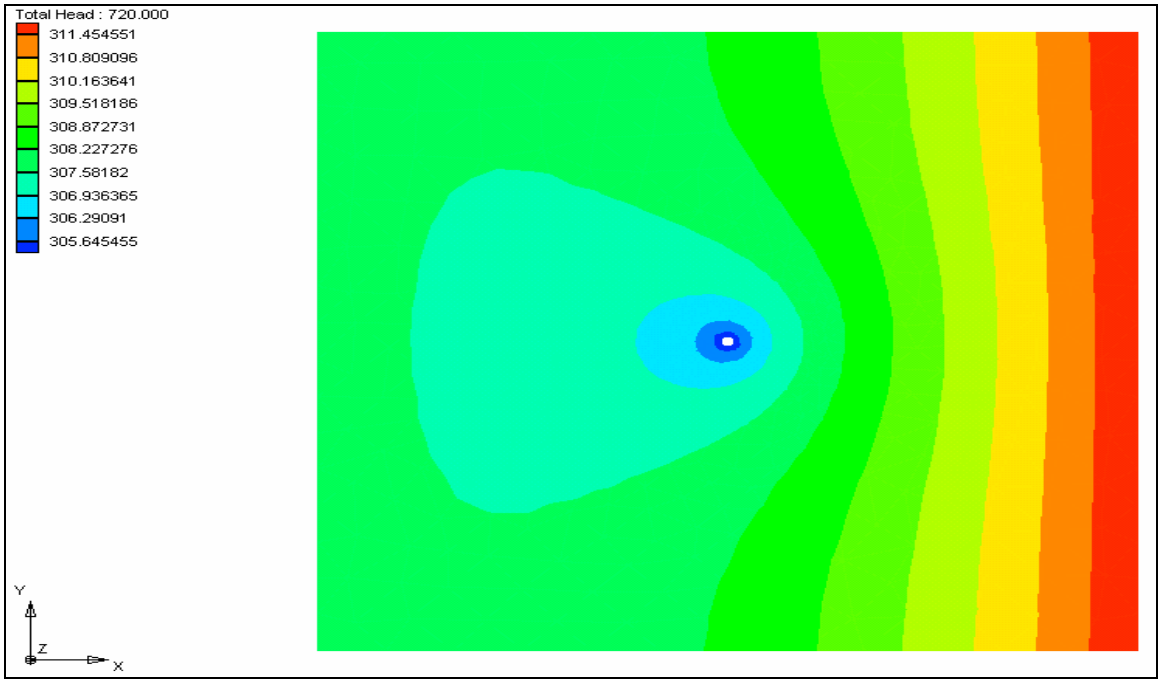

Fig. 4.3.1-5. Total Head Distribution (Time = 720 hours)

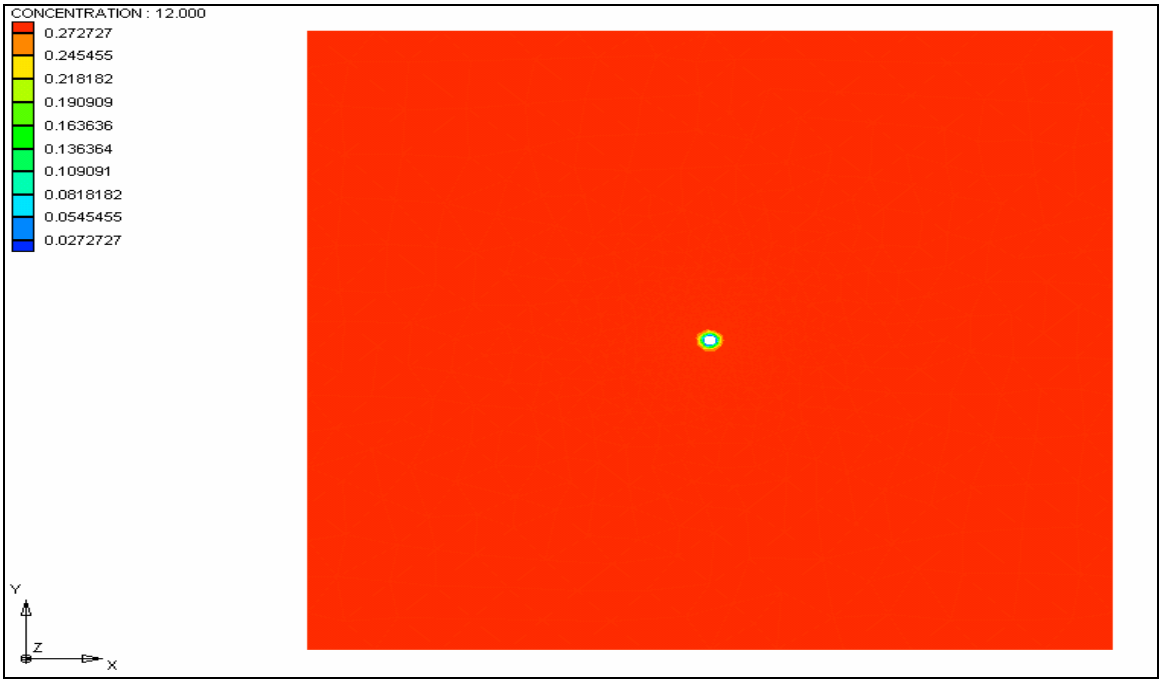

Fig. 4.3.1-6. Saline Concentration at Time = 12 hours

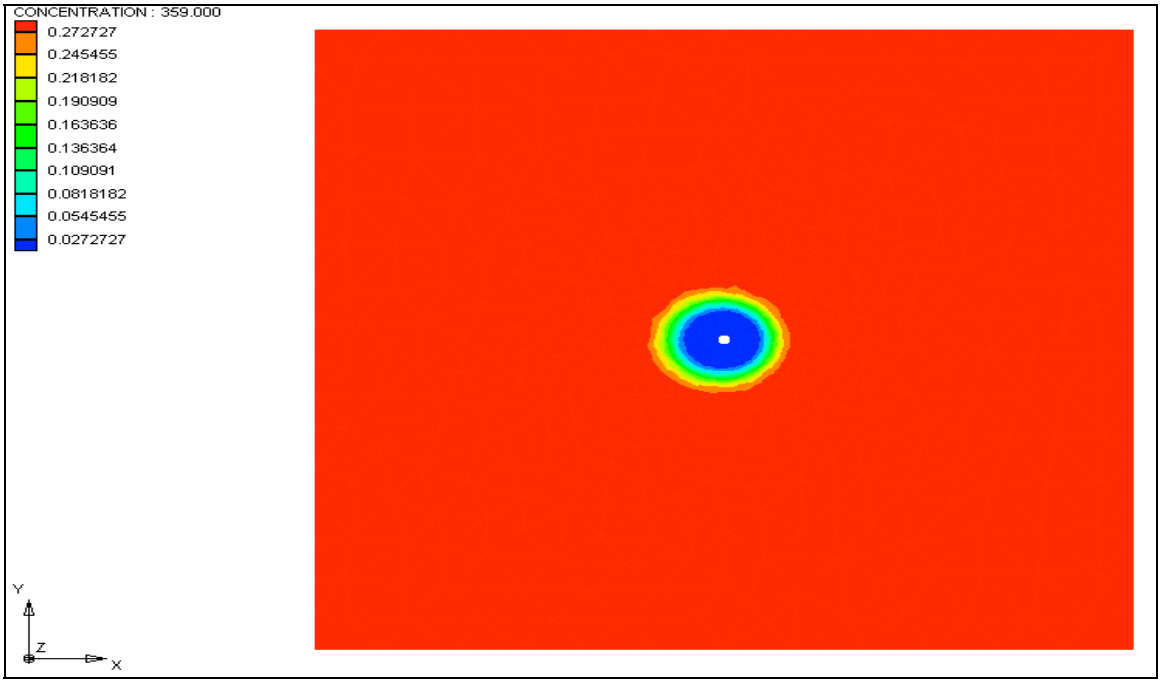

Fig. 4.3.1-7. Saline Concentration at Time = 359 hours

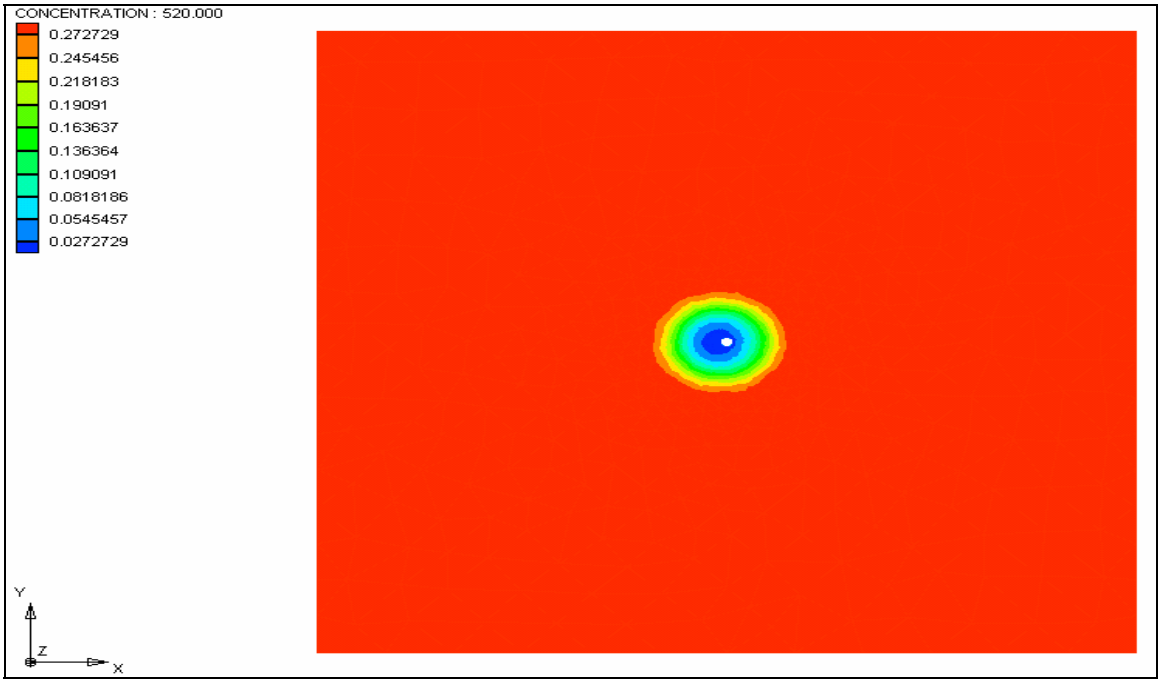

Fig. 4.3.1-8. Saline Concentration at Time = 520 hours

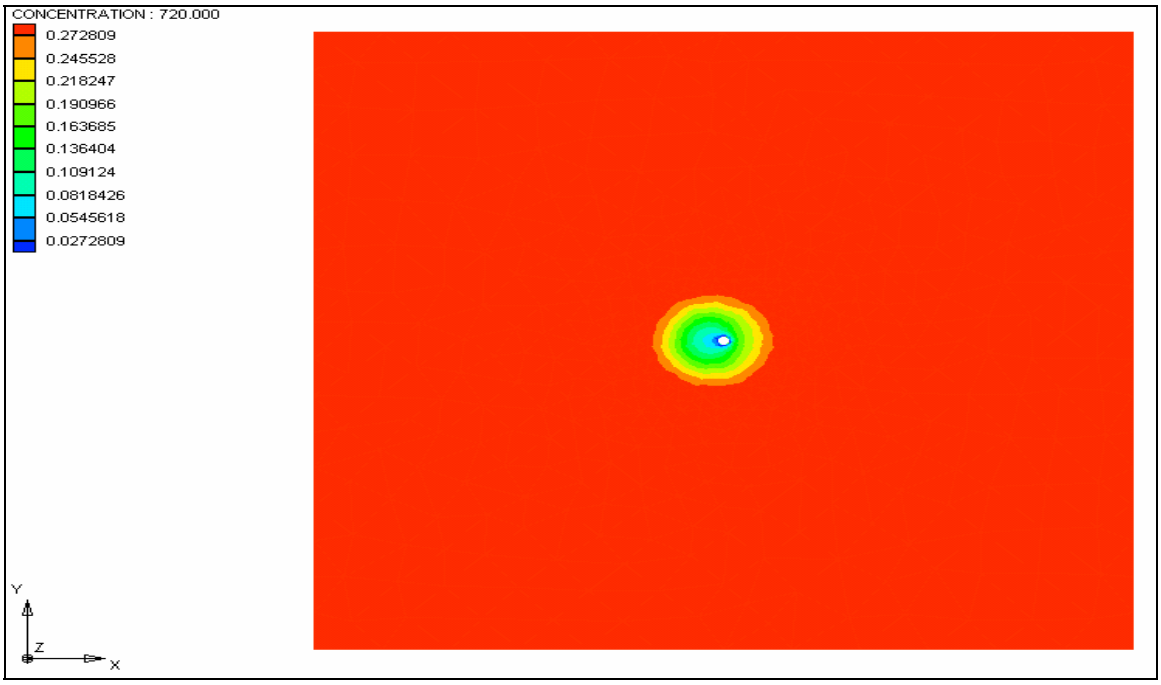

Fig. 4.3.1-9. Saline Concentration at Time = 720 hours

4.3.2 Design of a Spread Canal

The Biscayne Bay Coastal Wetlands (BBCW) Project is one component of the more than 60 restoration plans and has a goal to restore the coastal wetlands area in Central and South Biscayne Bay along its western shoreline. In the existing condition, fresh water plumes emanating from the mouths of canals and well-defined ditches can create local freshening of Biscayne Bay that can be harmful to sea grasses and the ecology of Biscayne Bay. Current restoration efforts in southern Florida are examining alternative water management plans that could change the quantity and the timing (Q & T) of freshwater delivery to the bay by restoring coastal wetlands along its western shoreline of the Biscayne Bay. In contrast to these well-defined surface features, shallow water wetlands can diffuse the introduction of fresh water into Biscayne Bay. Using wetlands to recharge fresh water into the groundwater system can be useful to minimize fresh water plumes extending into Biscayne Bay and to help minimize and/or impede saltwater intrusion. One scenario to address this effort is to create a spreader canal system to redistribute available surface water entering the area from the regional canal system (Cheng, et al., 2004). The spreader canal system would consist of a delivery canal and shallow swales (i.e., spreader canals) where water flows across the swale banks and becomes a more natural overland flow through existing coastal wetlands. Studying such a scenario on a design level involves the modeling of a coupled flow system of 1D canal network, 2D overland, and 3D subsurface.

The top of Figure 4.3.2-1 depicts a conceptual model of a spreader canal system. As water is introduced from a delivery canal, the spreader canal is designed to distribute water to its downstream wetland area in order to reduce the impact to the ecological system of the bay that is further downstream. The bottom of Figure 4.3.2-1 presents two scenarios that are associated with the spreader canal and need to be accounted for by the computational model: the left one shows a scene in which canal water is kept in canal, while the right one has canal water stage high enough to contribute to the downstream overland area. In the left case, the canal collects water from its upland surface (overland and canal waters are separate here) but has no contribution to its downland surface area. In the right case, the canal receives water from its upland surface on one hand and gives out water to its downland surface (canal and overland waters are connected here) on the other hand. When the subsurface is also taken into account, surface-subsurface interactions through infiltration and seepage (red arrows in Figure 4.3.2-1) may play crucial roles in determining subsurface water table, overland water depth, and canal water stage. In WASH123D, flux continuity is ensured on the medium interfaces, while state variable continuity is imposed when waters between two media are connected.

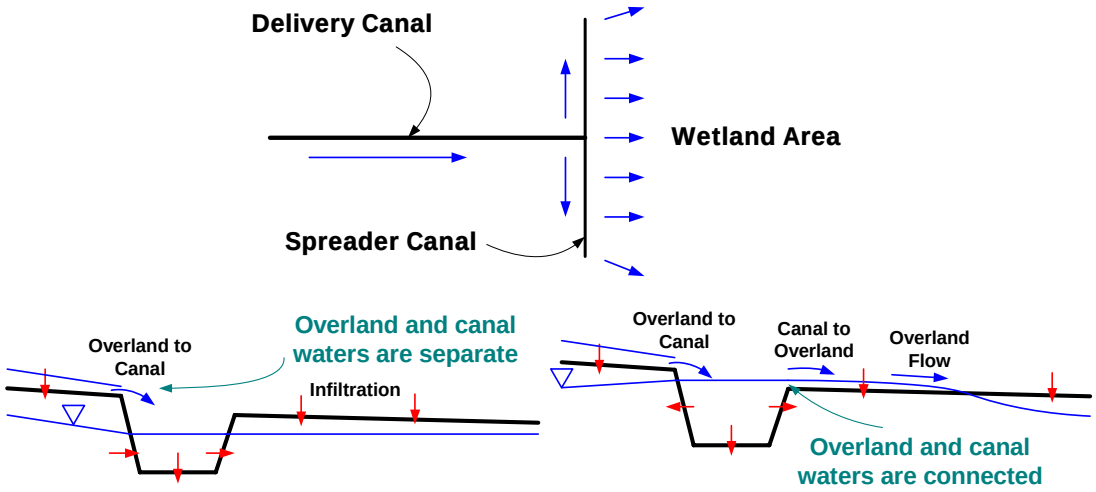

Fig. 4.3.2-1. A Conceptual Model (top) and Two Scenarios (bottom) of the Spreader Canal

This hypothetical example demonstrates how WASH123D may help model and design a spreader canal system that includes one-dimensional canal, two-dimensional overland, and three-dimensional subsurface flow. It used the topographic data in the BBCW project area (Fig. 4.3.2-2) to construct the discretized domain of interest. The study area of this example is marked in Figure 4.3.2-2. A spreader canal was placed in the domain to distribute water that came in from the west boundary (marked with a red A in Figure 4.3.2-3). The two-dimensional overland domain, which covered an area of approximately 1.1 square miles, was discretized with 28,340 elements and 14,390 nodes, where the mesh size was about 50 ft. The one-dimensional canal embraced 91 elements, 94 nodes, one upstream boundary node (A in Figure 4.4.2-3), two dead ends (DE1 and DE2 in Figure 4.3.2-3), and one junction (J in Figure 4.3.2-3) to connect the three canal reaches. The underlying three-dimensional domain contained 113,360 elements and 71,950 nodes. The width of the assumed rectangular canal was set 90 ft for Reach 1, 20 ft for Reach 2, and 60 ft for Reach 3 (Figure 4.3.2-3). The cross-sectional area was proportional to the depth, where the depth of the spreader canal was computed by solving one-dimensional diffusive wave equations.

The Manning's roughness was set to 0.015 for two-dimensional overland flow and 0.008 for one-dimensional canal flow. The subsurface medium was sandy loam and was assumed homogeneous through the entire domain, where the saturated hydraulic conductivity was 1,000 ft/day. The soil retention curves for the unsaturated zone were generated with the van Genuchten functions.

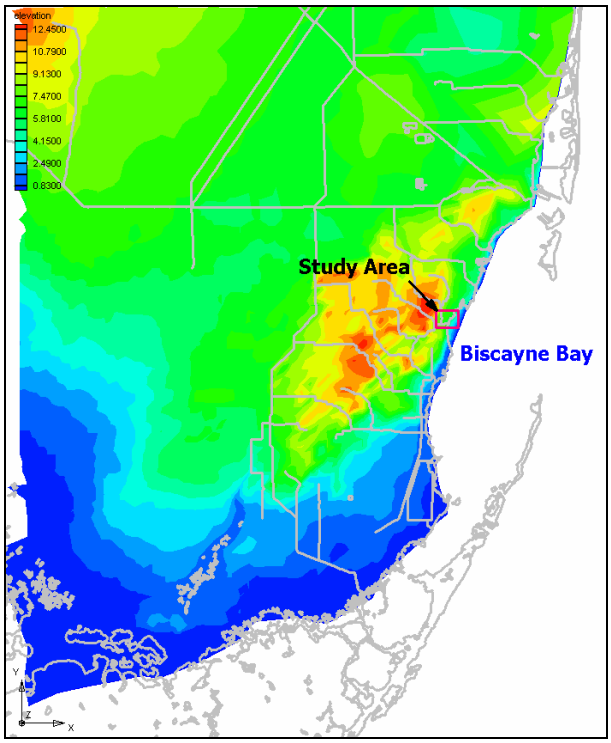

Fig. 4.3.2-2. Location of the Simulated Area of the Demonstration Example

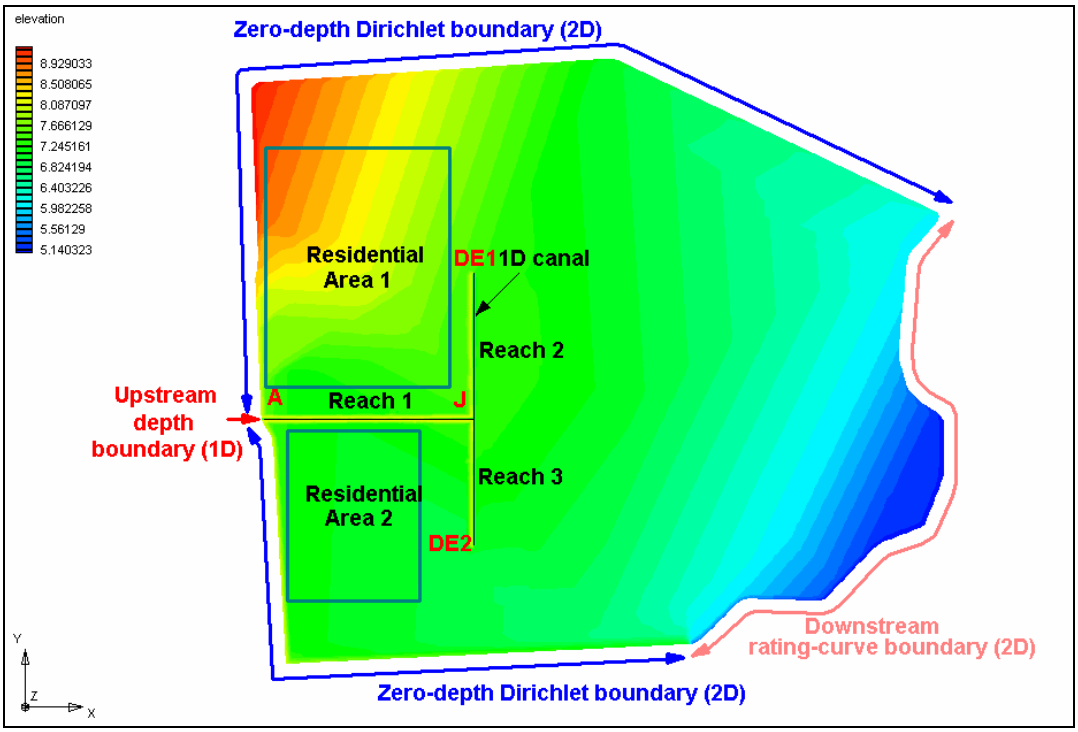

Fig. 4.3.2-3. 1D canal and 2D Overland Boundary Conditions Used for the Demonstration Example

In computing one-dimensional canal flow, a time-dependent water depth was given in Table 4.3.2-1 as the upstream boundary condition for the incoming water as indicated in Figure 4.3.2-3; a zero-velocity condition was applied at the two downstream dead-end nodes; and the continuity of both flow rate and water stage was enforced at the canal junction. In computing two-dimensional overland flow, its north, west, and south boundaries were imposed the zero-depth boundary condition throughout the simulation; a depth-dependent flux (i.e., rating curve) was given on the downstream depth-dependent (rating curve) boundary (Fig. 4.3.2-4); and a canal-overland interaction boundary condition was specified for the canal-related overland boundary sides, which includes (1) a depth-dependent flux when water flowed from overland to canal and overland water and canal water were separated and (2) a canal stage condition when flooding occurred (i.e., when overland water and canal water were connected). In computing three-dimensional subsurface flow, an interface boundary condition that accounted for the interaction between surface and subsurface waters was applied to the top boundary face of the three-dimensional domain; three total head boundary conditions were employed for (1) the subsurface boundary nodes associated with the one-dimensional canal upstream boundary node on the west vertical boundary face (time-dependent head that matches one-dimensional upstream boundary condition at the inlet (i.e., A in Fig. 4.3.2-3), (2) all the subsurface nodes, except those mentioned in (1), on the west boundary (a constant head of 7.12 ft), and all the subsurface nodes on the east boundary face (a constant head of 4.95 ft) as shown in Figure 4.3.2-4; and an impermeable boundary condition for the rest of the vertical boundary face and the bottom boundary. It is noted that for the vertical boundary face with total head specified, the Dirichlet boundary condition applied only to the boundary nodes below water table (i.e., in the saturated zone). For the vertical boundary face that was above water table, an impermeable boundary condition was assumed.

Table 4.3.2-1 Upstream Water Depth Boundary Condition used for the 1D Canal Flow

Time (seconds)	0	600	3600	7200
Depth (ft)	0.5	0.58	0.88	1.28

The initial pressure head in the subsurface was computed by solving the steady-state version of Richards' equation with a constant rainfall rate of 1.0×10^{-9} ft/s, while a constant water depth of 0.5 ft was enforced at the three-dimensional boundary nodes that were corresponding to one-dimensional spreader canal nodes and zero water depth was assumed at those corresponding to two-dimensional overland nodes. For a demonstration purpose, such setup allowed us to expect water flow from the spreader canal to its neighboring overland regime within a short period of time after the transient simulation began. As the transient simulation began, the rainfall rate of 1.0×10^{-9} ft/s was applied throughout the entire simulation period of 2 hours. The time-step size was 60 seconds for computing three-dimensional subsurface flow, 2 seconds for computing two-dimensional overland flow, and 0.01 second for computed one-dimensional canal flow. The absolute error tolerance was 1.0×10^{-5} ft for determining nonlinear convergence in computing one-dimensional, two-dimensional, and three-dimensional flow, respectively.

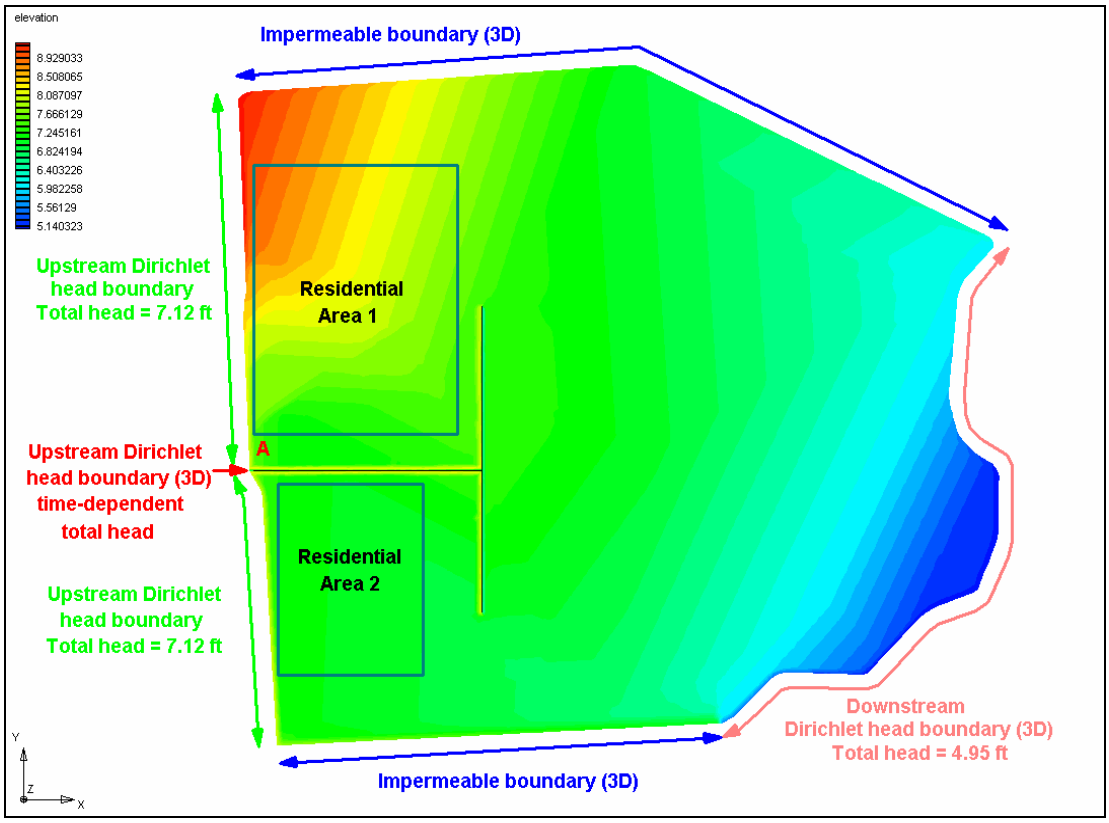

Fig. 4.3.2-4. 3D Subsurface Boundary Conditions used for the Demonstration Example

Figure 4.3.2-5 shows the distribution of water depth on the 2D overland (left) and 3D subsurface pressure head on ground surface (right) at time = 2 hours. On the right half of the figure, the portion shaded with blue color has groundwater below ground surface, while the portion without shade has water table reach ground surface. It is seen that most water coming out from Reach 3 of the spreader canal to overland is due to natural terrain (the north ground was higher than the south ground). And because the ground south to the second dead end (i.e., DE2) was so flat, water coming out of spreader canal near DE2 could flow westward and affect the southeast corner of Residential Area 2. Moreover, as water stage increased with time in Reach 1 (not shown), which was subject to the increasing upstream water depth over time (Table 1), seepage through levee was observed around the upstream section of Reach 1 even though there was no water flow over the bank of Reach 1 throughout the simulation. This, as a result, would cause problems for people living in the north part of Residential Area 2 based on the topography around this area (Fig. 4.3.2-6).

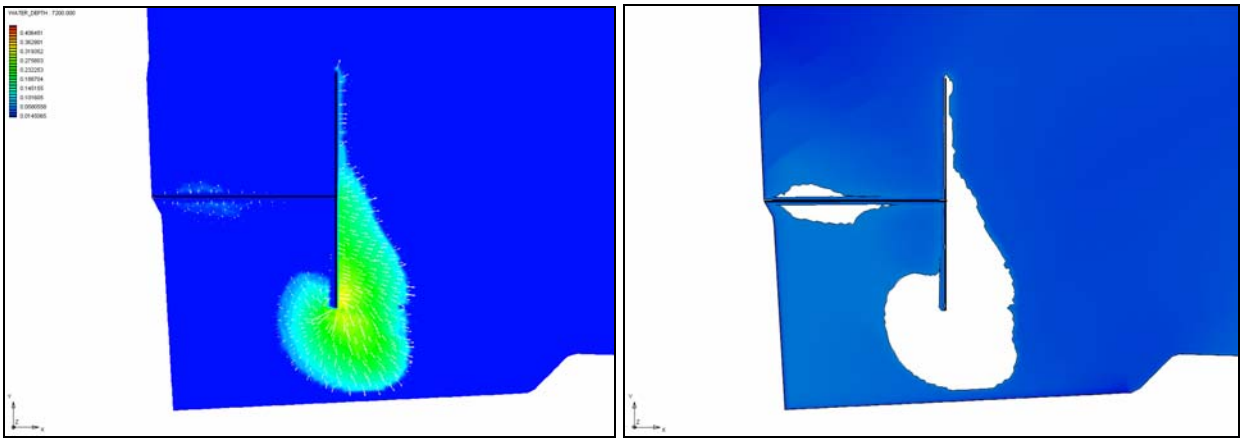

Fig. 4.3.2-5. 2D Overland (left) and 3D Subsurface (right) Flow results of Case 1 at Time = 2 hr

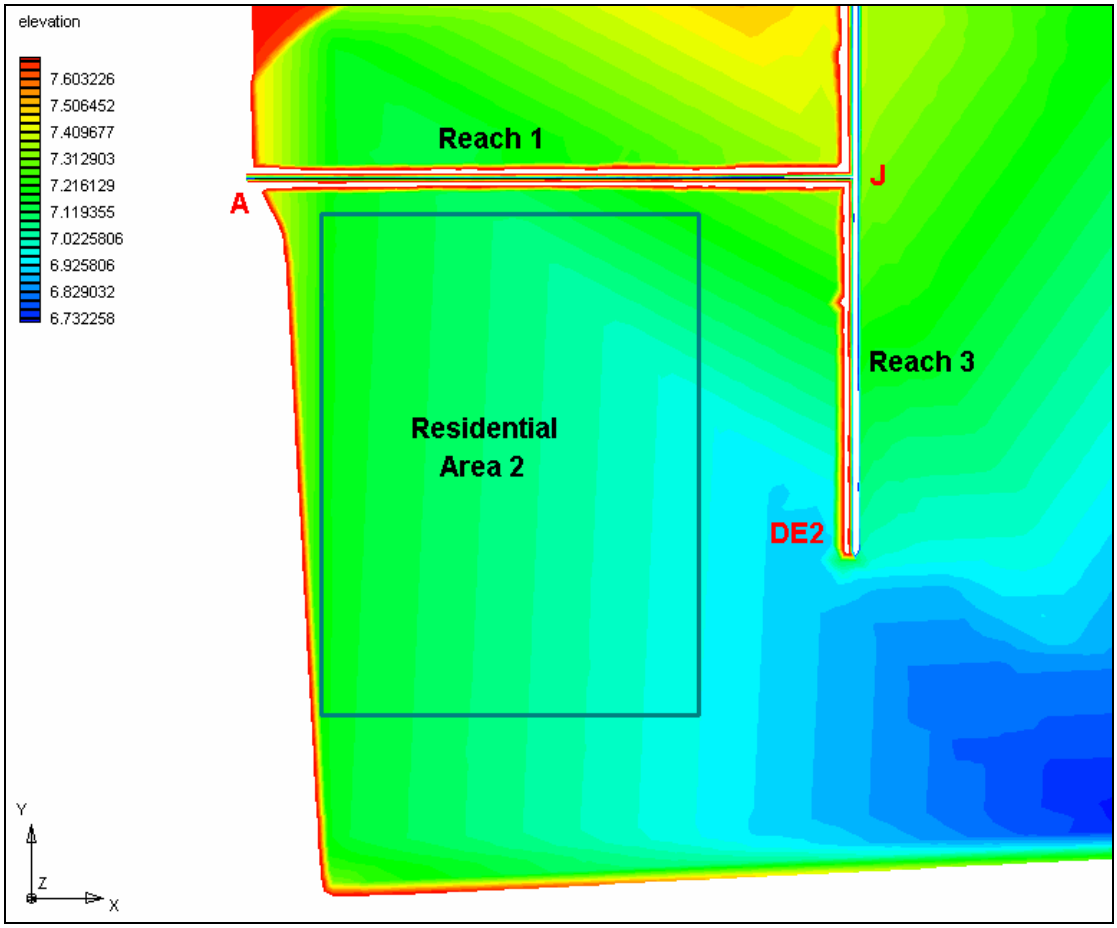

Fig. 4.3.2-6. Topo of Residential Area 2 and its Neighborhood Before an Extended Levee Was Applied

To protect Residential Area 2 from getting flooded, a waterproof liner was installed in Reach 1 and an additional levee from DE2 to the south overland boundary (Fig. 4.3.2-7) was considered in this study. Table 4.3.2-2 lists the three cases included in this study: Case 1 serves as the base case where neither a liner nor an additional levee is adopted; Case 2 has the liner; and Case 3 has both. Figure 4.3.2-7 shows the topography around Residential Area 2 after an additional levee was applied. Figures 4.3.2-8 and 4.3.2-9 show the computational results of Cases 2 and 3, respectively, which are corresponding to Figure 4.3.5 for comparison. It is obvious from Figure 4.3.2-8 that the waterproof liner has prevented seepage from occurring. From Figure 4.3.2-9, the extended levee has successfully stopped overland water from entering Residential Area 2.

Table 4.3.2-2 Three Cases in the Demonstration Example

Case 1 (base case)	Case 2	Case 3
No liner in Reach 1	Liner in Reach 1	Liner in Reach 1
No extended levee	No extended levee	Extended levee applied

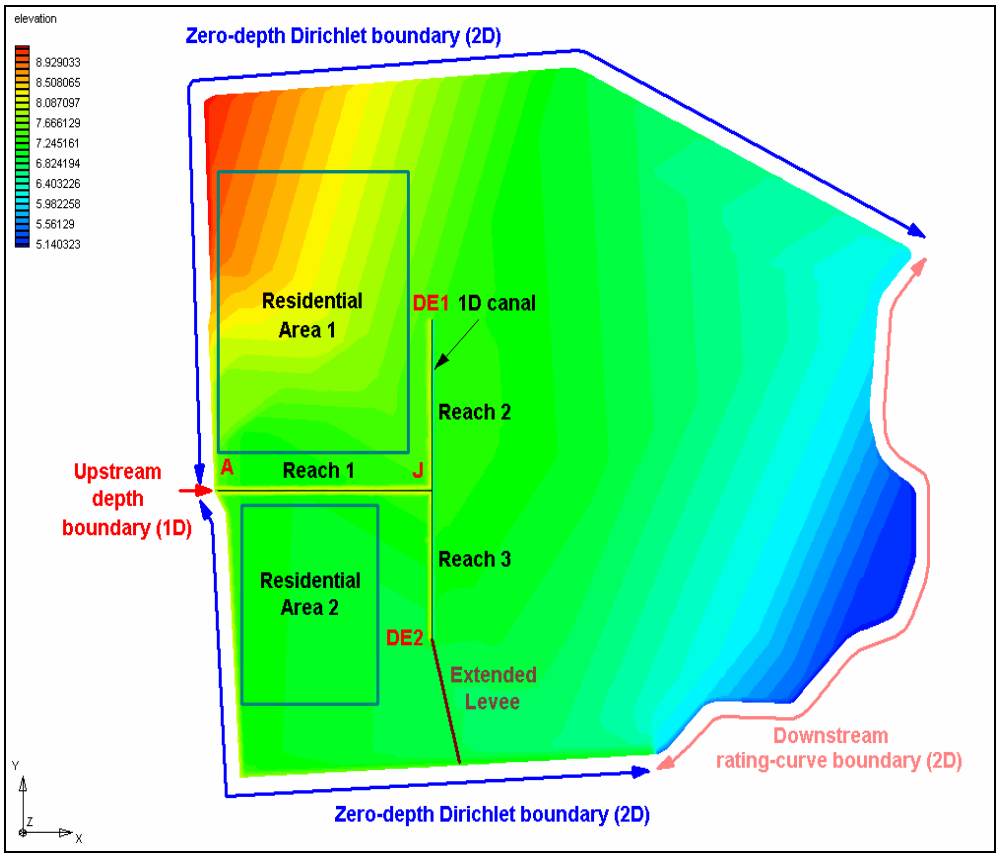

Fig. 4.3.2-7. With an Extended Levee to Prevent Flooding in Residential Area 2 (left) and the Topography of Residential Area 2 and its Neighborhood after an Extended Levee Was Applied.

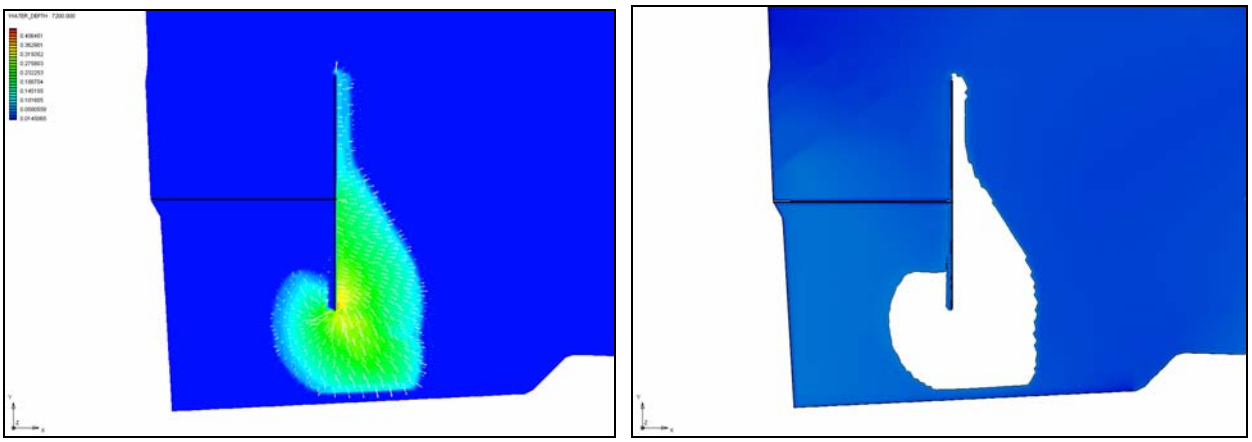

Fig. 4.3.2-8. 2D Overland (left) and 3D Subsurface (right) Flow Results of Case 2 at Time = 2 hr

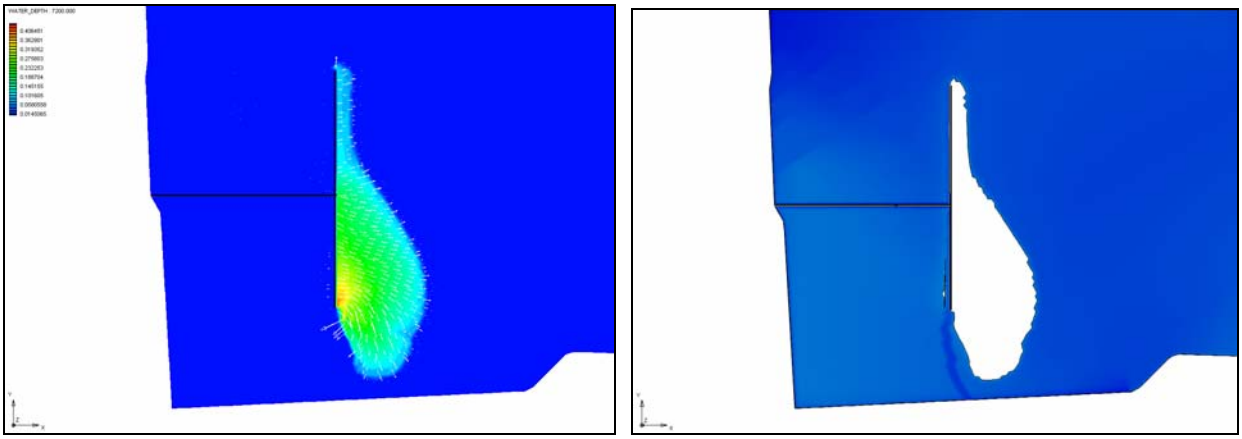

Fig. 4.3.2-9. 2D Overland (left) and 3D Subsurface (right) Flow Results of Case 3 at Time = 2 hr

In studying a spreader canal system on the design level, such as the demonstration example above, a couple of important issues were revealed. First, a high-resolution mesh is needed to achieve desired goals on the design level. In the demonstration example, for instance, canal water was successfully directed to the downstream overland without impacting Residential Area 2 after a liner and an additional levee were installed. However, canal water was not evenly distributed to overland (Fig. 4.3.2-9) as desired. To accurately determine what alternatives may help evenly distribute water, a high-resolution mesh that allows modelers to adequately catch most important physical processes and necessary details is a MUST.

Animations showing the spatial-temporal distribution of water depths and groundwater tables for Cases 1 (DE_1_wd.avi and DE_1_wt.avi), Case 2 (DE_2_wd.avi and DE_2_wt.avi), and Case 3 (DE_3_wd.avi and DE_3_wt.avi), respectively, are attached in Appendix A. Readers can visualize these moves by clicking the file contained in the attached CD.

4.3.3 Biscayne Bay Coastal Wetland (BBCW) Watershed Modeling.

The Biscayne Bay Coastal Wetland (BBCW) Project is one of more than 60 projects included in the federally approved Comprehensive Everglades Restoration Plan and has a ultimate goal to restore or enhance freshwater wetland, tidal wetland, and near shore bay habitat. The primary purpose of the BBCW project is to redistribute runoff form the watershed into the Biscayne Bay, away from the canal discharge that exists today and provide a more natural and historical overland flow through the existing and or improved coastal wetlands. This example presents the modeling effort to restore the wetlands including modeling approaches, building hydro-geologic conceptual model, selecting model domain and boundaries and calibrating model parameters. Discussions of calibration and preliminary results were given elsewhere (Lin et al., 2004).

WASH123D (Yeh et al., 2003) was used to develop the BBCW flow model. This flow model conceptualizes the BBCW watershed as a combination of 1D canal network, 2D overland flow regime, and 3D subsurface media. The graphical user interface GMS5.1 was used to construct the hydro-geologic conceptual model for the BBCW project area. Figure 4.3.3-1 shows the BBCW project area. Figure 4.3.3-2 shows the solids model generated from borehole data. Figure 4.3.3-3 shows the computational mesh for the BBCW flow model.

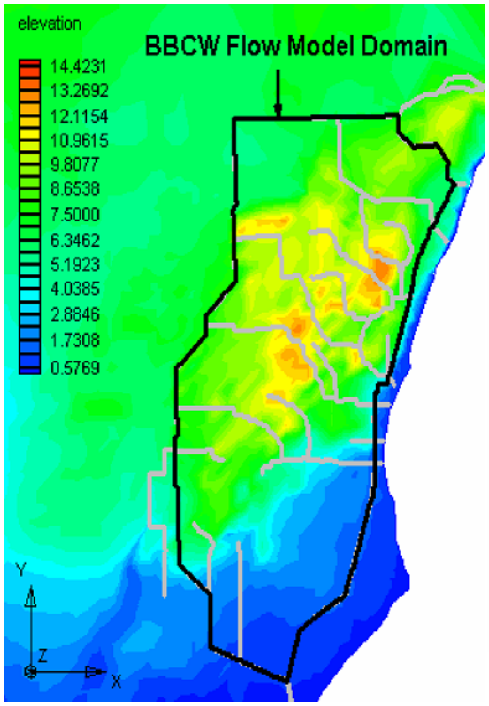

Fig. 4.3.3-1. BBCW Project Area

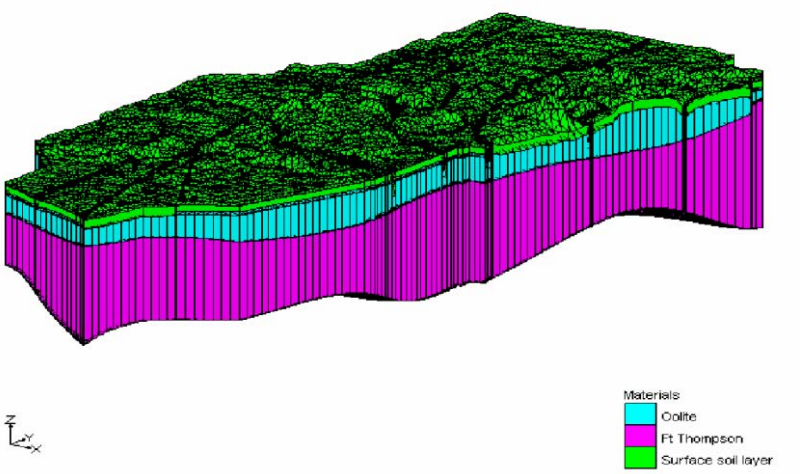

Fig. 4.3.3-2. Solid Model for the BBCW Project Area

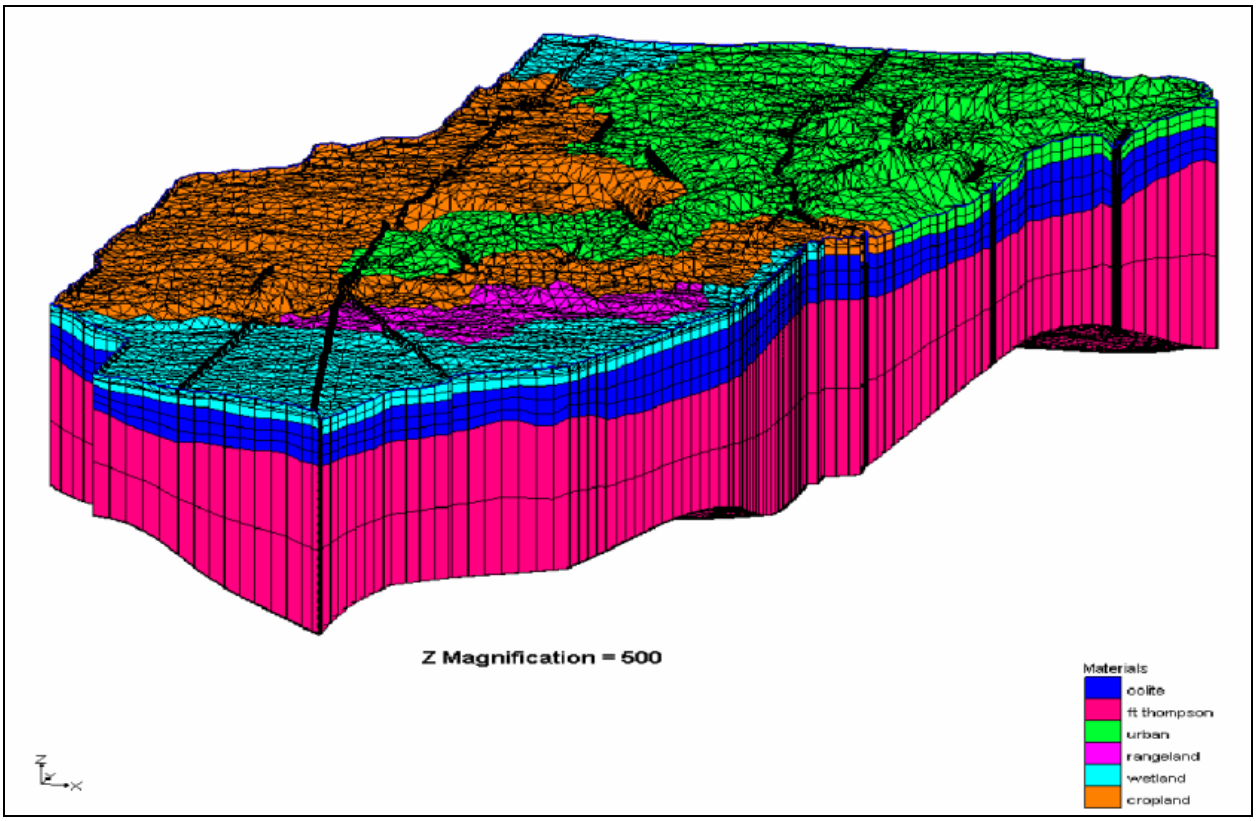

Fig. 4.3.3-3. Computational Mesh
(2D Nodes = 8,339; 2D Elements = 16,388; 3D Nodes = 66,712; 3D Elements = 114,716)

Figure 4.3.3-4 shows the 2D boundary conditions assigned to the model. Flux boundary was specified at the east side of model boundary. Observed stages were prescribed at the internal canals. Time-dependent rainfall and evapotranspiration (ET) were obtained from field measurements. Figure 4.3.3-5 shows the locations of rain gages and Figure 4.3.3-6 depicts the locations of ET gates.

Figure 4.3.3-7 shows the 3D boundary conditions assigned to the model. Continuity of flux and/or heads were imposed on the surface-subsurface interface. Observed heads and stages were specified on the 3D vertical side boundary. Impermeable condition was assumed on the bottom boundary. Internal head boundary conditions were prescribed along the canals. Time-dependent pumping rates and water levels in observation wells were obtained from field measurements. Figure 4.3.3-8 shows the locations of pumping wells and Figure 4.3.3-9 depicts the locations of observation wells.

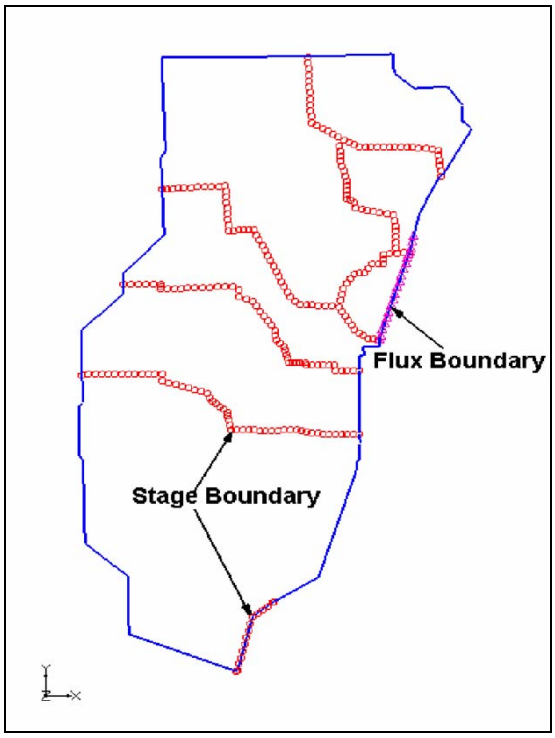

Fig. 4.3.3-4. 2D Boundary Conditions

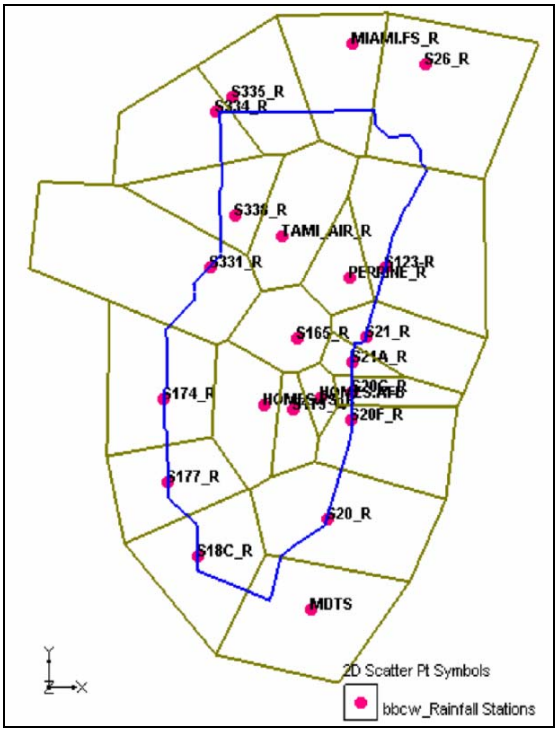

Fig. 4.3.3-5. Locations of Rain Gages

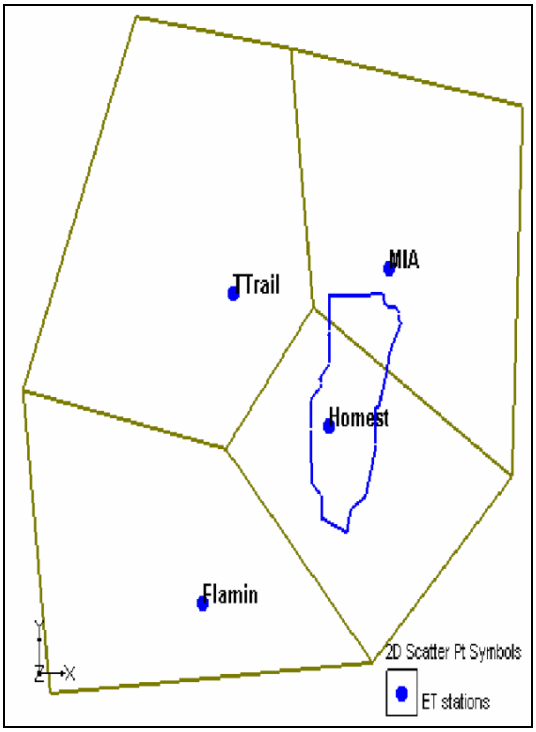

Fig. 4.3.3-6. Locations of ET Gages

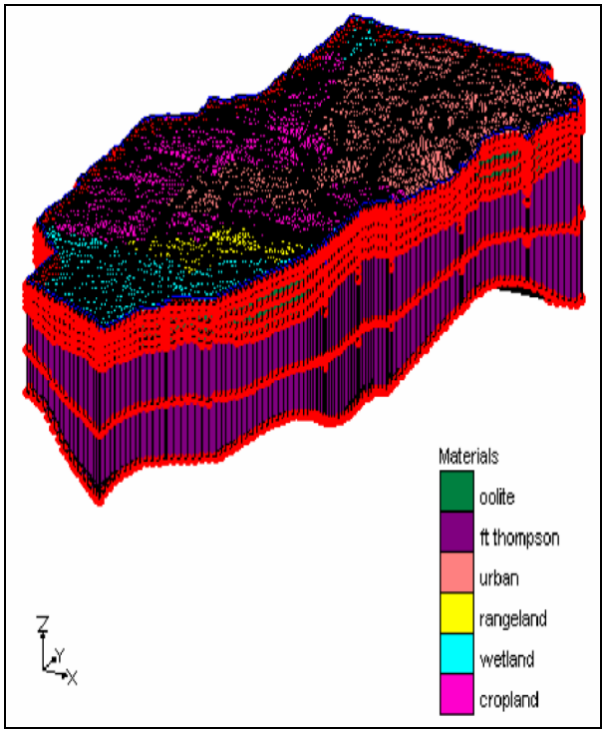

Fig. 4.3.3-7. 3D Boundary Conditions

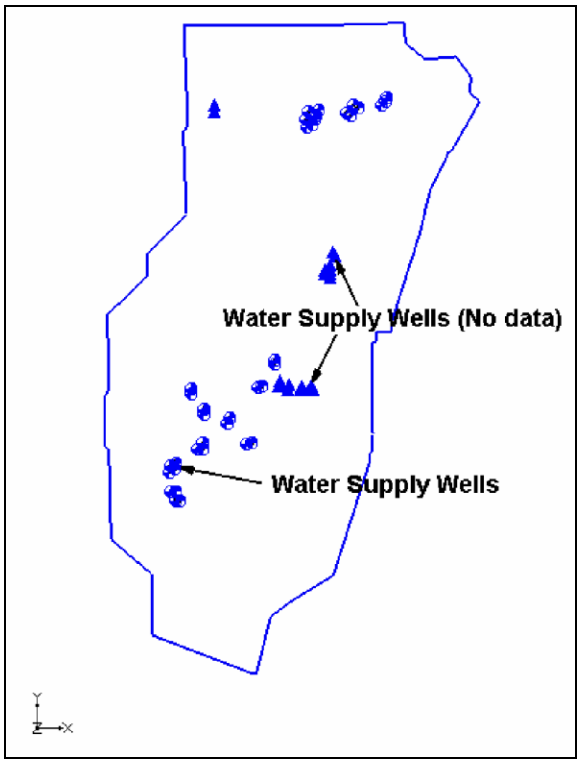

Fig. 4.3.3-8. Locations of Pumping Wells

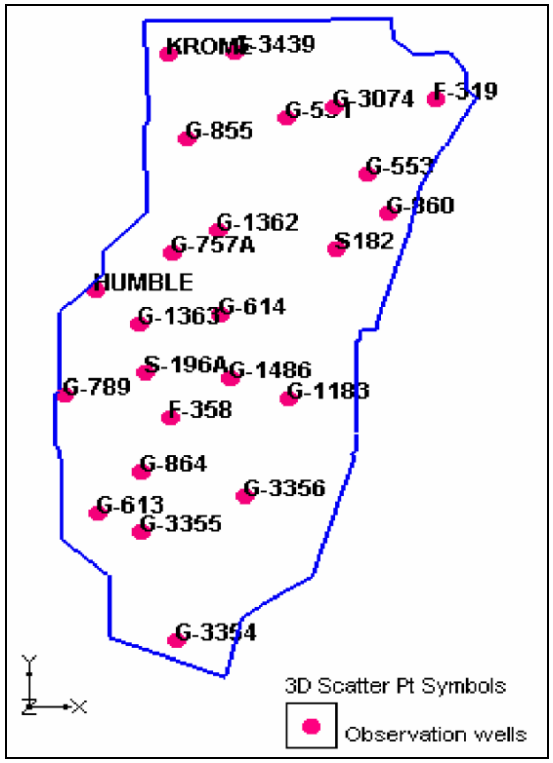

Fig. 4.3.3-9. Locations of Observation Wells

In model calibration with WASH123D, an approach of four steps is employed so that the more model runs can be performed and run time can be saved. Step 1: Calibrating coupled 2D/3D flow model. Step 2: Calibrating the 1D flow model. Step 3: Verifying the calibrated model obtained from Step 1 and Step 2. Step 4: Validating the coupled 1D/2D/3D model. This report presents primary results of Step 1. The complete modeling activity of the BBCW project is still undergoing and should be referred elsewhere (Cheng et al., 2006).

Table 4.3.3-1 lists the estimated range of hydraulic conductivities used in the beginning of the calibration processes.

Table 4.3.3-1 Estimated Hydraulic Conductivity for Initial Guesses in Calibration

Geologic Unit	Hydraulic Conductivity range (ft/day)
Top surface soil layers	0.01 to 10
Miami Oolite	10,000 to 40,000
Ft Thompson Formation	1000 to 20,000

The observed stages of overland flow and groundwater wells from May 1, 1999 through April 30, 2000 are used for the model calibration. Four samples of plotting the computed and the observed values at four represented locations are shown. Figure 4.3.3-10 shows the plotting results in east coastal ridge area (S-182). Figure 4.3.3-11 shows the plotting results in the water supply wells area

(G-551). Figure 4.3.3-12 shows the plotting results in the east of Homestead airport (G-1363). Figure 4.3.3-13 shows the plotting results of Model Land area (G_3354)

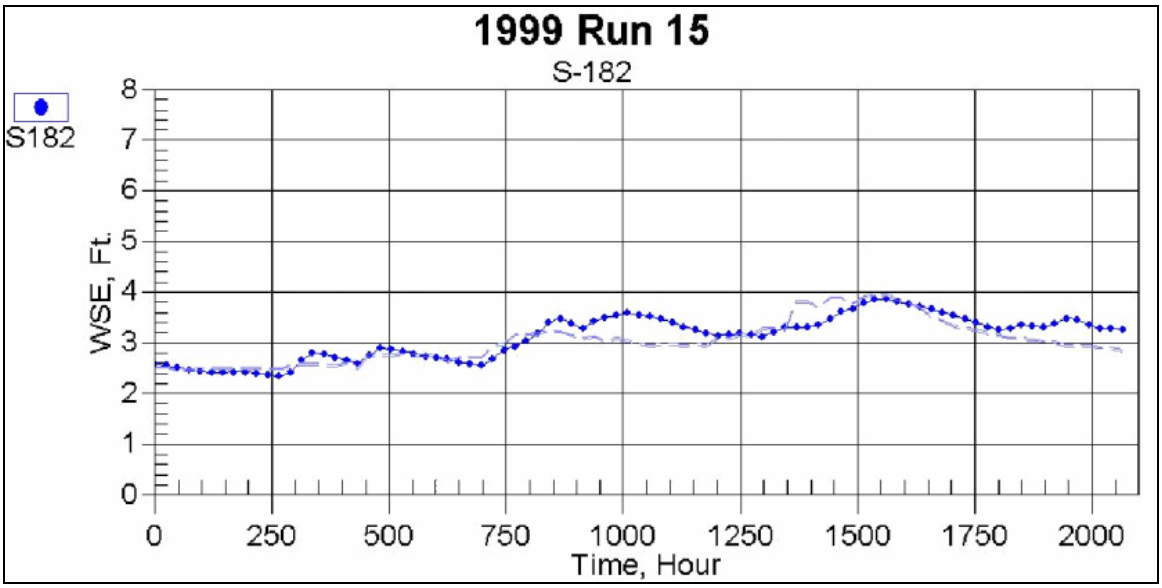

Fig. 4.3.3-10. Results in the East Coastal Ridge Area (S-182)

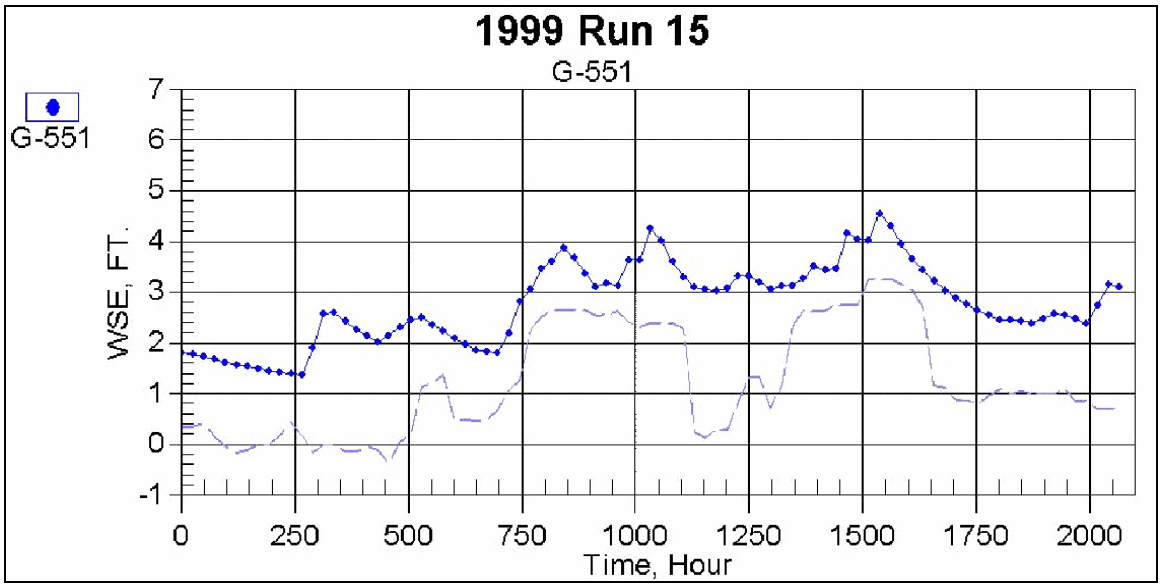

Fig. 4.3.3-11. Results in the Water Supply Area (G-551)

Fig. 4.3.3-12. Results in the East of Homestead Airport (G-1363)

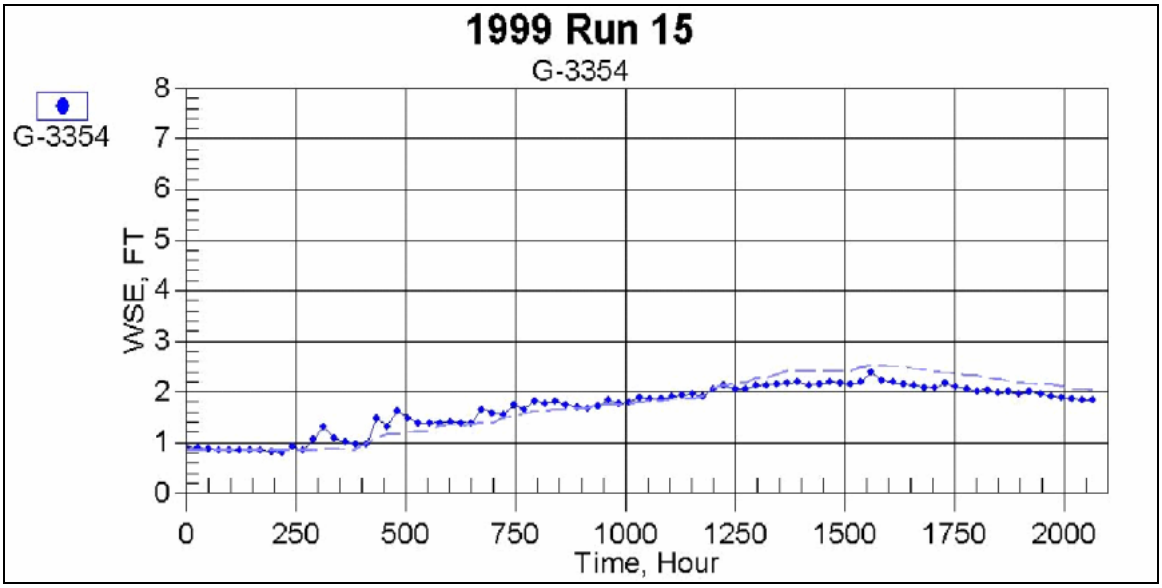

Fig. 4.3.3-13. Results in the Model Land Area (G-3354)

Figures 4.3.3-10 through 4.3.3-13 indicate that the model responds well to the observed stage fluctuations except for the case near the water supply wells and the computed stages are sensitive to the rainfall events as comparison to observed stages. Further investigation is needed to find out the discrepancies between simulations and measurements near the supply wells.

4.3.4 Stormwater Treatment Area.

Artificial treatment wetlands have been extensively used for wastewater treatment or stormwater nutrient removal in the United States of America. Typically, these surface water impoundments are built for flow-through treatment of stormwater by plant intakes of nutrients or pollutants.

In south Florida, the Everglades restoration effort has led to the design and construction of a series of constructed wetlands called Stormwater Treatment Areas (STAs) to reduce phosphorus level from stormwater runoff before they can enter the Everglades protection areas (SFWMD, 2004a). These constructed wetlands were located on former natural wetlands or farmlands that have strong hydraulic connection with the underlying highly conductive surficial aquifers.

Until recently, the hydraulic models applied for the design and management of these STAs are quite limited in scope and details. Most built models are two-dimensional model for steady state flow (for example, Burns & Mcdonell, 2000, 2003 and SFWMD, 2001). They are good for design purpose or as a screening tool but lack some important details. More detailed two-dimensional hydraulic models of existing STAs are being built for management and operation needs. They are calibrated and validated with historic time series data, considering only the two-dimensional surface flow (Sutron Corporation, 2004).

RMA2 (Norton, et al., 1973) and FEMWMS-FLO2DH (Froehlich, 2002) are the two popular two-dimensional surface water flow model codes for modeling wetland hydraulics. They were originally developed for coastal hydrodynamic modeling. Some limitations need to be addressed before they can be applied for wetland simulations. The incorporation of hydraulic structures, explicit representation of rainfall and evaporation, and treatment of wetting and drying are some examples. Swain et al. (2004) has described their experience in adapting and modifying the USGS SWIFT2D (Leendertse, 1987) originally developed for coastal tidal flow, to simulate the southern Everglades wetland hydrology. WASH123D does not have these limitations (Yeh et al., 2005).

This WASH123D application is an example of coupled surface/subsurface water flows in a constructed wetland for stormwater treatment in south Florida. Stormwater generated from farmlands is flown through the wetland for nutrient removal by wetland plants. The inflow and outflow rates are controlled by hydraulic structures. A significant portion of the inflow volume can be infiltrated into the highly conductive surficial aquifer.

Current two-dimensional hydraulic models cannot handle seepage losses properly. An integrated surface/groundwater model is needed to study the losses through bottom and perimeter levees due to dynamic interactions of surface flow within and groundwater flow underneath the treatment area. One-dimensional canal flow is also needed to simulate inflow/outflow and seepage collection. The impact of neglecting seepage loss is a likely distorted hydraulic model.

The purpose of a hydraulic model of a constructed wetland is to evaluate the hydraulic performance under different flow conditions. The hydrodynamic component is also a pre-requisition of the reactive transport computation because the transport and fate of nutrients including phosphorus and nitrogen are described with biogeochemical reactive transport equations. All these modeling

objectives can be effectively acheved using WASH123D.

The study area selected for this demonstrative modeling study is a typically constructed wetland in south Florida. The background information is excerpted from the STA-6 data (SFWMD, 2004b). The total area of the treatment cells is about 870 acres. There is a supply canal along the western boundary and a discharge canal located at the eastern boundary. Stormwater runoff is pumped into the north end of the supply canal and enters the marsh area through three inflow weirs. Eventually, treated stormwater is collected by outflow structures and flows into the discharge canal (Figure 4.3.4-1). In Figure 4.3.4-1, the supply canal is adjacent to and in parallel to L-3 borrow canal. The three inflow weirs are labeled as G-601, G-602 and G-603. Stormwater runoff enters the supply canal via the G-600 pump station. The outflow structures are G-354A through G-354C and G-393A through G-393C. They connect the treatment cells 3 and 5 with the discharge canal.

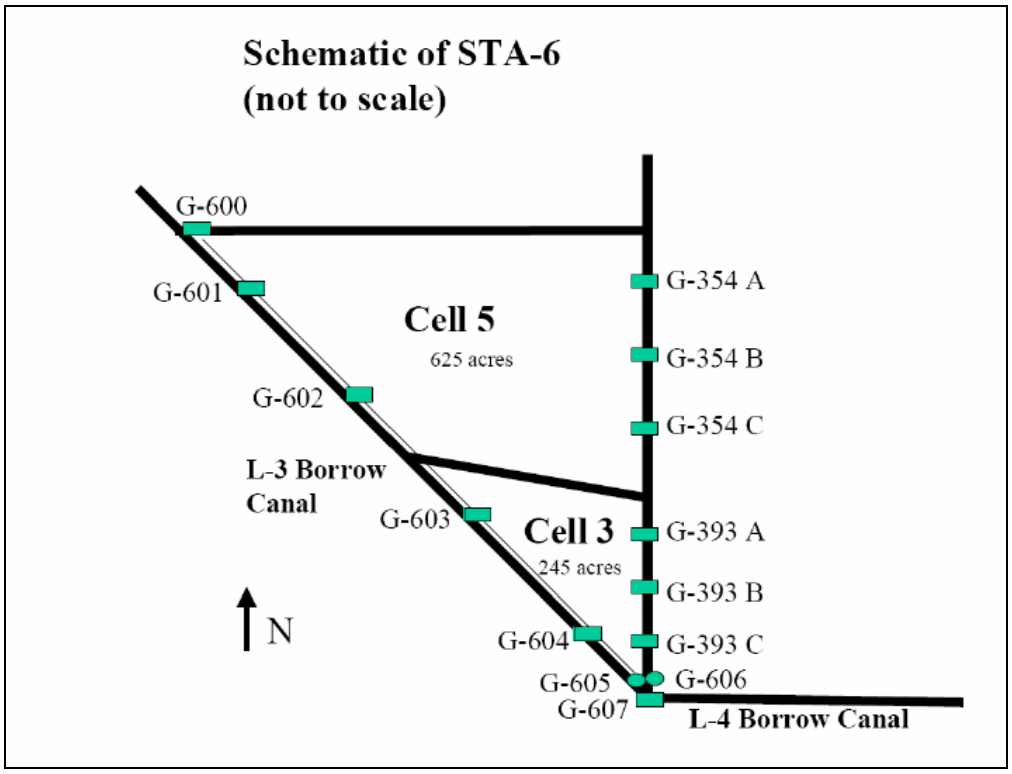

Fig. 4.3.4-1. Schematic Map of STA-6 Layout (SFWMD, 2004b)

The conceptualization of the study area leads to a relatively closed flow system. Stormwater runoff is pumped into the supply canal and flow into the treatment cells through control structures. The treated water is discharged at the downstream into the discharge canal and eventually enters the Everglades protection areas.

The surface water flows can be simulated by two-dimensional surface flow only or by coupled one-dimensional canal flow and two-dimensional flows. Vegetations were built into the treatment cells. They are categorized as emergent cattails and submerged aquatic vegetation (SAV). Previous studies have demonstrated that a water depth-dependent friction coefficient is appropriate for vegetation (Yen, 1992 and Wu et al., 1999). The base value of Manning's n used ranges from 0.095 to 0.95 for the above mentioned vegetation types.

For numerical simulations, the underlying surficial aquifer was vertically divided into several layers, the top two layers, extending from land surface to a few ft in thickness, are the poorly permeable peat and the lower layers are composed of sand or lime rock. Figure 4.3.4-2 shows the three-dimensional finite element mesh, which is made of 8,602 triangular elements with 5,302 nodes, for modeling subsurface flow. For this preliminary simulation, the model domain was selected up to the location of the supply canal and discharge canal. These canals are hydraulic divides for subsurface flow.

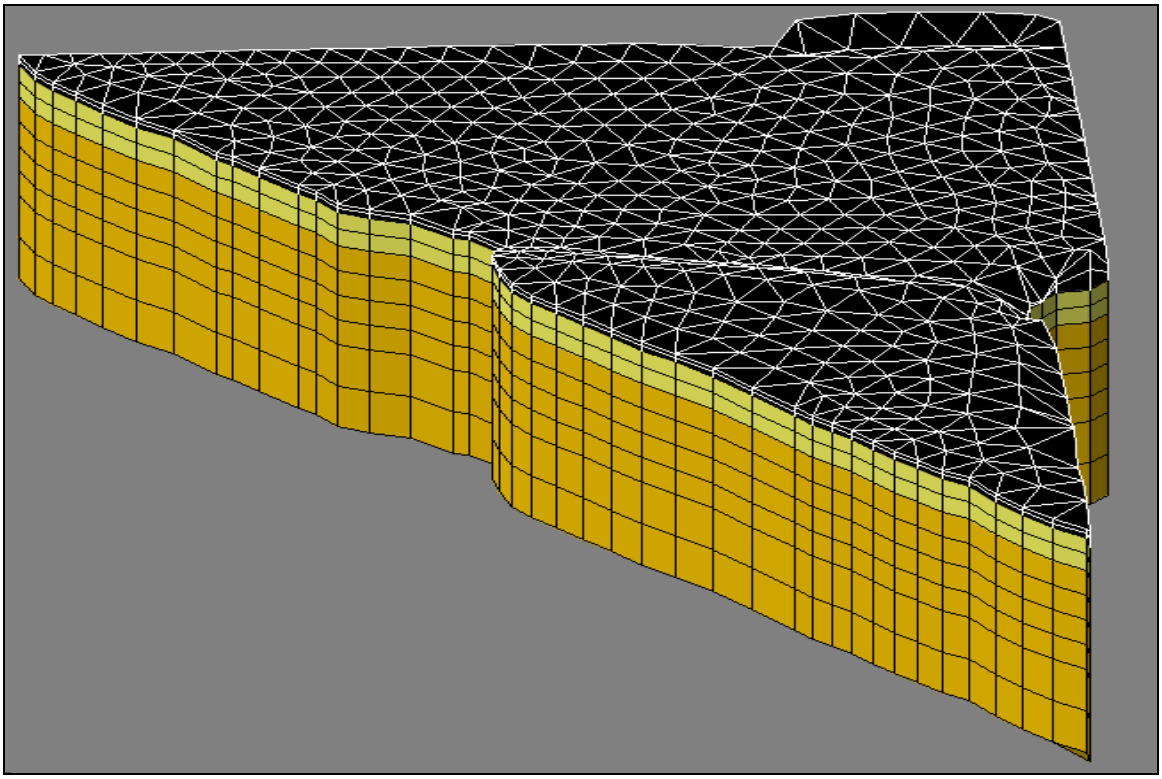

Fig. 4.3.4-2. Three-Dimensional Subsurface Finite Element Mesh

The hydrogeology was obtained from some relevant reference sources (Fish, 1988 and Harvey et al., 2002). Detailed local hydro-geological data was not available and an average value of hydraulic conductivity was applied. The initial value of saturated hydraulic conductivity used in the model runs is listed in Table 4.3.4-1.

Table 4.3.4-1 Value of Hydraulic Conductivity Used in the Simulation

Model Layer	horizontal	vertical	horizontal	Vertical
	Ft/hr	ft/hr	ft/day	ft/day
Layer 1	35	0.35	840	8.4
Layer 2-3	350	3.5	8400	84
Other layers	3500	35	84000	840

A 10-day simulation was carried out with historic flow and stage data. The total simulation time is 240 hours (10 days). A time step of 15 minutes was applied for one-dimensional canal and two-dimensional overland flows and a time step of 12.0 hours was used for three-dimensional subsurface flow. Three cases were simulated.

Firstly, two-dimensional surface flow only was modeled with the diffusive wave approximation. This was compared with model results from solving for the full shallow water equations by other two-dimensional surface water flow codes. Since the diffusive wave approach is applied in simulating the coupled surface and groundwater flows, for consistent, the diffusive wave option rather than the fully dynamic wave option is used in simulating two-dimensional surface water flow only. A by-product of this approximation is to assess the validity of the diffusive assumptions.

A different two-dimensional mesh from that shown in Figure 4.3.4-2 was designed for this case, in which the canals were included as a part of the two-dimensional finite element mesh rather than as an one-dimensional mesh. Simulation results show that the diffusive wave approximation can be applied to such a two-dimensional sheet flow and with the same Manning' n value; the diffusion wave model yields only a slightly higher water level than the full shallow water equations. The water surface elevation at time = 84.0 hours was plotted in Figure 4.3.4-3. Specified stage boundary conditions were applied to the northern end of the supply canal (upper left corner) and the downstream end of the discharge canal (lower right corner), respectively. An animation showing the spatial-temporal distribution of stages is attached in Appendix A (File Name: 2D_only(4-3-4).avi). Readers can visualize this move by clicking the file contained in the attached CD.

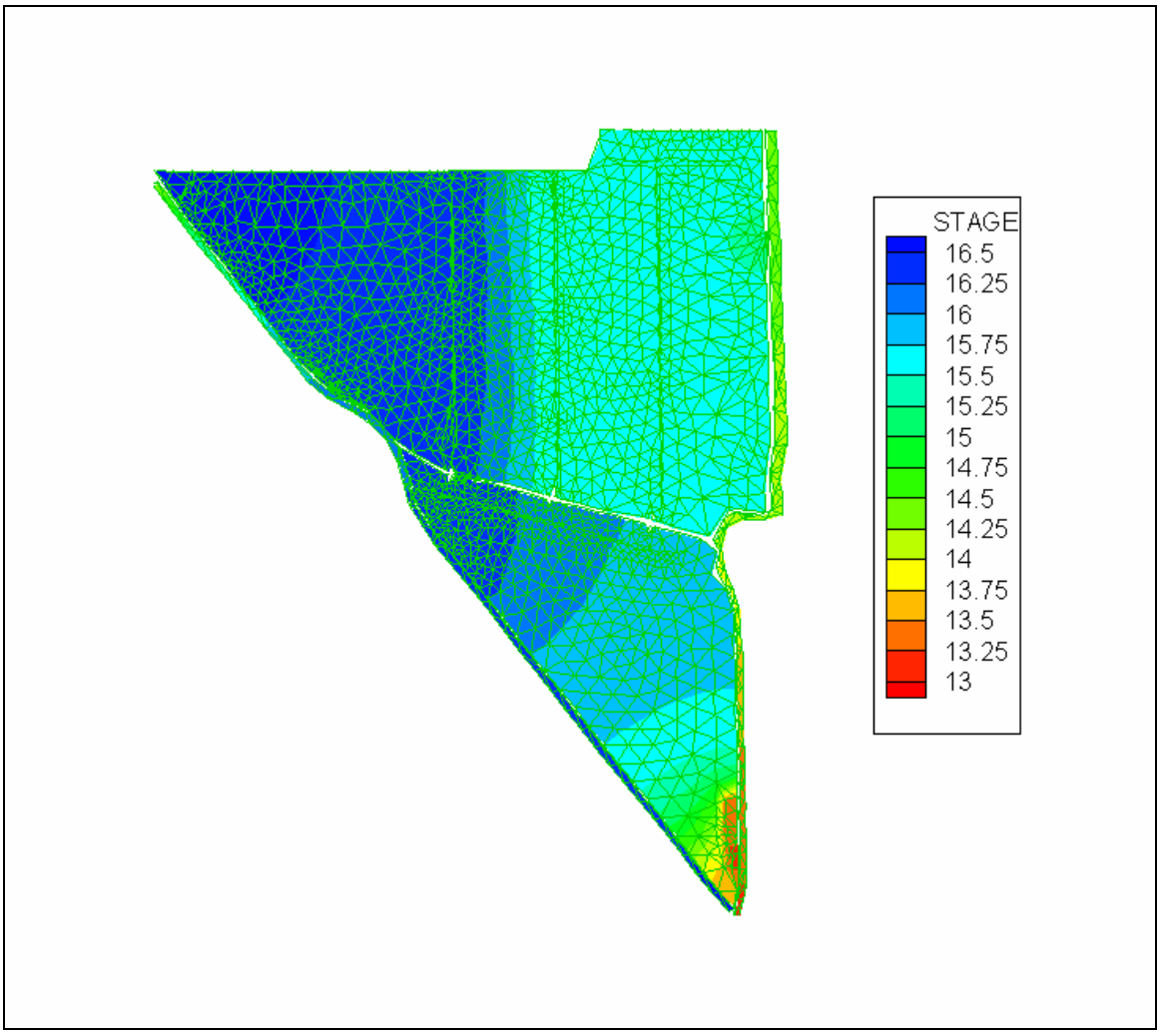

Fig. 4.3.4-3. Simulated Water Surface Elevation at Time = 84.0 hours (ft NGVD)

Secondly, two-dimensional surface flow was coupled with three-dimensional subsurface flow by using the finite element mesh in Figure 4.3.4-2. For this case, the top surface, consisting of 862 triangular elements with 482 nodes, is considered an internal boundary between the two-dimensional overland flow and three-dimensional subsurface flow on which the continuities of volumetric fluxes and pressure head/water depth are imposed. For subsurface flow, a constant specified total head of 10.5 ft NGVD was applied to the boundary nodes of the lower layers to represent the background groundwater flow in the region that is controlled by the maintained canal water level in the surrounding area. Only the vertical seepage through the bottom of the wetland is considered and the detailed geometry of the perimeter levee is not included.

The simulation results demonstrated the impact of seepage on water level in the marsh area (Fig. 4.3.4-4). The water depth at the interior marsh area (for example at node 103 in the overland regime) shows that the consideration of seepage losses has an obvious impact on water level. This indicates that without considering seepage losses, the calibration of two-dimensional hydraulic model may over-estimate model parameters (for example, Manning' n value). The magnitude of this

difference also depends on the hydraulic conductivity value.

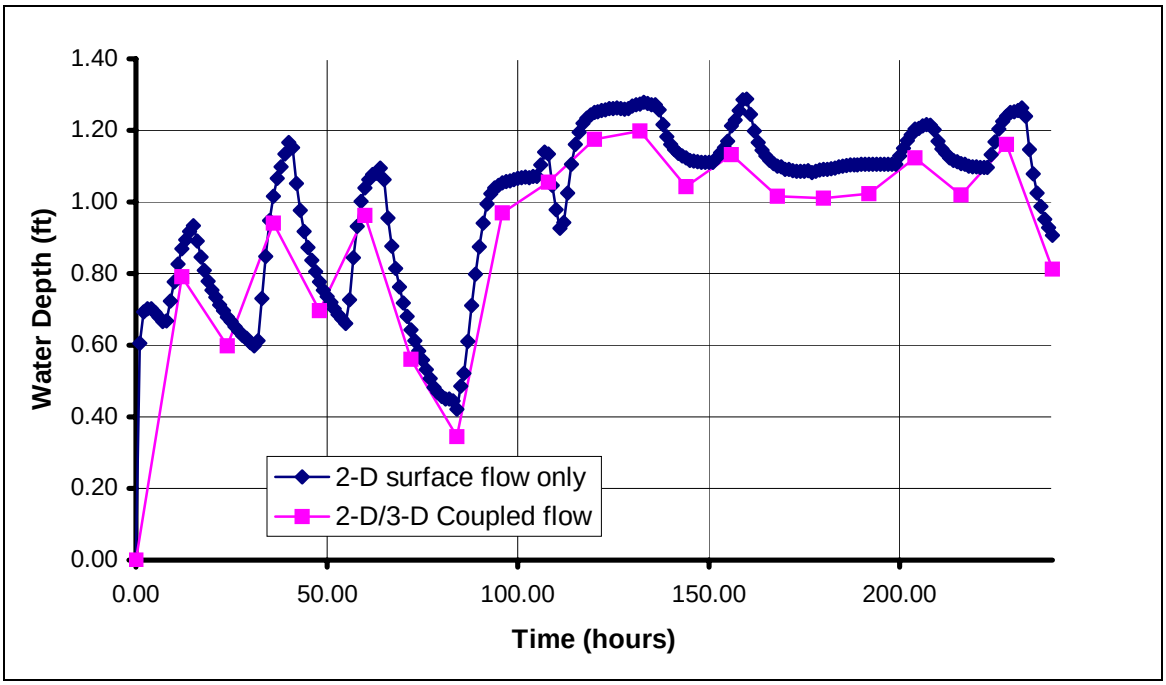

Fig. 4.3.4-4. Water Depth at 2-D Overland Node 103

Thirdly, the flow in supply canals was simulated as one-dimensional channel flow, not included as partial domains of two-dimensional overland flow. It is coupled with overland flow and groundwater flow. The one-dimensional canal flow interacts with two-dimensional overland flow and three-dimensional subsurface flow through their corresponding boundary nodes. In a test model run, the supply canal was simulated with 43 nodes and stormwater enters from the first node and the 43rd node is a dead end. Water was transferred from the supply canal to the treatment cells by two simplistic side weirs. However the discharge canal is considered as a part of the two-dimensional domain. Figure 4.3.4-5 is a contour plot of the vertical component of the subsurface Darcian velocity (ft/hr). It can be seen that the greater magnitude occurs at the vicinity of the supply canal and discharge canal.

The seepage rate depends on the hydraulic gradient and the hydraulic conductivity of the underlying porous media (peat, sand, and limerock). The canals are acting as hydraulic divides for the subsurface flow. The supply canal is a losing stream while the discharge canal is a gaining stream.

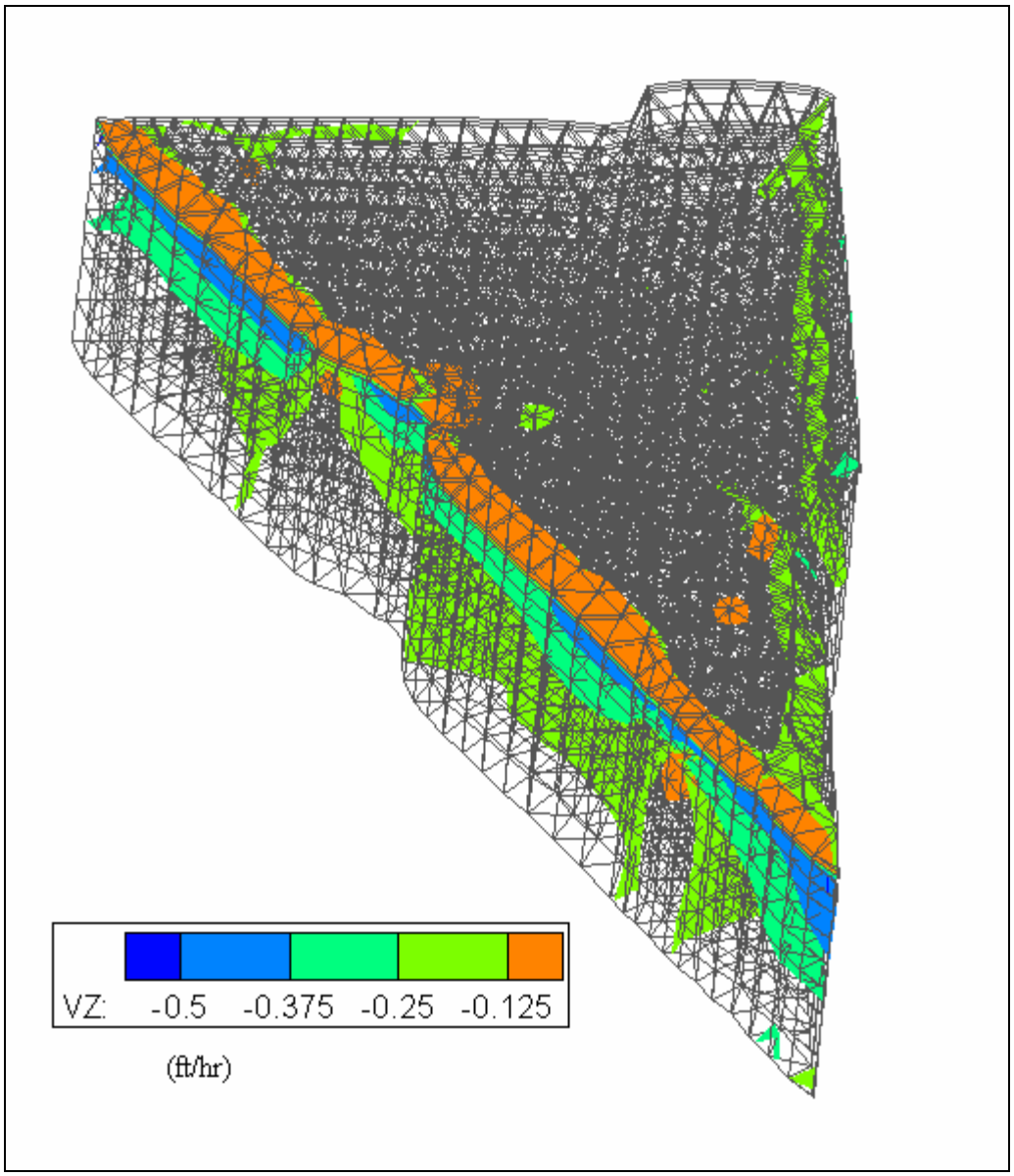

Fig. 4.3.4-5. Contour Map of Vertical Component of Subsurface Darcian Velocity (ft/hr) (Time = 228.0 hours)

4.3.5 Reservoir and Canal Networks Modeling for Evaluations of Storage Values in Northern Beach County in Florida.

The Reservoir Model and the River Model are two major components of WASH123D. The reservoir module takes an approach of water and energy budget, in which evaporation and transpiration modeled, not inputted. The Reservoir Model and the River Model were used for hydraulic modeling of surface water storage areas and canal networks in the study area of northern Palm Beach County (Fig. 4.3.5-1). The canal system is composed of the L-8 Canal, the M-Canal, and the East and West Branches of C-18 Canal. The surface water storage areas include a number of reservoirs within the study area. Details of this example can be found elsewhere (Wanielista et al., 2004).

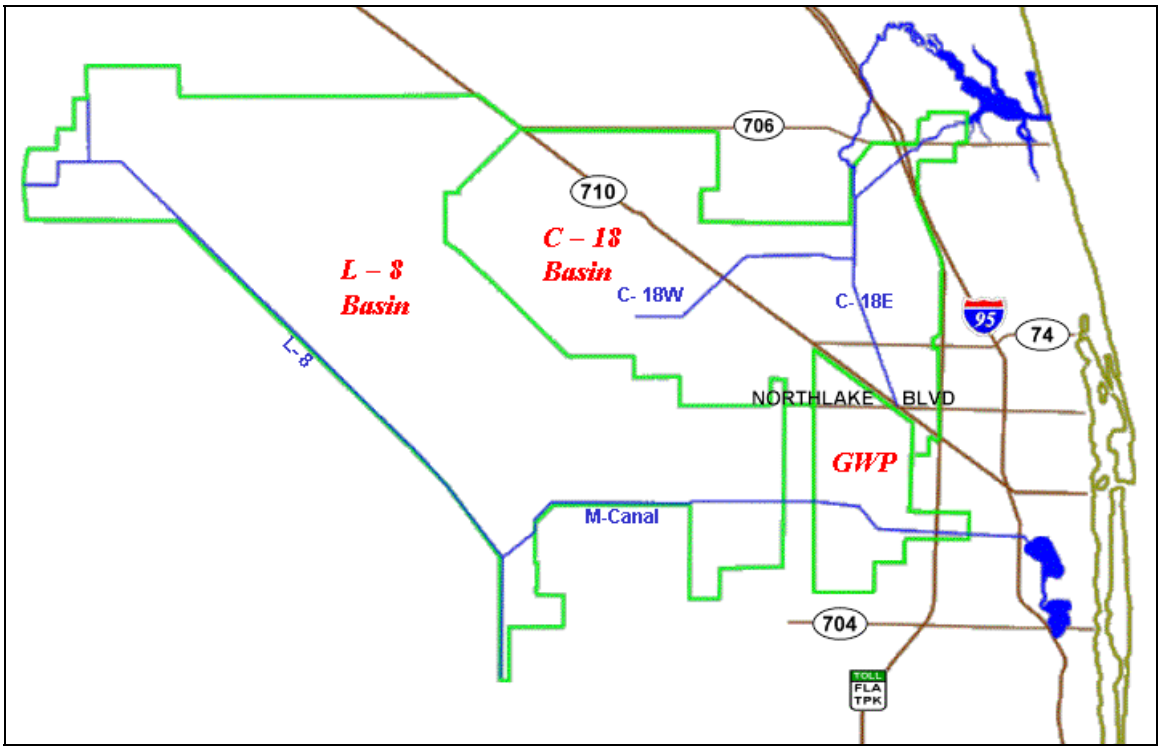

Fig. 4.3.5-1. Study Area Boundary and Local Roads and Landmarks in Northern Beach County

Many internal and external boundary conditions and pumping operations are included as shown Tables 4.3.5-1 and 4.3.5-2. In the River Model, the one-dimensional river channel is divided into reaches. A reach is a river channel segment bounded by hydraulic structures, river junctions, pump stations, or external boundaries of the modeling area. If the end node of a reach is an internal hydraulic structure or a river junction, the internal boundary conditions summarized in Table 4.3.5-1 are imposed. For internal hydraulic structures, the discharge is obtained from analytic formula or rating curve of the structure. Two types of river junctions are listed in Table 4.3.5-1. For a junction without storage capacity, the sum of discharge from all reaches connected at the junction should be zero. For a junction with storage capacity, such as a lake or a reservoir, the end node of the reach

will be treated as an external boundary node.

Table 4.3.5-1 Internal Boundary Conditions

Internal Boundary	Description	Boundary Conditions
Weir	Represents one-dimensional flow transfer by weirs.	Discharge is determined by weir formula or rating curve of the weir.
Gate	Represents one-dimensional flow transfer by gates	Discharge is determined by gate formula or rating curve of the gate.
Culvert	Represents one-dimensional flow transfer by culverts	Discharge is determined by culvert formula or rating curve of the culvert.
Non-Storage Junction	Represents non-storage junctions of one-dimensional river branches.	Sum of discharge from all reaches at the junction equals to zero.

If the end node of a reach is an external boundary, an external boundary condition is applied. There are six types of external boundary conditions showing in Table 4.3.5-2. The Dirichlet boundary condition gives the water depth or stage as a function of time in the simulation. The discharge at the external boundary can be given as a function of time or in the form of a general rating curve. Two special external boundary conditions are designed to simulate the elevation controlled gate and the demand controlled gate, where the gate openings and the rate at which the gate opens and closes are determine by water elevation and demanding discharge, respectively. On a river node where the river is connected directly to a reservoir or lake, the reservoir/lake boundary condition is imposed. Under this circumstance, the River Model is solved in coupling to the Reservoir Model.

The water transferred between these modules is modeled by coupling of the 1-D model and the 0-D model. Two types of coupling between the River Model (1-D model) and the Reservoir Model (0-D model), the on-line coupling and the off-line coupling, are identified. An on-line reservoir is defined as a reservoir that directly connects to river reaches as shown in Figure 4.3.5-2. In the River Model, the coupling is through the external boundary conditions for river nodes at the connection location, where water stage obtained from the Reservoir Model is imposed. In the Reservoir Model, the discharges obtained from the River Model at the connection location are used as inflow and outflow to update the water stage of reservoir. The coupling between the river and the on-line reservoir is modeled in the river-lake module.

Table 4.3.5-2 External Boundary Conditions

Boundary Type	Description	Boundary Conditions
Dirichlet	Water depth or stage is given at all time.	$h = h_B(t)$
Normal Flux	The volumetric flow rate is given at all time.	$Q = Q_B(t)$
General Rating Curve	The volumetric flow rate is given as a function of water depth or stage.	$Q = Q_B(h)$
Rating Curve of Elevation Controlled Gate	The volumetric flow rate is given as a function of water elevation and elevation controlled gate opening.	$Q = Q_B(h, Go(h))$
Rating Curve of Demand Controlled Gate	The volumetric flow rate depends on water elevation and demand controlled gate opening. The gate opening is given as a function water demanding discharge through the gate.	$Q = Q_B(h, Go(Q_D))$
Reservoir/ Lake	The river is connected to a lake/reservoir. It is used to couple the river flow with on-line reservoirs.	$H = H_R$

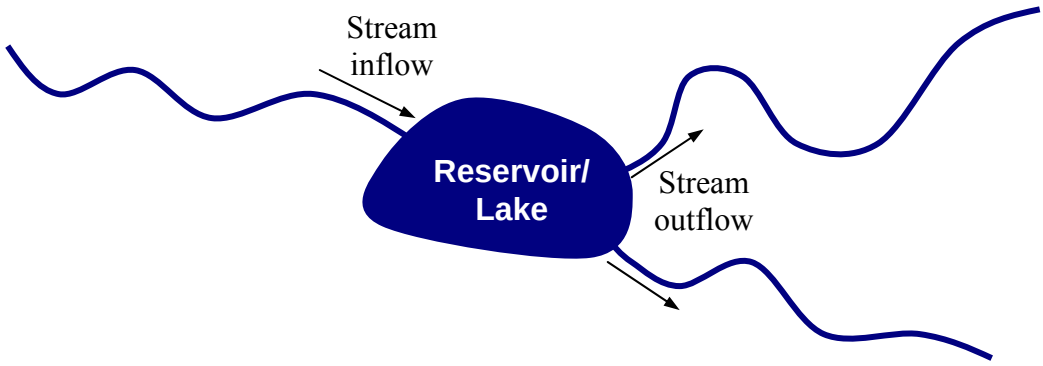

Fig. 4.3.5-2. Schematic Diagram of an On-line Reservoir/Lake

An off-line reservoir is defined as a reservoir that does not directly connect to rivers. A simple illustration of the off-line reservoir is shown in Figure 4.3.5-3. For an off-line reservoir, the water transfer between the reservoir and the river is accomplished through pump stations and/or hydraulic structures, which are implemented through two auxiliary modules: the pump module, and the

gravity-driven hydraulic structure module. A description of these modules can be found elsewhere (Wanielista, et al., 2004).

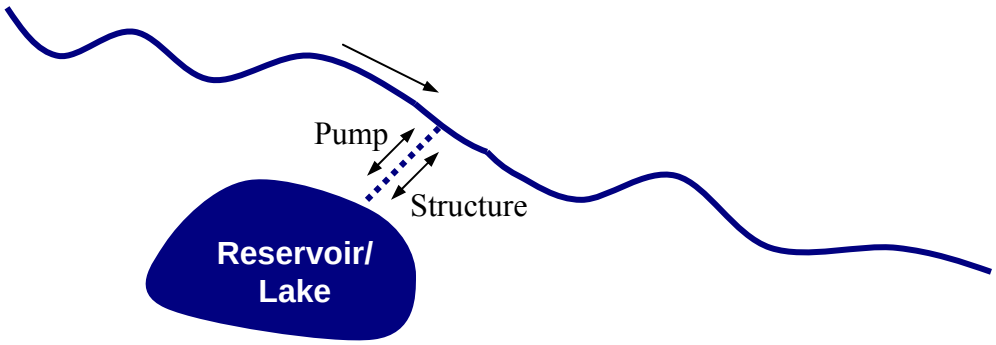

Fig. 4.3.5-3. Schematic Diagram of an Off-line Reservoir/Lake

Figure 4.3.5-4 provides a schematic representation of the model's layout. The primary canal network system consists of eight canals: the L-8 Canal, L-8 North Tieback Canal, L-8 South Tieback Canal, L-8 Outfall Canal, M-Canal, C-18 Canal West Branch, C-18 Canal East Branch, and SIRWCD C-14 Canal. There are four water storage areas: Indian Trail Improvement District (ITID) impoundment area, Grassy Waters Preserve (GWP), Southern L-8 Reservoir (Rock Pits), and C-18 Reservoir.

The L-8 Canal connects Lake Okeechobee to Water Conservation Area 1 (WCA 1). It starts at Culvert 10A at the north end. At the south end, the connection to WCA 1 is by way of S-5A structures.

The L-8 North Tieback Canal drains a small portion of the L-8 basin. It connected with L-8 Canal just east of structure S-76.

The L-8 Outfall Canal connects the ITID impoundment area and the L-8 Canal. On its east end, it makes connections with the impoundment through a culvert structure with riser. On its west end, the connection is also in the form of culvert with riser.

The L-8 South Tieback Canal connects the L-8 Canal and the M-Canal. The northeast end of the canal is a pump station PS-1 (Control #2) owned and operated by the City of West Palm Beach.

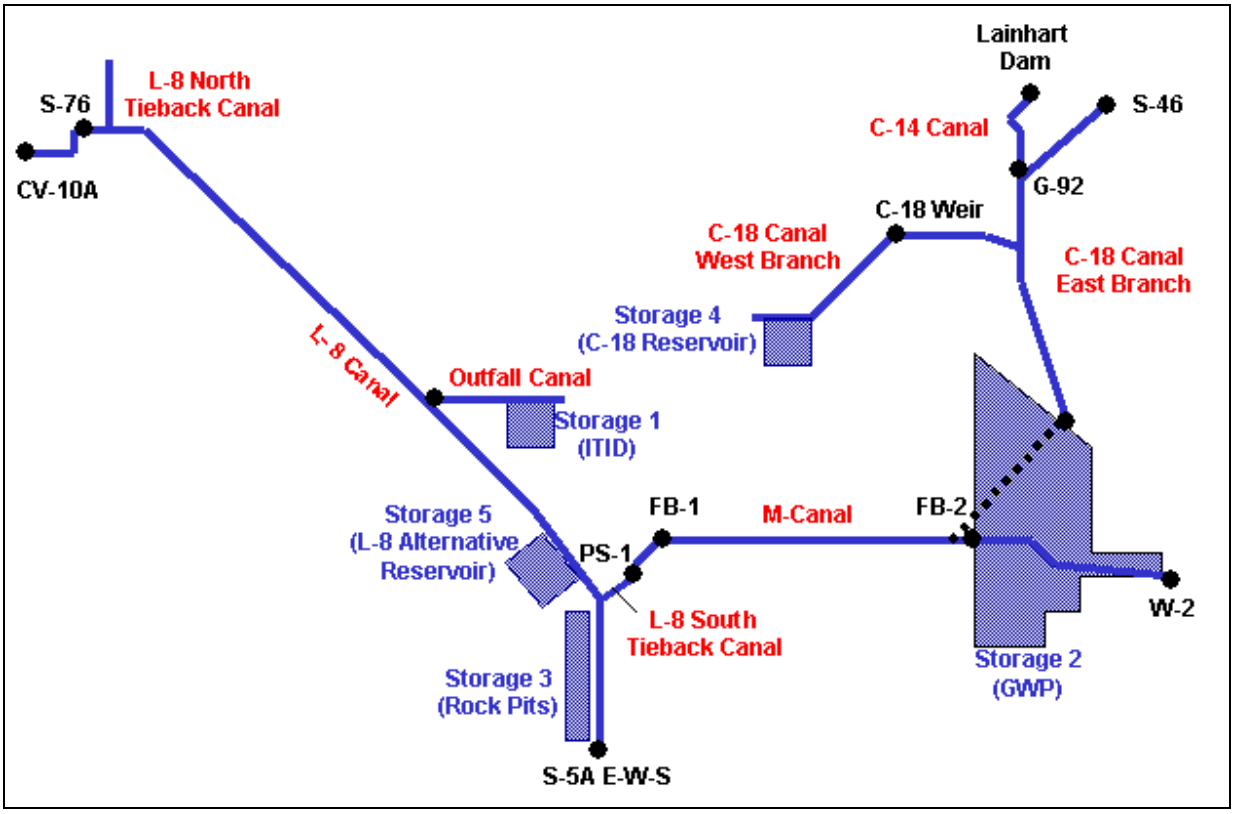

Fig. 4.3.5-4. Model layout of Northern Palm Beach County: Storage Values

The M-Canal starts at PS-1 and extends eastward. In the scope of this model, the east boundary of the M-Canal is a weir structure W-2 located west of the Haverhill Road.

The East Branch of C-18 Canal starts at GWP and extends northward. In the scope of current model, the C-18 Canal ends at structure S-46 which supplies water to the Southwest Fork of the Loxahatchee River.

The West Branch of C-18 Canal begins at the northeast corner of section of Range 40E-Township 42S. It extends eastward and confluences with the East Branch.

The SIRWCD C-14 Canal originates at the G-92 Structure and ends at Lainhart dam – a small weir structure (with a small culvert) located upstream of the Northwest Fork of the Loxahatchee River.

Fifteen canal reaches were created for modeling purpose as shown in Figure 4.3.5-5. Each reach is delimited either by structure, junction, dead end, or external boundary. The length and description of each reach are given elsewhere (Wanielista, et al., 2004).

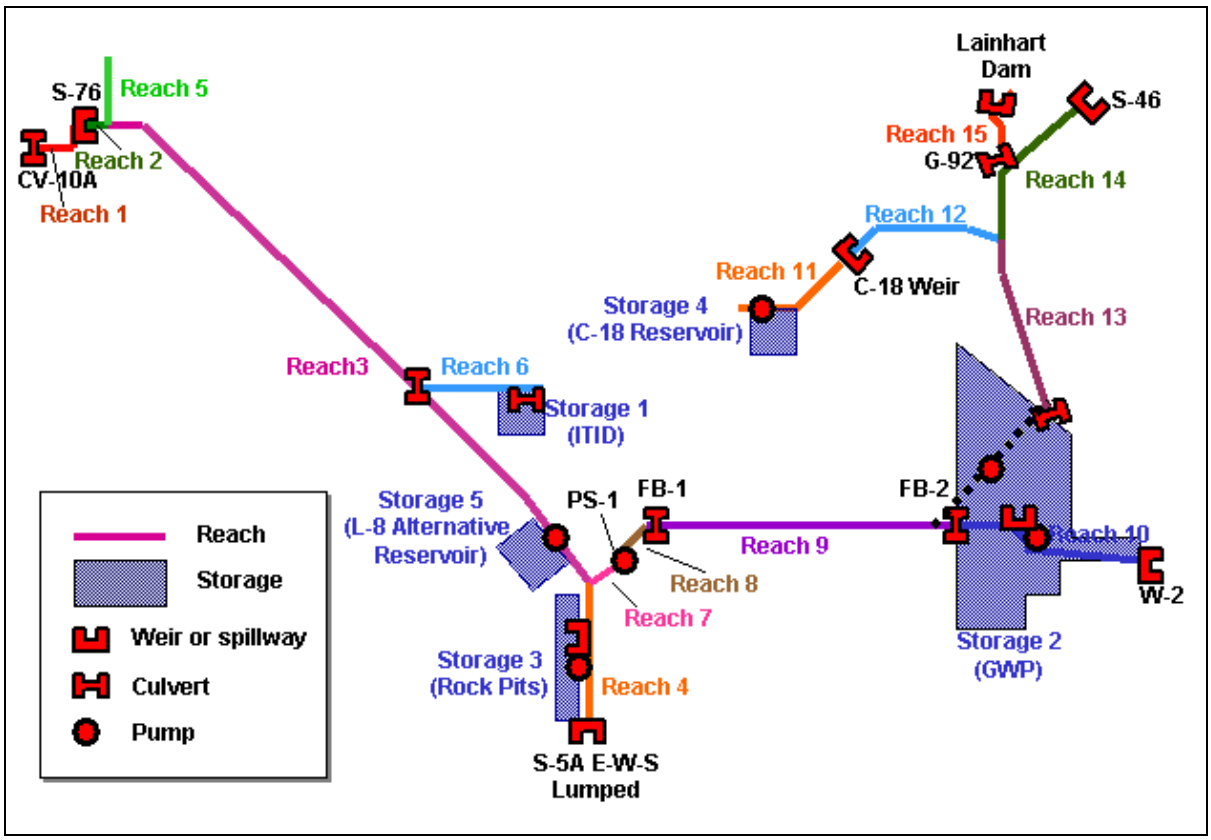

Fig. 4.3.5-5. Canal Reaches in the Model

Water storage area and reservoirs are considered as key components in a regional water management strategy. There are three existing water storage areas (Fig. 4.3.5-5): the Indian Trail Improvement District (ITID) impoundment area (Storage 1), the Grassy Waters Preserve (GWP) (Storage 2), and the Southern L-8 Reservoir (or Rock Pits) (Storage 3). The two proposed surface water reservoirs include the C-18 Reservoir (Storage 4) and the L-8 Alternative Reservoirs (Storage 5). The reservoir operations were simulated using the reservoir module in WASH123D. The connections between the reservoirs and canal reaches are by way of hydraulic structures and pump stations.

The Indian Trail Improvement District (ITID) impoundment area located at a sub-basin of the L-8 Basin (Fig. 4.3.5-1). The maximum storage of the area is around 3300 acre-feet at a water depth of 5 feet. The connection between the impoundment area and the L-8 Outfall Canal is by way of a culvert structure with riser. The riser is in the impoundment area and the culverts open to the L-8 Outfall Canal.

The Grassy Waters Preserve (GWP) formerly known as the City of West Palm Beach Water Catchment Area is an approximately 19 square mile impounded area that is predominantly wetland in nature. Currently, GWP is owned and maintained by the City of West Palm Beach and serves as a surface water storage reservoir for public water supply. Water from this wetland is discharged to the east through the M-Canal to Lake Mangonia and Clear Lake, and subsequently enters the City's water treatment plant in West Palm Beach.

The Southern L-8 Reservoir is proposed to use the abandoned rock mining pits to provide a combined above-ground and in-ground storage capacity of approximately 48,000 acre-feet. It is located immediately west of the L-8 Canal and near the junction of L-8 and C-51 Canals. An area of 1,200 acres may be available and the operation depth is 35 feet (20 feet in ground and 15 feet above ground). The purpose of this reservoir is to increase water supply availability, and attenuate discharge to Lake Worth Lagoon and provide compatible drainage benefits for northern Palm Beach County area. It will also provide flows to enhance hydroperiods in the Loxahatchee Slough, increase base flows to the Northwest Fork of the Loxahatchee River, and reduce high discharges to the Lake Worth Lagoon (SFWMD, 2002).

The C-18 Reservoir was modeled on a footprint of 1,000 acres or 2,000 acres with maximum depths ranging from 10 feet to 15 feet. The total storage volume ranges from 10,000 acre-feet to 30,000 acre-feet. The connection between the reservoir and C-18 Canal West Branch is by way of a pump station with a capacity of up to 100 cfs. This reservoir is designed for the purpose of catching and storing wet season water for use during the dry season to meet the minimum flow criteria to the Northwest Fork of the Loxahatchee River.

The L-8 Alternative Reservoir was placed near the junction of the L-8 Canal and the South L-8 Tieback Canal and west side of L-8 Canal. This reservoir was modeled with a foot print of 1,000 acres or 2,000 acres. Maximum depths ranging from 10 feet to 15 feet were evaluated. The total storage volume ranges from 10,000 acre-feet to 30,000 acre-feet. A pump station with a capacity of 100 cfs connected the reservoir to L-8 Canal.

For the purpose of calibration, the flow data recorded at several sites as described in Table 4.3.5-3 were downloaded from SFWMD's online database. Under the existing condition, the conveyance between the Grassy Waters Preserve (GWP) and the East Branch of C-18 Canal is severely constrained (< 10 cfs), thus the L-8 Canal system and C-18 Canal system can be considered as decoupled. Within this project, since the daily rainfall and evaporation data for the entire area were not available, the rainfall and evaporation input to the model was on a monthly basis. Thus it would be very difficult to calibrate the model against the daily field data but using monthly data as input. Therefore, one-year accumulative discharges through the three structures listed in Table 6.11 were used to calibrate the model.

Under the assumption that C-18 Canal system is isolated from the L-8 Canal system, the amount of water that enters the C-18 Canal system is thus divided among direct rainfall, surface runoff, and groundwater seepage. Water inflows to C-18 Canal system contributed by direct rainfall onto the canal and surface runoff from the thirty two sub-basins of the C-18 drainage area can be modeled or obtained from field data. The groundwater seepage is difficult to estimate without modeling. Though the three-dimensional groundwater module of WASH123D model is capable of precisely predicting the groundwater seepage to C-18 Canal, the time frame of the project would not allow us to do so (Wanielista, et al., 2004). Thus, the estimation of groundwater seepage became part of the calibration procedure. The outlet of the system consists of two structures: S-46 and G-92. The object of the calibration is to match the cumulative discharge and the base flow at structure G92.

Table 4.3.5-3 Surface water data for model calibration

Station/ Site	Interval	Description	Start Date	End Date
S46_S	Daily	At southwest fork of Loxahatchee River	11/8/1992	9/16/2002
G92_C	Daily	G-92 culvert from C-18 to west branch of Loxahatchee River	5/10/1988	1/26/2003
LNHRT	Daily	Lainhart Dam on Loxahatchee River	4/25/1995	9/17/2002

The year of 1995 was selected for calibration, since the rainfall and evaporation input was from 1965 through 1995 and there were more field data available in 1995. Table 4.3.5-4 gives the cumulative discharge at the structures.

Table 4.3.5-4 Measured cumulative flow in 1995

Station/Site	Start Date	End Date	Cumulated Discharge (acre-feet)
S46_S	1/1/1995	12/31/1995	124230
G92_C	1/1/1995	12/31/1995	59091
LNHRT	4/25/1995	12/31/1995	59920

Structure G-92 is a gated culvert; it diverts water from C-18 Canal to C-14 Canal. The structure is operated via remote telemetry from the SFWMD Operations Control Room under a joint agreement with the SIRWCD to permit conveyance of flows to the Northwest Fork of the Loxahatchee River through Lainhart Dam. In current simulation, since the operation rule of G-92 was not provided by SFWMD, the gate was set at fixed openings, as shown in Table 4.3.6-5, 12.5% for CASE A, and 15% for CASE B.

Table 4.3.5-5 Gate opening at Structure G-92

CASE	Gate Opening of G-92
A	12.5%
B	15%

The simulation results are shown in Table 4.3.5-6. The results indicate that when the gate opening of structure G-92 was 15%, the cumulative flow through the structure is very close to the field data. Therefore, the gate opening of 15% was chosen for a series of simulations. In 1995, the field data at Lainhart Dam starts on 4/25. The cumulative flows through the structures S-46, G-92 and Lainhart

Dam from 4/25/95 to 12/31/95 are displayed in Table 4.3.5-7. Though these numbers are not matched as well as for structure G-92, generally the model calibration is still acceptable.

Table 4.3.5-6 Cumulative flow through different structures

	Cumulative Flow through the Following Structures (acre-feet) (1/1/95 -12/31/95)		
	S-46	G-92	Lainhart Dam
Field Data	124230	59091	N/A
A	111795	52980	70507
B	104770	60027	77555

Table 4.3.5-7 Cumulative flow through Lainhart Dam compared with field data

	Cumulative Flow through the Lainhart Dam (acre-feet) (4/25/95 -12/31/95)
Field Data	59920
A	57244
B	63628

The goal of the project is to study the capability of water storage reservoirs of providing supplement water to the Northwest Fork of the Loxahatchee River to meet the minimum flow request in the dry season. The minimum flow request was tested at Lainhard Dam for both CASE A and B. The target minimum flows were set at 35 cfs, 65cfs, and 100 cfs. The percent of time the target flow was met under existing conditions in the year of simulation is shown in Table 4.3.5-8. The results are the same for both gate openings at structure G-92. The percent of time that the minimum flow of 35 cfs, 65cfs, and 100 cfs were met were 70%, 60%, and 54%, respectively. As indicated by the *Loxahatchee River Minimum Flows and Levels*, over the past decade, the 35 cfs and 65 cfs flow target for the Lainhart Dam, were met about 75% and 57% of the time. To compare with the field data, the percent of time was calculated again from 4/25/95 through 12/31/95. The results are displayed in Table 4.3.5-9. In simulation with both 12.5% and 15% gate openings, the simulated time percentage is higher than field data for 65 cfs and 100 cfs, but lower for 35 cfs.

Table 4.3.5-8 Percent of time the target minimum flow is met at Lainhart Dam

CASE	Percent of Time The Following Target Flow Is Met (1/1/95 -12/31/95)		
	≥ 35 (cfs)	≥ 65 (cfs)	≥ 100 (cfs)
1-A	70%	60%	54%

1-B	70%	60%	54%

Table 4.3.5-9 Percent of time the target minimum flow is met.
A comparison with field data

CASE	Percent of Time The Following Target Flow Is Met (4/25/95 -12/31/95)		
	≥ 35 (cfs)	≥ 65 (cfs)	≥ 100 (cfs)
Field Data	79%	60%	52%
1-A	72%	69%	67%
1-B	72%	69%	67%

Figure 4.3.5-6(a) shows the hydrograph at structure G-92 with a gate opening of 12.5% in 1995 obtained from CASE A in comparison with field flow data. The hydrograph at structure G-92 obtained from CASE B is displayed in Figure 4.3.5-6(b). In this case, the gate opening of G-92 was 15%. The data in Table 6.14 and 6.15 indicates that the larger gate opening allowed the passing of more water through structure G-92. But the Figure 4.3.5-6 shows that his only happens during the wet seasons, in the dry season, both openings pass the same amount of water. The large deviations between the simulation results and the field data can be attributed to the following two factors: 1) The rainfall data used for the simulation was on a monthly basis; 2) The operation rule the gate at structure G-92 was not clear, so the gate opening was fixed in the simulation. However, in both cases, the yearly cumulative flows were quite close to the field data as shown previously in Table 4.3.5-6.

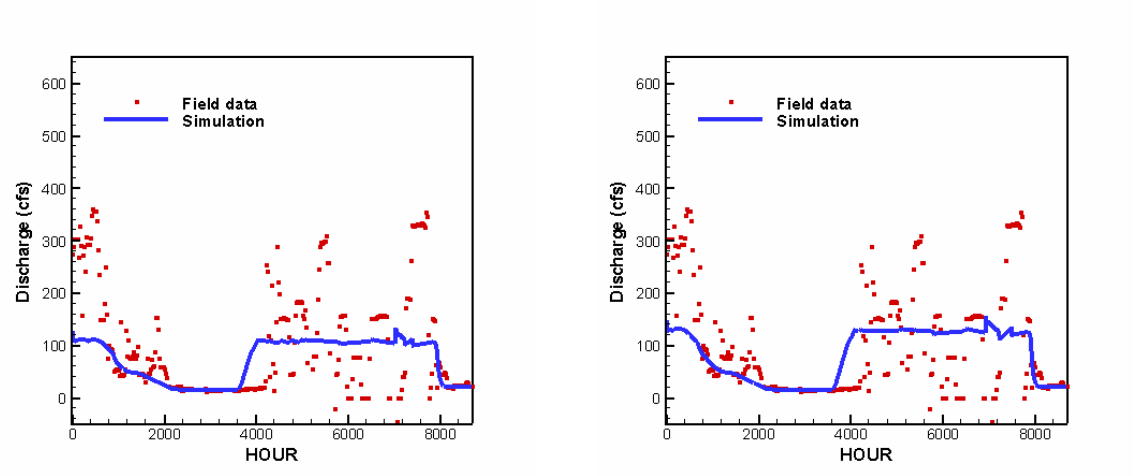

(a) CASE A (b) CASE B

Fig. 4.3.5-6. Hydrograph at structure G-92 from 1/1/95 through 12/1/95

The Lainhart Dam is an uncontrolled weir. The simulated hydrographs are displayed in Figures 4.3.5-7. Obviously the simulation results are in much better agreement with the field data than that of G-92 even though the input data was on monthly basis.

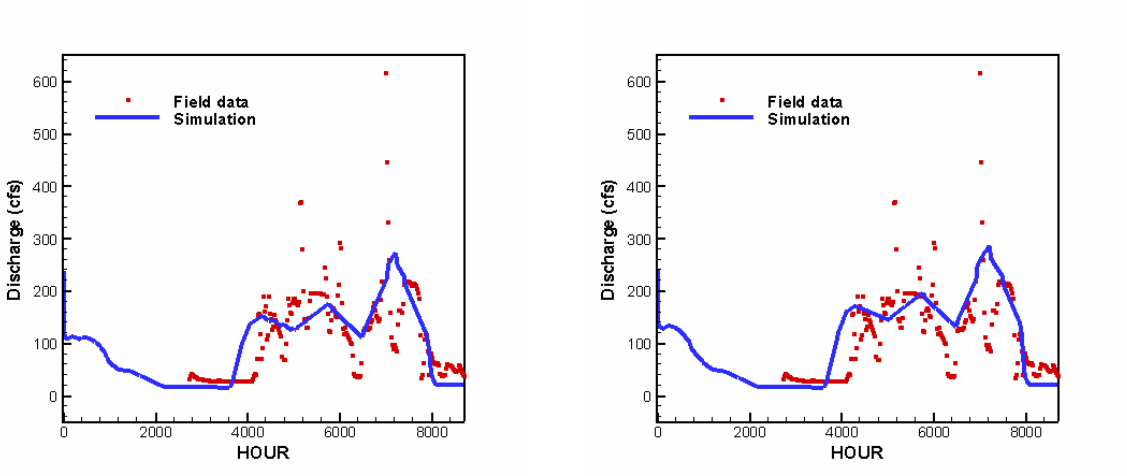

(a) CASE 1-A (b) CASE 1-B

Fig. 4.3.5-7. Hydrograph at Lainhart Dam from 1/1/95 through 12/1/95.

After successfully calibrate the model, various combinations of proposed reservoirs were investigated. The modeling of WASH123D coupled with an economic evaluation resulting in the recommendation of $2,500 per acre-ft of storage, which was in contrast to earlier studies, which estimated a cost of $5,500 per acre-ft. The study saved FDEP (Florida Department of Environmental Protection) of approximately $250 millions for the management.

4.3.6 Dade County Watershed Modeling.

This is a regional scale modeling effort for the South Florida wetlands. The Dade model domain extends from four miles west of the L-67 Extension dike to the western shore of Biscayne bay and from one mile north of the Tamiami canal south to Florida bay. Vertically, it extends from the land surface to the bottom of the surficial aquifer.

Some characteristics of this model are: (1) Strong interaction of overland flow/groundwater flow and canal flow in south Florida; (2) Complex hydraulic structure operations.

The 3-D finite element mesh for subsurface media (as shown in Figure 4.3.6-1) is complex: there are 37,760 global nodes, and 65,429 elements. There are 7 layers in vertical direction. And levees are incorporated as part of subsurface media.

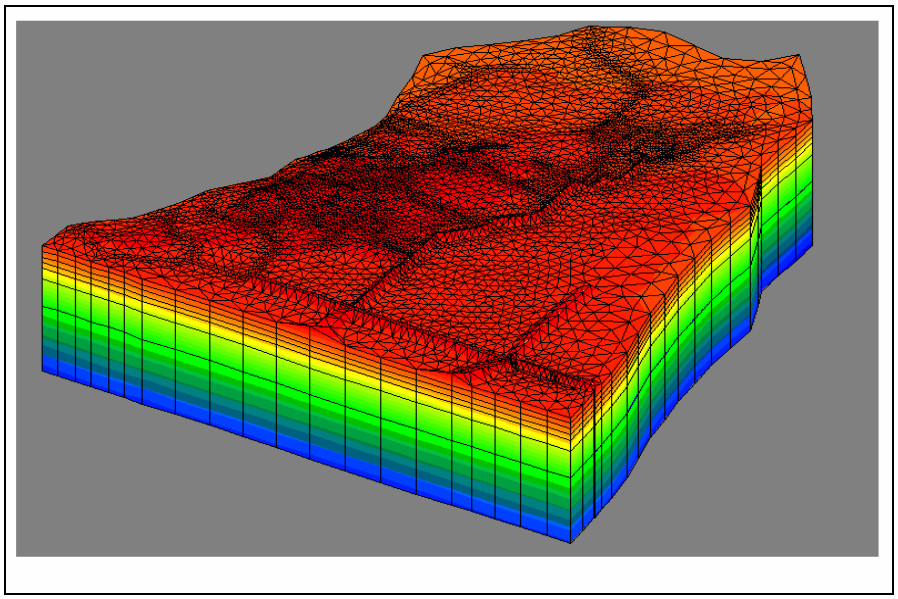

Fig. 4.3.6-1. 3-D Subsurface Media Finite Element Mesh

The boundary conditions for subsurface flow were determined from the SFWMM 2x2 model output for the northern boundary, and from structure operation records for the other sides of boundaries.

The 2-D overland flow domain consists of 4,720 nodes, and 9,347 triangular elements. Levees are included in the computation domain (Fig. 4.3.6-2). Boundary conditions were determined from structure operation records along the boundary.

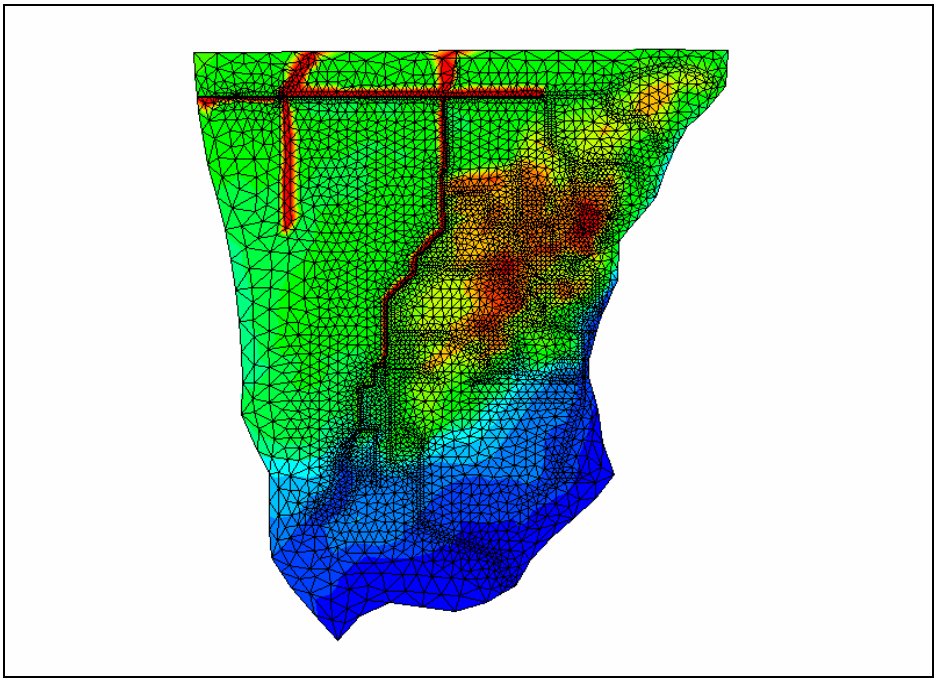

Fig. 4.3.6-2. 2-D Overland Regime Finite Element Mesh

The canal network as simplified in this simulation includes: Canal nodes: 560; Canal elements: 506; River reaches: 55; there are 20 canal junctions, and 11 interior Gates (Fig. 4.3.6-3).

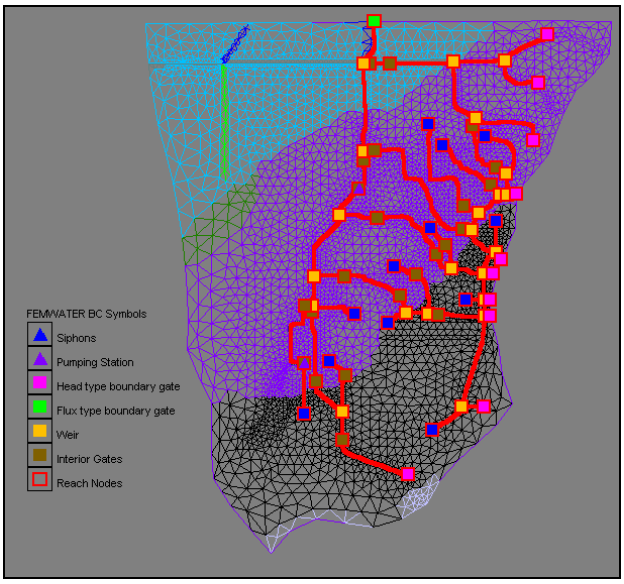

Fig. 4.3.6-3. Canal Network

The boundary conditions for subsurface flow were determined from the SFWMM 2x2 model output for the northern boundary, and from structure operation records for the other sides of boundaries.

The 1-D/2-D/3-D coupled flow simulation was first begun with a steady state of subsurface flow and the total head distribution of the steady state flow is shown in Figure 4.3.6-4. Then the steady state condition was used as the initial condition of the transient flow simulation.

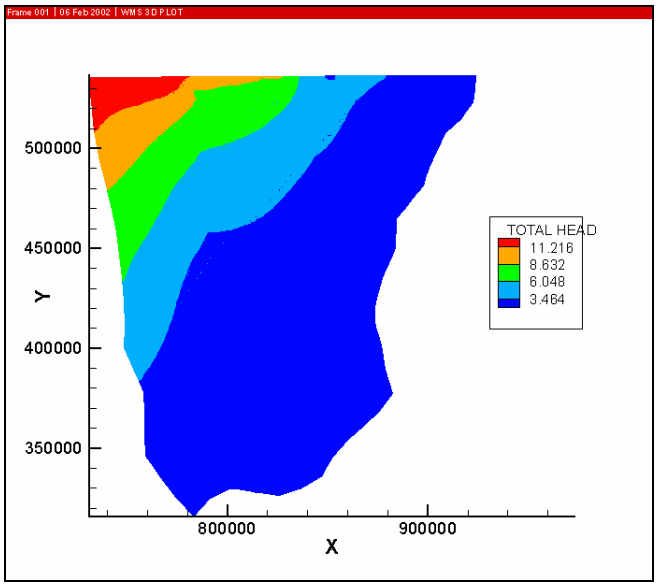

Fig. 4.3.6-4. Total Head at Steady State Subsurface Flow (feet)

Figure 4.3.6-5 and 4.3.6-6 depict the simulations result of a model run. Since the levee/dike are included as part of the subsurface media, it is demonstrated that the ground water flow from the northern boundary can bypass the less permeable levees via their underlying permeable media. It is also obvious that the canals recharge the ground water.

An animation showing the spatial-temporal distribution of water depth in surface runoff is attached in Appendix A (File Name: dade2ddepth.avi). Readers can visualize this move by clicking the file contained in the attached CD.

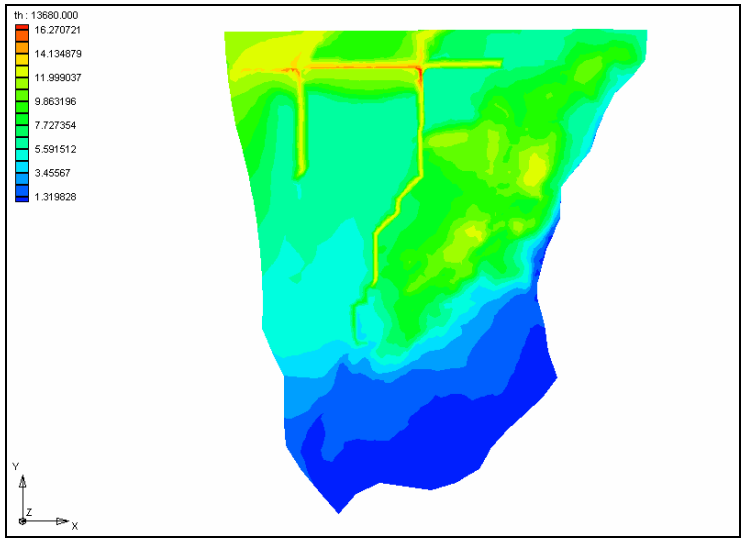

Fig. 4.3.6-5. Total Head Distribution (feet) at time=13,680 minutes (9.5 days)

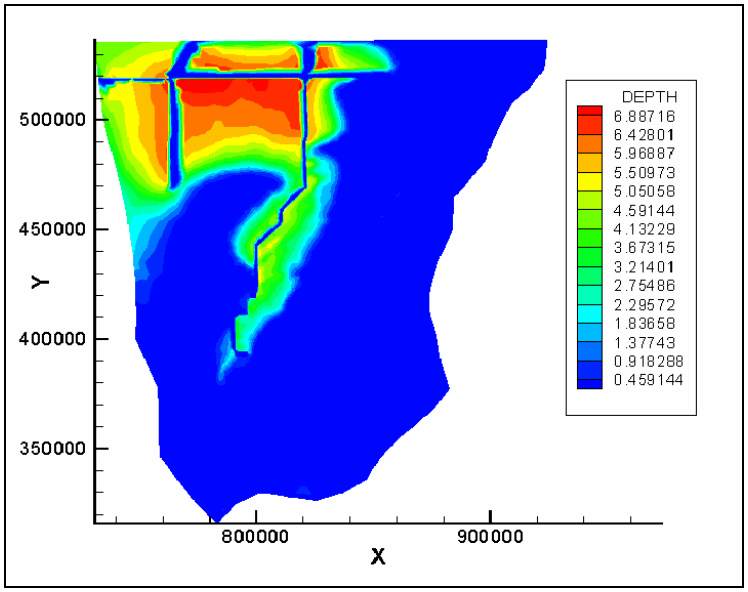

Fig. 4.3.6-6. Overland Water Depth (feet) at time = 7,000 minutes (4.86 days

5 WATER QUALITY TRANSPORT EXAMPLES

In this chapter, we are to present a total of 15 water quality transport problems: six examples for one-dimensional transport, four examples for two-dimensional transport, and five examples for three-dimensional transport.

5.1 One-Dimensional Examples

Six examples are used in this section. Two examples are compared with analytical solutions to verify the model and to emphasize the need of implementing various numerical options and coupling strategies to deal with different types of problems for different application circumstances. A hypothetical example with complexation, sorption and dissolution reactions is employed to demonstrate the capability of the model to handle complex reaction network involving both kinetic and equilibrium reactions. Two more example problems are employed to demonstrate the design capability of the model, in simulating sediment and chemical transport, chemicals in both mobile water phase and immobile water phase, and both kinetic and equilibrium reactions.

5.1.1 Comparison of Options to Solve Advective-dispersive Transport Equations

This example involves the transient simulation of chemical transport in a horizontally 50 km-long river/stream containing a uniform width of 10 m. The domain of interest is discretized into 1000 equal size elements (50 m each). We assume the water depth is 5 m and river/stream flow velocity is 0.4 m/s throughout the river/stream. There are two species, a dissolved chemical in the mobile water phase CMW and a dissolved chemical in the immobile water phase CIMW. The phase densities associated with both species are assumed to be 1.0. CMW and CIMW are considered to undergo the following equilibrium reaction.

$$\mathrm{CMW} \rightleftharpoons \mathrm{CIMW} \quad K_{eq} = 0.8 \tag{5.1.1}$$

Initially, no chemical exists in the domain of interest. Variable boundary conditions are applied to both the upstream and downstream boundary nodes for mobile species CMW. At the upstream boundary node, the incoming concentration of CMW is 1 g/m^3. The molecular diffusion coefficient is assumed to be zero. Three cases with different dispersivities of 3.125 m, 62.5 m, and 1000 m (grid Peclet number $Pe = \Delta x/\alpha L = 16$, 0.8 and 0.05 for case 1, 2, and 3, respectively) were considered. Simulations were performed with fixed time step size of 36 s (grid Courant number $Cr = V\Delta t/\Delta x = 0.288$) and total simulation time of 1800 s. For case 2, two more simulations were performed with different time step size of 120 s and 180 s ($Cr = 0.96$ and 1.44) in case 4 and 5, respectively.

Using the same coupling strategy, the fully-implicit scheme, to deal with reactive chemistry, simulations were performed with the five numerical options to solve the advective-dispersive equation. In Figure 5.1-1, simulation results of CMW in cases 1 through 3 are compared with the analytical solutions given by Lindstrom and Freed, 1967. R^2 values based on simulations and analytical results are also calculated and listed in the figure. In Figure 5.1-2, simulation results of CMW in cases 4 and 5 are plotted. R^2 and CPU time are also listed in the figure.

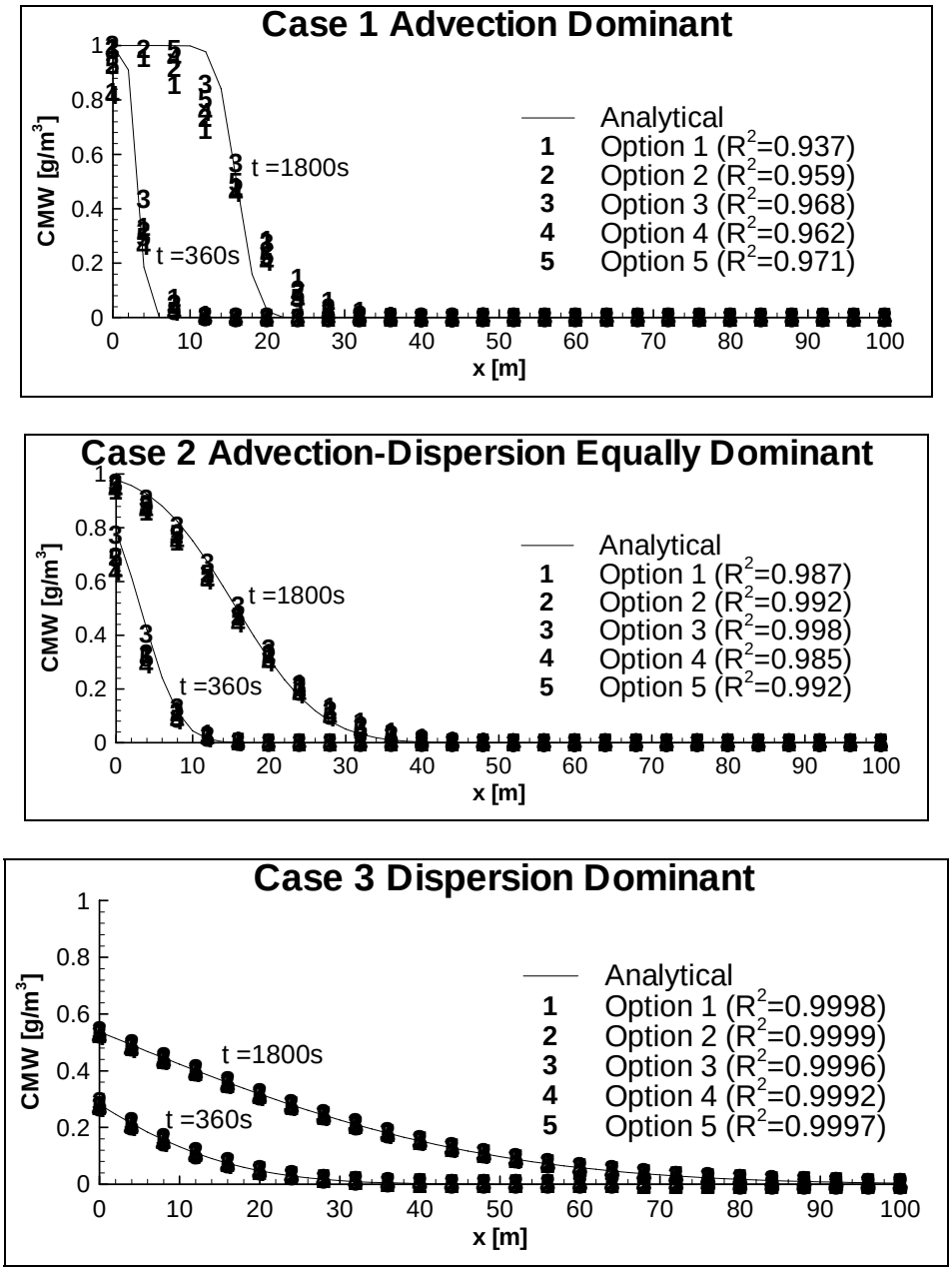

Fig. 5.1-1. Concentration Profiles of CMW in Cases 1, 2, and 3 of Example 5.1

It is seen that: (1) for advection dominant cases, Options 3 through 5 give more accurate simulation

than the other two; (2) for advection-dispersion equally-dominant cases, all five options yield almost same accurate results with Option 3 giving slightly better results than Option 2 and 5, and Option 2 and 5 yielding slightly better results than Option 1 and 4; (3) for dispersion dominant cases, all five options give approximately the same accurate simulation but with Option 1 and 2 giving slightly better results than the other three. Therefore, for advection dominant problems for research applications when accuracy is the primary concern, Options 3 through 5 are preferred. However, for dispersion dominant problems for research applications, Options 1 and 2 may be preferred. For practical applications when the efficiency is the primary concern, Option 3 is preferred under all transport conditions because it gives the most efficient computation in term of CPU time. The efficiency results from the fact that one can use a much larger time step size without having to worry about the limitation of time-step sizes imposed by advective transport. As shown in Figure 5.1-2, when the Courant number increases from 0.96 to1.44, Option 1 and 2 were not able to yield convergent solutions. Although, all of the other three options gave less accuracy results, only Option 3 yields accurate enough simulation. Since the time step size is enlarged, the total number of simulation time steps decreased, resulting in less CPU time.

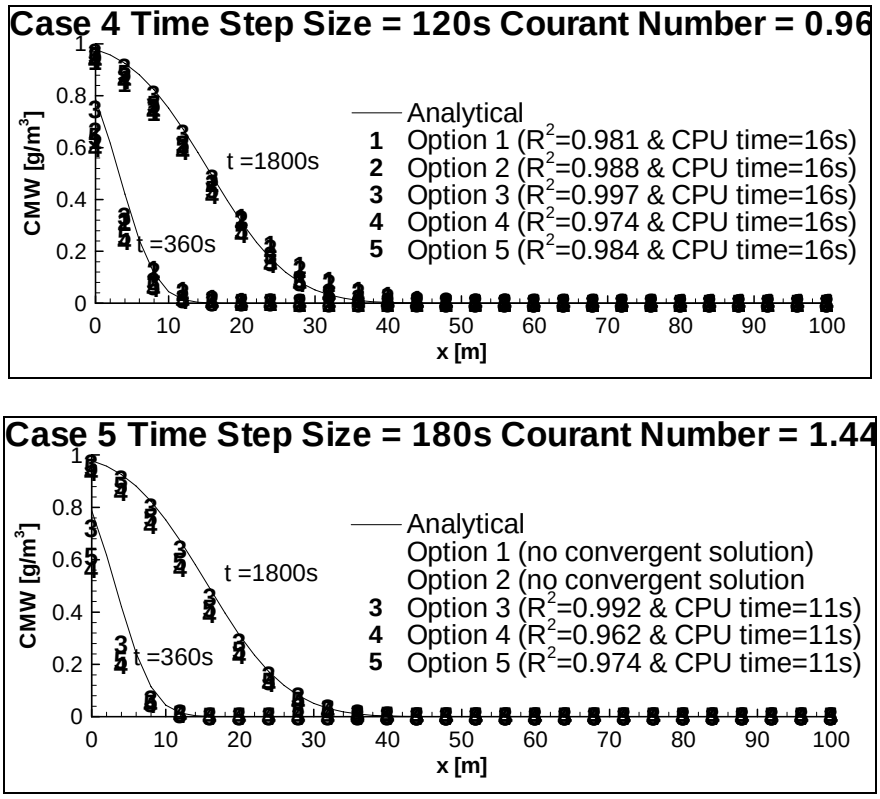

Fig. 5.1-2. Concentration Profiles of CMW in Cases 4 and 5 of Example 5.1

5.1.2 Comparison of Coupling Strategies to Deal with Reactive Chemistry

In this example, a horizontally 4 km-long river/stream containing a uniform width of 10 m is considered. The domain is discretized into 400 equal size elements (each 10 m). We assume the water depth is 2 m and river/stream flow velocity is 1.0 m/s throughout the river/stream. There are two species, a dissolved chemical in the mobile water phase CMW and a dissolved chemical in the

immobile water phase CIMW. The phase densities associated with both species are assumed to be 1.0. CMW and CIMW are considered to undergo the following reaction.

$$\text{Case1}: \text{CMW} \rightleftharpoons \text{CIMW} \quad K_{eq} = 1.0 \tag{5.1.2}$$

$$\text{Case2}: \text{CMW} \rightleftharpoons \text{CIMW} \quad K_f = 3h^{-1}, K_b = 3h^{-1} \tag{5.1.3}$$

$$\text{Case3}: \text{CMW} \rightleftharpoons \text{CIMW} \quad K_f = 1.0\times10^{-2}h^{-1}, K_b = 1.0\times10^{-2}h^{-1} \tag{5.1.4}$$

Initially, no chemical exists in the domain of interest. Dirichelet and Variable boundary conditions are applied to the upstream and downstream boundary nodes for mobile species CMW, respectively. At the upstream boundary node, the concentration of CMW is 1 mg/kg. Simulations were performed with fixed time step sizes of 360 s and total simulation time of 1800 s. The molecular diffusion coefficient and longitudinal dispersivity are assumed to be zero. Option 3 is used to solve the transport equations. With the grid size, time-step size and model parameters given above, the mesh Courant numbers are $Cr = V\Delta t/\Delta x = 36$. When the fully-implicit scheme with E_n^m written in terms of $(E_n^m/E_n)\bullet E_n$ is applied to Case 1, the mesh Courant number is $Cr = V/(1+K_{eq})\cdot(\Delta t/\Delta x) = 18$. With integral mesh Courant numbers, the numerical error is zero in solving the advective transport equation, thus numerical errors due to coupling strategies are isolated.

Using the same numerical option, Option 3 – the Modified LE approach, to solve the advective-dispersive equation, simulations were performed with three coupling strategies to deal with the reactive chemistry. In Figure 5.1-3, simulation results of CMW in Case 1, 2, and 3 are compared with the analytical solutions (Quezada et al, 2004). It is seen that the fully-implicit strategy gives accurate enough solution for all three cases although solution for Case 2 is less accurate than the other two. However, simulation accuracy using the mixed predictor-corrector/operator-splitting and operator-splitting strategies varies for the three cases. For Case 1, in which an equilibrium reaction involves, calculation results of these two strategies are far from the analytical values. For Case 2, in which a kinetic reaction with faster rate (compared to Case 3) involves, simulations of these two strategies are close to the exact solution although less accurate than the fully-implicit strategy. For Case 3, in which a kinetic reaction with slower rate (compared to Case 2) involves, accurate simulations are obtained with these two strategies.

For problems with reaction network involving only kinetic reactions with slower rates, all the three strategies can generate accurate solution. Because the fully-implicit strategy takes more time to achieve convergent simulations due to iteration between the advective-dispersive transport step and the reactive chemistry step, the other two strategies are recommended under this situation. However, for problems with reaction network involving equilibrium reactions, the fully-implicit strategy is recommended for both research and practical applications because the other two strategies simply cannot give enough accurate simulations. For problems involving only kinetic reactions with faster rates, the fully-implicit strategy is recommended when accuracy is the primary concern; on the other hand, the mixed predictor-corrector/operator splitting strategy and the operator splitting strategy are recommended for practical applications when efficiency is the primary concern.

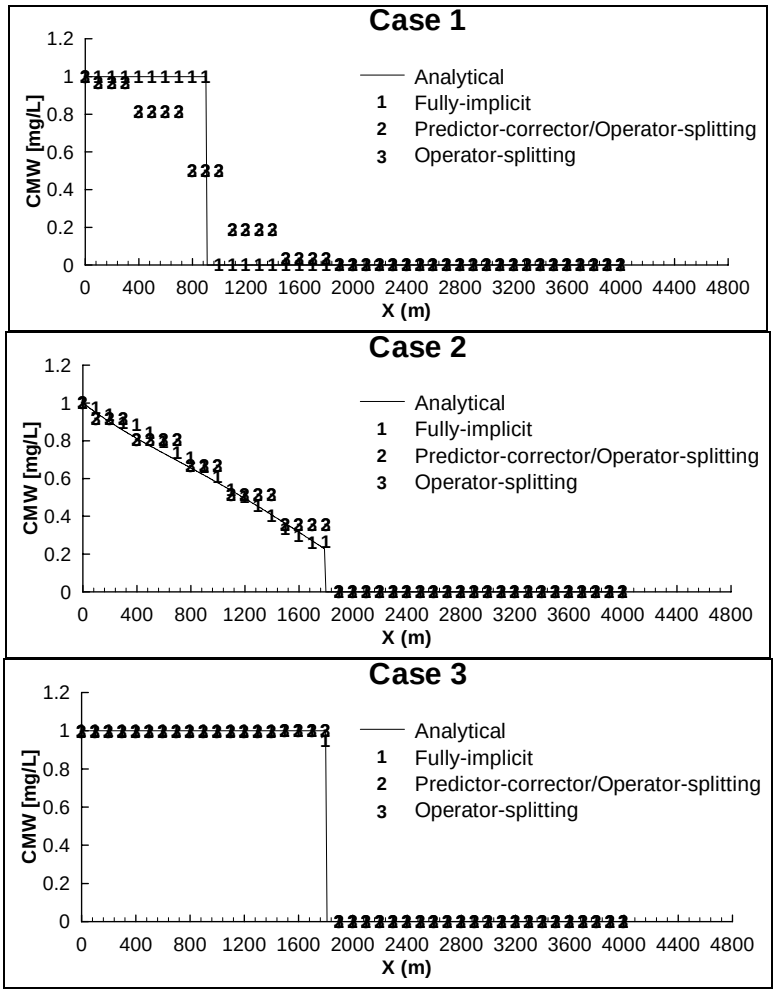

Fig. 5.1-3. Concentration Profiles of CMW in Cases 1, 2, and 3 of Example 5.2

5.1.3 Chemical Transport with Complexation, Sorption and Dissolution reactions

Reactive chemical transport, incorporating hypothetical aqueous complexation, sorption, and precipitate dissolution reactions in a system of mixed equilibrium and kinetic reactions, is simulated in this example. A horizontally 20 km-long river/stream containing a uniform width of 20 m is considered. The domain is discretized into 100 equal size elements (200 m each). To focus on transport, we assume water depth is 2 m and river/stream velocity is 1 m/s.

Forty-one chemical species are taken account, including 29 dissolved species in the mobile water phase (C_1~C_{27}, C_{29}, and C_{30}), 1 bed precipitate (M), and 11 particulates sorbed onto bed sediment (S_1~S_8, site-C_6, site-C_{29} and site-C_{30}). As shown in Table 5.1-1, the complex reaction network involves 33 reactions: including 1 dissolution reaction R1; 1 sorbing site forming reaction R2; 22 aqueous complexation reactions R3~R24; and 9 sorption reactions R25~R33.

Table 5.1-1 Reaction Network for Example 5.1-3

Reaction	Reaction parameters	No.
$M \leftrightarrow C_1 - 3C_2$	Rate= 5.787e-7M	R1
$M \leftrightarrow S_1$	$0.0047M=S_1+S_2+S_3+S_4+S_5+S_6+S_7+S_8$	R2
$C_3 \leftrightarrow C_4 + C_5$	$\text{Log } K_3^e = -17.97$	R3
$C_6 + C_5 \leftrightarrow C_7$	$\text{Log } K_4^e = 12.32$	R4
$C_2 + C_5 + C_6 \leftrightarrow C_8$	$\text{Log } K_5^e = 15.93$	R5
$C_6 \leftrightarrow C_2 + C_9$	$\text{Log } K_6^e = -12.6$	R6
$C_1 + C_5 \leftrightarrow C_{10}$	$\text{Log } K_7^e = 22.57$	R7
$C_1 + C_2 + C_5 \leftrightarrow C_{11}$	$\text{Log } K_8^e = 29.08$	R8
$C_1 + C_5 \leftrightarrow C_2 + C_{12}$	$\text{Log } K_9^e = 19.65$	R9
$C_1 + C_5 \leftrightarrow 2\,C_2 + C_{13}$	$\text{Log } K_{10}^e = -36.3$	R10
$C_1 \leftrightarrow C_2 + C_{14}$	$\text{Log } K_{11}^e = -2.19$	R11
$C_1 \leftrightarrow 2C_2 + C_{15}$	$\text{Log } K_{12}^e = -5.67$	R12
$C_1 \leftrightarrow 3C_2 + C_{16}$	$\text{Log } K_{13}^e = -13.6$	R13
$C_1 \leftrightarrow 4C_2 + C_{17}$	$\text{Log } K_{14}^e = -21.6$	R14
$2C_1 \leftrightarrow 2C_2 + C_{18}$	$\text{Log } K_{15}^e = -2.95$	R15
$C_2 + C_4 + C_5 \leftrightarrow C_{19}$	$\text{Log } K_{16}^e = 21.4$	R16
$C_4 \leftrightarrow C_2 + C_{20}$	$\text{Log } K_{17}^e = -9.67$	R17
$C_4 \leftrightarrow 2C_2 + C_{21}$	$\text{Log } K_{18}^e = -18.76$	R18
$C_4 \leftrightarrow 3C_2 + C_{22}$	$\text{Log } K_{19}^e = -32.23$	R19
$C_2 + C_5 \leftrightarrow C_{23}$	$\text{Log } K_{20}^e = 11.03$	R20
$2C_2 + C_5 \leftrightarrow C_{24}$	$\text{Log } K_{21}^e = 17.78$	R21
$3C_2 + C_5 \leftrightarrow C_{25}$	$\text{Log } K_{22}^e = 20.89$	R22
$4C_2 + C_5 \leftrightarrow C_{26}$	$\text{Log } K_{23}^e = 23.1$	R23
$\leftrightarrow C_2 + C_{27}$	$\text{Log } K_{24}^e = -14.0$	R24
$S_1 \leftrightarrow S_2 + C_2$	$\text{Log } K_{25}^e = -11.6$	R25
$S_1 + C_2 \leftrightarrow S_3$	$\text{Log } K_{26}^e = 5.6$	R26
$S_1 + 3C_2 + C_5 \leftrightarrow S_4$	$\text{Log } K_{27}^e = 30.48$	R27
$S_1 + C_1 + C_2 + C_5 \leftrightarrow S_5$	$\text{Log } K_{28}^e = 37.63$	R28
$S_1 + C_2 + C_4 + C_5 \leftrightarrow S_6$	$\text{Log } K_{29}^f = 25.0$, $\text{Log } K_{29}^b = -3.49$	R29
$S_1 - C_2 + C_4 \leftrightarrow S_7$	$\text{Log } K_{30}^f = -5.99$, $\text{Log } K_{30}^b = -3.30$	R30
$S_1 + C_2 + C_5 + C_6 \leftrightarrow S_8$	$\text{Log } K_{31}^f = 20.0$, $\text{Log } K_{31}^b = -3.81$	R31
$C_{29} + 2\text{Site-}C_{30} \leftrightarrow \text{Site-}C_{29} + 2C_{30}$	$\text{Rate}=10^{-5.75}\,C_{29}\cdot(a_{30}\text{Site-}C_{30})^2-10^{-5.5}a_{29}\text{Site-}C_{29}\cdot C_{30}^2$ $a_{29}= \text{Site-}C_{29}/(\text{Site-}C_6+\text{Site-}C_{29}+\text{Site-}C_{30})$ $a_{30}= \text{Site-}C_{30}/(\text{Site-}C_6+\text{Site-}C_{29}+\text{Site-}C_{30})$	R32
$C_6 + 2\text{Site-}C_{30} \leftrightarrow \text{Site-}C_6 + 2C_{30}$	$a_6\text{Site-}C_6\cdot C_{30}^2=10^{0.6}C_6\cdot(a_{30}\text{Site-}C_{30})^2$ $a_6= \text{Site-}C_6/(\text{Site-}C_6+\text{Site-}C_{29}+\text{Site-}C_{30})$ $a_{30}= \text{Site-}C_{30}/(\text{Site-}C_6+\text{Site-}C_{29}+\text{Site-}C_{30})$	R33

Totally, we have 41 species, 28 equilibrium reactions, and 5 kinetic reactions. Thus, 13 kinetic-variable transport equations (Table 5.1-2) and 28 equilibrium reaction algebraic equations (Table 5.1-3) were set up through decomposition and solved for 41 species. Among the 13 kinetic-variables, the 6th, 7th, 9th, and 11th contain no mobile species and are thus not solved in the advective-dispersive transport step. Therefore, instead of solving 29 advective-dispersive transport equations for 29 mobile species in a primitive approach, we only need to solve 9 advective-dispersive transport equations for 9 kinetic-variables. Since the fast reaction is decoupled and not included in the transport equations any more, robust numerical integration can be achieved.

Table 5.1-2 Kinetic-variable Transport Equations for Example 5.1-3

Equations	No.
$\partial(AE_1)/\partial t + L(E_1^m) = A(-R31+R32)$ where $E_1 = E_1^m = \rho_{C_6}C_6 + \rho_{C_7}C_7 + \rho_{C_8}C_8 + \rho_{C_9}C_9 + 0.5\rho_{C_{30}}C_{30}$	1
$\partial(AE_2)/\partial t + L(E_2^m) = A(-R29-R30)$ where $E_2 = E_2^m = \rho_{C_3}C_3 + \rho_{C_4}C_4 + \rho_{C_{19}}C_{19} + \rho_{C_{20}}C_{20} + \rho_{C_{21}}C_{21} + \rho_{C_{22}}C_{22}$	2
$\partial(AE_3)/\partial t + L(E_3^m) = A(0.5R29+0.5R30-R31)$ where $E_3 = -\rho_{C_1}C_1 - 0.5\rho_{C_2}C_2 - 1.5\rho_{C_4}C_4 + \rho_{C_5}C_5 + \rho_{C_7}C_7 + 0.5\rho_{C_8}C_8 + 0.5\rho_{C_9}C_9 - 0.5\rho_{C_{11}}C_{11}$ $+0.5\rho_{C_{12}}C_{12} + \rho_{C_{13}}C_{13} - 0.5\rho_{C_{14}}C_{14} + 0.5\rho_{C_{16}}C_{16} + \rho_{C_{17}}C_{17} - \rho_{C_{18}}C_{18} - \rho_{C_{19}}C_{19} - \rho_{C_{20}}C_{20}$ and $-0.5\rho_{C_{21}}C_{21} + 0.5\rho_{C_{23}}C_{23} - 0.5\rho_{C_{25}}C_{25} - \rho_{C_{26}}C_{26} + 0.5\rho_{C_{27}}C_{27} + 0.5\rho_M M + 0.5\rho_{S_1}S_1 + \rho_{S_2}S_2$ $E_3^m = -\rho_{C_1}C_1 - 0.5\rho_{C_2}C_2 - 1.5\rho_{C_4}C_4 + \rho_{C_5}C_5 + \rho_{C_7}C_7 + 0.5\rho_{C_8}C_8 + 0.5\rho_{C_9}C_9$ $-0.5\rho_{C_{11}}C_{11} + 0.5\rho_{C_{12}}C_{12} + \rho_{C_{13}}C_{13} - 0.5\rho_{C_{14}}C_{14} + 0.5\rho_{C_{16}}C_{16} + \rho_{C_{17}}C_{17} - \rho_{C_{18}}C_{18}$ $-\rho_{C_{19}}C_{19} - \rho_{C_{20}}C_{20} - 0.5\rho_{C_{21}}C_{21} + 0.5\rho_{C_{23}}C_{23} - 0.5\rho_{C_{25}}C_{25} - \rho_{C_{26}}C_{26} + 0.5\rho_{C_{27}}C_{27}$	3
$\partial(AE_4)/\partial t + L(E_4^m) = A(-R1-0.5R29-1.5R30+R31)$ where $E_4 = \rho_{C_1}C_1 + 0.5\rho_{C_2}C_2 - 0.5\rho_{C_3}C_3 + 1.5\rho_{C_4}C_4 - 2\rho_{C_5}C_5 - 2\rho_{C_7}C_7 - 1.5\rho_{C_8}C_8 - 0.5\rho_{C_9}C_9$ $-\rho_{C_{10}}C_{10} - 0.5\rho_{C_{11}}C_{11} - 1.5\rho_{C_{12}}C_{12} - 2\rho_{C_{13}}C_{13} + 0.5\rho_{C_{14}}C_{14} - 0.5\rho_{C_{16}}C_{16} - \rho_{C_{17}}C_{17} + \rho_{C_{18}}C_{18}$ and $+\rho_{C_{20}}C_{20} + 0.5\rho_{C_{21}}C_{21} - 1.5\rho_{C_{23}}C_{23} - \rho_{C_{24}}C_{24} - 0.5\rho_{C_{25}}C_{25} - 0.5\rho_{C_{27}}C_{27} + 0.5\rho_M M + 0.5\rho_{S_1}S_1 + \rho_{S_3}S_3$ $E_4^m = \rho_{C_1}C_1 + 0.5\rho_{C_2}C_2 - 0.5\rho_{C_3}C_3 + 1.5\rho_{C_4}C_4 - 2\rho_{C_5}C_5 - 2\rho_{C_7}C_7 - 1.5\rho_{C_8}C_8$ $-0.5\rho_{C_9}C_9 - \rho_{C_{10}}C_{10} - 0.5\rho_{C_{11}}C_{11} - 1.5\rho_{C_{12}}C_{12} - 2\rho_{C_{13}}C_{13} + 0.5\rho_{C_{14}}C_{14} - 0.5\rho_{C_{16}}C_{16}$ $-\rho_{C_{17}}C_{17} + \rho_{C_{18}}C_{18} + \rho_{C_{20}}C_{20} + 0.5\rho_{C_{21}}C_{21} - 1.5\rho_{C_{23}}C_{23} - \rho_{C_{24}}C_{24} - 0.5\rho_{C_{25}}C_{25} - 0.5\rho_{C_{27}}C_{27}$	4
$\partial(AE_5)/\partial t + L(E_5^m) = AR1$ where $E_5 = \rho_{C_1}C_1 + \rho_{C_{10}}C_{10} + \rho_{C_{11}}C_{11} + \rho_{C_{12}}C_{12} + \rho_{C_{13}}C_{13} + \rho_{C_{14}}C_{14} + \rho_{C_{15}}C_{15} + \rho_{C_{16}}C_{16} + \rho_{C_{17}}C_{17} + 2\rho_{C_{18}}C_{18} + \rho_{S_5}S_5$ and $E_5^m = \rho_{C_1}C_1 + \rho_{C_{10}}C_{10} + \rho_{C_{11}}C_{11} + \rho_{C_{12}}C_{12} + \rho_{C_{13}}C_{13} + \rho_{C_{14}}C_{14} + \rho_{C_{15}}C_{15} + \rho_{C_{16}}C_{16} + \rho_{C_{17}}C_{17} + 2\rho_{C_{18}}C_{18}$	5
$\partial(AE_6)/\partial t + L(E_6^m) = AR29$ where $E_6 = \rho_{S_6}S_6$ and $E_6^m = 0$	6
$\partial(AE_7)/\partial t + L(E_7^m) = AR30$ where $E_7 = \rho_{S_7}S_7$ and $E_7^m = 0$	7
$\partial(AE_8)/\partial t + L(E_8^m) = A(-R1-R29-R31)$ where $E_8 = -\rho_{C_1}C_1 + \rho_{C_3}C_3 + \rho_{C_5}C_5 + \rho_{C_7}C_7 + \rho_{C_8}C_8 - \rho_{C_{14}}C_{14} - \rho_{C_{15}}C_{15} - \rho_{C_{16}}C_{16}$ and $-\rho_{C_{17}}C_{17} - 2\rho_{C_{18}}C_{18} + \rho_{C_{19}}C_{19} + \rho_{C_{23}}C_{23} + \rho_{C_{24}}C_{24} + \rho_{C_{25}}C_{25} + \rho_{C_{26}}C_{26} + \rho_{S_4}S_4$ $E_8^M = -\rho_{C_1}C_1 + \rho_{C_3}C_3 + \rho_{C_5}C_5 + \rho_{C_7}C_7 + \rho_{C_8}C_8 - \rho_{C_{14}}C_{14} - \rho_{C_{15}}C_{15} - \rho_{C_{16}}C_{16}$ $-\rho_{C_{17}}C_{17} - 2\rho_{C_{18}}C_{18} + \rho_{C_{19}}C_{19} + \rho_{C_{23}}C_{23} + \rho_{C_{24}}C_{24} + \rho_{C_{25}}C_{25} + \rho_{C_{26}}C_{26}$	8
$\partial(AE_9)/\partial t + L(E_9^m) = AR31$ where $E_9 = \rho_{S_8}S_8$ and $E_9^m = 0$	9
$\partial(AE_{10})/\partial t + L(E_{10}^m) = A(-R32)$ where $E_{10} = E_{10}^m = \rho_{C_{29}}C_{29}$	10
$\partial(AE_{11})/\partial t + L(E_{11}^m) = AR32$ where $E_{11} = \rho_{Site-C_{29}}Site - C_{29}$ and $E_{11}^m = 0$	11
$\partial(AE_{12})/\partial t + L(E_{12}^m) = 0$ where $E_{12} = \rho_{C_{30}}C_{30} + \rho_{Site-C_{30}}Site - C_{30}$ and $E_{12}^m = \rho_{C_{30}}C_{30}$	12

$\partial(AE_{13})/\partial t + L(E_{13}^{m}) = A(-R32)$ where $E_{13} = -0.5\rho_{C_{30}}C_{30} + \rho_{Site-C_6}Site-C_6$ and $E_{13}^{m} = -0.5\rho_{C_{30}}C_{30}$	13

Note: $\rho_i = \rho_w$ for C_1~C_{27}, C_{29}, and C_{30}; $\rho_i = Ph_b\rho_{wb}\theta_b/A$, for M; and $\rho_i = PBS/A$, for S_1~S_8, site-C_6, site-C_{29} and site-C_{30} ($\rho_w = \rho_{wb} = 1.0$ kg/L, $h_b = 0.2$ m, $\theta_b = 0.6$, and BS = 1 kg/m^2).

Table 5.1-3 Equilibrium Reaction Algebraic Equations for Example 5.1-3

Equations	No.
$0.0047M = S_1 + S_2 + S_3 + S_4 + S_5 + S_6 + S_7 + S_8$	1
$Site\text{-}C_6^{2} \cdot C_{30}^{2} = 10^{0.6}C_6 \cdot Site\text{-}C_{30}^{4} / (Site\text{-}C_6 + Site\text{-}C_{29} + Site\text{-}C_{30})$	2
$C_4 = (K_{25}^e)^{1.5} / \left[K_{19}^e (K_{26}^e)^{1.5} \right] \cdot C_{22}S_3^{1.5} / S_2^{1.5}$	3
$C_5 = (K_{26}^e)^2 / (K_{25}^e K_{27}^e) \cdot S_2S_4 / S_3^2$	4
$C_2 = (K_{25}^e)^{0.5} / (K_{26}^e)^{0.5} \cdot S_3^{0.5} / S_2^{0.5}$	5
$C_7 = K_4^e (K_{26}^e)^2 / (K_{25}^e K_{27}^e) \cdot C_6S_2S_4 / S_3^2$	6
$C_1 = K_{25}^e K_{27}^e / (K_{26}^e K_{28}^e) \cdot S_3S_5 / (S_2S_4)$	7
$C_9 = K_6^e K_{26}^e / (K_{25}^e)^{0.5} \cdot C_6S_2^{0.5} / S_3^{0.5}$	8
$C_{10} = K_7^e K_{26}^e / K_{28}^e \cdot S_5 / S_3$	9
$C_{11} = K_8^e (K_{25}^e)^{0.5} (K_{26}^e)^{0.5} / K_{28}^e \cdot S_5 / (S_2^{0.5}S_3^{0.5})$	10
$C_8 = K_5^e (K_{26}^e)^{1.5} / \left[(K_{25}^e)^{0.5} K_{27}^e \right] \cdot S_2^{0.5}S_4 / S_3^{1.5}$	11
$C_{12} = K_9^e (K_{26}^e)^{1.5} / \left[(K_{25}^e)^{0.5} K_{28}^e \right] \cdot S_2^{0.5}S_5 / S_3^{1.5}$	12
$C_{14} = K_{11}^e (K_{25}^e)^{0.5} K_{27}^e / \left[(K_{26}^e)^{0.5} K_{28}^e \right] \cdot S_3^{0.5}S_5 / (S_2^{0.5}S_4)$	13
$C_{15} = K_{12}^e K_{27}^e / K_{28}^e \cdot S_5 / S_4$	14
$C_{16} = K_{13}^e (K_{26}^e)^{0.5} K_{27}^e / \left[(K_{25}^e)^{0.5} K_{28}^e \right] \cdot S_2^{0.5}S_5 / (S_3^{0.5}S_4)$	15
$C_{17} = K_{14}^e K_{26}^e K_{27}^e / (K_{25}^e K_{28}^e) \cdot S_2S_5 / (S_3S_4)$	16
$C_{13} = K_{10}^e (K_{26}^e)^2 / (K_{25}^e K_{28}^e) \cdot S_2S_5 / S_3^2$	17
$C_3 = (K_{25}^e)^{0.5} (K_{26}^e)^{0.5} / (K_3^e K_{19}^e K_{27}^e) \cdot C_{22}S_4 / (S_2^{0.5}S_3^{0.5})$	18
$C_{20} = K_{17}^e K_{25}^e / (K_{19}^e K_{26}^e) \cdot C_{22}S_3 / S_2$	19
$C_{19} = K_{16}^e K_{25}^e / (K_{19}^e K_{27}^e) \cdot C_{22}S_4 / S_2$	20
$C_{21} = K_{18}^e (K_{25}^e)^{0.5} / \left[K_{19}^e (K_{26}^e)^{0.5} \right] \cdot C_{22}S_3^{0.5} / S_2^{0.5}$	21
$C_{23} = K_{20}^e (K_{26}^e)^{1.5} / \left[(K_{25}^e)^{0.5} K_{27}^e \right] \cdot S_2^{0.5}S_4 / S_3^{1.5}$	22
$C_{24} = K_{21}^e K_{26}^e / K_{27}^e \cdot S_4 / S_3$	23
$C_{25} = K_{22}^e (K_{25}^e)^{0.5} (K_{26}^e)^{0.5} / K_{27}^e \cdot S_4 / (S_2^{0.5}S_3^{0.5})$	24
$S_1 = S_2^{0.5}S_3^{0.5} / \left[(K_{25}^e)^{0.5} (K_{26}^e)^{0.5} \right]$	25
$C_{27} = K_{24}^e (K_{26}^e)^{0.5} / (K_{25}^e)^{0.5} \cdot S_2^{0.5} / S_3^{0.5}$	26
$C_4 = K_{23}^e K_{25}^e / K_{27}^e \cdot S_4 / S_2$	27
$C_5 = K_{15}^e K_{25}^e (K_{27}^e)^2 / \left[K_{26}^e (K_{28}^e)^2 \right] \cdot S_3S_5^2 / (S_2S_4^2)$	28

As simulation starts, variable boundary conditions are applied to both the upstream and downstream

boundary nodes. Initial and coming-in concentrations are listed in Table 5.1-4. The longitudinal dispersivity is 80 m. A 90,000-second simulation is performed with a fixed time step size of 150-second.

The concentration distributions of M, C_1, and S_1 at different simulation time are plotted in Figure 5.1-4. Due to the dissolution reaction R1, the bed precipitate M gradually dissolutes into dissolved chemical C_1 in the mobile water phase. Therefore, we observe decreasing concentration of M with time and increasing concentration of C_1 along the down stream direction. Due to the sorbing site forming reaction R2, the concentration of S_1 decreases with time as the surface area of M decreases along with dissolution. Since S_1 involves in seven sorption reactions R25~R31, its concentration distribution is also affected by these reactions and related species.

Table 5.1-4 Initial and Boundary Concentrations for Example 5.1-3

Species	Initial	Boundary
C_1	1.0e-7 mol/Kg	1.0e-7 mol/L
C_2	1.0e-5 mol/Kg	1.0e-5 mol/L
C_3	1.0e-7 mol/Kg	1.0e-4 mol/L
C_4	1.0e-5 mol/Kg	1.0e-5 mol/L
C_5	1.0e-5 mol/Kg	1.0e-5 mol/L
C_6	1.0e-5 mol/Kg	1.0e-4 mol/L
C_{10}	1.0e-5 mol/Kg	1.0e-5 mol/L
C_{29}	1.0e-5 mol/Kg	1.0e-5 mol/L
C_{30}	1.0e-5 mol/Kg	1.0e-4 mol/L
M	2.0e-5 mol/Kg	-
Site-C_6	1.4e-4 mol/g	-
Site-C_{29}	7.0e-4 mol/g	-
Site-C_{30}	1.5e-4 mol/g	-

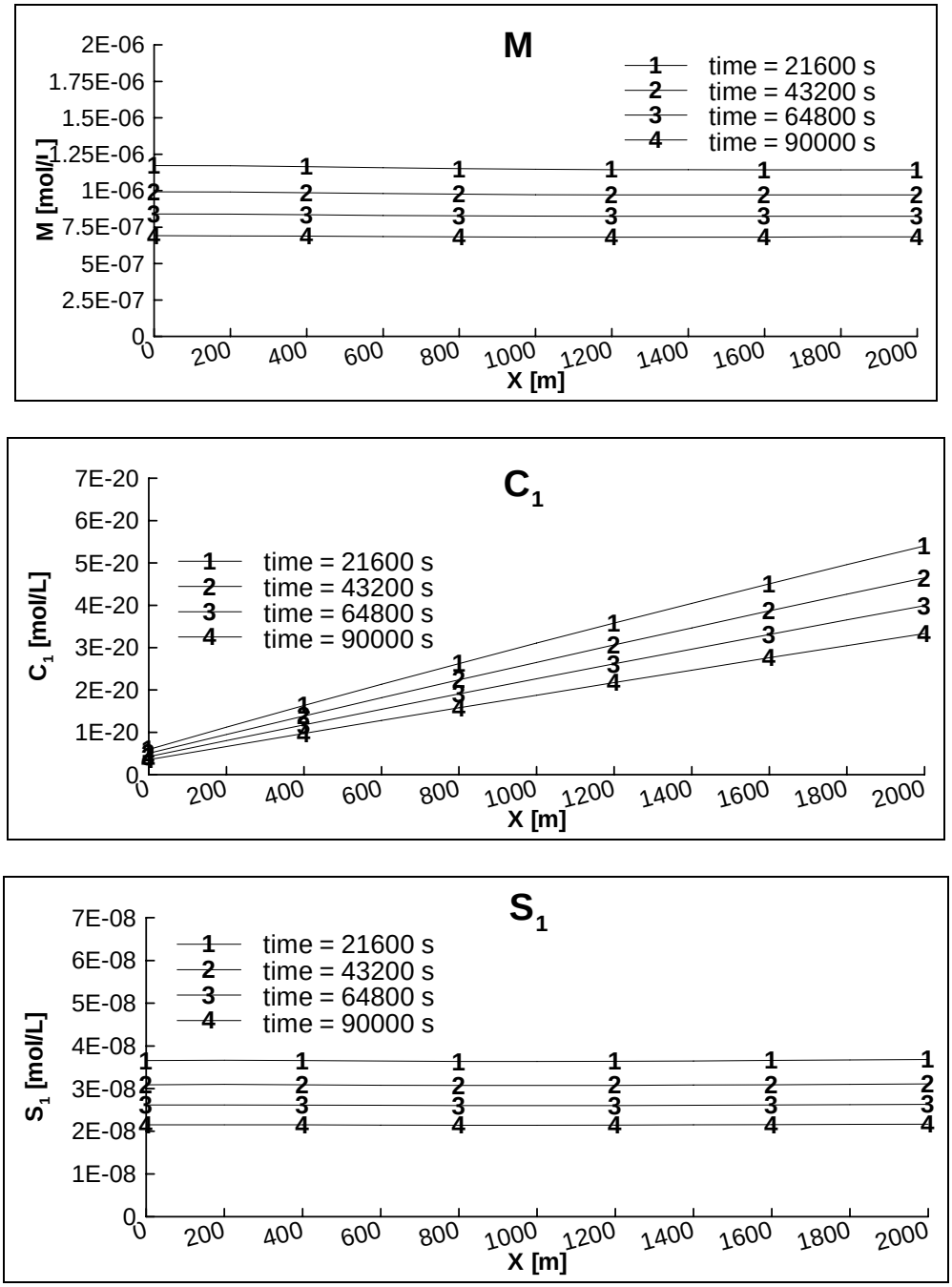

Fig. 5.1-4. Concentration Profiles for Species M, C_1, and S_1 for Example 5.1-3

5.1.4 River/Stream Transport with all Ten Types of Reactions

This example is to demonstrate the capability of the model in simulating sediment and reactive chemical transport subjected to all ten types of reactions presented in Figure 2.5-2.

A horizontally 20 km-long river/stream containing a uniform width of 20 m is considered. The domain is discretized into 100 equal size elements (200 m each). To focus on transport, we assume water depth is 2 m, and river/stream velocity is 1 m/s throughout the river/stream. Only one size of cohesive sediment is taken into account with settling speed of 1.0×10^{-6} m/s, erodibility of 0.15 $g/m^2/s$, critical shear stresses for deposition of 2.85 $g/m/s^2$, and critical shear stresses for erosion of 2.48 $g/m/s^2$. Manning's roughness is 0.02.

Fourteen chemical species are taken account including three dissolved chemicals in the mobile water phase (CMW1, CMW2, and CMW3), three dissolved chemicals in the immobile water phase (CIMW1, CIMW2, and CIMW3), three particulate chemicals in the suspended sediment phase (CS1, CS2, and CS3), three particulate chemicals in the bed sediment phase (CB1, CB2, and CB3), one suspension precipitate (SP3) and one bed precipitate (BP3). As shown in Table 5.1-5, these species are considered to undergo all ten types of reactions illustrated in Figure 2.5-2. Totally, there are twenty reactions, among which, R1 is an equilibrium aqueous complexation reaction among three dissolved chemicals in the mobile water phase; R2 through R4 are kinetic adsorption reactions of three dissolved chemicals in the mobile water phase onto the suspended sediment; R5 through R7 are kinetic adsorption reactions of three dissolved chemicals in the mobile water phase onto the bed sediment; R8 through R10 are kinetic sedimentation reactions of three particulates between suspended and bed sediment phases; R11 through R13 are kinetic diffusion of three dissolved chemicals between mobile and immobile water phases; R14 is a kinetic aqueous complexation reaction among three dissolved chemicals in the immobile water phase; R15 through R17 are kinetic adsorption reactions of three dissolved chemicals in the immobile water phase onto the bed sediment; R18 is a kinetic volatilization reaction of the second dissolved chemical in the mobile water phase; R19 is a kinetic precipitation/dissolution reaction between the third dissolved chemical in the mobile water phase and suspended precipitate; and R20 is a kinetic precipitation/dissolution reaction between the third dissolved chemical in the immobile water phase and bed precipitate;.

Totally, we have 14 species, one equilibrium reaction, and 19 kinetic reactions. Thus, 13 kinetic-variable transport equations and one equilibrium-reaction mass action equation were set up through decomposition and solved for 14 species (Table 5.1-6). Among the 13 kinetic-variables, the 6th through 11th and the 13th contain no mobile species and are thus not solved in the advective-dispersive transport step. Therefore, instead of solving seven advective-dispersive transport equations for mobile species in a primitive approach, we only need to solve six advective-dispersive transport equations for kinetic-variables. Since the fast reaction is decoupled and not included in the transport equations any more, robust numerical integration is enabled.

Table 5.1-5 Chemical Reactions Considered in Example 5.1.4

Reaction and rate parameter	Type	No.
CMW1 + CMW2 $\leftrightarrow$ CMW3 (k_{eq} = 0.4 m^3/g)	1	R_1
CMW1+ SS $\leftrightarrow$ CS1 + SS CMW2+ SS $\leftrightarrow$ CS2 + SS CMW3+ SS $\leftrightarrow$ CS3 + SS (k_f = 0.001 m^3/gSS/s, k_b = 0.0 s^{-1})	2	R_2 R_3 R_4
CMW1+ BS $\leftrightarrow$ CB1 + BS CMW2+ BS $\leftrightarrow$ CB2 + BS CMW3+ BS $\leftrightarrow$ CB3 + BS (k_f = 0.00001 m^2/gBS/s, k_b = 0.0P/A $m^{-1}s^{-1}$)	4	R_5 R_6 R_7
CS1 $\leftrightarrow$ CB1 (k_f = $Depo_1$P/A gSS/m^3/s, k_b = $Eros_1$P/A gBS/m^3/s) CS2 $\leftrightarrow$ CB2 (k_f = $Depo_2$P/A gSS/m^3/s , k_b = $Eros_2$P/A gBS/m^3/s) CS3 $\leftrightarrow$ CB3 (k_f = $Depo_3$P/A gSS/m^3/s, k_b = $Eros_3$P/A gBS/m^3/s)	10	R_8 R_9 R_{10}
CMW1 $\leftrightarrow$ CIMW1 CMW2 $\leftrightarrow$ CIMW2 CMW3 $\leftrightarrow$ CIMW3 (k_f = 0.0001 s^{-1}, k_b = 0.0$Ph_b\theta_b$/A s^{-1})	9	R_{11} R_{12} R_{13}
CIMW1+ CIMW2 $\leftrightarrow$CIMW3 (k_f = 0.0002$Ph_b\theta_b$/A m^3/g/s , k_b = 0.0005$Ph_b\theta_b$/A s^{-1})	5	R_{14}
CIMW1 + BS $\leftrightarrow$ CB1 + BS CIMW2 + BS $\leftrightarrow$ CB2 + BS CIMW3 + BS $\leftrightarrow$ CB3 + BS (k_f = 0.00001$Ph_b\theta_b$/A m^2/gBS/s, k_b = 0.0P/A $m^{-1}s^{-1}$)	6	R_{15} R_{16} R_{17}
CMW2 $\leftrightarrow$ P (k_f = 0.0002 s^{-1}, k_b = 0.02 g/m^3/ATM/s, P=0.0025ATM)	8	R_{18}
CMW3 $\leftrightarrow$ SP3 (k_f = 0.001 s^{-1}, k_b = 0.000001 s^{-1})	3	R_{19}
CIMW3 $\leftrightarrow$ BP3 (k_f = 0.0001$Ph_b\theta_b$/A s^{-1}, k_b = 0.0000001$Ph_b\theta_b$/A s^{-1})	7	R_{20}

Note: the reaction types are defined in Figure 2.5-2.

Table 5.1-6 Equations Obtained through Decomposition in Example 5.1-4

Equations	Type
$\partial(AE_1)/\partial t + L(E_1^m) = A(-R_2 - R_4 - R_5 - R_7 - R_{11} - R_{13} - R_{19})$ where $E_1 = E_1^m = \rho_{CMW1}C_{CMW1} + \rho_{CMW3}C_{CMW3}$	1
$\partial(AE_2)/\partial t + L(E_2^m) = A(-R_3 - R_4 - R_6 - R_7 - R_{12} - R_{13} - R_{18} - R_{19})$ where $E_2 = E_2^m = \rho_{CMW2}C_{CMW2} + \rho_{CMW3}C_{CMW3}$	1
$\partial(AE_3)/\partial t + L(E_3^m) = A(R_2 - R_8)$ where $E_3 = E_3^m = \rho_{CS1}C_{CS1}$	1
$\partial(AE_4)/\partial t + L(E_4^m) = A(R_3 - R_9)$ where $E_4 = E_4^m = \rho_{CS2}C_{CS2}$	1
$\partial(AE_5)/\partial t + L(E_5^m) = A(R_4 - R_{10})$ where $E_5 = E_5^m = \rho_{CS3}C_{CS3}$	1
$\partial(AE_6)/\partial t + L(E_6^m) = A(R_5 + R_8 + R_{15})$ where $E_6 = \rho_{CB1}C_{CB1}$ and $E_6^m = 0$	1
$\partial(AE_7)/\partial t + L(E_7^m) = A(R_6 + R_9 + R_{16})$ where $E_7 = \rho_{CB2}C_{CB2}$ and $E_7^m = 0$	1
$\partial(AE_8)/\partial t + L(E_8^m) = A(R_7 + R_{10} + R_{17})$ where $E_8 = \rho_{CB3}C_{CB3}$ and $E_8^m = 0$	1
$\partial(AE_9)/\partial t + L(E_9^m) = A(R_{11} - R_{14} - R_{15})$ where $E_9 = \rho_{CIMW1}C_{CIMW1}$ and $E_9^m = 0$	1
$\partial(AE_{10})/\partial t + L(E_{10}^m) = A(R_{12} - R_{14} - R_{16})$ where $E_{10} = \rho_{CIMW2}C_{CIMW2}$ and $E_{10}^m = 0$	1
$\partial(AE_{11})/\partial t + L(E_{11}^m) = A(R_{13} + R_{14} - R_{17} - R_{20})$ where $E_{11} = \rho_{CIMW3}C_{CIMW3}$ and $E_{11}^m = 0$	1
$\partial(AE_{12})/\partial t + L(E_{12}^m) = AR_{19}$ where $E_{12} = E_{12}^m = \rho_{SP3}C_{SP3}$	1
$\partial(AE_{13})/\partial t + L(E_{13}^m) = AR_{20}$ where $E_{13} = \rho_{BP3}C_{BP3}$ and $E_{13}^m = 0$	1
$C_{CMW3} = 0.4C_{CMW1}C_{CMW2}$	2

Note: the equation type 1 is kinetic-variable transport equation and type 2 is equilibrium reaction mass action equation.
$\rho_i = \rho_w$ for CMW1~CMW3, and SP3; ρ_i = SS for CS1~CS3; $\rho_i = Ph_b\rho_{wb}\theta_b/A$, for IMW1~CIMW3, and BP3; and ρ_i = PBS/A, for CB1~CB3 ($\rho_w = \rho_{wb}$ = 1.0 kg/L, h_b = 0.1 m, and θ_b = 0.5).

Initially, only sediment exists in the domain of interest with suspended concentration SS of 1 g/m^3 and bed concentration BS of 50 g/m^2. As simulation starts, Dirichlet boundary conditions are applied to the upstream boundary node, where suspended sediment has a constant concentration of 1 g/m^3 and dissolved chemicals in mobile water phase have constant concentrations of 1 mg/kg and all the other mobile chemicals have zero concentration. Out-flow variable boundary conditions are applied to the downstream boundary node. The longitudinal dispersivity is 80 m. A 90,000-second simulation is performed with a fixed time step size of 150-second. Simulation results are shown in Figure 5.1-5.

Figure 5.1-5 shows trend of increasing concentration of the suspended sediment along down stream direction, and depicts decrease of the bed sediment with increase of time. It indicates that deposition is less than erosion under the condition set for this example.

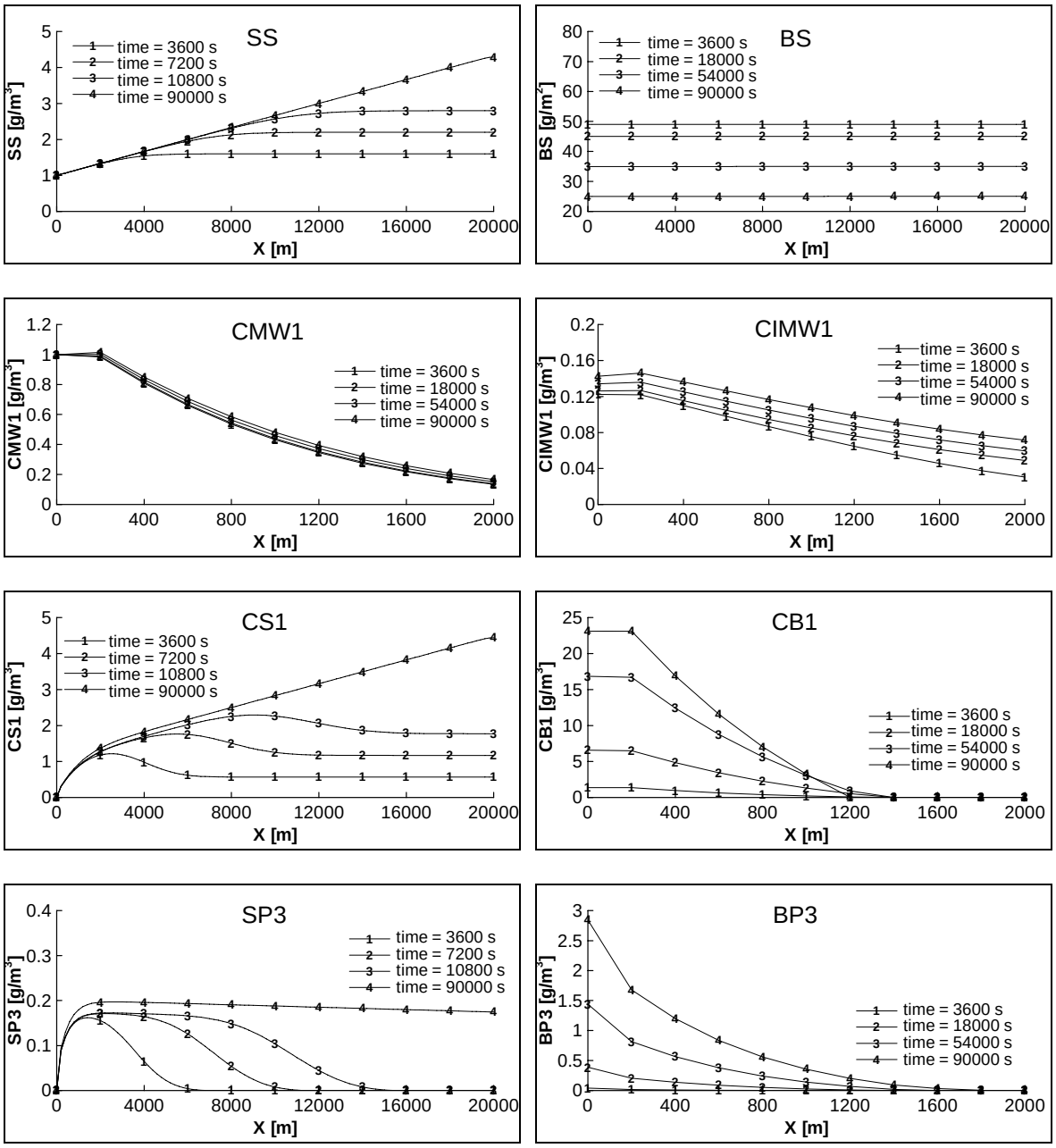

Fig. 5.1-5. Concentration Profiles of Various Species for Example 5.1-4

Figure 5.1-5 shows the decreasing concentration of CMW1 along the downstream direction. This is because we allow the adsorption to happen, but do not allow desorption from particulate chemicals to dissolved chemicals to occur. In the zone near the Dirichlet boundary, the concentration distribution curve of CMW1 is not smooth. Due to the fast reaction among the three dissolved chemicals in the mobile water phase, the concentration of CMW1 increases to its equilibrium value. The only source of dissolved chemicals in the immobile water phase is the corresponding dissolved chemicals in the mobile water phase. Therefore, concentration distribution of CIMW1 shows the similar pattern of CMW1.

Since the dissolved chemicals are little in the downstream region, the major source of chemicals is the particulate chemicals on suspended sediments that are transported from the upstream region along with water. Because erosion is greater than deposition, we observe increase of CS1 with time and decrease of CB1 along the downstream direction. Since the particulate chemicals on bed sediment result not only from dissolved chemicals in mobile water phase, but also from those in the immobile water phase, the decrease of CB1 along the downstream also reflects the similar pattern of CMW1 and CIMW1.

Since the major source of suspension precipitate in the downstream region is transported from the upstream region along with water, we observe an increase of suspension precipitate concentration with time. Since bed precipitate is involved in the precipitation reaction only, Figure 5.1-5 also shows decreasing bed precipitate concentration along the downstream direction reflecting the similar decrease of dissolved chemical concentration in the immobile phase.

5.1.5 River/Stream Transport with Eutrophication

This example is to demonstrate the capability of the model in simulating the chemical transport related to eutrophication reported in WASP5 (Ambrose et al., 1993).

WASP5, the Water quality Analysis Simulation Program, is a three-dimensional conventional water quality analysis simulation program. It is a group of mechanistic models capable of simulating water transport and fate and transport of water quality constituents and toxic organics for aquatic systems. Various components of WASP5 have been used to study a variety of river, lake, reservoir, and estuarine issues including ecological characterization, the effects of anthropogenic activities, and the impact of mitigation measures (Bierman and James, 1995; Lung and Larson, 1995; Tufford and McKellar, 1999; and Zheng et al., 2004).

EUTRO5 is a general operational WASP5 model used to simulate nutrient enrichment, eutrophication, and dissolved oxygen in the aquatic environment. It constitutes a complex of four interacting systems: dissolved oxygen, nitrogen cycle, phosphorus cycle, and phytoplankton dynamics. It can simulate up to eight eutrophication constituents in both water column and benthic layer, including: (1) Ammonia NH_3 and $NH_{3(b)}$, (2) Nitrate NO_3 and $NO_{3(b)}$, (3) Inorganic Phosphorus OPO_4 and $OPO_{4(b)}$, (4) Phytoplankton PHYT and $PHYT_{(b)}$, (5) Carbonaceous CH_2Ot and $CH2Ot_{(b)}$, (6) Oxygen O_2 and $O_{2(b)}$, (7) Organic Nitrogen ONt and $ONt_{(b)}$, and (8) Organic Phosphorus OPt and $OPt_{(b)}$, where 't' means total and '(b)' means benthic.

According to our definition of chemical phases and forms, the total concentration of a species is the sum of the dissolved chemical and the particulate sorbed onto sediments, such as $CH2Ot = CH_2O + CH2Op$, $CH2Ot_{(b)} = CH2O_{(b)} + CH2Op_{(b)}$, $ONt = ON + ONp$, $ONt_{(b)} = ON_{(b)} + ONp_{(b)}$, $OPt = OP + OPp$, and $OPt_{(b)} = OP(b) + OPp_{(b)}$), where 'p' means particulate. Therefore, the 16 species simulated in EUTRO5 were transformed into 22 chemical species listed in Table 5.1-7 and simulated in our model. The sixteen working equations of EUTRO5 were recast in terms of reaction network used in our eutrophication simulation. The reaction network includes 32 kinetic reactions and 6 equilibrium reactions (Zhang, 2005).

Table 5.1-7 Chemical Species in Example 5.1.5

Notation	Conc.	Initial Conditions	Boundary Conditions	ρ_i
NH_3	C_1	0.1 mg N/kg	1 mg N/kg	ρ_w
$NH_{3(b)}$	C_2	0.1 mg N/kg	-	$Ph_b\rho_{wb}\theta_b/A$
NO_3	C_3	0.1 mg N/kg	1 mg N/kg	ρ_w
$NO_{3(b)}$	C_4	0.1 mg N/kg	-	$Ph_b\rho_{wb}\theta_b/A$
OPO_4	C_5	0.01 mg P/kg	0.1 mg P/kg	ρ_w
$OPO_{4(b)}$	C_6	0.01 mg P/kg	-	$Ph_b\rho_{wb}\theta_b/A$
PHYT	C_7	0.2 mg C/kg	2 mg C/kg	ρ_w
$PHYT_{(b)}$	C_8	0.2 mg C/kg	-	$Ph_b\rho_{wb}\theta_b/A$
CH_2O	C_9	1.0 mg O_2/kg	10 mg O_2/kg	ρ_w
$CH_2O_{(p)}$	C_{10}	1.0 mg O_2/mg	10 mg O_2/mg	SS
$CH_2O_{(b)}$	C_{11}	1.0 mg O_2/kg	-	$Ph_b\rho_{wb}\theta_b/A$
$CH_2O_{(bp)}$	C_{12}	0.01 mg O_2/mg	-	PBS/A
O_2	C_{13}	0.2 mg O_2/kg	2 mg O_2/kg	ρ_w
$O_{2(b)}$	C_{14}	0.2 mg O_2/kg	-	$Ph_b\rho_{wb}\theta_b/A$
ON	C_{15}	0.2 mg N/kg	2 mg N/kg	ρ_w
$ON_{(p)}$	C_{16}	0.0 mg N/mg	0 mg N/mg	SS
$ON_{(b)}$	C_{17}	0.2 mg N/kg	-	$Ph_b\rho_{wb}\theta_b/A$
$ON_{(bp)}$	C_{18}	0.0 mg N/mg	-	PBS/A
OP	C_{19}	0.035 mg P/kg	0.35 mg P/kg	ρ_w
$OP_{(p)}$	C_{20}	0.015 mg P/mg	0.15 mg P/mg	SS
$OP_{(b)}$	C_{21}	0.035 mg P/kg	-	$Ph_b\rho_{wb}\theta_b/A$
$OP_{(bp)}$	C_{22}	0.00015 mg P/mg	-	PBS/A

Note: $\rho_w = \rho_{wb} = 1$ kg/L, $h_b = 0.12$ m, and $\theta_b = 0.6$

The canal considered is 4738 m-long with width of 4.6~12.2 m. It is descretized with nine elements of size of 515~549 m. The flow pattern was simulated using the flow module of WASH123D. The calculated water depth is 2.17~2.81 m and river/stream velocity is 0.06~0.88 m/s. To focus on reactive chemical transport, we assume that the temperature is 15˚C, suspended sediment concentration SS is $1g/m^3$, and bed sediment concentration BS is 15 g/m^2 throughout the canal. Dirichlet boundary condition is applied to the upstream boundary node. Flow-out variable boundary condition is applied to the downstream boundary node. Initial concentrations of all species and Dirichlet boundary concentrations of mobile species are listed in Table 5.1-7. The longitudinal dispersivity is 90 m. A 12-day simulation is performed with a fixed time step size of 6 minutes.

Figure 5.1-6 plots the concentration distribution of phytoplankton and dissolved oxygen. The similar concentration pattern of PHYT and DO indicates that these mobile species concentration change is mainly controlled by the advective-dispersive transport rather than the biogeochemical reactions. However, the concentration change of immobile benthic species $PHYT_{(b)}$ and $DO_{(b)}$ is mainly affected by the biogeochemical reactions.

In the benthic immobile water phase, the concentration change of PHYT(b) is due to its decomposition and PHYT settling. Figure 5.1-6 shows increasing concentration of PHYT(b) with time, demonstrating that the settling rate of PHYT is greater than PHYT(b) decomposition rate. In the benthic immobile water phase, the concentration change of DO(b) is due to the consumption of oxidation and diffusion of DO. Figure 5.1-6 shows decreasing concentration of DO(b) at upstream. This indicates that at the upstream the diffusion rate of DO is less than the consumption rate of oxidation. As the simulation time increases, there is more DO at downstream. Figure 5.1-6 shows increasing concentration of DO(b) at downstream, demonstrating that the increased diffusion rate of DO is greater than the consumption rate of oxidation.

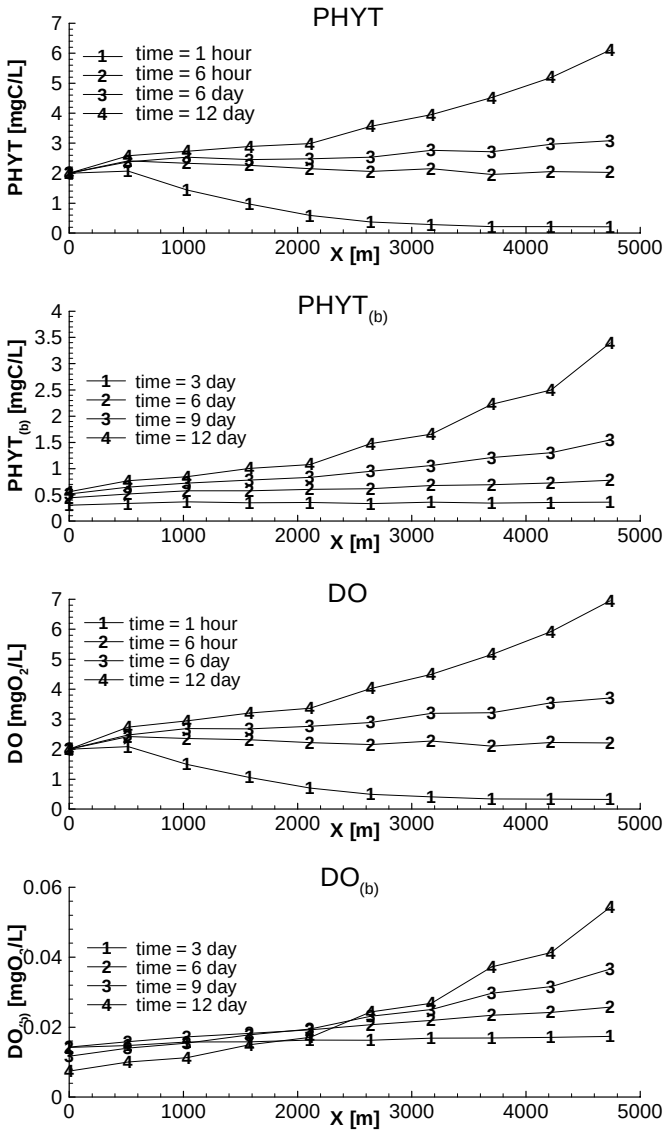

Fig. 5.1-6. Concentration Profiles of PHYT, $PHYT_{(b)}$, DO, and $DO_{(b)}$ for Example 5.1.5

5.1.6 River/Stream Transport with Junction

This example is to demonstrate the capability of the model in simulating sediment and chemical transport in river/stream network system with junction.

The system is composed of three river/stream reaches that are connected through a junction (figure 5.1-7). Each reach is 100 m long and is discretized with 11 nodes and 10 elements: Nodes 1 through 11 for Reach1, 12 through 22 for Reach 2, and 23 through 33 for Reach 3. Nodes 11, 12, and 23 coincide with one another and are located at the junction. The junction covers the area between

Node 11 and median of Nodes 10 and 11, Node 12 and median of Nodes 12 and 13, and Node 23 and median of Nodes 23 and 24.

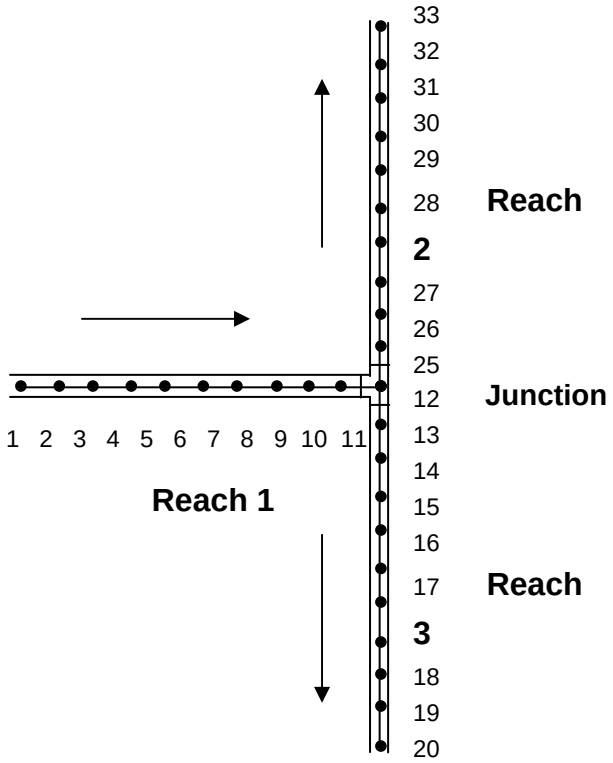

Fig. 5.1-7. River/stream Network for Example 5.1.6

Reach 1 has a uniform river/stream width of 2 m, while Reaches 2 and 3 contain a uniform river/stream width of 1 m. Manning's roughness is 0.028375 for all three reaches. To focus on transport, we assume water depth is 2 m and river/stream velocity is 1 m/s throughout the river/stream system under isotherm condition. Two dissolved chemicals are considered to undergo the following reaction:

$$CMW \rightleftharpoons CIMW \quad k_f = 0.001, \;\; k_b = 0 \qquad \textbf{(5.1.5)}$$

where CMW and CIMW represent dissolved chemicals in mobile water phase and immobile water phase, respectively.

Only one size of cohesive sediment is taken into account with settling speed of 1.2×10^{-6} m/s, critical shear stresses for deposition of 2.75 g/m/s^2 and critical shear stresses for erosion of 2.68 g/m/s^2. The following sorption reactions are included:

$$CMW + SS \rightleftharpoons CS + SS \quad k_f = 0.001, \; k_b = 0 \tag{5.1.6}$$

$$CMW + BS \rightleftharpoons CB + BS \quad k_f = 0.0001, \; k_b = 0 \tag{5.1.7}$$

$$CIMW + BS \rightleftharpoons CB + BS \quad k_f = 0.0001, \; k_b = 0 \tag{5.1.8}$$

where SS is suspended sediment, BS is bed sediment, CS is particulate chemical associated with CMW on SS, and CB is particulate chemical associated with CMW or CIMW on BS. We have, therefore, 4 species and 4 kinetic reactions in total.

Initially, only bed sediment exists in the domain of interest with initial concentration of 50 g/m^2. Dirichlet boundary conditions are applied to the upstream boundary node, where dissolved chemical in mobile water phase has a constant concentration of 1 mg/kg, suspended sediment and particulate on suspended sediment have zero concentration at this boundary node. The longitudinal dispersivity is 10 m. A 1000 second simulation is performed with a fixed time step size of 2 seconds. A relative error of 10^{-4} is used to determine the convergence for iterations involved in the computation.

Figures 5.1-8 through 5.1.13 plot the numerical results at various time, for concentration distributions of (1) suspended sediment (Figure 5.1-8), (2) bed sediment (Figure 5.1-9), (3) dissolved chemical in mobile water phase (Figure 5.1-10), (4) dissolved chemical in immobile water phase (Figure 5.1-11), (5) particulate chemical on suspended sediment (Figure 5.1-12), and (6) particulate chemical on bed sediment (Figure 5.1-13). Since Reaches 2 and 3 are symmetric in geometry, have identical river/stream width, velocity, and Manning's roughness, and are given same initial and boundary conditions for both sediments and chemicals, they have identical sediment and chemical concentration distribution patterns. Sediment and chemical concentration distribution patterns in Reaches 1 and 2/3 are provided through figures 5.1-8 and 5.1-13, where Reach 1 is the region with x-coordinate ranging from 0m to 100 m and Reach 2/3 is the region with x-coordinate ranging from 100 m to 200 m.

Figure 5.1-8 shows the trend of increasing concentration of suspended sediment along the down stream direction in Reach 1, while Figure 5.1-9 depicts the concentration decrease of bed sediment in Reach 1 with the increase of time. Figures 5.1-8 and 5.1-9 tell that the deposition is less than the erosion in Reach 1 under the condition set for this example. Figure 5.1-8 shows no change of bed sediment concentration either with simulation time or along the river/stream in Reach 2. This indicates that there are same amount of deposition and erosion in Reach 2. Since all the suspended sediment in Reach 2 is transported from upstream, its concentration increases with the simulation time and is approaching a steady state shown in figure 5.1-8. This steady state is maintained until the bed sediment upstream is depleted and no more suspended sediment is transported. At the junction, Figure 5.1-8 and figure 5.1-9 show increasing and decreasing concentrations of suspended and bed sediment, respectively. This tells that erosion is greater than deposition at the junction.

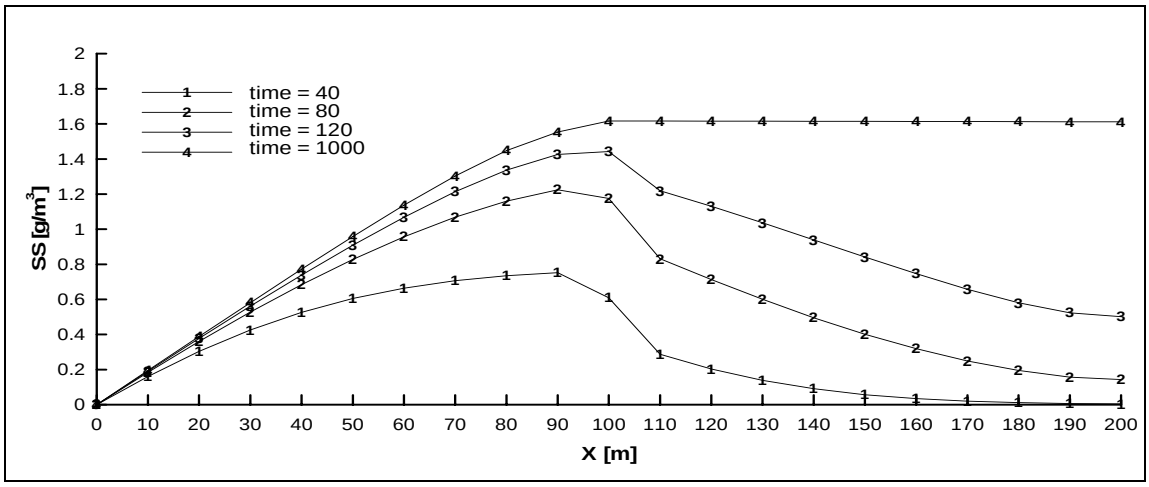

Fig. 5.1-8. Concentration of the Suspended Sediment for example 5.1.6

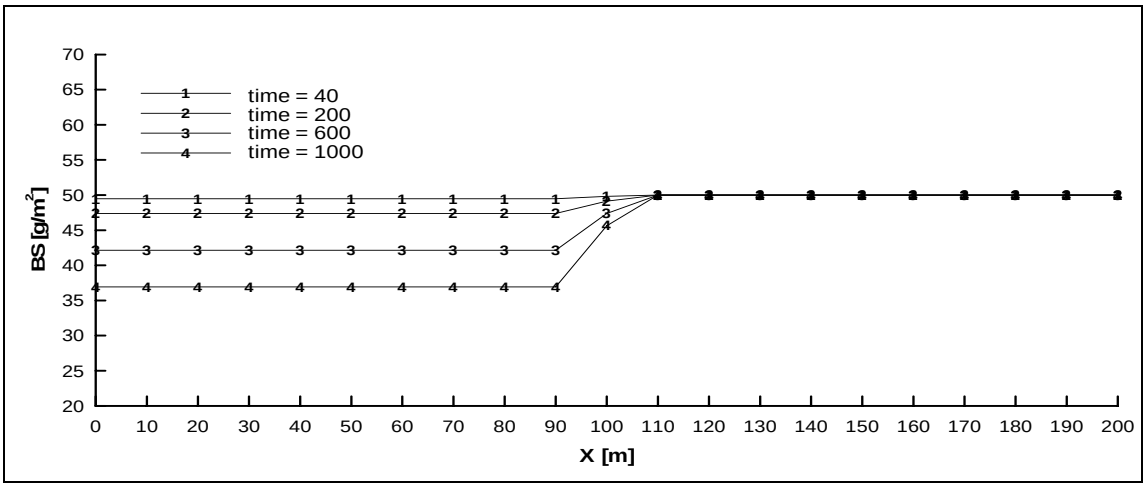

Fig. 5.1-9. Concentration of the Bed Sediment for Example 5.1.6

Figures 5.1-10 shows decreasing dissolved chemical concentration in mobile water phase along the downstream direction. This is because we allow the forward changing of dissolved chemical from mobile water phase to immobile water phase but not backward changing to occur (see equation 5.1.5), and the adsorption but not desorption from particulate chemicals to dissolved chemicals to happen (see equations 5.1.6 through 5.7.8). Due to the transform of dissolved chemical from mobile water phase into immobile water phase, the concentration of chemical in immobile water phase increases with time and shows similar pattern along the river/stream in figure 5.1.11 as that of chemical in mobile water phase. Since chemical in immobile water phase also involves in the reaction with bed sediment forming particulate on bed sediment, its concentration pattern in figure 5.111 also reflects this reaction. At the junction, figure 5.1-10 and figure 5.1-11 shows the decrease of chemical concentrations in both mobile and immobile water phase, due to the adsorption.

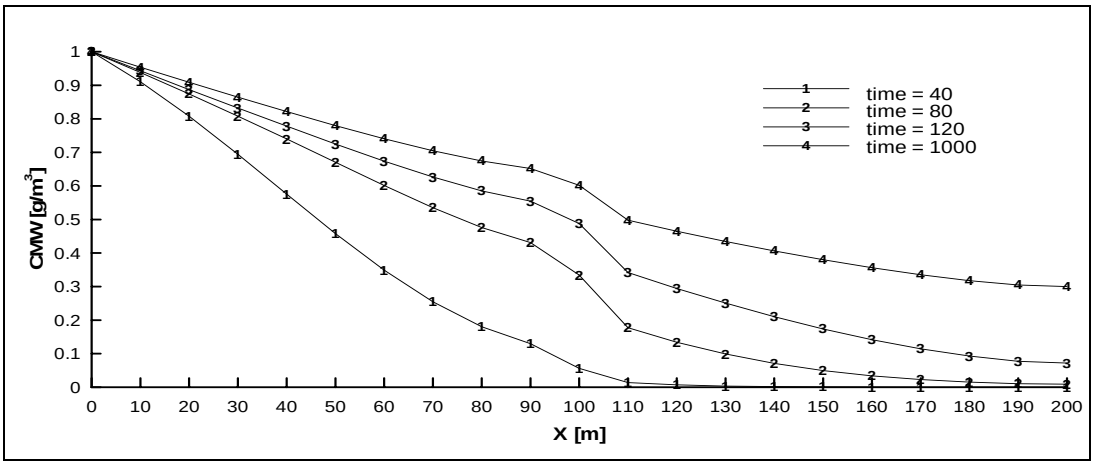

Fig. 5.1-10. Concentration of Dissolved Chemical in Mobile Water for Example 5.1.6

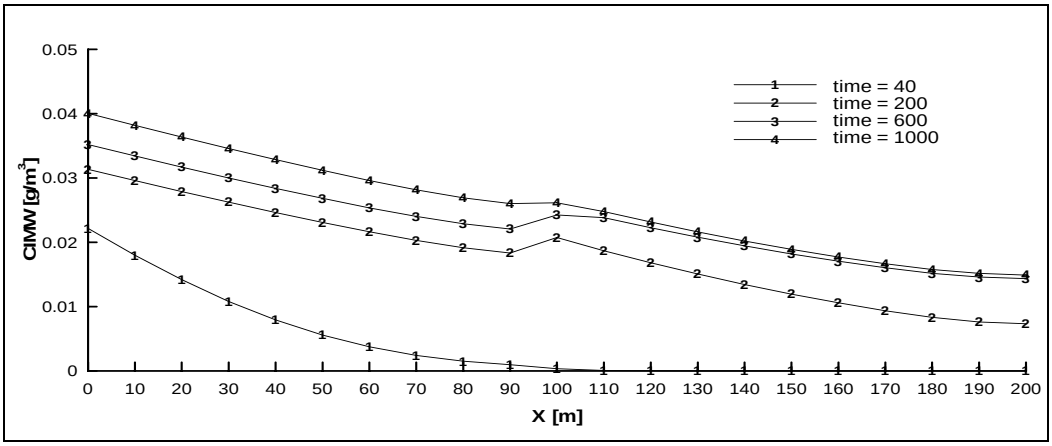

Fig. 5.1-11. Concentration of Dissolved Chemical in Immobile Water for Example 5.1.6

Particulate on suspended sediment results from adsorption/desorption, erosion/deposition, and transport. In reach 1, because erosion is greater than deposition, along the downstream direction, we observe an increase of particulate chemical on suspended sediments (figure 5.1-12). In Reach 2, erosion rate is the same as deposition rate and there is little dissolved chemical, so that most of the particulate on suspended sediment is transported from upstream and hardly transforms into particulate on bed sediment, and its concentration changes little along the reach (figure 5.1-12). At the junction, the increasing concentration of particulate chemical on suspended sediment (figure 5.1-12) is caused by not only adsorption but also erosion.

Particulate on bed sediment results from adsorption/desorption and erosion/deposition. In Reach 1, since deposition is less than erosion, the particulate on bed sediment is obtained from the adsorption of dissolved chemical in either mobile water phase or immobile water phase and reflects the same pattern in figure 5.1-13 as those of chemical in both mobile and immobile water phase (figure 5.1-10 and 5.1-11, respectively). In Reach 2, because erosion rate is the same as deposition rate, particulate on bed sediment is also formed through the adsorption and shows the same pattern in figure 5.1.13 as those of chemical in both mobile and immobile water phase (figure 5.1-10 and 5.1-11, respectively).

At the junction, the increasing concentration of particulate chemical on bed sediment (figure 5.1-12) indicates that its concentration increase due to adsorption is greater than the decrease caused by erosion.

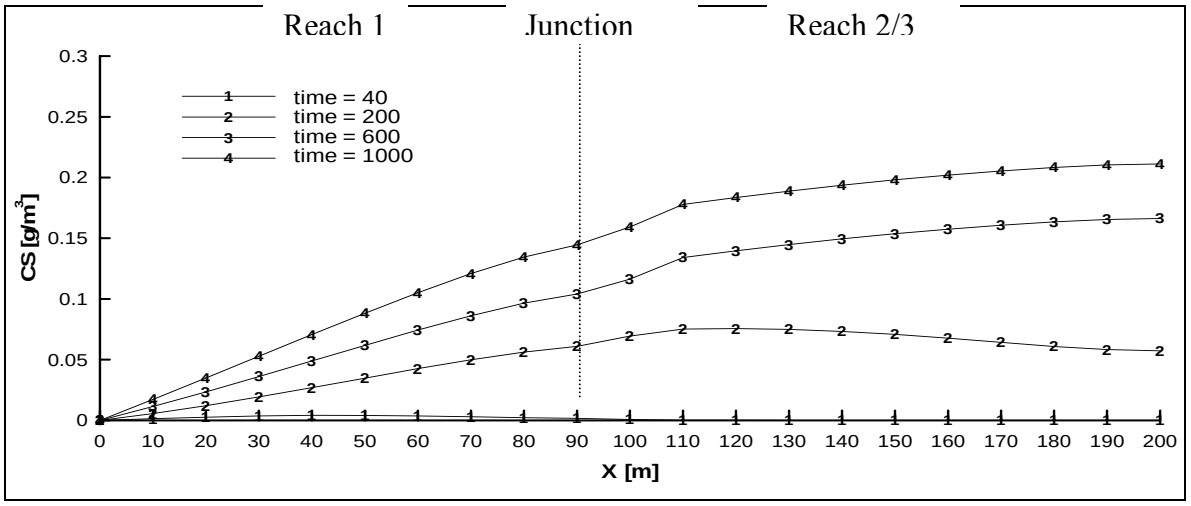

Fig. 5.1-12. Concentration of Particulate on Suspended Sediment for example 5.1.6

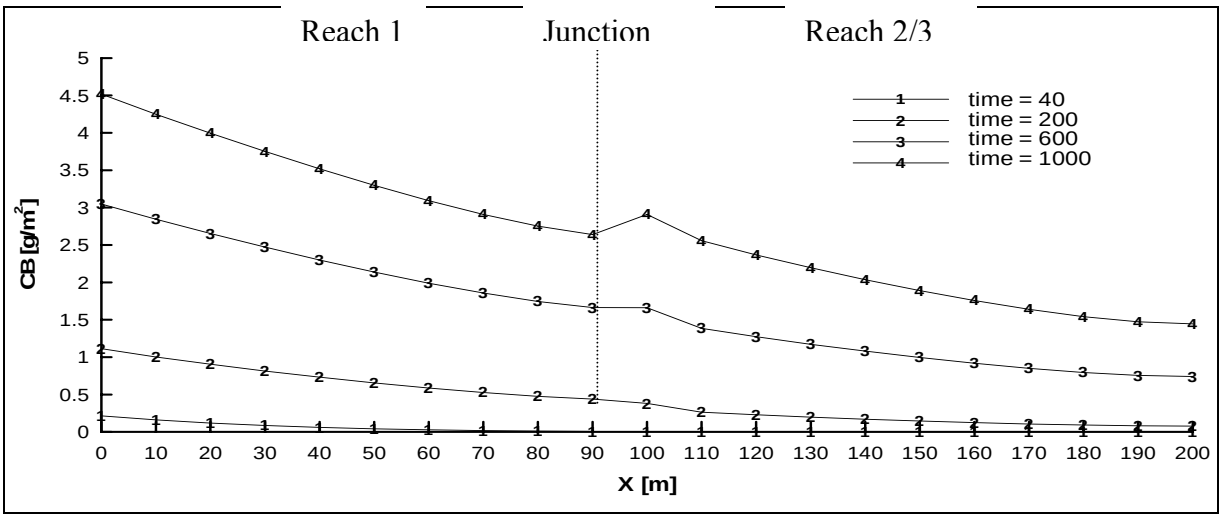

Fig. 5.1-13. Concentration of Particulate on Bed Sediment for example 5.1.6

5.2 Two-Dimensional Examples

Four examples are employed to demonstrate the design capability of the model in this section. The first example is used to demonstrate that the model can simulate all ten types of reactions described in Chapter 2. The second, third, and fourth examples are used to illustrate that the model has the design capability of simulate different eutrophication models reported in QUAL2E, WASP5, and CE-QUAL-ICM, respectively. Biogeochemical cycles, biota kinetics, and sediment-column water interactions in these eutrophication models have been successfully transformed into reaction networks. Based on the application of these eutrophication examples, the deficiency of current practices in water quality modeling is discussed and potential improvements over current practices using the current model are addressed.

5.2.1 Overland Transport with Ten Types of Reactions

This example is to demonstrate the capability of the model in simulating sediment and reactive chemical transport subject to complex reaction network involving both kinetic and equilibrium reactions, under the effect of temperature.

The domain of interest has covered a horizontal area of 5,000 m × 1,000 m and is discretized with 125 square elements of size 200 m × 200 m. To focus on transport, water depth is set to be 2.0 m, and flow velocity is 0.5 m/s in the x-direction and 0.0 m/s in the y-direction everywhere. Manning's roughness is 0.05. Two cases are considered with different temperature distribution. As shown in Figure 5.2-1, in case 1, temperature is set to be 15 °C throughout the region; and in case 2, temperature ranges from 15 °C to 25 °C at different locations.

One size of cohesive sediment is taken into account with settling speed of 1.2×0^{-6} m/s, critical shear stress for deposition of 4.15 g/m/s^2, critical shear stress for erosion of 4.08 g/m/s^2, and erodibility of 0.1 g/m^2/s. A reaction network of 20 reactions is considered for this example problem (Table 5.2-1). From the reaction network, it is seen that there are 14 species, including 3 dissolved chemicals in mobile water phase (CMW1, CMW2, and CMW3); 3 dissolved chemicals in immobile water phase (CIMW1, CIMW2, and CIMW3); 3 particulate chemicals sorbed onto suspended sediment (CS1, CS2, and CS3); 3 particulate chemicals sorbed onto bed sediment (CB1, CB2, and CB3); 1 suspension precipitate (SP3); and 1 bed precipitate (BP3).

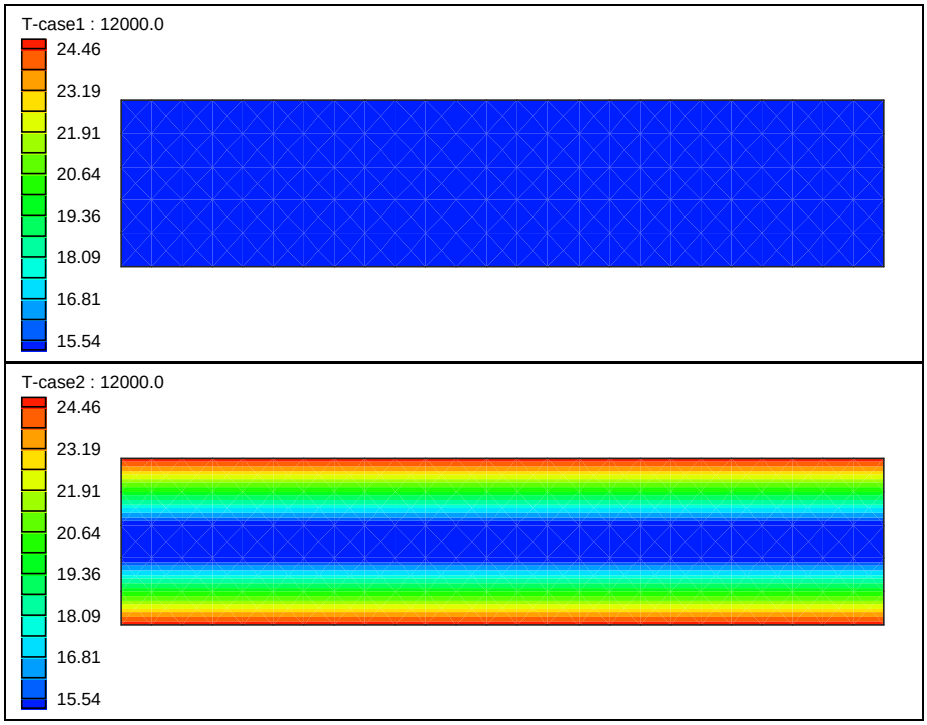

Fig. 5.2-1. Distribution of Temperature (ºC) for Example 5.2.1
Upper: case 1; Lower: case 2

As shown in Table 5.2-1, these species are considered to undergo all ten types of reaction illustrated in Figure 2.6-2, including aqueous complexation reactions, adsorption/desorption reactions, ion-exchange reactions, precipitation/dissolution reactions, volatilization reactions, diffusion reactions, and sedimentation reactions taking place between different chemical phases. Reaction rates of R11 through R13 are closely related to temperature (Table 5.2-1). Totally, we have 14 species, 1 equilibrium reaction, and 19 kinetic reactions. Thus, 13 kinetic-variable transport equations and 1 equilibrium reaction mass action equation were set up through decomposition and solved for 14 species, which are listed in Table 5.2-2. Among the 13 kinetic-variables, the 6th through 11th and the 13th contain no mobile species and are thus not solved in the advective-dispersive transport step. Therefore, instead of solving 7 advective-dispersive transport equations for mobile species in a primitive approach, we only need to solve 6 advective-dispersive transport equations for kinetic-variables. Since the fast reaction is decoupled and not included in the transport equations any more, robust numerical integration can be performed.

Initially, only bed sediments, BS, exist in the domain of interest. The initial concentration is 50 g/m^2 for the bed sediment. As the simulation starts, in-flow variable boundary conditions are applied to the upstream boundary sides, where all dissolved chemicals have a constant incoming concentration of 1 g/m^3 and all other mobile species and suspended sediment, SS, have zero incoming concentration. Out-flow variable boundary conditions are applied to the downstream boundary sides. The longitudinal dispersivity is 10.0 m. A 12,000-second simulation is performed with fixed time step size of 200 seconds. A relative error of 10^{-4} is used to determine the convergence for iterations involved in the computation.

Table 5.2-1 Chemical Reactions Considered in Example 5.2.1

Reaction type	Reaction and rate parameter	No.
Aqueous complexation reaction in mobile water phase	CMW1 + CMW2 $\leftrightarrow$ CMW3 (k_{eq} = 0.4 m^3/g)	R_1
Adsorption/desorption or ion-exchange reaction between mobile water and suspended sediment phases	CMW1+SS $\leftrightarrow$ CS1 + SS CMW2+SS $\leftrightarrow$ CS2 + SS CMW3+SS $\leftrightarrow$ CS3 + SS (k_f = 0.0001 m^3/g SS /s, k_b = 0.0 s^{-1})	R_2 R_3 R_4
Adsorption/desorption or ion-exchange reaction between mobile water and bed sediment phases	CMW1+BS $\leftrightarrow$ CB1 + BS CMW2+BS $\leftrightarrow$ CB2+ BS CMW3+BS $\leftrightarrow$ CB3 + BS (k_f = 0.00001 m^2/g BS /s, k_b = 0.0/h $m^{-1}s^{-1}$)	R_5 R_6 R_7
Sedimentation of particulate chemical between suspended and bed sediment phases	CS1 $\leftrightarrow$ CB1 (k_f = Depo/h g SS/m^3/s , k_b = Eros/h g BS/m^3/s) CS2 $\leftrightarrow$ CB2 (k_f = Depo/h g SS/m^3/s , k_b = Eros/h g BS/m^3/s) CS3 $\leftrightarrow$ CB3 (k_f = Depo/h g SS/m^3/s , k_b = Eros/h g BS/m^3/s)	R_8 R_9 R_{10}
Diffusion of dissolved chemical between mobile and immobile water phases	CMW1 $\leftrightarrow$ CIMW1 CMW2 $\leftrightarrow$ CIMW2 CMW3 $\leftrightarrow$ CIMW3 ($k_f = 0.0001\theta^{T-15^{\circ}C}$ s^{-1}, $k_b = 0.0h_b\theta_b/h\theta^{T-15^{\circ}C}$ s^{-1}, θ = 1.2)	R_{11} R_{12} R_{13}
Aqueous complexation reaction in immobile water phase	CIMW1+ CIMW2 $\leftrightarrow$ CIMW3 ($k_f = 0.002h_b\theta_b$/h m^3/g /s, $k_b = 0.005h_b\theta_b$/h s^{-1})	R_{14}
Adsorption/desorption or ion-exchange reaction between immobile water and bed sediment phases	CIMW1+BS $\leftrightarrow$ CB1 + BS CIMW2+BS $\leftrightarrow$ CB2 + BS CIMW3+BS $\leftrightarrow$ CB3 + BS ($k_f = 0.00001h_b\theta_b$/h m^2/g BS/s, k_b = 0.0/h /m/s)	R_{15} R_{16} R_{17}
Volatilization reaction of dissolved chemical from mobile water phase	CMW2 $\leftrightarrow$ P (k_f = 0.00002 /s, k_b = 0.02 g/m^3/ATM/s) (P=0.0025ATM)	R_{18}
Precipitation/dissolution reaction between mobile water and suspension precipitate phases	CMW3 $\leftrightarrow$ SP3 (k_f = 0.0001 /s, k_b = 0.0000001 /s)	R_{19}
Precipitation/dissolution reaction between immobile water and bed precipitate phases	CIMW3 $\leftrightarrow$ BP3 ($k_f = 0.0001\ h_b\theta_b$/h s^{-1}, $k_b = 0.0000001\ h_b\theta_b$/h s^{-1})	R_{20}

Table 5.2-2 Equations Obtained through Decomposition in Example 5.2.1

Kinetic-Variable Transport Equations
$\frac{\partial(hE_1)}{\partial t} + L(E_1^m) = h(-R_2 - R_4 - R_5 - R_7 - R_{11} - R_{13} - R_{19})$ where $E_1 = E_1^m = \rho_{CMW1}C_{CMW1} + \rho_{CMW3}C_{CMW3}$
$\frac{\partial(hE_2)}{\partial t} + L(E_2^m) = h(-R_3 - R_4 - R_6 - R_7 - R_{12} - R_{13} - R_{18} - R_{19})$ where $E_2 = E_2^m = \rho_{CMW2}C_{CMW2} + \rho_{CMW3}C_{CMW3}$
$\frac{\partial(hE_3)}{\partial t} + L(E_3^m) = h(R_2 - R_8)$ where $E_3 = E_3^m = \rho_{CS1}C_{CS1}$
$\frac{\partial(hE_4)}{\partial t} + L(E_4^m) = h(R_3 - R_9)$ where $E_4 = E_4^m = \rho_{CS2}C_{CS2}$
$\frac{\partial(hE_5)}{\partial t} + L(E_5^m) = h(R_4 - R_{10})$ where $E_5 = E_5^m = \rho_{CS3}C_{CS3}$
$\frac{\partial(hE_6)}{\partial t} + L(E_6^m) = h(R_5 + R_8 + R_{15})$ where $E_6 = \rho_{CB1}C_{CB1}$ and $E_6^m = 0$
$\frac{\partial(hE_7)}{\partial t} + L(E_7^m) = h(R_6 + R_9 + R_{16})$ where $E_7 = \rho_{CB2}C_{CB2}$ and $E_7^m = 0$
$\frac{\partial(hE_8)}{\partial t} + L(E_8^m) = h(R_7 + R_{10} + R_{17})$ where $E_8 = \rho_{CB3}C_{CB3}$ and $E_8^m = 0$
$\frac{\partial(hE_9)}{\partial t} + L(E_9^m) = h(R_{11} - R_{14} - R_{15})$ where $E_9 = \rho_{CIMW1}C_{CIMW1}$ and $E_9^m = 0$
$\frac{\partial(hE_{10})}{\partial t} + L(E_{10}^m) = h(R_{12} - R_{14} - R_{16})$ where $E_{10} = \rho_{CIMW2}C_{CIMW2}$ and $E_{10}^m = 0$
$\frac{\partial(hE_{11})}{\partial t} + L(E_{11}^m) = h(R_{13} + R_{14} - R_{17} - R_{20})$ where $E_{11} = \rho_{CIMW3}C_{CIMW3}$ and $E_{11}^m = 0$
$\frac{\partial(hE_{12})}{\partial t} + L(E_{12}^m) = hR_{19}$ where $E_{12} = E_{12}^m = \rho_{SP3}C_{SP3}$
$\frac{\partial(hE_{13})}{\partial t} + L(E_{13}^m) = hR_{20}$ where $E_{13} = \rho_{BP3}C_{BP3}$ and $E_{13}^m = 0$
Mass Action Equation
$C_{CMW3} = 0.4C_{CMW1}C_{CMW2}$

Note: $\rho_i = \rho_w$ for CMW1~CMW3, and SP3; $\rho_i = SS$ for CS1~CS3; $\rho_i = h_b\rho_{wb}\theta_b/h$, for CIMW1~CIMW3, and BP3; and $\rho_i = BS/h$, for CB1~CB3. ($\rho_w = \rho_{wb} = 1$ kg/L, $h_b = 0.2$ m, and $\theta_b = 0.5$)

Figures 5.2-2 through 5.2-4 depict the concentration contour at the end of simulation of SS, CMW1, and CIMW1, respectively. Figure 5.2.-2 shows trend of increasing concentration of the suspended sediment along down stream direction. It indicates that deposition is less than erosion under the condition set for this example. Because the reactive chemical transport was assumed having no effect on sediment transport, concentration distribution of SS in case 1 is the same as case 2. Figure 5.2-3 shows a decreasing concentration of CMW1 along the downstream direction. This is because we allow the adsorption to happen, but do not allow desorption from particulate chemicals to dissolved chemicals to occur. The only source of dissolved chemicals in the immobile water phase is the corresponding dissolved chemicals in the mobile phase. Therefore, Figure 5.2-4 also shows decreasing concentration of CIMW1 along the downstream direction.

Due to the temperature factor $\theta^{T-15^{\circ}C}$ in Table 5.2-1, reaction rates of R11 through R13 increase 6.19 times as temperature increases from 15˚C at the center of the domain to 25˚C at the top and bottom edges for case 2. Increase of these reaction rates means more dissolved chemicals will diffuse from mobile water phase to immobile water phase, therefore, we observe greater CMW1 concentration at the center than at the edges in Figure 5.2-3 and less CIMW1 at the center than at the edges in Figure 5.2-4.

Animations showing the spatial-temporal distribution of suspended sediment SS (Figure 5.2-2_case 1.avi and Figure 5.2-2_Case 2.avi), dissolved Chemical No. 1 in mobile water CMW1 (Figure 5.2-3_Case 1.avi and Figure 5.2-3_Case 2.avi), and dissolved Chemical No. 1 in immobile water CIMW1 (Figure 5.2-4_Case 1.avi and Figure 5.2-4_Case 2.avi), respectively, are attached in Appendix A. Readers can visualize these moves by clicking the file contained in the attached CD.

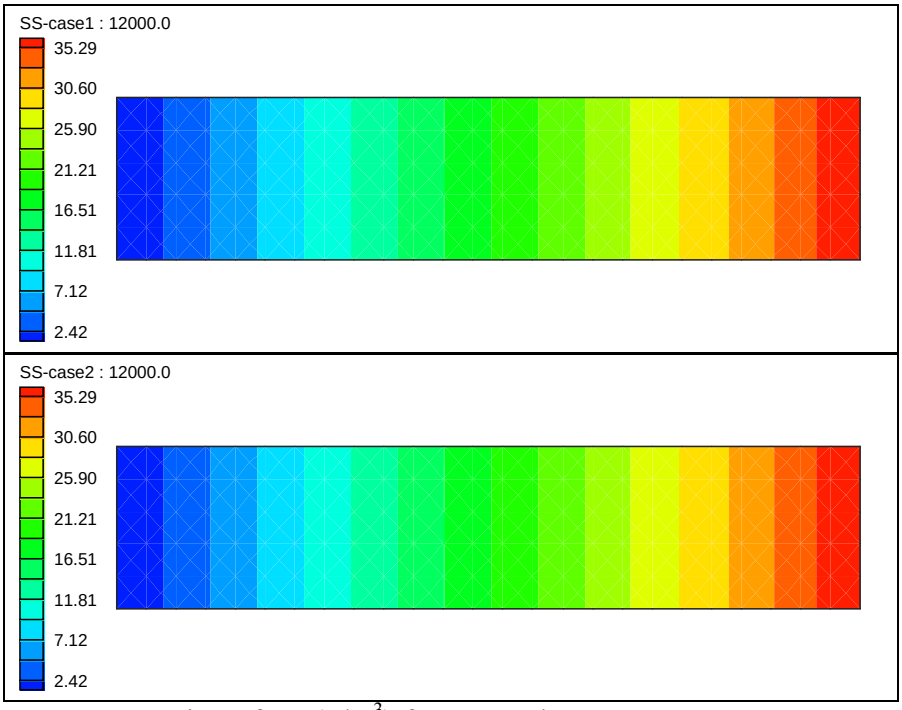

Fig. 5.2-2. Concentration of SS (g/m^3) for Example 5.2.1 Upper: case 1; Lower: case 2

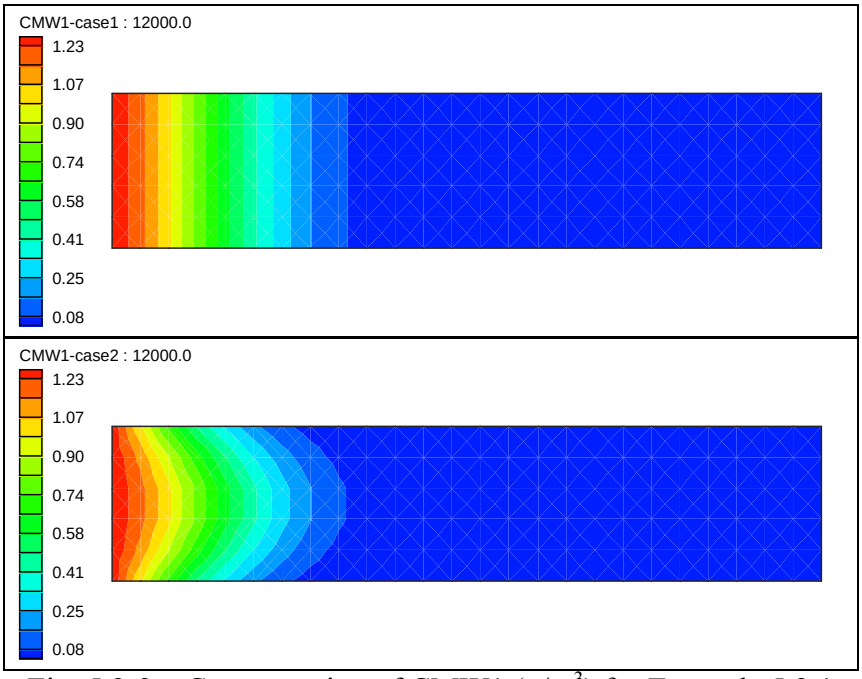

Fig. 5.2-3. Concentration of CMW1 (g/m^3) for Example 5.2.1
Upper: case 1; Lower: case 2

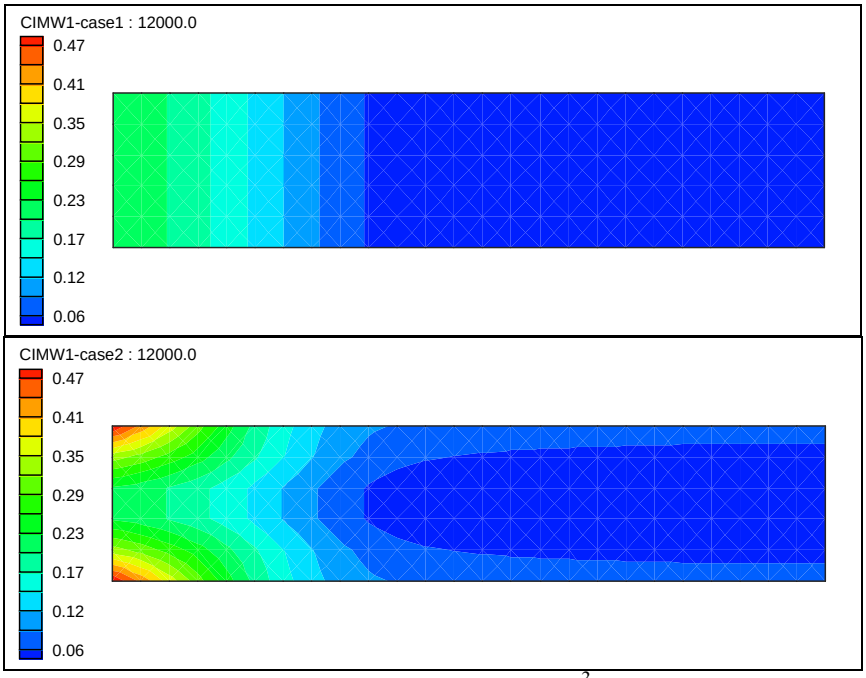

Fig. 5.2-4. Concentration of CIMW1 (g/m^3) for Example 5.2.1
Upper: case 1; Lower: case 2

5.2.2 Overland Transport with Eutrophication in QUAL2E

The Stream Water Quality Model QUAL2E (Brown and Barnwell, 1987) is a typical eutrophication model for stream systems. It is the most recent version of the model QUAL-II (Roesner et al., 1981), which was developed from the model QUAL-I in the 1960s. QUAL2E was first released in 1985 (Brown and Barnell, 1985) and has been successfully applied in many water quality studies since then (Lung, 1986; Wagner et al., 1996; Yang et al., 2000; Ning et al., 2001; Park and Lee, 2002; McAvoy et al., 2003; Ng and Perera, 2003; and Park et al., 2003). In QUAL2E, nine working equations were used to solve for nine water qualities (state variables) that related to eutrophication kinetics (Table 5.2-3).

Table 5.2-3 QUAL2E Original Working Equations

No.	Species	Notation	Working Equations
1	Dissolved Oxygen	O	$\frac{dO}{dt} = K_2\theta^{T\text{-}20}\left(O^* - O\right) + \left(\alpha_3\mu\theta^{T\text{-}20} - \alpha_4\rho\theta^{T\text{-}20}\right)\frac{Chl\underline{a}}{\alpha_0} - K_1\theta^{T\text{-}20}L - K_4\theta^{T\text{-}20}/d - \alpha_5\beta_1 CORDO\theta^{T\text{-}20}N_1 - \alpha_6\beta_2 CORDO\theta^{T\text{-}20}N_2$
2	Biochemical oxygen demand	L	$\frac{dL}{dt} = -K_1\theta^{T\text{-}20}L - K_3\theta^{T\text{-}20}L$
3	Chlorophyll a	$Chl\underline{a}$	$\frac{dChl\underline{a}}{dt} = \mu\theta^{T\text{-}20}Chl\underline{a} - \rho\theta^{T\text{-}20}Chl\underline{a} - \frac{\sigma_1}{d}\theta^{T\text{-}20}Chl\underline{a}$
4	Organic nitrogen	N_4	$\frac{dN_4}{dt} = \alpha_1\rho\theta^{T\text{-}20}\frac{Chl\underline{a}}{\alpha_0} - \beta_3\theta^{T\text{-}20}N_4 - \sigma_4\theta^{T\text{-}20}N_4$
5	Ammonia nitrogen	N_1	$\frac{dN_1}{dt} = \beta_3\theta^{T\text{-}20}N_4 - \beta_1 CORDO\theta^{T\text{-}20}N_1 + \sigma_3\theta^{T\text{-}20}/d - F\alpha_1\mu\theta^{T\text{-}20}\frac{Chl\underline{a}}{\alpha_0}$
6	Nitrite nitrogen	N_2	$\frac{dN_2}{dt} = \beta_1 CORDO\theta^{T\text{-}20}N_1 - \beta_2 CORDO\theta^{T\text{-}20}N_2$
7	Nitrate nitrogen	N_3	$\frac{dN_3}{dt} = \beta_2 CORDO\theta^{T\text{-}20}N_2 - (1-F)\alpha_1\mu\theta^{T\text{-}20}\frac{Chl\underline{a}}{\alpha_0}$
8	Organic phosphorus	P_1	$\frac{dP_1}{dt} = \alpha_2\rho\theta^{T\text{-}20}\frac{Chl\underline{a}}{\alpha_0} - \beta_4\theta^{T\text{-}20}P_1 - \sigma_5\theta^{T\text{-}20}P_1$
9	Dissolved phosphorous	P_2	$\frac{dP_2}{dt} = \beta_4\theta^{T\text{-}20}P_1 + \sigma_2\theta^{T\text{-}20}/d - \alpha_2\mu\theta^{T\text{-}20}\frac{Chl\underline{a}}{\alpha_0}$

The eutrophication model of QUAL2E is recast in terms of a network of 16 reactions involving 19 reaction constituents (O, L, Chla, N_4, N_1, N_2, N_3, P_1, P_2, $O_{(b)}$, $L_{(b)}$, $Chla_{(b)}$, $N_{4(b)}$, $N_{(1b)}$, $P_{(1b)}$, $P_{(2b)}$, CO_2, H_2O, and $O_{2(g)}$) in this report (Table 5.2-4). These 16 reactions (Table 5.2-4) address four interacting biogeochemical processes: algae growth kinetics (Reactions R1 through R4), nitrogen cycles (Reactions R5 through R9), phosphorus cycle (Reactions R10 through R12), and carbon cycles (Reactions R13 through R16).

Table 5.2-4 QUAL2E Eutrophication Model Cast in Reaction Network

No.	Mechanism	Reaction	Rate
1	Algae growth	$\alpha_1 N_1 + \alpha_2 P_2 + H_2O + CO_{2(g)} \rightarrow \alpha_0 \underline{Chla} + \alpha_3 O + (\alpha_4 - \alpha_3) O_{(g)}$	$R = \frac{\mu}{\alpha_0} \theta^{T-20} \underline{Chla}$
2	Diatom growth related nitrate reduction	$N_3 + 1.5H_2O \rightarrow N_1 + (\alpha_5 + \alpha_6) O_{(g)}$	$R = (1-F)\alpha_1 \frac{\mu}{\alpha_0} \theta^{T-20} \underline{Chla}$
3	Algae respiration	$\alpha_0 \underline{Chla} + \alpha_4 O \rightarrow \alpha_1 N_4 + \alpha_2 P_1 + H_2O + CO_{2(g)}$	$R = \frac{\rho}{\alpha_0} \theta^{T-20} \underline{Chla}$
4	Algae settling	$\underline{Chla} \rightarrow \underline{Chla}_{(b)}$	$R = \frac{\sigma_1}{d} \theta^{T-20} \underline{Chla}$
5	Mineralization of organic nitrogen	$N_4 \rightarrow N_1$	$R = \beta_3 \theta^{T-20} N_4$
6	Organic nitrogen settling	$N_4 \rightarrow N_{4(b)}$	$R = \sigma_4 \theta^{T-20} N_4$
7	Biological oxidation of ammonia nitrogen	$N_1 + \alpha_5 O \rightarrow N_2 + 1.5H_2O$	$R = \beta_1 CORDO \theta^{T-20} N_1$
8	Benthos source to ammonia nitrogen	$N_{1(b)} \rightarrow N_1$	$R = \sigma_3 \theta^{T-20} / d$
9	Oxidation of nitrate nitrogen	$N_2 + \alpha_6 O \rightarrow N_3$	$R = \beta_2 CORDO \theta^{T-20} N_2$
10	Organic phosphorus decay	$P_1 \rightarrow P_2$	$R = \beta_4 \theta^{T-20} P_1$
11	Organic phosphorus settling	$P_1 \rightarrow P_{1(b)}$	$R = \sigma_5 \theta^{T-20} P_1$
12	Benthos source to dissolved phosphorus	$P_{2(b)} \rightarrow P_2$	$R = \sigma_2 \theta^{T-20} / d$
13	Deoxygenating of BOD	$O + L \rightarrow CO_{2(g)} + H_2O$	$R = K_1 \theta^{T-20} L$
14	BOD settling	$L \rightarrow L_{(b)}$	$R = K_3 \theta^{T-20} L$
15	Re-aeration	$O_{(g)} \rightarrow O$	$R = K_2 \theta^{T-20} (O^* - O)$
16	Sediment oxygen demand	$O \rightarrow O_{(b)}$	$R = K_4 \theta^{T-20} / d$

The aforementioned 16 reactions are characterized by seven reaction stoichiometries (Table 5.2-5) and a total of 36 reaction parameters (Table 5.2-6).

Table 5.2-5 QUAL2E Example Reaction Coefficients

Variable	Description	Value	Unit
α_0	Ratio of chlorophyll-a to algae biomass	55	μg-Chla / mg-A
α_1	Fraction of algae mass that is nitrogen	0.08	mg-N / mg-A
α_2	Fraction of algae mass that is phosphorus	0.015	mg-P / mg-A
α_3	O_2 production per unit of algae growth	1.6	mg-O / mg-A
α_4	O_2 uptake per unit of algae respired	1.95	mg-O / mg-A
α_5	O_2 uptake per unit of NH_3 oxidation	3.5	mg-O / mg-N
α_6	O_2 uptake per unit of NO_2 oxidation	1.0	mg-O / mg-N

Table 5.2-6 QUAL2E Example Reaction Rate Parameters

Variable	Description	Value	Unit
M	Algae growth rate	μ_{max}(FL) (FN) (FP)	day^{-1}
μ_{max}	Maximum algae growth rate	2.0	day^{-1}
FL	Algae growth limitation factor for light	$\min\{(1/\lambda d)\ln[(K_L+I)/(K_L+Ie^{-\lambda d})],1\}$	-
λ	Light extinction coefficient	2.0	ft^{-1}
d	Depth of flow	Variable	ft
K_L	Half saturation light intensity	5	Btu/ft^2-hr
I	Surface light intensity	5	Btu/ft^2-hr
FN	Algae growth limitation factor for N	$(N_1+N_3)/(N_1+N_3+K_N)$	-
K_N	Half saturation constant for N	0.155	mg-N/L
FP	Algae growth limitation factor for P	$P_2/(P_2+K_P)$	-
K_P	Half saturation constant for P	0.0255	mg-P/L
θ_μ	Temperature correction for algae growth	1.047	-
F	Fraction of algae N taken from ammonia	$P_N N_1/[P_N N_1+(1-P_N)N_3]$	-
P_N	Preference factor for ammonia nitrogen	0.5	-
ρ	Algae respiration rate	0.275	day^{-1}
θ_ρ	Temperature correction for algae respiration	1.047	-
σ_1	Algae settling rate	3.25	ft/day
$\theta_{\sigma 1}$	Temperature correction for algae settling	1.024	-
β_3	Rate constant for organic N decay	0.21	day^{-1}
$\theta_{\beta 3}$	Temperature correction for organic N decay	1.047	-
σ_4	Organic N settling rate	0.0505	day^{-1}
$\theta_{\sigma 4}$	Temperature correction for organic N settling	1.024	-
β_1	Rate constant for ammonia oxidation	0.55	day^{-1}
CORDO	Nitrification rate correction factor	$1-e^{-KNITRF*O}$	-

$\theta_{\beta 1}$	Temperature correction for ammonia oxidation	1.083	-
KNITRF	First order nitrification inhibition coefficient	0.65	L/mg
σ_3	Benthic source rate for ammonia	0	mg-N/ft^2/day
$\theta_{\sigma 3}$	Temperature correction for ammonia source	1.074	-
β_2	Rate constant for nitrite oxidation	1.10	day^{-1}
$\theta_{\beta 2}$	Temperature correction for nitrite oxidation	1.047	-
β_4	Rate constant for organic P decay	0.355	day^{-1}
$\theta_{\beta 4}$	Temperature correction for organic P decay	1.047	-
σ_5	Organic P settling rate	0.0505	day^{-1}
$\theta_{\sigma 5}$	Temperature correction for organic P settling	1.024	-
σ_2	Benthic source rate for dissolved P	0	mg-P/ft^2/day
$\theta_{\sigma 2}$	Temperature correction for dissolved P source	1.074	-
K_1	BOD deoxygenating rate constant	1.71	day^{-1}
θ_{K1}	Temperature correction for BOD decay	1.047	-
K_3	BOD settling rate constant	0	day^{-1}
θ_{K3}	Temperature correction for BOD settling	1.024	-
K_2	Re-aeration rate constant	$\text{Min}(5.026u^{0.969}d^{-1.673}2.31,10)$	day^{-1}
U	Flow velocity	Variable	ft/day
O^*	Equilibrium oxygen concentration	$e^{-139.3441+1.575701\times10^5/T_k-6.642308\times10^7/T_k^2+1.2438\times10^{10}/T_k^3-8.621949\times10^{11}/T_k^4}$	mg/l
T_k	Temperature	T+273.15	°K=°C+273.15
θ_{K2}	Temperature correction for re-aeration	1.024	-
K_4	Benthic oxygen uptake	0	mg-O/ft^2/day
θ_{K4}	Temperature correction for SOD uptake	1.060	-

An incomplete decomposition of the QUAL2E reaction network would result a total of 19 reaction-extent equations. Because reaction rates of all 16 reactions are function of only the first nine constituents (O, L, Chla, N_4, N_1, N_2, N_3, P_1, and P_2), the governing equations for these nine constituents are decoupled from those for the other 10 constituents ($O_{(b)}$, $L_{(b)}$, $Chla_{(b)}$, $N_{4(b)}$, $N_{(1b)}$, $P_{(1b)}$, $P_{(2b)}$, CO_2, H_2O, and $O_{2(g)}$). These equations are listed in Table 5.2-7. It is noted that because there is no fast reaction involved in the reaction network of QUAL2E, the incompletely decomposed equations of new paradigm are reduced to the generally used primitive reaction-based working equations.

Table 5.2-7 New Paradigm Working Equations for QUAL2E

No.	Species	Notation	Working Equations
1	Dissolved Oxygen	*O*	$d[O]/dt = \alpha_3 R_1 - \alpha_4 R_3 - \alpha_5 R_7 - \alpha_6 R_9 - R_{13} + R_{15} - R_{16}$
2	Biochemical oxygen demand	*L*	$d[L]/dt = -R_{13} - R_{14}$
3	Chlorophyll a	*Chla*	$d[Chla]/dt = \alpha_o R_1 - \alpha_o R_3 - R_4$
4	Organic nitrogen	N_4	$d[N_4]/dt = \alpha_1 R_3 - R_5 - R_6$
5	Ammonia nitrogen	N_1	$d[N_1]/dt = -\alpha_1 R_1 + R_2 + R_5 - R_7 + R_8$
6	Nitrite nitrogen	N_2	$d[N_2]/dt = R_7 - R_9$
7	Nitrate nitrogen	N_3	$d[N_3]/dt = -R_2 + R_9$
8	Organic phosphorus	P_1	$d[P_1]/dt = \alpha_2 R_3 - R_{10} - R_{11}$
9	Dissolved phosphorous	P_2	$d[P_2]/dt = -\alpha_2 R_1 + R_{10} + R_{12}$

As shown in Figure 5.2-5, the domain of interest is a shallow water body discretized with 462 elements and 275 nodes. Region A, B, and C are illustrated for simulation results discussion. The flow is allowed to reverse direction every 12 hours (T = 12 hours). The flow pattern was simulated with a flow-reversal boundary condition implemented on the open boundary side and with the rest of the boundary treated as closed. It was also assumed subject to 10 point sources each with an injection rate of 1 m^3/s. As shown in Figure 5.2-6, water depth varies from 0.7 m to 10.3 m during one flow-reversal cycle. The calculated flow velocity ranges from 0.02 m/s to 1.6 m/s at various times during one flow-reversal cycle (Fig. 5.2-7).

To focus on transport, we assume that the temperature is 15 ^oC throughout the simulation region. Variable boundary conditions are applied to the open boundary sides. Initial and variable boundary incoming concentrations of the 9 simulated constituents are listed in Table 5.2-8. The dispersion coefficient is 5.2 m^2/s. Each point source injected the biochemical oxygen demand L at a rate of 20.0 $g/m^2/s$. A 30-day simulation is performed with a fixed time step size of 10 minutes.

Figure 5.2-8 plots the concentration contours of L and Chla at different simulation time. It is seen that at the point sources, the concentration of L increases due to injection, and at the open boundary, the concentration of L decreases due to the low incoming concentration. According to the reaction network of QUAL2E, the source of Chla is algae growth, and the sink of Chla includes algae respiration and settling. The Chla concentration decrease shown in Figure 5.2-8 indicates that the source is less than the sink. Because the settling rate of algae increases when water depth decreases, settling rate in region A is greater than in region C and settling rate in region C is greater than in region B. Therefore, we observe less Chla concentration in region A than in region C and less Chla concentration in region C than in region B. As the simulation time increases, when only small amount of Chla is left, the concentration distribution is mainly affected by advective-dispersive transport rather than reactions.

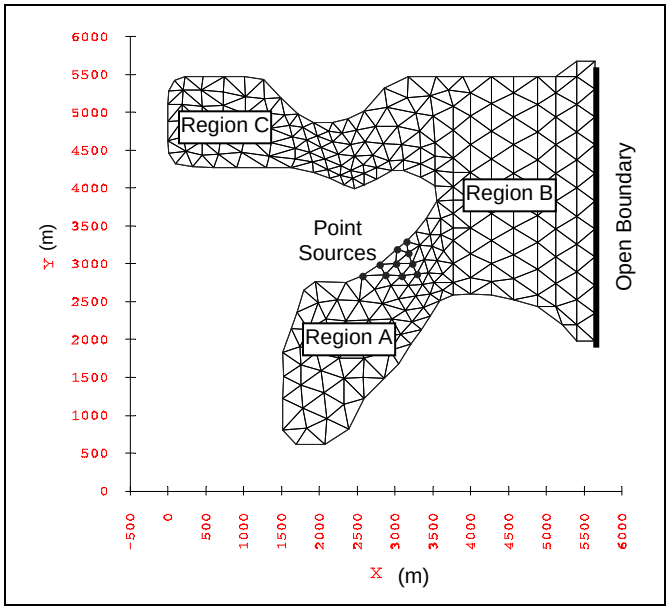

Fig. 5.2-5. Simulation Domain Descretization for Example 5.2.2

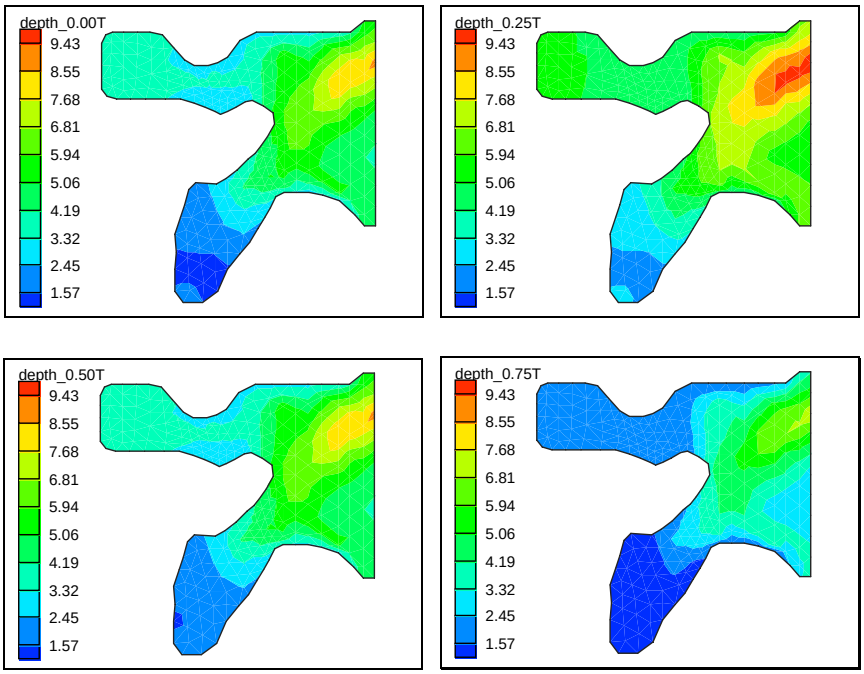

Fig. 5.2-6. Water Depth (m) at Various Times for Example 5.2.2:
0 T (upper left), 0.25T (upper right), 0.5T (lower left), and 1.0T (lower right)

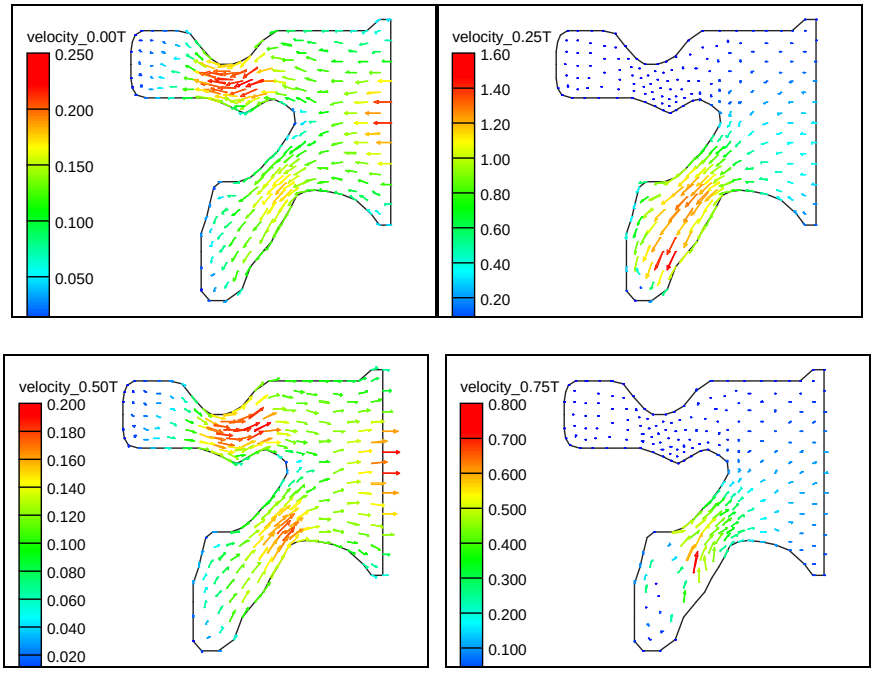

Fig. 5.2-7. Flow Velocity (m/s) at Various Times for Example 5.2.2: 0 h (upper left), 3 h (upper right), 6 h (lower left), and 12 h (lower right)

Table 5.2-8 Initial and Boundary Concentration in Example 5.2.2

No.	Species	Notatio	Initial	Boundary	ρ_i
1	Dissolved oxygen	O	5 mg-O_2 /kg	0.5 mg-O_2 /L	ρ_w = 1 kg/L
2	Biochemical oxygen	L	0.8 mg-O_2 /kg	0.08 mg-O_2 /L	ρ_w = 1 kg/L
3	Algae as chlorophyll a	Chla	20.0 µg-	2.0 µg-Chla/L	ρ_w = 1 kg/L
4	Organic nitrogen as N	N_4	2.0 mg-N /kg	0.2 mg-N /L	ρ_w = 1 kg/L
5	Ammonia as N	N_1	1.0 mg-N /kg	0.1 mg-N /L	ρ_w = 1 kg/L
6	Nitrite as N	N_2	0.1 mg-N /kg	0.01 mg-N /L	ρ_w = 1 kg/L
7	Nitrate as N	N_3	1.0 mg-N /kg	0.1 mg-N /L	ρ_w = 1 kg/L
8	Organic phosphorus as P	P_1	0.5 mg-P /kg	0.05 mg-P /L	ρ_w = 1 kg/L
9	Dissolved phosphorus as P	P_2	0.1 mg-P /kg	0.01 mg-P /L	ρ_w = 1 kg/L

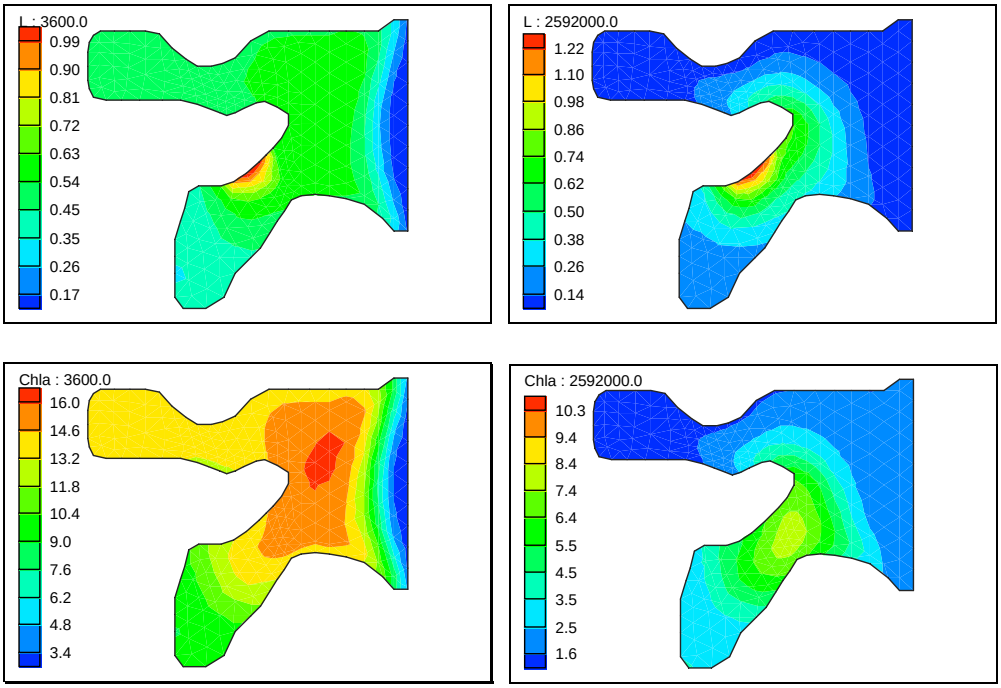

Fig. 5.2-8. Concentration Contours at 1hour (left) and 720 h (right) in Example 5.2.2: Upper: L (mg-O_2/L); Lower: Chla (µg-Chla/L)

Animations showing the spatial-temporal distribution of BOD (File Name: QUAL2E BOD.avi) and Chla (File Name: QUAL2E Algae.avi), respectively, are attached in Appendix A. Readers can visualize these moves by clicking the file contained in the attached CD.

5.2.3 Overland Transport with Eutrophication in WASP5

WASP5, the Water quality Analysis Simulation Program (Ambrose et al., 1993), is a three-dimensional conventional water quality analysis simulation program. It is a group of mechanistic models capable of simulating water transport and fate and transport of water quality constituents and toxic organics for aquatic systems. Various components of WASP5 have been used to study a variety of lake, reservoir, and estuarine issues including ecological characterization, the effects of anthropogenic activities, and the impact of mitigation measures (Bierman and James, 1995; Lung and Larson, 1995; Tufford and McKellar, 1999; Carroll et al., 2004; and Zheng et al., 2004). EUTRO5 is a general operational WASP5 model used to simulate nutrient enrichment, eutrophication, and dissolved oxygen in the aquatic environment. Sixteen working equations were used in EUTRO5 to simulate 16 state variables (NH_3, $NH_{3(b)}$, NO_3, $NO_{3(b)}$, OPO_4, $OPO_{4(b)}$, PHYT, $PHYT_{(b)}$, CH_2Ot, $CH_2Ot_{(b)}$, O_2, $O2_{(b)}$, ONt, $ONt_{(b)}$, OPt, and $OPt_{(b)}$) related to eutrophication kinetics (Zhang, 2005).

The eutrophication model of WASH5 was recast in terms of a network of 38 reactions involving 27 reaction constituents (NH_3, $NH_{3(b)}$, NO_3, $NO_{3(b)}$, OPO_4, $OPO_{4(b)}$, PHYT, $PHYT_{(b)}$, CH_2O, CH_2Op,

$CH_2O_{(b)}$, $CH_2Op_{(b)}$, O_2, $O_{2(b)}$, ON, ONp, $ON_{(b)}$, $ONp_{(b)}$, OP, OPp, $OP_{(b)}$, $OPp_{(b)}$, CO_2, H_2O, H^+, N_2, and $O_{2(g)}$). Details of these reactions can be found elsewhere (Zhang, 2005). These 38 reactions address sediment-biogeochemical interactions and four interacting biogeochemical processes: phytoplankton growth kinetics, nitrogen cycles, phosphorus cycle, and carbon cycles (Zhang, 2005). They are characterized by three reaction stoichiometries and a total of 66 reaction parameters (Zhang, 2005).

The simulation domain, descretization, flow field and temperature distribution are same as example 5.2.2. Variable boundary conditions are applied to the open boundary sides. Initial concentrations of the 22 simulated species and variable boundary incoming concentrations of mobile species are listed in Table 5.2-9. It is noted that only 22 species out of 27 species are simulated because the governing equations for CO_2, H_2O, H^+, N_2, and $O_{2(g)}$ are decoupled from those for the other 22 species. The decoupling of two sets of state variable is due to the formulation of rate equations that depend on only 22 species.

Table 5.2-9 Species Initial and Boundary Concentration in Example 5.2.3

No.	Species	Notation	Initial	Boundary	ρ_i
1	NH_3	C_1	1 mg N/kg	0.1 mg N/L	ρ_w
2	NO_3	C_3	1 mg N/kg	0.1 mg N/L	ρ_w
3	OPO_4	C_5	0.1 mg P/kg	0.01 mg P/L	ρ_w
4	PHYT	C_7	2 mg C/kg	0.2 mg C/L	ρ_w
5	CH_2O	C_9	10 mg O_2/kg	1.0 mg O_2/L	ρ_w
6	O_2	C_{13}	2 mg O_2/kg	0.2 mg O_2/L	ρ_w
7	ON	C_{15}	2 mg N/kg	0.2 mg N/L	ρ_w
8	OP	C_{19}	0.35 mg P/kg	0.035 mg P/L	ρ_w
9	$CH_2O_{(p)}$	C_{10}	0.2 mg O_2/mg	1.0 mg O_2/L	SS
10	$ON_{(p)}$	C_{16}	0.0 mg N/mg	0 mg N/L	SS
11	$OP_{(p)}$	C_{20}	0.003 mg P/mg	0.015 mg P/L	SS
12	$NH_{3(b)}$	C_2	1 mg N/kg	-	$h_b\rho_{wb}\theta_b$/
13	$NO_{3(b)}$	C_4	1 mg N/kg	-	$h_b\rho_{wb}\theta_b$/
14	$OPO_{4(b)}$	C_6	0.1 mg P/kg	-	$h_b\rho_{wb}\theta_b$/
15	$PHYT_{(b)}$	C_8	2 mg C/kg	-	$h_b\rho_{wb}\theta_b$/
16	$CH_2O_{(b)}$	C_{11}	10 mg O_2/kg	-	$h_b\rho_{wb}\theta_b$/
17	$O_{2(b)}$	C_{14}	2 mg O_2/kg	-	$h_b\rho_{wb}\theta_b$/
18	$ON_{(b)}$	C_{17}	2 mg N/kg	-	$h_b\rho_{wb}\theta_b$/
19	$OP_{(b)}$	C_{21}	0.35 mg P/kg	-	$h_b\rho_{wb}\theta_b$/
20	$CH_2O_{(bp)}$	C_{12}	0.002 mg O_2/mg	-	BS/h
21	$ON_{(bp)}$	C_{18}	0.0 mg N/mg	-	BS/h
22	$OP_{(bp)}$	C_{22}	0.00003 mg P/mg	-	BS/h

The dispersion coefficient was 5.2 m^2/s. Each point source injected NO_3 at a rate of 10.0 g/m^2/s. A 30-day (60T) simulation is performed with a fixed time step size of 10 minutes. A relative error of 10^{-4} is used to determine the convergence for iterations involved in the computation.

Figure 5.2-9 plots the concentration contours of NO_3 and PHYT at different simulation time. It is seen that at the point sources, the concentration of NO_3 increases due to the injection, and at the

open boundary, the concentration of NO_3 decreases due to the low incoming concentration. According to the reaction network of WASP5, PHYT growth consumes NO_3. Due to the light effect, the depth averaged growth rate of PHYT increases when water depth decreases. Thus, NO_3 consumed in region A is greater than in region C and NO_3 consumed in region C is greater than in region B. Therefore, we observe less NO_3 concentration in region A than in region C and less NO_3 concentration in region C than in region B.

According to the reaction network, the source of PHYT is its growth, and the sink of PHYT includes its death and settling. The PHYT concentration decrease shown in Figure 5.2-8 indicates that the source is less than the sink. Comparing the concentration distributions of PHYT (Figure 5.2-9) and Chla (Figure 5.2-8), we can see that relative decreasing rate of Chla (compared to the concentration) is greater than that of PHYT. This indicates that the rate of (algae respiration + settling – growth) in the QUAL2E example is greater than the rate of (PHYT death + settling – growth) in this example. The rate difference is due to the different rate formulation and parameterization of the two models.

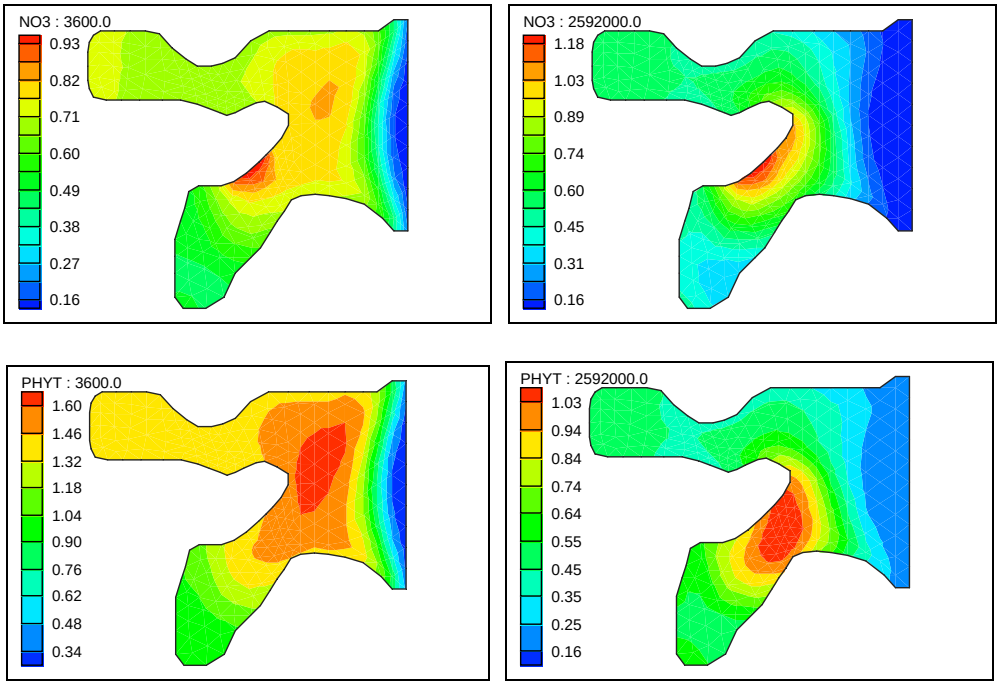

Fig. 5.2-9. Concentration Contours at 1hour (left) and 60T (right) in Example 5.2.3
Upper: NO_3 (mg-N/L); Lower: PHYT (mg-C/L)

Animations showing the spatial-temporal distribution of nitrate (File Name: WASP5 Nitrogen.avi) and phytoplankton (File Name: WASP5 PHYT.avi), respectively, are attached in Appendix A. Readers can visualize these moves by clicking the file contained in the attached CD.

5.2.4 Overland Transport with Eutrophication in CE-QUAL-ICM

The CE-QUAL-ICM (Cerco and Cole, 1995) water quality model was developed as one component of a model package employed to study eutrophication processes in Chesapeake Bay (Cerco and Cole, 1993; and Cerco and Cole, 2000). Eutrophication processes modeled with the CE-QUAL-ICM were also used to study phosphorus dynamics for the St. Johns River (Cerco and Cole, 2004). Fourty one working equations were used in CE-QUAL-ICM to simulate 41 state variables (Bc, Bd, Bg, DOC, LPOC, RPOC, NH_4, NO_3, DON, LPON, RPON, PO_4t, DOP, LPOP, RPOP, COD, DO, SU, SA, TAM, $POC_{(1b)}$, $POC_{(2b)}$, $POC_{(3b)}$, $NH_{4(1b)}$, $NH_{4(2b)}$, $NO_{3(1b)}$, $NO_{3(2b)}$, $PON_{(1b)}$, $PON_{(2b)}$, $PON_{(3b)}$, $PO_{4(1b)}$, $PO_{4(2b)}$, $POP_{(1b)}$, $POP_{(2b)}$, $POP_{(3b)}$, $COD_{(1b)}$, $COD_{(2b)}$, $SU_{(1b)}$, $SU_{(2b)}$, $SA_{(1b)}$, and $SA_{(2b)}$) related to eutrophication kinetics (Zhang, 2005).

The CE-QUAL-ICM eutrophication model was recast in terms of a network of 90 reactions involving 66 reaction constituents (Bc, Bd, Bg, DOC, LPOC, RPOC, NH_4, NO_3, DON, LPON, RPON, PO_4d, PO_4p, DOP, LPOP, RPOP, COD, DO, SU, SAd, SAp, TAMd, TAMp, $POC_{(1b)}$, $POC_{(2b)}$, $POC_{(3b)}$, $NH_{4(1b)}$, $NH_{4(2b)}$, $NO_{3(1b)}$, $NO_{3(2b)}$, $PON_{(1b)}$, $PON_{(2b)}$, $PON_{(3b)}$, $PO_4d_{(1b)}$, $PO_4p_{(1b)}$, $PO_4d_{(2b)}$, $PO_4p_{(2b)}$, $POP_{(1b)}$, $POP_{(2b)}$, $POP_{(3b)}$, $COD_{(1b)}$, $COD_{(2b)}$, $SU_{(1b)}$, $SU_{(2b)}$, $SAd_{(1b)}$, $SAp_{(1b)}$, $SAd_{(2b)}$, $SAp_{(2b)}$, CO_2, H_2O, N_2, $O_{2(g)}$, $Bc_{(b)}$, $Bd_{(b)}$, $Bg_{(b)}$, $TAMp_{(b)}$, BPOC, BNH_4, BNO_3, BPON, BPO_4, BPOP, BCOD, BSU, BSA, and BTAM). Eighty seven of the 90 reactions were considered slow/kinetic reactions and the other seven were fast/equilibrium reactions. Details of these reactions can be found elsewhere (Zhang, 2005). These 90 reactions address sediment-biogeochemical interactions and 6 interacting biogeochemical processes: plant and bacterial growth kinetics, nitrogen cycles, phosphorus cycle, carbon cycles, silica cycles, and metal cycles (Zhang, 2005). They are characterized by 45 reaction stoichiometries and a total of 86 reaction parameters (Zhang, 2005).

The simulation domain, descretization, flow field and temperature distribution are same as example 5.2.2. Variable boundary conditions are applied to the open boundary sides. Initial concentrations of the 48 simulated species and variable boundary incoming concentrations of mobile species are listed in Table 5.2-10. It is noted that only 48 species out of 66 species are simulated because the governing equations for CO_2, H_2O, N_2, $O_{2(g)}$, $Bc_{(b)}$, $Bd_{(b)}$, $Bg_{(b)}$, $TAMp_{(b)}$, BPOC, BNH_4, BNO_3, BPON, BPO_4, BPOP, BCOD, BSU, BSA, and BTAM are decoupled from those for the other 48 species. The decoupling of two sets of state variable is due to the formulation of rate equations that depend on only 48 species.

The dispersion coefficient was 5.2 m^2/s. Each point source injected PO_4d with a rate of 5.0 $g/m^2/s$. A 2.5-day (5T) simulation is performed with a fixed time step size of 10 minutes. A relative error of 10^{-4} is used to determine the convergence for iterations involved in the computation.

Table 5.2-10 Species Initial and Boundary Concentration in Example 5.2.4

No.	Species	Notati	Initial	Boundary	ρ_i
1	Cyan bacteria	Bc	0.1 mg-C/kg	0.01 mg-C/m^3	ρ_w
2	Diatoms	Bd	1.0 mg-C/kg	0.1 mg-C/m^3	ρ_w
3	Green algae	Bg	2.0 mg-C/kg	0.2 mg-C/m^3	ρ_w
4	Dissolved organic carbon	DOC	5.0 mg-C/kg	0.5 mg-C/m^3	ρ_w
5	Dissolved organic phosphorus	DOP	0.5 mg-P/kg	0.05 mg-P/m^3	ρ_w
6	Dissolved phosphate	PO_4d	0.05 mg-P/kg	0.005 mg-	ρ_w
7	Dissolved organic nitrogen	DON	2.0 mg-N/kg	0.2 mg-N/m^3	ρ_w
8	Ammonium	NH_4	1.0 mg-N/kg	0.1 mg-N/m^3	ρ_w
9	Nitrate	NO_3	1.0 mg-N/kg	0.1 mg-N/m^3	ρ_w
10	Dissolved available silica	SAd	1.0 mg-Si/kg	0.1 mg-Si/m^3	ρ_w
11	Chemical oxygen demand	COD	2.0 mg-O_2/kg	0.2 mg-O_2/m^3	ρ_w
12	Dissolved oxygen	DO	8.0 mg-O_2/kg	0.8 mg-O_2/m^3	ρ_w
13	Dissolved active metal	TAMd	0.000005 mol	0.0000005	SS
14	Labile particulate organic carbon	LPOC	0.02 mg-C/mg	0.1 mg-C/m^3	SS
15	Refractory particulate organic	RPOC	0.02 mg-C/mg	0.1 mg-C/m^3	SS
16	Labile particulate organic	LPOP	0.004 mg-P/mg	0.02 mg-P/m^3	SS
17	Refractory particulate organic	RPOP	0.004 mg-P/mg	0.02 mg-P/m^3	SS
18	Particulate phosphate	PO_4p	0.00006 mg-	0.0003 mg-	SS
19	Labile particulate organic nitrogen	LPON	0.0002 mg-	0.001 mg-	SS
20	Refractory particulate organic	RPON	0.0002 mg-	0.001 mg-	SS
21	Particulate available silica	SAp	0.0012 mg-	0.006 mg-	SS
22	Particulate biogenic silica	SU	0.0002 mg-Si/mg	0.01 mg-Si/m^3	SS
23	Particulate active metal	TAMp	0.0002 mol /mg	0.001 mol /m^3	SS
24	Benthic dissolved phosphate	$PO_4d_{(1}$	0.9 mg-P/kg	-	$h_b\rho_{wb}\theta_b/h$
25	Benthic dissolved phosphate	$PO_4d_{(2}$	1.8 mg-P/kg	-	$h_b\rho_{wb}\theta_b/h$
26	Benthic ammonium layer 1	$NH_{4(1b)}$	1.0 mg-N/kg	-	$h_b\rho_{wb}\theta_b/h$
27	Benthic ammonium layer 2	$NH_{4(2b)}$	2.0 mg-N/kg	-	$h_b\rho_{wb}\theta_b/h$
28	Benthic nitrate layer 1	$NO_{3(1b)}$	1.0 mg-N/kg	-	$h_b\rho_{wb}\theta_b/h$
29	Benthic nitrate layer 2	$NO_{3(2b)}$	2.0 mg-N/kg	-	$h_b\rho_{wb}\theta_b/h$
30	Benthic dissolved available silica	$SAd_{(1b)}$	0.6 mg-Si/kg	-	$h_b\rho_{wb}\theta_b/h$
31	Benthic dissolved available silica	$SAd_{(2b)}$	1.2 mg-Si/kg	-	$h_b\rho_{wb}\theta_b/h$
32	Benthic chemical oxygen demand	$COD_{(1}$	2.0 mg-O_2/kg	-	$h_b\rho_{wb}\theta_b/h$
33	Benthic chemical oxygen demand	$COD_{(2}$	4.0 mg-O_2/kg	-	$h_b\rho_{wb}\theta_b/h$
34	Benthic particulate organic carbon	$POC_{(1b}$	0.0195 mg-C/mg	-	BS/h
35	Benthic particulate organic carbon	$POC_{(2b}$	0.0075 mg-C/mg	-	BS/h
36	Benthic particulate organic carbon	$POC_{(3b}$	0.003 mg-C/mg	-	BS/h
37	Benthic particulate organic	$POP_{(1b}$	0.0039 mg-P/mg	-	BS/h
38	Benthic particulate organic	$POP_{(2b}$	0.0015 mg-P/mg	-	BS/h
39	Benthic particulate organic	$POP_{(3b}$	0.0006 mg-P/mg	-	BS/h
40	Benthic particulate phosphate layer	$PO_4p_{(1}$	0.0000099 mg-	-	BS/h
41	Benthic particulate phosphate layer	$PO_4p_{(2}$	0.0000198 mg-	-	BS/h
42	Benthic particulate organic nitrogen	$PON_{(1b}$	0.000195 mg-N/mg	-	BS/h
43	Benthic particulate organic nitrogen	$PON_{(2b}$	0.000084 mg-N/mg	-	BS/h
44	Benthic particulate organic nitrogen	$PON_{(3b}$	0.000021 mg-N/mg	-	BS/h
45	Benthic particulate available silica	$SAp_{(1b)}$	0.0000066 mg-	-	BS/h
46	Benthic particulate available silica	$SAp_{(2b)}$	0.0000132 mg-	-	BS/h
47	Benthic particulate biogenic silica	$SU_{(1b)}$	0.003 mg-Si/mg	-	BS/h
48	Benthic particulate biogenic silica	$SU_{(2b)}$	0.006 mg-Si/mg	-	BS/h

Figure 5.2-10 plots the concentration contours of PO_4d at different simulation time. It is seen that at the point sources, concentration of PO_4d increases due to the injection, and at the open boundary, concentration of PO_4d decreases due to the low incoming concentration.

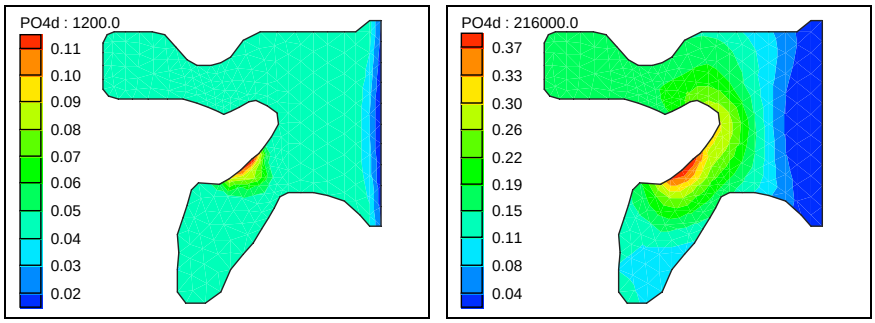

Fig. 5.2-10. Concentration of PO_4d (mg-P/L) in Example 5.2.4
Left: 20 minutes; Right: 5T

Figure 5.2-11 plots the concentration contours of Bc, Bd, and Bg. According to the reaction network of CE-QUAL-ICM, the source of Bc, Bd, and Bg is the growth, and the sink of Bc, Bd, and Bg includes basal metabolism, predating, and settling. The concentration decrease of Bc, Bd, and Bg shown in the Figure 5.2-11 indicates that the source is less than the sink. Among these three groups of algae, Bd has special need of silica to form cell walls. The similar concentration distribution of Bc, Bd, and Bg indicates that under the condition set for this example, there is enough silica, which does not limit the growth of Bd.

Comparing the concentration distributions of Bc (bacteria), Bd (diatom), and Bg (green alage) (Figure 5.2-11), PHYT (Figure 5.2-9) and Chla (Figure 5.2-8), we can see that relative decreasing rate of Chla is greater than Bc, Bd, Bg, and PHYT. This indicates that the rate of (algae respiration + settling – growth) in the QUAL2E example is greater than the rate of (PHYT death + settling – growth) in the WASP5 example and the rate of (Bc, Bd, and Bg basal metabolism + predating + settling – growth) in this example. The rate difference is due to the different rate formulation and parameterization of the models. For example, in QUAL2E, there is only transfer of chemicals from water column to bed. However, WASP5 and CE-QUAL-ICM include both column and benthic interactions. Thus, the algae settling speed in QUAL2E example is greater than the PHYT settling speed in WASP5 example and the Bc, Bd, and Bg settling speeds in CE-QUAL-ICM example.

Animations showing the spatial-temporal distribution of dissolved phosphorus (File Name: CE-QUAL-ICM PO4d.avi), bacteria (File Name: CE-QUAL-ICM Bc Bacteria.avi), diatom (File Name: CE-QUAL-ICM Bd diatom.avi), and green alage (File Name: CE-QUAL-ICM Bg Green algae.avi), respectively, are attached in Appendix A. Readers can visualize these moves by clicking the file contained in the attached CD.

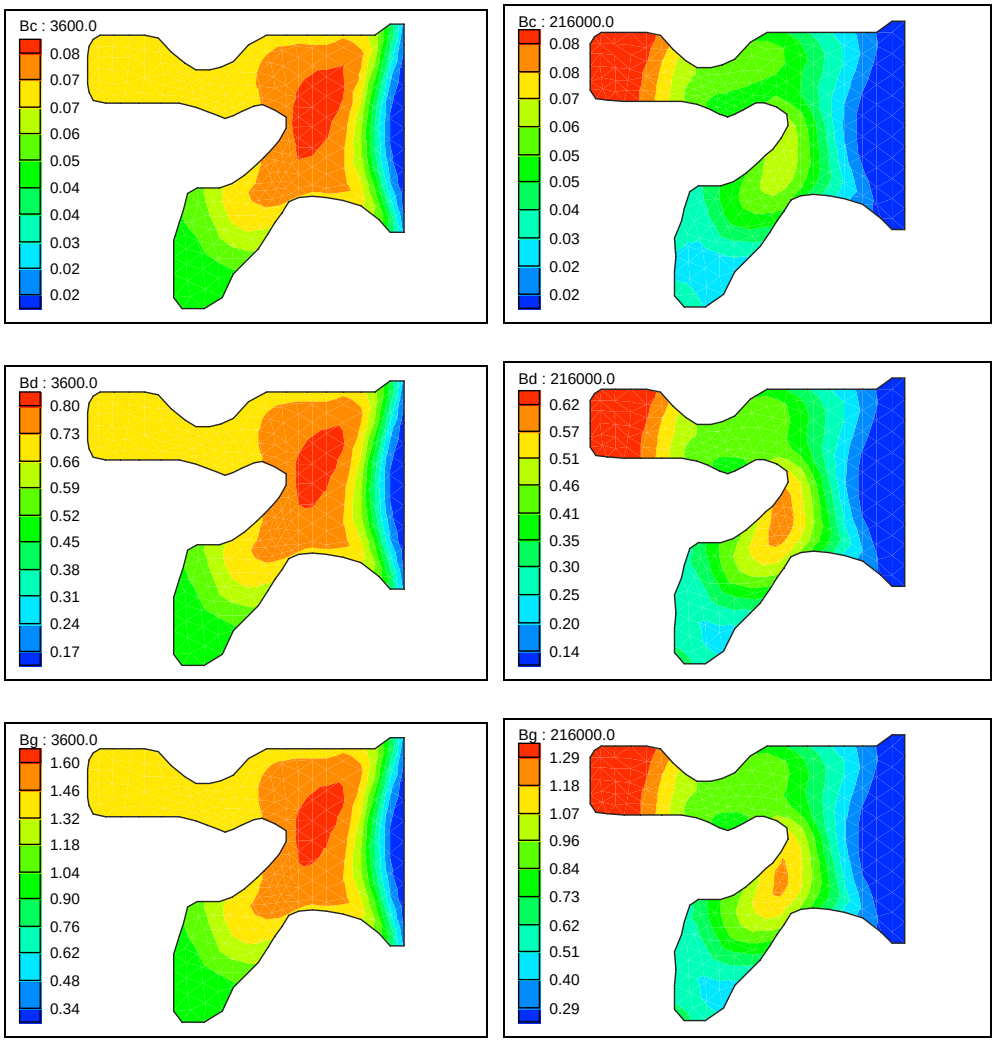

Fig. 5.2-11. Concentration of Algae (mg-C/L) at 1 hour (Left) and 5T (Right) in Example 5.2.4: Upper: Bc; Middle: Bd; Lower: Bg

5.2.5 Discussions on Diagonalization Approaches to Water Quality Modeling

To demonstrate flexibility of the general paradigm to model water quality, the eutrophication kinetics in three widely used models, QUAL2E, WASP5, and CE-QUAL-ICM, were recast in the mode of reaction networks and employed as examples. Table 5.2-11 lists the comparison of the three models via a reaction point of view.

Table 5.2-11 Comparison of QUAL2E, WASP5, and CE-QUAL-ICM

Model	QUAL2E	WASP5	CE-QUAL-ICM
Number and types of reactions	**16 kinetic reactions and 0 equilibrium reactions:** Algal kinetics: 4 Dissolved Oxygen Balance: 4 Nitrogen Cycle: 5 Phosphorus Cycle: 3	**32 kinetic reactions and 6 equilibrium reactions:** Phytoplankton Kinetics: 11 Dissolved Oxygen Balance: 9 Nitrogen Cycle: 11 Phosphorus Cycle: 7	**83 kinetic reactions and 7 equilibrium reactions:** Plant and bacterial Kinetics: 14 Dissolved Oxygen Balance: 16 Nitrogen Cycle: 20 Phosphorus Cycle: 21 Silica Cycle: 16 Metal Cycle: 3
No. of reactive water quality related to eutrophication kinetics in the report	**9** O, L, Chla, N_4, N_1, N_2, N_3, P_1, and P_2.	**16** NH_3, $NH_{3(b)}$, NO_3, $NO_{3(b)}$, OPO_4, $OPO_{4(b)}$, PHYT, $PHYT_{(b)}$, CH_2Ot, $CH_2Ot_{(b)}$, O_2, $O2_{(b)}$, ONt, $ONt_{(b)}$, OPt, and $OPt_{(b)}$.	**41** Bc, Bd, Bg, DOC, LPOC, RPOC, NH_4, NO_3, DON, LPON, RPON, PO_4t, DOP, LPOP, RPOP, COD, DO, SU, SA, TAM, $POC_{(1b)}$, $POC_{(2b)}$, $POC_{(3b)}$, $NH_{4(1b)}$, $NH_{4(2b)}$, $NO_{3(1b)}$, $NO_{3(2b)}$, $PON_{(1b)}$, $PON_{(2b)}$, $PON_{(3b)}$, $PO_{4(1b)}$, $PO_{4(2b)}$, $POP_{(1b)}$, $POP_{(2b)}$, $POP_{(3b)}$, $COD_{(1b)}$, $COD_{(2b)}$. $SU_{(1b)}$, $SU_{(2b)}$, $SA_{(1b)}$, and $SA_{(2b)}$
No. of water quality from the reaction point of view	**19** (first 9 modeled) O, L, Chla, N_4, N_1, N_2, N_3, P_1, P_2, $O_{(b)}$, $L_{(b)}$, $Chla_{(b)}$, $N_{4(b)}$, $N_{(1b)}$, $P_{(1b)}$, $P_{(2b)}$, CO_2, H_2O, and $O_{2(g)}$	**27** (first 22 modeled) NH_3, $NH_{3(b)}$, NO_3, $NO_{3(b)}$, OPO_4, $OPO_{4(b)}$, PHYT, $PHYT_{(b)}$, CH_2O, CH_2Op, $CH_2O_{(b)}$, $CH_2Op_{(b)}$, O_2, $O_{2(b)}$, ON, ONp, $ON_{(b)}$, $ONp_{(b)}$, OP, OPp, $OP_{(b)}$, $OPp_{(b)}$, CO_2, H_2O, H^+, N_2, and $O_{2(g)}$.	**66** (first 48 modeled) Bc, Bd, Bg, DOC, LPOC, RPOC, NH_4, NO_3, DON, LPON, RPON, PO_4d, PO_4p, DOP, LPOP, RPOP, COD, DO, SU, SAd, SAp, TAMd, TAMp, $POC_{(1b)}$, $POC_{(2b)}$, $POC_{(3b)}$, $NH_{4(1b)}$, $NH_{4(2b)}$, $NO_{3(1b)}$, $NO_{3(2b)}$, $PON_{(1b)}$, $PON_{(2b)}$, $PON_{(3b)}$, $PO_4d_{(1b)}$, $PO_4p_{(1b)}$, $PO_4d_{(2b)}$, $PO_4p_{(2b)}$, $POP_{(1b)}$, $POP_{(2b)}$, $POP_{(3b)}$, $COD_{(1b)}$, $COD_{(2b)}$, $SU_{(1b)}$, $SU_{(2b)}$, $SAd_{(1b)}$, $SAp_{(1b)}$, $SAd_{(2b)}$, $SAp_{(2b)}$, CO_2, H_2O, N_2, $O_{2(g)}$, $Bc_{(b)}$, $Bd_{(b)}$, $Bg_{(b)}$, $TAMp_{(b)}$, BPOC, BNH_4, BNO_3, BPON, BPO_4, BPOP, BCOD, BSU, BSA, and BTAM
No. Reaction Parameters	**36**	**66**	**86**

In the context of reaction network, there are 16, 38, and 90 biogeochemical reactions included in QUAL2E, WASP5, and CE-QUAL-ICM, respectively. All three models include the major interactions of the nutrient cycles; algae kinetics modified by temperature, light, and nutrient limitation; and dissolved oxygen balance under the effect of benthic oxygen demand, carbonaceous oxygen uptake, and atmospheric aeration. Therefore, under the similar conditions set for three eutrophication examples, we obtained similar algae concentration distributions in Figures 5.2-8, 5.2-9, and 5.2-11, for QUAL2E, WASP5, and CE-QUAL-ICM, respectively.

In QUAL2E, sediment-biogeochemical interactions are not considered. However, WASP5 and CE-QUAL-ICM include both column and benthic interactions. In QUAL2E, there is transfer of chemicals from water column to bed, but no chemicals transferred from benthic bed to column. In WASP5 and CE-QUAL-ICM, dissolved fractions are subject to diffusion, particulate fractions can settle and re-suspend, and inorganic nutrients can also enter into column water by benthic release.

In QUAL2E and WASP5 model, nutrient cycles include nitrogen cycles and phosphorus cycles. In addition to these two nutrient cycles, CE-QUAL-ICM also includes silica cycle and metal cycle. Consideration of silica cycle makes it possible to include kinetics of diatoms, which are distinguished by their requirement of silica as a nutrient. In QUAL2E and WASP5, all algae or phytoplankton are simulated as one group. However, in CE-QUAL-ICM, algae are grouped in to three classes: cyan bacteria, diatoms, and greens. Therefore, concentration distributions of three algae groups rather than one are plotted in Figure 5.2-11 for CE-QUAL-ICM.

In the original reports, there are 9, 16, and 41 water quality state-variables related to eutrophication kinetics simulated in QUAL2E, WASP5, and CE-QUAL-ICM, respectively. In the context of reaction network, there are 19, 27, and 66 constituents involved in QUAL2E, WASP5, and CE-QUAL-ICM, respectively. In the case of QUAL2E, all 16 rate equations depend only on the first nine constituents; thus, the other 10 constituents can be decoupled from the first 9 in any simulation. Had evidence indicated that the rate formulation of the 16 kinetic reactions also depended on the other 10 constituents in a system, all 19 constituents would have been modeled simultaneously. Therefore, when QUAL2E is applied to any system, the first order of business is to check if the rate formulation for the 16 kinetic reactions is valid. If it is, then one can consider other issues involved in applying the model to the system. If any of the 16 rate equations is invalid, then one should not apply the model to the system.

In the case of WASP5, rates of the 32 kinetic reactions were assumed not affected by the last 5 constituents. Thus, these 5 constituents can be decoupled from the other 22. Therefore, one only needs to simulate 22 constituents simultaneously from the reaction point of view. The question is then why WASP5 only considered 16 water quality state-variables. Examination of 6 fast equilibrium reactions would reveal that the adsorption reactions of aqueous CH_2O, $CH_2O_{(b)}$, ON, $ON_{(b)}$, OP, and $OP_{(b)}$ onto sediments were formulated with a simple partition. Furthermore, rate equations are only functions of the aqueous fractions of CH_2Ot ($=CH_2O + CH_2Op$), $CH_2Ot_{(b)}$ ($=CH_2O_{(b)} + CH_2Op_{(b)}$), ONt ($=ON + ONp$), $ONt_{(b)}$($= ON_{(b)} + ONp_{(b)}$), OPt ($=OP + OPp$), and $OPt_{(b}$($=OP_{(b)} + OPp_{(b)}$); not functions of 12 individual species in the parentheses. Thus, if we eliminate these 12 species using the 6 partition equations and 6 equations defining the total, the reaction-based approach would yield 16 identical equations as those in the WASP5 report. In our reaction-based approach, we prefer to model all 22 species. This allows us, if necessary, the flexibility of more mechanistically modeling the sorption reactions and formulating the rate equations as functions of all individual species. Similarly, for CE-QUAL-ICM, we prefer to model 48 species out of the total 66 species, rather than 41 constituents. This reaction-based approach alleviates the need of modeling 7 sorption reactions with a simple partition. In the decomposition of reaction-matrix, the elimination of 7 fast equilibrium reactions is performed automatically rather then manually. Ideally, one should model all of the 66 species if any of the reaction rates is affected by the other 18 species.

No attempts were made to compare the simulation results with field measurements because this is not the main objective of this report. It is almost certain that the simulations presented above will not match with field measurements using all reaction parameters reported in QUAL2E, WASP5, or CE-QUAL-ICM. The important question then is what we should do to calibrate the model. There may be three ways out. Take QUAL2E as an example. First we can abuse the model by optimizing all 36 rate parameters characterizing 16 reaction rate equations with the best optimization technique disregarding the physics involved in the system. Second we can justify the model by fine-tuning some of the 36 rate parameters or better reformatting some of the rate equations based on our understanding of the system. Third, we can wise the model by researching if there are new mechanisms that are operating in the system under investigation but not included in QUAL2E. In order not to abuse the model, a general paradigm is developed that has the design capability to include any number of reactions involving any number of species and that provides a protocol for formulating the rates of reactions and discovering the assumptions and limitations of the model employed.

The reaction network for QUAL2E system includes 16 kinetic reactions involving 19 species. Substitution of this reaction network into Equation (2.6.30) results in 19 ordinary differential equations for 19 species in a well-mixed system. Because the rates of all 16 reactions depend on only the first 9 species, equations governing the last 10 species are decoupled from the equations governing the first 9 species. Thus, only the first 9 species were considered in QUAL2E. The exclusion of the last 10 species has an important implication when QUAL2E is applied to a new system other than the one QUAL2E was developed for.

In a "true" reaction-based approach, governing equations for all species involved in the reaction network must be considered. The diagonalization of the reaction matrix for all 19 species would result in a set of 15 kinetic-variable equations [Equations (1) through (9) and (14) through (19) in Table 5.2-12] and 4 component equations [Equations (10) through (13) in Table 5.2-12].

If we substitute Equations (14) through (19) into Equations (1) through (9) in Table 5.2-12, the resulting first 9 equations are then decoupled from the last 10 equations. Once the resulting 9 equations are solved for C_1 through C_9, Equations (14) through (19) are used to calculated the dynamics of $Chla_{(b)}$, $N_{4(b)}$, $P_{2(b)}$, $L_{(b)}$, $O_{2(g)}$, and $O_{(b)}$, and Equations (10) through (13) can be used to calculate the amount of H_2O, CO_2, $N_{1(b)}$, and $P_{1(b)}$ that must be supplied to maintain the conservation principle for water, carbon dioxide, benthic organic nitrogen, and benthic organic phosphorus. In a large water body, the amount of water needed to maintain its conservation due to biogeochemical processes can be met without much problem. The nagging question is what would be the source of CO_2, $N_{1(b)}$, and $P_{1(b)}$ to maintain their conservation with respective to reactions. For any system, if this nagging question cannot be answered, then the partial pressure of CO_2 and the concentrations of $N_{1(b)}$ and $P_{1(b)}$ would probably be important factors in controlling reaction rates and inducing additional biogeochemical processes. Under such circumstances, one probably has to revisit the rate equations and to conduct research to uncover additional reaction networks for the system under investigations.

Table 5.2-12 Governing Equations for the Reaction-based Diagonalization Approach

Decomposition Equations	No.
$dE_1/dt = d\left[0.00027\left(C_3 + Chla_{(b)}\right) + C_9 + P_{2(b)}\right]/dt = -0.015R_3 + R_{10}$	(1)
$dE_2/dt = d\left[C_9 + P_{2(b)}\right]/dt = -0.015R_1 + R_{10}$	(2)
$dE_3/dt = d\left[-0.21\left(C_1 - C_2 + O_{2(g)} + O_{(b)} - L_{(b)}\right) + 0.0078\left(C_3 + Chla_{(b)}\right) - 0.77C_6 - C_7 + 5.1\left(C_9 + P_{2(b)}\right)\right]/dt = R_2 + 5.1R_{10}$	(3)
$dE_4/dt = d\left[0.00032\left(C_3 + Chla_{(b)}\right) + 0.22\left(C_4 + N_{4(b)}\right) + 1.2\left(C_9 + P_{2(b)}\right)\right]/dt = -0.22R_5 + 1.2R_{10}$	(4)
$dE_5/dt = d\left[-0.22\left(C_1 - C_2 + O_{2(g)} + O_{(b)} - L_{(b)}\right) + 0.0078\left(C_3 + Chla_{(b)}\right) + 0.23C_6 + 5.1\left(C_9 + P_{2(b)}\right)\right]/dt = R_7 + 5.11R_{10}$	(5)
$dE_6/dt = d\left[0.0094\left(C_1 - C_2 + O_{2(g)} + O_{(b)}\right) - 0.00033\left(C_3 + Chla_{(b)}\right) + 0.033C_6 - 0.22\left(C_9 + P_{2(b)}\right)\right]/dt = -0.043R_9 - 0.22R_{10}$	(6)
$dE_7/dt = d\left[0.0015\left(C_3 + Chla_{(b)}\right) + C_4 + C_5 + C_6 + C_7 + N_{4(b)}\right]/dt = R_8$	(7)
$dE_8/dt = d\left[0.00027\left(C_3 + Chla_{(b)}\right) + C_8 + C_9 + P_{2(b)}\right]/dt = -R_{11}$	(8)
$dE_9/dt = d\left(C_2 + L_{(b)}\right)/dt = -R_{13}$	(9)
$dT_1/dt = d\left(C_2 + L_{(b)} + H_2O\right)/dt = 0$	(10)
$dT_2/dt = d\left(C_2 + L_{(b)} + CO_2\right)/dt = 0$	(11)
$dT_3/dt = d\left[0.0015\left(C_3 + Chla_{(b)}\right) + C_4 + C_5 + C_6 + C_7 + N_{1(b)} + N_{4(b)}\right]/dt = 0$	(12)
$dT_4/dt = d\left[0.00027\left(C_3 + Chla_{(b)}\right) + C_8 + C_9 + P_{1(b)} + P_{2(b)}\right]/dt = 0$	(13)
$dE_{10}/dt = dChla_{(b)}/dt = R_4$	(14)
$dE_{11}/dt = dN_{4(b)}/dt = R_6$	(15)
$dE_{12}/dt = dP_{2(b)}/dt = -R_{12}$	(16)
$dE_{13}/dt = dL_{(b)}/dt = R_{14}$	(17)
$dE_{14}/dt = dO_{2(g)}/dt = -R_{15}$	(18)
$dE_{15}/dt = dO_{(b)}/dt = R_{16}$	(19)

C_1 = O, C_2 = L, C_3 = Chl<u>a</u>, C_4 = N_4, C_5 = N_1, C_6 = N_2, C_7 = N_3, C_8 = P_1, and C_9 = P_2

The use of diagonalization approaches allows one to formulate some rate equations one by one. For example, the reaction rate R_8 can be calculated by plotting the concentration of E_7 versus time in which E_7 is the linear combination of C_3, C_4, C_5, C_6, C_7, $Chla_{(b)}$ and $P_{2(b)}$ [see Equation (7) in Table 5.2-12]. Similarly, reaction rates R_{11}, R_{13}, R_4, R_6, R_{12}, R_{14}, R_{15}, and R_{16} can be calculated from the dynamics of E_8 through E_{15}, respectively [see Equations (8), (9) and (14) through (19) in Table 5.2-12]. Because linearly dependent reactions are present in the system, one cannot formulate all rate equations independently. To do so, one has to design an experimental system such that only linearly independent reactions are present to individually and mechanistically formulate rate equations.

5.3 Three-Dimensional Examples

Three examples are employed in this section. The first two examples involving simulations of uranium transport in soil columns are presented to evaluate the ability of the model to simulate reactive transport with reaction networks involving both kinetically and equilibrium-controlled reactions. The third example is a hypothetical three-dimensional problem and is presented to demonstrate the model application to a field-scale problem involving reactive transport with a complex reaction network.

5.3.1 Packed Column Breakthrough Curve Simulation for Uranium (VI) Sorption

A glass column of approximately one cm in diameter by 3 cm long was filled with 2.483 g crushed and sieved (< 2 mm) soil material with a porosity of 0.66. The soil contained 1.9 percent Fe oxides on a mass basis. A solution with 10 μM U(VI) and 50 mM $NaNO_3$ was injected at a specific discharge of 1.235 cm/h until breakthrough was observed. The inlet solution was switched to a U(VI) free solution after 614.7 PV (Pace et al., 2005).

In the simulation, the column is discretized with 20 nodes and 4 equal size elements (0.886 cm × 0.886 cm × 0.779 cm each) (Fig. 5.3-1). Other parameters for the experiments are summarized in Figure 5.3-1. The simulation was performed for a total duration of 2,500 hours with a constant time-step size of 0.25 hour.

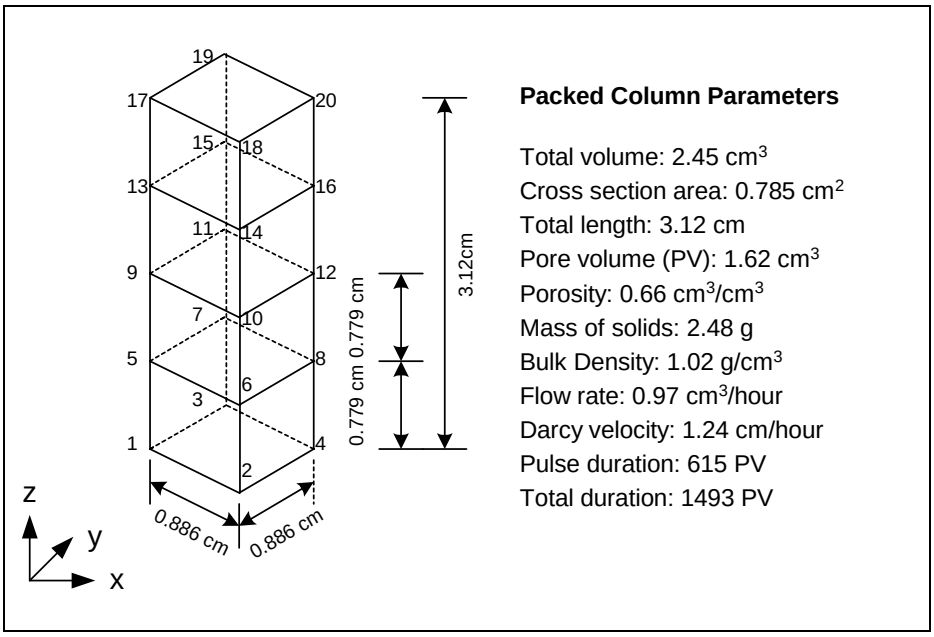

Fig. 5.3-1. Simulation Domain and Descretization for Example 5.3.1
Note: the column parameters are from Pace et al. (2005)

The reaction network utilized in the model is described in Table 5.3-1 (Lindsay, 1979, Brooks, 2001, Waite et al., 1994, and Langmuir, 1997), which utilizes 46 species and 39 equilibrium reactions. Because the activity of H_2O is assumed to be 1.0, it is decoupled from the system; hence only 45 chemical species are considered. The system involves 6 kinetic-variable transport equations (Table 5.3-2) and 39 equilibrium reaction mass action equations or user specified nonlinear algebraic equations (Table 5.3-3) set up through decomposition for 45 species.

Among the kinetic-variables, the fifth involves no mobile species and is not solved in the advection-dispersion transport step. Therefore, instead of solving 27 advection-dispersion transport equations for mobile species in a primitive approach, we only solve 5 advection-dispersion transport equations for kinetic-variables. Furthermore, one of the kinetic variables, E_6, involves only mobile species, which makes its transport equation linear allowing its solution to be solved outside the nonlinear iteration loop between transport and reactions when the fully-implicit scheme is used to deal with reactive chemistry. Since all reactions are equilibrium reactions, kinetic-variables are equivalent to components.

The experimental data and simulation results are shown in Figure 5.3-1. The simulation results closely follow the data, reflecting retardation due to reactions on both the leading and tailing portions of the breakthrough curve. The results provide validation of the reaction network employed to simulate uranium (VI) transport and the numerical implementation.

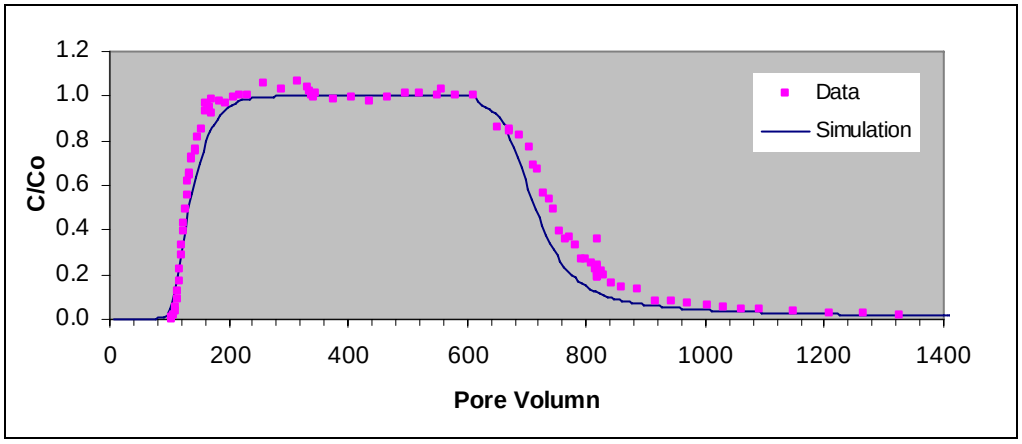

Fig. 5.3-2. U(VI) Breakthrough Curve for the Packed Column
Note: the experiment data are from Pace et al. (2005)

Table 5.3-1 Chemical Reactions Considered in Example 5.3.1

Reactions and Parameters	No.
$Fe(OH)_3 + 3H^+ = Fe^{3+} + 3H_2O \quad logK = 2.7$	(1)
$UO_2^{2+} + H_2O = UO_2OH^+ + H^+ \quad logK = -5.2$	(2)
$UO_2^{2+} + 2H_2O = UO_2(OH)_{2(aq)} + 2H^+ \quad logK = -10.3$	(3)
$UO_2^{2+} + 3H_2O = UO_2(OH)_3^- + 3H^+ \quad logK = -19.2$	(4)
$UO_2^{2+} + 4H_2O = UO_2(OH)_4^{2-} + 4H^+ \quad logK = -33.0$	(5)
$2UO_2^{2+} + H_2O = (UO_2)_2OH^{3+} + H^+ \quad logK = -2.7$	(6)
$2UO_2^{2+} + 2H_2O = (UO_2)_2(OH)_2^{2+} + 2H^+ \quad logK = -5.62$	(7)
$3UO_2^{2+} + 4H_2O = (UO_2)_3(OH)_4^{2+} + 4H^+ \quad logK = -11.9$	(8)
$3UO_2^{2+} + 5H_2O = (UO_2)_3(OH)_5^+ + 5H^+ \quad logK = -15.5$	(9)
$3UO_2^{2+} + 7H_2O = (UO_2)_3(OH)_7^- + 7H^+ \quad logK = -31.0$	(10)
$UO_2^{2+} + CO_3^{2-} = UO_2CO_{3(aq)} \quad logK = 9.68$	(11)
$UO_2^{2+} + 2CO_3^{2-} = UO_2(CO_3)_2^{2-} \quad logK = 16.94$	(12)
$UO_2^{2+} + 3CO_3^{2-} = UO_2(CO_3)_3^{4-} \quad logK = 21.6$	(13)
$3UO_2^{2+} + 6CO_3^{2-} = (UO_2)_3(CO_3)_6^{6-} \quad logK = 54.0$	(14)
$2UO_2^{2+} + 4H_2O + CO_{2(g)} = (UO_2)_2CO_3(OH)_3^- + 5H^+ \quad logK = -19.01$	(15)
$>Fe_sOH + H^+ + CO => Fe_sOH_2^+ \quad logK = 6.51$	(16)
$>Fe_sOH => Fe_sO^- + H^+ + CO \quad logK = -9.13$	(17)
$>Fe_s(OH)_2 + UO_2^{2+} = (>Fe_sO_2)UO_2 + 2H^+ \quad logK = -2.57$	(18)
$>Fe_w(OH)_2 + UO_2^{2+} = (>Fe_wO_2)UO_2 + 2H^+ \quad logK = -6.28$	(19)
$>Fe_sOH + H_2CO_3 => Fe_sCO_3H + H_2O \quad logK = 2.90$	(20)
$>Fe_sOH + H_2CO_3 => Fe_sCO_3^- + H_2O + H^+ + CO \quad logK = -5.09$	(21)
$>Fe_s(OH)_2 + UO_2^{2+} + H_2CO_3 = (>Fe_sO_2)UO_2CO_3^{2-} + 4H^+ + 2CO \quad logK = -13.0$	(22)
$>Fe_w(OH)_2 + UO_2^{2+} + H_2CO_3 = (>Fe_wO_2)UO_2CO_3^{2-} + 4H^+ + 2CO \quad logK = -17.10$	(23)
$FeOH^{2+} + H^+ = Fe^{3+} + H_2O \quad logK = 2.19$	(24)
$Fe(OH)_2^+ + 2H^+ = Fe^{3+} + 2H_2O \quad logK = 5.67$	(25)
$Fe(OH)_3^0 + 3H^+ = Fe^{3+} + 3H_2O \quad logK = 12.56$	(26)
$Fe(OH)_4^- + 4H^+ = Fe^{3+} + 4H_2O \quad logK = 21.6$	(27)
$H_2O + CO_{2(g)} = H_2CO_3^0 \quad logK = -1.47$	(28)
$H_2CO_3^0 = H^+ + HCO_3^- \quad logK = -6.35$	(29)
$HCO_3^- = H^+ + CO_3^{2-} \quad logK = -10.33$	(30)
$>Fe_wOH + H^+ + CO => Fe_wOH_2^+ \quad logK = 6.51$	(31)
$>Fe_wOH => Fe_wO^- + H^+ + CO \quad logK = -9.13$	(32)
$>Fe_wOH + H_2CO_3 => Fe_wCO_3H + H_2O \quad logK = 2.90$	(33)
$>Fe_wOH + H_2CO_3 => Fe_wCO_3^- + H_2O + H^+ + CO \quad logK = -5.09$	(34)
$0 \cdot Fe(OH)_3 = 0 \cdot [>Fe_sOH_2^+ + >Fe_sO^- + >Fe_sCO_3H + >Fe_sCO_3^- + (>Fe_sO_2)UO_2 + (>Fe_sO_2)UO_2CO_3^{2-}] + >Fe_sOH,\ 0.0018C_{Fe(OH)_3} = C_{>Fe_sOH} + C_{>Fe_sOH_2^+} + C_{>Fe_sO^-} + C_{>Fe_sCO_3H} + C_{>Fe_sCO_3^-} + 2(C_{(>Fe_sO_2)UO_2} + C_{(>Fe_sO_2)UO_2CO_3^{2-}})$	(35)
$0 \cdot Fe(OH)_3 = 0 \cdot [>Fe_wOH_2^+ + >Fe_wO^- + >Fe_wCO_3H + >Fe_wCO_3^- + (>Fe_wO_2)UO_2 + (>Fe_wO_2)UO_2CO_3^{2-}] + >Fe_wOH,\ 0.8732C_{Fe(OH)_3} = C_{>Fe_wOH} + C_{>Fe_wOH_2^+} + C_{>Fe_wO^-} + C_{>Fe_wCO_3H} + C_{>Fe_wCO_3^-} + 2(C_{(>Fe_wO_2)UO_2} + C_{(>Fe_wO_2)UO_2CO_3^{2-}})$	(36)
$0 \cdot > Fe_sOH => Fe_s(OH)_2 \quad C_{Fe_sOH} = 2C_{Fe_s(OH)_2}$	(37)
$0 \cdot > Fe_wOH => Fe_w(OH)_2 \quad C_{Fe_wOH} = 2C_{Fe_w(OH)_2}$	(38)
$UO_2^{2+} + NO_3^- = UO_2NO_3^+ \quad logK = -0.300$	(39)

Table 5.3-2 Kinetic-variable Transport Equations Solved in Example 5.3.1

Kinetic-Variable Transport Equations	No.
$\frac{\partial(\theta E_1)}{\partial t} + L(E_1^{\,m}) = 0$ $E_1 = \rho_w \begin{bmatrix} H^+ - HCO_3^- - 2CO_3^{2-} - UO_2OH^+ - 2UO_2(OH)_{2(aq)} - 3UO_2(OH)_3^- - 4UO_2(OH)_4^{2-} - (UO_2)_2OH^{3+} \\ -2(UO_2)_2(OH)_2^{2+} - 4(UO_2)_3(OH)_4^{2+} - 5(UO_2)_3(OH)_5^+ - 7(UO_2)_3(OH)_7^- - 2UO_2CO_{3(aq)} - FeOH^{2+} \\ -4UO_2(CO_3)_2^{2-} - 6UO_2(CO_3)_3^{3-} - 12(UO_2)_3(CO_3)_6^{6-} - 5(UO_2)_2CO_3(OH)_3^- - 2Fe(OH)_2^+ - 3Fe(OH)_3^0 \end{bmatrix}$ $- 3\rho_w Fe(OH)_3 + \rho_S \begin{bmatrix} > Fe_sOH_2^+ - > Fe_sO^- - 2(> Fe_sO_2)UO_2 - 2(> Fe_wO_2)UO_2 - 4(> Fe_sO_2)UO_2CO_3^{2-} \\ -4(> Fe_wO_2)UO_2CO_3^{2-} - > Fe_sO_3^- - 4Fe(OH)_4^- + > Fe_wOH_2^+ - > Fe_wO^- - > Fe_wCO_3^- \end{bmatrix}$ $E_1^{\,m} = \rho_w \begin{bmatrix} H^+ - HCO_3^- - 2CO_3^{2-} - UO_2OH^+ - 2UO_2(OH)_{2(aq)} - 3UO_2(OH)_3^- - 4UO_2(OH)_4^{2-} - (UO_2)_2OH^{3+} \\ -2(UO_2)_2(OH)_2^{2+} - 4(UO_2)_3(OH)_4^{2+} - 5(UO_2)_3(OH)_5^+ - 7(UO_2)_3(OH)_7^- - 2UO_2CO_{3(aq)} - FeOH^{2+} \\ -4UO_2(CO_3)_2^{2-} - 6UO_2(CO_3)_3^{3-} - 12(UO_2)_3(CO_3)_6^{6-} - 5(UO_2)_2CO_3(OH)_3^- - 2Fe(OH)_2^+ - 3Fe(OH)_3^0 \end{bmatrix}$	(1)
$\frac{\partial(\theta E_2)}{\partial t} + L(E_2^{\,m}) = 0 \qquad E_2 = \rho_w \left[Fe^{3+} + FeOH^{2+} + Fe(OH)_2^+ + Fe(OH)_3^0 + Fe(OH)_4^- \right] + \rho_P Fe(OH)_3$ $E_2^{\,m} = \rho_w \left[Fe^{3+} + FeOH^{2+} + Fe(OH)_2^+ + Fe(OH)_3^0 + Fe(OH)_4^- \right]$	(2)
$\frac{\partial(\theta E_3)}{\partial t} + L(E_3^{\,m}) = 0$ $E_3 = \rho_w \begin{bmatrix} UO_2^{2+} + UO_2OH^+ + UO_2(OH)_{2(aq)} + UO_2(OH)_3^- + UO_2(OH)_4^{2-} + 2(UO_2)_2OH^{3+} \\ +2(UO_2)_2(OH)_2^{2+} + 3(UO_2)_3(OH)_4^{2+} + 3(UO_2)_3(OH)_5^+ + 3(UO_2)_3(OH)_7^- \\ +UO_2CO_{3(aq)} + UO_2(CO_3)_2^{2-} + UO_2(CO_3)_3^{3-} + 3(UO_2)_3(CO_3)_6^{6-} + 2(UO_2)_2CO_3(OH)_3^- \end{bmatrix}$ $+ \rho_S \left[(> Fe_sO_2)UO_2 + (> Fe_wO_2)UO_2 + (> Fe_sO_2)UO_2CO_3^{2-} + (> Fe_wO_2)UO_2CO_3^{2-} \right]$ $E_3^{\,m} = \rho_w \begin{bmatrix} UO_2^{2+} + UO_2OH^+ + UO_2(OH)_{2(aq)} + UO_2(OH)_3^- + UO_2(OH)_4^{2-} + 2(UO_2)_2OH^{3+} \\ +2(UO_2)_2(OH)_2^{2+} + 3(UO_2)_3(OH)_4^{2+} + 3(UO_2)_3(OH)_5^+ + 3(UO_2)_3(OH)_7^- \\ +UO_2CO_{3(aq)} + UO_2(CO_3)_2^{2-} + UO_2(CO_3)_3^{3-} + 3(UO_2)_3(CO_3)_6^{6-} + 2(UO_2)_2CO_3(OH)_3^- \end{bmatrix}$	(3)
$\frac{\partial(\theta E_4)}{\partial t} + L(E_4^{\,m}) = 0 \qquad E_4^{\,m} = \rho_w \begin{bmatrix} CO_{2(g)} + H_2CO_3 + HCO_3^- + CO_3^{2-} + UO_2CO_{3(aq)} + 2UO_2(CO_3)_2^{2-} \\ +3UO_2(CO_3)_3^{3-} + 6(UO_2)_3(CO_3)_6^{6-} + (UO_2)_2CO_3(OH)_3^- \end{bmatrix}$ $E_4 = \rho_w \begin{bmatrix} CO_{2(g)} + H_2CO_3 + HCO_3^- + CO_3^{2-} + \\ UO_2CO_{3(aq)} + 2UO_2(CO_3)_2^{2-} + 3UO_2(CO_3)_3^{3-} \\ +6(UO_2)_3(CO_3)_6^{6-} + (UO_2)_2CO_3(OH)_3^- \end{bmatrix} + \rho_S \begin{bmatrix} > Fe_sCO_3H + (> Fe_sO_2)UO_2CO_3^{2-} \\ +(> Fe_wO_2)UO_2CO_3^{2-} + > Fe_sCO_3^- \\ + > Fe_wCO_3H + > Fe_wCO_3^- \end{bmatrix}$	(4)
$\frac{\partial(\theta E_5)}{\partial t} + L(E_5^{\,m}) = 0 \qquad E_5 = \rho_S \begin{bmatrix} > Fe_sOH_2^+ - > Fe_sO^- - 2(> Fe_sO_2)UO_2CO_3^{2-} - > Fe_sO_3^- + CO \\ -2(> Fe_wO_2)UO_2CO_3^{2-} + > Fe_wOH_2^+ - > Fe_wO^- - > Fe_wCO_3^- \end{bmatrix} \qquad E_5^{\,m} = 0$	(5)
$\frac{\partial(\theta E_6)}{\partial t} + L(E_6^{\,m}) = 0 \qquad E_6 = E_6^{\,m} = \rho_w (NO_3^- + UO_2NO_3^+)$	(6)

Note: as defined in Eq. (2.5.7.4), $\rho_s = \rho_b S_A/\theta$.

Table 5.3-3 Equilibrium Reaction Algebraic Equations Solved in Example 5.3.1

Equilibrium Reaction Algebraic Equations	No.	Equilibrium Reaction Algebraic Equations	No.
$0.0018C_{Fe(OH)_3} = C_{>Fe_sOH} + C_{>Fe_sOH_2^+} + C_{>Fe_sO^-} + C_{>Fe_sCO_3H} + C_{>Fe_sCO_3^-} + 2C_{(>Fe_sO_2)UO_2} + 2C_{(>Fe_sO_2)UO_2CO_3^{2-}}$	(1)	$0.8732C_{Fe(OH)_3} = C_{>Fe_wOH} + C_{>Fe_wOH_2^+} + C_{>Fe_wO^-} + C_{>Fe_wCO_3H} + C_{>Fe_wCO_3^-} + 2C_{(>Fe_wO_2)UO_2} + 2C_{(>Fe_wO_2)UO_2CO_3^{2-}}$	(2)
$C_{(>Fe_sO_2)UO_2CO_3^{2-}} = \frac{10^{-13.0} C_{>Fe_s(OH)_2} C_{UO_2^{2+}} C_{H_2CO_3}}{C_{H^+}^4 C_{CO}^2}$	(3)	$C_{(>Fe_wO_2)UO_2CO_3^{2-}} = \frac{10^{-17.10} C_{>Fe_w(OH)_2} C_{UO_2^{2+}} C_{H_2CO_3}}{C_{H^+}^4 C_{CO}^2}$	(4)
$C_{(UO_2)_2(OH)_2^{2+}} = 10^{-5.62} C_{UO_2^{2+}}^2 / C_{H^+}^2$	(5)	$C_{(UO_2)_3(OH)_4^{2+}} = 10^{-11.9} C_{UO_2^{2+}}^3 / C_{H^+}^4$	(6)
$C_{(UO_2)_3(OH)_5^+} = 10^{-15.5} C_{UO_2^{2+}}^3 / C_{H^+}^5$	(7)	$C_{(UO_2)_3(OH)_7^-} = 10^{-31.0} C_{UO_2^{2+}}^3 / C_{H^+}^7$	(8)
$C_{UO_2CO_{3(aq)}} = 10^{-7} C_{UO_2^{2+}} C_{H_2CO_3} / C_{H^+}$	(9)	$C_{UO_2(CO_3)_2^{2-}} = 10^{-16.42} C_{UO_2^{2+}} C_{H_2CO_3}^2 / C_{H^+}^4$	(10)
$C_{UO_2(CO_3)_3^{4-}} = 10^{-28.44} C_{UO_2^{2+}} C_{H_2CO_3}^3 / C_{H^+}^6$	(11)	$C_{>Fe_sO^-} = 10^{-9.13} C_{>Fe_sOH} / C_{H^+} C_{CO}$	(12)
$C_{(>Fe_sO_2)UO_2} = 10^{-2.57} C_{>Fe_s(OH)_2} C_{UO_2^{2+}} / C_{H^+}^2$	(13)	$C_{(>Fe_wO_2)UO_2} = 10^{-6.28} C_{>Fe_w(OH)_2} C_{UO_2^{2+}} / C_{H^+}^2$	(14)
$C_{>Fe_sCO_3^-} = 10^{-5.09} C_{>Fe_sOH} C_{H_2CO_3} / C_{H^+} C_{CO}$	(15)	$C_{(UO_2)_2CO_3(OH)_3^-} = 10^{-17.54} C_{UO_2^{2+}}^2 C_{H_2CO_3} / C_{H^+}^5$	(16)
$C_{(UO_2)_3(CO_3)_6^{6-}} = 10^{-46.08} C_{UO_2^{2+}}^3 C_{H_2CO_3}^6 / C_{H^+}^{12}$	(17)	$C_{>Fe_wO^-} = 10^{-9.13} C_{>Fe_wOH} / (C_{H^+} C_{CO})$	(18)
$C_{>Fe_wCO_3^-} = 10^{-5.09} C_{>Fe_wOH} C_{H_2CO_3} / (C_{H^+} C_{CO})$	(19)	$C_{Fe_sOH} = 2C_{Fe_s(OH)_2}$	(20)
$C_{Fe(OH)_3} = 10^{-2.7} C_{Fe^{3+}} / C_{H^+}^3$	(21)	$C_{Fe_wOH} = 2C_{Fe_w(OH)_2}$	(22)
$C_{UO_2OH^+} = 10^{-5.2} C_{UO_2^{2+}} / C_{H^+}$	(23)	$C_{UO_2(OH)_{2(aq)}} = 10^{-10.3} C_{UO_2^{2+}} / C_{H^+}^2$	(24)
$C_{UO_2(OH)_3^-} = 10^{-19.2} C_{UO_2^{2+}} / C_{H^+}^3$	(25)	$C_{UO_2(OH)_4^{2-}} = 10^{-33.0} C_{UO_2^{2+}} / C_{H^+}^4$	(26)
$C_{(UO_2)_2OH^{3+}} = 10^{-2.7} C_{UO_2^{2+}}^2 / C_{H^+}$	(27)	$C_{CO_3^{2-}} = 10^{-16.68} C_{H_2CO_3} / C_{H^+}^2$	(28)
$C_{>Fe_sOH_2^+} = 10^{6.51} C_{>Fe_sOH} C_{H^+} C_{CO}$	(29)	$C_{CO_{2(g)}} = 10^{1.47} C_{H_2CO_3^0}$	(30)
$C_{>Fe_sCO_3H} = 10^{2.90} C_{>Fe_sOH} C_{H_2CO_3}$	(31)	$C_{FeOH^{2+}} = 10^{-2.19} C_{Fe^{3+}} / C_{H^+}$	(32)
$C_{Fe(OH)_2^+} = 10^{-5.67} C_{Fe^{3+}} / C_{H^+}^2$	(33)	$C_{Fe(OH)_3^0} = 10^{-12.56} C_{Fe^{3+}} / C_{H^+}^3$	(34)
$C_{HCO_3^-} = 10^{-6.35} C_{H_2CO_3^0} / C_{H^+}$	(35)	$C_{Fe(OH)_4^-} = 10^{-21.6} C_{Fe^{3+}} / C_{H^+}^4$	(36)
$C_{>Fe_wOH_2^+} = 10^{6.51} C_{>Fe_wOH} C_{H^+} C_{CO}$	(37)	$C_{>Fe_wCO_3H} = 10^{2.90} C_{>Fe_wOH} C_{H_2CO_3}$	(38)
$C_{NO_3^-} = 10^{0.3} C_{UO_2NO_3^+} / C_{UO_2^{2+}}$	(39)		

5.3.2 Undisturbed Column Breakthrough Curve Simulation for Uranium (VI) Sorption

This problem involves similar geochemistry to that of the packed column, but involves an undisturbed soil core. A miscible displacement experiment was conducted at pH 4 under atmospheric CO_2(g). The core was 15.2 cm in length and 6.19 cm in diameter and was water-saturated from the bottom at 0.1 ml/h to ensure the removal of trapped air. A non-pulsing medical pump was used to deliver a flush solution to the bottom of the column. Approximately 10 L of 50 mM $CaCl_2$ was used to flush the core. Upon completion of the flush, the influent solution consisted of 50 mg/L U(VI) in 50 mM $CaCl_2$ was pumped through the column at a flow rate of 7 ml/h. The residence time of U(VI) in the column was 26.5 h. The pH of the carrier solution was adjusted to 4 with HCl. Uranium (VI) analysis was conducted using an Inductively Coupled Plasma Mass Spectrometer (ICPMS) (Brooks et al, 2005).

The column was numerically discretized with a simulation grid of 20 nodes and 4 equal sized elements (5.49 cm × 5.49 cm × 3.8 cm each) (Fig. 5.3-3). The experiment duration was 2,448 hours, which was simulated with a constant time-step size of 12 hours. Simulations were initially performed assuming the same equilibrium reactions as in Example 5.3.1. The equilibrium sorption simulation results (upper part of Figure 5.3-4) did not accurately predict U(VI) transport through the undisturbed column, indicating that some of the sorption sites may be kinetically hindered resulting in less sorption. Reactions 18 and 19 (Table 5.3-1) are considered to be the most kinetically limiting reactions. Therefore, a second simulation was performed with these two reactions as rate-limited.

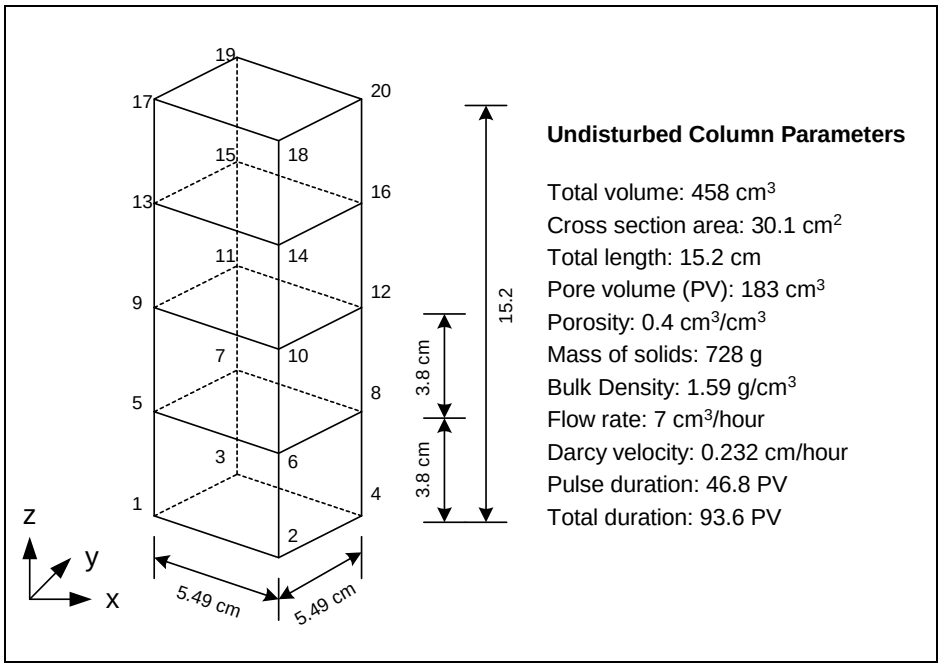

Fig. 5.3-3. Simulation Domain and Descretization for Example 5.3.2

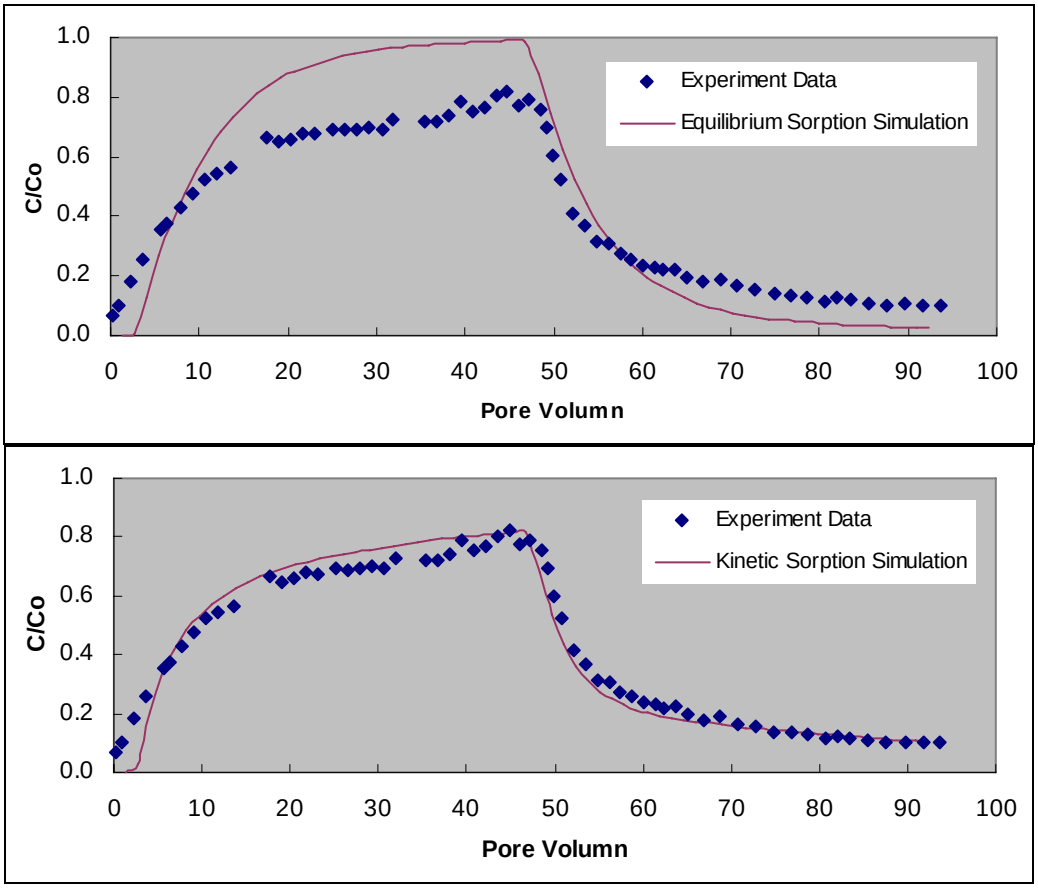

Fig. 5.3-4. U(VI) Breakthrough Curve for the Undisturbed Column
Note: the experiment data are from Brooks et al. (2005)

For the kinetic simulation, we have 46 species, 37 equilibrium reactions and 2 kinetic reactions. As in the previous example, H_2O activity is assumed constant and hence eliminated from the simulation leaving 8 kinetic-variable transport equations (Table 5.3-4) and 37 equilibrium reaction nonlinear algebraic equations (Table 5.3-5) obtained through decomposition.

Among the 8 kinetic-variables, the fifth and the last two involve only immobile species, so that no advection-dispersion equations are needed to solve for them. Therefore, instead of solving 27 mobile species advection-dispersion transport equations, we only need to solve 5 kinetic-variable advection-dispersion transport equations, and the reaction terms related to these kinetic-variables are all simplified. Compared to the previous example, two additional kinetic-variables result from the two linearly independent kinetic reactions. As with the previous example, E_6 can be solved outside the nonlinear iteration loop between hydrologic transport and reactive chemistry when the fully-implicit scheme is used.

Table 5.3-4 Kinetic-variable Transport Equations Solved in Example 5.3.2

Kinetic-Variable Transport Equations	No.
$\frac{\partial(\theta E_1)}{\partial t} + L(E_1^{\,m}) = 0$ $E_1 = \rho_w \begin{bmatrix} H^+ - HCO_3^- - 2CO_3^{2-} - UO_2OH^+ - 2UO_2(OH)_{2(aq)} - 3UO_2(OH)_3^- - 4UO_2(OH)_4^{2-} - (UO_2)_2OH^{3+} \\ -2(UO_2)_2(OH)_2^{2+} - 4(UO_2)_3(OH)_4^{2+} - 5(UO_2)_3(OH)_5^+ - 7(UO_2)_3(OH)_7^- - 2UO_2CO_{3(aq)} - FeOH^{2+} \\ -4UO_2(CO_3)_2^{2-} - 6UO_2(CO_3)_3^{3-} - 12(UO_2)_3(CO_3)_6^{6-} - 5(UO_2)_2CO_3(OH)_3^- - 2Fe(OH)_2^+ - 3Fe(OH)_3^0 \end{bmatrix}$ $- 3\rho_w Fe(OH)_3 + \rho_S \begin{bmatrix} > Fe_sOH_2^+ - > Fe_sO^- - 2(> Fe_sO_2)UO_2 - 2(> Fe_wO_2)UO_2 - 4(> Fe_sO_2)UO_2CO_3^{2-} \\ -4(> Fe_wO_2)UO_2CO_3^{2-} - > Fe_sO_3^- - 4Fe(OH)_4^- + > Fe_wOH_2^+ - > Fe_wO^- - > Fe_wCO_3^- \end{bmatrix}$ $E_1^{\,m} = \rho_w \begin{bmatrix} H^+ - HCO_3^- - 2CO_3^{2-} - UO_2OH^+ - 2UO_2(OH)_{2(aq)} - 3UO_2(OH)_3^- - 4UO_2(OH)_4^{2-} - (UO_2)_2OH^{3+} \\ -2(UO_2)_2(OH)_2^{2+} - 4(UO_2)_3(OH)_4^{2+} - 5(UO_2)_3(OH)_5^+ - 7(UO_2)_3(OH)_7^- - 2UO_2CO_{3(aq)} - FeOH^{2+} \\ -4UO_2(CO_3)_2^{2-} - 6UO_2(CO_3)_3^{3-} - 12(UO_2)_3(CO_3)_6^{6-} - 5(UO_2)_2CO_3(OH)_3^- - 2Fe(OH)_2^+ - 3Fe(OH)_3^0 \end{bmatrix}$	(1)
$\frac{\partial(\theta E_2)}{\partial t} + L(E_2^{\,m}) = 0 \qquad E_2 = \rho_w \left[Fe^{3+} + FeOH^{2+} + Fe(OH)_2^+ + Fe(OH)_3^0 + Fe(OH)_4^- \right] + \rho_P Fe(OH)_3$ $E_2^{\,m} = \rho_w \left[Fe^{3+} + FeOH^{2+} + Fe(OH)_2^+ + Fe(OH)_3^0 + Fe(OH)_4^- \right]$	(2)
$\frac{\partial(\theta E_3)}{\partial t} + L(E_3^{\,m}) = 0$ $E_3 = \rho_w \begin{bmatrix} UO_2^{2+} + UO_2OH^+ + UO_2(OH)_{2(aq)} + UO_2(OH)_3^- + UO_2(OH)_4^{2-} + 2(UO_2)_2OH^{3+} \\ +2(UO_2)_2(OH)_2^{2+} + 3(UO_2)_3(OH)_4^{2+} + 3(UO_2)_3(OH)_5^+ + 3(UO_2)_3(OH)_7^- \\ +UO_2CO_{3(aq)} + UO_2(CO_3)_2^{2-} + UO_2(CO_3)_3^{3-} + 3(UO_2)_3(CO_3)_6^{6-} + 2(UO_2)_2CO_3(OH)_3^- \end{bmatrix}$ $+ \rho_S \left[(> Fe_sO_2)UO_2 + (> Fe_wO_2)UO_2 + (> Fe_sO_2)UO_2CO_3^{2-} + (> Fe_wO_2)UO_2CO_3^{2-} \right]$ $E_3^{\,m} = \rho_w \begin{bmatrix} UO_2^{2+} + UO_2OH^+ + UO_2(OH)_{2(aq)} + UO_2(OH)_3^- + UO_2(OH)_4^{2-} + 2(UO_2)_2OH^{3+} \\ +2(UO_2)_2(OH)_2^{2+} + 3(UO_2)_3(OH)_4^{2+} + 3(UO_2)_3(OH)_5^+ + 3(UO_2)_3(OH)_7^- \\ +UO_2CO_{3(aq)} + UO_2(CO_3)_2^{2-} + UO_2(CO_3)_3^{3-} + 3(UO_2)_3(CO_3)_6^{6-} + 2(UO_2)_2CO_3(OH)_3^- \end{bmatrix}$	(3)
$\frac{\partial(\theta E_4)}{\partial t} + L(E_4^{\,m}) = 0 \qquad E_4^{\,m} = \rho_w \begin{bmatrix} CO_{2(g)} + H_2CO_3 + HCO_3^- + CO_3^{2-} + UO_2CO_{3(aq)} + 2UO_2(CO_3)_2^{2-} \\ +3UO_2(CO_3)_3^{3-} + 6(UO_2)_3(CO_3)_6^{6-} + (UO_2)_2CO_3(OH)_3^- \end{bmatrix}$ $E_4 = \rho_w \begin{bmatrix} CO_{2(g)} + H_2CO_3 + HCO_3^- + CO_3^{2-} + \\ UO_2CO_{3(aq)} + 2UO_2(CO_3)_2^{2-} + 3UO_2(CO_3)_3^{3-} \\ +6(UO_2)_3(CO_3)_6^{6-} + (UO_2)_2CO_3(OH)_3^- \end{bmatrix} + \rho_S \begin{bmatrix} > Fe_sCO_3H + (> Fe_sO_2)UO_2CO_3^{2-} \\ +(> Fe_wO_2)UO_2CO_3^{2-} + > Fe_sCO_3^- \\ + > Fe_wCO_3H + > Fe_wCO_3^- \end{bmatrix}$	(4)
$\frac{\partial(\theta E_5)}{\partial t} + L(E_5^{\,m}) = 0 \qquad E_5 = \rho_S \begin{bmatrix} > Fe_sOH_2^+ - > Fe_sO^- - 2(> Fe_sO_2)UO_2CO_3^{2-} - > Fe_sO_3^- + CO \\ -2(> Fe_wO_2)UO_2CO_3^{2-} + > Fe_wOH_2^+ - > Fe_wO^- - > Fe_wCO_3^- \end{bmatrix} \qquad E_5^{\,m} = 0$	(5)
$\frac{\partial(\theta E_6)}{\partial t} + L(E_6^{\,m}) = 0 \qquad E_6 = E_6^{\,m} = \rho_w (NO_3^- + UO_2NO_3^+)$	(6)
$\frac{\partial(\theta E_7)}{\partial t} + L(E_7^{\,m}) = R_{18} \qquad E_7 = \rho_S (> Fe_sO_2)UO_2 \qquad E_7^{\,m} = 0$	(7)
$\frac{\partial(\theta E_8)}{\partial t} + L(E_8^{\,m}) = R_{19} \qquad E_8 = \rho_S (> Fe_wO_2)UO_2 \qquad E_8^{\,m} = 0$	(8)

Note: as defined in equation (5.4), $\rho_s = \rho_b S_A/\theta$.

Table 5.3-5 Equilibrium Reaction Algebraic Equations Solved in Example 5.3.2

Equilibrium Reaction Algebraic Equations	No.	Equilibrium Reaction Algebraic Equations	No.
$0.0018C_{Fe(OH)_3} = C_{>Fe_sOH} + C_{>Fe_sOH_2^+} + C_{>Fe_sO^-} + C_{>Fe_sCO_3H} + C_{>Fe_sCO_3^-} + 2C_{(>Fe_sO_2)UO_2} + 2C_{(>Fe_sO_2)UO_2CO_3^{2-}}$	(1)	$0.8732C_{Fe(OH)_3} = C_{>Fe_wOH} + C_{>Fe_wOH_2^+} + C_{>Fe_wO^-} + C_{>Fe_wCO_3H} + C_{>Fe_wCO_3^-} + 2C_{(>Fe_wO_2)UO_2} + 2C_{(>Fe_wO_2)UO_2CO_3^{2-}}$	(2)
$C_{(>Fe_sO_2)UO_2CO_3^{2-}} = \frac{10^{-13.0} C_{>Fe_s(OH)_2} C_{UO_2^{2+}} C_{H_2CO_3}}{C_{H^+}^4 C_{CO}^2}$	(3)	$C_{(>Fe_wO_2)UO_2CO_3^{2-}} = \frac{10^{-17.10} C_{>Fe_w(OH)_2} C_{UO_2^{2+}} C_{H_2CO_3}}{C_{H^+}^4 C_{CO}^2}$	(4)
$C_{(UO_2)_2(OH)_2^{2+}} = 10^{-5.62} C_{UO_2^{2+}}^2 / C_{H^+}^2$	(5)	$C_{(UO_2)_3(OH)_4^{2+}} = 10^{-11.9} C_{UO_2^{2+}}^3 / C_{H^+}^4$	(6)
$C_{(UO_2)_3(OH)_5^+} = 10^{-15.5} C_{UO_2^{2+}}^3 / C_{H^+}^5$	(7)	$C_{(UO_2)_3(OH)_7^-} = 10^{-31.0} C_{UO_2^{2+}}^3 / C_{H^+}^7$	(8)
$C_{UO_2CO_{3(aq)}} = 10^{-7} C_{UO_2^{2+}} C_{H_2CO_3} / C_{H^+}$	(9)	$C_{UO_2(CO_3)_2^{2-}} = 10^{-16.42} C_{UO_2^{2+}} C_{H_2CO_3}^2 / C_{H^+}^4$	(10)
$C_{UO_2(CO_3)_3^{4-}} = 10^{-28.44} C_{UO_2^{2+}} C_{H_2CO_3}^3 / C_{H^+}^6$	(11)	$C_{>Fe_sO^-} = 10^{-9.13} C_{>Fe_sOH} / C_{H^+} C_{CO}$	(12)
$C_{>Fe_sCO_3^-} = 10^{-5.09} C_{>Fe_sOH} C_{H_2CO_3} / C_{H^+} C_{CO}$	(13)	$C_{(UO_2)_2CO_3(OH)_3^-} = 10^{-17.54} C_{UO_2^{2+}}^2 C_{H_2CO_3} / C_{H^+}^5$	(14)
$C_{(UO_2)_3(CO_3)_6^{6-}} = 10^{-46.08} C_{UO_2^{2+}}^3 C_{H_2CO_3}^6 / C_{H^+}^{12}$	(15)	$C_{>Fe_wO^-} = 10^{-9.13} C_{>Fe_wOH} / (C_{H^+} C_{CO})$	(16)
$C_{>Fe_wCO_3^-} = 10^{-5.09} C_{>Fe_wOH} C_{H_2CO_3} / (C_{H^+} C_{CO})$	(17)	$C_{Fe_sOH} = 2C_{Fe_s(OH)_2}$	(18)
$C_{Fe(OH)_3} = 10^{-2.7} C_{Fe^{3+}} / C_{H^+}^3$	(19)	$C_{Fe_wOH} = 2C_{Fe_w(OH)_2}$	(20)
$C_{UO_2OH^+} = 10^{-5.2} C_{UO_2^{2+}} / C_{H^+}$	(21)	$C_{UO_2(OH)_{2(aq)}} = 10^{-10.3} C_{UO_2^{2+}} / C_{H^+}^2$	(22)
$C_{UO_2(OH)_3^-} = 10^{-19.2} C_{UO_2^{2+}} / C_{H^+}^3$	(23)	$C_{UO_2(OH)_4^{2-}} = 10^{-33.0} C_{UO_2^{2+}} / C_{H^+}^4$	(24)
$C_{(UO_2)_2OH^{3+}} = 10^{-2.7} C_{UO_2^{2+}}^2 / C_{H^+}$	(25)	$C_{CO_3^{2-}} = 10^{-16.68} C_{H_2CO_3} / C_{H^+}^2$	(26)
$C_{>Fe_sOH_2^+} = 10^{6.51} C_{>Fe_sOH} C_{H^+} C_{CO}$	(27)	$C_{CO_{2(g)}} = 10^{1.47} C_{H_2CO_3^0}$	(28)
$C_{>Fe_sCO_3H} = 10^{2.90} C_{>Fe_sOH} C_{H_2CO_3}$	(29)	$C_{FeOH^{2+}} = 10^{-2.19} C_{Fe^{3+}} / C_{H^+}$	(30)
$C_{Fe(OH)_2^+} = 10^{-5.67} C_{Fe^{3+}} / C_{H^+}^2$	(31)	$C_{Fe(OH)_3^0} = 10^{-12.56} C_{Fe^{3+}} / C_{H^+}^3$	(32)
$C_{HCO_3^-} = 10^{-6.35} C_{H_2CO_3^0} / C_{H^+}$	(33)	$C_{Fe(OH)_4^-} = 10^{-21.6} C_{Fe^{3+}} / C_{H^+}^4$	(34)
$C_{>Fe_wOH_2^+} = 10^{6.51} C_{>Fe_wOH} C_{H^+} C_{CO}$	(35)	$C_{>Fe_wCO_3H} = 10^{2.90} C_{>Fe_wOH} C_{H_2CO_3}$	(36)
$C_{NO_3^-} = 10^{0.3} C_{UO_2NO_3^+} / C_{UO_2^{2+}}$	(37)		

Forward and backward kinetic rate coefficients for U(VI) sorption reactions 18 and 19 of the reaction network (Table 5.1) were fitted to the U(VI) breakthrough curve data using a nonlinear parameter estimation procedure yielding

$$>Fe_s(OH)_2 + UO_2^{2+} = (>Fe_sO_2)UO_2 + 2H^+ \quad \log K_f = 3.04,\ \log K_b = -10.1 \qquad \textbf{(5.1.9)}$$

$$>Fe_w(OH)_2 + UO_2^{2+} = (>Fe_wO_2)UO_2 + 2H^+ \quad \log K_f = -0.494,\ \log K_b = 4.5 \qquad \textbf{(5.1.10)}$$

Simulations of U(VI) transport using kinetic parameters (lower part of Figure 5.3-4) yielded good agreement with the measured results indicating that U(VI) transport may be kinetically controlled in naturally heterogeneous media.

5.3.3 Three-dimensional Reactive Uranium Transport Simulation

This example was undertaken to assess the model capability to handle complex geochemistry within a three-dimensional subsurface domain. A 600 m long, 400 m wide, and 200 m deep region is considered (Figure 5.3-5) and discretized with uniform hexahedral elements with size of 60 m × 50 m × 40 m. A steady state flow field was simulated with the subsurface flow module.

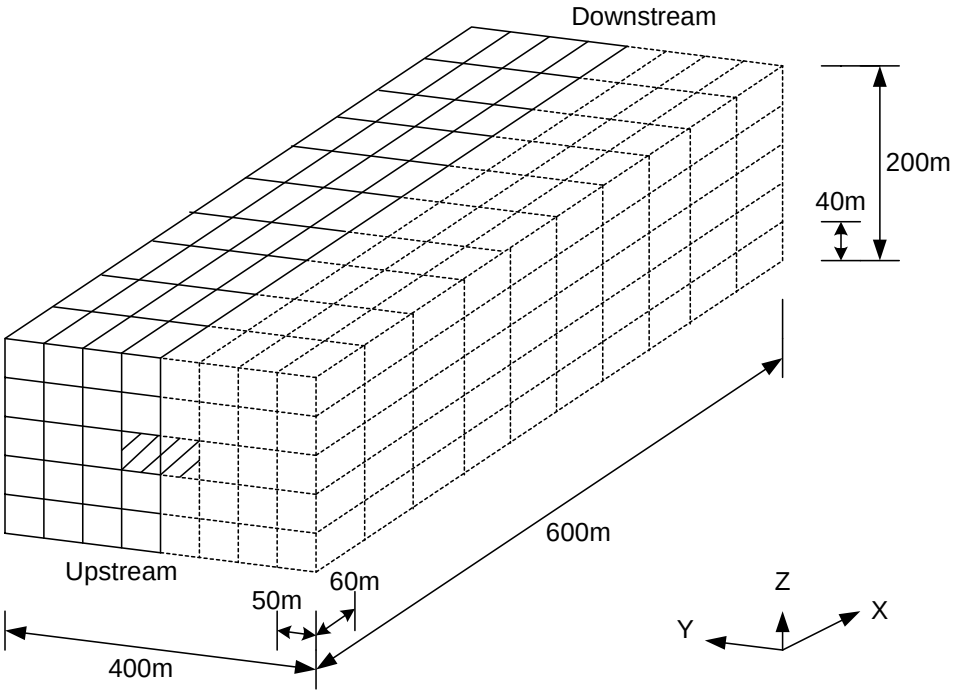

Fig. 5.3-5. Simulation Domain and Descretization for Example 5.3.3

For flow simulations, Dirichlet boundary conditions were applied to the upstream boundary (x = 0 m) with total head of 190 m and to the downstream boundary (x = 600 m) with total head of 180 m. Variable boundary conditions were applied to the top boundary (z = 200 m) with flux of 0.0015 m/d. We assumed a constant effective porosity of 0.3 and saturated hydraulic conductivity of $K_{xx} = K_{yy} =$ 1.0 and K_{zz} = 0.1 m/d. The following two equations were employed to describe the unsaturated hydraulic properties.

$$\theta = 0.1 + \left(0.3 - 0.1\right) \Big/ \left(1 + 4h^2\right) \qquad \textbf{(5.1.11)}$$

$$Kr = \left[0.1 + \left(0.3 - 0.1\right) \Big/ \left(1 + 4h^2\right)\right] \Big/ 0.3 \qquad \textbf{(5.1.12)}$$

where θ is the moisture content and Kr is the relative conductivity. The calculated moisture content is between 0.1 and 0.3 and Darcy velocity is between 0.0014 and 0.021 m/day.

In addition to the chemical species and reactions considered in Example 5.3.2, one more dissolved

species A is assumed to undergo a hypothetic kinetic reduction/oxidation reaction

$$UO_2^{2+} = A \quad \log K_f = -10.0,\ \log K_b = -5.0 \qquad \textbf{(5.1.13)}$$

Initial aqueous and adsorbed concentrations are assumed to be zero. The initial concentration of $Fe(OH)_3$ is assumed to be 0.0523 mol/L and the pH is 4.6 throughout the region. The boundary conditions for the transient simulation are: no flux at the bottom (z = 0 m), the front (y = 0 m) and the back (y = 400 m) boundaries; flow-out variable boundary condition for the downstream boundary (x = 600 m); flow-in variable boundary condition for the top (z = 200 m) and the upstream boundary (x = 0 m) with zero concentration for each mobile species except at the two shaded boundary faces shown in Figure 5.3-5, where the inflow contains UO_2^{2+} of 1.15×10^{-5} mol/L, NO_3^- of 0.05 mol/L, and a nonreactive tracer of 1.15×10^{-5} mol/L. The longitudinal dispersivity is 60 m, the transverse dispersivity is 6 m, and the molecular diffusion coefficient is assumed to be zero. A 100 years simulation is performed with a fixed time-step size of 1 year.

Simulation results within the bisected simulation domain are illustrated in Figure 5.3-6 for nonreactive tracer, aqueous uranium, and sorbed uranium. The two variable boundary faces on the upstream boundary (Shaded in Figure 5.3-5) represent the source of tracer and aqueous uranium. The nonreactive tracer is transported into the domain along with subsurface flow. However, due to the sorption reactions, most of the mobile aqueous uranium is transformed into immobile sorbed uranium in the region close to the two boundary faces. Therefore, uranium plume migration is much slower than that of the nonreactive tracer. The calculated percentage of sorbed uranium ranges from 56% to 96%, which illustrates that a single value of the distribution coefficient is not able to simulate the spatially variable retardation under the condition set for this example.

Using the fully-implicit scheme to deal with reactive chemistry, it took Option 1 (the FEM applied to the conservative form of the transport equations) 611 seconds to perform the simulation with a fixed time-step size of 1 year (maximum Courant number of 0.6). The same accurate simulation could be obtained through Option 3 (the modified LE approach) with a much larger time-step size of 5 years taking CPU time of 156 seconds. Comparison of CPU time verified the efficiency of Option 3.

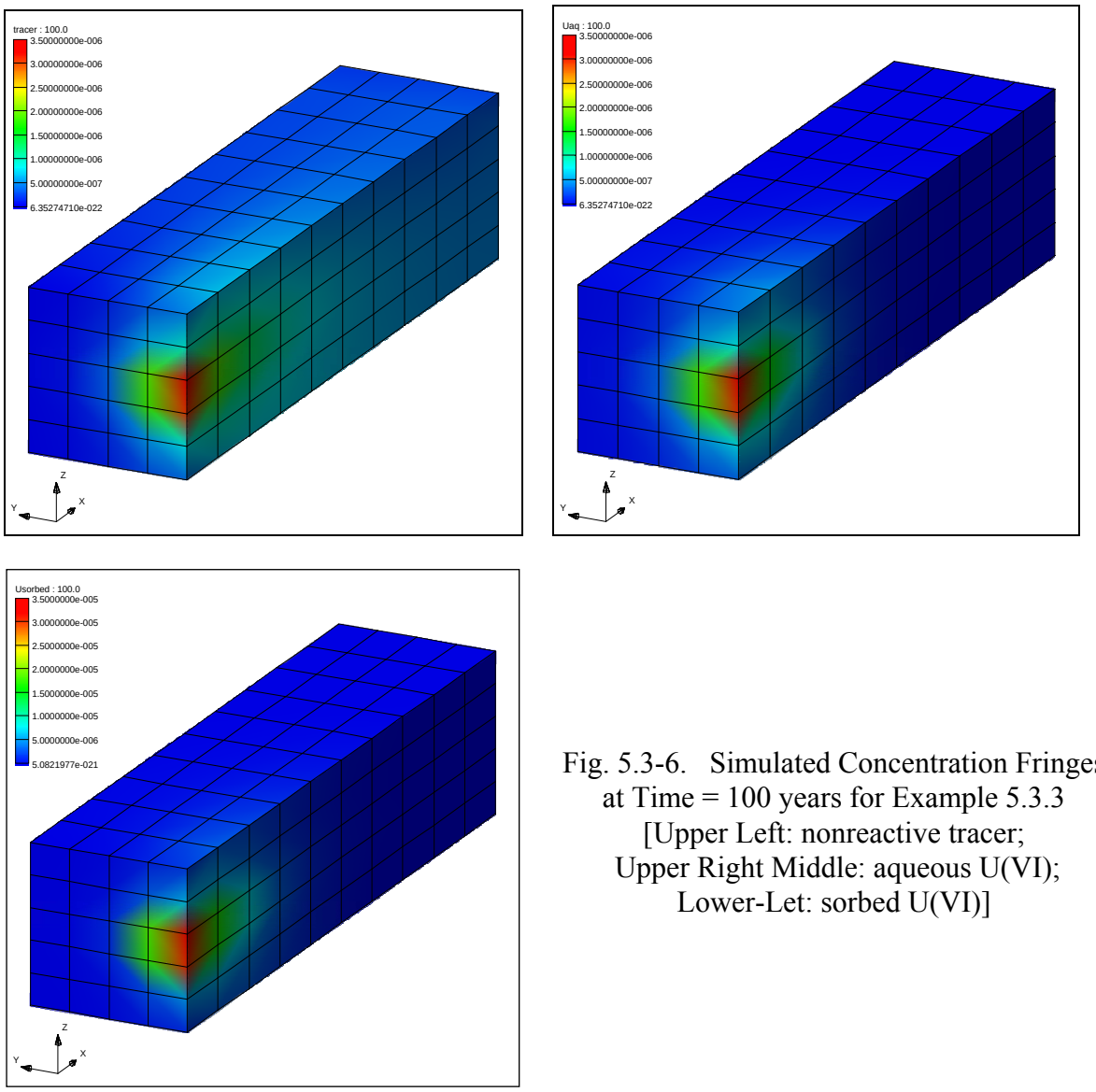

Fig. 5.3-6. Simulated Concentration Fringes at Time = 100 years for Example 5.3.3 [Upper Left: nonreactive tracer; Upper Right Middle: aqueous U(VI); Lower-Let: sorbed U(VI)]

Animations showing the spatial-temporal distribution of tracer (File Name: Figure 5.3-6 Tracer.avi), sorbed uranium (File Name: Figure 5.3-6 Uranium sorbed.avi), and aqueous uranium (File Name: Figure 5.3-6 Uranium Aqueous.avi), respectively, are attached in Appendix A. Readers can visualize these moves by clicking the file contained in the attached CD.

6 SUMMARY AND DISCUSSION

6.1 Summary

WASH123D has taken a step beyond previous models. It was developed to cover dentric river/stream/canal networks and overland regime (land surface) and subsurface media including vadose and saturated (groundwater) zones. It incorporates natural junctions and control structures such as weirs, gates, culverts, levees, and pumps in river/stream/canal networks. It also includes management structures such as storage ponds, pumping stations, culverts, and levees in the overland regime. In the subsurface media, management devices such as pumping/injecting wells, drainage pipes, and drainage channels are also included. Numerous management rules of these control structures and pumping operations have been implemented.

WASH123D is designed to deal with physics-based multi-processes occurring in watersheds. These include density dependent flow and thermal and salinity transport over the entire hydrologic cycle. The processes include (1) evaporation from surface waters (rivers, lakes, reservoirs, ponds, etc) in the terrestrial environment; (2) evportransipiration from plants, grass, and forest from the land surface; (3) infiltration to vadose zone through land surface and recharges (percolations) to groundwater through water tables; (4) overland flow and thermal and salinity transport in surface runoff; (5) hydraulics and hydrodynamics and thermal and salinity transport in densdric river networks; and (6) subsurface flow and thermal and salinity transport in both vadose and saturated zones.

Physics-based fluid flows in stream/river network, overland regime, and subsurface media are considered. Kinematic, diffusive, and fully dynamic wave approaches are all included for applications to dentric rivers and overland regime. Richards' quation is employed for subsurface flow. Junctions and control structures including weirs, gates, culverts, levees, pumping, and storage ponds are included to facilitate management. Boundary conditions for junctions and internal structures are implemented to explicitly enforce mass balance. Interface boundary conditions are rigorously dealt with by imposing the continuity of fluxes and the continuity of state variables or the formulation of fluxes when the state variables are discontinuous. Many optional numerical methods were employed for robust and efficient simulations and for application-dependent simulations.

New paradigms of diagonalizing reaction-based transport equations were employed to simulate water quality transport equations governed by advection-dispersion-reaction transport equations. As a result of these generic approaches, WASH123D can easily be employed to model bigogeochemical cycles (including nitrogen, oxygen, phosphorous, and carbon cycles and biota kinetics (including Algae, Phyotoplankton, Zooplakton, Caliform, Bacteria, Plants, etc.). In fact, once one's ability to transform biogeochemical processes into reaction networks and come up with rate equations for every reaction is achieved, one can employ WASH123D to model his/her system of reactive transport in surface runoff, surface water, and subsurface flows on watershed scales.

WASH123D can be applied to (1) one-dimensional river/stream network only, (2) two-dimensional overland regime only, (3) three-dimensional subsurface media only, (4) coupled one-dimenional

river networks and two-dimensional overland regime, (5) coupled two-dimensional overland regime and three-dimensional subsurface media, (6) coupled three-dimensional subsurface meida and one-dimensional river networks, and (7) coupled one-dimensional river networks, two-dimensional overland regime, and three-dimensional subsurface media. For each application one can simulate flows alone, sediment transport alone, water quality transport alone, or flow and sediment and water quality transport simultaneously. When both flow and transport are simulated, the flow fields are computed first. Then the transport is calculated using the computed flow fields at respective times. Temperature- and salinity-dependent flow is considered.

A total of 17 flow examples were given, which could serve as templates for users in applying WASH123D to either research problems or real-world field applications. These examples are presented to demonstrate the design capability of WASH123D, to show the needs of various approaches to simulate flow in river networks and overland flow problems, and to illustrate some realistic problems using WASH123D.

A total of 13 water quality transport problems were given: six examples for one-dimensional problems, four examples for two-dimensional problems, and three examples for three-dimensional problems. These examples are used to (1) verify the correctness of computer implementation, (2) demonstrate the need of various numerical options and coupling between transport and biogeochemical processes depending on application circumstances, (3) show the generality of the water quality modeling paradigm that embodies the widely used water quality models as specific examples, (4) validate the capability of the models to simulate laboratory experiments, and indicate its potential applications to field problems.

WASH123D could also be applied to (1) Design of flood protection works, (2) Design of wetlands and water conservation areas, (3) Assessment of impacts of tropical storms on flooding, (4) Investigationn of deep injection of fresh water for future use, (5) Dredge material disposal facility design, (6) Study of hazardous and toxic waste remediation, (7) Wellhead protection area definition, (8) Environmental restoration plans, and etc.

WASH123D has been coupled with a bay/estuary model and is ready for coupling with atmospheric models.

6.2 Discussion

Further refinements and enhancements can be made of WASH123D in several areas. First the governing equations for surface water flows and scalar transport should be cast in curvilinear coordinates along river directions for one-dimensional river networks (straightforward) and land surface fitted curvilinear coordinate (not so straightforward) for two-dimesnional overland regime. These modifications will make the model applicable to landscapes of steep slopes. Second high performance parallel computing (partially done by US Army Corps) should be implemented to make the application of the model to large scale problems computationally more tractable. Third, robust and user's friendly graphical interface pre- and post-processors (almost done by US Army Corps)

should be developed to make the learning curves of the model much shorter. Fourth, adaptive local grid refinement algorithms such as LEZOOMPC (Yeh 1990; Yeh, et al., 1992; Yeh, et al., 1995; Cheng, et al., 1996a, 1996b; Cheng et al, 1998a) should be incorporated in the discretization of sharp moving front problems to greatly speed up the computations. Fifth, optimal matrix solvers with computational efforts proportional to N (where N is the number of unknowns) such as algebraic-based multigrid method (Ruge and Stuben, 1985, 1987; Stuben and Trottenberg, 1982; Stuben, 1999a, 1999b) or geometric-based multigrid methods (Brandt, 1984; Bramble, et al., 1988; Xu and Zikatanov, 2000; Cheng, et al., 1998b; Li, et al., 2000, 2005) should be provided to greatly increase the computational speed. The algebraic-based multigrid methods will demand excessive CPU storages and are in general very difficult to achieve optimal performances for matrix equations resulting from generic nonlinear problems. On the other hand, geometric-based multigrid methods require extensive problem specific developments.

REFERENCES

Abbott, M., J. Bathurst, J. Cunge, P. O'Connell, and R. Rasmussen, 1986a. An Introduction to the European Hydrological System, "System Hydrologique European", (SHE), 1: A structure of a physically based, distributed modeling system. Journal of Hydrology 87, 61-67.

Abbott, M., J. Bathurst, J. Cunge, P. O'Connell, and R. Rasmussen, 1986b. An Introduction to the European Hydrological System, "System Hydrologique European", (SHE), 2: History and philosophy of a physically based, distributed modeling system. Journal of Hydrology 87, 45-59.

Adeel, Z., R.G. Luthy, and D.A. Edwards, 1995. Modeling transport of multiple organic compounds: Segregated transport-sorption/solubilization numerical technique, Water Resour. Res., 31(8), 2035-2045.

Ambrose, R.B., Wool, T.A., and Martin, J.L., 1993. The Water Quality Analysis Simulation Program, WASP5 Part A: Model Documentation. Environmental Research Laboratory, US Environmental Protection Agency, Athens, GA.

Bierman, V.J., Jr., James, R.T., 1995. A preliminary modeling analysis of water quality in Lake Okeechobee, Florida: diagnostic and sensitivity analysis. Water Res. 29 (12): 2767–2775.

Bonnet, M. P. and Wessen, K., 2001. ELMO, a 3-D water quality model for nutrients and chlorophyll: first application on a lacustrine ecosystem. Ecological Modeling, 141(1-3): 19-33.

Bramble, J. H., J. E. Pasciak, and J. Xu, 1988. The analysis of multigrid algorithms for nonsymmetric and indefinite elliptic problems. Math. Comp., 51:389-414, 1988.

Brandt, A., 1984. Multigrid Techniques: 1984 Guide with Applications to Fluid Dynamics. Department of Applied Mathematics, The Weizman Institute of Sciences, Rehovot 76100, Israel.

Brooks, S.C, (2001).Waste Characteristics of the Former S-3 Ponds and outline of Uranium Chemistry Relevant to NABIR FRC Studies. Available from: http://public.ornl.gov/nabirfrc/other/brooks_rpt.pdf (date of access: 15 Feb. 2005).

Brown, L.C., and Barnwell, T.O., 1985. Computer Program Documentation for the Enhanced Stream Quality Model QUAL2E, Athens, GA. EPA/600/3-85/065.

Brown, L.C., and Barnwell, T.O., 1987. The Enhanced Stream Water Quality Models QUAL2E and QUAL2E-UNCAS: Documentation and User Manual. US Environmental Protection Agency, Report No. EPA/600/3–87/007.

Brun, A., and P. Engesgaard, 2002. Modeling of transport and biogeochemical processes in pollution plumes: literature review and model development, J. Hydrol., 256, 211-227,.

Burns & McDonnell, 2000. 2D Hydrodynamic Modeling Stormwater Treatment Area 3/4 and East

WCA-3A Hydropattern Restoration, January 2000.

Burns & McDonnell, 2003. Long Term Plan for Achieving Water Quality Goals, October 27, 2003.

Carroll, R., A. James, J. Warwick, and J. Miller, 2004. Modeling erosion and overbank deposition during extreme flood conditions on the Carson River, Nevada. Journal of Hydrology, 297(1-4): 1-21

Cederberg, G.A., R.L. Street, and J.O. Leckie, 1985. A groundwater mass transport and equilibrium chemistry model for multicomponent systems, Water Resour. Res., 21, 1095-1104.

Cerco, C., and Cole, T., 1993. Three-dimensional eutrophication model of Chesapeake Bay. J. Environ. Eng. 119 (6): 1006–1025.

Cerco, C.F., and Cole, T., 1995. User's Guide to the CE-QUAL-ICM Three-Dimensional Eutrophication Model, Release Version 1.0. Technical Report EL-95-15, US Army Engineer Waterways Experiment Station, Vicksburg, MS, 1995.

Cerco, C., 2000. Phytoplankton kinetics in the Chesapeake Bay eutrophication model. Water Qual. Ecosystem Modeling 1: 5–49.

Cerco, C.F, Noel, M.R., and Tillman, D.H., 2004. A practical application of Droop nutrient kinetics (WR 1883). Water Research, 38: 4446–4454.

CH_2M Hill, 1989. Construction and Testing of the Aquifer Storage Recovery (ASR) Demonstration Project for Lake Okeechobee, Florida. South Florida Water Management District, P. O. Box 24680, 3301 Gun Club Road, West Palm Beach, Florida 33416-4680. Prepared by CH_2M Hill, Hillsboro Executive Center North, 800 Fairwaty Drive, Suite 350, Deerfield Beach, Florida 33441, December 1989. SEF24270.BO.61. Volume 1 Engineering Report.

Cheng, J. R., H. P. Cheng, and G. T. Yeh. 1996a. A Lagrangian-Eulerian Method with Adaptively Local Zooming and Peak/Valley Capturing Approach to Solve Two-Dimensional Advection-Diffusion Transport Equations. International J. of Numerical Methods in Engineering, Vol. 39, No. 6, 987-1016.

Cheng, H. P., J. R. Cheng, and G. T. Yeh, 1996b. A particle tracking technique for the Lagrangian-Eulerian finite element method in multi-dimensions. International J. Numerical Methods in Engineering in January, Vol. 39, No. 7, 1115-1136.

Cheng, H. P., J. R. Cheng, and G. T. Yeh, 1998a. A Lagrangian-Eulerian Method with Adaptively Local Zooming and Peak/Valley Capturing Approach to Solve Three-Dimensional Advection-Diffusion Transport Equations. International Journal of Numerical Methods in Engineering, 41:587-615.

Cheng, H. P., G. T. Yeh, M. H., Li, J. Xu, and R. Carsel. 1998b. A study of incorporating the multigrid method into the three-dimensional finite element discretization. International Journal of Numerical Methods in Engineering, Vol. 41, 499-526.

Cheng, H.-P., Yeh, G.-T., and Cheng J.-R., 2000. A numerical model simulating reactive transport in shallow water domains: model development and demonstrative applications. Advances in Environmental Research 4: 187-209.

Cheng, H. P., H. C. Lin, G. T. Yeh, E. Edris, and M. Granat, 2004. Using WASH123D to Design Spreader Canals for Water Management in Watersheds. CD. Proc. World Water & Environmental Resources Congress 2004, Salt Lake City, June 27-July 1, 2004. ASCE, 1801 Alexander Bell Drive, Reston, VA 20191-4400.

Cheng, H-P., J-R., Cheng, D. R. Richards, and G. T. Yeh, 2006. Numerical Strategies to Model Surface and Groundwater Interactions for the Biscayne Bay Coastal Wetlands Project Alternatives. Proc. (CD), XVI International Conferences on Computational Method in Water Rsources, Copenhagen, Denmark, June 19-22, 2006.

Chilakapati, A., 1995. RAFT: A Simulator for ReActive Flow and Transport of Groundwater Contaminants, PNL Report 10636.

Chilakapati, A., T. Ginn, and J. Szecsody, 1998. An analysis of complex reaction networks in groundwater modeling, Water Resour. Res., 34(7), 1767-1780.

Ewen, J., G. Parkin, and P. E. O'Connell, 2000. SHETRAN: Distributed River Basin Flow and Transport Modeling System. J. Hydrologic Engineering, 5(3):250-258.

Falconer, R.A., and Lin, B., 1997. Three-dimensional modeling of water quality in the Humber estuary. Water Res. 31(5): 1092-1102.

Fang, Y. L., Yeh, G. T. and Burgos, W. D., 2003. A Generic Paradigm to Model Reaction-Based Biogeochemical Processes in Batch Systems. Water Resources Research 33(4): 1083-1118.

Fish, J.E., 1988, Hydrogeology, aquifer characteristics, and ground-water flow of the Surficial Aquifer system, Broward County, Florida: U.S. Geological Survey Water Resources Investigations Report 87-4034, 92 p.

Froehlich, D. C., 2002. User's Manual for FESWMS Flo2DH, Release 3, Publication No. FHWA-RD-03-053, Federal Highway Administration, September 2002.

Gerritsen, H., Vos, R.J., Kaaij, T., Laneand A., and Boon, J.G., 2000. Suspended sediment modeling in a shelf sea (North Sea). Coastal Engineering, 41:317-352

Harris, C.K., and Wiberg, P.L, 2001. A two-dimensional, time-dependent model of suspended sediment transport and bed reworking for continental shelves. Computers & Geosciences 27: 675–690.

Harvey, J.W., et. Al, 2002, Interactions between Surface Water and Ground Water and Effects on Mercury Transport in the North-central Everglades: U.S. Geological Survey Water Resources

Investigations Report 02-4050, 91 p.

Hergarten, P. S. G. and H. J. Neugebauer, 1995, An integrated model for the surface runoff and the infiltration of water, EOS, transc. Am. Geophys. Union. Vol. 76, No. 46, F320.

HydroGeoLogic, Inc., 2001. MOD-HMS: A Comprehensive MODFLOW-based Hydrologic Modeling System. Version 1.1. Document and Users Guide, HydrolGeoLogic Inc., Herndon, Virginia.

Keum, D.K., and P.S. Hahn, 2003. A coupled reactive chemical transport model: mixing cell model with two solid phases and its application, Computers & Geosciences, 29, 431-445.

Leendertse, J.J., 1987, Aspects of SIMSYS2D, a system for two-dimensional flow computation: Santa Monica, Calif., Rand Corporation Report R-3572-USGS, 80 p.

Lensing, H. J., M. Voyt, and B. Herrling, 1994. Modeling of biologically mediated redox processes in the subsurface, J. Hydrol., 159, 125-143.

Li, M. H., H. P. Cheng, and G. T. Yeh, 2000. Solving 3-d subsurface density-dependent flow and transport problems with an adaptive multigrid approach. ASCE J. Hydrologic Engineering. Vol. 5, No. 1, 74-81.

Li, M. H., H. P. Cheng, and G. T. Yeh, 2005. An adaptive multigrid approach for the simulation of contaminant transport in 3D subsurface. Computer and Geoscience. 31:1028-1041.

Lin H. C., D. R. Richards, G. T. Yeh, J. R. Cheng, H. P. Cheng, and N. L. Jones, 1997. FEMWATER: A Three-Dimensional Finite Element Computer Model for Simulating Density-Dependent Flow and Transport in Variably Saturated Media. Report CHL-97-12, U. S. Army Corps of Engineers, 3909 halls Ferry Road, Vicksburg, MS 39180-6199.

Lin, H-C J., H. P. Cheng, E. V. Edris, and C. M. Hansen, 2004. Modelign the Water Flow of the Biscayne Bay Coastal Wetland Watershed System for Ecosystem Restoration. Poster Presentation. First National Conference on Ecosystem Restoration. Orlando, Florida, December 6-10, 2004. IFAS, University of Florida, Gainsville, FL.

Liu, C., and T. Narasimhan, 1989. Redox-controlled multiple-species reactive chemical transport, 1, Model development, Water Resour. Res., 25(5), 869-882.

Lung, W.S., 1986. Assessing phosphorus control in the James River basin. J. Envir. Engrg. Div. ASCE 12 (1): 44–60.

Lung, W.-S., and Larson, C.E., 1995. Water quality modeling of the upper Mississippi River and Lake Pepin. J. Environ. Eng. 121(10): 691–699.

MacDonald I., Baines M., Nichols N. and Samuels P. (1997). "Analytical benchmark solutions for open-channel flows", Journal of Hydraulic Engineering, ASCE, Vol. 123, No.11, November, 1997.

MacQuarrie, K.T.B., E.A. Sudicky, and E.O. Frind, 1990. Simulation of biodegradable organic contaminants in groundwater, 1, Numerical formulation in principal directions, Water Resour. Res., 26, 207–222.

McAvoy, D.C., Masscheleyn, P., Peng, C., Morrall S.W., Casilla, A.B., Lim, J.M.U., and Gregorio, E.G., 2003. Risk assessment approach for untreated wastewater using the QUAL2E water quality model, Chemosphere 52: 55–66

McCuen, R. H. 1989. Hydrologic Analysis and Design, Prentice-Hall, Englewood Cliffs, NJ.

McDonald, E.T., and Cheng, R.T., 1994. Issues related to modeling the transport of suspended sediments in Northern San Francisco Bay, California. Proceedings of the 3rd International Conference of Estuarine and Coastal Modeling, 551-564.

Ng, A.W.M., and Perera, B.J.C., 2003. Selection of genetic algorithm operators for river water quality model calibration, Engineering Applications of Artificial Intelligence 16: 529–541.

Ning, S.K., Chang, N.B., Yang, L., Chen H. W., and Hsu, H. Y., 2001. Assessing pollution prevention program by QUAL2E simulation analysis for the Kao-Ping River Basin, Taiwan Journal of Environmental Management (2001) 61: 61–76.

Norton, K. and I. Orlob, 1973. RMA-2, version 1: U.S. Army Corp of Engineers, Walla-Walla District, Walla-Walla, Washington.

Pace, M.N., P.M. Jardine, T.L. Mehlhorn, J. Parker, F. Zhang, S. Graves. 2005. Quantification of the fate and transport of uranium at the U.S. Department of Energy's NABIR site, Oak Ridge, TN. J. of Cont. Hydrol. (in preparation).

Park, S.S., and Lee, Y.S., 2002. A water quality modeling study of the Nakdong River, Korea. Ecological Modeling 152: 65–75.

Park, S.S., Na, Y. and Uchrin, C.G., 2003. An oxygen equivalent model for water quality dynamics in a macrophyte dominated river. Ecological Modeling, 168(1-2)-12.

Parkhurst, D. L., 1995. User's guide to PHREEQC, A computer model for speciation, reaction-path, advective-dispersive transport and inverse geochemical calculations, U.S. Geol. Surv. Water Resour. Invest. Rep., 95-4227.

Parkhurst, D. L., and C.A. J. Appelo, 1999. User's guide to PHREEQC (version 2)-A computer program for speciation, batch-reaction, one-dimensional transport, and inverse geochemical calculations, U.S. Geol. Surv. Water Resour. Invest. Rep., 99-4259.

Prandle, D., Hargreaves, J.C., McManus, J.P., Campbell, A.R., Duwe, K., Lane, A., Mahnke, P., Shimwell, S., and Wolf, J., 2000. Tide, wave and suspended sediment modeling on an open coast — Holderness. Coastal Engineering, 41: 237-267.

Roesner, LA, Giguere, PR, and Evenson, DE, 1981. Computer program documentation for the stream quality model QUAL-II. Report EPA 600y9-81-014. Athens, Georgia, USA: USEPA; 1981.

Ruge, J. W. and K. Stuben, 1985. Efficient solution of finite difference and finite element equations by algebraic multigrid (AMG). Multigrid Methods for Integral and Differential Equations, Paddon, D.J., Holstein H., eds., The Institute of Mathematics and its Applications Conference Series, New Series Number 3, pp. 169-212, Clarenden press, Oxford, 1985.

Ruge, J. W. and K. Stuben, 1987. Algebraic multigrid. In S.~F. McCormick, editor, Multigrid methods, Frontiers in applied mathematics, Vol 5, pages 73--130, Philadelphia, Pennsylvania, 1987. SIAM.

Rubin, J., 1983. Transport of reacting solutes in porous media: relation between mathematical nature of problem formulation and chemical nature of reactions. Water Resours. Res., 19: 493-502.

Saiers, J.E., H. Guha, P. Jardine, and S. Brooks, 2000. Development and evaluation of a mathematical model for the transport and oxidation-reduction of CoEDTA, Water Resour. Res., 31(11), 3151-3165.

Segel, I. H., 1975. Enzyme Kinetics. John Wiley & Sons, Inc. 957 pp.

SFWMD (South Florida Water Management District), 2001. Two dimensional Hydraulic Analysis for Cell 3 of STA-2, an SAV-dominated Treatment Cell, March 21, 2001.

SFWMD (South Florida Water Management District), 2002. Northern Palm Beach County Comprehensive Water Management Plan, Planning Document Volume I.

SFWMD (South Florida Water Management District), 2004a. 2004 Everglades Consolidated Report, West Palm Beach, FL

SFWMD (South Florida Water Management District) 2004b. Stormwater Treatment Area 6 Operation Plan, April, 2004, West Palm Beach FL.

SFWMD (South Florida Water Management District), 2005. Regional Simulation Model (RSM): Theory Manual. South Florida Water Management District (SFWMD), Office of Modeling, 3301 Gun Club Road, West Palm Beach, FL 33406.

Shen, Y., Zheng, Y., Komatsu, T., and Kohashi, N., 2002. A three-dimensional numerical model of hydrodynamics and water quality in Hakata Bay. Ocean Engineering, 29 (4): 461-473.

Singh, V. P., 1996, Kinematic Wave Modeling in Water Resources, John Wiley & Sons, Inc.

Somlyody, L., Henze, M., Koncsos, L., Rauch, W., Reichert, P., Shanahan, P. and Vanrolleghem, P., 1998. River water quality modeling III: future of the art. Water Research 38(11): 253-260.

Steefel, C.I., and A.C. Lasaga, 1994. A coupled model for transport of multiple chemical species and kinetic precipitation/dissolution reactions with application to reactive flow in single phase hydrothermal systems, Am. J. Sci., 294, 529-592.

Steefel, C. I., and Cappellen, V.P., 1998. Preface: Reactive transport modeling of natural systems. J. Hydrol. 209: 1–7.

Stüben, K. and U. Trottenberg, 1982. Multi-grid methods: Fundamental algorithms, model problem analysis and applications. Multigrid Methods (W. Hackbusch and U. Trottenberg, eds.), Springer Verlag, Berlin, 1982.

Stüben, K., 1999a. Algebraic multigrid (AMG): experiences and comparisons, GMD Rep. 53 (1999), St. Augustin.

Stüben, K., 1999b. A review of algebraic multigrid, GMD Rep. 69 (1999), St. Augustin.

Sutron Corporation, 2004. STA-2 two-dimensional Hydraulic Modeling Final Report, prepared for SFWMD, May 2004.

Swain, E. D., Wolfert M. A., Bales J. D., and Goodwin C. R., 2004. Two-Dimensional Hydrodynamic Simulation of Surface-Water Flow and Transport to Florida Bay through the Southern Inland and Coastal Systems (SICS), U.S. Geological SurveyWater-Resources Investigations Report 03-4287, 2004.

Tebes-Stevens, C., A. J. Valocchi, J. M. VanBriesen, and B. E. Rittmann, 1998. Multicomponent transport with coupled geochemical and microbiological reactions: Model description and example simulations, J. Hydrol., 209, 8-26.

Thomann R. V., 1998. The future “golden age” of predictive models for surface water quality and ecosystem management. Journal of Environmental Engineering, ASCE 124(2): 94-103.

Tompson, A.F.B., 1993. Numerical Simulation of Chemical Migration in Physically and Chemically Heterogeneous Porous Media, Water Resour. Res., 29, 3709-3726.

Tufford, D.L., and McKellar, H.N., 1999. Spatial and temporal hydrodynamic and water quality modeling analysis of a large reservoir on the South Carolina (USA) coastal plain. Ecological Modeling, 114 (2-3): 137-173.

VanderKwaak, J. E., 1999. Numerical Simulation of Flow and Chemical Transport in Integrated Surface-Subsurface Hydrologic Systems. Ph.D. Thesis, Dept. of Earth Science, University of Waterloo, Waterloo, Ontario, Canada.

Wagner, R.A., Tisdale, T.S., and Zhang, J., 1996. A framework for phosphorus transport modeling in the Lake Okeechobee watershed evaluation. Water Res. Bull. 32 (1): 57–73.

Walton, R., E. Wexler, and R. Chapman, 1999. An integrated groundwater-open channel flow

model (MODNET). Tech. Recport, West Consultants, Bellevue, Washington.

Wang, J. D. and J. J. Connor, 1975, Mathematical Modeling of Near Coastal Circulatioin, MITSG 75-13, Massachusetts Institute of Technology, Cambridge, Massachusetts 02109.

Wanielista, M., W. Milon, H. Shan, O. Nnadi, D. Finnoff, and G. Yeh, 2004. Evaluation of the Storage Value of Reservoirs in South Florida. Stormwater Management Academy, University of Florida, Orlando, FL 32816. June 2004.

Wigmosta, M. S. and Perkins, 1997. A GIS-Based Modeling System for Watershed Analysis. Final Report to the National Council of the Paper Industry for Air and Stream Improvement. 160 pp.

Wood, B.D., C.N. Dawson, J.E. Szecsody, and G.P. Streile, 1994. Modeling contaminant transport and biodegradation in a layered porous media system, Water Resour. Res., 30(6), 1833– 1845.

Wu F., Shen H.W. and Chou Y., 1999. Variation of Roughness Coefficients for Unsubmerged and Submerged Vegetations., ASCE Journal of Hydolrogic Engineering, Vol. 125, No. 9, September 1999.

Xu, J. and L. Zikatanov, 2000. "A Monotone Finite Element Scheme for Convection Diffusion Equations", Math. Comp., 68:1429-1446, 2000

Yang, M.D., Sykes, R.M., and Merry, C.J., 2000. Estimation of algal biological parameters using water quality modeling and SPOT satellite data Ecological Modeling 125: 1–13

Yeh, G. T., 1969. Turbulent Diffusion by Forced Convection. Ph.D. Dissertation. School of Civil and Environmental Engineering, Cornell Universtiy, Ithaca, New York. 124 pp.

Yeh, G. T., Verma, A. P., and F. H. Lai, 1973. Unsteady temperature predictions in cooling ponds, Water Res. Res. 9:1555 63.

Yeh, G. T., 1987. 3DFEMWATER: A Three-Dimensional Finite Element Model of Water Flow through Saturated-Unsaturated Porous Media. Report 2904, Oak Ridge National Laboratory, U.S.A.

Yeh, G. T., 1990. A Lagrangian-Eulerian method with zoomable hidden fine-mesh approach to solving advection-dispersion equations, Water Resources Res. Vol. 26, No. 6, 1133-1144.

Yeh, G.T. and V.S. Tripathi, 1991. A model for simulating transport of reactive multispecies components: model development and demonstration, Water Resour. Res., 27, 3075-3094.

Yeh, G. T., J. R. Chang, and T. E. Short. 1992. An Exact Peak Capturing and Essentially Oscillation-Free Scheme to Solve advection-dispersion-reactive transport equations. Water Resour. Res.. Vol. 28, No. 11, 2937-2951.

Yeh, G. T., J. R. Chang, J. P. Gwo, H. C. Lin, W. Martin, and D. Richards. 1994. 3DSALT: A Three-dimensional Salt Intrusion Model in Saturated-Unsaturated Media. Instruction Report HL-94-

1. Waterway Experiment Station, U. S. Army Corps of Engineers, Vicksburg, MS.

Yeh, G. T., J. R. Chang, H. P. Cheng, and C. H. Sung. 1995. An adaptive local grid refinement based on the exact peak capturing and oscillation free scheme to solve transport equations, Computers and Fluids, Vol. 24, No. 3, 293-332.

Yeh, G. T., J. R. Cheng, M. H. Li, H. P. Cheng, and H. C. Lin, 1997. COSFLOW: A Finite Element Model Coupling One-Dimensional Canal, Two-Dimensional Overland, and Three-Dimensional Subsurface Flow. Technical Report CHL-97-20. U. S. Army Corps of Engineers, Waterways Experiment Station, 39909 Halls Ferry Road, Vicksburg, MS 39180-6199. 188 pp.

Yeh, G. T., H. P. Cheng, J. R. Cheng, and Jerry H. Lin. 1998. A Numerical Model to Simulate Water Flow and Contaminant and Sediment Transport in Watershed Systems of 1-D Stream-River Network, 2-D Overland Regime, and 3-D Subsurface Media (WASH123D: Version 1.0). Technical Report CHL-98-19. Waterways Experiment Station, U. S. Army Corps of Engineers, Vicksburg, MS 39180-6199.

Yeh, G.T., Burgos, W.D., and Zachara, J.M., 2001a. Modeling and measuring biogeochemical reactions system consistency, data needs, and rate formulation. Advances in Environmental Research, 5: 219-237.

Yeh, G.T., M.D. Siegel, and M.H. Li, 2001b. Numerical modeling of coupled fluid flows and reactive transport including fast and slow chemical reactions, J. Contam. Hydrol., 47, 379-390.

Yeh, G. T., G. B. Huang, and H. C. Lin, 2003. A first principle, physics-based watershed model of various temporal and spatial scale. Proc. (CD) World Water Resources and Environment Conference, ASCE, Philadelphia, June 23-26, 2003.

Yeh, G.T., J.T. Sun, P.M. Jardine, W.D. Burger, Y.L. Fang, M.H. Li, and M.D. Siegel, 2004. HYDROGEOCHEM 5.0: A Three-Dimensional Model of Coupled Fluid Flow, Thermal Transport, and HYDROGEOCHEMical Transport through Variable SaturatedConditions - Version 5.0, ORNL/TM-2004/107, Oak Ridge National Laboratory, Oak Ridge, TN 37831.

Yeh, G.T., G. B. Huang, H. P. Cheng, F. Zhang, H. C. Lin, E. Edris, and D. Richards. 2005. A first principle, physics-based watershed model: WASH123D, in Watershed Models. Eds. By Singh VP and Frevert DK, CRC Press, Boca Raton, FL, September 2005.

Yen, B. C., 1992. ‘‘Hydraulic resistance in open channels.’’ Channel flow resistance: Centennial of Manning’s formula, B. C. Yen, ed., Water Resources Publications, Littleton, Colo.

Zeng, W., and Beck, M.B., 2003. STAND, a dynamic model for sediment transport and water quality. Journal of Hydrology 277: 125–133.

Zhang, F. 2005. A New Paradigm of Modeling Watershed Water Quality. Ph.D. Dissertation. Department of Civil and Environmental Engineering, University of Central Florida, Orlando, FL 32816.

Zheng, L., Chen, C. and Zhang, F.Y., 2004. Development of water quality model in the Satilla River Estuary, Georgia. Ecological Modeling, 178 (3-4): 457-482.